

Abstract Volume 14th Swiss Geoscience Meeting

Geneva, 18th – 19th November 2016

Time in Geosciences:
Knowledge for a new beginning



sc | nat 

Swiss Academy of Sciences
Akademie der Naturwissenschaften
Accademia di scienze naturali
Académie des sciences naturelles



**UNIVERSITÉ
DE GENÈVE**

FACULTÉ DES SCIENCES
Section des sciences de la Terre
et de l'environnement

Big Picture: The Geologic Time Spiral, A Path to the Past

The Earth is very old—4.5 billion years or more according to scientific estimates. Most of the evidence for an ancient Earth is contained in the rocks that form the Earth's crust. The rock layers themselves—like pages in a long and complicated history—record the events of the past, and buried within them are the remains of life—the plants and animals that evolved from organic structures that existed 3 billion years ago.

Also contained in rocks once molten are radioactive elements whose isotopes provide Earth with an atomic clock. Within these rocks, «parent» isotopes decay at a predictable rate to form «daughter» isotopes. By determining the relative amounts of parent and daughter isotopes, the age of these rocks can be calculated. Thus, the scientific evidence from rock layers, from fossils, and from the ages of rocks as measured by atomic clocks attests to a very old Earth.

REFERENCE: Graham, Joseph, Newman, William, and Stacy, John, 2008, The geologic time spiral—A path to the past (ver. 1.1): U.S. Geological Survey General Information Product 58, poster, 1 sheet. (Also available online at <http://pubs.usgs.gov/gip/2008/58/>.)

Small Picture: «the Pillars of cration»

Astronomers using NASA's Hubble Space Telescope have assembled in 2015 a bigger and sharper photograph of the iconic Eagle Nebula's "Pillars of Creation" from 1995.

Credits: NASA/ESA/Hubble Heritage Team (STScI/AURA)/J. Hester, P. Scowen (Arizona State U.)

14th Swiss Geoscience Meeting, Geneva 2016

Table of contents

Organisation 2

Abstracts

0	Plenary Session	4
1	Structural Geology, Tectonics and Geodynamics	10
2	Mineralogy, Petrology, Geochemistry	52
3	Gemmology	120
4	Palaeontology	126
5	The Sedimentary Record of Tectonic, Climatic and Environmental Change From Deep to Modern Times	176
6	Stratigraphy	214
7	Timing of Earth Processes: from dates to rates	226
8	Rock mechanics, Rock physics and Geophysics	286
9	Subsurface Geology & Geo-Energy	326
10	Open Session in Geomorphology	378
11	Quaternary environments: landscapes, climate, ecosystems, human activity during the past 2.6 million years	406
12	Cryospheric Sciences	458
13	Hydrology, Limnology and Hydrogeology	506
14	Environmental Biogeochemistry of Trace Elements	562
15	Linking Trace Element and Carbon Biogeochemistry	592
16	Trace elements in aquatic ecosystems: from legacy to emerging pollutants	606
17	Atmospheric Processes and Interactions with the Biosphere	620
18	Phenology and seasonality (merged with 19)	632
19	Earth Observation addressing key Earth System processes (merged with 18)	632
20	Geoscience and Geoinformation – From data acquisition to modelling and visualisation	648

Organisation

Host Institution

Section of Earth and Environmental Sciences of the University of Geneva

Patronnage

Platform Geosciences of the Swiss Academy of Sciences SCNAT

Local Organizing Committee

Sébastien Castelltort (president SGM 2016)

Stéphanie Girardclos (core team)

Edwin Gnos (core team)

Elias Samankassou (core team)

Susanne Schmidt (onsite registrations desk and receipts)

Matteo Lupi (communication, publicity and outreach)

Corine Frischknecht (exhibitors)

Massimo Chiaradia (posters)

Guy Simpson (posters)

Rossana Martini

Urs Schaltegger

Daniel Ariztegui

Coordination

Pierre Dèzes

Sponsors

Swiss Geological Survey, swisstopo

CHGEOL

Faculty of Sciences of the University of Geneva

Frontiers in Earth Science

International Association of Sedimentologists (IAS)

International Union of Geodesy and Geophysics (IUGG)

International Union of Geological Sciences (IUGS)

Natural History Museum of Geneva

Services Industriels de Genève (SIG)

Swiss Academy of Sciences (SCNAT)

Swiss Drilling

Swiss Gemmological Institute (SSEF)

Société académique de Genève (sacad)

Tescan Orsay France

University of Geneva (fond général)

Participating Societies and Organisations

Commission of Limnology and Oceanography

Federal office of Topography (swisstopo)

International Union of Geodesy and Geophysics, Swiss Committee (IUGG)

International Union of Geological Sciences, Swiss Committee (IUGS)

Kommission der Schweizerischen Paläontologischen Abhandlungen (KSPA)

Muséum National d'Histoire Naturelle

ProClim – Forum for Climate and Global Change

Swiss Association of Energy Geoscientists (SASEG)

Swiss Association of Geographers (ASG)

Swiss Commission on Atmospheric Chemistry and Physics (ACP)

Swiss Commission for Phenology and Seasonality (CPS)

Swiss Commission for Remote Sensing (SCRS)

Swiss Committee for Stratigraphy (Platform Geosciences/SCNAT)

Swiss Gemmological Society (SGG-SSG)

Swiss Geodetic Commission (SGC)

Swiss Geological Society (SGG/SGS)

Swiss Geological Survey (swisstopo)

Swiss Geomorphological Society (SGGm/SSGm)

Swiss Geophysical Commission (SGPK)

Swiss Geotechnical Commission (SGTK)

Swiss Hydrogeological Society (SGH)

Swiss Hydrological Commission (CHy)

Swiss Paleontological Society (SPG/SPS)

Swiss Snow, Ice and Permafrost Society (SIP)

Swiss Society for Hydrology and Limnology (SGHL/SSHL)

Swiss Society for Quaternary Research (CH-QUAT)

Swiss Society of Mineralogy and Petrology (SMPG/SSMP)

Swiss Tectonics Studies Group (Swiss Geological Society)

0. Plenary Session

- 1 Klaus Mezger: A Time-Line for the Formation of Terrestrial Planets
- 2 Andrew Knoll: The Proterozoic Eon: Life and Environments in Earth's Middle Age
- 3 Edouard Bard: Radiocarbon as a geochronometer and as a tracer in paleoclimatology, geophysics and astrophysics
- 4 Ulrike Niemeier: The Anthropocene: May we cure the symptoms of a changing climate

1

A Time-Line for the Formation of Terrestrial Planets

Klaus Mezger

Institut für Geologie, Universität Bern, Baltzerstrasse 1+3, CH-3012 Bern (klaus.mezger@geo.unibe.ch)

The discovery of numerous exoplanets in the last two decades created renewed interest in a detailed understanding of the process that can lead to the formation of planetary systems consisting of rocky and gas-dominated planets. Exoplanet can only be observed via telescopes and their formation and evolution can only be understood through modelling since in-situ analyses by space crafts is currently not feasible and material for direct study in the laboratory is, and will be for a long time, unavailable. The only planetary system that can be study directly via space missions and meteorites delivered to Earth is our own solar system, which, could serve as a model for other planetary systems. However, a concern is the possibility that it is an unusual or a rare type of planetary systems in the universe.

A key problem towards a robust model for planetary origin and evolution is the combination of physical parameters and chemical evolution of material with the time of important events and processes in the early solar system starting from the formation of dust to the differentiation of rocky bodies. The different materials from planetary bodies of our solar system available for direct study in the laboratory preserve valuable information on these early processes, their timing and duration. In order to obtain reliable and meaningful time constraints for the sequence of chemical differentiation processes that led to planet formation, high precision and high resolution ages are crucial. Improvements in analytical techniques in the last decade for the analyses of small variations in isotope abundances generated by short-lived isotopes were essential to obtain precise and accurate ages.

Time constraints can be derived from chemical and isotopic analyses of primitive meteorites and their components using long and short-lived isotope systems. The time line for early solar system processes and events derived from these materials has significantly changed the physical and chemical models describing the evolution of the solar nebula from its formation to the formation of planets. Key findings include the discovery that some planetesimals formed and differentiated into metal cores and silicate mantles within the first Ma of the beginning of the solar system. The observation that chondrites, the chemically and mineralogically most primitive materials of the solar system, formed over a time interval of several Ma and after the first highly differentiated planetary bodies had formed. The time needed to form the planets from a cloud of dust and gas was long thought to have taken around 100 Ma, but the new geochronological constraints reveal that the processes involved had a duration that is about one order of magnitude shorter.

2 The Proterozoic Eon: Life and Environments in Earth's Middle Age

Knoll A.H.

Harvard University Botanical Museum, Cambridge MA 02138, USA

the Proterozoic Eon began, Earth was already two billion years old. Nonetheless, Proterozoic rocks provide our first clear chronicle of evolutionary history, documented by well-preserved microfossils, biomarker molecules, isotopic signatures, and sedimentary structures, especially stromatolites.

Cyanobacteria radiated in oxygenated surface oceans, but recurring anoxia within the photic zone supported regionally extensive primary production by anoxygenic photosynthetic bacteria. By 1700-1600 million years ago (Ma), eukaryotic cells had gained a foothold in the oceans, adding new morphological and ecological complexity to marine ecosystems.

Although unambiguous eukaryotic microfossils occur in mid-Proterozoic rocks, protistan diversity remained relatively low until about 800 Ma, when new types of fossils, including testate and scale-forming taxa, radiated. It is hypothesized that the evolution of eukaryovory – predation by eukaryotic cells on other eukaryotes -- provided an ecological driver for Neoproterozoic eukaryotic diversification. Ecology also played a key role in the ensuing radiation of animals, with carnivores playing a role comparable to that eukaryovores in earlier Neoproterozoic ecosystems.

The environments within which cyanobacteria, eukaryotes and animals sequentially diversified differed from both those of the Archean Eon and those familiar to us today. In particular, the basal Proterozoic rise of oxygen in the atmosphere and surface oceans permitted innovations in energy metabolism and biosynthetic pathways, although persistent subsurface anoxia likely provided a continuing challenge to early aerobic organisms.

Following a prolonged interval of low pO_2 , the atmosphere and oceans began their transition to a more modern redox state near the end of the Eon. Oxygen availability placed significant constraints on Proterozoic evolution, and renewed oxygenation near the end of the eon likely facilitated animal radiation, not least by making carnivory possible. Thus, the ecological theater of Proterozoic environments and the evolutionary play recorded by fossils appear to have influenced each other throughout Earth's long middle age.

3

Radiocarbon as a Geochronometer and as a Tracer in Paleoclimatology, Geophysics and Astrophysics

Edouard Bard*

* Collège de France & CEREGE, Technopôle de l'Arbois, 13545 Aix-en-Provence, France (bard@cerege.fr)

An accurate chronometer that covers the past 50,000 years is of paramount importance in fields such as geophysics, geochemistry, and paleoclimatology. Since the 1950s, radiocarbon measurements have been used to obtain accurate dates for various archives of past events. While alive, organisms equilibrate with the atmospheric $^{14}\text{C}/^{12}\text{C}$ ratio, but when they die, the ratio starts to decrease as ^{14}C decays. The ^{14}C content of biological remains therefore correlates with their age. However, we now recognize that the atmospheric $^{14}\text{C}/^{12}\text{C}$ ratio varies with time. To calculate accurate ages, atmospheric ^{14}C fluctuations must be corrected for with a calibration curve obtained by comparing the raw ^{14}C measurements with true calendar ages derived from independent dating methods (e.g. counting tree-rings or another radiometric methods such as uranium-thorium).

The high frequency variations in ^{14}C composition, from a year to a millennium, are related to changes in the production rate of ^{14}C in response to fluctuations of the Sun, which modulates the arrival of protons on Earth. Over the long term, the dominant factor is the variation of the geomagnetic field. Any reduction in this field allows penetration of more cosmic rays into the atmosphere, thus enhancing the formation of cosmogenic nuclides. The maximum of ^{14}C production corresponds to the Laschamp magnetic excursion, during which the geodynamo weakened very sharply. The short and long term ^{14}C variations in the atmosphere can be compared with those observed for other cosmogenic isotopes, notably the beryllium 10 record in ice cores from Antarctica.

In addition, the ^{14}C and ^{10}Be production signal is often perturbed by other sources of variations linked to the geochemical cycles of these elements on Earth. For example, atmospheric precipitations and volcanic eruptions can affect ^{10}Be observations. Geochemical cycles of both elements are vastly different so that it is useful to combine ^{10}Be and ^{14}C data to reconstruct the past geomagnetic and solar variabilities. This comparison is indeed crucial because the atmospheric $^{14}\text{C}/^{12}\text{C}$ ratio also varies in response to climate changes, which affected the global carbon cycle as illustrated by large variations of the pCO_2 measured in bubbles occluded in ice cores from Antarctica.

If the geological clock can be inferred independently, the ^{14}C can be used as a tracer to probe the past carbon cycle and to reconstruct the variations of fluxes between its various reservoirs. For example, the sea surface reservoir age varies spatially in the ocean as it depends on air-sea gas exchange and oceanic mixing. It is thus sensitive to climate parameters such as sea-surface temperature, wind strength, sea-ice cover and air-sea pCO_2 gradient. ^{14}C measurements in various shells of organisms living at the sea surface allow showing that its reservoir age varied in the past, notably during the deglaciation characterized by low pCO_2 and large reorganizations of the atmosphere-ocean couple. In parallel to ^{14}C measurements in surface shells, it is possible to probe the interior of the ocean by measuring ^{14}C in benthic foraminifera and deep-water corals. A coherent picture is beginning to emerge from a growing number of data showing large changes of the residence time of the deep and intermediate ocean water masses.

To illustrate the progress in this research field, I will review several key and ongoing studies documenting short and long-term ^{14}C variations on Earth and providing invaluable insights on climatological, biogeochemical, geophysical and astrophysical processes.

4 The Anthropocene: May we cure the symptoms of a changing climate?

Ulrike Niemeier,

Max Planck Institute for Meteorology, Bundesstr 53, D-20146 Hamburg

About two hundred years ago the first industrial revolution started introducing serious anthropogenic emissions by humans. Burning coal to run the first steam-engine was one of the first anthropogenic emissions of CO₂. Since then, anthropogenic CO₂ emissions are steadily rising. The consequence is a changing climate.

Concentrations of CO₂ on Earth are changing also naturally. CO₂ reached even higher concentrations on Earth before, but when discussing climate change, the quality of human life on Earth matters. Rising temperatures have an impact on the daily live of people. Changing precipitation amount and pattern may cause increasing numbers of floods and droughts. Furthermore, increasing temperatures coincide with a rising sea level, which also bears the danger of loosing valuable land.

Last year, 2015, in Paris politicians agreed on a 1.5 K goal of maximum temperature rise, which would require a very fast transition to a fossil-free economy. But attempts to initiate the decrease of CO₂ emissions have not been very successful in the last years. In this situation climate engineering may become an important issue.

Climate engineering is the deliberate large-scale manipulation of the climate to counteract anthropogenic climate change. Climate engineering techniques have been proposed in order to prepare for the case that attempts to limit projected climate change by the reduction of greenhouse gas concentrations may not be sufficient, or that consequences of climate change may prove worse than expected. A climate-engineered climate differs from a natural one of the same global mean temperature. Therefore, numerical model studies on possible risk and side effects for crucial parts of the Earth system and human kind were performed.

Different climate-engineering techniques of reducing incoming solar radiation, the so called solar radiation management (SRM), have been proposed to possibly counteract global warming. Among them are the injection of sulfur into the stratosphere, mirrors in space, and marine cloud brightening through artificial emissions of sea salt. The injection of sulfur will be taken as an example for performing climate engineering within model studies and to discuss climate impacts, limits and uncertainties, as well as consequences of stopping climate engineering and an estimate of a time frame how long climate engineering may have to be performed when started.

1. Structural Geology, Tectonics & Geodynamics

Guido Schreurs, Neil Mancktelow, Paul Tackley

Swiss Tectonics Studies Group of the Swiss Geological Society

TALKS:

- 1.1 Bergemann C., Gnos E., Berger A., Whitehouse M.: Exhumation and brittle deformation of the Lepontine area dated through ion probe on hydrothermal cleft monazite
- 1.2 Cardello G.L., Lupi M., Makhloufi Y., Do Couto D., Clerc N., Moscariello A., Sartori M. & Meyer M.: Fault evolution and fluid circulation in the Great Geneva Basin (Jura fold-and-thrust belt, France & Switzerland)
- 1.3 Fischer Gy., Kindler P., Baldessin E., Godefroid F.: Tectonic control on carbonate sedimentation on the Mayaguana Bank (SE Bahamas) during the Neogene
- 1.4 Fomin I., Tackley P.: Melting and melt segregation at the core-mantle boundary
- 1.5 Frehner M.: Fold axis rotation during transpressional folding: Insights from numerical modeling and application to the Zagros Simply Folded Belt
- 1.6 Gauthiez-Putallaz L., Rubatto D., Hermann J., Martin L., Whitney D.: Water and trace element exchanges in the subducting slab: a SHRIMP oxygen isotope study in the Tavsanli zone, Turkey
- 1.7 Gruber M., Sommaruga A., Mosar J.: Structural style of the Western Swiss Molasse Basin
- 1.8 Manzotti P., Ballèvre M., Dal Piaz G.V.: Continental gabbros in the Dent Blanche klippe (Western Alps): inferences for the pre-Alpine crustal structure of the Adriatic palaeo-margin
- 1.9 Miller S.A.: Fluid-driven aftershocks and Omori's Law
- 1.10 Mosar J., Sommaruga A., Abenego M., Egli D., Gruber M., Ibele T., Kurmann-Matzenauer E., Nguyen V.-T., Schmitt N., Verbeken B., Vouillamoz N.: Swiss Molasse Basin: on faults and stress
- 1.11 Nibourel L., Herwegh M., Berger A., Egli D., Schreurs G.: The role of mechanical anisotropies in the Neogene exhumation history of the Aar massif
- 1.12 Sanan P., May D.A., Schenk O., Bollhöfer M., Rupp K., Tackley P.J.: Robust Multigrid Solvers for Highly Heterogeneous Stokes Flow
- 1.13 Zwaan F., Schreurs G.: Effects of oblique extension and structural inheritance on rift interaction: results from 4D analogue models

POSTERS:

- P 1.1 Beaussier S., Gerya T., Burg J-P.: 3D Thermomechanical modeling of the Wilson Cycle: From intraoceanic subduction initiation to obduction
- P 1.2 Bower D.J., Wolf A.S., Sanan P.D., Tackley P.J.: Terrestrial magma ocean crystallisation: bottom-up or middle-out?
- P 1.3 Diehl T., Kraft T., Lee T., Kissling E., Wiemer S.: Structure and mechanics of seismogenic fault zones in Switzerland: insights from microearthquake imaging

- P 1.4 Duretz T., Petri B., Mohn G., Schmalholz S.M., Schenker F.L., Müntener O.: Evolution and architecture of continental passive margins: the role of structural softening
- P 1.5 Hawemann F., Mancktelow N., Wex S., Pennacchioni G., Camacho A.: Intracontinental seismicity from 550 Ma to present day in the Musgrave Ranges of Central Australia
- P 1.6 Kiss D., Duretz T., Podladchikov Y., Schmalholz S.M.: Dimensional analysis for the evolution of temperature and thickness of shear zones caused by shear heating
- P 1.7 Liao, J., Gerya, T.: Oblique versus orthogonal collision influenced by lateral variations: 3D numerical modeling
- P 1.8 Luyet M., Vouillamoz N., Blascheck P., Abednego M., Mosar J.: Seismotectonic study of microseismic sequences in North-Western Switzerland using sonograms and waveform similarity analysis.
- P 1.9 Magott R., Fabbri O., Fournier M.: Polyphase ductile/brittle deformation along a major tectonic boundary in an ophiolitic nappe, Alpine Corsica: Insights on subduction zone intermediate-depth asperities
- P 1.10 Manzotti P., Ballèvre M., Poujol M.: Sediment travel paths in the Carboniferous as recorded by detrital zircon geochronology in the Dora-Maira and Zone Houillère
- P 1.11 Mauvilly J., Koiava K., Gamkrelidze I., Mosar J.: Tectonics in the Georgian Greater Caucasus: a structural cross-section in an inverted rifted basin setting
- P 1.12 Mohammadi A., Burg J.-P., Guillong M.: Provenance, detrital zircon U-Pb geochronology, and tectonic significance of Eocene-Miocene sequence of onshore west Makran, South Iran
- P 1.13 Munch J., Ueda K., Göğüş O.H., Burg JP., Gerya T.: Physical parameters controlling orocline development: Insights from numerical modelling
- P 1.14 Nguyen V.-T., Gruber M., Schmitt N., Mosar J.: Structural and kinematic study of the strike-slip fault of Pontarlier
- P 1.15 Preuss S.: Seismic cycle modeling on evolving faults: The question of fault branching
- P 1.16 Ruh J.B., Vergés J.: Tectonic inversion of a basement-involved fold-and-thrust belt: Numerical modelling applied to the Kopet Dagh Mountains
- P 1.17 Schmitt N., Verbeken B., Grassi R., Miller S., Perrochet L., Valley B., Mosar J.: Fault anatomy and microtectonics of the La Sarraz strike-slip fault system
- P 1.18 Schierjott J., Rozel A., Tackley P.: Influence of grain size evolution on the self-consistent generation of LLSVPs from primordial material and subducted MORB
- P 1.19 Schmalholz S.M., Duretz T.: Impact of grain size reduction on pinch-and-swell formation
- P 1.20 Schori M., Sommaruga A., Mosar J.: Triassic thickness compared to topography of the Swiss-French Alpine Foreland (Jura and Molasse Basin)
- P 1.21 Spitz R., Schmalholz S.M., Kaus B.J.P.: 3D numerical modeling with application to the Helvetic nappe system: Transition of viscous overthrusting to folding and oblique basal overthrusting
- P 1.22 Stalder, N.F., Herman, F., Reiners, P.W., Aguilar, G.: Late Cenozoic acceleration of erosion in the Southern Central Andes revealed by low-temperature thermochronology
- P 1.23 Tackley P.J.: Scaling of Mixing Rate in Mantle Convection Models: Influence of Plate Tectonics, Melting and Crustal Production
- P 1.24 Ueda K., Gerya T., Willett S.: Delamination, upper plate extension, and plate margin complexity
- P 1.25 Rickenbacher M., Ziegler M.: Exfoliation fracture geometry as a new tool to infer principal stress ratios ?
- P 1.26 Zwaan F., Schreurs G.: 4D analogue modeling of scissor tectonics

1.1

Exhumation and brittle deformation of the Lepontine area dated through ion probe on hydrothermal cleft monazite

Christian Bergemann¹, Edwin Gnos¹, Alfons Berger² & Martin Whitehouse³

¹ *University of Geneva, Rue des Maraichers 13, 1220 Geneva, Switzerland (christian.bergemann@unige.ch)*

² *Natural History Museum of Geneva, Geneva, Switzerland*

³ *University of Bern, Bern, Switzerland*

⁴ *Swedish Museum of Natural History, Stockholm, Sweden*

Hydrothermal monazite from open alpine type fissures (clefths) is an excellent mineral for unraveling the brittle tectonic history of an area. It has the advantage of recording the age of crystallization without the risk of diffusional lead-loss at the prevalent temperatures. Due to partial dissolution-reprecipitation in the often mm-sized crystals, they have the additional potential to record more than one age in the temperature range of ca. 350-200 °C. Following internal zonation patterns more than 500 ion-probe analyses were performed on 22 monazite samples in order to capture as wide an age range recorded in the crystals as possible.

The study area in the Central Alps encompasses the Lepontine metamorphic dome and the eastern half of the Rhone-Simplon fault. The region has a complex tectonic history, with greenschist to amphibolite facies metamorphism predated by and partly overlapping with nappe stacking. This was followed by exhumation, particularly in the central part and further folding and thrusting. The Lepontine area's famous mineralized Alpine clefths formed later during brittle deformation affecting the entire region combined with hydrothermal fluid flow. The westernmost part of the region was dominated by dextral strike-slip deformation along the Rhone-Simplon Line, one of the major fault systems of the Alps.

The dating of cleft monazites revealed a range of ^{232}Th - ^{208}Pb ages between 19 and 5 Ma distributed over four age groups. A general decrease in ages from east to west is visible, with the westernmost areas recording significantly younger ages than the rest of the region. Ages from almost all samples suggest an event affecting the entire area at around 10 to 13 Ma. Later activity is largely restricted to the western Lepontine as well as the central Aare massif/southern Gotthard nappe areas and is likely related to activity along the Rhone-Simplon Line. Combined with other chronological methods, these new monazite data provide an overview over part of the uplift and brittle tectonic history of much of the Central Alps.

1.2

Fault evolution and fluid circulation in the Great Geneva Basin (Jura fold-and-thrust belt, France & Switzerland)

Cardello G.L.¹, Lupi M.¹, Makhloufi Y.¹, Do Couto D.¹, Clerc N.¹, Moscariello A.¹, Sartori M.¹ & Meyer M.²

¹ *Section des sciences de la Terre et de l'environnement, Université de Genève, Rue des Maraichers 13, CH-1205 Genève (luca.cardello@unige.ch)*

² *Services Industriels de Genève (SIG)*

The Canton of Geneva is exploring the opportunity to exploit geothermal energy in the Great Geneva Basin (GGB). The GGB is an Oligo-Miocene siliciclastic basin tightened between the Alps and the southern Jura fold-and-thrust belt. The outcropping relieves represent good field analogues of buried faulted structures identified after seismo-stratigraphic analysis. In this frame, we review the regional tectonics to:

- (1) understand the present-day structural setting with a special focus on fault properties and;
- (2) assess preferential paths for fluid flow.

Hereby, we present new field observations, kinematic analysis, and petrographic determination of the deformation processes. Field and geophysical evidences confirmed that the Molasse siliciclastic deposits progressively seal the growing anticlines constituted of Mesozoic carbonates. Those are shaped by a set of fore- and back-thrusts usually having little veining association.

Structural analysis indicates that syn-kinematic mineralisations and pressure-solution planes occur far from the thrust zones, concentrating on the strike-slip faults. In relation to the presence of shale-rich interlayers, bed-to-bed flexural slip is the main mechanism accompanying shortening. Locally, a consistent transition from less to well-developed en échelon fracture sets can be recognised. The study of their arrangement leads to a regional fault-evolution model. The coalescence of mode-I veins is associated with larger amount of accumulated displacement. This is the result of strain localisation and fluid circulation that created progressively longer and mature faults. Some of these faults acted as proper tear-faults that can reach a few kilometers in fault length. They can be distinguished on the base of: orientation, amount of displacement, spacing and fault fabric. Preliminary data highlight the occurrence of two main transversal fault-sets, showing veining and mineralisation.

The first set (1) strikes NNW-SSE. It has fault length up to 60 km in map view, cutting the whole Mesozoic-Cenozoic cover, and possibly also the Quaternary deposits (i.e., Vuache fault system). Most notably, it is associated with brittle-ductile transition textures and crack-and-seal carbonate mineralization. This fabric was probably inherited during the exhumation (in the order of a few km). The Vuache fault later evolved into brittle faulting that is traced by shallow earthquakes (i.e. less than 5 km deep) reaching a local magnitude as high as ML 5.3. This involves change in fluid-flow regime (i.e., Epagny earthquake in 1996; Gratier et al. 2013).

The second set (2) is constituted by W/NW-striking 10 km long tear-faults. Those are associated in places with up to few meters thick calcitic and brecciated polyphase mineralisations. Such faults are most likely confined at the upper thrust sheets and limited to the Meso-Cenozoic formations although we track the continuity of some of them up to the surface. In addition, as visible on the Digital Elevation Model and satellite images, smaller size (up to 4 km fault length) N-S and NE-striking faults are associated with dry and tightly spaced (5-10 cm) open joints. Those are possibly good candidates for recent activity and water infiltration. Uprising fluids occur too, as indicated by natural geothermal upwelling (e.g. Divonne-les-Bains) being, vertical fracture connectivity enhanced at strike-slip fault intersection.

In conclusion, our observations show that:

- 1) on the outcropping relieves, WNW- and NNE-striking systems are vein-rich and therefore “wet” whereas N- and NE-striking systems are “dry”;
- 2) within the buried structures, similarly oriented fault-zones act as conduits that may have opposite fluid-flow directivity depending on the structural position;
- 3) from a dynamic point of view, most of the faults are coherent with the present day stress regime orientation;
- 4) at a regional scale, the kinematics of the fault systems may have evolved during time with the indentation of the Jura arc.

REFERENCES

Gratier, J. P., Thouvenot, F., Jenatton, L., Tourette, A., Doan, M. L., & Renard, F. (2013). Geological control of the partitioning between seismic and aseismic sliding behaviours in active faults: Evidence from the Western Alps, France. *Tectonophysics*, 600, 226-242.

1.3

Tectonic control on carbonate sedimentation on the Mayaguana Bank (SE Bahamas) during the Neogene

Gyöngyvér Fischer¹, Pascal Kindler¹, Erika Baldessin¹ and Fabienne Godefroid¹

¹ *Département des Sciences de la Terre, University of Geneva, Rue des Maraichers 13, CH-1205 Genève (Gyongyver.Fischer@unige.ch)*

Our stratigraphic study of Neogene strata from both surface exposures and core borings on the island of Mayaguana (SE Bahamas) reveals two episodes of carbonate sedimentation separated by a protracted interval of exposure that cannot be explained by eustatic sea-level fluctuations, but more likely by tectonic factors.

The Mayaguana Bank is a small, elongated (57x13 km) carbonate platform in the SE Bahamas that comprises only one large island, Mayaguana, and lies ca. 300 km to the north of the North Caribbean Plate Boundary Zone. Our database results from a multi-approach study comprising lithostratigraphy, biostratigraphy, sedimentology and Sr-isotope dating of both surface exposures and 15 core borings between 17 and 44 m in length.

The stratigraphic record of Mayaguana is much more extensive than that of other Bahamian islands, and extends from the Early Miocene (Burdigalian) to the Holocene (Godefroid, 2012). Core studies further showed that Early Miocene (Aquitanian) rocks occur down to a depth of 44 m. Interestingly, Middle Miocene rocks have not been found neither on outcrops nor in core borings.

The bank evolved from a southward dipping ramp in the Miocene to a flat topped platform in the Quaternary. Carbonate accumulation rates varied from 36.3 m/my to 9.5 during the Early Miocene to <1 m/my during the Late Miocene to 6.7 in the Early Pleistocene.

The Middle Miocene discontinuity cannot be explained by a protracted episode of sea-level lowstand as high eustatic sea-levels have been documented during this time interval (e.g. Miller et al., 2005). Therefore, we propose that the peculiar stratigraphy of the Mayaguana Bank results from tectonic controls, possibly from alternating regimes of transpression and transtension related to the northward migration of a forebulge developed in response to the subduction of the North American Plate under the Caribbean Plate.

REFERENCES

- Godefroid, F. 2012 : Géologie de Mayaguana, SE de l'archipel des Bahamas : Terre & Environnement, v. 108, xxv + 230 pp.
Miller, K.G., Kominz, M.A., Browning, J.V., Wright, J.D., Mountain, G.S., Katz, M.E., Sugarman, P.J., Cramer, B.S., Christie-Blick, N., Pekar, S.F., 2005. The Phanerozoic record of global sea-level change. *Science* 312, 1293-1298.

1.4

Melting and melt segregation at the core-mantle boundary

Ilya Fomin¹, Paul Tackley

¹ *Institute of Geophysics, ETH Zurich, Sonneggstrasse 5, CH-8092 Zurich (ilya.fomin@erdw.ethz.ch)*

Temperatures at the Core-Mantle Boundary (CMB) are close to the onset of melting. Presence of such partially molten patches is proposed both by models of long-term Earth evolution (Labrosse et al., 2007) and geophysical models of ULVZ (e.g. (Beuchert & Schmeling, 2013)). We perform long-term (millions of years) numerical simulations of the Earth's mantle for a possible range of CMB temperatures to understand plausibility of melting and its consequences.

We've built an empirical model of solid-liquid transition. Physical properties (liquid-solid density differences) are adjusted with data of (de Koker et al., 2013; Mosenfelder et al., 2007; Stixrude & Lithgow-Bertelloni, 2011; Thomas & Asimow, 2013). This model was incorporated in StagYY numerical code (e.g. (Tackley, 2008)) to simulate convection within the Earth mantle.

Melt segregation (rock's permeability, directions and velocities, and adiabatic heating and viscous dissipation effects) is considered using equations listed in (Abe, 1995; Solomatov, Stevenson, 1993; Martin & Nokes, 1989).

Our model predicts, that in case of melting iron-rich dense liquid forms a thin layer around CMB, which consequently splits to separated batches piles. Atop them a layer of iron-depleted material forms, which solidus temperatures are high enough to restrict further melting.

Thickness of molten or partially molten material piles strongly depends on the actual CMB temperature (reaching up to 8 to 20 km at $T(\text{CMB})=4300\text{-}4500\text{K}$, while at $T(\text{CMB})=3800\text{K}$ no melt forms).

REFERENCES

- Abe Y. 1995: Basic equations for the evolution of partially molten mantle and core, *The Earth's central part, its structure and dynamics*, 215-230.
- Beuchert, M. J. & Schmeling, H. 2013: A melting model for the lowermost mantle using Clapeyron slopes derived from experimental data: Consequences for the thickness of ultralow velocity zones (ULVZs), *Geochemistry, Geophysics, Geosystems*, 14, 197-208.
- de Koker, N., Karki, C.C. & Stixrude, L. 2013: Thermodynamics of the MgO-SiO₂ liquid system in Earth's lowermost mantle from first principles, *Earth and Planetary Science Letters*, 361, 58-63.
- Labrosse, S., Hernlund, J. W. & Coltice, N. 2007: A crystallizing dense magma ocean at the base of the Earth's mantle, *Nature*, 450, 866-869.
- Martin D. & Nokes, R. I. 1989: A Fluid-Dynamical Study of Crystal Settling in Convecting Magmas, *Journal of Petrology*, 30, 1471-1500.
- Mosenfelder, J. L., Asimow, P. D. & Ahrens, T. J. 2007: Thermodynamic properties of Mg₂SiO₄ liquid at ultra-high pressures from shock measurements to 200 GPa on forsterite and wadsleyite, *Journal of geophysical research*, 112.
- Stixrude, L. & Lithgow-Bertelloni, C. 2011: Thermodynamics of mantle minerals II, Phase equilibria, *Geophysical Journal International*, 184, 1180-1213.
- Solomatov, V. S. & Stevenson, D. J. 1993: Suspension in Convective layers and style of differentiation of a terrestrial magma ocean, *Journal of geophysical research*, 98, 5375-5390.
- Tackley, P. J. 2008: Modelling compressible mantle convection with large viscosity contrasts in a three-dimensional spherical shell using the yin-yang grid, *Physics of the Earth and Planetary Interiors*, 171, 7-18.
- Thomas, C. W. & Asimow, P. D. 2013: Direct shock compression experiments on premolten forsterite and progress toward a consistent high-pressure equation of state for CaO-MgO-Al₂O₃-SiO₂-FeO liquids, *Journal of geophysical research: solid earth*, 118, 5738-5752.

1.5

Fold axis rotation during transpressional folding: Insights from numerical modeling and application to the Zagros Simply Folded Belt

Marcel Frehner¹

¹ Geological Institute, ETH Zurich, Sonneggstrasse 5, CH-8092 Zurich (marcel.frehner@erdw.ethz.ch)

Transpression is the combination of strike-slip deformation and shortening orthogonal to the deformation zone. Whereas in the upper crust transpression is dominantly accommodated by faulting, viscous parts of the lithosphere dominantly deform by folding. In some cases, transpressional strain is geographically partitioned (Tikoff and Teyssier, 1994) between a strike-slip domain lacking major shortening structures and a neighboring pure-shear domain (e.g., fold-and-thrust belt) lacking major strike-slip structures.

Here, the growth and rotation of folds during transpression as a function of the convergence angle is investigated using 3D numerical finite-element models (Figure 1; Frehner, in press). The model setup comprises upright single-layer buckle folds in Newtonian materials, which grow from an initial point-like perturbation due to a combination of in-plane shortening and shearing (i.e., transpression). The numerical results suggest that fold axes are always parallel to the major horizontal principal strain axis (λ_{\max}), and that sequential folds appearing later form parallel to already existing folds and rotate with λ_{\max} with increasing strain. This suggests that fold axes are not passive material lines and that fold hinge migration occurs during transpression.

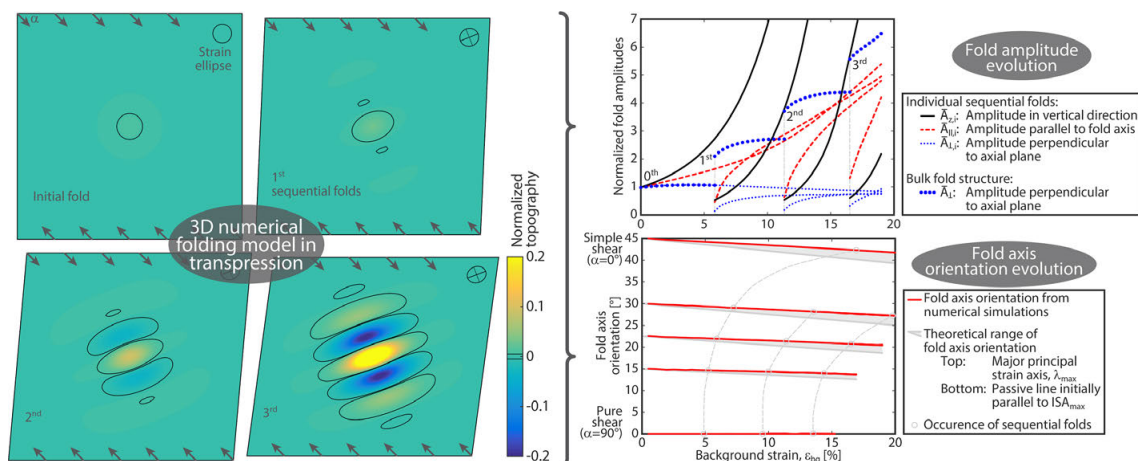


Figure 1: Graphical abstract of main results. Left: Top view snapshots of example simulation with a convergence angle, $\alpha=45^\circ$. With increasing background strain, the fold structure grows in all three dimensions. Top right: Fold amplitude evolution in three directions: vertical (fold growth), parallel to fold axis (fold elongation) and perpendicular to axial plane (sequential fold growth). Bottom right: Fold axis orientation with increasing background strain for different convergence angles ($\alpha=0^\circ-90^\circ$). For all cases, the fold axis is always parallel to the major principal strain axis, λ_{\max} ; hence it is not a passive marker line.

Because the fold axis is always parallel to λ_{\max} , there is an analytical triangular relationship between the convergence angle, the amount of strain, and the fold axis orientation. If two of these values are known, the third can be determined. Importantly, this relationship is independent of the viscosities and viscosity ratios involved in the folded layers.

For the Zagros Simply Folded Belt (ZSFB) in NE Iraq, the far-field convergence angle (from GPS; Vernant and Chéry, 2006) is $\alpha=35^\circ$. Strain is partitioned between the ZSFB and the bordering strike-slip fault-system. However, the degree of partitioning is disputed, ranging from full partitioning ($\alpha=90^\circ$ in the ZSFB; Talebian and Jackson, 2004) to intermediate partitioning ($\alpha=60^\circ$ in the ZSFB; Vernant and Chéry, 2006). Zero strain partitioning ($\alpha=35^\circ$ in the ZSFB) is unrealistic because some strike-slip movement along bordering strike-slip fault-system is clearly documented (Talebian and Jackson, 2002). The above mentioned triangular relationship is applied to the Zagros fold-and-thrust-belt to estimate the degree of strain partitioning (Figure 2). Despite some data scatter, the orientation of the majority of fold axes indicates a convergence angle within the ZSFB of $\alpha=60^\circ-90^\circ$, confirming the proposed range. However, the data covers this entire range and it is not clear which end-member model is more appropriate.

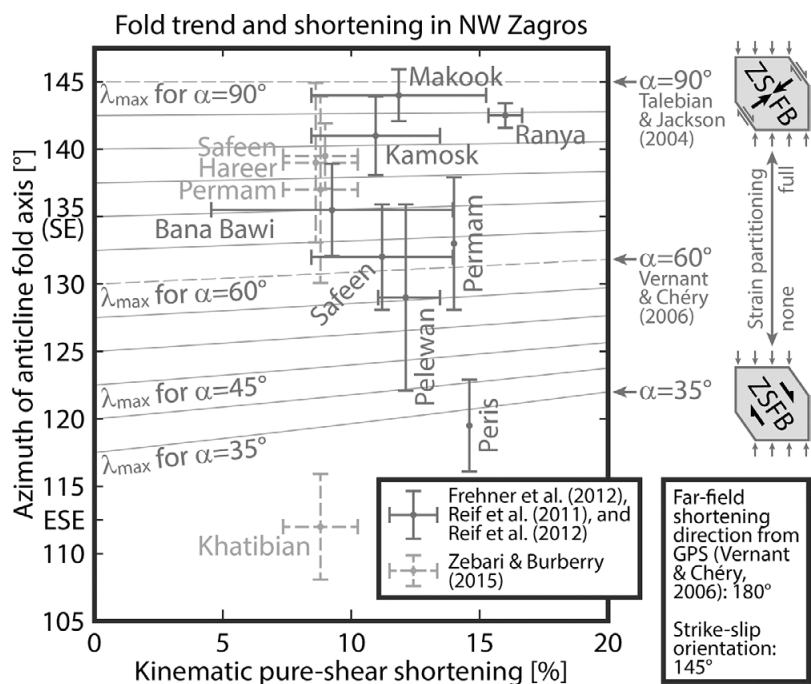


Figure 2: Fold axis orientations versus strain estimates in the ZSFB. In the back, theoretical fold axis orientations, λ_{\max} , are plotted for different convergence angles. End-member convergence angles are sketched on the right based on the far-field shortening direction and strike-slip fault orientation: 90° (pure shear; full strain partitioning), 35° (zero strain partitioning).

REFERENCES

- Frehner, M. in press: 3D fold growth in transpression, *Tectonophysics*, doi:10.1016/j.tecto.2016.01.002.
- Talebian, M. & Jackson, J. 2004: A reappraisal of earthquake focal mechanisms and active shortening in the Zagros mountains of Iran, *Geophysical Journal International*, 156, 506–526.
- Tikoff, B. & Teyssier, C. 1994: Strain modeling of displacement-field partitioning in transpressional orogens, *Journal of Structural Geology* 16, 1575–1588.
- Vernant, P. & Chéry, J. 2006: Mechanical modelling of oblique convergence in the Zagros, Iran, *Geophysical Journal International*, 165, 991–1002.

1.6

Water and trace element exchanges in the subducting slab: a SHRIMP oxygen isotope study in the Tavsanlı zone, Turkey

Laure Gauthiez-Putallaz¹, Daniela Rubatto², Joerg Hermann², Laure Martin³, Donna Whitney⁴

¹ *Research School of Earth Sciences, The Australian National University, Canberra, ACT 0200 Australia (laure.gauthiez-putallaz@anu.edu.au)*

² *Institute of Geological Sciences, University of Bern, Baltzerstrasse 1-3, 3012 Bern*

³ *Centre for Microscopy, Characterisation and Analysis, UWA, 35 Stirling Highway, Crawley WA6009 Australia*

⁴ *Earth Sciences, University of Minnesota, Minneapolis USA*

Elemental and isotopic exchanges within the subducting slab are key to understanding slab dehydration, melting and the broader crust-mantle geochemical cycling. In order to investigate large scale metasomatism in subduction, we choose to look at smaller scale exchanges in a low temperature – high pressure metamorphic area of central Turkey: the Tavsanlı zone. In the Halilbagi Formation (max. 530°C, ~23 kbar), layers of characteristic subduction slab lithologies (metasediments, metabasites, ultramafics) are juxtaposed at the scale of meters or hundreds of meters (Davis and Whitney, 2008). Moreover, these lithologies preserve their subduction assemblages including abundant fresh lawsonite, which allows for an observation window that is free of exhumation and weathering overprints.

We use oxygen isotopes as a monitor for fluid circulations. Oxygen, the only major element shared by rocks and fluids, yields direct information about fluid-rock interaction. The components of the subducting slab - sediments and altered mafic-ultramafic rocks – are of contrasting oxygen isotope compositions on the seafloor: 15-25 ‰_{VSM} O_W and 2-8 ‰_{VSM} O_W respectively. Fluid-induced interaction between these rocks can thus be tracked by identifying relative changes in the bulk rock values. Within a single sample, this can also be done by looking at zoning within metamorphic minerals, measuring δ¹⁸O in situ (e.g. Martin et al., 2014). We analysed δ¹⁸O in garnet, zircon, apatite and lawsonite using the SHRIMP II, SHRIMP SI and CAMECA 1280 ion microprobes. The oxygen isotope results are then combined to microprobe major elements LA-ICP-MS trace element analysis to identify fluid-rock exchanges between lithologies.

In the Tavsanlı zone HP-LT rocks, we observe the homogenisation of both oxygen isotope ratios and fluid-mobile trace-element ratios during subduction. In high-pressure zoned garnet and lawsonite, we see both the influx of high δ¹⁸O sediment-equilibrated water into mafic pods, and the influx of lower-δ¹⁸O water in a sedimentary layer. Chemical changes correlating with the fluid influx are mainly Sr/Pb, Fe³⁺ and potentially Ca. This raises important flags for thermobarometry, as addition of Ca, H₂O and changes in oxygen fugacity could stabilise lawsonite over epidote, and modify the stability field of glaucophane and omphacite. Not all fluid exchanges happen at high-pressure: we observe a substantial shift of δ¹⁸O between the growth of magmatic minerals (zircon) and metamorphic minerals (garnet, lawsonite), which is also reflected in the mixed bulk-rock δ¹⁸O composition of most lithologies in the Tavsanlı zone. This data suggests that the main pulse of fluid-rock interaction happens at low pressure in the near-seafloor area - where rocks are hydrous, porous and fine-grained.

We identify fluid-rock interactions both at low pressure and high pressure in a subducted slab. These fluids homogenise δ¹⁸O and Sr/Pb between mafic and sedimentary lithologies. They also favour the formation of lawsonite which can carry water and a wide array of trace elements deeper in the mantle.

REFERENCES

- Davis, P.B., & Whitney, D.L., 2008: Petrogenesis and structural petrology of high pressure metabasalt pods, Sivrihisar, Turkey: *Contributions to Mineralogy and Petrology*, 156, 217-241.
- Martin, L.A., Rubatto, D., Crépeau, C., Hermann, J., Putlitz, B., & Vitale-Brovarone, A., 2014: Garnet oxygen analysis by SHRIMP-SI: matrix corrections and application to high-pressure metasomatic rocks from Alpine Corsica: *Chemical Geology*, 374, 25-36.

1.7

Structural style of the Western Swiss Molasse Basin

Marius Gruber¹, Anna Sommaruga¹, Jon Mosar¹

¹ *Department of Geosciences, Earth Sciences, University of Fribourg, Chemin du Musée 6, CH-1700 Fribourg, Switzerland (marius.gruber@unifr.ch, anna.sommaruga@unifr.ch, jon.mosar@unifr.ch)*

This study focusses on the structural style of the Western Swiss Molasse Basin (WSMB) in the area of the Canton Fribourg, Canton Vaud and Canton Bern (Switzerland). Our structural analysis is based on the interpretation of more than 200 2D seismic reflection lines, deep borehole data and surface data (bedding dip data, fault data).

The most prominent structural elements in the study area are: [1] a NE-SW to N-S striking synsedimentary normal fault system confined to the Mesozoic and lowermost Cenozoic units, [2] a décollement zone in Middle to Upper Triassic evaporite units dipping at low angle towards the SE parallel to the Base Mesozoic horizon, [3] a N-S to WNW-ESE striking conjugated strike-slip fault system crosscutting the Mesozoic and the Cenozoic units, [4] a NE-SW listric reverse fault system located in Mesozoic and Cenozoic units and [5] a NE-SW striking thrust fault system confined to the Cenozoic units in the SE part of the study area (eg. Subalpine Molasse).

These different structural elements are the results of the multiphase tectonic evolution of the WSMB during Mesozoic and Cenozoic times. Thickness variations in Liassic and Dogger units along NE-SW to N-S oriented lineaments suggest an enhanced subsidence phase which may be related to normal faulting [1] during Liassic and Dogger times (eg. spreading of the alpine Tethys, (Stampfli, 2000)). This normal fault system [1] was reactivated during Late Eocene to Oligocene times in relation to the flexural down-bending of the European lithosphere (Pfiffner, 1986) and/or the initiation of the European Cenozoic rift system (Ziegler, 1992). This is supported by metres sized Lower Cretaceous olistoliths in Rupelian / Lower Chattian Molasse sediments on the hanging wall side of a N-S striking fault system (also referred to as the Fribourg zone).

The conjugated strike-slip fault system [3] and the listric reverse fault system [4] are related to the décollement zone [2] which led to the formation of the Jura-fold-and-thrust-belt (JFTB) in the distal part of the Alpine Foreland Basin during Miocene times. Both, the strike-slip fault system [3] and the listric reverse fault system [4] are at least partly reactivated normal faults which were active during Liassic to Dogger and/or during Eocene to Oligocene times.

REFERENCES

- Pfiffner, O. A. (1986). Evolution of the north Alpine foreland basin in the Central Alps. Special Publication of the international Association of sedimentologists, 8, 219-228.
- Stampfli, G. M. (2000). Tethyan oceans. Geological Society of London, Special Publication, 173, 1-23.
- Ziegler, P. A. (1992). European Cenozoic rift system. Tectonophysics, 208, 91-111.

1.8

Sediment travel paths in the Carboniferous as recorded by detrital zircon geochronology in the Dora-Maira and Zone Houillère

Paola Manzotti¹, Michel Ballèvre² & Marc Poujol²

¹ *Institute of Earth Sciences, University of Lausanne, Géopolis, Quartier Mouline, Lausanne 1015, Switzerland (paola.manzotti@gmail.com)*

² *Géosciences Rennes, UMR CNRS 6118, Université Rennes1, Campus de Beaulieu, Rennes Cedex 35042, France*

In the internal zone of the European Alps, late Carboniferous to Permian sediments have been detached from their basement (e.g. the Zone Houillère in the Briançonnais Zone). The Pinerolo Unit (Dora-Maira Massif) is the deepest unit exposed in the stack of the Western Alps and is considered to be Carboniferous in age based on lithological considerations (Franchi & Novarese, 1895; Argand, 1911). The blueschist-facies Pinerolo Unit occupies a key tectonic position in the Alpine belt, being overthrust by the coesite-eclogite and quartz eclogite units of the Dora-Maira Massif.

Detrital zircon grains from the Pinerolo Unit and the Zone Houillère (located along the external margin of the Briançonnais domain) display similar age patterns, with the youngest and largest population being Carboniferous (340-330 Ma). The distribution of Carboniferous magmatism in the Alps and surrounding areas suggests that the detritus was transported from Maures-Corsica and possibly from the Helvetic Zone into the Zone Houillère and the Pinerolo basin. Our results highlight the potential of detrital zircon geochronology for deciphering the sources of detrital material in meta-sediments, even if they have been affected by metamorphic overprints.

1.9

Fluid-driven Aftershocks and Omori's Law

Stephen A. Miller¹*Center for Hydrogeology and Geothermics (DHYN)*

I propose a new physical explanation for the temporal decay of aftershocks following large earthquake, known as Omori's Law. I show that Omori's Law arises naturally through the permeability, where permeability is treated as an exponential function of the effective normal stress combined with an exponential decrease in permeability with time following a co-seismic step. The temporal decay represents precipitation processes that shut down the permeable network. Solving a non-linear diffusion equation using this functional form for permeability, I find excellent correlations in both space and time between model and data for over 10,000 aftershocks from 1992 Joshua Tree (M6.1), the 1992 Landers (M7.3), the 1994 (M6.7) Northridge, and 1999 (M7.1) Hector Mine earthquakes. The only fitting parameter to match the observed Omori Law is shown to be the permeability recovery rate α .

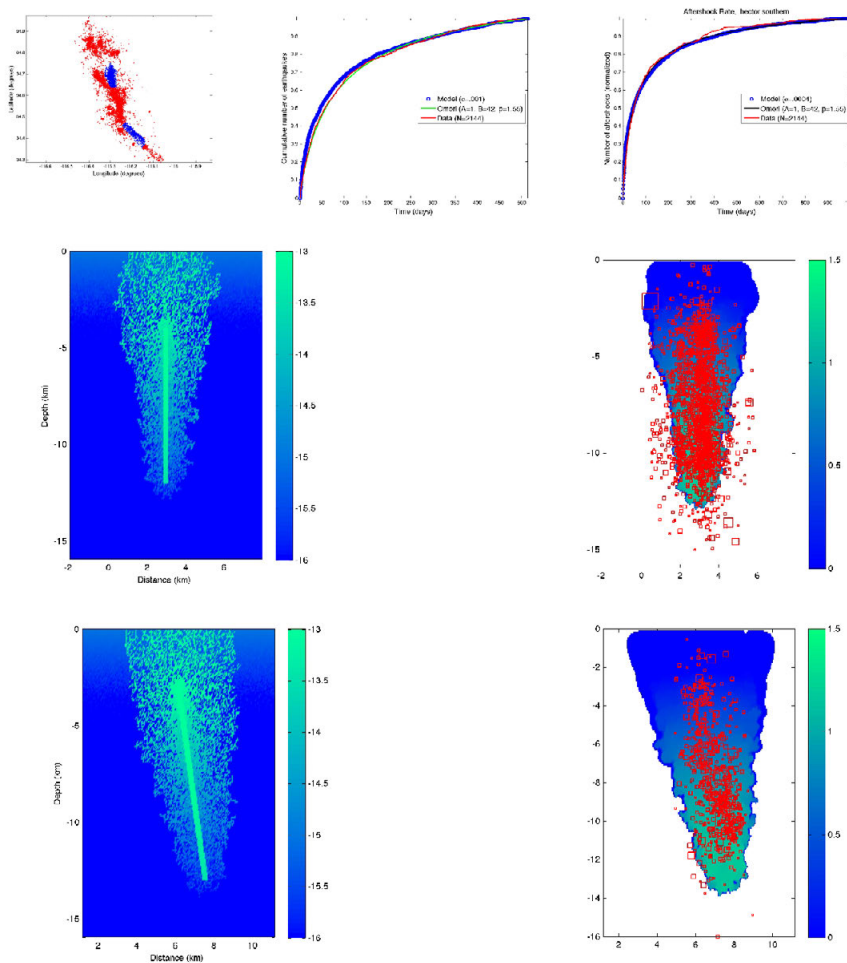


Figure 1. Top row: Aftershocks (in blue) from two sections of the 1999 M7.1 Hector Mine earthquake used for comparison with Omori's Law. Middle row: Calculated permeability field and the calculate fluid pressure field compared with measured aftershocks for the northern section. Bottom row: Calculated permeability field and the calculate fluid pressure field compared with measured aftershocks for the southern section.

1.10

Swiss Molasse Basin: on faults and stress

Jon Mosar¹, Anna Sommaruga¹, Martinus Abenego¹, Daniel Egli², Marius Gruber¹, Tobias Ibele³, Eva Kurmann-Matzenauer⁴, Viet-Thang Nguyen¹, Nicole Schmitt¹, Benjamin Verbeke¹, Naomi Vouillamoz⁵

¹ *Département de Géosciences - Sciences de la Terre, Université de Fribourg, Chemin du Musée 6, CH-1700 Fribourg (jon.mosar@unifr.ch)*

² *Institut für Geologie - Universität Bern, Baltzerstrasse 1+3, CH-3012 Bern*

³ *Ibele Geologie, Volksbadstrasse 17b, CH-9000 St. Gallen*

⁴ *Landesgeologie – swisstopo, Seftigenstrasse 264, CH-3084 Wabern*

⁵ *Institut für Geophysik – Universität Stuttgart, Azenbergstr. 16, D-70174 Stuttgart*

The western Alpine Molasse basin is a classic Molasse-type, overfilled, flexural foreland basin that evolved during the Tertiary in front of the Alpine orogeny and developed on Mesozoic platform sediments (mainly carbonates). Due to the “distant push” linked to the exhumation and imbrication of the External Crystalline Massifs in the Alps, the foreland, including the Tertiary Molasse Basin deposits, detached along the Middle Triassic evaporite horizon leading to the formation to the NW of the Jura foreland fold-and-thrust-belt to the NW. The Molasse basin thus evolved from a purely flexural basin to a wedge top basin. Unlike the Jura Mountains, and due to its tapered geometry and important sediment thickness the Molasse Basin did not develop major fault-related folds, but only gentle, often evaporite-cored anticlines. To the SE the Molasse Basin terminates against the thrust and imbricated Subalpine Molasse. Like the Jura Mountains, important tear faults have also developed in the Molasse Basin. Two main directions, N-S sinistral such as the Pontarlier or Vuache Faults and its conjugate movement the NW-SE dextral such as the La Sarraz or the La Lance Faults, are in agreement with present-day stress field. These faults connect from the Jura into the Molasse basin, are active only in the detached cover and have a polyphase history. To the SW the Molasse basin is “involved” in the folding of the Chaînes Subalpines, whereas to the E the limit of the detached basin extends beyond the eastern termination of the Jura Mountains s.str. This eastern zone is characterized by large strike-slip faults zone affecting the sedimentary cover and the underlying basement (Freiburg-Bonndorf-Bodensee Fault Zone or the St. Gallen Fault).

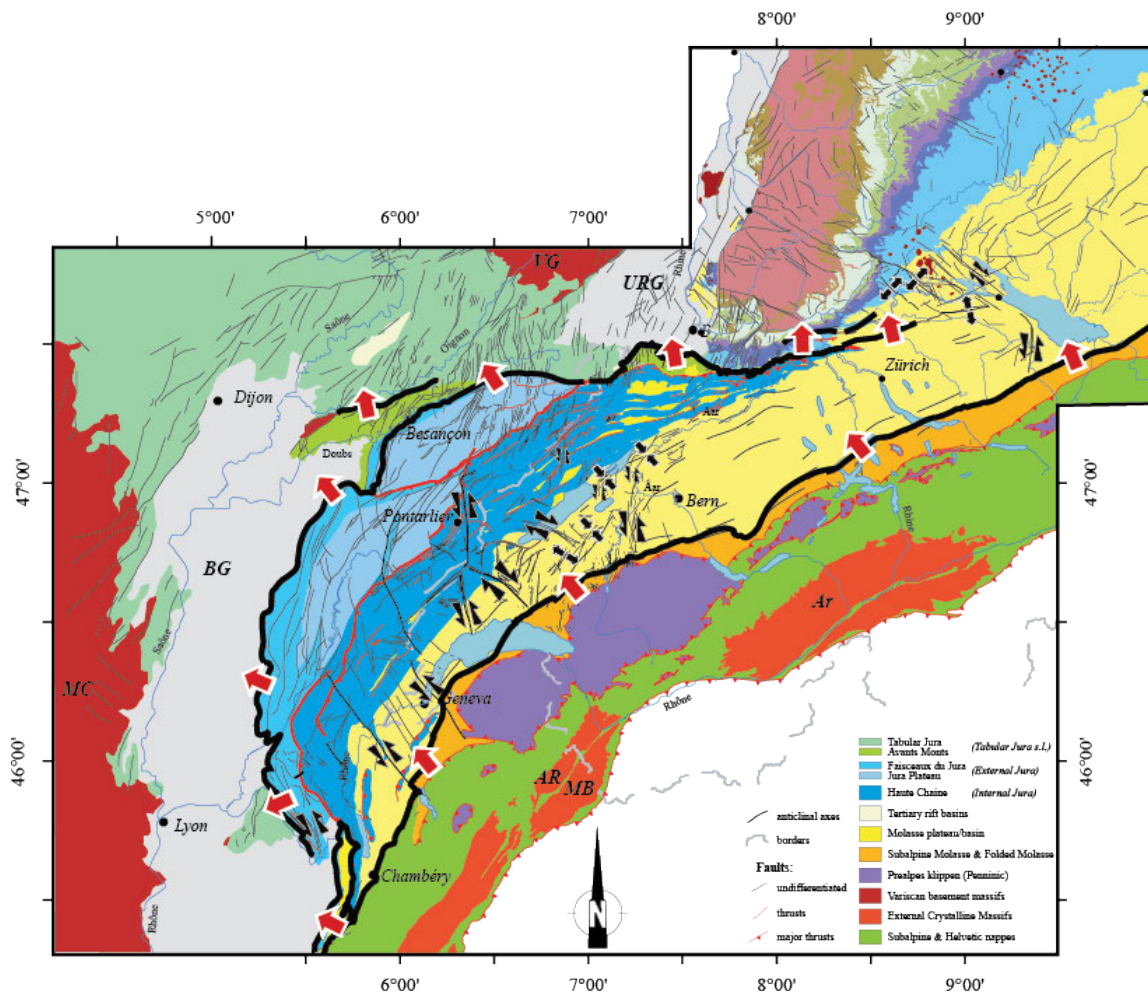


Figure 1 Simplified tectonic map of the alpine foreland with main fault systems.

Based on field data, earthquake analysis and 3D stress modelling we will discuss:

- the geometry and kinematics of the eastern termination of the decollement-related tectonics with examples from the Freiburg-Bonndorf-Bodensee Fault Zone and the St. Gallen strike-slip fault (abandoned geothermal site) and the transition from the eastern Jura Mountains to the Molasse basin in relation with an important E-W Permo-Carboniferous graben;
- the tectonic context of the large strike-slip/tear fault systems connecting the Jura to the Molasse Basin and their kinematic significance;
- the changes in stress and paleostress orientation due to complex fault patterns and complexity along individual faults. We will use data from earthquakes studies, stress modelling and paleostress analysis applied to local regional examples (Randen Fault, Fribourg Zone, La Sarraz fault system)
- the possibility that the whole of the Western Alpine Molasse Basin, and especially all the strike-slip/tear faults may be critically stressed.

Beyond the scientific interest of understanding the tectonic development of the alpine foreland, these issues are relevant for projects of hydrocarbon exploration, especially when associated to invasive techniques such as hydrofracking, projects for deep geothermal energy, CO₂ sequestration and earthquake hazard mitigation.

1.11

The role of mechanical anisotropies in the Neogene exhumation history of the Aar massif

Lukas Nibourel¹, Marco Herwegh¹, Alfons Berger¹, Daniel Egli¹ & Guido Schreurs¹

¹ *University of Bern, Institute of Geological Sciences, Baltzerstrasse 1+3, 3012 Bern, Switzerland*
(lukas.nibourel@geo.unibe.ch)

The Aar massif is a large ENE-WNW striking dome-like bulge, which is strongly dissected by massif-subparallel fault zones. Its structural evolution and exhumation history has been discussed over several decades and is still controversial. Estimates on kinematics and dynamics are difficult to obtain, because good markers for unraveling the Alpine history are scarce, especially in its external parts that are dominated by polymetamorphic crystalline basement rocks.

We present new field observations and structural analyses from the Faernigen-Maderanertal-Windgaellen Zone, which is the most prominent tectonic boundary of the northern Aar massif (Meiental-Reuss-Maderanertal area). It comprises synclines and wedges of Upper Pennsylvanian sedimentary and volcanoclastic rocks, Mesozoic sediments and is surrounded by polymetamorphic crystalline basement. In the field, sedimentary and basement units show a very contrasting mechanical behavior. These differences in rheology and the well-constrained age of the sediments make them suitable markers for the study of the Neogene evolution of the Aar massif.

Our investigations at the basement-cover contact show that at least some of the Permo-Carboniferous to Mesozoic half-grabens acted as crustal-scale instabilities dictating the position and nature of subsequent Alpine shortening.

1.12

Robust Multigrid Solvers for Highly Heterogeneous Stokes Flow

Patrick Sanan^{1,2}, Dave A. May¹, Olaf Schenk², Matthias Bollhöfer³, Karl Rupp, Paul J. Tackley¹

¹ *Department Erdwissenschaften, ETH Zürich, Sonneggstrasse 5, 8092 Zürich, Switzerland*

² *Institute of Computational Science, Università della Svizzera italiana, Via Buffi 6, 6900 Lugano, Switzerland*

³ *Institute of Computational Mathematics, TU Brunswick, Pockelsstrasse 14, 38106 Brunswick, Germany*

Multigrid methods provide scalable solvers for this problem, essential for large-scale simulation. However, optimal (“textbook”) multigrid solvers can be elusive for problems with non-grid-aligned and large coefficient jumps, yet these problems are often those of greatest scientific interest. In addition to absolute performance, robustness, here characterized by acceptable performance over a set of related problems, is key. To this end, we first present results of using complex preconditioners for a Q2-Q1 finite element code, focusing on the novel component of using incomplete factorizations for local smoothing. We show that this can exhibit useful robustness to geometric distribution of high-viscosity inclusions, when compared to an approximate block factorization (ABF) approach. Secondly, we present results of software development to make these tools available via the composable solver library PETSc: we present a wrapper for the ILUpack library to make approximate factorization of saddle point matrices available, and finally show results of attempts to increase the robustness of the multigrid solver within StagYY by wrapping it in an outer Krylov method.

1.13

Effects of oblique extension and structural inheritance on rift interaction: results from 4D analogue models

Frank Zwaan¹, Guido Schreurs¹,

¹ *Institut für Geologie, Universität Bern, Baltzerstrasse 1 + 3, CH- 3012 Bern (frank.zwaan@geo.unibe.ch)*

Introduction

During the early stages of rifting, rift segments may form along non-continuous and/or offset pre-existing structures. They can link in various ways to form a continuous rift system. Here we test the effects of 1) dextral and sinistral oblique extension as e.g. observed in the East African Rift System and 2) various geometries of structural inheritance on rift segment linkage. We use a similar method as Zwaan et al. (2016) that allows distributed deformation in the overlying model materials: sand layers for the brittle upper crust and a viscous sand/silicone mixture for the lower crust. Above the basal viscous layer we apply right stepping offset lines (seeds) of the same viscous mixture, representing inherited weaknesses in the sand, along which deformation focuses. Selected models are run in a CT-scanner to reveal their 3D internal

Results

Our models show that rift segments initiate along the main seeds and then propagate ca. parallel to the extension direction (Fig. 1a). With sinistral transtension they grow apart, orthogonal extension has them propagating in a parallel fashion and with dextral transtension rift segments grow together. When we apply a secondary seed that connects the main seeds, the former seed seldom activates. This is in contrast with previous studies (e.g. Acocella et al., 1999), but in line with the notion that inherited structures do not always reactivate during a next tectonic phase (e.g. Nalpas & Brun, 1995). Furthermore, in our sinistral transtension models without rift-connecting seeds and with the initial seeds laterally far apart, a surprising phenomenon occurs: instead of rifts that grow apart, a strike-slip transfer zone develops, connecting both rift segments (Fig. 1ax1-4 and 1b). Some models develop a hybrid system with both a strike-slip transfer zone and a rift arm propagating away. This might indicate that these models are close to a transition between two modes: propagating apart or strike-slip transfer zone mode. The latter resembles the Tanganyika-Malawi fault zone in East Africa (Fig. 1c): we observe 1) a similar extension direction, 2) a strike-slip transfer zone with the same motion with 3) a similar orientation to the main rifts and 4) rift segments that grow apart.

REFERENCES

- Acocella, V., Facenna, C., Funiciello, R., Rosetti, F., 1999. Sand-box modelling of basement-controlled extensional domains. *Terra Nova*, 11, 149-156.
- Nalpas, T., Le Douaran, S., Brun, J.-P., Unternehr, P., Richter, J.-P., 1995. Inversion of the Broad Fourteens Basin (offshore Netherlands), a small-scale model investigation. *Sedimentary Geology*, 95, 237-250.
- Zwaan, F., Schreurs, G., Naliboff, J., Buiters, S.J.H., 2016. Insights in the effects of oblique extension on continental rift interaction from 3D analogue and numerical modeling, *Tectonophysics*.

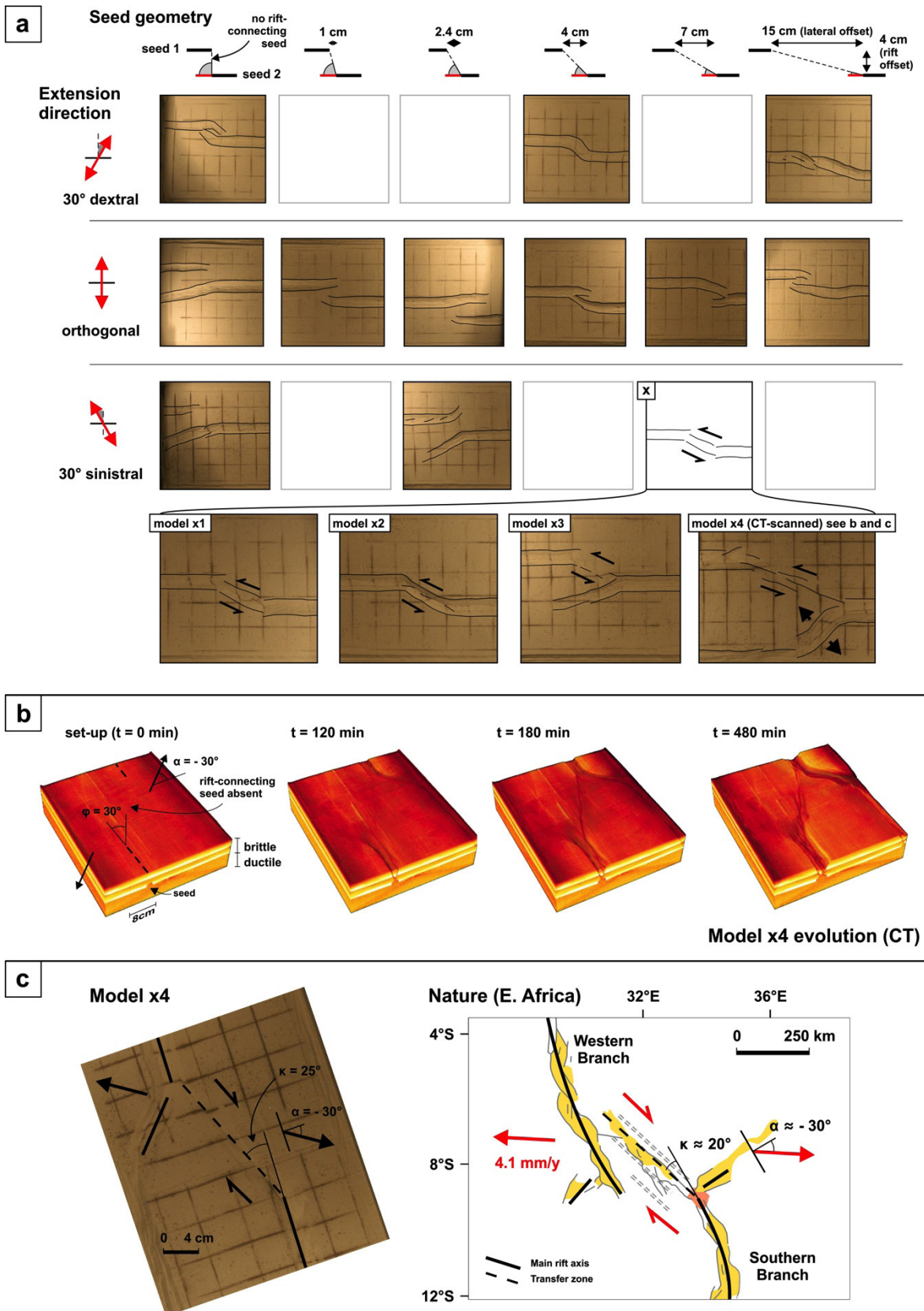


Figure 1. a) Final top view structures as a function of seed geometry and extension direction; b) CT-derived 3D evolution of model x4 (NB: mirrored with respect to Fig. 1a-b); c) Model-nature comparison, image modified after Acocella et al., 1999.

P 1.1

3D thermomechanical modeling of the Wilson Cycle: from intraoceanic subduction initiation to obduction

Stephane Beaussier¹, Taras Gerya², Jean-Pierre Burg¹

¹ *Geological Institute, ETH Zurich, Sonneggstrasse 5, CH-8092 Zurich
(stephane.beaussier@erdw.ethz.ch, jean-pierre.burg@erdw.ethz.ch)*

² *Institute of Geophysics, ETH Zurich, Sonneggstrasse 5, CH-8092 Zurich
(taras.gerya@erdw.ethz.ch)*

Obduction describes the emplacement of fragments of oceanic lithosphere, known as ophiolites, onto continental lithosphere.

Geological evidence recorded in Tethys ophiolites suggests that obduction started during the early stages of subduction, advocating that those two processes are strongly linked. Subduction initiation remains a controversial topic. Thus, a better understanding of subduction initiation may provide insight on the mechanisms leading to obduction.

Using the thermo-mechanical code, I3ELVIS (Gerya and Yuen, 2007) T.V., Yuen, D.A., 2003. Characteristics-based marker-in-cell method with conservative finite-differences schemes for modeling geological flows with strongly variable transport properties. *Phys. Earth Planet. Interiors* 140, 295-320], which is a combination of conservative finite-differences with marker-in-cell techniques to include the effects of visco-elasto-plastic rheology, self-gravitation and a self-consistently derived evolving curvilinear planetary surface. This code is called I2ELVIS and can solve a new class of computationally challenging problems in geodynamics, such as shear localization with large strains, crustal intrusion emplacement of magmas, bending of realistic visco-elasto-plastic plates and core-formation by vigorous shell tectonics activities related to a global Rayleigh-Taylor instability of a metal layer formed around silicate-rich lower density (primordial), in three-dimensions, we have developed a new approach in which the full "Wilson Cycle" is spontaneously simulated from continental extension and oceanic spreading to convergence and subduction. The model allows tracking the complex effects of inherited tectono-magmatic structures on subsequent subduction and provides a new near-ridge subduction initiation mechanism that can lead to obduction.

In our model, the convergence induces a swelling of the former ridge until it becomes a gravitational instability that drive the oceanic lithosphere down into subduction a few tenth of km away from the former ridge. The ridge swell can later be overthrust onto the continental lithosphere at the margins forming an ophiolite. The subduction initiation and obduction obtained from our model is compatible with the geological records of the Oman ophiolites and shown that obduction depends on the strength difference between the continental and oceanic lithosphere as well as on the geometry of the ridge swell formed during subduction initiation that is mainly controlled by convergence rate and the oceanic lithosphere rheology.

REFERENCES

Gerya, T. V., Yuen, D. a., 2007. Robust characteristics method for modelling multiphase visco-elasto-plastic thermo-mechanical problems. *Phys. Earth Planet. Inter.* 163, 83–105. doi:10.1016/j.pepi.2007.04.015 Beograd.

P 1.2

Terrestrial magma ocean crystallisation: bottom-up or middle-out?

Dan J. Bower¹, Aaron S. Wolf², Patrick D. Sanan³, and Paul J. Tackley¹

¹ *Institut für Geophysik, ETH Zürich, Zürich, Switzerland (dan.bower@erdw.ethz.ch)*

² *Earth and Environmental Sciences, University of Michigan, Ann Arbor, USA*

³ *Institute of Computational Sciences Università della Svizzera italiana Lugano, Switzerland*

Earth has likely experienced several episodes of magma ocean formation early in its history due to planetary accretion, core-formation, and large impacts. However, the evolution from an initially molten to solid mantle has not been explored in a physical model that adequately treats the high temperature and pressure behaviour of melts and solids. In particular, the shape of the liquidus and solidus relative to the adiabat determines whether a magma ocean will crystallise from the bottom-up or middle-out. These end-member scenarios give different predictions for the longevity of melt at the base of the mantle and thus the origin of small-scale seismic heterogeneity (“ultra-low velocity zones”) observed at present day.

Modelling the evolution of a magma ocean is challenging due to the vastly different timescales and lengthscales associated with turbulent convection (magma ocean) and viscous creep (present-day mantle), in addition to uncertainties in material properties and chemical partitioning. We therefore devise a fast, flexible, and portable code to calculate magma ocean cooling scenarios to explore the wide parameter space. The code utilises an energy-conserving finite volume method to solve for energy flow by tracking conductive and convective heat flow in addition to energy transfer associated with convective mixing and gravitational separation. Preliminary results suggest that a middle-outward crystallisation scenario experiences rapid cooling by convective heat transport until the rheological transition is reached. Subsequent cooling at the base of the mantle proceeds most efficiently by gravitational separation of melt and solid which can form a subadiabatic region near the core-mantle boundary.

P 1.3

Structure and mechanics of seismogenic fault zones in Switzerland: insights from microearthquake imaging

Tobias Diehl¹, Toni Kraft¹, Timothy Lee¹, Edi Kissling², Stefan Wiemer¹

¹ *Swiss Seismological Service, ETH Zurich, CH-8092, Switzerland (tobias.diehl@sed.ethz.ch)*

² *Institute of Geophysics, ETH Zurich, 8092, Switzerland*

Information on structure and mechanics of faults and their connection with present-day seismicity is key to the understanding of neotectonic processes in the Swiss Alps and the northern Swiss Foreland. Precisely determined focal depths in combination with high-resolution structural models can provide important insight into deformation styles of the uppermost crust (e.g. thin-skinned versus thick-skinned tectonics) and detailed images of seismogenic fault zones will also improve the assessment of the hazard related to natural and induced earthquakes in those regions. In the framework of various projects, studies have been recently undertaken or initiated to image seismogenic fault zones in southwest and northeast Switzerland at high resolution. Both regions were chosen because of their high societal relevance. Southwest Switzerland, especially the Valais, is the region with one of the highest natural seismic hazard in Switzerland and a large part of the present-day seismic activity is related to a transtensional earthquake lineament located in the Rawil depression. The possibility of large magnitude earthquakes critically depends on the question as to whether this activity is related to a single fault of considerable lateral and vertical extension or not. Studies of seismogenic structures and neotectonic processes in the northeastern Molasse basin, on the other hand, are of special interest, since the region is one of the target sites for radioactive waste repositories and future geothermal plants.

In this presentation, we use the results derived from the induced earthquake sequence of St. Gallen in 2013 to demonstrate, how high-precision earthquake locations and seismic tomography can be combined to resolve structures and fluid interactions in a seismogenic fault zone. In addition, we will present high-precision earthquake relocations and seismotectonic interpretations of recent earthquake sequences in the Valais and northeast Switzerland. Finally, we will give an overview of on-going projects aiming to image seismogenic fault zones in Switzerland. These projects include temporal densification of the national seismic network operated by the Swiss Seismological Service (SED) in the area of the Rawil depression and Eglisau (ZH), mainly to improve detection and location qualities of microearthquakes in those regions.

P 1.4

Evolution and architecture of continental passive margins: the role of structural softening

Thibault Duret¹, Benoit Petri¹, Geoffroy Mohn², Stefan Markus Schmalholz¹, Filippo Luca Schenker³, Othmar Müntener¹

¹ *Institute of Earth Sciences, University of Lausanne, Géopolis, CH-1015 Lausanne (thibault.duret@unil.ch)*

² *Université de Cergy-Pontoise, 33 boulevard du Port, F-95011 Cergy-Pontoise*

³ *SUPSI, University of Applied Sciences and Arts of Southern Switzerland, Via Trevano, CH-6952 Canobbio*

Numerous geological and geophysical studies have drawn attention to the multi-stage and depth-dependent character of lithospheric thinning. During rifting, a variety of structures are generated to accommodate lithospheric thinning (normal faults, low angle detachments, extensional shear zones, extraction faults), leading to complex passive margin architectures (e.g. necking zones, extremely thinned continental crust, mantle exhumation, continental allochthons). It is generally accepted that the lithosphere bears mechanical heterogeneities inherited from previous tectonic events (i.e. tectonic inheritance). During deformation, the presence of mechanical heterogeneities may induce mechanical instabilities and trigger structural softening. The influence of such processes on the dynamics of lithospheric extension and passive margin formation is so far incompletely understood.

We have designed two-dimensional thermo-mechanical models of lithospheric thinning to study the role of inherited mechanical heterogeneities on the development of passive margins. We represent first order heterogeneities by mechanical layering at the kilometre scale. The entire lithosphere incorporates several mechanically strong layers. The rheologies are voluntarily kept simple (temperature, stress, and strain rate-dependent visco-plastic) and we do not consider any material strain softening parameterisation nor damage model.

Our numerical simulations demonstrate that mechanical layering induces depth-dependent multi-stage lithospheric extension. Firstly the overall deformation style is decoupled and symmetric: both upper crustal and lithospheric layers undergo thinning by brittle (frictional-plastic) faults independently, while lower crustal and lithospheric levels accommodate extension by ductile necking. Secondly a low angle extensional structure develops across the Moho causing the overall deformation style to be coupled and asymmetric. Consequently subcontinental mantle exhumation takes place along the low angle extensional structure. At later stages, crustal allochthons form at the edges of the conjugate passive margins and competent mid-crustal levels are laterally extracted from the hyper-extended domain

These results stress the primordial role of mechanical heterogeneities and associated structural softening for lithospheric thinning. The incorporation of mechanical heterogeneities in lithospheric extension models can explain the formation of numerous observed geological features (necking zones, mantle exhumation, continental allochthons) regardless of the usage of a simple rheological model. Structural softening can hence alone give an explanation for the complex structuration and evolution of passive margins.

P 1.5

Intracontinental seismicity from 550 Ma to present day in the Musgrave Ranges of Central Australia

Friedrich Hawemann¹, Neil Mancktelow¹, Sebastian Wex¹, Giorgio Pennacchioni², & Alfredo Camacho³

¹ *Department of Earth Sciences, ETH Zurich, Sonneggstrasse 5, CH-8092 Zurich*

² *Department of Geosciences, University of Padua, Via Gradenigo 6, 35131 Padua*

³ *Department of Geological Sciences, University of Manitoba, 125 Dysart Rd, Winnipeg, Manitoba, R3T 2N2 Canada*

The Petermann Orogeny (~550 Ma) in Central Australia represents an outstanding example of an intracontinental orogeny, yet the reasons for localized deformation far removed from the plate margins are still poorly understood. In the Musgrave Ranges, located between the North, West and South Australian cratons, the exposed rocks were at middle to lower crustal levels during the Petermann Orogeny. The earlier (~1.2 Ga) Musgravian Orogeny already stitched together the Australian cratons and resulted in amphibolite to granulite facies metamorphism in the study area. This high-temperature

metamorphism and associated local partial melting induced dehydration of the lower crust. As a result, the crust that localized deformation within the continent interior during the subsequent Petermann Orogeny was relatively dry and (at least transiently) strong, as seen by the absence of any partial melting for conditions up to $\sim 650^{\circ}\text{C}$ and 1.2 GPa and from the presence of abundant synkinematic pseudotachylytes, generally taken as indicators of palaeo-seismicity. The Petermann Orogeny was associated with a dominant N-S compression, resulting in the E-W trend observed today in the Musgrave Ranges. Lower crustal rocks in the south are juxtaposed against middle crustal rocks in the north across the Woodroffe Thrust, which extends for about 600 km along strike and dips shallowly to the south. The Woodroffe Thrust zone consists of several hundred meters of mylonites, ultramylonites and multiple generations of pseudotachylyte, without evidence for marked rehydration. Pseudotachylyte is developed as precursors to localized ductile shearing, during shearing, and as undeformed injections, demonstrating repeated seismic events at middle to lower crustal depths.

The Musgrave Ranges continue to be seismically active in modern times, with large earthquakes occurring at relatively short intervals ($M_w > 5$ in 2012 and 2013, $M_w \sim 6.2$ in 2016). The two events from 2012 and 2013 were in close proximity to the Woodroffe Thrust, but their fault plane solutions do not match the geometry on the Woodroffe Thrust, although they still indicate overall NE-SW convergence. The most recent and largest event is potentially located on the old thrust plane, with similar kinematics. These earthquakes were the largest on the Australian continent since 1997, raising the same questions with regard to the cause of intracontinental earthquakes as with the Proterozoic examples.

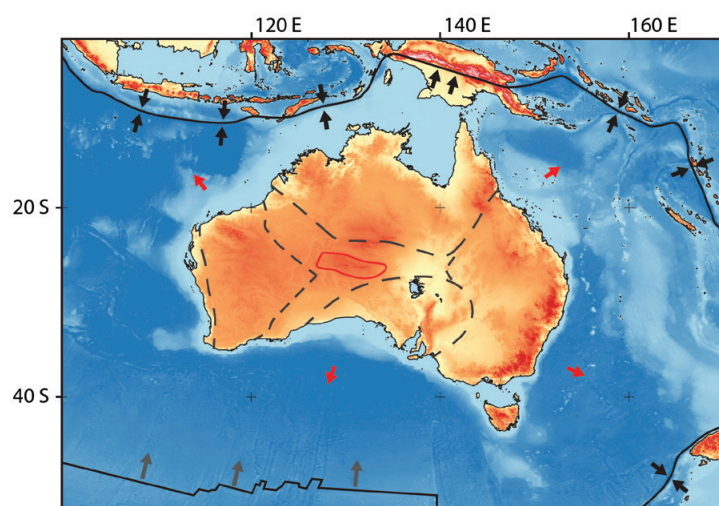
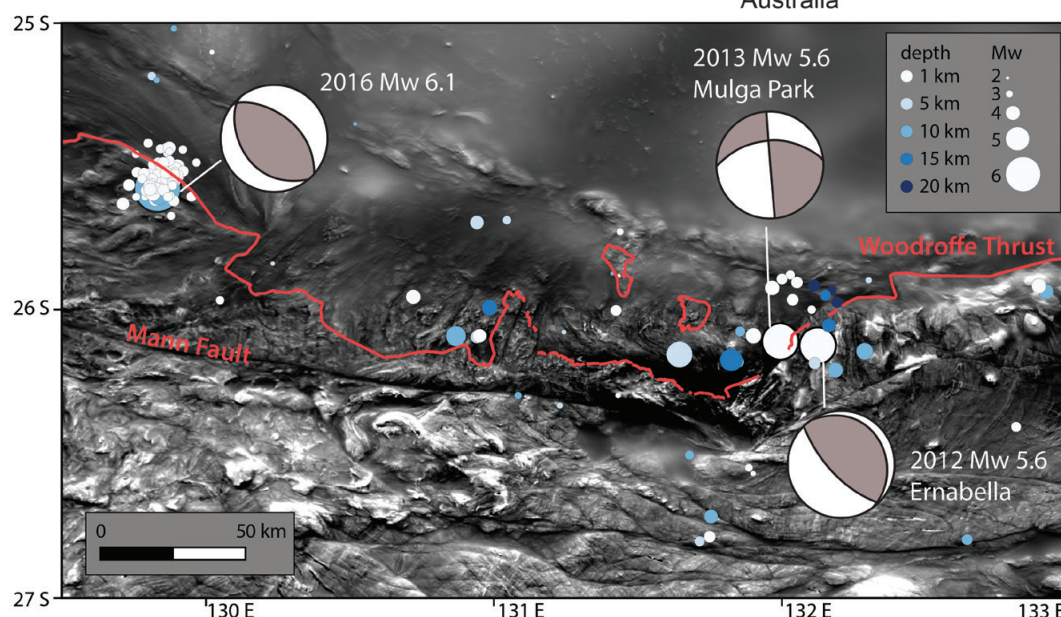


Figure 1 (left): Location of the Musgrave Ranges between the cratons (boundaries as dashed lines). Plate boundary forces as arrows, red arrows show buoyancy force. Topography and bathymetry from ETOPO1, provided by NOAA.

Figure 2 (below): Earthquakes in the Central Musgraves are located in close proximity to the Woodroffe Thrust. Background: Total magnetic intensity map, Geoscience Australia



P 1.6

Dimensional analysis for the evolution of temperature and thickness of shear zones caused by shear heating

Dániel Kiss, Thibault Duretz, Yuri Podladchikov, and Stefan M. Schmalholz

Institute of Earth Sciences, University of Lausanne, Lausanne, Switzerland (daniel.kiss@unil.ch)

Localization of deformation plays a major role during tectonic processes at all scales, from the formation of deformation bands within single grains up to crustal and lithospheric scale shear zones. It has been shown that in a sheared heterogeneous media (e.g.: sedimentary sequences on the top of a strong basement) so-called kinematic shear localization is present. If we consider also the temperature gradient, this type of shear localization can explain the formation of tectonic nappes to the first-order. This kind of kinematic shear localization is highly prescribed, as it can happen only in “weak zones”, while shear heating can be a mechanism of spontaneous shear localization in a quasi-homogenous material (e.g.: strike-slips). Shear heating can significantly amplify the small perturbations that are initially present, resulting in locally elevated temperature and strongly localized shear deformation. In nature both localization mechanisms are present - sometimes simultaneously - but in this presentation we focus on shear localization by thermal softening related to shear heating.

We show some important features of shear zones formed by shear heating and we also perform a dimensional scaling analysis of the equations that describe the 1D spontaneous shear zone model to determine the dimensionless parameters that are controlling the process. We consider a 1D configuration where the bulk shear deformation is controlled by a constant shear velocity. The initial configuration exhibits small thermal perturbations. (1) For linear viscous material after a transient stage a constant maximum temperature is reached, regardless of the initial state. (2) The width of the shear zone is not constant, but is increasing with time due to thermal diffusion. (3) The shear zone thickness with respect to the finite strain is always significantly thinner than the thickness of the temperature perturbation. (4) The maximum temperature in the shear zone is controlled by only one dimensionless number, and (5) the dimensionless thickening rate of the temperature perturbation can be predicted by only one dimensionless number. This number can be used to estimate *a priori* whether shear heating is important or not. The 1D shear zone model is also applied to geological data of natural shear zones, to assess whether shear heating may be an important mechanism of shear localization or resulting in significantly elevated temperatures.

P 1.7

Oblique versus orthogonal collision influenced by lateral variations: 3D numerical modeling

Jie Liao¹, Taras Gerya¹

¹ *Geophysical Fluid Dynamics, Institute of Geophysics, ETH Zurich, Sonneggstrasse 5, CH-8092, Zurich, Switzerland (jie.liao@erdw.ethz.ch)*

Continental collision is an important tectonic process that builds up high mountain ranges. A principal understanding of collisional dynamics can be gained through two dimensional numerical modeling and analogue modeling. Many of these assume quasi-infinite homogeneity in the third dimension. Three dimensional numerical studies on continental collision are limited, but are essential in investigating the full dynamics of realistic, three-dimensional orogenic systems, in particular the controls of lateral heterogeneities on collisional dynamics. Lateral variations (e.g., curvature and metamorphic grade) are widely revealed along the strike of orogenic belts worldwide. They imply that initial variations like margin geometry, thermal differences, and kinematic gradients, significantly controlled the dynamic evolution of continental collision and surface expressions. However, the influence of lateral variations on collisional dynamics remains enigmatic and requires quantitative understanding through three dimensional modeling.

In this study, we employ 3D thermomechanical numerical models to investigate the effect of lateral variation on continental collision in three model series (i.e., compositional variations, oblique collision, and thermal variations). All these three lateral variations expose a first-order control on model evolution and produce large lateral variations in lithospheric deformation. Continental crust is shortened in the shallow depth, and crustal shortening varies along strike. Mantle lithosphere of the lower plate subducts beneath the upper plate, and lateral variation is shown on slab geometry.

P 1.8

Seismotectonic study of microseismic sequences in North-Western Switzerland using sonograms and waveform similarity analysis.

Marie Luyet¹, Naomi Vouillamoz², Patrick Blascheck², Martinus Abednego¹, Jon Mosar¹

¹ *Department of Geosciences, University of Fribourg, Switzerland, marie.luyet@unifr.ch*

² *Institute of Geophysics, University of Stuttgart, Germany, naomi.vouillamoz@geophys.uni-stuttgart.de*

The SED (Swiss Seismological Service) recently reported 30 earthquakes close to the city of Biel. The seismic activity was clustered in periods of a few days – weeks in January 2014 and January-February 2015. Two events reaching local magnitudes (ML) above 3 were largely felt by the local population.

With the aim to complete the catalog in the lower magnitude range, continuous broadband data of four local Swiss stations are reprocessed in the form of sonograms. Sonograms are spectrograms with a frequency-dependent noise adaptation on which earthquakes display typical frequency-time signatures that are easily recognized by the analyst down to the background seismic noise threshold. Events are then evaluated in HypoLine and better constrained by additional seismic-array records at the Mont-Terri rock laboratory in 2015.

170 low magnitude events ($ML < 1$) were positively correlated and associated to the two earthquake sequences. The events of interest show emergent P-onsets due to their low energies. Therefore, an approach that focuses on S-phase cross-correlation is used to derive event clustering. A linkage function applied on the cross-correlation matrices with correlation threshold above 80% returns several earthquake families, suggesting that ruptures occurred on different fault segments. This is supported by the focal mechanisms computed by the SED which show different fault plane solution for the main events. The matrices also suggest a reactivation of the same faults, some signals being more than 90% identical between 2014 and 2015.

REFERENCES

- Edwards, B., Kraft, T., Cauzzi, C., Kastli, P., Wiemer, S. 2015 : Seismic Monitoring and Analysis of a Deep Geothermal Project in St. Gallen, Switzerland, *Geophys. J.Int.*
- Joswig, M. 2008: Nanoseismic monitoring fills the gap between microseismic networks and passive seismic, *First Break*, 26, 117–124.
- Kradolfer, U. 1984 : Magnitudenkalibrierung von Erdbebenstationen in der Schweiz, Diplomarbeit, ETHZ, Zürich.
- Sick, B., Walter, M., Joswig, M. 2012: Visual Event Screening of Continuous Seismic Data by Supersonograms, *Pure Appl. Geophys.*
- Vouillamoz, N. 2015: Microseismic characterization of Fribourg area (Switzerland) by Nanoseismic Monitoring. PhD thesis. *GeoFocus*, 38, Département de Géosciences - Sciences de la Terre, Université de Fribourg, Suisse, 276 pp.

P 1.9

Polyphase ductile/brittle deformation along a major tectonic boundary in an ophiolitic nappe, Alpine Corsica: Insights on subduction zone intermediate-depth asperities

Rémi Magott¹, Olivier Fabbri¹ & Marc Fournier²

¹ *Laboratoire Chrono-environnement UMR CNRS 6249, Université Bourgogne Franche-Comté, F-25000 Besançon, France (remi.magott@univ-fcomte.fr)*

² *Sorbonne Universités, UMR 7193, UPMC Univ. Paris VI, ISTEP, F-75005 Paris, France*

In an ophiolitic nappe of Alpine Corsica, a major pseudotachylytes-bearing fault zone separates an upper metagabbro unit from a lower serpentinite and peridotite unit (Austrheim & Andersen, 2004). This fault zone recorded ductile and brittle deformation events associated to the alpine subduction. In the hanging-wall metagabbro damage zone, early deformation occurred under greenschist to blueschist or eclogite facies conditions and consisted of west-verging ductile shear alternating with pseudotachylyte-forming faulting with undetermined vergence. This deformation is likely coeval with west-verging seismic (pseudotachylyte-forming) faulting in the footwall peridotite or with ductile (distributed) deformation of footwall serpentinite (Magott et al., 2016). Early structures are interpreted as the result of reverse faulting/shear in the east-dipping subducting oceanic lithosphere in Cretaceous to Eocene times. Late deformation events consist of ductile shear and seismic faulting having occurred under retrograde greenschist conditions. Kinematics of the ductile shear is top-to-the-east. These events are interpreted as the result of syn- to post-collision extension of the Alpine Corsica in Eocene to Miocene times. Regarding the early events, the uneven distribution of pseudotachylyte veins along the fault zone (abundant at peridotite-metagabbro interfaces, rare or absent at foliated serpentinite-metagabbro interfaces) is interpreted as the result of contrasted frictional properties of the rocks in contact. High-friction peridotite-metagabbro contacts are patches characterized by large seismic ruptures (asperities; Seno, 2003) whereas low-friction serpentinite-metagabbro are creeping zones.

REFERENCES

- Austrheim, H., & Andersen, T.B. 2004: Pseudotachylytes from Corsica: fossil earthquakes from a subduction complex, *Terra Nova*, 16, 193-197.
- Magott, R., Fabbri, O. & Fournier, M. 2016: Subduction zone intermediate-depth seismicity: Insights from the structural analysis of Alpine high-pressure ophiolite-hosted pseudotachylytes (Corsica, France), *Journal of Structural Geology*, 87, 95-114.
- Seno, T. 2003: Fractal asperities, invasion of barriers, and interplate earthquakes, *Earth Planet Space*, 55, 649-665.

P 1.10

Sediment travel paths in the Carboniferous as recorded by detrital zircon geochronology in the Dora-Maira and Zone Houillère

Paola Manzotti¹, Michel Ballèvre² & Marc Poujol²

¹ *Institute of Earth Sciences, University of Lausanne, Géopolis, Quartier Mouline, Lausanne 1015, Switzerland (paola.manzotti@gmail.com)*

² *Géosciences Rennes, UMR CNRS 6118, Université Rennes1, Campus de Beaulieu, Rennes Cedex 35042, France*

In the internal zone of the European Alps, late Carboniferous to Permian sediments have been detached from their basement (e.g. the Zone Houillère in the Briançonnais Zone). The Pinerolo Unit (Dora-Maira Massif) is the deepest unit exposed in the stack of the Western Alps and is considered to be Carboniferous in age based on lithological considerations (Franchi & Novarese, 1895; Argand, 1911). The blueschist-facies Pinerolo Unit occupies a key tectonic position in the Alpine belt, being overthrust by the coesite-eclogite and quartz eclogite units of the Dora-Maira Massif.

Detrital zircon grains from the Pinerolo Unit and the Zone Houillère (located along the external margin of the Briançonnais domain) display similar age patterns, with the youngest and largest population being Carboniferous (340-330 Ma). The distribution of Carboniferous magmatism in the Alps and surrounding areas suggests that the detritus was transported from Maures-Corsica and possibly from the Helvetic Zone into the Zone Houillère and the Pinerolo basin. Our results highlight the potential of detrital zircon geochronology for deciphering the sources of detrital material in meta-sediments, even if they have been affected by metamorphic overprints.

P 1.11

Tectonics in the Georgian Greater Caucasus: a structural cross-section in an inverted rifted basin setting

Jeremiah Mauvilly¹, Kakhaber Koiava², Irakli Gamkrelidze² & Jon Mosar¹

¹ *Département de Géosciences - Sciences de la Terre, Université de Fribourg, Chemin du Musée 6, CH-1700 Fribourg (jon.mosar@unifr.ch)*

² *Ivane Javakishvili State University, Alexandre Janelidze Institute of Geology, A. Politkovskaia str. 5, GEO-0186 Tbilisi (gamkrelidzei@yahoo.com)*

The Greater Caucasus is Europe's highest mountain belt (Mount Elbrus, 5642 m.a.s.l.) and stretches from east to west from the Caspian Sea to the Black Sea. The present-day orogen has evolved from a Mesozoic back-arc rifted continental basin into a doubly vergent intracontinental orogenic wedge during the Alpine collisional event due to the north-south convergence of the Arabian and the Eurasian plates. No subduction zone under the Greater Caucasus and no remnants of Jurassic oceanic floor are known over a 200 year old history of geological exploration. The Greater Caucasus has its origin most likely in an extensively stretched and heavily intruded crust during Early Jurassic that has subsequently been inverted. Unlike the Greater Caucasus, both the South Caspian Sea and the East Black Sea show incipient subductions of oceanic lithosphere towards the north. To the north and the south the orogen is bordered by deep flexural molasse-type basins. The main orogenic transport direction (prowedge) is to the south. North-directed thrusting is unevenly spread on the northern flanks of the orogen and is best developed in the Dagestan. The imbrication of different tectonic nappes generated a post-Sarmatian uplift of some 4 km and has been accompanied since the Late Miocene by important volcanic activity.

The Georgian Military Road, as a major route crossing the central Greater Caucasus, is ideal for an insight into its different tectonics units. These tectonic zones are delimited by large thrust and correspond to different paleogeographic domains. Those are, from the core of the mountain belt towards the Trans-caucasian foreland, or from north to south respectively, the Main Range Zone (deepest part of the basin), the Kazbegi-Lagodekhi Zone (transition towards the flysch slope), the Mestia-Tianeti Zone (southern flysch slope), and the Kartli Zone (tertiary molassic basin fill superimposed on the southern edge of the basin).

Our poster presents a north-south oriented structural cross-section of the central Greater Caucasus based on our field investigation along the Georgian Military Road. Derived from this new cross-section and from existing data and knowledge about the Caucasus orogen, we also present a first attempt at a paleogeographic reconstruction of the Caucasus region (southern Eurasian margin) before the Alpine collisional event.

This new north-south oriented paleogeographic crustal scale cross-section shows an overall asymmetric rifting and highlights the complex inherited structure of the southern Eurasian margin with its rifted basins, basement highs and platforms. Several tectonic domains corresponding to the present-day tectonic zones were thus identified. The stable Scythian Platform was only moderately affected by rifting and is delimited to the south by the Bechasyan and Fore Range basement high, which forms today's crystalline massifs in the core of the mountain belt. The deepest part of the Greater Caucasus Basin, where the crust was thinned most and intruded intensely, is located in the present-day Main Range Zone. The Kazbegi-Lagodekhi, Mestia-Tianeti, and Gagra-Java Zones correspond to the southern portion of the former Greater Caucasus rifted basin. To the south, the Greater Caucasus Basin was separated from the smaller Ajara-Trialeti Basin by the Dzirula basement high, which corresponds to an outcropping Transcaucasian massif. The Ajara-Trialeti Basin is delimited to the south by the Artvin-Bolinis Block where the Mesozoic Transcaucasian magmatic arc was located.

Linking the paleogeographic cross-section with the present-day structural cross-section, we conclude that the major thrusts of the Caucasus orogen (e.g. the Main Caucasus Thrust and the Racha Fault) are large scale normal rifting faults that were reactivated as thrusts during the collisional events of the Arabia-Eurasia convergence.

REFERENCES

- Adamia, Sh., Zakariadze, G., Chkhotua, T., Sadradze, N., Tsereteli, N., Chabukiani, A. & Gventsadze, A., 2011: Geology of the Caucasus: A Review. *Turkish J. Earth Sci.*, 20, 489-544.
- Gamkrelidze, I. P., Pruidze, M. P., Gamkrelidze, M. I. & Loladze, M. I., 2013: Tectonic Map of Georgia, 1:500'000. Georgian National Academy of Sciences, Alexandre Janelidze Institute of Geology, Ivane Javakhsishvili Tbilisi State University.
- Mosar, J., Kangarli, T., Bochud, M., Glasmacher, U. A., Rast, A., Brunet, M.-F. & Sosson, M., 2010: Cenozoic-Recent tectonics and uplift in the Greater Caucasus: a perspective from Azerbaijan. *Geological Society, London, Special Publications*, 340, 261-280
- Somin, M. L., 2011: Pre-Jurassic Basement of the Greater Caucasus: Brief Overview. *Turkish J. Earth Sci.*, 20, 545-610.
- Sosson, M., Stephenson, R., Sheremet, Y., Rolland, Y., Adamia, Sh., Melkonian, R., Kangarli, T., Yegorova, T., Avagyan, A., Galoyan, G., Danelian, T., Hässig, M., Meijers, M., Müller, C., Sahakyan, L., Sadradze, N., Alania, V., Erukidze, O. & Mosar, J., 2016: The eastern Black Sea-Caucasus region during the Cretaceous: New evidence to constrain its tectonic evolution. *C. R. Geoscience* 348, 23-32.

P 1.12

Provenance, detrital zircon U-Pb geochronology, and tectonic significance of Eocene-Miocene sequence of onshore west Makran, South Iran

Ali Mohammadi¹, Jean-Pierre Burg¹, Marcel Guillong¹

¹ Department of Earth Sciences, ETH Zurich, Sonneggstrasse 5, 8092, Zurich, Switzerland

The ~ 1000 km long Makran Accretionary Wedge in SE Iran and SW Pakistan results from the convergence between the Arabian and Eurasian plates since Late Cretaceous. The present work aims to reconstruct the Mesozoic and Cenozoic geological history of the western part of the wedge in south Iran. We determined the provenance of Eocene-Miocene deep marine turbiditic and shelf sandstones, describe the sandstone framework and heavy minerals, and report a geochronological and geochemical study including LA-ICP-MS U-Pb zircon ages and 200 Hf isotopic analyses of 2500 in-situ detrital zircons.

Sandstone framework compositions reveal a magmatic arc provenance as main source of detritus. Heavy mineral assemblages and Cr-spinel reveal ultramafic rocks, likely ophiolites, as a subsidiary source. Detrital zircon yielded three main U-Pb age groups: (1) Eocene grains with major peak at 49 Ma, (2) Late Cretaceous grains with major peak at 106 Ma, and (3) Neoproterozoic zircons span between 500 and 1000 Ma. These new detrital zircon U-Pb age data are similar to the detrital zircon U-Pb of east Makran (Mohammadi et al. 2016). Miocene sediments are recycled (cannibalism) from accreted Late Cretaceous-Oligocene units of the basin.

REFERENCES:

- Mohammadi, A., Burg, J.P., Winkler, W., Ruh, J. and von Quadt, A., 2016. Detrital zircon and provenance analysis of Late Cretaceous– Miocene onshore Iranian Makran strata: Implications for the tectonic setting. *Geological Society of America Bulletin*, doi:10.1130/B31361.1.

P 1.13

Physical parameters controlling orocline development: Insights from numerical modelling

Jessica Munch¹, Kosuke Ueda¹, Oğuz H. Göğüş², Jean-Pierre Burg¹, & Taras Gerya¹

¹ *Earth Sciences department, ETH Zurich, Sonneggstrasse 5, 8092 Zurich (jessica.munch@erdw.ethz.ch)*

² *Eurasia Institute of Earth Sciences, Istanbul Technical University 34469 Maslak - Istanbul, Turkey*

Oroclines are formed along highly curved convergent systems often associated with mountain ranges and oceanic arcs. The oroclinal bending process may occur at different times and length scales in distinct geodynamic settings. For instance, 1) the several thousands of kilometers long Bolivian orocline in the Andes which has been suggested to have formed during the Eocene-Oligocene along the subduction of an oceanic plate beneath the continental plate South America, and 2) the few hundreds of kilometers long Gibraltar Alborán orocline, which was formed less than 35 Ma ago in a continental domain. Previous works principally studied orocline formation in the context of retreating subduction and possibly in lithospheric removal (delamination). Therefore, the understanding of the physical mechanisms that lead to orocline formation is a key to the comprehension of regional geodynamics in several places on Earth.

We used the thermomechanical code I3ELVIS (Gerya and Yuen, 2007) to model plume-induced retreating subduction initiation and geodynamic evolution in 3D. A series set of model simulations involving oceanic and continental lithosphere were analyzed to determine the physical parameters that control the orocline formation. Some models developed curved surface uplifts at the trenches, synchronously with slab retreat. Simulation results also show the narrowing of the slab width during its retreat. Retreating subduction is not the only way to generate oroclines: in analogue models, asthenospheric flow triggered by delamination of the lithospheric mantle also favors curved orogens. The parallel use of different kinds of modeling with varying controlling parameters in both subduction and delamination processes is likely to allow us to better understand the formation of oroclines and the geodynamic processes they are related to.

REFERENCES

Gerya, T. V. & Yuen, D. A. 2007. Robust characteristics method for modelling multiphase visco-elasto-plastic thermo-mechanical problems. *Physics of the Earth and Planetary Interiors* 163(1), 83-105.

P 1.14

Structural and kinematic study of the strike-slip fault of Pontarlier

Viêt-Thang Nguyen¹, Marius Gruber¹, Nicole Schmitt¹, Jon Mosar¹

¹ *Département de Géosciences - Sciences de la Terre, Université de Fribourg, Chemin du Musée 6, CH-1700 Fribourg
(viet-thang.nguyen@unifr.ch, marius.gruber@unifr.ch, nicole.scheidt@unifr.ch, jon.mosar@unifr.ch)*

The western Alpine Molasse Basin (WAMB) is an overfilled flexural foreland basin which is filled with detrital sediments of Tertiary age (Sinclair et al., 1991). During the exhumation and the imbrication of the external Crystalline Massifs in the Alps, the western Alpine Molasse Basin was detached along a decollement horizon located in Triassic evaporites (Burkhard and Sommaruga, 1998). This thin-skinned detachment is believed to be the cause of the formation of the Jura Fold-and-Thrust Belt (JFTB) ("Fernschub theory") (Buxtorf, 1916). The WAMB evolved from a classical flexural foreland basin to a wedge top basin. The presence of Molasse deposits in synclines of the JFTB strongly supports the idea of a post-depositional formation of the JFTB since the Serravallian (Burkhard and Sommaruga, 1998).

Cretaceous and Jurassic units of the JFTB and the WMAB are mainly composed of shallow water carbonate rich sediments (marls and limestones), whereas Triassic sediments are mainly composed of evaporites (anhydrite and salt).

The JFTB is cut by several large-scale vertical strike-slip faults which extend into the WAFB. This study focusses in particular on the fault of Pontarlier which is a vertical, N-S striking strike-slip fault of 80 km length in the central part of the JFTB and the WAMB. The aim of this study is to investigate the structural and the kinematic configuration of the fault of Pontarlier by creating a simplified 3D model. For this, based on the Swiss and the French geological maps at 1:25'000 and 1:50'000, we create a new generalized and simplified geological map. The following stratigraphic units are represented on the map: The Quaternary, the Tertiary, the Cretaceous, the Upper and the Lower Malm as well as the Dogger and the Liassic. These units are interpreted in 2D seismic lines in the Molasse Basin (Gruber, 2016). Moreover, we analyze the Swiss side of the fault of Pontarlier using the Swiss digital elevation model (DEM, SwissAlti3D). This allows to observe the surface expression of the fault of Pontarlier. The surface expression of the fault of Pontarlier is further investigated using satellite images. Finally, a simplified 3D model is created based on existing geological profiles and 2D seismic lines (Gruber, 2016). As a next step, we will validate this 3D model using newly acquired surface data. Further we will analyze the slip tendency of the fault surface using 3Dstress software and compare the results with surface fracture data.

REFERENCES

- Burkhard, M., & Sommaruga, A. (1998). Evolution of the western Swiss Molasse basin: structural relations with the Alps and the Jura belt. Geological Society, London, Special Publications 1998, v. 134, p. 279-298.
- Buxtorf, A. (1916). Prognosen und Befunde beim Hauensteinbasis und Grencherberg-tunnel und die Bedeutung der letzteren für die Geologie des Juragebirges. Verh, Naturforsch. Ges. Basel, 27, 184-205.
- Gruber, M. (in prep.). Structural Investigations of the Western Swiss Molasse Basin – From 2D Seismic Interpretation to a 3D Geological Model. Thèse de doctorat de l'Université de Fribourg, Géologie.
- Sinclair, H.D., & al. (1991). Simulation of Foreland Basin stratigraphy using a diffusion model of mountain belt uplift and erosion: and example from the central Alps, Switzerland. Tectonics, Vol.10, n°3, 599-620.

P 1.15

Seismic cycle modeling on evolving faults: The question of fault branching

Simon Preuss¹, Taras Gerya¹, Ylona van Dinther¹, Jean Paul Ampuero², Yannick Caniven³

¹ *Institute of Geophysics, ETH Zürich, Sonneggstrasse 5, CH-8092 Zurich, Switzerland (sipreuss@ethz.ch)*

² *Seismological Laboratory, California Institute of Technology, Pasadena CA (United States)*

³ *Géosciences Montpellier, Université de MontpellierMontpellier 34095 (France)*

Even in well documented fault zone regions like California, ~30% of the total displacement occurs off the main fault and large earthquakes have generated on unknown fault branches (e.g. 2010 Baja California earthquake). A severe issue is the determination of their location and estimation of their potential risk as well as proneness to rupture.

To answer such questions we first need a better physical understanding of the long-term evolution of branching fault structures. Our goal is to quantify the parameters influencing branching structure.

In our approach we will bridge long-term fault structure evolution and short-term seismicity generation using the tools of Seismo-Thermo-Mechanical (STM) modeling (van Dinther et al., 2013).

To start, we adopt a model with 2D plane view mature strike-slip geometry based on the laboratory model of Caniven et al. (2015) using visco-elasto-plastic material behavior to investigate and compare seismicity patterns and evolution. The numerical simulation results are comparable to the ones of the lab model and reproduce stick-slip behavior, seismic events, nucleation and propagation of ruptures.

Next, we implemented strain weakening of cohesion to analyze evolving fault structure in a 2D top view natural scale model. First results of this model show more complex fault pattern giving rise to Riedel shears, R¹ shears and sub parallel faults isolated by offsets from the main fault. Linkage of en échelon fault segments causes extensional bends and contractional bends.

Finally, these results will be compared to a 2D and 3D long-term geodynamic thermo-mechanical model in terms of fault structure on the surface to analyze the role of a visco-plastic structure with depth and short term seismic cycle. Once we have an appropriate setup to study the problem of fault branching, we ultimately plan to explore the role of different friction, material and tectonic parameters on branching structure.

P 1.16

Tectonic inversion of a basement-involved fold-and-thrust belt: Numerical modelling applied to the Kopet Dagh Mountains

Jonas B. Ruh¹ & Jaume Vergés¹

¹ *Institut de Ciències de la Terra Jaume Almera, Consejo Superior de Investigaciones Científicas, Barcelona, Spain*

In the last decades, much effort has been made towards understanding thin-skinned evolution of mountain belts, i.e. without taking into account any involvement of basement deformation, applying analogue, numerical, and analytical solutions (Davis et al., 1983; Gwinn, 1964; Hsu, 1979). Recent studies have shown that basement-involvement during orogenic growth can strongly influence the structural and mechanical evolution of mountain belts (e.g., Bauville and Schmalholz, 2015). Furthermore, focus is often limited on purely compressive systems, although new studies emphasize the importance of inversion of pre-orogenic extensional basins and inheritance of basement normal faults for the dynamics of evolving mountain belts (e.g., Boutoux et al., 2014). Numerical studies show proposed that even old and thermally strong basins could potentially be inverted if they are associated to weak shear zones (Buitter et al., 2009).

The Kopet Dagh mountain belt in NE Iran is an excellent example of an inverted fold-and-thrust belt and suits perfect to investigate and understand long-term processes and evolution of a basement-involvement and tectonic inversion (Figure 1; Robert et al., 2014, and references therein). The Kopet Dagh underwent a short period of extension in the Middle Jurassic, when the northern branch of the Tethys (Paleotethys) closed. Subduction of the southern branch of the Tethys (Neotethys) initiated and the Kopet Dagh Mountains developed although their timing is not clear yet: late Eocene-Oligocene or Miocene during continental collision. Therefore, the temporal and structural evolution of the Kopet Dagh is an important key towards understanding the large-scale tectonic history of the Arabia-Eurasia continental collision.

We apply a fully staggered, marker-in-cell, finite difference numerical code with a framework written after a text book for numerical geodynamic modelling (Gerya, 2010) that was further developed. The presented model exhibits a visco-elasto-plastic rheology and simplified strain-dependent plastic softening. Initial extension and subsequent tectonic inversion towards convergence is applied to a 30 km thick crustal sequence. Syn-tectonic sedimentation during extension as well as filling-up of the basin during the tectonically quiet phase is applied to investigate the effect of deep-rooted inherited basement faults on the structural evolution of the overlying sedimentary sequence (Figure 1). We test the effects of varying thermal gradients, crustal rheology, and amount of (non-physical) rock softening.

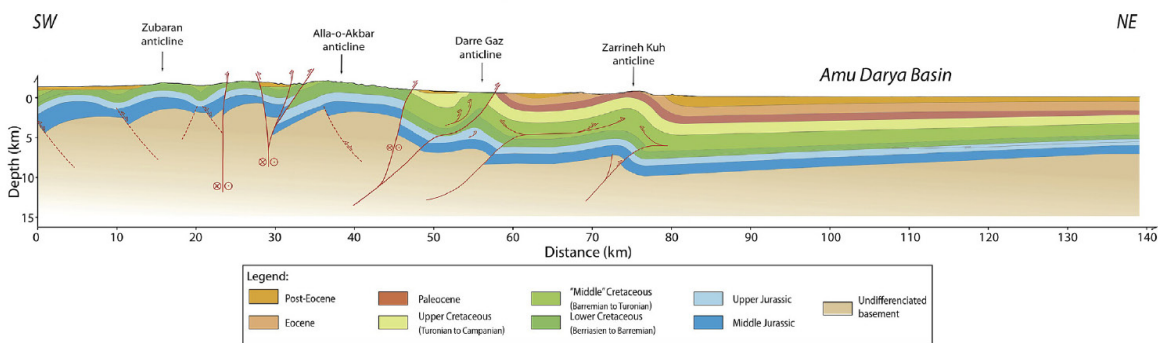


Figure 1: Regional cross-section showing inversion of inherited basement structures in the Kopet Dagh. Structural framework of Mesozoic and Cenozoic stratigraphy is strongly dependent on basement deformation. Adapted from Robert et al. (2014).

REFERENCES

- Bauville, A., and S. M. Schmalholz (2015), Transition from thin- to thick-skinned tectonics and consequences for nappe formation: Numerical simulations and applications to the Helvetic nappe system, Switzerland, *Tectonophysics*, 665, 101-117.
- Boutoux, A., N. Bellahsen, O. Lacombe, A. Verlaquet, and F. Mouthereau (2014), Inversion of pre-orogenic extensional basins in the external Western Alps: Structure, microstructures and restoration, *J Struct Geol*, 60, 13-29.
- Buiter, S. J. H., O. A. Pfiffner, and C. Beaumont (2009), Inversion of extensional sedimentary basins: A numerical evaluation of the localisation of shortening, *Earth Planet Sc Lett*, 288(3-4), 492-504.
- Davis, D., J. Suppe, and F. A. Dahlen (1983), Mechanics of Fold-and-Thrust Belts and Accretionary Wedges, *J Geophys Res*, 88(Nb2), 1153-1172.
- Gerya, T. (2010), *Introduction to Numerical Geodynamic Modelling*, 345 pp., Cambridge University Press.
- Gwinn, V. E. (1964), Thin-Skinned Tectonics in the Plateau and Northwestern Valley and Ridge Provinces of the Central Appalachians, *Geol Soc Am Bull*, 75(9), U863-&.
- Hsu, K. J. (1979), Thin-Skinned Plate Tectonics during Neo-Alpine Orogenesis, *Am J Sci*, 279(4), 353-366.
- Robert, A. M. M., J. Letouzey, M. A. Kavooosi, S. Sherkaty, C. Muller, J. Vergés, and A. Aghababaei (2014), Structural evolution of the Kopeh Dagh fold-and-thrust belt (NE Iran) and interactions with the South Caspian Sea Basin and Amu Darya Basin, *Mar Petrol Geol*, 57, 68-87.

P 1.17

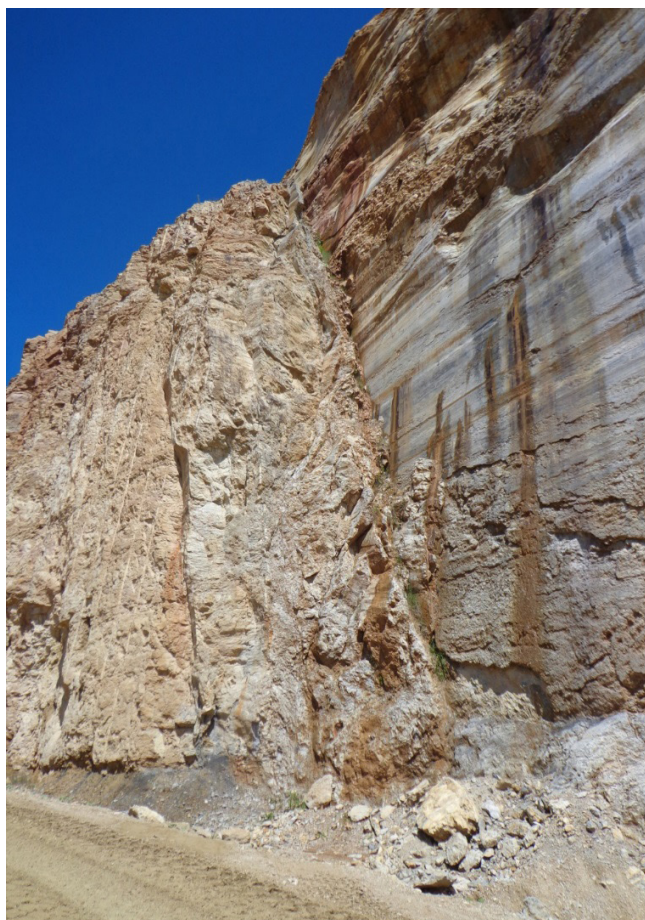
Fault anatomy and microtectonics of the La Sarraz strike-slip fault system

Nicole Schmitt¹, Benjamin Verbeken¹, Renata Grassi¹, Stephen A. Miller², Lea Perrochet¹, Benoît Valley² & Jon Mosar¹

¹ *Département de Géosciences - Sciences de la Terre, Université de Fribourg, Chemin du Musée 6, CH-1700 Fribourg, (jon.mosar@unifr.ch)*

² *Center for Hydrogeology and Geothermics, University of Neuchâtel, Rue Emile-Argand 11, CH -2000 Neuchâtel*

The comprehension of the distance to failure (criticality) of the faults in the Alpine foreland is of strategic importance for the development of geothermal resources in Switzerland. Fault maturity consists of several processes leading to a complex anatomy. In turn, this complex anatomy will have an important impact on the fault properties, behaviour and stability.



Our study is part of a larger joint venture between Swisstopo, the Department of Geosciences of the University of Fribourg and the Center for Hydrogeology and Geothermics of the University of Neuchâtel on Stress State, Fault Criticality and Fluids.

The subproject of Fault anatomy, porosity and pore connectivity: the La Sarraz Fault system combines different laboratory and field techniques to better understand the porosity and permeability associated to fault zones. The objective is to identify and describe deformation in outcrops, in hand samples and in thin sections from the undeformed edges of the fault zones to the highly strained fault core.

The Mormont – La Sarraz fault system located at the transition of the Jura Mountains and Molasse Basin; is an outstanding natural laboratory for this purpose. This NW-SE oriented dextral strike-slip fault system is exposed in the Eclépens quarry and is sinistrally conjugated to the Pontarlier N-S fault system.

At marco-scale we can observe striation fibers along a polished undulating fault plane. Variable sized lenses ranging from centimeter to meter scale are seen inside the fault zone and main fault plane. Lonzenge-shaped locally sigmoid lenses are found to be parallel to foliation and confirm the dextral sense of shear on the main fault. These structural features aid in identifying stress/shear direction and facilitate quantifying the displacement offset along the numerous faults.

Several rock samples were taken from carefully chosen locations in the fault gouge with which we identified the Mormont strike-slip fault to be molded by cataclasis and pressure dissolution.

Evidence of cataclasis is most visible at meso-scale, where the abundance of stylolites, microfractures, displacements, and rotations of rigid particles with no permanent lattice distortion are observed. The majority of stylolites and microfractures are NE-SW orientated which are oblique to the WNW-ESE oriented main fault plane. Interconnecting network of stylolites is abundant in the oolitic limestone and reflects an increase in porosity from the fault edge to the core fault zone.

It can be shown in ooid-rich samples (Urgonian formation) that pressure solution is a major process. Calcite crystals reveal double twinning (twinning inside twinning) indicating intracrystalline deformation mechanisms. Calcite veins with variable quantities of pyrite transect the rock samples at all scales indicating the presence of sulphur-rich fluid circulation in the quarry.

P 1.18

Influence of grain size evolution on the self-consistent generation of LLSVPs from primordial material and subducted MORB

Jana Schierjott¹, Antoine Rozel¹ & Paul Tackley¹

¹ *Institute of Geophysics, ETH Zurich, Sonneggstrasse 5, CH- 8092 Zurich (jana.schierjott@erdw.ethz.ch)*

Seismic studies show two antipodal regions of low shear velocity at the core-mantle boundary (CMB), one beneath the Pacific and one beneath Africa. These regions, called Large Low Shear Velocity Provinces (LLSVPs), are thought to be chemically distinct and thus have a different density and viscosity. Whereas there is a general consensus about the density of the LLSVPs the viscosity is still debated.

So far, in numerical studies the viscosity is treated as either depth- and/or temperature-dependent but the potential grain size- dependence of the viscosity is neglected most of the time. In this study we use a self-consistent convection model which includes a grain size- dependent rheology based on the approach by Rozel et al. (2011) and Rozel (2012). For our set of numerical simulations we include the phase transition from perovskite to post-perovskite whose influence on the stability of primordial reservoirs was investigated by Li et al. (2014). Further, we consider both a primordial layer and a time-dependent basalt production at the surface to dynamically form the present-day chemical heterogeneities, similar to earlier studies, e.g by Nakagawa & Tackley (2014).

We test the influence of density and viscosity of both, subducted MORB and the primordial layer, on the morphology of the LLSVPs. Also, we are able to show some of their characteristics such as the effective viscosity, average grain size, overall rheology (diffusion or dislocation creep) and the composition. This information will be used for coupling our geodynamic modelling with seismic studies. We also report observations of the competition between intense grain growth close to the CMB due to large core temperature and the presence of the post-perovskite phase transition which tends to diminish grain size.

REFERENCES

- Li, Y., Deschamps, F., Tackley, P. J., 2014: Effects of low-viscosity post-perovskite on the stability and structure of primordial reservoirs in the lower mantle, *Geophys. Res. Lett.*, 41.
- Nakagawa, T. & Tackley, P. J., 2014: Influence of combined primordial layering and recycled MORB on the coupled thermal evolution of Earth's mantle and core, *Geochem. Geophys. Geosyst.*, 15, 619–633.
- Rozel, A., 2012: Impact of grain size on the convection of terrestrial planets, *Geochem. Geophys. Geosyst.*, 13, Q10020.
- Rozel, A., Ricard, Y., Bercovici, D., 2011: A thermodynamically self-consistent damage equation for grain size evolution during dynamic recrystallization, *Geophys. J. Int.*, 184, 719–728.

P 1.19

Impact of grain size reduction on pinch-and-swell formation

Stefan Markus Schmalholz, Thibault Duretz

Institut of Earth Sciences, University of Lausanne, Géopolis, CH-1015 Lausanne (stefan.schmalholz@unil.ch)

Strain localization in the ductile (creep) regime plays an important role during the formation of shear and necking zones across a wide range of geological scales (cm to km), but the mechanisms of ductile strain localization are still debated. One potential mechanism of ductile strain localization is grain size reduction (GSR) and the related viscosity decrease during diffusion creep dominated deformation. Many natural pinch-and-swell structures in calcite veins show a reduction of grain size from the swells towards the pinches. Pinch-and-swell formation is usually considered as the result of localized thinning due to a necking instability which takes place when a competent layer is extended. We investigate here the impact of GSR on necking and pinch-and-swell formation with 1D and 2D numerical simulations.

We consider a combination of grain size sensitive-diffusion and dislocation creep flow laws. To model grain size reduction we use the paleowattmeter equations and also the paleopiezometer equation. In the paleowattmeter the GSR-rate is proportional to the dislocation work rate whereas in the paleopiezometer the grain size is inversely proportional to stress.

Simulations are performed for calcite flow laws, an ambient temperature of 350 °C and bulk extension rates between 10^{-12} and 10^{-14} s⁻¹. For dislocation creep both a standard flow law and a flow law with a grain size sensitive Peierls stress are applied. The numerical simulations show GSR from the swells towards the pinches in broad agreement with natural observations. For the paleowattmeter, the equilibrium grain size is achieved after the first few percent of extension. However, GSR does not significantly amplify the necking instability such that results with GSR and with a constant grain size are similar. The results hence suggest that GSR has a minor-to-moderate impact on pinch-and-swell formation and on localized thinning related to necking.

Numerical implementation of grain size sensitive flow laws described by the paleowattmeter causes considerable nonlinearities in the governing equations. The impact of various numerical iteration schemes (e.g. global iterations, local iterations, non-linear tolerance) on the results are discussed.

P 1.20

Triassic thickness compared to topography of the Swiss-French Alpine Foreland (Jura and Molasse Basin)

Marc Schori¹, Anna Sommaruga¹, Jon Mosar¹

¹ *Department of Geosciences, Earth Sciences, University of Fribourg, Chemin du Musée 6, CH-1700 Fribourg, Switzerland (marc.schori@unifr.ch)*

We used existing thickness contour maps and models from various authors, cross checked them with available drill core logs and compiled them into a homogenized model of the European Alpine Foreland (Jura and Molasse Basin) that extends across Switzerland, France, Germany and Austria. A new set of thickness maps for the three classical Triassic units is presented: Keuper, Muschelkalk and Buntsandstein.

The Buntsandstein unit with a mean thickness of 48 m shows a deposition center situated at the western front of the Jura Mountains with a maximum depth of about 270 m. It is linked to a half graben related to the Bresse Graben. To the north the thickness increases generally (Germanic Basin) and another depocenter with a max. thickness up to 250 m is visible in the Rhine Graben close to Freiburg (D) and Colmar (F). In the Molasse Basin, the Buntsandstein unit disappears roughly 30 km south of the Jura Mountains.

The Muschelkalk unit shows a depositional thickness of 100 – 200 m (mean thickness 129 m). Thickness occurrences of more than 200 m are seen to be due to tectonic processes rather than depocenters. The Muschelkalk unit is thickest (more than 700 m) in a narrow region just north of Zurich in the Eastern Jura Mountains. A larger region of plainly increased thickness is seen in the Molasse Basin west of Bern and in the central Jura west of Lake Neuchâtel.

The Keuper unit with a mean thickness of 179 m increases drastically in thickness at the northwest of Lausanne, with a maximum thickness of more than 950 m (SW of Yverdon). A second region of increased thickness due to tectonic processes is above the Buntsandstein unit depocenter situated at the western front of the Jura Fold and Thrust belt. Wells in the Jura Mountains display that the Keuper unit is repeated several times due to thrusts.

The depositional thickness across Europe was roughly between 150 – 200 m. We relate thicknesses more than 250 m to tectonic processes.

In total, it is seen that the Triassic sequence is thickest at the center of the Jura Mountains and a second thickness increase is seen at the front of the Western Jura. The Triassic sequence experienced tectonic thickening especially in the area of the Jura Mountains whereas large parts of Europe show Triassic thickness changes due to deposition.

The décollement zone of the Jura FTB and the Molasse Basin is located in the Triassic units and two main décollement horizons can be discriminated: the Muschelkalk unit and the overlying Keuper unit. The Muschelkalk layers act as main décollement zone in the East, whereas the Keuper layers in the West (Sommaruga et al. submitted).

REFERENCES

Sommaruga, A., Schori M., Gruber M. & Mosar J. (submitted): The role of the Triassic evaporites underneath the North Alpine foreland. In J.I. Soto, J.F. Flinch & G.C. Tari (Eds.): *Permo-Triassic Salt Provinces of Europe, North Africa, and Central Atlantic: Tectonics and Hydrocarbon Potential*. Elsevier.

P 1.21

3D numerical modeling with application to the Helvetic nappe system: Transition of viscous overthrusting to folding and oblique basal overthrusting

Richard Spitz¹, Stefan M. Schmalholz¹ & Boris Kaus²

¹ *Institute of Earth Sciences, University of Lausanne, Bâtiment Géopolis, CH-1015 Lausanne (richard.spitz@unil.ch)*

² *Institute of Geosciences, Johannes Gutenberg University Mainz, J.-J.-Becher-Weg 21, D-55128 Mainz*

The Helvetic nappe system in Switzerland is generally described as fold and thrust belt. While the overall geology has been studied in detail, the tectonic development and mechanical interconnection between overthrusting and folding is still not fully understood. One important clue comes from the mechanical stratigraphy (Pfiffner, 1993) and the corresponding lateral transition from overthrusting to folding, which is characteristic for the Helvetic nappe system. In addition the Morcles and Doldenhorn nappes, two prominent fold nappes, feature a divergent plunging of their respective fold axes. The plunging orientation can be linked to the Rawil depression located between the two nappes. Several different explanations for the evolution of the Rawil depression exist. Burkhard (1988) for examples suggests oblique overthrusting in the basement to facilitate the Rawil depression.

We employ a three-dimensional numerical model with linear and non-linear viscous rheology to (I) investigate the control of the lateral variation in the thickness of a weak detachment horizon on the transition from folding to overthrusting during bulk shortening and (II) the impact of an oblique ramp on overthrusting to generate a depression. All simulations are conducted with LaMEM (Fernandez & Kaus, 2014), a three-dimensional parallel staggered-grid finite difference code, which allows for coupled nonlinear thermomechanical modeling of lithospheric deformation with visco-elasto-plastic rheology.

For (I) our model configuration is based on published work based on 2D numerical simulations (Jaquet et al., 2014). The configuration consists of a stiff

viscous layer, with a pre-existing weak zone, resting within a weaker viscous matrix. The reference viscosity ratio μ_L/μ_M (for the same strain rate) between the layer and matrix ranges from 10 to 200. The simulations were run with several distinct initial geometries by altering laterally the thickness of the detachment horizon below the stiff layer. For (II) the configuration is based on a model by Burkhard (1988) and consists of a rigid viscous thrust sheet embedded within a weaker viscous matrix. The sheet is thrust over a parallel ramp complex, which contains an oblique ramp in the middle of the structure. We investigate the effect of the oblique ramp by varying the angle and width across different simulations.

First results of the simulations show:

(I) The importance of mechanical stratigraphy in the lateral transition between overthrusting and folding. An increase of detachment horizon thickness in relation to the layer thickness shifts the deformation regime from overthrusting to folding. (II) The connection between angle and width of an oblique ramp in the formation of depressions. Ramps with low obliqueness ($\sim 30^\circ$) produce no significant depressions. Stronger obliqueness for the same ramp width creates a larger offset between the two frontal parts of the thrust sheet, which is reflected in depressions concordant to the oblique ramp.

REFERENCES

- Burkhard, M. 1988: L'Helvétique de la bordure occidentale du massif de l'Aar (évolution tectonique et métamorphique). *Eclogae Geol. Helv.*, 81(1), 63– 114.
- Fernandez, N., & Kaus B. J. P. 2014, Fold interaction and wavelength selection in 3D models of multilayer detachment folding, *Tectonophysics*, 632, 199–217.
- Jaquet, Y., Bauville, A., & Schmalholz, S. M. 2014: Viscous overthrusting versus folding: 2-D quantitative modeling and its application to the Helvetic and Jura fold and thrust belts. *Journal of Structural Geology*, 62, 25-37.
- Pfiffner, O. A. 1993. The structure of the Helvetic nappes and its relation to the mechanical stratigraphy. *Journal of structural Geology*, 15(3-5), 511-521.

P 1.22

Late Cenozoic acceleration of erosion in the Southern Central Andes revealed by low-temperature thermochronology

Nadja F. Stalder¹, Frédéric Herman¹, Peter W. Reiners², German Aguilar³

¹ *Institute of Earth Surface Dynamics, University of Lausanne, 1015 Lausanne, Switzerland*

² *Department of Geosciences, University of Arizona, 85271 Tucson, USA*

³ *Advanced Mining Technology Center, Facultad de Ciencias Físicas y Matemáticas, Universidad de Chile, Santiago, Chile*

The Earth's topography results from feedback mechanism between tectonics, climate, and surface processes. To understand the influence of such interactions on mountain building processes, one can quantify the temporal and spatial history of exhumation. The Andes are a suitable natural laboratory to study these feedbacks, because they result from the steady subduction of the Nazca plate below the South American plate and their meridional extent crosses several global climate zones. Furthermore, the recent growth of regional low-temperature thermochronological studies led to an extensive data coverage, which can now be inverted to estimate the exhumation history at the scale of a mountain range. In this study, we present 50 new apatite (U-Th)/He bedrock ages filling remaining data gaps between 26°S and 34°S latitude. Intrusion ages decrease from Cretaceous in the North to Miocene in the South. From about 31°S to 34°S, the study area covers a key transitional zone where topography decreases, the subduction zone changes from flat to steep dip angle, and precipitation increases. The data acquired north of 33°S include 28 valley bottom samples and 3 elevation profiles, the southern samples represent 2 elevation profiles with 4 samples each. Ages are highly variable to the north of 33°S with average ages from 4 to 52 Ma, but only two of them (at ~32°S) are < 9.5 Ma. In contrast, the southern elevation profiles reveal average ages from 0.5 to 3.5 Ma. This observed decrease in ages over about 300 km suggests intensified erosion south of 33°S latitude during the Plio-Pleistocene. The transition occurs more than 150 km to the south of the tectonic change in the subduction regime. However, the establishment of the modern atmospheric circulation pattern in the late Pliocene led to increased moisture transport to the North. Higher precipitation in the area south of 33°S latitude could thus explain the intensified erosion in the Plio-Pleistocene. Coinciding with decreasing topography and a narrowing of the Andean mountain belt, these preliminary results may indicate a climatic control on exhumation, and potentially tectonics, in the Southern Central Andes.

P 1.23

Scaling of Mixing Rate in Mantle Convection Models: Influence of Plate Tectonics, Melting and Crustal Production

Paul J. Tackley¹

¹ *Institut für Geophysik, Departement Erdwissenschaften, ETH Zürich, CH-8092 (ptackley@ethz.ch)*

It is generally thought that the early Earth's mantle was hotter than today, which using conventional convective scalings should have led to vigorous convection and mixing. Geochemical observations, however, suggest that mixing was not as rapid as would be expected, leading to the suggestion that early Earth had stagnant lid convection [Debaille et al., 2003]. Additionally, the mantle's thermal evolution is difficult to explain using conventional scalings because early heat loss would have been too rapid, which has led to the hypothesis that plate tectonics convection does not follow the conventional convective scalings [Korenaga, 2003]. One physical process that could be important in this context is partial melting leading to crustal production, which has been shown to have the major effects of buffering mantle temperature and carrying a significant fraction of the heat from hot mantle [Nakagawa & Tackley, 2012], making plate tectonics easier [Lourenco et al., 2016], and causing compositional differentiation of the mantle that can buffer core heat loss [Nakagawa & Tackley, 2010]. Here, the influence of this process on mantle mixing is examined, using secular thermo-chemical models that simulate Earth's evolution over 4.5 billion years. Mixing is quantified both in terms of how rapidly stretching occurs, and in terms of dispersion: how rapidly initially close heterogeneities are dispersed horizontally and vertically through the mantle. These measures are quantified as a function of time through Earth's evolution. The results will then be related to geochemically-inferred mixing rates for different stages of Earth evolution.

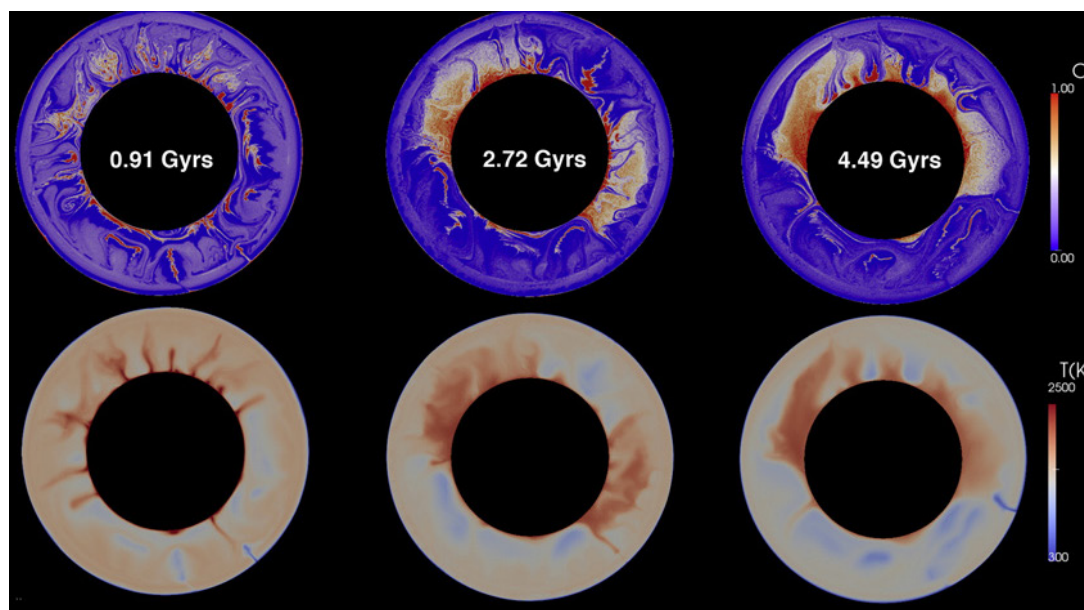


Figure 1. Time evolution of mantle composition and temperature in a simulation in Nakagawa and Tackley (2012).

REFERENCES

- V. Debaille V., O'Neill C., Brandon A. D., Haenecour P., Yin Q.-Z., Mattielli N., & Treiman A. H., 2003: Stagnant-lid tectonics in early Earth revealed by ¹⁴²Nd variations in late Archean rocks, *Earth Planet. Sci. Lett.* **373**, 83-92.
- Korenaga J., 2003: Energetics of mantle convection and the fate of fossil heat, *Geophys. Res. Lett.* **30**, 1437.
- Nakagawa T. & Tackley P. J., 2012: Influence of magmatism on mantle cooling, surface heat flow and Urey ratio, *Earth Planet. Sci. Lett.* **329-330**, 1-10.
- Lourenco D., Rozel A. & Tackley P. J., 2016 : Melting and crustal production helps plate tectonics on terrestrial planets, *Earth Planet. Sci. Lett.*, 439, 18-28.
- Nakagawa, T. & Tackley P. J., 2010: Influence of initial CMB temperature and other parameters on the thermal evolution of Earth's core resulting from thermo-chemical spherical mantle convection, *Geophys. Geochem. Geosyst.* **11** (Q06001).

P 1.24

Delamination, upper plate extension, and plate margin complexity

Kosuke Ueda¹, Taras Gerya¹, Sean Willett¹

¹ *Departement Erdwissenschaften, ETH Zürich, Sonneggstrasse 5, CH-8092 Zürich (kosuke.ueda@erdw.ethz.ch)*

Removal of lithospheric mantle at depth may have major consequences for the geodynamic evolution of a plate margin and associated crustal tectonics, but it is difficult to document convincingly. Strong indications can be obtained from topography, magmatic activity (Kay and Kay, 1993), and seismic tomography. A reduction or removal of lithosphere may be achieved by means of coherent delamination or viscous drip-type convective thinning (e.g., Ueda et al., 2012), but can also accompany syn-convergent extension in an approximate back-arc position (Gögüs, 2015). The geometry of many suspected delaminating plate margins exhibits curvature, such as the Aegean subduction system, the Carpathians, or the Western Mediterranean. In order to better evaluate the viability of delamination as potential mechanism in convergent settings, it is therefore important that self-consistent forward models are improved in terms of expectable observations, and are performed in three-dimensions.

We present geodynamic models of subduction-collision zone evolution to delamination retreat/spreading stages that are produced in three dimensions at high resolution. The thermomechanical models include melting, melt extraction, phase changes (Gerya and Yuen, 2007). They show complex interaction and geometric entanglement, between upper mantle, lithosphere, and partially molten rocks over hundreds of kilometers across the plate contact. Long-term foundering of lithospheric mantle changes from a wholesale, retreating “peeling” delamination to slower convective removal. Models in which the passive margin geometry of the lower plate is varied, exhibit consistent and inherited differences in dynamic evolution. Where promontories exist along the margin, they tend to localize three stages of evolution: 1) a magmatic arc; 2) a lower plate, exhumation-like exhumation of buried continental crust in domal patterns of few tens of km wavelength; and subsequently, 3) the formation of extended zones on the upper plate which lack a lithospheric mantle, undergo partial extension, and feature lower crustal melting (Fig. 1a). In contrast, slab break-off is consistently favoured in locations where the lower plate margin is relatively recessed. In all models, predicted plateau elevations reach up to 3 km and overlay regions of extended partial melting.

The numerical experiments suggest also that the resulting lithosphere-asthenosphere-boundary (LAB) has a complex geometry, with elongated anomalies at scales of few tens to hundred kilometers (Fig. 1b). If a region like this was imaged by means of seismic tomography, the anomaly pattern would likely be also complex. A simple estimate is obtained by calculating seismic velocities from a thermodynamic tabulation according to composition, temperature, and pressure, and then coarsening these fields to more appropriate imaging cell sizes of ca. 20 km (Fig. 1c). While these estimates can be expected to differ greatly from proper propagation with variable coverage, they show complex anomaly patterns larger than imaging voxels, which would sufficiently elude smearing.

Overall, results indicate that transitions and co-evolution between delamination, convective thinning, and upper-plate extension are gradual and these modes are not mutually exclusive. This is likely reflected in observations. Mixed-mode removal and extension is similar to the Aegean, where both upper plate extension, and drastic, albeit not complete reduction of the lithospheric mantle have been reported. If the curved Apenninic system converged passive margins with originally variable geometries, predictions from our model would be in good agreement with incipient necking of the slab below central Calabria and its surface expressions (Faccena et al., 2014).

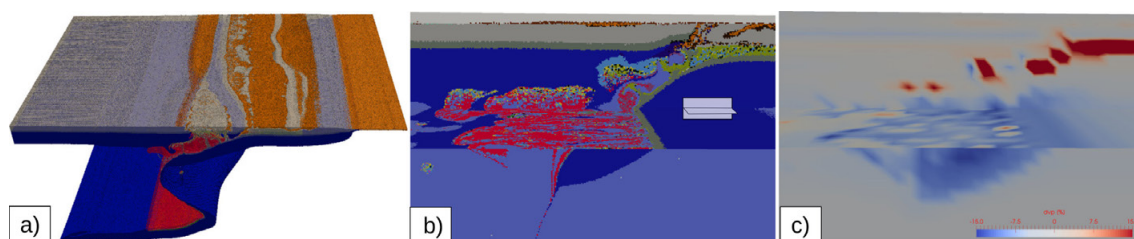


Figure 1. Three-dimensional delamination geometry. a) Upper plate thinning and magmatic plateau where initial lower plate margin was protruding. Slab in the back has already started to detach. b) Detail of margin complexity at depth, and c) simple estimate of p -velocity anomaly from regrided composition, temperature, and pressure from b), assuming infinitely good coverage.

REFERENCES

- Faccena, C., Becker, T.W., Miller, M.S., Serpelloni, E., & Willett, S.D., 2014: Isostasy, dynamic topography, and the elevation of the Apennines of Italy. *Earth and Planetary Science Letters*, 407, 163-174.
- Gerya, T.V., & Yuen, D., 2007: Robust characteristics method for modelling multiphase visco-elasto-plastic thermo-mechanical problems. *Physics of the Earth and Planetary Interiors*, 163, 83-105.
- Gögüs, O., 2015: Rifting and Subsidence following lithospheric removal in continental back-arcs. *Geology*, 43, 3-6.
- Kay, R.W., & Kay, S.M., 1993: Delamination and delamination magmatism. *Tectonophysics*, 219, 177-189.
- Ueda, K., Gerya, T.V., & Burg, J.-P., 2012: . *Journal of Geophysical Research*, 117, B08202, doi:10.1029/2012JB009144.

P 1.25

Exfoliation fracture geometry as a new tool to infer principal stress ratios ?

Michael Rickenbacher¹, Martin Ziegler¹

¹ *Department of Earth Sciences, ETH Zurich, Sonneggstrasse 5, CH-8092 Zurich
(rmichael@student.ethz.ch; martin.ziegler@erdw.ethz.ch)*

Exfoliation fractures, also known as sheeting joints, are restricted to shallow rock masses as deep as about 200 m below the bedrock surface. In the last years these fractures were investigated in great detail in the granites and gneisses along the upper Aar valley, south of Guttannen (Grimsel region, Switzerland). The focus was on fracture occurrence, timing of fracture formation (multiple exfoliation fracture generations were found), and on fracture mechanics (Ziegler et al., 2013, 2014). Ziegler et al. (2016) found that numerical models simulating gravitational (topographic) and far-field compressive stresses yield maximum principal stress orientations within the shallow bedrock of the inner U-shaped valleys of the Grimsel region, which are similar to those inferred from exfoliation joint fractographic markings (i.e., the orientation of the fracture plumose axis can be used as proxy for the maximum compressive principal stress, σ_1). Owing to the widespread occurrence of exfoliation fractures and their geologically recent (Pleistocene) ages, we gained new insights into stress patterns in morphologically complex Alpine valleys. Yet, the magnitudes and the ratios of principal stresses within shallow bedrock are not well understood.

The shape of an exfoliation fracture is an expression of the isotropy or anisotropy of the principal stresses (i.e., ratio of the maximum and intermediate principal stress, σ_1/σ_2 ; σ_3 is oriented perpendicular to the fracture plane) and the rock's fracture toughness. Thus, an interpretation of the geometry of Pleistocene exfoliation fractures could be used to constrain the today's principal stress ratios of near-surface bedrock. During summer 2016 we collected a first set of geometric data of five well-exposed exfoliation fractures at two locations (at Kunzentennlen and east of Lake Grimsel) using 3D photogrammetric models obtained from aerial images taken with a UAV (Unmanned Aerial Vehicle) (Rickenbacher, 2016; Figure 1A). Our main interest was to measure the shapes of the fractures. Since many of the previously identified exfoliation fractures formed in a stepwise stable manner, with fracture increments separated by mostly elliptical or parabolic fracture arrest marks, we were able to study the geometric evolution of selected exfoliation joints.

In order to extract fracture geometrical information we fitted ellipses to the approximately elliptical exfoliation fracture arrest marks in our 3D models (Figure 1B). In parts, where no arrest marks were seen, we used plumose striations on the fracture planes, which are oriented perpendicular to the fracture tip and the arrest marks (e.g., Pollard and Aydin, 1988; Ziegler et al., 2014). Then, we calculated the ratios of 33 obtained ellipse axes. This axes ratio is defined as the ratio between the lengths of the longer to the shorter ellipse axes. The mean axes ratio is 2.1 and the majority of ratios (73%) ranges between 1.5 and 2.5 (Figure 1C). Such ratios are very similar to the numerical model results of near-surface stress conditions at the two sites by Ziegler et al. (2016; Figure 1D). Thus, our preliminary result suggests that the axes ratio of exfoliation fracture surfaces could be used as a tool to infer σ_1/σ_2 . Future work will focus on more field data and 3D fracture numerical modelling.

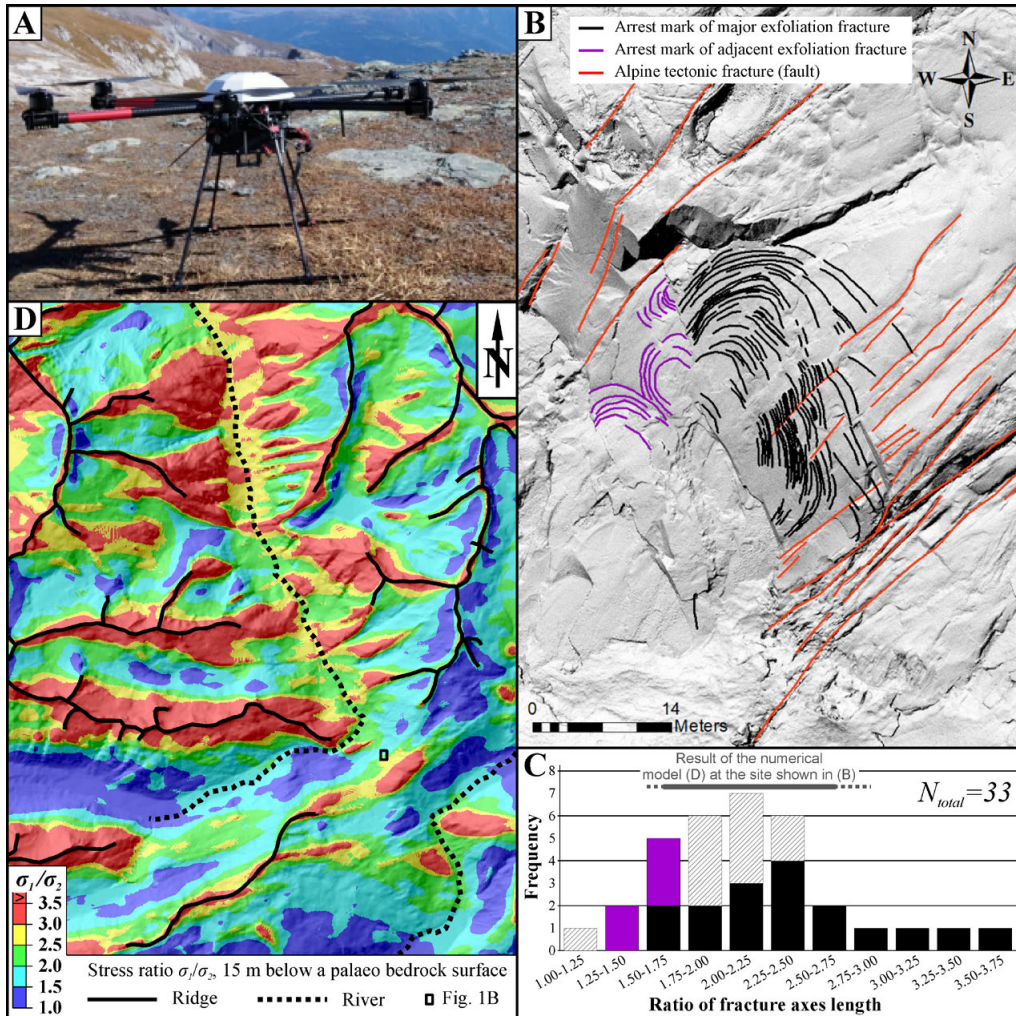


Figure 1. A) Photo of the used UAV (XR6, Airborne Robotics), B) Digital surface model and identified exfoliation fracture arrest marks, C) Histogram of fracture axes ratios (data shown in B is black or purple), D) Principal stress ratio (σ_1/σ_2) results from elastic finite difference modelling by Ziegler et al. (2016:Fig. 7M).

REFERENCES

- Pollard, D.D. & Aydin, A. 1988: Progress in understanding jointing over the past century, *GSA Bulletin*, 100, 1181–1204.
- Rickenbacher, M. 2016: 3D-Analysis of hydraulic and mechanic fracture propagation, B.Sc. Thesis, Department of Earth Science, ETH Zurich, 41 pp.
- Ziegler, M., Amann, F. & Loew, S. 2016: Near-surface patterns of rock stress orientations in morphologically complex Alpine valleys – The Grimsel region of Switzerland as a case study, *Rock Mech. Rock Eng.*, 85, 129–151.
- Ziegler, M., Loew, S. & Bahat, D. 2014: Growth of exfoliation joints and near-surface stress orientations inferred from fractographic markings observed in the upper Aar valley (Swiss Alps), *Tectonophysics*, 626, 1–20.
- Ziegler, M., Loew, S. & Moore, J.R. 2013: Distribution and inferred age of exfoliation joints in the Aar Granite of the central Swiss Alps and relationship to Quaternary landscape evolution, *Geomorphology*, 201, 344–362.

P 1.26

4D analogue modeling of scissor tectonics

Frank Zwaan¹, Guido Schreurs¹,

¹ *Institut für Geologie, Universität Bern, Baltzerstrasse 1 + 3, CH- 3012 Bern, Schweiz (frank.zwaan@geo.unibe.ch)*

Introduction

Although tectonic modelers generally apply constant deformation velocities throughout their models, natural settings can involve along-strike velocity variations. In extensional regimes (e.g. the North Atlantic), we often observe the propagation and associated “scissor-like” opening of a rift, as older rift parts are further evolved than the rift tip. In some cases, this extension can result in compression on the other side of the rotation axis to complete a full scissor tectonic system (e.g. Pyrenees).

Methods

To model scissor tectonics, we apply a foam base that allows distributed deformation at the base of overlying brittle-ductile model material: quartz sand sieved upon a layer of a viscous PDMS/sand mixture (Fig. 1a). Both layers are 4 cm thick (1 cm = 5 km in nature), representing upper and lower crust respectively. Rotation of the model sidewalls around a rotation point induces extension at one side of the model and compression at the other side (Fig. 1b). Seeds of ductile material (diameter ca. 1 cm) on top of the basal model layer control where faulting occurs in the overlying brittle sand (Fig. 1c). The sidewall tips move apart with 4 mm/h during 7.5 h. These 30 mm of extension translate to 30 km of extension at a natural strain rate. X-Ray computer tomography allows 3D analysis of the internal structural evolution (hence 4D).

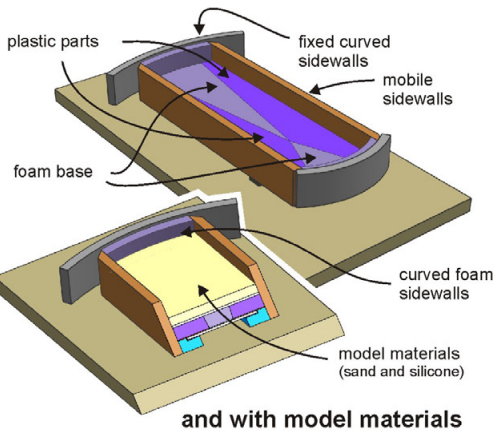
Results

Top views show that our model produces rifting in the extensional domain, no visible deformation near the scissor axis and thrusting in the compressional domain (Fig. 1c). These structures are also well visible on a horizontal section through the brittle sand layer (Fig. 1d). It also shows the development of a second thrust as part of a pop-up structure that is evident on vertical CT-sections (Fig. 1e, panel I). The vertical CT-sections also show no deformation near the scissor axis (Fig. 1e, panel II). In the extension domain, rift structures occur (Fig. 1e, panel III). The rift becomes more developed farther away from the scissor axis, as total extension increased and rift-internal faulting occurs. Towards the model edge, we observe a 36 mm wide and 8 mm deep basin, horst structures, and a strongly deformed seed (Fig. 1e, panels IV-VI). Some boundary effects are present in the shape of faulting along the sidewalls.

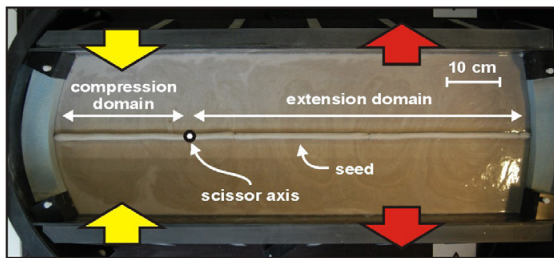
Outlook

These initial model results show the functionality of our model set-up. Future modeling will involve syn-rift sedimentation, various weak zone geometries and the testing of another possible set-up with rigid base plates that our new machine allows. Both 3D surface scanning and particle-tracing analysis will be used for surface evolution mapping and to quantify surface and internal model deformation.

a) 3D set-up sketch (without model materials)



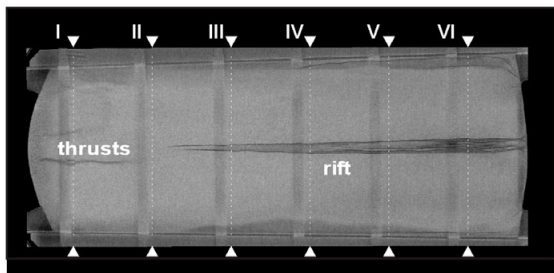
b) Seed geometry (without sand cover)



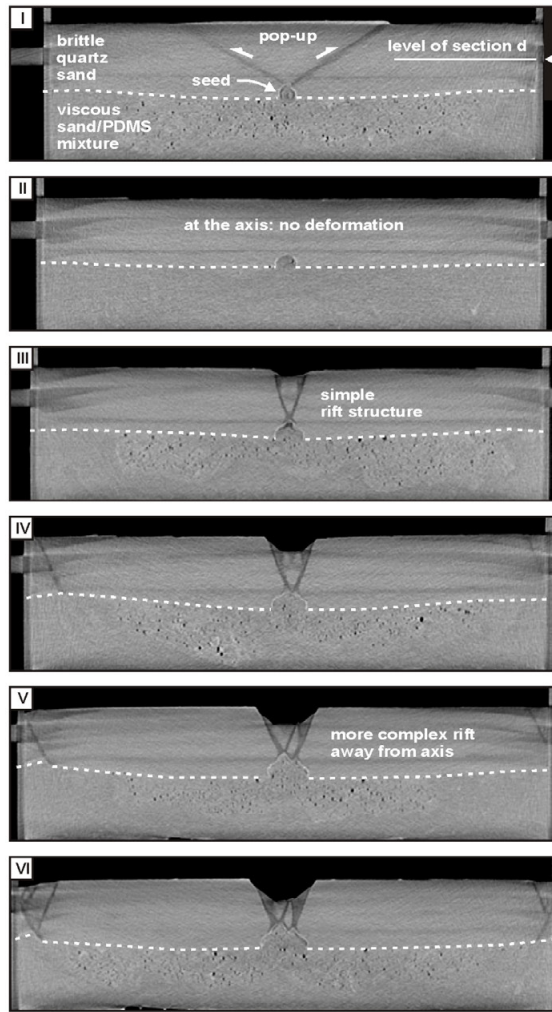
c) Model final top view



d) horizontal CT-section (section level shown in e, panel I)



e) horizontal CT-sections



f) 3D final topography (CT-derived)

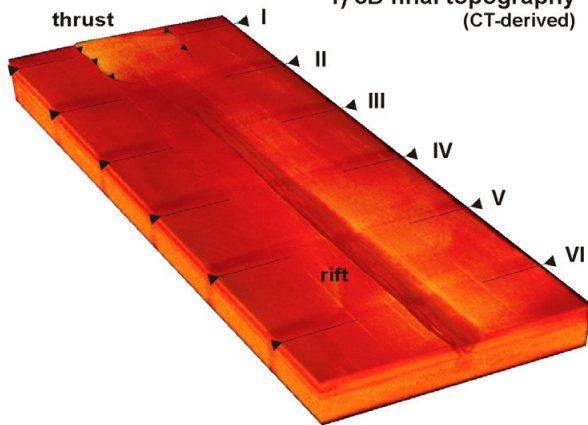


Figure 1. (a) 3D model set-up sketch. (b) Top view showing seed geometry without sand cover. (c) Final top view, showing surface structures at the end of the model run. (d) Horizontal CT-section through the sand layer, showing structures at ca. 2 cm depth (see Fig. 1e). Vertical stripes are CT-artifacts. (e) Vertical CT-sections showing internal model structures. Section locations are depicted on Figs. 1d and f. (f) CT-derived 3D topography at the end of the model run.

2. Mineralogy, Petrology, Geochemistry

Sébastien Pilet, Bernard Grobéty, Eric Reusser

Swiss Society of Mineralogy and Petrology (SSMP)

TALKS:

- 2.1 Bégue F., Baumgartner L., Bouvier A.-S., Putlitz B., Vennemann T.: Stable isotope exchange and reactive fluid-flow around hydrothermal veins
- 2.2 Bouvier A.-S., Manzini M., Métrich N., Baumgartner L.P.: Deciphering the different sources of Cl input into the mantle beneath St. Vincent (Lesser Antilles Arc): insight from B, O and Cl isotopes
- 2.3 Brett A., Diamond L.W.: Porosity and permeability evolution during epidosite alteration of the oceanic crust, Semail ophiolite, Oman
- 2.4 El Korh A., Luais B., Deloule E., Cividini D.: Iron stable isotope fractionation during subduction of basic rocks
- 2.5 Ewing T.A., Müntener O., Schaltegger U.: The mantle source of the early stages of island arc magmatism: evidence from Hf isotopes in rutile from the Kohistan complex
- 2.6 Hartung E., Caricchi L., Roggero D., Floess D., Wallis S., Harayama S.: The plutonic-volcanic connection: Insights from central Japan
- 2.7 Hovakimyan S., Moritz R., Tayan R., Melkonyan R., Harutyunyan M.: Regional strike-slip tectonics and porphyry Cu-Mo and epithermal ore deposit formation during Cenozoic subduction to post-collisional evolution of the southernmost Lesser Caucasus, Tethyan belt
- 2.8 Kong X.-Z., Saar M.O.: Implications of hydrothermal flow-through experiments on deep geothermal energy utilization
- 2.9 Leuthold J., Lissenberg J., Falloon T., Ulmer P., O'Driscoll B., Klimentyeva D.: Partial melting of the mafic lower oceanic crust
- 2.10 Maltese A., Mezger K., Pandey O.P., Upadhyay D.: Zircon U-Pb ages from the Bastar Craton, central India: A Paleoproterozoic patchwork terrane.
- 2.11 McCarthy A., Othmar M.: Decompression-driven crystallization of superheated melts: The formation of orbicules and comb layers in shallow subvolcanic conduits (Fisher Lake, USA)
- 2.12 Pape J., Mezger K., Bouvier A.-S., Baumgartner L.: Analytical method development of high precision Mg isotope measurements by SIMS for in-situ ^{26}Al - ^{26}Mg mineral isochron dating of chondrites
- 2.13 Popkhadze N., Moritz R., Kekelia S.: Evolution of Volcanism at the Late Cretaceous Madneuli Copper gold-polymetallic deposit, Lesser Caucasus, Georgia
- 2.14 Richter L., Gutzmer J., Atanasova P., Banks D.: Xenotime formation in a low-temperature hydrothermal environment, Browns Range, WA
- 2.15 Schenker F.L., Ambrosi C., Scapozza C., Maino M., Castelletti C., Antognini M. & Gouffon Y.: The core of the Lepontine dome: new geological, structural, metamorphic and geochronological data (sheet Osogna, no. 1293,1:25'000)
- 2.16 Siron G., Baumgartner L., Bouvier A.-S., Vennemann T.: Control of water activity on the hydroxyl content of biotite

- 2.17 Tedeschi M., Lanari P., Rubatto D., Hermann J., Pedrosa-Soares A., Dussin I., Pinheiro M.A.P.: Reconstruction of high-pressure metamorphic conditions from symplectites: insights from Pouso Alegre mafic rocks (Brasília Belt, Brazil)
- 2.18 Tollan P.M.E., O'Neill H.St.C.: The role of trace and major element chemistry in controlling the solubility of water in upper mantle olivine
- 2.19 Zanoni G., Šegvić B., Moscariello A.: Clay mineral diagenesis in Cretaceous Dentale and Gamba clastic reservoirs from the South Gabon Basin (West African passive margin) – new insights on the regional geology and basin evolution history

POSTERS:

- P 2.1 Edwards M., Pioli L., Andronico D., Cristaldi A., Scollo S.: Characterising the May 2016 eruption of Mt Etna, Italy
- P 2.2 Scignari M., Pioli L., Andronico D., Caricchi L.: Driving Mechanisms of 1651-53 and 2002 Eruptions at Etna Volcano (Italy)
- P 2.3 Demers-Roberge A., Kaczmarek M.-A., Pilet S., Roggero D., Müntener O.: Peridotite xenoliths from Sierra Baguales: Insights into melting and refertilization processes into the mantle wedge
- P 2.4 Roggero D., Müntener O., Pilet S.: Neogene back-arc basaltic magmatism in the Sierra Baguales (southern Patagonia): are there alternatives to teared slabs and slab window models ?
- P 2.5 Curry A., Caricchi L., Lipman P.: Determining the physical processes behind four large eruptions in rapid sequence
- P 2.6 Nformidah-Ndah S.S., Kaba M., Tene Djoukam J.F., Borba de Carvalho B.M., Kovacs I., Kirali E., Tchouankoue J.P., Hermann J.: Petrography and mineral chemistry of mantle xenoliths from maars in Cameroon: implications for the nature of the mantle and CO₂ concentrations below the Cameroon Volcanic Line
- P 2.7 Kaufmann A., Pettke T., Baumgartner L.: The magmatic-hydrothermal transition at the Torres del Paine igneous complex, Chile – first results of an on-going fluid/melt inclusion study
- P 2.8 Lechmann A.K., Burg J.-P., Ulmer, P., Guillong, M., Faridi M.: Middle Miocene to Quaternary volcanism in NW Iranian Azerbaijan: implications for the evolution of the Turkish-Iranian Plateau from geochemical, isotopic and geochronological data
- P 2.9 Pandey O.P., Mezger K., Upadhyay D., Singh A.K., Maltese A.: Mafic dyke swarms in global geodynamics: Examples from Singhbhum and Bastar cratons, India
- P 2.10 Probst L., Pioli L., Bali E., Simpson G., Caricchi L.: Temporal variations of mineral chemistry during the 2014-2015 Holuhraun-Bárðarbunga eruption
- P 2.11 Seitz S., Putlitz B., Baumgartner L., Bouvier A.-S.: The role of crustal melting in the formation of rhyolites: constraints from SIMS oxygen isotope data (Chon Aike Province, Patagonia)
- P 2.12 Belgrano T.M., Diamond L.W., Vogt Y., Gilgen S.A., Brett A., Al-Tobi K.: A new volcanic map of the Semail Ophiolite, Oman using a combined field, geochemical and aeromagnetic approach
- P 2.13 Bonta, M., Serneels, V.: Historical Iron smelting in Kaniasso, Ivory Coast: technological change and exchange at Siola and Doumbala
- P 2.14 Chalal Y., Lerari N.: ElBema-East Taourirt granite (Hoggar central-Algeria) : RMG or not RMG
- P 2.15 Pujol Solà N., Chairadia M., Aiuppa A., Paonita A., Rizzo A.: Metal geochemistry and Cu-Zn isotope compositions of volcanic gas condensates and volcanic rocks: Vulcano Island, Italy

- P 2.16 Jollands M.C., Ulyanov A., Müntener O.: Protocol for Be analysis by LA-ICP-MS and Be distribution in some olivine- and pyroxene-bearing rocks
- P 2.17 Farré de Pablo J., Chiaradia M., Rizzo A., Landi P.: Geochemistry and Cu, Zn isotope composition of volcanic rocks in Stromboli Island, Italy
- P 2.18 Weber G., Probst L., Schaltegger U., Arce J.L., Caricchi L.: Construction, architecture and evolution of the plumbing system of Nevado de Toluca volcano (Mexico)
- P 2.19 Mirza A., Ilbeyli N.: Field, Mineralogical and Petrographical Characteristics of the Ladakh Batholith in NW India
- P 2.20 Shengelia D., Tsutsunava T., Chichinadze G., Beridze G., Vardanashvili K., Javakhishvili I.: Petrogenetic and geodynamic types of Late Paleozoic (Sudetic) granitoids of the Caucasus
- P 2.21 Frøystein M., Heinrich C.: Relative timing and characterization of Au-associated veins in the Gotthard Massif, Graubünden, Switzerland
- P 2.22 Fisch M., Eggenberger U., Kündig R.: Inventory of Swiss gravel wash mud
- P 2.23 Schlatter D.M., Schläglöva K., Hughes J.: Comparisons of Paleoproterozoic orogenic gold deposits/occurrences of Nalunaq and Vagar in South Greenland and Svartliden in Northern Sweden
- P 2.24 Huseynova A.: Correlation of reservoir properties of productive series and the red series within Absheron-Pribalkhan threshold
- P 2.25 Ivanić M., Škapin S.D., Vdović N., Mikac N. & Sondi I.: Size Dependent Physico-Chemical and Geochemical Characteristics of Two Distinct Carbonate-Rich Marine Sediments (Adriatic Sea)
- P 2.26 Kempf E., Hermann J., Reusser E.: Monitoring dehydration reactions in subducted serpentinites by metamorphic olivine formation in the Zermatt-Saas Ophiolites
- P 2.27 Lafay R., Baumgartner L.P.: Textural characterization of forsterite + talc assemblage resulting from antigorite breakdown in the bergell contact aureole (Italy)
- P 2.28 Ricchi E., Gnos E., Bergemann C.: Crystallization ages of Alpine cleft monazite; correlation with exhumation history and shear zone activity
- P 2.29 Oliveras M., Kouzmanov K., Schläglöva K., De los Santos M.: Composition, origin and time evolution of ore-forming fluids and trace element geochemistry of enargite in the Lepanto epithermal high-sulfidation deposit (Philippines)
- P 2.30 Perroud P., Schmidt S.Th., Süssenberger A.: OPTiCMin©: a new electronic teaching tool for optical mineral identification
- P 2.31 Peters, D., Pettke, T.: Evaluation of major to ultra trace element bulk rock chemical analysis of nanoparticulate pressed powder pellets by LA-ICP-MS
- P 2.32 Ordóñez L., Ariztegui D., Chiaradia M., Vogel H., Morlock M., Melles M., Russell J.M., Bijaksana S., & the TDP scientific team: Fe isotopes as indicators of bio-geochemical cycling in Lake Towuti (Indonesia)
- P 2.33 DuPasquier A., Grolimund D., Pena J., Verrecchia E.P.: Manganese oxides in travertines from Skoura (Morocco): geochemical or biological deposits?

2.1

Stable isotope exchange and reactive fluid-flow around hydrothermal veins

Florence Bégué¹, Lukas Baumgartner¹, Anne-Sophie Bouvier¹, Benita Putlitz¹ & Torsten Vennemann²

¹ *Institute of Earth Sciences, University of Lausanne, Géopolis, 1015 Lausanne*
(florence.begue@unil.ch)

² *Institute of Earth Surface Dynamics, University of Lausanne, Géopolis, 1015 Lausanne*

Stable isotopes have proven to be an efficient tool in tracing fluid-rock interaction. Carbonates in contact aureoles are ideally suited for this kind of study, since significant (>10‰) oxygen isotope variations are present between magmatic fluids and the carbonate host rocks.

Here, we present a detailed petrologic, Secondary Ion Mass Spectrometry (SIMS), and cathodoluminescence (CL) study of reactions driven by infiltration of magmatic fluids in carbonate host-rocks of the Bergell and Adamello intrusions (Central Alps, Italy). We focus on olivine veins, where fluid infiltration occurred along an open crack - now filled with olivine (Ol), calcite (Cc) and retrograde tremolite and talc - forming a central zone. This zone is symmetrically framed by a replacement zone, with Ol+Cc replacing the original dolomite (Do). Traditional stable isotope analyses across the veins show overlapping and steep $\delta^{18}\text{O}$ and $\delta^{13}\text{C}$ fronts, which also coincide with the mineralogical front (Taylor & Bucher, 1986; Bégué, 2008). A formation temperature of ~550°C for the Ol+Cc pairs has been established, which is in agreement with phase petrology.

Numerous $\delta^{18}\text{O}$ profiles in Cc and Do, acquired with SIMS, combined with CL imaging, show that stable isotope exchange occurs only through mineral reaction and recrystallization. We also observe that: (1) partial dissolution and recrystallization of Do occurs a few mm to cm further into the dolomitic protolith and beyond the Ol+Cc mineralogical front; and (2) sharp $\delta^{18}\text{O}$ fronts at the core-rim interface of Do are mirrored by different CL intensities, with brighter rims (low $\delta^{18}\text{O}$) around darker cores (high $\delta^{18}\text{O}$).

The lack of Ol further into the replacement zone suggests that the silica front lagged behind the Do recrystallization front, and since there is no new mineral phase that precipitates in the Do dissolution/recrystallization zone, the reaction must be driven by small chemical changes or optimization of the crystal lattice only. Furthermore, progressive re-equilibration between Cc and Do at the interface between the replacement zone and the original Do supports the presence of only small amounts of fluid during the dissolution/recrystallization reactions.

REFERENCES

Bégué, 2008, MSc Thesis, University of Lausanne.

Bucher K. 1998: Growth mechanisms of metasomatic reaction veins in dolomite marbles from the Bergell Alps. *Mineral. Petrol.* 63, 151–171.

Taylor, B. E., & Bucher-Nurminen, K. 1986: Oxygen and carbon isotope and cation geochemistry of metasomatic carbonates and fluids—Bergell aureole, Northern Italy. *Geochimica et Cosmochimica Acta*, 50(6), 1267-1279.

2.2

Deciphering the different sources of Cl input into the mantle beneath St. Vincent (Lesser Antilles Arc): insight from B, O and Cl isotopes

Anne-Sophie Bouvier¹, Mélina Manzini¹, Nicole Métrich², Lukas Baumgartner¹

¹ *Institut des Sciences de la Terre, University of Lausanne, UNIL-Mouline, CH-1015 Lausanne (anne-sophie.bouvier@unil.ch)*

² *Institut de Physique du Globe de Paris, Sorbonne Paris Cité, Université Paris-Diderot, CNRS UMR 7154, Paris, France*

The effect of recycling crust and sediments on the composition of the mantle wedge, in particular for volatiles, is still debated. Chlorine is an important fluid mobile element. Its stable isotopes have different concentrations in the terrestrial reservoirs making Cl-isotopes potential tracers of slab-derived fluids (e.g., John et al., 2010). Despite its potential as a tracer, only a few studies report $\delta^{37}\text{Cl}$ in terrestrial rocks, mainly due to the analytical challenge to accurately determined the $^{35}\text{Cl}/^{37}\text{Cl}$ ratios.

Olivine-hosted melt inclusions provide a first order constraint on the $\delta^{37}\text{Cl}$ of primary magmas, since they were unaffected by near surface processes. However, due to their small size, an in situ technique is required. $\delta^{37}\text{Cl}$ analyses were conducted with a CAMECA IMS 1280-HR at the SwissSIMS laboratory. First results show that melt inclusions from the Lesser Antilles, Aeolian and Vanuatu arcs range from -1.9 to +0.6‰, -3.3 to -1.4‰ and -1.7 to +0.4‰, respectively. These first $\delta^{37}\text{Cl}$ dataset on melt inclusions from arc settings suggest that Cl addition mainly originates from serpentinites in the Lesser Antilles and Vanuatu arcs. In contrast, Cl added to the mantle wedge beneath the Aeolian Islands may record a higher proportion of fluids derived from the subducting sediments (Manzini et al., submitted). However, based on $\delta^{37}\text{Cl}$ only, it is difficult to estimate the respective contributions of the different slab end-members, especially for altered oceanic crust and serpentinites, which have similar $\delta^{37}\text{Cl}$.

Here, we used a well-studied sample from St. Vincent (Lesser Antilles) (Bouvier et al., 2008), for which melt inclusions display a large range of $\delta^{37}\text{Cl}$ (up to 2.5‰, Manzini et al., submitted). The previously determined $\delta^{37}\text{Cl}$ were coupled with new $\delta^{11}\text{B}$ and $\delta^{18}\text{O}$ analysis, providing a unique dataset to better constrain the different sources of Cl input into the mantle wedge and to understand the large $\delta^{37}\text{Cl}$ variation in melt inclusions from a single sample.

The coupling between $\delta^{11}\text{B}$ and $\delta^{37}\text{Cl}$ suggests Cl addition by fluids from serpentinites, and minor altered oceanic crust (AOC) and sediments. These results are in agreement with previous study (Bouvier et al., 2008). Comparison of $\delta^{18}\text{O}$ and $\delta^{37}\text{Cl}$ points towards serpentinitized mantle wedge as the major source of fluids, which inherited the Cl isotopic sediment signature during their early dehydration. Coupling the 3 isotopic systems in melt inclusions leads thus to coherent and complementary results and could be used to better constrain the Cl cycle in the mantle.

REFERENCES

- Bouvier, A.-S., Deloule, E., Métrich, N., 2008. Slab-Derived Fluids in the Magma Sources of St. Vincent (Lesser Antilles Arc): Volatile and Light Element Imprints. *J. Petrol.* 49, 1427–1448. doi:10.1093/petrology/egn031
- John, T., Layne, G.D., Haase, K.M., Barnes, J.D., 2010. Chlorine isotope evidence for crustal recycling into the Earth's mantle. *Earth Planet. Sci. Lett.* 298, 175–182. doi:10.1016/j.epsl.2010.07.039
- Manzini, M., Bouvier, A.-S., Barnes, J.D., Bonifacie, M., Rose-Koga, E.F., Ulmer, P., Métrich, N., Bardoux, G., Williams, J., Layne, G.D., Straub, S., Baumgartner, L.P., John, T., n.d. SIMS chlorine isotope analyses in melt inclusions from arc settings. *Submitt. to Chem. Geol.*

2.3

Porosity and permeability evolution during epidosite alteration of the oceanic crust, Semail ophiolite, Oman

Alannah Brett¹ & Larryn W. Diamond¹

¹ *Institute of Geological Sciences, University of Bern, Baltzerstrasse 3, 3012 Bern*

Basaltic rocks underlying spreading ridges in the oceanic crust undergo hydrothermal alteration due to circulation of hot, chemically altered seawater. Epidosites (rocks consisting of epidote + quartz ± hematite ± titanite) are extreme examples of this alteration. Established models envisage epidosite formation in high-temperature upflow zones at the base of the sheeted dike complex (Richardson et al. 1987; Alt, 1995). Because of their pervasive metasomatism and depletion in Cu and Zn, epidosites have been postulated as source rocks for metals in seafloor volcanogenic massive sulfide (VMS) deposits (Richardson et al. 1987; Jowitt et al. 2012).

In the Semail Ophiolite (Oman), epidosites are rare and small in the sheeted dikes but they are numerous and far larger (up to ~ 1 km² in outcrop) in the overlying pillow lavas. Moreover, their timing relative to crust-forming events suggests they are not directly related to spreading (Gilgen et al. 2016). These deviations from the conventional model raise the question of the significance of epidosites in the hydrothermal circulation system in the oceanic crust. In order to elucidate this issue, we are mapping pillow lavas in the Semail Ophiolite and tracking changes in alteration mineralogy, bulk chemistry, porosity and permeability. The results will be used as input for reactive-transport modelling of the epidotisation process.

A first step in understanding the significance of epidosites is to reconstruct the rock–water reaction by which they formed. An important constraint is the change in volume of solids attending epidosite metasomatism. For example, Harper (1988) noted a 10 vol.% decrease when albite is altered to epidote. Most pillow lavas in Oman show regionally distributed chlorite-albite hydrothermal alteration, which is attributed to seawater recharge. The epidosites, which presumably represent discharge alteration, overprint the chlorite-albite alteration. Inter-pillow hyaloclastites are first converted to epidosites, followed by pillow cores and finally pillow rims. Our helium-pycnometry measurements show that pillows altered to chlorite-albite have porosities of 3 – 8 vol.%. In contrast, epidotised pillows have porosities up to twice as high. Similarly, dikes altered to chlorite-albite have between 0.5 and 4 vol.% porosity, but the epidotised equivalents have up to two times higher porosity.

Digital processing of SEM back-scattered electron images has largely confirmed our pycnometry results and helped characterize pores into four types: intra-crystalline pores (fluid inclusions), open inter-crystalline pores, inter-crystalline pores clogged by post-epidotization calcite (precipitated during or after obduction of the ophiolite), and open micro-fractures that post-date epidotization. Whereas fracture porosity is inevitably included in the bulk He-pycnometry measurements and calcite-clogged porosity is inevitably excluded, the image-processing permits correction of these effects. We conclude that pristine epidosites contain up to ~12 vol.% intra-crystalline porosity and up to ~1.5 vol.% intra-crystalline fluid inclusions, resulting in $\Delta V \sim -9$ vol.% for the overall epidotization reaction in pillow basalts.

Our measurements of permeability reveal the same trends as those found for porosity in the pillow lavas. The chlorite-albite precursor rocks have permeabilities of $1 \times 10^{-20} - 1 \times 10^{-18}$ m² whereas epidosites have values up to four orders of magnitude higher, at $1 \times 10^{-18} - 1 \times 10^{-15}$ m². These observations confirm the suggestion of Harper (1988), that the epidosite reaction strongly increases the permeability of oceanic rocks. We also see that epidotisation is a self-reinforcing process, in that the metasomatic replacement creates its own porosity and thereby facilitates pervasive alteration of huge volumes of the pillow lavas.

REFERENCES

- Alt, J.C., 1995. Sub-seafloor processes in mid-ocean ridge hydrothermal systems. In: Humphris, S.E., Zierenberg, R.A., Mullineaux, L.S., Thomson, R.E. (Eds.), *Seafloor Hydrothermal Systems: Physical, Chemical, Biological, and Geological Interactions*. Geophysical Monograph 91, 85–114.
- Gilgen, S.A., Diamond, L.W., & Mercogli, I., 2016. Sub-seafloor epidosite alteration: Timing, depth and stratigraphic distribution in the Semail ophiolite Oman. *Lithos*, 260, 191–210.
- Harper, G.D., 1988. Reaction-enhanced Permeability by Formation of Epidosites in Seafloor Hydrothermal Systems. *Abstract EOS*, 69, 527.
- Jowitt, S.M., Jenkin, G.R.T., Coogan, L.A., & Naden, J., 2012. Quantifying the release of base metals from source rocks for volcanogenic massive sulphide deposits: effects of protolith composition and alteration mineralogy. *Journal of Geochemical Exploration*, 118, 47–59.
- Richardson, C.J., Cann, J.R., Richards, H.G., & Cowan, J.G., 1987. Metal-depleted root zones of the Troodos ore-forming hydrothermal systems, Cyprus. *Earth and Planetary Science Letters*, 84 (2–3), 243–253.

2.4

Iron stable isotope fractionation during subduction of basic rocks

Affé El Korh, Béatrice Luais, Etienne Deloule, Damien Cividini

Centre de Recherches Pétrographiques et Géochimiques (CRPG), UMR 7358 CNRS-Université de Lorraine, 15 rue Notre Dame des Pauvres, BP 20, F-54501 Vandœuvre-lès-Nancy Cedex, France (elkorh@crpg.cnrs-nancy.fr)

During subduction, the hydrothermally altered oceanic crust dehydrates progressively. Mass transfers from the oceanic rocks to the deep mantle may be responsible for compositional heterogeneities of the upper mantle.

Significant Fe stable isotope fractionation may occur during low-temperature (low-T; < 350°C) hydrothermal processes, as well as during high-T magmatic processes. Fe is strongly sensitive to variations in Fe redox state, the heavier Fe isotopes being preferentially incorporated into the Fe³⁺-phases.

This study employs Fe isotopes as a geochemical tracer of mass transfers during pre-subduction and syn-subduction metasomatic processes. We have analysed Fe isotopes in series of high-pressure (HP) metamorphic basic rocks of MORB affinity from the Ile de Groix (France) Variscan terrane (peak P–T conditions: 1.6–2.5 GPa; 500–600°C; El Korh et al., 2009). Blueschist, eclogite and retrograde greenschist facies were investigated in order to determine if and how the subducted basaltic crust may contribute to the mantle Fe isotope heterogeneity.

Fe isotopes ($\delta^{56}\text{Fe}_{\text{IRMM-014}} \pm 0.01\text{--}0.03\text{‰}$ at 2σ SE) were measured in bulk samples using a NeptunePlus MC-ICPMS (ThermoFisher Scientific) after sample dissolution and Fe separation through ion exchange chromatography column at the CRPG (Liu et al., 2014). The studied metabasites have $\delta^{56}\text{Fe}$ values (+0.16 to +0.33‰) heavier than those of MORBs-OIBs (+0.07 to +0.18‰; Teng et al., 2013). The heavy Fe compositions may be explained by the formation of isotopically heavy Fe³⁺-rich secondary products during the pervasive seafloor low-T hydrothermal alteration that occurred prior to subduction. Besides, our values are also consistent with the heavy $\delta^{56}\text{Fe}$ values (up to +0.34‰) of Samoan differentiated lavas, which could reflect either oxidising conditions or metasomatism of their mantle source, in addition to magmatic processes (Konter et al., 2016).

A good correlation between the $\delta^{56}\text{Fe}$ values and HFSE ratios (such as Y/Nb or Zr/Nb) reveals compositional heterogeneities in the initial magmatic protolith compositions. The $\delta^{56}\text{Fe}$ values decrease from blueschists (+0.19–0.33‰) to eclogites (+0.16–0.18‰). Eclogites have higher SiO₂ abundances and lower Al₂O₃ and Y/Nb contents than blueschists (El Korh et al., 2009). Thus, the different $\delta^{56}\text{Fe}$ values between blueschists and eclogites can be explained by: 1) small variations in the protolith composition, and/or 2) Fe isotope fractionation during high-pressure metasomatic processes related to dehydration reactions.

The $\delta^{56}\text{Fe}$ values of retrograde greenschists (+0.17 to +0.27‰) are similar to those of eclogites and blueschists, even in samples that show evidence of intensive interaction with Na-Al-Si bearing and Fe-poor fluids.

Fe isotope fractionation in the HP metabasites is limited by the restricted range of Fe₂O₃^{tot} abundances (El Korh et al., 2009) and Fe³⁺/ΣFe. In blueschists and eclogites, Fe is mainly distributed between the main metamorphic phases: Fe²⁺-rich garnet, Fe³⁺-rich epidote, Fe²⁺-Fe³⁺-bearing glaucophane and Fe²⁺-Fe³⁺-bearing omphacite. While Fe³⁺-richer omphacite is formed at the expense of Fe²⁺-richer glaucophane in eclogites, epidote is generally richer in Al and poorer in Fe³⁺ than in blueschists (El Korh et al., 2009). In greenschists, chlorite, Fe³⁺-rich epidote, Fe²⁺-Fe³⁺-bearing barroisite and actinolite, and magnetite formed at the expense of garnet, glaucophane and omphacite. No significant Fe amount was lost during the dehydration and rehydration reactions, owing to Fe partitioning and Fe²⁺/Fe³⁺ exchange between the metamorphic minerals stable under varying P–T conditions, and to the low mobility of Fe in low-Cl subduction zone fluids (Manning, 2004).

It is then suggested that the subducted metabasites have retained heavy Fe isotopic signatures until a depth of c. 60–70 km, where important dehydration occurs at the blueschist to eclogite transition. However, fluids derived from the subducted basic crust are not expected to carry significant amounts of Fe that would generate mantle Fe heterogeneities, because of the large stability field of Fe-bearing minerals in the source rock under subsolidus conditions. Our data predict that isotopically heavy Fe rocks are carried to deeper levels in the subduction zone, where they undergo disequilibrium partial melting (>100 km). Thus, the basic oceanic crust represents an important source for mantle Fe isotope heterogeneities through melt-induced metasomatism of the fore-arc mantle wedge.

REFERENCES

- El Korh, A., Schmidt, S.Th., Ulianov, A. & Potel, S. 2009: Trace element partitioning in HP–LT metamorphic assemblages during subduction-related metamorphism, Ile de Groix, France: a detailed LA-ICPMS study. *Journal of Petrology*, 50, 1107–1148.
- Manning, C.E. 2004: The chemistry of subduction-zone fluids. *Earth and Planetary Science Letters*, 223, 1–16.

- Konter, J.G., Pietruszka, A.J., Hanan, B.B., Finlayson, V.A., Craddock, P.R., Jackson, M.G., Dauphas, N. 2016: Unusual $\delta^{56}\text{Fe}$ values in Samoan rejuvenated lavas generated in the mantle. *Earth and Planetary Science Letters*, 450, 221-232.
- Liu, P.P., Zhou, M.F., Luais, B., Cividini, D., Rollion-Bard, C. 2014: Disequilibrium iron isotopic fractionation during the high-temperature magmatic differentiation of the Baima Fe–Ti oxide-bearing mafic intrusion, SW China. *Earth and Planetary Science Letters*, 399, 21-29.
- Teng, F.Z., Dauphas, N., Huang, S. & Marty, B. 2013: Iron isotopic systematics of oceanic basalts. *Geochimica et Cosmochimica Acta*, 107, 12-26.

2.5

The mantle source of the early stages of island arc magmatism: evidence from Hf isotopes in rutile from the Kohistan complex

Tanya Ewing¹, Othmar Müntener¹ & Urs Schaltegger²

¹ *Institute of Earth Sciences, University of Lausanne, CH-1015 (tanya.ewing@unil.ch)*

² *Department of Earth Sciences, University of Geneva, CH-1205*

Island arcs are one of the primary sites of generation of new continental crust, and are also key locations to understand the proportion of subducted sediment incorporated into the source of arc lavas versus recycled deep into the mantle. The Kohistan complex (northeastern Pakistan) preserves a remarkably complete ~50 km thick cross-section through an exhumed Jurassic–Cretaceous island arc. It affords a rare opportunity to study the chemical and isotopic evolution of island arc magmatism, from subduction initiation, through intra-oceanic subduction, to arc–continent collision.

In this study, we investigate the ultramafic–mafic Jijal Complex, which preserves part of the plutonic roots of the Kohistan complex formed over ~20 Ma of intra-oceanic subduction. We characterise the mantle source of the Jijal Complex using in situ LA-MC-ICPMS determination of the Hf isotope composition of rutile from mafic lithologies, which are zircon-free. This work exploits the superior sensitivity of the Neptune Plus, coupled with an improved analytical protocol, to improve precision of this novel technique and permit in situ analysis of rutile with only ~10–30 ppm Hf.

The analysed Jijal Complex samples are garnet-bearing gabbros and garnet-hornblendites with variable development of paragonite–quartz–epidote reaction textures attributed to interaction with residual hydrous melts. Rutile occurs included in early-formed minerals such as clinopyroxene and garnet, indicating crystallisation at high pressures and temperatures. Rutile from all samples, collected across ~3 km of former crustal depth, has indistinguishable Hf isotope compositions close to depleted mantle values. The Hf isotope composition shows no variation with degree of development of paragonite–quartz–epidote reaction textures, supporting their formation by interaction with in situ segregations of residual melt, and arguing against any role for late crustal fluids.

Integrating the new Hf isotope data for rutile with previously published whole rock Nd–Sr isotope data (Dhuime et al., 2009), we show that the Jijal Complex gabbros have an enriched Indian Ocean type mantle source. The Hf isotope data permit only a very limited contribution from subducted sediments to this source. This is in contrast to the previous interpretation of derivation of the Jijal gabbros from typical depleted MORB type mantle, which would require a significant sedimentary contribution to explain the isotope systematics (Dhuime et al., 2009). The distinction between these two scenarios, which is permitted by the new Hf isotope data, is of fundamental importance in understanding the relative proportions of juvenile mantle versus recycled crustal material in the source of the early stages of island arc magmatism.

REFERENCES

- Dhuime, B. et al., 2009. *Journal of Petrology*, 50(3): 531-569.

2.6

The plutonic-volcanic connection: Insights from central Japan

Eva Hartung¹, Luca Caricchi¹, Davide Roggero², David Floess¹, Simon Wallis³ & Satoru Harayama⁴

¹ *Department of Earth Sciences, University of Geneva, Rue Maraichers 13, CH-1205 Geneva (eva.hartung@unige.ch)*

² *Institute of Earth Sciences, University of Lausanne, Geopolis, CH-1015 Lausanne*

³ *Department of Earth and Planetary Sciences, Nagoya University, Nagoya 464-8601, Japan*

⁴ *Department of Geology, Shinshu University, Matsumoto 390-8621, Japan*

The Takidani pluton in the Japan Alps is the potential source of large andesitic and rhyolitic eruptions and therefore provides a rare opportunity to investigate the petrogenesis of large silicic magmatic systems and the highly debated volcanic-plutonic connection.

Here we present new whole rock data from 103 samples of the Takidani pluton (including enclaves) and 11 samples of volcanic rocks that have been proposed to be its erupted equivalent (i.e. Nyukawa PFD and Ebisutoge-Chayano PD) together with glass analyses of pumices and trace element chemistry of plagioclase from the different volcanic and plutonic units.

Whole rock REE patterns for the plutonic and volcanic rocks are similar and dominated by plagioclase and amphibole fractionation. The segregated porphyritic unit near the roof of the Takidani pluton shows a more marked Eu anomaly compared to the other Takidani units and the volcanic deposits. Glass compositions of pumices from crystal-rich andesitic Nyukawa PFD and the crystal-poor rhyolitic Ebisutoge and Chayano eruptions are comparable.

Sr, Ba, Eu and La concentrations in plagioclase serve to distinguish two major populations in the volcanic products: high-Eu plagioclases abundant in the andesitic Nyukawa PFD and low-Eu abundant in the rhyolitic Chayano tuff. Plagioclases from the Ebisutoge deposits are typically high in Eu but also contain resorbed low-Eu plagioclase cores. The trace element trends in the plagioclases across the different units of the Takidani pluton are similar from core to rim, with the exception of plagioclase cores from marginal granodiorite at the roof contact of the intrusion. Trace element patterns of the Takidani plagioclases are nearly identical to the low-Eu plagioclases observed in the Nyukawa PFD (i.e. 40 to 50 mol.% anorthite).

Overall, REE trends indicate that a petrogenetic relationship exists between the Takidani pluton and the Nyukawa PFD and Ebisutoge-Chayano deposits. However, trace element and plagioclase chemistry clearly show that the Ebisutoge and Chayano magmas evolved separately. The plagioclase compositions from the Takidani granodiorite and Nyukawa PFD, however, suggest that plagioclases from the volcanic and plutonic systems crystallised from a similar or potentially the same magmatic system.

2.7

Regional strike-slip tectonics and porphyry Cu-Mo and epithermal ore deposit formation during Cenozoic subduction to post-collisional evolution of the southernmost Lesser Caucasus, Tethyan belt

Samvel Hovakimyan^{1,2}, Robert Moritz¹, Rodrik Tayan², Rafael Melkonyan², Marianna Harutyunyan²

¹ *Department of Earth Sciences, University of Geneva, Rue des Maraîchers 13, CH-1205 Genève, Switzerland (samvel.hovak@gmail.com)*

² *Institute of Geological Sciences of the Armenian National Academy of Sciences, 0019 Yerevan, Republic of Armenia*

The oblique convergence and final collision of Gondwana-derived terranes and the Arabian plate with Eurasia during the Cenozoic created a favorable setting for the formation of the highly mineralized Meghri-Ordubad composite pluton in the southernmost Lesser Caucasus, central segment of the Tethyan metallogenic belt. Regional strike-slip faults played a critical role in the control of the porphyry Cu-Mo and epithermal systems hosted by the Meghri-Ordubad pluton. Detailed structural field mapping, stereonet compilation of ore-bearing fractures and vein orientations, and paleostress reconstructions allow us to constrain the formation of ore deposits in the context of wrench fault tectonics.

During Eocene subduction-related evolution of the region (Moritz et al. 2016), a NE-oriented compressional setting was favorable for dextral displacements along the two major, regional NNW-oriented Khustup-Giratakh and Salvard-Ordubad strike-slip faults (Fig.1). This resulted in the formation of a NS-oriented transrotational basin, known as the Central magma and ore-controlling zone (Tayan, 1998). It caused a horizontal clockwise rotation of blocks. The EW-oriented faults separating the blocks formed as en-échelon antithetic faults (Voghji, Meghrasar, Bughakyar, and Meghriget-Cav faults), and controlled the rotation of the blocks. The Central zone consists of a network of EW-oriented sinistral and NS-oriented subparallel strike-slip faults (Tashtun, Spetry, Tey, Meghriget and Terterasar faults). They are active since the Eocene and were reactivated during the entire tectonic evolution of the pluton, but with different behaviors. The regional Tashtun transcurrent NS-oriented fault was active during all stages of evolution of the pluton. During the Eocene, dextral displacement along the NS-oriented strike-slip faults were favorable for the opening of NE-oriented en-échelon normal faults. The NS-oriented faults, in particular at their intersection with EW- and NE-oriented faults, were important ore-controlling structures for the emplacement of major porphyry Cu-Mo (Dastakert, Aygedzor and Agarak) and epithermal Au and base metal (Tey-Lichkvaz and Terterasar) deposits.

During the Oligocene to the Miocene, collisional to post-collisional geodynamic evolution (Moritz et al. 2016), and associated NS-oriented compression and EW-oriented extension, resulted in renewed dextral displacement along the NS-oriented ore-controlling faults, and sinistral displacement along the EW-oriented en-échelon antithetic faults. This setting created the favorable geometry for opening NS- EW- and NE-oriented extension fractures, and the adequate conditions for the emplacement of vein and stockwork-type porphyry Cu-Mo deposits, including the giant Kadjaran deposit. During the Lower Miocene, the Tashtun transcurrent fault had an oblique-slip behavior. It formed a negative flower structure with a strike-slip component, which resulted in the development of a pull-apart basin and the formation of the Lichk porphyry Cu-Mo deposit.

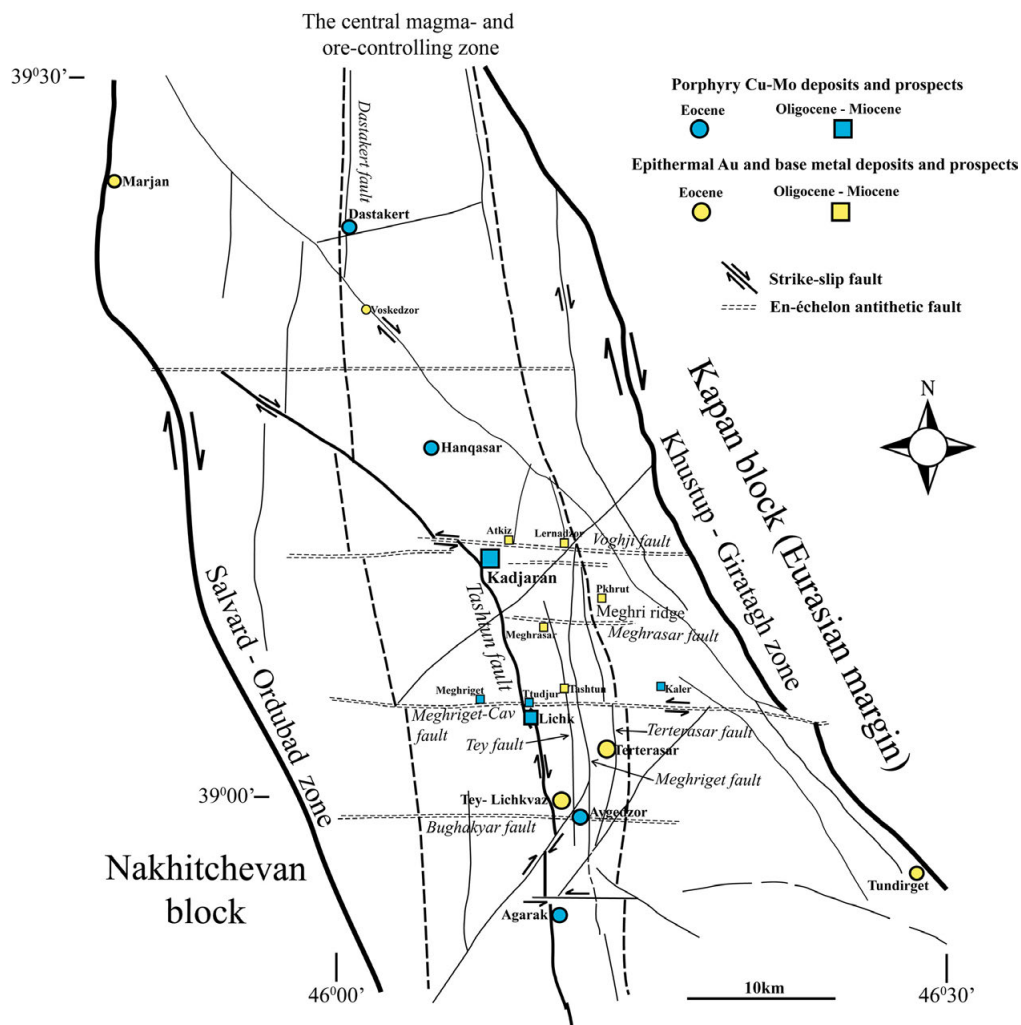


Figure 1. Schematic structural map of the Meghri-Ordubad pluton (modified after Karamyan et al., 1974; Tayan, 1998)

REFERENCES

- Karamyan, K.A., Tayan, R.N. & Guyumdjyan, H.P. 1974: The main features of intrusion magmatism of the Zangezur ore region of the Armenian SSR. Proceedings of the National Academy of Sciences of Arm.SSR, Earth Sciences, №1, p. 54-65. (in Russian).
- Moritz, R., Rezeau, H., Ovtcharova, M., Tayan, R., Melkonyan, R., Hovakimyan, S., Ramazanov, V., Selby, D., Ulianov, A., Chiaradia, M., & Putlitz, B. 2016: Long-lived, stationary magmatism and pulsed porphyry systems during Tethyan subduction to post-collision evolution in the southernmost Lesser Caucasus, Armenia and Nakhitchevan. *Gondwana Research*, 37, 465-503.
- Tayan, R.N. 1998: On central magma-ore controlling zone of the Zangezur ore region. Proceedings of the National Academy of Sciences of the Republic of Armenia, Earth Sciences, v. 51, №3, p.20-26 (in Russian with English abstract).

2.8

Implications of hydrothermal flow-through experiments on deep geothermal energy utilization

Xiang-Zhao Kong¹, Martin O. Saar²

¹ Institute of Geophysics, ETH-Zurich, Sonneggstrasse 5, 8092 Zurich, Switzerland (xkong@ethz.ch)

² Institute of Geophysics, ETH-Zurich, Sonneggstrasse 5, 8092 Zurich, Switzerland

Utilization of underground reservoirs for geothermal energy extraction, particularly using CO₂ as a working fluid, requires an in-depth understanding of fluid, solute (e.g., dissolved CO₂ and minerals), and energy (heat, pressure) transport through geologic formations. Such operations necessarily perturb the chemical, thermal, and/or pressure equilibrium between native fluids and rock minerals, potentially causing mineral dissolution and/or precipitation reactions with often immense consequences for fluid, solute, and energy transport, injectivity, and/or withdrawal in/from such reservoirs. The involved physico-chemico-thermo-mechanical processes often lead to modifications of permeability, one of the most variable and important parameters in terms of reservoir fluid flow and related advective solute/reactant and heat transport. Importantly, the amount of mineral dissolution/precipitation that can cause orders of magnitude in permeability reduction can be very small, if minerals are removed or deposited in pore throats or narrow fracture apertures. This potentially has detrimental consequences for geothermal energy usage.

However, analysing, understanding, and predicting reservoir evolution and flow properties are non-trivial, as they depend on complex chemical, thermodynamic, and fluid-dynamic feedback mechanisms. To achieve these goals, it requires the integration and extrapolation of thermodynamic, kinetic, and hydrologic data from many disparate sources. The validity, consistency, and accuracy of these data-model combinations are unfortunately often incomparable due to the relative scarcity of appropriate parameterizations in the literature. Here, we present some results of hydrothermal flow-through experiments on rock core samples. During the experiments, we fixed the flow rates, confinement and outlet pore-fluid pressures, and recorded inlet pore-fluid pressure. We also analysed the outlet fluid chemistry samples throughout the experiments and imaged our rock cores before and after the flow-through experiments using X-Ray Computed Tomography (XRCT). With all these data, we are able to interpret the changes in permeability, porosity, and (reactive) surface area at the core scale.

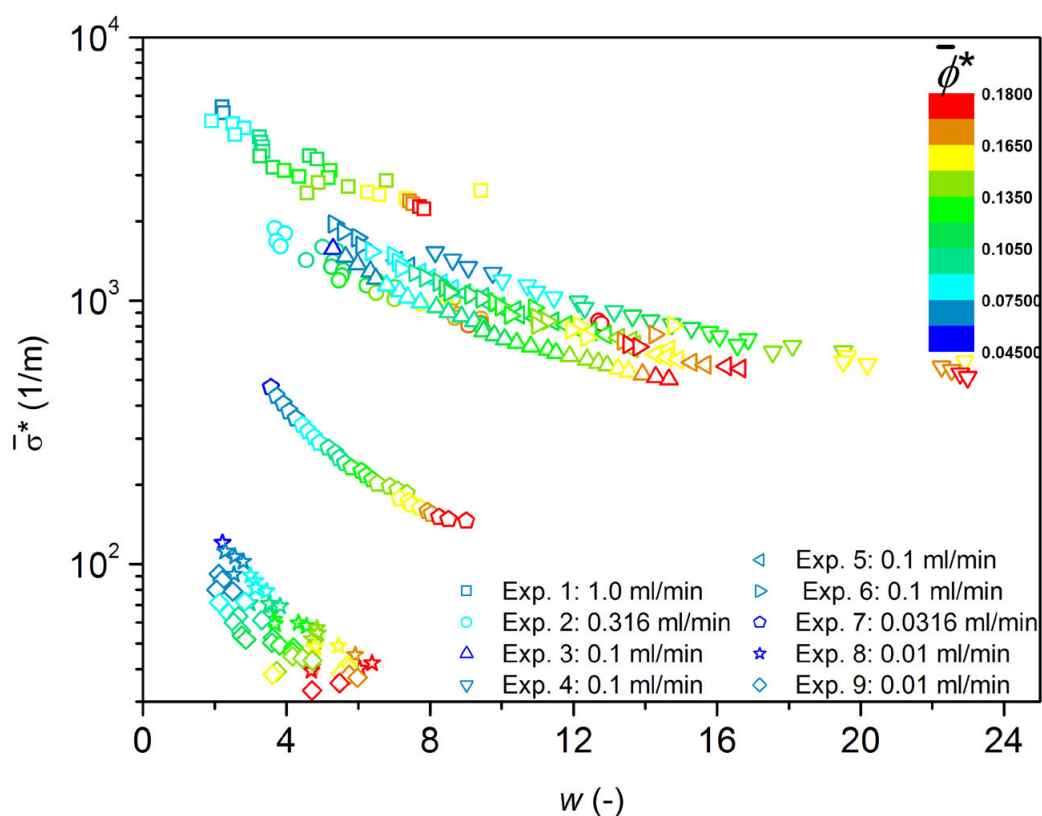


Figure 1. Dependency of the relationship between the fitted initial specific reactive surface area, $\bar{\sigma}^*$, and the fitted parameter, w , on initial porosity.

2.9

Partial melting of the mafic lower oceanic crust

Julien Leuthold¹, Johan Lissenberg², Trevor Falloon³, Peter Ulmer¹, Brian O'Driscoll⁴ & Dina Klimentyeva¹

¹ *Institute of Geochemistry and Petrology, ETH Zürich, Clausiusstrasse 25, 8092 Zürich (julien.leuthold@erdw.ethz.ch)*

² *School of Earth and Ocean Sciences, Cardiff University, Cardiff CF10 3YE, United Kingdom*

³ *Earth Sciences, University of Tasmania, Private Bag 79, Hobart 7001, Australia*

⁴ *School of Earth, Atmospheric and Environmental Sciences, University of Manchester, Manchester M13 9PL, United Kingdom*

Along oceanic spreading ridges, magma batches underplate, ascend, stall and erupt (see Fig.1). Although fractional crystallization is frequently considered the most important process, MASH processes characterize open-system igneous complexes and affects the crustal evolution of magmas. We examine the record of partial melting in lower oceanic crust gabbro cumulate from slow- (Atlantic ocean at Kane Megamullion) and fast-spreading ridges (Pacific ocean at Hess Deep).

At the crystal scale, eutectic minerals are most affected by partial melting (i.e. Cpx + Plg ± Ol). Cpx oikocryst microstructure show resorption embayments related to sharp geochemical variations: compatible Cr and Al and incompatible Ti, Zr and REE decrease from core to rim, with a late-stage TiO₂ and REE increase. Mg#, Eu* and Sr* increase from core to rim and strongly decrease towards the outer rim. Plg shows reverse zoning.

Textures and geochemical evolution are incoherent with processes such as fractional crystallization or crystallization from successive mantle-derived melts. Zoned Cpx oikocrysts result from 1) partial melting of REE-poor lower crust gabbroic cumulate, 2) hybridization with intrusive hot Cpx-undersaturated primitive mantle-derived melt and 3) refertilization. Reaction products are a Cpx-poor gabbro/troctolite residue and a hybrid melt saturated in Cpx and Plg (see Eq.1). Mineralogy, texture and chemistry of cumulate primocrysts and hot intrusive melt are modified. Outer rim crystallized from a distinct percolating late-stage reacted melt, close to solidus conditions.

Hybrid melt has high SiO₂ and Mg# contents and is Cr-, Zr- and REE-depleted. MELTS calculations and geochemical modelling of the hybrid melt liquid line of descent match N-MORB chemistry. Hybridization with co-genetic gabbro partial melt is a valid alternative/complementary process to explain variations in the primitive MORB geochemistry. However, the lacks of strong mineralogical and geochemical contrast between co-genetic invading melt and cumulate make it difficult to distinct in erupted lavas alone.

Eq.1: initial rock (Cpx₁+Plg₁+Ol₁) + hot primitive basalt = restite (Ol₁±Plg₁±Cpx₁) + Cpx-rich hybrid melt => crystallization of secondary and new phases (Ol₂+Plg₂+Cpx₂±Spl)

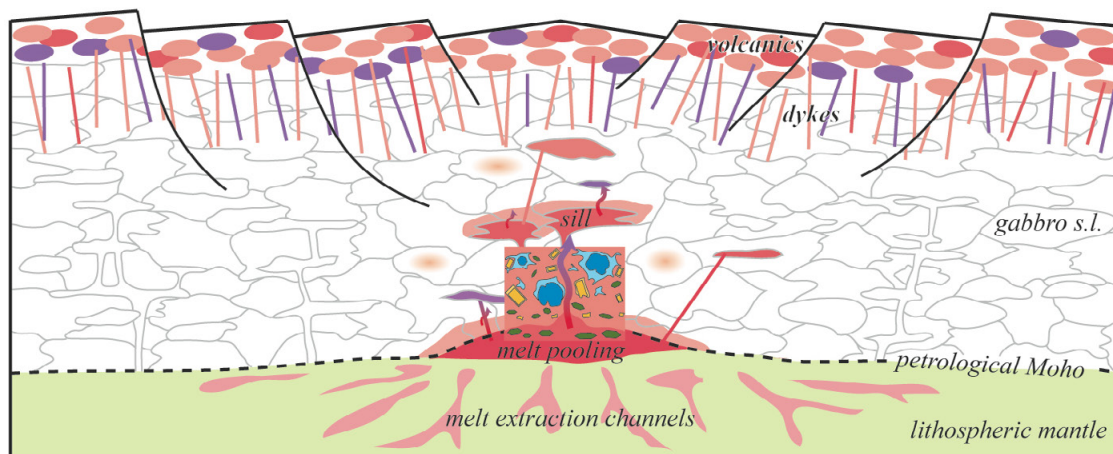


Figure 1. Cross-section of slow-spreading ridges, showing the different occurrences of melt in the oceanic crust (based on Sinton & Detrick, 1992; Dick et al., 2008). Gabbro s.l. includes troctolite, gabbro, gabbronorite and oxide gabbro. Also dunite occurs along the Moho. Young hot crustal gabbro reacts (i.e. partial melting, hybridization, re-crystallization) with invading primitive mantle-derived melt. Crystals, rocks and melt chemistry and texture are modified.

REFERENCES

- Sinton, J. & Detrick, R. 1992. Mid-ocean ridge magma chambers, *Journal of Geophysical Research* 97, 197-216.
 Dick, H.J.B., Tivey, M.A. & Tucholke, B.E. 2008. Plutonic foundation of a slow-spreading ridge segment: oceanic core complex at Kane Megamullion, 23°30'N, 45°20'W, *Geochemistry, Geophysics, Geosystems* 9.

2.10

Zircon U-Pb ages from the Bastar Craton, central India: A Paleoarchaeoan patchwork terrane.

Alessandro Maltese¹, Klaus Mezger¹, Om Prakash Pandey¹, Dewashish Upadhyay²

¹ *Institut für Geologie, Universität Bern, Baltzerstrasse 1+3, CH-3012 Bern (alessandro.maltese@geo.unibe.ch)*

² *Department of Geology and Geophysics, Indian Institute of Technology, 721302 Kharagpur, India*

Reconstruction of Earth's early crustal evolution is tied to the identification and precise and accurate age determination of the Archaean rock record. The Bastar Craton (BC) in Central India is an Archaean terrane that comprises some of the oldest domains of the Indian subcontinent. Granitoids from central Bastar yield zircon U-Pb dates of 3.56 and 3.58 Ga (Ghosh 2004, Rajesh et al. 2009). Another sample from southern Bastar yields a date of 3.51 Ga (Sarkar et al. 1993). However, due to the low amount of available data, it is still unclear whether the dates coincide with actual crust-forming events, represent a time of reworking or interaction of juvenile melts with older crustal components.

In order to better constrain the timing of crustal growth in the BC we conducted U-Pb, LA-ICP-MS analyses on zircon grains separated from all exposed rock types from a large area. For a suite of granites and gneisses zircon grains yielded dates of ca. 3.50 Ga. Some samples also preserve older cores (ca. 3.58 Ga). One gneissic sample uniformly hosts 3.58 Gyr old zircon. Other granitic rocks from the region yielded zircon dates of ca. 2.48 and 2.50 Ga without inheritance of older components. In every sample, the degree of concordance is highly variable, but the upper intercept with Concordia is always well-defined by the data array.

Despite some samples having older cores, the zircon dates within an individual sample are strikingly uniform indicating a major addition of crust and reworking (assimilation) of slightly older material (3.58 Ga) at ca. 3.50 Ga. The intrusion of Neoarchaeoan granites into the Paleoarchaeoan unit may have locally altered the host rock, but not its zircon. This simple petrogenetic evolution of the older granitoids makes them particularly suitable to study crust-mantle differentiation processes in the early Archaean.

REFERENCES

- Ghosh, J. G. 2004: 3.56Ga tonalite in the central part of the Bastar Craton, India: oldest Indian date. *J. Asian Earth Sci.* 23(3), 359–364.
- Rajesh, H. M., Mukhopadhyay, J., Beukes, N. J., Gutzmer, J., Belyanin, G. A. & Armstrong, R. A. 2009: Evidence for an early Archaean granite from Bastar craton, India. *J. Geol. Soc.* 166(2), 193–196.
- Sarkar, G., Corfu, F., Paul, D. K., McNaughton, N. J., Gupta, S. N. & Bishui, P. K. 1993: Early Archean crust in Bastar Craton, Central India—a geochemical and isotopic study. *Precambrian Res.* 62(1-2), 127–137.

2.11

Decompression-driven crystallization of superheated melts: The formation of orbicules and comb layers in shallow subvolcanic conduits (Fisher Lake, USA)

Anders McCarthy¹, Othmar Müntener¹

¹ *Institute of Earth Sciences, University of Lausanne, UNIL-MOULINE, CH-1015, Lausanne*

Understanding the formation of igneous layering in shallow arc plutons is key to constraining the migration and emplacement of melts within the mid-to upper crust and their relationship with volcanic complexes. At intraplutonic contacts, magma flow structures commonly separate more homogeneous bodies. Some of these features include orbicules and comb layers, which are enigmatic features formed by the crystallization of elongated minerals (comb-textures) perpendicular to the layering either on a wall rock (comb layers) or on pre-existing xenoliths (orbicules). By studying comb layers and orbicules from Fisher Lake, Sierra Nevada (USA), we provide new insights regarding the mechanisms responsible for the growth of comb layers and orbicules in shallow arc settings.

Comb layers and orbicules show a significant diversity in terms of layer thickness, mineralogy and texture. The majority of comb textured layers show plagioclase as the initial mineral to crystallize, forming a plagioclase-dominated cumulate, with crystal fractionation leading to interstitial pyroxene and oxide saturation. Conductive cooling will lead to the saturation of amphibole, thereby forming plagioclase- and plagioclase-amphibole comb layers. The lack of comb textured amphibole in orbicule rims suggests that the presence of a thermal gradient is important in diversifying comb layer mineralogy and texture.

Comb layers and orbicules are formed in subvertical dykes at shallow emplacement depths (ca. 2kbar depth), and are associated with high-An plagioclase (An85-97), magma-breccia bodies and orbicule cores (xenoliths) originating from local lithologies, suggesting hydrous conditions and dyke propagation through hydraulic fracturing. We therefore propose that comb layers and orbicules are formed by the adiabatic ascent of moderately hydrous mafic melts (ca. 4 wt% H₂O) through the crust, inducing dissolution of pre-existing crystals and nuclei and the formation of a superheated melt. Upon reaching the upper crust, this superheated melt will reach volatile saturation. Degassing will induce heterogeneous nucleation and growth of plagioclase on solid rocks (wall rocks or locally remobilized xenoliths), forming plagioclase-dominated comb layers and orbicule rims.

The rarity of comb layers and orbicules worldwide is suggested to be related to i) their local formation in subvolcanic conduits upon volatile saturation, ii) their formation in highly dynamic environment and iii) the rarity of adiabatic ascent leading to superheating in arc settings.

2.12

Analytical method development of high precision Mg isotope measurements by SIMS for in-situ ^{26}Al - ^{26}Mg mineral isochron dating of chondrites

Jonas Pape¹, Klaus Mezger¹, Anne-Sophie Bouvier², Lukas Baumgartner²

¹ *Institute of Geological Sciences, University of Bern, Baltzerstrasse 1 + 3, CH-3012 Bern (jonas.pape@geo.unibe.ch)*

² *Institute of Earth Sciences, University of Lausanne, UNIL-Mouline, 1015 Lausanne*

Chondrites are primitive undifferentiated meteorites, which contain chondrules, calcium-aluminum-rich inclusions (CAIs) and matrix that belong to the most pristine components of the solar system. Models propose that chondrules were formed by either collisions of planetesimals or by shock-induced remelting of dust agglomerates in the disk and that they may record a key step towards planet formation. Because condensation of CAIs, formation of chondrites and differentiation of first planetesimals occurred within a few million years only, high precision crystallization ages of chondrules with an age resolution of a few tens to hundreds of thousands of years are needed to understand the relative timing of chondrite formation. This project aims to date chondrules from different types of the most pristine chondrites using the $^{26}\text{Al}/^{26}\text{Mg}$ extinct radionuclide system. Precise chondrule ages in chondrules will lead to a better chronology of the earliest processes in the solar system and to the timing of formation processes of planetary systems in general.

Chondrules, viewed as closed systems that formed by melting followed by rapid cooling of mm to sub-mm sized objects, comprise different minerals with distinct compositions (i.e. $^{27}\text{Al}/^{24}\text{Mg}$). The short-lived (and now extinct) ^{26}Al decays to ^{26}Mg (i.e. in situ excess ^{26}Mg). This decay results in increasing $^{26}\text{Mg}/^{24}\text{Mg}$ that correlates with Al/Mg ratios of the host material (minerals, glass, mesostasis). Mineral isochrons constructed from different components of chondrules in pristine meteorite samples that have different Al/Mg yield information about the age of last crystallization and thus chondrule formation.

The set of samples selected for this study comprises some of the least metamorphosed carbonaceous (CO3 and CV3) as well as ordinary chondrites (L/LL3.05, L3.05, L3.10, L3.15, L3.00). Reference materials, which are used to determine instrumental mass fractionation laws, comprise natural high-T minerals (olivines and pyroxenes), international standard glasses (BCR-2G, BHVO-2G) and synthetic glasses. First analytical sessions at the SwissSIMS laboratory were performed in order to adopt and develop analytical protocols (e.g. Villeneuve et al., 2009) for high precision Mg isotope measurements using the Cameca IMS 1280-HR large radius secondary ion microprobe.

Here we present first results of reference material measurements and correction for instrumental mass fractionation as well as preliminary Mg isotope data for chondrite samples. A typical external reproducibility (2 s.d.) for ^{26}Mg excess of better than $\pm 0.07\%$ and a 2σ error on the mean of all standard materials (2 s.e.) of better than $\pm 0.011\%$ was achieved during the first sessions, which, however, needs to be improved by modifying the analytical routine in order to reach the high precision needed for ^{26}Al - ^{26}Mg mineral isochron dating of single chondrules.

REFERENCES

Villeneuve, J., Chaussidon, M., Libourel, G. 2009: Homogeneous distribution of ^{26}Al in the solar system from the Mg isotopic composition of chondrules. *Science*, 325, 985 – 988.

2.13

Evolution of Volcanism at the Late Cretaceous Madneuli Copper gold-polymetallic deposit, Lesser Caucasus, Georgia

Nino Popkhadze¹, Robert Moritz², Sergo Kekelia¹

¹ Al. Janelidze Institute of Geology of I.Javakishvili Tbilisi State University, A. Politkovskaya 31, 0186, Tbilisi, Georgia (nino_popkhadze@yahoo.com)

² Department of Earth sciences, University of Geneva, Rue de Maraîchers 13, CH-1205 Geneva

The Madneuli polymetallic deposit, Bolnisi mining district in Southern Georgia is a part of the Artvin-Bolnisi tectonic zone, located between the Somkheto-Karabakh island arc of the Lesser Caucasus in the East, the Eastern Pontides to the west and the Santonian-Campanian Adjara-Trialeti back-arc to the North. The formation of the Madneuli deposit is tightly linked to the evolution of Late Cretaceous island arc magmatism in the Bolnisi district, where calc-alkaline to tholeiitic rocks are characterised by a bimodal mafic-felsic composition. The Madneuli deposit is hosted by volcanic and volcano-sedimentary rocks of rhyodacitic composition of the Mashavera suite interpreted as Coniacian to Santonian in age. Our field-oriented detailed studies were based on facies analyses, and enabled us to collect and interpret different volcanic and sedimentary structures, outline their distribution and their relationship in the open pit, and finally classify them into two facies assemblages: volcanic and volcano-sedimentary (Popkhadze et al., 2014). This allowed us to constrain the evolution of volcanism in the Madneuli deposit and adjacent areas (Fig.1).

Cycle I consists of a phreatomagmatic eruption, documented by ash fall deposits, including a pumice-rich pyroclastic flow interfingering with beds of fine-grained tuff and vesiculated tuff, associated with accretionary lapilli horizons. Cycle II is associated with the formation of a submarine dome-like structure, produced during several eruptive pulses, and was accompanied by the emplacement of isolated lobes. Two types of hyaloclastite flows were described for the first time in the Madneuli deposit: (i) hyaloclastite with glass-like selvages and (ii) hyaloclastite with pillow-like forms, representing the external part of individual lobes (Popkhadze et al., 2014). During Cycle III, the bedded volcano-sedimentary sequence and lobe structure was crosscut by a rhyodacitic extrusion, and later by dikes, which outcrop in the eastern part of the open pit. A columnar-jointed ignimbrite in the northern part of the open pit is described for the first time and was connecting to Cycle IV. Reliable evidence for the hot emplacement is columnar jointing and high-temperature devitrification textures (e.g. spherulites), which was followed by the emplacement of a welded ignimbrite pyroclastic flow in the uppermost part of the Madneuli deposit.

In conclusion, the phreatomagmatic eruption centre of Cycle I was located in the Bolnisi area, at a distance of several kms away from the Madneuli open pit. The volcanic activity producing the dome structure and the rhyodacitic extrusion in the open pit might be connected to a granodiorite to quartz diorite porphyry intrusion, crosscut by drilling at a depth of 800-900 m beneath the Madneuli deposit.

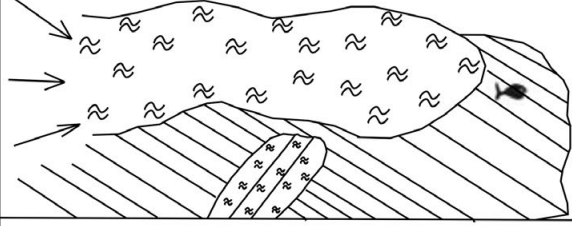
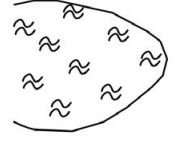
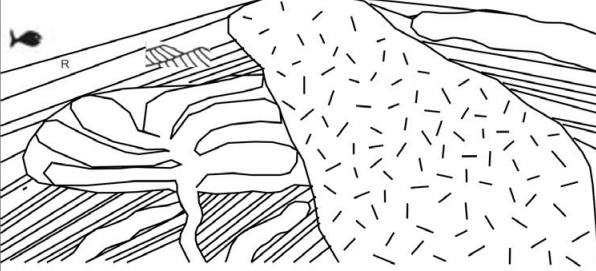
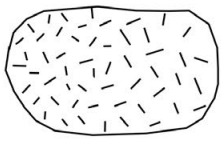
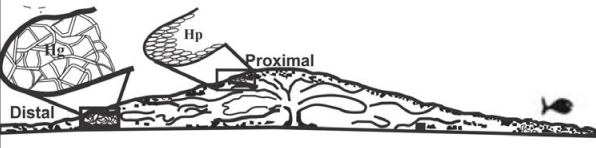
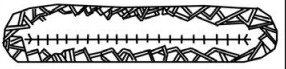
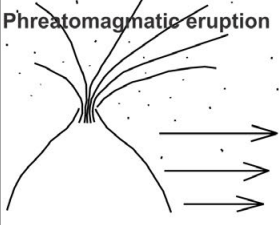
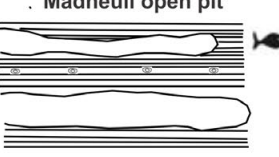
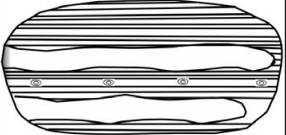
Silicic volcanism	Processes	Products
Cycle IV	Entrance of Ignimbrite pyroclastic flow in shallow-marine environment; emplacement of columnar jointing ignimbrites. 	Ignimbrite pyroclastic flow 
Cycle III	Injection of rhyodacitic extrusion 	Massive lava 
Cycle II	Lava dome emplacement in unconsolidated banded VS sequence; cooling, hyaloclastite fragmentation. 	Hyaloclastite with pillow like forms  Hyaloclastite with glass-like selvages 
Cycle I	Phreatomagmatic eruption  Madneuli open pit 	Pyroclastic flow interfingering with banded rhyodacitic products of phreatomagmatic eruption and volcanoclastic turbidities. 

Figure 1. Schematic evolution of magmatism at the Madneuli deposit and adjacent areas, and the processes and facies architecture during Late Cretaceous volcanic activity (scheme based on Soriano et al., 2013).

REFERENCES

- Soriano, C., Giordano, G., Ray Gas., Riggs, N., Porreca, M. 2013. Facies architecture, emplacement mechanisms and eruption style of the submarine andesite EL Barronal complex, Cabo de Gata, SE Spain. *Journal of Volcanology and Geothermal Research*, 264, 210-222.
- Popkhadze N., Moritz R., Gugushvili V., 2014. Architecture of Upper Cretaceous Rhyodacitic Hyaloclastite at the polymetallic Madneuli deposit, Lesser Caucasus, Georgia. *Central European Journal of Geosciences*, 6, 308-329.

2.14

Xenotime formation in a low-temperature hydrothermal environment, Browns Range, WA

Lisa Richter^{1,2}, Jens Gutzmer^{1,3}, Petya Atanasova³ and David Banks⁴

¹ *Institute of Mineralogy, TU Bergakademie Freiberg, Brennhausgasse 14, 09599 Freiberg (lisa.richter@gmx.net)*

² *Water–Rock Interaction Group, Institute of Geological Sciences, University of Bern, Baltzerstr. 3, CH-3012 Bern, Switzerland*

³ *Helmholtz-Zentrum Dresden - Rossendorf, Helmholtz Institute Freiberg for Resource Technology, 09599 Freiberg, Germany*

⁴ *School of Earth and Environment, University of Leeds, Woodhouse Lane, Leeds LS2 9JT, UK*

The Browns Range district is located in the northernmost part of Western Australia. The district comprises of a cluster of mineralized, steeply dipping breccia bodies and veins, hosted by sedimentary rocks, which are presumably part of the ca. 6 km thick Birrindudu Group (Blake et al. 1975). Sedimentation of the host rocks took place from 1.735 to 1.64 Ga (Blake et al. 1975). The age of xenotime-quartz mineralization has been constrained to 1646±5 Ma (SHRIMP U-Pb dating of xenotime, Morin-Ka et al. 2016), corresponding to the final deposition stage of the Gardiner Sandstone (Blake et al. 1995). The mineralogy is dominated by xenotime and quartz, with subordinate hematite, zircon and florencite-goyacite. We observed two major textural types of xenotime: (I) fine-grained xenotime impregnating the host rock and (II) coarser-grained, euhedral xenotime growing within open veins, or as syntaxial overgrowth onto the oldest of three generations of vein quartz. The quartz generations can be readily distinguished by their cathodoluminescence (CL) color. Quartz A predates xenotime and shows dark blue CL. Quartz B is cogenetic with xenotime and emits light blue CL with distinct oscillatory zoning and inclusions of xenotime along distinct growth zones. Quartz C is distinguished by yellow to light blue CL, overgrows Quartz A and B and clearly postdates xenotime formation.

Fluid inclusion studies were carried out on Quartz A and Quartz B in order to constrain the conditions of xenotime precipitation. Quartz A hosts fluid inclusion clusters and trails of pseudosecondary origin (according to criteria in Roedder 1984). They are H₂O ± salt mixtures consisting of liquid-vapor (L-V) or liquid-vapor-solid (L-V-S) (accidental trapped solid crystals), with ca. 10 vol.-% vapor at room temperature. Freezing data of individual fluid inclusion assemblages (FIAs; Goldstein and Reynolds 1994) reveal a salinity range from 1 to 8 wt.-% NaCl_{eq} (Steele-MacInnis et al. 2012). Temperatures of homogenization (Th_{TOT}) into the liquid phase range between 190 and 165 °C. Regarding homogeneous trapping, Th_{TOT} constitute minimum trapping temperatures. Fluid inclusions in Quartz B are located along growth zones and are therefore primary. Their assemblages comprise H₂O±salt L-V inclusions and coexisting monophasic vapor (H₂O) inclusions. The liquid is of high salinity (23.6-25.8 wt.-% NaCl_{eq}) and the L-V inclusions homogenize into the liquid phase at 120 to 100 °C. The coexistence of L-V and mono-phase V inclusions in the growth zones in Quartz B suggests boiling of the low-salinity fluid. Thus Th_{TOT} represents the trapping temperature for Quartz B inclusions.

LA-ICP-MS analysis of fluid inclusions trapped in Quartz A and B (L-V fluid inclusions) reveals the dominance of Na, K, Mg and Ca. Fluid inclusions in both quartz generations contain detectable Y, U, Fe, Cu, Zn, Pb and REE. Higher salinity fluids hosted by Quartz B contain significantly greater amounts of Y, U and LREE compared to the low salinity inclusions in Quartz A. However, not only the absolute abundance of REE changes between the two quartz generations. Normalization of the analyses to equal salinities reveals that the fluid inclusions in Quartz A are markedly enriched in HREE vs. LREE, whereas no such enrichment is recorded by fluid inclusions in Quartz B.

Although the ultimate source of REE remains unknown, detrital REE-bearing minerals in the lower portion of the Birrindudu Group or U and REE mineralization in underlying basement rocks are suitable metal sources. Xenotime-quartz assemblages evidently formed in a low-temperature environment from a fluid that was already enriched in REE in general and in HREE in particular. Low-grade burial metamorphism of the sediments (Blake et al. 1979) led to mineral dehydration and pore fluid mobilization. The mobilized aqueous fluid migrated along the basal unit of the Gardiner sandstone into structural pathways. Xenotime-quartz mineralization coincides in age (Morin-Ka et al. 2016) with the final stages of the sedimentation of the Birrindudu Group (Blake et al. 1995) and D6 deformation (Ahmad and Dunster, 2013). It is evidently due to this regional tectonic event that SiO₂- and REE-rich oxidizing pore fluids cooled and decompressed, resulted in fluid boiling below hydrostatic pressure conditions (closed system) and precipitation of abundant Quartz B and xenotime. Mobilization of fluids and precipitation of Quartz A could have taken place between 190 to 270 °C and 0.5 to 1.7 kbar, under hydrostatic to lithostatic pressure conditions. The presence of hematite suggests oxidizing conditions.

Results of this study reveal that xenotime-quartz mineralization of the Browns Range District owes its origin to an HREE-enriched, low salinity, oxidizing basinal fluid. Heavy REE may have been remobilized by this fluids during diagenesis/metamorphism and concentrated by the mineralizing system. Whilst cooling is thought to be responsible for the precipitation of large volumes of quartz (Quartz A), it was evidently boiling that led to extreme enrichment of HREE as an entirely new mode of REE deposit formation.

REFERENCES

- Ahmed, M. and Munson, T.J. (compilers) 2013: Geology and mineral resources of the Northern Territory. Northern Territory Geological Survey, Special Publ. 5.
- Blake, D.H., Hodgson, I.M. and Smith, P.A. 1975: Geology of the Birrindudu and Tanami 1:250 000 Sheet Areas, Northern Territory. Bureau of Mineral Resources, Australia, Canberra, Report 174.
- Goldstein, R.H. and Reynolds, T.J. 1994: Systematics of fluid inclusions in diagenetic minerals: Society for Sedimentary Geology Short Course 31, 199 pp.
- Morin-Ka, S., Beardsmore, T.J., Hancock, E.A., Rasmussen, B., Dunkley, D., Zi, J., Muhling, J., Wilson, R. and Chapman, J. 2016: Alteration and age of the Browns Range heavy rare earth element deposits. GSWA extended abstracts 2016, (2), 21-25.
- Roedder, E. 1984: Fluid inclusions. Reviews in Mineralogy, Vol. 12, 644 pp. Mineralogical Society of America, Washington.
- Steele-MacInnis, M., Lecumberri-Sanchez P. and Bodnar, R.J. 2012: HOKIEFLINCS-H₂O-NaCl: A Microsoft Excel spreadsheet for interpreting microthermometric data from fluid inclusions based on the PVTX properties of H₂O–NaCl. Computers & Geosciences, 49, 334-337.

2.15

The core of the Lepontine dome: new geological, structural, metamorphic and geochronological data (sheet Osogna, no. 1293,1:25'000)

Filippo Luca Schenker¹, Christian Ambrosi¹, Cristian Scapozza¹, Matteo Maino², Claudio Castelletti¹, Marco Antognini³ & Yves Gouffon⁴

¹ *Institute of Earth Sciences, University of Applied Sciences and Arts of Southern Switzerland (SUPSI), Via Trevano, CH-6952 Canobbio (filippo.schenker@supsi.ch)*

² *Dipartimento di Scienze della Terra e dell'Ambiente, University of Pavia, via Ferrata 1, I-07100 Pavia*

³ *Museo Cantonale di storia naturale, Viale C. Cattaneo 4, CH-6901 Lugano*

⁴ *Swiss Geological Survey, Federal Office of Topography swisstopo, Seftigenstrasse 264, CH-3084 Wabern*

The central part of the Lepontine dome includes, from bottom-to-top, the subpenninic gneissic nappes of the Leventina, Simano, Adula/Cima-Lunga and Maggia. These nappes derive from the same post-Variscan gneissic crust complicating their lithological distinction within the nappe pile.

We present the geological map of the Osogna sheet (Swiss National Map no. 1293,1:25'000) together with structural and metamorphic data and magmatic and metamorphic U-Pb zircon ages of ortho- and paragneisses laying along the Leventina-Simano boundary.

The geological map shows lithological boundaries that are locally incongruent with the tectonic contact of the published maps. In particular, the boundary between the Leventina and the Simano gneisses is not clear. Generally, the boundary was traced within leucogneisses by joining a carbonate lens with quartzite, amphibolite or paragneiss lenses. Nevertheless, we could not find any quartzite and the amphibolite and paragneiss lenses are vertically distributed in the tectonostratigraphy and do not form a single folded horizon. Within these two units the strain related to top-to-the-foreland shearing is rather distributed. Such deformation occurred at peak metamorphic conditions between 570 and 620 °C and below ~6000 bar (conditions constrained with equilibrium thermodynamics).

Magmatic Early Permian U-Pb zircon ages from a folded granitic dike discordant within the paragneisses that separate the Leventina and the Simano units attest moderate deformation along the boundary during the Alpine orogen. Therefore, we present evidence that the top-to-the-foreland deformation between the Leventina and the Simano units was more distributed than commonly assumed, limiting the allochthonous character of the Simano unit.

2.16

Control of water activity on the hydroxyl content of biotiteGuillaume Siron¹, Lukas Baumgartner¹, Anne-Sophie Bouvier¹ & Torsten Vennemann²¹ *Institute of Earth Sciences, University of Lausanne, Lausanne, CH-1015 (guillaume.siron@unil.ch)*² *Institute of Earth Surface Dynamics, University of Lausanne, Lausanne, CH-1015*

Water activity is an important variable controlling metamorphic processes. Water can be present as a fluid phase, but its activity is reduced by dilution with CO₂ or dissolved salts, for example. Alternatively, water activity can also be reduced due to undersaturation of the system, e.g. no free fluid phase is present. Such variations have been called upon to explain processes as diverse as melting in the crust, granulite formation, equilibrium or the kinetics of mineral reactions. Water activity is typically inferred from low-variance mineral assemblages or fluid inclusions, but it requires an independent determination of both temperature and pressure. Here we present another approach: hydrous minerals can, in principle, monitor a_{H₂O} through a change in hydroxyl ion concentrations by the reaction $2 \text{OH}^-_{\text{bt}} \rightarrow \text{O}^{2-}_{\text{bt}} + \text{H}_2\text{O}_{\text{fluid}}$ (here for biotite, for example). To evaluate this hypothesis, we have analyzed water content in biotite from two different contact aureoles using SIMS.

The OH⁻ content of biotite in pelitic schists from the mid-crustal contact aureole of the western Adamello (Floess and Baumgartner 2013) decrease slightly with increasing temperature of biotite crystallization. In these biotites Ti content increases, while no correlation with Cl or F was observed. Such an evolution has been attributed to Ti-oxygen substitutions (Cesare et al. 2008). Nevertheless, here we demonstrate that Ti-content varies within an individual sample (outside EPMA uncertainty), but these variations are not correlated with OH⁻, since OH⁻ content is constant. Hence, Ti-oxygen substitution is not solely responsible for water decrease in biotite of the Adamello contact aureole. We rather interpret the decrease of OH⁻ content from 3.41 ± 0.09 p.f.u. for sub-solidus samples to 3.27 ± 0.08 p.f.u. for partially molten rocks as an indication of a decrease in water activity due to fluid absent partial melting.

In the Ubehebe Peak contact aureole, infiltration of a water-rich fluid from the intrusion (Roselle et al. 1999) produced metacarbonate assemblages containing phlogopite in two different metacarbonate samples, metamorphosed at the same temperature, but different fluid composition, as determined by phase petrology. Water content decreases in biotite with increasing CO₂ in the fluid phase from 2.8-3.8 p.f.u. to 1.5-2.2 p.f.u. Since there is virtually no Fe or Ti in these phlogopites we interpret this clear trend of OH⁻ content in biotite to monitor water activity during crystallisation.

In conclusion, water content in biotite is a powerful tool to constrain the relative evolution of water activity of a system, but it still requires a good experimental calibration of the relation between these two variables to be of absolute value.

REFERENCES

- Cesare, B., Satish-Kumar, M., Cruciani, G., Pocker, S., & Nodari, L. 2008: Mineral chemistry of Ti-rich biotite from pegmatite and metapelitic granulites of the Kerala Khondalite Belt (southeast India): Petrology and further insight into titanium substitutions. *American Mineralogist*, 93, 327–338.
- Floess, D., & Baumgartner, L. 2013: Formation of garnet clusters during polyphase metamorphism. *Terra Nova*, 25, 144–150.
- Roselle, G. T., Baumgartner, L. P., & Valley, J. W. 1999: Stable isotope evidence of heterogeneous fluid infiltration at the Ubehebe Peak contact aureole, Death Valley National Park, California. *American Journal of Science*, 299, 93–138.

2.17

Reconstruction of high-pressure metamorphic conditions from symplectites: insights from Pouso Alegre mafic rocks (Brasília Belt, Brazil)

Mahyra Tedeschi^{1,2,3}, Pierre Lanari¹, Daniela Rubatto¹, Jörg Hermann¹, Antônio Pedrosa-Soares², Ivo Dussin⁴, Marco Aurélio P. Pinheiro³

¹ *Institute of Geological Sciences, University of Bern, Baltzerstrasse 1+3, Bern, Switzerland (mahyratecheschi@gmail.com)*

² *Programa de Pós-Graduação em Geologia, Universidade Federal de Minas Gerais, Av. Antônio Carlos 6627, Belo Horizonte, Brazil*

³ *Geological Survey of Brazil, Avenida Brasil 1731, Belo Horizonte, MG, Brazil*

⁴ *Multilab, Universidade do Estado do Rio de Janeiro, R. São Francisco Xavier 524, Rio de Janeiro, Brazil*

Mafic rocks within crustal sections that underwent polycyclic tectono-metamorphic evolutions may be used as markers for suture zones, particularly if they preserve relict of high-pressure metamorphism. Reconstructing the metamorphic history of such mafic rocks is challenging because they are commonly retrogressed and are scarce in supercrustal sequences. The mafic rocks from Pouso Alegre in the Meridional Brasília Orogen (SW-Brazil), outcrop as rare lenses within (Ky)-Sil-Grt gneiss, Amp-Grt orthogneiss and Bt granite and are heavily weathered. It has been previously suggested that the Pouso Alegre garnet amphibolites are “retro-eclogites”, based on a characteristic symplectite texture and mineralogical observations, and thus they have been interpreted to mark the suture zone between the Paranapanema and São Francisco cratons. However, no quantitative estimates of the pressure is available to support this conclusion. In this study we investigated in detail these samples to refine their P-T-t history.

The Grt-Cpx amphibolite from Pouso Alegre shows symplectite and corona textures overprinting a former Grt-Cpx1 paragenesis, as commonly observed in retrogressed eclogites. Bulk rock chemistry indicates a tholeiitic gabbroic composition, with a MORB-like signature. The bulk-rock composition was used for P-T modelling with THERIAK-DOMINO (De Capitani & Petrakakis 2010). The Grt-Cpx1 assemblage is stable at 700°C and 14 kbar. The symplectite is developed from the reaction $\text{Omp} + \text{Qz} + \text{H}_2\text{O} \rightarrow \text{Cpx} + \text{Amp} + \text{Pl} + \text{Qz}$. Local compositions of the symplectite domains were used to retrieve the jadeite content of Cpx1. This value is in line with the predictions of the model and confirms a maximum pressure of 14 kbar. The P-T conditions for the formation of the symplectite are between 600-750°C and less than 7kbar as estimated using XMapTools (Lanari et al. 2014) and BINGO-ANTIDOTE (Lanari & Duesterhoeft 2016). This program compares the metamorphic assemblage, mineral modes and composition observed in a given domain of the rock to those predicted by the thermodynamic models.

Rutile is a good candidate to preserve relict metamorphic stages that have been completely obliterated in the matrix. Zr-in-rutile thermometry (Tomkins et al. 2007) indicates that rutile forms at temperature of ca. 715°C. The Zr-in-rutile data are consistent with the T from modelling, without evidence of a preceding, higher grade stage.

The inclusions trapped in the garnet porphyroblast, rutile and in zircon were systematically analyzed to search for relicts of a metamorphic stage predating the Grt-Cpx1 assemblage. Inclusions of Cpx, Amp, Grt, Ttn, Zrn and Bt are similar in composition to the matrix minerals, supporting the results of the thermodynamic models with a maximal pressure of 14 kbar. We thus conclude that this sample equilibrated at lower crustal conditions.

U-Pb zircon age (LA-ICP-MS) of zircon cores spread along concordia from ca. 1.7 to 1.0 Ga with a significant cluster at 1518±9 Ma (MSDW = 1.3), which is interpreted as the protolith crystallization age. Zircon rim ages in the interval 660-590 Ma are correlated to the metamorphic event based on CL imaging and Th/U ratios. U-Pb geochronology of the samples provide a crystallization age for the orthogneiss and granite of ca. 2.1 Ga, a maximum sedimentation age of the (Ky)-Sil-Grt gneiss at 794±4 Ma and metamorphism in the orthoderivated rocks at 626±5 Ma.

In the mafic rocks, the significant time span between protolith crystallization and metamorphism (ca. 800 Ma), the lack of evidence of a collision in this period and the bulk-rock chemistry indicate a continental basalt/gabbro origin. The mafic magma intruded the granitic country rocks at ca. 1.5Ga, and sediments deposited on this basement by 800Ma. The sequence was involved in the collision at ca. 630Ma, when it reached the peak metamorphic conditions.

REFERENCES

- de Capitani, C. & Petrakakis, K. 2010: The computation of equilibrium assemblage diagrams with Theriak/Domino software. *Am. Mineral.* 95, 1006–1016.
- Lanari, P. & Duesterhoeft, E. 2016: Thermodynamic modeling using Bingo-Antidote: A new strategy to investigate

metamorphic rocks. EGU-2016-11363.

Lanari, P., Vidal, O., De Andrade, V., Dubacq, B., Lewin, E., Grosch, E. G. & Schwartz, S. 2014: XMapTools: a MATLAB©-based program for electron microprobe X-ray image processing and geothermobarometry. *Comput. Geosci.* 62, 227–240.

Tomkins, H.S., Powell, R. & Ellis, D.J., 2007: The pressure dependence of the zirconium-in-rutile thermometer, *Journal of Metamorphic Geology*, 25, 703–713.

2.18

The role of trace and major element chemistry in controlling the solubility of water in upper mantle olivine

Peter Tollan^{1,2}, Hugh O'Neill²

¹ *Institut für Geologie, University of Bern, Bernoullistrasse 32, CH-4056 Basel*

² *Research School of Earth Sciences, The Australian National University, Canberra, Australia*

Experiments in simple systems (SiO₂-MgO-*Tr*) have demonstrated that when doped with appropriate levels of a trace element (*Tr*), the solubility of water in forsterite is substantially enhanced (Berry et al. 2005). Despite the clear relationship in synthetic systems, studies investigating natural olivines have concluded that the ability of trace elements to influence water incorporation is minimal (Gaetani et al. 2014). We have attempted to reconcile this discrepancy by conducting a series of experiments on natural mantle olivines from a single locality with a range of trace and major element compositions, representative of typical depleted upper mantle.

Six optically-clear crystals of San Carlos olivine (Arizona, USA) were cut into cubes with dimensions of 15x15x15 mm, with each face orientated parallel to a principle crystallographic direction. Cubes from each olivine were packed in platinum capsules surrounded by olivine-orthopyroxene powder and heated at 1400 °C and atmospheric pressure for 24 hours. The cubes were then extracted and sealed inside silver capsules containing distilled water. The capsules were held at 800 °C and 15 Kbar for 72 hours, allowing hydrogen to diffuse into the crystal structure and decorate existing point defects. The cubes were subsequently mounted in epoxy and double-polished such that profiles along the *a* and *c* axes could be measured by Fourier transform infrared spectroscopy (FTIR) in order to ascertain both the water content and the nature of the hydrous defect populations present. The FTIR data was then compared to laser-ablation ICP-MS data for the same cubes to deduce the relationship between water content and crystal composition.

Spectra along each axis consists of four main groups of bands in the water stretching region (3650-3000 cm⁻¹). The sum of the integrated absorbance of all of these bands (proportional to total water content) shows no clear relationship with composition, similar to previous studies (Gaetani et al. 2014). However, when the absorbance beneath individual bands is compared to composition, distinct relationships are found. The single band at 3612 cm⁻¹ shows a negative correlation with Cr and positive correlation with Mn. The intensity of bands centred at 3572 cm⁻¹ and 3525 cm⁻¹, which are typically dominant in upper mantle olivine, have very strong positive correlations with the Ti content and negative correlations with Mg. Bands between 3400 cm⁻¹ and 3300 cm⁻¹ show a positive correlation with Cr/Na and negative correlations with Fe_{Tot} and Mg#. The broad band at 3250 cm⁻¹ has a weak positive correlation with Mn and a weak negative correlation with MgO. There were no correlations between any of the band intensities and Al concentration.

These results illustrate the often overlooked complexity of hydrous point defect populations in olivine. The positive and negative relationships between different bands and trace elements act to cancel each other out such that over the compositional range investigated, trace element concentration would appear to have minimal impact on water solubility when only measurements of total water are performed. However, when the total water content is broken down into water associated with different point defects as done here, a substantial control from composition is apparent. Most significant is the relationship with Ti, since formation of this hydrous defect results in the generation of Si vacancies and thus is a principle weakening mechanism of the olivine structure (Faul et al. 2016). The substantial range of Ti contents and associated hydrous defect concentration between olivine crystals extracted from such a limited volume of mantle suggests that interaction of fluids with typical upper mantle peridotite may lead to weakening effects over much smaller scales than previously thought. Any models considering total mantle water content and consequential weakening must therefore incorporate trace element variability on both large and small scales in order to accurately model mantle dynamics and water recycling.

REFERENCES

- Berry, A.J., Hermann, J., O'Neill, H.St.C., Foran, G.J. 2005: Fingerprinting the water site in mantle olivine. *Geology*, 33, 869-872
- Gaetani, G.A., O'Leary, J.A., Koga, K.T., Hauri, E.H., Rose-Koga, E.F., Monteleone, B.D. 2014: Hydration of mantle olivine under variable water and oxygen fugacity conditions. *Contrib. Mineral. Petrol.* 167:965-979
- Faul, U.H., Cline II, C.J., David, E.C., Berry, A.J., Jackson, I. 2016: Titanium-hydroxyl defect-controlled rheology of the Earth's upper mantle. *Earth Planet. Sci. Lett.* 452, 227-237

2.19

Clay mineral diagenesis in Cretaceous Dentale and Gamba clastic reservoirs from the South Gabon Basin (West African passive margin) – new insights on the regional geology and basin evolution history

Giovanni Zaroni¹, Branimir Šegvić¹, Andrea Moscariello¹

¹ *Department of Earth Sciences, University of Geneva, Rue de Maraichers 13, 1205 Geneva, Switzerland*

The Gabon coastal region located along the equatorial West African continental margin, hosts several sedimentary basins with well-developed and prolific petroleum systems whose two key elements (source and reservoir) developed prior, during and after the opening of the South Atlantic Ocean in Cretaceous time. In this study, we focus on the Early Cretaceous Dentale and Gamba Formations in the onshore part of the South-Gabon sub-basin formed during the syn-rift and transition to post-rift time respectively. The two formations are both consisting of siliciclastic rocks thought to be accumulated in fluvial and lacustrine environments. The exceptional access to core material from two wells from these two reservoirs allowed us to provide unprecedented information on their mineralogy, geochemistry and thus origin and post-depositional diagenetic processes that controlled the distribution of clay parageneses. The latter is considered to be of high importance for the understanding of the basin's burial history and geotectonic development. Sampled material was analysed by X-ray diffraction, automated electron microscopy, and inductively coupled plasma mass spectrometry in order to reconstruct early and burial diagenetic variations directing the formation of clay assemblages in the basin. The clay content in both cores consists of authigenic mixed-layer minerals like illite-smectite (I-S), chlorite-smectite (C-S) and berthierine-chlorite (B-C) and some minor detrital illite/mica and chlorite. Illite-smectite and C-S phase chemistry are interpreted as the product of progressive evolution from the dioctahedral (I-S) and trioctahedral (C-S) smectitic precursors formed out of acid volcanic feedstock during early diagenesis. Different magmatic fractionation degrees, from rhyodacite to trachyandesite, reflected in the uniform REE curves of the volcanic glass conform to an active geotectonic development of the Cretaceous margins of Africa. If this is confirmed, this will be the first account of active volcanism recorded during Barremian-Aptian times in the eastern coast of South Atlantic.

Finally, the study on clay minerals allowed us to provide accurate description and quantification of pore filling minerals, a new controlling factor for log calibration, all of which having a direct impact on porosity calculation.

Overall the findings provide new insights and ideas at regional and reservoir scale that may assist the future exploration and development of hydrocarbons in these two 'mature' reservoirs formations.

P 2.1

Characterising the May 2016 eruption of Mt Etna, Italy

Matt Edwards¹, Laura Pioli¹, Daniele Andronico², Antonio Cristaldi² & Simona Scollo²

¹ *Department of Earth Sciences, University of Geneva, 1205 Geneva, Switzerland (matthew.edwards@unige.ch)*

² *Istituto Nazionale di Geofisica e Vulcanologia, Catania, Italy*

Activity at open vent basaltic volcanoes is highly variable, ranging from outgassing, to small ash explosions, larger paroxysmal events, and lava flows. Mount Etna is a type example basaltic volcano characterized by frequent eruptions of variable magnitude, intensity, and explosivity. This variability can occur among and within individual eruptions, with no apparent shift in vent position and/or magma composition, suggesting that each eruption is the product of several pre-eruptive processes and their non-linear interaction. Unraveling these processes and the specific parameters controlling explosivity of basaltic magmas requires specific studies on complex style eruptions.

We have investigated the eruptive dynamics of the May 2016 episode, which represents a relatively short eruption (1 week) alternating both explosive and effusive phases. Strombolian explosions occurred at three of the summit craters at various times during the episode. Among the summit vents, the Voragine Crater (VOR) displayed the greatest variability in style, alternating between explosions, pulsating lava fountains, lava flows and elevated outgassing from 18 to 21 May. The three lava fountains at VOR led to the formation of plumes to the east on 18 and 19 May and south-east on 21 May.

Compositional and physical magma properties were assessed on the tephra deposited from the 21 May plume and the lava flow of the same day in order to determine any variability present and rheological change controlling explosivity. The explosive phases are characterised by coupling field data with recordings from fixed monitoring cameras to constrain plume heights, eruption phase durations, total erupted masses and fallout boundaries. Particle size distributions of tephra from different locations were measured via CAMSIZER and used to compute the total grain-size distribution of the deposit. The curve was then compared to the distribution obtained by conventional methods.

Results suggests that even in the case of small volume eruptions, an abrupt shift in magma properties results in a rapid increase in explosivity with onset of efficient fragmentation and formation of a few km high plumes.

P 2.2

Driving Mechanisms of 1651-53 and 2002 Eruptions at Etna Volcano (Italy)

Milena Scrignari¹, Laura Pioli¹, Daniele Andronico², Luca Caricchi¹

¹ *Department of Earth Sciences, University of Geneva, Geneva, Switzerland*

² *Istituto Nazionale di Geofisica e Vulcanologia (INGV), Sezione di Catania, Osservatorio Etneo, Catania, Italy*

Mount Etna is a type case of open vent basaltic volcano. It shows a large range of eruptive styles as lava flows, Strombolian explosions, lava fountains, Subplinian and Plinian eruptions (Branca and Del Carlo, 2005). We compare two eruptions characterised by different styles. The 1651-1653 is a large volume, long lasting effusive eruptions fed by a crystal-rich (46.5 vol %) magma with up to 66.5. vol% cm- sized plagioclase crystals. The 2002-2003 eruption had a shorter duration, with a strongly explosive phase and contemporaneous smaller lava effusion. Lava flows and explosions were fed by lower crystallinity (25.6 vol%) magmas with different volatile content (Andronico et al., 2005; Spilliaert et al., 2006). These two eruptions represent ideal end-members in the volcanic activity of Etna because of the contrasting composition and petrography.

We performed a detailed sampling of both 1651-3 lavas and 2002-3 tephra and lavas to analyse the properties of the feeding magmas, their variations with time and at different eruptive vents. Moreover, the physical and textural properties of the lava and scoria of these two eruptions (e.g. density, vesicularity, grain size distribution and componentry), compared with their geochemical and petrological properties (bulk and phenocryst composition, CSDs) provide fundamental information on conduit and magma chamber processes and how they affected the eruptive dynamics.

Our results suggest that the 1651-1653 lavas are more evolved, with higher content of SiO₂, Al₂O₃ and Na₂O and lower TiO₂, Fe₂O₃ and K₂O concentrations with respect to the 2002 lavas. Two distinct chemical groups can be established considering the products of the 2002 eruption: the southern flank lavas are more primitive (MgO-rich and K₂O-poor) than those emitted on the Northern flank. Plagioclase compositions range from 0.42 to 0.87, and 0.72 to 0.88 An mol % in the 1651 lavas 2002 tephra and lava, respectively. All crystals show complex zoning and resorption patterns. Clinopyroxenes of 1651-1653 lavas have a Mg-richer composition, reaching in some cases 15 wt% of MgO. 2002 clinopyroxenes are characterized by a lower MgO content, generally ranging from 12 to 13.5wt%. Clinopyroxenes also reveal resorption textures, especially at the core and strong oscillatory zoning. Different CSDs for the three phenocryst species are also indicative of very distinct crystallization conditions.

Finally, heterogenous properties (vesicularity and groundmass crystallinity) of the scoria erupted during the Strombolian phase of the 2002 eruption suggest recycling, shallow magma mixing and non homogenous crystallization in the volcanic conduit as effective syn-explosive processes.

REFERENCES

- Andronico, D., Branca, S., Calvari, S., Burton, M., Caltabiano, T., Corsaro, R., Del Carlo, P., Garfi, G., Lodato, L., Miraglia, L., Murè, F., Neri, M., Pecora, E., Pompilio, M., Salerno, G., Spampinato, L., 2005. A multi-disciplinary study of the 2002-03 Etna eruption: insights into a complex plumbing system. *Bull Volcano* (2005)67:314-330
- Branca, S., Del Carlo, P., 2005. Types of eruptions of Etna volcano AD 1670-2003: implications for short-term eruptive behavior. *Bull Volcano* (2005)67:732-742
- Spilliaert N., Allard P., Métrich N., Sobolev A., 2006. Melt inclusion record of the conditions of ascent, degassing and extrusion of volatile-rich alkali basalt during the powerful 2002 flank eruption of Mount Etna (Italy). *J Geophys Res* (2006)111.

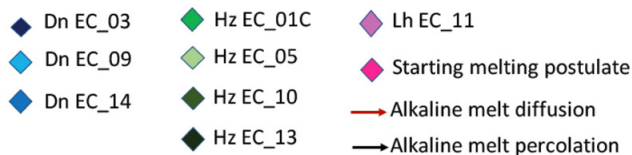
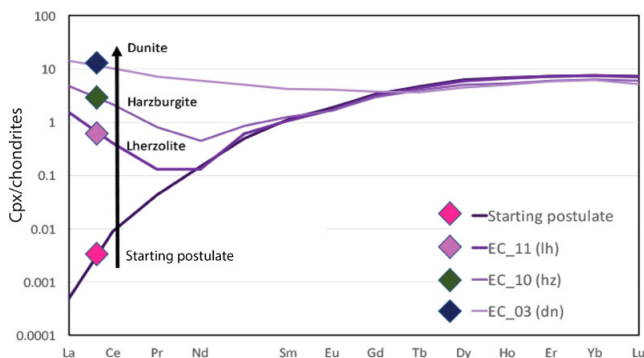
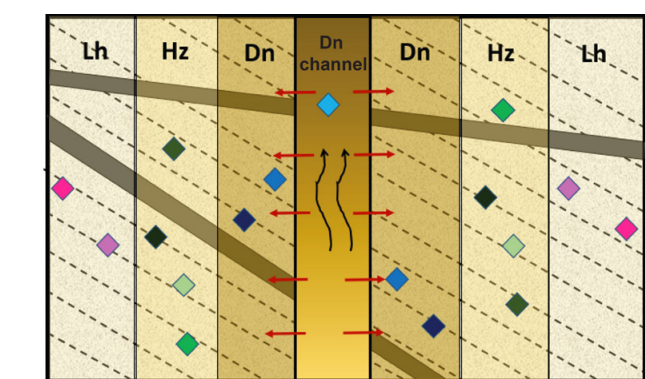
P 2.3

Peridotite xenoliths from Sierra Baguales: Insights into melting and refertilization processes into the mantle wedge

Alexandra Demers-Roberge¹, Mary-Alix Kaczmarek¹, Sébastien Pilet¹, Davide Roggero¹ and Othmar Müntener¹

¹ Earth Sciences Institute, University of Lausanne, CH-1015, Lausanne (alexandra.demers-roberge@unil.ch)

Mantle xenoliths are abundant in many different localities throughout the Patagonia area. They are found in plateau and post plateau alkaline volcanism (Miocene to Pleistocene) from Patagonian back-arc region. The latter is due to the subduction of the Chile triple junction point, where the Nazca and the Antarctica plates subduct under the South American plates, leading to the opening of a slab window. Mantle xenoliths from these localities are important because they provide information about the processes happening in the Andean mantle wedge and in back-arc volcanism. In the present study, mantle xenoliths, which include spinel bearing dunites, harzburgites and lherzolites, were collected in Sierra Baguales, Austral Patagonia, around 300 km east of the subduction trench in Chile, really close to the volcanic arc. We use petrographic analyses, geothermometry as well as major and trace elements geochemistry to identify the different processes which have affected the lithospheric mantle.



Harzburgites and lherzolites yield equilibration temperatures between 850°C and 950°C using the Wells (1977) and Brey and Köhler (1990) thermometers. Olivine, cpx and orthopyroxene Mg# range from 90 to 92.3, 89 to 94.7 and 90.5 to 92.6 respectively. Spinel is magnesiochromite and has Cr# between 25 to 50% from the most fertile to the most depleted peridotite. There are 3 distinct groups of REE patterns in cpx: lightly convex-shaped (group 1), lightly convex with LREE enrichment (group 2) and flat (group 3). We estimate, based on the best fit of HREE content in these cpx, that the initial melting process which depleted these peridotites start in the garnet stability field (0-7%) following by moderate melt extraction in the spinel stability field (6-9%). Secondary melt enrichment associate to chromatic effects related to melt circulation explain the LREE enrichment observed in cpx from various xenoliths. Refertilization simulations have been made with a melt having the same geochemistry as the host basalts (alkaline with a slab component) and yielded really good fits, linking all the samples together. The main different processes seen by the lithospheric mantle under Sierra Baguales are transition to porous to focused flow creating dunitic channels, partial melting in the garnet and spinel facies and refertilization by melt.

Figure 1. Interpretation of the processes (creation of a dunite channel, refertilization and partial melting) seen by the lithospheric mantle under Sierra Baguales, including all the samples and a comparison with their Cpx REE patterns. The initial setting of the figure is based on a figure of Müntener and Piccardo (2003).

REFERENCES

- Bjerg, E.A. et al. 2005: The upper mantle beneath Patagonia, Argentina, documented by xenoliths from alkali basalts, *Journal of South America Earth Sciences*, 18, 125-145.
- Breitsprecher, K., Thorkelson, DJ. 2009 : Neogene kinematic history of Nazca-Antarctica-Pheonix slab window beneath Patagonia and the Antarctic Peninsula, *Tectonophysics*, 464, Issue 1-4, 10-20.
- Gorring, M. L et al. 1997: Neogene Patagonian plateau lavas: continental magmas associated with ridge collision at the ChileTriple Junction, *Tectonics*, 16, 1-17.
- Müntener, O., Piccardo, G.B. 2003: Melt migration in ophiolitic peridotites: the message from Alpine-Apennine peridotites and implications for embryonic ocean basins, *Geological Society*, 218, 69-89.
- Rivalenti, G. et al. 2004:The backarc mantle lithosphere in Patagonia, South America, *Journal of South America Earth Sciences*, 27, 121-152.

P 2.4

Neogene back-arc basaltic magmatism in the Sierra Baguales (southern Patagonia): are there alternatives to teared slabs and slab window models ?

Davide Roggero¹, Othmar Müntener¹, Sébastien Pilet¹

¹ *Institute of Earth Sciences, University of Lausanne, 1015 Lausanne, Switzerland (davide.roggero@unil.ch)*

The Neogene back-arc magmatism in southern Patagonia (South America) has been associated to the melting of OIB type asthenospheric mantle, related to the opening of a slab window and/or slab tearing beneath South America as a consequence of the subduction of the Chile ridge. This back-arc magmatism produced alkaline to subalkaline transitional lavas – magmas with geochemical characteristics intermediate between alkaline and calc-alkaline geochemistry – yet the spatial and temporal evolution of the geochemical signatures are largely unconstrained. Slab tear and/or slab windows however, should produce a spatially and temporally resolvable signature in back-arc lavas, since the thermal structure of the mantle above the subducting plate will be strongly influenced by the presence or absence of a subducting slab.

Here we use detailed field investigations and new geochemical data from the back-arc lavas of the Sierra Baguales (southern Patagonia), that are located about 100 km east of the active volcanic arc, to test the potential relationships between the geochemical signature and tectonic models.

New geochemical analysis show that basaltic lavas and mafic rocks from Sierra Baguales are primitive magmas (up to Mg# = 70, Ni = 250-300 ppm and Cr = 500-550) with subalkaline to high-K calc-alkaline signature. Positive Pb and negative Nb anomalies suggest a connection with calc-alkaline magmas, but the OIB like general enriched trace element patterns distinct them from typical arc volcanoes. These basaltic magmas show, therefore, an unusual transitional signature with relatively high Nb content (Nb = 15 ppm) regarding calc-alkaline basalts but high La/Nb (1.3-1.5) and low Ce/Pb (6-8) regarding typical alkaline intraplate magmas (La/Nb < 1 and Ce/Pb > 15).

Studies have demonstrated that melting of amphibole-rich metasomatic veins or cumulates located in the lithospheric mantle could represent an alternative hypothesis for the origin of intra-plate alkaline volcanism. In particular, Pilet et al. (2011) have shown that the trace element signature of the alkaline magma are directly related to the metasomatic process that form the amphibole-rich veins. Amphibole-rich cumulate could also be produced by calc-alkaline arc magma differentiation at depth, and their potential delamination (e.g. Müntener & Ulmer, 2006) in a Ma time-scale could be an alternative to produce transitional magmas characterize by low Nb high Pb content. This hypothesis provide an alternative mantle source, linking the arc and back-arc magmatism with a coupled petrogenetic model, that differ from slab window and/or slab tearing models.

REFERENCES

- Guivel, C., Morata, D., Pelletier, E., Espinoza, F., Maury, R. C., Lagabrielle, Y., et al. 2006: Miocene to Late Quaternary Patagonian basalts (46–47°S): Geochronometric and geochemical evidence for slab tearing due to active spreading ridge subduction. *Journal of Volcanology and Geothermal Research*, 149(3-4), 346-370.
- Gorring, M.L., Kay, S.M., Zeitler, P.K., Ramos, V.A., Rubiolo, D., Fernandez, M.I., Panza, J.L. 1997: Neogene Patagonian plateau lavas: Continental magmas associated with ridge collision at the Chile Triple Junction. *Tectonics*, 16, 1-17.
- Kilian, R., Weigand, O., & Altherr, R. 1997: Tertiary to Quaternary chemical trends of basalts from the Cordillera Baguales (50° S): constraints on the geotectonic evolution of southernmost Andes. VIII Congreso Geológico Chileno.
- Müntener, O. & Ulmer, P. 2006: Experimentally derived high-pressure cumulates from hydrous arc magmas and consequences for the seismic velocity structure of lower arc crust. *Geophysical Research Letters*, 33(21), L21308.
- Pilet, S., Baker, M. B., Müntener, O., & Stolper, E. M. 2011: Monte Carlo Simulations of Metasomatic Enrichment in the Lithosphere and Implications for the Source of Alkaline Basalts. *Journal of Petrology*, 52(7-8), 1415–1442.

P 2.5

Determining the physical processes behind four large eruptions in rapid sequence

Adam Curry¹, Luca Caricchi¹, & Peter Lipman²

¹ Department of Earth Sciences, University of Geneva, Rue des Maraichers 13, CH-1205 Geneva (adam.curry@unige.ch)

² U.S. Geological Survey, 345 Middlefield Road, Menlo Park, California 94025, USA

Large, explosive volcanic eruptions can have both immediate and long-term negative effects on human societies. A primary goal of volcanology is to understand the frequency (f) and magnitude (M) of such events to mitigate their impact on human society. Statistical analyses of volcanic eruptions show that the f - M relationship observed for the largest eruptions on Earth ($> \sim 450 \text{ km}^3$) differs from that observed for smaller eruptions, suggesting different physical processes leading to eruption. Recent studies also show that the average flux of magma (Q_{av}) into a given volcanic-magmatic system fundamentally controls the f and M of volcanic eruptions, yet this parameter is unknown for many volcanic regions on Earth. This project will characterize the petrography, geochemistry, and geochronology of four caldera-forming ignimbrites from the Southern Rocky Mountain volcanic field, Colorado, to determine the physical processes leading to eruption, including the Q_{av} for the system. We collected outflow samples along stratigraphy of the three caldera-forming ignimbrites of the San Luis caldera complex: the Nelson Mountain Tuff ($>500 \text{ km}^3$), Cebolla Creek Tuff ($\sim 250 \text{ km}^3$), and Rat Creek Tuff ($\sim 150 \text{ km}^3$); and we collected samples of both outflow and intracaldera facies of the Snowshoe Mountain Tuff ($>500 \text{ km}^3$), which formed the Creede caldera. Single-crystal sanidine $^{40}\text{Ar}/^{39}\text{Ar}$ ages show that these large eruptions occurred in rapid succession between $26.91 \pm 0.02 \text{ Ma}$ (Rat Creek) and $26.87 \pm 0.02 \text{ Ma}$ (Snowshoe Mountain). This rapid succession of ignimbrite eruptions within the central San Juan caldera cluster provides a unique opportunity to investigate the physical processes leading to large, explosive volcanic eruptions. Our detailed study of whole-rock geochemistry, mineral chemistry, and zircon geochronology of these four ignimbrites will quantify the average rate of magma input (Q_{av}) and the frequency of magma recharge that preceded these eruptions. The results of this study will be used to understand the role of magma flux and periodicity of magma injection in determining the f - M relationship of volcanoes within the central San Juan caldera cluster.

P 2.6

Petrography and mineral chemistry of mantle xenoliths from maars in Cameroon: implications for the nature of the mantle and CO₂ concentrations below the Cameroon Volcanic Line

Siggy Signe Nformidah-Ndah¹, Mélanie Kaba¹, Joelle Flore Tene Djoukam¹, Borba de Carvalho Bruna Maria², Istvan Kovacs³, Edit Kirali³, Jean Pierre Tchouankoue¹, Jörg Hermann⁴

¹ *Department of Earth Sciences, University of Yaounde 1, Yaounde-Cameroon*

² *Department of Geology, Federal University of Pernambuco, Recife-Brazil*

³ *Geological and Geophysical Institute of Hungary, Budapest-Hungary*

⁴ *Institute of Geological Sciences, University of Bern- Switzerland (joerg.hermann@geo.unibe.ch)*

Petrography and mineral chemistry studies of mantle xenoliths from Kuk, Wum and Etome volcanoes (Southern continental part of the Cameroon Volcanic Line) were carried out to better understand the origin of magmatic CO₂ and the nature and the geodynamic environment of the mantle source. Massive CO₂ burst in two maars volcanoes lakes have led to the sudden death of 37 people (Monoun) and 1746 people (Nyos) in 1984 and 1986 respectively, making the study about the mantle source below the Cameroon Volcanic Line particularly relevant.

The studied rocks are spinel lherzolites of protogranular to porphyroclastic textures with olivine (64-75%), orthopyroxene (15-20%), clinopyroxene (8-17%) and spinel (2-3%). Chemically, olivine is forsteritic (88.4-90.8%) and the orthopyroxene has a slightly lower Mg# (85.6-90.0%). Clinopyroxenes show chemical variations in composition; they are diopside and augite with En (37-54%), Wo (42-50%) and Fs (4.4-15.7%). Fluid inclusions occur in clinopyroxene that are aligned along exsolution lamellae and at the rims (Nformidah-Ndah, 2016). Pargasitic amphibole, as observed at Nyos maar mantle xenoliths (Pinter et al., 2015), were not found in the studied xenoliths.

Trace and rare earth elements concentrations in olivines show differences in Sc and Cr (higher in Kuk), Yb, Er and Gd (lower in Kuk). Clinopyroxenes show a continuous trend from higher to lower Al and Na contents that fit the general trend for sub-continental lithospheric mantle. The good correlation between enrichment of Al₂O₃, TiO₂ and Na₂O, provide evidence for metasomatism of the peridotite xenoliths. Trace and rare earth elements for clinopyroxene are generally higher in Etome samples while Th and U values are higher in Wum. Trace element patterns are characterised by a general enrichment in large ion lithophile elements (LILE) except for Ba and light rare earth elements (LREE) relatively to primitive mantle and chondrite values. Nb is depleted with respect to LREE and U, as typical for subduction-related metasomatism. However, Pb and Sr do not show enrichments and thus the nature of the metasomatic agent remains enigmatic.

Petrographical, mineralogical and geochemical characteristics of the studied xenoliths thus indicate that the sub-continental lithospheric mantle below the Cretaceous Cameroon Volcanic Line was metasomatized probably during a Precambrian convergent episode by a fluid phase. This is supported by recent Archean to Paleoproterozoic ages obtained for mantle xenoliths from the Nyos region (Liu et al., 2016). While all samples display clear evidence for a metasomatic addition of some LILE, Th, U and LREE, the origin of the metasomatic imprint is not yet resolved. Nevertheless, our study provides evidence that the Precambrian geodynamics and related metasomatism of the mantle might create a modified subcontinental lithosphere. We suggest that the investigation of this metasomatism will contribute to the better understanding of CO₂ generation below the Cameroon Volcanic Line.

REFERENCES

- Liu C. Z., Yang L.Y., Li X.H., Tchouankoue J.P. (2016). Formation age and Sr-Nd-Hf isotopes of the subcontinental lithospheric mantle beneath the Cameroon Volcanic Line: constraints from the Nyos mantle xenoliths. *Chemical Geology*, in press.
- Nformidah-Ndah Siggy Signe (2016). Mineralogic and fluid inclusion study of mantle xenoliths from Kuk, Wum and Etome (North West Cameroon): implications for CO₂ concentrations. MSc Thesis, University of Yaounde 1, 92 p.
- Pinter Z., Levente Patko L., Tene Djoukam J. F., Kovacs I., Tchouankoue J. P., Falus G., Konc Z., Tommasi A., Barou F., Mihaly J., Nemeth C., Jeffries T. (2015). Characterization of the sub-continental lithospheric mantle beneath the Cameroon volcanic line inferred from alkaline basalt hosted peridotite xenoliths from Barombi Mbo and Nyos Lakes. *Journal of African Earth Sciences*, Vol. 111, 170-193.

P 2.7

The magmatic-hydrothermal transition at the Torres del Paine igneous complex, Chile - first results of an on-going fluid/melt inclusion study

Anne Kaufmann¹, Thomas Pettke¹, Lukas Baumgartner²

¹ *Institute of Geological Sciences, University of Bern, Baltzerstrasse 1+3, CH-3012 Bern (anne.kaufmann@geo.unibe.ch)*

² *Institute of Earth Sciences, University of Lausanne, CH-1015 Lausanne*

The study of coexisting inclusions of multiple fluid phases (aqueous liquid, vapour, salt or silicate melt) allows for direct observation of the partitioning behaviour of elements between residual water-saturated melt and aqueous fluid at the magmatic hydrothermal transition. This stage is decisive for the mass transfer of elements between geological reservoirs and is relevant to ore deposit forming processes.

The Torres del Paine bimodal igneous complex intruded as laccoliths at a depth of 2-3 km (~0.75 kbar) between 12.43 and 12.59 Ma (Leuthold et al. 2013). It is an ideal study area due to the numerous fluid exsolution features exposed in the field area, such as miarolitic cavities as well as pegmatoid and frothy zones, which document hydrothermal processes from 750 °C down to <300 °C as revealed by local occurrence of zeolite minerals. The complex is thus a perfect natural laboratory to investigate processes in shallow subvolcanic magma reservoirs that may ultimately trigger porphyry-type ore (Cu,Mo) deposit formation (e.g. Audétat et al. 2008).

During field work, numerous miarolitic cavities have been found and sampled in the exposed parts of magma-mingled mafic-felsic units, as well as in the lowest granite unit and in fallen blocks of all three granite units. These cavities range in size from mm up to about 1 m, and free-grown minerals are typically in the mm to cm range. The mineral assemblages of the cavities are mainly dominated by free-grown quartz and feldspar, in several cases also featuring a narrow eutectic graphic texture in the transition zone from the cavity into the surrounding rock. A few cavities show a more diverse mineralogy exhibiting also titanite, biotite, needle-shaped amphibole, allanite-epidote and locally various zeolites.

In order to quantify element distribution between residual melt and an exsolving aqueous fluid phase the sequence of inclusion entrapment and the different types of inclusions are characterised in detail using transmitted light microscopy. The studied samples cover several generations of quartz, including unaltered igneous rock, graphic texture, and free-grown crystals in cavities.

Vapour-rich inclusions (Type I) are found throughout all examined samples, while 2-phase vapour-liquid (Type II) and silicate melt (Type VI) inclusions are less common. The latter mostly occur in areas showing graphic texture. Additionally, a large number of inclusions are comprised of several types of brines, all of which are characterised at room temperature by the presence of a vapour bubble and a halite crystal in aqueous liquid (Type III), and many feature additional crystal phases (Type IV). In a few samples 3-phase-fluid inclusions (Type V) containing liquid H₂O, liquid CO₂ and CO₂ at room temperature are also observed.

Very promising for subsequent analysis are inclusion assemblages consisting of more than one type of inclusion. So far several coexisting brine + vapour-rich fluid inclusions ("boiling assemblages"), as well as coexisting silicate melt + aqueous vapour-rich inclusion trails have been identified in the samples from Torres del Paine.

Preliminary microthermometry was done using a Linkham THMS 600 heating freezing stage to obtain temperatures of significant phase transitions in fluid inclusions, which provide bulk salinity data expressed as NaCl_{equivalent} as well as first estimations of entrapment conditions. Preliminary results were obtained from inclusions in smoky quartz of sample TdP04. Type IV brine inclusions exhibit $T_{m,halite}$ at 346 °C, corresponding to 42 wt% NaCl_{eq} (Driesner & Heinrich 2007) - and total homogenisation into the liquid phase at $T_{H,tot}$ of 424 °C, which represents a minimum entrapment temperature. The inclusions also contain a cluster of small black needle-shaped crystals that melt around 355 °C, thus representing most likely daughter crystals.

So far, total homogenisation temperatures for another set of brine inclusions lie outside of the T range (>580 °C) accessible by our microthermometry stage, but they confirm fluid entrapment at high temperatures close to or even at the magmatic-hydrothermal transition.

Future work will include measurements of the chemical composition of inclusions by LA-ICP-MS following procedures documented in Pettke et al. (2012). Coexisting aqueous fluid and hydrous melt inclusions present in assemblages allow for the direct measurement of element distribution coefficients at the magmatic-hydrothermal transition, and entrapment temperatures are obtained from coexisting liquid-vapour fluid inclusion assemblages. Having determined the succession of

inclusion entrapment will then allow the reconstruction of the temporal evolution of melt-fluid chemistry upon cooling in this shallow intrusion.

REFERENCES

- Audétat, A., Pettke, T., Heinrich, C. A. & Bodnar, R. J. 2008: The composition of magmatic-hydrothermal fluids in barren and mineralized intrusions. *Economic Geology* 103, 877-908.
- Driesner, T. & Heinrich, C. A. 2007: The system H₂O-NaCl. Part I: Correlation formulae for phase relations in temperature-pressure-composition space from 0 to 1000 degrees C, 0 to 5000 bar, and 0 to 1 X-NaCl. *Geochimica Et Cosmochimica Acta* 71, 4880-4901.
- Leuthold, J., Müntener, O., Baumgartner, L. P., Putlitz, B. & Chiaradia, M. 2013: A detailed geochemical study of a shallow arc-related laccolith; the Torres del Paine Mafic Complex (Patagonia). *Journal of Petrology* 54, 273-303.
- Pettke, T., Oberli, F., Audétat, A., Guillong, M., Simon, A. C., Hanley, J. J. & Klemm, L. M. 2012: Recent developments in element concentration and isotope ratio analysis of individual fluid inclusions by laser ablation single and multiple collector ICP-MS. *Ore Geology Reviews* 44, 10-38.

P 2.8

Middle Miocene to Quaternary volcanism in NW Iranian Azerbaijan: implications for the evolution of the Turkish-Iranian Plateau from geochemical, isotopic and geochronological data

Anna Katharina Lechmann¹, Jean-Pierre Burg¹, Peter Ulmer², Marcel Guillong², Mohammad Faridi³

¹ *Geological Institute, ETH Zurich, Sonneggstrasse 5, CH-8092 Zurich (anna.lechmann@erdw.ethz.ch)*

² *Institute for Geochemistry and Petrology, ETH Zurich, CH-8092 Zurich, Switzerland*

³ *Geological Survey of Iran, Northwestern Regional Office, IR-5133-4359 Tabriz*

The Turkish-Iranian Plateau, shaped by the northward subduction of the Neo-Tethys Ocean during convergence and subsequent collision between Arabia and Eurasia, is covered over vast areas by Miocene to Quaternary magmatic rocks. Occurrence of Oligocene to lower Miocene limestones, indicating marine conditions across eastern Turkey to central Iran (Reuter et al., 2009), restrict the uplift of the Turkish-Iranian Plateau to be later than ~ 16 Ma (Gelati, 1975, Okay et al., 2010), coinciding with the first occurrence of Neogene volcanism (e.g. Keskin et al., 2006). For Azerbaijan Province in NW Iran, 22 new U-Pb zircon ages show two distinct age clusters, in middle Miocene (~16-10 Ma) and latest Miocene-late Pleistocene (~5.6-0.4 Ma). Samples are calc-alkaline with a wide compositional range, the SiO₂ contents ranging between 48 – 70 wt%. The rocks are commonly Na-rich (Na₂O 2-7.5 wt%) and show a large variety in K₂O content (0.4-7 wt%), plotting in low-K to high-K and shoshonitic fields. Plots of primitive mantle normalized trace elements systematically show negative Nb-Ta and Ti anomalies, indicating a subduction-modified component in the mantle source and/or crustal contamination (Pearce and Peate, 1995). These positive anomalies are less distinct in Quaternary samples. Very steep negative LREE patterns that flatten into a spoon-shaped, strongly depleted HREE pattern indicate the presence of garnet (± amphibole) in the source region or during fractionation. Some samples have adakite compositions as defined by Defant and Drummond (1990) and Martin et al. (2005). Adakitic melts can be produced as primary melts from direct slab melting or from a common andesitic primary melt travelling through the mantle wedge and experiencing high-pressure garnet fractionation. 7 representative rock powders have been analyzed for Sr, Nd and Pb isotopic compositions. ⁸⁷Sr/⁸⁶Sr values vary between 0.704802 and 0.708743, ²⁰⁶Pb/²⁰⁴Pb and ²⁰⁷Pb/²⁰⁴Pb values between 18.8512 and 19.0694 and 15.6557 and 15.7026, respectively. All analyzed samples show lower to upper crustal compositions. The adakitic samples should exhibit a depleted mantle (DM) or MORB-like signature if they were derived from primary slab melts. The presence of numerous small patched lava flows with a wide range in composition, the ubiquitous subduction zone signature, the lack of an age and geographic correlation in the field area and the compositions with a highly depleted HREE pattern typical for deep melting indicate that a heterogeneously metasomatized mantle produced small amounts of melts. Those experienced small to higher degrees of crustal contamination on their way up into the crust.

This work is supported by SNF Research Grant (project 200021_153124/1).

REFERENCES

- Defant, M. J., Drummond, M. S., 1990. Derivation of some modern arc magmas by melting of young subducted lithosphere. *Nature* 347, 662-665.
- Gelati, R., 1975. Miocene marine sequence from the Lake Van area, eastern Turkey. *Rivista Italiana di Paleontologia e Stratigrafia* 81, 477-490.
- Keskin, M., Pearce, J. A., Kempton, P. D., Greenwood, P., 2006. Magma-crust interaction and magma plumbing in a postcollisional setting: Geochemical evidence from the Erzurum-Kars volcanic plateau, eastern Turkey. *Geological Society of America Special Paper* 409, 475-505.
- Martin, H., Smithies, R. H., Rapp, R., Moyen, J.-F., Champion, D., 2005. An overview of adakite, tonalite-trondhjemite-granodiorite (TTG), and sanukitoid: relationships and some implications for crustal evolution. *Lithos* 79, 1-24.
- Okay, A., Zattin, M., Cavazza, W., 2010. Apatite fission-track data for the Miocene Arabia-Eurasia collision. *Geology* 38, 35-38.
- Pearce, J. A., Peate, D. W., 1995. Tectonic implications of the composition of volcanic arc magmas. *Annual Review of Earth and Planetary Sciences* 23, 251-285.
- Reuter, M., Piller, W. E., Harzhauser, M., Mandic, O., Berning, B., Rögl, F., Kroh, A., Aubry, M.-P., Wielandt-Schuster, U., Hamedani, A., 2009. The Oligo-/Miocene Qom formation (Iran): evidence for an early Burdigalian restriction of the Tethyan Seaway and closure of its Iranian gateways. *International Journal of Earth Sciences* 98, 627-650.

P 2.9

Mafic dyke swarms in global geodynamics: Examples from Singhbhum and Bastar cratons, India

Om Prakash Pandey¹, Klaus Mezger¹, Dewashish Upadhyay²,
Ajay Kumar Singh², Alessandro Maltese¹

¹ *Institute of Geological Sciences, University of Bern, Baltzerstrasse 1+3, CH-3012 Bern* (om.pandey@geo.unibe.ch)

² *Department of Geology and Geophysics, Indian Institute of Technology, Kharagpur, India*

The emplacement of mafic dyke swarms has been a common occurrence at least in the last 3 billion years of Earth's history. Such dyke swarms are observed on all continents. The dykes are largely of basaltic composition, occur as straight lineaments that can be several hundred kilometres long and are generally unaltered and unmetamorphosed, which makes them ideal for geophysical and geochemical studies (Halls 1982). These extensive basaltic magmatic intrusions commonly cut across all pre-existing geologic heterogeneities and thus can be used to reconstruct the formation and destruction of supercontinents through geologic time (e.g. Ernst et al. 2016) if they can be correlated between now separated continental fragments. There is a general acceptance that dykes are the result of rifting or at least some degree of crustal extension. The attitude of a dyke is controlled by the regional stress field. As a consequence, dykes may have a common orientation in a direction normal to the regional minimum principal stress (Anderson 1951).

The Archean Indian cratons have experienced mafic magmatism spanning from early Archean to Proterozoic, but due to scarcity of high quality isotopic age data, the history of the spatial growth of the cratons is not well established in which mafic magmatism has played a very crucial role (Bose 2009). Mafic magmatism in the Singhbhum craton spreads from ca. 3.3 Gyr old orthoamphibolite enclaves to younger dolerite dyke swarms (Bose 2009). These spectacular dyke swarms are known as 'Newer Dolerites' and occur in at least four distinct strike patterns, NE-SW, NW-SE, NNE-SSW and WNW-ESE and are readily visible in satellite images due to their large extent. The Bastar craton also has a history of episodic mafic magmatism spanning the Precambrian which is evidenced by exposed mafic volcanic masses and dykes in the craton. The Bastar Craton has at least three distinct mafic dyke swarms of Precambrian age (Srivastava & Gautam 2009). In order to describe the origin of these dykes high quality bulk rock geochemical data are required.

A total of 12 dykes from the Singhbhum craton were sampled covering almost all major mafic dykes of all strike trends. Six samples from the Bastar craton were collected from two dyke swarms trending NW-SE (prominent) and ENE-WSW. Bulk rock geochemical data shows that these rocks are of alkaline basaltic nature evolved from heterogeneous source. The trace element abundances indicate an origin by low degrees of melting possibly in a mantle plume. This implies that the cause of dyke emplacement is due to mantle upwelling rather than melting of upper mantle material due to crustal extension.

REFERENCES

- Anderson, E.M. 1951: The dynamics of faulting and dyke formation with application to Britain: London, England, Oliver and Boyd Ltd., 206.
- Bose, M.K. 2009: Precambrian mafic magmatism in the Singhbhum craton, eastern India, *Journal Geological Society of India*, 73, 13-35.
- Ernst, R.E., Hamilton, M.A., Söderlund, U., Hanes, J.A., Gladkochub, D.P., Okrugin, A.V., Kolotilina, T., Mekhonoshin, A.S., Bleeker, W., LeCheminant, Buchan, K.L., Chamberlin, K.R., Didenko, A.N. 2016: Long-lived connection between southern Siberia and northern Laurentia in the Proterozoic, *Nature Geoscience*, 9, 464–470.
- Halls, H.C. 1982: The Importance and Potential of Mafic Dyke Swarms in Studies of Geodynamic Processes, *Geoscience Canada*, 9, 3, 145-154.
- Srivastava, R.K., Gautam, G.C. 2009: Precambrian Mafic Magmatism in the Bastar Craton, Central India, *Journal Geological Society of India*, 73, 52-72.

P 2.10

Temporal variations of mineral chemistry during the 2014-2015 Holuhraun-Bárðarbunga eruption

Line Probst¹, Laura Pioli¹, Eniko Bali², Guy Simpson¹ & Luca Caricchi¹

¹ *Department of Earth Sciences, University of Geneva, Geneva, Switzerland*

² *Institute of Earth Sciences, University of Iceland, Reykjavík*

The Holuhraun-Bárðarbunga eruption is the largest lava flow produced in Iceland since the 1783-1784 Laki eruption. The eruption started at the end of August 2014 and lasted until the end of February 2015, releasing >1.5 km³ of magma. The eruption was associated with the synchronous progressive collapse of the Bárðarbunga caldera, which is located about 50 km from the fracture that released the magma. Geophysical and geochemical data suggest that volcanic activity was fed by the lateral migration of magma originating from the plumbing system of the Bárðarbunga volcano.

The lava field covers a total surface of about 85 km² and several lobes were produced at different times during the eruption. In September 2015 we collected samples from the lobes emplaced at different times during the eruption. The series was completed with samples collected at the onset of the eruption to obtain a full set of specimens representative of the entire duration of the eruption. Existing geochemical data show no geochemical variation of the whole rock composition of the samples during the eruption.

We performed a detailed petrographic investigation of the mineral phases present in the sample focusing on clinopyroxenes. Clinopyroxenes show distinct oscillatory zoning and electron microprobe analyses show that they are divided in two main populations with distinct trends of Cr₂O₃ vs MgO content. The test for equilibrium based on Fe-Mg partitioning between groundmass glass and clinopyroxene shows that the most mafic clinopyroxene compositions are not in equilibrium with the carrier liquid.

To establish whether the variation of the relative proportions or chemistry of the two main groups of pyroxenes are statistically significant, we are currently performing a study using the cross correlation of chemical profiles and images collected on the clinopyroxenes. The results of this study may highlight the processes occurring during the progressive drainage of magma from crustal magma reservoirs.

P 2.11

The role of crustal melting in the formation of rhyolites: constraints from SIMS oxygen isotope data (Chon Aike Province, Patagonia)

Susanne Seitz¹, Benita Putlitz¹, Lukas Baumgartner¹ & Anne-Sophie Bouvier¹

¹ *Institute of Earth Sciences, University Lausanne, CH-1015 Lausanne*

The origin of silica-rich magmas remains an important topic in igneous petrology. Here we report on a suite of Jurassic rhyolites (El Quemado Complex) in Patagonia. We use the oxygen composition of quartz and zircon - both from SIMS and laser fluorination analysis - to have a new look at the role of crustal contributions to the production of these silicic volcanics. The El Quemado Complex belongs to the Chon Aike Province, one of the largest - yet little explored - silicic igneous provinces known (Bryan & Ferrari 2013).

The studied rhyolites and ignimbrites are peraluminous in character and show a high $\delta^{18}\text{O}$ signature for both zircon (7.5‰ to 10.1‰) and quartz (10.8‰ to 12.5‰). This requires a significant contribution of supra-crustal (i.e., sedimentary or pelitic) material during rhyolite formation - a suggestion that contrasts with previous works (Pankhurst & Rapela 1995; Riley et al. 2001), arguing for smaller (< 20%) contribution from a mafic lower crust.

Another key observation is that zircon and quartz are not in high temperature (magmatic) isotopic equilibrium. It is then usually assumed that quartz has been reset due to late stage alteration processes (King et al. 1997). To verify this assumption, we carried out a series of SIMS profiles across several quartz phenocrysts, which showed magmatic cathodoluminescence zoning. The investigated profiles are mostly flat and pronounced enrichment along cracks - as expected for altered grains - are not evident. The SIMS data thus illustrate that the ^{18}O composition of quartz is not influenced by secondary alteration (in this case). This is true even for highly altered samples with high $\delta^{18}\text{O}$ whole rock values around 15‰; here the matrix and feldspar is replaced by carbonate minerals.

We also observe a large ^{18}O variation in zircon within single samples (up to 2.6‰) indicating either a heterogeneous source, an assembly of isolated magma batches or extraction of zircons together with interstitial melt from a crustal mush. We recognize that widespread crustal anatexis seems difficult to achieve due to the high thermal energy required, yet our data support partial melting of ^{18}O -rich crust to form the El Quemado rhyolites, probably reflecting the large-scale lower crustal reworking associated with the special tectonic and igneous setting of the Gondwana break-up (Mpodozis & Ramos 2008).

REFERENCES

- Bryan, S.E., Ferrari, L., 2013. Large igneous provinces and silicic large igneous provinces: Progress in our understanding over the last 25 years. *Geological Society of America Bulletin* 125 (7-8), 1053–1078.
- King, E.M., Barrie, C.T., Valley, J.W., 1997. Hydrothermal alteration of oxygen isotope ratios in quartz phenocrysts, Kidd Creek mine, Ontario: magmatic values are preserved in zircon. *Geology* 25 (12), 1079–1082.
- Mpodozis, C., Ramos, V.A., 2008. Tectónica Jurásica en Argentina y Chile: extensión, subducción oblicua, rifting, deriva y colisiones? *Revista de la Asociación Geológica Argentina* 63, 481–497.
- Pankhurst, R.J., Rapela, C.R., 1995. Production of Jurassic rhyolite by anatexis of the lower crust of Patagonia. *Earth and Planetary Sciences Letters* 134, 23–36.
- Riley, T.R., Leat, P.T., Pankhurst, R.J., Harris, C., 2001. Origins of large volume rhyolitic volcanism in the Antarctic Peninsula and Patagonia by crustal melting. *Journal of Petrology* 42 (6), 1043–1065.

P 2.12

A new volcanic map of the Semail Ophiolite, Oman using a combined field, geochemical and aeromagnetic approach

Thomas M. Belgrano¹, Larryn W. Diamond¹, Yves Vogt¹, Samuel A. Gilgen¹, Alannah Brett¹, Khalid Al-Tobi²

¹ Rock-Water Interaction Group, Institute of Geological Sciences, University of Bern, Baltzerstrasse 3, CH-3012 Bern, Switzerland (thomas.belgrano@geo.unibe.ch)

² Earth Secrets, P.O. Box 1242, PC 130 Athaibah, Muscat, Sultanate of Oman

The Oman Ophiolite provides the world's best surface exposure of the transition from axial-spreading to depleted-forearc seafloor volcanism. Previous petrologic studies have subdivided the lavas into axial, seamount, depleted forearc, and boninitic units (Alabaster et al. 1982; Ishikawa et al. 2002). However, current geological maps only differentiate two regionally occurring volcanic units. In light of the recent recognition of the volcanostratigraphic controls on VMS mineralisation (Gilgen et al. 2014), as well as debate on the tectonic setting of each magmatic phase, we have updated the existing maps to the stratigraphy defined by Gilgen et al. (2014; Fig. 1). We collected 103 rock samples and geochemically assigned each of them to one of the four recognized units using whole-rock XRF and ICP-MS and microprobe analyses of clinopyroxenes. In doing so we refined the lava discrimination parameters to be consistent and effective over the entire Ophiolite.

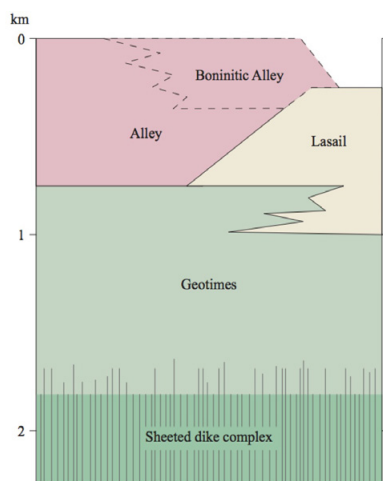


Figure 1. Volcanostratigraphy of the Semail Ophiolite after Gilgen et al. (2014)

We found that the extent of boninites is far greater than previously known, and that Lasail lavas intercalated deep in the Geotimes unit have a clear subduction component, showing that axial magmatism took place above a subduction zone. Furthermore, at certain sites we were able to correlate units with aeromagnetic features, allowing us to infer the presence of lava units under sedimentary cover. Considering that six of the recent VMS discoveries were buried deposits, our inferences should prove helpful for evaluating prospectivity and tracing potential ore horizons under the recent wadi gravels.

REFERENCES

- Alabaster, T., Pearce, J. A., & Malpas, J. 1982: The volcanic stratigraphy and petrogenesis of the Oman ophiolite complex, *Contributions to Mineralogy and Petrology*, 81, 168–183.
- Gilgen, S. A., Diamond, L. W., Mercolli, I., Al-Tobi, K., Maidment, D. W., Close, R., & Al-Towaya, A. 2014: Volcanostratigraphic Controls on the Occurrence of Massive Sulfide Deposits in the Semail Ophiolite, Oman, *Economic Geology*, 109, 1585–1610.
- Ishikawa, T., Nagaishi, K., & Umino, S. 2002: Boninitic volcanism in the Oman ophiolite: Implications for thermal condition during transition from spreading ridge to arc, *Geology*, 30, 899–9

P 2.13

Historical Iron smelting in Kaniasso, Ivory Coast: technological change and exchange at Siola and Doumbala

Madalina Bonta¹, Vincent Serneels¹

¹ Department of Geosciences, University of Fribourg, Chemin du Musée 6, CH-1700 Fribourg (madalina.bonta@unifr.ch)

The historical development of iron metallurgy has a special significance in West Africa. In the frame of the project “Origin and development of iron metallurgy in Burkina Faso and Ivory Coast”, the present study, which is ongoing, aims to study the remains excavated during the two field campaigns in 2013 (Siola) and 2015 (Doumbala).

Up to 1,000 years of iron smelting relics – slag heaps and furnaces – were discovered in the metallurgical region of Kaniasso, north-western Ivory Coast, marking a continuous commitment in this direction. Smelting, which is an essential step in obtaining iron metal for use in agriculture or defence, is the process where Fe³⁺ is reduced to metallic Fe within special furnaces, at high temperatures (of up to 1400° C), and in controlled atmospheres (subject to a prominent air supply). The samples (ores, slag and technical ceramics) were analysed in Fribourg for geochemistry (XRF with LOI corrections) and mineralogy (XRD and optical microscopy).

The series of techniques of both sites are comparable and demonstrate continuous exchange. The oldest technology, KAN 1 (small scale, mostly tapped slag) first appears in Siola (990 AD) and is borrowed in Doumbala. At the same time around 1450 AD, the technique is changed abruptly and simultaneously at Doumbala and Siola, for KAN 2 (a larger scale technology resulting exclusively in internal slag). 3 or 400 years later, KAN 2 of Siola is upgraded to KAN 3 (similar concept, larger scale), which is lent to Doumbala in the 18th century.

Different chemical and mineralogical compositions of the material demonstrate variability in the raw material sourcing and the *chaîne opératoire*. The ore is multiply sourced (« Fe-rich », « Fe-poor and Mn-rich », and « Fe-, Al-, and Ti-poor ») and suggests elaborate recipes of mixing. The slag marks variability in terms of resulting iron yields (KAN 3 the highest), lost iron in the process (KAN 2 the most economical), and the amount of reduction of Fe³⁺ to Fe²⁺ (KAN 2 the weakest).

The aim is to explore the variability between technologies KAN 1-2-3 in the two sites of Siola and Doumbala, its triggers, and its spread.

The project “The origin and development of iron metallurgy in Burkina Faso and Ivory Coast”, is funded by the Swiss-Liechtenstein Foundation for Archaeological Research Abroad (SLSA) and is supported by the Universities of Abidjan, Ouagadougou, and Fribourg.

P 2.14

EIBema-East Taourir granite (Hoggar central-Algeria) : RMG or not RMG

Chalal Youcef¹ and Lerari Nadjah

¹ Houari Boumediene Univeristy Algiers Algeria (Chalalyoucef@hotmail.com)

The granitic massif of EIBema-east is a particular granite, it belongs to the family of the so-called granites 'Taourirt' "Pan-African age (539-523 Ma) in the Tuareg Shield. The 'Taourirt' granites have been defined by Boissonnas, 1973 and Azzouni and al, 2003, they split into three groups based on their location (figure-1)

- Group I, of Silet: all granites are located to the West of 4° 50' shearzone
- Group II, of Laouni
- Group III of Tamanrasset.

The Groups II and III are located in the same Terrane 'Laouni' and are for many of them associated with the Sn -W (Ta-Nb) mineralization. While the granites of the first group are sterile (metallogenic sens) in their majority with the only one exception of the small group EIBema-AitOklane. These two massifs of AitOklane and Elbema show a mineralization essentially stanniferous (cassiterite) of vein morphology. The massif of Elbema-East is formed by three granitic facies

- granite type coarse to biotite leucogranite, it forms most of the massif
- similar gray granite and finer grain
- leucogranite with albite

Geochemical data of these granites show similarities with granites of RMG type with SiO₂ (74.46 - 76, 56%) levels and aluminous nature (Al₂O₃ (12, 54-13, 68) sodic with Na₂O (3, 5-2, 3). They are poor in P₂O₅.

Analyses to the microprobe of an opaque minerals in granites of EIBema and AitOklane has shown that these are special ilmenites by their composition rich in Manganese and Nb can permit rapprochement with the GMR

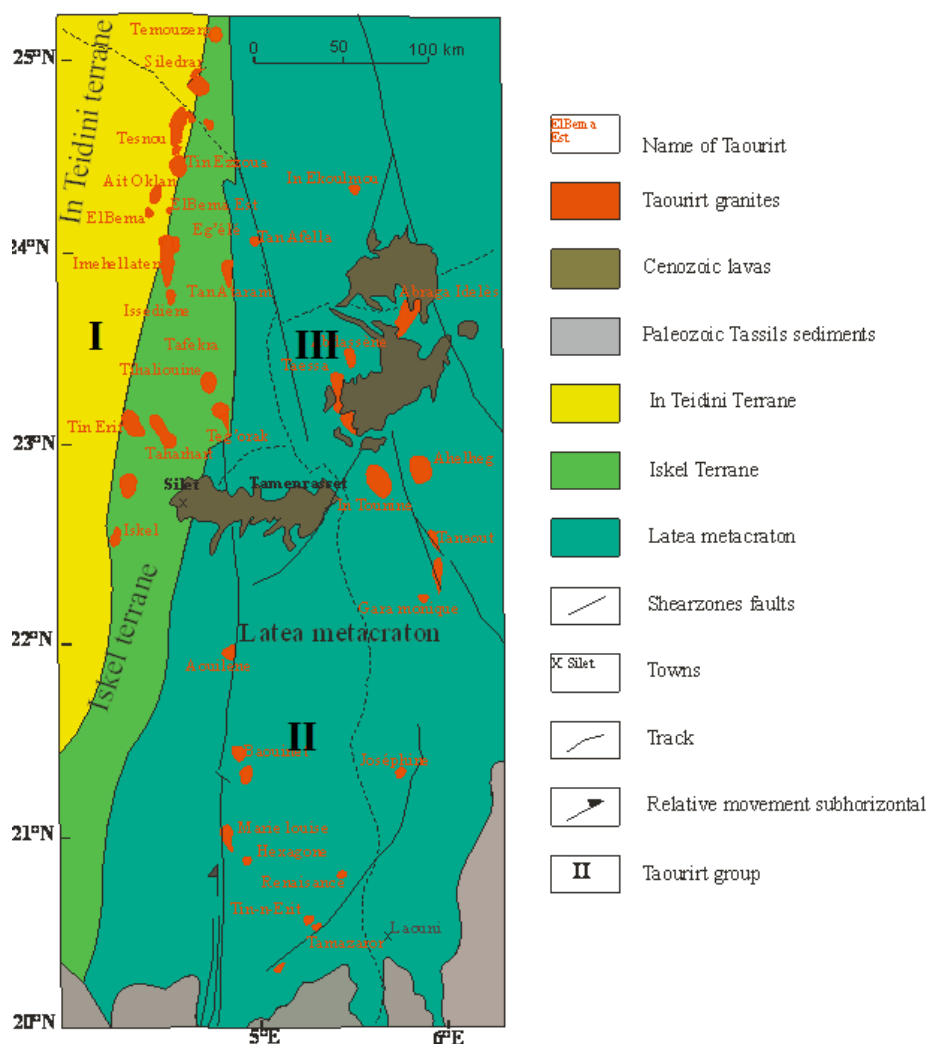


Figure 1- Taourirt plutons in the Central Hoggar with localization of the three groups and EIBema-AitOklane zone

P 2.15

Metal geochemistry and Cu-Zn isotope compositions of volcanic gas condensates and volcanic rocks: Vulcano Island, Italy

Núria Pujol Solà¹, Massimo Chairadia¹, Alessandro Aiuppa², Antonio Paonita² & Andrea Rizzo²

¹ *Department of Earth Sciences, Faculty of Earth and Environmental Sciences, University of Geneva, Rue des Maraichers, 13, 1205 Geneva, Switzerland (nurpss@gmail.com)*

² *Istituto Nazionale di Geofisica e Vulcanologia – Palermo, Italy.*

Cu and Zn isotope compositions have been measured by multiple collector inductively coupled plasma-mass spectrometry (MC-ICP-MS) for:

- a) Volcanic rocks representing various degrees of evolution within the high-potassium calc-alkaline and shoshonitic series of Vulcano Island (Aeolian Island Arc, Italy).
- b) Gas condensates and altered rocks from the fumaroles of La Fossa Cone (active magmatic-hydrothermal system in Vulcano Island).

The main goal was to investigate whether Cu and Zn isotope fractionation occurred during magma evolution and during the transfer of these metals from the magma to the fluids in the active system of Vulcano. Petrographic, major and trace elements whole-rock compositions, mineral chemistry, and radiogenic isotope studies have also been performed to establish the petrogenetic frame inside which interpretation of Cu and Zn isotope data could be carried out.

For Cu and Zn isotope compositions, different chromatographic purification methods were tested but the method developed by Maréchal et al. (1999) has been followed with two purification columns for Cu and one for Zn because it gave the best results in terms of purification and hence the minimal interferences. Standard bracketing correction was used for both elements. Due to incomplete purification and multiple polyatomic interferences, in-run correction was applied for Zn analyses but not for Cu analyses, because Ti-oxides and Ti-hydroxides interferences at several Zn atomic masses prevented the use of Zn for internal normalization.

Results for fresh volcanic rocks range between $-0.579 \pm 0.133\%$ and $+0.595 \pm 0.890\%$ for $\delta^{65}\text{Cu}$ and between $+0.059 \pm 0.106\%$ and $+1.145 \pm 0.101\%$ for $\delta^{68}\text{Zn}$. Variations within uncertainties are not observed for Cu isotopes, but Zn isotope variability is beyond analytical uncertainty and could reflect processes of magmatic differentiation. The main factor responsible of the observed variations is a source effect related to recycling of subducted crust.

Results for the high-temperature fumarolic field of La Fossa generally show higher $\delta^{65}\text{Cu}$ values for gas condensates than for altered rocks, and lower $\delta^{68}\text{Zn}$ for gas condensates than for altered rocks. These results can be explained by evaporation/condensation processes occurring at different levels of the magmatic-hydrothermal plumbing system of Vulcano: (i) equilibrium fractionation at surface levels and (ii) kinetic fractionation (precipitation) during gas ascent. Cu isotopes reflect the kinetic fractionation occurring during gas ascent and for this reason present heavier $\delta^{65}\text{Cu}$ in the measured gas phase because during kinetic reactions the lighter isotopes are incorporated preferentially into the reaction products. $\delta^{68}\text{Zn}$ values are mainly affected by equilibrium fractionation at surface levels, therefore, the gas phase is enriched in the lighter isotopes because the heavier isotopes are preferentially incorporated into the solid phase during equilibrium reactions. The different behaviors of the two metals are related to their different solubilities with respect to temperature (higher solubility for Zn than for Cu at a given temperature), so that, within the fumarole temperatures range (98–427°C), Cu tends to precipitate during gas ascent (at higher temperature) while Zn tends to remain in the solution and precipitate only near the surface at lower temperature. This explains the different concentrations of Cu (0.065–3.582 ppm) and Zn (28.0–2859 ppm) measured on the gas condensates.

REFERENCES

Maréchal, C.N., Telouk, P. & Albarede, F. 1999: Precise analysis of copper and zinc isotopic compositions by plasma-source mass spectrometry. *Chemical Geology*, 156, 251–273.

P 2.16

Protocol for Be analysis by LA-ICP-MS and Be distribution in some olivine- and pyroxene-bearing rocks

Michael C. Jollands¹, Alexey Ulianov¹ & Othmar Müntener¹

¹ *Institute of Earth Sciences, University of Lausanne*

Determining extremely low concentrations of trace elements in minerals *in situ* is a constant challenge in analytical geochemistry. When such trace elements are present only at the parts per billion or trillion levels, they may fall below detection limits of conventional methods, and hence be excluded from consideration. Beryllium (Be) is one such element. For example, beryllium, when at $> \mu\text{g g}^{-1}$ levels, has been a useful tool for understanding the nature of fluids released from subducting slabs (e.g. Johnson and Plank 1999, Pacquin et al 2004). Be diffusion profiles in olivine have potential to yield timescales of magmatic processes, without the complications of needing to constrain oxygen and water fugacities (Jollands et al, 2016). However, the behaviour of Be in mantle and lower crustal minerals is generally very poorly understood. We have thus developed a protocol for Be analyses using laser ablation inductively coupled plasma mass spectrometry (LA-ICP-MS). We show that this can have similar detection limits to ion probe techniques (albeit with poorer spatial resolution), which are more commonly used (e.g. Marschall et al., 2006) but has the advantages of much faster data acquisition and simpler sample preparation.

Signal enhancement (and background reduction) protocols were developed using both a sector field ICP-MS (Thermo Element XR) and a quadrupole (Agilent 7700) coupled to similar 193 nm excimer lasers, with hydrogen or nitrogen bled into the central gas flow (following Guillong and Heinrich, 2007; Hu et al., 2008).

By systematically varying the carrier gas flow and that of H_2 , sensitivity enhancements of up to 40 x from a base level (i.e. normal, non-specific tuning) have been achieved. Nitrogen has a lesser effect on signal enhancement, but is effective at reducing a surprisingly high background interference from $^{18}\text{O}^{++}$, which appears on the sector field instrument but not the quadrupole. In addition, using an X-type skimmer cone (rather than H-type) both increases the sensitivity and changes the response of the ICP-MS to H_2 or N_2 addition.

The best detection limits so far are obtained using the sector field instrument with sample gas flowing at $0.85\text{-}0.9 \text{ L min}^{-1}$, H_2 at $12\text{-}16 \text{ mL min}^{-1}$, with an X type cone. Coupled with only moderate laser ablation settings ($75 \mu\text{m}$ spot, 5 Hz, $\sim 8 \text{ J cm}^{-2}$ fluence), this technique gives $>400,000$ cps on NIST SRM 612 glass ($\sim 40 \mu\text{g g}^{-1}$ Be).

To show the potential of the new protocol, a variety of minerals from olivine and/or pyroxene bearing rocks, plus some other mineralogical samples were then analysed for their Be contents and inter- and intra-crystalline distributions.

REFERENCES

- Guillong, M., & Heinrich, C. A. 2007. Sensitivity enhancement in laser ablation ICP-MS using small amounts of hydrogen in the carrier gas. *Journal of Analytical Atomic Spectrometry*, 22, 1488-1494.
- Hu, Z., Gao, S., Liu, Y., Hu, S., Chen, H., & Yuan, H. 2008. Signal enhancement in laser ablation ICP-MS by addition of nitrogen in the central channel gas. *Journal of Analytical Atomic Spectrometry*, 23, 1093-1101.
- Johnson, M. C., & Plank, T. 2000. Dehydration and melting experiments constrain the fate of subducted sediments. *Geochemistry, Geophysics, Geosystems*, 1.
- Marschall, H. R., Altherr, R., Ludwig, T., Kalt, A., Gméling, K., & Kasztovszky, Z. 2006. Partitioning and budget of Li, Be and B in high-pressure metamorphic rocks. *Geochimica et Cosmochimica Acta*, 70, 4750-4769.
- Paquin, J., Altherr, R., & Ludwig, T. 2004. Li-Be-B systematics in the ultrahigh-pressure garnet peridotite from Alpe Arami (Central Swiss Alps): implications for slab-to-mantle wedge transfer. *Earth and Planetary Science Letters*, 216, 507-519.

P 2.17

Geochemistry and Cu, Zn isotope composition of volcanic rocks in Stromboli Island, Italy

Júlia Farré de Pablo¹, Massimo Chiaradia¹, Andrea Rizzo² & Patrizia Landi³

¹ *Department of Earth Sciences, Faculty of Earth and Environmental Sciences, University of Geneva, Rue des Maraîches 13, CH-1205 Geneva (jfarrededepablo@gmail.com)*

² *Istituto Nazionale di Geofisica e Vulcanologia, Sezione di Palermo, Palermo, Italy*

³ *Istituto Nazionale di Geofisica e Vulcanologia, 32 Via della Faggiola, 56126 Pisa, Italy*

Volcanic rocks from Stromboli volcano (Italy) were investigated in order to determine the processes the different magmas that have been feeding the volcano underwent, and to perform whole rock copper (Cu) and zinc (Zn) isotope analyses on the rocks. By first characterizing the magmas, it is possible to study the behaviour of Cu and Zn isotopes during magmatic processes and assess the potential of this isotopic system in tracing metal degassing processes. The samples from this study correspond to basalts and basaltic-andesites from the different Eruptive Epochs along Stromboli eruptive history, and represent the different magmatic series produced by the volcano: calc-alkaline (CA), high-K calc-alkaline (HKCA), shoshonitic (SHO), and potassic-alkaline (KS). Petrographic and geochemical studies have been performed on them, showing that open-system magmatic processes are widespread along the history of the volcano with some crustal contributions in some cases. Degassing processes occur in the present-day activity. From whole rock geochemistry, compatible behaviour is attributed to Cu and Zn elements during magmatic differentiation, showing a decrease of these elements content with increase of silica. However, Zn displays incompatible behaviour when studied along clinopyroxene phenocrysts.

Regarding Cu and Zn isotope analyses, the samples were prepared following the purification protocol for ion-exchange chromatography defined by Maréchal et al. (1999). Only one column of purification ion-exchange chromatography was used for chemical Zn isolation and two columns were used for Cu. The purified samples were measured on a Neptune PLUS MC-ICP-MS applying standard bracketing and external normalization corrections in the case of Zn and only standard bracketing correction in the case of Cu (to correct the mass bias of the machine). Purification was better achieved for Zn preparation, whereas Cu analyses still presented interferences from the matrix of the rocks, especially Na. The Cu and Zn isotopic compositions of the investigated samples of Stromboli are from $-0.212 \pm 0.063\text{‰}$ (2σ) and $0.456 \pm 0.387\text{‰}$ (2σ) for $\delta^{65}\text{Cu}$, and from $0.113 \pm 0.144\text{‰}$ (2σ) to $0.299 \pm 0.147\text{‰}$ (2σ) for $\delta^{68}\text{Zn}$. The values of the different units overlap in both cases. Cu isotope compositions seem to reflect fractionation towards heavier values with increasing magmatic differentiation, especially in the case of samples from present-day volcanic activity. This is attributed to fractionation of minerals introducing Cu in their structure, mainly sulphides. Zn isotope values of the samples do not show fractionation with magma fractionation. The effect of magmatic degassing is not reflected either on the $\delta^{68}\text{Zn}$ value of the residual magma relative to the volatile-rich one. On the other hand, the effect of a heterogeneous mantle source on the Cu and Zn isotope composition of volcanic rocks seems to be reflected on the variable $\delta^{65}\text{Cu}$ and $\delta^{68}\text{Zn}$ values observed among samples from Stromboli and Vulcano Island (Italy).

REFERENCES

Maréchal, C.N., Telouk, P., and Albarède, F. (1999). Precise analysis of copper and zinc isotopic compositions by plasma-source mass spectrometry. *Chem. Geol.* 156: 251–273.

P 2.18

Construction, architecture and evolution of the plumbing system of Nevado de Toluca volcano (Mexico)

Gregor Weber¹, Line Probst¹, Urs Schaltegger¹, José L. Arce², Luca Caricchi¹

¹ *Department of Earth Sciences, University of Geneva, Rue des Maraîchers 13, 1205 Geneva (Gregor.Weber@unige.ch)*

² *Departamento de Geología Regional, Instituto de Geología, UNAM, Cd. Universitaria, Coyoacán, México D.F., 04510, Mexico*

The factors that control the frequency, magnitude and style of volcanic eruptions can be linked to the physico-chemical properties of magmas, as well as to geodynamic processes, and crustal properties. However, our ability to forecast the recurrence rate and style of eruptions is veiled by the lack of data on key factors controlling the inner workings of magmatic systems.

Nevado de Toluca volcano in Mexico is a subduction-related volcano with an eruptive history spanning about 1.5 million years. Its activity is characterised by dacitic lava flows, and it is punctuated by explosive eruptions of up to 8 km³ in volume, making Nevado de Toluca an excellent laboratory to study the factors controlling the transition from effusive to explosive eruptions.

We collected samples spanning the entire eruptive history of the volcano and we will initially focus on the study of the largest eruption (12.5 ka) and two eruptions preceding and following this large volcanic event.

Detailed petrography, major and trace element geochemistry will be combined with in-situ high precision U-Th disequilibria dating and trace element analysis of zircon crystals, and cross correlation of chemical profiles in minerals. Zircon geochronology will be used to calculate average magma fluxes for eruptions of different magnitudes (Caricchi et al., 2014) while mineral chemistry will provide quantitative insights on the frequency at which intensive parameters changed within the magma reservoir before the eruptions.

Our results will be integrated in a global database including other volcanic systems and literature data to attempt to identify similarities and differences between magmatic reservoirs feeding volcanic eruptions of different magnitude. The final target of this project is to identify the physical factors controlling the recurrence rate of volcanic eruptions at regional and global scale.

REFERENCES

Caricchi, L., Simpson, G., & Schaltegger, U. 2014: Zircons reveal magma fluxes in the Earth's crust, *Nature* 511.7510, 457-461.

P 2.19

Field, Mineralogical and Petrographical Characteristics of the Ladakh Batholith in NW India

Azimuddin Mirza, Nurdane Ilbeyli

Department of Geological Engineering, Akdeniz University, Antalya 07058 Turkey (azimmirza786@gmail.com)

The Himalayan Mountain is a unique example of young continent-continent collision and the contradiction about ages has attracted the attention of geoscientist from all over the world. The Ladakh Batholith is located in the Trans-Himalayan Plutonic Belt (Fig. 1). The batholith has a Cretaceous-Paleogene in age and having Andean-type arc characteristics. It is bounded by the Indus suture zone in the south, the Shyok suture zone in the north and the Karakoram fault in the east. The Ladakh Batholith occurs as a linear body (Fig. 1) measuring about 600 km long and 25-75 km wide covers a major part of the Ladakh range (NW India). We have mainly focused on the mineralogy and petrography of the studied area which is located in westside of Leh district of Ladakh region.

The Ladakh Batholith is mainly composed of biotite granodiorite, hornblende granodiorite, quartz granodiorite, leucogranite, biotite-hornblende granite and hornblende biotite monzodiorite. The rocks are mainly medium- to coarse-grained and occasionally porphyritic with feldspar.

Main minerals of the studied rocks are alkali feldspar, plagioclase, quartz, biotite and hornblende. The accessory minerals of them are apatite, zircon, titanite, monazite, allanite, microcline, rutile, and opaque minerals. Secondary minerals are mainly chlorite, sericite, epidote, muscovite and clay minerals. Alkali feldspars are present in megacrysts with simple twinning. They have perthitic textures and having inclusions of biotite and plagioclase. Plagioclases have polysynthetic twinning and also dusty appearances due to sericite and clay minerals. They also show complex zoning (i.e. oscillatory). Quartz is anhedral showing that it occurred as a late mineral. Alkali feldspar, plagioclase and also quartz display intergrowth textures such as mymekites, microphyric and granophyric.

Biotite is subhedral, lath-shaped and is generally altered to chlorite. It has inclusions of hornblende crystals. Hornblende occurs as minor mafic minerals as compared to biotite. Apatite generally forms as a basal section of hexagonal system. Zircon is euhedral and prismatic in shape. Titanite is present as euhedral to subhedral crystals. Microcline typically shows tartan twinning.

Igneous enclaves are common in the Ladakh batholith and they have different shapes like rounded, elongated, lenticular etc. The presence of plagioclase xenocrysts and also acicular apatite could indicate that they are formed from magma mixing/ mingling process.

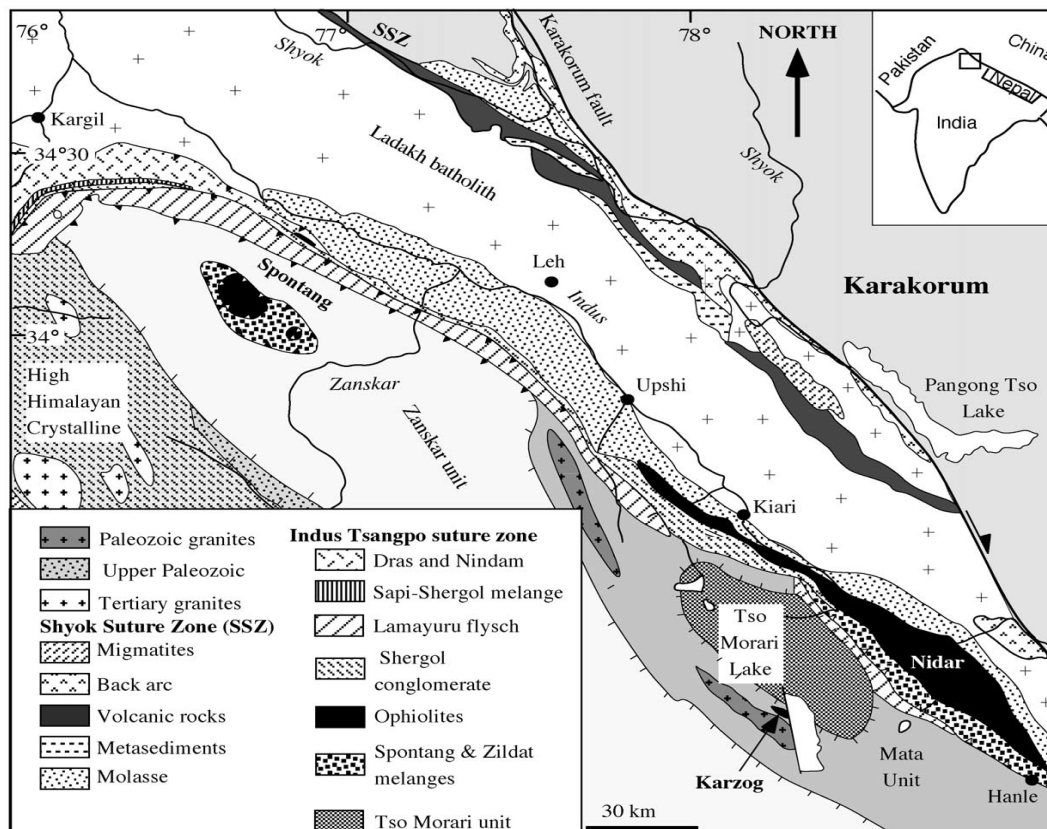


Figure 1. Geological map of Ladakh–Zaskar (modified after Mahe' o et al., 2000).

REFERENCES

- Kojima, S., Gozu, C., Itaya, T., Ahmad, T. & Islam, R. 2002: Geology of Ladakh Himalaya, northwestern India. *Jour. Geol. Soc. Japan*, 108: VII - VIII.
- Kumar, S., Singh, B., Wu, F.-Y., Ji, W.-Q. & Pathak, M., 2011: Geochemistry, zircon U–Pb geochronology and Hf isotope of granitoids and enclaves from Ladakh Batholith, Northwest Indian Higher Himalaya. *Symposium on Granites and Related Rocks*, Avila, Spain, 4–9 July 2011.
- Mahe' o, G., Bertrand, H., Guillot, S., Mascle, G., Pe'cher, A., Picard, C., de Sigoyer, J., 2000: Te'moins d'un arc immature te'thysien dans les ophiolites du Sud Ladakh (NW Himalaya, Inde). *C. R. Acad. Sci. Ser. II* 330, 289- 295.
- Singh, B. 1993: Geological set up of a part of the Ladakh Granitoid Complex, Ladakh Himalaya. *Journal of Himalayan Geology* 4, 57–62.
- Singh, S., Kumar, R., Barley, M.E. & Jain, A.K., 2007: SHRIMP U–Pb ages and depth of emplacement of Ladakh Batholith, Eastern Ladakh, India. *Journal of Asian Earth Sciences* 30, 490–503.

P 2.20

Petrogenetic and geodynamic types of Late Paleozoic (Sudetic) granitoids of the Caucasus

David Shengelia¹, Tamara Tsutsunava¹, Giorgi Chichinadze¹, Giorgi Beridze¹, Kristina Vardanashvili², Irakli Javakhishvili¹

¹ Alexandre Janelidze Institute of Geology, I. Javakhishvili Tbilisi State University, A. Politkovskaya 31, 0186 Tbilisi (d_shenge@yahoo.com)

² Ministry of Environment and Natural Resources Protection of Georgia, G. Gulua 6, 0114 Tbilisi

Late Paleozoic (Sudetic) granitoids within the Caucasus are spread in all outcrops of the pre-Alpine crystalline basement except Miskhan, Akhum and Asrikchay crystalline massifs. In particular, the granitoids crop out: in the southern part of the Scythian Platform and within the Greater Caucasian, Black Sea – Central Transcaucasian and Baiburt-Sevanian terranes (Figure 1).

Connection of the granitoids under consideration with the Sudetic orogeny is well-grounded by geological and isotope-geochronological data (Gamkrelidze & Shengelia 2005; Somin 2011; Shengelia et al. 2014). Geodynamic conditions of formation of Sudetic granitoids of the Caucasus are characterized mainly by thinning and unloading of the Earth's crust in one case and thickening and additional subsidence under the load of thick nappes in the other case. Therefore, despite the origin of the granitoids parent magma there are stated U and T (unloading and thickening of the Earth's crust) types of granitoids (Shengelia 1998). Most of these granitoids belong to S and I types of granites and to A, M etc. types as well. Sudetic granitoids from various structural units of the Caucasus differ from each other by mineralogical and petrological composition and isotope parameters (Th/U, $^{176}\text{Hf}/^{177}\text{Hf}$, $^{176}\text{Lu}/^{177}\text{Hf}$, $\epsilon\text{Hf}(T)$, TDM and TDMC (Gamkrelidze & Shengelia 2005; Shengelia et al. 2008).

Comprehensive investigation of Late Paleozoic granitoids of the Caucasus show that in spite of their belonging to the Sudetic orogeny, they considerably differ in petrogenetic parameters and geodynamic conditions of their formation.

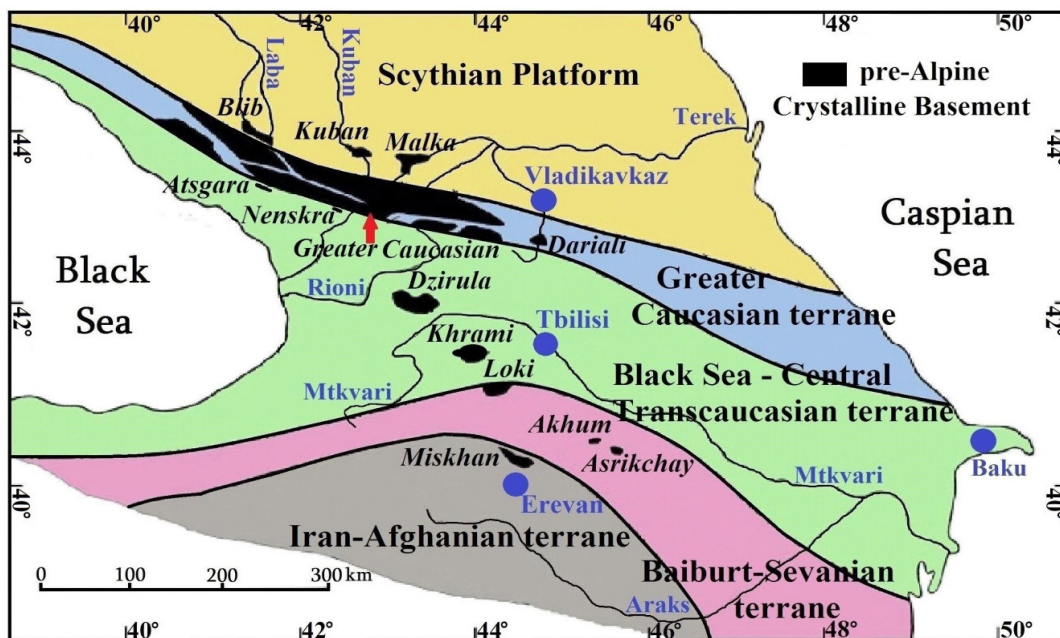


Figure 1. Tectonic zoning of the Caucasus with the exposures of pre-Alpine crystalline basement.

REFERENCES

- Gamkrelidze, I. & Shengelia, D. 2005: Precambrian-Paleozoic Regional Metamorphism, Granitoid Magmatism and Geodynamics of the Caucasus. "Nauchni Mir", Moscow, 479 p. (in Russian with English summary).
- Shengelia, D. 1998: The role of nappes in the process of formation of Late Hercynian granitoids of the Greater Caucasus. Proceed. Al. Janelidze Inst. of Geology, 163-169 (in Russian).
- Shengelia, D., Gamkrelidze, I., Tsutsunava, T., Shubitidze, L. 2008: Petrology and Geochemistry of Late Variscan Granitoids of the Caucasus. Proceed. Al. Janelidze Inst. of Geology, new ser., 124, 204-222.
- Shengelia, D., Tsutsunava, T., Chichinadze, G., Beridze G. 2014: Some Questions on Structure, Variscan Regional Metamorphism and Granitoid Magmatism of the Caucasian Terrane Crystallinicum. Bull. Georgian National Acad. Sci., 8-3, 56-63.
- Somin, M.L. 2011: Pre-Jurassic Basement of the Greater Caucasus: Brief overview. Turkish Journal of Earth Sciences, Geology of the Circum-Black Sea Region – Part A, Caucasus, 20, 545-611.

P 2.21

Relative timing and characterization of Au-associated veins in the Gotthard Massif, Graubünden, Switzerland

Maria Frøystein¹, Christoph A. Heinrich²

¹ *Institut für Geochemie und Petrologie, ETH Zürich, Sonneggstr. 5, CH-8006 Zürich (mariafr@student.ethz.ch)*

² *Institut für Geochemie und Petrologie, ETH Zürich, Sonneggstr. 5, CH-80 06 Zürich*

Metamorphic terranes are one of the most important sources of gold worldwide, associated with orogenic belts from Archean to Cenozoic time. Gold occurrences are found in association with sulfides in sericite and muscovite schists in the Surselva district of Graubünden, Switzerland (Jaffe, 2010 and references therein). They lie within the Gotthard Massif, a tectonic unit consisting of pre-Variscan, poly-metamorphic basement rocks with granitic cores that was deformed during the Alpine orogeny (Labhart 1977; Schmid et al. 2004). Additionally, native gold is found in the adjacent and highly sheared Tavetscher Zwischenmassif (Labhart 1977). Gold occur as either disseminated, in veinlets of quartz aligned or cross-cutting foliation and as layers of semi-massive sulfides. Alterations include sericitization, carbonatization and silicification. Despite the discovery of gold in the early 20th century, the understanding of the deposit is still in an early stage. In particular, the timing of the fluid leading to gold enrichment and precipitation remains debated (e.g., Della Valle and Haldemann, 1991; Stäheli, 2000; Jaffe, 2010). Some have argued for a pre-Alpine mineralization related to magmatic bodies, whereas others have suggested an Alpine timing of mineralization.

Here, we present evidence for an Alpine timing of gold precipitation, based on structural relationships and geochemical anomalies. We identified and mapped out cross-cutting veins of four generations on a scoured exposure of a pre-Alpine orthogneiss (9 by 4 meter) in Val Plattas, northern Gotthard Massif. The chl-biot-musc-KFsp-plag-qtz augengneiss has a penetrative foliation in E-W direction of Variscan age, as visible by its degree of deformation and mineral assemblage (amphibolite facies conditions). Discontinuous musc-KFsp-plag-qtz pegmatites are oriented parallel to foliation, and occasionally boudinaged. Quartz veins with rounded holes (< 1cm; often filled with carbonate and pyrite) are generally cross-cutting the pegmatite and foliation, indicative of a syn-Alpine timing. Contrastingly, they are also found parallel to foliation. The quartz bodies are deformed in a ductile-to-brittle regime by sulfide (pyrite-pyrrhotite) veinlets oriented in a conjugate-like manner in NE-SW and NW-SE. The sulfide veinlets displace pre-existing features in a predominantly sinistral manner, and is associated with discrete zones of limonitic alteration halo (rich in disseminated pyrite and minor chalcopyrite). Carbonate veinlets composed of calcite and ankerite is associated with the sulfide veinlets.

We studied the petrographic evolution using unpolished and polished thin sections, and alterations were identified – including a progressive evolution from biotite to chlorite, extensive sericitization of feldspars, sulfidation and carbonatization. Despite that the exposure is located several hundred meters from known gold occurrences in Val Plattas, geochemical gold up to 0.131 ppm was identified from the sulfide veins. Metallurgical assay and whole-rock geochemistry of major and trace elements (XRF and LA-ICP-MS) was carried out, and preliminary results suggest comparable geochemical anomalies to the mineralized zones. Mass balance calculations of least altered host rock versus altered is to be performed, and will contribute to quantify which elements were introduced and removed from the system during mineralization. On a larger scale, the work contributes to our understanding of the timing of gold mineralization within orogenic belts and metamorphic terranes worldwide.

REFERENCES

- Della Valle, G. & Haldemann, E.G. 1991: Metallogenie de l'or en Suisse. Rapport final: Disentis, Grisons. (unpublished report, Uni. Geneve).
- Jaffe, F. 2010: Gold mineralization in the Surselva region, Canton Grisons, Switzerland, *Swiss Journal of Geosciences*, 103, 1444-1451.
- Labhart, T. 1977: Aar und Gotthardmassiv, *Sammlung Geologische Führer*, 63, 1-173.
- Schmid, S.M., Fügenschuh, B., Kissling, E. & Schuster, R. 2004: Tectonic map and overall architecture of the Alpine orogeny, *Eclogae Geologicae Helvetiae*, 97, 93-117.
- Stäheli, P. 2000: Untersuchung der mesothermalen, alpin-syndeformativen, scherzonengebundenen Au-As-Sb Vererzungen in der Lukmanierschlucht bei Disentis (unpublished master thesis, ETH Zürich)

P 2.22

Inventory of Swiss gravel wash mud

Martin Fisch^{1,2}, Urs Eggenberger^{1,2} & Rainer Kündig^{1,3}

¹ *NEROS – Netzwerk mineralische Rohstoffe Schweiz, Institut für Geologie, Baltzerstrasse 1+3, CH-3012 Bern (martin.fisch@neros.ch)*

² *Fachstelle für Sekundärrohstoffe, Institut für Geologie, Universität Bern, Baltzerstrasse 1+3, CH-3012 Bern*

³ *Schweizerische Geotechnische Kommission, ETH Zürich, Sonneggstrasse 5, CH-8092 Zürich*

Swiss gravel industry produces ca. 2.5 Mt of pressed gravel wash mud per year (Behl & Bunge, 2013). Due to its characteristics, this material could be used as secondary raw material for various applications. Nevertheless, it is generally removed from value cycles by renaturation of gravel quarries or disposal in landfills. In both cases, valuable space is eliminated.

Gravel wash muds originate from the fine fraction of quaternary deposits. Consequently, their composition is regionally variable. In 1979, Mumenthaler has shown that mainly carbonate and clay mineral types are affected. In addition to local variabilities, a general East–West trend exists. In summary, there is no “average”, or “homogeneous” gravel wash mud in Switzerland. However, depending on the application as substitute raw material, different properties are of significance.

Subsequently, several applications of gravel wash mud have been successfully tested (e.g. Peters et al., 1982; Iberg et al., 1983; Bayer & Iberg, 1983): (a) The material can be used in brick factories. (b) Thermal treatment increases hydraulic properties of the material. Applications as mineral components in cement are technically feasible. (c) The chemical composition is close to that of clinker and the mineralogical composition is similar to conventional cement raw meal but energy-intensive milling is not required. Because of the large and locally dispersed availability of gravel quarries, lifetime of clinker raw material quarries could be extended.

Recently, gravel wash mud has been applied as soil-improver (www.kiwe-ca.ch) and as filler in construction materials (Logbau AG, Maienfeld). For its sustainability, such a building material has recently won the Swiss environmental award.

Since 1979, quarrying areas and material processing have significantly changed, technical requirements on material properties have increased and moreover, analytical techniques allow better material characterization. However, the inventory has not been updated.

NEROS – Netzwerk mineralische Rohstoffe Schweiz has launched a joint project together with FSKB (Fachverband der Schweizerischen Kies- und Betonindustrie) and gravel-industry partners that aims at pointing out the potential of gravel wash mud as substitute raw material, and finally increase its degree of recycling. In a first step, a new inventory is compiled, revealing local abundance and material parameters such as chemical and mineralogical composition as well as fineness. Preliminary results will be presented.

REFERENCES

- Bayer, G., Iberg, R. *Schweizer Ingenieur und Architekt* 101 (39), 1983, 917–924.
 Behl, M., Bunge, R. *Abklärung zum Inventar an umweltrelevanten Schlämmen in der Schweiz*, 2013, www.umtec.ch or www.bafu.admin.ch.
 Iberg, R., Peters, T., Mumenthaler, T. *Schweizer Ingenieur und Architekt* 101 (36) 1983, 845–850.
 Mumenthaler, T. *Dissertation Universität Bern* 1979, 83 pp.
 Peters, T., Iberg, R., Mumenthaler, T. *Schweizer Ingenieur und Architekt* 100 (19) 1982, 385–390.

P 2.23

Comparisons of Paleoproterozoic orogenic gold deposits/occurrences of Nalunaq and Vagar in South Greenland and Svartliden in Northern Sweden

Denis M. Schlatter*, Katerina Schläglova ** & Joshua W. Hughes***

¹ *Helvetica Exploration Services GmbH, Carl-Spitteler-Strass e 100, CH-8053 Zürich (denis.schlatter@helvetica-exploration.ch; http://www.helvetica-exploration.ch/)*

² *Institute of Geochemistry and Petrology, ETH Zürich, Clausiustr. 25, CH-8092 Zürich*

³ *Nanoq Resources Ltd, London, UK, http://www.nanoqresources.com/*

Paleoproterozoic gold deposits/occurrences occur in different host rocks in Northern Sweden (e.g. Svartliden) and in South Greenland (e.g. Nalunaq and Vagar). The Svartliden gold deposit (2.967 Mt., 4.26g/t; Fig. 1A, Schläglova et al. 2013) is located in the Lycksele-Storuman gold belt (LSGB), commonly referred to as the “Gold Line” and the Nalunaq gold deposit (0.713 Mt., 15g/t; Fig 1A, Bell et al. 2016) is located in the Nanortalik gold belt (NGB). The “Gold Line” trends in NW direction for 150 km within the Fennoscandian shield and is tentatively correlated with the NGB which can be followed for about 150 km from South-West to South-East Greenland (Fig. 1A, Lahtinen et al. 2008).

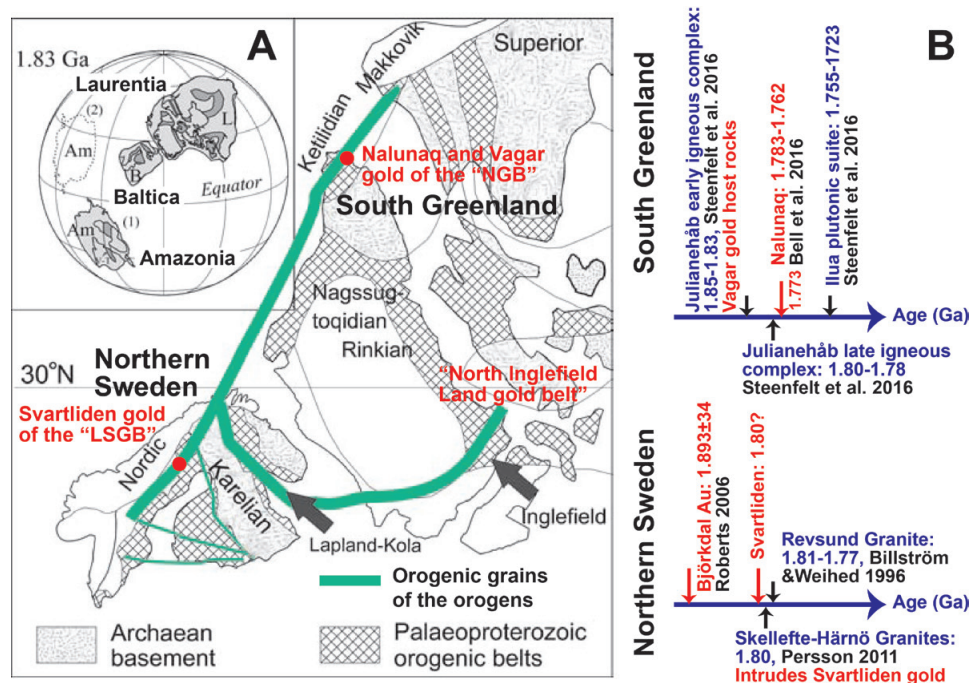


Figure 1. A: Plate reconstruction of Laurentia and Baltica at about 1.8 Ga and locations of Nalunaq and Vagar gold and Svartliden gold. Modified after Lahtinen et al. 2008. B: Sketch summarizing orogenic events and estimated timing of gold introduction in South Greenland and in Northern Sweden.

In this paper we discuss the similar geological environments of the LSGB and the NGB and depict the geological and geochemical characteristics of the gold deposits/occurrences of both gold belts. Gold mineralization occurs mainly in rocks of amphibolite metamorphic grade in all studied areas of the LSGB and the NGB. Gold of the NGB mainly occurs in quartz veins which are hosted in shear zones and a variety of rocks such as metabasalts (e.g. Nalunaq) and metagranitoids (e.g. Vagar) and the presence of auriferous quartz veins suggest an orogenic gold deposit. At Svartliden gold occurs in a shear zone at the contact between amphibolites and graphite-bearing schists and in boudinaged slivers of banded iron formation and is also considered to be an orogenic gold deposit (Schläglova et al. 2013).

The Svartliden gold deposit is dated indirectly by the intrusion ages of Skellefte-Härnö granites at 1.8 Ga (Fig. 1B) whereas the Nalunaq gold deposit has recently been dated to 1783 to 1762 Ma by Bell et al. (2016). Finally the Vagar gold occurrences of the NGB are suggested to be contemporaneous with the Ketilidian orogeny at about 1.85 to 1.83 Ga (Fig. 1B), hence the gold emplacement of the LSGB and NGB are roughly similar in ages. The most typical alteration minerals associated with the gold emplacement at the LSGB and the NGB are K-feldspar/biotite/sericite, arsenopyrite and pyrrhotite/löllingite reflecting addition of potassium, arsenic and sulphur at the time of the introduction of the gold. At Svartliden the

gangue of the gold mineralization comprises diopside-quartz, whereas at Nalunaq a similar calc-silicate alteration style that also comprises diopside pre-dates the mineralization (Bell et al. 2016). Both gold belts are characterized by abundant regional calc-alkaline granitoids which are in places sericite altered (Schlatter et al. 2013); but it is unclear if the granites were genetically related to gold mineralization. In summary gold deposits of the LSGB and the NGB are interpreted to be of orogenic type and share intriguing similarities with respect to their ages, their variety of host rocks and the similar hydrothermal alteration type and tectonic settings in shear zones.

Additional research including dating of the Svartliden deposit and the Vagar occurrences will add an argument in the discussion if there is a continuity of the LSGB and the NGB prior to the breakup of the Paleoproterozoic Columbia (Nuna) supercontinent. With respect to gold exploration a better understanding of the setting of the gold deposits of the "Gold Line" in Sweden will help the exploration efforts in remote South Greenland where much less data exist, and furthermore if the correlation of the proven prolific LSGB with the NGB can be demonstrated, such argument will favour investments for future exploration in South Greenland and elsewhere along the orogenic grains of the orogens, such as e.g. in Ingelfield (Fig. 1A).

REFERENCES

- Bell, R.-M., Kolb, J., Waight, T.E., Bagas, L. & Thomsen, T.B. 2016: A Palaeoproterozoic multi-stage hydrothermal alteration system at Nalunaq gold deposit, South Greenland. *Mineralium Deposita*: in press
- Lahtinen, R., Garde, A.A. and Melezhik, V. A. 2008: Paleoproterozoic evolution of Fennoscandia and Greenland. Episodes published by the IUGS, Vol.31 No.1, 20-28.
- Schlatter, D.M., Berger, A. & Christiansen, O. 2013: Geological, petrographical and geochemical characteristics of the granitoid hosted Amphibolite Ridge gold occurrence in South Greenland. Conference proceedings, "Mineral deposit research for a high-tech world." 12th Biennial SGA Meeting, pp 1189-1192.
- Schlöglöva, K., Gordon C., Hanes R., Ask H. & Broman, C. (2013): Svartliden gold mine: shear zone and BIF-hosted orogenic gold deposit, Gold Line, northern Sweden. Conf. Proceed. 12th Biennial SGA Meeting, Sweden: 1193-1196.

P 2.24

Correlation of reservoir properties of productive series and the red series within Absheron-Pribalkhan threshold

A.N.Huseynova

Institute of Geology & Geophysics of Azerbaijan National Academy of Science

Physico-chemical interaction in the system fluid and the enclosing rocks in sedimentary basins, are observed at all stages of their evolution and ontogenesis of hydrocarbons. Already at the stage of demolition and accumulation in marine reservoir precipitation, organic and plant residues, subsequent lithogenesis and diagenesis in the fluid-rock system, there are various physico-chemical interaction between the components of its material composition. Rocks of the lower Pliocene, formed on the Eastern edge of the South Caspian basin (Red-series - RS, South-Western Turkmenistan), differ from rocks of the same age on the West side (Productive series - PS, Azerbaijan) its brown color, which gives reason to assume about the various conditions of formation of RS and PS. In this regard, this article on the example of fields of the Absheron-Pribalkhan threshold of the South Caspian basin the comparative analysis of the physico-chemical properties of rocks and oil PT and CT.

Very specific conditions observed during the formation of signaling of sediments in the SCB. Isolation of the SCB in the late Miocene from the Black sea and the rest of the Paratethys contributed in the arid climate of intensification of the process of evaporation, leading to a dramatic lowering of sea level. From late Miocene up to present time the basin was filled with sediments with a total capacity of approximately 10 km, represented by alluvial, deltaic, shallow-marine to deep-water clastic sediments.

To study the spatial heterogeneity signaling most favorable reservoir object is the Absheron-Pribalkhan area that stretches from the Absheron Peninsula (in the West) to the Cheleken Peninsula (East), forming in the bottom topography peculiar latitudinal stretching stage – Absheron-Pribalkhan threshold. This underwater rise, sea is a continuation of the mountain ranges of the B. Caucasus (West) and Balkhan (in the East). According to its geological and geophysical characteristics of the considered area can be clearly divided into two sub — Absheron and Pribalkhan. Conventionally, the geological boundary between them and, accordingly, between PT and CT scan are conducted through the raising of the Kapaz (Bank intermediate). Within Absheron-Pribalkhan threshold identified some 20 petroleum structures, 8 of which are located within the Turkmen sector of the South Caspian.

Thus, it is considered a genetic indicator shows the relationship of oil PS and RS within Absheron-Pribalkhan zone, despite the various geochemical conditions of their location. Earlier came to the same conclusion and other researchers. Comparative analysis of rocks PS and RS in the SCB allowed to reveal the differences in their reservoir properties, which are explained as material composition of precipitation, demolished in the pool from a variety of power sources, physico-chemical interactions in the fluid - enclosing sedimentary rocks. It is established that the oil fields RS are not derived OM enclosing rocks and genetically similar to oil PS.

REFERENCES

- Ахмедов, А.Г., Нариманов, А.А., Сулейманов, А.И. 1992. О генетическом единстве нефтей Абшероно-прибалханской зоны поднятий. Геология нефти и газа, 3, 27-36.
- Фейзуллаев А., Тагиев М. 2008. Формирование залежей нефти и газа в продуктивной толще Южно-Каспийского бассейна: новые подходы и результаты. Азерб. нефть тасарруфаты, 3, с. 7-18
- Seewald, J.S. 2003. Review article Organic-inorganic interactions in petroleum-producing sedimentary basins. Nature 426, 327-333.
- Feyzullayev A.A., Guliyev I.S., Tagiyev M.F. Source potential of the Mesozoic-Cenozoic rocks in the South Caspian Basin and their role in forming the oil accumulations in the Lower Pliocene reservoirs // Petroleum Geoscience.- 2001.- V.7.- No.4.- P.409-417.

P 2.25

Size Dependant Physico-Chemical and Geochemical Characteristics of Two Distinct Carbonate-Rich Marine Sediments (Adriatic Sea)

Maja Ivanić¹, Srečo D. Škapin², Neda Vdovič¹, Nevenka Mikac¹ & Ivan Sondi³

¹ Division for Marine and Environmental Research, Ruđer Bošković Institute, Bijenička c. 54, 10 000 Zagreb, Croatia (mivanic@irb.hr)

² Department of Advanced Materials, Jožef Stefan Institute, Jamova cesta 39, 1000 Ljubljana, Slovenia

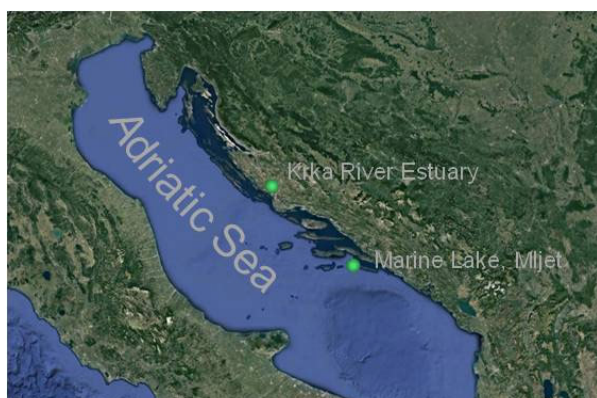
³ Faculty of Mining, Geology and Petroleum Engineering, Pierottijeva 6, University of Zagreb, 10 000 Zagreb, Croatia

Micron- and submicron-sized mineral particles, omnipresent in natural environments, comprise most of the potentially reactive surfaces responsible for transfer and removal of organic and inorganic contaminants [1]. On account of the size-related changes in surface reactivity, mineral particles occurring in the nanosized range (1-100 nm) are of considerable interest in investigations of fate of contaminants. In marine environment, micron- and submicron-sized mineral particles mostly consist of clay minerals, metal oxides and oxyhydroxides and sulphides while carbonate minerals more often occur as larger lithogenic and biogenic fragments. Even though investigations of their occurrence in the nanosized range are rare (Morse, 2007), authigenic precipitation can produce carbonate minerals in the submicron size (Sondi & Juračić, 2010).

This research investigates occurrence of carbonate minerals in different size fractions of two distinct sedimentological environments characterized by high carbonate content in sediment (Figure 1). One is a highly stratified karstic estuary (Krka River Estuary), supersaturated in calcite, with calc tufa barriers formed at the uppermost part of the estuary. The second is an enclosed marine lake (Mljet Lakes) with limited water exchange, where whiting events (drifting milky clouds of water) and the formation of aragonite-rich lake sediments have been the focus of previous investigations (Sondi and Juračić, 2010).

Recent marine sediments were retrieved using Uwitec gravity corer during different sampling campaigns. The upper 5 cm of sediment was treated with NaOCl for organic matter removal after which micron- and submicron-sized fractions were collected by gravitational settling. The size of each fraction was confirmed by laser-based granulometry and separated fractions were freeze-dried. Samples were mineralogically (XRD) and morphologically (FE-SEM) characterized, their physico-chemical properties (specific surface area, SSA and cation exchange capacity, CEC) and trace element concentrations (HR ICPMS) determined.

The results obtained showed that carbonate minerals resulting from weathering of carbonate rocks and disintegration of biomineral structures (i.e. Krka River samples) do not produce significant share of carbonates in the submicron and, especially, nanosized range. This is reflected in a very significant increase in concentrations of lithogenic trace elements (Al, Li) already in the fraction containing particles <8 µm, suggesting significant removal of carbonate minerals by settling. Their absence was accompanied by a sharp increase in SSA and CEC, as a result of higher concentration of clay minerals and Fe and Mn oxides/oxyhydroxides. Contrarily, in environment where carbonates (mostly aragonite) are produced as a result of authigenic processes (i.e. Mljet), their share is significant even in finest fractions. Incorporation of Sr in the aragonite crystal structure allows it to be used as a tracer of aragonite content. High levels of Sr were measured in all fractions collected from this sample, with a maximum of 4461 µg g⁻¹ determined in fraction containing particles <4 µm. Its concentration lowered only in the finest fraction (<0.45 µm; 1793 µg g⁻¹), where 90 % of particles were <200 nm. The sharp decrease in Sr concentration was accompanied by a 56 % increase in concentrations of Al. The prevalence of carbonate minerals in all size fractions collected from this sample is reflected in continuously low SSA and CEC values.



The study investigated influence of origin of carbonate mineral phases on their occurrence in various size-fractions. Carbonates were shown to be present in larger quantities in sub-micron sizes in environments where their authigenic formation occurs. Low surface reactivity of carbonate mineral phases of different origin was established.

Figure 1. Map showing sampling locations.

REFERENCES

- Hochella, M.F., Lower, S.K., Maurice, P.A., Penn, R.L., Sahai, N., Sparks, D.L. & Twining, B.S. 2008: Nanominerals, mineral nanoparticles, and Earth systems. *Science*, 319, 1631-1634
- Morse, J.W., Arvidson, R.F. & Lüttge, A. 2007. Calcium carbonate formation and dissolution. *Chem. Rev.* 107, 342-381.
- Sondi, I. & Juračić, M., 2010. Whiting events and the formation of aragonite in Mediterranean Karstic Marine Lakes: New evidence on its biologically induced inorganic origin. *Sedimentology* 57, 85-95.

P 2.26

Monitoring dehydration reactions in subducted serpentinites by metamorphic olivine formation in the Zermatt-Saas Ophiolites

Elias Kempf¹, Jörg Hermann¹, Eric Reusser²

¹ Institute of Geological Sciences, University of Bern, Baltzerstrasse 1+3, CH-3012 Bern
(elias.kempf@geo.unibe.ch, joerg.hermann@geo.unibe.ch)

² Institute of Geochemistry and Petrology, ETH Zurich, Clausiusstrasse 25, CH-8092 Zurich
(eric.reusser@erdw.ethz.ch)

Serpentinization at mid-ocean ridges involves hydration of mantle peridotite and the formation of magnetite, hydrous silicates such as chrysotile and lizardite ± chlorite and brucite. The hydrated mantle contains up to 12 wt% water bound in these hydrous minerals. Upon subduction, these hydrous minerals break down at various reactions. Every metamorphic olivine-forming reaction liberates water and hence the study of major and trace elements in olivine permit to reconstruct dehydration reactions in subducted serpentinites. Since olivine is stable to 660 km in the earth's mantle it is an important phase to study the deep water cycle.

The Zermatt-Saas serpentinite, a unique location nearly unaffected by Alpine deformation, preserves the history from mantle hydration at the seafloor to subduction and exhumation. The early history from the mantle to peak metamorphism is best preserved within a 50 m wide zone between two shear zones. In this domain, mantle textures escaped Alpine overprint. 0.5-2 cm sized olivines grow over the relict mesh texture, recognized as polygonal magnetite rims produced through the oceanic serpentinization of mantle olivine. The metamorphic olivines show iron-rich cores and magnesium-rich rims. The iron rich centers grow over the relict mesh texture, thus proving its metamorphic origin. Moreover, they occasionally contain sub-microscopic titanium-clinohumite patches. These olivines contain numerous inclusions of magnetite, chlorite, antigorite, diopside and sub-micron sized fluid inclusions. At peak temperature, the large olivines recrystallize into a second generation of olivine along discrete shear zones. They are unzoned regarding iron and magnesium contents and form a mosaic texture between polygonal 0.05-0.15 mm sized olivines with occasional diopside and magnetite inclusions, discrete titanium-clinohumite grains, antigorite and chlorite blades. The mesh texture in the newly formed olivine zone has vanished, the magnetite veins formed during serpentinization shrink and they are free of fluid inclusions. The shear zones contain also 0.1-0.75 mm wide titanium-chondrodite/titanium-clinohumite-olivine veins some of which are aligned en echelon. Olivines form a mosaic texture together with chlorite, antigorite and titanium-clinohumite/chondrodite grains.

Iron-rich cores in the first generation of olivines show Mg# of 0.95-0.96. The rims of these olivines have a Mg# of 0.96-0.98. Titanian-clinohumite-rich patches within the iron-rich cores have Mg# of 0.95-0.96 and contain 0.29-2.33 wt% TiO₂. The recrystallized olivines show Mg# values between 0.95-0.96. Recrystallized titanian-clinohumites have Mg# between 0.95-0.97 and contain 2.3-3.5 wt% TiO₂. Olivines in the shear zones show Mg# between 0.95-0.96. Titanian-clinohumites have Mg# of 0.97 and 1.9-4.9 wt% TiO₂. Titanian-chondrodites have Mg# between 0.95-0.96 and contain 7.7-7.8 wt% TiO₂.

The very high Mg# of all described phases are interpreted to be a product of the initial amount of iron preserved in the reactive phases antigorite and brucite and hence are thought to be dependent on the degree of serpentinization. This indicates that large amounts of Fe are sequestered into magnetite that formed during the extensive serpentinisation of the mantle rocks at the ocean floor. With increasing temperatures during Alpine convergence chrysotile transforms into antigorite and brucite. Upon further subduction temperatures increase and antigorite + brucite react to olivine + water ± chlorite at around 450°C. The observed zoning of olivine with increasing Mg# indicates continuous growth in a divariant field, as first reported by Kunugiza (1982), and occurs typically within a temperature interval of 20-40°C (Shen *et al.*, 2015). Titanian-clinohumite patches form by the dissolution of titanium-bearing magnetite. The higher iron content in the second generation of homogeneous recrystallized olivines is explained by the partial reaction of oxides with serpentine, shown by the disappearance of the relic magnetite mesh rims. Temperature estimates using the olivine-antigorite iron-magnesium exchange thermometer from Evans *et al.* (2012) indicates peak temperatures of the recrystallized olivines of around 600°C. Grains of titanian-clinohumite and titanian-chondrodite in equilibrium with antigorite and olivine suggest that pressures might have exceeded 25 kbar (Shen *et al.*, 2015).

Our detailed investigation of textures and composition shows that the first metamorphic olivine grows during a continuous dehydration reaction over 20-40°C where brucite disappears. The second generation of olivine with lower Mg# is interpreted to form through a redox reaction involving reduction of magnetite. This dehydration reaction has not been documented in subducted serpentinites before. It occurs close to peak conditions of ca. 25 kbar, 600°C, well before the terminal breakdown of antigorite and liberates small amounts of water-rich fluid.

REFERENCES

- Evans, B.W., Dyar, M.D., Kuehner, S.M. 2012: Implications of ferrous and ferric iron in antigorite, *American Mineralogist*, 97, 184-196.
- Kunugiza, K. 1982: Formation of zoning of olivine with progressive metamorphism of serpentinite-an example from the Ryumon peridotite body of the Sanbagawa metamorphic belt, Kii peninsula. *Journal of the Japanese Mineralogists, Petrologists and Economic Geologists*, 77, 157-170.
- Shen, T., Hermann J., Zhang L., Lü Z., Padron-Navarta JA., Xia B., Bader T. 2015: UHP Metamorphism documented in Ti-Chondrodite- and Ti-Clinohumite-bearing Serpentinized Ultramafic Rocks from Chinese Southwestern Tianshan, *Journal of Petrology*, 56:7, 1425-1458.

P 2.27

Textural characterization of forsterite + talc assemblage resulting from antigorite breakdown in the bergell contact aureole (Italy)

Romain Lafay & Lukas P. Baumgartner

Institut des Sciences de la Terre, Université de Lausanne, Lausanne, CH-1015, Switzerland

The Malenco serpentinite unit (Central Alps, Italy) suffered contact metamorphism within aureole of the Bergell tonalite. In this context, the dominant dehydration reaction is represented by antigorite (atg) breakdown to forsterite (fo) and talc (tc) (Trommsdorff & Evans 1972).

A detailed field and petrologic study provide interesting results to delineate processes controlling the fo + tc metamorphic assemblage development.

In this unit, the protolith chemistry remains linked to the primary layering of the mantle rocks (dunite/lherzolite/clinopyroxenite). In turn, the spatial distribution and textural characteristics of metamorphic assemblage reveals different textures for rocks with different modal abundance of tc produced.

Peculiar jack-straw (spinifex-like) fo of up to 15 centimeters in size with an aspect ratios of up to 20 developed at or near the fo + tc isograd. Moreover, fo mineral size decreases towards the intrusion and olivines tend to become equigranular. Metamorphic fo is homogeneous, but contains inclusions of atg, which is often Al-rich and the external part of the fo contains tc.

Our observations are very similar to the carbonate-hosted olivines of the Ubehebe peak contact aureole (Death Valley, California, Roselle et al., 1997). The similarity between those two locations indicates that the texture observed in the Bergell contact aureole is due to limited nucleation at the isograd. The shape of the fo is an inherent growth form, rather than due to the specifics of the dehydration/decarbonation reaction. Overstepping of the reaction increases toward the intrusion favor abundant fo nucleation (Roselle et al., 1997).

Atg breakdown initiation can develop vein-like reaction zones composed of weakly foliated, fine-grained tc and equigranular fo aggregates. The formation of wavy tc veinlets of centimeter to decimeter length and few millimeter width is characteristic of lithologies with abundant fo. These tc veins likely acted as exfiltration channels for fluid produced by the atg breakdown.

REFERENCES

- Trommsdorff V., & Evans B. 1972, Progressive metamorphism of antigorite schist in the Bergell tonalite aureole (Italy), *Amer. J. Sci* 272, 423-437;
 Roselle G. T., Baumgartner L. P., Chapman J. A., 1997, Nucleation-dominated crystallization of forsterite in the Ubehebe Peak contact aureole, California, *Geology* 823-826

P 2.28

Crystallization ages of Alpine cleft monazite; correlation with exhumation history and shear zone activity

Emmanuelle Ricchi¹, Edwin Gnos², C. Bergemann¹

¹ *Department of Earth Sciences, University of Geneva, Rue des Maraichers 13, 1205 Geneva, Switzerland (Emmanuelle.Ricchi@unige.ch)*

² *Natural History Museum Geneva, 1 Route de Malagnou, 1208 Geneva, Switzerland*

Alpine clefts are open fissures created during tectonic movements under peak to retrograde metamorphic conditions. They occur in all types of rocks and form at temperatures below the ductile/brittle transition of a rock (e.g., Mullis et al., 1996; Stalder, 1998), probably by fluid-assisted cracking (e.g., Cox, 2010). Monazite-bearing alpine clefts are of major interest for geochronology because the monazite, (LREE,Th)PO₄, is very resistant to radiation damage (e.g., Meldrum et al., 1998), and the Th- U-Pb system is not affected by diffusion at <450°C recorded in clefts (Cherniak et al., 2004). However, its isotopic system will be reset by recrystallization or dissolution/reprecipitation, notably in the presence of hydrous fluids (e.g., Seydoux-Guillaume et al., 2002, 2012; Grand'Homme et al., 2016). Due to the presence of a hydrous fluid in an Alpine cleft, retrograde mineral reaction is common. Monazite dissolution/precipitation occurs in clefts while this is rarely observed in the surrounding rocks. This permits to date the duration of brittle deformation (Berger et al., 2013; Bergemann et al., in review) occurring at temperatures below ~300°C.

Individual growth domains are revealed in cleft monazite by BSE images representing trace element variations (REE+Y, Th, U and Pb). SIMS Th-U-Pb age dating of these domains revealed that stepwise growth (and dissolution) can last up to 20 Ma, that cleft monazite crystallization in the Alps occurred between 90 and 6 Ma and that the age steps recorded can be correlated with tectonic activity (Janots et al., 2012; Berger et al., 2013; Gnos et al., 2014; Bergemann et al., 2015; Bergemann et al., in review). Interestingly, recent studies indicate that crystallization of monazite starts in most cases at the closure temperature of the zircon fission track system (Berger et al., 2013; Gnos et al., 2014) and that crystallization ceases at higher temperatures than those recorded by the zircon (U-Th)/He system (Gnos et al., 2014).

We collected cleft monazite from the Argentera Massif, Alpine high-pressure regions, the Tauern Window and the Aar- and Gotthard Massifs in order to acquire SIMS monazite growth domain ages, and to compare them with zircon fission track and (U-Th)/He data and to use them for constraining shear zone activity. Moreover, we will try to better define monazite growth conditions using monazite-quartz and other oxygen isotope thermometers, Ti-in-quartz thermometry in TiO₂-buffered monazite associations, and fluid inclusions. The interaction of host-rock REE minerals and cleft monazite will be investigated for selected cases in order to better understand fluid-rock interaction.

REFERENCES

- Bergemann, C., Gnos, E., Berger, A., Whitehouse, M., Wehrens, P., Pettke, T. and Janots, E. (in review). Th-Pb ion probe dating of zoned cleft monazite: Implications for shear zone activity in the Grimsel area of the Aar Massif, Switzerland. *Tectonics*.
- Bergemann, C., Gnos, E., Berger, A., Whitehouse, M., Walter, F., and Bojar, H. P. (2015). Monazite Th-Pb dating reveals eo-Alpine evolution in the Eastern Alps during brittle deformation. Abstract, 25th Goldschmidt Conference, Prague.
- Berger, A., Gnos, E., Janots, E., Whitehouse, M., Soom, M., Frei, R. and Waight, T.E. (2013). Dating brittle tectonic movements with cleft monazite: Fluid-rock interaction and formation of REE minerals. *Tectonics* 132: 1-14.
- Cherniak, D.J., Watson, E.B., Grove, M. and Harrison, T.M. (2004). Pb diffusion in monazite: A combined RBS/SIMS study. *Geochimica and Cosmochimica Acta* 68: 829-840.
- Cox, S. (2010). The application of failure mode diagrams for exploring the roles of fluid pressure and stress states in controlling styles of fracture-controlled permeability enhancement in faults and shear zones. *Geofluids*, 2, 217-233.
- Gnos, E., Janots, E., Berger, A., Whitehouse, M., Walter, F., Pettke, T. and Bergemann, C. (2014). Age of cleft monazites in the eastern Tauern Window: constraints on crystallization conditions of hydrothermal monazite. *Swiss Journal of Geosciences* 108: 55-74.
- Grand'Homme, A., Janots, E., Seydoux-Uillome, A.-M., Guillaume, D., Bosse, V. and Magnin, V., (2016). Partial resetting of the U-Th-Pb systems in experimentally altered monazite: Nanoscale evidence of incomplete replacement. *Geology*, doi: 10.1130/G27770.1.
- Meldrum, A., Boatner, L.A., Weber, W.J. and Ewing, R.C. (1998). Radiation damage in zircon and monazite. *Geochimica and Cosmochimica Acta* 62: 2509-2520.
- Janots, E., Berger, A., Gnos, E., Whitehouse, M., Lewin, E. and Pettke, T. (2012). Constraints on fluid evolution during metamorphism from U-Th-Pb systematics in Alpine hydrothermal monazite. *Chemical Geology* 326-327, 61-71.
- Mullis, J. (1996). P-T-t path of quartz formation in extensional veins of the Central Alps. *Scheizerische Mineralogische und*

Petrographische Mitteilungen 76: 159-164.

Seydoux-Guillaume, A.M., Paquette, J.L., Wiedenbeck, M., Montel, J.M. and Heinrich, W. (2002). Experimental resetting of the U-Th-Pb system in monazite. *Chemical Geology* 191, 165-181.

Seydoux-Guillaume, A.M., Montel, J.M., Bingen, B., Bosse, V., de Perseval, P., Paquette, J.L., Janots, E., and Wirth, R. (2012). Low-temperature alteration of monazite: Fluid mediated coupled dissolutionprecipitation, irradiation damage, and disturbance of the U-Pb and Th-Pb chronometers. *Chemical Geology*, 330-331: 140-158.

Stalder, H. A., Wagner, A., Graeser, S. and Stuker, P. (1998). *Mineralienlexikon der Schweiz*. Basel, Wepf Verlag.

P 2.29

Composition, origin and time evolution of ore-forming fluids and trace element geochemistry of enargite in the Lepanto epithermal high-sulfidation deposit (Philippines).

Oliveras, M.¹, Kouzmanov, K.¹, Schlöglová, K.² & De los Santos, M.³

¹ Department of Earth Sciences, University of Geneva, rue de Maraichers 13, 1205 Geneva, Switzerland

² Institute of Geochemistry and Petrology, ETH Zürich, Clausiusstrasse 25, 8092 Zürich, Switzerland

³ Lepanto Consolidated Mining Company, Manila, Philippines

The Lepanto-Far Southeast (FSE)-Victoria cluster in the Mankayan district, Philippines, offers an excellent opportunity to study fluid processes at the porphyry-epithermal interface (Tejada, 1989; Hedenquist *et al.* 1998). The district is centered on the FSE porphyry system and the Lepanto high-sulfidation epithermal ore body is developed outwards in NW direction. In the present study the Lepanto ore body has been subdivided into three main areas according to their distance from the FSE porphyry center – proximal, intermediate and distal.

The combination of near-infrared (NIR) microscopy and microthermometry with LA-ICP-MS analysis of enargite-hosted fluid inclusions (Kouzmanov *et al.* 2010) allowed studying composition, metal content, and P-T parameters of real ore-precipitating fluids at Lepanto. Such information is unique and can be used for a better understanding of ore precipitation mechanisms in the shallow epithermal environment. In addition, a detailed mineral geochemistry study of enargite from the three areas of the ore body has been performed in order to investigate the trace element pattern of the mineral as a function of distance to the supposed porphyry center.

Fluid inclusion microthermometry of enargite- and quartz-hosted fluid inclusions revealed a trend of decreasing temperature of formation from the proximal area (250°C) towards the distal areas of the deposit (125°C) and a slightly oscillating salinity of the mineralizing fluids (3.3 wt. % NaCl eq. on average for enargite-hosted and 0.88 wt. % NaCl eq. for quartz-hosted fluid inclusion assemblages), with no clear dilution pattern over the 2 km distance, as previously reported (Mancano and Campbell, 1995). Salinities measured for enargite-hosted fluid inclusions show a much wider range of values than previously reported for the deposit, with a maximum of 6 wt. % NaCl eq.

LA-ICP-MS analyses of enargite- and quartz-hosted fluid inclusions from the Lepanto ore body reveal high metal contents, especially in Pb, Zn, Ag, Bi and Au. Lead and zinc appear in anomalously high concentrations in fluid inclusions from the distal parts of the deposit and decrease towards the FSE porphyry center.

A combined NIR microscopy, electron microprobe and LA-ICP-MS study of enargite crystals from various parts of the ore body revealed a common oscillatory and/or complex sector zoning of the mineral. Systematic study of trace-element signatures of enargite along different sectors indicates a preferential incorporation of some trace elements in one specific sector with concentrations varying within several orders of magnitude. Therefore the potential of enargite trace element chemistry as a vectoring tool for porphyry-style mineralization (Deyell and Hedenquist, 2011) needs to be carefully reevaluated taking in account the complex internal growth features of the mineral.

REFERENCES

- Deyell C.L. Hedenquist J.W. (2011) Trace element geochemistry of enargite in the Mankayan district, Philippines. *Economic Geology*, v. 106, p. 1465-1478.
- Hedenquist J.W. Arribas A., Jr., Reynolds, T.J. (1998) Evolution of intrusion-centered hydrothermal systems: Far Southeast-Lepanto porphyry and epithermal Cu-Au deposits, Philippines. *Economic Geology*, v. 93, p. 373-404.
- Kouzmanov K. Pettke T., Heinrich C.A. (2010) Direct analysis of ore-precipitating fluids: Combined IR microscopy and LA-ICPMS study of fluid inclusions in opaque ore minerals. *Economic Geology*, v. 105, p. 351-373.
- Mancano D.P., Campbell A.R. (1995) Microthermometry of enargite-hosted fluid inclusions from the Lepanto, Philippines, high-sulfidation Cu-Au deposit. *Geochimica et Cosmochimica Acta*, v. 59, p. 3909-3916.
- Tejada, M.L.G. (1989) Characteristics and paragenesis of luzonite in the Lepanto copper-gold deposit, Mankayan Benguet, Philippines. Unpubl. MSc. thesis, Univ. Philippines, 89 p.

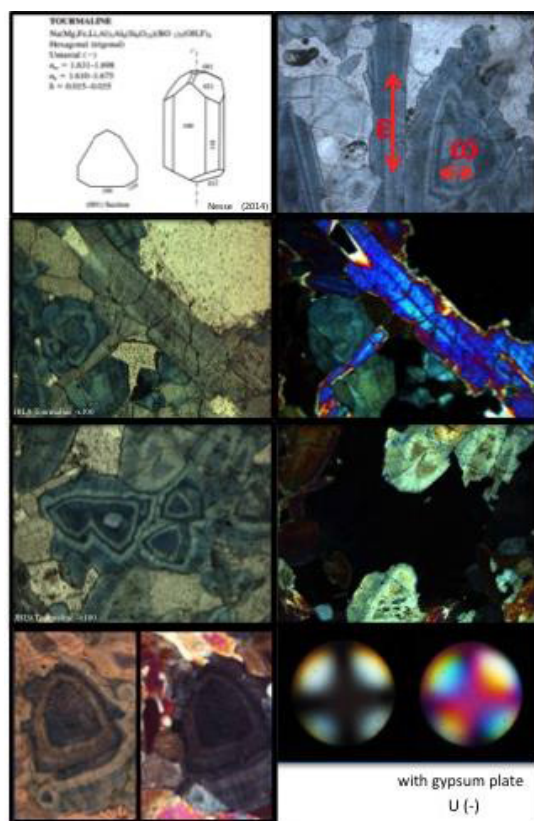


Figure 2. Example of tourmaline as it appears in OPTICMin©.

REFERENCES

- Nesse, W.D. (2014) Introduction to optical mineralogy, Oxford University Press, 4th edition, 361p.
- Phillips, Wm. R. & Griffen, Dana T. (1981) Optical Mineralogy The Nonopaque Minerals, W.H. Freeman and Company, 678 p.
- Schmidt, S. Th. (2016) Le P'tit Guide de Minéralogie optique, Université de Genève, 132p.
- W. A. Deer, R. A. Howie, J. Zussman (1993) An Introduction to the Rock-Forming Minerals, 2nd edition, Longman, 696 p.

P 2.31

Evaluation of major to ultra trace element bulk rock chemical analysis of nanoparticulate pressed powder pellets by LA-ICP-MS

Daniel Peters¹, Thomas Pettke¹

¹ Institute of Geological Sciences, University of Bern, Baltzerstrasse 1+3, CH-3012 Bern (daniel.peters@geo.unibe.ch)

An efficient, clean procedure for bulk rock major to trace element analysis by 193 nm Excimer LA-ICP-MS analysis of nanoparticulate pressed powder pellets (PPPs) employing a binder is presented (Peters & Pettke, 2016). Sample powders are milled in water suspension in a planetary ball mill, reducing average grain size by about one order of magnitude compared to common dry milling protocols (Garbe-Schönberg & Müller, 2014). Microcrystalline cellulose (MCC) is employed as a binder, improving the mechanical strength of the PPP and the ablation behaviour, because MCC absorbs 193 nm laser light well. Use of MCC binder allows for producing cohesive pellets of materials that cannot be pelletized in their pure forms, such as quartz powder. Rigorous blank quantification was performed on synthetic quartz treated like rock samples, demonstrating that procedural blanks are unproblematic except for a few elements at the 10 ng g⁻¹ concentration level. The LA-ICP-MS PPP analytical procedure was optimised and evaluated using six different SRM powders (JP-1, UB-N, BCR-2, GSP-2, OKUM, and MUH-1). External calibration using SRM 610, SRM 612, BCR-2G, and GSD-1G glasses allows for evaluation of possible matrix effects during LA-ICP-MS analysis.

The measurement trueness of the PPP LA-ICP-MS analytical procedure compares well to that achieved for liquid ICP-MS and LA-ICP-MS glass analysis (Fig. 1), except for element mass fractions below ~30 ng g⁻¹, where liquid ICP-MS offers more precise data and in part lower limits of detection. 1 σ standard deviations on the measurement repeatability of LA-ICP-MS PPP element concentrations are of the order of 0.5 to 2 % (n = 6) for mass fractions exceeding ~1 μ g g⁻¹. For lower element concentrations these uncertainties increase to 5-10% or higher when analyte-dependent limits of detection (LOD) are approached, and LODs do not significantly differ from glass analysis. Sample homogeneity is demonstrated by the high analytical precision, except for very few elements where grain size effects can rarely still be resolved analytically.

Matrix effects are demonstrated for PPP analysis of diverse rock compositions and basalt glass analysis when externally calibrated based on SRM 610 and SRM 612 glasses; employing basalt glass GSD-1G or BCR-2G for external calibration basically eliminates these problems. Perhaps the most prominent progress of the LA-ICP-MS PPP analytical procedure presented here is the fact that trace elements not commonly analysed, i.e. new, unconventional geochemical tracers, can be measured straightforwardly, including volatile elements, the flux elements Li and B, the chalcophile elements As, Sb, Tl, Bi, and elements that alloy with metal containers employed in conventional glass production approaches. The method presented here thus overcomes many common problems and limitations in analytical geochemistry and is shown to be an efficient alternative for bulk rock trace elements analysis.

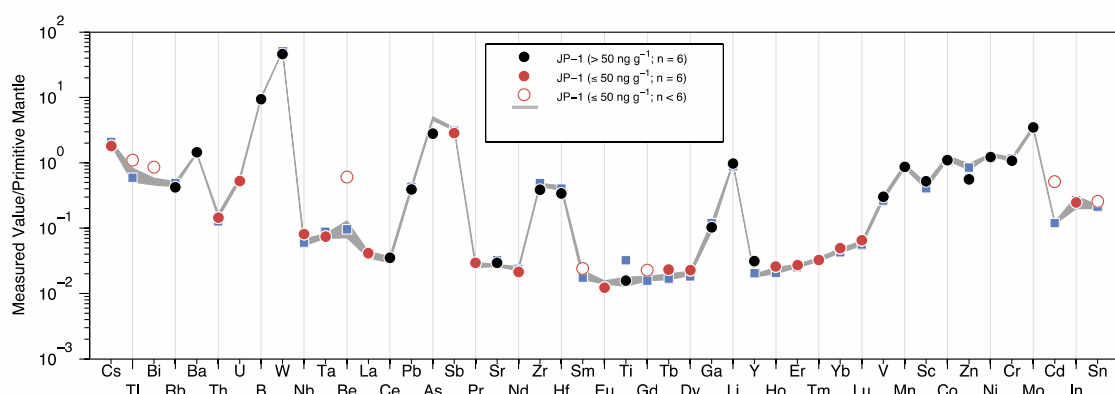


Figure 1. Comparison of MCC-PPP data from this study vs. liquid ICP-MS data (bomb digestion) from Kodolányi et al. (2012), based on JP-1, plotted as a primitive mantle (PM)-normalised spider diagram (PM values from Palme and O'Neill 2014). MCC-PPP data were calculated with GSD-1G as calibrator and internally standardised to the sum of major element oxide mass fractions. Most analytical uncertainties are smaller than symbol size.

REFERENCES

Garbe-Schönberg D., Müller S. 2014: Nano-particulate pressed powder tablets for LA-ICP-MS. *Journal of Analytical Atomic Spectrometry*, 29, 990–1000.

- Kodolányi J., Pettke T., Spandler C., Kamber B.S., Gméling K. 2012: Geochemistry of ocean floor and fore-arc serpentinites: Constraints on the ultramafic input to subduction zones. *Journal of Petrology*, 53, 235–270.
- Palme H. & O'Neill H.St.C. 2014: Cosmochemical estimates of mantle composition. In: Holland H.D. and Turekian K.K. (eds), *Treatise on geo- chemistry*. Elsevier (Amsterdam), 2, 1–39.
- Peters, D., Pettke, T. 2016: Evaluation of major to ultra trace element bulk rock chemical analysis of nanoparticulate pressed powder pellets by LA-ICP-MS. *Geostandards and Geoanalytical Research*, doi:10.1111/ggr.12125.

P 2.32

Geochemical cycles in Lake Towuti (Indonesia) Disentangling the dominant factors ruling Fe isotopes fractionation

Luis Ordoñez¹, Massimo Chiaradia¹, Daniel Ariztegui¹, Marina Morlock², Hendrik Vogel², Martin Melles³, James M. Russell⁴, Satria Bijaksana⁵ & the TDP scientific team

¹ *Department of Earth Sciences, University of Geneva, 1205 Geneva, Switzerland*

² *Institute of Geological Sciences and Oeschger Centre for Climate Change Research, University of Bern, 3012 Bern, Switzerland*

³ *Institute of Mineralogy and Geology, University of Cologne, 50674 Köln, Germany*

⁴ *Department of Geological Sciences, Brown University, Providence, RI 02912*

⁵ *Faculty of Mining and Petroleum Engineering, Institut Teknologi Bandung, Bandung 40132, Indonesia*

* Email address of corresponding author: luis.ordonez@unige.ch

Located in the center of the Indo-Pacific Warm Pool (IPWP) Lake Towuti provides an excellent archive that records the changes of the region's hydroclimate on orbital to millennial time-scales during the Quaternary. Hyposulfidic, ferruginous, partially stratified and anoxic Lake Towuti offers the opportunity to study the (bio-)geochemical cycling of redox sensitive elements such as iron. Owing to the, in many ways, unique water chemistry of Lake Towuti, the lake may be considered as an analogue of early Earth environments, opening the doors to Archean ocean's studies and interplanetary sciences. Identifying the main processes that drive isotopic variability and fractionation of iron in Towuti's sedimentary record is one of the main goals of our research endeavors.

Lake Towuti (2.75°S, 121.5°E; 318 m a.s.l.; 560 km² surface area; 203 m maximum water depth) is a tectonic lake located on the island of Sulawesi, central Indonesia. Its catchment area is primarily composed of intensely weathered ultramafic rocks from the East Sulawesi Ophiolite belt. Therefore, Lake Towuti is anomalously rich in iron and other redox-sensitive metals. Today the lake is anoxic below 140 meters depth, hyposulfidic, and is one of the least productive lakes on Earth.

The high contents of iron and other heavy metals in Towuti's water makes this lake an ideal place to study redox conditions during sediment deposition. The reduction and re-oxidation of iron is a common process in anoxic environments and iron fractionation occurs during this dynamic cycle. However, it is poorly constrained in lacustrine, low-sulfur and iron rich environments. Many studies in short cores or lab experiments tried to disentangle Fe-isotope fractionation in the many phases involved in redox reactions. Our work focusses on a long sedimentary record from the Towuti Drilling Project (TDP) Site 1 that was drilled in May-July 2015 at Lake Towuti in course of a scientific deep drilling project under the umbrella of the ICDP. Pelagic sedimentation in our sediment record is thought to span several glacial interglacial cycles, possibly reaching back to 600 kyr.

Constraining Fe-fractionation is challenging due to the many potential abiotic and biotic drivers of the redox reactions. Fe-reducing bacteria have been suggested as one of the most important drivers for the Fe-fractionation which may occur during the dissimilatory iron reduction (DIR). Thus, it is crucial to characterize the bulk nature of the organic matter (OM) as a main support for microbial development and to determine the dominating microbial communities in the subsurface sediments of the lake. As a first step we performed Rock Eval and CHN (Carbon-Hydrogen-Nitrogen) analyses on bulk samples as a means of characterizing OM in our samples. Additionally, qPCR analyses and DNA sequencing will be performed at the Geomicrobiology Laboratory of GFZ-Potsdam. These data, along with detailed mineralogical analyses and characterization of the depositional environment, will set the framework in which the DIR bioproducts occurred.

Two approaches will be compared to define the iron isotopic signatures on sediments: mechanically separated magnetite and iron recovered from chemical sequential extraction. While magnetite is an important biogenic endproduct of DIR, high amounts of detrital magnetite in Lake Towuti sediments may limit its significance to better understand Fe-fractionation during DIR. A depositional model, which incorporates source to sink element fluxes and cycling, will provide quantitative information on the amount of detrital material reaching our coring site through time. Preliminary SEM and XRD analyses of separate extracts show a mixture of magnetite and serpentine. Our planned sequential acid digestion extraction has the advantage of focusing on particular bioproducts such as siderite. Finally, our results from the sediment cores will be compared with the Fe-isotope signature of the catchment-characteristic bedrocks.

Combining the Fe-isotope datasets with the paleoclimatic reconstruction of Lake Towuti will be critical to define how Fe-fractionation relates to the dominant redox reactions taking place in this particular environment and further use it as an analogue for Archean oceans.

P 2.33

Manganese oxides in travertines from Skoura (Morocco): geochemical or biological deposits?

Armelle DuPasquier¹, Daniel Grolimund², Jasquelin Pena³, Eric P. Verrecchia³

¹ *Institut F.-A. Forel, University of Geneva, Boulevard Carl-Vogt 66 CH-1205 Genève, armelle.dupasquier@unige.ch*

² *Beamline MicroXAS, Paul Scherrer Institute, CH-5232 Villigen Switzerland*

³ *Institute of Earth Surface Dynamics IDYST, University of Lausanne, CH-1002 Chavannes-près-Renens*

Travertines, defined as continental carbonates rocks precipitating from oversaturated rocks, as CO₂ degasses, are extremely sensitive to deposit conditions, especially to water chemistry and temperature, but also to climate and tectonics. Skoura travertines precipitated during Quaternary from thermal waters and are composed by a succession of various layers, varying in color (pink, orange, white, and grey), thickness (mm to cm) and texture (coarsely to fine-grained). Manganese and iron oxides commonly occur in these travertines either as diffuse or well-developed shrubs (up to 1 cm). Microbes are known to be present in travertines and are often the main drivers in Mn and Fe oxidation. In a former study at Skoura, Chafetz et al. (1998) reported that the Mn-shrubs in the travertines resulted from bacterially-induced precipitation. Mn-oxides appeared as spherical and rod-shaped bodies under scanning electron microscope (SEM). Their interpretation was based on the fact that microenvironments around bacterial bodies induced precipitation due to variations in pH and Eh. However, a geochemical model expressing stability fields of Fe and Mn-carbonates and oxides as a function of partial pressure of O₂ and CO₂ could explain chemical phases (modified after Garrels & Christ, 1967). The aim of this study is to determine whether the precipitation of Mn and Fe oxides in travertine samples is biologically induced or purely geochemical in origin. To do so, two main axes have been studied: (i) characterization of chemical phases and comparison to the geochemical model; (ii) search of indices associated with biological activity, including the reproduction of observations of Chafetz et al. (1998). Analyses included XRD, XRF, stable isotopes, observations using optical and electronic microscopy, and precise mineralogical analyses and elemental mapping performed on microsites of interest, using the synchrotron facilities at the Paul Scherrer Institute (Villigen, Switzerland).

Chemical analyses show that shrubs are mainly composed of cryptomelane, which is consistent with the geochemical model. The reproduction of results from Chafetz et al. (1998) was not possible: no rod-shaped or spherical bodies have been found. Instead, TEM reveals that Mn oxides appear as nm-scale needles. Diffusion Limited Aggregation (DLA) processes could explain the geometry of the shrubs. Results show that (i) there is no need for bacterial mediation to explain the presence of Mn-rich shrubs in Skoura travertines; (ii) the morphology observed is not consistent with bio-induced precipitation; (iii) bacterial precipitation remains unlikely.

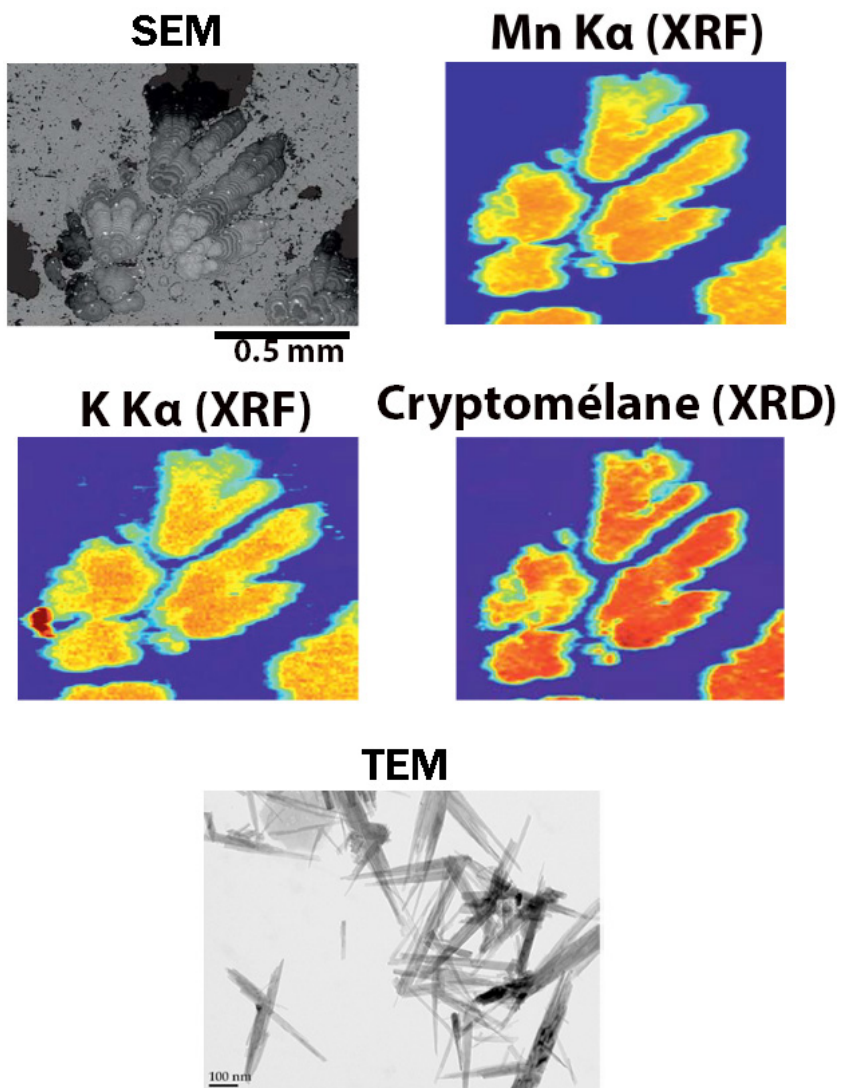


Figure 1. Pictures of Mn-rich shrubs under SEM, corresponding elemental XRF maps of Mn and K, mineralogical XRD map of Cryptomelane and pictures of nanoscale needles of Mn-shrubs observed using TEM.

REFERENCES

- Akdim, B., Desrochers, A. and Geurts, M. A. (1994), 'Morphogénèse et pétrogénèse des travertins hydrothermaux de Skoura au Maroc méridional', *Z. Geomorph. N.F* 38(3), 355-372.
- Chafetz, H. S., Akdim, B., Julia, R. and Reid, A. (1998), 'Mn- and Fe-rich black travertine shrubs ; bacterially (and nanobacterially) induced precipitates', *Journal of Sedimentary Research* 68(3), 404-412.
- Garrels, R. M. and Christ, C. L. (1967), *Equilibre des minéraux et de leurs solutions aqueuses*, Gauthier-Villars, Paris.

3. Gemmology

Michael S. Krzemnicki, Laurent E. Cartier

*Swiss Gemmological Society (SGG),
Swiss Society of Mineralogy and Petrography (SSMP)*

TALKS:

- 3.1 H. A.O. Wang, M. S. Krzemnicki, J.-P. Chalain, P. Lefèvre, W. Zhou, L.E. Cartier: Simultaneous High Sensitivity Trace Element and Isotopic Analysis for Gemstones using Laser Ablation Inductively Coupled Plasma Time-Of-Flight Mass Spectrometry
- 3.2 L. Franz, H.A. Hänni, W. Zhou: Sannan-Skarn: a new ornamental gemstone from Pakistan
- 3.3 M.S. Krzemnicki, D. Mannes, R. Marti, I. Jerjen, E. Lehmann: 3D Visualisation of inclusion features in emerald with neutron and X-ray tomography
- 3.4 L.E. Cartier, M.S. Krzemnicki: Golden South Sea Cultured Pearls: Cultivation, Species Determination and Treatment Detection

3.1

Simultaneous High Sensitivity Trace Element and Isotopic Analysis for Gemstones using Laser Ablation Inductively Coupled Plasma Time-Of-Flight Mass Spectrometry

Hao A.O. Wang, Michael S. Krzemnicki, Jean-Pierre Chalain, Pierre Lefèvre, Wei Zhou, Laurent Cartier

Swiss Gemmological Institute SSEF, Aeschengraben 26, 4051, Basel, Switzerland (hao.wang@ssef.ch)

GemTOF, installed at the Swiss Gemmological Institute SSEF, is a next-generation elemental analytical technique – Laser Ablation Inductively Coupled Plasma Time-Of-Flight Mass Spectrometry (LA-ICP-TOF-MS). The system enables full elemental mass spectrum acquisition at an ultra-high acquisition speed. Nearly all elements in the periodic table can be simultaneously acquired and accurately quantified with low limit of detection. Major to trace, even ultra-trace elements can be captured and slight concentration differences can be distinguished. As a result, multi-element information can be applied in multivariate statistical analysis thereby increasing the reliability of origin determination as well as detection of any possible new diffusion treatment methods. Additionally, higher precision in isotopic analysis is expected than with sequential acquisition Quadrupole-MS, especially for short transient signals. Novel research directions in gemstone age dating, analysis of inclusions and chemical zoning will benefit from the advantages of this system.

In the presentation, we aim to introduce this novel technique to gemmological testing and researches, illustrate key advantages of LA-ICP-TOF-MS comparing to conventional LA-ICP-Q-MS. We are going to demonstrated gemmological/geological applications using actual case studies.

3.2

Sannan-Skarn: a new ornamental gemstone from Pakistan

Leander Franz¹, Henry A. Hänni² & Zhou Wei²

¹ *Mineralogisch-Petrographisches Institut, University of Basel, Bernoullistrasse 30, CH-4056 Basel
(leander.franz@unibas.ch)*

² *SSEF Swiss Gemmological Institute, Aeschengraben 26, CH-4051 Basel*

At the Hong Kong Jewellery and Gem Fair September 2015 a significant volume of complex fine grained green rock material from Western Pakistan was sold to gemstone dealers under the name Maw Sit Sit. The new material originates from a remote area in Belochistan, about 60 km from the Muslim Bagh Chromite mine. The productive area lies in a thrust zone (Kazmi & Snee 1989) known as Karakorum Suture Zone. There, sediments from the Tethys were welded on the Eurasian Plate when the Indian continent collided some 65 Mio years ago. Triassic carbonate sediments and oceanic crust were imbricated in a tectonic movement going along with strong brecciation and mylonitization of the rocks. During this imbrication, intense fluid activity led to a replacement of carbonate by calcsilicate minerals. A common term to name the material is skarn, as it describes a rock formed by metasomatic replacement of a parent rock. Sannan is a specific modifier that describes the skarn from the new occurrence.

After a preliminary test, it became clear that this material has nothing in common with Maw Sit Sit, i.e. kosmochlor jade (e.g. Hänni & Meyer 1997; Franz et al. 2014), although specific gravity and refractive index may show overlaying data. Three samples (JG1– JG3) were selected and prepared for petrographic thin sections and investigated by polarization microscopy and micro-Raman spectroscopy. Each sample has a strongly different mineralogical composition.

Sample JG 1 (specific gravity 3.26 g/cm³) is of greenish-grey to dark green colour and has a fine grained, randomly oriented texture. Euhedral crystals of zoned green, up to 0.6 mm wide hydrogrossular (Ca₃(Al,Fe³⁺)₂(OH)₄/(SiO₃)₂) are surrounded by large prismatic diopside. Streaks and bands of chlorite are often cut by veins filled with calcite. The rock is a calcite-chlorite-hydrogrossular-diopside skarn. Sample JG 2 (specific gravity 2.98 g/cm³) is of medium green colour with a light green margin. Radiating clusters of short prismatic, up to 0.3 mm long aegirine crystals (Na-Fe-pyroxene, NaFe³⁺Si₂O₆) show a strong pleochroism from luminous green to yellow-green. In interspaces, subordinate fillings of agglomerated, yellow-brown prismatic pectolite crystals (NaCa₂Si₃O₈(OH)) occur. The lighter green margin shows a mylonitic texture with lenticular and linear concentrations of pectolite and chlorite as well as heavily fractured aegirine. The rock is a chlorite-pectolite-aegirine skarn. Sample JG 3 (specific gravity 2.67 g/cm³) shows an inhomogeneous patchy texture with green, dark greyish-green and whitish domains. Pale green winchite crystals (sodic-calcic amphibole, (CaNa)Mg₄(Al,Fe³⁺)Si₈O₂₂(OH)₂) of up to 1 mm size are intergrown with smaller, dark green aegirine crystals. In the darker areas, winchite prisms and fine aegirine needles lie in a groundmass of colourless natrolite (Na₂Al₂Si₃O₁₀ * 2H₂O). The white zones consist purely of sodalite (Na₈(Al₆Si₆O₂₄)Cl₂). The rock is thus an aegirine-natrolite-winchite skarn with sodalitic parts. The results of the crystal-optical analysis were confirmed by micro-Raman spectroscopy.

Qualitative chemical results were performed with ED-XRF. The analyses vary from sample to sample, due to their inhomogeneous composition. In all samples, the presence of Cr is identified and Ca is a main constituent, which represents a main difference to Maw Sit Sit.

The rocks described in this paper mainly consist of calc-silicates, which formed by tectonic movements and metasomatic processes in a thrust zone between carbonate sediments and descendants from the oceanic crust. The minerals that are identified are typical for metasomatic processes leading to skarn formation (e.g. Henmi et al, 1971; Nysten & Skogby, 1994). The green colour is due to chromium that is present in most of the constituent minerals.

Sannan-Skarn will have its position among other green stones, such as jadeite, Maw Sit Sit, nephrite a.s.o. It seems, however, clear that it has to be identified correctly and shall be sold under its correct name Sannan-Skarn, the recommended trade name for this new ornamental gemstone. The opaque material is suitable for cabochons, spheres, carvings and other jewellery items. Sannan-Skarn can either be differentiated from Maw Sit Sit by polarization microscopy of thin sections, by EDXRF by checking for Ca, or by micro-Raman spectroscopy through the identification of aegirine, winchite, hydrogrossular and the other minerals listed above.

REFERENCES

- Franz, L., Tay, T.S., Hänni, H.A., De Capitani, C., Theerapongs, T. & Atichat, W. 2014: A comparative study of jadeite, omphacite and kosmochlor jades from Myanmar, and suggestion for a practical nomenclature. *J. Gemmol.* 34, 210-229.
Hänni, H.A. & Meyer, J. 1997: Maw-sit sit (kosmochlor jade): A metamorphic rock with a complex composition from Burma.

Proceedings of the 26th International Gemmological Conference Idar-Oberstein, Germany, 22-24.

Henmi, K., Kusachi, I. & Numano, T. 1971: Contact minerals from Kushiro, Hiroshima prefecture, (I) gehlenite and hydrogrossular. *J. Min. Soc. Japan* 10, 160-169 (in Japanese).

Kazmi, A.H. & Snee, L.W. 1989: Emeralds of Pakistan, geology, gemology and genesis. Geological survey of Pakistan. Van Nostrand Reinhold Company, Melbourne, Australia, ISBN 0-442-30328-9.

Nysten, P. & Skogby, H. 1994: Manganese ferro-ferri-winchite from Harstigen, Filipstad, central Sweden. *Mineral. Mag.* 58, 168-172.

3.3

3D Visualisation of inclusion features in emerald with neutron and X-ray tomography

Michael S. Krzemicki^{1,2}, David Mannes³, Ralph Marti, Iwan Jerjen⁴, E. Lehmann³

¹ *Swiss Gemmological Institute SSEF, Aeschengraben 26, CH-4051 Basel (michael.krzemicki@ssef.ch)*

² *Institute of Mineralogy & Petrography, University of Basel, Bernoullistrasse 30, CH-4056 Basel*

³ *Laboratory for Neutron Scattering and Imaging, Paul Scherrer Institute, CH-5232 Villigen*

⁴ *X-ray tomography TOMCAT, Paul Scherrer Institute, CH-5232 Villigen*

Emerald, the green chromium-bearing variety of beryl $\text{Be}_3\text{Al}_2(\text{Si}_6\text{O}_{18})$, is highly valued as gemstone, although it is known to contain often quite large amounts of inclusion features, such as fluid and solid inclusions and fissures. Especially, in emeralds from Colombia, such features can be very prominent (Ottaway et al. 1994) and reduce the transparency – and thus beauty and value of the gemstone considerably. There is a long established tradition in the trade to fill open fissures in emeralds with colourless fillers, such as oil, wax and (artificial) resins, to reduce their visibility (Ringsrud 1983, Kiefert et al. 1999).

For this preliminary study on the 3D-visualisation of internal features in emeralds, we have analysed seven emeralds originating from Colombia, Brazil, and Zimbabwe, and one hydrothermal synthetic emerald at the ICON, the cold neutron imaging facility of the PSI in Villigen (Switzerland). Three emeralds were further analysed by X-ray micro-tomography, to compare the neutron images with X-ray absorption.

The study revealed that it is possible to visualise the complex pattern of internal features in emeralds with reasonable resolution and get 3D insight in their geometric relation. Furthermore we gained direct insight in the extent and spatial distribution of fissures fillings in our studied emeralds.

Although a thorough microscopic observation assisted with FTIR and microraman spectroscopy is in most cases sufficient for the characterisation of internal features and the identification of fissure filling, this new approach opens up further possibilities in gemstone research (Mannes et al. 2016), such as the characterisation of “Trapiche” growth patterns in gemstones, jadeite textures and impregnation, and pearl identification.

REFERENCES

- Kiefert, L., Hänni, H.A., Chalain, J-P., Weber, W. 1999: Identification of filler substances in emeralds by infrared and Raman spectroscopy. *Journal of Gemmology*, 26, 8, 501-520.
- Mannes, D., Hanser, C., Krzemicki, M., Harti, R., Jerjen, I. & Lehmann, E. 2016: Gemmological investigations on pearls and emeralds using neutron imaging. Abstract Proceedings of the 8th International Topical Meeting on Neutron Radiography (ITMNR-8), Beijing, China, 4–8 September, poster no. PA9 ID53.
- Ottaway, T.L., Wicks, F.J., Bryndzia, L.T., Kyser, T.K., Spooner, E.T.C. 1994: Formation of the Muzo hydrothermal emerald deposit in Colombia. *Nature*, 369, 552–554.
- Ringsrud, R., 1983: The oil treatment of emeralds in Bogota, Colombia. *Gems & Gemology*, 19, 3, 149-156.

3.4

Golden South Sea Cultured Pearls: Cultivation, Species Determination and Treatment Detection

Laurent E. Cartier^{1,2}, Michael S. Krzemnicki^{1,3}

¹ Swiss Gemmological Institute SSEF, Aeschengraben 26, CH-4051 Basel (laurent.cartier@ssef.ch)

² Institute of Earth Sciences, University of Lausanne, Géopolis, CH-1015 Lausanne

³ Institute of Mineralogy & Petrography, University of Basel, Bernoullistrasse 30, CH-4056 Basel

The South Sea pearl oyster *Pinctada maxima* is known to produce white (silver-lipped pearl oyster), cream and yellow pearls (gold-lipped pearl oyster). Careful breeding selection has even resulted in cultured pearls of saturated yellow - known and highly appreciated in the trade as golden cultured pearls (Müller, 1997; Shor, 2007). South Sea pearls are cultured mainly in Australia, Burma (Myanmar), Indonesia and Philippines at present. This study focuses on cultured pearl production of golden pearls from *Pinctada maxima* and gemmological investigations –including species determination and treatment detection- of such pearls.

The cause of colour of *Pinctada maxima* nacre is not fully understood (Karampelas, 2008; Scarratt, 2012), but is not only linked to the presence of natural colour pigments but also due to optical effects such as reflection and refraction (Dakin, 1913; Snow et al., 2004) at the surface and within the sub-surface nacre layer. It is however most unlikely, that the colour of *Pinctada maxima* is related to the presence of polyenes, as characteristic Raman peaks for these colour pigments at approx. 1135 cm⁻¹ and 1530 cm⁻¹ are absent in *Pinctada maxima*, very much in contrast to pearls from freshwater mussels (e.g. *Hyriopsis schlegeli*) and many other marine molluscs coloured by polyenes, such as Queen Conch (*Strombus Gigas*), Horse Conch (*Triplofusus giganteus*), Melo, Quahog (*Mercenaria Mercenaria*), and Scallop.

Apart from grading the colour of *Pinctada maxima* pearls into different categories of hue, saturation, and overtones, the main question remains the authenticity of colour, which is commonly tested in laboratories by a combination of UV-Vis-NIR reflectance, Raman spectroscopy, photoluminescence, and trace element analysis. These analyses provide complementary information about the nature of the colouration and its authenticity as has been well documented in literature (Elen 2001 & 2002; Karampelas 2008; Mamangkey 2009; Strack & Krzemnicki 2011; Scaratt et al., 2012).

Pearls oysters such as *Pinctada margaritifera*, *Pinctada maculata* and others can also produce these types of colours. Yellow *Pinctada maxima* are characterised by two broad Raman bands at about 1385 cm⁻¹ and 1540 cm⁻¹, not found in *Pinctada margaritifera* or the many molluscs species coloured by polyenes, such as freshwater pearls from *Unio*.

Given the high appreciation for golden South Sea pearls and the difficulty with harvesting intense colours, it is no surprise that lower-quality South Sea pearls have been treated to achieve a golden colour. All of these treated pearls could be identified positively by a combination of UV-Vis-NIR reflectance and Raman spectra. Part of these colour-treated pearls from *Pinctada maxima* showed a flat reflectance spectrum in the range from 330 nm to 460 nm as described by Elen (2001 & 2002) to be characteristic for treated pearls of this species. All of the treated pearls – even the ones with a non-specific reflectance spectrum – showed a distinctly stronger luminescence in Raman spectra when compared to their untreated yellow counterparts and in addition to this were lacking the small and broad Raman bands at about 1385 cm⁻¹ and 1540 cm⁻¹ characteristic for the natural yellow colour pigment of *Pinctada maxima*.

REFERENCES

- Dakin, W.J., 1913. Pearls. Cambridge University Press, Cambridge
- Elen, S., 2001. Spectral reflectance and fluorescence characteristics of natural-color and heat-treated “golden” South Sea cultured pearls. *Gems & Gemology*, Vol. 37, No. 2, pp. 114–123.
- Elen, S., 2002. Update on the Identification of Treated “Golden” South Sea Cultured Pearls. *Gems & Gemology*, 38(2), pp.156-159.
- Karampelas, S., 2008. Etude du changement de couleur des perles par traitement. (Doctoral dissertation, Université de Nantes (France) and Thessaloniki (Greece))
- Mamangkey, N., 2009. Improving the quality of pearls from *Pinctada maxima* (Doctoral dissertation, James Cook University).
- Müller, A. and Golay-Buchel (Lausanne), 1997. Cultured pearls: The first hundred years. Golay Buchel.
- Scarratt, K., Bracher, P., Bracher, M., Attawi, A., Safar, A., Saeseaw, S., Homkrajae, A. and Sturman, N., 2012. Natural pearls from Australian *Pinctada maxima*. *Gems Gemol*, 48, pp. 236-261.
- Shor, R., 2007. From single source to global free market: the transformation of the cultured pearl industry. *Gems & Gemology*, 43(3).
- Snow, M.R., Pring, A., Self, P. and Losic, D., 2004. The origin of the color of pearls in iridescence from nano-composite structures of the nacre. *American Mineralogist*, 89(10), pp.1353-1358.
- Strack, E., Krzemnicki, M.S., 2011. Experimental treatments involving dye and heat for Chinese freshwater cultured pearls and their detection by Raman spectrometry. *Gems & Gemology*, Gem-Research Conference abstract.

4. Palaeontology

Christian Klug, Torsten Scheyer, Lionel Cavin

*Schweizerische Paläontologische Gesellschaft,
Kommission des Schweizerischen Paläontologischen Abhandlungen (KSPA)*

TALKS:

- 4.1 Anquetin Jérémy, Tong H., Claude J.: The neck of the Late Jurassic *Platycheilus oberndorferi* and the origin of neck retraction mechanisms in turtles
- 4.2 Antcliffe Jonathan B.: The Ecology of the Ediacaran Biota
- 4.3 Baumgartner Peter O., Dumitrica P., Kukoc D., Andjic G.: Revision of some Late Cretaceous multicystid Nassellaria, a contribution to the biostratigraphy the Caribbean Large Igneous Province
- 4.4 Belvedere Matteo, Marty D., Stevens K., Ernst S., Razzolini N.L., Paratte G., Cattin M., Lovis C., Meyer C.A.: Minute sauropod tracks from the Late Jurassic of Canton Jura: babies or dwarfs? Morphological and behavioural evidences
- 4.5 Brosse Morgane, Baud A., Bucher H., Goudemand N., Nützel A., Ware D., Frisk Å., Hagdorn H.: Basal Triassic exotic blocks from Oman: The promised land, no raft of the Medusa
- 4.6 Carrillo Briceño Jorge D., Luz Z., Hendy A., Jaramillo C., Vennemann T.W., Kocsis L., Sánchez-Villagra M.R.: Colombian fossil elasmobranchs from the “last days” of the Central America Seaway and their environmental significance
- 4.7 Carrillo Juan D.: Endemic South American mammals from the Neotropics: phylogeny, diversity, and implications for the Great American Biotic Interchange
- 4.8 Costeur Loic, Mennecart B.: The ear before birth: morphology, ossification timing, and allometry
- 4.9 Daley Allison C.: The ecology and evolution of the anomalocaridids
- 4.10 Drage Harriet B., Holmes J.D., García-Bellido D.C., Daley A.C.: Detailed trilobite moulting behaviour preserved in the Emu Bay Shale, South Australia
- 4.11 Etter Walter: Palaeoecology of the Lower Jurassic Schambelen member of northern Switzerland
- 4.12 Ferrante Christophe, Vennemann T., Cavin L., Martini R.: Histology and geochemical study of bones of an *Allosaurus* (Dinosauria: Theropoda)
- 4.13 Foth Christian, Joyce W.G.: Skull shape variation in recent and fossil turtles through time and its relation to climate, habitat and feeding ecology
- 4.14 Frey Linda, Coates M., Ginter M., Klug C.: The first skeletal remains of *Phoebodus politus* Newberry 1889 (Chondrichthyes: Elasmobranchii) and its ecology
- 4.15 Jattiot Romain, Bucher H., Brayard A., Brosse M., Jenks J., Bylund K.G.: A new key Smithian (Early Triassic) quantitative ammonoid biochronology from the western USA basin
- 4.16 Klug Christian, Frey L., Korn D., Jattiot R., Rücklin M.: No fossil record? Yes fossil record! Konservat-Lagerstätten of the End-Devonian Hangenberg Black Shale in the eastern Anti-Atlas (Morocco)
- 4.17 Martini Pietro, Geraads D., Le Tensorer J.-M., Costeur L.: Cranial morphology of Recent and Pleistocene camels

- 4.18 Menecart Bastien, Costeur L.: How does bony labyrinth morphology help resolve the phylogeny and diversification timing of deer?
- 4.19 Pates Stephen, Daley A.C.: The taxonomy and ecology of *Caryosyntrips*, a radiodontan from the Cambrian of Canada, Spain and the USA
- 4.20 Vasilyan Davit: Herpetofauna of the early MP 16, Bartonian, Middle Eocene of Switzerland

POSTERS:

- P 4.1 Burek I., Comment G., Anquetin J.: A paleontological field school organized in Canton Jura
- P 4.2 Becker D., Tissier J., Costeur L., Antoine P.-O.: Mid-Oligocene Rhinocerotidae from Bumbach (Switzerland)
- P 4.3 Bischof E.A.: Insights into the Cidarid Echinoids from the Middle Oxfordian St. Ursanne Formation of the Swiss Jura Mountains
- P 4.4 Boivin S., Lathuilière B., Durllet C., Lazar I., Martindale R., El Khmidi K., Martini R.: Hettangian-Sinemurian coral association of Amellago area (High Atlas, Morocco): first approach.
- P 4.5 Burek, I.: Comparative cranial morphology of *Desmatochelys lowii* and modern marine turtles
- P 4.6 Chacko M.R., Carrillo-Briceño J.D.: A marine bony fish assemblage (Teleostei) from the early Miocene of the Southern Caribbean (Cocinetas Basin, Guajira Peninsula)
- P 4.7 Bapst L., Costeur L., Becker D.: Tooth mesowear highlights perissodactyl diets and environments in the Palaeocene of Europe
- P 4.8 Menecart B., Jouve S., Douteau J., Jalil N.-E.: The oldest durophagous Thalattosuchian (Crocodylomorpha, Machimosaurini) from the lower Bathonian of Central High Atlas, Morocco
- P 4.9 Peyrotty G., Peybernes C., Onoue T., Ueda H., Martini R.: Upper Triassic limestones from central and SW Hokkaido, Japan: a new insight on the Panthalassa Ocean
- P 4.10 Scherz K.: An assessment of the phylogeny of cats (Felidae), including *Smilodon gracilis*, using the morphology of the petrosal bone
- P 4.11 Scheyer T.M., Neenan J.M., Bodogan T., Furrer H., Plamondon, M.: A new, exceptionally preserved juvenile reptilian fossil (Diapsida) from the Middle Triassic of Ducan, Canton Grisons, Switzerland
- P 4.12 Tissier J., Becker D., Codrea V., Costeur L., Fărcaș C., Solomon A., Venczel M., Maridet O.: New material of amynodontids (Mammalia, Perissodactyla) from Romania
- P 4.13 Hoffmann R., Weinkauf M.F.G., Fuchs D.: Grasping the shape of belemnoid arm hooks – a quantitative approach

4.1

The neck of the Late Jurassic *Platycheilus oberndorferi* and the origin of neck retraction mechanisms in turtles

Jérémy Anquetin^{1,2}, Haiyan Tong³ & Julien Claude⁴

¹ JURASSICA Museum, Route de Fontenais 21, CH-2900 Porrentruy (jeremy.anquetin@jurassica.ch)

² Department of Geosciences, University of Fribourg, Chemin du Musée 6, CH-1700 Fribourg

³ Palaeontological Research and Education Centre, Mahasarakham University, Kantarawichai, Mahasarakham 44150, Thailand

⁴ Institut des Sciences de l'Evolution de Montpellier, UMR 5554 CNRS, Montpellier, France

Modern turtles are divided into two main clades, which find their origin as early as the Middle Jurassic. These two groups have independently developed complex double-bend neck retraction mechanisms. Pleurodires (side-necked turtles) fold the neck sideways and tuck the head under the anterior margin of the carapace. Cryptodires (hidden-necked turtles) withdraw the neck and head in the vertical plane between the shoulder girdles. Since each neck retraction mechanism offers some measure of protection for the neck and head in extant turtles, it is usually assumed that these mechanisms evolved mainly for protective reasons.

Here, we describe the neck of *Platycheilus oberndorferi*, a Late Jurassic stem pleurodire from Germany and Switzerland, and find major morphological similarities with modern cryptodires in the posterior part of the neck. A biomechanical analysis reveals that this taxon was able to withdraw the neck in the vertical plane, but that this retraction was incomplete. The head and anterior part of the neck cannot be withdrawn within the shell, which undermines the potential protective value of neck retraction in this taxon.

Platycheilus oberndorferi is a peculiar turtle that shows remarkable morphological convergences with the modern matamata (*Chelus fimbriata*) and the snapping turtles (*Chelydra serpentina* and *Macrochelys temminckii*). This strongly suggest that *Platycheilus* was an ambush predator practising ram and/or suction feeding. We therefore suggest that vertical neck retraction primarily evolved in this taxon to enable fast forward projection of the head and improve capture of darting prey.

The functional origin of neck retraction mechanisms in turtles has never been fully explored. The apparition of the complex double-bend mechanisms of pleurodires and cryptodires for purely protective reasons is relatively unlikely. The horizontal folding of pleurodires actually offers little more protection than the lateral head tuck of stem turtles, whereas in cryptodires the protection is only effective when the retraction is complete, which necessitates substantial morphological changes from the ancestral cervical morphotype.

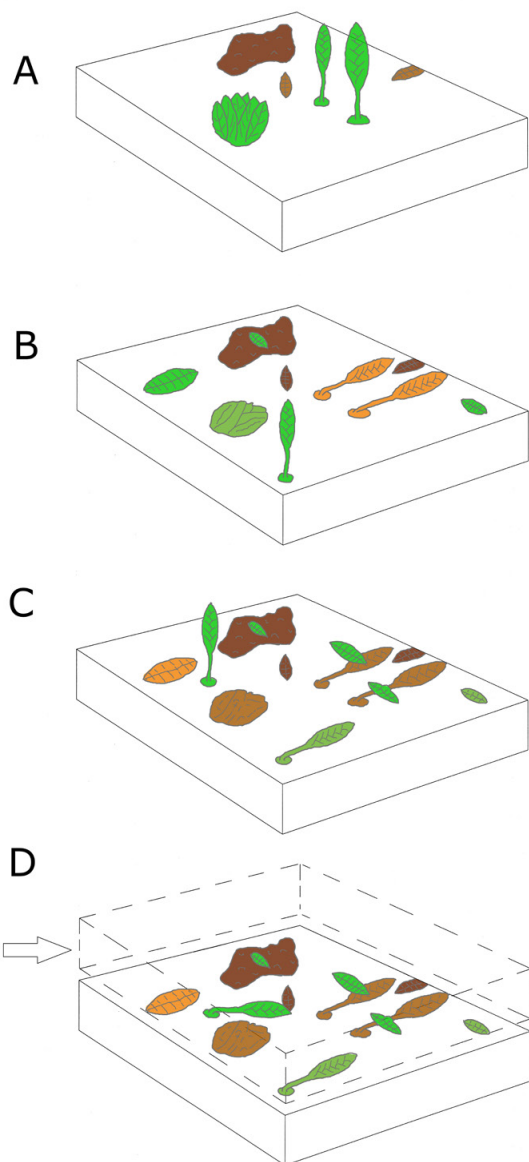
The case of *Platycheilus* offers a likely explanation to the origin of complex neck retraction mechanism in turtles, especially for cryptodires. Neck retraction could have evolved gradually as a way to enable fast forward thrust of the head during prey capture in the water. Partial neck retraction would already provide an advantage, as demonstrated by the very specialized ecological niche occupied by *Platycheilus*. Once a primary mechanism of neck retraction was in place, it would be easier to obtain complete head withdrawal for protection via natural selection. We therefore suggest that vertical neck retraction in cryptodires may have evolved primarily in order to enable fast forward projection of the head during underwater feeding, and that protection of the head by complete withdrawal within the shell is actually an exaptation.

4.2

The Ecology of the Ediacaran Biota

Jonathan B. Antcliffe¹¹ Faculty of Geosciences and Environment, University of Lausanne, UNIL – Sorge Géopolis - 1015 Lausanne, Switzerland

Ediacaran macrofossils immediately precede the first animal ecosystems of the Cambrian Period and have excited much attention for potentially containing ancestors of the modern animal phyla. Ediacaran fossil surfaces have been variously interpreted as vertically tiered census populations comparable to animal ecosystems, or as osmotrophic ecosystems exploiting turbulent flow regimes. These hypotheses are highly dependent upon the taphonomic interpretation of critical fossil surfaces



as consensus populations representing the association of the organisms in life. Reanalyses of these surfaces, however, indicate that this taphonomic model is inconsistent with the range of preservation states seen in each taxon. A new taphonomic model, for Mistaken Point surfaces in Newfoundland Canada is presented (Antcliffe et al 2015), described using an index of decay. This is then compared to other sites around the Avalonian palaeogeographic terrane. This reveals a complex history of life, death, and decay at these sites. Data gathered from large scale casting projects in Newfoundland show that only 15-40% of individuals were killed by ash flows, rather than the whole population as previously interpreted. This shows that Ediacaran organisms had a diverse range of ecological relationships with the microbial mat system. Frondose organisms, such as *Charnia*, are engaged in chemical exchange with the sediment and the water column with the stem penetrating through the microbial mat. Reclining forms, such as *Fractofusus*, lived exclusively above the microbial mat and drew nutrients from the dead organisms on which they typically grew. This ecology is based on organism interaction with the sediment-water interface quite unlike that of modern vertically tiered metazoan communities that have developed since the start of the Cambrian Period. When coupled with evidence for the growth dynamics of Ediacaran organisms these data are beginning to suggest which modern organisms maybe relatives of the Ediacaran biota.

Figure 1. Schematic succession of the biota as seen on the Mistaken Point E surface: a) colonisation of surface by fronds such as *Charniodiscus* and *Bradgatia*; b) Death and decay of fronds felled in orientation by current, development of more fronds and overgrowth by *Fractofusus*; c) Death and further decay of fronds felled in orientation of current, development of more fronds and overgrowth by *Fractofusus*; d) influx of ash fells fronds in direction of ash flow (shown by arrow), snapshot preservation of surface showing differential decay profiles. Colours indicate progress decay from green to brown.

REFERENCES

Antcliffe, J.B., Hancy, A., & Brasier, M.D. 2015: A new ecological model for the ~565Ma Ediacaran biota of Mistaken Point, Newfoundland. *Precambrian Research*, 268, 227-242.

4.3

Revision of some Late Cretaceous multicyrtyd Nassellaria, a contribution to the biostratigraphy the Caribbean Large Igneous Province

Peter O. Baumgartner¹, Paulian Dumitrica^{1,2}, Duje Kukoc¹, & Goran Andjic¹

¹ Institut des Sciences de la Terre, Université de Lausanne, Géopolis, 1015 Lausanne

² mailing address: Dennigkofenweg 33, 3073 Gümligen, Switzerland (peter.baumgartner@unil.ch)

A revised Late Cretaceous radiolarian biochronology is essential for more accurate and non-controversial dating of many radiolarian-rich siliceous sediments associated with effusive phases of the Caribbean Large Igneous province (CLIP, Fig. 1), as well as with, partly coeval, arc-derived tuffaceous and volcano-clastic sediments. These sediments usually lack planktonic foraminifera. Hence, the reconstruction of the CLIP evolution is until now largely based on ³⁹Ar/⁴⁰Ar-ages, often contradicted by fossil ages, when available.

Multicyrtyd Nassellaria (Fig. 2) are commonly used in the biostratigraphy of the Cretaceous. However, many species have holotypes defined by drawings from thin sections in classical work published at the turn of the 19th to the 20th century, or by transmitted light images in 1950-1985. The comparison of the now most widely used SEM images with this earlier work is often ambiguous. As a consequence, the “semantics” of many species has broadened by inclusion of morphotypes that more or less loosely compare with the original descriptions. Yet, the broader the species concept, the longer tends to be the species range.

To obtain a better resolution for a global, low-latitude, Late Cretaceous radiolarian biochronology, we are using the following strategies:

1. Obtain topotypic material from DSDP-ODP and land sites, where Late Cretaceous radiolarian taxa were described.
2. Compare SEM and transmitted light illustrations of topotypic material with original descriptions.
3. Use morphometrics to try to separate closely related forms in well-preserved material.
4. Construct evolutionary lineages for selected taxa.

So far we have been working on the following taxa (Fig.2): “*Dictyomitra*” *formosa* group, including “*D. torquata*”, “*D. duodecimcostata*”, “*D. koslovae*” and other similar taxa. *Dictyomitra multicostata*, *D. densicostata*, and other similar taxa. “*Pseudo-dictyomitra*” *pseudomacrocephala* group and related “*Pseudodictyomitra*” spp. We define several new genera and species.

Several local radiolarian biostratigraphies for the Late Cretaceous have been proposed in the last 40 years e.g. Pesagno (1976), Taketani (1986) and the low-latitude synthesis by Sanfilippo and Riedel (1985), which was based on DSDP Sites and land samples. These zonations have been used for a long time, although zonal marker taxa used are now known to have longer ranges. In addition, many species co-occurrences observed in samples from Central America, DSDP Sites and Southern Europe are incompatible with the ranges expressed in the fore-mentioned zonations. Several ranges are also shorter than those expressed in earlier publications.

Until now, we have used the stacked chronostratigraphic ranges of several authors with the hope to get close to the “full” global range of each taxon. To assess the age of a sample we have used the concurrent “full” range of the species recorded in each sample (e.g. (Baumgartner 1984, Bandini et al. 2006, 2008, Denyer & Baumgartner 2006, etc.). This method is, however, very unsatisfactory, because of the important differences in the quality of calibration to other fossil groups and ultimately to the time scale.

To overcome this situation, we propose to create a new, Late Cretaceous radiolarian biochronology based on Unitary Associations, a concept that has proven to be specially adapted to both temporally and spatially incomplete radiolarian fossil record (Baumgartner, 1984; Baumgartner et al., 1995; Carter et al., 1998; O’Dogherty, 1994).

At present, we work with a database consisting of >12,000, mostly unpublished, SEM images from some hundred Upper Cretaceous samples from low latitude DSDP/ODP Sites and land sections in Central and South America, the Caribbean and the Mediterranean area.

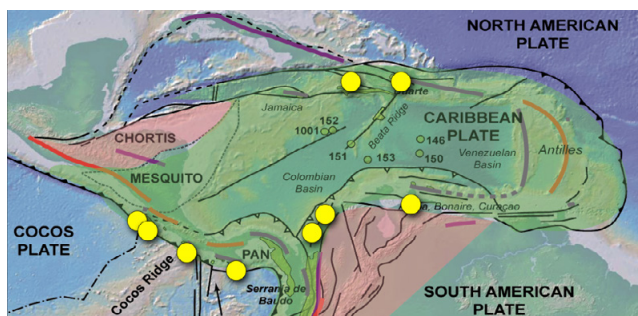


Figure 1. Map of the Caribbean Plate with published Upper Cretaceous radiolarian occurrences related to CLIP-like plateaus.

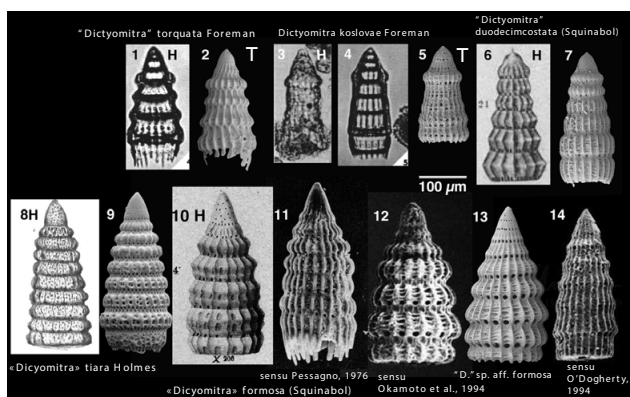


Figure 2. Comparison of some Late Cretaceous holotypes (H) and published specimens with topotypic material from DSDP sites. 1-2. "*Dictyomitra*" *torquata* Foreman. 3-5. "*Dictyomitra*" *koslovae* Foreman. 6-7. "*Dictyomitra*" *duodecim-costata* (Squinabol). 8-9. "*Dictyomitra*" *tiara* Holmes. 10-14. "*Dictyomitra*" *formosa* (Squinabol), 10. holotype. 11. sensu Pessagno. 12. sensu Okamoto et al. 13. "*D.*" sp. aff. *formosa*. 14. "*D.*" *formosa* sensu O'Dogherty, 1994.

4.4

Minute sauropod tracks from the Late Jurassic of Canton Jura: babies or dwarfs? Morphological and behavioural evidences

Matteo Belvedere¹, Daniel Marty¹, Kent Stevens², Scott Ernst¹, Novella L. Razzolini³, Géraldine Paratte¹, Marielle Cattin¹, Christel Lovis¹, Christian A. Meyer⁴

¹ Office de la Culture, Paléontologie A16, Hôtel des Halles, P.O. Box 64, CH-2900 Porrentruy 2, Switzerland

² Department of Computer and Information Science, University of Oregon, OR 97403, USA

³ Institut Català de Paleontologia Miquel Crusafont (ICP), Mesozoic Research Group, Carrer Escola Industrial, 23, 08201 Sabadell, Spain

⁴ Naturhistorisches Museum Basel, Augustinergasse 2, 4001 Basel, Switzerland

Excavations along Highway A16 (NW Switzerland) in Kimmeridgian tidal-flat deposits of the Jura carbonate platform revealed more than 650 sauropod and tridactyl (mostly theropod) trackways (Marty 2008, Marty et al., 2015), from huge (PL>1 m for sauropod, PL>50 cm for theropods) to tiny footprints (PL<10 cm for both sauropod and tridactyl trackmakers). Since the small tracks may have been left either by small adults or by young individuals of a larger species, 'baby' dinosaur tracks are not easy to be identified as such in the fossil record.

We present a group of 8 subparallel tiny sauropod trackways, of equal preservation, in very close association to each other, suggesting that the animals were moving together. The tracks are very small (mean PL: 11.6 cm; PW: 7.8 cm; ML: 4.4 cm, MW: 7.6 cm; small heteropody) and well-preserved (dI-IV, dI-II claws, manus ungual). A slightly larger trackway (PL: 22.9 cm) is in close vicinity to the smaller ones on the same level. Additionally, 17 small sauropod trackways (PL between 30 and 45 cm) have a similar configuration and track morphology (digits and claws of pes, manus ungual), but proportionally shorter digits. These slightly larger trackways are subparallel to the group of tiny trackways, and all but four proceed in the opposite direction from the tiny trackways.

We attribute the tiny tracks to very young sauropods of the same species as had left the small tracks, based on their morphological similarities (where the observed proportional differences of the digits compared to overall track length reflect allometric growth). The presence of very large sauropod (PL>1 m) and huge theropods (PL>50 cm) tracks on a level only about 10 cm higher supports our conclusion that the very small tracks were created by juveniles. Because most of the larger sauropod trackways are not heading in the same direction, at a first glance this ichnoassemblage of tiny tracks may provide evidence for separated gregarious behaviour (Myers & Fiorillo, 2009), although the question of if and how 'baby' sauropods were protected against large predators in an open tidal-flat environment should not be disregarded.

REFERENCES

- Marty D. 2008: Sedimentology, taphonomy, and ichnology of Late Jurassic dinosaur tracks from the Jura carbonate platform (Chevenez-Combe Ronde tracksite, NW Switzerland): insights into the tidal-flat palaeoenvironment and dinosaur diversity, locomotion and palaeoecology. *GeoFocus*, 21, 1-278.
- Marty, D., Stevens, K., Ernst, S., Paratte, G., Cattin, M., Lovis, C., Hug, W., & Meyer C.A. 2015: Processing and analysis with 'Cadence Toolse' of Late Jurassic dinosaur track data systematically acquired during ten years of excavation prio to construction of highway A16, NW Switzerland. 13th Swiss Geological Meeting 2015, Abstract book, 149.
- Myers, T. S., & Fiorillo, A. R. 2009: Evidence for gregarious behavior and age segregation in sauropod dinosaurs. *Palaeogeography, Palaeoclimatology, Palaeoecology*, 247, 96-104

4.5

Basal Triassic Exotic Blocks from Oman: The Promised Land, no Raft of the Medusa

Morgane Brosse¹, Aymon Baud², Hugo Bucher¹, Nicolas Goudemand³, Alexander Nützel⁴, David Ware¹, Åsa Frisk⁵ & Hans Hagdorn⁶

¹ Paleontological Institute and Museum, University of Zurich, Karl Schmid-Strasse 4, Zürich, 8006, Switzerland

² Geol Museum, UNIL-BFSH2, Lausanne, CH-1015, Switzerland

³ University Lyon, ENS de Lyon, CNRS, University Claude Bernard Lyon 1, Institut de Génomique Fonctionnelle de Lyon, UMR 5242, 46 allée d'Italie, Lyon Cedex 07, F-69364, France

⁴ Bayerische Staatssammlung für Paläontologie und Geologie, Richard Wagner Strasse 10, Munich, D-80333, Germany

⁵ Department of Earth Sciences, Palaeobiology, Uppsala University, Villavägen 16, Uppsala, SE 752 36, Sweden

⁶ Muschelkalk Museum Ingelfingen, Schlossstraße 11, Ingelfingen, 74653, Germany

In Oman, Griesbachian marine faunas were first reported from an exotic block at Wadi Wasit in the Hawasina nappes (Krystyn et al. 2003). Here, we document a new exotic boulder of the same age discovered in the Batain mélange (eastern Oman).

The Asselah boulder is a 1 metre-thick crinoidal limestone, which yields an abundant and diversified fauna including crinoids, ammonoids, gastropods and conodonts:

- Typical conodont index species such as *Hindeodus parvus* and several *Isarcicella* species allow to give the entire succession a Griesbachian age (= base of Induan).
- Few small specimens of ammonoids including *Episageceras* sp., *Metopliceras subdemissum*, *Aldonoceras* sp. and *Ophiceras* sp. have been retrieved from the block. This association documents the co-occurrence of taxa of both Permian and Triassic affinities. Size analyses of the gastropod *Naticopsis* sp. provide further evidence against the Lilliput effect hypothesis (e.g. Brayard et al. 2010).
- Crinoid ossicles suggest the occurrence of a holocrinid with subpentagonal proximal columnals and long cylindrical cirrals with transverse articulation ridges. The distal columnals are cylindrical with multiradiate facets; culmina may bifurcate as typical for Holocrinidae. Obviously, this crinoid is conspecific with *Baudicrinus krystyni* Oji and Twitchett, 2015 from the Wadi Wasit block. However, the Asselah material suggests holocrinid assignment of *Baudicrinus* rather than dadocrinid. Holocrinids had hitherto not been documented until the Olenekian (Hagdorn 2011), and this discovery pushes their origin back into the Griesbachian

Deposition of this crinoidal limestone on off-shore sea mounts was contemporaneous with the “anachronistic” microbial limestone known from shallow shelves of equatorial Cimmerian blocks, a facies that has been interpreted as devastated environments illustrating complete diversity collapses in the immediate aftermath of the Permian-Triassic boundary mass extinction (Schubert and Bottjer 1992; Schubert and Bottjer 1995, but see Hautmann et al 2015 for contradictory results and interpretations).

The Asselah and Wasit blocks record basal Triassic fossil assemblages that are unknown from continental shelves during this post-extinction transgressive interval. The associated community was living in well oxygenated shallow marine waters. These neritic off shore plateaus harboured dense prairies of crinoids and various skeletal organisms and functioned as healthy carbonate factories. They escaped the siliclastic fluxes that prevailed on epicontinental platforms, slopes and basins. Moreover, absence of any indication of oxygen depletion does not support a rise of the oxygen minimum zone.

Griesbachian offshore sea-mounts from Oman evidently escaped the alleged “devastation” and “lethally hot” temperatures that are supposed to have delayed the biotic recovery. A Griesbachian cold and dry global climate is indicated by the plant record from NE Greenland, Pakistan, and Australia (Hochuli et al. 2016), which together with the prosperous marine environment described here, demonstrate that the deleterious conditions of the Permian-Triassic boundary mass extinction were short-lived.

REFERENCES

- Brayard, A., Nützel, A., Stephen, D. A., Bylund, K. G., Jenks, J., & Bucher, H. 2010: Gastropod evidence against the Early Triassic Lilliput effect. *Geology*, 38(2), 147-150.
- Hagdorn, H., 2011: Triassic: the crucial period of post-Palaeozoic crinoid diversification: *Swiss Journal of Palaeontology*, v. 130, no. 1, p. 91-112.
- Hautmann, M., Bagherpour, B., Brosse, M., Frisk, Å., Hofmann, R., Baud, A., Nützel, Goudemand, N. & Bucher, H. 2015: Competition in slow motion: The unusual case of benthic marine communities in the wake of the end-Permian mass

- extinction. *Palaeontology* 58(5): 871-901.
- Krystyn, L., Richoz, S., Baud, A., & Twitchett, R. J., 2003: A unique Permian–Triassic boundary section from the neotethyan Hawasina basin, Central Oman Mountains: *Palaeogeography, Palaeoclimatology, Palaeoecology*, v. 191, no. 3, p. 329-344.
- Hochuli, P. A., Sanson-Barrera, A., Schneebeli-Hermann, E., & Bucher, H. 2016: Severest crisis overlooked—Worst disruption of terrestrial environments postdates the Permian–Triassic mass extinction. *Scientific Reports*, 6.
- Oji, T., & Twitchett, R. J., 2015: The Oldest Post-Palaeozoic Crinoid and Permian-Triassic Origins of the Articulata (Echinodermata): *Zoological science*, v. 32, no. 2, p. 211-215.
- Schubert, J. K., Bottjer, D. J., & Simms, M. J., 1992: Paleobiology of the oldest known articulate crinoid. *Lethaia*, v. 25, no. 1, p. 97-110.
- Schubert, J. K., & Bottjer, D. J. 1995. Aftermath of the Permian-Triassic mass extinction event: Paleocology of Lower Triassic carbonates in the western USA. *Palaeogeography, Palaeoclimatology, Palaeoecology*, 116(1), 1-39.

4.6

Colombian fossil elasmobranchs from the “last days” of the Central America Seaway and their environmental significance

Jorge Domingo Carrillo-Briceño¹, Zoneibe Luz², Austin Hendy³, Carlos Jaramillo⁴, Torsten W. Vennemann², László Kocsis⁵ & Marcelo Ricardo Sánchez-Villagra¹

¹ Palaeontological Institute and Museum, University of Zürich, Karl-Schmid-Strasse 4, 8006 Zürich
(jorge.carrillo@pim.uzh.ch; m.sanchez@pim.uzh.ch).

² Institut des Dynamiques de la Surface Terrestre, Université de Lausanne, Rue de la Mouline, 1015 Lausanne
(zoneibe.luz@gmail.com; torsten.vennemann@unil.ch)

³ Natural History Museum of Los Angeles County, 900 Exposition Blvd, Los Angeles, California 90007 USA
(ahendy@nhm.org)

⁴ Smithsonian Tropical Research Institute, Av. Gorgas, Ed. 235, 0843- 03092 Balboa, Ancón, Panamá (jaramillo@si.edu)

⁵ University of Brunei Darussalam, Faculty of Science, Geology Group, Jalan Tungku, BE 1410, Brunei Darussalam
(laszlokocsis@hotmail.com)

The Central America Seaway was a deep oceanic connection between the Pacific and Atlantic Oceans along the tectonic boundary of the South America and Caribbean plates that existed through the Cenozoic until the middle-Late Miocene, when it constricted coincident with the rising of the Panama Isthmus (Montes et al., 2012). During this time, large areas of the northern margin of South America were submerged including Cocinetas Basin, located in the eastern flank of La Guajira Peninsula, northern Colombia (South Caribbean). This region presents extensive and well-exposed Neogene deposits that have yielded a rich record of invertebrates and vertebrates (Moreno et al., 2015; Hendy et al., 2015; Carrillo-Briceño et al., 2016) and has been well dated using Sr isotopes (Hendy et al. 2015). Recent expeditions (2010-2014) collected early-middle Miocene fossil elasmobranchs from Jimol (Burdigalian), Castilletes (late Burdigalian-Langhian) and Ware (Gelasian-Piacenzian) formations that are presented here.

The assemblages are characterized by at least 32 taxa of sharks (Dalatiidae, Pristiophoridae, Ginglymostomatidae, Lamnidae, †Otodontidae, Alopiidae, Hemigaleidae, Carcharhinidae and Sphyrnidae) and rays (Rhynchobatidae, Pristidae, Dasyatidae, Aetobatidae, Myliobatoidea, Rhinopteridae, and Mobulidae). Twenty-five taxa are reported from Colombian Neogene deposits for the first time. The habitat preferences of the living representatives evidence tropical coastal-shallow marine environments. These shallow paleoenvironments could suggest a decrease in relative sea level or basin shallowing, contrasting with the underlying Aquitanian deposits of the Uitpa Formation, which lower part was probably accumulated at a water depth of 100 to 200 m (Carrillo-Briceño et al., 2016).

†*Carcharocles megalodon* was found in the Castilletes Formation and this record support the presence of the species as early as 16.2 Ma., during the later Burdigalian. Paleotemperature estimation was performed using oxygen in phosphate stable isotopes on shark's teeth. Preliminary results of shallow water shark species were homogeneous and range from 19.8‰ to 20.1‰ (VSMOW) reflecting temperatures between 25 to 26°C approximately.

REFERENCES

- Carrillo-Briceño, J.D., Argyriou, T., Zapata, V., Kindlimann, R. & Jaramillo, C.A. 2016: A new Early Miocene (Aquitanian) Elasmobranchii assemblage from the Guajira peninsula, Colombia. *Ameghiniana*, 53, 77-99.
- Hendy, A.J.W., Jones, D.S., Moreno, F., Zapata, V. & Jaramillo, C. 2015: Neogene molluscs, shallow marine paleoenvironments, and chronostratigraphy of the Guajira Peninsula, Colombia. *Swiss Journal of Palaeontology*, 134, 1, 45-75.
- Montes, C., Bayona, G., Cardona, A., Buchs, D.M., Silva, C., Morón, S., Hoyos, N., Ramírez, D.A., Jaramillo, C.A. & Valencia, V. 2012: Arc-continent collision and orocline formation: Closing of the Central American seaway. *Journal of Geophysical Research: Solid Earth*, 117, B4, B04105.
- Moreno, F., Hendy, A.J.W., Quiroz, L., Hoyos, N., Jones, D.S., Zapata, V., Zapata, S., Ballen, G.A., Cadena, E., Cárdenas, A.L., Carrillo-Briceño, J.D., Carrillo, J.D., Delgado-Sierra, D., Escobar, J., Martínez, J.I., Martínez, C., Montes, C., Moreno, J., Pérez, N., Sánchez, R., Suárez, C., Vallejo-Pareja, M.C. & Jaramillo, C. 2015: Revised stratigraphy of Neogene strata in the Cocinetas Basin, La Guajira, Colombia. *Swiss Journal of Palaeontology*, 134, 1, 5-43.

4.7

Endemic South American mammals from the Neotropics: phylogeny, diversity, and implications for the Great American Biotic Interchange

Juan D. Carrillo^{1,2}

¹ *Paläontologisches Institut und Museum, Universität Zürich, Karl-Schmid-Strasse 4, CH-8006 Zurich (juan.carrillo@pim.uzh.ch)*

² *Museum of Zoology, University of Cambridge, Downing St, CB2 3EJ Cambridge UK*

South America (SA) was isolated during most of the Cenozoic and was home to a highly endemic fauna, which include caviomorph rodents, xenarthrans (sloths, anteaters and armadillos) and South American native ungulates (SANUs), among others. SANUs are a conspicuous faunal element in the continent fossil record and exhibit a high taxonomic diversity and large morphological disparity. However, the phylogenetic relationships of this group with other placentals is not fully resolved. The isolation of SA ceased during the late Neogene after the formation of the Isthmus of Panama and the establishment of a land connection with North America (NA). As result, one of the greatest biological experiments of biota exchange at a continental scale took place, the Great American Biotic Interchange (GABI). The Neotropical fossil record is essential to better understand the diversity patterns and mammal evolution in SA. However, there is a fossil sampling bias in the continent, and is little what we know from the tropics when compared with the temperate faunas. This obscures our understanding of the GABI and the palaeobiogeography of the endemic groups in the continent. In this contribution I study the palaeobiology and phylogenetic relationships of an exceptionally complete SANU representative, and present new findings from northern SA and its implications for the GABI.

Notoungulata is the major clade within SANUs. The earliest notoungulates are mostly known by isolated teeth. I describe one of the oldest skeletons of a notoungulate with associated craniodental and postcranial elements: *Thomashuxleya externa* (Isotemnidae) from Cañadón Vaca in Patagonia, Argentina (middle Eocene). The estimated body size is ~212 kg, and bone histology reveals features associated with increase loading in large mammals and shows the new specimen was skeletally mature. The new anatomical data together with amino acid sequences in a comprehensive dataset is used to examine the phylogenetic relationship of *Thomashuxleya* and other SANUs with other placentals. *Thomashuxleya* is placed either within Afrotheria or within a clade with Perissodactyla.

I investigate biogeographic patterns in SA and review the temporal and geographical distribution of fossil mammals during the GABI. There is a differentiation between tropical and temperate mammal faunas in SA at least since the middle Miocene (Carrillo et al. 2015). In addition, I present new findings from the Urumaco sequence (late Miocene-late Pliocene) of Venezuela and from the Cocinetas basin (middle Miocene and early Pliocene) of Colombia. These localities serve to characterize changes of Neotropical mammal communities during the GABI (Amson et al. 2016, Moreno et al. 2015). Middle Miocene remains from the Castilletes Formation include several groups of SANUs (uruguaytheriine astrapotheres, leontinid notoungulates, proteroterid litopterns), representing the earliest records in the tropics for these clades. Material from the late Miocene deposits of Urumaco documents higher diversity of giant neoepiblemid rodents (Carrillo & Sánchez-Villagra, 2015). Pliocene remains from Colombia (Ware Formation) and Venezuela (San Gregorio Formation) provide the oldest records of North American mammals in the tropics (procyonids and camelids), and includes a diverse assemblage of sloths and hydrochoerid rodents. Toxodonts from San Gregorio represents a new taxon belonging to a tropical clade which includes a GABI participant. The Miocene and Pliocene mammalian assemblages represent diverse and distinct mammal communities in the northern SA, and reveal multi-directional migration dynamics during the GABI.

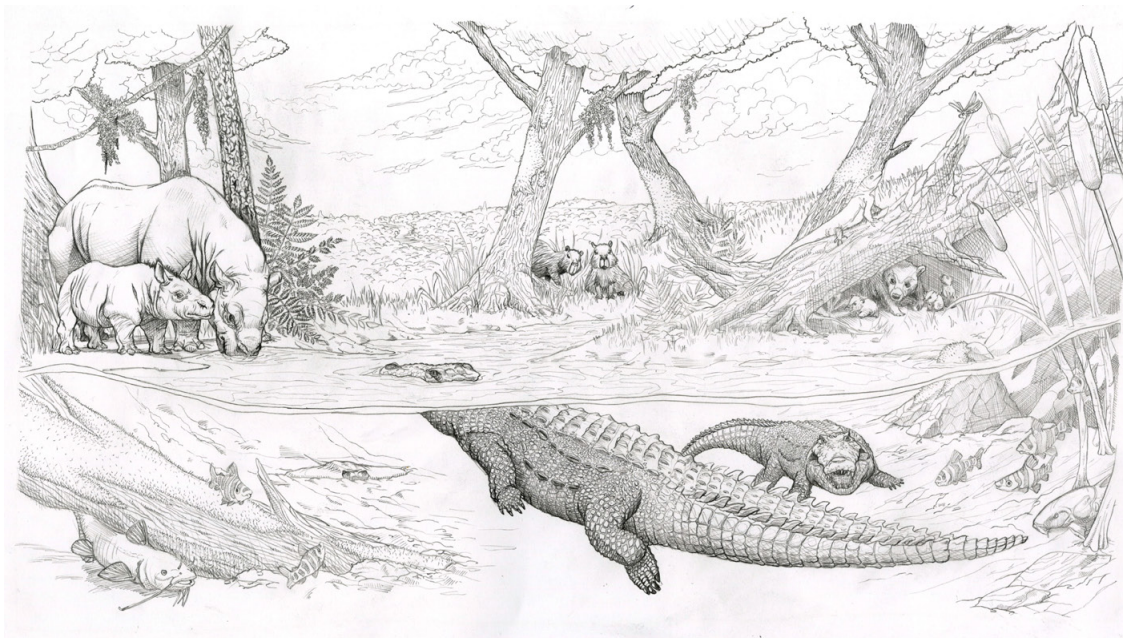


Figure 1. Vertebrate fauna of the San Gregorio Formation (late, Pliocene) from Urumaco, Venezuela. Illustration by Stjepan Lukac.

REFERENCES

- Amson, E., Carrillo, J.D., Jaramillo, C. 2016. Neogene sloth assemblages (Mammalia, Pilosa) of the Cocinetas basin (La Guajira, Colombia): implications for the Great American Biotic Interchange. *Palaeontology*, 59(4): 563-582. doi: 10.1111/pala.12244
- Carrillo, J.D., Forasiepi, A., Jaramillo, C., & Sánchez-Villagra, M.R. 2015: Neotropical mammal diversity and the Great American Biotic Interchange: spatial and temporal variation in South America's fossil record, *Frontiers in Genetics*, 5, 451. doi: 10.3389/fgene.2014.00451
- Carrillo, J.D., & Sánchez-Villagra, M.R. 2015: Giant rodents from the Neotropics: diversity and dental variation of late Miocene neopiblemid remains from Urumaco, Venezuela. *Palaontologische Zeitschrift*, 89 (4), 1057-1071. doi: 10.1007/s12542-015-0267-3
- Moreno, F., et al. 2015. Revised stratigraphy of Neogene strata in the Cocinetas Basin, La Guajira, Colombia. *Swiss Journal of Palaeontology* 134(1), 5-43. doi: 10.1007/s13358-015-0071-4

4.8

The ear before birth: morphology, ossification timing, and allometry

Loïc Costeur¹, Bastien Mennecart¹

¹ *Naturhistorisches Museum Basel, Augustinergasse 2, CH-4001 Basel (loic.costeur@bs.ch)*

Foetuses are a source of scientific information to understand the development and evolution of anatomical structures. The bony labyrinth, surrounding the organ of balance and hearing, is a phylogenetically and ecologically informative structure for which still little concerning growth and shape variability is known in many groups of vertebrates. The same is true for the middle ear bones, i.e., the stapes, incus and malleus, which are the smallest bones of the mammalian skeleton and constitute the chain of bones conducting sound from the outer ear to the inner ear. Except in humans, these structures are poorly known in most placentals and their prenatal growth has almost never been studied.

Ruminants are a diversified group of placentals and represent an interesting case study to understand the prenatal growth of the ear region. We CT-scanned five cow foetuses and an adult petrosal bone (*Bos taurus*, Artiodactyla, Mammalia) and describe the bony labyrinth when already ossified. The foetuses encompass the second half of the 9.3 months long gestation period of the cow. They were sampled at different ontogenetic stages to understand how and when the petrosal bone and bony labyrinth ossify in ruminants.

The petrosal bone and bony labyrinth ossify within about 20 days in the fourth month of gestation. The bony labyrinth is already fully ossified at least in the 6th month, while only the cochlea, most of the vestibule, and the common crus are already ossified at the beginning of the 4th month (Fig. 1). The pars canicularis of the petrosal thus ossifies last. The size and volume of the bony labyrinth stay similar from the 6th month (possibly even from the 5th). From the end of the 4th month of gestation, a progressive lengthening of the cochlear aqueduct and endolymphatic sac occurs culminating in the adult form and partly explaining the larger volume of the later. The inner ear in the cow ossifies quickly during the gestation period, being fully ossified around mid-gestation time, as in humans. The adult size and most of its volume are reached by mid-gestation time, while the petrosal bone and skull still grow. A negative ontogenetic allometry, between the bony labyrinth and both the petrosal bone and the skull, is thus observed. It matches the evolutionary negative allometry of the structure observed in earlier studies. Few changes occur after ossification is achieved; only open structures (i.e., cochlear aqueduct and endolymphatic sac) continue to grow after birth and reflect size increase of the petrosal bone (Costeur et al., in press).

In the middle ear, while the ossicles are the tiniest of all bones in the placental mammal skeleton, ossification occurs at the same time as the bony labyrinth and petrosal bone. All three ossicles are ossified and identifiable at the species level at the end of the fourth month of gestation although they still haven't reached their full size (Fig. 1), in line with previous results obtained in humans. In particular, the stapes is smaller than in the adult and its footplate is smaller than the membrane of the oval window where it comes in contact to stimulate the inner ear (Costeur et al., submitted).

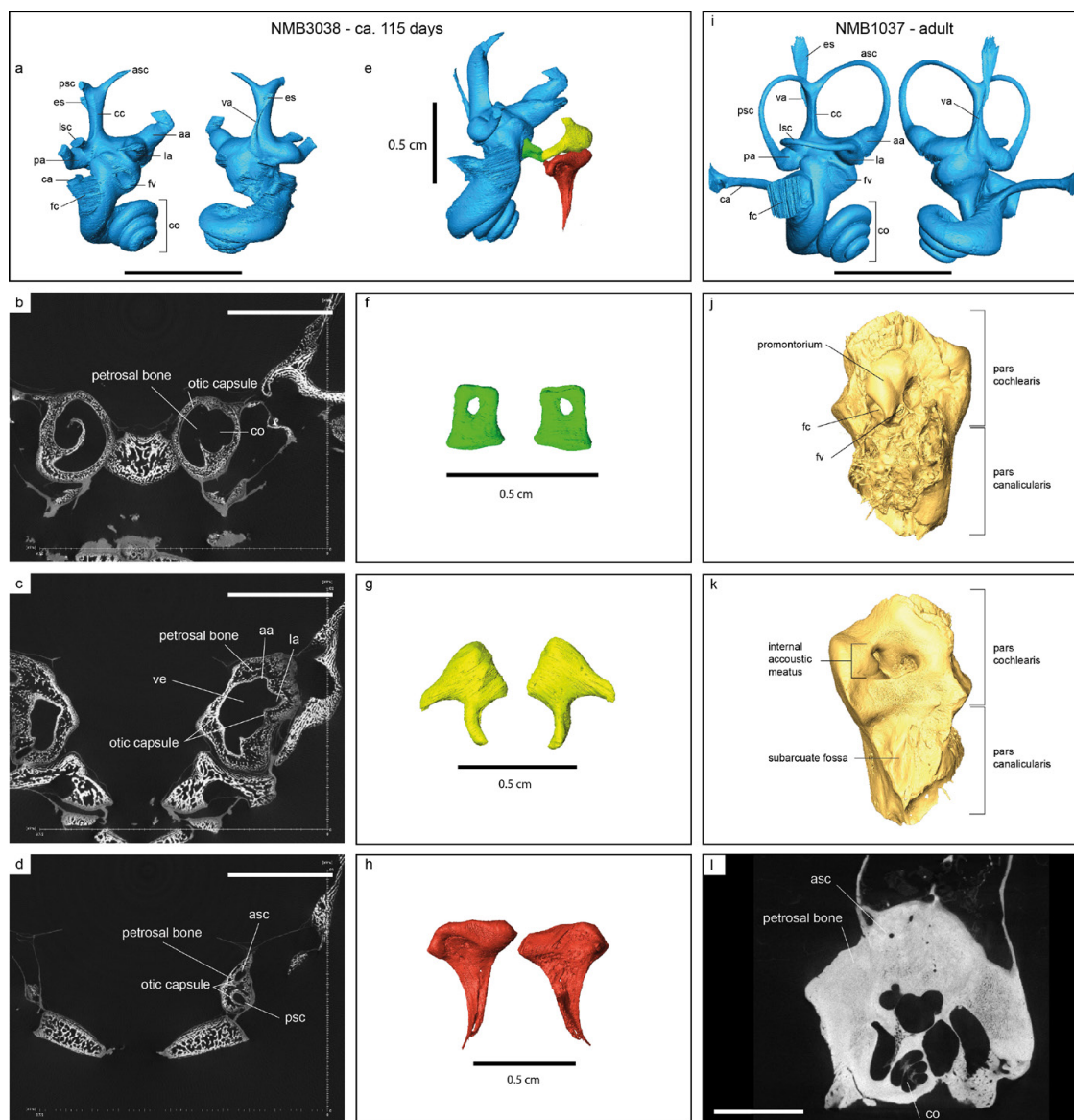


Figure 1. Reconstructed right bony labyrinth (a, e) and ossicles (f-h), together with micro-CT images (b-d) through the petrosal bone of a *Bos taurus* foetal stage (NMB3038) at about 115 days of gestation; and left bony labyrinth (i) and petrosal bone (j, k) of an adult (NMB 1037, mirrored in the picture); j: micro-CT image through its cochlea . **aa**, asc ampulla; **asc**, anterior semi-circular canal; **ca**, cochlear aqueduct; **cc**, common crus; **co**, cochlea; **es**, endolymphatic sac; **fc**, fenestra cochleae; **fv**, fenestra vestibuli; **la**, lsc ampulla; **lsc**, lateral semi-circular canal; **pa**, psc ampulla; **psc**, posterior semi-circular canal; **va**, vestibular aqueduct. When not indicated, scale bars are 1 cm long. Figure modified after Costeur et al. (in press, submitted)

REFERENCES

- Costeur, L., Mennecart, B., Müller, B., & Schulz, G. in press: Prenatal growth stages show the development of the ruminant bony labyrinth and petrosal bone, *Journal of Anatomy*.
- Costeur, L., Mennecart, B., Müller, B., & Schulz, G. submitted: Middle ear bones of a mid-gestation ruminant foetus extracted from X-Ray computed tomography, *Proceedings of SPIE*.

4.9

The ecology and evolution of the anomalocaridids

Allison C. Daley¹

¹ Institut des sciences de la Terre, Faculté des géosciences et de l'environnement, University of Lausanne, Bâtiment Géopolis, CH-1015 Lausanne (allison.daley@hotmail.com)

The Cambrian Explosion was a major biodiversification event that saw the rise of nearly all animal phyla in a rapid burst over 500 million years ago. The anomalocaridids (Radiodonta) are iconic members of these early animal ecosystems, owing to their large size, bizarre morphology and complicated history of description. These pelagic animals had a segmented body bearing swim flaps, and a head with a prominent pair of grasping appendages, stalked eyes, and circular mouthparts (Whittington & Briggs 1985). Taxa such as *Anomalocaris* were first described from the Burgess Shale in Canada, but have since been found globally at many other Cambrian fossil lagerstätten. Much work has been undertaken on the anomalocaridids in the last 10 years, and these animals have proved important for understanding Cambrian ecology and the early evolution of arthropods.

The anomalocaridids were originally interpreted as highly specialised apex predators attacking trilobites, but the diversity of appendage and mouthpart morphologies instead suggests that they actually employed a diverse range of feeding strategies. While taxa such as *Anomalocaris* may have been highly specialised predators, other taxa such as *Hurdia* were more generalised in their feeding approach, employing both scavenging and predation (Daley & Budd 2010). The early Ordovician taxon *Aegirocassis* is a suspension feeder and reached a gigantic body size of 2 metres, equivalent to the ecological niche of whales today (Van Roy et al. 2015).

Anomalocaridids occupied a basal position in the stem lineage leading to Arthropoda, the phylum that today includes chelicerates, crustaceans, myriapods and insects (Daley et al. 2009). Some aspects of anomalocaridid morphology are remarkably similar to characteristics of extant arthropods, such as the multi-faceted compound eyes consisting of over 15,000 lenses seen in *Anomalocaris* (Paterson et al. 2014). Other features provide insight into the early evolutionary stages of key arthropod features, such as the biramous limb, head appendages and exoskeleton (Daley et al. 2009). For example, the two branches of the arthropod biramous limb were once separate structures protruding from the body wall, which in the Ordovician anomalocaridid taxon *Aegirocassis* can be seen at two pairs of body flaps (Van Roy et al. 2015). These separate body flaps eventually fused to form the arthropod biramous limb, but the anomalocaridid condition allows us to see an important early stage in the evolution of this morphological feature. Ultimately, understanding the ecology and evolution of the anomalocaridids can inform on how arthropods achieved such great success both in the earliest animal ecosystems of the Cambrian, and in the modern day.

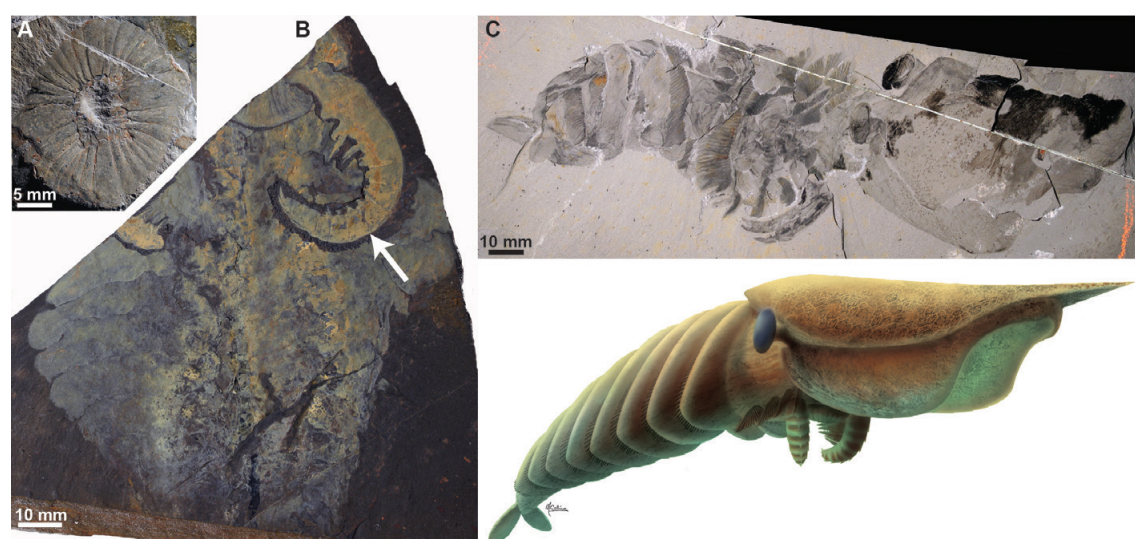


Figure 1. Anomalocaridids from the Burgess Shale, Canada. A: Circular mouthparts of *Peytoia nathorsti*. B: Full body specimen of *Anomalocaris canadensis*, with the prominent grasping appendage indicated by the white arrow. C: Fossil image and reconstruction of *Hurdia victoria*. Reconstruction by Marianne Collins.

REFERENCES

- Daley, A.C. & Budd G.E. 2010: New anomalocaridid appendages from the Burgess Shale, Canada. *Palaeontology* 53, 721–738.
- Daley, A.C., Budd, G.E., Caron, J.-B., Edgecombe, G.D. & Collins D. 2009: The Burgess Shale anomalocaridid *Hurdia* and its significance for early euarthropod evolution. *Science* 323, 1597–1600.
- Paterson, J.R., García-Bellido, D.C., Lee, M.S.Y., Brock, G.A., Jago, J.B. & Edgecombe G.D. 2011: Acute vision in the giant Cambrian predator *Anomalocaris* and the origin of compound eyes. *Nature* 480, 237–240.
- Van Roy, P., Daley, A.C. & Briggs D.E.G. 2015: Anomalocaridid trunk limb homology revealed by a giant filter-feeder with paired flaps. *Nature* 522, 77–80.
- Whittington, H.B. & Briggs D.E.G. 1985: The largest Cambrian animal, *Anomalocaris*, Burgess Shale, British Columbia. *Philos. T. Roy. Soc. B.* 309, 569–609.

4.10

Detailed trilobite moulting behaviour preserved in the Emu Bay Shale, South Australia

Harriet B Drage^{1,2}, James D Holmes³, Diego C García-Bellido⁴, Allison C Daley^{1,2,5}

¹ Department of Zoology, University of Oxford, Tinbergen Building, South Parks Road, Oxford, UK, OX1 3PS
(harriet.drage@zoo.ox.ac.uk)

² Oxford University Museum of Natural History, Parks Road, Oxford, UK, OX1 3PW

³ Department of Biological Sciences, University of Adelaide, South Australia, SA 5005

⁴ South Australian Museum, North Terrace, Adelaide, South Australia, SA 5000

⁵ Faculty of Geosciences and Environment, University of Lausanne, Sorge Géopolis, CH-1015 Lausanne, Switzerland

The Emu Bay Shale (EBS; Kangaroo Island, South Australia) is an early Cambrian (c. 514 Ma) locality with exceptional preservation of soft tissues (Konzervat-Lagerstätte). The locality is important for expanding our knowledge of the earliest evolved animals, and is particularly interesting for its unique preservation. This resulted from rapid burial at an active tectonic margin and sediment anoxia, facilitated by low levels of abiotic (water currents) and biotic (bioturbation, predation) disruptive processes (Gehling *et al.*, 2011).

The EBS displays a diverse Burgess Shale-type fauna, however the composition is dominated by both preserved carcasses and moulted exoskeletons of two trilobite species, *Estiaingia bilobata* in the majority, and *Redlichia takoensis* (Paterson *et al.*, 2016). The excellent preservational conditions at the EBS have produced a great number of virtually undisturbed moulted exoskeleton assemblages for these taxa. These assemblages capture the moment of exuviation, describing the sequence of movement and pattern of sclerite disarticulation during moulting. This has allowed for an unprecedented interpretation of detailed behavioural information from trilobite moults.

Extensive field collections of *E. bilobata* and *R. takoensis* housed in the South Australian Museum (Adelaide) were surveyed. Moulting assemblages of both species displaying the total observable range of variation in moulting behaviour were chosen for closer examination. Moulting behaviour and movement during exuviation were described and interpreted for each specimen. These data were then compared to the observable moulting behaviour for the extremely numerous species *Ogygopsis klotzi* (Burgess Shale) and *Elrathia kingii* (Wheeler Shale, Utah) from other localities with exceptional preservation.

The resulting observations and inferences made for movement during moulting are much more detailed for the EBS trilobites than those from the other localities. Very rare moulting events requiring unusual patterns of movement are discernable for *E. bilobata* and *R. takoensis*, because of the style of preservation at the EBS. For example, both species usually disarticulate the free cheeks (these are often associated with the cranidium and form a lower cephalic unit in *E. bilobata*, and laterally inverted for *R. takoensis*). However, they also rarely demonstrate moulting through disarticulation of the entire cephalon (=Salter's configuration). The latter assemblages are not observed at the other localities, which often show non-moulting related disruption in the placement of disarticulated sclerites.

The EBS assemblages suggest that trilobite moulting behaviour, even within a single species, was more variable than expected. As a group, trilobites displayed flexibility in moulting, presumably to adapt to different conditions and circumstances. This only becomes obvious through the observation of large collections of moulting assemblages from localities with exceptional preservation and almost no transportation of exoskeletal sclerites prior to preservation.

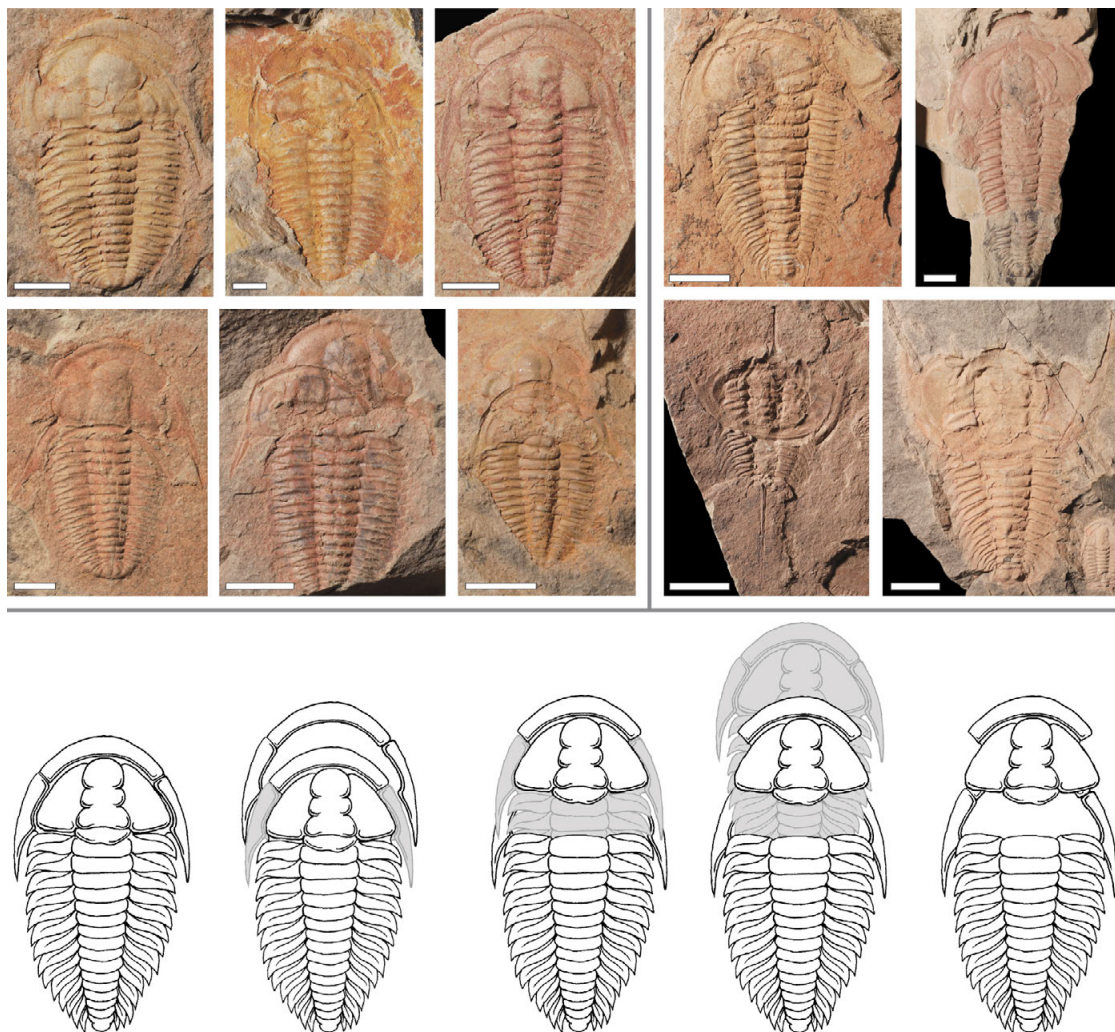


Figure 1. Moulded exoskeleton assemblages of *Estaingia bilobata* (top left) and *Redlichia takoensis* (top right) from the Emu Bay Shale. The bottom two specimens of *R. takoensis* display the rare Salterian moult configuration (disarticulation and inversion of entire cephalon). The bottom panel interprets exuvial movement (grey) for *E. bilobata*, leaving the moult assemblage (white). Scale bars 5mm for *E. bilobata*, 10mm for *R. takoensis*. Photographs: HBD.

REFERENCES

- Paterson, J.R., García-Bellido, D.C., Jago, J.B., Gehling, J.G., Lee, M.S.Y. & Edgecombe, G.D. 2016: The Emu Bay Shale Konservat-Lagerstätte: a view of Cambrian life from East Gondwana. *J. Geol. Soc.*, 173, 1-11.
- Gehling, J.G., Jago, J.B., Paterson, J.R., García-Bellido, D.C. & Edgecombe, G.D. 2011: The geological context of the Lower Cambrian (Series 2) Emu Bay Shale Lagerstätte and adjacent stratigraphic units, Kangaroo Island, South Australia. *Aust. J. Earth Sci.*, 58, 243-257.

4.11

Palaeoecology of the Lower Jurassic Schambelen member of northern Switzerland

Walter Etter

Natural History Museum Basel, Augustinergasse 2, CH-401 Basel (walter.etter@bs.ch)

In his "Urwelt der Schweiz", Oswald Heer (1865) devoted a whole chapter to the fossils from the "Schambelen" south of Brugg/Windisch. These fossils were then a sensation: Jurassic insects were previously only known from England. Additional finds included articulated ophiuroids, crustaceans, fishes, echinoids preserved with the spines still attached and dozens of different insect remains. These confirmed the exceptional status of this locality, and Heer gave a lively reconstruction of the marine life at the time. The beds were named "Insect marls" (Moesch 1857; today Schambelen member, Reisdorf et al. 2011) and occur in the canton Aargau and Baselland in a thickness between 0.5 and 10 m.

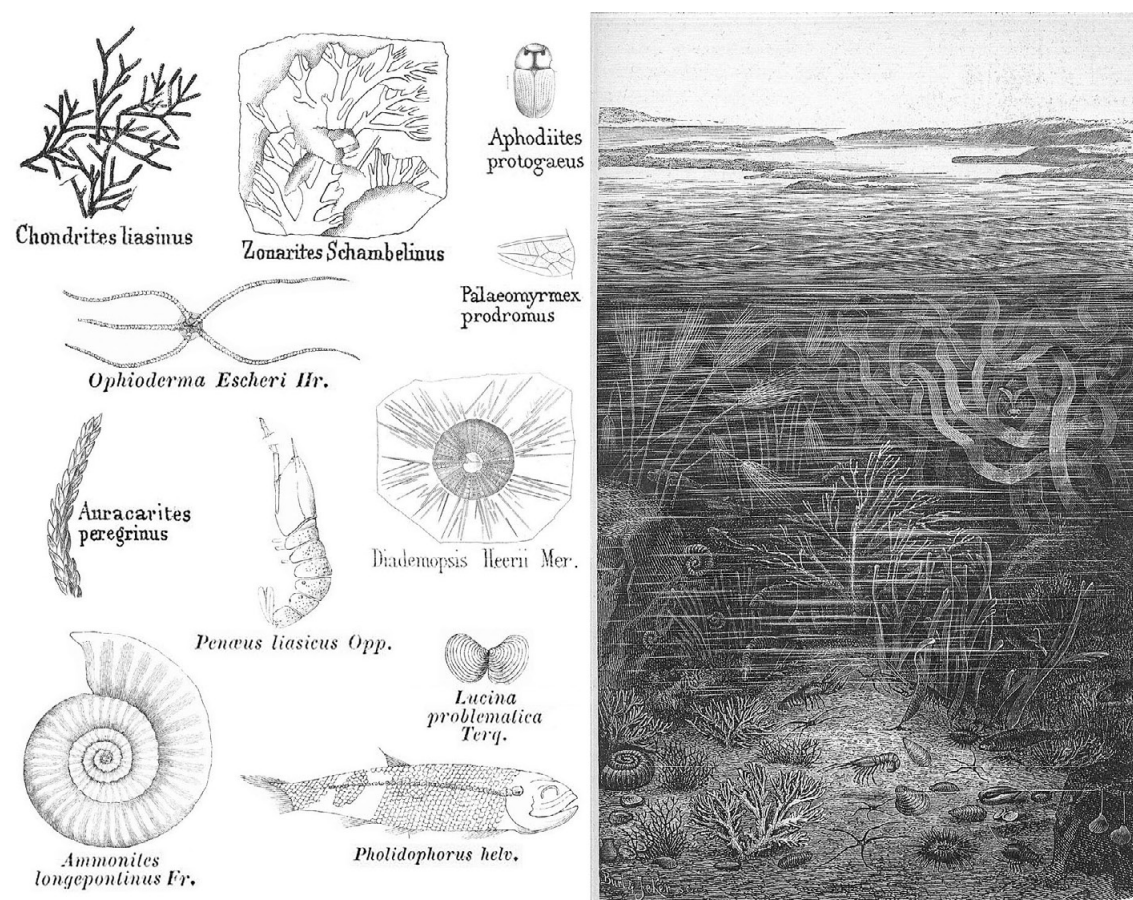


Fig. 1. Fossils found in the "Insect marls" at the locality Schambelen as documented by Heer (1865), together with a reconstruction of the depositional environment by the same author.

In surface exposures, the soft marls decay to small chips. A re-evaluation of Heer's findings is only possible through systematic excavations.

Ammonites are not uncommon, and they indicate a middle Hettangian age (liasicus-zone). The benthic fauna is sparse and dominated by thin-shelled, small epi- and shallow endobenthic bivalves. Small gastropods and various echinoderms regularly occur in washed residues. Trace fossils are of low diversity. Insects appear to be exceedingly rare, and the several hundred specimens of Heer must have accumulated over many years of intense sampling.

Although most fossils are flattened and the aragonitic shells were dissolved, fossil preservation is good, and articulated preservation of crustaceans and echinoderms is not uncommon. Delicate organic structures like the ammonite periostracum and anaptychi survived. The analysis of the benthic fauna and of the taphonomic pattern indicates a depositional environment with very soft substrate and lowered oxygen content of the bottom water but never anoxic bottom water (cf. Schwab & Spangenberg 2007).

REFERENCES

- Heer, O. 1865: Die Urwelt der Schweiz. Zürich, Schulthess, 622 pp.
- Moesch, C. 1857: Das Flözgebirge im Kanton Aargau. Neue Denkschriften der allgemeinen schweizerischen Gesellschaft für die gesamten Naturwissenschaften, 15, 1-80, Taf. 1-3.
- Reisdorf, A. G., Wetzel, A., Schlatter, R. & Jordan, P. 2011: The Staffelegg Formation: a new stratigraphic scheme for the Early Jurassic of northern Switzerland. *Swiss Journal of Geosciences*, 104, 97-146.
- Schwab, V. F. & Spangenberg, J. E. 2007: Molecular and isotopic characterization of biomarkers in the Frick Swiss Jura sediments: A palaeoenvironmental reconstruction on the northern Tethys margin. *Organic Geochemistry*, 38, 419-439.

4.12

Histology and geochemical study of bones of an *Allosaurus* (Dinosauria: Theropoda)

Christophe Ferrante^{1,3}, Torsten Vennemann², Lionel Cavin³, Rossana Martini¹

¹ Department of Earth Sciences, University of Geneva, Rue de Maraichaire 13, 1205 Genève

² Institute of Earth Surface Dynamics, University of Lausanne, UNIL-GEOPOLIS, 1015 Lausanne

³ Department of Geology and Palaeontology, Natural History Museum of Geneva, CP 6434, 1211 Genève 8

The Muséum d'Histoire Naturelle de la Ville de Genève (MHNG), Switzerland, houses in its collection a partial skeleton of the theropod dinosaur *Allosaurus* (MHNG GEPI V2567) from the Cleveland-Lloyd Dinosaur Quarry (CLDQ; Emery County, Utah, USA) in the Upper Jurassic Morrison Formation.

An osteological description, histological examinations of two limb bones, and geochemical and O-isotopic analyses of the bones were recently completed.

The osteological description, together with investigations in the archives of the MHNG, indicate that MHNG GEPI V2567 corresponds to a composite skeleton. Histological observations show that bone-tissues of the tibia have preserved their primary structure, in contrast to the femur, which displays important in vivo bone remodeling. The tibia recorded cyclic variations of the oxygen isotopic composition, which seem to vary according to the nature of bone-tissues and with respect to growth marks. Generally, zones of fast growth provide low values of $\delta^{18}\text{O}$ whereas annuli, corresponding to slower growth rates, have higher $\delta^{18}\text{O}$ values reflecting potential temperature and/or humidity variations. Zinc contents measured on the tibia, which is a biomarker associated to bone formation, show that zones of fast growth have generally higher zinc contents compared to annuli. REE concentrations and the cyclic variations of the oxygen isotope composition support a primary signal, which may have been overprinted slightly from its original values during diagenesis.

The combined study of histology and geochemistry demonstrates that fossil bones can record seasonal variations of the climate. These results provide a better understanding of climatic influence on bone growth as well as information on lifestyle of the studied animal.

4.13

Skull shape variation in recent and fossil turtles through time and its relation to climate, habitat and feeding ecology

Christian Foth¹, Walter G. Joyce¹

¹ *Department of Geosciences, University of Fribourg/Freiburg, Chemin du Musée 6, 1700 Fribourg, Switzerland*

Turtles (Testudinata) represent a diverse group of reptiles with a rich fossil record that extends back to the Late Triassic. Over the course of their evolutionary history they conquered a broad set of habitats and feeding ecologies, but little is known about their evolutionary disparity and the relationship between cranial shape and ecological preferences in general. We here investigate the cranial shape of 171 representatives of the turtle lineage in dorsal, lateral and ventral view, their shape variation through time (= temporal disparity) and the relationship to different habitat and diet preferences using two-dimensional geometric morphometrics. Cranial shape was superimposed, and subjected to principal component analyses, in which principal components containing the most significant shape variation were identified with help of the broken-stick method. To increase the temporal resolution for disparity analyses the principal components were mapped onto a time-calibrated supertree estimating ancestral skull shapes, which were included into the final data set. All taxa were then grouped into 20 equal time bins ranging from the Late Triassic until the Recent, before sum of variance was calculated for each bin. The course of disparity curves was compared with climate data from the same period. Furthermore, the correlation between cranial shape and ecological preferences (habitat and diet) were tested for recent taxa with help of npMANOVA. Afterwards, the morphospace of each extant ecological group was defined on the basis of the principal components containing relevant shape information. The classification of fossil turtles was then realized by calculating the Euclidean distance of each taxon to the mean of each ecological group.

Disparity was found to be greatest in lateral view and smallest in ventral view. However, in all three anatomical views, three evolutionary phases are apparent in all three anatomical views investigated. In the first phase, disparity increases gradually from the Late Triassic to the Palaeogene with only a minor decline at the K/T border. Although global warming was previously suggested to cause an increase in diversity, and by extension in disparity, we find only little evidence for this correlation and hypothesize that the fragmentation of Pangaea during the Mesozoic to be a more plausible factor for this development. After its maximum, disparity decreases strongly towards the Miocene, only to recover partially towards the Recent. This collapse in disparity is probably a result of habitat destruction due to global drying, combined with the homogenization of global turtle faunas through increased transcontinental dispersal in the Tertiary. The disparity minimum in the Miocene, marking the beginning of the third phase, is probably an artefact of the methods employed herein caused by the poor fossil record of turtles in the Miocene and Oligocene. Interestingly, turtles show no significant shift of their position within morphospace through time. However, when comparing the two major lineages, disparity of pan-cryptodires is generally higher than that of pan-pleurodires, while both groups occupy significantly different areas in morphospace for each time bin.

Furthermore, the skull shape of recent turtles correlates with both habitat and feeding preferences, but is more affected by habitat than diet. However, the application of these correlations to extinct turtles produces mostly inconsistent results, especially for stem-turtles, highlighting that morphospace held by extant turtles is not necessarily the optimal location in tree space for a particular ecological adaptation in the cranium. The inability to correctly predict the ecology of fossil turtles is probably related to the fact that the shape of turtle skulls is highly dominated by the emarginations and jaw closure mechanisms, two shape features unrelated to habitat or feeding ecology. This indicates that various specializations that are nevertheless apparent in the skull only contribute minor to overall shape.

Bullet list: Testudinata, skull shape, cranial disparity, ecology, climate, evolution, geometric morphometrics

4.14

The first skeletal remains of *Phoebodus politus* Newberry 1889 (Chondrichthyes: Elasmobranchii) and its ecology

Linda Frey¹, Michael Coates², Michał Ginter³ and Christian Klug¹

¹ Paläontologisches Institut und Museum, University of Zurich, Karl-Schmid-Strasse 4, CH-8006 Zürich
(linda.frey@pim.uzh.ch; chkflug@pim.uzh.ch)

² Department of Organismal Biology and Anatomy, University of Chicago, 1027 E. 57th St., USA-60637 Chicago

³ Faculty of Geology, University of Warsaw, al. Żwirki i Wigury 93, PL-02-089 Warszawa

Phoebodus is a chondrichthyan, which was widely distributed during the Devonian. It includes around 13 species that are largely based on their characteristic tricuspid teeth so far (Ginter et al. 2010). Teeth associated to remains of skulls and a few axial skeletons were recently found in Famennian (Late Devonian) outcrops of the eastern Anti-Atlas of Morocco. The skulls are often three-dimensionally preserved enabling CT-scanning and subsequent reconstruction of brain endocasts, branchial arches, orbits and jaws. The teeth of these specimens show some important characteristics of *Phoebodus politus* that was found in the Cleveland Shales of Ohio before (Newberry, 1889). First examinations on the remains show affinities to hyodontiform sharks and to the Carboniferous *Thrinacoselache gracia* Grogan & Lund, 2007 that already was suggested to be closely related to *Phoebodus* (by, e.g., Ginter et al. 2010). Moreover, morphological similarities to the modern, only distantly related, thinned sharks (*Chlamydoselache*) such as the tooth morphology and the elongated body indicate similar functional morphology of the jaws and dentition.

The here described remains of *Phoebodus politus* are associated with skeletons of cladoselachian and ctenacanthid chondrichthyans, several placoderm species (*Dunkleosteus*, *?Driscollaspis*, undescribed placoderm taxon) sarcopterygians, and possibly acanthodians. Phyllocarid crustaceans occur also in great abundance and likely were an important food source for the chondrichthyans. The body sizes and the massive fin spines of some chondrichthyans in combination with their abundance show that they likely competed with giant armored fish during the Late Devonian.

REFERENCES

- Ginter, M., Hampe, O., & Duffin, C., 2010: Chondrichthyes, Paleozoic Elasmobranchii: Teeth, Handbook of Paleoichthyology, 3D, 1-168.
- Grogan, E.D., & Lund, R., 2007: A basal elasmobranch, *Thrinacoselache gracia* n. gen & sp., (Thrinacodontidae, new family) from the Bear Gulch Limestone, Serpukhovian of Montana, USA, Journal of Vertebrate Paleontology, 28(4), 970-988.
- Newberry, J. S., 1889: The Paleozoic fishes of North America, Monograph of the U.S. Geological Survey, 16, 1-340.

4.15

A new key Smithian (Early Triassic) quantitative ammonoid biochronology from the western USA basin

Romain Jattiot^{1,2}, Hugo Bucher¹, Arnaud Brayard², Morgane Brosse¹, Jim Jenks³ & Kevin. G. Bylund⁴

¹ *Paläontologisches Institut der Universität Zürich, Karl Schmid-Strasse 4, CH-8006 Zürich (romain.jattiot@pim.uzh.ch)*

² *UMR CNRS 6282 Biogéosciences, Université de Bourgogne Franche-Comté, 6 boulevard Gabriel, 21000 Dijon, France*

³ *1134 Johnson Ridge Lane, West Jordan, Utah 84084, United States of America*

⁴ *140 South 700 East, Spanish Fork, Utah 84660, United States of America*

Since the pioneer work of Silberling and Tozer (1968), the western USA basin is known as including an excellent record of Early Triassic ammonoids. Smithian marine fossiliferous strata are widely distributed and cover southwestern Montana, southeastern Idaho, Utah, Wyoming and northeastern Nevada. The Smithian is a crucial time interval, recording the first global, major diversification-extinction cycle after the Permian-Triassic boundary mass extinction (PTBME). In the Tethys, early and middle Smithian corresponds to the main re-diversification of ammonoids and conodonts, whereas the late Smithian witnessed the most severe intra-Triassic crisis for the nekton, ca. 2 myr after the PTBME. Our intensive sampling of the lower portion of the Thaynes Group within the Palomino Ridge area (northeastern Nevada) yielded abundant and well-preserved Smithian ammonoid faunas. Based on new data from Palomino Ridge and previous data from neighboring localities in Utah, we provide here the first quantitative Smithian ammonoid biochronological scheme for the western USA basin. This new zonation is based on the Unitary Associations (UA) method. The biochronological sequence comprises five unitary association zones that can be correlated with other localities from the Northern Indian Margin (Salt Range, Pakistan; Spiti northern India; and Tulong, South Tibet). Three unitary association zones (UAZ₁, UAZ₂ and UAZ₃) are defined for the early Smithian, one (UAZ₄) spans the entire middle Smithian and one (UAZ₅) comes into the first part of the late Smithian. Finally, a provisional UAZ₆ would represent the second part of the late Smithian.

This zonation stands in contrast to the fourteen Smithian UA zones previously established in the Northern Indian Margin (Brühwiler et al. 2010). The latter is shaped by much higher turnover rates, especially during the middle Smithian. This pronounced difference is discussed in terms of biogeography in the framework of the Early Triassic ammonoid biotic recovery.

REFERENCES

- Brühwiler, T., Bucher, H., Brayard, A. & Goudemand, N. 2010: High-resolution biochronology and diversity dynamics of the Early Triassic ammonoid recovery: the Smithian faunas of the Northern Indian Margin. *Palaeo* 3. 297, 491-501.
- Silberling, N. J. & Tozer, E. T. 1968: Biostratigraphic classification of the marine Triassic in North America. *Geol. Soc. Am. Spec. Pap.* 110, 1-63.

4.16

No fossil record? Yes fossil record! Konservat-Lagerstätten of the End-Devonian Hangenberg Black Shale in the eastern Anti-Atlas (Morocco)

Christian Klug¹, Linda Frey, Dieter Korn², Romain Jattiot¹ and Martin Rücklin³

¹ *Paläontologisches Institut und Museum, Universität Zürich, Karl Schmid-Strasse 4, CH-8006 Zürich (chklug@pim.uzh.ch; linda.frey@pim.uzh.ch)*

² *Museum für Naturkunde Berlin, Leibniz-Institut für Evolutions- und Biodiversitätsforschung, Invalidenstraße 43, D-10115 Berlin, Germany*

³ *Naturalis Biodiversity Center, Postbus 9517, 2300 RA Leiden, The Netherlands*

Things are not always what they seem. For example, in the arid areas of the Anti-Atlas, black shales may appear whitish to pinkish due to weathering. This deep weathering may also destroy fragile fossils close to the surface, creating the impression that these sediments are devoid of fossils. In the case of the latest Devonian Hangenberg Black Shale of Morocco, its sediments contain abundant deformed fossils lacking carbonatic shells but with remains of organic matter. Since the fossils are completely flattened, weathering quickly destroys the nearly two-dimensional fossils in the top 30 to 50 centimeters below the surface. Excavations at three localities revealed that, in contrast to published opinions, the Hangenberg Black Shale in the eastern Anti-Atlas contains abundant remains of marine invertebrates including ammonoids, bivalves, bactritids, trilobites, bryozoans, and crinoids as well as rare chondrichthyan teeth and plant remains (Klug et al. 2016).

Most remarkably, the claystones of the late Famennian Hangenberg Black Shale yielded flattened but otherwise well-preserved ammonoid conchs of at least four species. In spite of the dissolved shell, these fossils display morphological details such as sutures, growth lines, details of the shell surface such as the wrinkle layer and epizoans. The most interesting aspect, however, is the in situ jaws found in three species. The jaws were originally chitinous and are preserved as carbonaceous films, sometimes with a wealth of morphologic detail. Additionally, some originally organic shell parts are visible; this includes organic films in the body chamber and other black stripes linked either to mature growth or injuries.

The documented ammonoid jaws belong to three different orders and suborders, from two of which jaws were previously unknown (Tanabe et al. 2015). This is of interest because, presuming jaws did not evolve independently in three cephalopod groups, this supports the hypothesis that a chitinous jaw is a plesiomorphic character of the Ammonoidea. In turn, this suggests that the cephalopod jaw evolved at the latest at the root of the crown group of the Cephalopoda in the Silurian. Possibly, the diversification of jawed fish in the Silurian and Devonian (Klug et al. 2010) was the indirect ecological driver behind the evolution of cephalopod mouthparts.

Further research will focus on details of the ecological changes around the Hangenberg mass extinction and the impact on vertebrate communities as well as marine food webs across the Devonian Carboniferous boundary.

REFERENCES

- Klug, C., Frey, L., Korn, D., Jattiot, R. & Rücklin, M., 2016: The oldest Gondwanan cephalopod mandibles (Hangenberg Black Shale, Late Devonian) and the Mid-Palaeozoic rise of jaws, *Palaeontology*, 19 pp. doi: 10.1111/pala.12248
- Klug, C., Kröger, B., Kiessling, W., Mullins, G. L., Servais, T., Frýda, J., Korn, D. & Turner, S., 2010: The Devonian nekton revolution, *Lethaia*, 43, 465-477.
- Tanabe, K., Kruta, I. & Landman, N. H., 2015: Ammonoid buccal mass and jaw apparatus. In: Klug, C., Korn, D., De Baets, K. Kruta, I. & Mapes, R. H. (Eds.), *Ammonoid paleobiology, Volume I: from anatomy to ecology*. Springer, Dordrecht, *Topics in Geobiology*, 43, 429-484.

4.17

Cranial morphology of Recent and Pleistocene camels

Pietro Martini^{1,2}, Denis Geraads³, Jean-Marie Le Tensorer¹ & Loïc Costeur²

¹ *Institut für Prähistorische und Naturwissenschaftliche Archäologie, University of Basel, Spalenring 145, CH-4055 Basel (pietro.martini@unibas.ch)*

² *Naturhistorisches Museum Basel, Augustinergasse 2, CH-4001 Basel*

³ *Muséum National d'Histoire Naturelle, 8 rue Buffon, FR-75231 Paris*

Camels are two charismatic species of domestic large mammals, but their anatomy, history and evolution are poorly known. Only few works have tried to describe and compare the osteology of Bactrian camel and dromedary, and there is a general dearth of knowledge regarding their domestication, the origins of the genus *Camelus*, its fossil species and their evolutionary relationships.

The family Camelidae colonized Eurasia from North America in the late Turolian (~6 Ma), with some large-sized forms assigned to the poorly defined genus *Paracamelus*. There are only four described fossil species of *Camelus*: *C. grattardi* (Ethiopia, 2.2 Ma), *C. sivalensis* (Indian subcontinent, 2 Ma), *C. thomasi* (Algeria, middle Pleistocene) and *C. knoblochi* (Russia and central Asia, middle-late Pleistocene). However, the mostly undescribed fauna of the El Kowm Basin (Central Syria, dated from ~2 Ma to ~50 Ka) includes a greater number of forms, with at least 5 species in the sequence (Martini et al. 2015). Clearly, the diversity of fossil *Camelus* is currently underestimated.

In our presentation, we focus on the evolutionary anatomy of Camelidae and compare the cranial morphology of the two Recent species *C. bactrianus* (the Bactrian camel) and *C. dromedarius* (the dromedary) with undescribed material of the Pleistocene forms *Camelus* sp. (undescribed, from Nadaouiye Ah Askar, Syria) and *Camelus thomasi* (from Tighenif/Ternifine, Algeria).

Nadaouiye Ah Askar, in the El Kowm Basin (central Syria) was excavated from 1989 to 2003 by a team directed by the University of Basel (Jagher 2011). The site was an artesian well in an arid steppe of Central Syria. The main focus of the excavations has been the lithic tool of the Acheulean industry; only preliminary faunal studies have been published yet. The age of the site is archaeologically constrained between ~0.5 and ~0.2 Ka (with lower, poorer layers possibly up to 1.0 Ma); the cranium itself is dated close to 0.43 Ka.

The locality of Tighenif (also known as Ternifine or Palikao) has been excavated on three occasions: from 1872 to 1882, then in 1954-1956, and finally in 1981-1983 (Geraads et al. 1986). It has yielded a fauna rich in African species, indicative of an arid, open habitat, and also signs of human activity. The site is reconstructed as a small artesian lake, prone to drying out. According to the most recent publication, the site was dated to the beginning of the middle Pleistocene, at 0.7 Ma; however, our reconsideration of the fauna suggests an age closer to 1.0 Ma in the Jaramillo subchron. *C. thomasi* has been described since 1893, but never studied in detail.

Between the two modern species, a large number of significant differences can be recognized. In general, the cranium is larger in Bactrian camels, with a "smooth" outline; in dromedaries it is narrower, with a longer face, but appears more irregular, with stronger angles and deeper concavities. Further diagnostic characters of dromedaries, relatively to the Bactrian camel, include: maxillary crest absent, larger nasal opening, larger ethmoidal fissure, orbits placed lower and more rostrally, different conformation of the orbits, thinner zygomatic arch, postorbital constriction closer to the orbits, narrower braincase, longer palate, smaller diastema between C and caniniform P1, palatine foramina at the level of P4 (instead of M1), wider choana, nasal caudal spine frequent (rather than rare), shorter optic foramen spine, glenoid fossa triangular (rather than rectangular), relatively large occipital condyles, nuchal tubercle absent and other minor differences. No significant difference was found in the dentition. Major differences are also found in the mandibula (here not shown). Sexual dimorphism is evident in the dentition, but in the cranium is limited to few subtle metric characters, not shared between both species.

The cranium from Nadaouiye Ah Askar is larger than that of dromedaries. The low sagittal crest and small erupting P1 suggest that the specimen was a female 6-7 years old. Its characters are: maxillary crest present, laterally bulging maxilla, broad face and forehead, dorsally convex supraorbital notch (rather than concave), conformation of the orbit close to dromedary but much stronger, postorbital constriction shallow and distant from the orbits, narrow braincase, palatine foramina at the level of M1, narrow palate, narrow choana but caudal nasal spine present, triangular glenoid fossa, broad mastoid foramina, average-sized condyles, nuchal tubercle absent. M1 is large, M2 and M3 have broader mesial than distal lobes, M3 is small.

The cranium from Tighenif is also large. Its large left canine, large alveoles for I3 and P1, slightly worn M3 and developed

sagittal crest indicate that the specimen was a middle-age adult male. It has a smooth outline, maxillar crest present, broad forehead, shallow postorbital constriction, low placement of the orbita, palatine foramina at the level of P4, P1 in rostral position, occipital condyles rostrally narrow but caudally wide and massive, nuchal tubercle absent. M1 and M2 have broad mesial lobes.

Both fossil crania show a mosaic of characters found in either modern species, traits in common among themselves and unique traits. Together they confirm that the two Recent species of *Camelus* are only the remains of a former diversity brought about by a complex evolution.

REFERENCES

- Geraads, D., J.-J. Hublin, J.-J. Jaeger, H. Tong, S. Sen and P. Toubeau (1986). The Pleistocene hominid site of Ternifine, Algeria: New results on the environment, age, and human industries. *Quaternary Research* 25(3): 380-386.
- Jagher, R. (2011). Nadaouiyeh Aïn Askar - Acheulean variability in the Central Syrian Desert. The Lower and Middle Palaeolithic in the Middle East and Neighbouring Regions. J. M. Le Tensorer, R. Jagher and M. Otte. Liège, *Etudes et Recherches Archéologiques de l'Université de Liège (ERAUL)*. 126.
- Martini, P., L. Costeur, J.-M. Le Tensorer, and P. Schmid (2015). Pleistocene camelids from the Syrian Desert: The diversity in El Kowm. *L'Anthropologie* 119(5): 687-693.

4.18

How does bony labyrinth morphology help resolve the phylogeny and diversification timing of deer?

Bastien Mennecart¹, Loïc Costeur¹

¹ Natural History Museum, Basel, Augustinergasse 2, CH-4001 Basel, Switzerland (mennecartbastien@gmail.com)

Phylogenetic relationships within extant deer (family Cervidae) appear to be well resolved based on molecular data (mitochondrial and nuclear). Molecular clock analyses calibrate the origin of crown Cervidae within the Late Miocene (7-10 Mya). However, no phylogenetic hypothesis, based on morphological characters only, reflects the molecular-based topology. For example, *Megaloceros* is either part of the basal radiation of *Cervus* (molecular data), of the *Dama* radiation (combined analyses of molecular and morphological data), or closely related to the “basal Cervini” *Eucladoceros* (morphological data). In addition, palaeontological evidence indicates that stem Cervidae occurred 19 Mya and crown Cervidae could have arisen in the Middle Miocene, 4 My earlier than inferred from molecular data.

We investigated the shape of the cervid bony labyrinth performing 3D geometric morphometrics and cladistic analyses. Phenetic patterns of the bony labyrinth of 12 extant and 4 stem undisputed species of cervids do not coincide with phylogenetic hypotheses. However, a clear distinction between the stem and crown Cervidae, based on the shape of the bony labyrinth, can be drawn. Interestingly, the morphospace occupied by the Capreolinae is larger than the one occupied by the stem Cervidae and the Cervinae respectively, indicating a wider variation in the shape of the bony labyrinth.

Cladistic analyses based on bony labyrinth characters in other ruminants recover a consensual topology of the phylogenetic hypotheses (Mennecart & Costeur 2016, Mennecart et al. 2016). For this reason, we have performed a cladistic analysis including 26 characters of the bony labyrinth (12 on the semi-circular canals, 7 on the vestibule, 7 on the cochlea) and 28 species of Cervidae (12 extant species in all tribes and 16 fossil species from Europe, Asia, and America). Discrete characters were selected and continuous characters were found using canonical analyses based on specific regions of the bony labyrinth (semi-circular canals, oval window, cochlea) for species for which subfamily attribution is known. Recovered characters were then applied to debated fossil cervids.

The Nelson consensus compromise of the 20 minimum length trees distribution of the characters is structured following the ontogeny of the bony labyrinth (Costeur et al. in press). It supports monophyletic Capreolinae and Cervinae, as well as the Lagomerycinae, Procervulinae, and Dicrocerinae as stem deer. The “Old World” Capreolinae form a distinct clade including *Hydropotes*, while the phylogenetic position of the American capreolines remains unclear within the subfamily. The disparity of the bony labyrinth of the latter may reflect their recent evolutionary radiation in the New World, in line with previous suggestions made from their morphology and life history traits. Within Cervinae, the morphology of the bony labyrinth supports the already proposed clades: *Axis-Metacervoceros*, *Dama-Pseudodama-Megaloceros*, *Cervus-Eucladoceros*. However, the position of the insular *R. timorensis* and *C. nippon* is different from the hypothesis based on molecular data (forcing *Muntiacus* within the Cervini). As already proposed based on external morphology, *Euprox furcatus* is recovered as a stem Cervinae. This species appeared ca. 13.8 Mya pushing back the origin of crown deer by at least 4 My. A new molecular-based dating of the deer tree is then proposed. It suggests an origin of the Ruminantia at the base of the Middle Eocene (ca. 46 Mya) and an origin of the Pecora during the Late Oligocene-earliest Miocene (26-22 Mya). The diversification of the living Cervidae clades occurred after that of the Bovidae, during the Pliocene global climatic change.

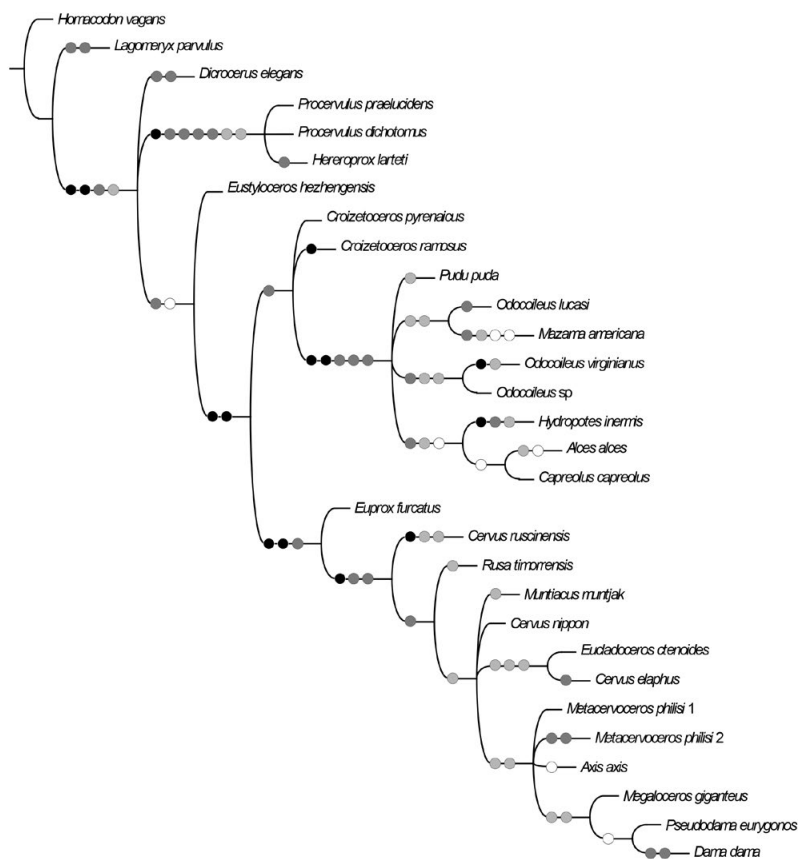


Figure 1. Phylogenetic tree (Nelson consensus compromise of the 20 minimum length trees) of selected Cervidae based on 26 characters of the bony labyrinth with repartition of the characters used. Black dots: cochlea; dark grey dots: semi-circular canals; light grey dots: vestibular aqueduct and endolyphatic sac; white dots: cochlear aqueduct. Consistency Index: 33; Retention Index: 72.

REFERENCES

- Costeur, L., Mennecart, B., Müller, B., & Schulz, G. in press: Prenatal growth stages show the development of the ruminant bony labyrinth and petrosal bone, *Journal of Anatomy*.
- Mennecart, B., & Costeur, L. 2016: A *Dorcatherium* (Mammalia, Ruminantia, Middle Miocene) petrosal bone and the tragulid ear region. *Journal of Vertebrate Paleontology*. DOI 10.1080/02724634.2016.1211665
- Mennecart, B., Rössner, G.E., Métais, G., DeMiguel, D., Schulz, G., Müller, B., & Costeur, L. 2016: The Petrosal Bone and Bony Labyrinth of Early to Middle Miocene European Deer (Mammalia, Cervidae) Reveal their Phylogeny. *Journal of Morphology*. DOI 10.1002/jmor.20579

4.19

The taxonomy and ecology of *Caryosyntrips*, a radiodontan from the Cambrian of Canada, Spain and the USA

Stephen Pates¹, Allison C. Daley^{1,2,3}

¹ Department of Zoology, University of Oxford, The Tinbergen Building, South Parks Road, Oxford, OX1 3PS, UK (stephen.pates@zoo.ox.ac.uk)

² Oxford University Museum of Natural History, Parks Road, Oxford, OX1 3PW, UK

³ Faculty of Geosciences and Environment, University of Lausanne, Sorge Géopolis, CH1015, Lausanne, Switzerland

Caryosyntrips is a genus of radiodontan (Cambrian apex predators in the stem lineage of arthropods) with two elongate and tapering frontal appendages of 14 podomeres. Each podomere has two large spines on the inner margin. Each appendage has a convex shaped proximal margin, and a rounded distal end. The etymology of the name (=nutcracker) suggests a crushing predation style.

Caryosyntrips appendages have previously been reported from the Burgess Shale, of the Middle Cambrian of Canada (Daley and Budd 2010). New specimens of the genus are here reported from the Wheeler Formation and Langston Formation, Spence Shale Member of the Middle Cambrian of Utah. A single specimen previously described as a lobopodian (Gamez-Vintaned et al. 2011) from the Lower Cambrian upper Valdemiedes Formation of Spain is reinterpreted as a *Caryosyntrips* appendage. These new finds increase the temporal and geographic ranges for the genus into the Lower Cambrian, and to a new continent (Gondwana).



Three species are recognised based on differences in appendage morphology. *Caryosyntrips serratus* Daley and Budd 2010 (Figure 1A) has small spines along the outer edge, and large spines along the inner edge with clear flexible membrane between the podomeres. *C. durus* nov. sp. (Figure 1B) has small spines along the outer edge, large spines along both edges, and does not have a clear flexible membrane between podomeres. *C. camurus* nov. sp. (Figure 1C) has no spines along the outer edge, large spines along the inner edge and clear flexible membrane between the podomeres on the outer edge. *C. camurus* also has a thin, flexible distal tip.

These differences in appendage morphology may indicate feeding specialisations. *C. durus*, which has no clear flexible membrane, is interpreted to have used a simple crushing technique. *C. serratus*, flexible along the length of the appendage, would have been able to manipulate prey items. *C. camurus*, with a flexible distal end, would have had some ability to manipulate prey items, but also appears adapted for crushing.

Caryosyntrips serratus and *C. camurus* are both reported from the Burgess Shale. *C. durus* is only known from the Wheeler Formation. *C. camurus* is also reported from the Langston Formation, Spence Shale Member and upper Valdemiedes Formation, Spain, and so has the widest geographic and temporal range of the species.

Figure 1. Isolated appendages of the three species of *Caryosyntrips*. A: *Caryosyntrips serratus* Daley and Budd 2010. B: *C. durus* nov. sp.. C: *C. camurus* nov. sp.. Scale bars 10mm.

REFERENCES

- Daley, A. C., & Budd, G. E. 2010: New anomalocaridid appendages from the Burgess Shale, Canada, *Palaeontology*, 53(4), 721-738.
- Gámez-Vintaned, J. A., Linán, E., & Zhuravlev, A. 2011: A new Early Cambrian lobopod-bearing animal (Murero, Spain) and the problem of the ecdysozoan early diversification. In *Evolutionary Biology—Concepts, Biodiversity, Macroevolution and Genome Evolution*, 193-219.

4.20

Herpetofauna of the early MP 16, Bartonian, Middle Eocene of Switzerland

Davit Vasilyan^{1,2}

¹ JURASSICA Museum, Route de Fontenais 21, 2900 Porrentruy (davit.vasilyan@jurassica.ch)

² Department of Geosciences, University of Fribourg, Chemin du musée 6, 1700 Fribourg, Switzerland.

Since the XIXth century, due to the industrial mining of the quarries of the Jurassic and Cretaceous limestone, many karstic pockets of Eocene age have been exposed. Some of them provided rich vertebrate faunas, mainly large mammals, whereas the other groups of vertebrates were scarcely studied or are entirely unstudied. In the present study the amphibian and reptile faunas of three localities, la Verrerie de Roches (several pockets), Les Alleveys, and Eclépens Gare have been studied. The localities provided mammalian fauna referable to the base of the Paleogene mammal level MP16, mid Bartonian, Middle Eocene. Among them the Les Alleveys is the oldest, whereas the La Verrerie de Roches is the youngest (Becker et al., 2013). The studied fossils come both from historical collections as well as newly screen-washed sediments.

The study of the material revealed a rather rich fauna of amphibians and reptiles, including salamanders, frogs, different lizards, snakes, and crocodile remains. Among the three localities, the most diverse fauna is that from La Verrerie de Roches, most probably because it is the most well-sampled site. The fauna of the locality includes: a small-sized salamandrid (Salamandridae indet.); frogs – *Thaumastosaurus* sp., Bufonidae indet. and Pelobatidae indet.; lizards – Varanidae indet. (?*Saniwa*), *Plesiolacerta* sp., *Geiseltalielius* sp., Gekkonidae indet., Amphisbaenidae indet., Glyptosaurini indet., Anguinae indet. Anguidae indet.; snakes – Boidae indet. (small-sized), Serpentes indet. 1 and 2; as well as a ziphodont crocodyliform.

The locality of Les Alleveys provides similar groups of vertebrates, but less taxa: a frog – *Thaumastosaurus* sp.; lizards – Lacertilia A and Lacertilia B., Glyptosaurini indet., Anguidae indet.; a snake – a large-sized pythonid snake; as well as a ziphodont crocodyliform.

The karstic fissure Eclépens Gare yielded fragmentary preserved lizard material - Glyptosaurini indet., remains of crocodyles, and turtles.

In summary, the amphibian and reptiles faunas from these localities are similar to each other. They represent the oldest known faunas among the known localities of the MP16 level. The herpetofauna from the studied localities does not differ strongly from that of the other middle Eocene fossil sites of Europe (Augé, 2005; Boret & Evans 2013). It is interesting to note the presence of *Thaumastosaurus* sp., representing the earliest stratigraphic occurrence of this frog. Few fragments of Bufonidae indet. represent so far the first stratigraphic occurrence of the group in MP16. The ziphodont crocodyliform remains, present probably in all three studied localities, represent one of the latest occurrences of this extinct crocodyliform group. Overall the studied amphibian and reptile fauna suggests warm and humid conditions, based on presence of groups like varanids, python, diverse lizard fauna.

REFERENCES

- Augé, M. L. 2005. Évolution des lézards du Paléogène en Europe, Mémoires du Muséum national d'Histoire naturelle, 192, 1-365.
- Becker, D., Rauber, G., & Scherler, L. 2013. New small mammal fauna of late Middle Eocene age from a fissure filling at La Verrerie de Roches (Jura, NW Switzerland), *Revue de Paléobiologie*, 32, 433-446.
- Bolet, A., & Evans, S. E. 2013. Lizards and amphisbaenians (Reptilia, Squamata) from the late Eocene of Sossís (Catalonia, Spain), *Palaeontologica Electronica*, 16, 1-23.

P 4.1

A paleontological field school organized in Canton Jura

Irena Burek¹, Gaël Comment^{2,1} & Jérémy Anquetin^{2,1}

¹ Department of Geosciences, University of Fribourg, Chemin du Musée 6, CH-1700 Fribourg (Irenajadwiga.burek@unifr.ch)

² JURASSICA Museum, Route de Fontenais 21, CH-2900 Porrentruy

Since 2015, the JURASSICA Museum in Porrentruy (Canton Jura) hosts an academic unit in geosciences consisting of five permanent researchers and several postgraduate students and postdocs. In addition to the study of regional geology and paleontology, one of our main objective is the training of students interested in different aspects of paleontology (from scientific research to fossil preparation), as well as the curation of natural history collections and museography.

Paleontological field techniques are rarely taught at university. In order to learn these techniques, students interested in paleontology usually participate to fieldwork during the summer vacation, but such opportunities are scarce. In August 2016, the JURASSICA Museum organized its first paleontological field school. We received more than 60 applications from all over Europe and selected 13 students to participate to the two weeks of fieldwork. Selected candidates came from different countries (Switzerland, France, Germany, United Kingdom, and Spain) and were at different stages in their university curriculum (from first-year Bachelor to finishing Master students).

The fieldwork focussed on a late Kimmeridgian layer of marls, the Lower *Virgula* Marls (Reuchenette Fm.; Comment et al. 2015), which was known to produce a rich assemblage of marine invertebrates and vertebrates (chondrichthyans, osteichthyans, turtles, and crocodylomorphs). This layer has previously been extensively excavated during the construction of the A16 Transjurane highway. The new locality, named Nova (Fig. 1), is located in Courtedoux (Canton Jura) and was first identified in 2010 thanks to exploratory diggings. Remains of a relatively complete turtle shell were found at that time and left in place. The purpose of the field school was therefore to extract this specimen, open a new surface for digging, and complete the sampling of this locality.

The collected material consists mostly of invertebrates, but about a hundred remains of vertebrates were also found. This assemblage is relatively congruent with the data already gathered in the past fifteen years concerning this particular stratigraphical interval. Among the most prominent finds made by the students are two new sub-complete plesiochelyid turtle shells (Fig. 2), some isolated *Steneosaurus* teeth, as well as several “*Lepidotés*”-like, pycnodontiform, and shark teeth.

Participating students were able to experiment different aspects of fossil extraction. Small specimens were usually extracted from the marls using trowels and dentist tools, whereas larger specimens were protected on the field with a plaster jacket before extraction. Mechanical extraction was also used in some parts of the locality. Several hundreds of kilograms of sediments were sampled for microrests at different horizons within the marls, and fragments of turtle shells were selected for geochemical analysis. Documentation related to the excavation (recording and identification of the finds, mapping of the site, etc.) was realized by the main author as part of an internship at the JURASSICA Museum.

It is our objective that such a paleontological field school will be organized every year from now on. Different stratigraphical intervals (Mesozoic or Cenozoic) will be targeted in the next few years and will, as much as possible, be linked to ongoing research projects in our institution.



Figure 1. The digging site during the excavation. Nova locality, Courtedoux, Canton Jura, Switzerland.



Figure 2. One of the new sub-complete turtle shells found by the students. Posterior part of the plastron (right) and scattered bones of the carapace.

REFERENCES

Comment, G., Lefort, A., Hantzpergue, P. & Koppka, J. 2015: Le Kimméridgien d'Ajoie (Jura, Suisse) : lithostratigraphie et biostratigraphie de la Formation de reuchenette, *Revue de Paléobiologie*, 34, 161-194.

P 4.2

Mid-Oligocene Rhinocerotidae from Bumbach (Switzerland)

Damien Becker^{1,2} Jérémy Tissier^{1,2} Loïc Costeur³ & Pierre-Olivier Antoine⁴

¹ *Jurassica Museum, Route de Fontenais 21, CH-2900 Porrentruy (damien.becker@jurassica.ch)*

² *Département des Géosciences, Université de Fribourg, Chemin du Musée 6, CH-1700 Fribourg*

³ *Department of Geosciences, Naturhistorisches Museum Basel, Augustinergasse 2, CH-4001 Basel*

⁴ *Institut des Sciences de l'Évolution, Université Montpellier 2, Place Eugène Bataillon, F-34095 Montpellier*

The first observations on the mid-Oligocene mammal remains of Bumbachgraben (Canton Bern, Switzerland) were published in Rüttimeyer (1855). Since then, the Bumbach locality has become a well-known mammal site of the Swiss Molasse Basin, in particular thanks to the numerous works on the Anthracotheriidae (e.g. Rüttimeyer 1855). During the first decades of the 20th century, Hans Georg Stehlin has regularly cited this locality, giving a first nearly complete faunal list in an overview on the mammal localities of the Swiss Molasse Basin in 1914. However it is only in the 80s, when small mammals were taken into account in the biostratigraphy that Bumbach was renamed as Bumbach 1 and became the Swiss reference level for MP25. More recent studies have focused on the large mammals, permitting the reassessment of the faunal list (see electronic supplementary material in Scherler et al. 2013). Despite this relatively high scientific productivity, the systematics of some recorded taxa is still questionable, especially those referred to Rhinocerotidae. Generally, two species, a large-sized form, often assigned to *Ronzotherium filholi*, and a small sized form, were considered by previous studies.

Recent studies on rhinocerotids of the European Oligocene (Ménouret & Guérin 2009, Becker et al. 2013) led to the description of two new taxa, the enigmatic "*Diaceratherium*" *massiliae* of teleoceratine affinities from Marseille (France) and *Molassitherium delemontense* from Poillat (Jura Canton, Switzerland), sister taxon of *Molassitherium albigenae* (junior synonym of *Protaceratherium albigenae*), which shows strong affinities with some specimens from Bumbach. Besides, new preparations of the rhinocerotid material of Bumbach stored at the Natural History Museum in Bern, offer a significantly better preservation quality for systematic descriptions. In the present work, we revise the complete collection of rhinocerotid specimens from Bumbach, and we identify for the first time three species: *Ronzotherium romani*, *Molassitherium delemontense* and "*Diaceratherium*" *massiliae*. The latter assemblage encompasses a mixture of Western European rhinocerotids of Palaeogene affinities and possibly of taxa previously only known in the Miocene. We present detailed results of systematics and general characteristics (morphology, ecology, stratigraphical and geographical ranges), which provide insights into (1) the phylogeny of Oligocene Western European rhinocerotids, (2) the taxonomic and ecological palaeodiversity of rhinocerotids (3) the mid-Oligocene palaeoclimate and ecosystem in Western Europe, based on the complete mammal assemblage of Bumbach.

REFERENCES

- Becker, D., Antoine, P.-O., & Maridet, O. 2013: A new genus of Rhinocerotidae (Mammalia, Perissodactyla) from the Oligocene of Europe. *Journal of systematic palaeontology*, 11, 947-972.
- Ménouret, B., & Guérin, C. 2009: *Diaceratherium massiliae* nov. sp. des argiles oligocènes de Saint-André et Saint-Henri à Marseille et de Les Milles près d'Aix-en-Provence (SE de la France), premier grand Rhinocerotidae brachypode européen. *Geobios*, 42, 293-327.
- Rüttimeyer, L. 1855: Über schweizerische *Anthracotherium*. *Verhandlungen der naturforschenden Gesellschaft Basel*, 3, 1-19.
- Scherler, L., Mennecart, B., Hiard, F., & Becker, D. 2013: Evolutionary history of hoofed mammals during the Oligocene–Miocene transition in Western Europe. *Swiss Journal of Geosciences*, 106, 349-369.
- Stehlin, H.G. 1914: Übersicht über die Säugetiere der schweizerischen Molasseformation, ihre Fundorte und ihre stratigraphische Verbreitung. *Verhandlungen der naturforschenden Gesellschaft Basel*, 25, 179-202.

P 4.3

Insights into the Cidarid Echinoids from the Middle Oxfordian St. Ursanne Formation of the Swiss Jura Mountains

Eva Alexandra Bischof

Department of Geosciences, University of Fribourg, Chemin du Musée 6, 1700 Fribourg, Switzerland (eva.bischof@unifr.ch)

Echinoids have a calcitic endoskeleton and are therefore well represented in the fossil record. The group first appeared in the Late Ordovician. Whereas the diversity of echinoids was low during the Palaeozoic, the group reached its highest diversity in the Mesozoic (Smith, 1984). Even though echinoids are primarily known for inhabiting shallow shelf areas, they also populated the full spectrum of other marine habitats throughout their history, ranging from the poles to the equator and from the intertidal zone to the deep-sea. The calcitic endoskeleton of echinoids is composed of a large number of individual elements with complex microarchitecture and therefore provides a rich basis for morphological studies. Since echinoids are morphologically adapted to the local environmental conditions (Sumrall & Brochu, 2008) they furthermore can be used as palaeoenvironmental indicators (Smith, 1984).

The goal of this study is to find a possible correlation between the carbonate facies in the St. Ursanne Formation and the echinoid species associated with this facies. For this purpose, eleven sections were measured and the rocks they contain classified in three primary facies: the coral reef facies, the reef debris facies, and the lagoonal facies. Given that the echinoids of the St. Ursanne formation have been neglected since the 19th century, the alpha taxonomy of the group was revised before identifying the sample. Particular attention was paid to representatives of the family of Cidaridae. In the coral reef and the reef debris facies of the St. Ursanne Formation at least five cidarid taxa can be distinguished. These can be assigned to the four genera *Diplocidaris*, *Paracidaris*, *Plegiocidaris* and *Rhabdocidaris*. Amongst these five taxa is one new species, namely *Diplocidaris bernasconii* nov. sp.

REFERENCES

- Sumrall, C. D. & Brochu, C. A. 2008: Viewing paleobiology through the lens of phylogeny. *Paleontological Society Papers*, 14, 165–183.
- Smith, A. B. 1984: *Echinoid palaeobiology*, 1. London, Taylor & Francis.

P 4.4

Hettangian-Sinemurian coral association of Amellago area (High Atlas, Morocco): first results.

Simon Boivin¹, Bernard Lathuilière², Christophe Duret³, Iuliana Lazar⁴, Rowan Martindale⁵, Khalid El Khmidi⁶ & Rossana Martini¹

¹ *Department of Earth Sciences, University of Geneva, 13 rue des Maraîchers, 1205 Geneva, Switzerland (Simon.Boivin@unige.ch)*

² *UMR CNRS 7359 Géoressources, Université de Lorraine, BP 70239,*

4506 Vandœuvre-lès-Nancy, France

³ *UMR CNRS 6282 Biogéosciences 6 Bd Gabriel, FR-21000 Dijon, France*

⁴ *University of Bucharest Faculty of Geology and Geophysics Department of Geology and Paleontology, 1, N. Balcescu Ave., RO – 010041 Bucharest, Romania*

⁵ *Department of Geological Sciences, University of Texas at Austin, 1 University Station C1100 Austin, TX 78712, U.S.A.*

⁶ *Département de l'Energie et des Mines Direction de la Géologie, Rue Abou Marouane Essaadi BP 6208, Haut Agdal, Rabat, Morocco*

This contribution is part of the long-term research project on reef and carbonate build-up development (REEFCADE to RM), started in 2007 and supported by the SNSF.

The end-Triassic mass extinction is one of the five largest mass extinctions of the Phanerozoic. The end of the Triassic and Early Jurassic are intervals with profound biotic and environmental changes, characterised by a dramatic decrease in marine fauna diversity. Corals especially suffered very high extinction rates; thus, compared with those of the Upper Triassic, the Early Jurassic is traditionally defined as exhibiting a “reef gap”.

In the literature, there are few occurrences of reefs in the Early Jurassic. In order to better understand these stages, the aim of the REEFCADE project is to study these poorly known corals. The Alpine Tethys area is investigated because genuine frameworks for colonial coral are scarce and concentrated in the western Tethys. During the previous research, conducted as part of a PhD thesis (M. Gretz, 2014), three localities have been investigated: the Isle of Skye in Scotland (Gretz et al. 2013), the Ardèche region in South of France (Gretz et al. 2015) and the Mas de Messier in Languedoc, South of France. In the Hettangian and Sinemurian time, these sites were located in the northern margin of the Tethys (Figure 1).

During this project (S. Boivin, PhD Thesis), we investigate the Hettangian-Sinemurian series cropping out in the Amellago area (Moroccan High Atlas), located in the southern margin of the Tethys (Figure 1). The geological context of Amellago is already known (Sarih et al. 2007; Lachkar et al. 2009; Pierre et al. 2010), but the coral associations have not been studied. To reach the set goals of the on-going project, and taking into account the good results already obtained, an integrated approach involving palaeontology and palaeoecology alongside sedimentology and biogeochemistry, is used to study the new coral association of Amellago. Hettangian-Sinemurian corals from Apuseni Mountains (Romania) discovered by Popa (1981) will be also considered. The poster presents the first results from the field work in Morocco.

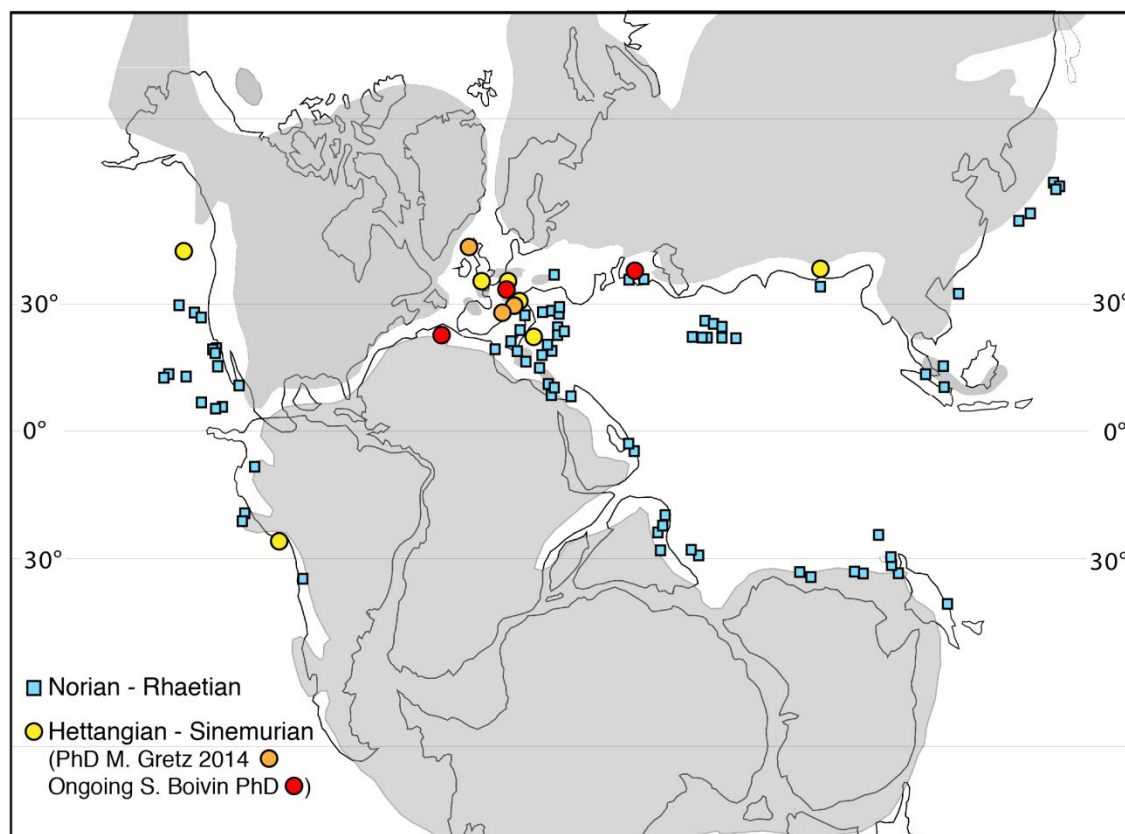


Figure 1. Distribution of coral reefs during Late Triassic and Early Jurassic. Among the Hettangian and Sinemurian reefs plotted with circle, our contributions are showed in red and orange (modified after Lathuilière & Marchal 2009, updated with Popa 1981).

REFERENCES

- Gretz, M. 2014: Biotic, environmental and climatic changes across the Triassic-Jurassic boundary: causes and effects highlighted via the Liassic coral reef associations. Thèse N°4644, Université de Genève.
- Gretz, M., Lathuilière, B., Martini, R & Bartolini A. 2013: The Hettangian corals of the Isle of Skye (Scotland): An opportunity to better understand the palaeoenvironmental conditions during the aftermath of the Triassic–Jurassic boundary crisis. *Palaeogeography, Palaeoclimatology, Palaeoecology*, 376: 132–148.
- Gretz, M., Lathuilière, B., & Martini, R. 2015 : A new coral with simplified morphology from the oldest known Hettangian (Early Jurassic) reef in southern France. *Acta Palaeontologica Polonica*, 60 (2): 277–286.
- Lachkar, N., Guiraud, M., El Harfi, A., Dommergues, J.-L., Dera, C., & Durllet, C. 2009 : Early Jurassic normal faulting in a carbonate extensional basin: characterization of tectonically driven platform drowning (High Atlas rift, Morocco). *Journal of the Geological Society, London*, 166: 413–430.
- Lathuilière, B. & Marchal, D. 2009 : Extinction, survival and recovery of corals from the Triassic to Middle Jurassic time. *Terra Nova*, 21 : 57-66.
- Pierre, A., Durllet, C., Razin, P. & Chellai, E. H. 2010 : Spatial and temporal distribution of ooids along a Jurassic carbonate ramp: Amellago outcrop transect, High-Atlas, Morocco. *Geological Society, London, Special Publications*, 329 : 65-88.
- Popa E. 1981. La biostratigraphie des formations mésozoïques de la partie orientale de Padurea craiului (monts Apuseni). *Anuarul institutului de Geologie si geofizica* 58: 203–281, pl. 13–16
- Sarih, S., Dommergues, J.-L., El Hariri, K., Garcia, J.-P. & Quiquerez, A. 2007 : Pseudoskirroceras, a remarkable but poorly known Early Pliensbachian Tethyan ammonite genus: New data from the High Atlas (Morocco). *Journal of African Earth Sciences*, 49 : 90–102.

P 4.5

Comparative cranial morphology of *Desmatochelys lowii* and modern marine turtles

Irena Burek

Department of Geosciences, University of Fribourg, Chemin du Musée 6, CH-1700 Fribourg (Irenajadwiga.burek@unifr.ch)

The phylogenetic placement of Cretaceous marine turtles, especially the clade of giant marine turtles, Protostegidae, has been a contentious subject among paleontologists. Whereas protostegids were traditionally thought to be situated within the clade of recent marine turtles (Cheloniodea) (e.g., Gaffney and Meylan 1988; Hirayama 1998), recent morphological and molecular studies theorize that protostegids are not directly related with chelonioids, but rather with stem cryptodires (Joyce 2007 Joyce et al. 2013; Rabi et al. 2013; Parham et al. 2014; Crawford et al. 2015). One reason why the evolution of marine turtles remains a complex enigma is a lack of insights into the cranial anatomy of protostegids, in particular the basicranium. However, a general availability of high quality fossil material, combined with modern analysis techniques, like X-ray microtomography (μ CT), provide ample opportunity to improve this situation.

For this study, I am describing the external and internal cranial morphology of the extinct protostegid turtle *Desmatochelys lowii* based on its beautifully preserved holotype, KU1200, from the Turonian Greenhorn Limestone of Kansas, currently housed in the collections of the University of Kansas. The skulls of two recent marine turtles, *Eretmochelys imbricata* (Cheloniidae) and *Dermochelys coriacea* (Dermochelyidae), serve at the comparative basis. All three skulls were scanned using micro CT scanners at the University of Fribourg, Switzerland and the University of Chicago, USA and the scans were then processed with the 3D Software Amira to create three dimensional skull models. Applying segmentation techniques, each skull bone was then virtually isolated (e.g., fig.1) to allow observing it from all angles. The final result will be an exhaustive comparative osteology of the three ingroup taxa highlighting all anatomical structures and notable morphological similarities and differences (e.g., fig. 2). This will then hopefully serve as a basis for future phylogenetic work.

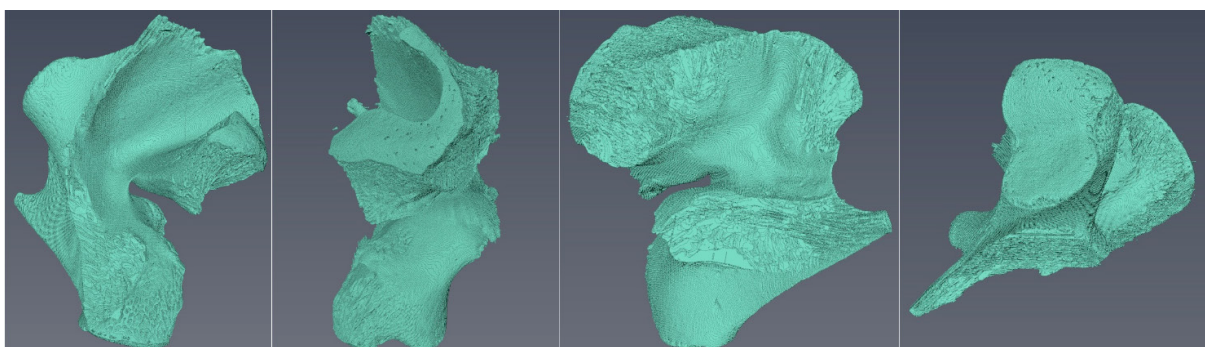


Figure 1. Non-edited 3D model of a virtually isolated skull bone (left quadrate) of *Eretmochelys imbricata*. Shown from four different perspectives: lateral, posterior, medial and ventral. (Screenshots taken within the Amira 3D Software)

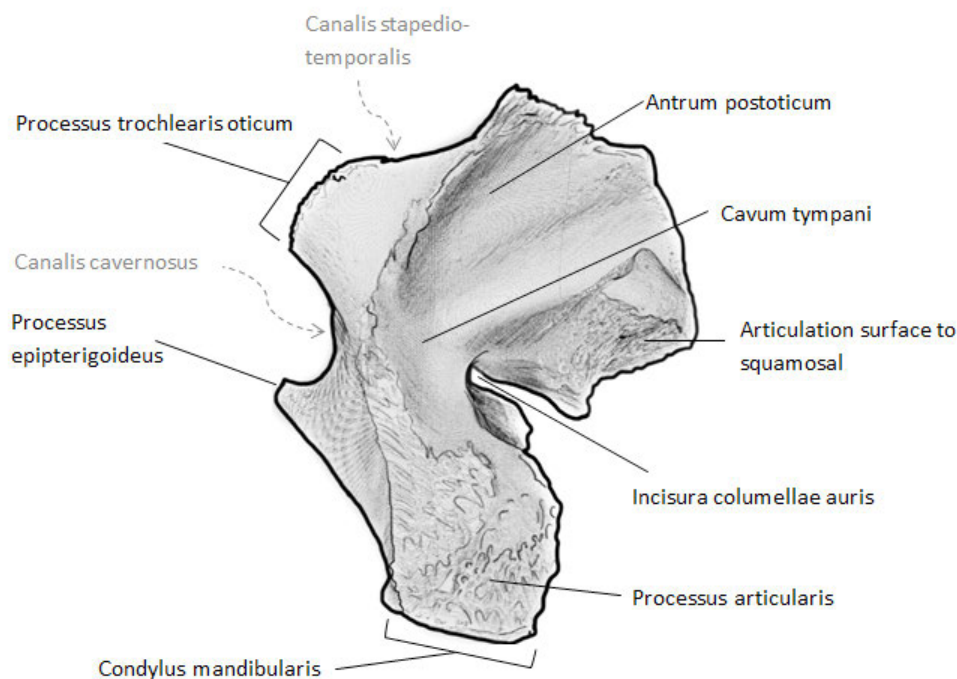


Figure 2. Illustration of the left quadrate of *Eretmochelys imbricata* with description

REFERENCES

- Crawford, N.G., Parham, J.F., Sellas, A.B., Faircloth, B.C., Glenn, T.C., Papenfuss, T.J., Hederson, J.B., Hansen M.H. & Simison, W.B. 2015: A phylogenetic analysis of turtles. *Molecular Phylogenetics and Evolution*, 83, 250–257.
- Joyce, W.G. 2007. Phylogenetic relationships of Mesozoic Turtles. *Bulletin of Peabody Museum of Natural History*. 48 (1): 3 – 102.
- Joyce, W.G., Parham, J.F., Lyson, T.R., Warnock, R.C.M., & Donoghue, P.C.J. 2013. A divergence dating analysis of turtles using fossil calibrations: an example of best practices. *Journal of Paleontology* 87: 612–634.
- Parham, J.F., Donoghue, P.C.J., Bell, C.J., Calway, T.D., Head, J.J., Holroyd, P.A., Inoue, J.G., Irmis, R.B., Joyce, W.G., Ksepka, D.T., Patané, J.S.L., Smith, N.D., Tarver, J.E., Van Tuinen, M., Yang, Z., Angielczyk, K.D., Greenwood, J., Hipsley, C.A., Jacobs, L., Makovicky, P.J., Müller, J., Smith, K.T., Theodor, J.M., Warnock, R.C.M., & Benton, M.J.. 2012. Best practices for justifying fossil calibrations. *Systematic Biology* 61(2):346-359.
- Rabi, M., Zhou, C.F., Wings, O., Ge, S. & Joyce, W.G.. 2013. A new xinjiangchelyid turtle from the Middle Jurassic of Xinjiang, China and the evolution of the basiptyergoid process in Mesozoic turtles. *BMC Evolutionary Biology* 13:203.

P 4.6

A marine bony fish assemblage (Teleostei) from the early Miocene of the Southern Caribbean (Cocinetas Basin, Guajira Peninsula)

Merin Reji Chacko¹; Jorge Domingo Carrillo-Briceño¹

¹ *Paleontological Institute and Museum, University of Zürich, Karl-Schmid-Strasse 4, 8006 Zürich (jorge.carrillo@pim.uzh.ch)*

The Cocinetas Basin is located in the eastern flank of La Guajira Peninsula, in northern Colombia. During the Miocene, large areas of this region had been submerged; the best evidence of this is represented by extensive and well-exposed deposits that have yielded a rich record of invertebrate and vertebrate fauna (Moreno et al., 2015; Hendy et al., 2015; Carrillo-Briceño et al., 2016). We report the discovery of a new marine bony fish assemblage from a single locality (~16 Ma) of the Burdigalian Jimol Formation. We document at least eight taxa, including Acanthuridae, Labridae, Scaridae, Sparidae, Sphyrnidae, Balistidae and Diodontidae — many of which are reported from the Colombian Neogene deposits for the very first time. In this assemblage, the most abundant feeder group is a durophagous one. The habitat preferences of their living representatives, as well as of other associated assemblages such as corals, bryozoans, echinoderms, mollusks and elasmobranchs (~20 shark and ray taxa), suggest a tropical shallow subtidal marine environment with conditions protected from major freshwater input. The new assemblage provides insight into the coastal bony fish diversity that had inhabited the northwestern margin of South America, from when the region had been a gateway between the Atlantic and Pacific Oceans.

REFERENCES

- Carrillo-Briceño, J.D., Argyriou, T., Zapata, V., Kindlimann, R., and Jaramillo, C.A. 2016. A new Early Miocene (Aquitania) Elasmobranchii assemblage from the Guajira peninsula, Colombia. *Ameghiniana* (53):77-99.
- Hendy, A.J.W., Jones, D.S., Moreno, F., Zapata, V., and Jaramillo, C. 2015. Neogene molluscs, shallow marine paleoenvironments, and chronostratigraphy of the Guajira Peninsula, Colombia. *Swiss Journal of Palaeontology*, 134(1):45-75.
- Moreno, F., Hendy, A.J.W., Quiroz, L., Hoyos, N., Jones, D.S., Zapata, V., Zapata, S., Ballen, G.A., Cadena, E., Cárdenas, A.L., Carrillo-Briceño, J.D., Carrillo, J.D., Delgado-Sierra, D., Escobar, J., Martínez, J.I., Martínez, C., Montes, C., Moreno, J., Pérez, N., Sánchez, R., Suárez, C., Vallejo-Pareja, M.C., and Jaramillo, C. 2015. Revised stratigraphy of Neogene strata in the Cocinetas Basin, La Guajira, Colombia. *Swiss Journal of Palaeontology*, 134(1):5-43.

P 4.7

Tooth mesowear highlights perissodactyl diets and environments in the Palaeocene of Europe

Laure Bapst¹, Loïc Costeur², Damien Becker^{1,3}

¹ *Département des Géosciences, Université de Fribourg, Chemin du Musée 6, CH-1700 Fribourg*

² *Naturhistorisches Museum Basel, Augustinergasse 2, CH-4001 Basel (loic.costeur@bs.ch)*

³ *Jurassica Museum, Route de Fontenais 21, CH-2900 Porrentruy*

The evolution of diets and environmental conditions in terrestrial realms can be estimated from the study of tooth morphology. Mesowear analysis records the cusps sharpness on the occlusal surface of the teeth, or “occlusal relief” (Fortelius & Solounias, 2000). Pointed and sharp cusps indicate animals with browsing diets, mostly composed of leaves or fruits while flat occlusal surfaces characterize animals with grazing abrasive diets, often composed of abrasive grasses. Mixed-feeders with a less extreme diet composed of both abrasive and non-abrasive food items have intermediate tooth occlusal surfaces. Combining this type of data to the hypsodonty index, a measure of tooth crown height related to food abrasiveness (see Mithbachler et al., 2011), brings insights into the environment and diet of a taxon.

Mithbachler et al. (2011) have reconstructed tooth occlusal relief in horses along the whole Cenozoic of North America showing a clear evolution from browsing, forest-dwelling horses in the Eocene towards larger cursorial grazing horses in the late Cenozoic, paralleling the global climatic trend of more seasonal, more arid and temperate environments towards the present.

Using a similar approach, we reconstruct diet types in perissodactyls (horses, rhinoceroses, tapirs, and their extinct relatives) across the Eocene and Oligocene (from MP10 to MP30) of western Europe. A total of 66 localities were investigated (mostly in France, Switzerland and Germany) and 1683 single measurements were done on 79 species of perissodactyls.

Our results parallel those of Mithbachler et al. (2011) for the Palaeocene with a first period in the Eocene where most of the taxa have low crowned teeth and folivore-frugivore diets followed by browser to mixed-feeder types of diets with slightly higher tooth crowned heights in the Oligocene where more abrasive food items play a larger role in the diets. It corresponds to the generally accepted picture of a tropical Eocene with closed humid forests followed by a more open and less tropical Oligocene. An interesting result is a difference in mesowear scores in Eocene taxa. While pachynolophids and palaeotheres have low mesowear scores indicating a folivore to frugivore diet devoid of any abrasive particles, lophodontids show slightly higher scores indicative of a slightly more abrasive diet. Feeding directly on trees in the former vs. feeding on the ground for the latter may explain the incorporation of more abrasive particles and thus of higher mesowear scores. This indicates resource partitioning where lophodontids probably use more open areas, like clearings, than the denser forested areas that remain vastly spread during the European Eocene. Rhinoceroses appear in Europe early in the Oligocene and their mesowear scores are higher or in the range of the by then extinct lophodontids. They are browsers to mixed feeders and confirm the more open environmental picture of the Oligocene.

REFERENCES

- Fortelius, M., & Solounias, N. 2000: Functional Characterization of Ungulate Molars Using Abrasion-Attrition Wear Gradient: A new Method for Reconstructing Paleodiets, *American Museum Novitates* 3301, 1-36.
- Mithbachler, M. C., Rivals, F., Solounias, N., & Semperebon G. M. 2011: Dietary change and Evolution of Horses in North America, *Science* 331, 1178-1181.

P 4.8

The oldest durophagous Thalattosuchian (Crocodylomorpha, Machimosaurini) from the lower Bathonian of Central High Atlas, Morocco

Bastien Mennecart¹, Stéphane Jouve², Julien Douteau³, Nour-Eddine Jalil²

¹ *Naturhistorisches Museum Basel, Augustinergasse 2, 4001 Basel, Switzerland (mennecartbastien@gmail.com)*

² *Sorbonne Universités, Département Histoire de la Terre, Muséum National d'Histoire Naturelle, CR2P, CNRS-MNHN-UPMC, CP38, 57 rue Cuvier, 75005, France*

³ *le pontet 03160 Franchesse, France*

The marine crocodylomorphs were particularly abundant in Europe during the Middle Jurassic, but were very scarce in Africa. New finds of thalattosuchians cranial elements in Morocco suggest that this scarcity is probably related to poor sampling. These remains pertain to the coastal thalattosuchians, the teleosauroids, and particularly to the clade grouping the blunt-toothed “*Steneosaurus*” *obtusidens* and the genus *Machimosaurus*. A new tribe is erected grouping these two taxa: Machimosaurini Tribe. Nov (Jouve et al. accepted). Until now the machimosaurins were only known from the middle Callovian.

The described thalattosuchian material has been collected 2.5 km Northeast from the town of Isseksi in the Taguelft syncline (Central High Atlas mountains, Morocco), at an approximated altitude of 1350m. In the central part of the basin, red marls and sandstones dominate the landscape. These red sediments are the so-called Middle Jurassic to Early Cretaceous “Red Beds”. The “Red Beds” provided some of the more spectacular African dinosaurs remains, such as the complete *Atlasaurus imelakei*, and numerous trackways dating from the late Middle Jurassic (Bathonian and ?Callovian) (e.g. Belvedere *et al.* 2010). The Tillouquit Formation is directly underneath the “Red Beds”. This formation is characterized by variegated silty marls and sandstones. On the top of this, a very fossiliferous limestone contains brachiopods. This is the last record of marine deposits during the Jurassic of the Central High Atlas Mountains. They are dated to the lower Bathonian by brachiopods. Some Jurassic terrestrial vertebrate remains and ichnofossils have also been found in the Tillouquit formation.

The studied specimens were embedded in a thin marly layer inserted in-between silty limestone. Just a few meters above it, we can observe red marls and sandstones from the “Red Beds”. Other fossils have been observed 1,5 m below the studied specimen. A limestone bank full of brachiopods provided rhombic teeth, probably belonging to an *Asteracanthus*-type shark. The silty limestone corresponds to the uppermost part of the Tillouquit Formation, lower Bathonian in age. The new remains extend the presence of the Machimosaurini further back to the lower Bathonian, nearly 5 Myr earlier (Jouve et al. accepted).

REFERENCES

Belvedere M., Mietto P., Ishigaki S. 2010. A Late Jurassic diverse ichnocoenosis from the siliciclastic Iouaridene Formation (Central High Atlas, Morocco). *Geological Quarterly*, 54(3), 367–380.

Jouve S., Mennecart B., Douteau J., Jalil N.-E. accepted. The oldest durophagous Thalattosuchian (Crocodylomorpha, Thalattosuchia) from the Lower Bathonian of Central High Atlas, Morocco. *Palaeontology*.

P 4.9

Upper Triassic limestones from central and SW Hokkaido, Japan: a new insight on the Panthalassa Ocean

Giovan Peyrotty¹, Camille Peybernes¹, Tetsuji Onoue², Hayato Ueda³, Rossana Martini¹

¹ *Department of Earth Sciences, University of Geneva, Rue des Maraichais 13, CH-1205 Genève (giovan.peyrotty@unige.ch)*

² *Department of Earth & Environmental Sciences, Kumamoto University, 2-39-1 Kurokami, Kumamoto 860-8555, Japan*

³ *Department of Geology, Niigata University, 8050 Ikarasi-ninocho, Nishi-ku, Niigata, 950-2181 Japan*

In comparison with the well-known Tethyan domain, Upper Triassic limestones from the Panthalassa realm are still poorly known. However, these carbonates represent a unique opportunity to have a more accurate view of the Panthalassa ocean during the Triassic, allowing comparison and correlation of biotic assemblages, diagenesis, and depositional settings of different Triassic localities from Tethyan and Panthalassic domains. Moreover, investigation of these panthalassic carbonates provides data for taxonomic revisions and helps to better constrain palaeogeographical models.

One of the best targets for the study of these carbonates is Hokkaido Island (northern part of Japan). Indeed, this island is a part of the South-North continuity of Jurassic to Paleogene accretionary complexes, going from the Philippines to Sakhalin Island (Far East Russia). Jurassic and Cretaceous accretionary complexes of Japan and Philippines contain Triassic mid-oceanic seamount carbonates from the western Panthalassa realm (Peybernes et al., 2016; Kiessling & Flügel, 2000). They have been accreted either as isolated limestone slabs or as clasts and boulders and are associated with mudstone, cherts, breccias and basaltic rocks.

Two of the major accretionary complexes forming Hokkaido Island (Fig. 1) containing Triassic limestone have been accurately explored and extensively sampled: the Oshima Belt, a Jurassic accretionary complex, and the Sorachi-Yezo Belt, a Cretaceous accretionary complex. A third zone, corresponding to the extension of the Oshima Belt to the North, has also been investigated in the northern part of Honshu Island. More than one hundred limestone samples were collected in these areas in July 2016 to perform sedimentological and micropaleontological analyses. The diagenetic aspect, interesting for the reconstruction of the evolution of these carbonates from their deposition to their subduction-generated accretion, will be investigated for the first time on both samples from previous studies and new samples. Extraction and identification of conodonts from selected samples is also an important part of the project. Indeed, this is essential to improve the dating of these Upper Triassic carbonates and refine the correlations with coeval limestones from the Tethys and Panthalassa oceans.

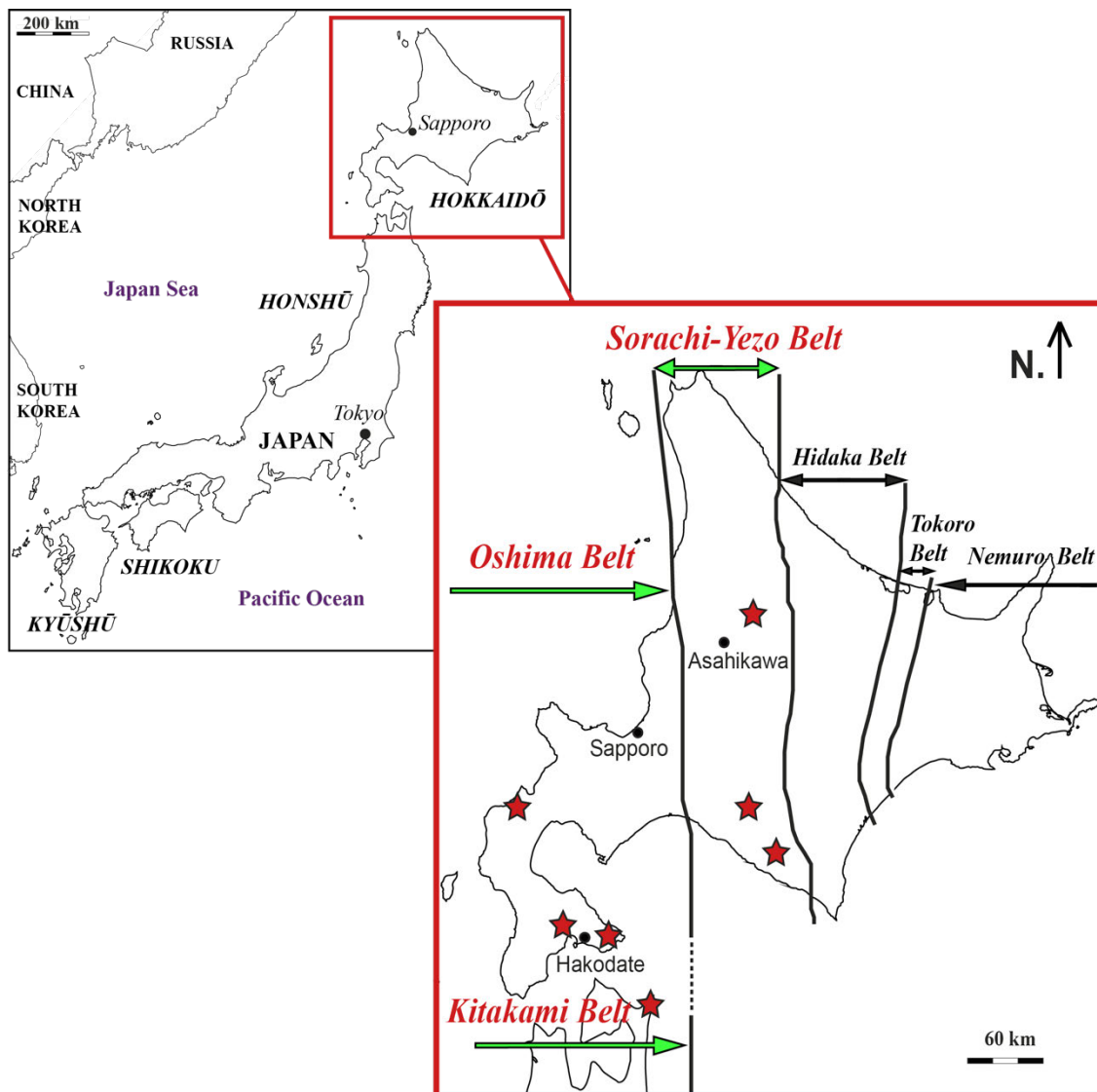


Figure 1. Map of the study area. Distribution of the Jurassic to Paleogene (West to East) accretionary complexes (belts) in Hokkaido Island. In red and yellow, the three investigated belts, containing Triassic limestone. Modified after The Geology of Japan, 2016.

REFERENCES

- Kiessling, W., & Flügel, E. 2000: Late Paleozoic and Late Triassic Limestones from North Palawan Block (Philippines): Microfacies and Paleogeographical Implications. *Facies*, 43, 39-78.
- Peybernes, C., Chablais, J., Onoue, T., Escarguel, G., & Martini, R. 2016: Paleoecology, biogeography and evolution of reef ecosystems in the Panthalassa domain during the Late Triassic: Insights from the reef limestone of the Sambosan Accretionary Complex, Shikoku, Japan. *Palaeogeography, Palaeoclimatology, Palaeoecology*, 457, 31-51.
- Ueda H. 2016: *The Geology of Japan*. Geological Society, London, 2g, 203-223.

P 4.10

An assessment of the phylogeny of cats (Felidae), including *Smilodon gracilis*, using the morphology of the petrosal bone

Karin Scherz

Department of Geosciences, University of Fribourg, Chemin du Musée 6, CH-1700 Freiburg (karin.scherz@unifr.ch)

The sabertooth cat *Smilodon gracilis* belongs to the extinct clade Machairodontinae, which is a subgroup of Felidae. *Smilodon gracilis* was a common, large predator in the late Pleistocene of North and South America that is thought to be similar to the extant jaguar, *Panthera onca*, in its general size and ecology (e.g., Martin et al. 2000; Christiansen & Harris 2005). There are many studies on the cranial, dental, and general anatomy of cats in general and *S. gracilis* in particular (e.g., Anyonge 1993; Martin et al. 2000; Christiansen & Harris 2005), but only little is known about the morphology of their petrosals. The phylogenetic relationships of felids were originally constructed using morphological data, but molecular techniques have more recently converged upon an alternative hypothesis (e.g., Zhang & Zhang 2013). Given that phylogenetic relationships of fossil cats can only be evaluated using morphology, current research is now focused on finding a consensus among morphological and molecular data and exploring new character complexes. The petrosal bone, a composite structure that surrounds the ear of mammals, has proven to be a particularly rich source of new phylogenetic characters, as it is morphologically complex, but had previously been neglected, because it is hidden within the skull (e.g., Costeur 2014).

To explore the utility of the petrosal bone for reconstructing the phylogeny of cats, the skulls of a sample of extant felids, *S. gracilis*, and the outgroup taxon *Prionodon linsang* were scanned using a Bruker-Skyscan 2211, a nano/micro-CT scanning system (x-ray computed tomography) housed at the University of Fribourg. CT-scanning allows documenting the internal morphology of the skull without damaging the specimen. 3D surface and volume models of the petrosal bone can then be rendered using specialized software. Apparent morphological differences were then encoded into a character/taxon matrix consisting of 47 character with 53 derived characters states for 10 taxa, including the outgroup. 6 multistate characters form morphoclines that can be ordered.

Preliminary phylogenetic analysis using petrosal characters alone yields a result that is broadly incongruent with recent molecular data. *Smilodon gracilis* is retrieved as sister to *Caracal caracal*, which contradicts traditional ideas, but may be influenced by ecological convergence. Future work will validate the use of petrosal characters for cats by integrating the data matrix into molecular and morphological hypotheses with broader sampling.

REFERENCES

- Anyonge, W. 1993: Body mass in large extant and extinct carnivores. *Journal of Zoology*, 231, 339–350.
- Christiansen, P. & Harris, J. M. 2005: Body size of *Smilodon* (Mammalia: Felidae). *Journal of Morphology*, 266, 369–384.
- Costeur, L. 2014: The petrosal bone and inner ear of *Micromeryx flourensianus* (Artiodactyla, Moschidae) and inferred potential for ruminant phylogenetics. *Zitteliana*, 32, 99–114.
- Martin, L. D., Babiarz, J. P., Naples, V. L. & Hearst, J. 2000: Three ways to be a saber-toothed cat. *Naturwissenschaften*, 87, 41–44.
- Zhang, W. Q. & Zhang, M. H. 2013: Complete mitochondrial genomes reveal phylogeny relationship and evolutionary history of the family Felidae. *Genetics and Molecular Research*, 12, 3256–3262.

P 4.11

A new, exceptionally preserved juvenile reptilian fossil (Diapsida) from the Middle Triassic of Ducan, Canton Grisons, Switzerland

Torsten M. Scheyer¹, James M. Neenan², Timea Bodogan¹, Heinz Furrer¹, & Mathieu Plamondon³

¹ Paläontologisches Institut und Museum der Universität Zürich, Karl Schmid-Strasse 4, CH-8006 Zürich (tscheyer@pim.uzh.ch)

² Oxford University Museum of Natural History, Parks Road, Oxford, OX1 3PW, UK

³ EMPA, Center of X-ray Analytics, Überlandstrasse 129, CH-8600 Dübendorf

The Prosanto Formation exposed at the Ducanfurrga near Davos, Canton Grisons, recently gained importance as another Swiss locality yielding outstanding Middle Triassic fossils. Some of the vertebrate faunal elements, including land-dwelling reptiles, marine sauropterygian reptiles, as well as fishes, are similar to those known from the slightly older Besano Formation at the World Heritage Site of Monte San Giorgio, Canton Ticino and Northern Italy, whereas others are novel findings (e.g., Furrer 2009; Fraser and Furrer 2013; Cavin et al. 2013). Here we report on such a new finding; a small diapsid reptile, which is exceptionally preserved and almost completely articulated. The complete skeleton, exposed in ventral view, is less than 20 cm long, and was scanned using computed microtomography to also reveal its dorsal components. The specimen is characterised by a deep skull with a short rostrum, stout cervical ribs, extremely elongated transverse processes of the thoracic vertebrae, a T-shaped interclavicle, a straight humeral shaft, radius and ulna forming a small spatium interosseum, a slightly curved femoral shaft, a very short and broad tail and only two carpal and tarsal ossifications. Because the animal is considered to be a juvenile, the condition of the latter two might still be prone to change during ontogeny. The most outstanding feature of the new reptile, however, is the presence of extensive body armour, including conical osteoderms on the vertebrae and along the thoracic ribs, as well as a row of flat and keeled osteoderms lateral to the gastralia. Preliminary anatomical comparison indicates affinities of the new specimen with the type material of *Eusaurosphargis dalsassoi* from the Middle Triassic of Besano, Varese Province, Italy (Nosotti and Pinna 2003).

REFERENCES

- Cavin, L., Furrer, H., & Obrist, C. 2013: New coelacanth material (Sarcopterygii, Actinistia) from the Middle Triassic of eastern Switzerland, and comments on the diversity of post-Palaeozoic coelacanths, *Swiss Journal of Geosciences*, 106, 161-177.
- Fraser, N., & Furrer, H. 2013: A new species of *Macrocnemus* from the Middle Triassic of the eastern Swiss Alps. *Swiss Journal of Geosciences*, 106, 199-206.
- Furrer, H. 2009: So kam der Fisch auf den Berg – Eine Broschüre über die Fossilfunde am Ducan, Bündner Naturmuseum Chur und Paläontologisches Institut und Museum Universität Zürich, 2. aktualisierte Auflage, 32 pp.
- Nosotti, S., & Rieppel, O. 2003: *Eusaurosphargis dalsassoi* n. gen n. sp., a new, unusual diapsid reptile from the Middle Triassic of Besano (Lombardy, N Italy). *Memorie della Società Italiana di Scienze Naturali e del Museo Civico di Storia Naturale di Milano*, 31, 3-33.

P 4.12

New material of amynodontids (Mammalia, Perissodactyla) from Romania

Jérémy Tissier^{1,2} Damien Becker^{1,2} Vlad Codrea³, Loïc Costeur⁴, Cristina Fărcaș⁵, Alexandru Solomon³, Marton Venczel⁶ & Olivier Maridet^{1,2}

¹ *Jurassica Museum, Route de Fontenais 21, CH-2900 Porrentruy (jeremy.tissier@jurassica.ch)*

² *Département des Géosciences, Université de Fribourg, Chemin du Musée 6, CH-1700 Fribourg*

³ *Department of Geology, Faculty of Biology-Geology, Babeş-Bolyai University, 1 Kogălniceanu Str., RO-400084 Cluj-Napoca*

⁴ *Department of Geosciences, Naturhistorisches Museum Basel, Augustinergasse 2, CH-4001 Basel*

⁵ *Faculty of Environment Science, Babeş-Bolyai University, 30, Fântânele Str., RO-400294 Cluj-Napoca*

⁶ *Department of Natural History, Țării Crișurilor Museum, Dacia Av. 1-3, RO-410464 Oradea*

Amyodontidae is a peculiar family of perissodactyls (“odd-toed ungulates”), known from the middle Eocene to early Miocene of North America and Eurasia. They are generally considered as derived from rhinocerotoids, although some authors have proposed a relationship with tapiroids (e.g. Radinsky 1969). The monophyly of the family is well-accepted and it is clearly diagnosed by having a preorbital fossa, four digits on the manus, several dental characteristics such as a quadratic M3, the absence of first premolars and developed canines, and by being hornless. Some of the species might have developed a proboscis, similar to that of tapirs as suggested by several skull characteristics (e.g. expansion of nasal incision). In addition they were long thought to have hippo-like amphibious lifestyle, but it may be an erroneous generalisation (Wall 1989).

Here, we present new material of amynodontids from Romania. It comprises a cranial fragment from Morlaca (Valea Nadășului Formation) of Priabonian age with complete right M1-M3 (Fig. 1), as well as a new incomplete skull from Dobârca (Transylvania; Priabonian-Rupelian age) bearing a left M3 associated to the already published mandible of “*Cadurcodon*” *zimborensis* (Codrea & Șuraru 1989). The specimens of Morlaca and Dobârca differ by the angle of the zygomatic arch and the slightly different shape of the M3.

A parsimony analysis of Amyodontidae based on morphological characters showed that the referred specimens from Dobârca could be closer to *Sianodon* than *Cadurcodon* by having a reduction of the lower premolars (only p3-p4 are present), low teeth crowns, wide zygomatic arches compared to frontals as well as a sharp angle of the *processus zygomaticus*. Nevertheless, they may belong to a new genus of amynodontidae, characterized by the presence of a strongly developed posterolateral “collar”, unknown until now among amynodontids. The Morlaca specimen on the other hand, is very similar to the type of *Amyndon reedi*, but both are too incomplete to undoubtedly validate this affinity.

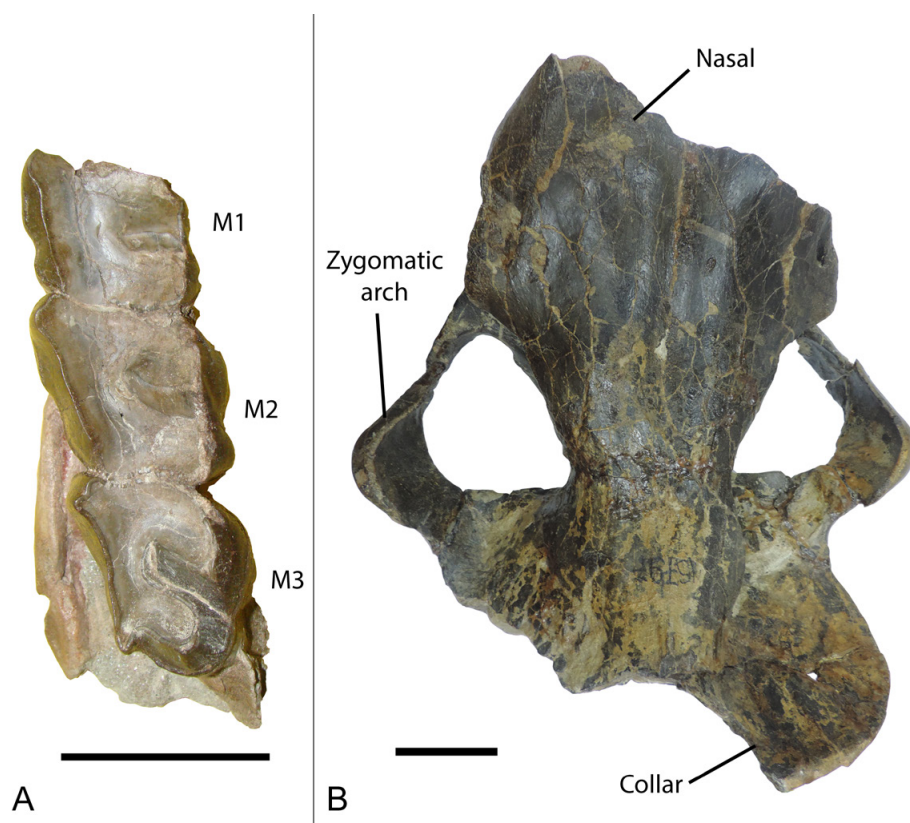


Figure 1. Amynodontidae from Romania. A) Cranial fragment from Morlaca (Priabonian) with right M1-M3 in ventral view. B = Incomplete skull from Dobârca (Priabonian-Rupelian) in dorsal view. Scale bars = 5cm.

REFERENCES

- Codrea, V. & Şuraru, N. 1989: Über einen Amynodontiden: "*Cadurcodon*" *zimborensis* n. sp. in den Zimborer-Schichten von Zimbor, kreis Salaj im Nord-Westen des Transsylvanischen Beckens. In Petrescu, I. (Ed.), The Oligocene from the Transylvanian Basin. University of Cluj-Napoca, Geology-Mineralogy Department, Special Issue, 319-338.
- Radinsky, L.B. 1969: The Early Evolution of the Perissodactyla. *Evolution*, 23(2), 308-328.
- Wall, W.P. 1989: The phylogenetic history and adaptive radiation of the Amynodontidae. In: *The Evolution of Perissodactyls*, 341-354, New-York.

P 4.13

Grasping the shape of belemnoid arm hooks – a quantitative approach

René Hoffmann¹, Manuel F. G. Weinkauf² & Dirk Fuchs³

¹ *Institut für Geologie, Mineralogie & Geophysik, Ruhr-Universität Bochum, Universitätsstrasse 150, DE-44780 Bochum (rene.hoffmann@rub.de)*

² *Section des Sciences de la Terre et de l'Environnement, Université de Genève, Rue des Maraîchers 13, 1205 Genève*

³ *Department of Earth and Planetary Sciences, Hokkaido University, Kita-10 Nishi-8 Kita-ku, JP-060-0810 Sapporo*

Chitinous arm hooks (onychites) of belemnoid coleoids are widely distributed in Mesozoic sediments. Due to their relative abundance and variable morphology compared to the single, bullet-shaped belemnite rostrum, arm hooks came into the focus of micropalaeontologist as a promising index fossil group for the Jurassic–Cretaceous rock record and have been the target of functional, ecological, and phylogenetic interpretations in the past (e.g. Reitner & Engeser 1982; Fuchs et al. 2013; Hammer et al. 2013).

Based on three well-preserved arm crowns of the Toarcian diplobelid *Chondroteuthis wunnenbergi*, we analyzed the shape of a total of 87 micro-hooks. The arm crown of *Chondroteuthis* is unique in having uniserial (rather than biserial) hooks. The first application of elliptic Fourier shape analysis to the arm weapons of belemnoid coleoids allows for the distinction of four micro-hook morphotypes and the quantification of shape variation within these morphotypes. Based on the best preserved arm crown, we reconstructed the distribution of morphotypes within the arm crown as well as along a single arm.

Our quantitative data support former observations that smaller hooks were found close to the mouth and at the most distal arm parts, while the largest hooks were found in the central part of the arm crown. Furthermore, we found a distinct arm differentiation, as not every arm was equipped with the same hook-morphotypes. Here, we report the functional specialisation of the belemnoid arm crown for the first time and speculate about the potential function of the four morphotypes.

Our analyses suggest a highly adapted functional morphology and intra-specimen individual distribution of belemnoid hooks, serving distinct purposes mainly during prey capture, prey digestion, as well as reproduction. In this regard, hooks at the distal end of the arms show stronger curvature to effectively catch and hold the prey, while hooks closer to the belemnoids mouth are more suitable for prey dissection and for transporting food to the mouth.

We speculate that this highly specialised arrangement is an adaptation of *Chondroteuthis* towards its uniserial hook-arrangement. This is supported by the fact that belemnoids with biserial hook armament do not show inter-individual changes in micro-hook morphology (Engeser 1987).

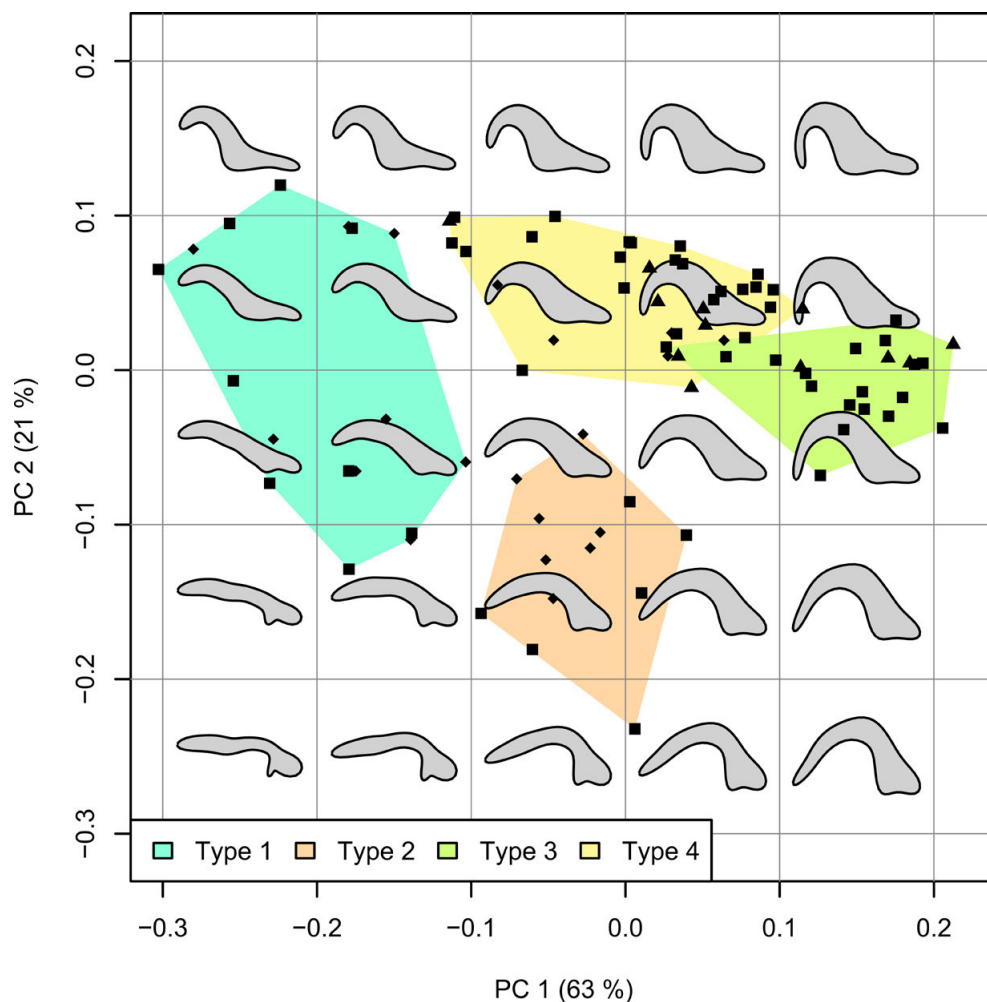


Figure 1. Principal component analysis of *Chondroteuthis wunnenbergi* micro-hook morphology. Symbols represent the individual hooks, grey silhouettes represent the theoretical mean form of the respective 0.1×0.1 square. The positions of the four distinguished morphotypes are indicated.

REFERENCES

- Engeser, T. 1987: Belemnoid arm hooks (onychites) from the Swabian Jurassic – a review. *Neues Jahrbuch für Geologie und Paläontologie Abhandlungen* 176, 5–14.
- Fuchs, D., Donovan, D. T. & Keupp, H. 2013: Taxonomic revision of “*Onychoteuthis*” *conocauda* Quenstedt, 1849 (Cephalopoda: Coleoidea). *Neues Jahrbuch für Geologie und Paläontologie Abhandlungen* 270, 245–255.
- Hammer, Ø, Hryniewicz, K., Hurum, J. H., Hoyberget, M., Knudsen, E. M. & Nakrem, H. A. 2013: Large onychites (cephalopod hooks) from the Upper Jurassic of the Boreal Realm. *Acta Palaeontologica Polonica* 58, 827–835.
- Reitner, J. & Engeser T. 1982: Zwei neue Coleoidea-Arten aus dem Posidonienschiefer (Untertoarcium) aus der Gegend von Holzmaden (Baden-Württemberg). *Stuttgarter Beiträge zur Naturkunde Serie B (Geologie und Paläontologie)* 84, 1–19.

5. The Sedimentary Record of Tectonic, Climatic and Environmental Change From Deep to Modern Times

Sébastien Castelltort, Samuel Jaccard, Adrian Gilli, Karl Föllmi

*Schweizerische Paläontologische Gesellschaft,
Kommission des Schweizerischen Paläontologischen Abhandlungen (KSPA)*

TALKS:

- 5.1 Adatte T., Font E., Mbabi Bitchong A., Sordet V., Keller G., Schoene B., Samperton, K., Khadri S.: Timing and tempo of Deccan volcanism, evidence from mercury anomalies
- 5.2 Baldessin E., Machel H., Kindler P., Chiaradia M.: New constraints on the timing of dolomitization episodes in the Bahamas during the Neogene: the Sr-isotope data from Mayaguana.
- 5.3 Baumgartner-Mora C., Andjic G., Baumgartner P.O.: Punctuated chlorozoan carbonate paleo-environments – A biotic response to accretion tectonics and stalled arc activity (Late Cretaceous-Cenozoic, Caribbean Plate)
- 5.4 Cartapanis O., Galbraith E.D., Bianchi D., Jaccard S.L.: Changes in the global burial rate of carbon in marine sediments and atmospheric CO₂ variations over the last glacial cycle
- 5.5 Charbonnier G., Morales C., Duchamp-Alphonse S., Westermann S., Adatte T., Föllmi K.B.: Mercury enrichment indicates volcanic triggering of the Valanginian Weissert episode
- 5.6 Chen C., Castelltort S., Guerit L., Paola C., Foreman B.: Grain size evolution in fluvial deposits during global warming at the Paleocene-Eocene boundary, Tremp formation, Spain
- 5.7 Fantasia A., Föllmi K.B., Adatte T., Scasso R.A., Spangenberg J.E., Schoene B., Barker R.T.: The Cañadón Asfalto Formation, Argentina: sedimentology and paleoenvironments
- 5.8 Hunger G., Moscariello A., Ventra D., Veiga G.D.: Compositional changes related to non-steady state conditions during deposition of a Miocene sedimentary basin infill, Central Argentinian Foreland (Mendoza province)
- 5.9 Kindler P., Revillon S., Vimpere L., Godefroid F.: Elevated coralgall bioherms from Long Island (Bahamas): a testimony of recent tectonic uplift or of a high sea level during Marine Isotope Stage 7
- 5.10 Litty C., Lanari P., Burn M., Schlunegger F.: Climatic control on sediment provenance inferred from detrital zircon ages, Western Peruvian Andes
- 5.11 Malatesta L.C., Avouac J-P., Brown N., Berger Q., Breitenbach S., Pan J., Chevalier M-C., Rhodes E., Saint-Carlier D., Zhang W., Poisson B.: Buffering and mixing of sediment flux across the north piedmont of the Tian Shan
- 5.12 Meier, M.M.M. (Recipient Paul Niggli Medal): Meteorites and micrometeorites from sediments – identification and characterization using noble gases
- 5.13 Perret M., Segvic B., Puigdefabregas C., Moscariello A., Clark J., Fildani A., Dykstra M., Castelltort S.: Petrography and clay mineralogy of Eocene clastic rocks from the Tremp-Graus-Ainsa basin, Southern Pyrenean Foreland (Spain) – Reconstruction of sediment provenance and burial diagenesis
- 5.14 Schöllhorn I., Gertsch B., Adatte T., Houben A., Spangenberg J., Schwennicke T., Föllmi K.B.: Depositional mechanisms and environmental conditions leading to the formation of phosphorite in the El Cien Formation (Oligocene-Miocene; Baja California-Mexico)

POSTERS:

- P 5.1 Blattmann F., Schenker T., Picotti V., Cobianchi M.: Reconstructing the Evolution of the Northwestern Friuli Platform Margin Based on Microfacies
- P 5.2 Fentimen R., Lim A., El Kateb A., Wheeler A., Spezzaferri S.: Benthic foraminiferal assemblages from small scaled Cold-water coral habitats : the Moira Mounds
- P 5.3 Foubert A., Jaramillo-Vogel D., De Boever E., Feenstra E., Hamaekers H., Krause S.: High-resolution visualization of microbial carbonates using μ -CT: Insights from field and lab experiments
- P 5.4 Chen C., Castellort S., Guerit L., Paola C., Foreman B.: Laboratory experiments of autogenic fluvial progradation above incised-valley fills during sea-level rise
- P 5.5 Lathion R., Le Cottonnec A., Moscariello A.: Sedimentology and stratigraphic architecture of an incised valley fill, Late Carboniferous (Eastern Kentucky, USA).
- P 5.6 Honegger L., Castellort S., Clark J., Adatte T., Puigdefàbregas C., Dykstra M, Fildani A., Spangenberg J.: $\delta^{13}\text{C}$ as a tool for sequence stratigraphy correlations in the South Pyrenean foreland basin, Spain
- P 5.7 Hunger T., Adatte T., Kouzmanov K., Castellort S.: Climatic signals in the Paleocene fluvial formation of Tresp, Pyrenees, Spain.
- P 5.8 Shawwa N.A, Chesnel V., Merino-Tomé Ó., Fernández L.P., Šegvić B., Samankassou E.: Linking subaerial exposures to paleoenvironments and paleoclimates (Valdorria carbonate platform, northern Spain)
- P 5.9 Läubli C., Garcès M., Valero L., Clark J., Puigdefabregas C., Adatte T., Castellort S.: Multiproxy approach to climate signals in the middle-upper Eocene deposits of the Ainsa Basin, Spain
- P 5.10 Ambrosi C., Bernoulli D., Scapozza C., Schenker F., Dall'Agnolo S.: The new geological map of the area between Mendrisio (Switzerland), Como and Varese: 300 million years of geological history.
- P 5.11 Stutenbecker L., Berger, A., Schlunegger, F.: Detrital garnet fingerprint of the Central Swiss Alps
- P 5.12 Madella A., Delunel R., Blard P-H., Akçar N., Schlunegger F., Christl M.: Paleo-erosion rates and paleo-elevation inferred through cosmogenic ^{10}Be and ^{21}Ne in northernmost Chile
- P 5.13 Amsler H.E., Jaccard S.L., McCave I.N., Ikehara M.: Variations in near-bottom flow of ACC during past glacial cycle in SW Indian Ocean
- P 5.14 Oesch L., Sigman D.M., Studer A.S., Haug G.H.: Nitrogen isotope changes in the equatorial Atlantic during Plio-Pleistocene Transition
- P 5.15 Kremer K., Wirth S.B., Reusch A., Fäh D., Bellwald B., Anselmetti F.S., Girardclos S., Strasser M.: Epicentres and magnitudes of possible paleoearthquakes based on lacustrine sediment records in Switzerland

5.1

Timing and tempo of Deccan volcanism, evidence from mercury anomalies

Adatte T.¹, Font E.², Mbabi Bitchong A.¹, Sordet V.¹, Keller G.³, Schoene B.³, Samperton, K. ³, Khadri S.⁴

¹ *Institute of Earth Sciences, ISTE, GEOPOLIS building University of Lausanne, Switzerland (thierry.adatte@unil.ch)*

² *Universidade de Lisboa, IDL, Lisbon, Portugal*

³ *Department of Geosciences, Princeton University, Princeton NJ 08540, USA*

⁴ *Department of Geology, Amravati University, Amravati, India*

Mercury is a very toxic element, with a long residence time (1-2 years) and wide distribution by aerosols. Volcanic emissions and coal combustion are the two main natural sources of mercury. Several studies [e.g. Sanei et al., 2012, Grasby et al, 2013, Percival et al., 2016, Font et al., 2016,] evaluated the relationship between Hg anomalies in sediments and LIP activity across mass extinction horizons. The bulk (80%) of Deccan Trap eruptions occurred over a relatively short time interval in magnetic polarity C29r. U-Pb zircon geochronology reveals the onset of this main eruption phase 250 ky before the Cretaceous-Tertiary (KT) mass extinction and continued into the early Danian suggesting a cause-and-effect relationship [Schoene et al, 2015]. In a related study we investigate the mercury (Hg) contents of sections in France (Bidart), Spain (Zumaya), Denmark (Nye Klov), Austria (Gams), Italy (Gubbio), Tunisia (Elles, El Kef), Egypt (Sinai), India (Megalaya), Texas USA (Brazos River) and Mexico (La Parida). In all sections, results show Hg concentrations are more than 2 orders of magnitude greater during the last 100ky of the Maastrichtian up to the early Danian P1a zone (first 380 Ky of the Paleocene). These Hg anomalies are correlative with the main Deccan eruption phase. Hg anomalies generally show no correlation with clay or total organic carbon contents, suggesting that the mercury enrichments resulted from higher input of atmospheric Hg species into the marine realm, rather than organic matter scavenging and/or increased run-off. At Gams, Bidart and Elles, Hg anomalies correlate with high shell fragmentation and dissolution effects in planktic foraminifera indicating that paleoenvironmental and paleoclimate changes drastically affected marine biodiversity. These observations provide further support that Deccan volcanism played a key role in increasing atmospheric CO₂ and SO₂ levels that resulted in global warming and acidified oceans, increasing biotic stress that predisposed faunas to eventual extinction at the KTB. Global documentation of Deccan volcanism-related proxies and environmental effects preceding the KTB mass extinction is now possible and brings much needed clarity and improved understanding of the catastrophic effects of Large Igneous Province (LIP) volcanic eruptions during four of the five big mass extinctions in Earth's

REFERENCES

- Font, E., Adatte, T., Sial, A.N., Lacerda, L.D., Keller, G., Puneekar, J., 2016. Mercury anomaly, Deccan Volcanism and the end-Cretaceous Mass Extinction. *Geology* 44, 171–174.
- Grasby, S.E., Sanei, H., Beauchamp, B., and Chen, Z.H., 2013, Mercury deposition through the Permo-Triassic biotic crisis: *Chemical Geology*, v. 351, p. 209–216.
- Sanei, H., Grasby, S.E., and Beauchamp, B., 2012, Latest Permian mercury anomalies: *Geology*, v. 40, p. 63–66.
- Schoene, B., Samperton, K.M., Eddy, M.P., Keller, G., Adatte, T., Bowring, S.A., Khadri, S.F.R., Gertsch, B., 2015, U-Pb geochronology of the Deccan Traps and relation to the end-Cretaceous mass extinction: *Science*, v. 347, p. 182–184.
- Percival, L.M.V. Witt, M. L. I. T., Mather, A., Hermoso, M., Jenkyns, H. C. , Hesselbo, S. P., Al-Suwaidi, A. H. , Storm, M. S. , Xu, W., Ruhl, M. 2015: Globally enhanced mercury deposition during the end-Pliensbachian extinction and Toarcian OAE: A link to the Karoo–Ferrar large igneous province. *Earth and Planetary Science Letters*. 428, 267–280.

5.2

New constraints on the timing of dolomitization episodes in the Bahamas during the Neogene: the Sr-isotope data from Mayaguana.

Erika Baldessin¹, Hans Machel², Pascal Kindler¹, Massimo Chiaradia¹

¹Department of Earth Sciences, University of Geneva, Rue des Maraîchers 13, CH-1205 Genève (Erika.Baldessin@unige.ch)

²Department of Earth and Atmospheric Sciences, University of Alberta, Edmonton, AB T6G 2E3, Canada

Sr-isotope data recently obtained on Neogene dolostones from the surface and the subsurface of the Mayaguana Bank (SE Bahamas) reveal the occurrence of four short-lived (< 1.2 Myr) dolomitization phases during this time interval that contrast with the long-lasting episodes of dolomitization previously identified in this area.

The Mayaguana Bank is located in the SE Bahamas, and bears one single island: Mayaguana. The latter contrasts with all other Bahamian islands because it exposes three lithostratigraphic units consisting of, or comprising dolostone: (1) the Timber Bay Formation (TBF) consists of mimetically dolomitized boundstone and grainstone that have been biostratigraphically dated from the Pliocene; (2) the Little Bay Formation (LBF) is made of laminated dolomicrite (i.e. caymanite) whose age is constrained between the Burdigalian and the Pliocene; (3) the Mayaguana Formation (MYF) includes foraminiferal grainstone and packstone dated from the Early Miocene (Aquitania – Burdigalian) that comprise several dolostone intervals at depth.

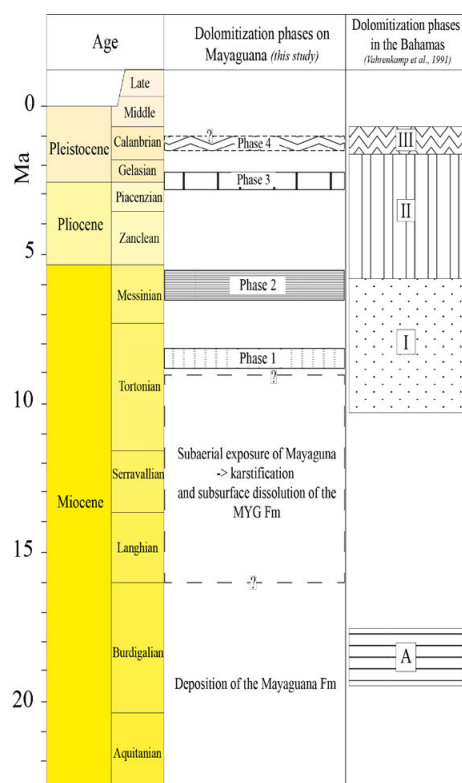
We made two assumptions: (1) like other Bahamian occurrences, the Mayaguana dolostones result from the interaction of a parent limestone with seawater, and (2) the ⁸⁷Sr/⁸⁶Sr ratio of pure dolomite samples reflect that of the dolomitizing fluid, and thus indicate the age of dolomitization.

We thus selected thirteen dolostone samples collected from the aforementioned formations, and containing 100% dolomite as checked by XRD analysis. ⁸⁷Sr/⁸⁶Sr ratios from whole-rock powders obtained from these samples were measured with an ICP Multi-Collector Mass Spectrometer Neptune Plus at the University of Geneva. Numerical ages were then obtained by comparison with the Sr-isotope evolution of global seawater for the Neogene reported as the look-up table Version 4:08/04 (McArthur et al. 2001).

⁸⁷Sr/⁸⁶Sr ratios of pure dolomite samples range from 0.708922 to 0.709082, and delineate four phases of dolomitization on Mayaguana (Figure 1). Phase 1 lasted ca. 0.3 Ma during the early Late Miocene (Tortonian), and caused partial dolomitization of the MYF. Phase 2 was longer (ca. 1.2 Ma), and occurred in the Latest Miocene (Messinian). This second event resulted in the partial dolomitization of the MYF and the complete dolomitization of the LBF. Phase 3 spanned the Latest Pliocene and the Earliest Pleistocene (ca 0.7 Ma), and affected the TBF and part of the MYF.

A fourth phase based on samples containing less than 100% dolomite was identified in the Early Pleistocene, but its precise timing and duration could not be determined. Part of the TBF was dolomitized during this episode.

Although in general agreement with the dolomitization events previously recognized in the Bahamas, the episodes identified on Mayaguana differ by their short duration, and the lack of the late Early Miocene event (Phase A; Vahrenkamp et al., 1991) despite deposition of part of the MYF before that time. These findings bring new constraints on the dolomitization events in the Bahamas, and will contribute to a better understanding of the relationship between these episodes and eustatic sea-level changes.



Exposure surface observed in the Aquitanian on Mayaguana, but the timing is based on Miller et al. (2009) due to broad biostratigraphic ages. The dolomitization event in the Mid-late Miocene includes Sr-datation of Vahrenkamp (1991) on Pierson's samples (MA-10 and/or MA-18).

Figure 1 – Comparison of dolomitization phases on Mayaguana and in the Bahamas.

REFERENCES

- McArthur, J.M., Howard, R.J. and Bailey, T.R., 2001. Strontium Isotope Stratigraphy: LOWESS Version 3. Best-fit line to the marine Sr-isotope curve for 0 to 509 Ma and accompanying look-up table for deriving numerical age. *Journal of Geology*, Vol. 109, No. 2, pp. 150-170.
- Vahrenkamp, V.C., Swart, P.K. and Ruiz, J., 1991. Episodic dolomitization of late Cenozoic carbonates in the Bahamas: Evidence from strontium isotopes. *Journal of Sedimentary Petrology*, Vol. 61, pp. 1002-1014.

5.3

Punctuated chlorozoan carbonate paleo-environments - A biotic response to accretion tectonics and stalled arc activity (Late Cretaceous-Cenozoic, Caribbean Plate)

Claudia Baumgartner-Mora¹, Goran Andjic¹, & Peter O. Baumgartner¹

¹ *Institut des Sciences de la Terre, Université de Lausanne, Géopolis, 1015 Lausanne (claudia.baumgartner@unil.ch)*

We propose a new model for “punctuated chlorozoan carbonate paleo-environments”, inspired by the model of punctuated equilibria in evolution, Eldredge & Gould (1972). They are characterized by a very rapid appearance and disappearance of stable conditions favorable to chlorozoan carbonate production, modest size and a geologically short life span. Late Cretaceous – Cenozoic carbonate-producing paleo-environments in the “oceanic” areas of the Caribbean Plate (Fig. 1) were short-lived (1-10 Ma). This is particularly the case along the intra-oceanic subduction zones of Central America and the Caribbean, areas largely floored by a CLIP-type (Caribbean Large Igneous Province) thickened oceanic crust.

The small carbonate banks were mainly built by rock-forming LBF (larger benthic foraminifera) and rhodophycean algae, while rudists in the Upper Cretaceous and corals in the Oligocene-Miocene may have produced framework. These banks are fundamentally different from long-lived (10-60 Ma), large carbonate shelves set on (often thinned) continental crust along passive margins, such as Florida, Yucatan, Nicaragua Rise etc. Hence, models developed for the latter do not apply to the small carbonate banks. Oceanic basements, such as basalt plateaus, oceanic seamounts and proto-island arcs in isostatic equilibrium formed at subphotic depths and subsided thermally, unless tectonic or volcanic activity produced uplift or sufficient buoyancy to make them temporarily reach the photic zone. Once oceanic and arc rocks reached the subaerial realm – either by accretion/collision or in volcanic edifices – they were highly affected by tropical weathering, producing high discharge of clays and silt into the surrounding seas. In addition, explosive volcanic activity of island arcs produced suspended clays in surface waters, as well as abundant dissolved nutrients, creating unfavorable conditions for the growth of LBF. Hence, both the rapid appearance and disappearance of chlorozoan carbonates built largely by LBF on uplifted accretionary prisms, island arcs and intra-plate volcanic edifices, provide valuable markers of the geodynamic, tectonic and paleo-environmental evolution of the active margins and the Caribbean Plate as a whole.

Here, we synthesize in chronologic order the biotic - sedimentary record observed (O1-6)) in short-lived carbonate banks and relate it primarily to endogenic processes (P1-6):

(O1): Oldest sediments on oceanic basements are pelagic, hemipelagic or turbiditic. Their depth of formation was clearly below storm wave base and the photic zone. (P1): Basaltic basements form normally at subphotic depths and subside rapidly after formation.

(O2): Deep water sediments are sometimes overlain by shelfal, arc-derived, sandy to pebbly tempestites and mudstones formed above storm wave base. (P2): Tectonic uplift occurs due to accretion and/or underplating, or collision.

(O3): Coarsening upwards tempestites, progressive unconformities and/or (bio-) erosion of lithified and tilted sediments in the inter-tidal zone. (P3): Further tectonic uplift and land-ward tilting as a consequence of collision or incorporation of accreted material into the upper plate, fore-arc area.

(O4): Pure chlorozoan limestones encroach with an angular unconformity on deep-water and shelfal deposits. Arc-derived material is rare or absent. (P4): Accumulation due to relative sea level rise, owing to tectonic subsidence after an accretion event and/or due to eustatic sea-level rise. Scarcity of volcano-detrital input implies stalling of the nearby arc activity due to collision, underplating or back-stepping of the arc.

(O5): Carbonate facies show increasing water energy up-section, i.e. evolution from restricted to open marine paleo-environments. Topmost carbonate levels show interbedded ash layers. (P5): Continued subsidence produces accommodation space for carbonates. Renewed explosive arc activity starts to interfere with carbonate production.

(O6): A sharp change to volcano-detrital offshore or deep water turbiditic sediments marks the abrupt end of carbonate production (“drowning”). (P6): Increasing volcano-detrital input causes low water transparency and eutrophication of surface waters, stopping the carbonate factory.

Our new model relates biotic and sedimentary responses, preserved in short-lived carbonate banks, with endogenic processes, such as tectonic uplift and subsidence and fluctuation of nearby arc-volcanic activity, all related to the state of the subduction factory. Paleo-climatic and eustatic sea-level variations come second in their influence on the development of punctuated chlorozoan carbonates.

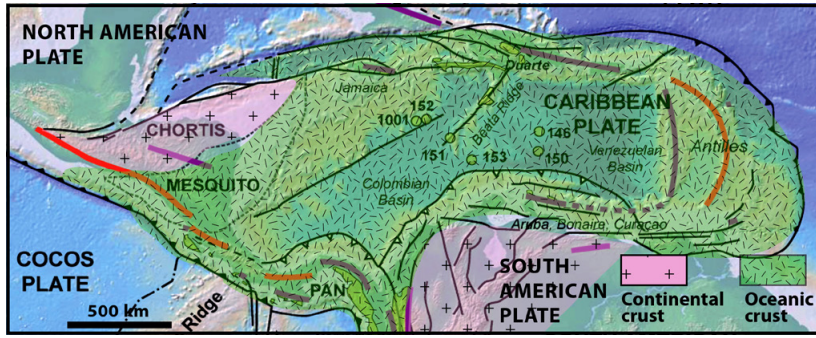


Figure 1. Tectonic map of the Caribbean Plate with types of basement

5.4

Changes in the global burial rate of carbon in marine sediments and atmospheric CO₂ variations over the last glacial cycle

Olivier Cartapanis¹, Eric D. Galbraith², Daniele Bianchi³, and Samuel L. Jaccard¹

¹ *Institute of Geological Sciences and Oeschger Centre for Climate Change Research, University of Bern.*
(oliviercartapanis@yahoo.fr)

² *ICREA, Barcelona, Spain; Institut de Ciència i Tecnologia Ambientals (ICTA) and Department of Mathematics, Universitat Autònoma de Barcelona.*

³ *Department of Atmospheric and Oceanic Sciences, University of California Los Angeles*

Carbon released from the solid Earth is removed from the active carbon pool as organic and inorganic carbon in marine sediments, and exerts a strong control on the climate over timescales of 100-1000ka, via its impact on atmospheric CO₂. However, global variations of carbon burial in oceanic sediment over glacial cycles remain poorly constrained.

Here we use a global sedimentary proxy database to quantify variation in organic and inorganic carbon burial in the deep ocean over the last 150ka.

We show that organic carbon burial increased by 50% during peak glacial conditions as compared to interglacial. Meanwhile carbonate burial in deep-sea sediments was reduced by 20%, reaching the lowest point during MIS4.

We use the reconstructed time series to perform transient simulations of the carbon system for the last glacial cycle, using an ocean-atmosphere box model. We show that increased burial of organic carbon combined with reduced burial of carbonates during glacials could have contributed to lower pCO₂ by 50ppm from the late MIS5 to MIS2. When combined with reconstruction of volcanic CO₂ emissions, and realistic scenarios for burial over shelves, changes in alkalinity and carbon inventories could explain a significant portion of the variations in atmospheric pCO₂ and δ¹³C of oceanic DIC during the last glacial cycle. Our results indicate that interactions between geological forcings and climate represent an effective process in driving pCO₂ variations on glacial-interglacial timescales, and that steady state is not a good assumption on periods shorter than a full glacial cycle.

5.5

Mercury enrichment indicates volcanic triggering of the Valanginian Weissert episode

Guillaume Charbonnier¹, Chloé Morales², Stéphanie Duchamp-Alphonse³, Stéphane Westermann⁴, Thierry Adatte¹, Karl B. Föllmi¹

¹ *Institute of Earth Sciences, Géopolis, University of Lausanne, CH-1015 Lausanne, Switzerland*

² *Marine Palynology Group, Institute of Earth Sciences, University of Utrecht, Heidelberglaan 24, 3584 CS Utrecht, The Netherlands*

³ *Laboratoire GEOPS, Bâtiment 504, Université Paris Sud, UMR 8148, Orsay F91405, France*

⁴ *Cantonal agency for environmental protection, Rue des Creusets 5 CH-1950 Sion, Switzerland*

The Valanginian stage (Early Cretaceous, ~137-132 Ma) recorded an episode of pronounced palaeoenvironmental change, which is marked by a globally recorded positive $\delta^{13}\text{C}$ excursion of 1.5 to 2‰ amplitude (Erba et al., 2004; Gröcke et al., 2005; Charbonnier et al., 2013), also known as the “Weissert event or episode” (Weissert, 1989; Erba et al., 2004; Föllmi, 2012). Its onset near the early/late Valanginian boundary (B. campylotoxus-S. verrucosum ammonite Zones) coincides with a phase of warmer climate conditions associated with enhanced humidity (Charbonnier et al., 2016), major changes in the evolution of marine plankton, and the drowning of tropical and subtropical marine shallow-water carbonate ecosystems (Föllmi et al., 1994, 2006). The globally recorded excursion indicates important transformations in the carbon cycle, which have tentatively been associated with Paraná-Etendeka large igneous province (LIP) volcanic activity. Uncertainties in existing age models preclude, however, its positive identification as a trigger of Valanginian environmental change.

Since very recently, mercury (Hg) chemostratigraphy offers the possibility to evaluate the role of LIP activity during major palaeoenvironmental perturbations (Sanei et al., 2012). In this study we investigate the distribution of Hg contents in four Valanginian reference sections located in pelagic and hemipelagic environments in the Central Tethyan Realm (Lombardian Basin, Breggia section), the northern Tethyan margin (Vocontian Basin, Orpierre and Angles sections), and the narrow seaway connecting the Tethyan and Boreal Oceans (Polish Basin, Wawal core).

All records show an enrichment in Hg concentrations at or near the onset of the Weissert Episode, with maximal values of 70.5 ppb at Angles, 59.5 ppb at Orpierre, 69.9 ppb at Wawal, and 17.0 ppb at Breggia. The persistence of the Hg anomaly in Hg/TOC and Hg/phyllsilicate ratios shows that organic-matter scavenging and/or adsorption onto clay minerals only played a limited role. We propose that volcanic outgassing was the primary source of the Hg enrichment and conclude that an important magmatic pulse triggered the Valanginian environmental perturbations.

REFERENCES

- Charbonnier, G., Boulila, S., Gardin, S., Duchamp-Alphonse, S., Adatte, T., Spangenberg, J.E., Föllmi, K.B., Colin, C., & Galbrun, B. 2013: Astronomical calibration of the Valanginian “Weissert” episode: the Orpierre marl-limestone succession (Vocontian Basin, southeastern France). *Cretaceous Research*. 45, 25–42.
- Charbonnier, G., Duchamp-Alphonse, S., Adatte, T., Föllmi, K.B., Spangenberg, J.E., Gardin, S., Galbrun, B., & Colin, C. 2016: Eccentricity paced monsoon-like system along the northwestern Tethyan margin during the Valanginian (Early Cretaceous): new insights from detrital and nutrient fluxes into the Vocontian Basin (SE France). *Palaeogeography, Palaeoclimatology, Palaeoecology*. 443, 145–155.
- Erba, E., Bartolini, A.C., & Larson, R.L. 2004: Valanginian Weissert oceanic anoxic event. *Geology*. 32, 149–152.
- Föllmi, K.B. 2012: Early Cretaceous life, climate and anoxia. *Cretaceous Research*. 35, 230-257.
- Föllmi, K.B., Weissert, H., Bisping, M., & Funk, H. 1994: Phosphogenesis, carbon-isotope stratigraphy, and carbonate-platform evolution along the Lower Cretaceous northern Tethyan margin. *Geological Society of American Bulletin*. 106, 729–746.
- Föllmi, K.B., Godet, A., Bodin, S., & Linder, P. 2006: Interactions between environmental change and shallow water carbonate buildup along the northern Tethyan margin and their impact on the early Cretaceous carbon isotope record. *Paleoceanography*. 21, 1–16.
- Gröcke, D.R., Price, G.D., Robinson, S.A., Baraboshkin, E.Y., Mutterlose, J., & Ruffell, A.H. 2005: The upper Valanginian (Early Cretaceous) positive carbon-isotope event recorded in terrestrial plants. *Earth and Planetary Science Letters*. 240, 495-509.
- Sanei, H., Grasby, S.E., & Beauchamp, B. 2012: Latest Permian mercury anomalies. *Geology*. 40, 63–66.
- Weissert, W. 1989: C-isotope stratigraphy, a monitor of palaeoenvironmental change: a case study from the early Cretaceous. *Surveys in Geophysics*. 10, 1–61.

5.6

Grain size evolution in fluvial deposits during global warming at the Paleocene-Eocene boundary, Tremp formation, Spain

Chen Chen*, Sébastien Castellort*, Laure Guerit**,*, Chris Paola***, Brady Foreman****

¹ *Department of Earth Sciences, University of Geneva, Rue des Maraichers 13, CH-1206 Geneva, Switzerland (chen.chen@unige.ch)*

² *Geoscience Environment Toulouse, Paul Sabatier University, 14 Avenue Edouard Belin, 31000 Toulouse, France*

³ *Department of Geology and Geophysics, and St. Anthony Falls Laboratory, University of Minnesota, Minneapolis, Minnesota 55414, USA*

⁴ *Department of Geology & Geophysics, Western Washington University, Bellingham, WA, USA*

Sedimentary records across the PETM have been found in the southern Spanish Pyrenees. Based on outcrops and borehole information (Pujalte, Schmitz et al. 2014) from the Tremp-Graus Basin, it is shown that a sea-level fall of at least 20 m occurred less than 75 kyr prior to the PETM. In the central part of the Tremp-Graus basin, the Paleocene to early Eocene record can be documented at the Esplugafreda section. A paleo-incised valley carved into the Esplugafreda formation and is interpreted as a sequence boundary produced in response to the pre-PETM sea level fall. The valley was then filled by channel-like conglomeratic sandbodies at the bottom and finer reddish floodplain deposit in the rest of the section. The incised valley is capped by the Claret Conglomerate — an extensive sheet-like unit which ranges in thickness between 1m and 4m and is generally interpreted as the river response to a dramatic climate change at the PETM because of its occurrence at or close to the PETM signal recorded in the stable isotope composition of paleosoil nodules (Pujalte, Schmitz et al. 2014). The conglomerate unit ends abruptly and is overlaid by fine-grained yellowish soil which is mainly made up of silty mudstones with abundant small size carbonate nodules suggesting another shift in the hydrological cycle after the PETM. Sea level kept rising after the PETM and all of the section was inundated by the ocean leading eventually to deposition of Ilerdian marine limestone on the top of the section.

Several studies (Schmitz and Pujalte 2003, Schmitz and Pujalte 2007, Pujalte, Schmitz et al. 2014) suggested that grain size increased significantly across the PETM based essentially on the observation of the coarse-grained Claret Conglomerate. We tested this assumption by performing a systematic quantification of grain size within conglomerates in the formations below and at the Claret conglomerate.

Our results show that there is no significant grain size variation across the PETM in the studied section. Given our data on channel depth and width, this implies that the intensity of river discharge during effective flood events was not significantly altered. We will discuss the possible other forcing factors that may be responsible for the observed changes in stratigraphy.

REFERENCES

- Pujalte, V., B. Schmitz and J. I. Baceta (2014). „Sea-level changes across the Paleocene–Eocene interval in the Spanish Pyrenees, and their possible relationship with North Atlantic magmatism.“ *Palaeogeography, Palaeoclimatology, Palaeoecology* 393: 45-60.
- Schmitz, B. and V. Pujalte (2003). „Sea-level, humidity, and land-erosion records across the initial Eocene thermal maximum from a continental-marine transect in northern Spain.“ *Geology* 31(8): 689.
- Schmitz, B. and V. Pujalte (2007). „Abrupt increase in seasonal extreme precipitation at the Paleocene-Eocene boundary.“ *Geology* 35(3): 215-218.

5.7

The Cañadón Asfalto Formation, Argentina: sedimentology and paleoenvironments

Fantasia Alicia ¹, Föllmi Karl B. ¹, Adatte Thierry ¹, Scasso Roberto A. ², Spangenberg Jorge E. ³, Schoene Blair⁴, Barker Ryan T. ⁴

¹ *Institute of Earth Sciences, University of Lausanne, 1015 Lausanne, Switzerland (alicia.fantasia@unil.ch)*

² *IGEBA-Departamento de Ciencias Geológicas, Universidad de Buenos Aires, Argentina*

³ *Institute of Earth Surface Dynamics, University of Lausanne, 1015 Lausanne, Switzerland*

⁴ *Department of Geosciences, Princeton NJ 08544, United States*

The Cañadón Asfalto Formation represents terrestrial environments (fluvial to lacustrine) and is known for its fossil preservation and for the presence of organic-rich sediments (e.g., Cabaleri et al., 2013; Oliveira et al., 2015; Figari et al., 2016). The successions are composed of thick series of sediments interbedded with basaltic flows accumulated in the Cañadón Asfalto Basin, which is situated in central Patagonia (Chubut Province). We sampled three sections located at different stratigraphic levels within the sedimentary succession intercalated in the basaltic flows: the Quebrada Barreño section, the Alice Creek section, and the Quebrada Subsidiaria section. These sections are characterized by silicified carbonate, organic-rich sediments, mudstone, sandstone, conglomerates and tuffaceous material. A high-resolution multidisciplinary approach has been chosen including sedimentological observations, mineralogy, phosphorus, carbon isotopes and organic-matter content. Moreover, we provide absolute U-Pb zircon ages of a selection of volcanogenic deposits, which place the Cañadón Asfalto Formation in the late Toarcian (179.4 ±0.2 Ma; 180.3±0.1; 180.1±0.1), which is in agreement with previous studies (Cúneo et al., 2013). Total organic carbon (TOC) content shows values up to 7 wt.% and the HI-OI crossplots show typical values for terrestrial and lacustrine organic matter. A strong correlation between preservation, organic matter type and carbon-isotope record is observed. The isotopic composition of carbonates ($\delta^{13}\text{C}$ and $\delta^{18}\text{O}$) indicates variable origins: typical freshwater values are recognized but other values are more difficult to interpret (e.g., pedogenic carbonate, hydrothermalism). The clay assemblages is dominated by smectites, resulting from basalt alteration under warm climate with dry and humid seasons (seasonal precipitations). These sediments may provide information on lacustrine organic-carbon preservation and its isotopic signature, the formation of lacustrine carbonates and the general climate in the region during this time. Since the continental record of the Toarcian is less well established, this study will provide important clues to better understand the development of organic-rich lacustrine successions in a volcanic context.

REFERENCES

- Cabaleri, N. G., Benavente, C.A., Monferran, M.D., Narvaez, P.L., Volkheimer, W., Gallego, O.F., and Do Campo, M.D. 2013: Sedimentology and palaeontology of the Upper Jurassic Puesto Almada Member (Cañadón Asfalto Formation, Fossati sub-basin), Patagonia Argentina: Palaeoenvironmental and climatic significance. *Sedimentary Geology* 296: 103-121.
- Cúneo, R., Ramezani, J., Scasso, R., Pol, D., Escapa, I., Zavattieri, A.M., and Bowring, S.A. 2013: High-precision U–Pb geochronology and a new chronostratigraphy for the Cañadón Asfalto Basin, Chubut, central Patagonia: Implications for terrestrial faunal and floral evolution in Jurassic. *Gondwana Research* 24: 1267-1275.
- Figari, E. G., Scasso, R.A., Cuneo, R.N., and Escapa, I. 2015: Estratigrafía y evolución geológica de la Cuenca de Cañadón Asfalto, Provincia del Chubut, Argentina. *Latin American Journal of Sedimentology and Basin Analysis*, volume 22 (2), 135-169.
- Oliveira, D. E., Zavattieri, A.M., and Quattrocchio, M.E. 2015: Palynology of the Cañadón Asfalto Formation (Jurassic), Cerro Cóndor depocenter, Cañadón Asfalto Basin, Patagonia, Argentina. *Paleoecology and paleoclimate based on ecogroup analysis*. *Palynology* 39: 362-386.

5.8

Compositional changes related to non-steady state conditions during deposition of a Miocene sedimentary basin infill, Central Argentinian Foreland (Mendoza province)

Gabriel Hunger ¹, Andrea Moscariello ¹, Dario Ventra ¹, Gonzalo D. Veiga ²

¹ *Earth and environmental Sciences, University of Geneva, rue des Maraichers 13, 1205 Geneva, Switzerland. (gabriel.hunger@unige.ch)*

² *Centro de Investigaciones Geológicas, Universidad Nacional de La Plata - CONICET, Argentina*

Sediments deposited in foreland basins are accurate recorders of processes acting at different temporal and spatial scales during orogenic uplift. The effects of allogenic forcing on foreland sedimentation are well known at basin-scale, but uncertainties remain in deciphering and interpreting them at higher resolution, and in differentiating them from the sedimentary changes due to autogenic processes.

Here, we present observations on the continental sedimentology and stratigraphy of the Central Argentinian Foreland. The majority of the basin infill is comprised by the Mariño Fm. and La Pilona Fm., which were deposited during the Miocene and cover almost 2000 m of stratigraphy. The large scale stratigraphy trend leads to interpret the entire alluvial system as a large fluvial fan that aggraded/prograded over the proximal margin of the foreland basin. The basin infill records a continuous sediment supply from the rising Principal Cordillera and the first stages of the uplift of the Frontal Cordillera. The interaction of different allogenic forcing factors, but also autogenic processes, is recorded in the compositional changes of the sedimentary infill.

This project aims to provide a detailed reconstruction of paleoenvironmental dynamics and unravel the relative roles of climate and tectonics, using a high-resolution, integrated compositional and sedimentological analysis of the Mariño Formation and the basal part of the La Pilona Formation. The main objectives are: (1) detect geochemical signatures of allogenic controls; (2) track changes in sediment provenance in relation to magmatism and exhumation of the uplifting Andes; and (3) recognize the effects of different allogenic drives on sedimentary processes and local environmental changes. The followed approach embodies a high-resolution geochemical and petrographical study, using automated QEMSCAN[®] technology, geochemistry, heavy-minerals and radiogenic isotope analysis. The use of statistical methods is also used to explain the element associations and mineralogical control on chemical composition.

Along 1500 m in stratigraphy, we identified different depositional environments, from floodplains and fluvial channels to an aeolian erg system that can be correlated throughout the foothills of the Andes.

The evolution of the basin infill (Fig.1) can be linked to recognizable compositional variations due to, at least, 3 phases of non-steady state weathering conditions. The A-CN-K ternary diagram displays low to moderate weathering values (CIA = 45-65) and shows the evolution of the composition towards the illite pole, in agreement with the QEMSCAN[®] results. Intermediate source rock composition is inferred using major and trace elements. Comparison between compositional changes in the sandstones and the associated mudstones indicate poor mineral and geochemical fractionation except in the upper part of the Mariño Fm. and in the La Pilona Fm., where Al_2O_3/TiO_2 and TiO_2/Zr mark a difference between depositional facies. La Pilona Fm. is characterized by more scarce composition certainly due to the advance of the thrust front coupled with inputs from the uplifting Frontal Cordillera, a tectonic province feeding the basin with different igneous sources. The next step will be the integration of heavy mineral and isotopic data to constrain the source area changes and to have a better understanding of the evolution of the uplifting Andes.

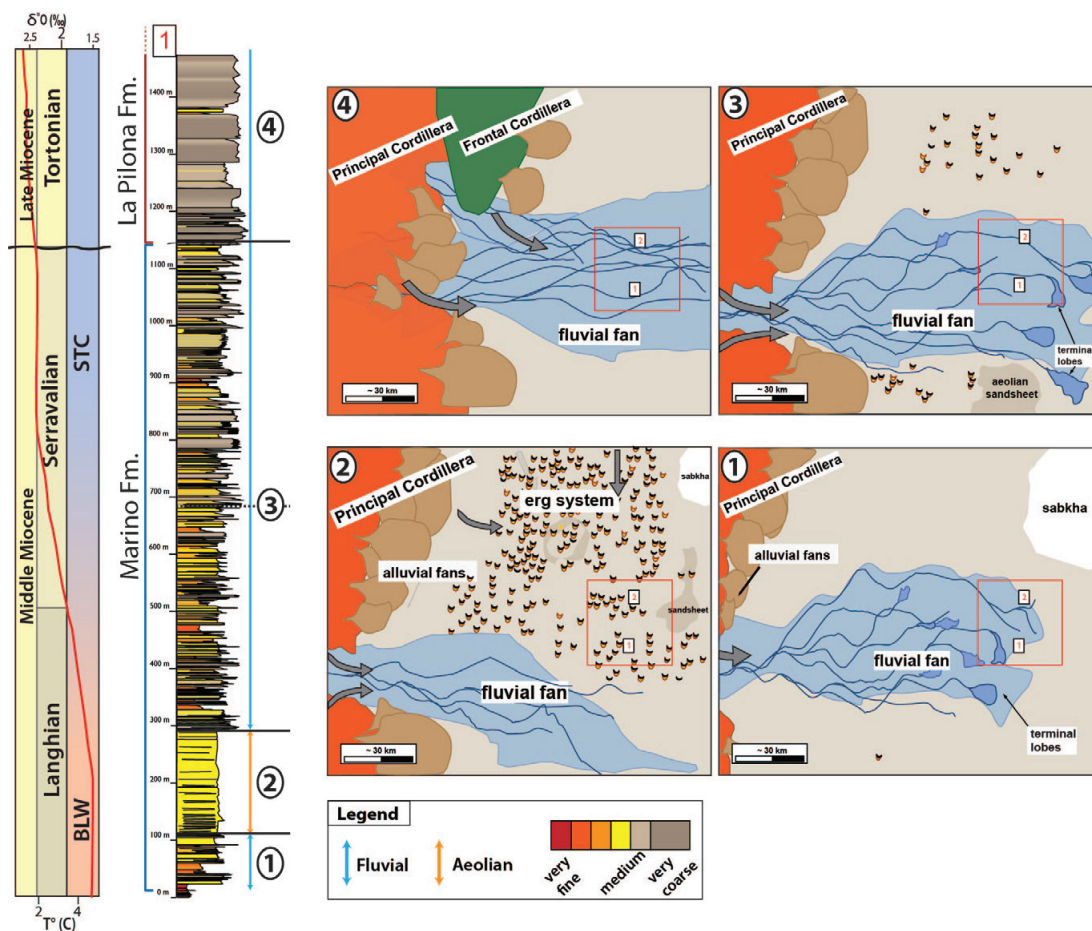


Figure 1. Long-term global climatic trend during part of the Miocene(after *Zachos et al. 2008*). 1500 m stratigraphic log showing the evolution of the depositional environment.

REFERENCE

Zachos, J. C., Dickens, G. R., & Zeebe, R. E. 2008. An early Cenozoic perspective on greenhouse warming and carbon-cycle dynamics. *Nature*, 451(January), 279–283.

5.9

Elevated coralg bioherms from Long Island (Bahamas): a testimony of recent tectonic uplift or of a high sea level during Marine Isotope Stage 7

Pascal Kindler¹, Sidonie Revillon², Lucas Vimperc¹ & Fabienne Godefroid¹

¹ Department of Earth Sciences, University of Geneva, rue des Maraichers 13, CH-1205 Geneva (pascal.kindler@unige.ch)

² Sedisor, Laboratoire Domaine Océaniques, Place Nicolas Copernic, 29280 Plouzane, France

Coralgal bioherms dating from the penultimate interglacial period (Marine Isotope Stage 7) have been found on Long Island (Bahamas). These features mark a relative sea-level datum that either corresponds to a yet unrecorded eustatic highstand during this time period, or provides evidence of unsuspected tectonic uplift in this portion of Great Bahama Bank (GBB).

Located along the subsiding SE margin of GBB, Long Island mostly consists of eolianites of Pleistocene and Holocene age (Hearty, 2010). Fossil marine facies (i.e. beaches and reefs) are scarce on Long Island (Curran et al., 2004).

Little Harbour is a protected, km-size cove along the SE coast of the island. Its central portion forms a low (+2m) terrace consisting of similarly oriented, m-sized, hard coralg bioherms, comprising a core of coral framestone (*Porites porites*, *Acropora cervicornis*, *Agaricia agaricites*, *Isophyllia* sp.) overlain by one thick bindstone cap (Figure 1) comprising red algae, vermetid gastropods, encrusting foraminifers (*Homotrema*, *Nubecularia*), and microbialite laminae. Interstitial cavities are occupied by oolitic grainstone that locally forms dm-thick beds set against the bioherms. Ooids are still aragonitic, and occasionally trapped in the tests of the encrusting foraminifers. The intervals between the bioherms are filled with pedogenically altered bioclastic eolianites.

The coral core of the bioherms gave a radiometric age of 212 ± 2 ka (U-series dating). $^{87}\text{Sr}/^{86}\text{Sr}$ ratios from the bindstone cap range between 0.709121 and 0.709168, suggesting an Early to Middle Pleistocene age. Alloisoleucine/Isoleucine ratios obtained from the oolite and the bioclastic eolianites are of 0.56 and 0.40, respectively, indicating a Middle Pleistocene age for the former, and a Late Pleistocene age for the latter.

Based on their geometry, the coralg bioherms and intervening intervals can be interpreted as shallow spurs and grooves at the frontal part of a reef. The $^{87}\text{Sr}/^{86}\text{Sr}$ ratios measured from the bindstone are not coherent with the physical stratigraphy, but both the U-Th date obtained from the coral core and the A/I ratios from the coeval oolite indicate a correlation with MIS 7, possibly MIS 7c. The fossil reef from Little Harbour provides a relative sea-level datum that is at odds with both the known sea-level history and the tectonic regime in this area.

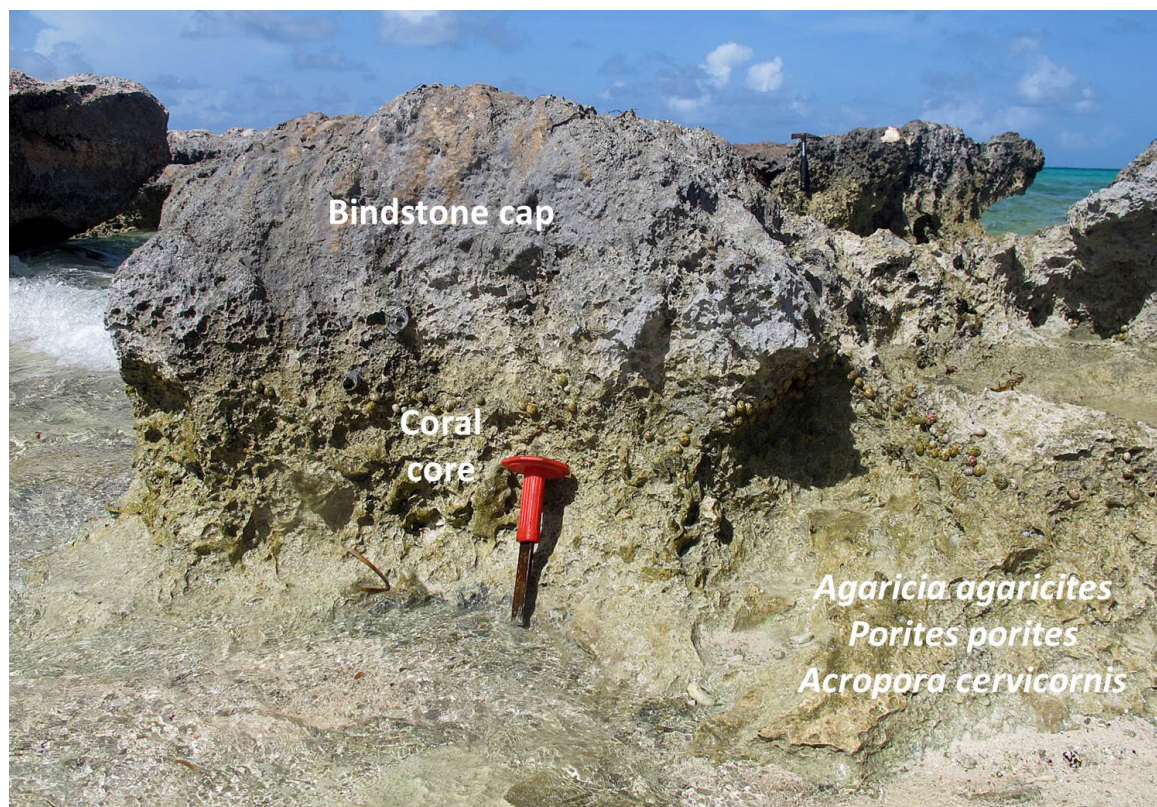


Figure 1. Internal structure of the Little Harbour bioherm revealed by recent marine erosion. Chisel is 20 cm long.

REFERENCES

- Curran, H.A., Mylroie, J.E., Gamble, D.W., Wilson, M.A., Davis, R.L., Sealey, N.E., Voegeli, V.J. (2004) Geology of Long Island, Bahamas: a field trip guide. Fieldtrip guidebook, 12th Symposium on the Geology of the Bahamas and other carbonate regions, Gerace Research Centre, San Salvador, Bahamas, 24 pp.
- Hearty, P.J. (2010) Chronostratigraphy and morphological changes in Cerion land snail shells over the past 130 ka on Long Island, Bahamas. *Quaternary Geochronology* 5: 50-64.

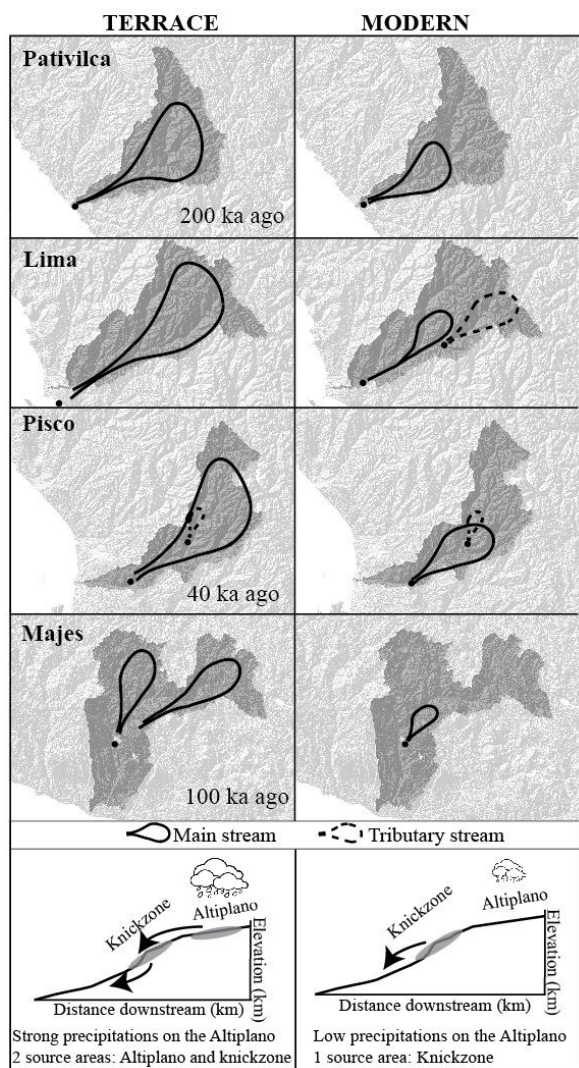
5.10

Climatic control on sediment provenance inferred from detrital zircon ages, Western Peruvian Andes

Camille Litty¹, Pierre Lanari¹, Marco Burn¹ & Fritz Schlunegger¹

¹ Institute of Geological Sciences, University of Bern, Baltzerstrasse 1+3, Bern

U-Pb ages measured on detrital zircon have become a frequently used method for the determination of provenance and for inferring sedimentary dynamics within erosional basins (e.g. Beranek et al., 2006; He et al., 2014). Because of their remarkable durability, zircon crystals may be reworked during multiple erosional and depositional cycles, thus providing a valuable indicator of sedimentary provenance of stream sediments.



Climatic changes are known to have major impacts on landscapes evolution and erosion rates. For example in the Andes, variations in precipitation rates and patterns during the Quaternary led to remarkable lake-level variations on the Altiplano and pulses of erosion on the western Andean margin. They have also resulted in the formation of cut-and-fill terrace systems, particularly in lower valley reaches along the western margin of the Peruvian Andes (Steffen et al., 2009; 2010). Provenance analysis of these terrace deposits, together with modern sediments from the same streams, from four catchments draining the Western margin of the Andes in Peru is used to infer changes in erosion between the past and the present period by matching *in situ* detrital U-Pb zircon ages obtained with LA-ICP-MS with crystallization ages of source rocks. Age populations suggest major changes in sediment provenance through the past 100 Ka: At present, sediment sources are mainly located along the steep middle reaches of the rivers whereas, during the Pleistocene, sources were additionally located in the low-relief headwaters of these catchments (Fig. 1).

These shifts in the loci of erosion are interpreted to reflect orbitally-driven changes in precipitation patterns, where periods of stronger precipitation on the Altiplano allowed the entrainment of material from the low-relief plateau in the past. In contrast, modern precipitation patterns result in negligible erosion rates on the Altiplano, and the site of material entrainment shifts to the knickzone reach where steeper slopes and higher stream power promote erosion. This study demonstrates that climate-controlled shifts in sediment provenance may be successfully inferred from *in situ* detrital zircon ages according that the age of the deposit are known.

Figure 1: Provenance of the sediment today and during the accumulation of the terrace material

REFERENCES

- Beranek, L. P., Link, P. K. & Fanning, C. M., 2006. Miocene to Holocene landscape evolution of the western Snake River Plain region, Idaho: Using the SHRIMP detrital zircon provenance record to track eastward migration of the Yellowstone hotspot. *Geological Society of America Bulletin*, v. 118(9-10), p. 1027-1050.
- He, M., Zheng, H., Bookhagen, B. & Clift, P. D., 2014. Controls on erosion intensity in the Yangtze River basin tracked by U-Pb detrital zircon dating. *Earth-Science Reviews*, v. 136, p. 121-140.
- Steffen, D., Schlunegger, F. & Preusser, F., 2009. Drainage basin response to climate change in the Pisco valley, Peru. *Geology*, v. 37, p. 491-494.
- Steffen, D., Schlunegger, F., & Preusser, F., 2010. Late Pleistocene fans and terraces in the Majes valley, southern Peru, and their relation to climatic variations. *International Journal of Earth Sciences*, v. 99(8), p. 1975-1989.

5.11

Buffering and mixing of sediment flux across the north piedmont of the Tian Shan

Luca C Malatesta^{1†}, Jean-Philippe Avouac¹, Nathan Brown², Quentin Berger³, Sebastian Breitenbach⁴, Jiawei Pan⁵, Marie-Luce Chevalier⁵, Edward Rhodes^{2,6}, Dimitri Saint-Carlier⁷, Wenjing Zhang⁵, Blanche Poisson⁸

¹ *Division of Geological and Planetary Sciences, California Institute of Technology, Pasadena, CA 91125, USA*

† *luca@caltech.edu*

² *Department of Earth, Planetary, and Space Sciences, University of California, Los Angeles, 595 Charles Young Drive East, Box 951567, Los Angeles, CA 90095-1567, USA*

³ *Laboratoire de Probabilités et Modèles Aléatoires, Université Paris 6, 4, Place Jussieu, 75005 Paris, France*

⁴ *Institut für Geologie, Mineralogie und Geophysik, Ruhr-Universität Bochum, Universitätsstrasse 150, 44801 Bochum, Deutschland*

⁵ *State Key Laboratory of Continental Tectonics and Dynamics, Institute of Geology, CAGS, 26 Baiwanzhuang St, Beijing 100037, China*

⁶ *Department of Geography, The University of Sheffield, Sheffield S10 2TN, United Kingdom*

⁷ *Université de Lorraine, Centre de Recherches Pétrographiques et Géochimiques, UMR 7358 CNRS-UL, 15 rue Notre Dame des Pauvres, B.P. 20, 54501 Vandœuvre lès Nancy, France*

⁸ *Hazard Mechanisms and Simulation Unit, Bureau de Recherches Géologiques et Minières, Orleans, France.*

The accurate interpretation of clastic sedimentary records hinges on a good understanding of the timescale and mode of sediment transport from source to sink. A forcing signal can be accurately recorded in the stratigraphy if it is transported quickly without being mixed with older sediments, or it can be entirely shredded by a slow transport and significant mixing along the way. We tackle this question in the north piedmont of the Eastern Tian Shan, a depositional fold-and-thrust belt, with 23 new luminescence ages of terrace abandonment and alluvial aggradation. We show that the piedmont incises and aggrades in reaction to changes in insolation at a 21 kyr period, through growth and melt of glaciers restricted to the high range and changing levels of moisture delivered by the Westerlies, without the necessity for monsoonal incursions deep in Central Asia. The partly glaciated valleys of the Tian Shan can amplify the effect of relatively weak changes in temperature and moisture, resulting in incision as fast as 5 cm/yr in canyons as deep as 330 m. We show that a significant fraction of sediments evacuated from the high range is temporarily deposited in the piedmont before a later incision phase can deliver it to the basin. We quantitatively constrain the effect of crossing the alluvial piedmont on the sediment flux: 1) the delivery of coarse sediments to the basin is delayed by at least 7 to 14 kyrs between being first evacuated from the mountain and later re-eroded and transported basinward; 2) the outflux of coarse sediments from the piedmont contains a significant amount of recycled material that was deposited on the piedmont as early as the Middle Pleistocene, smearing and buffering climatic signals. The delayed gravel front is separated by a hiatus from the initially contemporary fine-grained load where they overlap in the proximal basin. We finally devise both a numerical and an analytical model that capture the elemental components of the sediment transfer function. The function predicts the probability of sediment mixing in the outflux of alluvial zones undergoing cycles of aggradation and incision and informs better sampling strategies.

5.12

Meteorites and micrometeorites from sediments – identification and characterization using noble gases

Matthias M. M. Meier¹

¹ Institute of Geochemistry and Petrology, ETH Zurich, Clausiusstrasse 25, CH-8092 Zurich

The processes of erosion and sedimentation combined result in a continued renewal of the Earth's surface. This makes it possible for geologists to reconstruct the Earth's history and evolution – but it also enables us to trace, date and sometimes even recover, and characterize, extraterrestrial material falling to Earth in past eras (Merrihue, 1965). Without sediments, what we could learn from extraterrestrial material (predominantly meteorites, micrometeorites and Interplanetary Dust Particles = IDPs) would essentially be restricted to two time-windows: 1) a dynamical snap-shot of the solar system during the last few 10 Ma at most, i.e., the time during which these objects were released from their parent asteroids (or planets) and delivered to the Earth's surface, and 2) the first few Ma of the solar system, i.e., the processes important during the formation of these objects about 4.57 Ga ago. Terrestrial sediments can open a third, much larger time-window of investigation, spanning essentially the ~4.5 Ga between the other two. In some cases, it has been possible to find not only indirect traces of extraterrestrial material (e.g., peaks of ^3He , $^{187/188}\text{Os}$, and Ir abundance), but actual relict (surviving) extraterrestrial material, which can then be further characterized (in particular, chromite; Schmitz et al., 2001; Meier et al., 2014). In this presentation, I will first review what we have already learned from this “third window”, focusing on two events: the “L chondrite parent body” asteroid break-up event 470 Ma ago, tied to the discovery of >100 fossil meteorites in a limestone quarry in Sweden (Schmitz et al., 2001; 2014), as well as the break-up of a large carbonaceous asteroid ca. 8 Ma ago which likely resulted in a collisional family of asteroids on similar orbits (the Veritas asteroid family) in the outer asteroid belt, as well as a ^3He -peak in deep sea sediments (e.g., Farley et al., 2006). For both events, the analysis of noble gases (predominantly He and Ne) in very small amounts (on the order of ~20'000 atoms), possible thanks to a unique “compressor-source” instrument at ETH Zurich (Baur, 1999) have come to play an important role.

For the Ordovician event, He and Ne have allowed the determination of cosmic-ray exposure ages (CRE ages; the time these meteorites spent as meter-sized objects in space while exposed to highly energetic cosmic rays) in relict chromite grains from fossil meteorites (Heck et al., 2004; Schmitz et al., 2014) and micrometeorites (Meier et al., 2014). Chromite is the only mineral abundant in meteorites which can largely escape terrestrial alteration for 470 Ma. Its elemental (and later also O-isotopic) composition has allowed to determine that the fossil meteorites are all L-type ordinary chondrites (Schmitz et al., 2001), with a single exception (Schmitz et al., 2014). The CRE ages of all meteorites and many micrometeorites are very short (<~1 Ma), requiring that the parent asteroid family was located close to a powerful and “fast” orbital resonance. Furthermore, the observation of long (>1 Ma) CRE ages in sediment-dispersed “micrometeoritic” (solar-wind rich) chromite grains requires the presence of a thick layer of regolith on the surface of the disrupted parent asteroid.

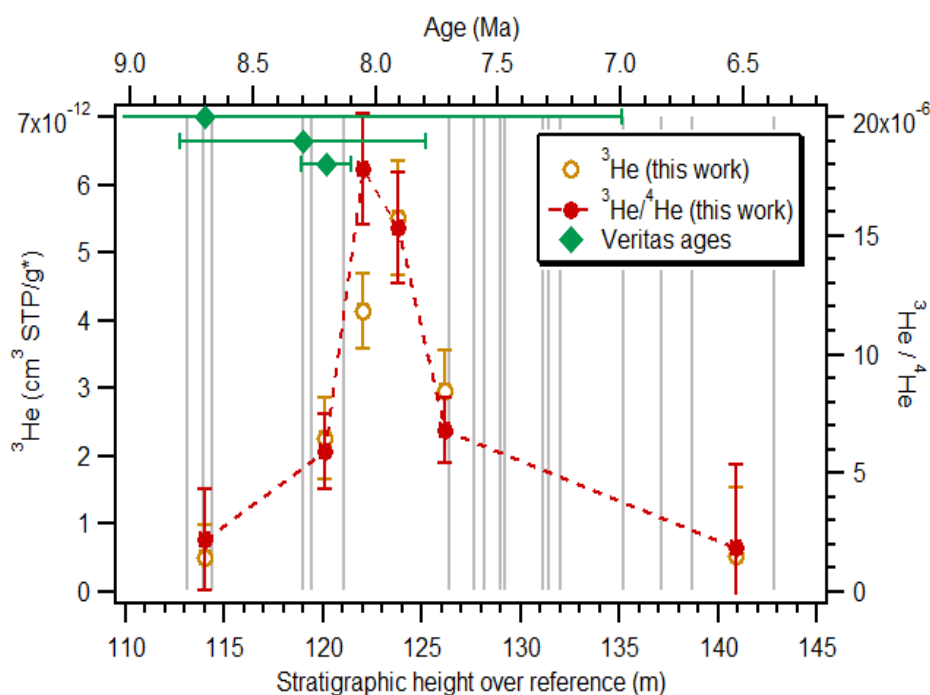


Figure 1: ^3He (and $^3\text{He}/^4\text{He}$) peak in the Tortonian section, allowing a much better constraint on the age of the Veritas break-up than dynamical approaches.

For the Tortonian event, which is thought to have been initiated by the break-up of the ca. 110-140 km-sized Veritas family parent asteroid ca. 8.1 Ma ago, so far only a ^3He peak has been identified in deep sea sediments by Farley et al. (2006; i.e., no fossil meteorites or micrometeorites yet), and most recently at the Tortonian GSSP section near Ancona (see Fig. 1; Meier et al., unpubl.). However, searches for relict extraterrestrial minerals within that section are on-going, and an update on that effort will be provided at the conference.

REFERENCES

- Baur H. 1999. A noble-gas mass spectrometer compressor source with two orders of Magnitude improvement in sensitivity. EOS Trans. AGU 46, #F1118.
- Farley K. A., Vokrouhlický D., Bottke W. F. & Nesvorný D., 2006. A late Miocene dust shower from the break-up of an asteroid in the main belt. *Nature* 439, 295-297.
- Heck, P. R., Schmitz, B., Baur, H., Halliday A. N. & Wieler R. 2004. Fast delivery of meteorites to Earth after a major asteroid collision. *Nature* 430, 323-325.
- Meier M. M. M., Schmitz B., Lindskog A., Maden C. & Wieler R. 2014. Cosmic-ray exposure ages of fossil micrometeorites from mid-Ordovician sediments at Lynna River, Russia. *Geochim. Cosmochim. Acta* 125, 338-350.
- Merrill, C. 1965. Rare Gas Evidence for Cosmic Dust in Modern Pacific Red Clay. *Ann. New York Acad. Sci.* 119, 351-367.
- Schmitz, B., Tassinari, M., & Peucker-Ehrenbrink B. 2001. A rain of ordinary chondritic meteorites in the early Ordovician. *Earth & Planet. Sci. Lett.* 194, 1-15.
- Schmitz B., Huss, G. R., Meier, M. M. M., Peucker-Ehrenbrink, B., Church, R. P., Cronholm, A., Davies, M. B., Heck, P. R., Johansen, A., Keil, K., Kristiansson, P., Ravizza, G., Tassinari, M., Terfelt, F. 2014. A fossil winonaite-like meteorite in Ordovician limestone: A piece of the impactor that broke up the L-chondrite parent body? *Earth & Planet. Sci. Lett.* 400, 145-152.

5.13

Petrography and clay mineralogy of Eocene clastic rocks from the Tremp-Graus-Ainsa basin, Southern Pyrenean Foreland (Spain) - Reconstruction of sediment provenance and burial diagenesis

Marc Perret¹, Branimir Segvic¹, Cai Puigdefabregas², Andrea Moscariello¹, Julian Clark³, Andrea Fildani³, Mason Dykstra³, Sébastien Castelltort¹

¹ Section of Earth and Environmental Sciences, University of Geneva, Rue des Maraîchers 13, 1205 Geneva, Switzerland

² Institut de Ciències de la Terra (CSIC), Carrer Lluis Solé Sabaris, 08028 Barcelona, Spain

³ Statoil, 6300 Bridge Point Parkway, Austin, TX, USA

Provenance studies improve our understanding of terrigenous material delivery and deposition into sedimentary basins. This information addresses problems of sediment distribution patterns and mountain range morphological evolution. Thanks to excellent outcrop continuity and stratigraphic constraints, the South Pyrenean foreland basin provides an ideal natural laboratory to study sediment pathways and provenance in a tectonically active basin during a period of important climate variations (e.g. early and middle Eocene climatic optima, Eocene-Oligocene transition).

Previous provenance studies have focused on sandstone petrography of the fluvial-alluvial deposits of the Tremp-Graus sub-basin and, separately, on the deep-marine turbiditic environment of the Ainsa sub-basin, without considering the continuum of their source-to-sink relationships.

Herein we present results from a range of analytical techniques on clastic and basement rocks from the whole source-to-sink system of the Tremp-Graus-Ainsa basin (Southern Pyrenees, Spain): optical mineralogy (OM), automated and classical electron microscopy (QEMSCAN® and SEM-EDS), and X-ray diffraction (XRD) on clay fraction. These tools allow us to study the sediment mineralogy and sediment provenance in order to understand the paleogeographic evolution of the Tremp-Graus-Ainsa basin during Eocene time. In addition, our results on clay mineral dynamics and albitization of K-feldspars shed new light on the thermal and geodynamic evolution of the basin and its diagenetic history.

Overall, we show that most of analysed clastic rocks are hybrid arenites consisting of high contents of quartz (up to 51%), feldspar (5-18%) and carbonate (11-86%), whereas mica (up to 7%) and clay minerals (up to 8%) are reported as minor phases. Clay parageneses in the different basins are similar in terms of smectite, mixed-layer illite-smectite (I-S), kaolinite, chlorite, and illite. Still, we observe that the total smectite content diminishes westwards, i.e. downstream the sediment routing system, with a lack of discrete smectite in the Ainsa basin, while I-S is progressively transformed into high-charged illite compositions.

Heavy-mineral (HM) content of analysed clastic rocks is dominated by pyrite, rutile, titanite, and apatite. Based on the composition of the adjacent crystalline basement (granites and gneisses) and pre-Mesozoic sedimentary or low-grade metamorphic rocks (sandstones, schists, and phyllites) no single source region or lithology, which might have served as a material feedstock, can be identified. However, the HM ratios (zircon-tourmaline-rutile vs. apatite vs. other heavy minerals) vary downstream deposition. The ratio of unstable heavy minerals (apatite and other heavy minerals) decreases whereas the proportion of stable heavy minerals remains equivalent or increases along the system indicating fractionation due to weathering and diagenesis.

The I-S proportions within the clay fraction of analysed sediments suggest that smectite was the starting material at deposition time, formed by weathering of feldspars and mica in the parent material. Once buried, the illitization of smectite is depth dependent, suggesting that the Tremp-Graus sediments were buried under 3-3.2 km of sediment, assuming a standard geothermal gradient of 25°C/km (foreland basin). Conversely, illitization of smectite in the Ainsa basin reveals that burial there exceeded 4 km of depth. Such a finding is consistent with the westwards deepening of the whole foreland depositional system in the Pyrenees. This result is corroborated by the observed prograde albitization of detrital K-feldspars, which is found to be total (100%) in the Ainsa basin, indicating burial temperatures higher than 100°C. By contrast, in the Tremp-Graus basin, albitization remained incomplete and simply shows a depth dependence relation. This comprehensive petrographic and diagenetic study allowed an in-depth comprehension of the properties and development of the potential sandstone reservoir rocks. Still, in order to better understand the complex provenance and interactions between sediment sources, more effort will be placed on the comparative geochemical – whole rock and phase chemistry – inquiry of basin sediments and of their surrounding basement rocks.

5.14

Depositional mechanisms and environmental conditions leading to the formation of phosphorite in the El Cien Formation (Oligocene-Miocene; Baja California-Mexico)

Iris Schöllhorn¹, Brian Gertsch², Thierry Adatte², Alexander Houben³, Jorge Spangenberg², Tobias Schwennicke⁴ and Karl B. Föllmi²

¹ *Geosciences and environment Institut, University of Lausanne, Quartier UNIL-Mouline Bâtiment Géopolis, CH-1015 Lausanne (iris.schoellhorn@unil.ch)*

² *Geosciences and environment Institut, University of Lausanne, Quartier UNIL-Mouline Bâtiment Géopolis, CH-1015 Lausanne*

³ *Centre for Earth, Environmental and Life Sciences, Netherlands Organization for Applied Scientific Research (TNO), Princetonlaan 6, 3584 CB Utrecht, Netherlands*

⁴ *Academic Department of Geology, University of Baja California Sur, Carretera al sur k.m. 5.5, Apartado Postal 19-B, C.P.: 23080, La Paz Baja California Sur, México*

Phosphogenesis and the accumulation of phosphorite is a widespread phenomenon in the Late Cenozoic and three main episodes have been discerned during the Late Oligocene-Pliocene interval. Phosphorites of the first episode (Late Oligocene-Early Miocene) occur in different regions in the southern part of Baja California, which have been previously studied for their mineralogy and sedimentology, but which are generally insufficiently dated to be correlated to records of climate and sea-level change.

In order to better constrain the sedimentary processes and environmental conditions which have led to phosphogenesis and the accumulation of phosphorites, and to obtain a better age control, two cores drilled in the phosphate mine of ROFOMEX in San Juan de la Costa (Baja California Sur, Mexico) were studied using sedimentological, mineralogical and geochemical techniques. This sedimentary succession, part of the El Cien formation, spans the Upper Oligocene and the lowermost Miocene, and is composed by muddy-siltstones with intercalated phosphorite beds, tuffs and coarse detrital wackestone.

The study of microfacies revealed that the El Cien formation was deposited on the outer shelf below the storm-wave base level. The siltstone was deposited as the result of hemipelagic sedimentation, whereas the phosphorite and wackestone were transported and brought in by turbidity currents. The turbidite deposits are generally associated with tuff layers, which suggests that their origin was often related to a phase of seismic activity linked to a phase of volcanic activity. The absence of benthic organisms, the presence of fine laminations, the enrichment in organic matter and redox-sensitive trace elements in the siltstone suggest deposition in a low-oxygen environment.

Palynofacies, Rock-Eval, carbon and nitrogen isotope records suggest the influence of fluctuations in oxygen contents, productivity and organic-matter sources. These variations were likely linked to phases of higher/lower upwelling intensity or to changes in nutrient input from the continent.

Laser-ablation ICP-MS-based age analyses on zircons from a selection of tuff layers is currently underway. The results will permit to correlate the phosphorites more precisely with global climate and environmental change during the Late Oligocene and earliest Miocene.

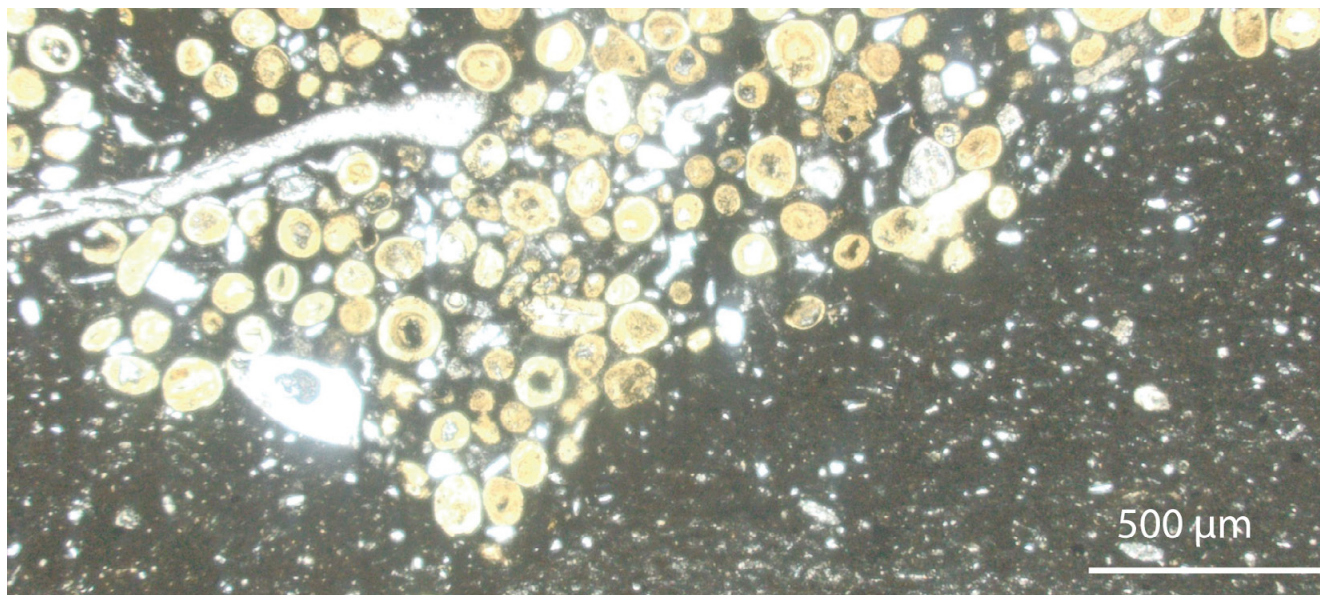


Figure 1. Turbidite composed of phosphate-coated grains deposited on top of a clay-rich siltstone.

P 5.1

Reconstructing the Evolution of the Northwestern Friuli Platform Margin Based on Microfacies

Franziska Blattmann¹, Tanja Schenker¹, Dr. Vincenzo Picotti¹, Prof. Dr. Miriam Cobianchi²

¹ *Department of Earth Sciences, Eidgenössische Technische Hochschule Zürich (ETHZ), Sonneggstrasse 5, 8092 Zürich, blattmaf@student.ethz.ch*

² *Department of Earth and Environmental Science, University of Pavia, Strada Nuova 65, Pavia*

The Friuli platform, a northwestern segment of the larger Adriatic platform, was located in the Tethys during the Mesozoic and Paleogene (Vlahović et al., 2005). Formation of the platform started after the disintegration of the wider Late Triassic Hauptdolomit (Bernoulli, 1974) and evolved throughout the Mesozoic until drowning in the Late Cretaceous (Masetti, 2012). The objective of this study is to shed light on the changing geometry of the northwestern Friuli platform margin from the Kimmeridgian to Paleogene. The main focus is on the Val Cellina section (CE), a well-known platform succession (Woodfine et al., 2008). This has been correlated with the Casso (CS) and Pieve di Alpago sections (T), two slope sections that allow planktonic biostratigraphy. To gain a better understanding of the evolving morphology of the margin, a microfacies and sedimentological analysis was performed within a previously conducted biostratigraphic frame, based on calcareous algae and foraminifera.

In the Late Jurassic to Early Cretaceous, tidal channels within a wide peritidal environment can be observed in CE, meaning that CE was within the platform interior and a rimmed margin must have been present. Important influence of fresh water is recorded throughout the Late Jurassic and Early Cretaceous. Possibly the first signs of back stepping can be seen in the platform region. Starting in the Cenomanian, a change in the stratal pattern of the CE section and stacking of mud and rudists mounds are observed. In CS, which is located in the lower slope, condensation is recorded in the Late Jurassic to Early Cretaceous. From late Albian to Cenomanian, reworked platform debris is recognized in CS and T, documenting a change in geometry of the former rimmed margin and the establishment of a distally steepened ramped margin (Burchette and Wright, 1992). The formation of mud mounds, which are generally located in the lower half of the ramped margin are a sure indication of a back stepping trend associated with important paleoceanographic variations. After the Santonian, carbonate production ceases in CE imply that the platform has finally drowned. A condensed succession is recorded in the upper slope (T section). In CS, the contrary is seen; here sedimentation rates strongly increase in the Santonian to Maastrichtian and consist predominantly of platform derived turbidites and pelagic reworked contourites. This lobe of reworked deposits in the lower slope cannot derive from the adjacent CE area, which has already drowned. Therefore, it is believed that the platform areas of the Adriatic carbonate platform some tens of kilometers east of CE was still producing up to Maastrichtian and supplied to the lower slope region of CS, with westward directed turbiditic/contour currents.

To sum up from the Late Jurassic to the Late Cretaceous, the Friuli platform recorded transition from a rimmed margin to a distally steepened ramp to final drowning, due to interplay of tectonic subsidence and paleoceanographic variations.

REFERENCES

- Bernoulli, D., Jenkyns, H.C. 1974: Alpine, Mediterranean and Central Atlantic Mesozoic facies in relation to the early evolution of the Tethys. *Spec. Publ. Soc. Econ. Paleont. Mineral.*, 19, 129-160.
- Burchette, T.P. & Wright, V.P. 1992: Carbonate ramp depositional systems. *Sedimentary Geology*, 79(1), 3-57.
- Masetti, D., Fantoni, R., Romano, R., Trevisani E. 2012: Tectonostratigraphic evolution of the Jurassic extensional basins of the eastern Southern Alps and Adriatic foreland based on an integrated study of surface and subsurface data. *AAPG Bulletin*, 96(11), 131.
- Vlahović, I., Tišljarić, J., Velić, I. & Matičec, D. 2005: Evolution of the Adriatic Carbonate Platform: Palaeogeography, main events and depositional dynamics. *Palaeogeography, Palaeoclimatology, Palaeoecology*, 220(3-4), 333-360.
- Woodfine, R.G., Jenkyns, H.C., Sarti, M., Baroncini, F. & Violante, C. 2008: The response of two Tethyan carbonate platforms to the early Toarcian (Jurassic) oceanic anoxic event: environmental change and differential subsidence. *Sedimentology*, 55(4), 1011-1028.

P 5.2

Benthic foraminiferal assemblages from small scaled Cold-water coral habitats : the Moira Mounds

Robin Fentimen¹, Aaron Lim², Akram El Kateb¹, Andrew Wheeler², Silvia Spezzaferri¹

¹ University of Fribourg, Department of Geosciences, Chemin du Musée 6, 1700 Fribourg, Switzerland
(robin.fentimen@unifr.ch)

² Department of Geology & Environmental Research Institute, University College, Cork, College Rd., Cork, Ireland

Cold-water coral ecosystems are particularly well developed along the North-east Atlantic continental margin, particularly along the Irish margin. Giant to small and numerous cold-water carbonate mounds are located in this deep sea environment. This work focuses on the Moira Mounds, these are small scaled (up to 10 m high and 35 m wide) cold-water carbonate mounds situated between 930 and 1070 m depth and located in the Belgica mound province, Porcupine Seabight. These small carbonate build-ups, mostly formed by living corals, colonize hard substrates creating a network of small patchy mounds. This in turn provides an ecological niche for a diverse fauna, including benthic foraminifera.

We are currently investigating stained (living) and unstained (dead) benthic foraminifera from surface samples (0-1 cm; >63 µm, >125 µm and >250 µm size fractions) from the Moira mounds (Eurofleets cruise, 2012) along a North-South transect. Living benthic foraminifera from the Moira mounds are entirely non-documented. Thus our aim is to provide a thorough inventory of live benthic foraminifera in this region in order to better understand these complex environments. Assessing taphonomical biases and different transport processes in such current influenced environments is also a main objective. Furthermore, foraminiferal assemblages combined to sedimentological work (Lim *et al.* submitted) and geochemical data (TOC, Phosphorous content) will allow us to better understand current dynamics in the region and their role on mound development.

The Moira Mounds were sampled during the cruise funded by the European Union Seventh Framework Programme (FP7/2007-2013), under the EUROFLEETS grant agreement n°228344 (to the University of Fribourg, University of Milano-Bicocca and University College Cork).

This study is funded by the Swiss National Science Foundation (projects n° FN- 200020_153125).

P 5.3

High-resolution visualization of microbial carbonates using μ -CT: Insights from field and lab experiments

A. Foubert¹, D. Jaramillo-Vogel¹, E. De Boever¹, E. Feenstra¹, H. Hamaekers^{1,2}, S. Krause³

¹ *Department of Geosciences, University of Fribourg, Switzerland, anneleen.foubert@unifr.ch*

² *Department of Earth and Environmental Sciences, K.U. Leuven, Belgium*

³ *GEOMAR – Helmholtz Centre for Ocean Research, Kiel, Germany*

Microbial carbonates are unique deposits formed by the direct or indirect action of microbes. They witness early Life since Precambrian times, occur in a wide variety of environments - from marine to continental settings – and recently gained interest by the energy sector as potential reservoir rocks. Recent studies evidence the difficulty in predicting their nature, occurrence and reservoir properties. Processes (microbial mediated versus physico-chemical precipitation) involved in the formation of such microbialites remain to be unveiled. Moreover, early diagenesis is often obliterating the primary facies and fabric, rendering the interpretation of microbial structures difficult.

This study highlights the potential of multi-scaled X-ray computed tomography combined with field (in-situ) and lab (in-vitro) experiments in (1) unravelling the petrophysical properties (from micro- to nano-scale) of microbial carbonates and, (2) understanding the precipitation mechanisms and early diagenesis of microbial mediated Ca-Mg carbonates in a wide variety of settings. Different case studies have been selected to test the potential of multi-scaled visualization and analysis of micro-porosity in microbial carbonates and showing the necessity of high-resolution 3D visualization to understand microbial-mediated precipitation mechanisms.

The first case study focuses on marine and hypersaline microbialites deposited in an active rift setting from the Danakil Depression in Ethiopia, Afar. The second case study presents field precipitation experiments on different substrates of continental tufa deposits in Gotteron Valley (Fribourg, Switzerland). The last case study visualizes microbial-mediated precipitates in biofilms produced under aerobic and anaerobic conditions in constrained lab experiments.

Samples have been measured with the Bruker Skyscan 2211 (multi-scale X-ray nano-CT system) using an open X-ray source (energies varying between 60 and 120 kV, <4W) with Be-window. Two types of detectors have been used (resp. the 6 Mp flatpanel detector and the 11Mp cooled CCD detector) and voxel resolution was varying between 500 nm and 10 micrometer. Filter-sets were evaluated to enhance the segmentation of different carbonate minerals (calcite, dolomite, aragonite). Defined carbonate standards have been added during the scans facilitating segmentation. Images have been reconstructed using InstaRecon. Image segmentation and visualization have been performed using resp. CT-An, CT-Vox and Avizo (FEI).

P 5.4

Laboratory experiments of autogenic fluvial progradation above incised-valley fills during sea-level rise

Chen Chen¹, Sébastien Castelltort¹, Chris Paola², Laure Guerit^{3,1}, Brady Foreman⁴

¹ Department of Earth Sciences, University of Geneva, Rue des Maraichers 13, CH-1206 Geneva, Switzerland (chen.chen@unige.ch)

² Department of Geology and Geophysics, and St. Anthony Falls Laboratory, University of Minnesota, Minneapolis, Minnesota, 55414, USA

³ Geoscience Environment Toulouse, Paul Sabatier University, 14 Avenue Edouard Belin, 31000 Toulouse, France

⁴ Department of Geology, Western Washington University, Bellingham, Washington, 98225, USA

Incised valleys have been widely recognized and studied by many researchers (Hansen 1984, Dalrymple, Zaitlin et al. 1992, Zaitlin 1994, Posamentier 2001, Li, Wang et al. 2002). The original description of incised valleys of the Mississippi River was established by Fisk in 1944 and later defined as a “*fluvial eroded, elongate topographic low that is typically larger than a single channel*” (Zaitlin 1994). Valley fills generally contain a complex range of alluvial architecture linked to laterally amalgamated sandy channel belts in lowstand systems tracts (Martinsen 1994, Zaitlin 1994, Posamentier 2001) to channel avulsion processes and backstepping deltaic deposit (Harris 1994) during highstand systems tracts.

A sea-level fall driven paleo-incised valley has been found in the Esplugafreda section of the central Tremp-Graus basin (Spanish South-Pyrenees) across the transition of Paleocene and Eocene (Pujalte, Schmitz et al. 2014). The incised valley fills in this section are composed of sandbodies and well-developed soils (Esplugafreda Fm.). An extensive gravel deposit (Claret Conglomerate unit) was preserved in the section immediately above the filling of incised valley during sea-level rise (Pujalte, Schmitz et al. 2014). The conglomerate unit ends abruptly and is overlain by fine-grained yellowish soil sequence. All of the section was inundated by the ocean eventually. The unknown question need to be investigated is that, the extensive fluvial progradation (Claret Conglomerate unit) during sea-level rise was driven by external perturbation of Paleocene Eocene Thermal Maximum (PETM) or it is a natural consequence of incised valley fill?

To address these questions, we performed several experiments of incised valley infilling deposition during a single base-level rise in the Saint Antony Falls Laboratory (SAFL, University of Minnesota). The experimental setup consists in a non-erodible V-shape valley of 2.05 m x 0.8 m x 0.10 m, with an original valley slope of 0.05, and placed inside a 5 m x 5 m tank. The sediment load ($4 \times 10^{-6} \text{ m}^3/\text{s}$) and water discharge ($7 \times 10^{-6} \text{ m}^3/\text{s} - 2 \times 10^{-5} \text{ m}^3/\text{s}$) is carried in by a computer-controlled sediment feeder and water pump respectively. Water discharge, the rate of base level rise and the model slope were changed systematically in the ten sets of experiments. Overhead images are collected every 30 s. In addition, the topography is digitally acquired every 10 min by a computer-controlled laser scanner. The geometry of the channel sandbodies is acquired by cross-section photos after each runs.

In our experiments the prismatic geometry of a theoretical V-shape widening seaward incised valley imposes a reduction of accommodation creation once sea-level rises above the slope. The diminution of accommodation space volume triggers a progradation of the alluvial feeders system over the valley fills. Our results imply that, the extensive fluvial progradation deposits (Claret Conglomerate unit) in the Esplugafreda section might be a signature of autogenic process in the incised-valley stratigraphy. The coarse-grained progradation of the Claret Conglomerate is actually a consequence of reduced accommodation imposed by the incised valley geometry.

REFERENCES

- Dalrymple, R. W., B. A. Zaitlin and R. Boyd (1992). „Estuarine facies models: conceptual basis and stratigraphic implications: perspective.“ *Journal of Sedimentary Research* 62(6).
- Hansen, A. (1984). „Engineering geomorphology: the application of an evolutionary model of Hong Kong’s terrain.“ *Z. Geomorphol., Suppl* 51: 39-50.
- Harris, P. T. (1994). „Incised valleys and backstepping deltaic deposits in a foreland-basin setting, Torres Strait and Gulf of Papua, Australia.“
- Li, C., P. Wang, H. Sun, J. Zhang, D. Fan and B. Deng (2002). „Late Quaternary incised-valley fill of the Yangtze delta (China): its stratigraphic framework and evolution.“ *Sedimentary Geology* 152(1): 133-158.
- Martinsen, O. J. (1994). „Evolution of an incised-valley fill, the Pine Ridge Sandstone of southeastern Wyoming, USA: systematic sedimentary response to relative sea-level change.“
- Posamentier, H. W. (2001). „Lowstand alluvial bypass systems: incised vs. unincised.“ *AAPG bulletin* 85(10): 1771-1793.
- Pujalte, V., B. Schmitz and J. I. Baceta (2014). „Sea-level changes across the Paleocene–Eocene interval in the Spanish Pyrenees, and their possible relationship with North Atlantic magmatism.“ *Palaeogeography, Palaeoclimatology, Palaeoecology* 393: 45-60.
- Zaitlin, B. A. (1994). „The stratigraphic organization of incised-valley systems associated with relative sea-level change.“

P 5.5

Sedimentology and stratigraphic architecture of an incised valley fill, Late Carboniferous (Eastern Kentucky, USA).

Lathion Rodolphe, Le Cottonnec Aymeric, Moscariello Andrea.

*Department of Earth Sciences, University of Geneva, 13 Rue des Maraîchers, 1205 Geneva.
(rodolphe.lathion@etu.unige.ch)*

Late Carboniferous fluvio-deltaic successions of the Breathitt Group in eastern Kentucky, has long been recognised as an excellent analogue outcrop for the hydrocarbons-rich systems in the Southern North Sea. It consists of an overall coarsening- and shallowing-upward succession of Lower to Middle Pennsylvanian fluvio-deltaic deposits. It has been divided into eight 3rd order Formations bounded by major marine units (Chesnut, 1996), within each Formation 4th order Milankovitch cycles are well expressed. The paleo-environmental location of the study area and the strong glacio-eustatic control over sea-level at the time of deposition, make of the Breathitt Group an incised valley prone succession of deposits. Incised valley mechanisms of formation are relatively well-known based on numerous Quaternary examples, however, the sedimentological details of their infill is less known. This is mostly due to the fact that i) the size of typical incised valleys (up to several kilometers in width and tens of meters in height) is typically much larger than an outcrop size in ancient incised valley fills, ii) there is often limitations in resolution or areal coverage (seismic and well data) of subsurface data for the study of Quaternary incised valley fills.

Sedimentology and sequence stratigraphy in the uppermost formations of the Breathitt Group (Pikeville, Hyden, Four Corners and Princess) have been studied since the 80's by numerous authors. On the other hand the sedimentology and architecture of the lower depositional sequences (Grundy Formation), characterised by large incised valleys systems are less known, mostly due to lack of outcrops. However recent (2014-2016) extensive roadworks in Eastern Kentucky unraveled several kilometers of new and continuous outcrops which allow a detailed examination of these poorly known units.

In this paper we present the detailed sedimentologic and stratigraphic study of an incised valley fill in the Grundy Formation. Indeed, an extensive new outcrop (over 2 km in width and 250 m in height) has been exposed by roadworks in the area of Elkhorn City, uncovering a very well exposed incised valley fill. Through dm-scale logging and photo panel correlations a complete sedimentological description and spatial distribution of facies associations in the incised valley fill has been performed. Furthermore, relation between specific facies associations and sequence stratigraphic stage has been established, thus unveiling in great details the complete anatomy of an ancient incised valley fill.



Figure 1: View of an incised valley fill in the studied outcrop

REFERENCES:

Chesnut, D.R., 1996. Geologic framework for the coal-bearing rocks of the Central Appalachian Basin. *Int. J. Coal Geol.* 31, 55–66. doi:10.1016/S0166-5162(96)00011-0

P 5.6

$\delta^{13}\text{C}$ as a tool for sequence stratigraphy correlations in the South Pyrenean foreland basin, Spain

Louis Honegger¹, Sébastien Castellort¹, Julian Clark², Thierry Adatte³, Cai Puigdefàbregas⁴, Mason Dykstra², Andrea Fildani², Jorge Spangenberg⁴

¹ *Département des Sciences de la Terre, Université de Genève, Rue des Maraîchers 13, CH-1205 Genève (louis.honegger@etu.unige.ch, sebastien.castellort@unige.ch)*

² *Statoil, 6300 Bridge Point Parkway, Austin, TX, USA*

³ *Institut des Sciences de la Terre, Université de Lausanne, CH-1015 Lausanne*

⁴ *Institut de Ciències de la Terra (CSIC), Carrer Lluis Solé Sabaris, 08028 Barcelona, Spain*

⁵ *IDYST, Geopolis, Université de Lausanne, 1015 Lausanne, Switzerland*

In the intent to unravel Earth's sedimentary history, sequence stratigraphy has proven to be a powerful tool providing useful insights on the sedimentary record and its response to external forcing (Milankovitch cycles, eustasy variations, climate change and tectonics). Sequence stratigraphy provides theoretical models allowing to predict the nature and timing of surfaces and sedimentary packages from marine to continental environments, thus contributing to global source-to-sink comprehension of Earth's dynamic response to environmental change. In recent years, although classic sequence stratigraphy models have evolved thanks to ground-truthing studies and advances of subsurface imaging, correlations of marine and continental stratigraphies at high-resolution remain challenging to establish on the field. Consequently, the debate about the nature of the factors controlling stratigraphic patterns fluvial successions are still debated (Sømme, 2009). To address this problem, a mapping and multi-proxy approach was undertaken in the Tresp-Graus and Ainsa basins in the South-Pyrenean foreland basin. We focused on the early Eocene Castissent formation, a major fluvial excursion and its deep marine time-equivalent; the turbiditic systems of Fosado, Arro and Gerbe with the intent to obtain a high resolution deposition timing of the fluvial and marine sand bodies.

Based on field work and previous mapping, we use carbon stable isotopes on bulk rock carbonates to trace a climatic signal in the sedimentary record on three sections representing the distal deep marine depositional system, the transitional shallow marine deltaic systems, and the fluvial feeder system at three different loci in the basin. This allows us to correlate environmental signals across the whole source-to-sink profile and discuss sequence stratigraphic models for the relative timing of deposition of sand in these different segments. The results and interpretations are supported by geochemistry of major and trace elements.

REFERENCES

- Loutit, T. S., Hardenbol, J., Vail, P. R., & Baum, G. R. (1988). Condensed sections: The key to age determination and correlation of continental margin sequences. *Sea-Level Changes* (Vol. 42). <http://doi.org/10.2110/pec.88.01.0183>
- Mutti, E., Séguret, M., & Sgavetti, M. (1988). Sedimentation and Deformation in the Tertiary Sequences of the Southern Pyrenees.
- Shanley, K., & McCabe, P. (1994). Perspectives on the sequence stratigraphy of continental strata. *AAPG Bulletin*, 4(4), 544–568. Retrieved from <http://archives.datapages.com/data/bulletns/1994-96/data/pg/0078/0004/0500/0544.htm>
- Somme, T. O., Helland-Hansen, W., & Granjeon, D. (2009). Impact of eustatic amplitude variations on shelf morphology, sediment dispersal, and sequence stratigraphic interpretation: Icehouse versus greenhouse systems. *Geology*, 37(7), 587–590. <http://doi.org/10.1130/G25511A.1>
- Vail, P. R. (1987). Seismic Stratigraphy Interpretation Using Sequence Stratigraphy Part I : Seismic Stratigraphy Interpretation Procedure. *AAPG Studies in Geology* #27, Volume 1: Atlas of Seismic Stratigraphy, 1(1), 1–10.

P 5.7

Climatic signals in the Paleocene fluvial formation of Tremp, Pyrenees, Spain.

Teodoro Hunger¹, Thierry Adatte², Kalin Kouzmanov¹ & Sébastien Castelltort¹.

¹ *Department of Earth Sciences, University of Geneva, 13 Rue des Maraîchers, 1205 Genève*

² *Institut des Sciences de la Terre, Université de Lausanne, CH-1015 Lausanne.*

(teodoro.hunger@etu.unige.ch)

The fluvial successions of the Tremp Group in the South Central Pyrenees preserves a nearly continuous record of climate evolution through the Paleocene and Eocene epochs, spanning the remarkable Paleocene-Eocene thermal maximum (PETM) at which a dramatic global warming event took place. These series thus represent an important repository of paleoenvironmental information that can be studied to help improve the understanding of the current global warming worldwide. In this work, we focus on two correlative sections, the Esplugafreda and Serraduy sections, which document sedimentation in an extended arid alluvial and coastal plain influenced by climate-controlled sediment supply, water discharge and sea-level fluctuation.

During fieldwork in July 2016, we sampled paleosoil carbonate nodules and fine-grained floodplain material with a resolution of 1.5 to 5 meters on the Esplugafreda section over a thickness of 300 meters. On the Serraduy section we focused on sampling material from 20 meters below and across the PETM in order to provide new constraints on paleoenvironmental change at this boundary.

We will present our preliminary study of these two sections with focus on their sedimentological evolution, whole rock geochemistry and stable isotope composition of the carbonate nodules. In addition, we intend to address the origin of the very specific red color of the Tremp formation. We will present paleogeographic maps document the possible relationship with exhumation and erosion of ophiolitic material of the now collapsed alpine orogen in the mediterranean domain. This hypothesis will be tested using XRF data on ophiolite samples from Elba.



Figure 1. Aerial view of the Esplugafreda section

REFERENCES

- Pujalte V., Schmitz B., Baceta J.I., 2013. Sea-level changes across the Paleocene-Eocene interval in the Spanish Pyrenees, and their possible relationship with North Atlantic magmatism. *Palaeogeography, Palaeoclimatology, Palaeoecology* 393. 45-60.
- Schmitz B., Pujalte V., 2003. Sea-level, humidity, and land-erosion records across the initial Eocene thermal maximum from a continental-marine transect in northern Spain. *Geology* 31, 689-692.
- Zachos J., Pagani M., Sloan L., Thomas E., Billups K., 2001. Trends, Rhythms, and Aberrations in Global Climate 65 Ma to Present. *Science* 292, 686-693.

P 5.8

Linking subaerial exposures to paleoenvironments and paleoclimates (Valdorria carbonate platform, northern Spain)

Nabil A. Shawwa¹, Valentin Chesnel¹, Óscar Merino-Tomé², Luis Pedro Fernández², Branimir Šegvić¹ & Elias Samankassou¹

¹ *Université de Genève, Département des Sciences de la Terre, CH-1205, Genève, Switzerland (Nabil.Shawwa@etu.unige.ch)*

² *Universidad de Oviedo, Departamento de Geología, Arias de Velasco, 33005, Oviedo, Spain*

The Valdorria carbonate platform is an isolated system found in the Cantabrian Mountains, Northern Spain. It is part of the Valdeteja Formation, which is stratigraphically overlying the Barcaliente Formation and underlying the San Emiliano Formation. The platform developed during the Bashkirian (Pennsylvanian) in the Variscan foreland basin and thrust belt, nowadays known as the Cantabrian Zone (Chesnel et al. 2016a).

Milankovitch cyclicity has recently been revealed throughout the carbonate platform exhibiting subaerial exposure features at the top of each cyclothem (Chesnel et al. 2016b). Subaerial exposures are of interest for a diagenetic interpretation of the history of platforms because they can display a complete paragenetic sequence of the lithification process. Features of interest observed range from marine deposition to vadose, phreatic and burial cementation along with tectonism and recent features that have developed after burying. At Valdorria, 13 different subaerial exposure surfaces have been identified, predominantly as subtle to deep immature dissolution surfaces and mature karstic and/or calcretic dissolution surfaces. Compacted immature dissolution surfaces are present but rare.

Transmitted light and optical cathodoluminescence petrographic studies show the presence of various cement generations. Furthermore, cathodoluminescence shows the presence of meteoric and burial cements within many samples. Vadose and upper phreatic cements can be confirmed due to a lack of luminescence indicating an oxidized environment where Mn and Fe are being incorporated into oxide minerals. Lower phreatic cements can also be confirmed where the brightest luminescence is found indicating reduced pore water because Mn is highly abundant in this environment. Burial cements can also be observed when cements are dimly luminescent indicating an enrichment in Fe, typical of the burial realm.

Furthermore, burial depths have been established using X-ray diffraction techniques to determine the smectite versus illite content of clay mineral assemblages found in karstic cavities and calcretic layers. The presence of calcrete along with its clay mineral assemblage has also been used to establish paleoenvironments of the platform.

Stable oxygen ($\delta^{18}\text{O}$) and carbon ($\delta^{13}\text{C}$) isotopes along with major and trace element geochemistry of Ca, Fe, Mg, Mn and Sr have been acquired to confirm the presence of cementation for the various diagenetic realms. Linking this information to the petrographic framework provides a paragenetic relationship related to the relative timing of diagenetic events.

REFERENCES

- Chesnel, V., Samankassou, E., Merino-Tomé, Ó., Fernández, L.P. & Villa, E., 2016a: Facies, geometry and growth dynamics of the Valdorria carbonate platform (Upper Carboniferous, N. Spain). *Sedimentology* 63, 60-104.
- Chesnel, V., Merino-Tomé, Ó., Fernández, L.P., Villa, E. & Samankassou, E., 2016b: Isotopic fingerprints of Milankovitch cycles in Pennsylvanian carbonate platform-top deposits: the Valdorria record, Northern Spain. *Terra Nova*, DOI: 10.1111/ter.12229

P 5.9

Multiproxy approach to climate signals in the middle-upper Eocene deposits of the Ainsa Basin, Spain

Charlotte Läubli, Miguel Garcès, Luis Valero, Julian Clark, Cai Puigdefabregas, Thierry Adatte, Sébastien Castelltort

¹ *Department of Earth Sciences, University of Geneva, Rue des Maraîchers 13, CH-1205 Genève*

Excellent exposure and preservation of entire source-to-sink systems make the south Pyrenean foreland basin an ideal research site to study sequence stratigraphy, climatic-cyclicity over multimillennial times scales and correlation between continental and deep basin deposits. The Ainsa basin, situated between the Tremp-Graus (fluvio-deltaic sediments) and the Jaca (distal deep marine sediments) basins, is composed of very well preserved syn-tectonic sediments typical of a proximal deep basin with submarine fans and hemipelagic slope deposits, bottom of slope and basin floor environments. The Ainsa succession is made of eight Sediment Gravity Flow systems (SGFs: Fosado, Los Molinos, Arro, Gerbe, Banaston, Ainsa, Morillo and Guaso), which were deposited during the Ypresian and the Lutetian epochs (early to middle Eocene). The total stratigraphic thickness reaches approximately 4 km. Each individual system is composed of a dominantly sandy interval of sandbodies channelized in submarine canyon fill, mass transport deposits and fan, and of a dominantly marly interval of hemipelagic slope wedge and interfan marlstones. Source of sediments in the Ainsa basin can thus be both intrabasinal or extrabasinal. These sediments thus preserve information about both environmental variables external to the basin, such as climate and regional tectonics, as well as intrabasin environmental variations such as burial history and diagenetic evolution..

The classical interpretation of the systematic cyclicity between periods of coarse sediments supply (channelised sandbodies, mass transport deposits) and periods with hemipelagic deposits invokes eustasy, pulsed tectonics, or a combination of both (Cantalejo and Pickering 2014). However, it remains difficult to isolate a purely eustatic signal in deep marine sediments, where quantifying paleo-waterdepth is challenging.

In the frame of a broader project aimed at deconvolving climate signals in the Ainsa submarine stratigraphic record, we sampled and logged in July 2016 a continuous section in the upper Hecho group (Gerbe, Banaston and Ainsa SGFs, thickness of ca 1.4 km). We will undertake a multiproxies approach based on stable isotope analysis, whole rock geochemistry (major and trace elements) and clay mineralogy. Stratigraphic constraints will be obtained from new magnetostratigraphic measurements performed at the University of Barcelona, in combination with existing data from the literature.

Results will help correlate lithological patterns and proxy signals with global climatic (Zachos et al., 2001) and eustatic records (e.g. Kominz et al., 2008).



Figure 1. Example of alternating with siliciclastic turbidite beds and interfan hemipelagic marlstones in the Ainsa basin. Such sections were samples with an average resolution of 10 meters for magnetostratigraphy and geochemistry.

REFERENCES

- Cantalejo, B., Pickering, K.T., 2014: Climate forcing of fine-grained deep-marine systems in an active tectonic setting: Middle Eocene, Ainsa Basin, Spanish Pyrenees, *Palaeogeography, Palaeoclimatology, Palaeoecology* 410, 351–371
- Kominz, M. A., Browning J. V., Miller, K. G., Sugarman, P. J., Mizintseva S., Scotese, C. R. , 2008: Late Cretaceous to Miocene sea-level estimates from New Jersey and Delaware coastal plain coreholes: An error analysis, *Basin Res.*, 20, 211-226
- Pickering, K.T., Bayliss, N.J., 2009: Deconvolving tectono-climatic signals in deep-marine siliciclastics, Eocene Ainsa basin, Spanish Pyrenees: Seesaw tectonics versus eustasy. *Geology* 37, 203–206.
- Scotchman, J.I., et al., 2014: A new age model for the middle Eocene deep-marine Ainsa Basin, Spanish Pyrenees, *Earth Science Reviews*, 1–13
- Zachos, J., Pagani M., Sloan L., Thomas E., Billups K., 2001: Trends, Rhythms and Aberrations in Global Climate 65 Ma to Present, *Science*, 686-693

P 5.10

The new geological map of the area between Mendrisio (Switzerland), Como and Varese: 300 million years of geological history.

Christian Ambrosi¹, Daniel Bernoulli², Cristian Scapozza¹, Filippo Schenker¹ and Stephan Dall'Agnolo³

¹ *Institute of Earth Sciences, University of Applied Sciences and Arts of Southern Switzerland (SUPSI), Campus Trevano, 6952 Canobbio, Switzerland*

(christian.ambrosi@supsi.ch, cristian.scapozza@supsi.ch, filippo.schenker@supsi.ch)

² *Department of Earth Sciences, Swiss Federal Institute of Technology (ETH) and University of Basel (Switzerland).*

(daniel.bernoulli@unibas.ch)

³ *Swiss Geological Survey, Federal Office for Topography swisstopo, Seftigenstrasse 264, 3084 Wabern, Switzerland*

(stephan.dallagnolo@swisstopo.ch)

The new sheet Mendrisio of the Swiss Geological Atlas of Switzerland 1:25 000 covers an area that is crucial for the understanding of the sedimentary and tectonic history of the western Southern Alps of Lombardy (northern Italy) and Ticino (Switzerland). Three major tectono-stratigraphic units can be distinguished: 1. The area of Monte San Giorgio that is characterized by a Mesozoic high exposing a stratigraphic succession from the Hercynian basement to the Cretaceous Flysch Lombardo; 2. The Generoso area, separated from the Monte San Giorgio area by a Liassic syn-sedimentary listric fault of several kilometres throw and dominated by 4 km basinal syn-rift (Lower Liassic) and post-rift (Middle Liassic–Cretaceous) sediments, and 3. The unit of the Gonfolite Lombarda Group, a Oligo–Miocene clastic wedge that was back-thrusted onto the Mesozoic successions in late Miocene times. The map documents the evolutionary steps from Permian transtension and volcanicity, Triassic basin formation accompanied by the deposition of hydrocarbon source rocks, late Triassic to middle Liassic rifting along syn-sedimentary crustal faults, and ocean-wide palaeo-oceanographic changes during post-rift thermal subsidence. Early Alpine pre-collisional orogenic movements are testified to by late Cretaceous flysch sediments; Oligo–Miocene post-collisional ones by the deep-water clastic wedge of the Gonfolite Lombarda Group that is part of the subsurface Milano fold belt below the Po Plain. Deep valleys, incised into the fold belt and flooded by the early Pliocene transgression are related to the Messinian salinity crisis of the Mediterranean.

Numerical dating of Quaternary sediments and climate proxies reflecting content-wide or global events allow establish a regional stratigraphy integrating the different glacial events into a coherent picture. Four major Quaternary chronostratigraphic units are distinguished from top to bottom:

4. Postglacial deposits ("*Depositi del Postglaciale*"; 0–0.0117 Ma) are referred entirely to the Holocene. 3. Deposits of the Last Glacial Maximum and the Late-glacial ("*Depositi dell'Ultimo Massimo Glaciale e del Tardoglaciale*"; 0.0117–0.029 Ma). 2. Deposits preceding the Last Glacial Maximum ("*Depositi precedenti all'Ultimo Massimo Glaciale*"; 0.029–0.781 Ma), both referred to the Middle and Late Pleistocene. 1. Deposits referred to the Early Pleistocene ("*Depositi del Pleistocene inferiore*"; 0.781–2.588 Ma).

In the detailed legend of the map, we represent both age and facies of the Quaternary deposits. This representation of the chronostratigraphical units enables a 'harmonised cartography' in a larger regional framework because it allows for a quick visualisation of the spatial extent of the main morphoclimatic events, as, for example, the maximal glacial extent during the Last Glaciation compared to the previous ones. It also facilitates the understanding of the dynamics and the recognition of the main glacial flow directions in the area, in particular of the important role played by the Larian lobe of the Adda glacier with respect to the glacial lobes of Lake Lugano.

P 5.11

Detrital garnet fingerprint of the Central Swiss Alps

Laura Stutenbecker¹, Alfons Berger¹, Fritz Schlunegger¹

¹ *Institut für Geologie, University of Bern, Baltzerstrasse 1+3, CH-3012 Bern (laura.stutenbecker@geo.unibe.ch)*

Ever since the convergence of the European and Adriatic continents started, the Alpine orogen has been one of the most important sediment factories in Europe. Associated sediments have been either incorporated into the orogenesis, deposited in the foreland basins, or have been transported out of the Alpine system into connected sedimentary basins. In the reconstruction of sediment sources, transport and dispersal patterns of any of those sedimentary archives, several fingerprinting techniques are available, ranging from heavy mineral analysis to pebble counting. The wide range of lithologies, and the similarity of some of those to other sediment factories in Europe, however, remains problematic in identifying and distinguishing Alpine-derived sediment.

Most sediments derived from sources within the Alps contain garnets in their heavy mineral assemblages. The chemical composition of garnets depends mostly on the composition and metamorphic grade of the source rock, and has been proven to be a useful fingerprinting tool. Because of the high variability of source rocks present in the Alps, a correspondingly high range of detrital garnet compositions can be expected. In the Swiss Alps, a number of studies have published garnet compositions from individual outcrops or lithologies, but an overall work on the entire range of detrital garnets supplied from the major lithological complexes has never been done.

This study aims to establish detrital garnet fingerprints for the three major lithological groups present in the Central Swiss Alps: the Helvetic nappes, the Penninic nappes and the External massifs. Modern river sand was collected from tributary basins draining these three units. Garnets were extracted from the samples, and analysed with a scanning electron microscope. Results show that most garnets derived from the External massifs are characterized by a high grossular- and spessartine-component, whereas Penninic garnets are rich in almandine. Garnets found in the Helvetic nappes are not distinguishable from the Penninic ones.

P 5.12

Paleo-erosion rates and paleo-elevation inferred through cosmogenic ¹⁰Be and ²¹Ne in northernmost Chile

Andrea Madella¹, Romain Delunel¹, Pierre-Henri Blard², Naki Akçar¹, Fritz Schlunegger¹, Marcus Christl³

¹ *Institut für Geologie, Universität Bern, Baltzerstrasse 1+3, CH-3012 Bern (andrea.madella@geo.unibe.ch)*

² *Centre de Recherches Pétrographiques et Géochimiques, Université de Lorraine, France*

³ *Laboratory for Ion Beam Physics, ETH Zurich, Switzerland*

The uplift history of the Central Andes has largely been addressed in both structural, sedimentological and paleoclimatic studies during the past decades. The timing of uplift and the possible links to paleo-climatic changes, however, need better resolution and remain a matter of debate. A widely accepted scenario involves an episode of rapid uplift during the Late Miocene, paired with a shift from arid to hyperarid conditions in the western forearc. The El Diablo formation found in northern Chile (ca. 19°S) comprises fluvial mudstones, sandstones and conglomerates deposited between 17-11 Ma, and may represent a relevant sedimentary archive of the mentioned tectonic and paleo-climatic event.

We measured in situ cosmogenic ¹⁰Be and ²¹Ne concentrations in quartz extracted from 10 units of known age within the El Diablo formation, which have been dated to 13-11 Ma through magnetostratigraphy (von Rotz et al., 2005). Combining the data from these two isotopes we aim to infer paleo-erosion rates and paleo-elevation of the Chilean forearc during the depositional time of the El Diablo formation. This will therefore provide exceptional insights into the Late Miocene tectonic and climatic history of the Western Central Andes.

REFERENCES

von Rotz, R., Schlunegger, F., Heller, F. & Villa, I. (2005) Assessing the age of relief growth in the Andes of northern Chile: magneto-polarity chronologies from neogene continental sections. *Terra Nova*, 17, 462–471.

P 5.13

Variations in near-bottom flow of ACC during past glacial cycle in SW Indian Ocean

Helen Eri Amsler¹, Samuel L. Jaccard¹, Ian Nicholas McCave² & Minoru Ikehara³

¹ *Institute of Geological Sciences and Oeschger Centre for Climate Change Research, University of Bern, Baltzerstrasse 1+3, CH-3012 Bern, Switzerland (helen-eri.amsler@geo.unibe.ch)*

² *Department of Earth Sciences, University of Cambridge, Downing Street, Cambridge, Cambridgeshire, CB2 3EQ, United Kingdom*

³ *Center for Advanced Marine Core Research, Kochi University, 200 Monobe-otsu, Nankoku, 783-8502 Japan*

The meridional overturning circulation of the ocean plays a key role in global climate variability by storing and redistributing heat, fresh water, carbon and nutrients. In the North Atlantic surface water sinks to the abyss, but a major part of this cycle is the return path from the ocean's interior through upwelling in the Southern Ocean. This upwelling is largely regulated by the latitudinal position of the Southern westerly winds associated with the deep-reaching Antarctic Circumpolar Current (ACC) (Rintoul et al. 2001).

Climate model studies show progressively poleward intensifying winds, related to increased ACC transport and southward shifting of its mean position and increased upwelling. However, a number of recent numerical studies have shown that the sensitivity of the large-scale circulation in the Southern Ocean may be reduced by eddy-effects (Böning et al 2008).

As there remains significant uncertainty regarding the degree of sensitivity of the Southern Ocean circulation to wind stress and the response of the Antarctic circumpolar transport, our aim is to investigate the temporal and latitudinal evolution of the ACC dynamics over the last glacial cycle.

Previous studies suggested a stronger ACC during glacials in the Indian Ocean (Mazaud et al. 2010), but more recent studies in the Drake Passage and Scotia Sea indicate less throughflow during glacials and lateral differences in current speeds (McCave et al. 2014, Lamy et al. 2012). Here we present the sortable silt mean-size of a series of cores across the ACC in the SW Indian Ocean, the mean-size of the re-deposited silt fraction being proportional to the near-bottom flow velocity.

REFERENCES

- Böning C.W., Dispert A., Visbeck M., Rintoul S. R., Schwarzkopf F. U. (2008) *Nature Geoscience*, 1, 864-869.
- Lamy F., Arz H. W., Kilian R., Lange C. B., Lembke-Jene L., Wengler M., Kaiser J., Baeza-Urrea O., Hall I. R., Harada N., Tiedemann R. (2015) *PNAS*, 112, 13496–13501.
- Mazaud A., Michel E., Dewilde F., Turon J. L. (2010) *G3*, 11, doi:10.1029/2010GC003033.
- McCave I. N., Crowhurst S. J., Kuhn G., Hillenbrand C-D., Meredith M. P. (2014) *Nature Geoscience*, 7, 113-116.
- Rintoul S. R., Hughes C., Olbers D. (2001) in Siedler, G., Church, J., Gould, J. (eds). *Ocean Circulation and Climate*, Academic Press, 271-302.

P 5.14

Nitrogen isotope changes in the equatorial Atlantic during the Plio-Pleistocene Transition

Lukas E. Oesch¹, Daniel M. Sigman², Anja S. Studer³ and Gerald H. Haug^{1,3}

¹ *Geological Institute, ETH Zürich, Zürich, Switzerland, lukas.oesch@erdw.ethz.ch*

² *Department of Geosciences, Princeton University, Princeton, NJ, USA*

³ *Max Planck Institute for Chemistry, Mainz, Germany*

During the Plio-Pleistocene transition (2.9-2.4Ma), Earth's climate and ocean circulation underwent substantial changes. Focusing here on the equatorial Atlantic Ocean, upon the intensification of northern hemisphere glaciation at 2.7 MyrBP, proxies indicate cyclic maxima in productivity with the 41 kyr period of obliquity [Lawrence *et al.*, 2013], correlating with minima in sea surface temperature [Herbert *et al.*, 2010]. As a result of global cooling, an equator ward shift of the westerly wind belt as proposed by Brierley *et al.* (2009) may have lead to a basin-wide contraction of the Atlantic warm pool, allowing nutrient rich Sub Antarctic Mode Water (SAMW) to be upwelled into the euphotic zone in the equatorial Atlantic. At ODP Site 662 in the central equatorial Atlantic, foraminifera-bound d15N was measured on two species of planktonic foraminifera through the Plio-Pleistocene transition. The main feature is an onset of obliquity paced 41kyr cycles at 2.7MyrBP, with minima in d15N coinciding with maxima in benthic d18O. Glacial periods with lower sea surface temperatures, higher productivity, and lower FB-d15N alternated with interglacial phases, characterized by warm sea surface water, low production and higher d15N. These simple correlations of d15N with climate parameters are not observed over the last 160 kyr of the late Pleistocene at this site. Moreover, the mean FB-d15N between 2.4 and 2.9 Ma is 1-2‰ lower than over the last 160 kyr.

We propose that the cyclic change in FB-d15N starting at ~2.7 Ma is due to obliquity paced changes in the volume of the Atlantic warm pool, with colder climate reducing this volume, resulting in higher nitrate concentration in the waters upwelled in the equatorial Atlantic (Lawrence 2013). Unlike in the late Pleistocene, the nitrate concentration in the water below the warm pool (which is ultimately sourced from SAMW) was adequately high that nitrate consumption was incomplete along the equator during the obliquity-paced Plio-Pleistocene cold intervals, causing the observed decline in FB-d15N during those intervals. The lower mean FB-d15n over the entire investigated Plio-Pleistocene period suggests that SAMW nitrate d15N was lower during this period, consistent with Sub Antarctic nitrate consumption being weak during the Pliocene and early Pleistocene due to a lack of dust-derived iron input at that time (Martinez Garcia 2011; Lawrence 2013).

REFERENCES:

- Brierley, C. M., a V Fedorov, Z. Liu, T. D. Herbert, K. T. Lawrence, and J. P. LaRiviere (2009), Greatly Expanded Tropical Warm Pool and Weakened Hadley Circulation in the Early Pliocene, *Science* (80-.), 323(5922), 1714–1718, doi:10.1126/science.1167625.
- Herbert, T. D., L. C. Peterson, K. T. Lawrence, and Z. Liu (2010), Tropical ocean temperatures over the past 3.5 million years., *Science*, 328(5985), 1530–1534, doi:10.1126/science.1185435.
- Lawrence, K. T., D. M. Sigman, T. D. Herbert, C. a. Riihimaki, C. T. Bolton, A. Martinez-Garcia, A. Rosell-Mele, and G. H. Haug (2013), Time-transgressive North Atlantic productivity changes upon Northern Hemisphere glaciation, *Paleoceanography*, 28(4), 740–751, doi:10.1002/2013PA002546.
- Martínez-García, A. et al. (2014), Iron Fertilization of the Subantarctic Ocean During the Last Ice Age, *Science* (80-.), 343(6177), 1347–1350, doi:10.1126/science.1246848.

P 5.15

Epicentres and magnitudes of possible paleoearthquakes based on lacustrine sediment records in Switzerland

Katrina Kremer^{1,2}, Stefanie B. Wirth³, Anna Reusch^{1,4}, Donat Fäh², Benjamin Bellwald⁵, Flavio S. Anselmetti⁶, Stéphanie Girardclos⁷ & Michael Strasser⁸

¹ *Geological Institute, ETH Zurich, Sonneggstrasse 5, 8092, Switzerland*

² *Swiss Seismological Service, ETH Zurich, Sonneggstrasse 5, 8092 Zurich, Switzerland*

³ *Centre for Hydrogeology and Geothermics, University of Neuchâtel, Emile-Argand 11, 2000 Neuchâtel, Switzerland*

⁴ *Department of Geosciences, University of Bremen, Gebäude GEO, Klagenfurter Strasse 2, 28359 Bremen, Germany*

⁵ *Department of Earth Sciences, University of Bergen, Postboks 7803, 5020 Bergen, Norway*

⁶ *Institute of Geological Sciences and Oeschger Centre for Climate Change Research, University of Bern, Baltzerstrasse 1+3, 3012 Bern, Switzerland*

⁷ *Department of Earth sciences and Institute for Environmental Sciences, University of Geneva, Rue des Maraîchers 13, 1205 Geneva, Switzerland*

⁸ *Institute of Geology, University of Innsbruck, Innrain 52, 6020 Innsbruck, Austria*

In regions with moderate seismicity and long intervals between strong earthquakes, paleoseismological archives that exceed the historical and instrumental timescale are required to establish reliable estimates of earthquake recurrence. In several regions, studies have shown that lake sediments are very suitable for paleoseismological studies by causally linking characteristic sedimentological features to historic earthquakes calibrating the paleoseismic archive. Studies on single lakes, however, do neither allow determining the paleoepicentre nor the paleomagnitude for the potential paleoearthquakes.

Here we compile the sedimentary paleoseismic records of 11 lakes from Switzerland covering the last 10'000 years using shaking-induced mass movements and microdeformations. These data allow determining periods of enhanced mass-movement occurrence that is likely related to earthquakes. However, the large dating uncertainty attributed to such deposits does not allow to clearly define single earthquake events when comparing the different lake records and therefore represents one of the major limitations of this approach. However, areas of possible epicentres and ranges of magnitudes of paleoearthquakes can be reconstructed with a model using the geographical distribution of earthquake-related sedimentary impacts detected during the period with historical and/or instrumental records. This allows us to propose a catalogue of large events with respect to paleoearthquake scenarios including plausible epicentre locations and ranges of magnitudes.

6. Stratigraphy

Alain Morard, Reto Burkhalter, Oliver Kempf & Ursula Menkveld-Gfeller

*Swiss Committee for Stratigraphy (SKS/CSS),
Swiss Palaeontological Society (SPG/SPS),*

TALKS:

- 6.1 Adams A., Diamond L., Aschwanden L.: Dolomitization in an Inverted Mixing Zone (Stamberg-Member)
- 6.2 Baud A., Plasencia P., Hirsch F., Richoz S.: Middle Triassic stratigraphy of the Swiss Prealps revisited
- 6.3 Brack P., Wotzlaw J.-F., Storck J.-C.: Bedding patterns in hemipelagic carbonates: the case of the Middle Triassic Buchenstein Formation (Southern Alps, Italy)
- 6.4 Jordan P., Brugger J., Pietsch J., Abdelsayed M., Fuchs G., Neubert M.: Preliminary results from the Grandfontaine deep borehole (Ajoie, Canton of Jura, Switzerland)
- 6.5 Pictet A., Mojon P.-O., Spangenberg J.: A critical revision of the Hauterivian to Aptian sediments of the Jura Mountains (France and Switzerland)

POSTERS:

- P 6.1 Khojastehfar M., Aharipour R.: Study of microfacies, sedimentary environment and diagenetic processes of the Qom Formation in the southwest of Sorkheh (Semnan)
- P 6.2 Koiava K., Mosar J., Kvaliashvili L., Mauvilly J.: About the Konkian/Sarmatian boundary of Georgia based on Foraminifera

6.1

Dolomitization in an Inverted Mixing Zone

Arthur Adams¹, Larry Diamond¹, Lukas Aschwanden¹

¹ *Institute of Geological Sciences, Baltzerstrasse 1+3, 3012 Bern, Switzerland (arthur.adams@geo.unibe.ch)*

The recently reclassified Stamberg member (former *Trigonodus Dolomit*) of the Schinznach formation (former Upper Muschelkalk) of north-eastern Switzerland is a geochemically complex dolomitic unit. It forms part an extensive deep saline aquifer in the Molasse Basin of northern Switzerland, which is under investigation for its potential for geothermal energy production and for industrial CO₂ storage. The formation represents the sediments of a gently inclined carbonate ramp, situated in an extensive middle Triassic epeiric sea. Dolomitization of the formation is complete near Triassic paleoshorelines and wanes towards the centre of the seaway. Spatial distributions and facies analysis of these dolomites indicate that they formed through seepage-reflux mechanisms. Geochemical and isotopic evidence however, points to a more complex dolomitization mechanism.

Strontium isotopes of matrix dolomites range from 0.70844 to 0.7117, significantly higher than the Triassic marine ⁸⁷Sr/⁸⁶Sr ratio (0.70775), while oxygen isotope ratios range from -6.56 to -1.05‰_{VPDB}. A number of geochemical, petrographical and isotopic patterns are consistently observed in each borehole with depth: (1) strontium isotopic values paradoxically increase; (2) oxygen isotopic ratios decrease; (3) carbon isotopes values increase; (4) strontium concentrations decrease; (5) crystal size increases; (6) UV-fluorescence decreases; and (7) stoichiometry increases. While features 3 – 7 can be explained by seepage reflux, both sets of isotopic data are inconsistent with such a hypothesis. In light of new evidence, recrystallization can no longer account for the geochemical and isotopic signals of the dolomites.

The coupling of all geochemical, petrographic and isotopic data indicates that dolomite formed from waters, which progressively graded from dense refluxing saline brines to meteoric fluids from the top to the bottom of the unit. This paradox of saltwater overlying freshwater, despite their stark density differences, is present in a number of modern day settings. Most analogously, Australian hypersaline lakes often display inverted salinity gradients, whereby hypersaline brines reflux into underlying flowing freshwaters. Dolomite is known to be produced in these mixing zones and oxygen isotope ratios of these waters show remarkably similar ranges to those inferred by Triassic dolomites (Jacobson et al. 1991). Due to the proximity of the Vindelician High, the regressive nature of the carbonate ramp and its low angle of inclination, salinas, partially separated from the open sea, provided the unique hydrological settings for the formation of extensive Stamberg member dolomites.

REFERENCES

Jacobson, G., Jankowski, J. & Abell, R.S. 1991: Groundwater and surface water interaction at Lake George, New South Wales. *Journal of Australia Geology & Geophysics*, 12, 161-190.

6.2

Middle Triassic Stratigraphy of the Swiss Prealps revisited

Aymon Baud¹, Pablo Plasencia², Francis Hirsch³ and Sylvain Richoz⁴

¹ Parc de la Rouvraie, CH-1018 Lausanne

² Departamento de Botánica y Geología, Universidad de Valencia, Dr. Moliner, 50 Burjassot, 46100 Valencia, Spain

³ Laboratory of Geology, Naruto University of Education, Naruto, 772-8502, Japan

⁴ Institute of Earth Sciences, University of Graz, Heinrichstr. 26, 8010 Graz, Austria

The Middle Triassic in the “Médianes rigides” Nappe of the Swiss Prealps, belonging to the Briançonnais realm of the Western Alps, consists of a several hundred meters thick carbonate succession. More than 50 years ago Ellenberger (1950, 1958) proposed for it the dasycladacean biostratigraphic scheme that Baud & Mégard-Galli (1975) and Mégard-Galli & Baud (1977) followed in establishing the lithostratigraphic units.

Geological mapping and a recent conodont discovery lead us to revise thoroughly the Middle Triassic stratigraphy of the Swiss Prealps (Baud et al., submitted). At the localities Wiriehorn and Rothorn, about 600 m above the basal thrust, the *Costatoria goldfussi* limestone, a remarkable coquina and widespread transgressive marker bed, yields the key conodont *Sephardiella truempyi* (HIRSCH), a proxy for the Curionii - lower Gredleri ammonoid Zones (Early Ladinian). This remarkable *Costatoria goldfussi* coquina is a widespread marker bed that corresponds to the main flooding surface (MFS) of the large marine transgression. It is correlated biostratigraphically to the now well-dated Upper Muschelkalk transgression in Provence, Sardinia and Spain and with the basal Ladinian type locality at Bagolino in the Southern Alps.

This new correlation has deep implications on the age of the different Triassic formations in the Swiss Prealps:

- Late Anisian. Below the *S. truempyi* level, the Wiriehorn Formation, a mighty platform carbonate sequence, is built up by 2 members, the Wildgrimmi Member, a set of restricted upwards-shallowing carbonate para-sequences, 20 to 50 m thick (“calcaires rubanés”) and the Bodeflue Member a 20 to 80 m thick peritidal regressive dolostone (“Dolomies claires ou cendrées”) ending with mud-cracks beds. The coeval Champcella Formation in the Briançonnais realm is consequently also reassigned to the Late Anisian.
- Ladinian. The newly proposed Pralet Formation comprises the Balmi Member with the Lower Ladinian *Costatoria goldfussi* limestone at its base, followed by the dolomitic breccias of the Erpilles Member.

This revisited Middle Triassic Stratigraphy of the “Médianes rigides” thrust sheet is summarized in the Fig. 1.

REFERENCES

- Baud, A. & Mégard-Galli, J. 1975: Modèle d'évolution d'un bassin carbonate du domaine alpin durant la phase pré-océanique: cycles et rythmes dans le Trias de la zone briançonnaise des Alpes occidentales et des Préalpes. Proceeding of the 9th International Sedimentological Congress, Nice, 5/1, 45 - 50.
- Baud, A., Plasencia, P., Hirsch, F. & Richoz, S., submitted: Revised Middle Triassic Stratigraphy of the Swiss Prealps based on Conodonts and correlation to the Briançonnais (Western Alps). Swiss J. of Geosciences.
- Ellenberger, F. 1950: Horizons paléontologiques du Trias à faciès radical des Préalpes médianes vaudoises (coupes de la Grande Eau et de Saint-Triphon). C. r. Acad. Sci. 231, 1326 - 1328.
- Ellenberger, F. 1958: Etude géologique du Pays de Vanoise. Imprimerie nationale, Orléans, France, pp. 679.
- Mégard-Galli, J. & Baud, A. 1977: Le Trias moyen et supérieur des Alpes nord-occidentales et occidentales: données nouvelles et corrélations stratigraphiques. - Bulletin du BRGM, 2ème série. 4/3, 233 - 250.

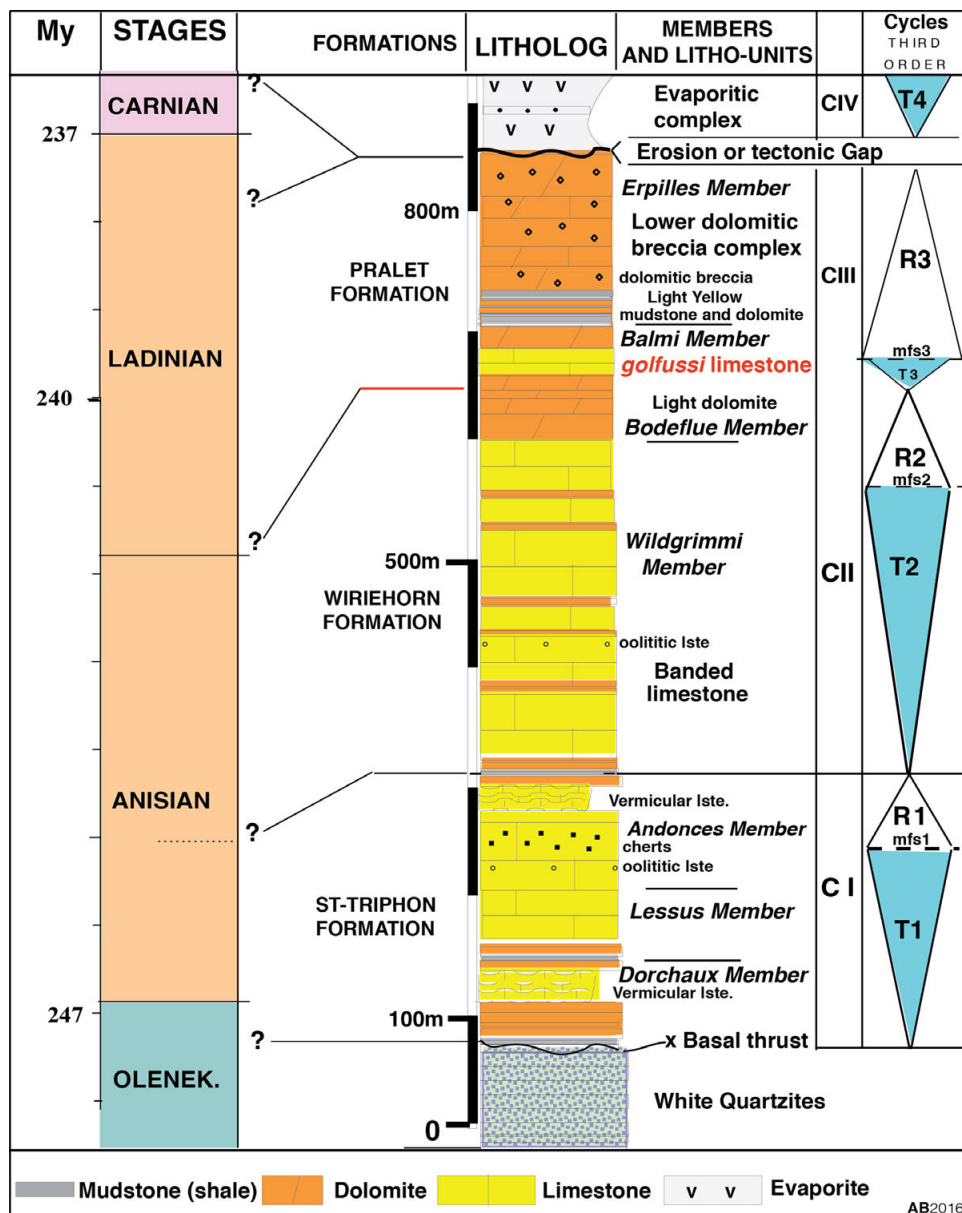


Figure 1. New composite section of the Middle Triassic sediments of the Western Swiss Prealps («Medianes rigides»). In red, the position of the remarkable «goldfussi» coquina unit. Main flooding surface: -mfs. Numerical age according to the Triassic time chart, in Ogg et al. (2016).

6.3

Bedding patterns in hemipelagic carbonates: the case of the Middle Triassic Buchenstein Formation (Southern Alps, Italy)

Peter Brack¹, Jörn-Frederik Wotzlaw¹, Julian-Christopher Storck¹

¹ *ETH Zurich, Institute of Geochemistry and Petrology, 8092 Zurich, Switzerland*

Hemipelagic carbonates of the 30-80 meters thick Middle Triassic Buchenstein Formation accumulated at slow rates in deep basins over wide areas of the Southern Alps. Geochronologic data suggest a time span close to four million years for this stratigraphic interval (Brack et al., 2007).

In the Dolomites the Buchenstein basins were bordered by rapidly aggrading carbonate platforms. Basin depth increased from a few tens to hundreds of meters. In the immediate vicinity of these buildups, platform-derived debris represent a substantial contribution to the Buchenstein carbonates (Maurer et al., 2003). In more distal successions, the sediments of the Buchenstein Fm. consist of lime mud, biogenic particles (mainly thin shells of pelecypods and radiolaria), fine-grained non-volcanic siliciclastic materials and volcanic debris in the form of discrete ash layers. The correlation of tephra layers and magnetic reversals along with biostratigraphic constraints demonstrates that bedding patterns persist over tens of kilometers throughout the Buchenstein basins in the Dolomites (Brack & Muttoni, 2000). Extension of these correlations to distant sections (> 100 km) elsewhere in the Southern Alps now reveals that similar patterns prevail over a much larger area and in supposedly not directly connected basin portions. The overall thickness of corresponding Buchenstein intervals varies by up to a factor of four and in expanded intervals individual beds tend to split into subsets of smaller layers.

These observations indicate an even sediment distribution throughout the Buchenstein basins with only gradual variation in the long-term subsidence. Distance to productive carbonate platforms seems to be a primary factor controlling the thickness of the carbonate fraction. The input of non-volcanic clastic materials appears to be punctuated but shows little areal variation. The persistence over a large area and the internal organization of stratal patterns in the Buchenstein Fm. suggests that the factors governing the bedding characteristics of the hemipelagic sediment are not related to local environments.

A Milankovitch type control has been suggested for Buchenstein bedding patterns in the Dolomites (Maurer et al., 2004) and variations in magnetic susceptibility of a short Buchenstein section in the central Dolomites (Spahn et al., 2013).

However, the results of both datasets cannot be readily reconciled. We expect that the new and extended correlations of Buchenstein successions will help improving the time frame for this and age-equivalent formations and the comprehension of their conspicuous bedding rhythms.

REFERENCES

- Brack, P. & Muttoni, G., 2000, *PPP*, 161, 361-380.
 Brack, P., Rieber, H., Mundil, R., Blendinger, W. & Maurer, F., 2007, *Swiss J. Geosci.*, 100, 327-347.
 Maurer, F., Reijmer, J.J.G. & Schlager, W., 2003, *Int. J. Earth Sci.*, 92, 593-609.
 Maurer, F., Hinnov, L. & Schlager, W., 2004, *SEPM Spec. Publ.* 81, 83-99.
 Spahn, Z.P., Kodama, K.P. & Preto, N., 2013, *G3*, 14/4, 1245-1257.

6.4

Preliminary results from the Grandfontaine deep borehole (Ajoie, Canton of Jura, Switzerland)

Peter Jordan^{1,2}, Julie Brugger¹, Johannes Pietsch^{1,2}, Mahmoud Abdelsayed^{1,2}, Gabor Fuchs³ & Wolfgang Neubert³

¹ Gruner Böhlinger AG, Mühlegasse 10, CH-4104 Oberwil (peter.jordan@gruner.ch)

² Geologisch-Paläontologisches Institut, University of Basel, Bernoullistrasse 32, CH-4056 Basel

³ Schweizer Salinen AG, Schweizerhalle, Postfach, Rheinstrasse 52, CH-4133 Pratteln 1 (gabor.fuchs@saline.ch)

Hundred years ago, the Buix deep borehole in northern Ajoie, prospecting for coal, reached an important rock salt deposit in Mid-Triassic strata (Schmidt et al. 1924). In adjacent France, about 40 km north of Swiss border, rock salt is exploited from Late Triassic deposits (e.g., Bichet & Campy, 2009). In the Buix borehole no rock salt is documented from this level. However, Late Triassic rocksalt is reported further south, from Essertine and Courtion deep boreholes south of Lake Neuchâtel and Lake Morat respectively (Büchi et al. 1965).

In the context of a campaign for ensuring long-term salt supply of Switzerland, the Swiss Saltworks (Schweizer Salinen AG) launched a deep well project in Western Ajoie to examine the extend of the Mid-Triassic salt deposit and to prospect for Late Triassic rock salt.

The 1200 m deep borehole close to Grandfontaine village, about 10 km west of Porrentruy, and 12.5 km south-west of Buix well site, was realised between January and July 2016. It started in Late-Jurassic Courgenay Formation and was mainly performed by destructive drilling. Coring was restricted to the Mid-Triassic Klettgau and Bänkerjoch Formation.

The Grandfontaine borehole provides the first record of considerable Late Triassic (Bänkerjoch Formation) rock salt layers in North-western Switzerland. Furthermore, it confirms the large extent of the Buix salt deposit in Mid-Triassic Zeglingen Formation. The drilling was stopped for technical reasons some meters below this salt deposit.

Though nearly fully destructively drilled, the Grandfontaine borehole gives a valuable insight in the lithology and thickness of Mid-Triassic to Mid-Jurassic formations not outcropping in the closer surroundings. The actual status of the on-going stratigraphic investigation will be presented.

REFERENCES

- Bicher, V. & Campy, M. 2009: Montagnes du Jura, Géologie et paysage. 2nd edition, Besançon (Neo Editions), 303 pages.
- Büchi, U.P., Lemcke, K., Wiener, G., Zimdars, J. 1965. Geologische Ergebnisse der Erdölexploration auf das Mesozoikum im Untergrund des schweizerischen Molassebeckens. Bull. Ver. Schweiz. Petrol-Geol. U. Ing., 32/82, p. 7 – 38.
- Schmidt, C., Braun, L., Paltzer, G., Mühlberg, M., Christ, P. & Jacob, F. 1924. Die Bohrungen von Buix bei Pruntrut und Allschwil bei Basel. Beiträge zur Geologie der Schweiz, Geotech. Serie, X. Lieferung, 73 pages.

6.5

A critical revision of the Hauterivian to Aptian sediments of the Jura Mountains (France and Switzerland)

Antoine Pictet¹, Pierre-Olivier Mojon², Jorge Spangenberg³

¹ Département des Sciences de la Terre, Université de Genève, 1205 Genève, Switzerland, (Antoine.Pictet@unige.ch)

² Rue du Centre 81, CH-2405 La Chaux-du-Milieu, Switzerland

³ Institut des dynamiques de la surface terrestre, Université de Lausanne, 1015 Lausanne, Switzerland

Since the 19th century, the Hauterivian to earliest Aptian sediments of the Jura mountains were very early divided in a succession of lithostratigraphic units defined on their facies and palaeontological content: the Marnes bleues d'Hauterive (MBH); the Pierre jaune de Neuchâtel (PJN); the Urgonien jaune (UJ); the marne de la Russille (MR); and the Urgonien blanc (UB). This succession was build as a synthetic sequence based on several stratotypic sections distributed on the whole Jura range, and considered as identical in any place. Although the dating of the Marnes d'Hauterive and the Pierre Jaune de Neuchâtel was roughly supported by the ammonites, the age attribution of the Urgonien Jaune and Urgonien Blanc has been riddled with incertitude and controversy (e.g., Arnaud-Vanneau and Arnaud 1990; Charollais et al. 2013).

Here we propose a new depositional model of this shallowing succession which frees itself from the confusion which was made between lithostratigraphic and chronostratigraphic concepts. During the last three years, more than thirty section

were relogged in high details, especially for the recognition of the discontinuity surfaces and marly layers which form isochronous time lines trough the Jura range (Figure 1). Additionally, robust palaeontological (cephalopods, ostracods, echinoids, and brachiopods) and geochemical data (carbon and oxygen stable isotopes, phosphorus) were used in order to calibrate these eustatic events.

First results unambiguously show a platform installation above hemipelagic sediments somewhere on the Burgey-Chartreuse area. This first phase is followed by a progradation of the platform, which moves toward the NE part of the Jura domaine. The MBH, the PJN, the UJ and the UB are diachronous and cogenetic facies which displace over time. A first phase of expansion is suddenly stopped by a drowning, the "Mid Barremian Event" (MBE; Coccioni et al., 2003) which lead to the deposition of condensed muddy sediments on the platform, the Russille marls. The platform recovered with a new oligotrophic carbonate production which purchased the initial progradation toward the NE before a final drowning event leading to the deposition of the Perte-du-Rhône Fm (PDR, Pictet et al. 2016). New datings show a diachronous age for each lithostratigraphic units which are older in the Meridional Jura and younger toward the Central Jura.

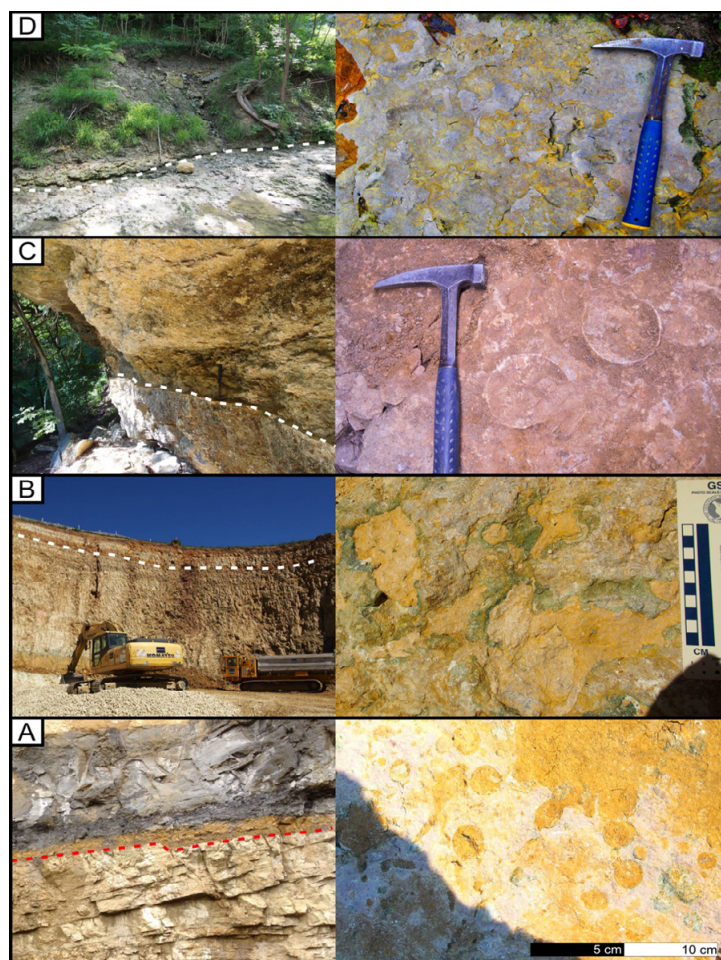


Figure 1. Discontinuity surfaces between: A) the Lower PJN and the Uttins Marl at Eclépens (VD, CH); B) the upper PJN and the UJ at St-Aubin (NE, CH); C) the UJ and the MR at Montcherand (VD, CH); D) the UB and the PDR Fm at Bellegarde-sur-Valserine (Ain, F).

REFERENCES

- Arnaud-Vanneau, A. & Arnaud, H. 1990: Hauterivian to Lower Aptian carbonate shelf sedimentation and sequence stratigraphy in the Jura and northern Subalpine chains (southeastern France and Swiss Jura). *Carbonate Platforms: Facies, Sequences and Evolution*. M. E. Tucker, J. L. Wilson, P. D. Crevello, J. R. Sarg and J. F. Read, Blackwell Scientific Publications, Special Publication of the International Association of Sedimentologists 9, 203-233.
- Charollais, J., Clavel, B., Granier, B., Busnardo, R. & Conrad, M.-A. 2013: Discussion of the paper by Godet et al., 2011, entitled "Reconciling strontium-isotope and K-Ar ages with biostratigraphy: the case of the Urgonian platform, Early Cretaceous of the Jura Mountains, Western Switzerland" (*Swiss Journal of Geosciences*, 104, 147-160). *Swiss. J. Geosci.* 106/3, 559-567.
- Coccioni, R., Galeotti, S. & Spovieri, M. 2003: The Mid-Barremian Event (MBE): the Prelude to the OAE1a. American Geophysical Union, Fall Meeting 2003, abstract #PP41B-0835.
- Pictet, A., Delamette, M. & Matron, B. 2016: The Perte-du-Rhône Formation, a new Cretaceous (Aptian-Cenomanian) lithostratigraphic unit in the Jura Mountains (France and Switzerland). *Swiss Journal of Geosciences* (in press).

P 6.1

Study of microfacies, sedimentary environment and Diagenetic processes of the Qom formation in the southwest of Sorkheh (Semnan)

Mohammad khojastefar¹, Reza aharipour²

¹ *Sedimentary petrology and sedimentology, M.Sc., Faculty of science, department of geology, Islamic azad university, Shahrood Branch, Shahrood, Iran. (moh.khojaste@yahoo.com)*

² *Assistant Professor, Faculty of geology science, Damghan university, Damghan, Iran.*

The early Miocene Qom Formation in southwest Sorkheh (south of the Abdullah Abad village) section includes succession of carbonate and evaporate rocks in the southern flank of Central Albourz Mountains. This formation located over the Lower Red Formation with a disconformity and the upper boundary of this formation in this region due to probably tectonic activity not visible (fig.1).

Qom Formation in the studied section contains 217 m. thick and is divided into four sedimentary units. Unit 1 is composed of alternation of white limestone and green marl. Unit 2 is composed of gray marl and thin layers gypsum and also more a thick layer of gypsum. Unit 3 is composed of alternation of white limestone and green and gray marl. Unit 4 is composed of thick layer of cream-colored limestone (fig.2).

In order to detailed analysis of sedimentary facies and sedimentary environment of the Qom Formation in the area, 35 thin sections had studied by using of polarized microscope. The results of study led to separation and recognition of 5 facies in the Qom Formation that have been deposited in 5 facies groups, involving: open marine (bioclastic wackestone-packstone), reef or bar (bioclastic packstone to grainstone and boundstone), lagoon (ostracod and bioclastic wackestone), tidal flat (gypsum). According to facies evidences, sediments of the Qom Formation in the study area is formed in Aquitanian to Burdigalian stages (Early Miocene) and deposited in carbonate ramp platform environment. Most facies represents the shallow water with a limited sea level changes (fig.3). The main diagenesis processes in the Qom Formation includes cementation, micritization, neomorphism, replacement and porosity that formed in meteoric, marine and funeral diagenetic environments (Tucker & Wright, 1990).

REFERENCES

Tucker, M., and V. P., Wright, 1990, Carbonate Sedimentology: Blackwell Scientific, 482 p.

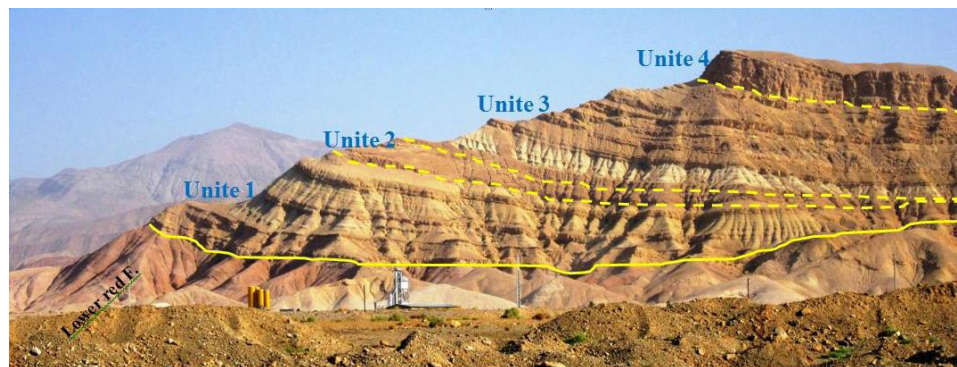


Figure 1. Overview and units, the Qom Formation in Abdullah Abad section in sight to the north

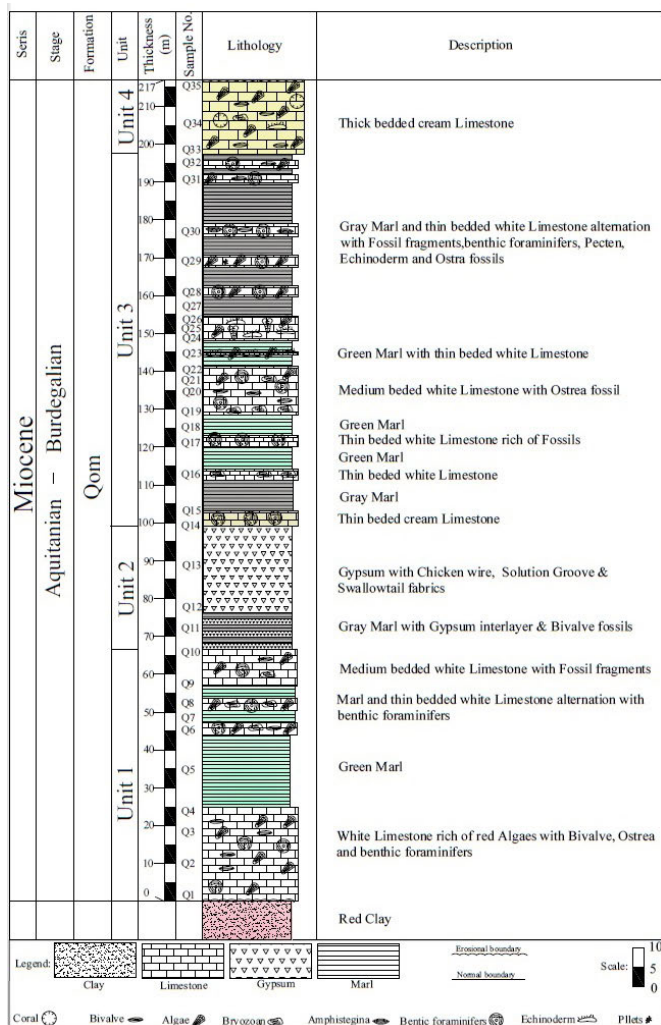


Figure 2. stratigraphic column of Qom Formation in the South West of Sorkeh

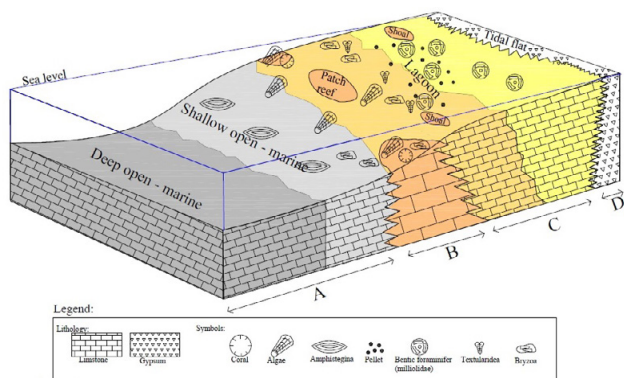


Figure 3. The environment of the Qom Formation in the South West of Sorkeh

P 6.2

About Konkian/Sarmatian Boundary of Georgia Based on Foraminifera

Kakhaber Koiava¹, Jon Mosar², Lia Kvaliashvili³ & Jeremiah Mauvilly²

¹ *Ivane Javakishvili State University, Alexandre Janelidze Institute of Geology, A. Politkovskaia str. 5, GEO-0186 Tbilisi (koiava_ka@yahoo.com)*

² *Département de Géosciences - Sciences de la Terre, Université de Fribourg, Chemin du Musée 6, CH-1700 Fribourg (mosar@unifr.ch)*

³ *LTD "GeoEngService", Ambrolauri str. 5, GEO-0160 Tbilisi*

In Eastern Paratethys the transition from the Konkian to the Sarmatian regional stage is characterized by a gradual change from rich Konkian stenohaline to poorer Sarmatian euryhaline foraminiferal assemblages. The reasons for this gradual replacement of the population are at present still being debated and it is responsible for the debate about the position of the Konkian/Sarmatian boundary. Some authors place the Konkian/Sarmatian boundary contemporaneously with the first occurrence of Sarmatian species whereas others place it at the level where a typical Sarmatian assemblage becomes well established.

The research material is collected in more than ten sections of Konkian and Sarmatian sediments in Eastern Georgia, besides, the study utilizes data on Konkian and Sarmatian foraminifera complexes of Eastern and Western Georgia, collected and specified by Djanelidze (1970) and Maissuradze (1971).

Analysis of the collected and existed data (Figure 1) indicates that foraminifera in Konkian sediments are presented by 56 species of 32 genera, out of them 38 species of 25 genera belong to Early Konkian (Sartaganian); 12 species of 7 genera to Early and Late Konkian, among them 9 species of 5 genera are also existed in Sarmatian age. 2 species of 2 genera belong to Late Konkian (Veseliankian), while the origin of the rest 4 species of 3 genera belongs to the Late Konkian and they continue existence in Sarmatian basin. Sarmatian sediments are characterized by small amount of foraminifera genera (17 types) and variety of species (93 species). It must be mentioned that the major portion of Lower Konkian foraminifera is presented by stenohaline species, while the most part of Late Konkian and Sarmatian foraminifera are presented by euryhaline species. Besides, from the phylogenesis viewpoint, the Late Konkian (Veseliankian) fauna is closer to Early Sarmatian rather than to Early Konkian. In Transylvania (Romania) on the boundary between Upper Badenian and Lower Sarmatian the «Tenuitellinata Zone» with planktonic foraminifera was distinguished (Filipescu & Silye, 2008). It should be noted that on the boundary between the Upper Sartaganian and Lower Veseliankian of Eastern Georgia (the gorges r. Arkhashen-su and r. Rusiani) the species *Tenuitella clemenciae* (Bermúdez) typical for «Tenuitellinata Zone» was discovered by us (Maissuradze et al., 2014). The similar foraminifera were also seen by O. Djanelidze in the same stratigraphical interval of Western Georgia in the gorge r. Dzimiti (unpublished data).

Based on the obtained results and taking into account the fact that existence of «Tenuitellinata Zone» in Georgia is indicated along the boundary of Upper Sartaganian and Lower Veseliankian, we can suggest that it will be correct to lay the boundary between the Konkian and Sarmatian regional stages along the Veseliankian bottom.

REFERENCES

- Djanelidze, O., 1970: Early and Middle Miocene Foraminifera of Georgia, "Mecniereba", Tbilisi, 172p. (In Russian)
- Filipescu, S., Silye, L. 2008: New Paratethyan biozones of planktic foraminifera described from the Middle Miocene of the Transylvanian Basin (Romania), *Geologica Carpathica*, 59, 6, 537–544.
- Maissuradze, L. S. 1971 Sarmatian Foraminifera of the West Georgia, "Mecniereba", Tbilisi, 120p. (In Russian)
- Maissuradze, L., Koiava, K., Kvaliashvili, L., & Spezzaferri, S. 2014: *Biodiversity, Evolution and Biostratigraphic Significance of Konkian Foraminifera of Eocene-Caspian Basin of Eastern Paratethys*, Proceedings of the Georgian National Museum, Natural Sciences and Prehistory Section, 6, 9-22.

7. Timing of Earth Processes: from dates to rates

Urs Schaltegger, Jörn-Frederik Wotzlav

TALKS:

- 7.1 Augland L.E., Jones M.T., Svensen H. & Tegner C.: Closing in on the Palaeocene-Eocene Thermal Maximum in the North Atlantic: chronostratigraphy and ash bed provenance through high precision U-Pb and Lu-Hf isotopic analyses of zircons
- 7.2 Baresel B., Bucher H., Bagherpour B., Brosse M., Guodun K., Schaltegger U.: Timing of global regression and microbial bloom marking the Permo-Triassic mass extinction
- 7.3 Buret Y., von Quadt A., Wotzlav J.F., Roozen S., Heinrich C.A.: Linking the timing of porphyry Cu deposit formation to nearby volcanism using zircon geochemistry and high-precision CA-ID-TIMS geochronology
- 7.4 Farina F., Dini A., Ovtcharova M., Bouvier AS., Baumgartner L., Schaltegger U.: Petrogenesis of the two mica-cordierite granites from the Larderello-Travale geothermal field revealed by oxygen isotopes and high-precision zircon U-Pb geochronology
- 7.5 Mintrone M., Moyen J.F., Chelle-Michou C., Caddick M., Couzinié S., Vézinet A., Laurent O.: Contrasted rates of melting and exhumation of a post-orogenic crust: an integrated thermodynamic, geochronologic and thermo-chronologic study
- 7.6 Naumenko-Dèzes M., Nägler T.F., Mezger K., Villa I.M.: Constraining the 40K decay constant for Ar-Ar dating
- 7.7 Rezeau H., Moritz R., Wotzlav J.F., Tayan R., Hovakimyan S., Ulianov A.: Timing of collisional magmatism in the southernmost Lesser Caucasus: Insights from geochronology and geochemistry
- 7.8 Rubatto D., Boston K., Hermann J., Engi M., Amelin Y.: U-Pb geochronology of mid-grade metamorphism in the Central Alps: when zircon is not an option
- 7.9 Schoene, B.: KEYNOTE: Evaluating and improving the gold standard: ID-TIMS U-Pb geochronology applied to the stratigraphic record
- 7.10 Szymanowski D., Wotzlav J.F., Ellis B.S., Bachmann O., von Quadt A.: Prolonged low-temperature storage of supervolcanic magma reservoirs recorded by zircon and titanite petrochronology

POSTERS:

- P 7.1 Shengelia D., Tsutsunava T., Chichinadze G., Beridze G., Javakishvili I.: LA-ICP-MS local zircon U-Pb dating of Late Variscan granites of the Dzirula and Khrami crystalline massifs (Georgia)
- P 7.2 Loretz M., von Quadt A., Peytcheva I.: In-situ Sr measurements and Zircon analysis of aplitic dykes in Cu-Au-(Mo) porphyry deposit Elatsite, Bulgaria
- P 7.3 Magalhães J., Pedrosa-Soares A., Dussin I., Müntener O., Knauer L.G.: Statherian bimodal volcanic and anorogenic intrusive rocks in northern Guanhães Block, SE Brazil: an episode of continental rift
- P 7.4 Palacz Z.: High precision Nd isotope ratio measurements by Thermal Ionization Mass Spectrometer with Faraday collectors equipped with $1e^{12}$ ohm feedback resistors
- P 7.5 Schaltegger U., Davies J.H.F.L., Palacz Z.: First high-precision U-Pb dates from the new Phoenix TIMS at University of Geneva
- P 7.6 Sheldrake T., Caricchi L.: Variations in the frequency and magnitude of volcanic eruptions at arc volcanoes
- P 7.7 Storck J.-C., Brack P., Wotzlaw J.-F., Ulmer P., von Quadt A.: A geochronologic framework for Middle Triassic magmatism and sedimentation in the Southern Alps
- P 7.8 von Quadt A., Wotzlaw J.F., Buret Y., Large S., Peytcheva I., Szymanowski D.: Zircon U-Pb geochronology at the 0.1 ‰ level by ID-TIMS using 1013 Ω resistors
- P 7.9 Widmann P., Davies J., Schaltegger U.: The effect of chemical abrasion on zircon chemistry, crystal structure and ID-TIMS-U-Pb ages
- P 7.10 Wotzlaw J.F., Kremer K.: From discrete dates to continuous age: A systematic comparison of currently available age modeling software
- P 7.11 Davies J.H.F.L., Seydoux-Guillaume A.M., Heaman L., Marzoli A., Schaltegger U.: The response of Baddeleyite to radiation damage, and how this relates to Pb loss
- P 7.12 Lu Gang, Di Capua A., Winkler W., Willett S., von Quadt A., Fellin M.G., Rahn M., Brack P.: Discriminating age and type of detrital sources in the Taveyannaz Formation (Northern Alpine early foreland basin)
- P 7.13 Large S.J.E., von Quadt A., Wotzlaw J.F., Heinrich C.A.: Zircon petrochronology revealing the shallow-crustal magmatic evolution and timescales of mineralization at the Ok Tedi porphyry-skarn Cu-Au deposit

7.1

Closing in on the Palaeocene-Eocene Thermal Maximum in the North Atlantic: chronostratigraphy and ash bed provenance through high precision U-Pb and Lu-Hf isotopic analyses of zircons

Lars E. Augland¹, Morgan T. Jones¹, Henrik Svensen¹ & Christian Tegner²

¹ Centre for Earth Evolution and Dynamics (CEED), University of Oslo, PO Box 1028 Blindern, 0315 Oslo, Norway

² Centre of Earth System Petrology, Department of Geoscience, Aarhus University, Høegh-Guldbergs Gade 2, 8000 Aarhus C, Denmark

Zircon is a powerful tool in geochronology and isotope geochemistry, as its affinity for U and Hf in the crystal structure and the low initial Pb and Lu allow for precise and accurate dating by U-Pb ID-TIMS and precise and accurate determination of initial Hf isotopic composition by solution MC-ICP-MS analysis. The U-Pb analyses provide accurate chronostratigraphic controls on the sedimentary successions and absolute age frames for the biotic evolution across geological boundaries. Moreover, the analyses of Lu-Hf by solution MC-ICP-MS may provide a powerful fingerprinting tool to test the provenance of individual ash beds. Here we focus on ash beds from the Palaeocene-Eocene Thermal Maximum (PETM) in Fur, Denmark. In combination with available isotopic data from potential source volcanoes, these data are used to evaluate the provenance of PETM ashes in Denmark. If explosive eruptions from volcanic centres such as the North Atlantic Igneous Province (NAIP) can be traced to distal basins as ash layers, they provide robust tests of hypotheses of global synchronicity of environmental changes and biotic crises. In addition, the potential correlation of ash layers with source volcanoes will aid in constraining the extent of explosive volcanism in the respective volcanic centres. When combined with stable isotope data and biostratigraphy the new integrated data sets will also contribute to establish a new reference section for the study of this boundary event.

7.2

Timing of global regression and microbial bloom marking the Permian-Triassic mass extinction

Björn Baresel¹, Hugo Bucher², Borhan Bagherpour², Morgane Brosse², Kuang Guodun³ & Urs Schaltegger¹

¹ Department of Earth Sciences, University of Geneva, Rue des Maraîchers 13, 1205 Geneva, Switzerland (bjorn.baresel@unige.ch)

² Paleontological Institute and Museum, University of Zurich, Karl Schmid-Strasse 4, 8006 Zurich, Switzerland

³ Guangxi Bureau of Geology and Mineral Resources, Jiangzheng Road 1, 530023 Nanning, China

New high-resolution U-Pb dates lead to a minimal duration of 68 kyr for the Permian part of the hiatus straddling the Permian-Triassic boundary (PTB) in shallow water settings of the Nanpanjiang Basin (South China) and to a duration of 37 ± 61 kyr for the next overlying microbial limestone. The timing of the hiatus is similar to that of the extinction interval in the Meishan Global Stratotype Section and Point. Sedimentation rates across the PTB indicate a seven-fold decrease compatible with a global cool climate during the Griesbachian and the glacio-eustatic low stand needed for the genesis of the worldwide hiatus straddling the PTB in shallow water sections. The timing of the hiatus is synchronous with the initial explosive phase of the Siberian Traps that likely released sulfur volatiles into the stratosphere, thus eliciting a short-lived ice age, a global low-stand, and acidified sea water. In a second step, the protracted build-up of volcanogenic CO₂ induced a transient cool climate until greenhouse conditions were reached not earlier than 500 kyr after the main extinction episode, as indicated by terrestrial plants.

7.3

Linking the timing of porphyry Cu deposit formation to nearby volcanism using zircon geochemistry and high-precision CA-ID-TIMS geochronology

Yannick Buret¹, Albrecht von Quadt¹, Jörn-Frederik Wotzlaw¹, Stan Roozen¹ & Christoph Heinrich¹

¹ *Institute of Geochemistry and Petrology, Department of Earth Sciences, ETH Zurich, Clausiusstrasse 25, 8092 Zurich, Switzerland. (yannick.buret@erdw.ethz.ch)*

Porphyry Cu deposits represent the interface between plutonic and volcanic domains of upper crustal magmatic systems. These deposits are typically composed of multiple porphyritic intrusions which bracket the maximum duration of ore formation to several 10⁴ years (Buret et al., 2016) and are commonly intruded into the base of volcanoes. The relationship between volcanic activity and porphyry stocks is often difficult to establish, as they are rarely exposed together unless later faulting and/or tilting occurred (Dilles, 1987). In order to investigate the relationships between extrusive magmatism and porphyry Cu formation we compare zircon petrochronology from late stage volcanic units with the nearby world class Bajo de la Alumbrera porphyry Cu deposit, from the Late Miocene Farallón Negro Volcanic Complex (FNVC).

In this study we texturally characterise zircon crystals by CL-imaging prior to obtaining in-situ geochemical and geochronological information by LA-ICP-MS. Analysed zircon grains were then extracted and analysed by high precision CA-ID-TIMS. This approach has the two-fold benefit of screening for inherited cores, and obtaining texturally defined geochemical information, prior to dissolution of the zircon crystal for CA-ID-TIMS analysis. This approach permits us to establish temporal and chemical links between studied volcanic and porphyry units in the FNVC.

The results of this study suggest a close temporal and genetic link between the Bajo de la Alumbrera porphyry Cu deposit and the late stage volcanism at the FNVC. Voluminous explosive volcanism immediately following porphyry formation has important implications for the thermal and rheological state of the magma that is parental to the porphyries and fed the eruption. Further work investigating the geochemistry of other accessory and major minerals could shed further light on the evolution of the magmatic body prior to eruption/ emplacement.

REFERENCES

- Buret, Y., von Quadt, A., Heinrich, C., Selby, D., Wälle, M. & Peytcheva, I. 2016: From a long-lived upper-crustal magma chamber to rapid porphyry copper emplacement: Reading the geochemistry of zircon crystals at Bajo de la Alumbrera (NW Argentina). *Earth and Planetary Science Letters*, 450, 120-131.
- Dilles, J. 1987: Petrology of the Yerington Batholith, Nevada; evidence for evolution of porphyry copper ore fluids, *Economic Geology*, 82, 1750-1789.

7.4

Petrogenesis of the two mica-cordierite granites from the Larderello-Travale geothermal field revealed by oxygen isotopes and high-precision zircon U-Pb geochronology

Federico Farina¹, Andrea Dini², Maria Ovtcharova¹, Anne-Sophie Bouvier³, Lukas Baumgartner³, Urs Schaltegger¹

¹ Department of Earth Sciences, University of Geneva, Rue de Maraîchaire 13, CH-1205 Genève, Switzerland.

² Istituto di Geoscienze e Georisorse, Area della Ricerca CNR di Pisa, Via Moruzzi 1, 56124, Pisa, Italy.

³ Institute of Earth Sciences, University of Lausanne, Géopolis, 1015 Lausanne, Switzerland.

The Larderello-Travale geothermal field in southern Tuscany (Italy), is the site of a large-scale steam-dominated geothermal anomaly which has been industrially exploited since the 1950s. The deepest part of the system (below ca. 2500-4000 m) is constituted by a plutonic complex built up incrementally between ca. 3.8 and 1.3 Ma by progressive stacking of granite magma batches having different isotopic and geochemical signature (Dini et al., 2005). The Larderello-Travale plutonic system is formed by high-silica (68-78% SiO₂) peraluminous two-mica and cordierite-bearing granites exhibiting pronounced crustal isotopic signature (⁸⁷Sr/⁸⁶Sr ranging 0.715-0.721).

We report the first results from zircon crystals of the Larderello-Travale plutonic system, obtained from granite samples cored at 3.0-4.5 km depths. In this study, we combine imaging of growth textures with in-situ oxygen isotopic data and high-precision U-Pb dates to constrain the petrogenetic evolution of the Larderello-Travale granites. Cathodoluminescence images of zircon grains reveal a complex magmatic crystallization history for these zircons; i.e. featureless CL-bright crystals, core-to-rim fine-scale oscillatory zoned grains, convoluted zoning and irregular and lobate cores overgrowth by oscillatory zoned rims.

Oxygen isotopic data were obtained from the SwissSIMS ion microprobe. Zircon δ¹⁸O values range between 7‰ and 13‰, and the different granites exhibit different mean oxygen isotopic values. The sample displaying the highest oxygen isotopic values has an average δ¹⁸O of 11.6‰ (SD = 1.0), the one with the lowest mean values has δ¹⁸O of 9.3‰ (SD = 0.6). Zircon grains exhibit significant inter- and intra-crystal oxygen isotopic heterogeneity, with intra-sample δ¹⁸O variability of 2-3‰. Noteworthy, this variability is one order of magnitude greater than the reproducibility determined on a Temora zircon reference material (2SD = 0.28‰).

High-precision zircon U-Pb geochronological data were performed through chemical abrasion thermal ionization mass spectrometry (CA-ID-TIMS) on the same grains previously analysed by SIMS. Preliminary results from two granites previously analysed by SIMS show that the Larderello-Travale granites record 200–300 kyr of zircon growth. This large spread in age suggests that most of the zircon crystals formed before the final shallow-level emplacement of the granites.

We propose a model in which zircon grains crystallized from isotopically distinct magma batches, reflected by the significant intra-sample range in δ¹⁸O, generated by partial melting of different fertile metasedimentary crustal sources. In our model, the different source rocks do not start melting synchronously. In fact, the exact time at which a rock start melting depends on the interplay between the evolution of the thermal anomaly in the crust and the position of the liquidus in the P-T space, with the latter parameter mostly depending on the composition of the source rock. The non-simultaneous melting of the different crustal sources reflects on their cooling paths and thus on the timing of zircon crystallization (i.e. on the U-Pb zircon ages). Finally, all these isotopically diverse zircon-bearing magma batches were assembled at shallow-level into a single pluton.

This study was performed in the frame of the Marie Skłodowska-Curie Project "MIGRATE" (Standrad EF – 701494) and Horizon 2020 European Project "DESCRAMBLE" (640573, Topic LCE-02-2014). Samples were kindly provided by ENEL Green Power (Italy).

REFERENCES

Dini, A., Gianelli, G., Puxeddu, M., Ruggieri, G., 2005: Origin and evolution of Pliocene–Pleistocene granites from the Larderello geothermal field (Tuscan Magmatic Province, Italy), *Lithos*, 81, 1-31.

7.5

Contrasted rates of melting and exhumation of a post-orogenic crust: an integrated thermodynamic, geochronologic and thermochronologic study

Michaël Mintrone¹, Jean-François Moyen¹, Cyril Chelle-Michou^{1,2}, Mark Caddick³, Simon Couzinié¹, Adrien Vézinet¹ & Oscar Laurent⁴

¹ Univ. Lyon, UJM-Saint-Etienne, UBP, CNRS, IRD, Laboratoire Magmas et Volcans UMR 6524, F-42023 Saint Etienne, France (michael.mintrone29@gmail.com)

² Department of Earth Sciences, UNIGE, 13 rue des Maraîchers, 1205 Geneva, Switzerland

³ Virginia Tech, Department of Geosciences, 1405 Perry ST, Blacksburg, VA 24061, USA

⁴ Université de Liège, Département de Géologie B20, Quartier Agora, allée du six Août 12, B-4000 Liège, Belgium. Now at ETH, Inst. für Geochemie und Petrologie, Clausiusstrasse 25, 8092 Zürich, Switzerland

Constraining the duration of metamorphic processes remains a challenge. Radiometric approaches, especially in-situ, are powerful tools but it remains difficult to tie a date to a specific point along a P–T path. An alternative consists in modelling garnet diffusion profiles to estimate metamorphic time scales (Caddick et al., 2010). This approach is anchored on the definition of a P–T path for the studied rock as precise as possible using phase equilibria modelling. Then, at each step of the P–T path, the composition of each new garnet increment will evolve as a function of P, T and X, but also by intra-crystalline diffusion which will similarly affect the previous garnet increments (largely a function of time and temperature). As a result, it is possible to build a synthetic garnet chemical zoning profile as a function of the P–T path defined for the whole sample and to constrain the rate of the metamorphic evolution that best matches the actual garnet zoning profiles.

We applied this approach to a high temperature (melting) episode in a tardi-orogenic crust, the Hercynian belt of the French Massif Central. There, a large anatectic core complex (the Velay dome) cuts across the Carboniferous nappe stack. We investigated three samples, one in the core of the dome, one from a klippe on top of it, and one from the nappe stack outside of the dome. Using diffusion modelling, we demonstrate that the duration of the exhumation from peak metamorphic conditions was on the order of 10–20 Ma for the samples outside and on top of the dome; but of only 1–10 Ma for the sample in the core of the dome, corresponding to an ultra-fast exhumation rate of 1–10 mm/a. In addition, the sample in the core of the dome record a rapid melting event (peak conditions) on the order of ~1 Ma.

Thermochronology (Ar–Ar on biotite and apatite fission tracks) within the dome also reveal comparably rapid exhumation and cooling rates at the end of the Carboniferous. In contrast, existing radiometric ages (U–Pb on monazites) outside of the dome, and in the klippen on top of it, point to a long-lived period of protracted monazite growth corresponding to a multi-million-year thermal anomaly in the orogenic crust. This further emphasizes the difference between the undisturbed nappe pile, that evolved at “normal” orogenic paces (10’s of Ma); and the anatectic dome, that reflects a very quick event of melting and exhumation (~1 Ma). Our study demonstrates the potential of the garnet diffusion approach to characterize the rate of metamorphic evolution and dynamics at play in an orogenic crustal segment.

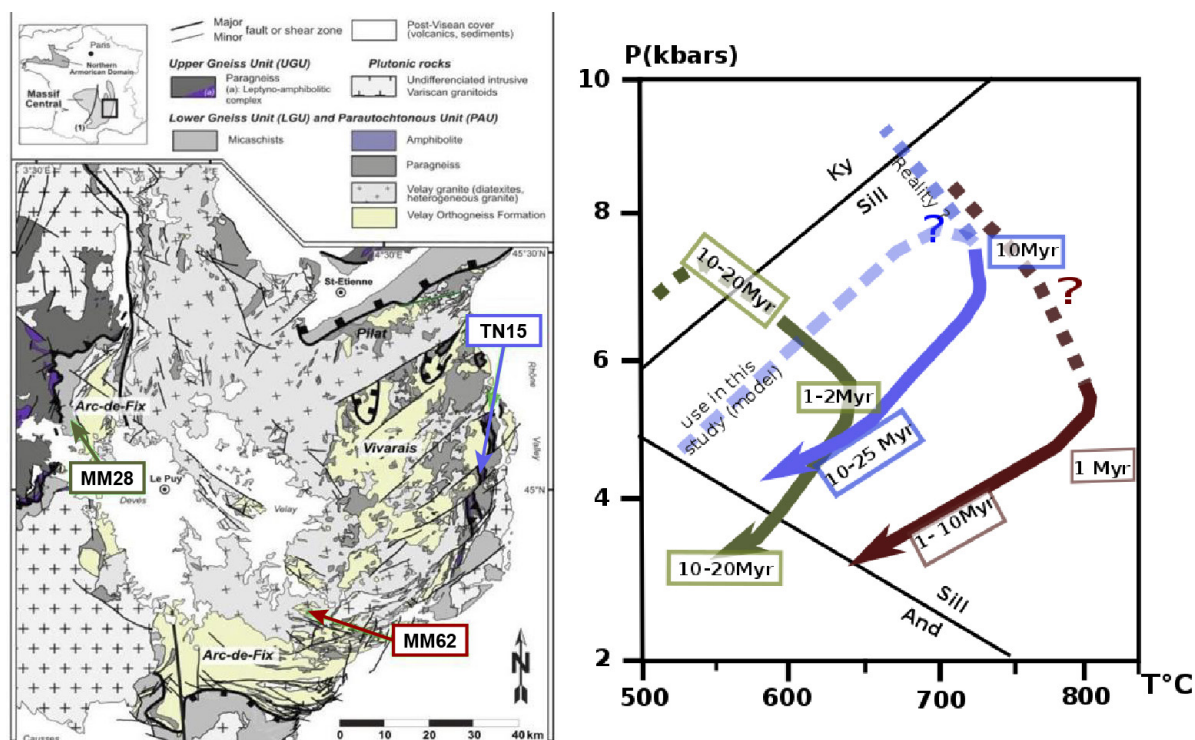


Figure 1. (left) Geological map of the Velay complex in French Massif Central (Couzinié et al., submitted), with sample locations. (right) P—T paths (and duration) of the « Velay » event in the core of the dome (red, MM62) ; outside of the dome (green, MM28) ; and in the klippe on top of it (blue, TN15).

REFERENCES

- Caddick, M.J., Konopásek, J. and Thompson, A.B., 2010. Preservation of garnet growth zoning and the duration of prograde metamorphism. *Journal of Petrology*, 51(11): 2327-2347.
- Couzinié, S. et al., submitted. The Neoproterozoic basement of the eastern Massif Central (Variscan belt, France). *Comptes Rendus Academie des sciences Geoscience*.

7.6

Constraining the ^{40}K decay constant for Ar-Ar dating

Maria Naumenko-Dèzes^{1,2}, Thomas F. Nägler¹, Klaus Mezger¹, Igor M. Villa^{1,3}

¹ Institut für Geologie, Universität Bern, Baltzerstrasse 1+3, 3012, Bern, Switzerland (marie@geosphere.ch)

² Université Nice Sophia Antipolis, Géoazur, Sophia Antipolis, 250 rue A. Einstein, 06560 Valbonne, France

³ Università di Milano Bicocca, Piazza della Scienza 4, 20126 Milano, Italy

Ar-Ar is one of the most used dating systems and its accuracy plays an important role in constraining the age of planets, duration of geological processes and their sequence of occurrence. This system has been reported to give ages that are ca. 1% younger than U-Pb ages. The discrepancies between the two mostly used and precise geochronometers, U-Pb and Ar-Ar, have been a subject of critical reviewing (e.g. Renne et al. 2010, and refs. therein) and were attributed to a systematic offset of the ^{40}K decay constant. Multiple attempts to recalibrate the constant did not achieve consistency and resulted in a prominent variance among the published values for the ^{40}K decay constant. Currently a few different ^{40}K decay constants are in use (e.g. Steiger and Jäger, 1977, Min et al., 2000, the discrepancy between ages calculated with these two constants being ca. 1.5 %).

The Ar-Ar geochronometer is based on the radioactive decay of the ^{40}K isotope to ^{40}Ar and ^{40}Ca . The intercalibrations of three dating systems: U-Pb (the main reference), Rb-Sr (the consistency check) and K-Ca (the unknown), allowed us to better constrain the ^{40}K decay constant.

Tree samples, selected from a shortlist of ten with known U-Pb ages, were investigated (a) to evaluate if they meet the requirement of a geological “point-like” history (Begemann et al, 2001) (i.e. “instantaneous” formation and subsequent ideal closure of chronometers) and (b) to narrow down the systematic uncertainty on the ^{40}K decay constant by investigating the metrologically traceable K-Ca decay constant. Only the samples from the Phalaborwa complex represent a “point-like” magmatic event and meet all criteria to make them suitable for the ^{40}K decay constant intercalibration. The Rb-Sr age of this sample is 2058.9 ± 5.2 Ma and agrees with the age determined by Nebel et al. (2010) and with published U-Pb ages.

Applying our refined Ca measurement protocol (Naumenko-Dèzes, 2015) the K-Ca age was determined to 2040 ± 13 Ma, applying the constants of Steiger&Jäger (1977). Forcing the K-Ca isochron slope to give an age coincident with the U-Pb and Rb-Sr ages (fig.1) gives one equation with two unknowns. Assuming that the branching ratio of the K-Ca branch, B_{Ca} , lies in the interval ($k=2$) of all published references, i.e. $0.8925 < B_{\text{Ca}} < 0.8963$, the most reliable uncertainty interval ($k=2$) for the total ^{40}K decay constant, λ_{tot} , is calculated as $5.484 \cdot 10^{-10} \text{ a}^{-1} < \lambda_{\text{tot}} < 5.498 \cdot 10^{-10} \text{ a}^{-1}$. This confirms that the presently used IUGS recommendation is inaccurate.

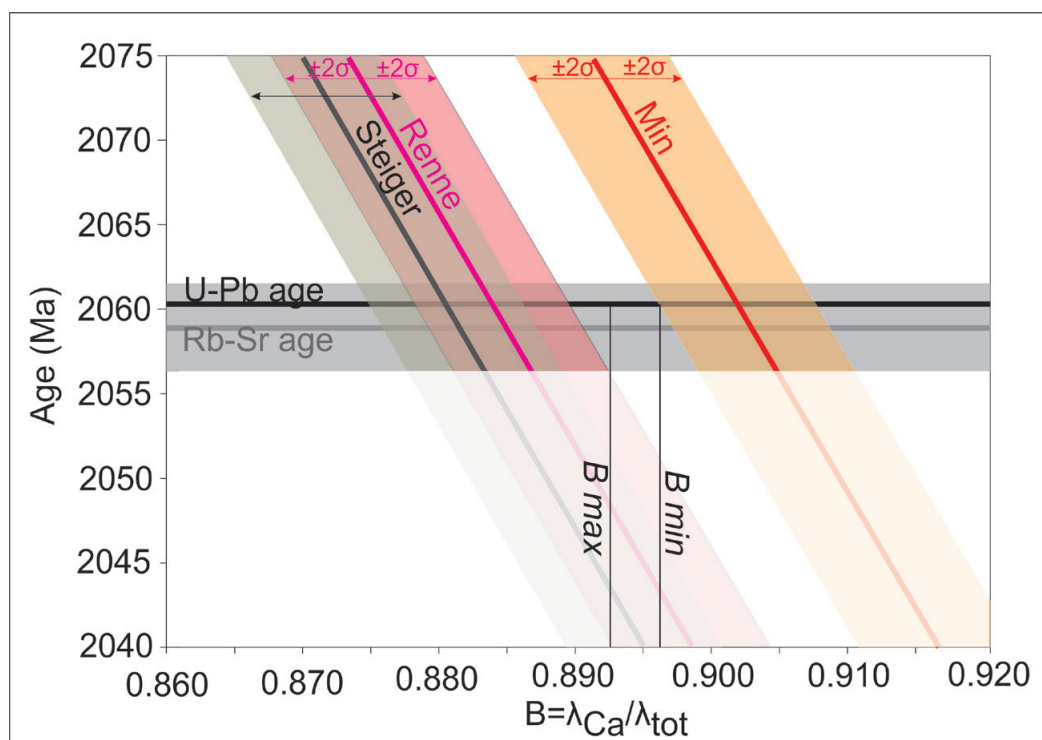


Figure 1. K-Ca age of Phalaborwa phlogopite changes along sloping lines as a function of assumed branching ratio B , calculated with the total ^{40}K decay constant of Steiger&Jäger (1977), Renne *et al.* (2011) and Min *et al.* (2000).

REFERENCES

- Begemann et al. (2001) *Geochim. Cosmochim Acta* 65, 111-121;
Min et al. (2000) *Geochim. et Cosmochim. Acta* 64, 73-9.
Naumenko-Dèzes et al. (2015) *Int. J. of Mass Spectr.* 387, 60-68;
Nebel et al (2010) *GCA* 74, 5349;
Renne et al. (2010) *Geochim. Cosmochim Acta* 74, 5349-5367;
Steiger&Jäger (1977) *Earth and Plan. Sci. L.* 36, 359-362.

7.7

Timing of collisional magmatism in the southernmost Lesser Caucasus: Insights from geochronology and geochemistry

Hervé Rezeau¹, Robert Moritz¹, Jörn-Frederik Wotzlaw², Rodrik Tayan³, Samvel Hovakimyan^{1,3}, & Alexey Ulianov⁴

¹ *Department of Earth Sciences, University of Geneva, CH-1205 Geneva, Switzerland (herve.rezeau@unige.ch)*

² *Institute of Geochemistry and Petrology, ETH Zurich, 8092 Zurich, Switzerland*

³ *Institute of Geological Sciences, National Academy of Sciences, 0019 Yerevan, Armenia*

⁴ *Institute of Earth Sciences, University of Lausanne, 1015 Lausanne, Switzerland*

The Meghri-Ordubad pluton (MOP) is exposed over ~1000 km² in southern Armenia, Lesser Caucasus. It is located in the central part of the Tethyan orogenic belt extending from the Alps through the Carpathians–Balkans, Turkey, Iran, and Pakistan, Tibet, and Indochina. The MOP is described as a composite pluton emplaced during a subduction-related to a post-subduction evolution (Moritz et al., 2016). A new exhaustive zircon U-Pb geochronology survey revealed an incremental growth of the MOP during three compositionally distinct magmatic episodes over ~30 m.y., including (1) Middle Eocene (48.9–43.1 Ma) calc-alkaline magmatism lasting 5.8 ± 0.8 m.y., followed by (2) Late Eocene–Middle Oligocene (37.8–28.1 Ma) shoshonitic magmatism over 9.7 ± 0.9 m.y., and (3) Late Oligocene–Early Miocene (26.6–21.2 Ma) adakitic magmatism consisting of lamprophyres and high-K calc-alkaline granodioritic magmas emplaced over 5.4 ± 0.4 m.y. (Rezeau et al., 2016). Despite the distinct geodynamic settings and magma compositions of these intrusive suites, complementary in situ zircon hafnium ($\epsilon\text{Hf}_{\text{zircon}} = +8$ to $+11.3$) and oxygen ($\delta^{18}\text{O}_{\text{zircon}} = +4.6\text{‰}$ to $+6.0\text{‰}$) isotope data support a mantle-dominated magma source with limited crustal contribution (Rezeau et al., 2016).

Both of these intrusive suites are enriched in LILE, U, Th and LREE and have pronounced negative Nb-Ta depletion, geochemical hallmarks of subduction zone-related magmas. However, whole-rock major and trace element geochemical ratios differ significantly over time. The first transition from Middle Eocene to Late Eocene–Middle Oligocene is marked by a substantial increase in $\text{K}_2\text{O}/\text{Na}_2\text{O}$, Nb/Ta (suprachondritic), Ba/Ce, Th/Yb, Sr/Y, La/Yb, Gd/Yb ratios for similar SiO_2 and Mg# content. The calc-alkaline serie points toward a metasomatism of the mantle wedge by a fluid-flux from the subducted slab during Middle Eocene magmatism, whereas the following Late Eocene–Middle Oligocene shoshonitic intrusions are either dominated by a slab-melt enrichment (oceanic crust/subducted sediments) that hybridized the mantle wedge source and/or by subsequent low partial melting of previously fractionated lower-crustal cumulates. The second transition from Late Eocene–Middle Oligocene to Late Oligocene–Early Miocene is characterized by a marked increase in Mg#, Ni and Cr content, and a decrease in Al_2O_3 content with similar high $\text{K}_2\text{O}/\text{Na}_2\text{O}$, Sr/Y, La/Yb ratios. These characteristics together with a high $\epsilon\text{Hf}_{\text{zircon}}$ values ($+9.5$ to $+11.3$) likely reflect an input of juvenile magma mixed with the previously metasomatized mantle wedge. Lamprophyres (minette, spessartite) are generally related to the melting of a phlogopite-rich mantle source and the combined high Sr/Y ratio and low Al_2O_3 content indicate a limited plagioclase fractionation due to partial melting initiated at higher pressure or with higher H_2O content (>4wt. %).

The geochemical composition variations of these intrusive suites emplaced at the same location over ~30 m.y. can be explained by a change in subduction geometry such as slab steepening and concomitant crustal growth, followed by an input of juvenile mantle during convective removal of the sublithosphere (Platt and England, 1994; Turner et al., 1999) or by slab break-off (Davies and von Blanckenburg, 1995) during the late stage of collisional magmatism. From a regional geodynamic point of view, it can be interpreted as an evolution from an active subduction-related transitional to a collisional/post-collisional magmatism. In this case, the first transition would correspond to the onset of the collision magmatism at ca. 42–38 Ma (Arabia–Eurasia collision) and the second transition is ascribed to the initiation of the orogen collapse at ca. 28–26 Ma. The timeframe of 10–15 m.y. for this geodynamic evolution is in agreement with the literature (Platt and England, 1994; Turner et al., 1996; Kaislaniemi et al., 2014) as well as the timing for the Arabia–Eurasia collision (e.g., Moritz et al. 2016).

REFERENCES

- Davies, J. H. & von Blanckenburg, F. (1995) Slab breakoff: a model of lithospheric detachment and its test in the magmatism and deformation of collisional orogens. *Earth and Planetary Science Letters*, 129, 85–102.
- Kaislaniemi, L., Van Hunen, J., Allen, M. B., & Neill, I. (2014) Sublithospheric small-scale convection - A mechanism for collision zone magmatism. *Geology*, 42, 291–294.
- Moritz, R., Rezeau, H., Ovtcharova, M., Tayan, R., Melkonyan, R., Hovakimyan, S., Ramazanov, V., Selby, D., Ulianov, A., Chiaradia, M., & Putlitz, B. (2016) Long-lived, stationary magmatism and pulsed porphyry systems during Tethyan subduction to post-collision evolution in the southernmost Lesser Caucasus, Armenia and Nakhitchevan. *Gondwana Research*, 37, 465–503.
- Platt, J. P. & England, P. C. (1994) Convective removal of lithosphere beneath mountain belts: thermal and mechanical consequences. *American Journal of Science* 294, 307–336.

- Rezeau, H., Moritz, R., Wotzlaw, J. F., Tayan, R., Melkonyan, R., Ulianov, A., Selby, D., d'Abzac, F-X., & Stern, R. A. (2016) Temporal and genetic link between incremental pluton assembly and pulsed porphyry Cu-Mo formation in accretionary orogens. *Geology*, 44, 627-630.
- Turner, S. P., Platt, J. P., George, R. M. M., Kelley, S. P., Pearson, D. G., & Nowell, G. M. (1999) Magmatism associated with orogenic collapse of the Betic–Alboran domain, SE Spain. *Journal of Petrology*, 40, 1011-1036.
- Turner, S., Hawkesworth, C., Gallagher, K., Stewart, K., Peate, D. & Mantovani, M. (1996) Mantle plumes, flood basalts, and thermal models for melt generation beneath continents: assessment of a conductive heating model and application to the Paraná. *Journal of Geophysical Research* 101, 11503–11518.

7.8

U-Pb geochronology of mid-grade metamorphism in the Central Alps: when zircon is not an option

Daniela Rubatto¹, Katherine Boston², Joerg Hermann¹, Martin Engi¹ & Yuri Amelin²

¹ *Institut für Geologie, University of Bern, Baltzerstrasse 1-3, CH-3012 Bern, (daniela.rubatto@geo.unibe.ch)*

² *Research School of Earth Sciences, Australian National University, Acton, 2601, ACT, Australia*

Large portions of the Earth's crust record mid-grade metamorphism under greenschist- to amphibolite-facies conditions. Geochronology of such terranes is complicated by overprinting deformation and recrystallization stages of minerals and possibly protracted metamorphic cycles. At this metamorphic grade zircon has low reactivity, hence accessory minerals such as monazite, allanite, rutile and titanite are more suitable for U-Th-Pb age determination. Multiple generations of these minerals commonly form in different rock types over the protracted evolution of Barrovian amphibolite-facies terranes. Age determination must thus be coupled with petrological constraints on mineral-forming reactions and P-T conditions. Geochronology of these minerals have different strengths and difficulties, such as the presence of common Pb, low U content, different reactivity and uncertain closure temperature, which may reduce accuracy and precision of age determinations. A mineral-specific approach to U-Th-Pb analysis and data treatment is required, and dating of multiple minerals in the same rock and comparison of ages from diverse lithologies, both locally and over regional scale, increase reliability of the ages.

Accessory minerals allanite, monazite and rutile from amphibolite facies rocks across the Barrovian sequence of the Central Alps (Switzerland) were investigated for composition and U-Th-Pb ages. Allanite and monazite preserve distinct growth zones and were dated in situ by SHRIMP ion microprobe. Rutile geochronology was performed by ID-TIMS to improve precision. The growth ages of these minerals record stages of prograde and peak metamorphism (Fig. 1) and give insights into the relative stability of monazite and allanite, as well as rutile closure temperature.

Allanite formed during the prograde path at 33-26 Ma. Allanite crystals are aligned along an early penetrative foliation that is overprinted by later generations of mica. Rutile from one metapelite at Alpe Sponda records the age of 33.45 ± 0.37 Ma, consistent with the age of allanite. Zr-in-rutile thermometry yields a temperature of 550 ± 20 °C, which is lower than the 620 °C deduced from the main mineral assemblage, indicating that rutile crystallized under prograde conditions. We interpret this early age as the time when the rocks reached maximum pressure conditions.

A later metamorphic stage at higher T is recorded in monazite and rutile, and in allanite rims in one sample. Monazite in two samples from the Western and Central Lepontine yields an age of ~22 Ma and grew at the expense of allanite and after the first stage of garnet growth. In monazite-bearing samples, allanite is preserved as inclusions in garnet, whereas monazite is part of the matrix. Zr-in-rutile thermometry suggests that ~23 Ma rutile in a calcschist records the timing of 560-600 °C in the western Lepontine at Robiei. Allanite rims in one metapelite from the same area crystallized at 19.7 ± 1.3 on older (27 Ma) cores, and are also interpreted to reflect the timing of peak to retrograde conditions.

Through multi-mineral geochronology a metamorphic history that spans 10 Ma can be reconstructed: from prograde greenschist-facies to peak amphibolite-facies conditions. The observation that 33 Ma prograde rutile is preserved despite the later temperature peak at 22 Ma suggests a closure temperature of Pb in rutile in excess of 620 °C.

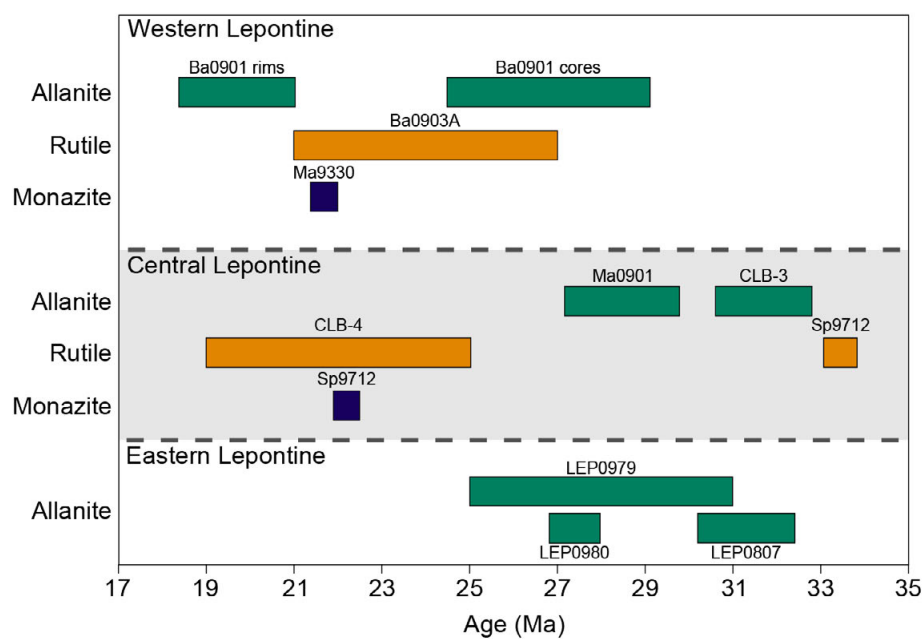


Figure 1. Summary of geochronology results grouped by area (Western, Central and Eastern Lepontine) and by mineral dated. Sample locations and numbers: Robiei (Ba0901/0903), Croveo (Ma9330), Campolungo (Ma0901, CLB-3/-4), Alpe Sponda (Sp9712), Forcola (LEP0979/0980/0807).

7.9

Evaluating and improving the gold standard: ID-TIMS U-Pb geochronology applied to the stratigraphic record.

Blair Schoene¹

¹ *Department of Geosciences, Princeton University, Princeton, NJ 08544, USA (bschoene@princeton.edu)*

U-Pb zircon ID-TIMS geochronology of volcanic ashbeds is a powerful and widespread method of calibrating processes recorded in the stratigraphic record, from biotic evolution to environmental change. There are more U-Pb dates pinning the geologic timescale than any other geochronologic method, and so assessing the accuracy of these dates while pushing for increased precision is an ongoing task. This contribution summarizes recent improvements in the precision and accuracy of ID-TIMS U-Pb geochronology, highlights current limitations, and offers some ways forward, giving examples from ongoing projects.

Driven by the EARTHTIME initiative, U-Pb ID-TIMS labs around the world have increased collaboration and communication to assess laboratory protocols, sample preparation techniques, and standard reproducibility. Mixing and distribution of community tracers for isotope dilution have helped eliminate sources of interlab biases and enable the traceability of U-Pb dates to first principle experiments, permitting more accurate comparison to other dating techniques and cyclostratigraphy. Synchronous increases in analytical precision have been facilitated by improved lab techniques and better mass spectrometry. Dates from single ashbed zircons and zircon fragments are commonly far more precise than the timescales of zircon growth within upper crustal magmatic systems that source eruptions. Thus, uncertainty in relating such data to the process we actually want to date – ashbed eruption – limits the accuracy of timescale calibration and global correlation of events.

There is currently no consensus on how to interpret a dataset where zircon dates span over 10,000 to 1,000,000 years, given recognition of both prolonged zircon growth and anticipated analytical scatter, but new tools are emerging that continue to increase the precision and accuracy of dates and age models. These include imaging and microsampling of zircon, integration of geochemical information from zircon into age interpretations, characterization of plutonic and volcanic zircon systematics to build a database of common age distributions from each, and application of Bayesian methods to assess zircon growth records and develop more robust age models for stratigraphic successions. For questions where the highest precision is required, for example those pertaining to the causes and consequences of mass extinction events, the interpretation of zircon U-Pb data can play a crucial role in how we understand the Earth system.

7.10

Prolonged low-temperature storage of supervolcanic magma reservoirs recorded by zircon and titanite petrochronology

Dawid Szymanowski¹, Jörn-Frederik Wotzlaw¹, Ben S. Ellis¹, Olivier Bachmann¹ & Albrecht von Quadt¹

¹ *Institute of Geochemistry and Petrology, Department of Earth Sciences, ETH Zürich, Clausiusstrasse 25, CH-8092 Zürich (dawid.szymanowski@erdw.ethz.ch)*

Clues about the timescales and thermal conditions associated with the growth and evacuation of large silicic magma reservoirs are frequently drawn from radiometric dating, diffusion modelling, or thermomechanical modelling. A growing amount of petrological and geochronological evidence, supported by thermal modelling, suggests that many silicic magma reservoirs may exist for some 10^4 – 10^6 years in the form of high-crystallinity mushes at relatively low temperatures (~700–750°C; Bachmann & Bergantz 2004; Gelman et al. 2013; Cooper & Kent 2014). Geochronological studies addressing this issue typically utilise the U–Pb system in zircon capable of recording extended periods of crystallisation, particularly in evolved calc-alkaline systems that spend most of their lifetime zircon-saturated.

In this study, we integrate U–Pb dating of zircon and titanite to investigate the longevity of the magma reservoir that produced the Kneeling Nun Tuff, a ~35 Ma, > 900 km³ crystal-rich rhyolitic super-eruption from the Mogollon–Datil volcanic field in New Mexico (USA). High-precision ID–TIMS U–Pb dates of single crystals of both zircon and titanite independently record a continuous crystallisation history over >400,000 years. We combine the dating of both accessory phases with textural, major, trace element and isotopic studies of single crystals, placing tight constraints on the thermal conditions of magma accumulation and storage while recording differentiation and rejuvenation processes within the magma reservoir. The results suggest a protracted ‘cool’ upper-crustal storage of magma prior to the Kneeling Nun Tuff eruption followed by a melting event which reduced the magma crystallinity and conditioned it for eruption.

REFERENCES

- Bachmann, O. & Bergantz, G. W. 2004: On the origin of crystal-poor rhyolites: Extracted from batholithic crystal mushes. *Journal of Petrology* 45, 1565–1582.
- Cooper, K. M. & Kent, A. J. R. 2014: Rapid remobilization of magmatic crystals kept in cold storage. *Nature* 506, 480–483.
- Gelman, S. E., Gutierrez, F. J. & Bachmann, O. 2013: On the longevity of large upper crustal silicic magma reservoirs. *Geology* 41, 759–762.

P 7.1

LA-ICP-MS local zircon U-Pb dating of Late Variscan granites of the Dzirula and Khrami crystalline massifs (Georgia)

David Shengelia¹, Tamara Tsutsunava¹, Giorgi Chichinadze¹, Giorgi Beridze¹, Irakli Javakhishvili¹

¹ *Alexandre Janelidze Institute of Geology, I. Javakhishvili Tbilisi State University, A. Politkovskaya 31, 0186 Tbilisi (d_shenge@yahoo.com)*

Late Variscan granites are widespread in the Dzirula and Khrami crystalline massifs of the Black Sea – Central Transcaucasian terrane (Gamkrelidze & Shengelia 2005). The age of the granites is well-grounded geologically by a number of geologists, but there are solitary isotope-geochronological data on these massifs (Dudaury & Togonidze 1985; Okrosvaridze 2002).

Late Variscan granites of the Dzirula crystalline massif is represented by porphyreous and epigranular granites and the Khrami massif is built up of biotite-hornblende-allanite bearing, biotite bearing and biotite-garnet bearing granites and alaskites. During the Bretonian orogeny the Dzirula crystalline underwent tectonic layering. In particular, according to geologic and geophysical data it is proved that sialic and mafic layers of the Earth's crust are overthrust on the sialic "inversional" layer (Ioseliani 1998; Gamkrelidze & Shengelia 2005). In the "inversional" sialic substratum at different depths initial magmas of epigranular eutectoid and porphyreous granites of T type were generated (Figure 1). Porphyreous granites by mineralogic and petrological characterization are formed in higher temperature conditions than epigranular granites and therefore they generated in most abyssal parts of the "inversional" layer and separately from one another as well.

Zircons of the Dzirula and Khrami massifs are fully corroborated by the authors with the help of U-Pb LA-ICP-MS method: 68 local age determinations in the zircons from the Dzirula massif and 26 – from the Khrami massif are done. In some cases the inherited ages of detrital zircons and zircons associated with various endogenic processes are recorded as well. The obtained results are as follows: the age of Dzirula massif granites is – 315-331 Ma, the inherited age recorded in 22 zircon grains occupies the interval of 396-2392 Ma. Th/U ratio in epigranular granites of the massif corresponds to the range 0,125-0,680, but in the porphyreous granites this ratio is considerably different – 0,02-1,493. $\epsilon_{\text{Hf}}(\text{T})$ parameter lays in the interval from -1,5 to -9,2 and TDmC – in the range 1426-1906. The same data for the Khrami massif are: the age varies in the interval of 319-331 Ma, inherited age fixed only in 1 zircon grain shows 931 Ma, Th/U ratio changes from 0,113 to 0,617, $\epsilon_{\text{Hf}}(\text{T})$ parameter varies from -0,1 to -6,9 and TDmC – occupies the range 1425-1767.

In addition, results obtained by 94 local zircon U-Pb LA-ICP-MS dating proves that the age data of both granites from the Dzirula massif and from the Khrami massif cover the same interval and correspond to Late Variscan orogeny. Despite the similarity of a number of geochronological parameters the differences exist as well. They are caused by various reasons, but mainly by the higher content of mantle material in the granites of the Khrami massif compared to the Dzirula massif granites.

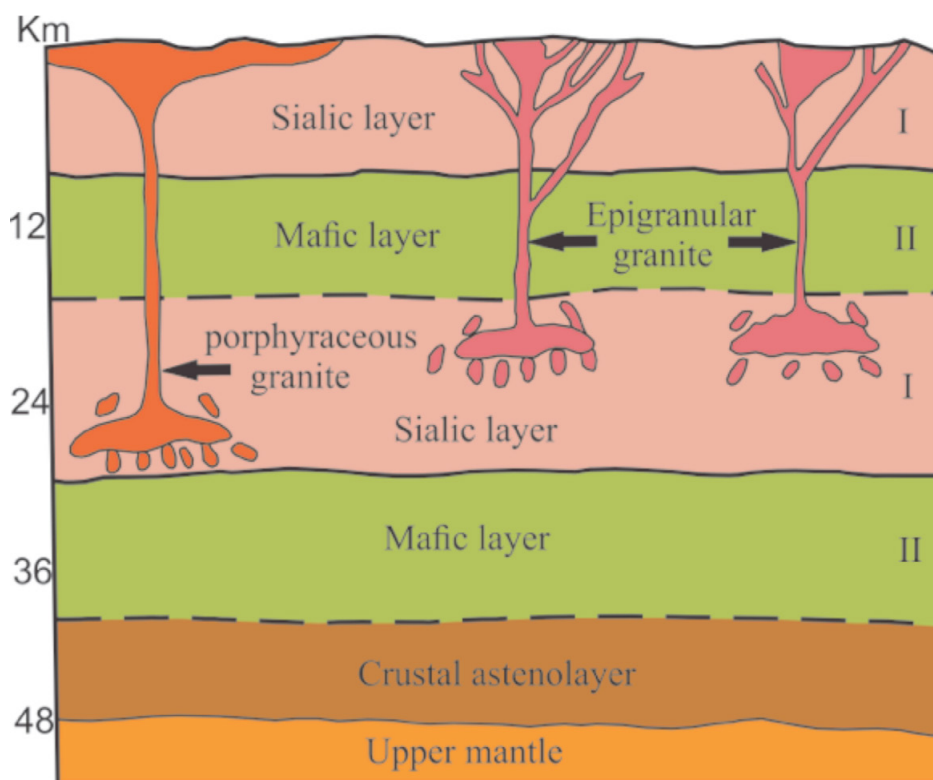


Figure 1. Principle scheme of formation of Late Variscan granites of the Dzirula crystalline massif.

REFERENCE

- Gamkrelidze, I. & Shengelia, D. 2005: Precambrian-Paleozoic Regional Metamorphism, Granitoid Magmatism and Geodynamics of the Caucasus. "Nauchni Mir", Moscow, 479 (in Russian with English summary).
- Gamkrelidze, I., Shengelia, D., Tsutsunava, T., Chung, S., Chiu, H., Chikhelidze, K. 2011: New Data on the U-Pb Zircon Age of the Pre-Alpine Crystalline Basement of the Black Sea – Central Transcaucasian Terrane and their Geological Significance. Bull. Georgian National Acad. Sci., 5-1, 64-76.
- Dudauro, O., Togonidze, M. 1985: Geochronology of Granitoids of the Dzirula Crystalline Massif. Tbilisi: GIN AN GSSR, 8-44.
- Ioseliani, M., Chichinadze, V., Diasamidze, Sh., Kveladze, Z., Onoprishvili, T. 1989: Structure of Lithosphere of the Territory of Georgia According to Seismic Data. "Metsniereba", Tbilisi, 150 (in Russian).
- Okrostsvaridze, A., Clarke, D., Reynolds, P. 2002: Sm-Nd, Rb-Sr and K-Ar Isotopic Systems and Ages of the Pre-Alpine Granitoids of the Dzirula Salient of the Transcaucasian Median Massif. Proceed. Al. Janelidze Inst. of Geology, new ser., 117, 137-186 (in Russian).

P 7.2

In-situ Sr measurements and Zircon analysis of aplitic dykes in Cu-Au-(Mo) porphyry deposit Elatsite, Bulgaria

Marco Loretz¹, Albrecht von Quadt¹, Irena Peytcheva^{1,2}

¹ *Institute of Geochemistry and Petrology, ETH Zurich, Clausiusstrasse 25, 8092 Zürich, Switzerland
(mloretz@student.ethz.ch)*

² *Geological Institute, Bulgarian Academy of Sciences, 1113 Sofia, Bulgaria*

Porphyry copper-gold deposits supply the major part of the world's demand for copper and molybdenum as well as one-fifth of all the gold production (Sillitoe, 2010). These deposits consist of large volumes of hydrothermally altered rock with extensive hydrothermal sulphide mineralisation, centered around multiple intrusions which evolved from an underlying magma chamber. The Elatsite Cu-Au-(Mo) deposit in Bulgaria was investigated by Fanger (2001) and Stefanova et al. (2014) who suggested, that the ore mineralization occurred after a transitional process between magmatic and hydrothermal stages.

The aim of this study was to investigate isotope analyses to define the time window of the ore formation, the isotopic element behaviour at the magmatic to hydrothermal stage in aplitic dykes in different host rock assemblages of the porphyry system in Elatsite to identify the magmatic evolution and linking to the formation of the deposit.

The study of Sr and Nd measurements on individual mineral micro-scale area is promised to probably find non-altered Sr/Nd compositions instead of whole rock data. For this purpose, we have selected to use a small scale hollow-drill sampling technique. Sr and Nd tracing analyses have been performed on a MC-ICP-MS (NU3) and on our Thermal Ion Mass Spectrometer (TritonPlus-RPQ, ThermoFischer Scientific). The Selected zircon grains of three selected magmatic rocks (granodiorite porphyry, aplitic dyke, monzodiorite porphyry) have been analysed in a first step by the LA-ICP-MS technique to identify chronology of the magmatic intrusives. Eight individual zircons of each sample, which are lying on the concordia have been selected for high-precision TIMS analysis.

Results of the isotopic investigations show that within single cm thick aplitic dykes variations in $^{87}\text{Sr}/^{86}\text{Sr}$ ratios from 0.706 to 0.710 may occur due to microscale segregation of early hydrothermal fluid from the late magmatic melt. On the other hand, a similar aplitic intrusion with a crosscutting quartz vein yield equal Sr ratios in the hydrothermal quartz as in the aplitic dyke.

The LA-ICP-MS measurements of the zircons yield a time window of the intrusive porphyry bodies of < 1.5 Ma, which reflects a small timeframe of ore formation. Preliminary U-Pb zircon ages demonstrate a shorter time life of the magmatic history as well as the ore formation.

Precise small-scale hollow drilling combined with MC-ICP-MS can provide a different approach in isotope distribution studies while the advantage over a conventional drilling lies clearly in the three-dimensional mineralogical control of the drilled sample. Single generations of late magmatic aplitic dykes may not yield equal distribution of isotopic content due to heterogeneous distribution of minerals which is related to the separation of hydrothermal fluid from the late magmatic melt. Transition from late magmatic to hydrothermal stage within an ore forming system is not clearly gradual along single dykes or intrusions, but segregationally within very late dykes or draining from magmatic batches.

REFERENCES

- Fanger, L., 2001. Geology of a porphyry copper (-Au-PGE) ore deposit: Elatsite, Bulgaria. Unpublished M.Sc. Thesis, Zurich, Switzerland, ETH Zürich: 167.
- Sillitoe, R. H. (2010). Porphyry copper systems. *Economic Geology*, 105(1), 3-41.
- Stefanova, E., Driesner, T., Zajacz, Z., Heinrich, C. A., Petrov, P., & Vasilev, Z. (2014). Melt and Fluid Inclusions in Hydrothermal Veins: The Magmatic to Hydrothermal Evolution of the Elatsite Porphyry Cu-Au Deposit, Bulgaria. *Economic Geology*, 109(5), 1359-1381.

P 7.3

Statherian bimodal volcanic and anorogenic intrusive rocks in northern Guanhões Block, SE Brazil: an episode of continental rift

Joana Magalhães^{1,2,3}, Antônio Pedrosa-Soares², Ivo Dussin⁴, Othmar Müntener¹, Luiz Guilherme Knauer²

¹ Institut des Sciences de la Terre, University of Lausanne, CH-1015 Lausanne, Switzerland (joana.magalhaes@unil.ch)

² Programa de Pós-graduação em Geologia, Universidade Federal de Minas Gerais, Av. Antônio Carlos 6627, 31270-901 Belo Horizonte, MG, Brazil

³ Geological Survey of Brazil, Av. Brazil 1731, 30140-003 Belo Horizonte, MG, Brazil

⁴ Faculdade de Geologia, Universidade do Estado do Rio de Janeiro, R. São Francisco Xavier 524, 20559-900 Rio de Janeiro, RJ, Brazil

Statherian (1.8-1.6 Ga) taphrogenic processes are well recorded on the east margin of São Francisco Craton and culminated with the opening of an intracontinental rift-sag basin. Volcanic and intrusive rocks related to the rift evolution are widespread in the Guanhões Block, southern Brazil (Figure 1). Detailed in situ zircon U–Pb and Hf isotopic data are presented for mafic and felsic volcanism in the Alto Rio Guanhões region, aiming to constrain their age, petrogenesis, and tectonic implications.

Felsic magmatism is represented in the Guanhões Block by voluminous anorogenic igneous activity such as meta-granite bodies and meta-rhyolites. Poorly synchronous mafic-ultramafic volcanism is characterized by restricted occurrences of meta-basalts, meta-gabbros and tremolite-talc schists.

LA-ICPMS zircon U–Pb ages indicate that the mafic and felsic volcanic rocks were erupted at 1725 ± 4 Ma and 1748 ± 3 Ma, respectively. The mafic rocks are tholeiitic in composition and exhibit overall moderate enrichments in most incompatible trace elements, resembling within-plate basaltic rocks in continental rifts. The felsic rocks have geochemical characteristics of A2-type granites suggesting an extensional tectonic regime (Dussin, 1994).

All analyzed zircons from meta-basalts yielded consistently negative $\epsilon_{\text{Hf}}(t)$ varying from -8.25 to -4.05, suggesting contamination during ascent through the crust. $\epsilon_{\text{Hf}}(t)$ from meta-rhyolite ranges from -17.58 to -12.32 and indicate that magma was essentially sourced from crustal rocks. The Hf model ages (TDM) of zircons from meta-basalt range between 2.28–2.44 Ga, while those for meta-rhyolite vary from 2.62–2.80 Ga, which is the age of the Archean basement defined as Guanhões Complex.

The mafic rocks were most likely generated by parental magmas derived from enriched lithospheric mantle and crystal fractionation during magma evolution. The genesis of felsic magmatism is related to partial melting of Archean continental crust. The heat is most probably provided by underplating mafic magmas. At that time, the bimodal volcanic rocks interlayered with the Guanhões Group were developed in a continental rifting environment in Statherian time.

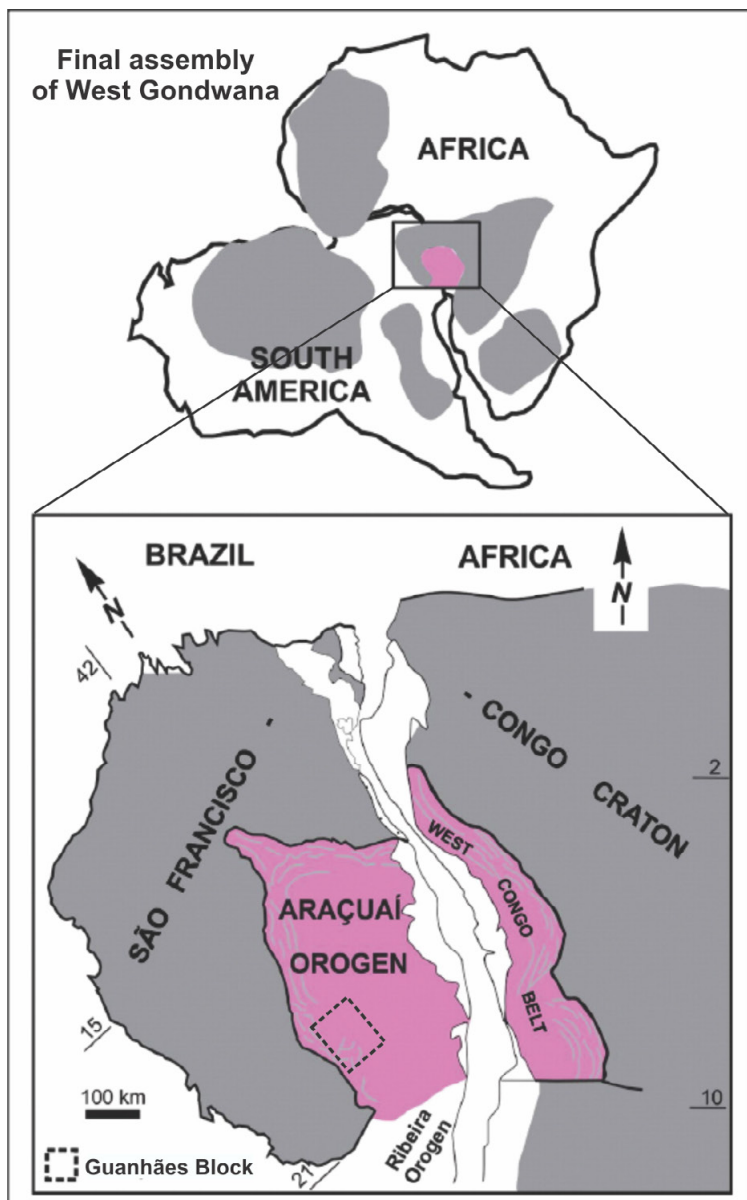


Figure 1. Geotectonic setting of the study area - Guanhões Block within Araçuaí–West Congo orogenic system and related cratons (modified from Alkmim et al. 2006).

REFERENCES

- Alkmim, F.F., Marshak, S., Pedrosa-Soares, A.C., Peres, G.G., Cruz, S.C.P. & Whittington, A. 2006: Kinematic evolution of the Aracuaí–West Congo orogen in Brazil and Africa: nutcracker tectonics during the Neoproterozoic assembly of Gondwana. *Precambrian Research* 149, 43–64.
- Dussin, T. M. 1994: Associações vulcano- plutônicas de l'Espinhaço Meridional (SE - Brasil). Université d'Orléans, Orléans, PhD Thesis.

P 7.4

High precision Nd isotope ratio measurements by Thermal Ionization Mass Spectrometer with Faraday collectors equipped with $1e^{12}$ ohm feedback resistors

Zenon Palacz¹

² *IsotopX Ltd., Milbrook Court, Midpoint 18, CW10 0GE Cheshire, UK (zenon.palacz@isotopx.com)*

We present the analytical performance of new amplifier boards equipped with $1e^{12}$ ohm resistors. Noise levels of ~ 3 to $4 e^{-18}$ amp (3 to 4 attoamp) can be achieved with noise integration of 12 minutes. The resistors have a dynamic range up to 1 volt ($1e^{11}$ ohm equivalent) or $6e^7$ cps. The relative gains between the resistors can be calibrated with a reference voltage rather than with an ion beam. For an ion signal of $5e^{-14}$ amp ^{143}Nd . Replicate measurements of $^{143}\text{Nd}/^{144}\text{Nd}$ yielded a reproducibility of 150ppm 2RSD, a factor of three better than for a $1e^{11}$ ohm resistor. Replicate measurements of 100pg Nd metal using single filaments with a carbon activator yielded $^{143}\text{Nd}/^{144}\text{Nd}$ 0.512111 \pm 62ppm 2RSD. With ion yields of 12%.

The precision of these measurements is better than can be obtained using a single ion counting Daly detector at the same ion intensity. The large dynamic range overlap between the ion counting Daly and the $1e^{12}$ ohm (1T) resistors makes them particularly well suited for high precision Pb and U measurements using a combination of the two detectors.

P 7.5

First high-precision U-Pb dates from the new Phoenix TIMS at University of Geneva

Urs Schaltegger¹, Joshua H.F.L.¹ & Zenon Palacz²

¹ *Earth Sciences, University of Geneva, Rue des Maraîchers 13, 1205 Genève (urs.schaltegger@unige.ch; Joshua.Davies@unige.ch)*

² *IsotopX Ltd., Milbrook Court, Midpoint 18, CW10 0GE Cheshire, UK (zenon.palacz@isotopx.com)*

We will present first U-Pb data from the new PHOENIX thermal ionisation mass spectrometer at University of Geneva, purchased in 2016. This instrument is optimized for lowest-level isotopic analyses for U-Pb geochronology. We are investigating different measurement techniques, involving single-collector Daly-based ion counting, and mixed Faraday-Daly multidynamic procedures using novel high-sensitivity and low-noise 1TOhm faraday cups.

P 7.6

Variations in the frequency and magnitude of volcanic eruptions at arc volcanoes

Tom Sheldrake¹, Luca Caricchi^{1°},

¹ *Department of Earth Sciences, University of Geneva, Geneva, Switzerland*
(thomas.sheldrake@unige.ch)

[°] *Presenting author*

Quantifying the frequency-Magnitude (f-M) relationship for volcanic eruptions is important to estimate volcanic hazard. Furthermore, understanding how this relationship varies between different groups of volcanoes can provide insights into the processes that exert control on the frequency and size of volcanic events. Using the LaMEVE record of large-magnitude volcanic eruptions we calculate the f-M relationship for sets of volcanoes according to factors such as morphology and tectonic setting. We use a Bayesian framework, which allows us to conceptualise the volcanic record as a series of individual and unique time series, associated by common group behaviour. We identify variations in f-M behaviour between different regions on Earth, with volcanic arcs where the crust is thicker associated with a higher proportion of larger-magnitude eruptions. Together with crustal magma fluxes, the crustal thickness is used to explain regional variations in the f-M relationship. The comparison between volcanic systems with different characteristics, across a variety of tectonic settings, will allow us to identify the main factors controlling the tempo of volcanism. Additionally, understanding the link between tectonic setting, physics of magmatic processes, and the recurrence rate of volcanic eruptions will serve to improve our capacity to quantify volcanic hazards in regions with limited geological and historical records of volcanic activity.

P 7.7

A geochronologic framework for Middle Triassic magmatism and sedimentation in the Southern Alps

Julian-Christopher Storck¹, Peter Brack¹, Jörn-Frederik Wotzlaw¹, Peter Ulmer¹ & Albrecht von Quadt

¹ *Department of Earth Sciences, Institute of Geochemistry and Petrology, ETH Zurich, Sonneggstrasse 5, CH-8092 Zurich (julian.storck@erdw.ethz.ch)*

The middle Triassic magmatism in the Southern Alps and particularly in the Dolomites and Lombardian Alps encompasses widespread felsic volcanoclastic deposits, basaltic lava flows and irregularly distributed intrusive complexes. The origin, petrogenesis and geodynamic setting as well as the timescales of this magmatic flare-up remain poorly understood. Felsic volcanic ash layers interbedded with Middle Triassic fossiliferous sedimentary successions have been traced over hundreds of kilometres in stratigraphic sections with litho-, bio- and magnetostratigraphic control (Brack & Rieber, 1993) and document a time interval of ca. four millions of years (e.g., Brack et al., 2007). Small intrusions, including those at Monzoni and Predazzo in the Dolomites, were emplaced during or immediately after the climax of the explosive volcanic activity.

Here we present a detailed stratigraphic framework and a comprehensive zircon petrochronology dataset that constrain the timing as well as the chemical evolution of this magmatic province. High precision zircon U-Pb geochronology obtained by CA-ID-TIMS provide absolute tie-points for felsic ash layers from various localities and also bracket the interval of effusion of several hundred metres thick piles of basaltic lava in the Dolomites. The new stratigraphic and geochronologic framework further allows linking these volcanic deposits with stratigraphically unconstrained intrusive complexes at Monzoni and Predazzo.

The new temporal framework with unprecedented resolution provides a firm basis for a quantitative analysis not only of the magmatic systems but also of sedimentary processes including the growth of carbonate platforms during the Middle Triassic.

REFERENCES

- Brack, P. & Rieber, H. 1993: Towards a better understanding of the Anisian/Ladinian boundary: New biostratigraphic data and age correlations of boundary sections from the Southern Alps, *Eclogae Geologicae Helveticae* 86(2), 415-527.
- Brack, P., Rieber, H., Mundil, R., Blendinger & W., Maurer, F., 2007: Geometry and chronology of growth and drowning of Middle Triassic carbonate platforms (Cenera and Bivera/Clapsavon) in the Southern Alps (northern Italy). *Swiss Journal of Geosciences* 100(3), 327-347.

P 7.8

Zircon U-Pb geochronology at the 0.1 ‰ level by ID-TIMS using 1013 Ω resistors

von Quadt, A.¹, Wotzlaw, J.-F.¹, Buret, Y.¹, Large, S., Peytcheva, I.^{1,2} and Szymanowski, D.¹

¹ *Institute of Geochemistry and Petrology, ETH Zurich, IGP, Clausiusstrasse 25, CH-8092 Zurich, (vonquadt@erdw.ethz.ch)*

² *Geological Institute, Bulgarian Academy of Sciences, Sofia, Bulgaria*

The accuracy and precision of U-Pb isotope analysis using newly available 10¹³ Ohm resistors by Thermal Ionisation Mass Spectrometry (TIMS) have been tested using a variety of reference materials. The TritonPlus-RPQ at the IGP (ETH Zurich) is equipped with five new 10¹³ Ohm resistors and one MasCom multiplier to measure the ²⁰²⁻²⁰⁴⁻²⁰⁵⁻²⁰⁶⁻²⁰⁷⁻²⁰⁸Pb masses in static mode; the ²⁶⁵⁻²⁶⁷⁻²⁷⁰UO₂ masses are measured during a second step, also in static mode. The new equipment has been tested using different natural zircon standard materials and synthetic U/Pb solutions (www.earthime.org).

High-precision zircon U-Pb data sets are limited by internal measurement uncertainties as well as the accuracy and precision of the correction of isobaric interferences from minor UO₂ isotopologues, which can become the major source of uncertainty. Here we present a direct comparison of high-precision U-Pb data obtained using different detector systems, including dynamic peak hopping on a secondary electron multiplier and static multi-collection routines that use 10¹³ ohm resistors in the amplifier feedback loop [von Quadt et al., 2016]. We also demonstrate precise and accurate measurement of the minor ²³⁸U¹⁸O¹⁶O isotopologue (i.e., ²⁷²(UO₂)) in a static and combined static-multi-collection routine, which permits precise and accurate determination of the ¹⁸O/¹⁶O ratio of UO₂ molecules during the U-isotope ratio measurement.

This study illustrates that the accurate and precise within-run correction of isobaric interferences from the minor UO₂ isotopologues eliminates one of the major sources of uncertainty in ultra-high-precision U-Pb data sets. This approach permits the determination of single U-Pb dates with uncertainties <0.2 ‰ and corresponding weighted mean dates with uncertainties <0.1 ‰.

REFERENCES

Von Quadt, A., Wotzlaw, J.-F., Buret, Y., Large, S.J.E., Peytcheva, I., Trinquier, A. 2016: High-precision zircon U/Pb geochronology by IDTIMS using new 1013 ohm resistors JAAS 31: 658-665.

P 7.9

The effect of chemical abrasion on zircon chemistry, crystal structure and ID-TIMS-U-Pb ages

Philipp Widmann¹, Joshua Davies¹, Urs Schaltegger¹

¹ *Department of Earth Sciences, University of Geneva, rue des Maraichers 13, CH-1205 Geneva, Switzerland (Philipp.widmann@unige.ch)*

It is customary in U-Pb-dating of ash layers to choose the youngest group of zircon U-Pb ages assuming that zircon crystallization is similar in age to volcanic eruption and ash deposition. However, loss of radiogenic Pb (Pb*) from the crystal lattice (Pb-loss) or the presence of old cores (inheritance) result in biased ages which are, respectively, either too young or too old. Therefore, reliable and meaningful ages require the control on factors that cause dispersion of ages. Grains with inherited cores can be easily excluded through careful pre-selection on the base of CL imaging. Recognition and mitigation of Pb-loss is more difficult and impacts directly on the final age of the grain.

Pb-loss occurs along altered zones of the crystal lattice as a consequence of the structural damage produced by Uranium decay, which provides pathways for Pb to diffuse through the lattice (Nasadala et al., 2005). Mattinson (2005) established the chemical abrasion technique (CA), comprising high temperature annealing to restore the damaged parts of the crystal lattice, followed by an acid attack to remove the remaining non-annealed zones, leaving an undisturbed (closed-system) residue. The Mattinson (2005) technique is purely empirical and is often modified by different laboratories. However, without a proper understanding on how (1) the applied annealing temperature and (2) the temperature and duration of partial dissolution affect metamict and non-metamict zones, data from different U-Pb geochronology laboratories following different procedures are problematic to compare quantitatively. Previous studies have investigated the effect of annealing on radiation damaged zones at different time and temperature conditions (e.g. Nasadala et al., 2002), or the effect of temperature at a fixed duration of the partial dissolution step (Huyskens et al., 2016) on the final reproducibility of U-Pb dates. However, no study has investigated the effect of the chemical abrasion procedure on the zircon trace element chemistry compared to the state of the crystal structure and the U-Pb date.

This study intends to develop protocols for chemical pre-treatment of zircon based on crystal structure, and also determines the effects of chemical abrasion on zircon chemistry. For this purpose we choose to study the Plešovice zircon, which is used as a reference material (Sláma et al., 2008). The Plešovice zircon is ideal due to its variations in trace element concentrations and because it contains domains rich in actinides. Plešovice grain fragments were annealed for 48h at 900°C. Four aliquots were separated and attacked in concentrated hydrofluoric acid at 180 °C for 6h, 12h, 18h and 24h. Additionally, we performed Raman mapping, EMPA, CL imaging and LA-ICP-MS trace element analysis on each of the fractions. The zircons treated by CA were compared to untreated and solely annealed zircons.

REFERENCES

- Huyskens, M.H., Zink, S., Amelin, Y., 2016: Evaluation of temperature-time conditions for the chemical abrasion treatment of single zircons for U–Pb geochronology, *Chemical Geology*, 438, 25-35.
- Mattinson, J.M., 2005: Zircon U–Pb chemical abrasion (“CA-TIMS”) method: Combined annealing and multi-step partial dissolution analysis for improved precision and accuracy of zircon ages, *Chemical Geology*, 220, 1–2, 12, 47-66.
- Nasadala, L., Lengauer, C.L., Hanchar, J.M., Kronz, A., Wirth, R., Blanc, P., Kennedy, A.K., Seydoux-Guillaume, A., 2002: Annealing radiation damage and the recovery of cathodoluminescence, *Chemical Geology*, 191, 1–3, 121-140.
- Nasadala, L.; Hanchar, J.M.; Kronz, A., Whitehouse, M.J., 2005: Long-term stability of alpha particle damage in natural zircon. *Chem. Geol.*, 220, 83–103.
- Sláma, J., Košler, J., Condon, D.J., Crowley, J.L., Gerdes, A., Hanchar, J.M. Horstwood, M.S.A., Morris, G.A., Nasadala, L., Norberg, N., Schaltegger, U., Schoene, B., Tubrett, M.N., Whitehouse, M.J., 2008: Plešovice zircon — A new natural reference material for U–Pb and Hf isotopic microanalysis, *Chemical Geology*, 249, 1–2, 1-35.

P 7.10

From discrete dates to continuous age: A systematic comparison of currently available age modeling software

Jörn-Frederik Wotzlaw¹, Katrina Kremer²

¹ *Institute of Geochemistry and Petrology, Department of Earth Sciences, ETH Zurich*
(joern.wotzlaw@erdw.ethz.ch)

² *Geological Institute, Department of Earth Sciences, ETH Zurich*

Temporal calibration of sedimentary sequences typically involves dating of several discrete horizons that contain dateable material such as volcanic ash beds for U-Pb or ⁴⁰Ar/³⁹Ar dating and organic-rich layers for ¹⁴C geochronology. However, in many cases, the events of interest such as paleoclimatic, environmental and evolutionary turnovers occur somewhere between these dated horizons. Accurate dating of such events therefore requires some sort of interpolation between dated horizons, thereby constructing a continuous age model for sediment deposition. For this purpose, different types of age-depth models and corresponding software applications have been developed. Most of these applications were developed within and for the ¹⁴C geochronology and paleoecology communities but are applicable to essentially all chronostratigraphic studies. We here present a systematic comparison of different age-depth modeling approaches using a variety of geochronologic data from different depositional settings. All software we test herein is freeware and uses R as an interface.

Two of the software packages, *Bchron* (Haslett and Parnell, 2008; Parnell et al., 2008) and *Bacon* (Blaauw and Christen, 2011) use bayesian approaches that take into account prior assumptions about sediment deposition while the third software, *Clam* (Blaauw, 2010), uses classical non-bayesian interpolation algorithms (e.g., linear interpolation, cubic spline fitting etc.).

We apply these different software applications to ¹⁴C dated lacustrine deposits, zircon U-Pb dated marine sections and ⁴⁰Ar/³⁹Ar dated continental sequences, some of which have independent age models from orbital tuning. Age models generated using the different approaches show some significant differences, particularly with respect to model uncertainties.

Age models generated using *Bchron* tend to have the largest uncertainties while *Clam*-generated models tend to have the smallest uncertainties. *Bacon*-generated age models strongly benefit from prior assumptions concerning the sediment accumulation rate (absolute rate and rate of change in accumulation rate) that can be derived from sedimentologic and stratigraphic data resulting in more realistic uncertainty estimates. The robustness of age models is tested by randomly removing and adding individual dates from the different data sets. The accuracy of all age models primarily depends on the number and distribution of discrete age constraints as well as the complexity of the depositional systems. Simple depositional systems with rather uniform sediment accumulation rates (e.g., pelagic/hemipelagic and lacustrine deposits) require only a small number of age constraints while complex depositional systems (e.g., fluvial deposits) require a large number discrete dates.

This comparison highlights the non-unique nature of stratigraphic age models and aims to motivate the wider geochronology and stratigraphy communities to find agreement concerning the use and interpretation of such models.

REFERENCES

- Blaauw, M., 2010: Methods and code for 'classical' age-modelling of radiocarbon sequences. *Quaternary Geochronology*, 5, 512-518.
- Blaauw, M., Christen, J.A., 2011: Flexible paleoclimate age-depth models using an autoregressive gamma process. *Bayesian Analysis*, 6, 457-474.
- Haslett, J., Parnell, A., 2008: A simple monotone process with application to radiocarbon dated depth chronologies. *Journal of the Royal Statistical Society: Series C*, 57, 1-20.
- Parnell, A., Haslett, J., Allen, J., Buck, C., and Huntley, B., 2008: A flexible approach to assessing synchronicity of past events using Bayesian reconstructions of sedimentation history. *Quaternary Science Reviews*, 27, 1872-1885.

P 7.11

The response of Baddeleyite to radiation damage, and how this relates to Pb loss

Davies, JHFL.¹ Seydoux-Guillaume, A-M.² Heaman, L.³ Marzoli, A.⁴ Schaltegger, U.¹

¹ *Department of Earth Sciences and the Environment, Université de Genève 13, Rue des Maraîchers 13, Geneva 1205, Switzerland*

² *Laboratoire Magmas et Volcans LMV, UMR 6524 CNRS-UBP-UJM-IRD, Faculté des Sciences et Techniques, 23 rue du Dr. Paul Michelon, 42023 Saint Étienne, France*

³ *Department of Earth & Atmospheric Sciences, University of Alberta, Edmonton, Alberta T6G 2E3, Canada*

⁴ *Dipartimento di Geoscienze, Università di Padova, via Matteotti 30, 35100 Padova, Italy*

Baddeleyite (ZrO₂) is the oxide form of zircon. It is a trace phase that incorporates U into its crystal structure whilst rejecting Pb and is dominantly found in mafic rocks. Baddeleyite U-Pb geochronology typically yields concordant or close to concordant results whereas untreated zircon from the same samples with similar U concentrations can record large and variable degrees of discordance (Davies and Heaman, 2014). Therefore, baddeleyite should be an ideal geochronometer, however, high precision U-Pb analysis of baddeleyite often uncovers age dispersions greater than expected from simple cooling models (Bloch et al. 2014), and much greater than co-existing zircon that has undergone chemical abrasion treatment. These findings suggest that baddeleyite records small degrees of open system behaviour (Pb loss) and should be used with caution to obtain precise and accurate age information.

Here we attempt to uncover the mechanism of Pb loss in baddeleyite with eventual the aim of removing the affected areas or identifying effected crystals before time and resource intensive ID-TIMS analysis. To identify the mechanisms for Pb loss we have structurally, chemically and geochronologically characterized a suite of crystals from gabbroic sills, dolerite dykes, carbonatites and metamorphosed limestones over an age range of 2 Ga using TEM, Raman spectroscopy, elemental analysis, electron imaging and U-Pb geochronology.

Our TEM analysis shows that all of the crystals are crystalline and non-metamict despite high alpha doses. However, older crystals show evidence of lattice distortion which is most likely related to Frenkel pairs, similar to monazite (see Seydoux-Guillaume et al. 2002; 2004). Raman spectral analysis of the same crystals show band broadening, intensity loss and the appearance of new bands suggesting that the short range order of the crystals is significantly altered, and this disturbance correlates with alpha dose. The combination of long range order with short range disorder is similar to that found in biotite radiohalos around zircon inclusions (Nasdala et al. 2001). Based on our exhaustive analysis of different baddeleyite crystals, we suggest the likely causes of open system behaviour, and also recommend the best ways for avoiding it and in the process, obtain the most reliable age information.

REFERENCES

- Bloch, E., Watkins, JM., & Van Orman, JA., 2014: Diffusion kinetics of geochronologically relevant species in baddeleyite AGU Fall Meeting Abstracts 1, 4872.
- Davies, JHFL., & Heaman, LM., 2014: New U–Pb baddeleyite and zircon ages for the Scourie dyke swarm: A long-lived large igneous province with implications for the Paleoproterozoic evolution of NW Scotland, *Precambrian Research*, 249, 180–198.
- Nasala, L., Wenzel, M., Andrut, M., Wirth, R., & Blaum, P., 2001: The nature of radiohaloes in biotite: Experimental studies and modeling, *American Mineralogist*, 86, 498-512.
- Seydoux-Guillaume A. M., Wirth, R., Nasdala, L., Gottschalk, M., Montel, JM., & Heinrich, W. 2002. An XRD, TEM and Raman study of experimentally annealed natural monazite, *Physics and Chemistry of Minerals*, 29, 240-253.
- Seydoux-Guillaume A. M., Wirth, R., Deutsch, A., & Schaerer, U. 2004: Microstructure of 24-1928 Ma concordant monazites; implications for geochronology and nuclear waste deposits, *Geochimica Cosmochimica Acta*, 68, 2517-2527.

P 7.12

Discriminating age and type of detrital sources in the Taveyannaz Formation (Northern Alpine early foreland basin)

Lu Gang¹, Andrea Di Capua², Wilfried Winkler¹, Sean Willett¹, Albrecht von Quadt³, Maria Giuditta Fellin³, Meinert Rahn⁴, Peter Brack³

¹ Department of Earth Sciences, Geological Institute, ETH Zürich, Sonneggstrasse 5, 8092 Zürich, Switzerland (gang.lu@erdw.ethz.ch)

² Università degli Studi di Milano-Bicocca, 4, Piazza della Scienza, 20126 Milano, Italy

³ Department of Earth Sciences, Sonneggstrasse 5, 8092 Zürich, Switzerland

⁴ Swiss Federal Nuclear Safety Inspectorate ENSI, Industriestrasse 19, 5200 Brugg, Switzerland

Paleogene syn-tectonic volcanic products sparsely occur in the Alpine orogen. They are located in three basinal settings: (1) the Northern Alpine early foreland basin (Late Eocene? to Oligocene Taveyannaz and Champsaur Fms.; e.g. Rahn et al. 1995), (2) the Southern Alps foreland basin (Oligocene-Miocene Como Formation and Gonfolite Lombarda Group, (e.g. Malusa et al. 2011), and (3) Middle to Late Eocene South Alpine turbiditic sandstones intercalated within deep-water successions of the Trento area (e.g. Sciunnach and Borsato 1994). The chronostratigraphic range of the formations correlates with the Cenozoic Alpine collision, however, the derivation and geodynamic significance of the volcanic material is poorly defined. It is likely that the Eocene-Oligocene volcanoclastic material was supplied from volcanic dykes related to the magma intrusions as well as eruptions along the palaeo-Insubric lines.

We investigate the Early Oligocene (Rupelian) turbidite deposits to evaluate their temporal and genetic relationship with the hypothetical magmatic provinces and basement. Detrital zircons from sandstones in three representative localities (Haute-Savoie, Alpe de Taveyannaz and Glarus area) have been dated by laser ablation ICP-MS analysis methods. The obtained age patterns are compared with trace element analysis of the detrital zircons (Eu, Th, U, REE) which indicate the magmatic environment of zircons crystallization. Time corrected $^{176}\text{Hf}/^{177}\text{Hf}$ isotope ratios allow revealing their origin from either mantle or crust (crustal contamination as a result of single or polyphase recycling).

The age of detrital zircons show two major populations: a large dominance (92%) of pre-Alpine zircons (Cadomian, Caledonian, Variscan and post-Variscan, ~ 650–252 Ma) as commonly observed in other Alpine flysch formations (e.g. Beltrán et al. 2013). Notably, the Caledonian zircons largely prevail and a derivation from Austroalpine basement units can be inferred (Frisch, 1984). For further evaluating the type of basement sources, we shall apply a double-dating on detrital zircons.

Neo-Alpine detrital zircons are quite rarely observed (8%) in the age range from Late Eocene to Early Oligocene (~ 39.8 ± 0.7 – 29.7 ± 0.8 Ma). Th/U, Ce, Eu (REE) signatures clearly imply that the zircons have an igneous origin. The obtained zircon ages correlate with geochronologic data from the Adamello (~ 43–29 Ma), Bergell (~ 32–28 Ma) and Biella (~ 33–30) intrusions, and their related dykes, respectively. Thermochronological data, however, indicate that these intrusions along the palaeo-Insubric line were still buried below the surface between 10 and 5 kms (e.g. Rosenberg 2004). Consequently, the detrital zircons were derived from dykes and surficial extrusions. Preliminary $\epsilon\text{Hf}(t)$ data in the Glarus area are ambiguous showing positive and negative values in two different samples.

The discovery of minor Neo-Alpine zircons presumably is due to low zircon production in the volcanic sources along the palaeo-Insubric line. The long distance transport of the syn-sedimentary volcanic material caused mixing with various Alpine basement sources. Thermochronological results in literature suggest that Austroalpine and South Alpine may have represented the major sources.

ACKNOWLEDGEMENTS: The support of LG by a Chinese Scholarship (CSC) is appreciated.

REFERENCES

- Beltrán-Triviño A., Winkler W. & von Quadt A. 2013: Tracing Alpine sediment sources through laser ablation U–Pb dating and Hf-isotopes of detrital zircons. *Sedimentology* 60, 197–224
- Malusà, M.G., Villa, I.M., Vezzoli, G. & Garzanti, E. 2011. Detrital geo-chronology of unroofing magmatic complexes and the slow erosion of Oligocene volcanoes in the Alps. *Earth and Planetary Science Letters* 301(1-2), 324–336.
- Rahn, M.K., Stern, W.B., & Frey, M. 1995. The origin of the Taveyannaz sandstone: arguments from whole-rock and clinopyroxene composition. *Schweiz. Mineral. Petrogr. Mitt.* 75, 213–224.
- Rosenberg, C. L. 2004. Shear zones and magma ascent: a model based on a review of the Tertiary magmatism in the Alps. *Tectonics*, 23(3).
- Sciunnach D. & Borsato A. 1994. Plagioclase-arenites in the Molveno Lake area (Trento): record of an Eocene volcanic arc. *Studi Trent. Sci. Nat.*, 69, 81–92.
- Frisch, W., Neubauer, F., & Satir, M. 1984. Concepts of the evolution of the Austroalpine basement complex (Eastern Alps) during the Caledonian-Variscan cycle. *Geologische Rundschau*, 73(1), 47–68.

P 7.13

Zircon petrochronology revealing the shallow-crustal magmatic evolution and timescales of mineralization at the Ok Tedi porphyry-skarn Cu-Au deposit

Simon J. E. Large¹, Albrecht von Quadt¹, Jörn-Frederik Wotzlaw¹ and Christoph A. Heinrich¹

¹ *Institute of Geochemistry and Petrology, ETH Zürich (simon.large@erdw.ethz.ch)*

Metal endowed porphyry deposits are the result of the magmatic-hydrothermal interplay in the upper crust. These porphyry stocks are small rapidly cooling apophyses of much larger magma chambers below that are the locus of zircon crystallization. Understanding the magmatic evolution in this magma reservoir together with the pace of emplacement of porphyry stocks are key questions in understanding these deposits. To fully quantify these processes we apply a combination of spatially resolved in-situ geochemistry with high precision CA-ID-TIMS geochronology on zircons from the Ok Tedi deposit, one of the youngest (~1.2 Ma) giant Cu-Au porphyry-skarn deposits.

Zircons from intrusive rocks associated with the Ok Tedi deposit, were imaged for internal textures (CL), followed by in-situ geochemical and geochronological data acquisition by LA-ICP-MS. We selected inclusion and inheritance free zircons to obtain high precision U-Pb CA-ID-TIMS dates. This combination of spatially resolved in-situ trace element analysis with high precision dating enables us to reconstruct the magma chamber evolution from zircon saturation to the emplacement of the porphyry intrusions at <10 ka years resolution.

Zircon ages of pre- and syn-mineralization intrusives indicates protracted zircon crystallization within the magma chamber over some 105 years and a rapid succession of emplacement and subsequent mineralization within few 104 years. Similar geochemical trends in zircons from all samples trace progressive fractional crystallization in the magma reservoir and indicate a common magmatic source. A portion of the youngest zircons record distinct chemical characteristics that are not coherent with the fractional crystallization trend and point to a rapid change of the chemical conditions towards the end of zircon crystallization. Rapid porphyry emplacement, crystallization and Cu-Au mineralization at Ok Tedi is consistent with numerical predictions and other geochronological studies (Weis et al., 2012; Buret et al., 2016; Tapster et al 2016).

REFERENCES

- Weis, P., Driesner, T., & Heinrich, C. A. 2012: Porphyry-copper ore shells form at stable pressure-temperature fronts within dynamic fluid plumes. *Science*, 338(6114), 1613-1616.
- Buret, Y., von Quadt, A., Heinrich, C., Selby, D., Wälle, M., & Peytcheva, I.: 2016. From a long-lived upper-crustal magma chamber to rapid porphyry copper emplacement: Reading the geochemistry of zircon crystals at Bajo de la Alumbrera (NW Argentina). *Earth and Planetary Science Letters*, 450, 120-131.
- Tapster, S., Condon, D. J., Naden, J., Noble, S. R., Petterson, M. G., Roberts, N. M. W., Saunders, A.J. & Smith, D. J.: 2016. Rapid thermal rejuvenation of high-crystallinity magma linked to porphyry copper deposit formation; evidence from the Koloula Porphyry Prospect, Solomon Islands. *Earth and Planetary Science Letters*, 442, 206-217.

8. Rock mechanics, Rock physics and Geophysics

Marie Violay, Brice Lecampion, Claudio Madonna, Matteo Lupi, György Hetényi

*Schweizerische Paläontologische Gesellschaft,
Kommission des Schweizerischen Paläontologischen Abhandlungen (KSPA)*

TALKS:

- 8.1 Barnhoorn A., Verheij J., Frehner M.: Transition from elastic to inelastic deformation identified by seismic attenuation, not seismic velocity
- 8.2 Carrier A., Lupi M., Haddad A., Baron L., Linde N.: Bouguer anomaly inversion at the Nirano Mud Volcanic Field, Italy, to infer depth and density variations of hydrocarbon and mud reservoirs
- 8.3 Duran J.A., Obermann A.: 2D sensitivity kernels for monitoring weak changes on highly heterogeneous elastic medium
- 8.4 Häusler M., Schmelzbach C., Sollberger D.: A new seismic vector source: the Galperin source
- 8.5 Malvoisin B., Podladchikov Y.Y., Connolly J.A.D.: Role of metamorphic reactions on deformation and fluid flow: a new fully-coupled model
- 8.6 Pirot G., Linde N., Mariethoz G., Bradford J.: Geophysical data inversion with graph cuts under geological realism constraint
- 8.7 Somogyvári M., Jalali M., Bayer P.: Fracture network characterization using a stochastic transdimensional algorithm
- 8.8 Zbinden D., Pio Rinaldi A., Urpi L. & Wiemer S.: Coupled hydro-mechanical modelling of seismicity induced by gas production

POSTERS:

- P 8.1 Acosta M., Passelegue F., Schubnel A., Violay M.: An experimental study of the influence of pore water on dynamic rupture processes.
- P 8.2 Wenning Q., Madonna C., Moulas E., Burg, J.P.: Petrophysical properties through a Grimsel granodiorite shear zone – Implications for geothermal reservoir evaluation and modelling
- P 8.3 Ciardo F., Lecampion B.: Modelling of fluid injection into a frictional weakening dilatant fault
- P 8.4 Hefny M., Zappone A., Madonna C., Moscariello A., Burg J.P.: Geothermal potential of the Geneva Basin: the aid of petrophysical laboratory data
- P 8.5 Nikolskiy, D., Lecampion, B.: Simulating fully three dimensional pressurized fracture propagation
- P 8.6 Cornelio C., Violay M., Spagnuolo E.: Viscosity fluid influence on stick-slip motions
- P 8.7 Dutler N., Valley B., Krietsch H., Amann F., Gischig V. & Evans K.: Stress Characterisation and stress modeling at the Grimsel Test Site for the In-situ Stimulation and Circulation Project

- P 8.8 Blum T., Lecampion B.: Acoustic monitoring of laboratory hydraulic fracture growth under stress and pore pressure
- P 8.9 Dombrowski E., Vogler D., Walsh S.D.C., Perras M.A.: Towards Replicating Rock Specimens: A Comparison of Tensile Fractures from 3D Printed and Natural Sandstones
- P 8.10 Hunziker J., Favino M., Caspari E., Quinta B.I, Krause R., Holliger K.: Numerical modeling of seismic attenuation in realistic fractured media
- P 8.11 Sprengel H., Ziegler M.: Analysis of surface roughness of Opalinus Clay extensional fractures
- P 8.12 Orellana L.F., Violay M., Gramajo E., Henry P., Guglielmi Y., Amann F., Nusbaum C.: Petro-physical characterization of the Main Fault at the Mont Terri Laboratory
- P 8.13 Kakurina M., Guglielmi Y., Nussbaum C., Valley B.: Architecture of a fault zone in Opalinus Clay at the Mont Terri laboratory (Switzerland)
- P 8.14 Heap M., Violay M., Wadsworth F.: Porosity and permeability reduction in conduit wall rock. A transition from localised cataclastic pore collapse to distributed viscous flow.
- P 8.15 Hartung E., Caricchi L.: The physical properties of evolved melts and implications for melt segregation and the built-up of large silicic eruptions
- P 8.16 Antunes V., Lupi M., Carrier A., Obermann A., Mazzini A., Ricci T., Sciarra A., Moretti M.: Seismic signals at the Nirano Mud Volcanic Field, Italy
- P 8.17 Haddad A., Lupi M., Gonzalez Vidal D., Ganas A., Kassaras I.: Tectonic and fluid-driven seismic activity in Western Peloponnese, Greece
- P 8.18 Hetényi G., Le Roux-Mallouf R., Berthet T., Cattin R., Cauzzi C., Phuntsho K., Grolimund R.: Mind the (seismic) gap: the 1714 Bhutan earthquake
- P 8.19 Tair S., Pitout F., Yahiat Y., Zaourar N.: Effect of tilt angle on the inter-hemispherical asymmetries: Study of the variations of the temperature and the electronic density
- P 8.20 Colavitti L., Hetényi, G.: 3-D shear-wave velocity model of the Central Alps using converted waves
- P 8.21 Hadjadj A., Benaïssa Z., Benaïssa A., Boudella A.: Gray-scale Hough transform for seismic wavefield separation?
- P 8.22 Schnydrig S., May D., Ueda K., Gerya T.: Topographic expressions of coupled surface process and 3Dtectonic models
- P 8.23 Chanard K., Hetényi G., Baumgartner L., Licul A., Herman F.: Constraints on the extent and kinetics of eclogitization processes in the Indian lower crust
- P 8.24 Incel S., Hilairet N., Labrousse L., John T., Deldicque D., Ferrand T., Wang Y., Renner J., Morales L., Schubnel A.: Laboratory earthquakes triggered during eclogitization of lawsonite bearing blueschist

8.1

Transition from elastic to inelastic deformation identified by seismic attenuation, not seismic velocity

Auke Barnhoorn¹, Jeroen Verheij¹ and Marcel Frehner²

¹ Department of Geoscience and Engineering, Delft University of Technology, Stevinweg 1, NL-2628 CN Delft (auke.barnhoorn@tudelft.nl)

² Geological Institute, ETH Zurich, Sonneggstrasse 5, CH-8092 Zurich

The transition from elastic to inelastic deformation occurs at the yield point in a stress-strain diagram. This yield point expresses the moment permanent deformation occurs and is marked by the onset of fracturing in the brittle field at relatively low pressures and temperatures or the onset of dislocation and/or diffusional creep processes in the ductile field at higher temperatures and pressures. Detection of this transition in materials under stress using an indirect measurement technique is crucial to predict imminent failure, loss of material integrity, or of approaching release of energy by seismic rupture.

Here we use a pulse transmission method at ultrasonic frequencies to record the change in acoustic wave form across the transition from elastic to inelastic deformation in a rock-fracturing experiment. In particular, we measure both the acoustic wave velocity (Figure 1B) and attenuation (Figure 1C) with increasing strain from the elastic regime all the way to macroscopic failure.

Our results (Figure 1) show that the transition from elastic to inelastic deformation coincides with a minimum in attenuation (Figure 1C). At the same time, the acoustic wave velocity continues to increase across the transition from elastic to inelastic deformation (Figure 1B). Therefore, the acoustic velocity is not a valid indicator for this elastic-to-inelastic transition. However, we observe a minimum in attenuation for a range of different rock types (Barnhoorn et al., submitted) and this seems to be an almost universal feature. Therefore, the change in attenuation is a valid indicator for the onset of permanent deformation and fracturing.

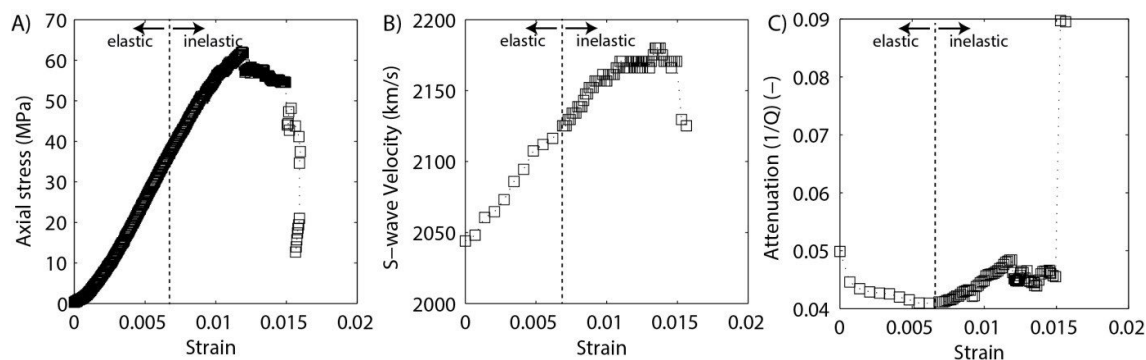


Figure 1: Example of mechanical and acoustic data for Whitby shale. A) Axial stress-strain data with shear wave velocity with strain (B) and shear wave attenuation with strain (C), both measured during the uniaxial compression experiment. The strain at which the transition from elastic to inelastic deformation behavior occurs is indicated with the dashed vertical line.

In Figure 2 we propose a conceptual model to explain our observations. Below the minimum in attenuation, pre-existing microfractures close, leading to a reduction of attenuation. Above this minimum, formation of new microfractures occurs and attenuation increases. In other words, attenuation is a function of the fracture density.

That the acoustic velocity does not react in the same way to the change in fracture density (Figure 1B) may be explained by the fracture orientation. For randomly oriented pre-existing microfractures, the fractures perpendicular to the uniaxial compression direction close preferentially. This leads to a preferred fracture orientation parallel to the sample axis at the onset of permanent deformation. New microfractures also preferentially form parallel to the sample axis, accentuating this preferred fracture orientation. This leads to a seismic anisotropy with the fast direction parallel to the sample axis, which increases throughout the experiment (i.e., crossing the elastic-to-inelastic transition).

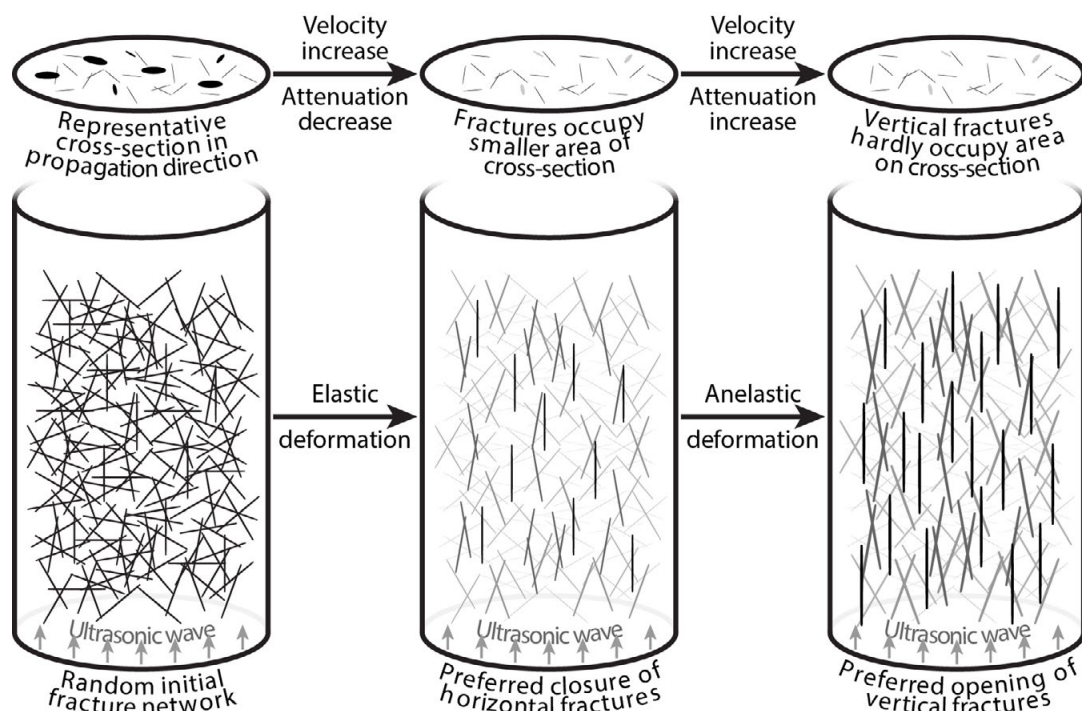


Figure 2: Conceptual model of fracture closure and opening of new fractures during a uniaxial compression experiment. The uniaxial compression results in a change in fracture density, but also in a change in fracture orientation from random to preferentially vertically oriented.

We propose that analysis of attenuation, not velocity, of acoustic waves through stressed materials may be used, for example, to detect imminent failure in materials, onset of crack formation in pipes or the cement casing in boreholes, or onset of fracturing in the near wellbore area. On a larger scale, attenuation monitoring may help predict the imminent release of energy by seismic rupture.

REFERENCE

Barnhoorn, A., Verheij, J., Frehner, M., Zhubayev, A. and Houben, M. submitted: Identification of the transition from elasticity to inelasticity from seismic attenuation analyses, *Geophysical Research Letters*.

8.2

Bouguer anomaly inversion at the Nirano Mud Volcanic Field, Italy, to infer depth and density variations of hydrocarbon and mud reservoirs

Aurore Carrier¹, Matteo Lupi¹, Antoine Haddad¹, Ludovic Baron², Niklas Linde²

¹ *Département des Sciences de la Terre et de Géophysique, University of Geneva, Rue des Maraîchers 13, CH-1205 Genève (aurore.carrier@unige.ch)*

² *Institut des Sciences de la Terre, University of Lausanne, Quartier UNIL-Mouline, Bâtiment Géopolis, CH-1015 Lausanne*

Mud volcanoes are often encountered in hydrocarbon provinces and considered as natural boreholes for sampling underlying reservoir formations. Mud volcanoes are still poorly investigated with geophysical methods. For example, little is known about their plumbing system or how fluids are transferred from the feeding reservoir to the surface.

To shed light on the underlying geometry of a logistically accessible mud volcanic system, the Nirano Mud Volcanic Field, Italy, we performed a gravity survey across the volcanic system. We used the gravimeter Scintrex CG5 and the GPS Leica 1200 to conduct two profiles striking N45 and N135.

The Bouguer Anomaly analysed with wavelength filtering indicate at least a 2000m-deep reservoir, two mid-depth reservoirs (i.e., 600 m deep) and three shallow ones (i.e., 100 m deep). Using these observations and previous studies as prior information, the Bouguer anomaly is then inverted via a gradient-based least-squares method that uses the LSQR algorithm and account for data and model covariances. Inversion results suggest two subspheroidal reservoirs at about 1500 m depth that are tilted by 30° that are overlaid by two reservoirs at intermediate depths (i.e. 600 m deep). Density variations range from 100 to 200 kg/m³. Due to the difficulty to constrain both geometry and density of the investigated reservoirs, complementary information (i.e. seismic and electrical resistivity tomography) may be used to further improve the results. Despite the degree of uncertainty of our investigations, this study represents the first attempt to provide a gravimetry-based geophysical image of the plumbing system of a mud volcanic field.

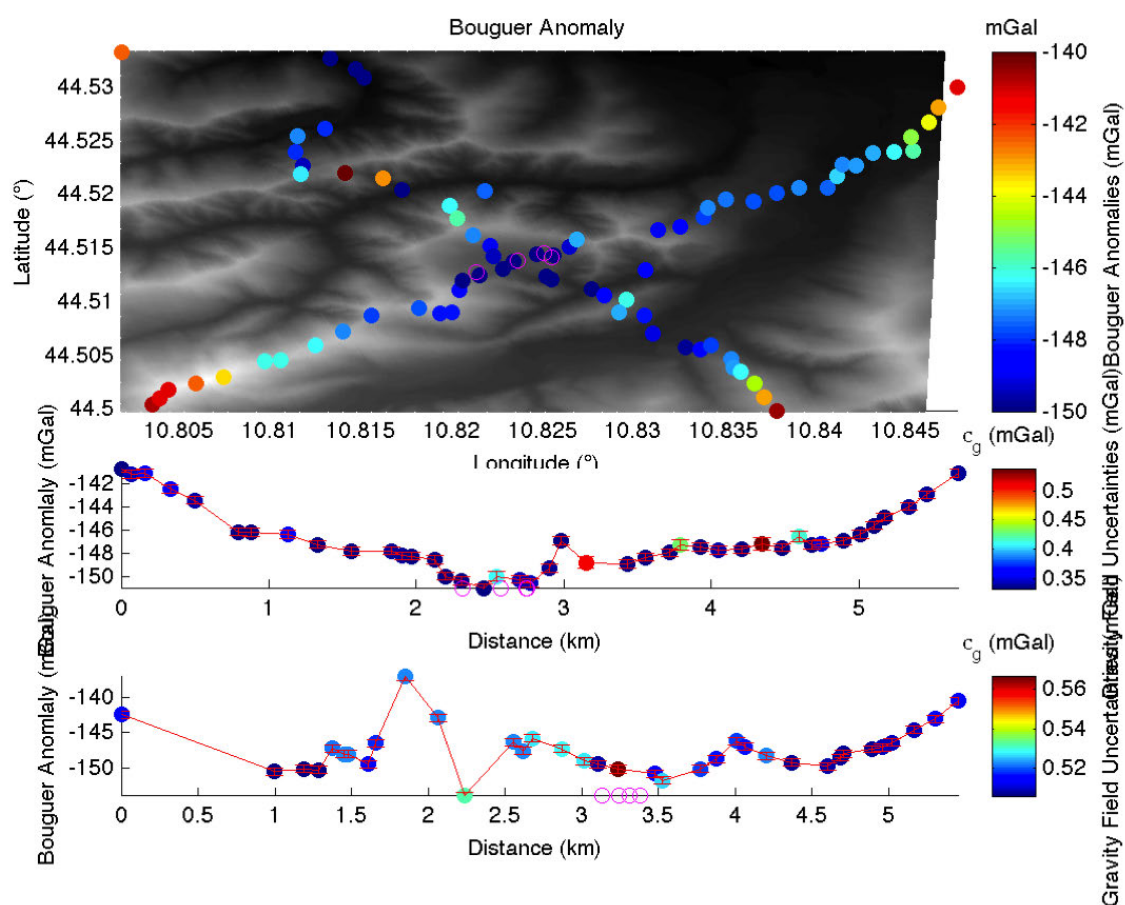


Figure 1. Top : Bouguer anomaly measured versus topography of the studied area (gray). Bottom : Two Bouguer Anomalies Lines Purple circles : mud volcanoes localization.

8.3

2D sensitivity kernels for monitoring weak changes on highly heterogeneous elastic medium

J. A. Duran¹, Anne Obermann¹

¹ *Institute of Geophysics, ETH Zurich, Sonneggstrasse 5, CH-8092 Zurich
(alejandro.duran@sed.ethz.ch)*

The main goal of most geophysical methods is an investigation and characterization of the subsurface. The most powerful geophysical tool hereby is the study of the passage of seismic waves through the Earth. The Earth is often assumed to be a simple stratified medium and the seismic waves will be reflected and refracted at the stratification boundaries. In classical seismic and seismology applications, this allows us to make direct conclusions about the subsurface from the traveltimes of the waves. However, the Earth is more complicated than the simple layer assumption and shows heterogeneities at different scales (mountain ranges (km), fractures (m), different grains (cm-mm)). These heterogeneities cause the late arriving waves to be multiply scattered within the medium, and wave propagation becomes very complex. These multiply scattered waves are called coda waves.

Besides their random character, coda waves are highly repeatable, such that if the medium remains unchanged over time, subsequent measurements of coda waveforms would be identical. Additionally, coda waves sample the medium very densely and become sensitive to even tiny perturbations of its mechanical (velocity, pressure, etc.) or structural (change of scatterer position, for instance due to fracturing) properties. This feature makes them ideal for monitoring purposes and has led to the development of the coda-wave interferometry (CWI) technique (Poupinet et al., 1984; Snieder et al., 2002; Snieder, 2006).

The technique makes use of coda waves to detect changes in the wave field due to a localized perturbation in the heterogeneous medium. This change is visible as a shift in the travel time between the perturbed and unperturbed wave fields.

Pacheco & Snieder (2005) developed a sensitivity Kernel which describes the relation between a localized perturbation in an acoustic medium and the change in the travel time. Since then, the detection of temporal changes with coda waves has been successfully applied in different areas in seismology such as: landslides (Mainsant et al. 2012), fault zones (Poupinet et al., 1984; Brenguier et al. 2008b), volcanoes (Grêt et al. 2005; Brenguier et al. 2008a), hydrocarbon reservoirs (Meunier et al. 2001), injection induced changes (Obermann et al. 2015; Hillers et al. 2015), as well as civil engineering applications (Larose et al. 2015, Salvermoser et al. 2015).

Despite the success obtained by the theoretical development of this Kernel, an extension on elastic medium is needed for a more complete description of the multiple scattering phenomena.

In a heterogeneous elastic medium, P and S waves are constantly converted from one state to another. A discrimination of the intensity contribution for each state is possible by an analytical approach which leads to a derivation of sensitivity kernels for each state individually. This means that travel time changes caused by a perturbation in the P-wave and S-wave velocities can be individually analyzed.

In the current study we address this problem from a numerical perspective. We developed 2D finite difference simulations over a synthetic highly heterogeneous elastic medium. The heterogeneity of the medium is characterized by verifying the equipartition of seismic waves (Hennino et al. 2001).

Then, P and S wave fields are recorded individually and each Kernel (K_p and K_s) is built from the intensity of the waves. Relative strength of K_p and K_s is studied, the effect of the source mechanism on the kernels as well as the sensitivity of the waves at different time steps.

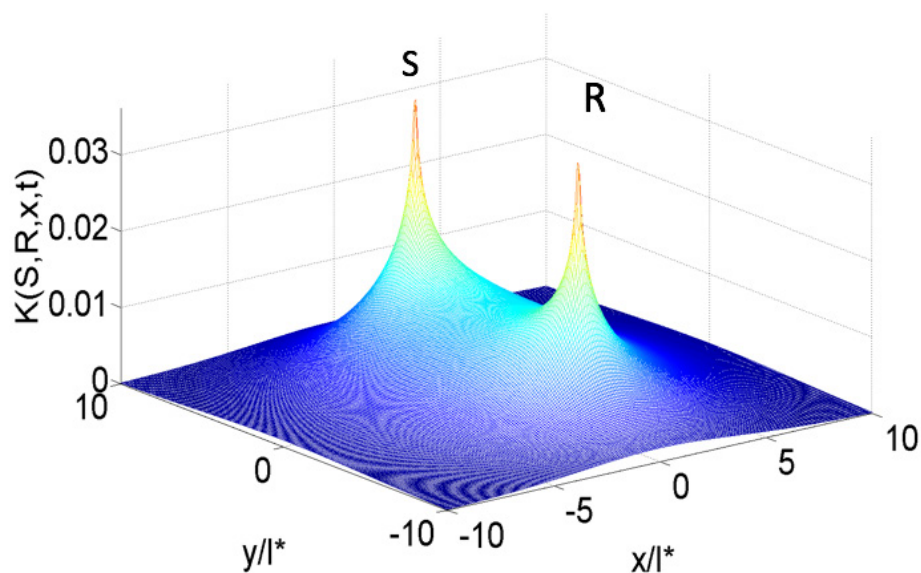


Figure 1. Spatial representation of the sensitivity kernel that describes the statistical time the waves spent in each part of the medium. The two peaks (R, S) indicate the position of the station pair. The time statistically spent in a region decreases with its distance to the stations (Obermann et al. 2013b).

REFERENCES

- Kanu, C. & Snieder R. 2015: Numerical computation of the sensitivity kernel for monitoring weak changes with multiply scattered acoustic waves. *Geophys. J. Int.* 203, 1923-1936.
- Obermann, A. et al. 2013a: Depth sensitivity of seismic coda waves to velocity perturbations in an elastic heterogeneous medium, *Geophys. J. Int.* 194(1), 372–382.
- Pacheco, C. & Snieder R. 2005: Time-lapse travel time change of multiply scattered acoustic waves. *J. Acoustic Soc. Am.* 118, 1300-1310.

8.4

A new seismic vector source: the Galperin source

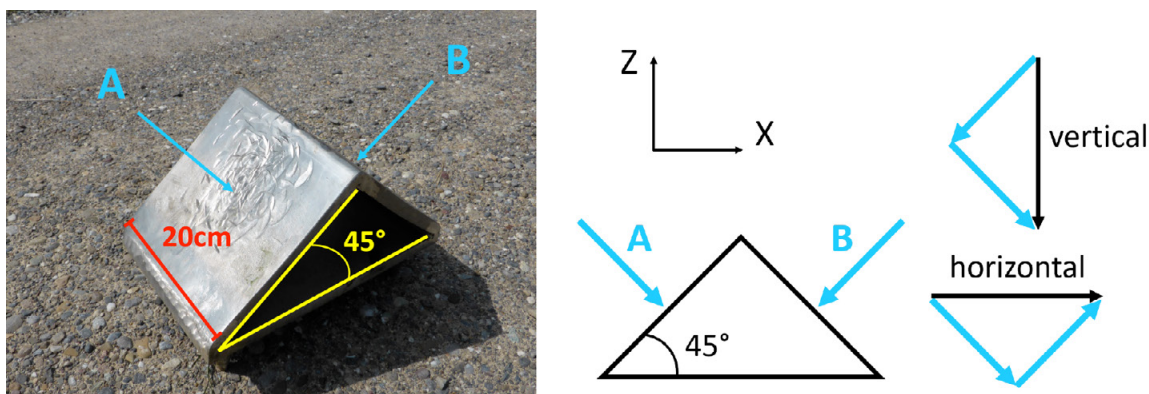
Mauro Häusler¹, Cedric Schmelzbach¹ & David Sollberger¹

¹ Institute of Geophysics, ETH Zurich, Sonneggstrasse 5, CH-8092 Zürich (cedric.schmelzbach@erdw.ethz.ch)

In the last decades, multicomponent seismic acquisition has experienced an increasing popularity in both exploration seismic surveying as well as in near-surface investigations (e.g., Hardage et al., 2011; Sollberger et al., 2014). Multicomponent measurements involve three-component (3C; vector) sources and/or 3C receivers and allow analysing the seismic wavefield in more detail than using single-component data only. For example, multicomponent data enable the analysis of shear waves to estimate elastic parameters for applications such as earthquake hazard and ground stability assessment. Furthermore, multicomponent data are critical for anisotropy and spatial seismic wavefield gradient studies.

Classic vertically-directed sources are, for example, a sledgehammer striking a steel plate and Vibroseis-sources. In order to excite horizontally polarized waves, shear beams and tilted or horizontal Vibroseis-sources have been employed. However, the source mechanism and source-to-ground coupling of these horizontally-directed sources may differ from vertically-directed sources, thus compromising a combined processing. Furthermore, horizontally-directed sources are usually more cumbersome in field operations. By hitting the two opposite sides of a metal wedge with 45°-inclined sides with a sledgehammer, a horizontal and a vertical source component can be obtained by either summing or subtracting the two records, which corresponds to a coordinate transformation (Figure 1a; Schmelzbach et al., 2016). Turning the wedge by 90° in the horizontal plane allows acquiring an additional transverse horizontal component. However, the re-positioning of the wedge is labour intensive and may change the source coupling. Furthermore, the total acquisition requires hits on four sites to obtain three directed source components; one vertical source-vector is redundant.

a)



b)

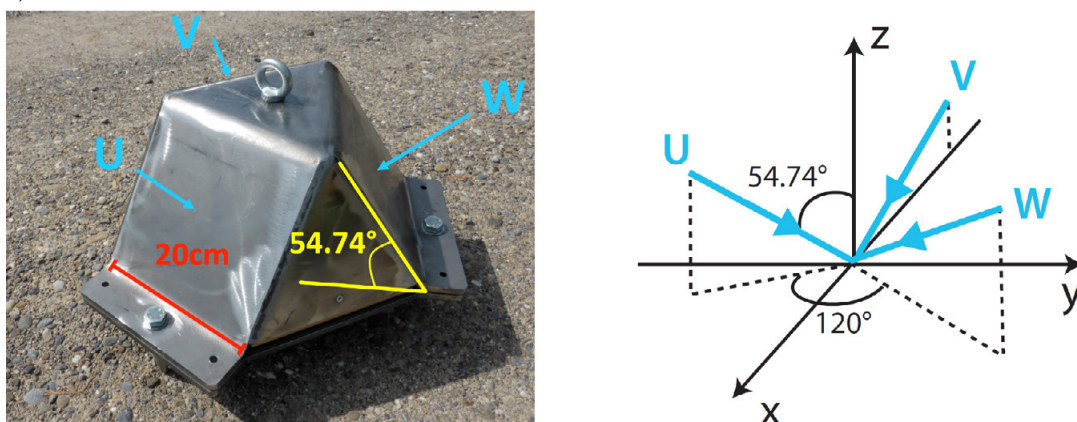


Figure 1. a) Metal wedge source as used, for example, in Schmelzbach et al. (2016). b) The Galperin source, a metal-wood construction using the Galperin configuration. Blue arrows indicate the source vector orientations.

With the motivation to develop an effective vector source with uniform source coupling for all three components, we designed a new source, called the Galperin source (Häusler, 2016). The acquisition principle is inspired by the Galperin receiver configuration known from, for example, the Streckeisen triaxial seismometer STS-2. The Galperin source consists of a three-sided steel pyramid that is struck with a sledgehammer (Figure 1b). The three normal vectors (corresponding to the source impact directions) are all orthogonal to each other with an angle of 54.74° to the vertical axis and separated by 120° in the horizontal plane. After acquisition, the seismic data is rotated into the Cartesian coordinate system to obtain source vectors parallel to all three coordinate axes. The Galperin geometry brings the advantage of identical impact patterns and consistent source coupling for all source components with three hits only.

To validate the Galperin source, we compared it to a metal plate and the metal wedge, all struck with the same sledgehammer. We found that the Galperin source compares well to these two sources when analysing, for example, amplitudes and phases, hodograms and frequency spectra. A possible limitation of the Galperin configuration is its sensitivity to errors in orientation, levelling and varying source strength. Synthetic-data studies indicate that the orientation and levelling error must not exceed 3° to keep the amplitude errors below 5%.

REFERENCES

- Häusler, M. 2016: 36 Component Seismic Data: Investigating Translational and Rotational Components in Exploration Seismology, MSc thesis ETH Zurich.
- Hardage, B. A., DeAngelo, M. V., Murray, P. E., & Sava, D. 2011: Multicomponent seismic technology, SEG, Tulsa.
- Schmelzbach, C., Sollberger, D., Greenhalgh, S. A., Horstmeyer, H., Maurer, H., & J. O. A. Robertsson 2016: 9C seismic data acquisition for near-surface applications: recordings, waveform reciprocity and 4C rotation, 78th EAGE Conference & Exhibition 2016, Vienna.
- Sollberger, D., C. Schmelzbach, H. Horstmeyer, F. Reiser, L. Rabenstein, H. Maurer, J. O. A. Robertsson, and S. A. Greenhalgh (2014), Mapping near surface-elastic parameters of quaternary sediments using multicomponent seismic techniques, EGU General Assembly 2014.

8.5

Role of metamorphic reactions on deformation and fluid flow: a new fully-coupled model

Benjamin Malvoisin^{1,2} Yury Y. Podladchikov¹, & James A. D. Connolly³

¹ *Institut des Sciences de la Terre, University of Lausanne, Géopolis, CH-1015 Lausanne (benjamin.malvoisin@unil.ch)*

² *Centre d'hydrogéologie et de Géothermie, University of Neuchâtel, Rue Emile Argand 11, CH-2000, Neuchâtel*

³ *Institut für Geochimie und Petrologie, Department of Earth Sciences, ETH Zürich, Clausiusstrasse 25, CH-8092 Zürich*

Metamorphic reactions do not only modify rock chemical and mineralogical compositions but they also have strong impacts on density and porosity. Therefore, the role of reactions on deformation and fluid flow has to be taken into account for modelling the evolution of metamorphic environments.

Here, we present a new model coupling reaction, deformation and fluid flow. Based on mass conservation and using a poro-viscoelastic rheology, new equations are derived for fluid pressure and porosity evolutions in reactive systems. The impact of reactions on density and porosity is predicted by using energy minimization calculations at the equilibrium. A delay in the achievement of equilibrium is introduced to model the effect of reaction kinetics. The validity of this model is demonstrated through the reproduction of the purely mechanic and equilibrium limits. Among the various parameters controlling the impact of reaction on deformation and fluid flow, the Clapeyron slope relating the evolution of porosity with pressure is shown to play a key role. This is well evidenced with the modelling of reacting porosity waves propagation in the crust providing a new complete mechanism for episodic tremor and slip events propagation.

8.6

Geophysical data inversion with graph cuts under geological realism constraint

Guillaume Pirot¹, Niklas Linde¹, Grégoire Mariethoz² & John Bradford³

¹ *Institut des sciences de la Terre et de l'environnement (ISTE), University of Lausanne, UNIL-Mouline, CH-1015 Lausanne (guillaume.pirot@unil.ch)*

² *Institut des dynamiques des surfaces terrestres (IDYST), University of Lausanne, UNIL-Mouline, CH-1015 Lausanne*

³ *Department of Geosciences, Boise State University, 1910 University Dr., Boise, ID 83725, USA*

In hydrogeological applications, flow path and mass transfer are strongly influenced by the subsurface connectivity. When using geophysics to characterize an aquifer, it becomes important that geophysical inversion results are in agreement with the expected geological setting. Another important aspect in such applications is the quantification of uncertainty. To achieve these, we combine two concepts. Within a Markov chain Monte Carlo (MCMC) method that enables inversion of geophysical data and uncertainty quantification, we embed a multiple-point statistics algorithm which allows to generate complex geological structures. Compared to iterative pixel-based multiple-point statistics technique, patch-based multiple-point statistics techniques such as graph cuts considerably speed-up the algorithm. The efficiency of the algorithm has already been proven on synthetic cases.

Here we propose a first-ever field application by estimating the porosity field from ground penetrating radar data at the Boise Hydrogeophysical Research Site, Boise, Idaho. We consider two different prior models (training images) : one multi-Gaussian and one outcrop-based that are in agreement with available porosity data. In both case, the posterior realizations honor the pattern characteristics of the related prior. Convergence of the multi-Gaussian model is much faster than for the outcrop-based prior model, but the latter is geologically more realistic and it better preserves the full porosity range of the prior.

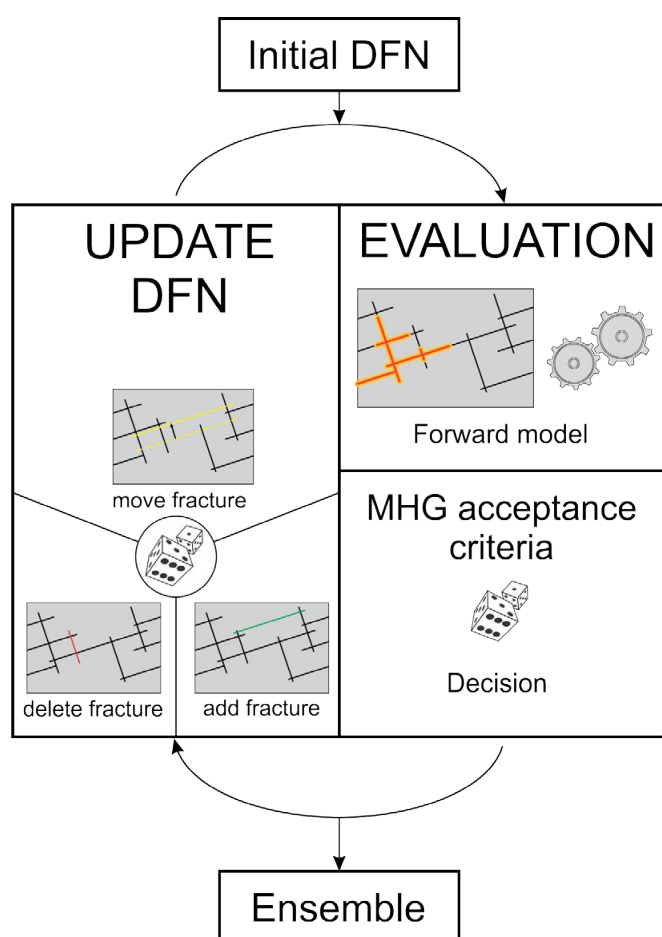
8.7

Fracture network characterization using a stochastic transdimensional algorithm

Márk Somogyvári*, Mohammadreza Jalali*, Peter Bayer*

¹ Department of Earth Sciences, ETH Zürich, Sonneggstrasse 5 CH-8092 Zürich (mark.somogyvari@erdw.ethz.ch)

Transport in fractured media is dominated by the geometry of the fracture network. While some geometrical properties of fractures like orientation and spacing can be easily captured from borehole logs, core images and outcrops, the assessment of the actual geometry of the fractured system (e.g. fracture length, height and width) is a great challenge, and could require the interpretation of transport related experiments. Existing interpretation methods are limited as they either approximate the fracture system as continuous media or provide fracture network realizations that are not conditioned to the measurements. Modern tomographic investigation methods in hydrogeology have proven to be able to provide insight into the distribution of the physical properties to infer the geometries of the fractures via introducing discrete fracture network (DFN) models which can be used for parametrization and rapid forward modelling. In this study we present a novel concept, using the reversible jump Markov Chain Monte Carlo (rjMCMC) method to characterize the fracture network geometry by interpreting tomographic tracer experiments in fractured aquifers.



A random initial DFN realization is generated using the statistical information on the fractured media, such as fracture intensity, fracture length distribution and fracture spacing. This fracture network is then evolved through an iterative stochastic inversion process. During each iteration a new DFN realization is proposed by updating the last accepted realization via deleting, adding or moving a fracture in the DFN. An implicit upwind finite difference method is used to simulate fluid and heat transport within the fracture network during the tomographic thermal tracer experiment – as the forward model of the inversion. To evaluate the proposed DFN realization, the Metropolis-Hastings-Green acceptance criterion is used which is the standard evaluation step of rjMCMC methods. A successful rjMCMC modelling requires large number of iterations and results in an ensemble of thousands of equally probable DFN realizations. From the ensemble of accepted realizations fracture probability maps are generated – showing the possible fracture locations thus highlighting the dominant transport conduits. Individual DFN realizations from the ensemble can be used for deterministic modelling whereas using the full ensemble it is possible to create stochastic flow and transport simulations for practical applications (e.g. risk assessment, efficiency studies).

Figure 1. Visual summary of the used reversible jump Markov Chain Monte Carlo method for discrete fracture network (DFN) reconstruction.

8.8

Coupled hydro-mechanical modelling of seismicity induced by gas production

Dominik Zbinden¹, Antonio Pio Rinaldi¹, Luca Urpi¹ & Stefan Wiemer¹

¹ *Institut für Geophysik, ETH Zürich, Sonneggstrasse 5, CH-8092 Zürich (dominik.zbinden@sed.ethz.ch)*

Induced seismicity due to natural gas exploitation has been observed at many sites around the world. It has been suggested that the pressure drop caused by gas production leads to compaction, which affects the stress field in the reservoir and the surrounding rock formations. This in turn can reactivate pre-existing faults and hence trigger earthquakes. Although these induced seismic events are often moderate in magnitude, some of them can be felt at the ground surface causing nuisance to the population and sometimes moderate damages to structures. A well-known example is the Groningen gas field in the Netherlands, where production-induced seismicity has caused damage to buildings close to the production site. Given the high public impact, it is crucial to understand the underlying processes during natural gas exploitation.

We carried out numerical simulations to better determine the conditions leading to fault reactivation. In our numerical model, gas is produced from a permeable reservoir, divided into two compartments by a low permeability fault zone and overlain by impermeable caprock. In contrast to previous modelling approaches, the fault in our model is serving as a bound for the gas reservoir, which is more realistic than assuming an unbounded, infinite reservoir. We used a simulator that couples multiphase fluid flow and geomechanics in order to account for gas and water flow within the reservoir and the fault. We performed a sensitivity analysis aimed at investigating different production scenarios and fault properties.

The results show that fluid flow plays a major role pertaining to pore pressure and stress evolution within the fault. Fluid inflow into the fault leads to bending of the stress path, causing rupture to occur at lower depletion levels and lower stresses than would be expected when neglecting fluid flow. In addition, the offset of the reservoir leads to uneven compaction, causing the shear stress in the fault to increase stronger compared to the case of a reservoir without offset. We also analysed the scenario of multiple production wells, and results show that simultaneous production does not prevent the fault to be reactivated. Actually, the rupture occurs at much higher stresses, because the contraction of the two offset reservoir compartments leads to an additional increase in shear stress in the fault. However, because the induced shear stress is opposing the tectonic stress in the upper part of the right reservoir compartment, the rupture is halted at the reservoir/caprock interface, leading to a smaller seismic event compared to the single well case.

P 8.1

An experimental study of the influence of pore water on dynamic rupture processes.

M.Acosta¹, F.Passelegue², A.Schubnel³ and M.Violay¹.

¹ LEMR, ENAC, École polytechnique fédérale de Lausanne (EPFL), Lausanne, Switzerland,

² School of Earth, Atmospheric and Environmental Sciences, University of Manchester, Manchester, UK,

³ Laboratoire de Géologie, Ecole Normale Supérieure de Paris, CNRS UMR8538, 24 rue Lhomond, 75005 Paris, France.

Fluids play a fundamental role in controlling fault strength and earthquake nucleation, propagation and arrest (Sibson, 1973, 2000; Lachenbruch, 1980; Rice, 1992, 2006; Hickman et al., 1995). The understanding of how the presence of fluid in faults affects the seismic cycle in the upper continental crust remains poor, especially in the case of induced seismicity due to engineering applications (Hydraulic stimulations). To examine the influence of pore water on dynamic rupture processes in the context of deep geothermal reservoirs, we conducted stick slip experiments on thermally-treated, saw-cut westerly granite samples under triaxial loading ($\sigma_1 > \sigma_2 = \sigma_3$) at confining pressures (σ_3) ranging from 10 to 95 MPa and pore water pressures ranging from 0 to 94 MPa (Schubnel et al. 2011 and Passelègue et al. 2013, 2016). The samples were instrumented with four strain gages recorded at high frequencies and one thermocouple located close to the fault plane, that allowed measuring respectively dynamic shear stress drops and temperature elevation. The nucleation point of slip and rupture speeds were assessed during the experiments through an acoustic monitoring array. The method consists in recording particle motion at high-frequencies for each acoustic emission event and inverting the arrival times for each sensor of the array. We recorded more than 200 stick slip events. Preliminary results showed that at a given effective confining pressure ($P_c - p_f$), the dynamic shear stress drops were about 20 to 30% higher and slip distances were about 30 to 40% longer in dry samples than in water saturated samples. Following the same tendency, higher temperature elevations were recorded during nominally dry experiments. These results highlight the importance of pore water pressure in frictional processes, and suggest that water might inhibit dynamic weakening and so, rupture propagation in granitic rocks.

P 8.2

Petrophysical properties through a Grimsel granodiorite shear zone – Implications for geothermal reservoir evaluation and modelling

Quinn Wenning¹, Claudio Madonna¹, Evangelos Moulas² & Jean-Pierre Burg¹

¹ Geological Institute, ETH Zurich, Sonneggstrasse 5, CH-8092 Zurich

Corresponding Author: Q. Wenning (quinn.wenning@erdw.ethz.ch)

² Institute of Geochemistry and Petrology, ETH Zurich, Clausiusstrasse 25, CH-8092 Zurich

This study focuses on measurements of elastic and fluid flow properties through a fault zone that first deformed ductilely and subsequently experienced brittle faulting. Measurements were performed on core material from the Grimsel Test Site (GTS) underground research laboratory. We measured the seismic velocities, porosity, and permeability, perpendicular and parallel to ductile foliation, systematically every 0.1 m in the 0.7 m transition zone between the host rock and the first fault core penetrated by the borehole. The studied fault zone consists of a foliated ductile transition zone grading from the host rock to the first ductile mylonitic fault core (also locally known as lamprophyres). A fractured damage zone (~3 m wide) formed between the first fault core and is bounded by another fault core at the base of the well. Foliation plane parallel p - and s -wave velocities and permeability systematically increase from the host rock towards the fault core. The positive correlation between foliation parallel velocity and permeability is contrary to what is typically shown in brittle fault damage zones. Although brittle deformation has persisted in recent times, antecedent ductile structures continue to control the matrix elastic and fluid flow properties instead of microfractures. The results demonstrate how physical characteristics of faults in crystalline rocks change in proximity to the fault core. In addition, insight is shed on the transient changes as fault rock properties undergo ductile to brittle transitions. In such crystalline rocks the elastic and fluid flow properties have important implications for natural crustal processes and exploitation and use in geothermal energy and waste storage. The characterization of such a system is particularly important to geothermal resource evaluation and reservoir modelling.

P 8.3

Modelling of fluid injection into a frictional weakening dilatant fault

Federico Ciardo & Brice Lecampion¹

¹ *Geo Energy Laboratory – Gaznat Chair on Geo-Energy (GEL), École Polytechnique Fédérale de Lausanne (EPFL), EPFL-ENAC-IIC-GEL Station 18, CH-1015 Lausanne (federico.ciardo@epfl.ch)*

Understanding the mechanism of nucleation of dynamic rupture is an important issue in seismology. It is the key factor in determining the seismic potential of pre-existing faults under long-term loadings. Furthermore, the activation of Mode II fracture by means of fluid injection is the way to enhance the permeability of deep geothermal reservoirs (Enhanced Geothermal Systems) whose efficacy rely on the shear-induced dilation.

Locally elevated pore pressure associated with fluid injection leads to a reduction of the fault frictional strength (product of the local normal effective stress and the slip-weakening friction coefficient) which may eventually falls below the background shear stress. As a result, a shear crack will start to propagate with an initially moderate velocity (quasi-static) as it is induced by fluid pressure diffusion. As slip accumulate, the quasi-static crack growth may become unstable due to the slip-weakening nature of friction, resulting in the nucleation of a dynamic rupture until residual frictional strength is reached (see Garagash & Germanovich, 2012). The size of such a dynamic rupture (associated with fluid injection) is intrinsically related to both the way the pore-pressure distribution evolves spatially and temporally along the fault and the initial background shear stress. Larger dynamic ruptures are actually obtained for lower overpressure that are spread over larger zones, while a dynamic rupture associated with larger (but more localized) peak overpressure reaches residual friction earlier. Moreover, for large values of overpressure (with respect to the initial effective stress state along the fault), the nucleation length is smaller for lower value of the background shear stress.

In this contribution, we investigate the effect of the shear dilatancy of the fault on the diffusion of pore pressure. Dilatancy may locally reduce pore-pressure depending on the ability of the fluid to flow in the newly created void space. Reduction in pore-pressure associated with dilatancy can result in increase of the fault shear resistance and thus can potentially arrest a dynamic rupture.

We formulate a 2D model of fluid injection in a shear dilatant fault exhibiting slip weakening friction. The model couples elastic deformation, shear weakening Coulomb friction with dilatancy and fluid flow along the fault. We develop a numerical scheme based on boundary element (Displacement Discontinuity Method) for elastic deformation and a finite volume scheme for fluid flow. We verify our solver first on the non-dilatant case by comparing our results with the solution of Garagash & Germanovitch (2012). We then investigate the effect of shear-dilatancy and its feedback on the nucleation of dynamic rupture.

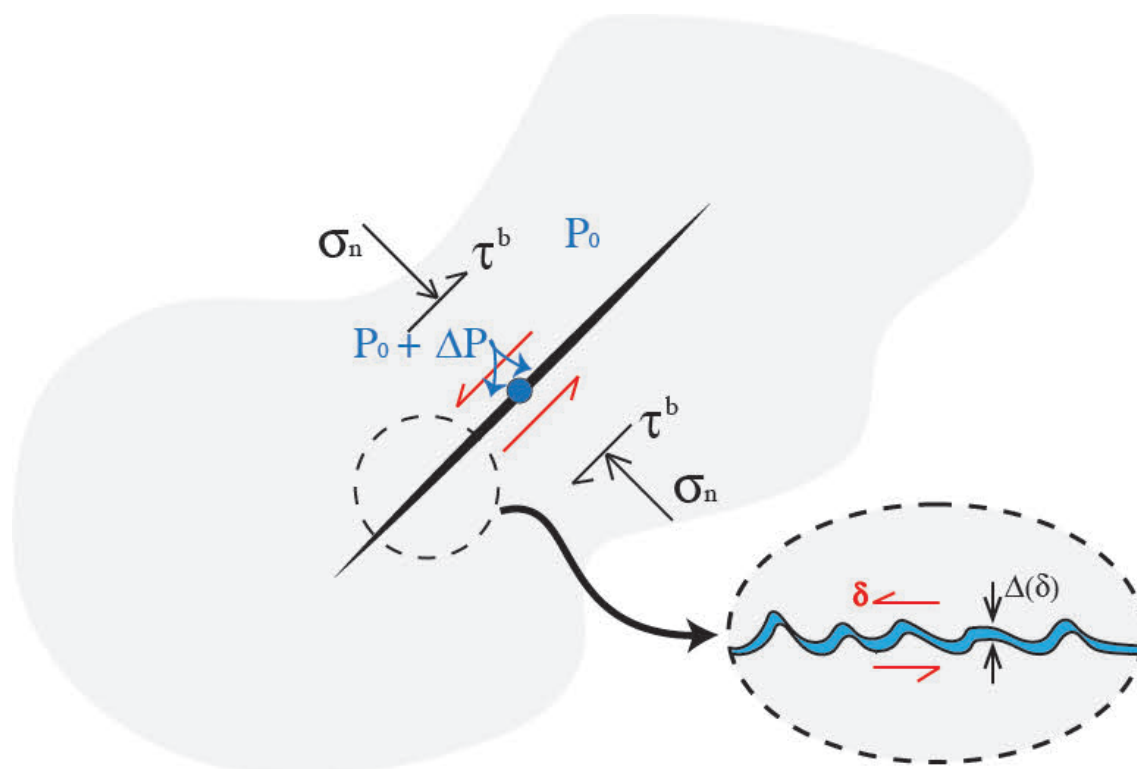


Figure 1. Sketch of frictional weakening dilatant fault under fluid injection.

REFERENCES

- Garagash, D.I., and J.W. Rudnicki. 2003: Shear heating of a fluid-saturated slip-weakening dilatant fault zone, 1, Limiting regimes. *J. Geophys. Res.* 108(B2), 2121.
- Garagash, D.I., and L.N. Germanovich. 2012: Nucleation and arrest of dynamic slip on a pressurized fault. *J. Geophys. Res.* 117(B10310).
- Hillers, G., and S.A. Miller. 2007: Dilatancy controlled spatiotemporal slip evolution of a sealed fault with spatial variations of the pore pressure. *Geophys. J. Int.* 168, 431-445.
- Rudnicki, J.W., and C-H. Chen. 1988: Stabilization of Rapid Frictional Slip on a Weakening Fault by Dilatant Hardening. *J. Geophys. Res.* 93(B5), 4745-4757.
- Segall, P. and J.R. Rice. 1995: Dilatancy, compaction, and slip instability of a fluid-infiltrated fault. *J. Geophys. Res.* 100(B11), 22,155-22,171.

P 8.4

Geothermal potential of the Geneva Basin: the aid of petrophysical laboratory data.

Mahmoud Hefny¹, Alba Zappone^{2,3}, Claudio Madonna¹, Andrea Moscariello⁴, Jean-Pierre Burg¹

¹ *Geological Institute, ETH Zurich, Sonneggstrasse 5, CH-8092 Zurich
(mahmoud.hefny@erdw.ethz.ch)*

² *Swiss Seismological Service, ETH Zurich, Sonneggstrasse 5, CH-8092 Zurich*

³ *Institute of Process Engineering, ETH Zurich, Sonneggstrasse 3, CH-8092 Zurich*

⁴ *Department of Earth Sciences, University of Geneva, rue des Maraichers 13, 1205 Geneva*

GEothermie 2020 (<http://www.geothermie2020.ch>) is an exploration program sponsored by the State of Geneva and SIG (Service industriel de Geneve), to integrate the subsurface geological and geophysical data and evaluate the potential of geothermal energy production in the Geneva basin (Moscariello, 2016). Under the umbrella of this program, the Department of Earth Sciences at UniGeneva together with the Rock Deformation Laboratory at ETH Zurich have undertaken a joint research project focussed on physical properties relevant for the assessment of the geothermal potential. We present some preliminary results, including petrography and porosity measurements. Aim of the research is to characterise the influence of the mineral composition and texture on the seismic response of the key lithologies of the Molasse Basin.

Particular attention is given to the following aquifer/aquitard pairs:

- Hauptrogenstein/Effinger member (Lower Oxfordian)
- Upper Marine Molasse/Upper Freshwater Molasse
- Buntsandstein/Anhydrite Group
- Upper Muschelkalk/ Gypskeuper
- Lower Cretaceous/Lower Freshwater Molasse

The samples to test derive from borehole plugs of the Humilly (France) borehole, made available from TOTAL S.A.. 59 cylindrical samples of 25.4 mm diameter and > 30 mm length were collected. Where possible the cores were cut parallel and perpendicular to sedimentary banding or layering, in order to investigate rock anisotropy. Thin sections were prepared from the heads of the cylinders and represent the starting material for mineralogical and modal composition assessment. Further on, quantitative petrography and image analysis with the QEMSCAN at UniGeneva allows characterizing the rock microtexture. Bulk and grain density has been measured with the aid of a helium pycnometer. Porosity and permeability have been measured on the same sample set. These new measurements add substantially in assessing the potential for geothermal challenges in the Geneva region.

This analyses will be followed by ultrasound velocity data (V_p and V_s) experimental tests on the same samples, at room temperature and at increasing pressure to reach reservoir conditions. The dataset that will be collected will help the interpretation of the seismic data available, and represent a complete and well constrained set of input parameters for numerical modelling of the Geneva basin subsurface.

REFERENCES

Moscariello A. 2016: Geothermal exploration in SW Switzerland, Proceeding of the European Geothermal Congress, Strasbourg 19-23 september 2016, 9 pp.

P 8.5

Simulating fully three-dimensional pressurized fracture propagation

Dmitry Nikolskiy¹, Brice Lecampion

*Geo-Energy Laboratory - Gaznat Chair on Geo-Energy, Ecole Polytechnique Fédérale de Lausanne, Switzerland
EPFL-ENAC-IIC-GEL, GC B1 391 (Bâtiment GC), Station 18, CH-1015 Lausanne*

¹ Corresponding author (dmitry.nikolskiy@epfl.ch)

We report the progress on a new computational technique for fully three-dimensional simulation of propagation of hydraulic fractures in the vicinity of a wellbore. One of the components of this technique is the boundary element code for modeling the elastic deformation of rock containing pressurized cracks developed previously by the first Author (see Nikolskiy, Mogilevskaya & Labuz, 2015). This code requires the use of only surface mesh, which facilitates its coupling with models of the fluid flow through the fractures. The code also features second order polynomial approximations of the boundary unknowns, which allow for accurate resolution of the cracks opening and sliding displacement near the tips and the stresses around these tips. The example of numerical solution of a problem of two pressurized cracks initiating from a borehole obtained with this code (the calculated boundary displacements) is given in Figure 1.

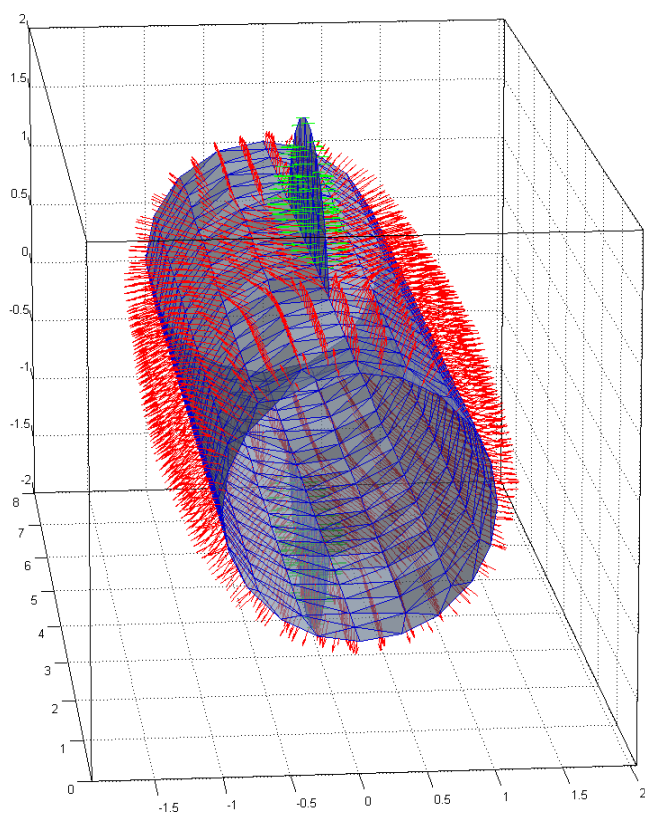


Figure 1. The boundary displacements (red) and displacement discontinuities (green) on two pressurized cracks initiating from a borehole.

In the present work, we further develop the code incorporating a fracture propagation algorithm that is capable of capturing the effects of mixed-mode loading (see Lazarus et al., 2001; Pham & Ravi-Chandar, 2016). In particular, we focus on the segmentation of the fracture front observed under combined opening (mode I) and anti-plane shear (mode III) load during fracture re-orientation from a wellbore. We discuss the importance of such fracture segmentation for the stimulation of unconventional reservoirs as well as for enhanced geothermal systems.

REFERENCES

- Nikolskiy, D.V., Mogilevskaya, S.G. & Labuz, J.F. 2015: Boundary element analysis of non-planar three-dimensional cracks using complex variables. *International Journal of Rock Mechanics and Mining Sciences*, 76, 44-54.
- Lazarus, V., Leblond, J.B. & Mouchrif, S-E. 2001: Crack front rotation and segmentation in mixed mode I+III or I+II+III. *Journal of the Mechanics and Physics of Solids*, 49, 1399-1443.
- Pham, K.H. & Ravi-Chandar, K. 2016: On the growth of cracks under mixed-mode I+III loading. *International Journal of Fracture*, 199, 105-134.

P 8.6

Viscosity fluid influence on stick-slip motions

Chiara Cornelio¹, Marie Violay¹, Spagnuolo Elena²,

¹ *Laboratory of Experimental Rock Mechanics, EPFL, Station 18 CH 1015 Lausanne* ¹(chiara.cornelio@epfl.ch)

² *Sezione di Sismologia e Tettonofisica, Istituto Nazionale di Geofisica e Vulcanologia, Via di Vigna Murata 605, 00143 Roma, Italy*

The Enhanced Geothermal System (EGS) offers a great potential for developing the use of geothermal energy, allowing the creation of hydrothermal reservoirs in deep and hot geological formations, where energy production was impossible due to a lack of fluid or permeability. In order to guarantee the economic flow rates of the system, this technology allows to improve the permeability of the rock pumping high-pressure fluid from an injection well.

With the injection of fluid, the stress equilibrium of the rock formation could change and lead to enhanced seismic activity. Thus making necessary to investigate the physical and chemical role of pore fluid (i.e., water pressure, flow rate water chemistry, and water density and viscosity) on the fault stability and lubrication, in order to optimise the hydraulic stimulation in a EGS.

With this purpose, a first series of experiment has been set up in dry and wet conditions using fluids with different viscosity for direct shear tests and rotary shear tests on pre-cut samples of Westerly granite. Normal stress varied from 0.3 MPa to 10 MPa. Slip velocity was set at ~ 0.008 mm/s. Water and glycerol with different concentrations (0% and 80%) have been used for the wet tests thereby the kinematic viscosity ranges between about $1 \text{ mm}^2\text{s}^{-1}$ to $50 \text{ mm}^2\text{s}^{-1}$. Glycerol has been chosen because it is fully miscible with water and is not considered as a lubricant.

First results show differences in stick-slip motions that occur with the different configurations. The amplitude of stress drops are larger for wet conditions than for dry one, in particular it grows as the viscosity increases. At the same time, the viscosity of the fluid layer negligibly affects the macroscopic frictional resistance, reducing the mean static friction coefficient of only 10% above the dry condition.

P 8.7

Stress Characterisation and stress modeling at the Grimsel Test Site for the In-situ Stimulation and Circulation Project

Nathan Dutler² now at ¹Benoît Valley¹, Hannes Krietsch², Florian Amann², Valentin Gischig² & Keith Evans²

¹ Centre for Hydrogeology and Geothermics, University of Neuchâtel, Rue Emile-Argand 11, CH-2000 Neuchâtel

² Geological Institute, ETH Zurich, Sonneggstrasse 5, CH-8092 Zurich

The controlled creation of permeability at great depth is a major challenge for the development of deep geothermal projects in Switzerland and worldwide. The interplay between an interconnected fracture network and the in-situ stress field governs the permeability creation processes. The In-situ Stimulation and Circulation (ISC) project taking place at the Grimsel Test Site (GTS) aims at enhancing our understanding of these processes. A good comprehension of the in-situ stress field is a prerequisite to design the ISC experiment.

Thus, a stress characterization campaign was performed in the target rock mass for the ISC experiment, which includes overcoring, and hydraulic fracturing methods. The stress determination from various methods do not agree on all stress parameters. The micro-seismicity cloud recorded during hydraulic-fracturing indicates the minimum principal stress is sub-horizontal and orientated in NNE direction, similar to the results of other measurements conducted in the vicinity (e.g. Pahl et al., 1989), although there are also indications of local heterogeneity of the stress field. This contribution presents results of numerical stress models based on the geological model that attempt to match and explain the observations made during the stress measurement campaign and possibly explain some of the observed discrepancies. The stress models permit an evaluation of the effect on the stress field of such factors as topographic and tectonic loading on the regional scale.

The modelling work was performed using the 3D distinct element code 3DEC from ITASCA. As a first step, an isotropic elastic model was developed that reproduced the results derived in earlier numerical studies at the GTS (Konietzky and Marschall, 1996; Ziegler et al, 2016). Tectonic loading was simulated by imposing shortening of the distance between opposite boundaries. Shortening in directions striking 105-285° (MOD105) and 150-330° (MOD150) was needed to reproduce the measurements from hydraulic-fracturing and overcoring respectively. In total four different constitutive models were applied: isotropic elastic, transversal elastic, linear plastic and bilinear plastic. The transversal elastic model indicates that anisotropy does not have a major influence compared to the results of the isotropic elastic models. The linear plastic behaviour represented by Byerlee's law for a normal tectonic regime provides questionable stress tensor results up to a depth of 1000 m. The bilinear plastic behaviour represented by a combination of Byerlee's law and micro-crack initiation threshold delivers similar stress tensors as the isotropic elastic models.

The stress model fails to explain the hydraulic fracture orientation inferred from the alignment of micro-seismic events monitored during the hydraulic fracturing tests. The stress models with a regional loading directions striking 150-330° fits best with the overcoring measurements from field campaign. The model leads to a maximum principal stress magnitude between 19.3 and 24.9 MPa with a dip direction of 142° and a dip of 12°. The intermediate axis is located sub-horizontal with a magnitude of 11.7-12.3 MPa. Dip and dip direction are both around 41°. The minimum principal stress has a magnitude between 9.1 and 9.3 MPa with a dip of 46° and 246° azimuth which is also in general agreement with the overcoring results. Generally, the models show the predominance of the topographic influence on the stress state at the GTS, and tend to validate the overcoring stress measurement results, because the tectonic loading is more consistent with the large-scale stress direction from the World Stress Map. Currently, the observed orientations of the hydraulic fractures remain unexplained.

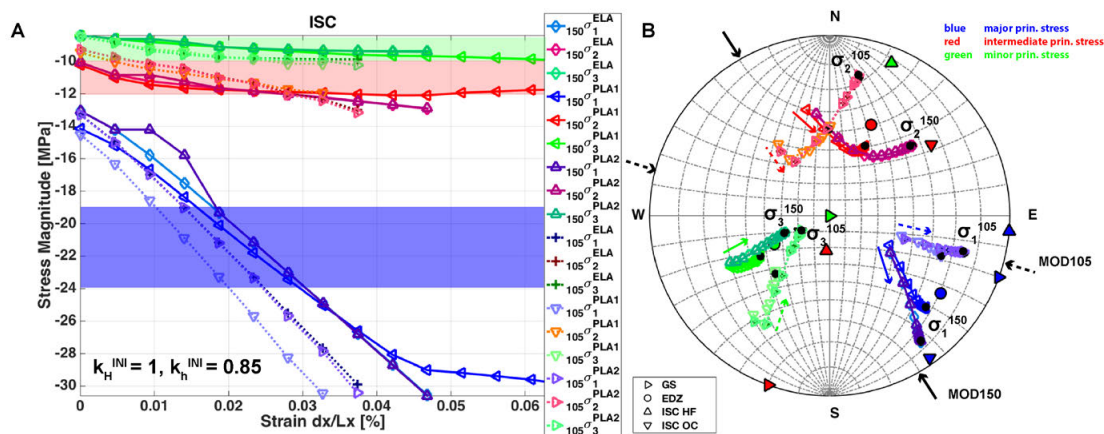


Figure. 1: A and B have an k_h^{ini} of 0.85. The shortcuts in the legends are for the elastic isotropic behavior (ELA), the linear plastic behavior (PLA1) and the bilinear plastic behavior (PLA2). The dashed lines indicate the results for MOD105 and the solid ones for MOD150. The transparency color bars in A display the most reliable observed magnitude range from the measurements.

REFERENCES

- Konietzky, H., & Marshall, P. (1996). Excavation disturbed zone around tunnels in fractured rock – Example from the Grimsel Test Site. In Z. Rakowski (Ed.), *Geomechanics* (p. 235 - 240). Rotterdam / Brookfield: A.A. Balkema.
- Krietsch, H., Doetsch, J., Amann, F., Gischig, V., Jalali, M., Evans, C. M. K., . . . Loew, S. (2016, 04). Preliminary stress characterization for an in-situ stimulation experiment at the Grimsel Underground Laboratory. Vienna.
- Leith, K., Moore, J. R., Amann, F., & Loew, S. 2014: In situ stress control on microcrack generation and macroscopic extensional fracture in exhuming bedrock. *J. Geophys. Res. Solid Earth*, 119, 594-615.
- Pahl, A., Heusermann, S., Bräuer, V., & Glöggler, W. (1989). *Rock Stress Investigations* (Tech. Rep. No. NTB88-39E). Wettingen: Nagra.
- Ziegler, M. and Loew, S. and Amann, F. (2016). Near-surface rock stress orientations in alpine topography derived from exfoliation fracture surface markings and 3D numerical modelling. *Intl J Rock Mech Mining Sci.ens*, 85, 129-151.

P 8.8

Acoustic monitoring of laboratory hydraulic fracture growth under stress and pore pressure

Thomas Blum¹ & Brice Lecampion¹

¹ *Geo-Energy Laboratory – Gaznat chair on Geo-Energy, Ecole Polytechnique Fédérale de Lausanne, EPFL-ENAC-IIC-GEL, Station 18, CH-1015 Lausanne (thomas.blum@epfl.ch)*

Fluid-driven fracturing is used in a wide range of applications, including oil and gas extraction, geothermal energy recovery, and CO₂ sequestration. In order to efficiently fracture the targeted rock formation, theoretical models provide estimates of the fracture size and shape. Carrying properly scaled laboratory experiments, on the other hand, allows to validate theoretical predictions by providing complete datasets of individual experiments performed under controlled conditions, and therefore to better understand the physics of fluid-driven fracturing. The DelFrac Consortium at TU Delft pioneered this field by building an acoustic monitoring setup inside a triaxial press applying three independent stresses on a cubic specimen (Groenenboom, 1998).

At the Geo-Energy Lab, we intend to further investigate the solid and fluid mechanics of hydraulic fractures by building a novel experimental setup in our EPFL facility. The fracturing setup will consist in a triaxial frame designed to accommodate cubic-shaped specimens of up to 250 mm in length, and to apply up to 20 MPa independently on each axis. We will also have the ability to pressurize a pore fluid up to 5 MPa inside the frame in order to simulate in-situ conditions. Our current high-pressure pump can inject fluids with a maximum pressure of 51 MPa and a flow rate ranging from 1 μ L/min to 90 mL/min through a high-pressure line and a cased wellbore inside the specimen.

We will monitor the growth of the fracture with a combination of compressional and shear piezoelectric transducers for a total of 64 units, that can be used to both generate and measure acoustic energy. We use a function generator connected to a high-power amplifier to generate an excitation signal, which is then routed to one of 32 excitation transducers through a multiplexer. The other 32 transducers are connected to a high-speed acquisition board in order to simultaneously record the measured ultrasonic signals. By carefully placing the transducers on all six faces of the specimen to be fractured, we expect to record transmitted, reflected and diffracted acoustic events (Figure 1). We intend to use these three types of event in order to estimate the spatial extent of the fracture, as well as its thickness along raypaths. Transmission measurements, where the wave travels across the specimen, provide fracture thickness information (Groenenboom & Fokkema, 1998; Kovalyshen et al., 2014). Diffraction events, where the wave propagates to the tip of the fracture and then towards the side of the block, carry information about the tip position, and in turn give an estimate of the fracture size (Groenenboom et al., 2001). Reflection events, where the acoustic energy is reflected back toward the same side of the block, let us discriminate between dry and fluid-filled fracture in the case where a fluid lag is present at the fracture tip.

With these unique laboratory capabilities, we plan to investigate complex fracturing problems that have not yet been investigated in laboratory experiments. This includes the case of fluid-saturated porous materials, where the porosity and properties of both injection and pore fluids have a strong influence on fracture growth, but also the case of fracture propagation in anisotropic or inhomogeneous materials, as well as the effects of mixed-mode fracturing with fracture reorientation, as well as the influence of existing fractures.

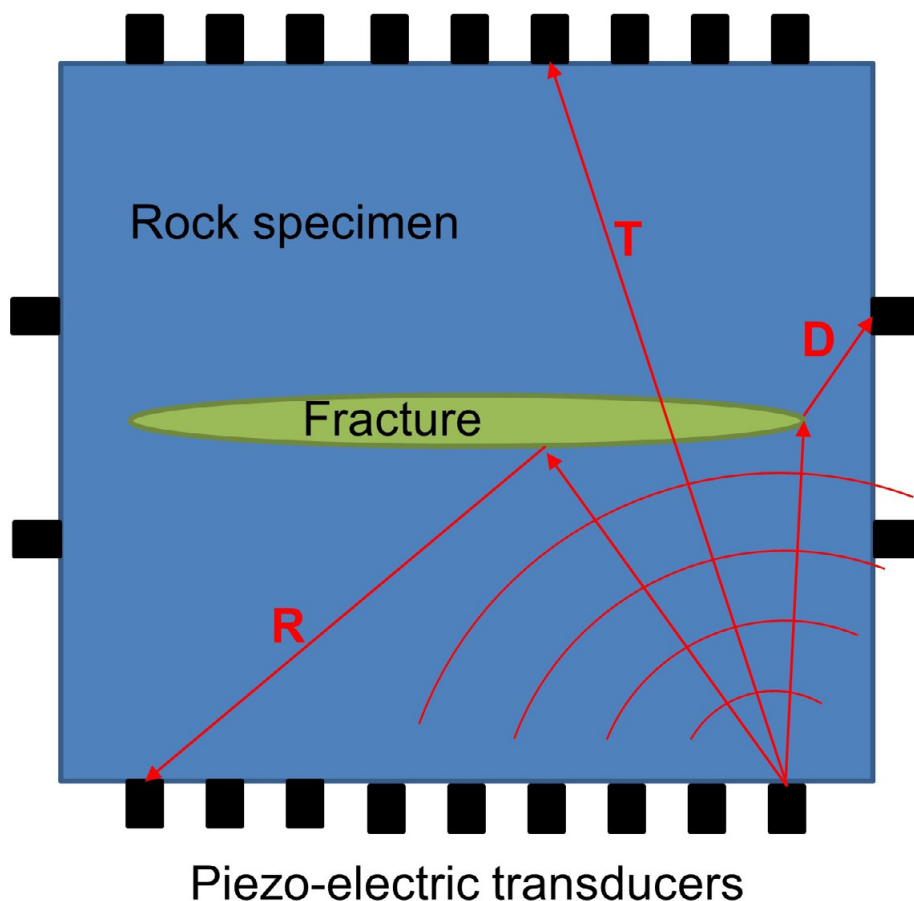


Figure 1. Schematic of the ultrasonic monitoring configuration. T: transmitted wave, R: reflected wave, D: diffracted wave.

REFERENCES

- Groenenboom, J. 1998: Acoustic monitoring of hydraulic fracture growth, PhD thesis, TU Delft, The Netherlands.
- Groenenboom, J. & Fokkema, J. T. 1998: Monitoring the width of hydraulic fractures with acoustic waves, *Geophysics*, 63, 139-148.
- Groenenboom, J., van Dam, D.B. & de Pater, C.J. 2001: Time-Lapse Ultrasonic Measurements of Laboratory Hydraulic-Fracture Growth: Tip Behavior and Width Profile, *Society of Petroleum Engineers Journal*, 6, 14-24.
- Kovalyshen, Y. Bunger, A.P., Kear J. & Kasperczyk D. 2014: Comparison between ultrasonic and photometric methods for hydraulic fracture laboratory monitoring, *International Journal of Rock Mechanics & Mining Sciences*, 70, 368-374.

P 8.9**Towards Replicating Rock Specimens: A Comparison of Tensile Fractures from 3D Printed and Natural Sandstones**

Elisaveta Dombrovski^{1,2}, Daniel Vogler¹, Stuart D.C. Walsh³, Matthew A. Perras¹

¹ *ETH Swiss Federal Institute of Technology Zurich, Department of Earth Sciences, Zurich, Switzerland*

² *Technical University of Munich, Faculty of Civil Environmental and Geo Engineering, Munich, Germany.*

³ *Stone Code Pty. Ltd., Sydney, Australia*

Recent advances in 3D printing technology have the potential to replicate the physical characteristics of natural sandstones, enabling the manufacturing of reproducible rock specimens. This process could be used to replicate heterogeneous specimens to perform destructive testing with different tests and testing configurations. In a first stage, a sand based printed material was examined to determine if its behaviour was similar to natural sandstones. For this purpose, we compare the tensile failure behavior of 3D printed and natural sandstone specimens.

We tested two different grain sizes of the same 3D printed material and three natural sandstones to compare: (1) tensile strength; (2) strain path to failure; (3) fracture surface roughness after failure; and (4) failure mode as analyzed with digital image correlation.

Tensile strength and failure modes of 3D printed sandstone and weak natural specimens was found to be comparable. Crack propagation paths during failure as measured with surface roughness of the 3D printed specimens were similar to those of natural specimens of comparable tensile strength. The findings of this study suggest similar grain- and macro-scale failure behaviour was found between the 3D printed and natural sandstone specimens and this 3D printed material could be a useful analogue material for future studies.

P 8.10

Numerical modeling of seismic attenuation in realistic fractured media

Jürg Hunziker¹, Marco Favino², Eva Caspari¹, Beatriz Quintal¹, Rolf Krause² & Klaus Holliger¹

¹ *Applied and Environmental Geophysics Group, Institute of Earth Sciences, University of Lausanne, Switzerland*

² *Institute of Computational Science, Università della Svizzera italiana, Switzerland*

Imaging of fractures is important for geothermal and hydrocarbon exploration as well as for nuclear waste disposal and CO₂ storage. As the fracture thickness is much smaller than the seismic wavelength, direct imaging of fractures with seismic methods is generally not possible. Indirect imaging is, however, potentially possible, because seismic waves experience velocity dispersion and attenuation in fractured media due to wave-induced fluid flow (WIFF).

Numerical upscaling experiments allow us to better understand the velocity dispersion and attenuation of seismic waves caused by WIFF. To this end we apply a compressibility test to a representative sample of the subsurface region of interest. The fractured numerical sample is compressed under undrained conditions vertically along its upper boundary with the lower and lateral boundaries remaining fixed. Fractures are modeled as a highly compliant and highly porous material embedded in a much stiffer and much less porous background material. The P-wave velocity dispersion and attenuation can then be obtained by solving the quasi-static poroelastic equations (Biot, 1941) in the space-frequency domain. Shear tests are used in a similar manner to obtain the S-wave velocity dispersion and attenuation.

So far, such numerical experiments have been limited to simple fracture models (e.g., Quintal et al. (2014), Rubino et al. (2013,2014)). Here, we present a new finite-element code called Parrot that allows us to model realistic 2D fracture geometries. This code is based on the Multiphysics Object Oriented Simulation Environment (MOOSE). Instead of creating a mesh with element boundaries coinciding with fracture boundaries, we create a mesh of rectangular elements, which are adaptively refined at fracture locations but otherwise independent of the geometry of the fractures. Note that our approach does not necessarily require structured meshes. Here, we just have chosen structured meshes as they are trivially to generate. This allows for a fast mesh generation that does not require user interaction, making the code amenable for the simulation of realistic, stochastic fracture networks.

We compare our results with those of the Comsol Multiphysics software for two interconnected fractures (Fig. 1a). The agreement between the two sets of results in terms of attenuation is very good (Fig. 1b). The small differences are most likely due to the different meshes. An example of a realistic fracture network is depicted in Fig. 1c. As for the case of only two fractures, the attenuation exhibits two peaks (Fig. 1d), one at low frequencies due to WIFF between the fractures and the background, and one at high frequencies due to WIFF between connected fractures. As there are not so many connections between the fractures in the second example, the low-frequency attenuation peak has a much higher amplitude than the one at higher frequencies.

In the future, we plan to use this code to explore relations between WIFF effects and the effective permeability of realistic, stochastic fracture networks featuring different statistical properties. An extension of this code to 3D is currently under development.

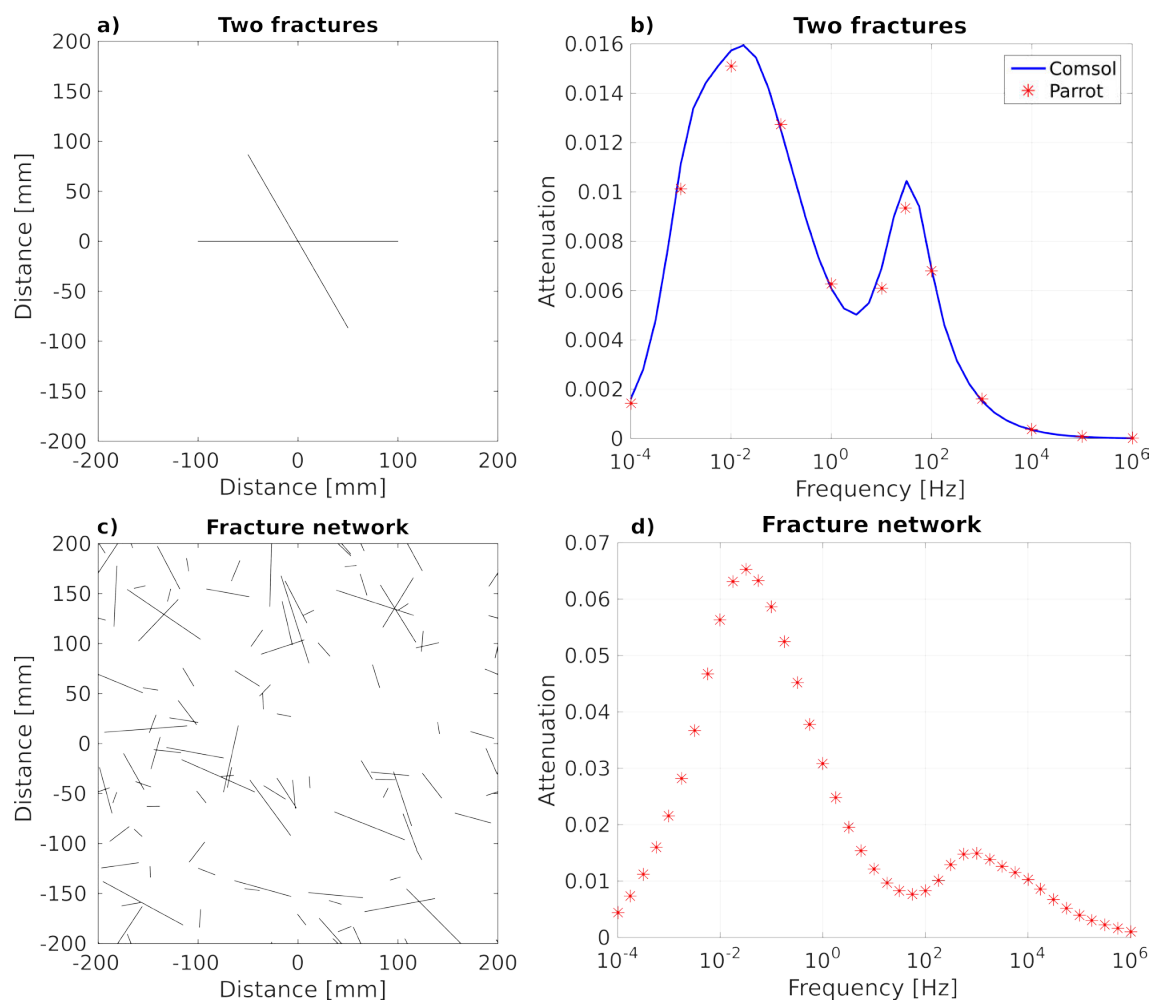


Figure 1. a) Fracture geometry for two interconnected fractures and b) corresponding frequency-dependent attenuation. c) Fracture geometry for a realistic fracture network and d) corresponding attenuation.

REFERENCES

- Biot, M. A. 1941: General theory of three-dimensional consolidation. *Journal of Applied Physics*, 12, 155-164.
- Quintal, B., Jänicke, R., Rubino, J. G., Steeb, H. & Holliger, K. 2014: Sensitivity of S-wave attenuation to the connectivity of fractures in fluid-saturated rocks. *Geophysics*, 79, WB15-WB24.
- Rubino, J. G., Guarracino, L., Müller, T. M. & Holliger, K. 2013: Do seismic waves sense fracture connectivity? *Geophysical Research Letters*, 40, 692-696.
- Rubino, J. G., Müller, T. M., Milani, M. & Holliger, K. 2014: Seismic attenuation and velocity dispersion in fractured rocks: The role played by fracture contact areas. *Geophysical Prospecting*, 62, 1278-1296.

P 8.11

Analysis of surface roughness of Opalinus Clay extensional fractures

Holger Sprengel¹, Martin Ziegler¹

¹ Department of Earth Sciences, ETH Zurich, Sonneggstrasse 5, CH-8092 Zurich
(sholger@student.ethz.ch, martin.ziegler@erdw.ethz.ch)

Opalinus Clay is the target rock formation for the high-level nuclear waste repository in Switzerland. Rock mass characterization experiments in Opalinus Clay at the Mont Terri underground rock laboratory have shown that tunnel excavation leads to formation of an Excavation Damage Zone (EDZ) around the underground galleries (e.g. Nussbaum et al., 2011). This EDZ contains newly formed brittle fractures of which some are extensional fractures aligned about tangential to the tunnel walls. Shortly after tunnel excavation rock mass support measures are installed in order to limit tunnel convergence and rock mass damage. Characterization and assessment of the system behavior of EDZ fractures and confining stress, e.g., due to tunnel support and/or later swelling of bentonite backfill, is highly relevant for the long-term storage of radioactive waste and repository safety since the EDZ fractures may form release paths for radionuclides. The impact of EDZ fractures on repository integrity has been subject to a wide range of scientific investigations at the Mont Terri underground rock laboratory and other research laboratories until today.

Mechanical and hydrological rock mass behavior is strongly influenced by the roughness of rock fractures (e.g. Grasselli and Egger, 2003; Scesi and Gattinoni, 2007). This study investigates the effect of suction pressure (and corresponding saturation) on the roughness of (1) newly-formed Opalinus Clay extensional fractures and of (2) fractures under confining pressure. The study aims at increasing our understanding of the fracture sealing processes, which are relevant for the long-term disposal of radioactive waste.

We used artificial fractures formed by Brazilian indirect tensile strength tests as analogues for extensional EDZ fractures (Figure 1a; Ulusay and Hudson, 2007). The fractures were produced parallel and perpendicular to bedding planes. To be able to analyze the influence of the suction pressure on the fracture roughness, sample material from the same sampling location at the Mont Terri underground rock laboratory was desaturated artificially to obtain five different water contents (>97 %, 85 %, 66 %, 43%, 15 %) using oversaturated salt solutions. 3D models of the fracture surfaces were created by the use of a photogrammetric scanner (GOM ATOS Core 300). Calculated surface models with resolutions on the order of 0.5 mm were used to determine different roughness parameters, such as Z_2S (Belem et al., 2000) and the standard deviation of the asperity height, to characterize the surface morphology quantitatively (Figure 1b). The scans were carried out before and after fracture-perpendicular compressive loading, simulating confining stress buildup during gallery closure. Different magnitudes of confinement were applied. We will present and discuss our investigation concept and laboratory loading equipment (Figure 1c), and aim at showing first results of the Opalinus Clay fracture roughness investigations.

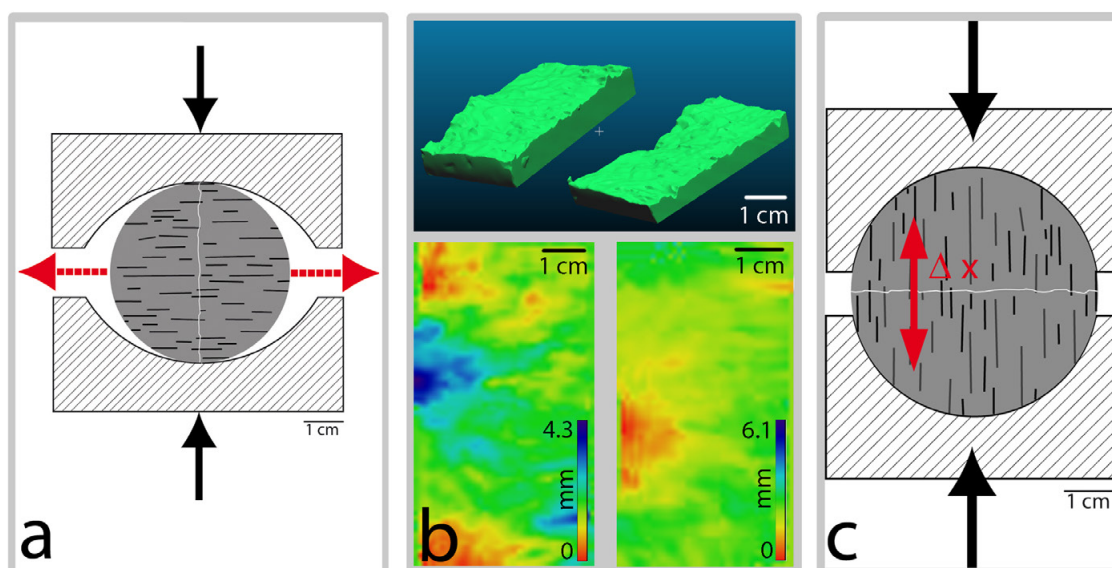


Figure 1. a) As analogue for EDZ extensional fractures new fractures were artificially formed by the Brazilian indirect tensile strength test. Tensile stress occurs perpendicular (red arrows) to the loading direction (black arrows). b) Both fracture surfaces were scanned by an optical 3D scanner. High resolution 3D models of the fracture surfaces (top) were used to calculate digital surface models (bottom) of each fracture surface. These were then used to determine surface roughness parameters. c) During a second experimental step fracture closure was simulated by uniaxial compressive loading of mated fractures, perpendicular to the mean orientation of the fracture. Strain between both sample parts was measured. After loading the fracture's roughness was investigated a second time.

REFERENCES

- Belem, T., Homand-Etienne, F. & Souley, M. 2000: Quantitative parameters for rock joint surface roughness, *Rock Mechanics and Rock Engineering*, 33, 217–242.
- Grasselli, G. & Egger, P. 2003: Constitutive law for the shear strength of rock joints based on three-dimensional surface parameters, *International Journal of Rock Mechanics and Mining Sciences*, 40, 25–40.
- Nussbaum, C., Bossart, P., Amann, F. & Aubourg, C. 2011: Analysis of tectonic structures and excavation induced fractures in the opalinus Clay, Mont Terri underground rock laboratory (Switzerland), *Swiss J Geosci*, 104, 187–210.
- Scesi, L. & Gattinoni, P. 2007: Roughness control on hydraulic conductivity in fractured rocks, *Hydrogeology Journal*, 15, 201–211.
- Ulusay, R. & Hudson, J. A. (ed.) 2007: *The complete ISRM suggested methods for rock characterization, testing, and monitoring: 1974–2006*. ISRM Turkish National Group, Ankara.

P 8.12**Petro-physical characterization of the Main Fault at the Mont Terri Laboratory**

Luis Felipe Orellana¹, Marie Violay¹, Eduardo Gramajo¹, Pierre Henry², Yves Guglielmi³, Florian Amann⁴, Christophe Nusbaum⁵.

¹ *Laboratory of Experimental Rock Mechanics, École Polytechnique Fédérale de Lausanne, Route Cantonale 1015, CH-1018, Lausanne (felipe.orellana@epfl.ch)*

² *Aix Marseille Université, CNRS, Collège de France, IRD, CEREGE UMR7330, 13545 Aix-en-Provence cedex 4, France*

³ *Earth and Environmental Sciences Area, Lawrence Berkeley National Laboratory, Berkeley, CA 94720, USA*

⁴ *Department of Earth Sciences, ETH Zurich, Sonneggstrasse 5, CH-8092 Zurich.*

⁵ *Federal Office of Topography (SWISSTOPO), Seftigenstrasse 264, CH-3084 Wabern*

Opalinus clay has been widely studied in the context of deep geological disposal. Its favorable hydro-mechanical properties made it a suitable material for the storage of nuclear waste. One of those key properties is its low permeability, being practically impermeable.

This work focuses on the petro-physical characterization of the Main Fault zone at the Mont Terri Laboratory, in Switzerland. The objective of the study is to constrain the cap rock sealing efficiency. The petro-physical properties were determined from sample measurements in the laboratory. Permeability was measured by transient pressure pulse method using fluid at chemical equilibrium with the rock. Connected porosity was measured using the triple-weight method and helium pycnometry. Porosity topology was assessed by mercury porosity technique. Preliminary results suggest that porosity along the fault structures suggest a layered system. Fault core was ~21 % porosity and dominated by small pores of size lower than 14 nm. Surrounding damage zone presented porosity values lower than 15%, and nano-pores of about 16 nm. Permeability far from the fault zone is in the order of $1e^{-20}$ and $1e^{-19}$ m², if measured perpendicular and parallel to bedding respectively.

P 8.13

Architecture of a fault zone in Opalinus Clay at the Mont Terri laboratory (Switzerland)

Maria Kakurina¹, Yves Guglielmi², Christophe Nussbaum³, Benoît Valley¹

¹ Center for Hydrogeology and Geothermics, University of Neuchâtel, Rue Emile-Argand 11, CH-2000 Neuchâtel (maria.kakurina@unine.ch)

² Lawrence Berkeley National Laboratory, University of California, 1 Cyclotron Rd, CA 94720 Berkeley

³ Swisstopo, Seftigenstrasse 264, CH-3084 Wabern

Opalinus Clay formation exposed in the Mont Terri underground rock laboratory gives an excellent opportunity to investigate the architecture of an unweathered clay fault zone. Since 20 years, about 150 experiments have been performed in Mont Terri in order to investigate the hydrogeological, geochemical and mechanical properties of argillous formations. The FS (Fault Slip) experiment aims at better understanding the stability of clay faults. This experiment has been conducted by injecting fluids in the upper, middle and lower parts of the main tectonic structure of the Opalinus Clay, so-called the Main Fault, using the SIMFIP probe (Guglielmi 2016). The present work contributes to a highly-detailed structural analysis of three FS fully cored and logged 35-to-50m long and 1.7-to-4.3m spaced boreholes intersecting the entire fault zone.

The Main fault core consists of a thrust zone of about 4.0-5.0 m wide, that includes scaly clay and non-scaly fabrics intersected by various density of secondary fault planes (Figure 1). The fault rocks are classified in 7 different fault facies: 2 scaly clay facies and 5 fractured rock facies:

- Scaly clays, including shear zones, microlithons, S-C bands and microfolds, mainly occur in larger zones at top and bottom of the Main Fault boundaries, and also as isolated lenses in the middle. The scaly clay facies 1 comprises a scaly fabric that has a relative low “tensile strength” since it can be easily broken by hands. The scaly clay facies 2 consists of larger microlithons, that are intersected by thin shear zones, and cannot be easily disintegrated.
- The fractured facies 1 is characterized by mainly non-deformed zones rarely intersected either by moderately SSE-dipping system or by low-angle SW-dipping fault planes. The fractured facies 2 consists of a sequence of the SSE-dipping faults intersected with the SW-low-dipping fault planes usually associated with calcite mineralisation. Slickenside analysis of SSE-dipping faults with well-striated surfaces indicates that the slip direction has a top-to-NNW shear sense, while the SW-low-dipping fault planes – NW shear sense. The fractured facies 3 includes moderately inclined N- to NNE-striking faults with mainly NW shear sense. The fractured facies 4 is specified by the rhombohedral undeformed blocks with low to moderately SSE-dipping fault planes with NW slip direction. It was noted that the higher the inclined angle of the fault plane, the larger are the shining strias. The fracture facies 5 is characterized by the very densified SSE-dipping fractures with a very shiny and well-striated surface with NNW slip direction. This facies usually occurs closed by the scaly clays. The three fault systems observed in the fractured facies have been identified in the galleries of the rock laboratory (Nussbaum et al. 2011).

These structural facies have been differentiated in order to correlate the structural features between the boreholes. Indeed, such a complex variability of the fractured zones as well as the continuity of the borders of the Main Fault are hard to correlate even with highly detailed geological data within the relatively small volume of the experiment. This high heterogeneity within the fault zone is likely to impact the fault rock response to fluid injection and its reactivation. It has been recently shown in Tournemire underground rock laboratory (France), that the rupture in faulted clay rich rocks is mainly associated with the reactivation of preexisting discontinuities (Guglielmi et al. 2015). It results in high potential instability of some fault planes to stress variability induced by galleries excavation, that are very important questions in many industrial applications and, therefore, need to be studied.

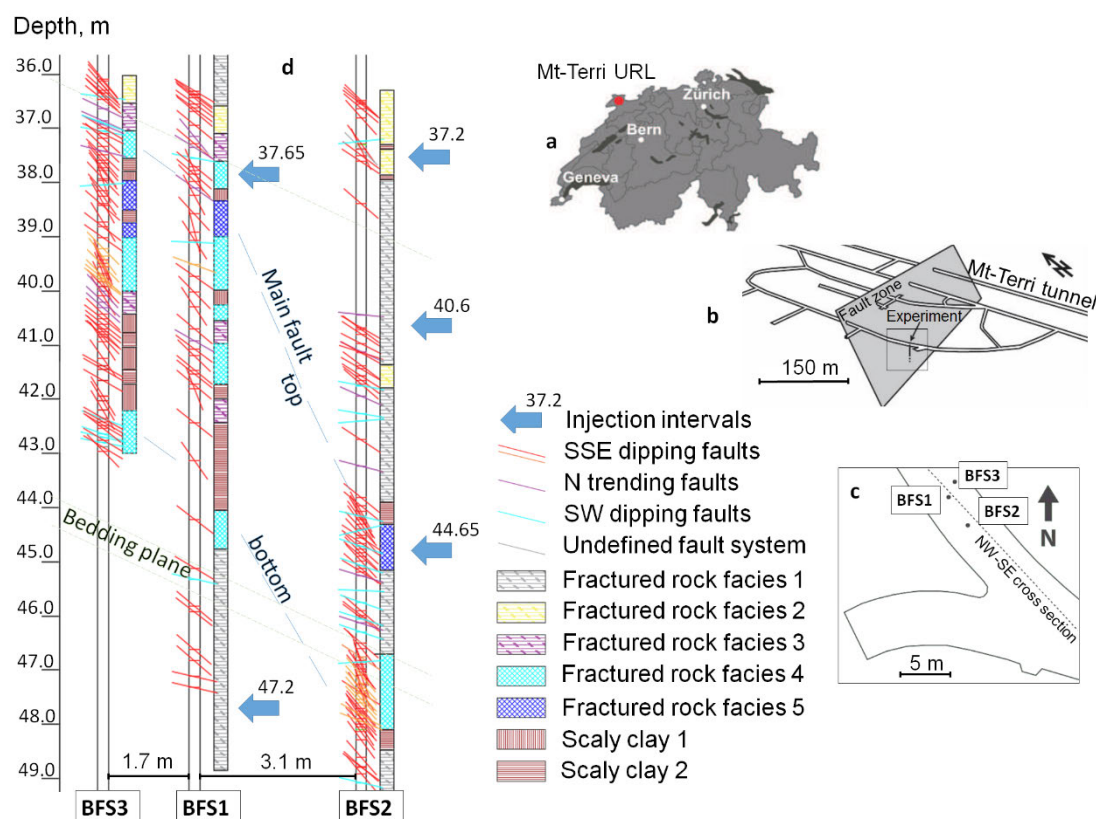


Figure 1. a,b - Experimental location in Mt-Terri URL; c - Map of the boreholes geometry in the FS experiment zone, d - Cross section of the Main Fault geometry

REFERENCES

- Guglielmi, Y. 2016: In-situ clay faults slip hydro-mechanical characterization (FS experiment), Mont Terri underground rock laboratory. Technical Note 2015-60, p. 1-63
- Guglielmi, Y. G., Henry, P., Nussbaum, C., Dick, P., Gout, C., & Amann, F. 2015: Underground Research Laboratories for conducting fault activation experiments in shales. In 49th US Rock Mechanics/Geomechanics Symposium. American Rock Mechanics Association.
- Nussbaum, C., Bossart, P., Amann, F., & Aubourg, C. 2011: Analysis of tectonic structures and excavation induced fractures in the Opalinus Clay, Mont Terri underground rock laboratory (Switzerland). Swiss Journal of Geosciences, 104(2), 187-210.

P 8.14

Porosity and permeability reduction in conduit wall rock. A transition from localized cataclastic pore collapse to distributed viscous flow.

Michael Heap¹, Marie Violay², and Fabian Wadsworth³

¹ *Géophysique Expérimentale, Institut de Physique de Globe de Strasbourg (UMR 7516 CNRS, Université de Strasbourg/EOST), 5 rue René Descartes, 67084 Strasbourg cedex, France.*

² *Laboratory of Experimental Rock Mechanics, École Polytechnique Fédérale de Lausanne, Station 18, CH-1015, Lausanne, Switzerland.*

³ *Earth and Environmental Sciences, Ludwig-Maximilians-Universität, Theresienstr. 41, 80333 Munich, Germany.*

The permeability of volcanic conduit walls can govern the outgassing and explosivity of eruptions. The destruction of the porosity and permeability of the materials within this zone could therefore promote explosive behaviour.

To examine the mechanisms of porosity and permeability loss in the region of the conduit margin zone, we conducted high-pressure (effective pressure of 40 MPa), high-temperature (up to 800 °C) triaxial deformation experiments on porous andesite. Porosity change was measured during deformation.

Mechanical and micro-structural observations (at experimental constant strain rate of 10^{-5} s^{-1}) indicate that andesite deforms by cataclastic pore collapse at temperatures that do not exceed the glass transition ($T_g = \sim 740 \text{ °C}$) of the amorphous groundmass phase. Localized cataclastic pore collapse produces bands of crushed pores orientated sub-perpendicular to the maximum principal stress. In this regime, porosity is only reduced within the bands; the host rock porosity remains unchanged. Although these features may disrupt the outgassing of the nearby magma-filled conduit, it is unclear whether they will form a coherent low-permeability barrier. At temperature higher than T_g , the deformation is distributed throughout the sample and no localized bands develop. This change in deformation mechanism is accompanied by a substantial reduction in strength and a substantial increase in porosity and permeability loss, the result of widespread viscous pore flattening and closure. A low-porosity, low-permeability viscously compacted layer within the conduit wall will severely inhibit the outgassing of the nearby magma-filled conduit and could allow pore pressure to build to that preparatory for the next Vulcanian explosion.

Our study therefore highlights that small changes in the temperature can result in a change in deformation micromechanism that drastically alters the mechanical and hydraulic properties of the wall rock adjacent to the conduit, with implications for pore pressure augmentation and explosive behavior.

P 8.15

The physical properties of evolved melts and implications for melt segregation and the built-up of large silicic eruptions

Eva Hartung¹ & Luca Caricchi¹

¹ *Department of Earth Sciences, University of Geneva, Rue de Maraichers 13, CH-1205 Geneva (eva.hartung@unige.ch)*

The extraction of residual melt from crystallising magmas is a mechanism commonly considered to precede the eruption of crystal poor magmas. A detailed petrographic, geochemical and structural study of the Takidani pluton suggests that a porphyritic granitic unit near the roof of the intrusion was produced by the extraction of residual melt from magma crystallised to about 50 wt.%.

The rheological properties of magma and residual melt depend on temperature, pressure, chemistry, water, crystal and bubble content, and the rate of deformation. In this study we calculate the physical properties of magma and residual melt during the progressive crystallization of magma with the composition of the Takidani granodiorite. Given the compositional similarity, the variation of chemistry and crystallinity as function of temperature was obtained from the experiments of Costa et al. (2004).

As a first step, we have calculated the density, viscosity and bubble volume fraction at 200MPa and different temperatures for water saturated melts. The water content at saturation for the residual melt increases with decreasing temperatures from 6.0 to 7.0 wt.%. The total initial volume of the magma and dissolved water triples from 1000°C (near liquidus) to 700°C (near solidus) because of water exsolution. However, the volume of the magma itself only increases by about six percent, while the density decrease from 2.30 to 2.17 g/ccm. The viscosity of the residual magma increases from about 2.4 to 4.2 between 1000°C and 800°C, and to about 5 at 700°C. In comparison, the viscosity for anhydrous melts increases exponentially from 5.2 to 13.1 from 1100°C to 700°C.

In the second step we will calculate the relative viscosities of the residual melt for a two- and three-phase system after the models of Pistone et al. (2012) and Truby et al. (2014), respectively. In addition, we will calculate the rheological properties for a water-undersaturated melt and discuss the implication for magma transport of silicic melts in the upper crust.

In summary, calculations of physical properties for magmas with different initial water contents will be presented to determine if the extraction of residual melt during magma crystallisation was triggered by the achievement of a particular set of physical properties of the residual melt.

REFERENCES

- Costa, F., Scaillet, B. & Pichavant, M. 2004: Petrological and Experimental Constraints on the Pre-eruption Conditions of Holocene Dacite from Volcan San Pedro (36°S, Chilean Andes) and the Importance of Sulphur in Silicic Subduction-related Magmas. *Journal of Petrology*, 45, 855–881.
- Pistone, M., Caricchi, L., Ulmer, P., Burlini, L., Ardia, P., Reusser, E., Marone, F. & Arbaret, L. 2012: Deformation experiments of bubble- and crystal-bearing magmas: Rheological and microstructural analysis. *Journal of Geophysical Research*, 117, B05208.
- Truby, J. M., Mueller, S. P., Llewellyn, E. W. & Mader, H. M. 2014: The rheology of three-phase suspensions at low bubble capillary number. *Proceedings of the Royal Society A: Mathematical, Physical and Engineering Sciences*, 471, 20140557.

P 8.16

Seismic signals at the Nirano Mud Volcanic Field, Italy

Verónica Antunes¹, Matteo Lupi¹, Aurore Carrier¹, Anne Obermann², Adriano Mazzini³, Tullio Ricci⁴, Alessandra Sciarra⁴, Milena Moretti⁴

¹ *Department of Earth Sciences, University of Geneva, Rue des Maraichers 13, CH-1205 Geneva (veronica.antunes@unige.ch)*

² *ETH Zürich, Erdbebendienst (SED), NO H 63, Sonneggstrasse 5, CH-8092 Zurich*

³ *Centre for Earth Evolution and Dynamics (CEED), University of Oslo, ZEB-bygningen, Sem Saelandsvei 2A, Blindern, NO-0371 Oslo*

⁴ *Istituto Nazionale di Geofisica e Vulcanologia (INGV), Via di Vigna Murata, IT-605-00143 Rome*

Mud volcanoes are geological systems characterized by elevated fluid pressures at depth. For this reason, mud volcanoes are often considered ideal natural laboratories to investigate the effects of passing seismic waves on fluid-saturated geological systems. We deployed a network of 7 temporary seismic stations around the Nirano Mud Volcanic Field, Italy, to capture the local effects of remote earthquakes. We notice that the seismic noise is increasing after the passage of the seismic waves. This is possibly indicating changes in the (shallow) fluid flow regime within the mud plumbing system.

Additionally, during the three months long deployment we repeatedly recorded drumbeat signals beneath the mud volcanic field. The signals were characterized by a high-frequency content in the range of 10-25 Hz. We attempt to locate and characterize the source generating such recurrent seismic signals. The amplitude of the events varies across the stations suggesting a conduit located in the NE-most part of the mud volcanic field.

P 8.17

Tectonic and fluid-driven seismic activity in Western Peloponnese, Greece

Antoine Haddad¹, Matteo Lupi¹, Diego Gonzalez Vidal², Dr Athanassios Ganas³, Ioannis Kassaras⁴

¹ *Crustal Deformation and Fluid Flow Group, University of Geneva, Rue des Maraichers 13, CH-1205 Genève. antoine.haddad@unige.ch – matteo.lupi@unige.ch*

² *Earth Sciences department, University of Concepción, Víctor Lamas 1290, Concepción – Chile diegogonzalezv@udec.cl*

³ *Research Director, National Observatory of Athens Lofos Nymfon, Thission P.O Box 20048 11810 Athens – Greece aganas@gein.noa.gr*

⁴ *Assistant Prof. Professor (Assistant) - University of Athens - Department of Geophysics and Geothermy Greece · Athens kassararas@geol.uoa.gr*

The interaction between fluid flow and seismic activity is modulated by the state of stress of the crust. Fluid-rich geological environments are often characterised by elevated pore pressure at depth. The heterogeneous distribution of pore pressure may be an important aspect to identify regions prone to generate fluid-driven seismic swarms.

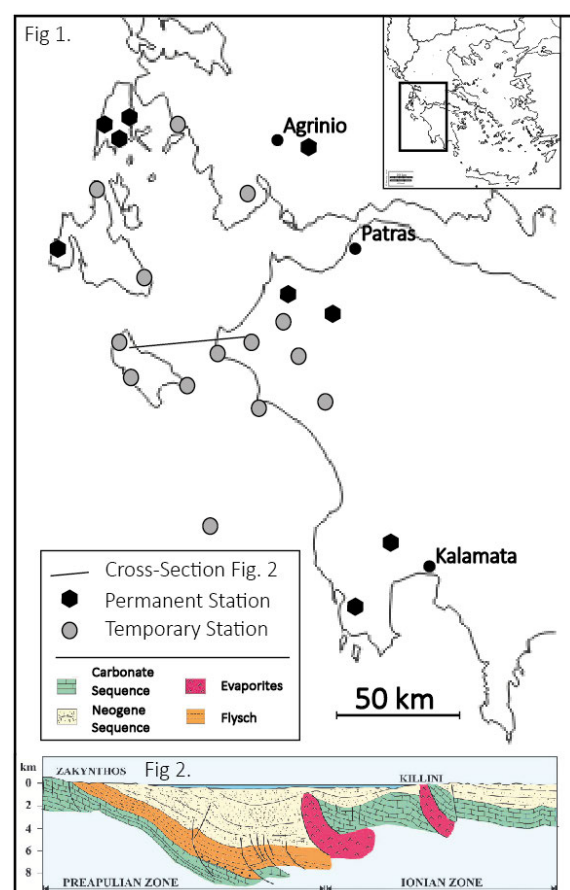


Figure 1. Map of the seismic stations distribution in Western Peloponnese – Greece _ Figure 2. Simplified cross-section between Zakyntos and Kyllii – Greece – (Etiopie et al. 2006)

This study investigates fluid-driven seismicity in the Western Peloponnese area (Fig.1) that is considered an ideal natural laboratory due to the abundance of crustal fluids and frequent occurrence of earthquakes. The basin is composed of thick Jurassic-Eocene carbonate and clastic sedimentary sequences underlain by Triassic evaporites (Fig.2.) that under tectonic stress penetrate through cataclastic zones generating diapiric structures. They likely control fluid migration/concentration processes. (Etiopie et al. 2006).

To capture the evolution of such fluid-driven seismic sequences we deployed a seismic network spanning 200 km from north to south and more than 100 km from east to west. The network is composed of 14 temporary and 7 permanent seismological stations (Fig.1).

Fluid-driven seismic sequences are often characterised by temporary permeability enhancements and may localise in regions affected by increase lithostatic pore pressures at depth. We couple numerical fluid flow models with accurate earthquake locations to highlight whether in this part of Western Peloponnese seismic sequences/swarms may be fluid driven as the result of anomalous P-T variations in the crust.

REFERENCES

- Etiopie G., Papatheodorou G., Christodoulou D., Ferentinos G., Sokos E., Favali P. (2006). Methane and hydrogen sulfide seepage in the NW Peloponnese petroliferous basin (Greece): origin and geohazard. *AAPG Bulletin.*, 90, 5, 701-713.
- Hill D. (2006). Dynamic Triggering – *Earthquake Seismology Volume 4.* U.S Geological Survey
- Lupi, M., S. Geiger, and C. M. Graham (2010), Hydrothermal fluid flow within a tectonically active rift-ridge transform junction: Tjornes Fracture Zone, Iceland, *J. Geophys. Res. B Solid Earth*, 115,
- Lupi, M., Geiger, S., & Graham, C. M. (2011). Numerical simulations of seismicity-induced fluid flow in the Tjornes Fracture Zone, Iceland. *Journal of Geophysical Research*, 116(B7), B07101.
- Miller, S. A., Collettini, C., Chiaraluce, L., Cocco, M., Barchi, M., & Kaus, B. J. P. (2004). Aftershocks driven by a high-pressure CO₂ source at depth. *Nature* 427(6976), 724-727

P 8.18

Mind the (seismic) gap: the 1714 Bhutan earthquake

György Hetényi¹, Romain Le Roux-Mallouf², Théo Berthet³, Rodolphe Cattin², Carlo Cauzzi⁴, Karma Phuntsho⁵, Remo Grolimund⁴

¹ *University of Lausanne, Institute of Earth Sciences, UNIL-Mouline Géopolis, CH-1015 Lausanne, Switzerland*

² *Géosciences Montpellier, Université de Montpellier, Place E. Bataillon, F-34095 Montpellier, France*

³ *Department of Earth Sciences, Uppsala University, Villavägen 17, S-75236 Uppsala, Sweden*

⁴ *Swiss Seismological Service, ETH Zürich, Sonneggstrasse 5, CH-8092 Zürich, Switzerland*

⁵ *Shejun Agency for Bhutan's Cultural Documentation and Research, Changangkha, Thimphu, Bhutan*

The region of Bhutan is thought to be the only segment of the Himalayas not having experienced a major earthquake over the past half millennium. A proposed explanation for this apparent seismic gap is partial accommodation of the India-Asia convergence further south across the Shillong Plateau, yet the seismic behavior of the Himalayan megathrust is unknown.

Here we present historical documents from the region reporting on an earthquake in 1714 AD and geological evidence of surface rupture to constrain the latest large event in this area. We compute various earthquake scenarios using empirical scaling laws relating magnitude with intensity and rupture geometry. Our results constrain the 1714 AD earthquake to have ruptured the megathrust in Bhutan, most likely during a M7.5-8.3 event. This finding reclassifies the apparent seismic gap to a former information gap, and implies that the entire Himalayan arc has a high level of earthquake potential.

P 8.19**Effect of tilt angle on the inter-hemispherical asymmetries:
Study of the variations of the temperature and the electronic density**Sabrina Tair¹, Frédéric Pitout², Yasmina Yahiat¹ & Naima Zaourar¹¹ *Faculté des Sciences de la Terre, Géographie et Aménagement du Territoire, Université des Sciences et de la Technologie Houari Boumediene, BP 32 El Allia 16111 bab ezzouar Alger, Algérie (sabrina_tar@yahoo.com)*² *Institut de recherche en Astropysique et Planétologie, 9 avenue du Colonel Roche, BP 44346, 31028 Toulouse cedex 4, France*

Geomagnetic activity is controlled by the angle (Φ), called tilt angle, which makes the magnetic axis of the Earth with regard to the perpendicular for the ecliptic. Indeed, if the equipotentiality of the lines of force of the ground magnetic field, in particular large-scale, is source of a symmetry between the combined regions, the causes of asymmetry between hemispheres are not rare. This asymmetry is due on one hand, in the slope of the axis of rotation of the Earth from the point of view of the ecliptic, leading a seasonal effect and on the other hand, in the slope of the axis of the geomagnetic dipôle with regard to the geographical axis, which leads a diurnal effect.

The seasonal effect due to the differences of conductivity between the polar summer and winter ionospheres is translated by a strong disparity between the capacities of the north and south hemispheres to close the magnetospheric currents, also leading to an asymmetry of electric fields and convection of the plasma.

In our study, we exploit average minutes of the Density and the electronic Temperature of the electric field during the period 2002 - 2004, measured by the probe Langmuir PLP aboard the satellite CHAMP.

We also use the index of the radio flow which represents the variations of the solar flow «ultraviolet ray» in a 10,7 cm wavelength. This flow has no influence on the structure of the atmosphere, but suits to represent the temperature variations observed in the thermosphere.

To show the influence of the slope of the magnetic axis (seasons) on the differences between hemispheres, we put a selection criterion of data according to the variability of the tilt angle and examined the relation enter the variation of the solar flow (F10.7) and the parameters of the electric field various intervals.

After a decomposition of the electric field values, measured by the probe Langmuir PLP aboard the satellite CHAMP, according to the variability of the angle of inclination (Φ), we show a correlation enter the sign of the tilt angle (Φ) and the inter-hemispherical asymmetries. These results are obtained from the cards of the average minutes of the meridian variation of the temperature and the density of electrons for the low heights.

The tilt angle plays a fundamental role on the geomagnetic activity which depends on the sign of this angle. Indeed, we were able to reveal a visible seasonal effect (asymmetry for the high latitudes marked by an increase of the effect Joule in the north hemisphere when (Φ) is positive and in the southern hemisphere when (Φ) is negative and less visible when the angle of inclination is zero.

REFERENCES:

- Nowada, M., & J.H. Shue, J.H and Russell,C.T. 2009 : Effect of dipole tilt angle on geomagnetic activity .Planetary and Space Science 57 (11), 1254-1259.
- Pitout, F., Escoubet, & C. P., Klecker, B., and Dandouras, I. 2009 : Cluster survey of the mid-altitude cusp – Part 2: Large-scale morphology . Annales Geophysicae, 27, 1875-1886.
- Rother, M. 2000 : CH-ME-2-PLP corrected magnetic field in ECEF/NEC system , Information System and Data Center, GeoForschungszentrum Potsdam, Germany . doi:10.5880/ISDC.
- Russell, C.T. 1971 : Geophysical coordinate transformations. Cosmic Electrodyn. 2, 184–196.
- Russell, C.T., & McPherron, R.L. 1973 : Semiannual variation of geomagnetic activity. J. Geophys. Res. 78 (1), 92-108.

P 8.20

3-D shear-wave velocity model of the Central Alps using converted waves

Leonardo Colavitti¹ & György Hetényi¹

¹ *Institut des sciences de la Terre, University of Lausanne, Quartier UNIL-Mouline, Bâtiment Géopolis, CH-1015 Lausanne (leonardo.colavitti@unil.ch)*

The Alpine geological chain represents the consequence of the collision and subduction process involving the European plate and the Adriatic (or Apulian) microplate, which is a promontory of the African plate. The whole process that initiated the formation of Alps orogen started during the Lower Eocene, about 55 million years ago. Although they represent a relatively young mountain belt, the structure of Alps is very complex both at the surface and at depth. Actual information about deep crustal structure has been provided through P-wave velocity models obtained combining active and passive seismic investigations (e.g. Wagner et al. 2012; Diehl et al. 2009 and references therein).

The aim of this work is to exploit converted waves (that represent the analogue of reflectivity from active seismics) and complementary geophysical investigations (e.g. gravity) to deliver a whole 3-D shear-wave velocity model of the crust. The first application is focused on the Central Alps, where active seismic data is widely available for control and also for comparison.

A 3-D model is very useful because orogenic structures are not frequently cylindrical and vary greatly laterally; therefore, it is indispensable to develop a new technique to try to improve structural images and to determine different lithologies and remark the geometry of discontinuities present in the Earth.

Here we adopt the technique of 'receiver function' RF (Langston, 1977) which has been developed during the last 40 years and is nowadays largely used for structural investigations based on passive seismic experiments.

We perform a new analysis of receiver functions using a data set composed of about 20 years of high-quality data from permanent broad-band stations of the Swiss Seismological Service. To get homogeneous coverage of the entire Central Alpine tectonic domain, we also added data from permanent broad-band stations operating in neighbouring countries. We selected data from teleseismic events in the 30-90° epicentral distance range and we chose a threshold magnitude of 5.2. By applying the H- κ stacking technique (Zhu & Kanamori, 2000), using timing of direct and multiple P-to-S converted phases derived from the crust-mantle interface, we compute the crustal features of Moho depth and average V_p/V_s ratio for tectonic units and we compare the results obtained with those of Lombardi et al. 2008 using the same approach. Our main goal is to develop a new technique to construct a fully 3-D V_s model from RFs, by applying a joint inversion strategy of converted waveforms sampling the study area.

The inversion method can either proceed directly, or can use *a priori* information such as existing Moho depth and high-quality 3-D P-wave velocity model (e.g. Diehl et al. 2009): in this case the inversion can focus on V_s (or V_p/V_s ratio). With our method, we aim to build an at least three-layer model including, for instance, sediments, upper crust and lower crust. S-wave information guarantees a much better correlation with rock density and mechanical properties than P-wave model only, reducing effectively the interpretation ambiguities.

The resulting model will be interpreted by taking into account the lithology and the physical properties of the main tectonic units of the region considered.

Finally, we plan to combine our results with the existing gravity anomaly data, controlled source seismology (CSS) profiles acquired during the years, studies of local earthquake tomography (LET) and geological data.

REFERENCES

- Diehl, T., Husen, S., Kissling, E. & Deichmann, N. 2009: High-resolution 3-D P-wave model of the Alpine crust. *Geophys. J. Int.*, 179, 1133-1147.
- Langston, C. A., 1977. Corvallis, Oregon, crustal and upper mantle receiver structure from teleseismic P-waves and S-waves. *J. Geophys. Res.*, 84, 4749-4762.
- Lombardi, D., Braunmiller, J., Kissling, E. & Giardini, D. 2008: Moho depth and Poisson's ratio in the Western-Central Alps from receiver function. *Geophys. J. Int.*, 173, 249-264.
- Wagner, M., Kissling, E. & Husen, S. 2012: Combining controlled-source seismology and local earthquake tomography to derive a 3-D crustal model of the western Alpine region. *Geophys. J. Int.*, 191, 789-802.
- Zhu, L. & Kanamori, H. 2000: Moho depth variation in southern California from teleseismic receiver functions. *J. Geophys. Res.-Solid Earth*, 105, 2969-2980.

P 8.21

Gray-scale Hough transform for seismic wavefield separation?

Asma Hadjadj¹, Zahia Benaïssa¹, Abdelkader Benaïssa¹ & Amar Boudella¹

¹ *University of Sciences and Technology Houari Boumediène, Geosciences Faculty, BP 32, El Alia, Bab-Ezzouar, 16000 Algiers, Algeria. E-mail: zabendz@yahoo.fr*

In a Vertical Seismic Profile (VSP) recording, the useful signal is composed of the superposition of a downgoing wavefield with positive apparent velocities, and an upgoing wavefield with negative apparent velocities. To make best use of them, they need to be separated. Several methods exist to perform this separation, each with its advantages and disadvantages (Kommedal & Jostheim, 1989). The most frequently used in the industry are median filtering which remains, however, unsuitable when amplitude preservation is critical, and (f-k) filter which needs a regular sampling.

In this study, we propose a new method based on the gray-scale Hough transform (GSHT) (Lo & Tsai, 1995; Kesidis & Papamarkos, 2000) which is an extension of the conventional Hough transform used to detect straight lines and other curves (Hough, 1962; Duda & Hart, 1972). The technique, we suggest here, directly maps the gray-scale VSP image, including the downgoing and upgoing linear events, in image coordinate space (x, t, g) to the gray Hough parameter counting space (θ, ρ, g) , where ρ and θ are, respectively, the distance and the orientation with respect to the x-axis of the normal vector to the line, and g represents the gray value. In this new space, the downgoing events appear in the negative angles θ quadrant and the upgoing in the positive quadrant.

The inverse GSHT algorithm, we developed, is then performed to extract the lines that satisfy the filtering conditions: θ negative for the downgoing VSP wavefield and θ positive for the upgoing VSP wavefield (Fig.1).

The experimental results on synthetic and real VSP datasets are convincing (Hadjadj et al., submitted). The wave separation is well performed, even in the presence of loud noise levels, with signal to noise ratio improvement and amplitude preservation.

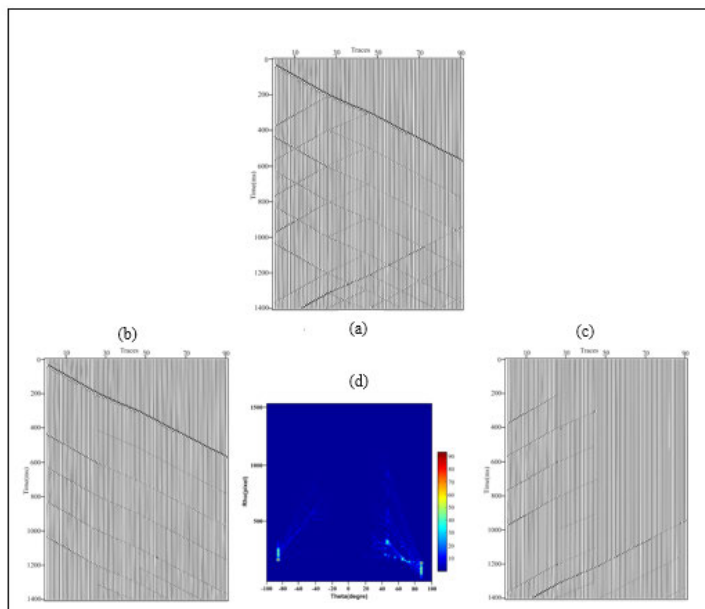


Figure 1. Wavefield separation using GSHT: (a) synthetic VSP seismogram; (b) downgoing wavefield from VSP seismogram after filtering with $(-90^{\circ} \leq \theta \leq 0^{\circ})$; (c) upgoing wavefield from VSP seismogram after filtering with $(0^{\circ} \leq \theta \leq 90^{\circ})$; (d) GSHT space of VSP image.

REFERENCES

- Duda, R. O. & Hart, P. E. 1972: Use the Hough transform to detect lines and curves in pictures. *Comm. Ass. Comput.* 15, 11-15.
- Hadjadj, A., Benaïssa, Z., Benaïssa, A. & Boudella, A. submitted: VSP wavefield separation using the gray-scale Hough

transform: synthetic data. A.J.G.

Hough, P. V. C. 1962: Method and means for recognizing complex patterns. U.S. Patent 306954.

Kesidis, A. L. & Papamarkos, N. 2000: On the gray-scale inverse Hough transform. *Image and Vision Computing* 18, 607-618.

Kommedal, J. H. & Tjøstheim, B. A. 1989: A study of different methods of wavefield separation for application to VSP data. *Geophysical Prospecting* 37, 117-142.

Lo, R. & Tsai, W. 1995: Gray scale Hough transform for thick line detection in gray-scale images. *Pattern Recognition* 28, 647-661.

P 8.22

Topographic expressions of coupled surface process and 3D-tectonic models

Stephanie Schnydrig¹, Dave May¹, Kosuke Ueda¹ & Taras Gerya¹

¹ *Departement Erdwissenschaften, ETH Zürich, Sonneggstrasse 5, CH-8092 Zürich (schnydrs@student.ethz.ch)*

The coupling between dynamics in the Earth's interior and surface processes over geodynamic time scales is widely accepted. Tectonic processes such as plate collision set up topography and in response surface processes redistribute significantly large volumes of sedimentary material. This may induce tectonic feedback due to the dynamic loading and unloading of the underlying crust.

To study the interaction between topographic evolution, surface processes and lithosphere/mantle dynamics, a 3D thermo-mechanical model (I3ELVIS: Gerya and Yuen, 2007) is fully coupled with a surface process model. To this end, we test and employ a new 2D surface process model, FDSM, which affects the physical surface of the model. It uses a diffusion-advection law to model erosion and sedimentation that approach a physical description of surface processes. Firstly, we evaluate the applicability of our landscape evolution model for large scale geodynamics. We also assess the most appropriate mathematical description to model the physics of erosion and sedimentation in large scale problems. Secondly, the role of surface processes on topographic expression is examined, i.e. we explore how surface processes modify large scale topographies. And lastly, we examine the influence of erosion and sedimentation on the behaviour of the lithosphere and the mantle flow dynamics, examined for the case of drip-type, convective removal of lithospheric mantle (Fig. 1).

Based on a comparison with analytical solutions, we show that the FDSM code is accurate and stable. Further, a linear diffusion model appears sufficient to capture the feedback under reasonable geological assumptions, and behaves virtually identical to a critical-slope non-linear diffusion model, while both outperform gross-scale, prescribed, erosion/sedimentation formulations.

Coupled models (Fig. 1) show that the steady-state elevation is similar for very different efficiencies of long-range surface redistribution, despite the fact the amount of uplift and exhumation varies significantly. The role of feedback is demonstrated by the decay time of topography, which is at least one order of magnitude longer in the case of active erosion-uplift feedback, as compared to static analytical predictions (Fig. 1b). Even for lowest effective diffusivity values, the erosional decay effects dominate over gravitational collapse (c.f. Jadamec et al., 2007). The developing stratigraphy is in agreement with principal observations from the Miocene Arizaro Basin in Argentina, which is indeed thought to have formed in response to partial lithospheric removal (DeCelles et al., 2015).

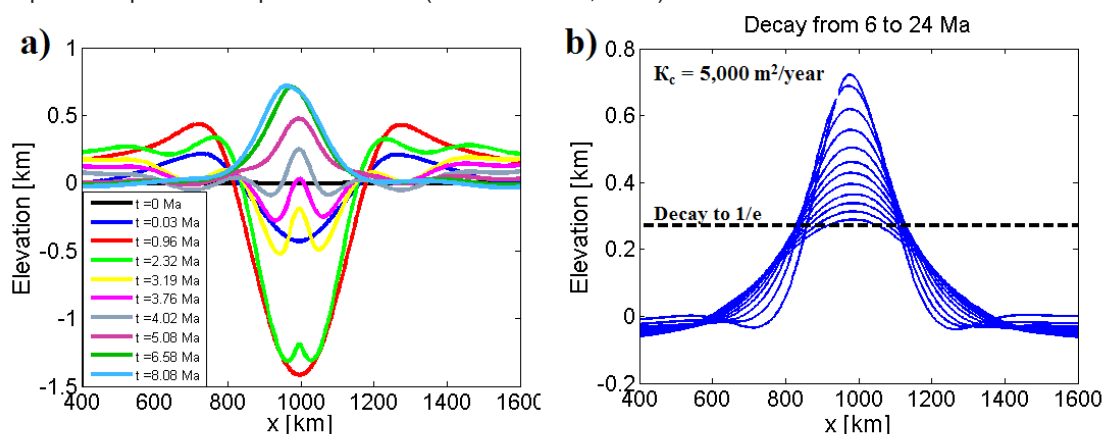


Figure 1. Coupled three-dimensional drip model. a) Model evolution from 0 to 8 Ma.. b) Decay time scales for drip models. Predicted time scales are 1 Ma; coupled model predictions are 17 times slower because of feedback, where erosion leads to localized crustal response due to unloading, counteracting the surface-driven lowering of topography.

REFERENCES

- DeCelles, P.G., Carrapa, B., Horton, B., McNabb, J., Gehrels, G.E., & Boyd, J. 2015: The Miocene Arizaro Basin, Central Andean hinterland: Response to partial lithosphere removal? *Geological Society of America Memoirs*, 212, 359-386.
- Gerya, T.V., & Yuen, D., 2007: Robust characteristics method for modelling multiphase visco-elasto-plastic thermo-mechanical problems. *Physics of the Earth and Planetary Interiors*, 163, 83-105.
- Jadamec, M.A., Turcotte, D.L., & Howell, P., 2007: Analytic models for orogenic collapse. *Tectonophysics*, 435, 1-12.

P 8.23

Constraints on the extent and kinetics of eclogitization processes in the Indian lower crust

Chanard K., Hétenyi G., Baumgartner L., Licul A., Herman F.

Earthquakes occurring in the Indian lower crust underthrusting Tibet can be related to the mineral transformations of subducted crustal rocks to denser eclogites. These intermediate-depth earthquakes are most likely linked to physical processes accommodating the significant volume change caused by dehydration reactions during eclogitization. However, while described by laboratory experiments and field samples, the kinetics of metamorphic reactions at large scale is not well known.

We propose to constrain the extent and kinetics of eclogitization processes in the Indian lower crust, at large spatial scales, by combining Bouguer anomaly data with 2-D thermokinematic and petrological modeling. We derive lithospheric density profiles by coupling thermokinematic modeling with a realistic multi-layer petrological model depending on mineralogical composition, pressure and temperature. The density estimates are then used to compute the associated Bouguer anomalies, which are then constrained by observed data along profiles perpendicular to the Himalayan arc. We explore model parameters (model geometry, mineralogical composition, water content) to best fit observations along 10 profiles spanning from NW India to Bhutan and discuss lateral variations in eclogitization processes along the Himalayan arc, in relation with seismic activity in the region.

P 8.24

Laboratory earthquakes triggered during eclogitization of lawsonite bearing blueschist

Sarah Incel¹, Nadège Hilairet², Loïc Labrousse³, Timm John⁴, Damien Deldicque¹, Thomas Ferrand¹, Yanbin Wang⁵, Joerg Renner⁶, Luiz Morales⁷ & Alexandre Schubnel¹

¹ *Laboratoire de Géologie de l'ENS -PSL Research University - UMR8538 du CNRS, 24 Rue Lhomond, 75005 Paris, France (incel@geologie.ens.fr)*

² *CNRS - UMET, Université Lille 1, 59655 Villeneuve d'Ascq, France*

³ *Université Pierre et Marie Curie, 4 place Jussieu, 75252 Paris, France*

⁴ *Freie Universität Berlin, Malteserstr. 74-100, 12249 Berlin, Germany*

⁵ *GeoSoilEnviroCARS, University of Chicago, Argonne, IL 60439, USA*

⁶ *Ruhr-Universität Bochum, Universitätsstraße 150, 44801 Bochum, Germany*

⁷ *GeoForschungsZentrum Potsdam, Telegrafenberg, 14473 Potsdam, Germany*

The origin of intermediate-depth seismicity has been debated for decades. Almost all of these events occurs within the upper plane of Wadati-Benioff double seismic zones believed to represent subducting oceanic crust. We deformed natural lawsonite-rich blueschist samples under eclogite-facies conditions ($1 < P < 3.5$ GPa; $583 \text{ K} < T < 1121 \text{ K}$), using a D-DIA apparatus installed at a synchrotron beam line continuously monitoring stress, strain and strain rate, phase proportions, and acoustic emissions (AEs). Two distinct paths were modelled: i) high pressure paths (> 2.5 GPa) under which lawsonite and glaucophane became gradually unstable while entering the stability field of lawsonite-eclogite ii) a low pressure path (< 2 GPa) without entering the lawsonite-eclogite stability field, but crossing the breakdown reaction of lawsonite and entering the stability field of epidote-blueschist and later eclogite-amphibolite. Upon entering the Lws-Ecl stability field samples exhibited brittle failure, accompanied by the radiation of AEs. In-situ X-ray diffraction and microstructural analysis demonstrate that fractures are topologically related to the formation of omphacite. Amorphous material filling out the fractures was detected by transmission-electron microscopy without evidence for free-water. Since the newly formed omphacite crystals are small compared to the initial grains, we suggest that grain-size reduction (transformational faulting) during the transition from lawsonite-blueschist to lawsonite-eclogite leads to brittle failure of the deviatorically loaded samples. In contrast, we find no microstructural evidence that the breakdown of lawsonite, and hence the liberation of water leads to the fracturing in the samples.

9. Subsurface Geology & Geo-Energy

Andrea Moscariello, Anneleen Foubert, Lyesse Laloui, Alex Hürlimann

TALKS:

- 9.1 Bataller F.J., McDougall N., Moscariello A.: Improved Late-Ordovician glacial reservoir prediction in North Africa using Spectral Decomposition on 3D Seismic data
- 9.2 Carrier A., Lupi M., Clerc N., Russillon E., Do Couto D., Moscariello A., Meyer M.: Inferring lateral depth variations of Tertiary formations within the Great Geneva Basin, western Switzerland.
- 9.3 Carvalho I., Erkman S.: Designing new business models for the geo-energy project
- 9.4 Caudroit J., Mondino F., Rex I.: New insights of Eastern Niger Delta reservoir based on core sedimentology and seismic stratigraphy.
- 9.5 Chao Li, Guillaume R., Laloui L.: Geomechanical modelling framework of CO₂ injection with consideration of salt precipitation and dissolution
- 9.6 Do Couto D., Moscariello A., Bou Daher S., Littke R., Weniger P.: Unconventional petroleum resources in the Geneva basin: myth or reality?
- 9.7 Ejderyan O.: Development and governance of deep geothermal energy. Insights from the social sciences
- 9.8 Le Cotonnec A., Ventra D., Moscariello A.: Incised valley fill reservoirs, from outcrop analogue to subsurface interpretations (Upper Carboniferous, Kentucky, USA)
- 9.9 Leila M., Moscariello A.: Sedimentological and petrophysical characterizations of the Messinian sandstones, onshore Nile Delta, Egypt
- 9.10 Makhnenko R., Mylnikov D., Vilarrasa V., Laloui L.: Thermo-hydro-mechanical aspects of caprock – CO₂ interaction for safe geological storage
- 9.11 Mondino F.: Surface structural analysis and relevance for the subsurface characterization of tight reservoirs (carbonate and clastics).
- 9.12 Perego R., Pera S., Belliardi M.: Multi-parameter low enthalpy geothermal mapping of Cantone Ticino
- 9.13 Wanner C., Alt-Epping P., Diamond L.W.: Thermal evolution of the Grimsel Pass hydrothermal system: insights from numerical modeling
- 9.14 Zia H., Lecampion B.: Implicit level set scheme to model the propagation of planar 3D hydraulic fractures

POSTERS:

- P 9.1 Alt-Epping P., Diamond L.W.: Numerical simulation of CO₂ injection into the U. Muschelkalk aquifer: implications of fluid–rock reactions in the aquifer and at the contact to an overlying clay formation
- P 9.2 Antunes V., Lupi M., Moscariello A., Meyer M., de Bono C.N., François M.: Searching for microseismic activity in the Great Geneva Basin
- P 9.3 Aschwanden L., Adams A., Diamond L.W., Mazurek M.: Anhydrite-dissolution porosity in the Upper Muschelkalk aquifer, NE-Switzerland: implications for geo-energy and geological storage of gas
- P 9.4 Brixel B., Jalali M., Klepikova M., Amann F., Loew S.: Hydraulic metrics & fingerprints: Development of sound test procedures & analytical framework to evaluate permeability enhancement
- P 9.5 Clerc N., Rusillon E., Cardello L., Moscariello A., Renard P.: Structural modeling of the Geneva Basin for geothermal resource assessment
- P 9.6 Dahrabou A., Valley B., Ladner F., Guinot F., Meier P.: Optimisation of borehole trajectory in order to minimize borehole failure
- P 9.7 De Boever E., Foubert A., Oligschlaeger D., Claes S., Soete J., Bertier P., Özkul M., Virgone A., Swennen R.: Combined μ -CT – NMR approach to (micro)porosity quantification in continental spring carbonates
- P 9.8 Egli D., Baumann R., Küng S., Berger A., Baron L., Herwegh M.: Fracture-controlled flow paths in an active hydrothermal system (Grimsel, Swiss Alps)
- P 9.9 Gaehwiler M., Preisig G., Volken S., Möri A.: GeoQuat project: From harmonization of unconsolidated rock data to 3D geological and parametric modelling
- P 9.10 Guglielmetti L., Moscariello A., Meyer M., de Bono C.N., Maurer H. & Dupuy D.: Geophysical characterisation of Cretaceous formations for underground thermal energy storage in the Geneva Basin
- P 9.11 Jalali M.R., Doetsch J., Gischig V., Krietsch H., Amann F.: Hydraulic Stimulation of Crystalline Rock – Grimsel Test Site
- P 9.12 Jansen G., Miller S.A.: Slip induced stress transfer in the embedded discrete fracture method
- P 9.13 Krietsch H., Doetsch J., Gischig V., Amann F.: Results from combined characterization based on geological mapping and geophysics: Grimsel Test Site
- P 9.14 Makhloufi Y., Samankassou E., Rusillon E., Meyer M.: Dolomitization of the Upper Jurassic sediments in the Great Geneva Basin
- P 9.15 Moukhtari F., Lecampion B.: The tip region of a hydraulic fracture driven by a power law fluid
- P 9.16 Rusillon E., Moscariello A.: Reservoir rock typing of the Late Jurassic Reef Complex, Greater Geneva Basin, (Switzerland and France)
- P 9.17 Sohrabi R., Jansen G., Miller S.A.: HULK – Simple and fast generation of structured hexahedral meshes for improved subsurface simulations
- P 9.18 Weidmann Y., Signorelli S., Grüniger A.: Country-wide analysis of geothermal potential for railway switch point heaters
- P 9.19 Rickenbacher M., Jalali M., Ziegler M.: Sensitivity analysis of hydraulic fracture propagation
- P 9.20 Leila M., Moscariello A.: Organic geochemistry of oil and natural gas in the West Dikirnis and El-Tamad fields, onshore Nile Delta, Egypt: Generation by Upper Cretaceous — Lower Tertiary terrigenous source rocks
- P 9.21 Ejderyan O., Stauffacher M.: Social discourses on deep geothermal energy

9.1

Improved Late-Ordovician glacial reservoir prediction in North Africa using Spectral Decomposition on 3D Seismic data

Francisco J. Bataller^{1,2}, Neil McDougall², Andrea Moscardello¹

¹ Department of Earth Sciences, University of Geneva, 13 Rue des Maraichers, 1205 Geneva, Switzerland.

² Repsol Exploración S.A. Mendez Alvaro 44, 28045, Madrid.

The study of ancient glacial reservoirs is of significant importance for several reasons, as oil and gas reservoirs in several parts of the world (most notably North Africa, Latin America, the Middle East, etc.), aquifers and as analogues for depositional models to improve the understanding of the processes underneath present-day ice sheets.

Oil and gas exploration in North Africa has, for many years, targeted a play focused on the sediment infilling glacial incisions of Late Ordovician age related to the Hirnantian glaciation. Exploration and production activities have provided a good data set for research aimed at improving our understanding of these depositional environments.

This paper focuses on methodologies for improving definition of intra-glacial reservoir depositional architectures using 3D seismic data from the Murzuq Basin in North Africa (Fig. 1). Seismic spectral decomposition was applied to this data set with the aim of significantly improving identification and mapping of glacially-related depositional features and suggesting comparisons of Red Green Blue (RGB) spectral decomposition responses with core data.

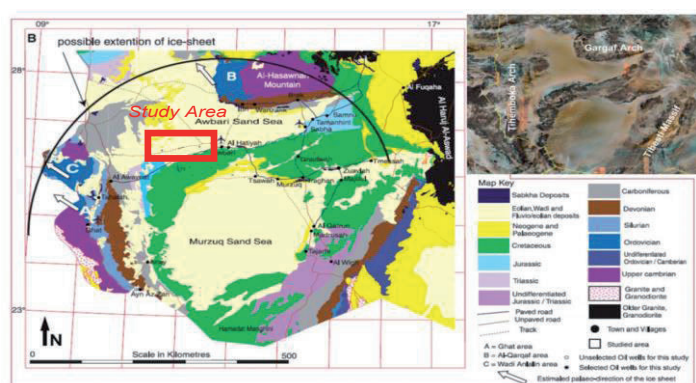


Figure 1. Murzuq Basin geological setting. Modified from El-Ghali, 2005.

Spectral decomposition workflows can significantly improve the mapping of paleogeographic highs and the associated glacial incisions infilled by reservoir sands. The workflow and tests carried-out in order to define the optimum frequency and algorithms selection, what to look for in the resultant RGB combinations (an example can be seen in Fig. 2) and how the results can be used as “cognitive pre-interpretation” providing a visual model which will improve our subsequent horizon picking is described; effectively providing a conceptual framework for “what” is being interpreted.

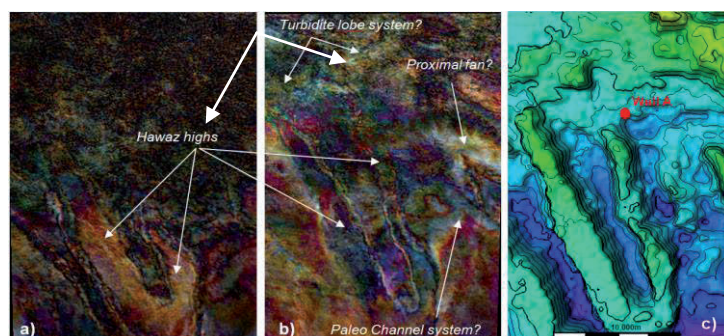


Figure 2. a) and b) RGB Spectral Decomposition of 2 different time slices showing a paleo tunnel valley and other sedimentological features. c) Tunnel Valley interpreted horizon map.

Also, the relationship between RGB responses and both core lithofacies and facies descriptions, which can provide us a calibration of the resultant seismic interpretation against hard data (Fig. 3) is highlighted. It should then be possible to extrapolate into areas with less or no data, always taking into account the significant difference in vertical resolution between the seismic data set and core-scale descriptions.

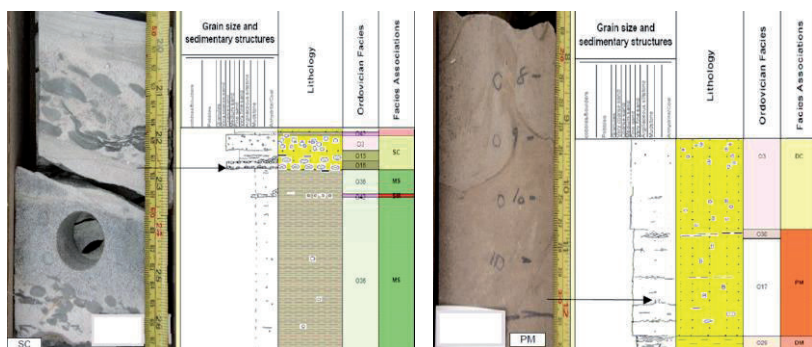


Figure 3. Core lithological and sedimentological description together with facies interpreted for Well A. (SC= Submarine Channel, MS= Muddy Shelf, DC= Distributary Channel, PC= Proximal Mouthbars, DM= Distal Mouthbars).

REFERENCES

- El-ghali, M.A.K., 2005: Depositional environments and sequence stratigraphy of paralic glacial, paraglacial and postglacial Upper Ordovician siliciclastic deposits in the Murzuq Basin, SW Libya. *Sedimentary Geology* 177, 145–173.
- Ghienne, J.-F. 2003: Late Ordovician sedimentary environments, glacial cycles, and post-glacial transgression in the Taoudeni Basin, West Africa. *Palaeogeography, Palaeoclimatology, Palaeoecology*, 189, 117–145.
- Le Heron, D. P., Craig, J. & Etienne, J. L. 2009: Ancient glaciations and Hydrocarbon accumulations in North Africa and the Middle East. *Earth-Science Reviews*, 93, 47–76.
- McDougall, N.D., Tawengi, K., Quin, J., Vipla Pont, J., 2005: Depositional environments and large-scale sediment architecture in the Upper Ordovician of the Murzuq Basin, SW Libya (Melaz Shuqran and Mamuniyat Formations, EAGE).
- Partyka, G, J Gridley & J Lopez, 1999: Interpretational applications of spectral decomposition in reservoir characterization. *The Leading Edge*, March 1999

9.2

Inferring lateral depth variations of Tertiary formations within the Great Geneva Basin, western Switzerland.

Aurore Carrier¹, Matteo Lupi¹, Nicolas Clerc¹, Elme Russillon¹, Damien Do Couto¹, Andrea Moscariello¹, Michel Meyer²

¹ *Département des Sciences de la Terre et de Géophysique, University of Geneva, Rue des Maraîchers 13, CH-1205 Genève (aurore.carrier@unige.ch)*

² *Services Industriels de Genève, CP: 2777, CH-1211 Genève*

The Swiss plan for a sustainable energy development supports the growth of renewable energies. In this framework, the Canton of Geneva began to investigate whether hydrothermal energy may be exploited in Western Switzerland. The Great Geneva Basin (GGB) shares geological and petrophysical similarities with the geological formations of the, already successfully exploited, such as the Munich area (Baviera, Germany) and Paris Basin (France). This led local Swiss authorities (State of Geneva and SIG, Services Industriels de Genève) to start an exploration phase in 2014 within the GGB (Moscariello, 2016). In this framework, the characterization of the relevant geological units including their geometries and geophysical characteristics is of prime importance.

This study aims at constraining and refining lateral and vertical heterogeneities of Tertiary and Quaternary formations using seismic and well data. In particular, we focus on Lower Cretaceous and possibly Tertiary formations that are considered promising target for hot water production and heat storage. Well data were used to build velocity laws by inverting a linear velocity law for each geological unit. We also combined Quaternary depths with seismic data from the GeoMol project to convert time to depth information by interpolating velocity law obtained at various wells within the GGB.

We produced a thickness (i.e. depth) map of the formations of the GGB focusing on Tertiary formations. For instance, computed Tertiary thickness ranges from 0 near the Jura mountains border to the NW to more than 3000m in the SE, at the border with the French Alps. These observations are consistent with field and wells observations. Our procedure allowed us to reduce the uncertainty of key target formation and represents an important step towards the development of geothermal energy in the Great Geneva Basin.

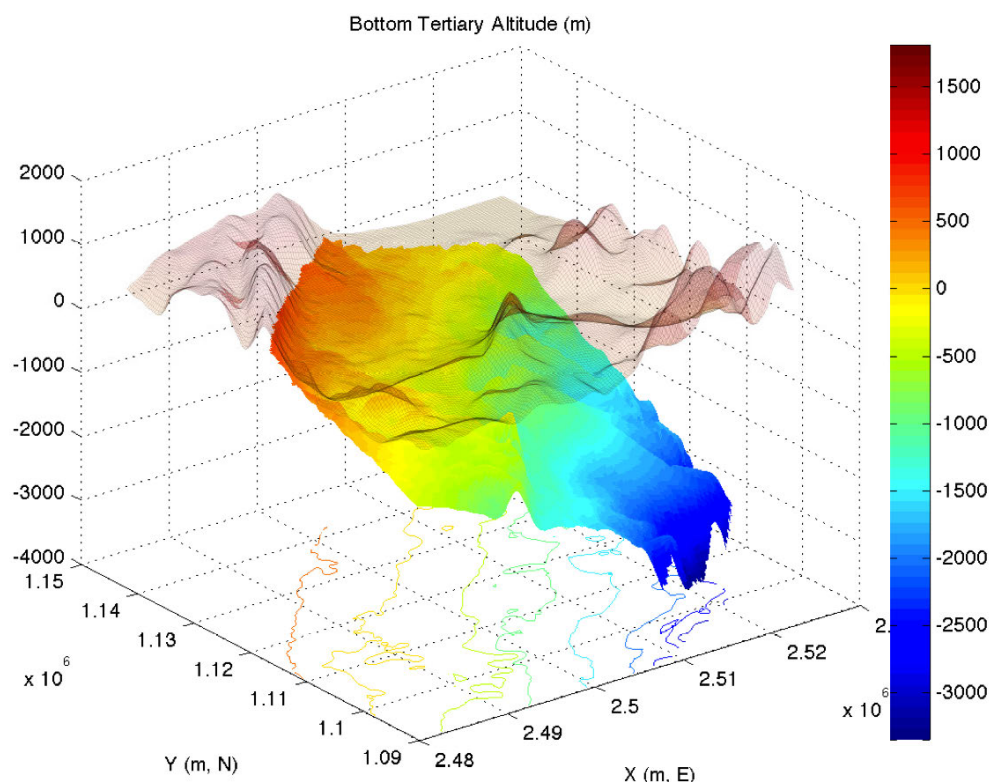


Figure 1. Iso-surface presenting Bottom Tertiary layer altitude (color mesh) compared to the topography (black mesh) of the Great Geneva Basin

REFERENCES

Moscariello A. 2016: Geothermal exploration in SW Switzerland, Proceeding of the European Geothermal Congress, Strasbourg 19-23 september 2016, 9 pp.

9.3

Designing business models for the geo-energy project

Ignes A. C. C. de Carvalho¹ & Suren Erkman¹

¹ *Institute of Earth Surface Dynamics, University of Lausanne, Géopolis, CH-1015 Lausanne (ignes.contreiras@unil.ch)*

² *Institute of Earth Surface Dynamics, University of Lausanne, Géopolis, CH-1015 Lausanne (suren.erkman@unil.ch)*

This study aims to understand the development and implementation of business models for the geo-energy project using the Industrial Ecology approach as a way to design processes, products, and services including natural environment and society as primary stakeholders of the organization. This can be translated in a way to re-think, re-design, and build business models that explore a sustainable industrial and social ecosystem, and reflect its complex structures and properties.

Industrial ecology draws an analogy between the functioning of ecosystems and industrial systems by revealing connections between production, consumption, and sustainability in a collaborative form. With this in mind, this approach can strive for mutuality to create, deliver, and capture not just economic value, but also environmental and social ones. This requires a long term system analysis adopting a broader meaning of value, bringing stakeholders inside (employees, shareholders, other collaborators) and outside (suppliers, partners, customers, government, society and others) of the firm to identify different perspectives and challenges.

Together, it is possible to observe different values that are missed, destroyed, absent or with a surplus in order to transform them into opportunities for everyone, including an environmental point of view. This can help organizations to understand and develop business models able to sustain economic value, considering growth, financial resilience and long-term viability and stability. Also embrace environmental values, considering resource use within regeneration rates, renewal of water and other resources, energy, emissions and waste levels, protection of the biodiversity, and seeking for not just to neutralize bad effects but also to promote positive benefits. The social value can promote poverty alleviation, social justice, equality, well-being, community development, long-term employment and labour standards and practices.

Figure 1 shows a Value mapping tool that helps to identify these values across different stakeholders, in a process, that start with setting the scene to map the value and to generate value opportunities for sustainability. Another approach is presented in Figure 2, presenting Environmental life cycle, Social stakeholder, and Economic business model design layers. Together, they suggest different forms to understand perspectives, challenges, and opportunities linked to the design of a business model for the geo-energy project, which is able to embrace different approaches in a win-win form to business, society, and environment.

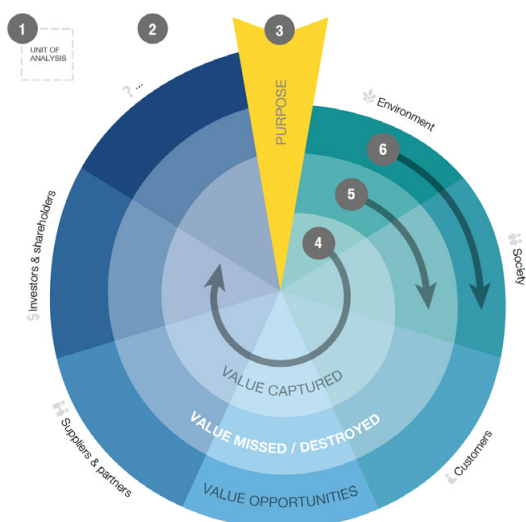


Figure 1. Value mapping tool (Bocken, Short Rana & Evans, 2015)

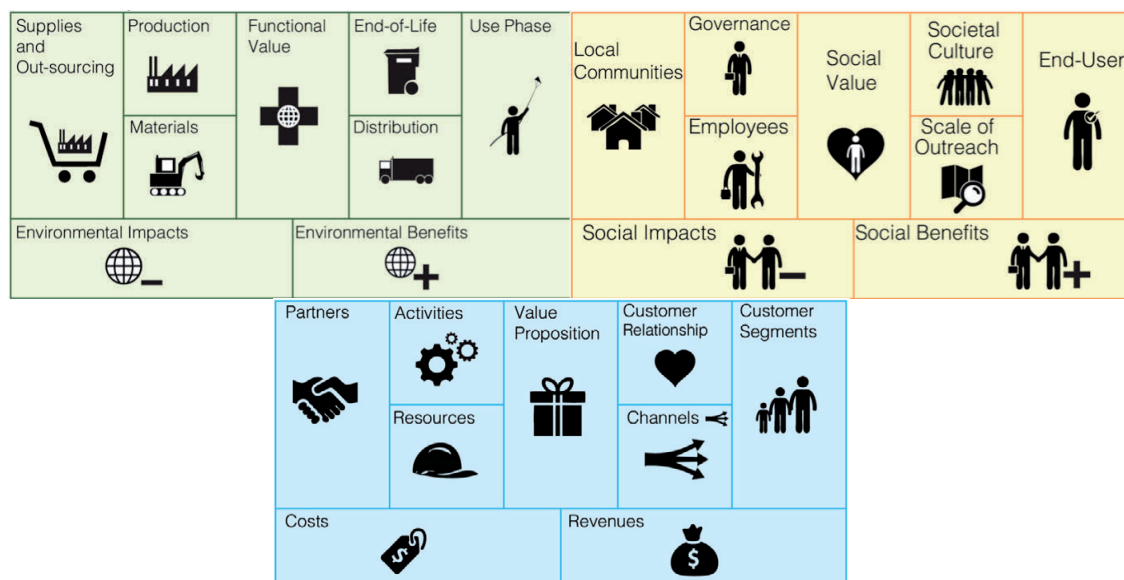


Figure 2. Environmental life cycle, Social stakeholder and Economic business model design layers (Joyce, Paquin & Pigneur, 2015).

REFERENCES

- Bocken, N., Short, S., Rana, P. & Evans, S. 2015: Value mapping for sustainable business thinking, *Journal of Industrial and Production Engineering*, 32:1, 67-81.
- Erkman, S. 2004: *Vers une écologie industrielle*, Paris: Éditions Charles Léopold Mayer.
- Joyce, A., Paquin, R. & Pigneur, Y. 2015: The triple layered business model canvas: a tool to design more sustainable business models, ARTEM Organizational Creativity International Conference, Nancy, France.

9.4

New insights of Eastern Niger Delta reservoir based on core sedimentology and seismic stratigraphy.

Caudroit Jerome¹, Mondino Fiammetta¹, Ilene Rex¹

¹ *Addax Petroleum Ltd, Route de Malagnou 101, 1224 Chêne-Bougeries, Switzerland*

Planning an infill well campaign in a mature and heavy oil field with current oil price under 50\$/bbl is a clear challenge for today's geologists. Success depends crucially on understanding reservoir composition, structural architecture and dynamic behaviour of fluids. In the Niger Delta, where complex shallow marine deposits create very high lateral and vertical heterogeneities, these factors become even more critical to understand and incorporate in static and dynamic modelling

The subsurface geology of a mature oil field situated in the OML 123 block in the Eastern Niger Delta is being re-examined to update the geological modelling in support of potential new infill wells.

Core, electric log and seismic stratigraphic analyses indicate that the reservoir rocks, interpreted to have been deposited in a tidally-influenced marginal marine environment, are characterised by a large vertical and lateral heterogeneity of sedimentary facies. Such heterogeneity may be explained by a complex interplay among deltaic authigenic processes, sea-level changes and tectonic activities.

In particular, the vertical distribution of what are interpreted as upper shoreface dominated parasequences, their overlying fluvial-dominated units, and bounding shale units have been described and correlated over the study area in order to assess their impact on fluid flow. Lateral and vertical facies changes may induce sudden variability in permeability and porosity causing baffles or barriers to flow.

Syn-sedimentary tectonic activity, mostly induced by gravitational processes and possibly deep strikeslip movements, have compartmentalised the study area in several structural blocks thus rendering the correlation across the blocks of stratigraphic units a challenging task.

As an additional challenge, well data distribution is mostly aligned in the crest of the structure and does not allow a clear understanding of the 3D facies distribution. The latter however, has been inferred by detailed seismic stratigraphic work which allows the extrapolation of key surfaces and sedimentary units in the interwell area and beyond well control.

Our studies to date indicate that lithofacies variations and structural barriers separating the blocks combined control reservoir connectivity as indicated by a variety of water-hydrocarbon contacts observed in the area.

9.5

Geomechanical modelling framework of CO₂ injection with consideration of salt precipitation and dissolution

Chao Li, Robert Guillaume and Lyesse Laloui

Laboratory of Soil Mechanics - Chair "Gaz Naturel" Petrosvibri, Swiss Federal Institute of Technology of Lausanne, EPFL, Switzerland

The precipitation of salt is observed to occur in pore throats of the host rock during CO₂ injection, and in return, it restricts fluid flows, limits the injectivity and causes an additional pressure build-up eventually. Such interplay between geochemistry and geomechanics is poorly understood, representing an important knowledge gap up to date.

This study presents a theoretical framework for describing the chemically induced geomechanical effects during the CO₂ injection. The framework makes it possible to take into account the salt precipitation due to CO₂ drying-out, the redistribution of stress with the presence of precipitated salts, the dissolution of essential minerals, strain development induced by the crystallization, as well as the effect of temperature. Each mechanism is analysed and is integrated together through mass, momentum and energy conservation and transport equations, leading to a set of fully coupled chemo-thermo-hydro-mechanical governing equations. Numerical implementation is also addressed to allow efficient resolution of the resulting complex system.

9.6

Unconventional petroleum resources in the Geneva basin: myth or reality?

Damien Do Couto¹, Andrea Moscariello¹, Samer Bou Daher², Ralf Littke² & Philipp Weniger³

¹ *Department of Earth Sciences, University of Geneva, Rue des Maraichers 13, CH-1205 Genève (damien.docouto@unige.ch)*

² *Institute of Geology and Geochemistry of Petroleum and Coal, EMR Group, RWTH Aachen University, Lochnerstr. 4-20, 52056 Aachen, Germany*

³ *Bundesanstalt für Geowissenschaften und Rohstoffe, Stilleweg 2, 30655 Hannover, Germany*

While the future provision of energy is challenging the scientific community, the interpretation of the Swiss subsurface geology and the assessment of the potential energetic resources (both fossil and renewable) appear essentials to avoid any conflict of use in the next future. The conventional petroleum exploration that took place in Switzerland and neighbouring France in the past century did not reveal the occurrence of major petroleum accumulation below the Molasse basin, despite numerous oil and gas shows at the surface and in the subsurface. However, and as long as unconventional resources represent a major new source of energy in countries around the globe, the potential discovery of unconventional oil and gas at depth sharpened many concerns in the past few years, in particular after the discovery of a tight gas accumulation in Paleozoic rocks near the Geneva Lake (Noville-1 well; Leu 2012).

In order to investigate the unconventional potential of the Molasse basin around Geneva, tens of samples made of cuttings, core fragments and plugs have been gathered from several wells in the southwestern Molasse Basin in which two major source-rocks in particular have been analysed: the Posidonia shale (Lower Jurassic) and the Permo-Carboniferous *sensu lato*. An evaluation of the organic geochemistry of these potential source-rocks (TOC, maturity, biomarker analysis, gas chromatography and isotopic analysis) has been realized both on well samples and bitumen and gas seeps occurring at the surface.

While most of the Posidonia shales hold a rather low amount of organic matter (<0.7%), an interval of about 12m in the Humilly-2 well show high organic content up to 4% TOC. Geochemical analyses show that the Posidonia shale formation below the Geneva Basin is currently in the oil window thus mature enough to generate oil and very few gas. On the contrary, the Posidonia shale of the Faucigny-1 well near the Alpine front thrust are supermature and have already generated large part of their oil and gas. Biomarker analyses of bitumen seeps in the Geneva canton reveal their origin from the Posidonia shale.

The Permo-Carboniferous beds encountered in the Jura have reached the oil and partially the gas windows, but there is no indication in the centre of the basin due to the lack of deep samples. Gas retrieved from an hydrocarbon pocket in the freshwater molasse unveil a biogenic and thermogenic origin. So far, the isotopic composition of the gas seems to indicate that it may originate from a mature Type II precursor or from an early mature Type III precursor.

These results show that two source-rocks are currently generating hydrocarbons at depth. The potential of unconventional petroleum accumulation are discussed below the Geneva basin, and are compared with Basin and Petroleum System Modelling simulations.

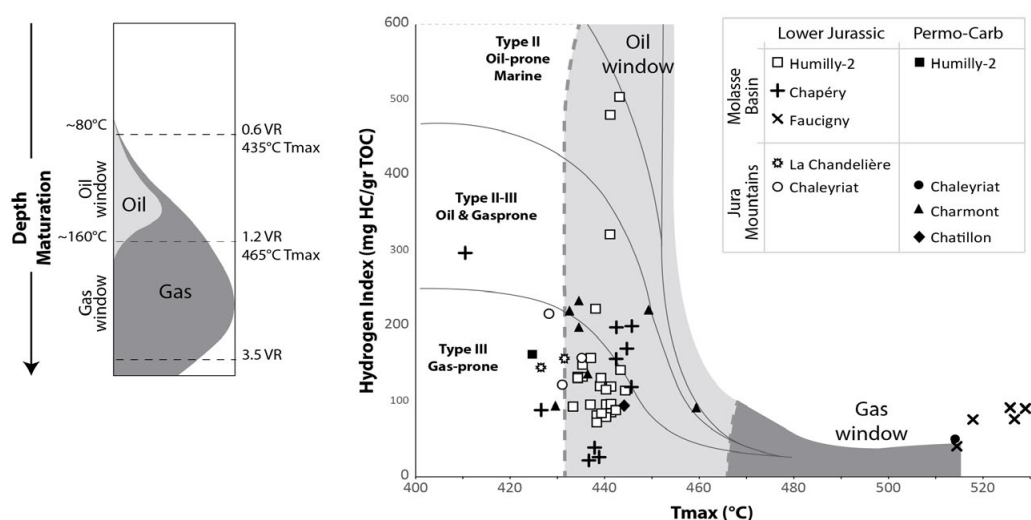


Figure XX3

Figure 1. Maturity diagram showing that most of the Posidonia shale analysed are in the oil window whereas the Permo-Carboniferous sandstones and coals spreads from the oil to the gas window.

REFERENCES

- Leu, W. 2012. Swiss oil/gas exploration and lessons learnt. *Swiss Bull. angew. Geol.*, 17, 49-59.
 Leu, W. & Gautschi, A., 2014: Shale gas potential of the Opalinus Clay and Posidonia Shale in Switzerland – A first assessment. *Swiss Bull. angew. Geol.*, 19/2, 95-107.

9.7

Development and governance of deep geothermal energy. Insights from the social sciences

Olivier Ejderyan

D-USYS Td-Lab / Swiss Competence Center for Energy Research - Supply of Electricity, ETH Zurich, Sonneggstrasse 5, NO F27, CH-8092 Zurich | Switzerland

Deep geothermal energy (DGE), is presented as a potential technology to decarbonize energy production worldwide. The 2007 IPCC 4th assessment report indicated that in 2050 8,3% of world electricity production should be covered by DGE. In Switzerland, the Federal Energy Strategy plans a development potential of DGE of up 4.4 TWh/year by 2050. These projections rely for a large part on the development of DGE production in non-volcanic areas and the use of new technologies such as EGS (engineered/enhanced geothermal systems) and/or petrothermal.

Despite those announcement, DGE development is slow with the exception of a few hotspots such as Southern-Germany. EGS power plants remain mainly at the level of pilot projects. In Switzerland there is no electricity produced by deep geothermal energy yet. Two major projects in Basel (2007) and St.Gallen (2013) triggered earthquakes, raising intense media attention and concern among local population and decision makers.

Actors active in the development of deep geothermal energy (DGE) have stressed that its large scale deployment does not depend only on technological innovation but also on its social acceptance (Majer et al. 2012;). Social sciences are enrolled to enquire social perceptions in order to anticipate acceptance when planning a geothermal project.

Social sciences can make valuable contributions to public engagement procedures for siting, planning, and risk management of DGE infrastructures. Here it is important to underline that “there is no “cookbook recipe” applicable to all projects that might imply induced seismicity and there can barely be one” (Trutnevyte & Ejderyan, submitted). This implies that taking into account the social dimension of DGE requires to address the specificities of various social contexts.

In this paper, I propose an overview of various methodologies used in order to assess the social dimension of DGE in Switzerland. The paper presents results of media analyses evaluating the social perception of DGE as well as insights from case studies that discuss strategies used to engage different publics.

REFERENCES

- Majer, E., Nelson, J., Robertson-Tait, A., Savy, J., & Wong, I. 2012. Protocol for Addressing Induced Seismicity Associated with Enhanced Geothermal Systems. Washington DC.
- Trutnevyte, E. & Ejderyan, O. Submitted. Managing Geoenergy-Induced Seismicity with Society. Journal of Risk Research.

9.8

Incised valley fill reservoirs, from outcrop analogue to subsurface interpretations (Upper Carboniferous, Kentucky, USA)

Le Cottonnec Aymeric, Ventra Dario, Moscariello Andrea

Department of Earth Science, University of Geneva, Switzerland

e-mail : Aymeric.LeCottonnec@unige.ch

Incised valleys are extensive geomorphological features with a high potential of encasing coarse grain sediments in muddy environments, therefore representing an interesting reservoir potential. Even though incised valleys have been recognized throughout the geological record, most of our knowledge on the geometry, genesis and infill of incised valleys comes from Quaternary case studies. This has led to a rather good understanding of the mechanisms of formation of incised valleys, but their internal stratigraphic architecture still needs investigation. From a reservoir point of view, the understanding of the stratigraphic architecture of the infill of incised valleys is necessary in order to better predict heterogeneities, as well as geometry and dimensions of sand-prone facies.

In order to improve the understanding of geometries, dimensions and heterogeneities of subsurface reservoirs, outcrop and modern analogues have proven to be a very useful tool. However, due to the size of incised valleys (up to several kilometres in width and tens of meters in height), ancient examples observable at outcrop are scarce and subsurface investigations of modern or recent cases are limited by data resolution and areal coverage (such as seismic and well data). In this context, Pennsylvanian successions of eastern Kentucky, a well-known as an outcrop analogue for Carboniferous fluvio-deltaic reservoirs in coal-bearing strata (e.g. Southern North Sea and onshore Europe), appears as an excellent field laboratory for the study of ancient incised valleys. The Breathitt Group is a coarsening- and shallowing-upward succession of Lower to Middle Pennsylvanian shallow-marine and fluvial deposits, representing the infill of an elongated foreland basin developed during the Alleghanian Orogeny punctuated by basin-wide marine units which allow the subdivision of the entire succession into eight formations. Stratigraphic cyclicity in the Breathitt Group is commonly attributed to high-magnitude glacioeustatic fluctuations driven by Gondwanan glaciations. Well-established, high-resolution correlations and previous work on regional geology make for an excellent stratigraphic framework, as well as extensive roadcuts and a large database of well/core data available from the Kentucky Geological Survey, enables detailed 3D analysis of architectural geometries and heterogeneities.

In this paper we are comparing field and well-logs data from the Upper Carboniferous of southeastern Kentucky with subsurface data from the Pennsylvanian of the Southern North Sea focusing on stacking patterns, dimensions and stratigraphical architecture of incised valleys.

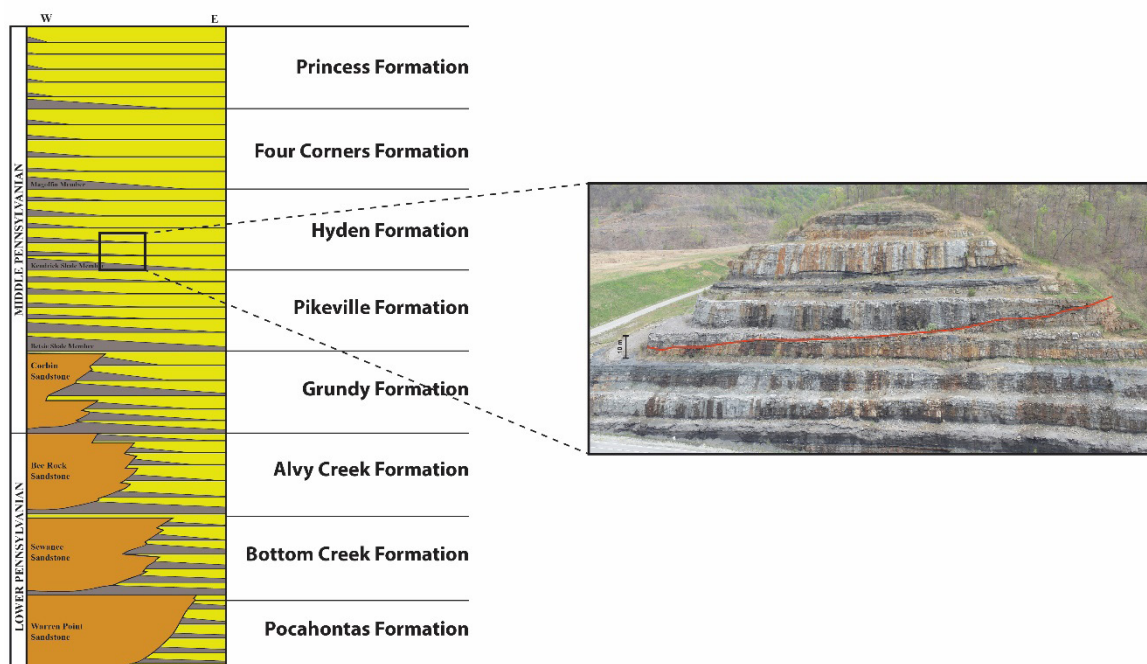


Figure 1. Stratigraphy of the Breathitt Group (left), example 1 of an incised valley in the Hyden Formation (right). Red line shows the base of the incised valley fill.

9.9

Sedimentological and petrophysical characterizations of the Messinian sandstones, onshore Nile Delta, Egypt

Mahmoud Leila¹, Andrea Moscariello¹

¹ *Department of Earth Sciences, University of Geneva, Rue de Maraîchère 13, CH-1205 Genève.*

Messinian sediments in the Nile Delta hosts excellent hydrocarbon reservoirs. Despite this they are still poorly studied. In this context, a multidisciplinary sedimentological and geochemical study is being carried out to unravel the depositional environment and tectonic setting before, during and after the Messinian Salinity Crisis (MSC) in the Eastern Mediterranean, and how this affected the eastern part of the onshore Nile Delta. The Lower Messinian Qawasim Formation consists of amalgamated channel fill sandstones capped by shallow marine lagoon mudstones deposited in an overall deltaic environment. The deeply incised valley infill, dating the Late Messinian consists of the Abu Madi Formation made of lowstand braided and meandering fluvial sandstone followed by tidally influenced shoreface sandstones as a result of sea level incipient rise. The base of this unit is erosional and contains large mud clasts embedded in fine-grained matrix. The Upper Messinian fluvial and shoreface sandstones are capped by estuarine horizontal and cross laminated mudstones, siltstones/mudstones followed by an open marine mudstones of the Lower Pliocene Kafr El-Sheikh Formation representing the end of the MSC and the subsequent transgression episode after the re-establishment of the connection between the Mediterranean and the Atlantic Ocean.

The Qawasim and Abu Madi sandstones were subjected to different diagenetic alterations, revealing a different pore water chemistry. Early smectite infiltration and its subsequent chloritization enormously decreased the permeability and pore throat radius of the Abu Madi sandstones. Qawasim sandstones underwent milder mechanical compaction preserving their original primary porosity. Dissolution of feldspars and carbonate lithoclasts enhanced the reservoir quality of the Qawasim and Abu Madi sandstones through the formation of well-developed secondary pore spaces. Carbonate and clay cements are the most diagenetic alterations that control the reservoir quality of the Messinian sandstones. Qawasim sandstones have better reservoir quality in terms of permeability, flow zone indicator and pore throat radius than the Abu Madi sandstones. Moreover, the channel fill Qawasim sandstones and the fluvial Abu Madi sandstones are the best reservoir quality facies for further exploration activities in the Messinian sequence of the Nile Delta.

9.10

Thermo-hydro-mechanical aspects of caprock – CO₂ interaction for safe geological storage

Roman Makhnenko¹, Danila Mylnikov¹, Victor Vilarrasa^{1,2} & Lyesse Laloui¹

¹ Soil Mechanics Laboratory - Chair "Gaz Naturel" Petrosvibri, École Polytechnique Fédérale de Lausanne, EPFL ENAC IIC LMS, GC – Station 18, CH-1015 Lausanne (roman.makhnenko@epfl.ch)

² Institute of Environmental Assessment and Water Research, Spanish National Research Council (IDAEA-CSIC), Jordi Girona 18-26, 08034 Barcelona, Spain

Security of carbon dioxide (CO₂) geological storage largely depends on the caprock integrity, especially at the early stages after the start of injection when the maximum overpressure is reached. The lower boundary of the caprock is in contact with CO₂ saturated pore water or pore fluid that consists almost of pure CO₂. Thermal and chemical interactions between the pore fluid and the caprock may change the material properties of the latter. Geomechanical stability is also crucial to maintain the caprock sealing capacity, since failure could lead to permeability increase and potentially induced microseismicity. Considering clay-rich materials (e.g., shales) as potential caprock has several advantages, including thermal, chemical, and inelastic deformations of the clay-rich (ductile) formation minimizing the affection on the sealing integrity as the upward movement of CO₂ through their pore system should be resisted by high capillary pressure.

Opalinus clay (Swiss shale) is studied as a representative caprock material because of its high (~ 60%) clay content and very small dominant pore size (~ 30 nm). Poromechanical properties of the shale are analysed by performing drained, undrained, and unjacketed conventional triaxial tests. Thermo-mechanical response is studied in drained and undrained heating and cooling experiments. It is shown that a potential shallow (~ 1 km) storage case with cold CO₂ injection leading to caprock cooling by 15 °C (from 40 °C to 25 °C) neither compromises shale integrity nor deteriorates its mechanical properties.

The breakthrough pressure values and effective permeability of liquid and supercritical CO₂ are measured for intact and reconstituted shale brought to in situ conditions in the oedometric cell. Breakthrough pressure is found to be effective stress-dependent and smaller for the intact material rather than for the reconstituted one (1.5 MPa and 4 MPa, respectively, at 18 MPa effective stress). This non-intuitive observation is explained by a non-uniform structure of the undisturbed material where CO₂ can find a path with larger than dominant pore sizes to flow through. CO₂ effective permeability of brine-saturated shale is an order of magnitude smaller than the one for brine and is on the order of 10⁻²¹ m² for the intact and reconstituted material loaded to in situ conditions.

Shales show interesting self-sealing features and their ductile-type failure allows often times to retain very small permeability. Since creep may become significant when assessing the long-term caprock integrity, viscous (time-dependent) deformation should be considered. The effective viscosity of Opalinus clay was found to be on the order of 10¹⁵ Pa•s, decreasing with temperature, and dropping to 10¹³ Pa•s in region where the pore fluid pressure gets closer to the total stress, which increases the probability of porosity waves creation.

9.11

Surface structural analysis and relevance for the subsurface characterization of tight reservoirs (carbonate and clastics).

Fiammetta Mondino^{1°}

^{1°}Shell International E&P, Kesslerpark 1, Rijswijk, The Netherlands

[°]Current address: Addax Petroleum Ltd, Route de Malagnou 101, 1224 Chêne-Bougeries | Switzerland

The impact of fractures and in-situ stresses on upstream operations has become more important with the advancement of technology and the shifting of frontiers to deeper and tighter reservoirs, with increasingly high temperature and high pressure. Fractured reservoirs constitute an important area for oil & gas exploration and production, but also for renewable energies (geothermal). Interpretation and analysis of these reservoirs using surface data (satellite, outcrops, etc.) offers an inexpensive approach to exploration strategies and can identify key insights into the nature of deformation represented by the fractures.

The aim of this talk is to demonstrate the impact of data integration and to illustrate the added value of a consistent structural characterization approach at regional scale to define development strategy of a fractured reservoir portfolio. The use of surface data (satellite image, outcrops, etc.) and the integration with subsurface data (seismic interpretation, core data, BHI images, etc.) is essential for the understanding of the structural setting of a field and to build conceptual and discrete fracture models, reducing the uncertainty range.

Two case studies from North Africa and Middle East will be presented where faults and fractures network were analysed in complex geological areas. These are generally not entirely newly formed structures, but represent reactivation of ancient structures. Changes in the orientation of stresses create selective activation of ancient faults with favorable orientations through time, resulting in complex fracture and fault patterns.

The satellite analysis shows that the studied outcrops have exposures of large sub seismic NW- SE trending structures remarkably similar in terms of their orientation, scale (both laterally and vertically) and widths to structures identified in the subsurface and the surface structures could therefore be used as a potential analogues. In such a setting the reservoir compartmentalization is a realistic structural scenario, due to combination of potentially sealing faults, presence of cemented fractures and the tight nature of (some of) the reservoir(s). Also, the difference in the deformation style/history can be related to the reology and age of the formations involved (mechanical stratigraphy).

9.12

Multi-parameter low enthalpy geothermal mapping of Cantone Ticino

Rodolfo Perego¹, Sebastian Pera¹, Marco Belliardi²

¹ *Institute of Earth Science, SUPSI, Via Trevano, CH-6952 Canobbio (rodolfo.perego@supsi.ch)*

² *Institute for Applied Sustainability to the Built Environment, SUPSI*

Low enthalpy geothermal energy is a type of renewable energy that is continuously growing in terms of exploitation within Europe, especially through the use of closed-loop systems. Currently the authorisation process for closed-loop systems in Cantone Ticino is based on maps taking into account the presence of restrictions arising from the enforcement of the water protection act and ordinance. It states that new closed-loop systems can not be installed within S groundwater protection zones, while they are always allowed in üB(“übriger Bereich”= remaining territory) sectors. Within the Au (usable groundwater) sector, a “sacrifice area” approach is adopted, allowing the installations of such systems in specific areas where the presence of conflicts precludes groundwater exploitation for drinking purposes. The described procedure, however, does not consider the subsurface potential. Therefore developing a multi-parameter geothermal mapping could give precious planning indications from both an energetic and socio-economic standpoint while fulfilling environmental protection requirements. Furthermore, an overall estimate of shallow geothermal potential in Canton Ticino is important due to the progressive diffusion of these kind of systems in the next years, since at least the 20% of energy requirements for new buildings will have to be provided from renewables (RUEn, 2008). The mapping procedure started with the realization of a ground surface temperature (GST) map using mean annual air temperature (MAAT) data retrieved by MeteoSwiss stations and a 25m DEM. Firstly we correlated MAAT measured in different stations with altitude in order to find a regression equation, then we applied it to the DEM to create a MAAT map. The GST map was then obtained by applying the formulas contained in SIA 384/6 regulation:

$$GST = \text{Mean Annual Air Temperature} + 1.55 \quad \text{for altitude} < 1000 \text{ m.a.s.l.}$$

$$GST = \text{Mean Annual Air Temperature} + 1.55 + \frac{(\text{Altitude} - 1000)}{800} * 2.45 \quad \text{for altitude} > 1000 \text{ m.a.s.l.}$$

Results were compared with real measured data of ground temperature coming both from IDAWEB database and undisturbed ground temperature values obtained by TRT tests executed in 6 spots. A digitalized geological map (Geologische Karte der Schweiz 1:500000, 2005) was used in order to define the main outcrop lithologies, while part of the sedimentary portion of the Canton Ticino region was characterized using hydraulic conductivity values extracted from pumping tests, interpolated using ordinary kriging and classified accordingly into gravels, sands and clays. A reference set of thermal properties was then assigned to each lithological unit (both rocky and sedimentary) according to SIA 384/6 regulation and a thermal conductivity map (for outcrops and equivalent Quaternary deposits) was realized. 128 simulations with EED varying λ , GST, heat flux and volumetric heat capacity were performed in order to calculate the total borehole length required to satisfy a hypothesized annual heat demand of 30 MWh/year. This value was estimated taking into account a residential unit composed of 5 flats of 100 m² each, with an equivalent operating annual time of 1200 hours, a heat pump peak power of 25 kW and an energetic index of 60 kWh/m² year (MINERGIE® standard for refurbished buildings). Maps of required borehole length and estimated extraction rate (W/m) were developed for Canton Ticino. Usually the most suitable areas match the most densely populated ones however, within Au sectors, most of the areas where closed-loops are authorised show lower potential as they are placed in alluvial fans, where the higher depth to the groundwater table results in lower λ values.

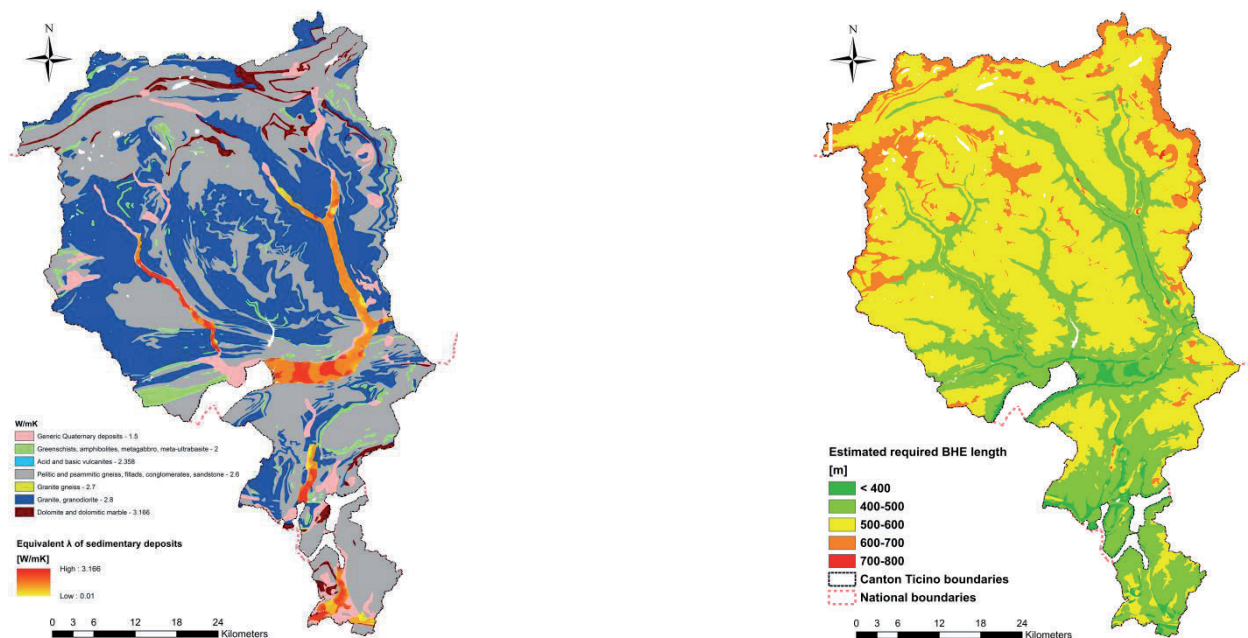


Figure 1 - Left) λ map for Cantone Ticino. The orange portion represents the equivalent λ of Quaternary deposits within monitored aquifers. Right) Estimated BHE length to satisfy the assigned annual heat demand for a reference residential unit

REFERENCES

- [1] BAFU, Wärmenutzung aus Boden und Untergrund, Wärmenutzung aus Boden und Untergrund: Vollzugshilfe für Behörden und Fachleute im Bereich Erdwärmennutzung, 2009
- [2] OFEFP (2004) Instructions pratiques pour la protection des eaux souterraines [Groundwater protection guide]. L'environnement pratique. SAEFL, Berne, Switzerland, 141 pp
- [3] SIA 384/6, 2009. Erdwärmesonden. Schweizer Norm SN/Bauwesen, Schweizerischer Ingenieur- und Architektenverein, Zürich, Switzerland, 76 pp.

9.13

Thermal evolution of the Grimsel Pass hydrothermal system: insights from numerical modeling

Christoph Wanner¹, Peter Alt-Epping¹ & Larryn W. Diamond¹

¹ *Institute of Geological Sciences, University of Bern, Baltzerstrasse 3, CH-3012 Bern (wanner@geo.unibe.ch)*

Hydrothermal springs with discharge temperatures of up to 28°C occur beneath the Grimsel Pass in the Transitgas AG tunnel crosscutting through para-autochthonous crystalline units of the Aar massif (Pfeifer et al., 1992). Located at about 1900 m.a.s.l., these springs are the highest thermal discharges documented in the entire Alps (Belgrano et al., 2016). The springs occur over a narrow tunnel section of <100 m and are associated with a major mylonitic shear zone that has experienced brittle overprint during uplift and cooling of the Aar massif. Stable and radiogenic isotope analyses ($\delta^{18}\text{O}$, $\delta^2\text{H}$, ^3H , ^{14}C) reveal a meteoric origin and suggest that the springs infiltrated more than 30,000 years ago at an elevation of about 2200-3000 m.a.s.l. (Waber et al., 2016). Moreover, these analyses show that the springs actually correspond to a mixture of an old thermal component with a surface-derived, young cold water component. Applying an enthalpy balance and assuming a contribution of 40-50% yield hypothetical spring temperatures of 45-50°C in the absence of cooling with cold water. Beside the occurrence of warm springs, hydrothermal activity is also manifested by the occurrence of a hydrothermal breccia which is widely exposed at and near the Grimsel Pass. Dating of this so-called Grimsel Breccia demonstrated that the hydrothermal system has been active for at least the last 3.3 Ma years (Hofmann et al., 2004). Furthermore, oxygen isotopes in quartz and adularia, combined with fluid inclusion data, indicate a maximum Breccia formation temperature of 160°C. Taking into account a geothermal gradient of 25°C per km and a mean annual surface temperature of 4°C this temperature estimation suggest that meteoric water infiltrates to a maximum depth of 6.25 km.

For this contribution we present results from a numerical modeling study aiming at (i) unraveling the thermal and hydrodynamic evolution of the Grimsel Pass hydrothermal system and (ii) at evaluating the general geothermal potential of fracture-flow driven hydrothermal systems. The latter is particularly important with respect to Switzerland's ongoing effort in accessing and/or creating such systems for geothermal power production. Numerical simulations were performed using two different approaches. Results obtained from a 3D (dual) continuum model using TOUGHREACT suggest that steady-state temperature distribution is approached in less than 2000 years, which is much faster than the lifetime of the Grimsel-Pass hydrothermal system. Moreover, these 3D simulations demonstrate that the extent of temperature anomalies induced by fracture-flow driven hydrothermal systems are mainly controlled by (i) the reservoir temperature, (ii) the upflow velocity, i.e., by the fault zone permeability as well as the hydraulic head driving hydrothermal circulation, and (ii) the 3D extent of the fault system. Results obtained from a 2D discrete fracture network model using ConnectFlow (AMEC, 2012) coupled to PFLOTTRAN (www.pfлотran.org) confirm the importance of the upflow velocity in controlling the temperature distribution and thus the geothermal potential of fracture-flow driven hydrothermal systems. Moreover, they demonstrate that the detailed fault-zone geometry such as fracture orientation, -spacing and -aperture plays a key role as well. In conclusions, applied to the Grimsel pass hydrothermal system, our models suggest that the small thermal anomaly observed in the Transitgas AG tunnel results from low discharge rates (<50 L/min) induced by the relatively low fault-zone permeability of about 10^{-13} m^2 .

REFERENCES

- AMEC, 2012. CONNECTFLOW Release 10.4 Technical summary document. AMEC/ENV/CONNECTFLOW/15, AMEC, UK.
- Belgrano, T.M.; Herwegh, M.; Berger, A. 2016. Inherited structural controls on fault geometry, architecture and hydrothermal activity: an example from Grimsel Pass, Switzerland. *Swiss Journal of Geosciences*. Doi:10.1007/s00015-016-0212-9
- Hofmann, B. A.; Helfer, M., Diamond, L. W.; Villa, I. M.; Frei, R.; Eikenberg, J. 2004. Topography-driven hydrothermal breccia mineralization of Pliocene age at Grimsel Pass, Aar massif, Central Swiss Alps. *Schweizerische Mineralogische und Petrographische Mitteilungen*, 84(3), 271–302.
- Pfeifer, HR; Sanchez A.; Degueldre, C. Thermal springs in granitic rocks from the Grimsel Pass (Swiss Alps): The late stage of a hydrothermal system related to Alpine Orogeny. In: Kharaka YK & Maest AS, editors, *Proceedings of Water-Rock Interaction WRI-7*, Park City, Utah, A.A. Balkema, Rotterdam, The Netherlands; 1992. p. 1327-1330
- Waber H.N, Schneeberger, R.; Mäder, U.K.; Wanner, C. 2016. Constraints on evolution and residence time of geothermal water in granitic rocks at Grimsel (Switzerland). *Procedia Earth and Planetary Science*. *Proceedings of the 15th Water-Rock Interaction Symposium WRI-15*, Evora, Portugal.

9.14

Implicit level set scheme to model the propagation of planar 3D hydraulic fractures

Haseeb Zia¹, Brice Lecampion¹

¹ *Geo-Energy Lab - Gaznat chair on Geo-Energy, EPFL-ENAC-IIC-GEL, Station 18, CH-1015 Lausanne (haseeb.zia@epfl.ch)*

We present a python implementation of the implicit level set algorithm to model propagation of planar hydraulic fractures. This algorithm was first introduced by Peirce & Detournay in (2008). The growth of a fluid driven planar fracture is modelled by coupling elasticity, described by a hypersingular integral equation (assuming a homogeneous medium) with fluid flow inside the fracture, described by the lubrication equation together with the mode I fracture propagation condition. The solution of the coupled system is numerically challenging due to a number of reasons. First, the lubrication equation describing the viscous fluid flow degenerate at the fracture tip (see e.g. Detournay and Peirce, 2014). Secondly, the elasticity results in a non-local relation between the pressure and the fracture width resulting in densely populated matrices causing the problem to be computationally intensive. Finally, the footprint of the fracture is not known as the resolution of the fracture front requires the velocity field, which is a-priori unknown. The Implicit Level Set Algorithm (ILSA) tracks the free boundary by implicitly enforcing the hydraulic fracture opening tip asymptote at the computational domain cells in the vicinity off the tip. The regular rectangular computational grid is divided into three types of cells. The tip cells, i.e. the cells containing the fracture tip, the ribbon cells comprising of a narrow band of cells adjacent to the tip cells inside the fracture and the channel cells containing the remaining cells inside the fracture. The boundary conditions for the Eikonal equations are prescribed by inverting the tip asymptote in the ribbon cells from the knowledge of the trial fracture opening in those cells. The fracture front is then located by solving the Eikonal equation using the Fast Marching Method (Sethian, 1996). Since the method is implicit, the Eikonal equation is solved iteratively in a time step until the correct position of the fracture front satisfying both the mass and momentum conservation of the fluid and the elasticity equation is located.

We have verified the algorithm by testing the propagation of a radial fracture in the toughness dominated regime for which an analytical solution exist (Abé et al., 1976). In this propagation regime, the viscous losses are negligible and the pressure is uniform throughout the fracture. Our results show that the numerical solution matches with the analytical solution.

We also present a number of others simulations for the case where the confining stresses is spatially varying, resulting in deviation of the fracture footprint from the initially radial geometry.

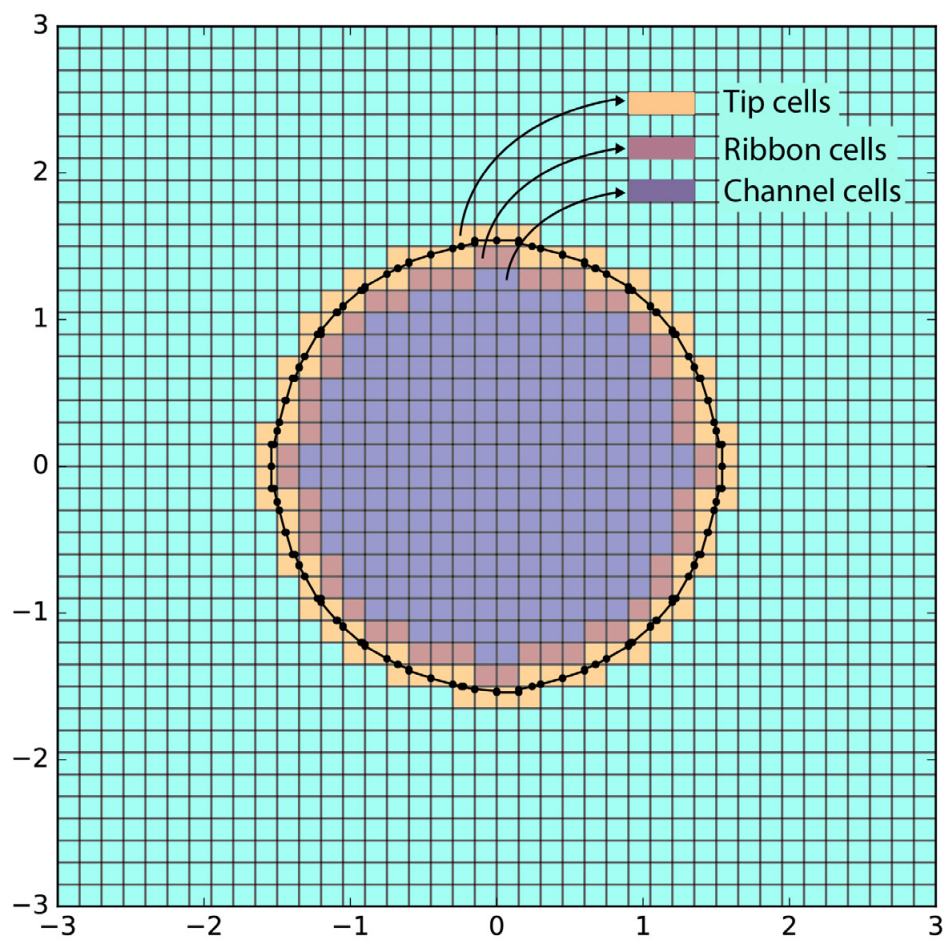


Figure 1. A snapshot of planar hydraulic fracture propagation using ILSA (Implicit level set Algorithm). The tip cells containing the fracture tip, the ribbon cells where the tip asymptote is inverted to get boundary conditions for the Eikonal equation and the channel cells are shown in different colors.

REFERENCES

- Peirce, A., & Detournay, E. 2008: An implicit level set method for modeling hydraulically driven fractures. *Computer Methods in Applied Mechanics and Engineering*, 197(33), 2858-2885.
- Detournay, E., and Peirce, A. 2014: On the moving boundary conditions for a hydraulic fracture. *International Journal of Engineering Science*, 84, pp.147-155.
- Sethian, J. A., 1996: A fast marching level set method for monotonically advancing fronts. *Proceedings of the National Academy of Sciences*, 93(4), 1591-1595.
- Abe, H., Keer, L. M., & Mura, T., 1976: Growth rate of a penny-shaped crack in hydraulic fracturing of rocks, 2. *Journal of Geophysical Research*, 81(35), 6292-6298.

P 9.1

Numerical simulation of CO₂ injection into the U. Muschelkalk aquifer: implications of fluid–rock reactions in the aquifer and at the contact to an overlying clay formation

Peter Alt-Epping & Larryn W. Diamond

Institute of Geological Sciences, University of Bern, Baltzerstrasse 3, CH-3012 Bern (alt-epping@geo.unibe.ch)

A study by (Chevalier et al., 2010) has identified several deep saline aquifers in the Swiss Molasse Basin, which may potentially be useful as reservoirs to store anthropogenic CO₂. One of these aquifers is the Trigonodus Dolomite of the U. Muschelkalk formation. Predictive numerical modelling, constrained by in-situ testing and laboratory measurements, constitutes an important step in the evaluation of the storage capacity, injectivity and the long-term isolation performance of the aquifer. We use the reactive transport code PFLOTRAN (www.pflotran.org) to assess the implications of the dynamics of the CO₂ plume, fluid-fluid and fluid-rock interaction and pressure and temperature conditions for the safe, long-term storage of CO₂.

More than 80% of the Trigonodus Dolomite is composed of dolomite with minor calcite and anhydrite and accessory quartz, kaolinite and sulphide minerals (pyrite, sphalerite) making up the remaining 20 %. Laboratory measurements on core samples of the Trigonodus Dolomite indicate porosities as high as 25 % and a strongly heterogeneous distribution of porosity and permeability. Furthermore, the Trigonodus Dolomite aquifer is intensely fractured implying that the migration of the CO₂ plume may be fracture controlled (Figure 1).

Previous simulations have indicated a strong dependence of the efficiency of solubility trapping on the permeability of the aquifer if the aquifer permeability is homogeneous. Here we look at the implication of fractures on the migration of the plume and the CO₂ trapping efficiency. We make use of the unstructured grid capability of PFLOTRAN to incorporate fracture networks into our simulations. PFLOTRAN is then used to simulate the evolution of the CO₂ plume and the ensuing changes in the brine composition and mineralogy. Changes in the mineralogy due to dissolution/precipitation reactions affect the porosity and permeability of the aquifer which feeds back onto the migration of the plume. By using different fracture sets we aim to identify those fracture properties having the strongest control on the CO₂ trapping capacity.

Preliminary simulations suggest that compared to homogeneous conditions aquifer heterogeneities reduce the rate of CO₂ solubility trapping. These simulations also suggest that, as the dissolution of CO₂ into the brine is associated with a decrease in *pH*, carbonate minerals dissolve releasing additional CO₂ into the brine thereby lowering the efficiency of CO₂ solubility trapping. Thus the chemical trapping capacity tends to be lower in carbonate aquifers than in silicate dominated aquifers. As a consequence, a plume of free CO₂ may exist for longer periods of time during which the tightness of the overlying seal needs to be ensured.

To address the issue of seal integrity we use a generic model of an interface between a carbonate aquifer and a clay rock. We simulate the arrival of a CO₂ plume and look at the reactive transport processes taking place on both sides of the interface. The infiltration of the CO₂ plume into the clay will be simulated with a new transport module that combines diffusive transport with electromigration to take into account the effect of the surface charge of clay minerals on solute transport. The surface charge of clay minerals induces an electrical potential extending into the pore space and affecting the distribution of charged ions. A diffuse layer enriched in cations and depleted in anions forms at mineral surfaces such that the pore water composition and mineral solubilities change with distance from clay mineral surfaces. We explicitly consider the diffuse layer in our simulations and compare the results with simulations involving conventional ion exchange. Although conventional ion exchange models can produce a similar breakthrough of cations as a diffuse layer model (provided that appropriate selectivities are chosen), the results differ strongly in terms of the breakthrough of anions.

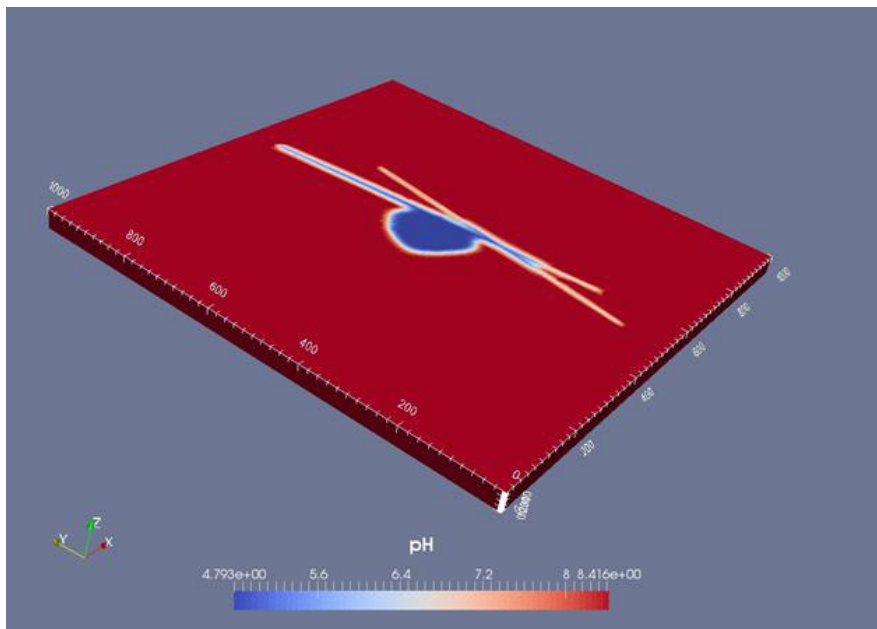


Figure 1. A CO₂ plume represented as a region of low *pH*. Permeable faults or fractures act as preferential pathways for the plume. Hence, tracking the pathway of CO₂ requires an understanding of the fracture distribution and fracture properties such as aperture, strike, dip, length and depth.

REFERENCES

- AMEC, 2012: CONNECTFLOW Release 10.4 Technical summary document. AMEC/ENV/CONNECTFLOW/15, AMEC, UK..
- Chevalier, G., Diamond, L. W. & Leu, W. 2010: Potential for deep geological sequestration of CO₂ in Switzerland: a first appraisal. *Swiss Journal of Geosciences* 103 (3).

P 9.2

Searching for microseismic activity in the Great Geneva Basin

Verónica Antunes¹, Matteo Lupi¹, Andrea Moscariello¹, Michel Meyer², Carole Nawratil de Bono², Martin François²

¹ Department of Earth Sciences, University of Geneva, Rue des Maraichers 13, CH-1205 Geneva
(veronica.antunes@unige.ch)

² Services industriels de Genève – SIG, Case postale 2777, CH-1211 Geneva 2

Switzerland is moving towards renewable energies growth and the Canton of Geneva is actively involved in such deployment. Yet, little is known about the seismic activity within the Great Geneva Basin (GGB) and the small number of seismic stations deployed in the region is a contributing factor for such shortening of knowledge.

To date there are only two seismic stations deployed around GGB: one from SED (Swiss Seismological Survey) and other from RESIF (French Seismologic and Geodetic Network). Such limited amount of stations, does not allow to capture and localize small magnitude (i.e. less than M2) seismic events. In a preliminary phase we analyzed the records of the currently deployed stations highlighting a seldom micro-seismic activity. Yet, it was not possible to understand the rate of seismic activity in the region and its relationship with the existing faults.

To understand where micro-seismic activity may be located around and within the GGB we deployed a temporary network composed of 8 broadband stations. We located the identified events using the available GeoMol velocity model that will be improved in a later time.

Current results indicate weak seismic activity in the GGB not showing a clear clustering. Further studies must be done to determine the baseline of the seismic activity before geothermal exploration takes place.

Epicenter Map

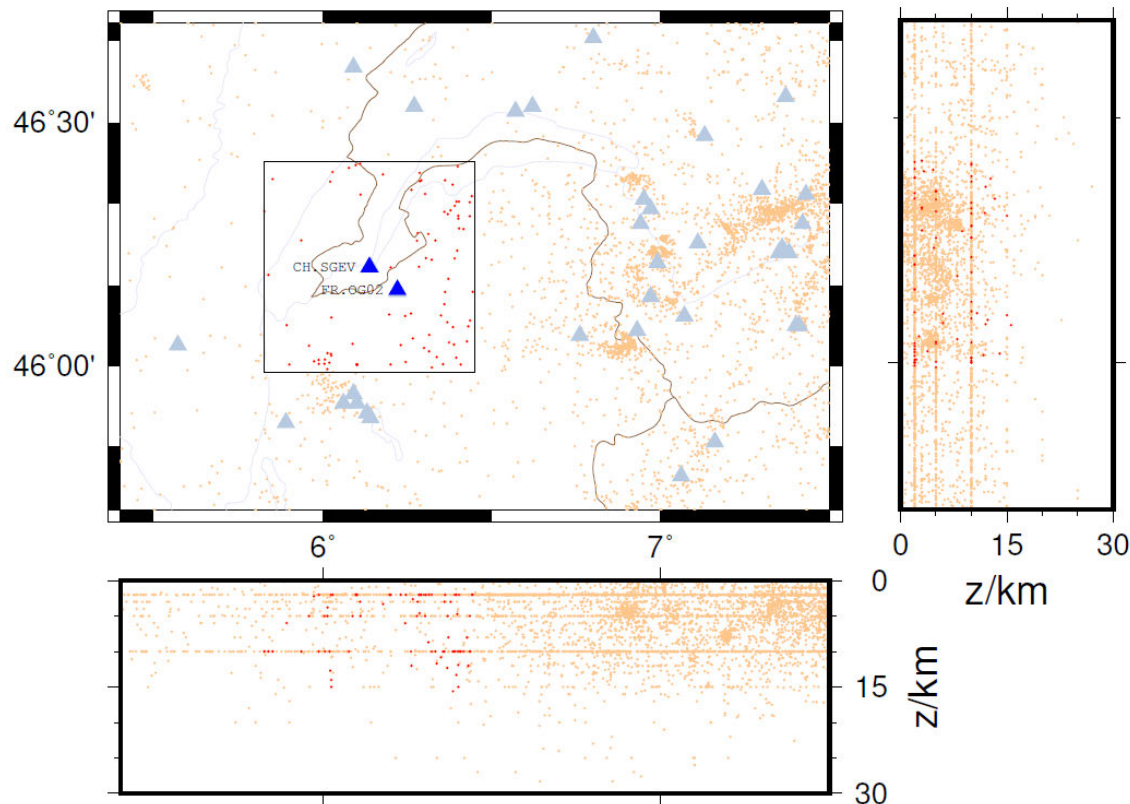


Figure 1. Epicenter map of events occurred from January 01 1966 to July 11 2016, according to the ISC (International Seismological Centre) catalogs. Red dots represent the earthquakes occurred in the Great Geneva Basin (represented by the black square) and orange dots the earthquakes occurred in the surrounding areas. The triangles show the location of the permanent seismic stations in the Great Geneva Basin (in blue) and in the surrounding areas (in grey).

P 9.3

Anhydrite-dissolution porosity in the Upper Muschelkalk aquifer, NE-Switzerland: implications for geo-energy and geological storage of gas

Lukas Aschwanden¹, Arthur Adams¹, Larryn W. Diamond¹ & Martin Mazurek¹

¹ Institute of Geological Sciences, University of Bern, Baltzerstrasse 1+3, CH-3012 Bern (lukas.aschwanden@geo.unibe.ch)

In the Swiss Molasse Basin (SMB), the Middle Triassic dolomite rocks within the Upper Muschelkalk (Trigonodus Dolomit) are currently being investigated for geothermal energy and geological storage of gas. At shallow levels along the northern margin of the SMB, these dolomites show locally high matrix porosities and permeabilities (≤ 25 vol.% and $\leq 10^{-13}$ m², respectively). These good reservoir properties are in part due to beds rich in cavities left by the dissolution of eogenetic anhydrite nodules. However, the distribution of this type of porosity is not well known. The present study reconstructs the genesis and evolution of these pores, thus providing conceptual understanding to support ongoing exploration in the deeper, hotter, southern regions of the SMB.

Our reconstruction of the genesis and evolution of the anhydrite-dissolution porosity is based on drill-core samples from two boreholes at Benken and Schlattingen and includes standard petrographic investigations, isotopic analyses (i.e. δD , $d^{18}O$, and $^{87}Sr/^{86}Sr$) of dolomite, quartz, calcite and kaolinite, and fluid inclusion studies of pore-filling quartz and calcite.

The results show that in some intervals of the Upper Muschelkalk at Benken and Schlattingen the anhydrite-dissolution pores have been affected by two events of mineral precipitation: (1) the first involved precipitation of quartz, which contains tiny inclusions of relict anhydrite, indicating that the quartz precipitated during anhydrite dissolution; (2) a younger event in which calcite and kaolinite precipitated, in part coevally.

Primary fluid inclusions in pore-filling quartz yield trapping temperatures in the range of 41–52 °C, whereas the salinity of the trapped fluid is highly variable, ranging from 5 to 23 wt.% NaCl_{eq}. In contrast, primary fluid inclusions in paragenetically younger calcite pore-fillings indicate trapping temperatures from 76 to 85 °C, whereas the salinity of the trapped fluid ranges from 0.2 to 6.5 wt.% NaCl_{eq}. The results of the stable and radiogenic isotope analyses of the various pore-filling minerals, as well as the calculated isotope signatures of corresponding parent-waters, are given in Fig. 1.

The highly variable salinity of fluid inclusions in quartz is interpreted to reflect mixing of two waters with contrasting salinities during anhydrite dissolution. The more saline endmember of this mixture is likely to have been seawater modified by evaporation and diagenesis, that was originally trapped within the rock pores during seepage-reflux dolomitization of the carbonate precursor of the Trigonodus Dolomit.

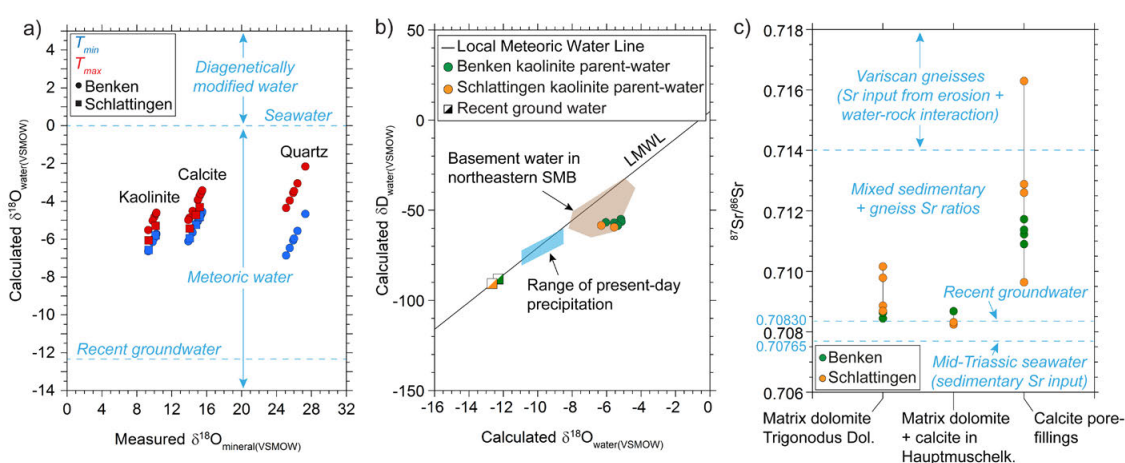


Figure 1. Results of the stable and radiogenic isotope analyses of the various pore-filling minerals, as well as of the calculated isotope signatures of the corresponding parent-waters.

The calculated $d^{18}O$ signatures of the parent-waters of pore-filling quartz and later calcite and kaolinite (Fig. 1a,b) reveal strong meteoric components. Thus, influx of meteoric water and dilution of the original porewater was evidently responsible for dissolution of the anhydrite nodules. This mixing scenario is consistent with the highly elevated $^{87}Sr/^{86}Sr$ ratios of the pore-filling calcite compared to the rock matrix (Fig. 1c). The only sources of radiogenic Sr in the local stratigraphy are the Buntsandstein and the Variscan gneiss basement, which have $^{87}Sr/^{86}Sr$ values up to 0.7285 (Matter et al., 1987). As a

consequence, radiogenic basement waters could have infiltrated the Upper Muschelkalk along deep fractures and caused anhydrite dissolution. An alternative explanation draws on the fact that the Buntsandstein and the Variscan gneisses are exposed in the Black Forest Highlands to the north of the SMB. Meteoric water has interacted with these rocks since they were uplifted by Miocene block-faulting, and such waters could have acquired radiogenic $^{87}\text{Sr}/^{86}\text{Sr}$ signatures. Topographically-induced southward flow of these chemically modified surface waters could have recharged the aquifer laterally and caused the anhydrite to dissolve. From the evidence available to date, neither the exact origin of the waters nor the timing of infiltration can be resolved. However, the two scenarios have totally different implications for exploration strategies: Infiltration along deep fractures would imply that the high matrix porosity and permeability are locally restricted to the vicinity of deep fractures, which hydrologically connect the Upper Muschelkalk and the crystalline basement. In contrast, lateral recharge of meteoric runoff from the Black Forest Highlands would imply that the high matrix porosity and permeability are likely to be restricted to the northern margin of the SMB, as hydraulic gradients inhibit lateral infiltration into the deeper, southern regions of the SMB. Further in-depth investigations will be required to reliably determine the origin of these waters and to define appropriate exploration strategies.

REFERENCES

Matter, A., Peters, T. & Ramseyer, K. 1987: $^{87}\text{Sr}/^{86}\text{Sr}$ -Verhältnisse und Sr-Gehalte von Tiefengrundwässern, Mineralien sowie Gesteinen aus dem Kristallin und der Trias der Nordschweiz. *Eclogae Geologicae Helveticae*, 80, 579–592.

P 9.4

Hydraulic metrics & fingerprints: Development of sound test procedures & analytical framework to evaluate permeability enhancement

Bernard Brixel¹, Mohammadreza Jalali¹, Maria Klepikova¹, Florian Amann¹, Simon Loew¹

¹ *Institute of Geology, Group of Engineering Geology, NO Building, Sonneggstrasse 5, ETHZ, 8092 Zurich, Switzerland (bernard.brixel@erdw.ethz.ch)*

The Swiss Competence Center for Energy Research – Supply of Electricity (SSCER-SoE), is carrying out a controlled hydraulic stimulation experiment at the Grimsel Test Site (GTS), in the canton of Bern, Switzerland. This experiment is part of a series of ongoing research programs aimed at evaluating the potential for implementing deep geothermal energy (DGE) technology as a viable source of base load power generation in Switzerland. Research activities at the GTS will rely on the design, monitoring and analysis of an in-situ fault stimulation experiment with the objective to improve our understanding of thermo-hydro-mechanical (THM) processes related to permeability enhancement and induced seismicity in stimulated granitic massifs (i.e. conditions similar to the ones expected at the depths targeted for enhanced geothermal systems (EGS)).

Presented herein are the results of an ongoing hydrogeological characterization field program designed to (i) provide high-resolution data for the development of a conceptual flow model for our experimental test volume (approx. 8000 m³) under baseline conditions, i.e. prior to hydraulic stimulation, and (ii) develop a set of hydraulic metrics and fingerprints as our basis for the quantification of permeability enhancement. To meet these objectives, extensive field measurements and hydraulic tests were completed throughout the year, including: monitoring formation pressures, automated tunnel inflow logging, and a comprehensive series of packer tests (both in single and cross-hole configuration). Interpretation of field data using head profiles, well test analysis and diagnostic plots allowed us in turn determining: (i) local hydraulic gradients and principal flow directions across our test volume, (ii) the transmissivity and storage parameters of known fractured zones and their surrounding rock mass, (iii) distinct conceptual fluid flow regimes/models, and (iv) the occurrence (or lack) of hydraulic connection between discrete geological structures (e.g. ductile lamprophyre contact zones and brittle fractures).

Preliminary test results indicate that flow across our experimental reservoir volume is oriented towards the northeast direction and takes place mainly through a network of discrete fractured zones, exhibiting in general only low-to-moderate transmissivity ($\sim 10^{-7}$ m²/s). The use of pressure derivative analysis (PDA) and diagnostic plots allowed us identifying various flow regimes, ranging from Infinite Acting Radial Flow (IARF) and double-porosity to linear and bilinear flow regimes, reflecting the heterogeneous nature of the local geological structures and their effect on local fluid flow patterns. In our view, the occurrence of such a broad range of hydraulic responses precludes the use of a single standard conceptual flow model, and calls instead for an assessment of discrete fractured network (DFN) versus continuum (e.g. double-porosity) modeling approaches. Related to that, and of particular interest to our research, is the quantitative evaluation of how to best calibrate numerical flow simulations, together with the reconstruction of fractured networks, using parameters generally hard to estimate and/or typically overlooked (e.g. the flow dimension (Barker, 1988; Le Borgne et al., 2004) and two-point hydraulic connection data (Day-Lewis, 2000)).

REFERENCES

- Barker, J. A. 1988: A generalized radial flow model for hydraulic tests in fractured rock, *Water Resources Research*, 24, 1976-1804.
- Day-Lewis, F. D., Hsieh, P. A., Gorelick, S. M. 2000: Identifying fracture-zone geometry using simulated annealing and hydraulic-connection data, *Water Resources Research*, 36, 1707-1721.
- Le Borgne, T., Bour, O. de Dreuzy, J. R., Davy, P., Touchard, F. 2004 : Equivalent mean flow models for fractured aquifers : Insights from a pumping tests scaling interpretation, *Water Resources Research*, 40, W03512

P 9.5

Structural modeling of the Geneva Basin for geothermal resource assessment

Nicolas Clerc¹, Elme Rusillon¹, Luca Cardello¹, Andrea Moscariello¹ & Philippe Renard²

¹ *Department of Earth Sciences, University of Geneva, Rue des Maraîchers 13, CH-1205 Genève (Nicolas.Clerc@unige.ch)*

² *Center for Hydrogeology and Geothermics (CHYN), University of Neuchâtel, Rue Emile-Argand 11, CH-2000 Neuchâtel*

In late 2015, 62 km 2D reflexion seismic data were acquired over the Geneva canton as part of the GEothermie 2020 Geneva State program, which aims at investigate and develop the deep geothermal potential of the Geneva basin (Moscariello, 2016). These newly acquired data complements the existing 2D seismic dataset partly recently reprocessed available over the the Swiss-French Geneva basin.

In the light of this most ever complete Swiss-French 2D seismic dataset (>500 km), the structural scheme of the Geneva basin, already depicted by various authors at either basin- or local-scale can be further refined. In this sense, the main left-lateral strike-slip fault zones known across the basin are confirmed, but detailed delineation of individual seismic faults geometries and extensions reveals a more complex structuration of these main fault zones, along with the presence of smaller-scale associated or conjugated fault systems. Despite this improved seismic data coverage, the connections, extensions and orientations of certain fault objects remain however uncertain in some areas. Indeed, some areas suffer from non-unique possible interpretation of fault traces between 2D seismic profiles. This issue, as well as the proposed refined structural scheme of the Geneva basin in its whole, is temptatively validated by observed surface fault expressions and fault-kinematics analysis from nearby outcrop observations (Cardello et al., 2016), in the context of the tectonic structuration history of the greater Geneva region.

This enriched 2D seismic dataset also provides better controll on the 3D geometries of the main Mesozoic stratigraphic units across the basin. Their respective seismic signature, coherent with their main lithological contents, is identified from the deep well Humilly-2 along a reference seismic line running through it. Petrophysical measurements on core and outcrop samples, coupled with well-log response analysis reveal that the Kimmeridgian – Tithonian *Reef Complex* and underlying *Calcaires de Tabalcon* units display the most encouraging geothermal reservoir properties within the Mesozoic sedimentary cover (Rusillon et al., 2016). For this reason, despite its limited thickness at seismic scale and some difficulty to track it with good precision within the seismically monotonous calcareous-prone Upper Malm interval, special emphasis is given in the 3D mapping of the Kimmeridgian unit in order to highlight its depth and thickness variations across the Geneva basin. Moreover, specific dome-shape structure patterns with irregular to chaotic internal reflexions, surrounded by onlapping reflectors can be repetively identified on certain seismic profiles. The stratigraphic position, thicknesses and lateral extension of these seismic objects is coherent with the Kimmeridgian *Reef-Complex* buildups observed in nearby outcrops. They are temptatively interpreted as such, while keeping in mind that the presence of numerous (subseismic) unit-bounded diffused fault discontinuities, commonly observed within the massive limestones of the Upper Malm and Cretaceous intervals, can also generate similar seismic artifacts. In both cases, whereas it is of depositional (*Reef Complex* buildups) or structural (increased fault density) origine, these percular zones likely correspond to enhance reservoir properties regions that deserve special mapping attention in the quest of geothermal reservoirs.

A clear mapping of the fault network and Kimmeridgian reservoir unit across the Geneva basin will play a kee role in the selection of future drilling location for deep geothermal heat production. Understanding the development of the fault network in terms of fault relationships and kinematics within the basin stress field evolution through time and present-day situation should also help to predict the development and preferential orientation of smaller-scale fault and fracture-related enhanced permeability zones, potentially acting as hydraulic conduits connecting most productive reservoir facies.

REFERENCES

- Cardello, G. L., Lupi, M., Makhloufi, Y., Do Couto, D., Clerc, N., Sartori, M. & Meyer, M. 2016: Fault evolution and fluid circulation in the Great Geneva Basin (Jura fold-and-thrust belt, France & Switzerland). Abstract 14th Swiss Geoscience Meeting, Geneva, Switzerland.
- Moscariello, A. 2016: Geothermal exploration in SW Switzerland. Proceeding of the European Geothermal Congress, Strasbourg, France, 19-23 September 2016, 9pp.
- Rusillon, E. & Moscariello, M. 2016: Reservoir rock typing of the Late Jurassic Reef Complex, Greater Geneva Basin, (Switzerland and France). Abstract 14th Swiss Geoscience Meeting, Geneva, Switzerland.

P 9.6

Optimisation of borehole trajectory in order to minimize borehole failure

Asmae Dahrabou¹, Benoît Valley¹, Florentin Ladner², Frédéric Guinot², Peter Meier²

¹ Centre for Hydrogeology and Geothermics (CHYN), University of Neuchâtel, Emile-Argand 11, CH-2000 Neuchâtel (asmae.dahrabou@unine.ch, benoit.valley@unine.ch)

² Geo-Energie Suisse AG, Reitergasse 11, 8004 Zürich. (f.ladner@geo-energie.ch, f.guinot@geo-energie.ch, p.meier@geo-energie.ch)

In the frame of a CTI-project the CHYN and Geo-Energie Suisse AG are developing a workflow and associated software tools that enable a fast decision process for selecting an optimal well trajectory while drilling deep inclined wells for EGS-projects. Optimal well trajectory is needed to minimize borehole instabilities and maximize the intersection with natural fractures. Minimizing borehole instabilities is mandatory for higher drilling performance and brings down risks and costs and on the other hand it is the key to allow the deployment of the innovative reservoir creation technology ("multi-stage stimulation concept" by Geo-Energie Suisse) that requires an almost in-gauge borehole for proper packer sealing.

In this paper are presented the results of an initial parameter study on the borehole stability that sets solid bases for the workflow development. For the moment, the parametric study was based on linear-elastic analytical solutions for the stress concentration around a borehole and the angular opening of the borehole breakouts (referred as breakout width) was used as a borehole stability indicator. Sensitivity analyses were performed by using MATLAB software and the framework UQlab. From both approaches, it can be concluded that the most influential parameters are the maximum horizontal stress SHmax, the uniaxial compressive strength UCS, and the mud pressure Pmud. In addition the sensitivity of borehole stability to borehole deviation is illustrated with the plots shown in figure 1. These figures show the impact that the drilling direction decision can have on the borehole stability.

In parallel, the data from the Deep Heat Mining project hole BS-1 were re-analyzed in order to extract additional information on the borehole geometry. More than 80% of the crystalline borehole section of BS-1 presents breakouts. The objective is to go beyond looking at breakout width only and to find borehole geometry descriptors that are potentially more relevant to packer sealing integrity. The geometric descriptor investigated were in addition to breakout width, breakout radial extend (also referred as breakout depth), borehole cross sectional area, borehole cross section ellipticity parameters and borehole cross section minimum radius of curvature (Figure 2). Correlations amongst these geometrical descriptors were assessed. Relatively low correlation between these parameters suggests that a combination of them will be required to assess the suitability of the borehole wall geometry for setting packers. These findings will serve at developing the rationale behind the workflow that will be developed and applied on the Haute-Sornes deep geothermal project.

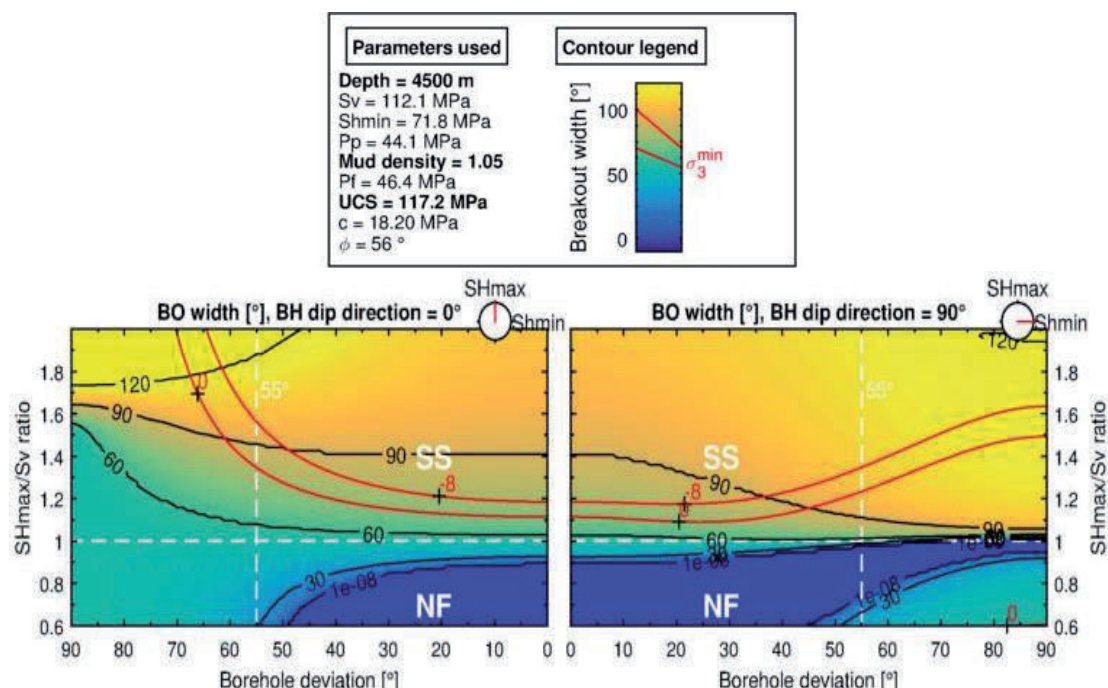


Figure 1. The parameters of the analyses listed in the top frame, breakout width contour plots for 2 drilling directions (0° 90°) are below for drilling direction toward SHmax or Shmin and assuming SHmax = 1.05 Sv mud density = 1.00 and the UCS = 167.3 MPa.

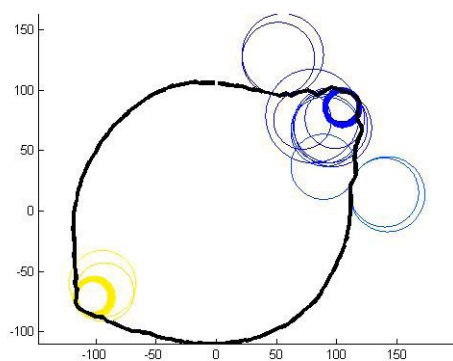


Figure 2. Example of different breakout geometries for a same minimum radius of curvature. To differentiate breakout geometries, which give similar minimum radius of curvature but will have different implications for the packers and their ability to seal a borehole section, the minimum radius of curvature must be combined with other parameters, like breakout width or depth.

REFERENCES

- Aadnoy & Looyeh, 2011, *Petroleum Rock Mechanics*, 1st edition, Drilling operations and well design.
- Barton, C. A., M. D. Zoback, and D. Moos, 1995, Fluid flow along potentially active faults in crystalline rock, *Geology*, 23(8), p. 683–686.
- Valley, B. and Evans, Keith F, 2009, Stress orientation to 5 km depth in the basement below basel (switzerland) from borehole failure analysis, *swiss J. Geosci.* 102, 467–480.

P 9.7

Combined μ -CT - NMR approach to (micro)porosity quantification in continental spring carbonates

Eva De Boever¹, Anneleen Foubert¹, Dirk Oligschlaeger², Steven Claes³, Jeroen Soete³, Pieter Bertier⁴, Mehmet Özkul⁵, Aurélien Virgone⁶, Rudy Swennen³

¹ Department of Geosciences, University of Fribourg, Fribourg, Switzerland (eva.deboever@unifr.ch; +41 26 300 89 73)

² Department of Earth and Environmental Sciences, KU Leuven, Leuven, Belgium

³ Institut für Technische und Makromolekulare Chemie (ITMC), RWTH Aachen University, Worringer Weg 1, 52074 Aachen, Germany

⁴ Clay and Interface Mineralogy, Energy and Mineral Resources Group, RWTH Aachen, Aachen, Germany

⁵ Geological Engineering, Pamukkale University, Kınıklı Campus, 20070, Denizli, Turkey

⁶ TOTAL E&P Recherche Développement, Paris, France

Travertine hot-spring depositional systems precipitate CaCO_3 at rates which are orders-of-magnitude higher than any other carbonate factories. Additionally, continental carbonate springs witness high rates and large magnitudes of physical and chemical gradients (e.g., temperature, pH and CO_2 degassing) along their downstream flow pathways. Recent investigations furthermore confirm the role of distinctive microbial communities in the formation of distinct downstream fabrics and facies (vent, apron and channel, pond, proximal slope and distal slope facies). These settings and their deposits gained renewed interest as certain facies and fabrics are comparable to those found in potential subsurface carbonate reservoirs.

As a result of those high rates of carbonate precipitation and high environmental gradients over small spatial scales, the primary fabrics and (micro)porosity encountered in them can be expected to reflect both abiotic and biotic factors. Secondary, early (and late) diagenetic processes may additionally influence this primary, porous networks. Understanding the different pore classes, their distribution, origin and evolution through time are of importance in the evaluation of their potential as subsurface reservoirs for energy applications.

One powerful technique to quantify the pore structure of representative rock plugs in 3D is microfocus computed tomography (μ -CT). This technique is combined with nuclear magnetic resonance (NMR) of miniplugs in addition to classical petrographical and petrophysical techniques, to investigate the pore network characteristics of two common and widespread ancient spring carbonate facies, as exposed in the Pleistocene Cakmak quarry (Denizli, Turkey). The results are compared to the pore network of recent travertine deposits at Mammoth Hot Springs (Yellowstone Park, USA). The results show that NMR T_2 distributions systematically display an uni- to bimodal MICP and bimodal NMR T_2 distribution with a single microporosity mode and a meso- to macroporosity mode. Micro-sized pore bodies (pore diameter $< 1\mu\text{m}$), make up between 6 and 33% of the pore space (average NMR T_2 cut-off value: 62ms) and are systematically located within crystal cores of granular and dendritic crystal textures or along common crystal nucleation points. The investigated properties did not reveal differences in micropore size or shape with respect to more or less biology-associated facies. Results show that to achieve a linked scale view on the porosity distribution and connectivity from sub-micron to millimeter scale, NMR and μ -CT are ideally combined.

P 9.8**Fracture-controlled flow paths in an active hydrothermal system (Grimsel, Swiss Alps)**

Daniel Egli¹, Rahel Baumann¹, Sulamith Küng¹, Alfons Berger¹, Ludovic Baron² & Marco Herwegh¹

¹ Institute of Geological Sciences, University of Bern, Baltzerstrasse 1+3, CH-3012 Bern (daniel.egli@geo.unibe.ch)

² Institute of Earth Sciences, University of Lausanne, Bâtiment Géopolis, CH-1015 Lausanne

Flow paths in fault-bound hydrothermal systems are strongly controlled by the spatial distribution and continuity of ductile and brittle structures (shear zones, fractures, joints) that can provide the main fluid pathways and enhance permeability of the rock mass by joining existing pores and creating new pore space but can also act as seals to fluid flow. In long-lived systems, these patterns are complex and dynamic in time and space, especially if they are subject to orogenic processes. However, better understanding of such naturally porous and permeable rocks at suitable depths could provide an alternative to enhanced geothermal systems for future geothermal exploration and eventually energy production in the northern Alpine foreland basin (NAFB). Direct observation of the rocks that constitute potential geothermal reservoirs in the NAFB is hindered by the up to km thick Molasse sediments and thus available outcrops of appropriate basement rocks (e.g. the in External Crystalline Massifs of the Alps) can serve as analogue study objects. This study focuses on an active fault-bound hydrothermal system in the crystalline basement of the Aar Massif (Swiss Alps) that has been exhumed from few km depth and which documents at least 3 Ma of hydrothermal activity (Hoffmann et al., 2004; Belgrano et al., 2016). On the basis of structural data collected from a 125 m long drillhole, the corresponding drill core as well as surface mapping, we evaluate the structural evolution with regard to porosity, permeability and fracture distribution around a central water-bearing breccia zone from the millimetre to decametre scale with main focus on the flow path evolution with time. The high variability of deformation structures and related fluid pathways at different scales emphasises the complex link between their mechanical evolution and hydraulic behaviour in time and space.

REFERENCES

- Belgrano, T.M., Herwegh, M. & Berger, A. 2016: Inherited structural controls on fault geometry, architecture and hydrothermal activity: an example from Grimsel Pass, Switzerland. *Swiss J. Geosci.* 1-20.
- Hoffmann, B.A., Helfer, M., Diamond, L.W., Villa, I.M., Frei, R. & Eikenberg, J. 2004: Topography-driven hydrothermal breccia mineralization of Pliocene age at Grimsel Pass, Aar massif, Central Swiss Alps. *Schweiz. Mineral. Petrogr. Mitt.*, 84, 271–302.

P 9.9

GeoQuat project: From harmonization of unconsolidated rock data to 3D geological and parametric modelling

Michael Gaehwiler¹, Giona Preisig¹, Stefan Volken¹, Andreas Möri¹

¹ Federal Office of Topography swisstopo, Swiss Geological Survey (SGS), Seftigenstrasse 264, CH-3084 Wabern bei Bern (Michael.Gaehwiler@swisstopo.ch)

In Switzerland, Quaternary deposits have been explored for hydrogeological, geotechnical or geothermal purposes. About 90 % of the underground uses take place in the mainly unconsolidated rock layer. These sediments accommodate about half of Switzerland's drinking water resources and they represent significant deposits of raw materials (gravels and sands). Furthermore, they are a source for shallow geothermal energy production and a significant part of housing and transport infrastructure takes place on and inside these rock bodies. Due to the increased demand on these deposits, use conflicts in the shallow subsurface are unavoidable. To plan and coordinate the different uses in these rock layers, knowledge about their composition and spatial distribution is essential. The GeoQuat project has been therefore launched by the Federal Office of Topography swisstopo in cooperation with the Federal Office for the Environment FOEN and the Federal Office of Energy SFOE in order to:

- i) Develop a system for structured storage of unconsolidated rock data (QLG database).
- ii) Realize 3D geological and parametric models (voxel models) of Quaternary deposits (Preisig et al., 2016).
- iii) Make them accessible to users working in the different fields of applied geology.

The focus is given on the development of a system, for homogeneous and structured storage of unconsolidated rock data in Switzerland, which constitute the basis of 3D geological and parametrical modelling.

Indeed, the unused potential of existing Quaternary deposit data needs to be made accessible to interested users working in the different fields of applied geology related to the shallow subsurface. In order to test the practicality of the currently developed GeoQuat infrastructure, four pilot regions (Birrfeld, Lake Lucerne, Upper Aar Valley and Visp) were defined.

The variety of data sources and data owners complicate the development and deployment of a central storage for Quaternary deposit data. Due to their different origin, the data is characterized by a large heterogeneity in their format, type and content, leading to a large variation of data quality. To make the data comparable a well-structured Quaternary deposit data model is needed. The QLG data model is currently implemented at the Swiss Geological Survey (SGS) in conjunction with the setup of the national borehole database that is based on the Borehole data model (Brodhag & Oesterling 2014).

Topographic maps (GA25), Geological vector datasets (GeoCover), top bedrock and digital elevation model (swissALTI3D) are also implemented in the QLG data model (Fig. 1).

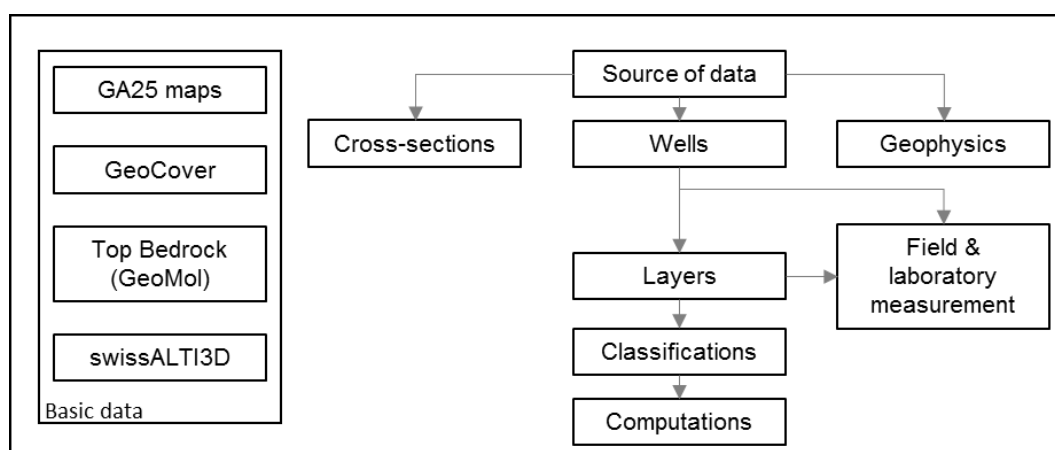


Fig. 1: Generalized overview of the QLG data model

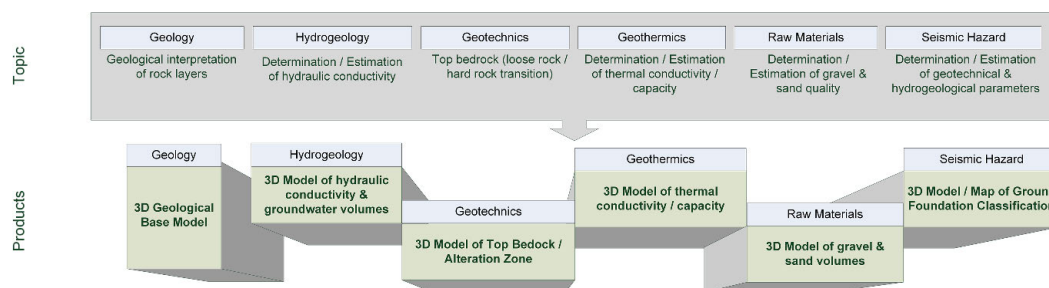


Fig. 2: Main topics and resulting products for each pilot region.

Wells, geological cross-sections and geophysical data are the main components of the QLG database. The original lithological description in the «Layers» table is followed by the «Classifications» which integrates material properties based on Swiss and European standards: VSS, SIA, EN, ISO. The table «Computations» integrates computed values from the «Classifications», such as hydraulic conductivity. Another group of relevant data is the «Field and laboratory measurement» group, which considers in situ measurements and laboratory analyses (Fig. 1). Observed, measured and analyzed data in the QLG database are a good basis for the characterization of Quaternary deposits and history, as well as for the elaborations of 3D geological and parametric models (Fig. 2 & Fig. 3).

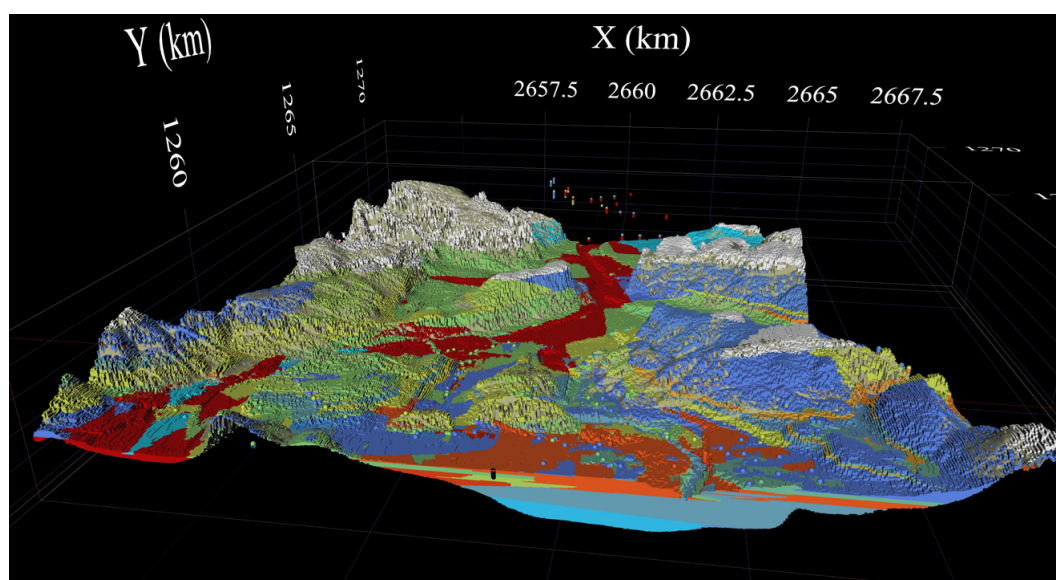


Fig. 3: 3D Geological Model, Region Birrfeld

REFERENCES

- Brodhag, S. & Oesterling, N. 2014: Borehole Data Model – Description UML-Format and object browser (German). Published by Federal Office of Topography swisstopo.
- Volken, S., Preisig, G. & Gaehwiler, M. 2016: GeoQuat: Developing a system for the sustainable management, 3D modelling and application of Quaternary deposit data. *Swiss Bull. angew. Geol.*, 21(1), 3-16.
- Giona Preisig, Stefan Volken, Michael Gaehwiler, Andreas Möri & Michael Sinreich: GeoQuat project: realization of groundwater volumes and vulnerability maps based on 3D parametric modeling. *Swiss Geoscience Meeting*, 2016.

P 9.10

Geophysical characterisation of Cretaceous formations for underground thermal energy storage in the Geneva Basin

Luca Guglielmetti¹, Andrea Moscariello¹, Michel Meyer², Carole Nawratil de Bono², Hansruedi Maurer³ & David Dupuy⁴

¹ *Earth Sciences Department, University of Geneva, Rue des Maraichers 13, CH1205 Geneva*

² *Services Industriels de Geneve, Chemin du Château-Bloch 2, CH1219, Le Lignon (GE)*

³ *Institute of Geophysics, ETH-Swiss Federal Institute of Technology, ETH Hoenggerberg, CH8093, Zurich*

⁴ *Geo2X SA Geophysics for Geology, Rue du Centre 6, CH1377, Oulens-sous-Echallens (VD)*

In the framework of the Swiss Competence Centers for Energy Research (SCCER) one of the action fields in energy research is Heat and Electricity Storage (HaE). The University of Geneva is an active member of SCCER and the Earth Sciences Department has been developing a geothermal exploration strategy (Moscariello, 2016) of the Geneva Canton in the framework of the Geothermie 2020 program, in collaboration with Services Industriels de Geneve (SIG), and the Geneva State Geological Survey. The main goal at this stage is to characterise the subsurface in support of geothermal energy exploration and development at different depth for both heat production, storage, and power generation.

The first main step in geothermal development is the understanding of the geothermal conditions at depth in order to provide feasibility scenarios to decision makers. Therefore the understanding of porosity, permeability and saturation of fluids is crucial to plan correctly a sustainable approach to the geothermal resource exploitation.

Within this large exploration effort, a specific 'geophysical acquisition and processing optimisation' project will aim at:

1. Developing an optimised exploration strategy in terms of geophysical data acquisition,
2. Producing a software tool able to manage the several geophysical datasets under a unique workflow in order to make it as a standard for future projects aiming at characterizing geothermal reservoirs in Switzerland and abroad.

The main goal of this project is to assess geophysical signatures of properties such as porosity, permeability, water saturation and reservoir connectivity which controls the reservoir compartmentalisation and fluid circulation at depth. In this project new seismic, gravity and MT data will be acquired and the data will be integrated to the 3D geological model available already (Figure 1). We estimate that our development will be applicable on the "Swiss Plateau", where 80% of the geothermal projects are planned.

Specifically, this project will include 3 main phases:

1) Acquisition of geophysical data:

- 3D high-resolution full range reflection seismic. The survey will cover an area of approximately 3x3km which will guarantee a 1km² full fold illumination of the geological target at about 1000m in depth.
- Gravity data acquisition with station spacing of 100 m is envisaged in the framework of this project.
- Magnetotelluric data will be collected in this project using the very far remote reference (Uchida et al, 2005) method.

2) Data Integration via Joint Inversion processing:

- 3D seismic reflection tomographic model, based on the inversion of both traveltimes and full wavefield of the seismic signal,
- 3D density model based on the 3D inversion of the gravity data,
- 3D resistivity model based on the 3D inversion of MT data.

3) Characterization of the 3D variations of velocity, density and resistivity

- Definition of the geometry of the brittle structures with seismic and gravity data
- Identification of the saturation conditions in the subsurface with seismic and MT data
- Definition of the permeability conditions in the subsurface
- Development of a replicable and site-specific exploration, processing and interpretation approach
- Testing the approach with real data
- Provide a geophysical exploration strategy to be applied also for 4D time-laps reservoir monitoring

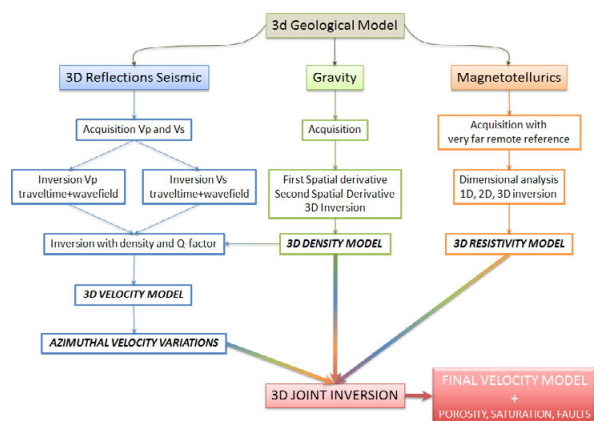


Figure 1. Workflow of the proposed project

REFERENCES

- Dell'Avesana (2007). Joint Inversion of Seismic, Gravity and magnetotelluric Data combined with depth seismic Imaging. EGM 2007 International Workshop, Capri, Italy
- Jegen, M.D. et al. (2009). Joint inversion of marine magnetotelluric and gravity data incorporating seismic constraints. Preliminary results of sub-basalt imaging off the Faroe Shelf, Earth planet. Sci. Lett., 282, 47–55
- Moorkamp, M et al. (2011). A framework for 3-D joint inversion of MT, gravity and seismic refraction data. Geophys. J. Int. (2011) 184, 477–493
- Moscariello A. 2016: Geothermal exploration in SW Switzerland, Proceeding of the European Geothermal Congress, Strasbourg 19-23 september 2016, 9 pp.
- Uchida et al, (2005). Magnetotelluric Survey in an Extremely Noisy Environment at the Pohang Low-Enthalpy Geothermal Area, Korea. Proceedings World Geothermal Congress 2005

P 9.11

Hydraulic Stimulation of Crystalline Rock – Grimsel Test Site

Mohammadreza Jalali¹, Joseph Doetsch¹, Valentin Gischig¹, Hannes Krietsch¹, & Florian Amann¹

¹ Swiss Competence Center for Energy Research – Supply of Electricity (SCCER-SoE), ETH Zürich, Sonneggstrasse 5, CH-8092 Zürich (jalalim@ethz.ch)

A decameter-scale In-situ Stimulation and Circulation (ISC) experiment has been initiated at the Grimsel Test Site (GTS, Figure 1) to study and address a wide-range of research questions related to the stimulation and production phases of a geothermal reservoir. The main objectives in this context consist of the physical understanding of permeability enhancement during hydraulic stimulation, related induced seismicity, and evaluation of the generated heat exchanger efficiency.

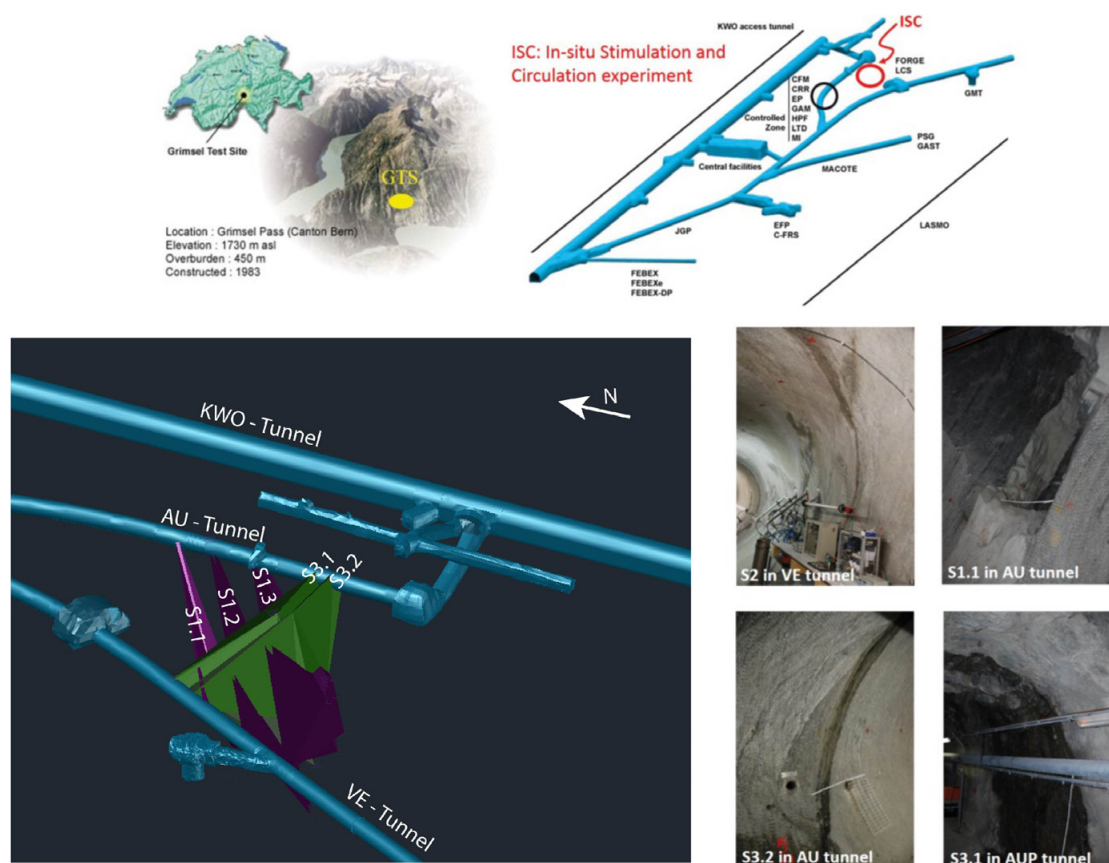


Figure 1. Grimsel Test Site (GTS) is located in the Swiss Alps in the central part of Switzerland. ISC experiment is conducted in the south part of the GTS in a low fracture density grimsel granodiorite. Three main intersecting sub-vertical ductile shear-zones exist in the stimulated volume.

The hydraulic stimulation part of the ISC experiment, which is the focus of this study, is split into three phases, i.e. pre-stimulation (phase I), stimulation (phase II) and post-stimulation (phase III) (Figure 2). Each phase includes planning and performing of intensive geological, geophysical, hydrogeological, geomechanical and seismological field investigations followed by data analysis that guides design of the subsequent phase.

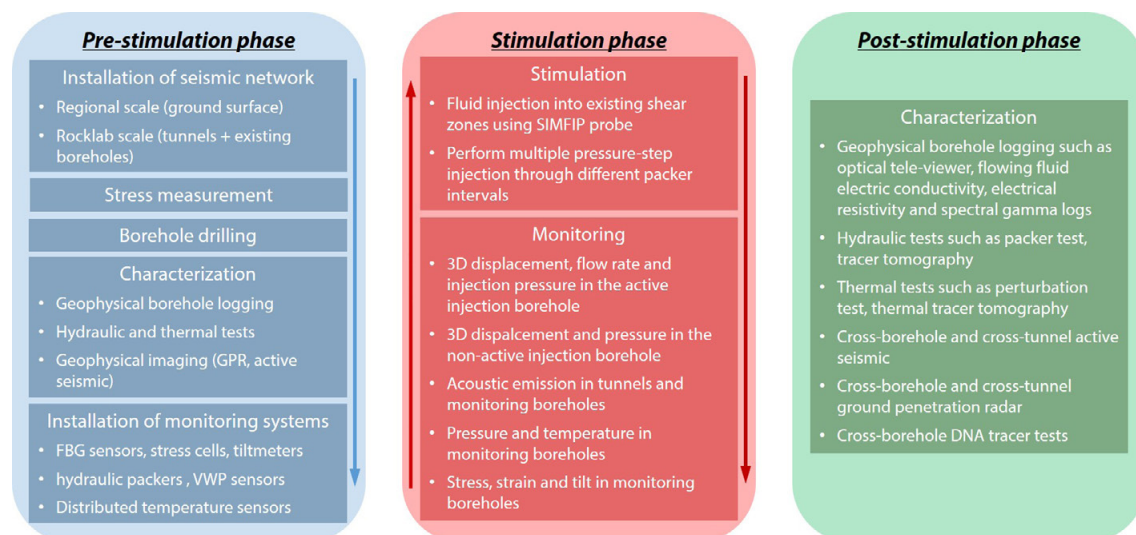


Figure 2. Workflow of the stimulation part of the ISC experiment

Phase I of the ISC experiment started in August 2015 to evaluate detailed characteristics of the target rock volume. Geophysical borehole logging, geophysical imaging (GPR and active seismic), hydraulic testing (packer tests, heat, solute, dye and DNA-tracer tests) and stress measurement have been performed to optimize the location of monitoring boreholes, improve anticipation of the experiment outcome and add more constraints on input parameters, boundary conditions and geometry for numerical models. In addition, three stress measurement boreholes, two injection boreholes and ten additional boreholes dedicated to pressure, temperature, strain, GPR, and active and passive seismic monitoring were drilled and characterized. After completion of all the monitoring boreholes, hydraulic stimulation using step-rate and pressure injection scenarios in various stimulation intervals in two dedicated injection boreholes will be carried out. Seismic activity, pressure propagation, strain and tilt measurements are carried out simultaneously during the hydraulic stimulation phase. The stimulation phase is followed by post-stimulation phase which mostly contains geophysical (e.g. borehole geophysical) and hydraulic characterization of the stimulated volume. This allows to analyze the stimulation induced changes in faults and rock mass controlling the fluid flow and heat exchanger properties, which define the stimulation efficiency.

The ISC experiment is designed such that stimulation processes, i.e. shear dilatancy, seismic and aseismic slip front propagation, and the resulting enhancement of the fracture conductivity, are recorded in a unique interdisciplinary dataset. The data will include information on THM coupled processes and induced seismicity that could not be obtained from stimulation experiments in deep reservoirs typically targeted for EGS. This dataset also allows us to address the objectives as well as validation and verification of the existing THM and induced seismicity models.

P 9.12

Slip induced stress transfer in the embedded discrete fracture method

Gunnar Jansen¹, Stephen A. Miller¹

¹ CHYN - Centre for Hydrogeology and Geothermics, Laboratory of Geothermics and Geodynamics, University of Neuchâtel, Rue Emile-Argand 11, CH-2000 Neuchâtel (gunnar.jansen@unine.ch)

A large fraction of the world's water and energy resources are located in naturally fractured reservoirs within the earth's crust. Depending on the lithology and tectonic history of a formation, fracture networks can range from dense and homogeneous highly fractured networks to single large scale fractures dominating the flow behaviour. Understanding the dynamics of such reservoirs in terms of flow and transport is crucial to successful application of engineered geothermal systems (also known as enhanced geothermal systems or EGS) for geothermal energy production in the future. Fractured reservoirs are considered to consist of two distinct separate media, namely the fracture and matrix space respectively. Fractures are generally thin, highly conductive containing only small amounts of fluid, whereas the matrix rock provides high fluid storage but typically has much smaller permeability.

Simulation of flow and transport through fractured porous media is challenging due to the high permeability contrast between the fractures and the surrounding rock matrix. However, accurate and efficient simulation of flow through a fracture network is crucial in order to understand, optimize and engineer reservoirs. It has been a research topic for several decades and is still under active research. Accurate fluid flow simulations through field-scale fractured reservoirs are still limited by the power of current computer processing units (CPU).

We present an efficient implementation of the embedded discrete fracture model, which is a promising new technique in modelling the behaviour of enhanced geothermal systems. An efficient coupling strategy is determined for numerical performance of the model. We provide new insight into the coupled modelling of fluid flow, heat transport of engineered geothermal reservoirs with focus on the slip-induced stress changes during the stimulation process. Further we account for thermo- and poro-elastic stress changes in the model to provide better estimations to the onset of fracture slip. We account for slip-induced stress changes based on Okada's analytical formulas derived from a Green's function solution to the elastic half space problem (Okada, 1992). Combined with a statistic displacement estimation, the stress changes induced during the injection period of reservoir development can be studied.

REFERENCES

Okada, Y. 1992: Internal deformation due to shear and tensile faults in a half-space. *Bulletin of the Seismological Society of America*, 82(2), 1018-1040.

P 9.13

Results from combined characterization based on geological mapping and geophysics: Grimsel Test Site

Hannes Krietsch¹, Joseph Doetsch¹, Valentin Gischig¹ & Florian Amann¹

¹ Swiss Competence Center for Energy Research – Supply of Electricity (SCCER-SoE), ETH Zurich, Sonneggstrasse 5, CH-8006 Zurich (hannes.krietsch@erdw.ethz.ch)

In the framework of the decameter In-situ Stimulation and Circulation (ISC) project at the Grimsel Test Site a detailed characterization phase was carried out, combining geological mapping with geophysical prospecting. Measurements were conducted in all boreholes and along the tunnels (see Figure 1). The geological characterization consisted of tunnel mapping, core-logging and optical televiewer borehole logging. The interpretation and classifications of the observations were mainly based on the report by Keusen et al. (1989). Along the tunnel walls five different ductile shear-zones were distinguished. With respect to their dip direction they could be separated into three S1 (142/77) and two S3 (183/65) oriented shear-zones. S1 shear zones are characterized by a more pronounced foliation, the S3 shear-zones are bound by 50 cm thick meta-basic dykes.

The tunnel to tunnel interpolation of these shear-zones, including the data points from the borehole logging, illustrated that the S1 shear-zones are relatively straight in strike, whereas the S3 shear-zones are slightly bended. From the core-logging it is known that a highly fractured zone is located east of the S1 shear-zones between the S3-shear-zones.

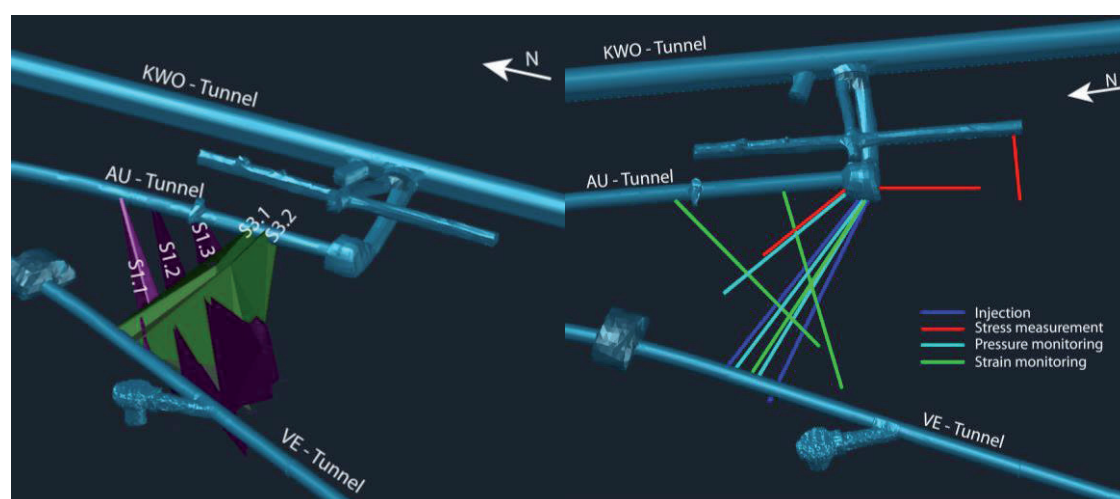


Figure 1. Test site overview, left: interpolated shear-zones, right: all used boreholes for logging and geophysical prospecting.

Geophysical measurements included Ground Penetrating Radar (GPR) reflection and transmission, as well as seismic cross-borehole and cross-tunnel transmission data. Reflection GPR measurements from tunnel walls and boreholes clearly image the meta-basic dykes as well as shear zones away from the tunnels, where direct characterization by mapping is impossible. The tunnel to tunnel seismic tomography reveals variations in velocity as well as variations in the strength of the anisotropy, which is closely related to the foliation.

The combination of the geophysical prospecting and geological mapping highlights several interesting geological features. In the seismic tunnel-tunnel tomography the highly fractured zone can be found as a low velocity zone (Figure 2). The ductile shear-zones can be traced as lower velocity zones as well (i.e. lower velocity than the host rock). These features along the shear zones are even clearer in the tomograms of the anisotropy strength (not shown), as it is directly linked to the foliation. This observation is great proof for the interpretation of the shear-zones through the volume of interest. In the GPR reflection images (e.g., measured from the VE-tunnel) the S1 shear-zones can be seen, whereas the S3 shear-zone cannot be resolved. Interestingly, a dextral shearing of the S1 shear-zone that was hitherto not proven is apparent in the GPR results (Figure 2). This observation fits the relative age of S1 and S3 (i.e. S1 is older than S3).

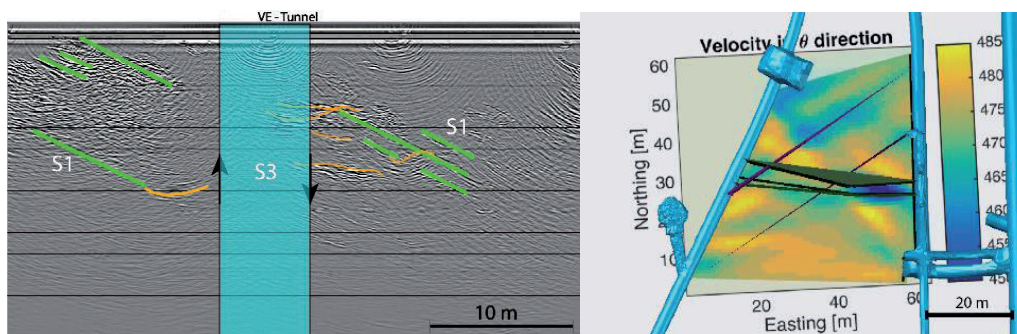


Figure 2. *left: Reflection GPR section recorded from the VE Tunnel; Dextral shearing of S1-shear-zones along S3-shear-zones; right: Seismic tomography results with blue colors indicating low velocities.*

Our results show that with the combination of geophysical characterization and geological mapping, the geological model can be considerably improved, even for rock volumes that are as well characterized as the Grimsel Test Site. While tunnel, core and optical televiewer logging can give detailed information at the accessible locations, GPR and seismic results can resolve the structural information between tunnels and boreholes. Only the careful joint interpretation can reveal details such as the dextral shearing of the S1 shear zone.

REFERENCES

Keusen, H., Ganguin, J., Schuler, P., and Buletti, M. (1989). Grimsel test site: Geology. Technical report, Nationale Genossenschaft fuer die Lagerung Radioaktiver Abfaelle (NAGRA).

P 9.14

Dolomitization of the Upper Jurassic sediments in the Great Geneva Basin

Yasin Makhloufi¹, Elias Samankassou¹, Elme Rusillon¹ & Michel Meyer²

¹ *Departement of Earth Sciences, University of Geneva, Rue des Maraichers 13, CH-1205 Geneva (yasin.makhloufi@unige.ch)*

² *Service Industriels de Genève (SIG), CP 2777, 1211 Geneva 2.*

Diagenesis of carbonate rocks can induce important modifications of the physicochemical, petrophysical and geomechanical properties. Dolomitization is a complex physico-chemical reaction leading to the formation of dolomite via the replacement of calcium by magnesium in calcite. This process can greatly affect the petrophysical properties (porosity, permeability) of the host rock. Assessing the diagenetic history of the rock is thus essential when working on any reservoir exploitation project.

The Canton of Geneva is currently exploring the opportunities for geothermal energy exploitation in the Great Geneva Basin (GGB) sub-surface. So far, other geothermal exploitation projects proved that dolomitized carbonate rocks can present good reservoir properties and are suitable for geothermal energy production (e.g. Bavaria, south Germany, Paris Basin, France).

This study main objectives are to: (1) describe and characterize the dolomitized bodies in the GGB and especially their diagenetic history and (2) quantify the reservoir properties of those bodies (porosity, permeability). Currently, the core target of our study is the Upper Jurassic sedimentary bodies of the GGB.

Through well and field study, our first results show that the dolomitization processes that occurred in the GGB are not ubiquitous. Those processes seem to follow constrained path of fluid migrations through faulting or exhumation during the basin's history.

First results from the petrographical analyses of the Kimmeridgian (Upper Jurassic) cores recovered in the Humilly-2 (France) well show that dolomitization affected only a part of the sediments. Samples recovered at the top of the Kimmeridgian present several stages of interparticular calcite cementation, preserving only a small fraction of the initial porosity. Samples presenting dolomitization tends to show that this process occurred in the late stages of diagenesis, without inducing modifications in the petrophysical or microstructural properties.

Further investigations of the dolomitized body in the close vicinity of the GGB and in its field analog will provide further informations on the chronological order of the diagenetic stages affecting the carbonate sediments. This preliminary work will orientate further analyses (mainly geochemistry) in order to determine the origin of the fluid responsible for the dolomitization processes.

P 9.15

The tip region of a hydraulic fracture driven by a power law fluid

Fatima-Ezzahra Moukhtari*, Brice Lecampion*

*Geo-Energy Laboratory – Gaznat Chair on Geo-Energy (GEL), École Polytechnique Fédérale de Lausanne (EPFL), EPFL-ENAC-IIC-GEL, Station 18, CH-1015 Lausanne (fatima-ezzahra.moukhtari@epfl.ch)

We investigate the tip region of a hydraulic fracture driven by a power law fluid propagating at a constant velocity V in an impermeable linear elastic medium. We account for the presence of a fluid lag of a priori unknown length at the tip of the fracture. The fluid pressurized fracture propagates perpendicular to the far-field compressive minimum stress σ_o in pure opening mode (see Fig.1a). The solution of this semi-infinite hydraulic fracture problem combines elastic deformation, lubrication flow in the filled region of the fracture and the quasi-static fracture propagation condition. It exhibits a multiscale structure related to the strong fluid solid coupling at play near the fracture tip. For a Newtonian fluid, the solution derived by Garagash & Detournay (2000) transition from the classical linear elastic fracture mechanics asymptote near the tip to the viscous asymptote (Desroches et al., 1994) away from the tip (see Fig.1b). The fluid lag was shown to vanish for large values of a dimensionless fracture toughness encapsulating all the problem parameters.

A lot of fluid used in industrial practice exhibit a shear-thinning rheology. Here, we extend the solution previously obtained for a Newtonian fluid to the case of a power-law shear-thinning fluid. For such a rheology, in simple shear, the fluid shear rate τ is related to the shear rate $\dot{\gamma}$ as:

$$\tau = M\dot{\gamma}^n$$

where n is the fluid power law index ($n \in [0,1]$ for shear-thinning fluid) and M is the consistency index.

We formulate the governing equations of the problem and derive a dimensionless form of these equations which only depends on the value of the power law index n and a dimensionless toughness κ defined as:

$$\kappa = 4 \left(\frac{2}{\pi V} \right)^{\frac{1}{2}} \left(\frac{\sigma_o^{2-n}}{M' E'^{n+1}} \right)^{\frac{1}{2n}} K_{IC}$$

where E' is the plain strain elastic modulus, K_{IC} is the mode I fracture toughness and $M' = \frac{2^{n+1}(2n+1)^n}{n^n} M$. The fracture width w and net pressure $p = p_f - \sigma_o$ are scaled by $\sigma_o/E' L_M$ and σ_o respectively, while the spatial coordinate x and the fluid lag size λ are scaled by the following viscous lengthscale L_M defined as

$$L_M = V \left(\frac{M'}{\sigma_o} \right)^{\frac{1}{n}} \left(\frac{E'}{\sigma_o} \right)^{\frac{n+1}{n}}$$

The integral elasticity equation is discretized using Gauss-Chebyshev polynomials (Ioakimidis & Theocaris, 1980). We notably transform the coordinates from the semi-infinite interval $[0, \infty[$ to the finite interval $[-1, 1]$ and use classical Gauss-Chebyshev method for solving singular integral equations for finite fractures. The lubrication flow equation is discretized via a collocation method using barycentric interpolation and derivation. The resulting non-linear system of equations is solved via a quasi-Newton root-finding scheme using the dimensionless net pressure at the collocation points as the primary unknown variables. For given values of the dimensionless toughness and power law index, our numerical results include the fracture opening w and fluid pressure p_f profiles over the whole fracture as well as the corresponding value of the fluid lag size.

We show that the solution is not only consistent with the square root singularity of linear elastic fracture mechanics near the tip ($x \ll L_M$), but that its asymptotic behaviour in the far field ($x \gg L_M$) corresponds to the solution of a semi-infinite hydraulic fracture driven by a power-law fluid constructed on the assumptions of zero toughness and zero fluid lag (Desroches et al., 1994). Our results also document how the power-law index modifies the variation of the lag size as a function of the dimensionless toughness κ , and its disappearance for large value of κ .

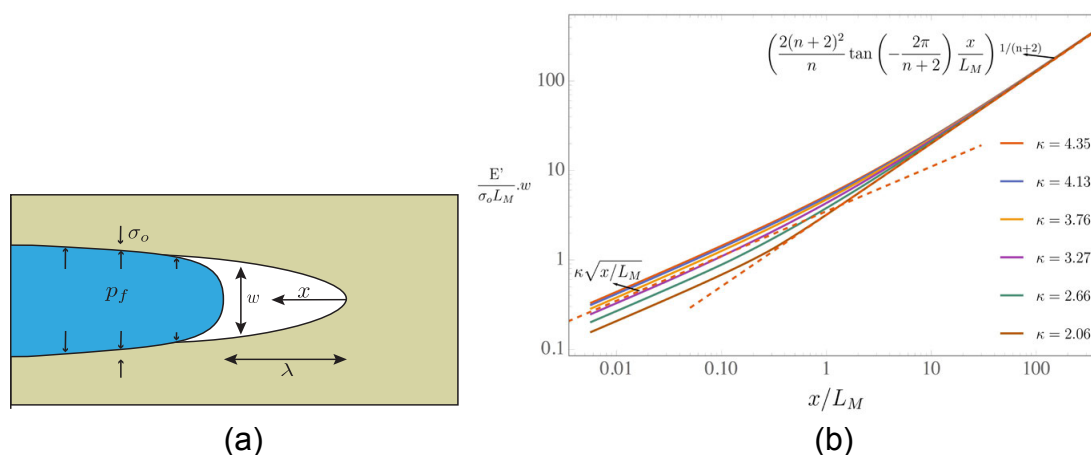


Figure 1. Semi-infinite fluid-driven fracture propagating at constant velocity V in an impermeable medium: a. Sketch of the problem, b. Dimensionless opening (in log-log scale) along the fracture ($n = 0.5$).

REFERENCES

Garagash, D. & Detournay, E. 2000: The tip region of a fluid-driven fracture in an elastic medium. *Journal of applied mechanics* 67(1), 183–192.

Desroches, J. & Detournay, E. & Lenoach, B. & Papanastasiou, P. & Pearson, J. & Thiercelin, M & Cheng, A. 1994: The crack tip region in hydraulic fracturing. In *Proceedings of the Royal Society of London A: Mathematical, Physical and Engineering Sciences* 447, 39–48.

Ioakimidis, N. & Theocaris, P. 1980: The practical evaluation of stress intensity factors at semi-infinite crack tips. *Engineering Fracture Mechanics* 13(1), 31–42.

P 9.16

Reservoir rock typing of the Late Jurassic Reef Complex, Greater Geneva Basin, (Switzerland and France)

Elme Rusillon¹, Andrea Moscariello¹

¹ *Department of Earth Sciences, University of Geneva, Rue des Maraîchers 13, CH-1205 Genève (Elme.Rusillon@unige.ch)*

In support for geothermal exploration, a first reservoir assessment was performed in the Greater Geneva Basin to develop low to medium enthalpy resources in the area (GEOthermie 2020 program, Moscariello, 2016). For this purpose, a specific rock typing workflow was designed, inspired from reservoir appraisal methodologies used in the oil and gas industry. This study is conducted simultaneously with a detail structural analysis of the basin (Clerc et al., 2016), as well as a review of the stratigraphical frame for the sake of data homogenization and correlations at regional scale (Brentini et al., 2016).

The first step of the reservoir assessment consists in describing both depositional and petrophysical characteristics of the sedimentary units ranging from the Permo-Carboniferous to the Lower Cretaceous. The material used includes both data from wells and outcrops: reports, cores and core samples (plugs, slices and cuttings), well logs and field rock samples (pieces and plugs). Firstly, microfacies and cathodoluminescence analyses were performed on thin sections. Then, porosity, permeability and grain density were measured on plug samples, and similar petrophysical measurements available in well reports were also supplemented to the database. In addition, modal mineralogy using Quantitative Evaluation of Mineral by SCANning electron microscopy (QEMSCAN) technology was carried out on one reference well that crosses the entire sedimentary column, as well as P- and S-wave velocity measurements. Finally, the pore network was further investigated with Scanning Electron Microscopy (SEM) images.

The second step consists in defining rock types in order to propagate and predict properly reservoir properties through 3D geological models. An integrated approach inspired from Skalinski & Kenter (2015) and Makhloufi (2013) is currently developed, combining depositional, diagenetic, petrophysical and electrical properties with pore network characteristics. Multivariate statistical analyses are used to discriminate rock types and propagate them along wells where no core material was available.

Petrophysical investigations on five potential reservoir intervals of the Greater Geneva Basin revealed that the Kimmeridgian - Tithonian *Reef Complex* and the underlying *Calcaires de Tabalcon* units are the most promising targets for low to medium enthalpy geothermal prospects (porosity range 10-20%; permeability to 1mD). Both on the outcrop and on the subsurface, best reservoir properties are measured in pure carbonated sediments formed in patch reefs and peri-reefal depositional environments, surrounded by synchronous tight lagoonal deposits. Associated highly porous dolomitized intervals reported in the western part of the basin also promote enhanced reservoir qualities. Accordingly, reservoir bodies display complex geometries and a scattered distribution that remain challenging to predict across the subsurface. To propagate these heterogeneous reservoir properties, rock types are currently defined. They will be integrated into 3D geological models based on 2D seismic lines interpretation, (Clerc et al., 2016).

Additionally to seismic facies identification, the detail structural characterization of the basin using available 2D seismic dataset confirmed the existence of several wrench fault zones and conjugate fault systems across the basin (Clerc et al., 2016). As promising reservoir bodies appear dispersed across the subsurface, these fault and fracture zones could act as hydraulic corridor, and play a key role in connecting the most productive reservoir facies.

These integrated rock type and structural studies allow us to understand better the distribution and properties of productive reservoir facies and hydraulic connectivity zones within the study area. The Kimmeridgian - Tithonian reef and peri-reefal facies appear to be the most promising reservoir targets, although lateral and vertical heterogeneities were recognized in this interval. Associated high-K fracture zones are thus essential to improve fluid circulation into and between reservoir bodies to assure the successful development of geothermal energy in the Greater Geneva Basin.

REFERENCES

- Brentini, M., Favre, S., Rusillon, E., & Moscariello, A. 2016: Tools for the Canton of Geneva to manage its subsurface resources : Relevance of geological data. Abstract 14th Swiss Geoscience Meeting, Geneva, Switzerland.
- Clerc, N., Rusillon, E., Moscariello, A., Renard, P., 2016: Structural Modeling of the Geneva Basin for Geothermal Ressource Assessment. Abstract 14th Swiss Geoscience Meeting, Geneva, Switzerland.
- Makhloufi, Y. 2013: Impact de la sédimentologie et de la diagenèse sur les propriétés pétrophysiques d'un réservoir carbonaté oolithique. Doctoral dissertation, Université Pierre et Marie Curie-Paris 6, 175p.

- Moscariello A. 2016: Geothermal exploration in SW Switzerland, Proceeding of the European Geothermal Congress, Strasbourg 19-23 september 2016, 9 pp.
- Skalinski, M. and Kenter, J.A.M. 2015: Carbonate petrophysical rock typing: integrating geological attributes and petrophysical properties while linking with dynamic behavior. Geological Society, Special Publications, London, 406, 229-259.

P 9.17**- HULK -****Simple and fast generation of structured hexahedral meshes for improved subsurface simulations**

Reza Sohrabi¹, Gunnar Jansen¹ & Stephen A. Miller¹

¹ CHYN - Centre for Hydrogeology and Geothermics, Laboratory of Geothermics and Geodynamics, University of Neuchâtel, Rue Emile-Argand 11, CH-2000 Neuchâtel (reza.sohrabi@unine.ch)

Short for **H**exahedra from **U**nique **L**ocation in **(K)**convex Polyhedra – HULK is a simple and efficient algorithm to generate hexahedral meshes from generic STL files describing a geological model to be used in simulation tools based on the finite difference, finite volume or finite element methods. Using binary space partitioning of the input geometry and octree refinement on the grid, a successive increase in accuracy of the mesh is achieved. HULK generates high accuracy discretizations with cell counts suitable for state-of-the-art subsurface simulators and provides a new method for hexahedral mesh generation in geological settings.

A geological model should incorporate structural information and rock properties for any kind of subsurface simulation because simulation accuracy strongly depends on the relevant rock properties and their distribution in space. Therefore, reliable results can only be expected when well-constrained structural and lithological information is used in the simulation. Due to complexities in both the geological modeling and subsurface simulation, an integrated approach of modeling the geology and the physics of the subsurface (e.g. flow, deformation, etc.) is in many cases not available. We address this problem for simulators using hexahedral grids by proposing an efficient mesh generation method. The method is based on octree refinement and provides for direct transfer of structural geological information to the numerical simulator of the underlying physics.

Accounting for structures in the subsurface using a geological model efficiently helps increase the accuracy of any kind of numerical subsurface simulation. We developed and implemented a fast and efficient hexahedral mesh generator for subsurface simulations. The simple structure of the algorithm makes it also possible to implement the algorithm directly in the discretization part of other simulation software. However, it can also be used as a stand-alone preprocessing unit. Simulators that use adaptive mesh refinement based on the physics can utilize our method within their simulations to dynamically resolve only those parts of the input geometry that are of interest in the current state of the simulation.

P 9.18

Country-wide analysis of geothermal potential for railway switch point heaters

Yvo Weidmann¹, Sarah Signorelli², Andrea Grüniger²

¹ Geoldee Geoinformatik, Postfach 1209, CH-8038 Zurich (yvo.weidmann@geoidee.ch)

² GEOWATT AG, Dohlenweg 28, CH-8050 Zurich (signorelli@geowatt.ch)

³ Grüniger PLUS GmbH, Flurweg 2a, CH-5034 Suhr (andrea@grueniger-plus.ch)

Important switch points of the Swiss railway network have to be heated during the winter month. The heating prevents the switch points of freezing due to snow and meltwater. The freezing of switch points makes a proper functioning impossible and would lead to troubles in the very dense timetable of the railway network.

Currently 10'000 – 11'000 switch point heaters are operated in Switzerland. Either with electricity or gas. The Federal Office of Transport (FOT) was launching a preliminary study to quantify the potential of geothermal resources for switch heating within Switzerland. The perimeter of the study covered 80 % of the Swiss railway system and included the lowlands, the Jura and alpine regions.

Based on existing and provided geodata of the government (swisstopo), geothermal base maps of the cantons and the railway network, the potential of geothermally heated railway switches was derived using spatial intersections and analysis of the vector-based geodata.

In a first step, the *theoretical potential* of geothermally heated switches was derived. This step took the location of each individual switch and intersected it with the prohibition zone maps for borehole heat exchangers. Three classes of locations were resulting: i) theoretically possible location for geothermal heating, ii) handicapped locations and iii) impossible locations.

In a second step, the *technical potential* was evaluated. Each of the individual locations of potentially possible heating's were intersected using sensitivity buffers around *waterbodies*, *buildings*, *land ownership* and *railway lines*. The technical potential includes therefore all locations which are suitable regarding the regulation of water conservation and basic technical limitations (e.g. distance to buildings and railway sections.).

Based on the spatial analysis, around 50 percent of the Swiss railway switch point heaters could be technically heated by geothermal resources.

Main challenge of the project was the acquisition and homogenisation of the geodata of the different cantons and railway companies. Regarding to the federalistic system of Switzerland, many of the needed geodata (e.g. geothermal energy maps) are available in different data formats, different level of detail or varying attribution. Often, the data are not consistent at the border between different cantons. Additional and demanding operations for data homogenisation and examination had to be included in the workflow.

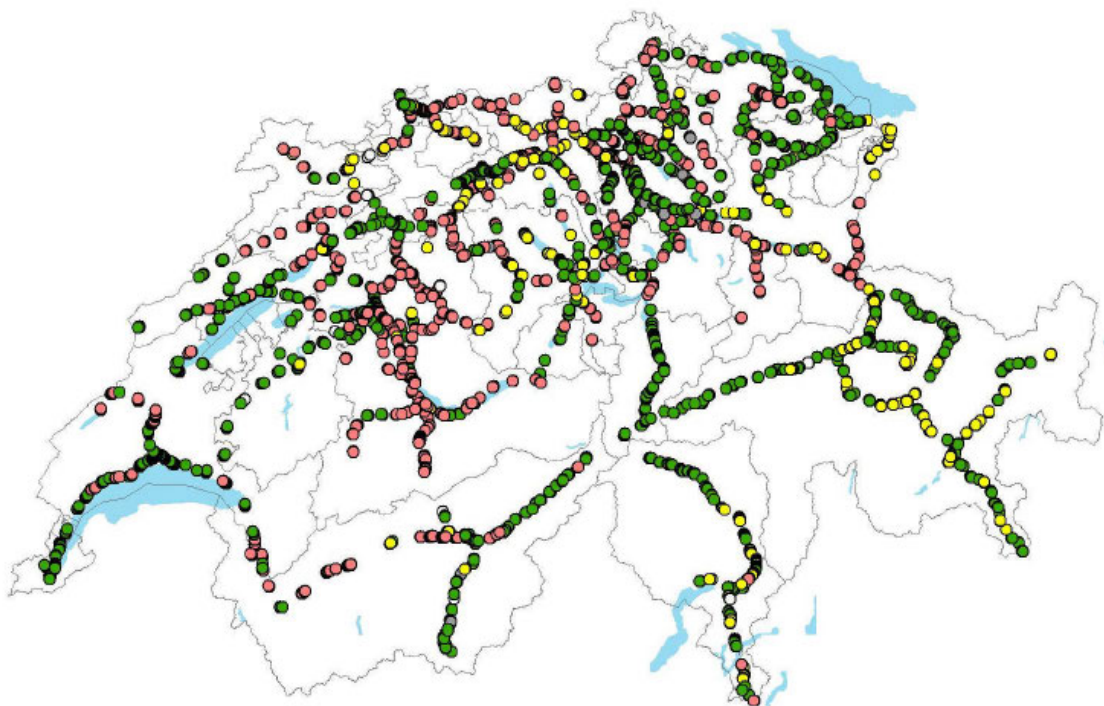


Figure 1. Map of the technical potential of railway switch point heaters (max. 50m distance from switch point to borehole and 3m distance to the centre of the railway tracks)

P 9.19**Sensitivity analysis of hydraulic fracture propagation**

Michael Rickenbacher¹, Mohammadreza Jalali¹, Martin Ziegler¹

¹ *Department of Earth Sciences, ETH Zurich, Sonneggstrasse 5, CH-8092 Zurich
(rmichael@student.ethz.ch; mohammadreza.jalali@erdw.ethz.ch)*

Rock fracture initiation and propagation is amongst one of the crucial physical processes in different Earth sciences related disciplines such as geothermal (e.g. enhanced geothermal systems), oil and gas industry (e.g. hydraulic fracturing in shale gas development), and mining industry (e.g. block caving and blasting). Comprehensive understanding of fracture behaviour plays a key role in the above-mentioned disciplines. The development of hydromechanical coupled models has made a big step in numerical simulation and physical understanding of fracture initiation and propagation. These numerical models are usually capable to simulate rock fracturing. In the last years these numerical models have been enhanced by rock mass anisotropy and simulation of pre-existing fractures in the rock mass (Shen et al., 2014; Xie et al., 2016). However, the complexity of natural rock masses (e.g. stress perturbations and rock mass heterogeneities) is still not fully reflected by numerical codes and an ongoing field of research.

In this study, a numerical code, which is called FRACOD, was used to simulate hydraulic fracture initiation and propagation. FRACOD is based on an indirect Boundary Element Method (BEM), which is called Displacement Discontinuity Method (DDM). This code enables modelling of rock failure processes in both tensile (mode-I) and shear (mode-II) mechanisms (Shen et al., 2014). In a simple 2D-hydraulic fracturing design, we modelled a single propagating fracture in an isotropic and homogeneous rock mass. In the case of hydraulic fracturing, the fracture tip failed under tensile manner as a consequence of excessive fluid pressure greater than tensile strength. Dependant on rock, fluid, and stress properties, the fracture geometry developed differently (Rickenbacher, 2016; Figure 1A). Our study focused on the interaction between these properties and the resulting fracture geometry. In order to quantify the influence of each property, we applied a sensitivity analysis. In this sensitivity analysis, different but realistic values were investigated for specific properties. As a result we were able to identify the key properties for fracture geometry (i.e. fracture length and fracture aperture) during propagation of a single hydraulic fracture. In a second approach we included rock mass anisotropy with the goal to study fracture propagation interacting with rock mass anisotropy. Thus, we placed a weak direction in order to simulate anisotropy. Owing to the fact that fractures propagate preferentially in direction of the major principal stress, σ_1 (i.e. a fracture in tensile manner prefers propagating perpendicular to σ_3), we were able to study complex anisotropic fracturing.

The analysis in FRACOD revealed a major influence of the fluid dynamic viscosity, hydraulic conductivity and Young's modulus on hydraulic fracture propagation (Rickenbacher, 2016; Figure 1B). This is consistent with former studies using other numerical codes (e.g. MFRAC). Moreover, the fracture orientation was found to be rather dependent on the direction of maximum principal stress, σ_1 , than on rock mass anisotropy. Future work will focus on 3D-numerical modelling as well as studying natural hydraulic fracturing.

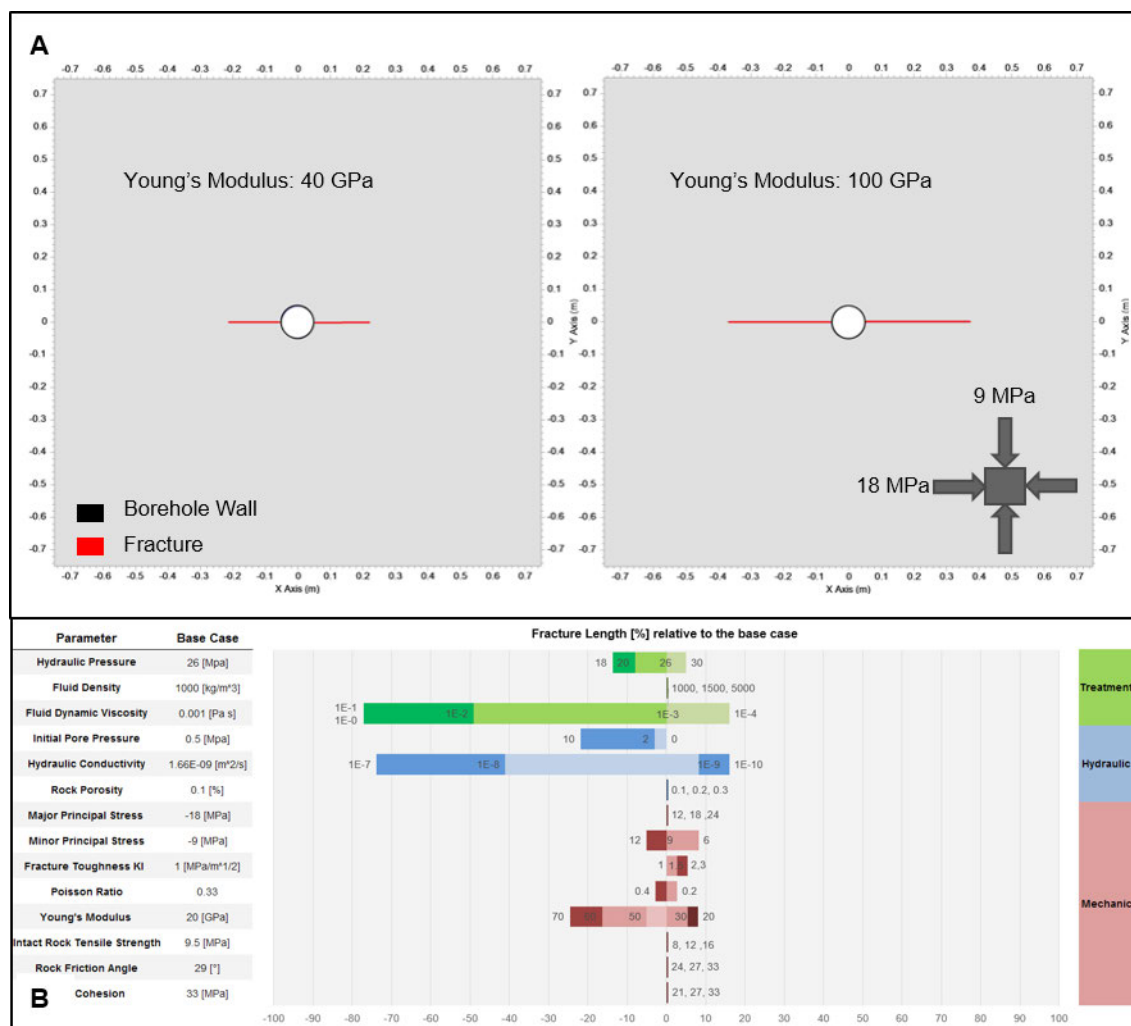


Figure 1. A) Variable fracture length with different Young's Modulus in a hydraulic fracturing model in FRACOD, B) Our sensitivity analysis revealed the relative influence of each property with respect to the fracture length. Fluid dynamic viscosity, hydraulic conductivity and Young's Modulus exhibit a major influence in a propagating fracture.

REFERENCES

- Rickenbacher, M., 2016: 3D-Analysis of hydraulic and mechanic fracture propagation, B.Sc. Thesis, Department of Earth Science, ETH Zurich, 41 pp.
- Shen, B., Siren, T., Rinne, M., 2014: Modelling Fracture Propagation in Anisotropic Rock Mass, Rock Mech Rock Eng, 48:1067-1081.
- Shen, B., Stephansson, O., Rinne, M., 2014: Modelling rock fracturing processes. Springer, 173 p.
- Xie, L., Min, K., Shen, B., 2016, in press: Simulation of hydraulic fracturing and its interaction with a pre-existing fracture using displacement discontinuity method, Journal of Natural Gas Science and Engineering.

P 9.20

Organic geochemistry of oil and natural gas in the West Dikirnis and El-Tamad fields, onshore Nile Delta, Egypt: Generation by Upper Cretaceous -- Lower Tertiary terrigenous source rocks

Mahmoud Leila¹, Andrea Moscariello¹

¹ *Department of Earth Sciences, University of Geneva, Rue de Maraîchère 13, CH-1205 Genève.*

Crude oil in the West Dikirnis field in the northern onshore Nile delta, Egypt, is present in the poorly-sorted Miocene sandstones of the Qawasim Formation. The geochemical composition and source of this oil is investigated in this study.

The reservoir sandstones are overlain by mudstones in the upper part of the Qawasim Formation and in the overlying Pliocene Kafr El-Sheikh Formation. However TOC and Rock-Eval analyses of these mudstones indicate that they have little potential to generate hydrocarbons, and mudstone extracts show little similarity in terms of biomarker compositions to the reservoir oils. The oils at West Dikirnis are interpreted to have been derived from an Upper Cretaceous -- Lower Tertiary terrigenous, clay-rich source rock, and to have migrated up along steeply-dipping faults to the Qawasim sandstones reservoir. This interpretation is supported by the high C₂₉/C₂₇ sterane, diasterane/sterane, hopane/sterane and oleanane/C₃₀ hopane ratios in the oils. Biomarker-based maturity indicators (Ts/Tm, moretanes/hopanes and C₃₂ homohopanes S/S+R) suggest that oil expulsion occurred before the source rock reached peak maturity. Previous studies have shown that the Upper Cretaceous -- Lower Tertiary source rock is widely distributed throughout the on- and offshore Nile Delta.

A wet gas sample from the Messinian sandstones at El-Tamad field, located near to West Dikirnis, was analysed to determine its molecular and isotopic composition. The presence of isotopically heavy δ^{13} methane, ethane and propane indicates a thermogenic origin for the gas which was cracked directly from a humic kerogen. A preliminary burial and thermal history model suggests that wet gas window maturities in the study area occur within the Jurassic succession, and the gas at El-Tamad may therefore be derived from a source rock of Jurassic age.

P 9.21

Social discourses on deep geothermal energy

Olivier Ejderyan & Michael Stauffacher

D-USYS Td-Lab / Swiss Competence Center for Energy Research - Supply of Electricity, ETH Zurich, Sonneggstrasse 5, NO F27, CH-8092 Zurich | Switzerland

Actors active in the development of deep geothermal energy (DGE) have stressed that its large scale deployment does not depend only on technological innovation but also on its social acceptance (Majer et al. 2012;) Social sciences are enrolled to enquire social perceptions in order to anticipate acceptance when planning a geothermal project. Social sciences can make valuable contribution to public engagement procedures for siting, planning, and risk management of DGE infrastructures. Here it is important to underline that “there is no “cookbook recipe” applicable to all projects that might imply induced seismicity and there can barely be one” (Trutnevyte & Ejderyan, submitted).

The assessment of social acceptance and the development of adequate public engagement procedures must link multiple scales. It is therefore always dependent on bringing together different contexts. Analyzing public discourses on DGE provides crucial information on these contexts. The goals of this research is to contribute conceptually and empirically to the development of public engagement procedures for DGE that are coherent from a general energy policy point of view, yet address local specificities.

This research combines media analyses and ethnographic case studies. Through media analysis it is possible to analyse how DGE is framed in the public sphere at various levels (Illustration 1). Ethnographic case studies in St. Gallen (Muratore et al. 2016), Haute-Sorne and Geneva, enable to analyse how such frames are mobilised on concrete DGE projects.

Frame	Statements	Articles
Technical	383	83
Governance	347	74
Risk	284	81
Transition	202	68
Knowledge	194	77
Cost	129	53

Media frames on DGE identified in *Le Temps*, *Tribune de Genève* and *Le Quotidien Jurassien* (1997-2015), with number of statements and number of articles found.

The media analysis shows that there are structuring elements in reporting on DGE. In order to evaluate in which respect these elements are central to social discourse on DGE, it is necessary to examine how frames are mobilised by concerned publics in actual DGE projects. First results of the case study in Haute-Sorne indicate the relevance of framing analysis to identify the main issues that will be raised. However they also show that media reports tend to homogenize actors categories and reduce the complexity of positions towards DGE. Must be addressed before designing public engagement procedures.

REFERENCES

- Majer, E., Nelson, J., Robertson-Tait, A., Savy, J., & Wong, I. 2012. Protocol for Addressing Induced Seismicity Associated with Enhanced Geothermal Systems. Washington DC.
- Muratore, S., Müller S., Kulla, H., Knüsel, B., Allemann, L., de Martino, A., Meier, N., Stoudmann, N., Tschanal, D. 2016. Tiefengeothermie: Das Projekt St.Gallen. USYS TdLab Transdisziplinäre Fallstudie 2015. Zürich.
- Trutnevyte, E. & Ejderyan, O. Submitted. Managing Geoenery-Induced Seismicity with Society. *Journal of Risk Research*.

10. Open Session in Geomorphology

C. Lambiel, C. Graf, I. Gärtner-Roer, N. Kuhn, R. Delaloye, M. Keiler, C. Scapozza, C. Levy, S. Castellort, I. Regolini-Bissig, I. Kull

Swiss Geomorphological Society (SGS)
Swiss Association of Geographers (ASG)

TALKS:

- 10.1 Bardou E., Favre-Bulle G., Ornstein P., Pache B., Délèze J.-Y., Mayoraz R.: A decision support tool to help prevent risks induced by permafrost degradation in high alpine environments
- 10.2 Delaney I.A., Weidmann Y., Huss M., Bauder A.: A sediment flux time series from a proglacial area: insights into sediment dynamics of glaciated catchments
- 10.3 Fehlmann M., Trappmann D., Moos C., Dorren L., Stoffel M., Bründl M., Huggel C.: Dynamics of rockfall hazards and risks from past to future: a case study in Täsch (VS), Switzerland
- 10.4 King G., Grujic D., Coutand I., Herman F.: Very low temperature OSL-thermochronometry applied to the Siwalik deposits in Nepal and Bhutan
- 10.5 Kummert M., Delaloye R.: Erosion and sediment transfer at the front of rapidly moving rock glaciers
- 10.6 Ramirez J.A., Zischg A.P., Schürmann S., Zimmermann M., Weingartner R., Keiler M.: Modelling geomorphic responses to human impacts and extreme floods: Application to the Kander river, Switzerland
- 10.7 Valla P.G., Lajeunesse E., Delunel R., Allemand P.: Coupling and feedbacks between orographic precipitations and landscape evolution: Basse Terre Island, Guadeloupe archipelago (Lesser Antilles Arc)
- 10.8 Walter F., Burtin A., McArdeall B., Hovius N., Weder B., Turowski J.: Rapid detection and location of debris flow initiation at Illgraben, Switzerland

POSTERS:

- P 10.1 Larsen, A., Capponi, M., Lane, S.N.: The hydro-geomorphic influence of beaver (*Castor fiber*) on Swiss low-order streams – first results
- P 10.2 Rieder M., Zimmermann M., Fuchs S., Keiler M.: Sediment yield estimation on a catchment scale in data-scarce regions – Rasht valley Tajikistan
- P 10.3 Schmutz D., Zimmermann M., Keiler M.: Assessment of sediment connectivity index in relation with hazardous events in alpine torrent catchments in Switzerland
- P 10.4 Chow C., Ramirez J.A., Zimmermann M., Barkwith A., Keiler M.: Debris flow modelling: How much model complexity is needed?
- P 10.5 de Palézieux L., Leith K., Loew S.: Reconnaissance study of landslide distribution with respect to erosional processes in northwestern Bhutan
- P 10.6 Meyrat R., Rüttimann S., Lane S.N., Lambiel C.: Using UAV for studying the dynamics of an active rock glacier
- P 10.7 Giaccone E., Mariethoz G., Lambiel C.: Interactions between geomorphology and vegetation in the Vaud Alps: first investigations
- P 10.8 Krenz J., Greenwood P., Kuhn B., Heckrath G., Foster I., Boardman J., Meadows M., Kuhn N.: In-filled reservoirs serving as sediment archives to analyse soil organic carbon erosion – Taking a closer look at the Karoo rangelands
- P 10.9 Vögtli M., Kuhn N.J., Franz L., de Capitani C., Koziol M.: Optical and geochemical analysis of the tephra layers from the Hinkelsmaar (Eifel region, Western Germany)
- P 10.10 Malatesta L.C., Lamb M.P.: Generation of waterfalls at intermittently alluviated fault scarps releases tectonic forcing on a climatic beat
- P 10.11 Reber R., Litty C., Madella A., Delunel R., Akçar N., Christl M., Schlunegger F.: Environmental control on erosion along the entire western margin of Peru

10.1

A decision support tool to help prevent risks induced by permafrost degradation in high alpine environments

Eric Bardou¹, Guillaume Favre-Bulle², Pascal Ornstein³, Barnabé Pache³, Jean-Yves Délèze³, Raphaël Mayoraz⁴

¹ DSM Consulting, Rte Barma 1, CH-1973 Nax (info@dsm-consulting.ch)

² CSD Ingénieurs, Rue de l'Industrie 54, CH-1950 Sion

³ CREALP, Rue de l'Industrie 45, CH-1950 Sion

⁴ Section H2G, DTEE-SRTCE, Canton du Valais, Rue des Creusets 5, CH-1950 Sion

In the framework of the Federal Office for the Environment (FOEN) pilot program “climate change adaptation” and with support from the canton of Valais, a computerized monitoring tool has been developed for the management of natural hazards inherent to the degradation of permafrost in Alpine environment. This tool is primarily intended to municipal and regional actors involved in local management of natural hazards. Ultimately, it is intended to integrate the future cantonal platform for the monitoring of slope instabilities, GUARDAVAL 2.0.

Following several years of high temperatures, 2015 was the warmest year ever recorded since the beginning of meteorological measurements (OMM, 2016). As demonstrated by recent observations of the Swiss Permafrost Monitoring Network (PERMOS), this has direct impact on the evolution of permafrost that never warmed as much as during the hydrological year 2014/2015 since the beginning of measurement. Besides the destabilization of high altitude rocky slopes, an additional effect of the permafrost melt is a significant increase in rock glacier creep rate that rose by 20% on average compared to the previous year (SCNAT, 2016). The purpose of the climate change adaptation FOEN pilot program, initiated in 2013 in Valais, is to provide an integrated concept for handling debris flows issued from permafrost degradation through the study of two sites (Figure 1): the debris covered glacier Bonnard located above the village of Zinal in the Val d'Anniviers and the rock glacier Bielzug located above the village of Herbriggen in the Mattertal.

This decision support system is based on the computation of a series of direct (rainfall, air/ground temperature, snowmelt) and indirect (rock glacier movements, photographic survey) weather/climate indicators. The aim of this system is to help municipal natural hazards specialists detect and anticipate a potentially hazardous situation based on operational data available (observations, forecasts) and, if necessary, to enter vigilance state.

Basic data are heterogeneous both in source and type:

- Land-based observation (federal, cantonal and local networks), rainfall radar measurements (MeteoSwiss data) or satellite imagery (MODIS),
- Rainfall and temperature forecasts (MeteoSwiss COSMO products)

They are fetched in real time from the different cantonal databases dedicated to natural hazards management. The collected data are consolidated, structured, enhanced and aggregated so they can be displayed to the user as tailored views (charts, maps, indicators) via a synthetic and interactive dashboard (Figure 1) providing an overview of the periglacial system's current hazard status.

The web portal development was conducted from the early design phase by a multidisciplinary team, including, in addition to computer scientists, experts in natural hazards and permafrost. They brought their knowledge of periglacial environments and dynamics for selecting the relevant parameters and to develop the calculation method for the indicators.

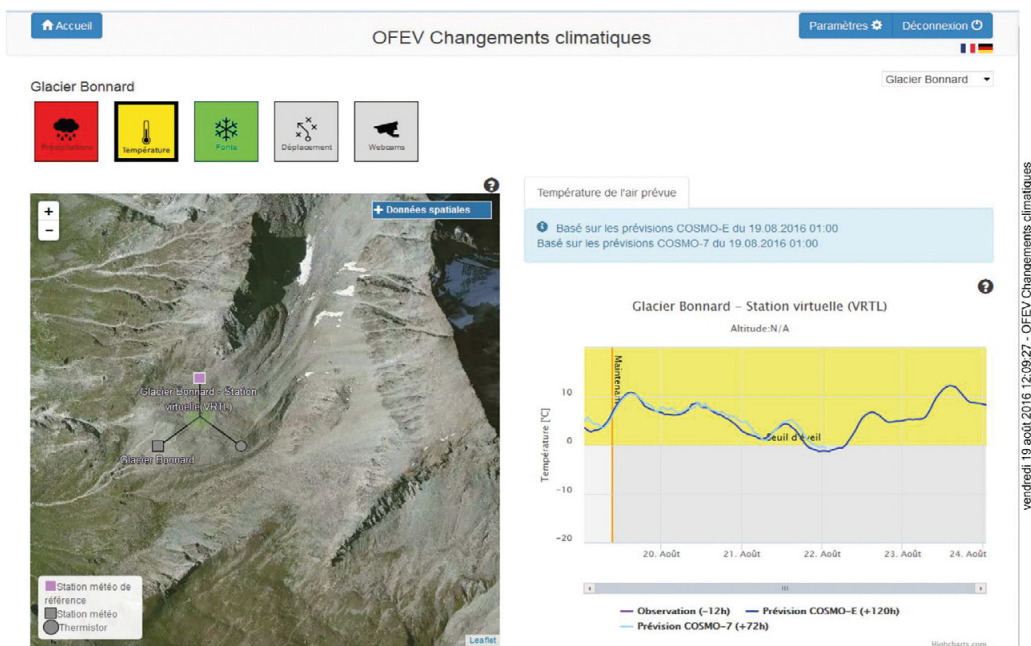


Figure 1 : Web portal OFEV-CC. Dashboard for interactive data visualizations

A first operational test was conducted during the spring-summer 2016 with the municipalities of St. Niklaus and Anniviers. It aimed, i) to control the behavior of various indicators and to assess whether the tool will be ad-hoc for evaluating the hazard situation and, ii) to evaluate the benefits of the tool in the monitoring process of potentially risky sites. The feedback that will follow should help us appraise and improve the adequacy of the tool to the needs and practices of local officials in charge of natural hazards management.

Near real-time access to environmental data from a single web portal facilitates the risk manager's work. Coupled with their own expertise, it optimizes and eases the decision making process linked to complex phenomena. As well as land use planning, this platform participates to the integrated risk management process of natural hazards.

10.2

A sediment flux time series from a proglacial area: insights into sediment dynamics of glaciated catchments

Ian A. Delaney¹, Yvo Weidmann¹, Matthias Huss¹ & Andreas Bauder¹

¹ *Laboratory for Hydraulics, Hydrology and Glaciology (VAW), ETH-Zürich, Hönggerberggring 28, CH-8093 Zürich (delaney@vaw.baug.ethz.ch)*

In recent years hydropower operators and others (e.g. Micheletti et al., 2015) in the Swiss Alps have observed increased erosion in glaciated regions, resulting sedimentation in reservoirs and abrasion of infrastructure downstream. This material could originate either subglacially or from newly created proglacial areas (PGA) formed as glaciers retreat and are often comprised of unconsolidated and easily erodeable material (e.g. Church and Ryder, 1972). To determine sediment fluxes from these PGAs, we examine the Griesgletscher in eastern Valais and compare these data with catchment characteristics, such as hydrology and glacier morphology, to better understand sedimentation and erosional processes.

By subtracting digital surface models made from annually-collected aerial photographs from 1986 to 2014 covering the PGA, we calculated annual sediment fluxes from the PGA. This data suggests that erosion has increased exponentially since 1986, a predominately product of the larger PGA caused by glacier retreat. However, six of the 26 years examined experience net deposition in the proglacial area, suggesting the importance of the subglacial sediment source or transport of material from other parts of the basin. Additionally, within the last seven years examined, three years experienced extreme amounts of erosion from the PGA, while two years experienced a comparable amount of deposition.

Catchment hydrology was modeled over the study period to better understand the relationship between sediment dynamics and runoff. When examined through the entire study period, erosion is correlated with maximum three to seven day discharge and higher runoff volume; these higher flows could provide the water necessary to remove large amounts of material from the PGA. Conversely, deposition is correlated with runoff variability and maximum discharge over short time periods (less than three days). These are associated with high subglacial water pressure (e.g. Iken and Bindenschadler, 1986), possibly increasing subglacial erosion, subsequently depositing sediment in the PGA as the water leaves glacier and its flow speed is reduced.

Lastly, comparison of four lake bathymetries from the Griesgletscher's proglacial reservoir, suggests that 10 to 50% of sediment deposited in the reservoir originates from the PGA. The remaining material must come from subglacial sources or other parts of the basin, which expel large quantities of sediment. By examining these relationships, we have been able to gain valuable insight into the processes controlling proglacial erosion and their relative importance in the catchment's sediment dynamics.

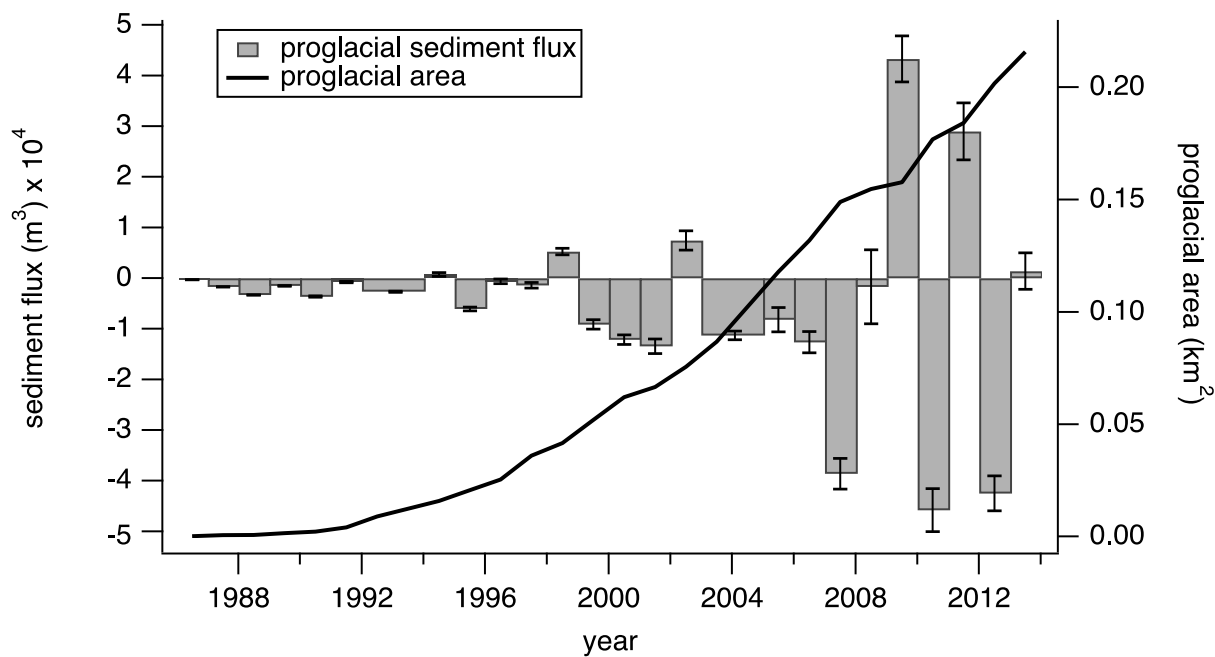


Figure 1. Annual volumetric sediment flux from the Greisgletscher's proglacial area from 1986 to 2014. Negative values denote net erosion, while positive values show net deposition in the proglacial area.

REFERENCES

- Micheletti, N., Lambiel, C. & Lane S. 2015: Investigating decadal-scale geomorphic dynamics in an alpine mountain setting, *JGR: Earth Surface* 120, 2155–2175, doi:10.1002/2015JF003656.C
- Church, M., & Ryder, J. 1972: Paraglacial Sedimentation: A Consideration of Fluvial Processes Conditioned by Glaciation. *GSA Bulletin*, 83, 3059-3072.
- Iken, A., & Bindschadler, R. 1986: Combined measurements of subglacial water pressure and surface velocity of Findelengletscher, Switzerland: conclusions about drainage system and sliding mechanism. *J. Glaciology*, 32, 110, 101-119.

10.3

Dynamics of rockfall hazards and risks from past to future: a case study in Täsch (VS), Switzerland

Michael Fehlmann¹, Daniel Trappmann², Christine Moos³, Luuk Dorren³, Markus Stoffel⁴, Michael Bründl⁵, Chrisitan Huggel¹

¹ *Department of Geography, University of Zurich, Winterthurerstrasse 190, CH-8057 Zürich (michael.fehlmann@uzh.ch)*

² *Institute of Geological Sciences, University of Berne, Baltzerstrasse 1-3, CH-3012 Bern*

³ *Division Forest Science, Bern University of Applied Sciences, Länggasse 85, CH-3052 Zollikofen*

⁴ *Institute for Environmental Sciences, University of Geneva, 66 boulevard Carl Vogt, CH-1205 Genève*

⁵ *WSL Institute for Snow and Avalanche Research SLF, Flüelastrasse 11, CH-7260 Davos Dorf*

Switzerland is exposed to a multitude of natural hazards. Mass movements such as snow and rock avalanches, landslides or rockfalls affect more than 6% of the country. To protect human lives, property and the environment from resulting damages, hazard and risk assessments provide an essential basis. However, such assessments are often only applied and representative for a certain time period, typically for present conditions. By contrast, multi-temporal analyses can provide valuable information about hazard and risk developments and their driving factors. The main purpose of this study is therefore to develop a consistent methodology to assess long-term developments of rockfall hazard and accompanying risk. To test the developed method, we applied it at “Täschgufer”, a highly active rockfall slope in the southern Swiss Alps, where release zones of rockfall are located in periglacial environments. We thereby created hazard and risk maps for distinct time periods (1880, 1940, 2010, 2060), depicting spatial patterns of past and likely future developments (Fig. 1).

In accordance with well-established concepts of hazard and risk in Switzerland (Bründl, 2009; Bründl et al., 2015), a general analytical framework was developed, integrating field observations, event reports, dendrochronological and socio-economic data as well as statistical and process-oriented models, and then adjusted to the different time periods. For the analysis of past time periods, information about rockfall frequencies were derived from dendrochronological data (Stoffel et al., 2005) of 255 sampled trees at the slope, and past exposure of infrastructure and people was inferred from historical maps. Furthermore, dendrochronological data allowed the establishment of relations between annual rockfall frequencies and mean annual summer temperatures over several decades of the 20th century. Future rockfall hazard and risk were then estimated based on both climatic and socio-economic scenarios. Results show that past development of rockfall risk in Täsch was mainly driven by socio-economic factors, more precisely by increasing exposure of infrastructure and people in the late 20th century. From present to 2060, however, projected rockfall risk is estimated to be equally driven by climatic and socio-economic factors, leading to an increase in rockfall risk by a factor of 2.2 over all scenarios.

Existing disaster loss studies (Bouwer, 2011; Bower, 2013) are mainly focusing on regional to global scales but risk has typically many local-scale characteristics, and therefore important aspects are likely not covered. Our study fills this gap by proposing a methodology for the assessment of local-scale risk evolution. Results for a periglacial rockfall site suggest, that a lacking climate signal in past losses from natural hazards does not necessarily imply the same finding for the future under continuing climate and socio-economic change. Despite well-founded theoretical understanding, however, the estimated climate impact on rockfall frequencies in periglacial environments remains highly uncertain and needs further investigation.

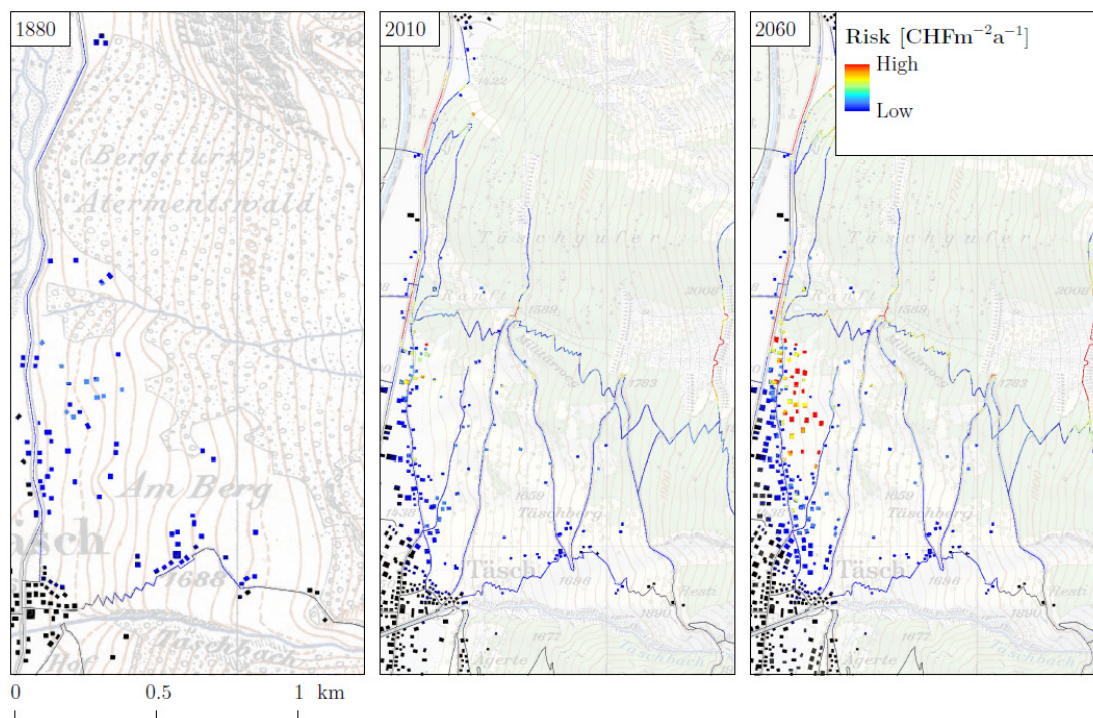


Figure 1. Rockfall risk maps for the village of Täsch (VS), modelled for the time periods of 1880, 2010 and 2060. The risk map of 2060 thereby depicts the situation under future climate warming (emission scenario A1B) and continuation of latest trends in socio-economic development.

REFERENCES

- Bouwer, L. M. 2011: Have disaster losses increased due to anthropogenic climate change?. *Bulletin of the American Meteorological Society*, 92(1), 39-46.
- Bouwer, L. M. 2013: Projections of future extreme weather losses under changes in climate and exposure. *Risk Analysis*, 33(5), 915-930.
- Bründl, M., Ettl, L., Burkard, A., Oggier, N., Dolf, F. & Gutwein, P. 2015: *EconoMe - Wirksamkeit und Wirtschaftlichkeit von Schutzmassnahmen gegen Naturgefahren. Formelsammlung*. 56 p.
- Bründl, M. (Ed.). 2009: *Risikokzept für Naturgefahren - Leitfaden*. Nationale Plattform für Naturgefahren PLANAT, Bern. 420 p.
- Stoffel, M., Schneuwly, D., Bollschweiler, M., Lievre, I., Delaloye, R., Myint, M., & Monbaron, M. 2005: Analyzing rockfall activity (1600–2002) in a protection forest—a case study using dendrogeomorphology. *Geomorphology*, 68(3), 224-241.

10.4

Very low temperature OSL-thermochronometry applied to the Siwalik deposits in Nepal and Bhutan

Georgina King¹, Djordje Grujic², Isabelle Coutand², Frédéric Herman³

¹ *Institute of Geology, University of Bern*

² *Department of Earth Sciences, Dalhousie University*

³ *Institute of Earth Surface Dynamics, University of Lausanne*

The Himalayan foreland fold-and-thrust belt is made of Neogene synorogenic sediments of the Siwalik Group and accommodates a large fraction of the India-Eurasia convergence. This region receives high precipitation and experiences seismic events of M8 and larger. Along the strike of the 2500-km-long orogenic arc, the eastward narrowing of the fold-and-thrust belt has been attributed to increasing annual rainfall and specific stream power, rather than to lateral changes in shortening rates. However, exhumation/erosion rates of this unit remain unknown. Precisely constraining the erosion rates of this unit at the scale of the orogen would allow an estimate of the relative contributions of tectonic and climatic processes to the erosion of the youngest and frontal part of the Himalayan orogen.

Thermochronometry enables the cooling, and therefore exhumation/erosion histories of rocks to be determined. However the exhumation histories of the Siwalik Group, which have experienced limited burial heating not exceeding ~100-50 °C remain very difficult to constrain using traditional thermochronometers. Optically stimulated luminescence (OSL)-thermochronometry is a recently developed very low temperature thermochronometer sensitive to temperatures of 30-90 °C. Consequently, its application to the Siwalik deposits may provide insights into their cooling and exhumation histories.

K-feldspar extracts from 18 sandstones samples of the Siwalik Group were investigated using a multi-OSL-thermochronometry approach, whereby four different signals, with different thermal stabilities were measured for each sample. The sandstone samples were collected along two traverses across the Himalayan fold-and-thrust belt in western Nepal, and eastern Bhutan. Using signals with different thermal sensitivities enables high precision Quaternary cooling histories to be derived. These data were inverted using a Bayesian approach resulting in preliminary cooling rates of ~100 °C/Myr during the last 0.2 Ma, which were broadly consistent between samples, indicating similar rates of cooling. These preliminary results suggest that estimated erosion rates over the foothills of the Himalaya are up to one order of magnitude higher than the longer-term erosion rates (1-3 mm/yr) documented in the hinterland of the orogen.

10.5

Erosion and sediment transfer at the front of rapidly moving rock glaciers

Mario Kummert¹ & Reynald Delaloye¹

¹ *Department of Geosciences/Geography, University of Fribourg, Chemin du Musée 4, CH-1700 Fribourg*

Covering many periglacial mountain slopes, rock glaciers are tongue-shaped or lobate landforms composed by a mix of rock debris and ice. Their movement can mainly be explained by the deformation of the interstitial ice (permafrost creep – e.g. Haeberli et al. 2006). Rock glaciers contribute to the alpine sediment cascade by slowly transferring rock debris from the rooting zone (talus-scrree, moraines or weathering deposits) towards their fronts (Delaloye et al. 2010). Typical rock glacier fronts are several meters high and show fine sediments at the surface. If located on top of a steep slope connected to a torrential gully, rock glacier fronts can act as sediment source for the triggering of hazardous gravitational processes such as rock fall and debris flow. The amount of sediment available for gravitational transport is then gradually renewed or increased as the rock glaciers advance. These cases are therefore very specific and ask for a better understanding of the erosion processes and the sediment transfer rates between the fronts and the torrential channels. These questions are especially relevant in the perspective of natural hazard assessment in the current context of climatically-driven rock glacier acceleration (e.g. Roer et al. 2008).

This contribution presents a comprehensive assessment of the erosion processes occurring at the front of three rapidly moving rock glaciers located in the Valais Alps (Dirru, Gugla and Tsarmine). In this study, a multi-method approach combining qualitative (observations via webcams) and quantitative (terrestrial laser scanning) data has been applied. The aim is (i) to determine the erosion mechanisms taking place at the front of rock glaciers, (ii) to quantify the sediment transfer rates between the fronts and the torrential channels and (iii) to understand the spatio-temporal behavior of these erosion and transfer processes.

The results show that even though their intensity and their exact timing are site-dependent, the same erosion processes can generally be observed at the front of the three investigated rock glaciers. Within one year, three main periods characterized by specific erosion activity and processes could be distinguished: the winter, the snow-melt, and the summer. At each site, a significant erosion rate was estimated thanks to the LiDAR data. Values range between 2000 m³/year (Dirru) and 6000 m³/year (Gugla). Finally, it was possible to assess the spatial behavior of the erosion of the front and to determine deposition patterns in the channels. At each site, the sediment tends to accumulate in storage areas in the upper part of the gullies nearby the fronts. These storage areas can be either permanent or temporary, depending on the sites and on the time scale.

REFERENCES

- Delaloye, R., Lambiel, C. & Gärtner-Roer, I. (2010). Overview of rock glacier kinematics research in the Swiss Alps. Seasonal rhythm, interannual variations and trends over several decades. *Geogr. Helv.* 65: 2, 135–145.
- Haeberli, W., Hallet, B., Arenson, L., Elconin, R., Humlum, O., Käab, A., Kaufmann, V., Ladanyi, B., Matsuoka, N., Springman, S. & Vonder Mühll, D. (2006). Permafrost creep and rock glacier dynamics. *Permafrost and Periglacial Processes*, 17, 189-214.
- Roer, I., Haeberli, W., Avian, M., Kaufmann, V., Delaloye, R., Lambiel, C. & Käab, A. (2008). Observations and considerations on destabilizing active rock glaciers in the European Alps. In: Kane, D.L. & Hinkel, K.M. (eds): *Proceedings of the 9th International Conference on Permafrost*, June 29-July 3, 2008, Fairbanks, Alaska, 2: 1505-1510.

10.6

Modelling geomorphic responses to human impacts and extreme floods: Application to the Kander river, Switzerland

Jorge Alberto Ramirez¹, Andreas Paul Zischg^{1,2}, Stefan Schürmann^{1,2}, Markus Zimmermann¹, Rolf Weingartner^{1,2} & Margreth Keiler¹

¹ Institute of Geography, University of Bern, Hallerstrasse 12, 3012 Bern, CH

² Oeschger Centre for Climate Change Research, Mobiliar Lab for Natural Risks, University of Bern

Originally, the Kander river flowed into the Aare river causing massive flooding in the region of Thun and this is why the Kander river was deviated to lake Thun by engineering works (Figure 1a). Besides the reduction of flooding, the goal of this deviation (Kander correction) was to prevent damming of the Aare from large sediment loads delivered by the Kander causing backwater effects and subsequent floodings in Thun upstream of the confluence. Moreover, the flood peaks occurring between Thun and Bern could be reduced. The Kander correction was pioneering, but it had unintended hydrological and geomorphic consequences. As a result of the correction the catchment area of Lake Thun increased by 50% and this additional discharge exceeded the limited storage capacity of the lake during floods. Direct sediment delivery to the Aare from the Kander ceased, but at the same time sediment flux to lake Thun increased forming the Kander delta. Furthermore, the correction shortened the Kander by 8 km and this substantially increased the slope and bed shear of the Kander upstream from the correction. Subsequently within four years the deviation itself quickly began to erode at an unprecedented rate (~30 m) and resulted in massive river bed changes that propagated up the Kander and Simme rivers.

Today we may have at our disposal the theoretical and empirical foundations to foresee the consequences of such a human intervention into a natural system. One method to investigate such geomorphic changes are numerical models that estimate the evolution of a river by simulating the movement of water and sediment. Although much progress has been made in the development of these geomorphic models, few models have been tested in circumstances with extreme forcings. As such, it remains uncertain if geomorphic models are useful and stable in extreme situations that include large movements of sediment and water over short periods of time. Resolving this uncertainty is particularly important as there is a need to estimate the geomorphic effects of river restoration efforts and resolve how river channels will respond to extreme floods that are becoming more frequent with climate change. Here, in this study, we use historic maps and documents to develop a detailed geomorphic model (CAESAR-Lisflood (Coulthard et al., 2013)) of the Kander river starting in the year 1714. We use this model to simulate the extreme geomorphic events that preceded the deviation of the Kander river into Lake Thun. We test our model by replicating the rates of incision within the correction (Figure 1b,c and Figure 2) and gauge the sensitivity of the model with floods of different magnitude and duration.

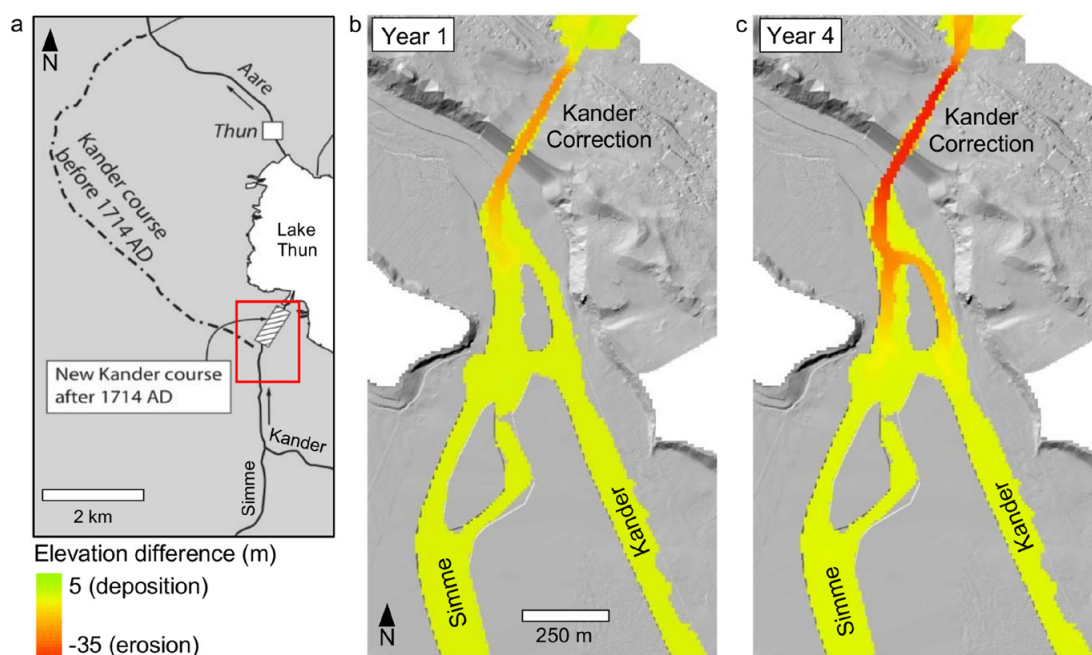


Figure 1. (a) Study site (map adapted from Wirth et al. (2011)) and modeled channel change within the Kander correction, Simme and Kander rivers after (b) year one, and (c) year four.

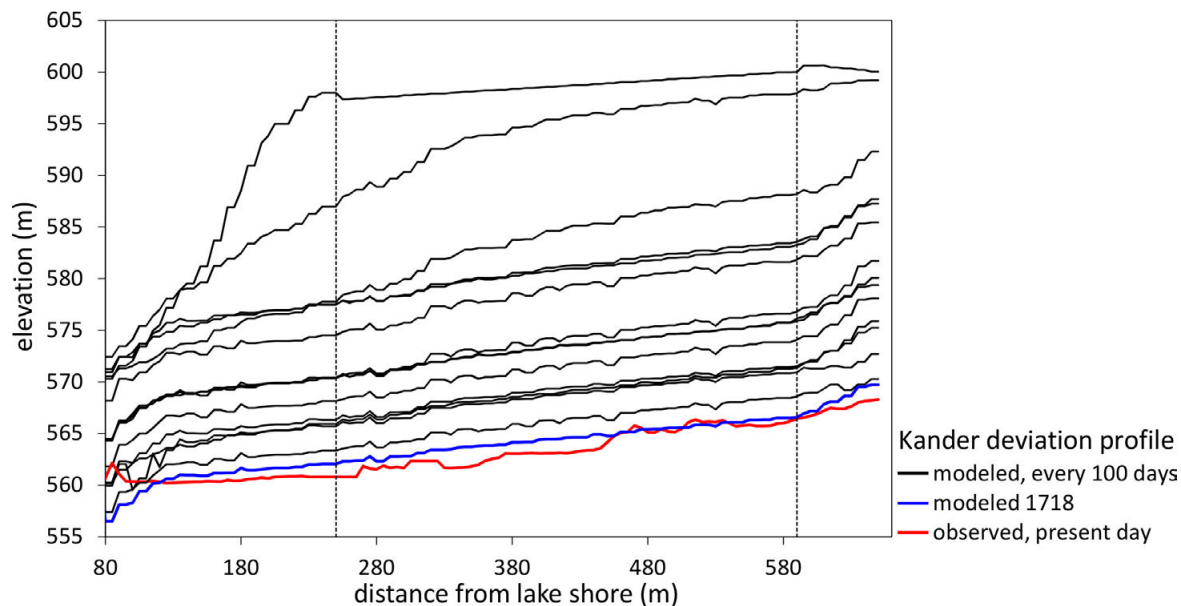


Figure 2. Comparison of modeled and observed elevation profile of the Kander correction. Modeling period between 1714-1718. Dashed lines represent the beginning and ending of Kander correction.

REFERENCES

- Coulthard, T.J., Neal, J.C., Bates, P.D., Ramirez, J., de Almeida, G.A.M., Hancock, G.R., 2013. Integrating the LISFLOOD-FP 2D hydrodynamic model with the CAESAR model: implications for modelling landscape evolution. *Earth Surf. Process. Landforms* 38, 1897–1906. doi:10.1002/esp.3478
- Wirth, S.B., Girardclos, S., Rellstab, C., Anselmetti, F.S., 2011. The sedimentary response to a pioneer geo-engineering project: Tracking the Kander River deviation in the sediments of Lake Thun (Switzerland). *Sedimentology* 58, 1737–1761.

10.7

Coupling and feedbacks between orographic precipitations and landscape evolution: Basse Terre Island, Guadeloupe archipelago (Lesser Antilles Arc)

Pierre G. Valla^{1,3}, Eric Lajeunesse², Romain Delunel³ & Pascal Allemand⁴

¹ *Institute of Earth Surface Dynamics, University of Lausanne, CH-1015 Lausanne (pierre.valla@unil.ch)*

² *Institut de Physique du Globe, Université Sorbonne Paris Cité, F-75005 Paris*

³ *Institute of Geological Sciences, University of Bern, CH-3012 Bern*

⁴ *Laboratoire de Géologie de Lyon Terre-Planète-Environnement, Université de Lyon, F-69100*

Tropical volcanic islands are interesting natural environments to investigate the interactions between endogenic and exogenic processes in the Earth's Surface evolution. Such interactions remain a scientific challenge, in part due to the intrinsic differences in spatial and temporal scales at which these processes operate. Tropical volcanic islands are small-scale settings, with relative spatially uniform basaltic/andesitic lithologies. They are also affected by a tropical humid climate with strong spatial variations in precipitations. Finally, detailed information on the volcanic activity exists, with independent knowledge on both the timing and spatial extent of eruptive events (i.e. dating of lava flow and topographic reconstruction of the initial volcanic edifice).

Here, we study the Basse Terre Island (Guadeloupe archipelago, Lesser Antilles Arc). It is composed of four successive andesitic edifices (Samper et al., 2007) that reveal the progressive southward migration of the volcanic activity from ~3 Ma until present-day. This unique setting offers a tight temporal framework for the quantification of erosional processes and landscape evolution after cessation of volcanism. Tropical humid climate is characterized by eastern trade-winds with strong orographic precipitations (Gaillardet et al., 2011) and storm events (Allemand et al., 2014). We present morphometric analysis conducted on a high-resolution DEM (10-m scale) that we combine with reconstruction of the volcanic activity from the literature (e.g. Samper et al., 2007) and modern precipitation data (source MeteoFrance). Our results show that topographic relief and drainage divide evolve with edifice age (erosional destruction) but more importantly that the precipitation patterns closely follow the island topography. This spatial correlation illustrates the co-evolution of both island topography and orographic effect. Preliminary analysis of river profiles and basin hypsometry confirms the spatial differences with both edifice age and precipitations, revealing that landscape dynamics is still active through drainage reorganization (Willett et al., 2014) and divide migration (Bonnet, 2009).

REFERENCES

- Allemand, P., Delacourt, C., Lajeunesse, E., Devauchelle, O., & Beauducel, F. 2014: Erosive effects of the storm Helena (1963) on Basse Terre island (Guadeloupe - Lesser Antilles Arc). *Geomorphology*, 206, 79-86.
- Bonnet, S. (2009). Shrinking and splitting of drainage basins in orogenic landscapes from the migration of the main drainage divide. *Nature Geoscience*, 2, 766-771.
- Gaillardet, J., Rad, S., Louvat, P., Rivé, K., Gorge, C., Allègre, C.J., & Lajeunesse, E. 2011: Orography-driven chemical denudation in the Lesser Antilles: evidence for a new feedback mechanism stabilizing atmospheric CO₂. *American Journal of Science*, 311, 851-894.
- Samper, A., Quidelleur, X., Lahitte, P., & Mollex, D. 2007: Timing of effusive volcanism and collapse events within an oceanic arc island: Basse-Terre, Guadeloupe archipelago (Lesser Antilles Arc). *Earth and Planetary Science Letters*, 258, 175-191.
- Willett, S.D., McCoy, S.W., Perron, J.T., Goren, L., & Chen, C.-Y. (2014). Dynamic Reorganization of River Basins. *Science*, 343.

10.8

Rapid Detection and Location of Debris Flow Initiation at Illgraben, Switzerland

Fabian Walter^{1,2}, Arnaud Burtin^{3,4}, Brian McArdell², Niels Hovius³, Bianca Weder¹, Jens Turowski³

¹ *Laboratory of Hydraulics, Hydrology and Glaciology, ETH Zurich, Switzerland*

² *Swiss Federal Institute for Forest, Snow and Landscape Research WSL, Switzerland*

³ *GFZ German Research Centre for Geosciences, Germany*

⁴ *Institut de Physique Du Globe de Paris, France*

Heavy precipitation can suddenly mobilize tens to hundreds of thousands of cubic meters of sediments in steep Alpine torrents. The resulting debris flows (mixtures of water, sediments and boulders) move downstream with velocities of several meters per second (Figure 1) and have a high destructive potential (e.g. Rickenmann and Zimmermann, 1993). Warning schemes for affected communities rely on raising awareness to the debris flow threat, precipitation monitoring and rapid detection methods (Deganutti et al., 2000; Fan et al., 2003; Badoux et al., 2009). The latter, in particular, remain an ongoing challenge, because debris-flow-prone torrents have their catchments in steep and inaccessible terrain, where installing and maintaining instrumentation is difficult. Here, we propose a simple processing scheme for seismic network data. We use debris flow and noise seismograms from Illgraben, Switzerland, a torrent, which produces several debris flow events per year (Badoux et al., 2009). Automatic in-situ detection is currently based on geophones and laser altimeters installed within the flow channel. The proposed approach has the advantage that it uses seismometers, which can be installed at more accessible locations, and where a stable connection to portable phone networks is available for data communication (Burtin et al., 2014). Our data processing uses time-averaged ground vibration amplitudes to estimate the location of the debris flow front. Applied to continuous data streams, inversion of the seismic amplitude decay (Battaglia et al., 2003) eliminates the need for single-station-based detection and knowledge of the local seismic velocity model. This makes the approach suitable for automation, as seismic phase identification is unnecessary and the amplitude averaging significantly reduces data volume. We apply our approach to a small debris flow event on 19 July 2011, which was captured with a temporary monitoring network. The processing rapidly detects the debris flow event half an hour before its front arrives at the torrent mouth and 8 minutes before detection by the current alarm system. An analysis of continuous seismic records furthermore indicates that detectability of Illgraben debris flows of this size are unaffected by changing environmental and cultural seismic noise. We therefore propose that our method reliably detects initiation of the Illgraben debris flows and can thus form an important ingredient in the next generation of early warning schemes.



Figure 1. Photo of Illgraben debris flow event. Source: Brian McArdell, WSL.

REFERENCES

- Badoux, A., Graf, C., Rhyner, J., Kuntner, R., & McArdell, B. W. (2009). A debris-flow alarm system for the Alpine Illgraben catchment: design and performance. *Natural hazards*, 49(3), 517-539.
- Battaglia, J., & Aki, K. (2003). Location of seismic events and eruptive fissures on the Piton de la Fournaise volcano using seismic amplitudes. *Journal of Geophysical Research: Solid Earth*, 108(B8).
- Burtin, A., Hovius, N., McArdell, B. W., Turowski, J. M., & Vergne, J. (2014). Seismic constraints on dynamic links between geomorphic processes and routing of sediment in a steep mountain catchment. *Earth Surface Dynamics*, 2(1), 21–33. <http://doi.org/10.5194/esurf-2-21-2014>.
- Deganutti AM, Marchi L, Arattano M (2000) Rainfall and debris-flow occurrence in the Moscardo basin (Italian Alps). In: Wieczorek GF, Naeser ND (eds) Debris-flow hazards mitigation: mechanics, prediction, and assessment. A.A. Balkema, Rotterdam, pp 67–72.
- Fan J-C, Liu C-H, Wu M-F, Yu SK (2003) Determination of critical rainfall thresholds for debris-flow occurrence in central Taiwan and their revision after the 1999 Chi-Chi great earthquake. In: Rickenmann D, Chen CL (eds) Debris-flow hazards mitigation: mechanics, prediction, and assessment. Millpress, Rotterdam, pp 103–114.

P 10.1

The hydro-geomorphic influence of beaver (*Castor fiber*) on Swiss low-order streams – first results

Annegret Larsen¹, Maxime Capponi¹, Stuart Lane¹

¹ *Institut des dynamiques de la surface terrestre, Université de Lausanne, 1015 Lausanne, Schweiz (annegret.larsen@unil.ch)*

The influence of beavers on river and floodplain hydrology, geomorphology and ecology are significant, but the processes leading to this impact, and its extent, are less well researched (Gurnell, 1998; Naiman et al., 1988). Beavers are known: i) to increase the number of channel bifurcations; ii) to decrease longitudinal channel connectivity and sediment transport through dam construction; and iii) to increase the in-channel water level. The latter combines with a higher lateral floodplain connectivity following from the creation of small channels to create a higher groundwater level in the floodplain. The result can be valley-width floodplain wetlands (beaver meadows), characterized by high surface heterogeneity and ecological significant ecological value. By creating wetlands, beavers also alter floodplain soil processes and the flux of nutrients in groundwater moving through the riparian zone to the channel. Hence, they may alter the flux of inputs from hillslopes to the stream channel. In this ongoing project, we aim to i) understand feedback processes between beaver, vegetation and streams and their floodplains, and also ii) quantify the impact of beaver in variable riparian settings. Here, we present a conceptual model of the existing types of beaver impact on European rivers and floodplains, which we argue depends strongly on previous Geomorphic conditions. We will also present first results from the hydraulic modelling of beaver influenced river sections, indicating that the largest influence of beaver dam structures is during low-medium flow. Ongoing research targets the influence of beaver on river channel pattern, water quality, and the role of beaver in Holocene river valley evolution.

REFERENCES:

- Gurnell AM. (1998) The hydrogeomorphological effects of beaver dam-building activity. *Progress in Physical Geography* 22: 167-189.
- Naiman RJ, Johnston CA and Kelley JC. (1988) Alteration of North American Streams by Beaver. *BioScience* 38: 753-762.

P 10.2

Sediment yield estimation on a catchment scale in data-scare regions - Rasht valley Tajikistan

Marco Rieder¹, Markus Zimmermann¹, Sven Fuchs² & Margreth Keiler¹

¹ *University of Bern, Institute of Geography, Hallerstrasse 12, CH-3012 Bern (marco.rieder@students.unibe.ch)*

² *University of Natural Resources and Life Sciences, Institute for Mountain Risk Engineering, Peter-Jordan-Straße 82, A-1190 Vienna*

In the arid area of Rasht valley, Tajikistan, several challenges for agriculture activities exist due to limited vegetation cover, intensive use of the limited space for pasture and consequently land degradation, and soil erosion. Moreover, during snow melt and intensive rain in steep channels transport considerable amounts of coarse sediments. In recent years, an increase of larger debris flows causing damages to the villages along the main valley is observed, and may be associated with rising soil erosion and thus the availability of fine material for torrential processes. Therefore, land management strategies as well as different basic conditions (geology, climate, vegetation, slope, soil type,...) are considered as contributing factors for increasing sediment yield.

In this study, an adapted PSIAC approach (de Vente et al. 2005) applying a combined method including remote sensing, GIS and field investigations was tested in 31 catchments of the Rasht valley. The approach considered factors such as geology, climate, vegetation cover, land use, soil type, precipitation, channel erosion, up-land erosion and slope, which were individually evaluated and weighted. In particular, the erosion parameters were adapted and specified to the local conditions. The approach allowed classifying those catchments which are sensitive to land management practices and overgrazing. A comparison between the catchments having same natural conditions but different land management strategies indicated best-practice examples. Consequently, this is also valuable information for hazard prevention and provides a basis for mainstreaming risk reduction and land management strategies in the area.

We will present the first results testing this adapted approach in data-scare areas by ranking the sediment yield and their sensitivity to land management for the different catchments.

REFERENCES

de Vente, J., Poesen, J. & Verstraeten, G. 2005. The application of semi-quantitative methods and reservoir sedimentation rates for the prediction of basin sediment yield in Spain. *Journal of Hydrology* 305(1), 63-86.

P 10.3

Assessment of sediment connectivity index in relation with hazardous events in alpine torrent catchments in Switzerland

Daria Schmutz¹, Markus Zimmermann¹, Margreth Keiler¹

¹ *University of Bern, Institute of Geography, Hallerstrasse 12, CH-3012 Bern (daria.schmutz@students.unibe.ch)*

Sediment connectivity is defined as the degree of coupling between sediment sources and sinks in a system and describes the effectiveness of the transfer of sediment from hillslopes into channels and within channels (Bracken et al. 2015). Borselli et al. (2008) developed a connectivity index (IC) based on digital terrain models (DTMs). Cavalli et al. (2013) adapted this index for mountainous catchments. These measures of connectivity provide an overall information about connectivity pattern in the catchment, thus the understanding of sediment connectivity can help to improve the hazard analysis in these areas. Considering the location of settlements in the alpine regions, high sediment transfer can pose a threat to villages located nearby of torrents or at the debris cones. However, there is still a lack of investigations on the linkage between IC and hazardous events with high sediment yield in alpine catchments.

In this study, the expressiveness and applicability of IC is tested in relation with hazardous events in several catchments of the Bernese and Pennine Alps. The IC is modelled based on DTMs showing the surface from the time before and after a documented event and analyzed with respect to changes in connectivity through the event. The spatial pattern of connectivity is compared with the observed sediment dynamic during the event using event documentations. In order to validate the IC, a semi-quantitative field connectivity (FIC) index is developed and applied in a selection of the case studies. Furthermore, this FIC is then compared with the IC modelled with GIS. First results and an evaluation will be presented.

REFERENCES

- Borselli, L., Cassi, P. & Torri, D. 2008: Prolegomena to sediment and flow connectivity in the landscape. A GIS and field numerical assessment. *CATENA* 75 (3), 268–277.
- Bracken, L. J., Turnbull, L., Wainwright, J. & Bogaart, P. 2015: Sediment connectivity. A framework for understanding sediment transfer at multiple scales. *Earth Surface Processes and Landforms* 40 (2), 177–188.
- Cavalli, M., Trevisani, S., Comiti, F. & Marchi, L. 2013: Geomorphometric assessment of spatial sediment connectivity in small Alpine catchments. *Geomorphology* 188, 31–41.

P 10.4

Debris flow modelling: How much model complexity is needed?

Candace Chow¹, Jorge Alberto Ramirez¹, Markus Zimmermann¹, Andrew Barkwith² and Margreth Keiler¹

¹ *University of Bern, Institute of Geography, Hallerstrasse 12, 3012 Bern, CH*

² *British Geological Survey, Environmental Science Centre, Keyworth, Nottingham, NG12 5GG, UK*

Debris flows occur with the rapid downslope transport of water and the entrainment of available solid materials. Future exposure to this hazard is unlikely to diminish as a greater occurrence of extreme precipitation events in the Alps is expected with respect to climate change (Rajczak et al., 2013). Consequently, debris flows of unprecedented magnitude may be triggered with increasing frequency (Stoffel et al., 2014). In particular, these hazardous events contribute to both economic losses and potential fatalities in settlements situated in mountain regions. In Switzerland alone, between 1972 and 2015, the average annual cost of damages due to floods, debris flows, landslides and rockfalls have already resulted in an estimated 312 million Euros, despite substantial investments in both technical and planning measures (Swiss Federal Institute for Forest, 2016).

One method to investigate the intensity and consequences of debris flow hazards involves the use of computer models to inform about the interaction of sediment and water with built structures. The information about the interactions and the outputs such as flow velocity, flow height and erosion and deposition is essential for subsequent risk assessment. Existing debris flow models are characterized by varying levels of physical rigour, complexity, and computational overhead. While physically-based models are capable of simulating greater system complexities, the definition and calibration of a wide range of model parameters is required, which inherently introduces uncertainty into model results. Furthermore, due to significant computational requirements, the possibility of investigating debris flow scenarios with different environmental forcings (e.g. precipitation) and initial model conditions (e.g. sediment availability) is limited. In contrast, reduced complexity models are characterized by simplified physics, fewer parameters and lower computational overhead. These simpler models can quickly simulate a greater quantity of debris flow scenarios, which supports identifying conditions that lead to non-linear responses associated with the initiation of catastrophic events.

Although reduced-complexity models offer many advantages, the accuracy associated with the outputs require further assessment. Additionally, there are few comparisons that identify the degree of model complexity required to accurately replicate an observed debris flow event. Herein we test two debris flow models, with variable amounts of model complexity, against detailed field data collected from the 2005 debris flow event that occurred along the Glyssibach in Brienz. The study compares the results from the more complex FLO-2D model (O'Brien et al., 1993) with the less complex SCIDDICA model (Di Gregorio et al., 1999). While the first is a finite difference model based on a quadratic rheologic law, the latter is a rule-based cellular automata implemented within the landscape evolution model CAESAR-Lisflood-DESC (Barkwith et al., 2015). Our results will determine if a reduced-complexity approach can accurately replicate debris flow processes or if a more complex model is required to obtain useful model outputs.

REFERENCES

- Barkwith, A., Hurst, M.D., Jackson, C.R., Wang, L., Ellis, M.A., Coulthard, T.J., 2015. Simulating the influences of groundwater on regional geomorphology using a distributed, dynamic, landscape evolution modelling platform. *Environ. Model. Softw.* 74, 1–20. doi:<http://dx.doi.org/10.1016/j.envsoft.2015.09.001>
- Di Gregorio, S., Kongo, R., Siciliano, C., Sorriso-Valvo, M., Spataro, W., 1999. Mount Ontake landslide simulation by the cellular automata model SCIDDICA-3. *Phys. Chem. Earth, Part A Solid Earth Geod.* 24, 131–137.
- Hilker, N., Badoux, A., Hegg, C., 2009. The Swiss flood and landslide damage database 1972–2007. *Nat. Hazards Earth Syst. Sci.* 9, 913–925.
- O'Brien, J.S., Julien, P.Y., Fullerton, W. T., 1993. Two-dimensional water flood and mudflow simulation. *Journal of Hydraulic Engineering* 119(2): 244–261.
- Rajczak, J., Pall, P., Schär, C., 2013. Projections of extreme precipitation events in regional climate simulations for Europe and the Alpine Region. *J. Geophys. Res. Atmos.* 118, 3610–3626.
- Stoffel, M., Mendlik, T., Schneuwly-Bollschweiler, M., Gobiet, A., 2014. Possible impacts of climate change on debris-flow activity in the Swiss Alps. *Clim. Change* 122, 141–155. doi:[10.1007/s10584-013-0993-z](https://doi.org/10.1007/s10584-013-0993-z)
- Swiss Federal Institute for Forest, Snow and Landscape Research (WSL), 2015. "Swiss flood and landslide damage database", http://www.wsl.ch/fe/gebirgshydrologie/HEX/projekte/schadendatenbank/index_EN.

P 10.5

Reconnaissance study of landslide distribution with respect to erosional processes in northwestern Bhutan

Larissa de Palézieux¹, Kerry Leith¹ & Simon Loew¹

¹ *Geological Institute, ETH Zurich, Sonneggstrasse 5, CH-8092 Zurich (larissa.depalezieux@erdw.ethz.ch)*

With elevations ranging from 97 m to 7570 m, the eastern Himalayas of Bhutan host very diverse geographical and climatic regions. The country can roughly be divided into three geomorphological zones, with the lowlands (100–3000 m), the mid reaches (3000–4200 m) and the high elevations above 4200 m. The higher latitudes and elevations are glacially overprinted with most end moraines above ca 4200 m, while the lower latitudes and below ca 3000 m show predominantly fluvial signals. Longitudinal profiles of rivers in the region show a consistent pattern with a marked topographic step covering 2000 m of elevation change within 10 km. This suggests a relatively recent and strong change in relative uplift or erosion rate, for which the signal is propagated upstream as a wave of increased incision. The steep topographic gradients and active incision lead to large instabilities, which can cover entire slopes in the high relief valleys. The glacially overprinted low relief areas show fewer instabilities, which are often suspended unlike those of the deeply incised valleys, which typically reach the valley floor. In this study we use satellite images in combination with a high resolution digital elevation model (5 m, ALOS-world 3D) for a regional scale landscape analysis. Field observations obtained in the scope of a first field campaign in the northwestern part of the country provide an opportunity to verify our findings. While the tectonic and erosional history of Bhutan is still under debate (e.g. Adams et al., 2016 and Grujic et al., 2006), this study aims to identify erosional markers in the landscape and evaluate the response of landslides to variations in key relief forming processes across the region.

REFERENCES

- Adams, B., Whipple, K. X., Hodges, K. V. & Heimsath, A. M. 2016: In situ development of high-elevation, low-relief landscapes via duplex deformation in the Eastern Himalayan hinterland, Bhutan, in *Journal of Geophysical Research: Earth Surface*, 925–938.
- Grujic, D., Coutand, I., Bookhagen, B., Bonnet, S., Blythe, A. & Duncan, C. 2006: Climatic forcing of erosion, landscape, and tectonics in the Bhutan Himalayas, *Geology*, 34, 801–804.

P 10.6

Using UAV for studying the dynamics of an active rock glacier

Régis Meyrat, Sébastien Rüttimann, Stuart Lane & Christophe Lambiel

Institut des Dynamiques de la Surface Terrestre (IDYST), Université de Lausanne, 1015 Lausanne
(regis.meyrat@unil.ch, sebastien.ruttimann@unil.ch, stuart.lane@unil.ch christophe.lambiel@unil.ch)

Active rock glaciers are landforms conveying large amounts of sediments downslope. The monitoring of their velocities is generally made with terrestrial geodetic methods such as differential GPS (dGPS). However, the spatial resolution offered by such methods is quite low and measurements are time-consuming and might be potentially dangerous in steep and active landforms. Besides, the development of UAVs (unmanned aerial vehicles) and Structure from Motion (SfM) photogrammetry has proven to be efficient for studying topographic movements such as landslides or river bed erosion with great accuracy. The main objective of this study is thus to investigate the potential of UAVs for investigating the dynamics and monitoring the velocities of active rock glaciers.

For this we are investigating the La Roussette rock glacier, located above Arolla (VS). This active rock glacier spreads from 2750 to 2380 meters and occupies an area of 13 ha. It is made of 5 lobes composed of (pluri-)metric gneissic blocks. dGPS surveys and a fixed GPS indicate velocity rates comprised between 50 cm/y and 150 cm/y.

Up to now, one scan was made in October 2015 with a DJI Inspire1. Two additional scans were made during early summer 2016 using two types of UAVs, one eBee RTK and one DJI Phantom3 Professional. The eBee RTK needs no ground control points (GCP) for georeferencing the digital elevation model (DEM) and only one flight was required to cover the entire rock glacier. However, some UAV overheating problems were encountered due to the high altitude difference between the take-off location and the highest flight line (500 m climb), as well as lower air density and slightly stronger solar radiation. Therefore, we used the Phantom3 quadcopter to continue the study, but 14 flights were necessary to cover the rock glacier. Thirteen GCPs were measured around the rock glacier for georeferencing the DEM and a final resolution of less than 3 cm per pixel was reached.

In addition to each flight, a dGPS survey of 20 points was carried out. An additional LiDAR scan of the rock glacier was also made and will be used as a ground truth data set. Both dGPS and LIDAR data will be used to evaluate the UAV – SfM approach. Special attention was put to avoid distortion in the construction of the photogrammetric DEM by strengthening image geometry.

P 10.7

Interactions between geomorphology and vegetation in the Vaud Alps: first investigations

Elisa Giaccone¹, Grégoire Mariéthoz¹, Christophe Lambiel¹

¹ *Institute of Earth Surface Dynamics (IDYST), University of Lausanne, UNIL Moulins, CH-1015 Lausanne (elisa.giaccone@unil.ch; gregoire.mariethoz@unil.ch; christophe.lambiel@unil.ch)*

The plant succession in the high altitude areas is controlled by time since deglaciation, grain size of debris, micro-relief and soil development (Burga et al. 2010). Furthermore, the influence of earth surface processes can modify the microhabitat conditions and the species richness, composition and distribution patterns of plant communities (Le Roux & Luoto 2014). It is therefore important to study how the geomorphological activity (permafrost, cryoturbation, solifluction, nivation) affects the distribution of plant species to predict future vegetation evolution in a context of climate change.

To better understand geomorphology-vegetation interactions, three focus sites in the Vaud Alps (Martinets, Perris Blancs and Outans, see Figure 1) have been comprehensively surveyed using different methodologies to record the most relevant environmental parameters related to temperature, permafrost, vegetation and granulometry.

A total of 60 miniature temperature loggers iButton® DS1922L (accuracy ± 0.5 °C, resolution 0.0625 °C) have been installed at the ground surface at 5/10 cm of depth in different geomorphological features to investigate the occurrence of permafrost, the snow duration and the micro-climate of the ground surface. In addition, three electrical resistivity tomography profiles (ERT) were carried out on the Martinets rock glaciers to detect and map ground ice.

15 vegetation surveys were performed in different environments to identify the main aspects of the plant communities. In some cases, old surveys (Vittoz & Dessimoz 2009) were repeated to observe possible changes in the floristic composition. Moreover, a complete floristic list was achieved on the rock glaciers.

The next step of this work will involve drone surveys to obtain high resolution images allowing for a detailed granulometry analysis. Furthermore, through the comparison of images of successive years, it will be possible to analyse rock glaciers movements.

The data achieved from geomorphological and vegetational surveys will be statistically analysed (e.g. with PCA). Then, they will be used together with drone images and the DEM to create a detailed semi-automated geomorphological map with geostatistical methods (Mariéthoz et al. 2010). This methodology will allow mapping extended areas and will be used for the entire Vaud Alps. Finally a model to quantify the interactions between the earth surface processes and the plant distribution will be elaborated.

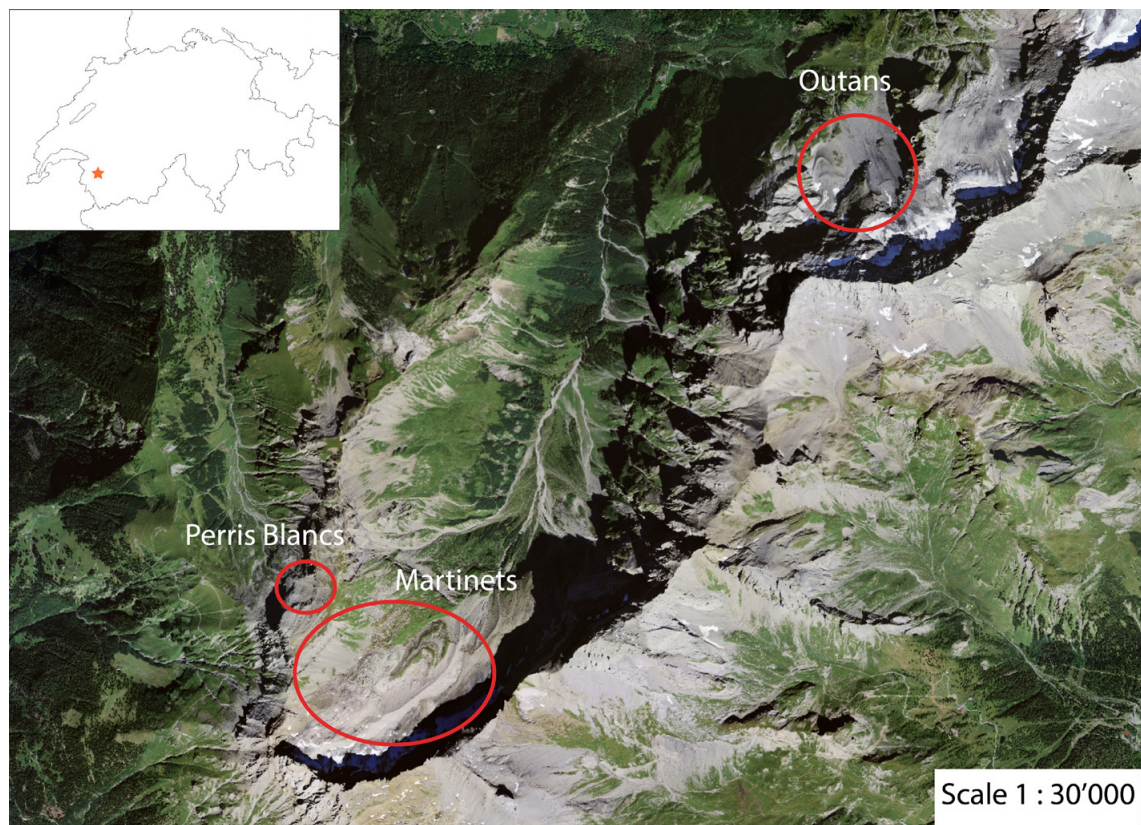


Figure 1. The focus sites.

REFERENCES

- Burga, C.A., Krüsi, B., Egli, M., Wernli, M., Elsener, S., Ziefle, M., Fischer, T., Mavris, C. 2010: Plant succession and soil development on the foreland of the Morteratsch glacier (Pontresina, Switzerland): Straight forward or chaotic? *Flora* 205, 561-576.
- Le Roux, P.C. & Luoto, M. 2014: Earth surface processes drive the richness, composition and occurrence of plant species in an arctic-alpine environment. *Journal of Vegetation Science* 25, 45-54.
- Mariethoz, G., Renard, P., Straubhaar, J. 2010: The direct sampling method to perform multiple-point geostatistical simulations. *Water Resources Research* 46, W11536.
- Vittoz, P. & Dessimoz, F. 2009: Flore vasculaire du Vallon de Nant. *Mémoire de la Société vaudoise de Sciences naturelles* 23, 85-114.

P 10.8

In-filled reservoirs serving as sediment archives to analyse soil organic carbon erosion – Taking a closer look at the Karoo rangelands

Juliane Krenz¹, Philip Greenwood¹, Brigitte Kuhn¹, Goswin Heckrath², Ian Foster³, John Boardman⁴, Michael Meadows⁵, Nikolaus Kuhn¹

¹ *Department of Environmental Sciences, Physiogeographie and Environmental Change, University of Basel, Klingelbergstrasse 27, 4056 Basel, Switzerland (juliane.krenz@unibas.ch)*

² *Department of Agroecology, Aarhus University, Blichers Allé 20, Postboks 50, 8830 Tjele, Denmark*

³ *School of Science and Technology, University of Northampton, Newton Building, NN2 6JD Northampton, United Kingdom*

⁴ *Environmental Change Institute, Oxford University Centre for the Environment, South Parks Road, OX1 3QY Oxford, United Kingdom*

⁵ *Department of Environmental and Geographical Sciences, University of Cape Town, Private Bag X3, Rondebosch 7701, South Africa*

The semi-arid rangelands of the Great Karoo region in South Africa, which are nowadays characterized by badlands on the foot slopes of upland areas and complex gully systems in valley bottoms, have experienced a number of environmental changes. With the settlement of European farmers in the late 18th century agricultural activities increased, leading to overgrazing which probably acted as a trigger to land degradation. As a consequence of higher water demands and shifting rainfall patterns, many dams and small reservoirs have been constructed to provide drinking water for cattle or to facilitate irrigation during dry periods. Most of these dams are now filled with sediment and many have become breached, revealing sediment archives that can be used to analyse land use changes as well as carbon erosion and deposition during the last ca. 100 years.

In this ongoing project, a combination of analytical methods that include drone imagery, landscape mapping, erosion modelling and sediment analysis have been employed to trace back the sediment origin and redistribution within the catchment, setting a special focus on the carbon history.

Sediment deposits from a silted-up reservoir were analysed for varying physicochemical parameters, in order to analyse erosional and depositional patterns. A sharp decrease in total carbon content with decreasing depth suggests that land degradation during and after the post-European settlement most likely triggered erosion of the relatively fertile surface soils which presumably in-filled the reservoirs. It is assumed that the carbon-rich bottom layers of the dam deposits originate from these eroded surface soils. A combination of erosion modelling and sediment analysis will be used to determine the source areas of the depositional material and might clarify the question if land degradation in the Karoo has resulted in its return from being a net sink of carbon into a net source of carbon.

P 10.9

Optical and geochemical analysis of the tephra layers from the Hinkelsmaar (Eifel region, Western Germany)

Martina Vögtli¹, Nikolaus J. Kuhn¹, Leander Franz², Christian de Capitani², & Martin Koziol³

¹ *Physiogeographie und Umweltwandel, University of Basel, Klingelbergstrasse 27, CH-4056 Basel (martina.voegtli@stud.unibas.ch)*

² *Mineralogisch-Petrographisches Institut, Bernoullistrasse 30, CH-4056 Basel*

³ *Maarmuseum Manderscheid & Rheinland-Pfälzische Umweltbildungsstation, Wittlicher Strasse 11, D-54531 Manderscheid*

Sediments deposited in Maar craters can often be used as environmental archives. To do so, dating the age of the maar and the sediment is critical. While methods such as isotope geochronology or thermoluminescence are widespread, their cost is often prohibitive, in particular within a small project and just a rough estimate is required. Identifying layers of sediment associated with a known event provides an inexpensive alternative, but also requires careful analysis.

The Hinkelsmaar is one of the five craters of the Mosenberg-group in the German Eifel region. Its vent was created through a phreatomagmatic explosion and the maar itself is built up from slag, tephra and lava shreds and filled with lake sediments and peat. The accumulation of the sediment started approximately 28'400 BP (Juvigné et al. 1988). In the course of practical studies in environmental reconstruction, drill cores were taken in the central part of the Maar using a Swedish rock drill. Each core recovered 0.5 meters to a depth of 7 meters. Three tephra layers were discovered at a depth of 2.85-2.93 m (T1), at 3.73-3.76 m (T2) and at 5.32-5.35 m (T3). These three layers offer the opportunity to date the sediments. The occurrence of three layers in the Hinkelsmaar has not been documented so far.

From the soft rock material of the three tephra layers, organics were removed by H₂O₂. Afterwards, the rock material was sieved and 25 grain mounts were prepared. The petrography of the grain mounts was investigated using a polarization microscope and Raman spectrometer while the chemical composition of volcanic glass shards was determined by electron microprobe analysis. For comparison, thin sections from tephra eruptions of nearby maar lakes were studied.

The grain mounts from the two upper tephra layers T1 and T2 are petrographically very similar with the dominant magmatic minerals aegirine-augite, Ti-hornblende and sanidine as well as accessory titanite. Shards of both layers revealed a trachytic to phonolitic composition. The mineral ratios and the geochemistry of the shards are characteristic for the MLST and ULST tephra units of the Laacher See (see Fig. 1; cf. Bogaard & Schmincke 1985), which erupted 12'900 years ago in the East Eifel region.

The deepest tephra layer T3 showed a totally different petrography with plenty of olivine, Ti-augite and very few ultramafic (tephritic to foiditic) volcanic glass shards. Most probably, this layer belongs to the ultramafic tephra eruption of the Schalkenmehrener Maar in the West Eifel region, which erupted 20'000 – 25'000 year BP (Sirocko et al. 2012).

The results show that the Hinkelsmaar has more tephra layers than previously documented. Their mineralogical, petrographic and geochemical analysis offers the opportunity to contribute to a better understanding of the sequence of late Holocene volcanic eruptions in the Eifel. Especially the geochemistry of relatively instable phases like volcanic glass is well suitable for the identification of specific eruptions.

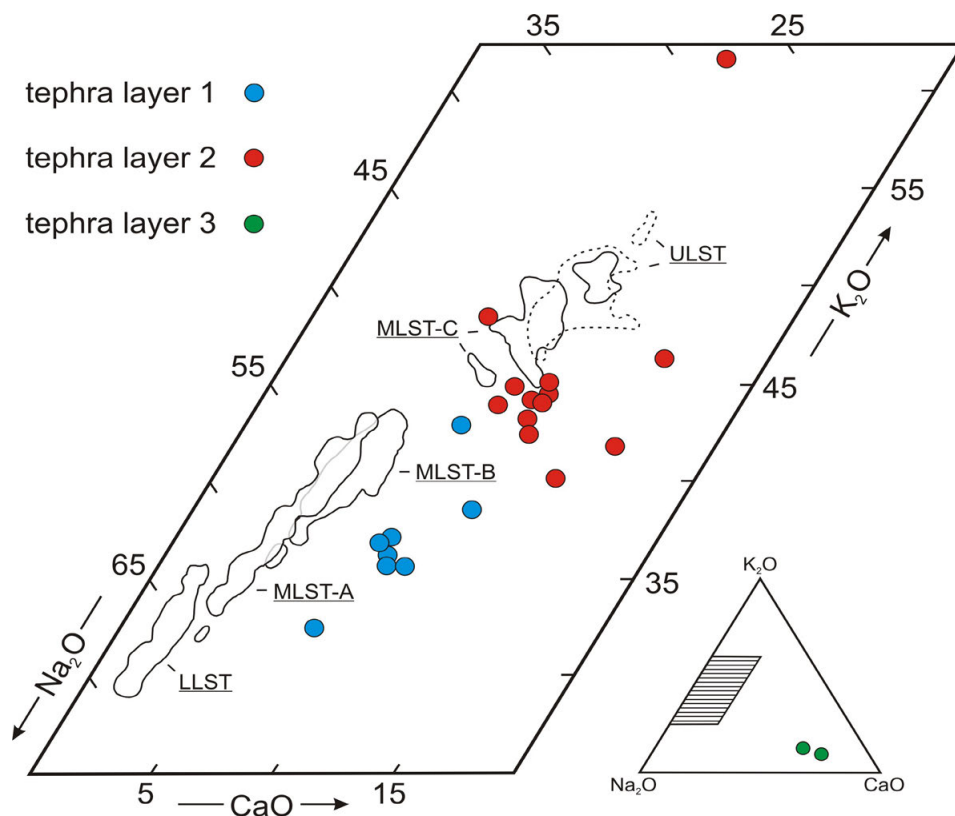


Figure 1: Microprobe analyses of glass shards from the three tephra layers of the Hinkelsmaar in the Na₂O-K₂O-CaO-plot. Distributive fields for glass shards from the LLST, MLST and ULST eruptions from the Laacher See are from Bogaard & Schmincke (1985).

REFERENCES

- Bogaard, P. & Schmincke, H.-U. (1985) Laacher See Tephra: A widespread isochronous late Quaternary tephra layer in central and northern Europe. *Geological Society of America Bulletin*, 96, 1554-1569.
- Juvigné, E., Boenigk, W., Brunnacker, K., Duchesne, J.C. & Windheuser, H. (1988) Zur Schlotfüllung des Hinkelsmaar (Eifel, Deutschland): Alter und Genese. *Stuttgart*, 544-561.
- Sirocko, F., Dietrich, S., Veres, D., Grootes, P.M., Schaber-Mohr, K., Seelos, K., Nadeau, M., Kromer, B., Rothacker, L., Röhrner, M., Krbetschek, M., Appleby, P., Hambach, U., Rolf, C., Sudo, M. & Grim, S. (2012) Multi-proxy dating of Holocene maar lakes and Pleistocene dry maar sediments in the Eifel, Germany. *Quaternary Science Review*, 62 (2013), 57.

P 10.10**Generation of waterfalls at intermittently alluviated fault scarps releases tectonic forcing on a climatic beat**

Luca C. Malatesta*†, Michael P. Lamb*

*Division of Geological and Planetary Sciences, California Institute of Technology, Pasadena, CA 91125, USA

† luca@caltech.edu

Waterfalls commonly exist near bounding faults of mountain ranges, where erosional bedrock catchments transition to depositional alluvial fans. We hypothesize that aggradation on alluvial fans can bury active faults, and that the faults accumulate slip in the subsurface to produce a bedrock scarp. Following entrenchment of the alluvial fan, the scarp can be exposed as a waterfall. To explore this hypothesis, we derive a geometric model for waterfall height which depends on alluvial fan length and the relative timescales of tectonic uplift, a forcing time for cycles of fan aggradation and entrenchment, and a response time for fan aggradation to respond to changes in sediment flux. We find that the model is consistent with observations at Gower Gulch, Death Valley, CA, where a man-made drainage capture event in 1941 caused rapid fan incision and exposed a waterfall at the canyon-fan transition. We also compare the model to 62 Pleistocene waterfalls in 18 catchments of the Death Valley area, and find that at least 15 of the waterfalls are best explained by the fault burial mechanism. Using field measurements of grain size and channel geometries, we show that the fault-burial mechanism can produce the observed waterfall heights, measuring 4 to 19 m, under a uniform climatic forcing requiring variations of 20% in precipitation during the Late Pleistocene. The fault burial mechanism, through the creation of upstream propagating waterfalls, may allow catchment-fan systems to experience frequent cycles of enhanced erosion in catchments and deposition on fans, that likely convolves tectonic and climatic signals.

P 10.11

Environmental control on erosion along the entire western margin of Peru

Regina Reber¹, Camille Litty¹, Andrea Madella¹, Romain Delunel¹, Naki Akçar¹, Marcus Christl² and Fritz Schlunegger¹,

¹ *Institut für Geologie, Universität Bern, Baltzerstrasse 1+3, CH-3012 Bern (rreber@geo.unibe.ch)*

² *Laboratory of Ion Beam Physics (LIP), ETH Zürich, Otto-Stern-Weg 5, CH-8093 Zürich*

We report catchment-wide denudation rates for 62 watersheds along the entire western Andean margin of Peru inferred from in-situ cosmogenic ¹⁰Be analyses. Spatially averaged denudation rates range from ca. 0.1 mm/kyr to 400 mm/kyr and positively correlates with the mean elevation and drainage area of the catchments. No correlations have been found with the tectonic settings in the sense that neither the subduction of the Buoyant Nazca ridge nor neo-tectonic uplift in southern Peru appear to drive erosion. Furthermore, valleys hosting cut and fill terrace sequences yield the highest denudation rates. We interpret the positive correlations observed between denudation and elevation and drainage area of the basins as the illustration of an environmental control on erosion, mainly because of the altitudinal dependency of modern precipitation. It thus appears that larger basins situated at higher elevations have large runoff and thus experience more erosion. Furthermore, cut and fill terraces in Peru have been related to shifts in the position of the Intertropical Convergence Zone (ITCZ), which adds a strong episodicity on climate, thereby driving the formation of terraces where high erosion rates have been measured (Bekaddour et al., 2014). Accordingly, the high modern rates reported here could either reflect the recycling of the terrace material or point to the erosive power of a more episodic and thus stormier climate.

REFERENCES

Bekaddour, T., Schlunegger, F., Vogel, H., Delunel, R., Norton, K., Akcar, N., & Kubik, P., 2014: Paleo erosion rates and climate shifts recorded by Quaternary cut-and-fill sequences in the Pisco valley, central Peru, *Earth and Planetary Science Letters*, 390, 103-115.

11. Quaternary environments: landscapes, climate, ecosystems, human activity during the past 2.6 million years

Irka Hajdas, Christine Pümpin, Susan Ivy Ochs, Naki Akçar, Gaudenz Deplazes, Jean Nicolas Haas, Stéphanie Girardclos

Swiss Society for Quaternary Research (CH-QUAT)

TALKS:

- 11.1 Abbott P., Davies S., Griggs A., Bourne A.: TRACEing Last Glacial Period (25-80 ka b2k) tephra horizons within North Atlantic marine cores
- 11.2 Boxleitner M., Maisch M., Brandova D., Egli M., Ivy Ochs S., Christl M.: Surface exposure dating of Lateglacial and Holocene glacier extents in the Canton of Uri, Switzerland
- 11.3 Claude A., Akçar N., Ivy-Ochs S., Schlunegger F., Kubik P.W., Christl M., Vockenhuber C., Dehnert A., Kuhlemann J., Meinert R., Schlüchter C.: Landscape evolution of the northern Alpine Foreland: constructing a temporal framework for early to middle Pleistocene glaciations
- 11.4 Diaz N., Dietrich F., Sebag D., King G.E., Valla P.G., Deschamps P., Herman F., Verrecchia E.P.: Evolution of a Sudano-Sahelian paleoenvironment since the late MIS-2 (Far N Cameroon, Chad Basin)
- 11.5 Dietrich F., Diaz N., Deschamps P., Sebag D., Verrecchia E.P.: Tracking the calcium over the last 20ky: the meaning of calcitic pedogenic nodules in a silicate watershed (northern Cameroon)
- 11.6 Dubois N., Jacob J.: Molecular biomarkers of anthropic impacts in natural archives
- 11.7 Gordijn T., Hippe K., Hajdas I., Ivy-Ochs S., Picotti V., Christl M.: Characterization of sediment storage with cosmogenic nuclides, a study of a fluvial catchment on the Bolivian Altiplano
- 11.8 Haas M., Baumann F., Reusch A., Strasser M., Eglinton T.I., Dubois N.: Historical evolution of human land-use in the catchment of Lake Murten
- 11.9 Lehmann B., Valla P.G., King G.E., Ivy-Ochs S., Christl M., Herman F.: Reconstruction of glacier fluctuations in the Mont-Blanc massif, western Alps: a multi-method approach
- 11.10 Morlock M., Vogel H., Nigg V., Hasberg A., Melles M., Russell J.M., Bijaksana S. & the TDP science team: Geochemical characterisation of Lake Towuti, Indonesia: setting the stage for climate reconstructions over several glacial-interglacial cycles
- 11.11 Mozafari Amiri N., Tikhomirov D., Özkaymak Ç., Sümer Ö., Uzel B., Ivy-Ochs S., Vockenhuber Ch., Sözbilir H., Akçar N.: Holocene seismic activity of the Yavansu fault, western Turkey
- 11.12 Normand R., Simpson G., Bahroudi A.: Tectonic geomorphology of the western Makran subduction zone: Evidence of past megathrust earthquakes?
- 11.13 Schwörer C., Gavin D., Walker I., Hu F.S.: Holocene treeline changes in the Canadian Cordillera are controlled by climate and local topography
- 11.14 Silva, T.A., Girardclos, S., Vogel, H., Loizeau, J.L.: Geochemical dataset of the Rhone River delta (Lake Geneva) sediments – disentangling human impacts from climate change

- 11.15 Spangenberg J.E., Vogiatzaki M., Zufferey V.: Effects of climate change on Swiss wine – a VOCs and multi-isotope study
- 11.16 Wüthrich, L., Hepp, J., Bromm, T., Benesch, M., Bliedtner, M., Schäfer, I.K., Zech, J., Glaser, B., Rozanski, K., Sirocko, F., Zech, R., Zech, M.: A relative humidity record for the Late Glacial to Holocene transition from the Gemündener Maar, Germany

POSTERS:

- P 11.1 Anspach J., Lupker M., Haghypour N., Eglinton T.: Biomarker Signature of Greenland Sediments: from modern Rivers and Soils to MIS 5e and 11 Records
- P 11.2 Bliedtner M., Suchodoletz H. v., Schäfer I.K., Zech J., Zielhofer C., Zech R.: Leaf waxes and compound-specific δD analyses in a Holocene fluvial sediment-paleosol sequence from the upper Alazani River, SE-Georgia
- P 11.3 Braakhekke J., Ivy-Ochs S., Hajdas I., Monegato G., Gianotti F., Christl M.: The Last Glacial Maximum around Lago d'Orta, Northern Italy; a multi method reconstruction
- P 11.4 Eggenschwiler L., Picotti V., Cherubini P., Hajdas I., Saurer M., Via G.B., Marabini S.: Using Stratigraphy and Dendrochronology near Tebano, Senio Northern Apennines to Analyze the Impact of Climatic Fluctuation at Certain Frequencies
- P 11.5 Eymard I., Alvarez M.d.P., Bilmes A., Dobra M.G., Suarez F., Vasconcelos C., Arizteguí D.: Stromatolites growth in a freshwater environment from Northeastern Patagonia (Argentina)
- P 11.6 Hajdas I., Maurer M., Röttig M.B., Chevrier B., Martinez M.L., Loukou S., Mayor A., Pollarol L., Rasse M., Garnier A., Lespez L., Tribolo C., Lebrun B., Camara A., Bocoum H., Huysecom E.: Radiocarbon Chronology of Human Settlement and paleo environment in Senegal, West Africa
- P 11.7 Ivy-Ochs S., Wirsig C., Zasadni J., Hippe K., Christl M., Akçar N., Schluochter C.: Into and out of the Last Glacial Maximum in the Alps
- P 11.8 Jiménez-Morillo N.T., Spangenberg J.E., González-Pérez J.A., Jordán A., Zavala L.M., González-Vila F.J.: Wildfire effects on lipid composition and hydrophobicity in bulk soil and soil size fractions
- P 11.9 Kronig O., Reitner J.M., Christl M., Ivy-Ochs S.: Dating the stabilisation age of relict rockglaciers
- P 11.10 LeKieffre C., Spangenberg J.E., Mabilieu G., Meibom A., Geslin E.: A benthic foraminifera species respond to anoxia with a strong metabolic shift suggesting a state of dormancy

- P 11.11 Marchegiano M., Horne D., Gliozzi E., Francke A., Ariztegui D.: Application of the Mutual Ostracod Temperature Range method (MOTR) to a sediment core from Lake Trasimeno (Umbria, central Italy)
- P 11.12 Moretti S., Jaccard S., Montluçon D., Martínez-García A., Eglinton I.T.: Iron fertilization in the Subantarctic Indian Ocean during the last glacial cycle and the drawdown of atmospheric CO₂
- P 11.13 Neugebauer I., Plessen B., Dinies M., Engel M., Tjallingii R., Brauer A.: Centennial-scale variability of the Early Holocene Humid Period in NW Arabia inferred from high-resolution geochemistry and microfacies of the Tayma palaeolake
- P 11.14 Opyrchał E., Zasadni J., Kłapyta P., Christl M., Ivy-Ochs S.: Lateglacial deglaciation of the High Tatra Mountains
- P 11.15 Patra S., Akçar N., Ivy-Ochs S., Monegato G.: Tracking the pace of Middle Pleistocene Revolution in the southern Alpine Foreland
- P 11.16 Saracoğlu D., Hajdas I., Maurer M., Röttig M.B., Ivy-Ochs S., Synal H.A.: Re-visiting radiocarbon ages of Oetzi the Ice Man
- P 11.17 Schäfer I.K., Bliedtner M., Wüthrich L., Wolf D., Zech J., Faust D., Zech R.: Leaf waxes and compound-specific isotopes indicate more humid conditions in Spain during the LGM
- P 11.18 Spangenberg J.E.: Multiple stable isotope analysis of vegetable oils from the southern and northern hemispheres: increasing an archaeological/paleoclimatic database
- P 11.19 Fabbri S.C., Weiss B.J., Hübscher C., Horstmeyer H., Schmelzbach C., Buechi M.W., Herwegh M., Schlunegger F., Anselmetti F.S.: Subaquatic moraine amphitheatre in Lake Thun
- P 11.20 Struck J., Sparrenberg S.F., Kühn P., Schneider R., Thiele-Bruhn S., Zech J., Zech R., Zander A., Weidenfeller M.: Multiproxy Analysis and Pedosedimentary Reconstruction of Loess-Paleosol Sequences on two Pleistocene Fluvial Terraces of the Mosel
- P 11.21 Strupler M., Hilbe M., Flavio S. Anselmetti, Fleischmann T., Kopf A.J., Strasser M.: Probabilistic stability evaluation and seismic triggering scenarios of submerged slopes in perialpine Lake Zurich
- P 11.22 Yeşilyurt S., Doğan U., Akçar N., Yavuz V., Ivy-Ochs S., Vockenhuber C., Schlunegger F., Schlüchter C.: Late Quaternary Glaciations of Kavuşşahap Mountains

11.1

TRACEing Last Glacial Period (25-80 ka b2k) tephra horizons within North Atlantic marine cores

Peter Abbott¹, Djordje Grujic², Isabelle Coutand², Frédéric Herman³

¹ *Institute of Geology, University of Bern*

² *Department of Earth Sciences, Dalhousie University*

³ *Institute of Earth Surface Dynamics, University of Lausanne*

The Himalayan foreland fold-and-thrust belt is made of Neogene synorogenic sediments of the Siwalik Group and accommodates a large fraction of the India-Eurasia convergence. This region receives high precipitation and experiences seismic events of M8 and larger. Along the strike of the 2500-km-long orogenic arc, the eastward narrowing of the fold-and-thrust belt has been attributed to increasing annual rainfall and specific stream power, rather than to lateral changes in shortening rates. However, exhumation/erosion rates of this unit remain unknown. Precisely constraining the erosion rates of this unit at the scale of the orogen would allow an estimate of the relative contributions of tectonic and climatic processes to the erosion of the youngest and frontal part of the Himalayan orogen.

Thermochronometry enables the cooling, and therefore exhumation/erosion histories of rocks to be determined. However the exhumation histories of the Siwalik Group, which have experienced limited burial heating not exceeding ~100-50 °C remain very difficult to constrain using traditional thermochronometers. Optically stimulated luminescence (OSL)-thermochronometry is a recently developed very low temperature thermochronometer sensitive to temperatures of 30-90 °C. Consequently, its application to the Siwalik deposits may provide insights into their cooling and exhumation histories.

K-feldspar extracts from 18 sandstones samples of the Siwalik Group were investigated using a multi-OSL-thermochronometry approach, whereby four different signals, with different thermal stabilities were measured for each sample. The sandstone samples were collected along two traverses across the Himalayan fold-and-thrust belt in western Nepal, and eastern Bhutan. Using signals with different thermal sensitivities enables high precision Quaternary cooling histories to be derived. These data were inverted using a Bayesian approach resulting in preliminary cooling rates of ~100 °C/Myr during the last 0.2 Ma, which were broadly consistent between samples, indicating similar rates of cooling. These preliminary results suggest that estimated erosion rates over the foothills of the Himalaya are up to one order of magnitude higher than the longer-term erosion rates (1-3 mm/yr) documented in the hinterland of the orogen.

11.2

Surface exposure dating of Lateglacial and Holocene glacier extents in the Canton of Uri, Switzerland

Max Boxleitner¹, Max Maisch¹, Dagmar Brandova¹, Markus Egli¹, Susan Ivy Ochs², Marcus Christl²

¹ Geographisches Institut, Universität Zürich, Winterthurerstrasse 190, CH-8050 Zürich

² Labor für Ionenstrahlphysik, ETH Zürich, Otto-Stern-Weg 5, CH-8093 Zürich

Moraines as witnesses of former climate-driven glacier-extents can be dated with the help of cosmogenic nuclides. Especially ¹⁰Be has been used in this context to constrain the deposition ages of glacial deposits throughout the Alps. Moraines built up during glacier readvance phases after the Last Glacial Maximum (LGM) can be found in many main valleys and their tributaries as in the catchment of the former Reuss-glacier (see Figure 1).

In order to develop an absolute post-LGM chronology of the local glacial development we identified and studied key sites (in the upper part) of the canton of Uri. Based on former work by Renner (1982) and Spillmann et al. (2011) we concentrated our efforts particularly on the Meiental and the Göscheneralp area, because various moraine sequences along these valleys are rather pronounced and well preserved.

So far we have dated more than 30 rock-samples from boulders of different moraine complexes. Our results show that the glacial deposits can be attributed to different distinct glacier readvances between the Oldest and the Younger Dryas, i.e. the time span between 10 – 16 kyrs BP.

With our research we want to contribute to a refined understanding of the glacier and climate history in Switzerland during the alpine Lateglacial. Combining the dating results with ongoing estimates of equilibrium line altitudes (ELA) of selected glacier stadials will certainly improve the knowledge about the time scale and the local to regional landscape evolution from the LGM to the beginning of the Holocene.

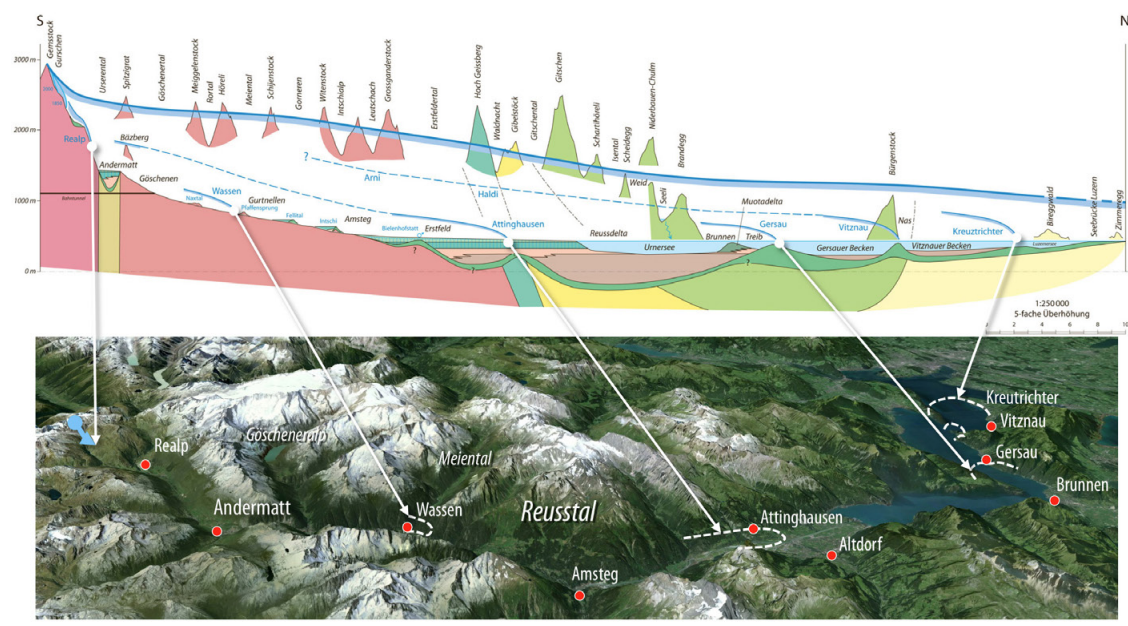


Figure 1. Longitudinal Profile and panoramic view of the Reuss-valley with Lateglacial glacier extents indicated (based on F. Renner; Spillmann et al., 2011; digital terrain model with Google Earth).

REFERENCES

- Renner, F. 1982: Beiträge zur Gletschergeschichte des Gotthardgebietes und dendroklimatologische Analysen an fossilen Hölzern. Physische Geographie, Vol. 8, Universität Zürich.
- Spillmann, P., Labhart, T., Brücker, W., Renner, F., Gisler, C. & Zraggen A. 2011: Geologie des Kantons Uri. Naturforschende Gesellschaft Uri – Bericht Nr. 24, 224 S.

11.3

Landscape evolution of the northern Alpine Foreland: constructing a temporal framework for early to middle Pleistocene glaciations

Anne Claude¹, Naki Akçar¹, Susan Ivy-Ochs², Fritz Schlunegger¹, Peter W. Kubik², Marcus Christl², Christof Vockenhuber², Andreas Dehnert³, Joachim Kuhlemann³, Meinert Rahn³ & Christian Schlüchter¹

¹ *Institute of Geological Sciences, University of Bern, Baltzerstrasse 1-3, CH-3012 Bern, (anne.claude@geo.unibe.ch)*

² *Laboratory of Ion Beam Physics (LIP), ETH Zurich, Otto-Stern-Weg 5, CH-8093 Zurich*

³ *Swiss Federal Nuclear Safety Inspectorate ENSI, Industriestrasse 19, CH-5200 Brugg*

The Deckenschotter deposits are believed to represent the oldest Quaternary sediments in the Alpine Foreland and are thus a sedimentary archives documenting palaeoenvironmental changes during the Quaternary. In the Swiss Alpine Foreland, sediments of the Deckenschotter represent proximal glaciofluvial gravels, which accumulated via meltwater during repeated glaciations of the Alps and the foreland. They lie unconformably on Tertiary Molasse or Mesozoic carbonate bedrock.

Lithostratigraphic positions of the Deckenschotter deposits in Switzerland have been extensively studied. However, compared to late Quaternary glaciations, the timing of these accumulations is poorly constrained. The aim of this study is to shed light on this timing and hence on the landscape evolution of the northern Alpine Foreland. We studied seven different sites: Hohle Gasse in Pratteln (BL), Mandach (AG), Ängi (AG), Rechberg, Siglistorf (AG), Stadlerberg (ZH) and Irchel (ZH) where different outcrops were investigated (Akçar et al. 2014; Claude et al. accepted; Claude et al. in review). We established their chronology using both depth-profile and isochron burial dating with ¹⁰Be, ²⁶Al and ³⁶Cl. Furthermore, detailed investigations of clast fabrics, petrographic compositions and clast morphometries enable the identification of sediment provenance and the interpretation of their transport mechanisms and depositional environments.

Our results show that a first gravel accumulation, depositing the sediments in Siglistorf, Stadlerberg and Irchel occurred at around 2 Ma, with most of the sediments originating from the northern central Alps or being reworked from the Miocene Molasse conglomerates (Claude et al., accepted). A fingerprint of the Linth paleoglacier is recognized in the sediments. At that time, the Alpine Rhine was draining through Lake Constance into the Danube River and eastwards into the Black Sea. A second phase of gravel accumulation was observed at around 1 Ma, coinciding with the Mid-Pleistocene Revolution, accumulating the gravels in Mandach, Ängi, Rechberg and Irchel. Sedimentological analyses showed that these sediments were derived either from the northern central and central eastern Alps or were reworked from the Molasse in the Alpine Foreland. In addition to the Linth paleoglacier, a fingerprint of the Rhaetian and Reuss paleoglaciers were observed. During the second accumulation phase, the Alpine Rhine was already redirected westwards into the Upper Rhine Valley from where it drained northwards into the North Sea.

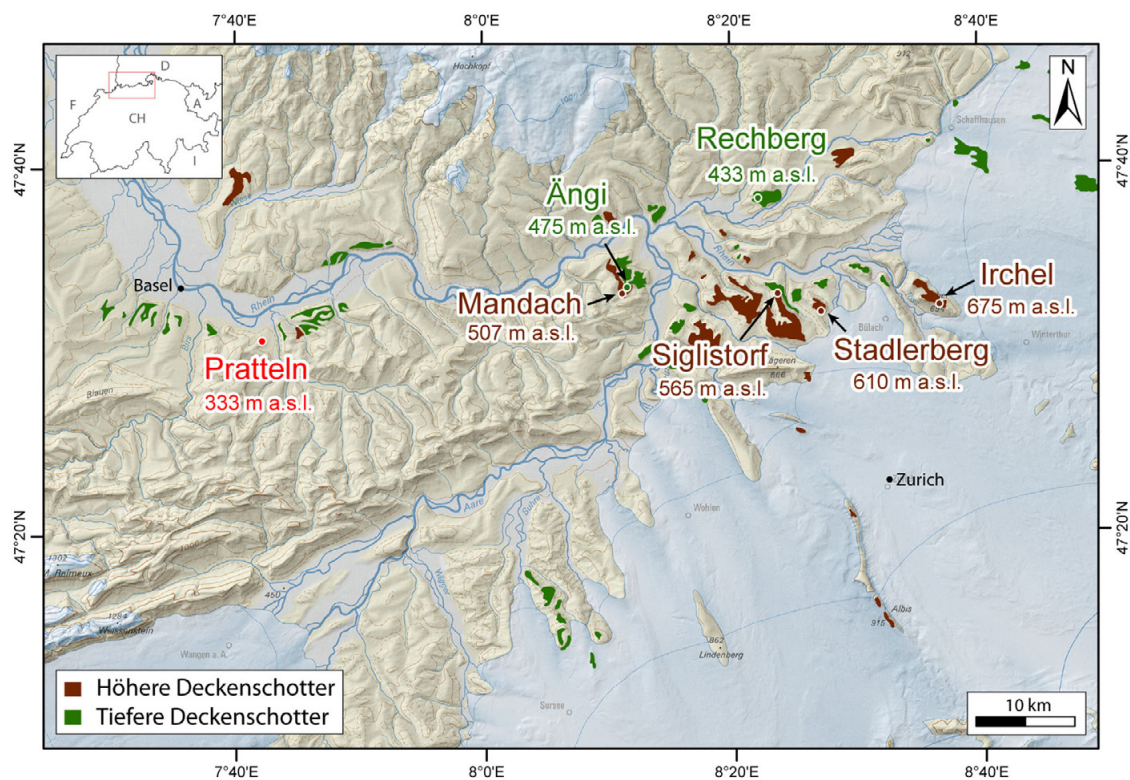


Fig. 1 Location of the study sites and distribution of the Deckenschotter in the northern Alpine Foreland (©Federal Office of Topography, swisstopo, CH-3084 Wabern).

REFERENCES

- Akçar, N., Ivy-Ochs, S., Alfimov, V., Claude, A., Graf, H.R., Dehnert, A., Kubik, P.W., Rahn, M., Kuhlemann, J., Schlüchter, C. (2014). The first major incision of the Swiss Deckenschotter landscape. *Swiss Journal of Geosciences*, 107, 337-347.
- Claude, A., Akçar, N., Ivy-Ochs, S., Schlunegger, F., Kubik, P.W., Dehnert, A., Kuhlemann, J., Rahn, M., Schlüchter, C. Timing of early Quaternary gravel accumulation in the Swiss Alpine Foreland. Accepted in *Geomorphology*.
- Claude, A., Akçar, N., Ivy-Ochs, S., Schlunegger, F., Rentzel, P., Pümpin, C., Tikhomirov, D., Kubik, P.W., Vockenhuber, C., Dehnert, A., Rahn, M., Schlüchter, C. Chronology of terrace formation in Pratteln, Hohle Gasse. In review at *Swiss Journal of Geosciences*.

11.4

Evolution of a Sudano-Sahelian paleoenvironment since the late MIS-2 (Far N Cameroon, Chad Basin)

Nathalie diaz¹, Fabienne Dietrich¹, David Sebag², Georgina E. King^{1,3}, Pierre G. Valla¹, Pierre Deschamps⁴, Frédéric Herman¹, Eric P. Verrecchia¹

¹ *Institute of Earth Surface Dynamics, University of Lausanne, Switzerland (corresponding author nathalie.diaz@unil.ch)*

² *Department of Geosciences and Environment, University of Rouen, France & IRD, Hydrosociences Montpellier, LMI Picass'Eau, University of Ngaoundéré, Cameroon*

³ *Institute of Geography, University of Cologne, Germany*

⁴ *CEREGE, Aix-Marseille Université-CNRS-IRD. France*

Soil relics enriched in pedogenic carbonate nodules occur in the southern part of Chad Basin in the Diamare piedmont (Far North Cameroon). They form widespread mima-like mound morphologies within stream networks. They are interpreted as Vertisol relics resulting from pedogenesis and erosion processes likely inherited from Quaternary climatic changes (Diaz et al., 2016). Vertisol relics are considered as pedo-sedimentary records and associated carbonate nodules are used as time and paleoenvironmental archives.

Pedogenic carbonate nodules are composed of a soil matrix (40-30 wt%), with primary and secondary minerals, and few organic matter (OM), cemented by calcite (60-70 wt%). The chronology was investigated with luminescence dating applied to K-feldspars with the aim of assessing the soil parent material deposition time. Radiocarbon dating of both OM and calcitic cements aim to estimate the time at which soils were developing and when carbonate precipitated, respectively. Finally, carbon ($\delta^{13}\text{C}_{\text{inorg}}$) and oxygen ($\delta^{18}\text{O}_{\text{inorg}}$) isotopic compositions of carbonate nodules, as well as carbon ($\delta^{13}\text{C}_{\text{org}}$) isotopic compositions of OM, aim to establish the paleoenvironmental conditions, precisely.

Results show that Vertisol relics registered four main environmental events during the last 20 ka: i) the soil parent material deposited from 18 to 12 ka BP, during the Bossoumian drier phase and the African Humid Period (AHP) onset, i.e. the end of Marine Isotopic Stage MIS-2 (Hervieu, 1969; DeMenocal et al., 2000; Holland et al., 2013); ii) the soil organic matter ages range from 11 to 8 ka cal BP, showing that soil dynamics were effective during the Main Humid phase (Armitage et al., 2015), i.e. onset of MIS-1; iii) the carbonate nodule precipitation occurs from 7 to 5 ka cal BP, at the end of the AHP, i.e. during a critical time; iv) finally, an erosion phase, not dated, but likely from the post-AHP, raises the question of a possible human impact.

The $\delta^{13}\text{C}_{\text{inorg}}$ values (9-7‰) shows that the carbonate C source is the soil OM and the $\delta^{13}\text{C}_{\text{org}}$ (20-25‰) suggest that the vegetation during the AHP corresponded to an open woodland (Cerling, 2014). $\delta^{13}\text{C}_{\text{inorg}}$ and $\delta^{18}\text{O}_{\text{inorg}}$ (8-7‰) become heavier with carbonate nodule ages at a critical time, suggesting that carbonate precipitation is likely linked to a shift in climatic conditions due to the southern monsoon front migration, inducing drier conditions and a decrease of the woodland cover. To conclude, pedo-sedimentary sequences are thus precious terrestrial archives and record environmental changes dating from the Late Pleistocene-Holocene climatic changes in the Chad Basin.

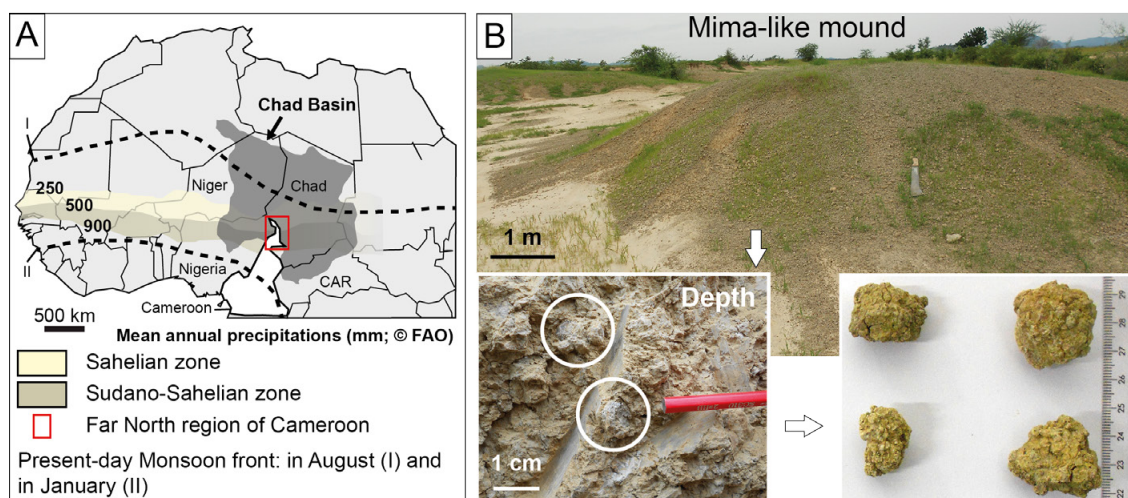


Figure 1. Study site and sample description. A) Study site (red square) is located in the southern part of the Chad Basin along the Sudano-Sahelian climatic zone. Dashed lines show the mean monsoon front position in August and in January (Nicholson, 2009). B) Mima-like mound and pedogenic carbonate nodules found at the surface and within soil.

REFERENCES

- Armitage, S.J., Bristow, C.S. & Drake, N.A., 2015: West African Monsoon Dynamics Inferred from Abrupt Fluctuations of Lake Mega-Chad. *PNAS* 112, 8543-8548.
- Cerling, T.E., 2014: Stable Isotope Evidence for Hominin Environments in Africa, in: Holland, H., Turekian, K. (Eds.), *Treatise on Geochemistry*. Elsevier, Amsterdam, Netherland.
- DeMenocal, P.B., Ortiz, J., Guilderson, T., Adkins, J., Sarnthein, M., Baker, L. & Yarusinsky, M., 2000: Abrupt onset and termination of the African Humid Period: rapid climate responses to gradual insolation forcing. *Quaternary Science Reviews* 19, 347-361.
- Diaz, N., Dietrich, F., Cailleau, G., Sebag, D., Ngounou Ngatcha, B., Verrecchia, E.P., 2016: Can mima-like mounds be Vertisol relics (Far North Region of Cameroon, Chad Basin)? *Geomorphology* 261, 41-56.
- Hervieu, J., 1969: *Le Quaternaire du Nord-Cameroun Schéma d'évolution Géomorphologique et Relations avec la Pédogenèse*. ORSTOM, Yaoundé, pp. 1-32.
- Holland, A.R., Petsch, S.T., Castaneda, I.S., Wilkie, K.M., Burns, S.J. & Birgham-Grette, J., 2013: A biomarker record of Lake El'gygytgyn, Far East Russian Arctic: investigating sources of organic matter and carbon cycling during marine isotope stage 1-3. *Climate of the Past* 9, 243-260.
- Nicholson, S.E., 2009: A revised picture of the structure of the "monsoon" and land ITCZ over West Africa. *Climate Dynamics* 32, 1155-1171.

11.5

Tracking the calcium over the last 20ky: the meaning of calcitic pedogenic nodules in a silicate watershed (northern Cameroon)

Fabienne Dietrich¹, Nathalie Diaz¹, Pierre Deschamps², David Sebag³ & Eric P. Verrecchia¹

¹ *Institute of Earth Surface Dynamics, University of Lausanne, Switzerland (corresponding author fabienne.dietrich@unil.ch)*

² *CEREGE, Aix-Marseille Université-CNRS-IRD. France*

³ *Department of Geosciences and Environment, University of Rouen, France & IRD, Hydrosociences Montpellier, LMI Picass'Eau, University of Ngaoundéré, Cameroon*

Calcium (Ca) is a key element of the earth system and is closely related to the carbon (C) cycle. The weathering of terrestrial silicate releases Ca that is exported to the ocean and sequestered in marine carbonate. However, a second Ca-trapping pathway involves some types of terrestrial carbonate.

The Diamaré piedmont (Far North Cameroon) provides an example of such pedogenic Ca-carbonate accumulations in silicate settings. Nodules are associated with a clay-rich parent material deposited between 18 and 12 ka BP, which covers either a granitic or a greenstone bedrock. They are related to Vertisols developed in the clay-rich parent material and are inherited from the African Humid Period (Diaz et al., 2016a, b). In the present-day, Vertisols are degraded soils and are not functioning as such anymore.

In this peculiar context, the amount of pedogenic calcitic nodules represents large quantities of Ca and C. This raises questions about the sources and dynamics of Ca through time. Moreover, the origin of the clay-rich parent material is also a key point in order to better understand the processes associated with the formation of Ca-carbonate nodules. To answer these questions, geochemistry of major elements, Sr and Nd isotopes have been applied to nodules, their surrounding soils, and the two different bedrocks.

Sr isotopes show that the main Ca source of carbonate nodules is the plagioclases from the local bedrocks, in contrast with other studies on terrestrial carbonate, emphasizing the dominance of allochthonous sources (Chiquet et al., 1999; Van der Hoven & Quade, 2000). The clay-rich parent material is a mixture of the local bedrock and aeolian dust. The distribution of the major elements in the soils highlights three main geochemical pathways: i) heritage from primary crystalline rocks; ii) weathering and secondary neoformation, iii) and then nodule precipitation.

Using this dataset, it is possible to propose a timeline for these different pathways involving Ca (Fig 1). First, a humid period produced weathering material, which is then mixed with aeolian dust between 18 and 12ky BP, to form the clay-rich parent material. Ca stocks were mainly in the granite (in plagioclases). Vertisols developed during a second stage between 11 and 8 ka cal BP (Diaz et al, 2016b). Ca was located mainly in the plagioclases found in the CRPM and the soil solution. Carbonate nodules precipitated between 7 and 5 ka cal BP. This time, Ca was relocated in carbonate nodules. Finally, an erosion phase led to the accumulation of carbonate nodules and the landscape observed today. Thus, the system being conservative through time, Ca is relocated from granite to carbonate nodules. Moreover, as the Ca sources of the carbonate nodules were silicates from bedrocks, these nodules represent a past C sink.

Finally, this system probably extends beyond Far North Cameroon. Indeed, similar features in other silicate watersheds have been observed all along the Sudano-Sahelian belt. Preliminary radiocarbon dates show that nodules from Mali, Niger, and Burkina Faso have similar ages to those from northern Cameroon. Thus, the impact of such carbonate nodules on the global carbon budget could be significant when considered at the African scale.

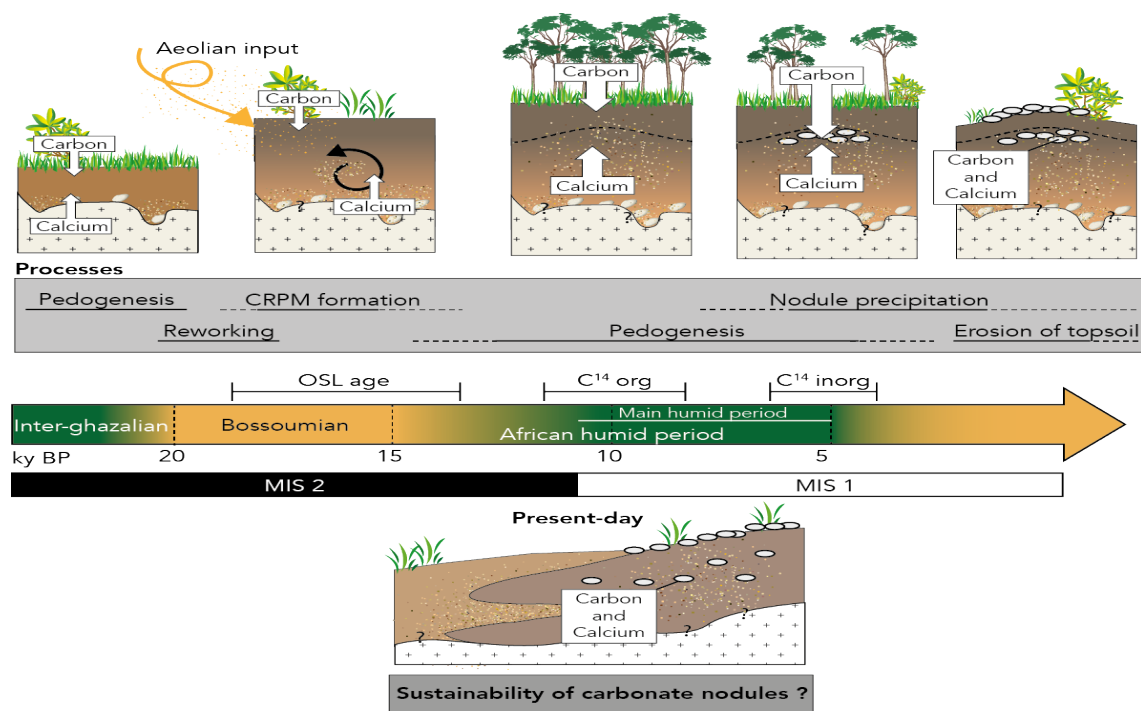


Figure 1 : Ca location through time in a soil profile. Ca is transferred from the granite to the carbonate nodules, emphasizing a conservative system through time. CRPM Clay-Rich Parent Material. Dates from Diaz et al. (2016b).

REFERENCES

- Chiquet, A., Michard, A., Nahon, D. & Hamelin, B., 1999. Atmospheric input vs in situ weathering in the genesis of calcretes: An Sr isotope study at Galvez (Central Spain). *Geochim Cosmochim Acta* 63, 311-323.
- Diaz, N., Dietrich, F., Cailleau, G., Sebag, D., Ngatcha, B.N. & Verrecchia, E.P., 2016a. Can mima-like mounds be Vertisol relics (Far North Region of Cameroon, Chad Basin)? *Geomorphology* 261, 41-56.
- Diaz, N., Dietrich, F., King, G.E., Valla, P.G., Sebag, D., F. Herman & Verrecchia, E. P., 2016b A 20-ka reconstruction of a Sahelo-Sudanian paleoenvironment using multi-method dating on pedogenic carbonate. EGU Conference. Vienna.
- Van der Hoven, S.J. & Quade, J., 2002. Tracing spatial and temporal variations in the sources of calcium in pedogenic carbonates in a semiarid environment. *Geoderma* 108, 259-276.

11.6

Molecular biomarkers of anthropic impacts in natural archives

Nathalie Dubois¹, Jérémy Jacob^{2,3,4}

*Surface Waters Research and Management, Eidgenössische Anstalt für Wasserversorgung, Abwasserreinigung und Gewässerschutz, CH-8600 Dübendorf (nathalie.dubois@eawag.ch)

**Institut des Sciences de la Terre d'Orléans, UMR7327, Université d'Orléans, Orléans, France,

***Centre National de la Recherche Scientifique / National Institute for Earth Sciences and Astronomy, Institut des Sciences de la Terre d'Orléans, UMR7327, Orléans, France,

****Bureau de Recherche Géologique et Minière, Institut des Sciences de la Terre d'Orléans, UMR7327, Orléans, France

Molecular fossils are becoming increasingly important tools in paleoenvironmental research, and over recent years, some were shown to be useful indicators of human activities. Common indicators of past human impacts include pollen, charcoal, sedimentation rates, and magnetic susceptibility, each of which has its limitations.

Thus the advent of novel molecular markers of human activities provides an additional set of tools to make the difficult distinction between anthropogenic and natural factors that have influenced the environment in the past. Fossil biomarkers preserved in natural archives provide valuable temporal and spatial insights on land use such as cultivation practices and pastoral activities, post-harvesting activities (e.g. retting), and their consequences on the environment and ecosystems.

Here we will present a review of the progress that has been made in developing novel biomarkers of human activities, differentiating those indicating environmental changes that can be related to human activities from those unambiguously attributable to human activities (Dubois and Jacob, 2016).

REFERENCES

Dubois, N., & Jacob J. 2016: Molecular biomarkers of anthropic impacts in natural archives: A review, *Frontiers in Ecology and Evolution*, 4, 92.

11.7

Characterization of sediment storage with cosmogenic nuclides, a study of a fluvial catchment on the Bolivian Altiplano

Tiemen Gordijn¹, Kristina Hippe², Irka Hajdas², Susan Ivy-Ochs², Vincenzo Picotti¹ & Marcus Christl²

¹ *Geological Institute, ETH Zürich, Clausiusstrasse 25, CH-8092 Zürich, Switzerland (gordijnt@student.ethz.ch)*

² *Laboratory of Ion Beam Physics, ETH Zürich, Otto-Stern-Weg 5, CH-8093 Zürich, Switzerland*

On the way from its source to its sink, a part of the sediment is temporarily stored in a fluvial catchment. The nature, age and spatial distribution of sediment storage is investigated in a catchment on the eastern border of the Bolivian Altiplano. The aim of this study is to identify climatic and tectonic conditions leading to the formation of storage compartments and to assess the effect on the concentration of multiple cosmogenic nuclides (i.e. *in situ* ¹⁴C, ¹⁰Be and ²⁶Al). Hippe et al. (2012) analyzed channel sediment samples in this catchment and recognized that the long-lived cosmogenic nuclides, ¹⁰Be and ²⁶Al, are not affected by sediment storage, but that *in situ* ¹⁴C possibly is.

Seven radiocarbon samples and two cosmogenic nuclide depth profiles were analyzed to constrain the age of the different sediment stores. Three terrace levels are present in the studied catchment, the lowest terrace level is dated at ~3.5-2.5 kyr BP, the highest terrace at ~34 kyr BP. The cosmogenic nuclide depth profiles are not applicable for dating due to too high variation in inheritance, but do provide information on the cosmogenic nuclide inventory in the catchment.

The ages of the terraces correlate with climatic records of nearby lakes (Baker et al., 2001; Abbott et al., 2003). A cycle of formation and incision of the fluvial terraces falls entirely in wet periods on the, otherwise rather dry, Altiplano. An incision rate of 0.33 mm/yr since the deposition of the highest terrace suggest that uplift might be higher than previously expected (Ege et al., 2007). A significant amount of sediment is stored in the catchment, and presently this sediment is being incised and transported out of the catchment. A model to quantify the effects of sediment storage on the cosmogenic nuclide inventory of the catchment is under construction.

REFERENCES

- Abbott, M. B., Wolfe, B. B., Wolfe, A. P., Seltzer, G. O., Aravena, R., Mark, B. G., Polissar, P. J., Rodbell, D. T., Rowe, H. D., and Vuille, M. (2003). "Holocene paleohydrology and glacial history of the central Andes using multiproxy lake sediment studies". In: *Palaeogeography, Palaeoclimatology, Palaeoecology*. 194.1–3, pp. 123–138.
- Baker, P. A., Rigsby, C. A., Seltzer, G. O., Fritz, S. C., Lowenstein, T. K., Bacher, N. P., and Veliz, C. (2001). "Tropical climate changes at millennial and orbital timescales on the Bolivian Altiplano". In: *Nature* 409.6821, pp. 698–701.
- Ege, H., Sobel, E. R., Scheuber, E., and Jacobshagen, V. (2007). "Exhumation history of the southern Altiplano plateau (southern Bolivia) constrained by apatite fission track thermochronology". In: *Tectonics* 26.1, TC1004.
- Hippe, K., Kober, F., Zeilinger, G., Ivy-Ochs, S., Maden, C., Wacker, L., Kubik, P. W., and Wieler, R. (2012). "Quantifying denudation rates and sediment storage on the eastern Altiplano, Bolivia, using cosmogenic ¹⁰Be, ²⁶Al, and *in situ* ¹⁴C". In: *Geomorphology* 179, pp. 58–70.

11.8

Historical evolution of human land-use in the catchment of Lake Murten

Mischa Haas¹, Franziska Baumann², Anna Reusch², Michael Strasser³, Timothy Ian Eglinton², Nathalie Dubois¹

¹ *Department of Surface Waters – Research and Management, Eawag, Überlandstrasse 133, CH-8600 Dübendorf (mischa.haas@eawag.ch)*

² *Department of Earth Science, ETH Zürich, Sonneggstrasse 5, CH-8006 Zürich*

³ *Institute of Geology, University of Innsbruck, Innrain 52, A-6020 Innsbruck*

The influence of human land-use on the Earth's surface started thousands of years ago with the spread of first agricultural societies. Agriculturally induced soil erosion has a strong influence on the global carbon cycle, however, the historical evolution of its extent and rate is rather poorly known. This study seeks to address this issue by investigating lacustrine sediments from Lake Murten to reconstruct past soil loss and soil degradation in the catchment and its influence on the soil carbon dynamics.

We applied a multi proxy approach including several geophysical, geochemical and biological methods on a 10 m sediment core from the deepest part of the Lake. Our first paleolimnological data show that the historical evolution of agriculture is well preserved in the sedimentary record. From 2.1 – 1.6 ky BP, slightly decreasing C/N ratios, but raising magnetic susceptibility, grainsizes and amount of detrital elements (Ti) were detected. At the same time, radiocarbon ages of the total organic carbon (TOC) fraction are increasing compared to the sediment ages, indicating a rapid flushing of old soil carbon from the surrounding catchment. Analyses on plant derived leaf waxes, such as *n*-alkanes, revealed a rough vegetation change from a tree to a more grass dominated landscape.

The findings are consistent with the development of first large-scale farming practices and the growing influence of the Roman city "Aventicum" 2000 years ago. Deforestation and soil cultivation led to increased runoff of terrestrial nutrient-rich material resulting in eutrophication of Lake Murten. Similar trends can be recognized from the medieval period until today. Since 1940, lake eutrophication occurred again, due to the growing human land-use in the Swiss Lowlands.

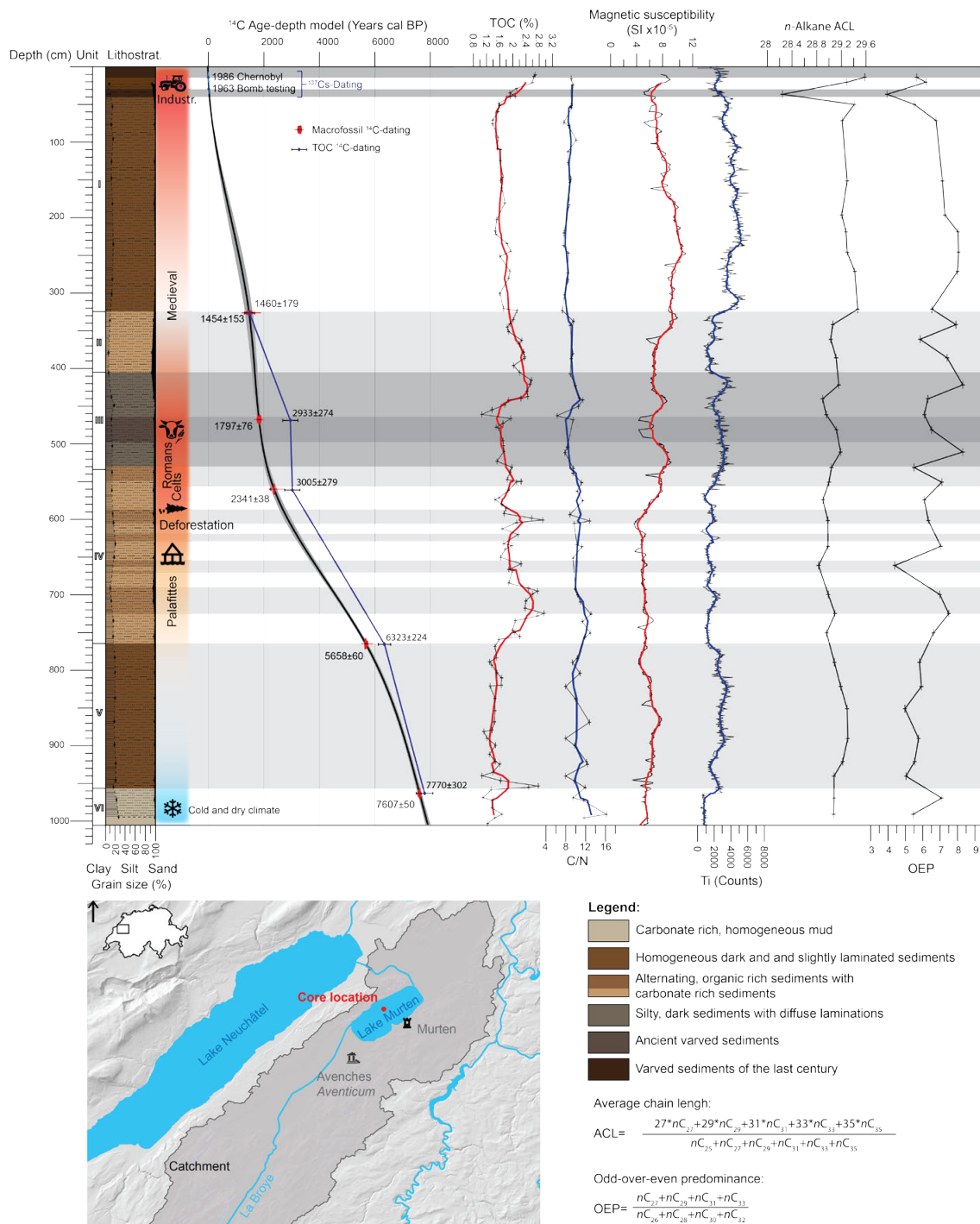


Figure 1. 10m Sediment core of Lake Murten. Shown are the age model based on radiocarbon dating, ²¹⁰Pb and ¹³⁷Cs, the total organic carbon content (TOC), the carbon to nitrogen ratio C/N, the magnetic susceptibility, the amount of detrital element Ti, ACL and OEP of n-alkanes (leaf wax biomarker).

11.9

Reconstruction of glacier fluctuations in the Mont-Blanc massif, w, western Alps: a multi-method approach

Benjamin Lehmann¹, Pierre G. Valla¹, Georgina E. King², Susan Ivy-Ochs³, Marcus Christl³ and Frédéric Herman¹

¹ *Institute of Earth Surface Dynamics, Faculty of Geosciences and Environment, University of Lausanne, CH-1012 Lausanne (benjamin.lehmann@unil.ch)*

² *Institute of Geography, University of Cologne, D-50923 Cologne, Germany*

^{***} *Laboratory of Ion Beam Physics, ETH Zurich, 8093 Zurich, Switzerland*

Providing tight spatial and temporal constraints on Late Pleistocene glacier fluctuations remains an important challenge for understanding glacier response to climatic change. In the Alps, paleo-glacier reconstructions are often scarce, non-continuous and spatially-limited during the Lateglacial and Holocene times, which makes their use as a paleoclimate proxy sometimes problematic.

Here, we focus on the Mer de Glace glacier (Mont-Blanc massif, France) where glacier reconstructions over the Little Ice Age (LIA, Vincent et al. 2014) and since the Mid Holocene (Le Roy et al., 2015) reveal important glacier fluctuations and ice thickness variations (~350 m over the last 4 ka). LGM trimline mapping (Coutterand et al., 2006) and cosmogenic ¹⁰Be exposure dating on the Italian side of the massif (Wirsig et al., 2016) give important indications on the maximum ice thickness at the LGM and the timing of ice surface lowering in this area. However, continuous records of the Mer de Glace fluctuations since the LGM are not precisely constrained. In order to better understand this complex deglaciation history, we collected seven samples of granitic polished bedrock surfaces between the LGM ice surface (~2505 m a.s.l., Coutterand et al., 2006) and the present-day glacier (1920 m a.s.l.) covering ~600 m of elevation for the ice surface fluctuations.

We first used cosmogenic ¹⁰Be dating on quartz (Gosse and Phillips, 2001) to constrain ice surface fluctuations during the Lateglacial and Holocene. Given that cosmic rays exposure produces ¹⁰Be over the first ~3 m below the rock surface, multiple exposure history from complex glacier fluctuations would be difficult to quantify using this chronometer.

To improve our temporal resolution for such complex exposure history, we combined cosmogenic ¹⁰Be dating on quartz with OSL surface exposure dating (Sohbati et al., 2011). OSL surface exposure dating is sensitive to light, based on the progressive bleaching of the OSL signal in a rock sample that depends on its exposure time, mineralogical properties and environmental conditions. Preliminary OSL results from rock slices show increasing exposure age (i.e. deeper bleaching of the OSL signal) with sample elevation. Moreover, our results reveal that the bleaching of the OSL signal is occurring within the first 1-3 cm below the rock surface, potentially offering high resolution to date the latest exposure following short-lived glacier fluctuations.

REFERENCES

- Coutterand S., Buoncristiani J.-F. (2006), Paléogéographie du dernier maximum glaciaire du Pléistocène récent de la région du Massif du Mont Blanc, France, *Quaternaire*, 17, (1), 2006, p. 35-43.
- Gosse, J.C. and F.M. Phillips (2001). Terrestrial in situ cosmogenic nuclides: theory and application. *Quaternary Science Reviews*, 20, 1475-1560.
- Le Roy, M., Nicolussi, K., Deline, P., Astrade, L., Edouard, J.-L., Miramont, C., Arnaud, F. (2015), Calendar dated glacier variations in the western European Alps during the Neoglacial: the Mer de Glace record, Mont Blanc massif, *Quaternary Science Review* 108 (2015) 1-22, doi:10.1016.
- Sohbati, R., Murray A., Jain M., Buylaert J.-P., and Thomsen K. (2011), Investigating the resetting of OSL signals in rock surfaces, *Geochronometria*, 38 (3), 249_258, doi:10.2478/s13386-011-0029-2.
- Vincent, C., Harter M., Gilbert A., Berthier D., Six D., (2014). Future fluctuations of Mer de Glace, French Alps, assessed using a parameterized model calibrated with past thickness changes. *Annals of Glaciology*, 55, 15-24.
- Wirsig C., Zasadni J., Christl M., Akçar N., Ivy-Ochs S. (2016), Dating the onset of LGM ice surface lowering in the High Alps. *Quaternary Science Reviews* 143 37-50.

11.10

Geochemical characterisation of Lake Towuti, Indonesia: setting the stage for climate reconstructions over several glacial-interglacial cycles

Marina Morlock¹, Hendrik Vogel¹, Valentin Nigg¹, Ascelina Hasberg², Martin Melles², James M. Russell³, Satria Bijaksana⁴ & the TDP science team

¹ *Institute of Geological Sciences and Oeschger Centre for Climate Change Research, University of Bern, 3012 Bern, Switzerland (marina.morlock@geo.unibe.ch)*

² *Institute of Mineralogy and Geology, University of Cologne, 50674 Köln, Germany*

³ *Department of Geological Sciences, Brown University, Providence, RI 02912*

⁴ *Faculty of Mining and Petroleum Engineering, Institut Teknologi Bandung, Bandung 40132, Indonesia*

In May-July 2015, more than 1000 m of sediment core capturing the entire sediment infill to bedrock have been recovered in the course of the ICDP Towuti Drilling Project (Russell et al. 2016). Hosted in the East Sulawesi Ophiolite, Lake Towuti is a large (560 km² surface area; 198 m max. water depth) ultraoligotrophic lake characterised by high iron and very low sulphur contents. The lake's catchment is characterized by several tens of metres thick, deeply weathered laterite soils and a closed-canopy rainforest. Today, Lake Towuti is a hydrologically open lake with one outflow draining into the Bay of Bone. The lake is split into two connected major basins, which are separated by fault controlled bedrock highs below and above the current water table. To the north, the Mahalona River dominates both water and sediment input to the basin. The river drains the upstream Lake Mahalona as well as a large catchment, which is characterised by partly serpentinised peridotites.

In order to characterise modern erosional processes and element cycling in the lake and its catchment, we collected catchment-characteristic bedrock samples with profiles of their overlying laterites, riverine sediments, and 85 surface sediment samples from the lake. All samples were analysed for their geochemical and clay-mineralogical composition in order to define the composition of erodible substrates, track source to sink changes in sediment composition, and assess the spatial variability in Lake Towuti. The relationships found in the modern system were then applied to two sediment cores, dating back 30,000 and 60,000 years BP, respectively. This work sets the foundation for work on the cores from the ICDP Towuti Drilling Project, which promise uninterrupted lacustrine sedimentation over several glacial-interglacial cycles (Russell et al., 2016).

The laterite soils in the catchment show a characteristic zonation with high concentrations of Al, Ti, Fe, and Cr in the uppermost horizon, while Mg is enriched in the saprolite zone directly above bedrock. Surface sediment samples show that the Mahalona River is the dominant sediment source to the northern basin. Its geochemical composition is characterised by high Mg concentrations, while concentrations of Al, K, and Ti are relatively low. This is contrasted by the Loeha River, which drains the only felsic catchment of the lake, and has a distinctly different geochemistry with high Al, K and Ti concentrations, while Mg, Fe, and Cr are low. In areas of the lake without major inlets and rather small and steep catchments, the elemental surface sediment composition more closely reflects that of evolved laterite horizons. Our data indicate that today's sediment composition at the coring sites is a mixture of Mahalona River sediments, material from the Loeha River, and direct laterite-derived input. Based on the river geochemistry we suggest that the Al/Mg ratio provides information about the importance of the Mahalona River relative to the Loeha River and the laterite-derived sediments.

Over time, changes in the relative importance of these three sediment sources are dependent on lake level fluctuations. A decrease in lake level lowers the hydrologic base level, which leads to a progradation of the Mahalona River Delta, deeper incision of river channels, and consequently a low Al/Mg ratio. Hence, bedrock erosion and remobilisation of poorly weathered substrates are dominant over laterite-derived sedimentation during dry periods. During lake level high stands, a higher proportional erosion of laterite soils compared to bedrock incision by the Mahalona River leads to an increase in Al/Mg in the lake sediments. Additionally, the Loeha River transports more material with high Al/Mg values to the coring sites during wet phases. This is because increased lake levels induce flooding of low-elevation areas in the eastern part of the lake, which can allow the Loeha River to change its course and drain into the northern basin. We thus propose that the Al/Mg ratio is an indicator for lake level fluctuations and can serve as a proxy for hydroclimatic changes in the region.

In the past 60,000 years, the Al/Mg ratio shows a cyclic pattern with lowest values in the mid-Holocene (3 - 5 kyr BP), between 15 - 27 kyr, and prior to 58 kyr BP. Following the interpretation of today's sediment composition this implies that conditions in central Sulawesi were significantly drier in the mid-Holocene, in MIS2, and MIS4. This is confirmed by earlier studies from Lake Towuti, which show that conditions were dry during the last glacial, causing a significant decrease in lake levels and an opening of the closed-canopy rainforest in the catchment.

REFERENCES

- Russell, J.M., Bijaksana, S., Vogel, H., Melles, M., Kallmeyer, J., Ariztegui, D., Crowe, S., Fajar, S., Hafidz, A., Haffner, D., Hasberg, A., Ivory, S., Kelly, C., King, J., Kirana, K., Morlock, M., Noren, A., apos, Grady, R., Ordonez, L., Stevenson, J., von Rintelen, T., Vuillemin, A., Watkinson, I., Wattrus, N., Wicaksono, S., Wonik, T., Bauer, K., Deino, A., Friese, A., Henny, C., Imran, Marwoto, R., Ngkoimani, L.O., Nomosatryo, S., Safiuddin, L.O., Simister, R. & Tamuntuan, G., 2016: The Towuti Drilling Project: paleoenvironments, biological evolution, and geomicrobiology of a tropical Pacific lake. *Scientific Drilling* 21, 29-40.
- Vogel, H., Russell, J.M., Cahyarini, S.Y., Bijaksana, S., Wattrus, N., Rethemeyer, J. & Melles, M., 2015: Depositional modes and lake-level variability at Lake Towuti, Indonesia, during the past ~29 kyr BP. *Journal of Paleolimnology* 54, 359-377.

11.11

Holocene seismic activity of the Yavansu fault, western Turkey

Nasim Mozafari Amiri*, Dmitry Tikhomirov*, Çağlar Özkaymak**, Ökmen Sümer**, Bora Uzel**, Susan Ivy-Ochs****, Christof Vockenhuber****, Hasan Sözbilir** & Naki Akçar*

¹ Institute of Geological Sciences, University of Bern, Baltzerstrasse 3, 3012 Bern, Switzerland (nasim.mozafari@geo.unibe.ch)

² Department of Geological Engineering, Afyon Kocatepe University, Ahmet Necdet Sezer Kampüsü, 03200 Afyonkarahisar, Turkey

³ Department of Geological Engineering, Dokuz Eylül University, 35160 İzmir, Turkey

⁴ Swiss Federal Institute of Technology, Institute for Particle Physics, Otto-Stern-Weg 5, 8093 Zürich, Switzerland

Seismic pattern modelling and estimation of the recurrence interval of significant rupture events requires a comprehensive paleoearthquake data over a long span of time. However, the oldest known earthquake in the Eastern Mediterranean and Middle East dates back to 464 B.C.³⁶Cl surface exposure dating is the only suitable method to date the paleoearthquake activities of the fault scarps, which are the best evidence of past ruptures, if built in carbonates. Following an earthquake, when a fault surface exposed to cosmic rays, the production rate of ³⁶Cl cosmogenic nuclides will accelerate during period of quiescence. By measuring of the distribution of cosmogenic ³⁶Cl versus height of the sample along fault surface, the timing of major seismic activities and their associated vertical displacements are identified.

The western Anatolia seismically active region with several major horst-graben systems built in carbonates formed in response to approximately N-S extensional regime since the early Miocene. The south-dipping WE-trending Yavansu fault is situated in the western part of the Büyük Menderes graben, about 6.5 km southeast of Kuşadası (Fig. 1) in this seismic-prone region. The fault juxtaposes the hanging wall of colluvial sediments against the limestone bedrock in the footwall. 67 samples of 10 cm height, 15 cm width and 3 cm thick continuously collected along a well-preserved 7.2 meters high fault starting from intersection of colluvium with the fault surface. The scarp dip, scarp height, top surface dip and colluvium dip as important geometrical factors as well as topographic shielding, density of the fault and colluvium were measured. Then, the sample preparation carried out in laboratory for elemental analysis and AMS measurements of ³⁶Cl.

FSDT- Fault Scarp Dating Tool- Matlab® code will be used to model the major ruptures of the fault scarp and their related vertical displacements. Our first results show the evidence of three or four major seismic activities of the Yavansu fault during Holocene.

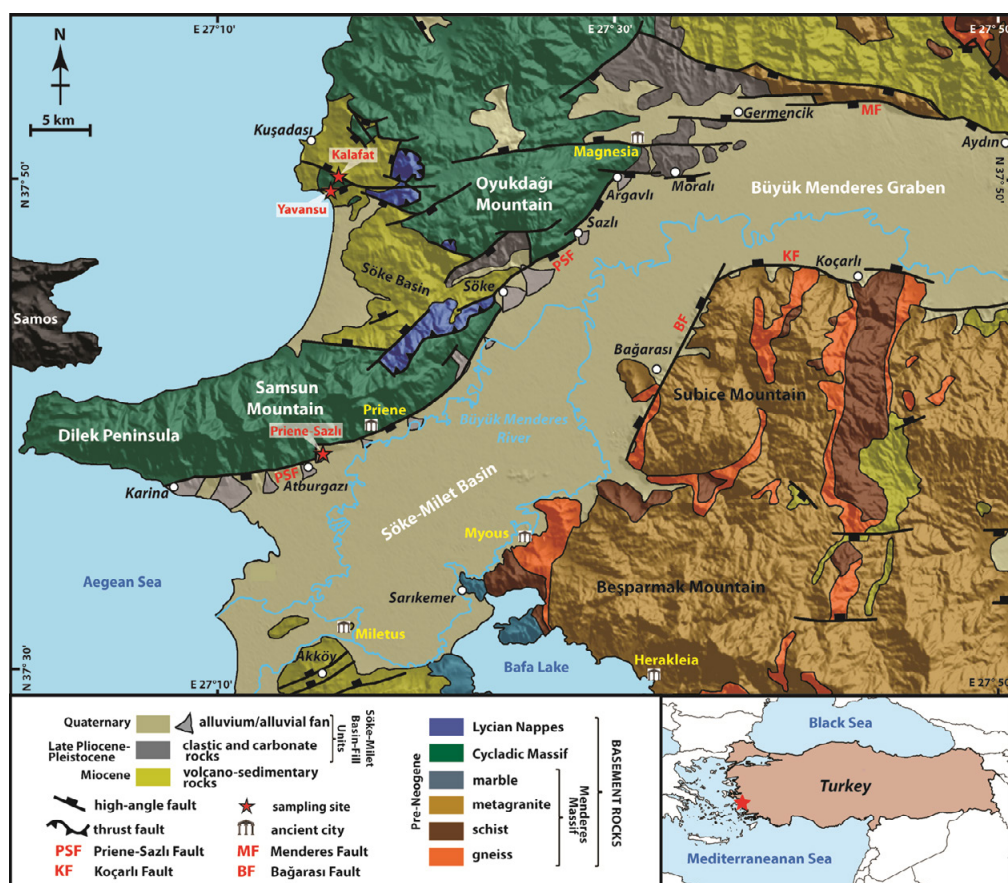


Figure 1. Geological map of the western Büyük Menderes graben

11.12

Tectonic geomorphology of the western Makran subduction zone: Evidence of past megathrust earthquakes?

Raphaël Normand¹, Guy Simpson¹ & Abbas Bahroudi²

¹ *Department of Earth Sciences, University of Geneva, Rue des Maraichers 13, CH-1205 Genève.
(Raphael.Normand@unige.ch)*

² *Exploration department, School of Mining Engineering, University of Tehran, Northern Kargar avn,
P.O. Box 11365-4563, Theran*

The western part of the Makran subduction zone (Iran) has not experienced a great megathrust earthquake in recent human history. We aim to find geological evidence of past earthquake activity to better assess the seismic hazard of the region. The presence of uplifted marine terraces along the coast indicates that the margin is still tectonically active over at least the Quaternary. Moreover, we observed that the terraces are offset and deformed by numerous trench parallel normal faults. We have mapped the faults and the marine terraces and collected samples for dating to determine surface uplift rates.

We consider the ¹⁴C ages obtained on the marine terraces to be minimum ages because they are close to the upper limit of the method. Therefore, the sea-level highstand(s) responsible for the formation of these surfaces could not be accurately determined. The presence of coast-parallel normal faults in a subduction context could be due to post-seismic stress field rotation in the overriding plate following a megathrust earthquake along a weak interface (e.g. due to high pore fluid pressures). The high pore fluid pressure of the Makran thrust is highly probable considering that the plate interface is overlain by 8 km of porous sediments at the surface of which numerous mud volcanoes are active. In that case, normal fault activity in the Pleistocene might suggest that megathrust events could happen again in the Makran subduction zone.

11.13

Holocene treeline changes in the Canadian Cordillera are controlled by climate and local topography

Christoph Schwörer^{1,2}, Daniel G. Gavin², Ian R. Walker³ & Feng Sheng Hu⁴

¹ *Institute of Plant Sciences and Oeschger Centre for Climate Change Research, University of Bern, Altenbergrain 21, CH-3013 Bern, Switzerland*

² *Environmental Change Research Group, Department of Geography, University of Oregon, Eugene, OR 97403-1251, USA*

³ *Biology and Earth & Environmental Sciences, University of British Columbia Okanagan, 3333 University Way, Kelowna, British Columbia, Canada V1V 1V7*

⁴ *Department of Plant Biology, University of Illinois, Urbana, IL 61801, USA*

Even though climate change is expected to lead to an upward shift of treelines in mountain areas, widespread evidence for treeline advances in response to rising temperatures remains scarce (Harsch et al. 2009). Secondary controls such as disturbances, competition, land-use legacies and topography or geomorphology might influence treeline dynamics at the local scale (Holtmeier & Broll 2005). In order to assess the impact of ongoing and future climate change on mountain forests, we studied treeline changes since the last ice age in the Canadian Cordillera (southeastern British Columbia, Canada). We aim to determine if top-down climatic factors were the main drivers of past treeline dynamics or if local bottom-up controls such as topography and/or geomorphology played a role as well.

To address this question, we analyzed post-glacial sediments from three lakes at or just below the present treeline for pollen, macrofossils and charcoal. We then compared the results to chironomid-inferred July temperature reconstructions from the same sediment cores (Chase et al. 2008).

At two lakes (Windy and Redmountain) highest macrofossil concentrations occurred in the warmer-than-present Early Holocene, indicating highest treeline position and forest density in response to higher temperatures. Individual peaks in macrofossil concentration at Windy Lake coincided with high solar activity and warmer summers. At the third lake (Thunder), a divergent vegetation history with highest macrofossil concentrations in the mid-Holocene suggests that local topography was an important control of mountain forest dynamics. During the dry and warm Early Holocene, moisture availability limited the establishment of closed forests on steep south-facing slopes or shallow soils near Thunder Lake. This is consistent with a number of other paleoecological studies in the region.

We conclude that summer temperature was the main driver of treeline dynamics over millennial to decadal timescales. However, closed forests occurred only in areas of adequate moisture availability, which is controlled by topography and geomorphology. We therefore expect a rapid upward shift of treelines during the 21st century in response to warmer temperatures, but only where deep soils or favorable aspects provide sufficient moisture for tree growth. Upward forest expansion will therefore be patchy and occur first in favorable microsites.

REFERENCES

- Chase M., Bleskie C., Walker I.R., Gavin D.G., & Hu F.S. (2008) Midge-inferred Holocene summer temperatures in Southeastern British Columbia, Canada. *Palaeogeography, Palaeoclimatology, Palaeoecology*, 257, 244–259.
- Harsch M.A., Hulme P.E., McGlone M.S., & Duncan R.P. (2009) Are treelines advancing? A global meta-analysis of treeline response to climate warming. *Ecology Letters*, 12, 1040–1049.
- Holtmeier F.-K. & Broll G. (2005) Sensitivity and response of northern hemisphere altitudinal and polar treelines to environmental change at landscape and local scales. *Global Ecology and Biogeography*, 14, 395–410.

11.14

Geochemical dataset of the Rhone River delta (Lake Geneva) sediments – disentangling human impacts from climate change

Tiago Adrião Silva^{*,***}, Stéphanie Girardclos^{**,***}, Hendrik Vogel^{****} & Jean-Luc Loizeau^{*,***}

¹ *Inst. F.-A. Forel, Uni. of Geneva, Switzerland (Tiago.Adriao@unige.ch);*

² *Dep. of Earth Sciences, Uni. of Geneva, Switzerland;*

³ *Inst. for Envir. Sciences, Uni. of Geneva, Switzerland;*

⁴ *Inst. of Geological Sciences & Oeschger Centre for Climate Change Research, Uni. of Bern, Switzerland*

Lake Geneva's sedimentary sequence functions as an archive that records changes in the lake watershed since deglaciation. In the Haut-Lac area the changes recorded are mainly linked to the sediment sourced from the Rhone River catchment, which contributes ~68% of the water and sediment inputs to the lake. Owing to its location in an alpine environment the Rhone River catchment experienced dramatic changes as a result of climate change but also due to upstream glacier dynamics, changes in the accessibility of sediment accumulated during the glacial as well as short-term seismic and exhumation processes. In the last 200 years (Anthropocene) this watershed was also impacted by anthropogenic activities (e.g. river channelization, hydropower dam construction, water flow regulation, water and sediment abstraction and land use changes). These recent changes are recorded as quantitative (sedimentation rate) and qualitative (mineralogy, geochemistry) sediment variations in Lake Geneva.

During this study, undertaken under the scope of the project SEDFATE (SNSF n°147689), 19 short sediment cores were collected in the subaqueous delta of the Rhone River (Switzerland/France) area in Lake Geneva. Six cores were dated using radiogenic isotopes (¹³⁷Cs and ²¹⁰Pb). The calculated sedimentation rates (SR) indicate a decrease starting in 1964, confirming results from Loizeau (1991) and Loizeau & Dominik (2000). This study found that those SR's increased from 1986 (Fig.1).

XRF and MSCL data were measured for all cores. Elemental data (linked to detrital sources, i.e. Al, Fe, K, Mn, Rb, Si, Ti) also point to a decrease in clastic input from 1964 to 1986 but indicate an increase from 1986 to the present (Fig.2). Other element ratios (Zr/Rb and Zr/K) added to magnetic susceptibility and lithology data were used to distinguish density flow deposits from hemipelagic sediments. Changes in the frequency and type of these deposits can also indicate a change in the sedimentation pattern in the Rhone River sublacustrine delta during the last century.

From these results we hypothesize that anthropogenic activities undertaken in the last century in the Rhone River watershed (mainly the construction of dams in the 1950-60's) have resulted in the abstraction of a substantial quantity of sediment from this system and have greatly changed the sediment flux between the river and the lake. The recent (from the 1990's) increase in sedimentation rates and in the detrital signal is interpreted as being a result of recent glacial melting due to global warming.

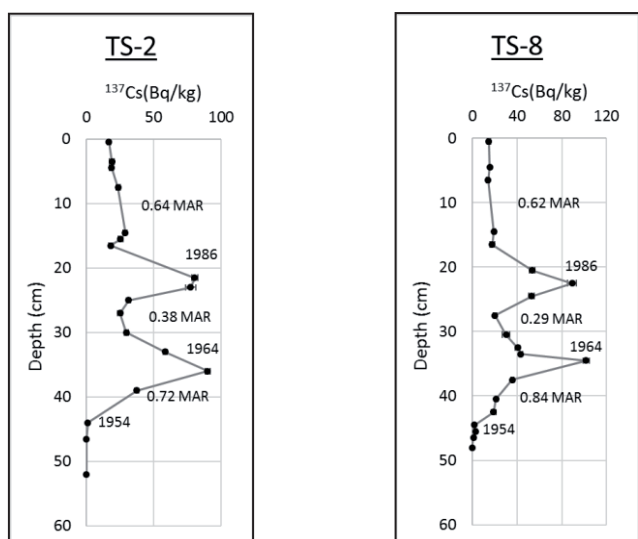


Figure 1. ¹³⁷Cs activity profiles from cores TS-2 and TS-8. The peaks of activity of ¹³⁷Cs (1986, 1964) and its first appearance (1954) allowed the calculation of mass accumulation rates (MAR's expressed in g.cm⁻².yr⁻¹) in the sediment cores.

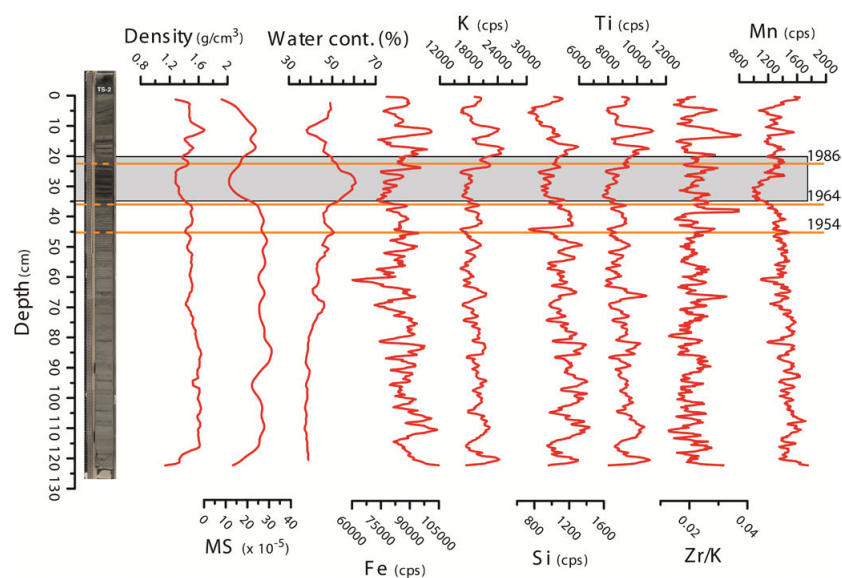


Figure 2. Elemental profile of the Core TS-2. We can observe that between 20-35cm of depth Fe, K, Si, and Ti show a decrease when compared to the base and to the very top of the core.

REFERENCES

- Loizeau, J.-L., 1991. La sédimentation récente dans le delta du Rhône, Léman: processus et évolution, unpublished PhD thesis. Institut Forel, Faculté des Sciences. Université de Genève, Genève, p. 209.
- Loizeau, J.-L., Dominik, J., 2000. Evolution of the Upper Rhone River discharge and suspended sediment load during the last 80 years and some implications for Lake Geneva. *Aquatic Sciences*, 62, 54-67.

11.15

Effects of climate change on Swiss wine - a VOCs and multi-isotope study

Jorge E. Spangenberg¹, Maria Vogiatzaki¹ & Vivian Zufferey²

¹ *Institute of Earth Surface Dynamics (IDYST), University of Lausanne, Géopolis, CH-1015 Lausanne (jorge.spangenberg@unil.ch)*

² *Agroscope, Institute of plant production sciences IPV, CH-1009 Pully*

While the interaction between the local climate, atmospheric CO₂ concentration, soil and site location (*terroir*) has a varied role in the physiology, biochemistry and yield of grapevine (*Vitis vinifera* L.), the general effect of macroclimate or regional climate (mesoclimate) appears to be better known (e.g., Jones et al., 2005). In this ongoing work, we investigate the biogeochemical changes induced during development of field-grown cultivars of white (cv. Chasselas) and red (cv. Pinot noir) grapes (vineyards of Agroscope-IPV station, Leytron, Valais, Switzerland) exposed to water stress controlled by monitoring the soil water status and leaving all the other key environmental variables constant. Three soil water status conditions were set by drip irrigation (9 L/m²), no irrigation and no irrigation and soil-water removal with a waterproof and non-reflective plastic cover (Zufferey et al., 2011).

Among the initial field and laboratory measurements was the carbon isotope composition ($\delta^{13}\text{C}$ values obtained by EA/IRMS) of the berry sugar at harvest (must sugar). The $\delta^{13}\text{C}$ values of must sugars (−27.6 to −22.5 ‰ VPDB) and leaf water potential (a direct measurement of the plant water status) during 10 growing seasons (2003 to 2012) were significantly correlated ($R^2=0.75$, $p<0.01$), indicating that these isotopic measurements allow a very sensitive detection of plant water status under natural conditions. These results motivated a study on possible similar chemical/isotopic response of (a) the vine leaf epicuticular waxes and (b) the volatile organic compounds (VOCs) in the derived monovarietal wines produced from each grapevine variety using the same vinification protocol. The molecular and isotopic composition of epicuticular waxes from leaves ($n = 42$) of Chasselas and Pinot noir collected monthly in 2014 were presented last year (Spangenberg et al., 2015). The changes in the distribution of alkanolic acids and neutral lipids (obtained by GC/MS and GC/FID), and compound specific $\delta^{13}\text{C}$ values of the individual n -alkanoic acids and n -alkanes (obtained by GC/C/IRMS) were correlated with the different soil water status and measured leaf water potentials. This year we present the results of a study of the monovarietal wines (Chasselas, Pinot noir) from vintages 2009-2014.

Wine aliquots were freeze-dried and the solid residue (SR) analyzed for their C/N and C and N isotope ratios ($\delta^{13}\text{C}$ and $\delta^{15}\text{N}$ values). The wine VOCs were extracted with organic solvents. For quantification purposes and standardization of the compound specific $\delta^{13}\text{C}$ values, the samples were spiked before extraction with a standard mixture of compounds of known $\delta^{13}\text{C}$. The main results are $(\text{C/N})_{\text{SR}}$, $\delta^{13}\text{C}_{\text{SR}}$, $\delta^{15}\text{N}_{\text{SR}}$, concentrations and $\delta^{13}\text{C}$ values of >50 VOCs, among them, alcohols are the most abundant, followed by fatty acid esters, fatty and other carboxylic acids, ketones and other esters, lactones, aldehydes, amides and phenols. They will be discussed in terms of different cultivars, leaf water potential, growing season, and potential application as indicators of plant abiotic stress (climate change) and wine *terroir*.

REFERENCES

- Jones, G. V., White, M. A., Cooper, O. R. & Storchmann, K. 2005: Climate change and global wine quality. *Climatic change*, 73, 319-343.
- Spangenberg, J. E., Schweizer, M. & Zufferey, V. 2015: Molecular and isotopic changes in leaf lipids of plants living under abiotic stress conditions – implications for organic geochemical proxies. 13th Swiss Geoscience Meeting, Basel 2015.
- Zufferey, V., Cochard, H., Ameglio, T., Spring, J.-L. & Viret, O. 2011: Diurnal cycles of embolism formation and repair in petioles of grapevine (*Vitis vinifera* cv. Chasselas). *Journal of Experimental Botany*, 62, 3885-3894.

11.16

A relative humidity record for the Late Glacial to Holocene transition from the Gemündener Maar, Germany

Lorenz Wüthrich^{1,2}, Johannes Hepp³, Tobias Bromm³, Marianne Benesch³, Marcel Bliedtner^{1,2}, Imke Kathrin Schäfer^{1,2}, Jana Zech¹, Bruno Glaser³, Kazimierz Rozanski⁴, Frank Sirocko⁵, Roland Zech^{1,2} & Michael Zech³

¹ *Geographical Institute, University of Bern, CH- Bern (lorenz.wuethrich@giub.unibe.ch)*

² *Oeschger Center for Climate Change Research, University of Bern, CH- Bern,*

³ *Institute for Agronomy and Nutritional Sciences, Martin Luther University Halle- Wittenberg, D- Halle*

⁴ *Faculty of Physics and Applied Computer Science, AGH University of Science and Technology, PL- Krakow*

⁵ *Institute of Geosciences, Johannes Gutenberg University, D- Mainz*

In terms of future climate change the large and rapid climate and environmental fluctuations during the Late Glacial to Holocene transition are of special interest in paleoclimate research. Many studies have focussed on the reconstruction of temperature, precipitation and vegetation, but not so much on relative humidity (RH) - although this is also an environmentally very relevant parameter. Here we present a RH record for the Late Glacial/Holocene transition (13 ka to 10 ka) based on a newly developed paleohygrometer (Turhorn et al., 2015), applied to sediments from the Gemündener Maar, Eifel, Germany. The method builds on the evapotranspirative enrichment of leaf water, as derived from coupled stable isotope analyses on plant material ($\delta^2\text{H}$ on *n*-alkanes and $\delta^{18}\text{O}$ on plant sugars). The reconstructed relative humidity (daytime and vegetation period: RH_{dv}) indicates relatively humid conditions during the early Younger Dryas (YD) and more arid conditions during the second half of the YD. However, RH_{dv} variability during the Preboreal (PB) is more pronounced than during the YD. Correlations found with North Atlantic Ocean temperature (Thornalley et al., 2010) and solar activity (Muscheler et al., 2014) are suggested to be the main drivers for the observed RH_{dv} fluctuations during the PB in middle Europe.

REFERENCES

- Turhorn, M., Zech, R., Ruppenthal, M., Oelmann, Y., Kahmen, A., de la Valle, H. F., Eglinton, T., Rozanski, K. & Zech, M. 2015: Coupling $\delta^2\text{H}$ and $\delta^{18}\text{O}$ biomarker results yields information on relative humidity and isotopic composition of precipitation- a climate transect study. *Biogeosciences*, 12, 3913-3924.
- Thornalley, D. J. R., McCave, I. N., & Elderfield, H. 2010: Freshwater input and abrupt deglacial climate change in the North Atlantic. *Paleoceanography*, 25
- Muscheler, R., Adolphi, F. & Knudsen, M. F. 2014: Assessing the differences between the IntCal and Greenland ice-core time scales for the last 14,000 years via the common cosmogenic radionuclide variations. *Quaternary Science Reviews*, 106, 81-87

P 11.1

Biomarker Signature of Greenland Sediments: from modern Rivers and Soils to MIS 5e and 11 Records

Jennifer Anspach¹, Maarten Lupker¹, Negar Haghipour¹ & Timothy Eglinton¹

¹ *Geological Institute, ETHZ, Sonneggstrasse 5, CH-8092 Zürich (jenny_anspach@hotmail.com)*

Better constraining the evolution of the Greenland Ice Sheet (GrIS) is crucial for a broader understanding of past and future climate changes. Previous studies reported that the GrIS was significantly smaller during interglacial periods MIS 5e and MIS 11 than at present (Colville et al. 2011, Reyes et al. 2014), which suggests that a bigger fraction of Greenland was covered by vegetation and soils. To investigate whether terrestrial biomarkers provide new constraints on the dynamics of the GrIS over the past interglacials, we characterised the biomarker composition (GDGTs and n-alkanes), as well as the bulk geochemistry (TOC, $\delta^{13}\text{C}$, C-14), of modern sediments from southwestern Greenland and of Eirik Drift core IODP-303-U1305 over MIS5e and 11.

Rivers in southwestern Greenland constitute the main link between the southwestern Greenland Ice Sheet (GrIS) and the ocean. Understanding the composition of suspended river sediments gives insights into the source of organic carbon that is mobilised and further exported to the ocean. To address these questions, biomarkers in suspended sediments and soils coming from Kangerlussuaq, southwestern Greenland, were measured. Kangerlussuaq is located in the most sensitive region of Greenland with regard to climate change, and is a good analogue for interglacials. Preliminary results (e.g. biomarker concentrations, MAT, CPI, ACL) show that modern soils or lakes are not the only source of organic matter in these rivers, and suggest that part of the biomarker signature is inherited from older, presently subglacial, organic pools.

The Eirik Drift accumulates material that is eroded from the eastern and southern Greenland margin, and it has been shown to record significant environmental changes of the GrIS over MIS 5e and MIS 11 (Colville et al. 2011, Reyes et al. 2014, de Vernal & Hillaire-Marcel 2008). However, the GDGT and n-alkane characterisation of drift sediments from IODP-303-U1305 do not show a significant response of the biomarker record to these interglacials.

REFERENCES

- Colville, E. J., Carlson, A. E., Beard, B. L., Hatfield, R. G., Stoner, J. S., Reyes, A. V., & Ullman, D. J. 2011: Sr-Nd-Pb isotope evidence for ice-sheet presence on southern Greenland during the Last Interglacial. *Science*, 333(6042), 620-623.
- de Vernal, A., & Hillaire-Marcel, C. 2008: Natural variability of Greenland climate, vegetation, and ice volume during the past million years. *Science*, 320(5883), 1622-1625.
- Reyes, A. V., Carlson, A. E., Beard, B. L., Hatfield, R. G., Stoner, J. S., Winsor, K., ... & Ullman, D. J. 2014: South Greenland ice-sheet collapse during Marine Isotope Stage [thinsp] 11. *Nature*, 510(7506), 525-528.

P 11.2

Leaf waxes and compound-specific δD analyses in a Holocene fluvial sediment-paleosol sequence from the upper Alazani River, SE-Georgia

Marcel Bliedtner¹, Hans v. Suchodoletz², Imke K. Schäfer¹, Jana Zech¹, Christoph Zielhofer² & Roland Zech¹

¹ *Institute of Geography and Oeschger Centre for Climate Change Research, University of Bern, Hallerstrasse 12, CH-3012 Bern (marcel.bliedtner@giub.unibe.ch)*

² *Institute of Geography, University of Leipzig, Johannisallee 19a, D-04103 Leipzig*

Leaf waxes of terrestrial plants are relatively resistant against degradation and serve as valuable biomarkers preserved in various sedimentary archives. Compound-specific D/H analyses on leaf waxes are increasingly used to reconstruct past climate and environmental conditions. Here, we present a n-alkane and compound-specific δD record from a Holocene fluvial sediment-paleosol sequence along the upper Alazani River in eastern Georgia.

Generally, such records from fluvial sedimentary archives must be divided into a catchment signal recorded in the fluvial sediment layers and a local in-situ signal recorded in the intercalated paleosols.

The n-alkane homologue pattern show a clear catchment versus in-situ signal. The paleosols are dominated by n-alkanes derived from the local vegetation, mainly grasses throughout the Holocene. Although the fluvial sediment layers contain mostly leaf waxes derived from the forested catchment, higher contributions from grasses between 8 and 5 ka possibly indicate more arid conditions during that time. The δD -values for the paleosols show more depleted values, whereas the δD -values for the fluvial sediment layers show a slight trend to more depleted values during the early Holocene and more enriched values during the mid and late Holocene.

Because of the well-known altitude-effect on the isotopic composition of precipitation, we had expected more depleted δD values for the fluvial sediment layers, i.e. the catchment-derived samples, and more enriched δD values for the paleosols, i.e. the low altitude, in-situ signal. As this is not the case, we hypothesize that this differences might be caused by different moisture proportions for the high mountainous catchment (up to >3000 m a.s.l.) and the investigated site (at 450 m a.s.l.). Air masses originating from the Black Sea might be affected by isotopic fractionation due to Luv-Lee and/or rainshadow effects at the investigated site. The mountainous catchment reflects the isotopic signal of the Black Sea during the Holocene.

P 11.3

The Last Glacial Maximum around Lago d'Orta, Northern Italy; a multi method reconstruction

Jochem Braakhekke¹, Susan Ivy-Ochs², Irka Hajdas², Giovanni Monegato³, Franco Gianotti⁴, and Marcus Christl²

¹ *Departement of Earth Sciences, Eidgenössische Technische Hochschule Zürich, Zürich, Switzerland
(jjm.braakhekke@gmail.com)*

² *Laboratory of Ion Beam Physics, ETH Zürich, Zürich, Switzerland*

³ *Istituto di Geoscienze e Georisorse, Consiglio Nazionale della Ricerche, Turin, Italy*

⁴ *Dipartimento di Scienze della Terra, Università degli Studi di Torino, Turin, Italy*

During the Quaternary multiple ice-ages saw the ice reaching the Alpine forelands. Glacial erosion created overdeepenings and during stable glacier positions moraines built up. Today we can recognize these landforms in the research area as a lake basin which accommodates Lago d'Orta and sets of moraines surrounding the southern lake tip, referred to as the amphitheatre. The glacier that used to fill the overdeepening during the Last Glacial Maximum (LGM) was a small branch of the Toce Glacier, which originated from the Simplon and Monte Rosa areas and which saw a bigger branch flowing down to the Lago Maggiore area. However, which moraines can be attributed to the LGM is variously discussed in the literature. To determine which ice-ages have formed the different moraines in the amphitheatre, we used cosmogenic nuclide exposure dating on the erratic boulders found on the frontal and lateral moraines.

On a nearby outcropping section of a Ticino River terrace in Castelnovate we applied radiocarbon dating over a profile depth of 5 meters to find ages of deposition. Whilst using multiple preparation methods on the radiocarbon samples we found large variations in the resulting ages. Possible reasons for these variations will be discussed. Combining results of both these dating methods, conventional geomorphological mapping and ArcGIS landscape analysis, we have constructed a spatial and temporal reconstruction of the LGM around Lago d'Orta. This research adds to our understanding of the termination of the LGM on the southern side of the Alps.

P 11.4

Using Stratigraphy and Dendrochronology near Tebano, Senio Northern Apennines to Analyze the Impact of Climatic Fluctuation at Certain Frequencies

Loren Eggenschwiler¹, Vincenzo Picotti², Paolo Cherubini³, Irka Hajdas⁴, Matthias Saurer⁵, Gian Battista Via⁶ & Stefano Marabini⁶

¹ Earth System Science, Department of Geography, UZH, Winterthurststr. 190, CH- 8057 Zürich
(loren.eggenschwiler@uzh.ch)

² Geological Institut, ETH, Sonneggstr. 5, CH- 8057 Zürich

³ Dendroecology, Landscape Dynamics, Swiss Federal Research Institute WSL, Zürcherstr. 111, CH- 8903 Birmensdorf

⁴ Laboratory of Ion Beam Physics ETH, Otto-Stern-Weg 5, CH- 8093 Zürich

⁵ Ecology Fluxes, Paul Scherrer Institute, CH- 5232 Villigen PSI

⁶ BiGEA, Università di Bologna, Via Zamboni 33, IT-40126 Bologna

The presence of *Pinus [sylvestris]* provides an insight into dramatic events due to climatic changes. Several major and minor climatic fluctuations have had a strong impact on terrestrial and marine environments since the last glacial period to present day (Ravazzi et al. 2006). This study aims to describe the response of a fluvial environment through the use of dendrochronology and stratigraphy. Here, we intend to get a better understanding of how these climatic fluctuations affect the behavior of the Senio River (Lotter et al. 1992).

In Tebano, Italy, several *Pinus sylvestris* subfossil trunks were discovered during excavation for an irrigation pool. Subfossil samples were collected to analyze the climate during the Younger Dryas (11,000 years BP) in detail. Charcoal samples from the Bubano clay quarry extend our research to further to 35,500 cal. years BP. The combination of dendrochronology along with stratigraphy allowed us to examine the climate at a detailed local and apply it to a broader spectrum. Tree-ring measurements and cross dating provided a better understanding and verification of extreme events that occurred during the lifespans of the trees. The use of stable isotopes indicates the extreme conditions that occurred. Radiocarbon dating validates the age of the samples and what geological period they come from. Along with stratigraphy, we were able to compile depth data to create a sediment curve. Using various methods throughout this study, we discovered the climatic situation of *Pinus* 11,000 years BP and are able to compare them with samples from today. These present day samples mark two of the southernmost extents of the *Pinus* population. We were then able to comprehend the magnitude of sediment supply and precipitation. Through this collection of methods and data, we are able to understand the influence of climate change in the past and the potential changes of the future.

REFERENCES

- Lotter, A. F.; Eicher, U.; Siegenthaler, U.; Birks, H. J. B. (1992): Late-glacial climatic oscillations as recorded in Swiss lake sediments. In *Journal of Quaternary Science* 7. DOI: 10.1002/jqs.3390070302.
- Ravazzi, Cesare; Donegana, Marta; Vescovi, Elisa; Arpentini, Enrico; Caccianiga, Marco; Kaltenrieder, Petra et al. (2006): A new Late-glacial site with *Picea abies* in the northern Apennine foothills. An exception to the model of glacial refugia of trees. In *Veget Hist Archaeobot* 15 (4), pp. 357–371. DOI: 10.1007/s00334-006-0055-9.

P 11.5

Stromatolites growth in a freshwater environment from Northeastern Patagonia (Argentina)

Inès Eymard¹, María del Pilar Alvarez², Andrés Bilmes², Mariano Gonzalez Dobra³, Fernando Suarez³, Crisogono Vasconcelos⁴, Daniel Ariztegui¹

¹ *Department of Earth Sciences, University of Geneva, Rue de Maraichaire 13, CH-1205 Geneva. (ines.eymard@unige.ch)*

² *CENPAT-CONICET, Puerto Madryn, Chubut, Argentina.*

³ *Universidad Nacional de La Plata, La Plata, Buenos Aires, Argentina.*

⁴ *Geologisches Institut, ETH Zürich, Sonneggstrasse 5, CH-8092 Zürich*

Stromatolites are laminated benthic microbial deposits. Formation and growth of those structures result from the interaction between environmental and microbial factors and is highly influenced by environmental factors allowing to use them as a proxy for paleoenvironmental conditions of the lake. Here fossils and living microbialites have been identified in the freshwater environment of the Maquinchao Basin.

The Maquinchao basin, is a closed lacustrine system located in Northeastern Patagonia at more than 700 above sea level. Today, the basin contains two main lakes, Cari Laufquen Grande and Cari Laufquen Chica, linked through the ephemeral Maquinchao River. However the presence of several paleoshorelines on the east side of Cari Laufquen Grande reports evidence of major water level fluctuations during recent times and the possibility of the presence of one main lake in the basin.

A field campaign has been lead in Austral spring of 2015 to identify preferential zones of development for fossils and living microbialites. Fossil stromatolites are found as individual buildsup, mostly covering basalt nucleus, of 10cm to 1m diameter with characteristic cauliflower and globular shapes and also in continuous metric banks. 3D drone mapping reveals preferential erosion of individual specimen as well as communities located along paleoshorelines at 830m high, south of Cari Laufquen Grande. Today, stromatolites have been replaced by living microbialites found in specific pounds of the Maquinchao River.

Ongoing investigations aim to compare the fossils and living microbialites through different methods: petrographic observations, geochemical analyses, identification of microbial communities, SEM observations. Those results will lead to understand the role of microbes in carbonate precipitation (organomineralisation; Pacton et al.) and defining the environmental and climatic changes contributing to replace microbialites from stromatolites.

REFERENCES

Pacton, M. G Hunger, V Martinuzzi, Cusminsky G, B Burdin, K Barmettler, C Vasconcelos and D Ariztegui, 2016.

Organomineralization processes in freshwater stromatolites: A living example from eastern Patagonia. *The Depositional Record* 1/2: 130–146 (*Open Access*)

P 11.6

Radiocarbon Chronology of Human Settlement and paleo environment in Senegal, West Africa

Irka Hajdas*, Mantana Maurer*, Maria Belen Röttig*, Benoît Chevrier**, Maria Lorenzo Martinez**, Serge Loukou**, Anne Mayor**, Luca Pollarolo**, Michel Rasse***, Aline Garnier****, Laurent Lespez****, Chantal Tribolo*****, Brice Lebrun*****, Abdoulaye Camara*****, Hamadi Bocoum***** & Eric Huysecom**

¹ *ETH Zurich, Laboratory of Ion Beam Physics, Switzerland*

² *APA, Department of Genetic and Evolution, University of Geneva, Switzerland*

³ *Archaeorient, University of Lyon 2, France*

⁴ *Department of Geography, University of Paris-Est Créteil, France*

⁵ *Laboratory IRAMAT-CRP2A, CNRS, University of Bordeaux-Montaigne, France*

⁷ *Institut Fondamental d'Afrique Noire (IFAN), Dakar, Senegal*

Research conducted in the Falémé Valley, East of Senegal, have shown the potential of this region for allowing joint studies on both new archaeological and local palaeoenvironmental data. Three main periods are addressed: Palaeolithic, Protohistory and pre-colonial history. Archaeological and palaeoenvironmental studies on a section of the lower Falémé Valley involve geochronological investigations, which apply 2 techniques: OSL and ¹⁴C.

Each year a set of radiocarbon ages obtained on organic matter collected during the January-March field seasons provide a timeframe for the sites surveyed and excavated. Typically, charcoal sample collected in the field are often of a very low size. Nearly 50 samples were analyzed during the last 3 years. The ages covered time from MIS2 (Chevrier et al., 2016; Lebrun et al., 2016) to the recent Holocene. We will discuss the data available so far and a potential for more precise chronologies of West African archeological sites, as we have started to do in the Dogon Country in Mali (Huysecom et al., 2015; Mayor et al., 2014).

For more information, see <http://www.ounjougou.org>

REFERENCES

- Chevrier, B., Rasse, M., Lespez, L., Tribolo, C., Hajdas, I., Figols, M.G., Lebrun, B., Leplongeon, A., Camara, A. & Huysecom, E., 2016. West African Palaeolithic history: New archaeological and chronostratigraphic data from the Faleme valley, eastern Senegal. *Quaternary International* 408, 33-52.
- Huysecom, E., Ozainne, S., Jeanbourquin, C., Mayor, A., Canetti, M., Loukou, S., Chaix, L., Eichhorn, B., Lespez, L., Le Drezen, Y., Guindo, N., 2015. Towards a Better Understanding of Sub-Saharan Settlement Mounds before Ad 1400: The Tells of Sadia on the Seno Plain (Dogon Country, Mali). *J Afr Archaeol* 13, 7-38.
- Lebrun, B., Chantal, T., Benoît, C., Michel, R., Laurent, L., Alice, L., Irka, H., Abdoulaye, C., Norbert, M., Éric, H., 2016. Establishing a West African chrono-cultural framework: First luminescence dating of sedimentary formations from the Falémé Valley, Eastern Senegal. *Journal of Archaeological Science: Reports* 7, 379-388.
- Mayor, A., Huysecom, E., Ozainne, S., Magnavita, S., 2014. Early social complexity in the Dogon Country (Mali) as evidenced by a new chronology of funerary practices. *J Anthropol Archaeol* 34, 17-41.

P 11.7

Into and out of the Last Glacial Maximum in the Alps

Susan Ivy-Ochs ¹, Christian Wirsig ¹, Jerzy Zasadni ², Kristina Hippe ¹, Marcus Christl ¹, Naki Akçar ³, and Christian Schlüchter ³

¹ *Ion Beam Physics, ETH, 8093 Zurich, Switzerland,*

² *Faculty of Geology, Geophysics and Environmental Protection, AGH University of Science and Technology, Kraków, Poland,*

³ *Geology, University of Bern, 3012 Bern, Switzerland*

Glaciers flowing out from local ice caps and extensive ice fields in the high Alps filled the main valleys and extended onto the forelands building piedmont lobes during the Last Glacial Maximum (LGM). The maximum extent at the outermost LGM moraines was reached by about 27-26 ka as shown by data from the Rhein Glacier area (Keller and Krayss, 2005). Abandonment of the outermost moraines at sites both north and south of the Alps was underway by 24 ka, as recorded at the Tagliamento (Monegato et al., 2007) and Orta amphitheatres on the Italian side (see SGM poster Braakhekke et al.) (cf. Scapozza et al., 2014). Similar dates are obtained for the Reuss Glacier area (Reber et al., 2014). Thereafter, glaciers oscillated at stillstand and minor re-advance positions on the northern forelands for several thousand years forming the LGM stadial moraines, for example, Killwangen, Schlieren, Zurich stadial moraines of the Linth-Rhein Glacier. Final recession to back within the mountain front took place by 19-18 ka. In the high Alps, systems of transection glaciers with transfluences over many of the Alpine passes, dominated. A good example is Grimsel Pass in the Central Alps (Switzerland). ¹⁰Be exposure ages of 23 ± 1 ka for glacially sculpted bedrock located just a few meters below the LGM trimline in the Haslital near Grimsel Pass suggest a pulse of ice surface lowering at about the same time that the outer foreland moraines were being abandoned (Wirsig et al., 2016). Widespread ice surface lowering, noted at our study sites near Mt. Blanc, Haslital, and Zillertal was well underway no later than 18 ka, with a similar timing to stabilization of the inner LGM moraines. Recalculation to a common basis of all published ¹⁰Be exposure dates related to LGM extents combined with recent data suggests a strong degree of synchrony for the timing of onset of ice decay both north and south of the Alps (Ivy-Ochs, 2015).

REFERENCES

- Ivy-Ochs S. 2015. Cuadernos de investigación geográfica 41: 295-315.
 Keller O., Krayss E. 2005. Vierteljahrschr. Naturforsch. Gesell. Zürich 150: 69-85.
 Monegato G. et al. 2007. Quat. Res. 68: 284-302.
 Reber R. et al. 2014. Swiss Journal of Geosciences 107: 293-307.
 Scapozza C. et al. 2014. Géomorphologie: relief, processus, environnement 20: 307-322.
 Wirsig C. et al. 2016. J. Quat. Sci. 31: 46-59.

P 11.8

Wildfire effects on lipid composition and hydrophobicity in bulk soil and soil size fractions

Nicasio T. Jiménez-Morillo¹, Jorge E. Spangenberg², José A. González-Pérez¹, Antonio Jordán³, Lorena M. Zavala³ & Francisco J. González-Vila¹

¹ Institute of Natural Resources and Agrobiology of Sevilla, IRNAS-CSIC, ES-41012 Sevilla, Spain
(njimenez@irnas.csic.es).

² Institute of Earth Surface Dynamics (IDYST), University of Lausanne, Géopolis, CH-1015 Lausanne, Switzerland
(Jorge.Spangenberg@unil.ch).

³ Department of Crystallography, Mineralogy and Agricultural Chemistry, University of Sevilla, ES-41012 Sevilla, Spain.

Low soil-water affinity and soil water repellency (SWR, hydrophobicity) prevents water from wetting or infiltrating soils in burnt and unburnt ecosystems, causing various changes on their hydrology, geomorphology, geochemistry, and biochemistry. Wildfire may destroy, develop or enhance SWR in previously wettable or water-repellent soils (e.g., Doerr et al., 2009; Jordán et al., 2013 and references therein). SWR is at least in part attributed to a lipid-like cover, rich in fatty acids (FAs). Recently, it was shown that FAs had a major role in increasing the water repellency of unburnt sandy soils in Doñana National Park (DNP, SW-Spain), with Mediterranean climate and developed under trees (*Quercus suber*, *Pinus pinea*) and shrubs (*Pteridium aquilinum*, *Halimium halimifolium*) dominated vegetation (Jiménez-Morillo et al., 2016).

To get further insight into how fire affect the distribution of soil lipids and their role in the SWR, a study was performed on different size fractions of a DNP sandy soil under *Quercus suber* canopy cover. Two soil samples were taken, one in a burnt site and another in an adjacent unburnt (control) one, both having the same physiographic characteristics. SWR was determined using water-drop-penetration-time test in the <2 mm sieved (bulk) soils and in six size fractions: 1-2 mm, 0.5-1 mm, 0.25-0.5 mm, 0.1-0.25 mm, 0.05-0.1 mm and <0.05 mm. Lipids were extracted from all samples ($n = 14$), and the FAs and neutral lipids were identified and quantified by GC/MS and GC/FID. The carbon isotope ratios ($\delta^{13}\text{C}$ values) for the individual fatty acids were determined by GC/C/IRMS.

The SWR values of soil samples and fractions were statistically different ($p < 0.01$), for both, the fire affected and unaffected soils, and different grain-size fractions. SWR values in burnt bulk soil and 0.05-0.1 mm fraction were higher than in unburnt homologues. The coarsest and finest soil fractions (1-2 mm and <0.05 mm, respectively) of the unburnt soil were the most hydrophobic; in contrast, the finer fractions (0.05-0.1 mm and <0.05 mm) were the most hydrophobic in burnt soils. The total amount of lipids and total FAs were higher in burnt bulk sample and all the size fractions, except the coarser one, which had twice the amount of lipids, compared to the burnt one. All samples showed similar distribution of saponifiable lipids, characterized by straight chain saturated acids in the C_{14} - C_{32} range and only differing in their relative abundance. In bulk soil and <0.5 mm fractions the concentrations (mg FA/g soil) of the FAs were higher in burnt compared to unburnt soil (this difference was small or absent in C_{22}). For the coarser fractions, the opposite trend was observed in most FAs, except C_{18} , and for $\text{C}_{<20}$ acids in the 0.5-1 mm fraction. All the samples showed generally very similar distribution of non-saponifiable lipids, dominated by C_{27} , C_{28} and C_{29} sterols and triterpenols, and a less abundant homologous series of n -alkan-1-ols in the C_{20} to C_{28} range and small amount of n -alkanes in the C_{23} to C_{28} range. Bulk soil and the size-fractions, except the coarser one, had higher concentrations in most neutral lipids. Principal component analysis (PCA) performed on lipid concentration, concentration ratios and SWR (Fig. 1A) indicated that hydrophobicity of soils were positively correlated to total amount of lipids, normal $\text{C}_{>24}$ FAs and branched $\text{C}_{>24}$ FAs, and negatively correlated with the even/odd FAs ratio. The scatterplot of the PC1 vs PC2 scores showed that all the burnt samples formed a cluster at values around 0, the unburnt coarse (>0.5 mm) and finest (<0.05 mm) fractions were positively correlated with SWR and total lipids, the bulk and intermediate fractions (0.5-0.05 mm) negatively (Fig. 1B). The biosynthetic origin of these lipids, and their transformation pathways during fire will be discussed with the results of the ongoing measurements of the $\delta^{13}\text{C}_{\text{FA}}$ values.

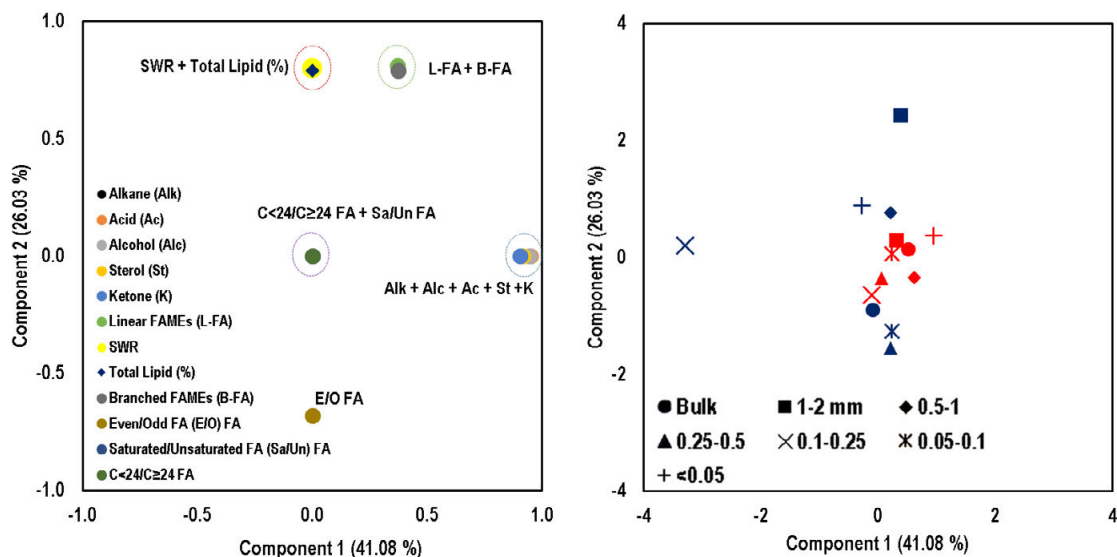


Figure 1. Principal components analysis (PCA) of lipid concentrations, concentration ratios and SWR. A. Loadings of variables; B. Scores of samples

REFERENCES

- Doerr, S.H., Shakesby, R.A., Blake, W.H., Chafer C.J., Humphreys, G.S., & Wallbrin, P.J. 2006: Effects of differing wildfire severities on soil wettability and implications for hydrological response. *Journal of Hydrology*, 319, 295–311.
- Jiménez-Morillo, N.T., González-Pérez, J.A., Jordán, A., Zavala, L.M., de la Rosa, J.M., Jiménez-González, M.A., & González-Vila, F.J. 2016: Organic Matter Fractions Controlling Soil Water Repellency in Sandy Soils From the Doñana National Park (Southwestern Spain). *Land Degradation and Development*, 27, 1413–1423.
- Jordán, A., Zavala, L.M., Mataix-Solera, J., Doerr, S.H. 2013: Soil water repellency: origin, assessment and geomorphological consequences. *Catena*, 108, 1–8.

P 11.9

Dating the stabilisation age of relict rockglaciers

Olivia Kronig¹, Jürgen M. Reitner², Marcus Christl¹, Susan Ivy-Ochs¹

¹ *Laboratory of Ion Beam Physics (LIP), ETH Zurich, Otto-Stern-Weg 5, CH-8093 Zurich (okronig@phys.ethz.ch)*

² *Geological Survey of Austria, Neulinggasse 38, A-1030 Vienna*

Rockglaciers are periglacial landforms and hence require permafrost conditions. The terminus of an active rockglacier is used to define the lower boundary of discontinuous permafrost and corresponds roughly to a mean annual air temperature of -2 °C to -1 °C in an environment where the annual precipitation is less than 2500 mm (Haeberli 1985). The stabilisation of a rockglacier describes the transition of an active to an inactive and finally to a relict rockglacier. Therefore, the time when a relict rockglacier stabilised and its position can be linked to past permafrost conditions, which reflect past climatic conditions. This makes rockglaciers an interesting source for regional paleoclimatic reconstructions.

The Tendl rockglacier is situated in the province of Carinthia (Austria), at the western valley side of the Maltatal, along the north-facing flank of the Reisseck mountain range. It is a relict rockglacier with a series of lobes. The highest lobe is at 2300 m above sea level (a.s.l) and the lowest reaches down to 1220m a.s.l., and thus lies nearly 1300 m below the modern permafrost limit. It is likely the lowest relict rockglacier of the Eastern Alps (Reitner 2007). A total of 20 samples of the entire succession, from the lowest up to the higher lobe, were taken for cosmogenic nuclide exposure dating. So far only few studies world-wide used exposure dating to date relict rockglaciers (Ivy-Ochs et al. 2009; Moran et al. 2016).

Additionally 14 samples were taken on another series of rockglaciers no further than 10 km to the south-west, in a side valley close to Mühldorf. They are located on a south-facing mountain. This offers the possibility to obtain further information about the influence of the geographic exposition to changes in the permafrost limit.

REFERENCES

- Haeberli, W. 1985: Creep of mountain permafrost, Mitteilungen der VAW der ETH Zürich, 77
- Ivy-Ochs, S., Kerschner, H., Maisch, M., Christl, M., Kubik, P. W. & Schlüchter, C. 2009: Latest Pleistocene and Holocene glacier variations in the European Alps. *Quaternary Science Reviews*, 28 (21-22), 2137-2149.
- Moran, A. P., Ivy-Ochs, S., Vockenhuber, C., & Kerschner, H. 2016: Rock glacier development in the Northern Calcareous Alps at the Pleistocene-Holocene boundary. *Geomorphology*, 273, 178-188.
- Reitner, J. M. 2007: Bericht 2005-2006 über geologische Aufnahmen im Quartär auf Blatt 182 Spittal an der Drau. *Jahrbuch der Geologischen Bundesanstalt* 147/3-4, Wien. 672-676.

P 11.10

A benthic foraminifera species respond to anoxia with a strong metabolic shift suggesting a state of dormancy

Charlotte LeKieffre¹, Jorge E. Spangenberg², Guillaume Mabilieu³, Anders Meibom^{1,4} & Emmanuelle Geslin⁵

¹ Laboratory for Biological Geochemistry, ENAC, Ecole Polytechnique Fédérale de Lausanne (EPFL), CH-1015 Lausanne (charlotte.lekieffre@epfl.ch)

² Institute of Earth Surface Dynamics (IDYST), University of Lausanne, Géopolis, CH-1015 Lausanne

³ SCIAM, Service Commun d'Imagerie et Analyses Microscopiques, IRIS-IBS Institut de Biologie en Santé, CHU d'Angers, LUNAM Université, France

⁴ Center for Advanced Surface Analysis, Institute of Earth Sciences, University of Lausanne, Géopolis, CH-1015 Lausanne

⁵ UMR CNRS 6112 - LPG-BIAF, University of Angers, France

Low-oxygenation events are more and more frequent and strong on continental shelves and in coastal areas where renewal of bottom waters is slow. Among the meiofauna living in such environments, foraminifera are among the most tolerant to the lack of oxygen. Some benthic foraminiferal species are able to survive hypoxia, and even anoxia, for weeks to months. Different species must have developed different mechanisms for survival - hypotheses include reduction of the metabolism, symbiosis with bacteria, or denitrification. *Ammonia tepida*, one of the most abundant species in intertidal environments, is able to survive up to 60 days in anoxia. Here we combined a 4 week feeding experiment using ¹³C-enriched microalgae (diatoms), with correlated transmission electron microscopy (TEM) and NanoSIMS (Secondary Ion Mass Spectrometry) imaging, and concentrations (GC/MS, GC/FFID), as well as bulk and compound specific carbon isotope ratios (¹³C/¹²C obtained by EA/IRMS and GC/C/IRMS) of individual fatty acids (FAs) to study the metabolic differences in intertidal *Ammonia tepida* exposed to oxic and anoxia conditions, respectively.

Strongly contrasting cellular-level dynamics of integration and transfer of the ingested biofilm components were observed under the two conditions. Under oxic conditions, within a few days, intact diatoms (i.e. including the frustule) were ingested, assimilated and consumed, in part for biosynthesis of different cellular components: ¹³C-labeled lipid droplets formed over a timescale of a few days and were then partly lost through respiration. In contrast, in anoxia, fewer diatoms were initially ingested and these were not assimilated or metabolized further, but remained visible within the foraminiferal cytoplasm even after 4 weeks. The compound specific ¹³C/¹²C ratios indicated substantial *de novo* synthesis by the foraminifera of polyunsaturated FAs (PUFAs), such as 20:4(*n*-6), in oxic conditions; very limited PUFA synthesis was observed under anoxia. Together, our results indicate that anoxia induced a greatly reduced rate of heterotrophic metabolism in *Ammonia tepida* on a time scale of about 24 hours, which seems consistent with a state of dormancy.

P 11.11

Application of the Mutual Ostracod Temperature Range method (MOTR) to a sediment core from Lake Trasimeno (Umbria, central Italy)

Marta Marchegiano¹, Dave Horne², Elsa Gliozzi³, Alexander Francke⁴, Daniel Ariztegui¹

¹ Department of Earth Sciences, University of Geneva, 13 rue de Maraichers, 1205 Geneva, Switzerland

² School of Geography, Queen Mary University of London, Mile End Road, London E1 4NS, UK

³ Department of Science, University Roma Tre, Largo S. Leonardo Murialdo 1, 00146 Rome, Italy

⁴ University of Cologne, Institute of Geology and Mineralogy, Cologne, Germany

Recent studies have shown that the Late Quaternary has been affected by numerous and rapid climate fluctuations. Different techniques have been developed to reveal their extent and associated effects on the environment. Here we present the application of the Mutual Ostracod Temperature Range (MOTR) method (Horne, 2007), on a 8.59 m long sediment core from Lake Trasimeno (Umbria, Italy; 43°09' N and 12°06' E). The MOTR is a non-analogue method for reconstructing paleotemperature using freshwater ostracod assemblages. It only considers the species still living today with a known climatic distribution. The temperature ranges, which enclose all the living records of the species, are determined by fitting WorldClim database (version 1.3) (Hijmans et al., 2001) to the mapped coordinate points of the species' distribution, and are expressed in terms of the maximum and minimum values of July and January temperature ranges. The mutual temperature range of all the species recovered in a fossil assemblage, representing the T interval in which they could have co-existed, provides the palaeotemperature reconstruction for that time interval. The Lake Trasimeno sediment core is ideal to be studied using the MOTR method because it contains the continuous presence of ostracods throughout the entire record. Thus, this new record will be an important tool for (still in progress) palaeoclimatic and palaeoenvironmental reconstruction since, until today only a few continental records provide high-resolution analyses of Late Quaternary climatic change. The 350 samples, which were analysed in this study, carried 19 different species of ostracods referable to 15 genera: *Cyprideis torosa*, *Candona angulata*, *Candona neglecta*, *Candona candida*, *Heterocypris incongruens*, *Cytheromorpha fuscata*, *Sarscypridopsis aculeata*, *Heterocypris salina*, *Ilyocypris sp.*, *Eucypris inflata (mareotica)*, *Darwinula stevensoni*, *Limnocythere inopinata*, *Limnocythere friabilis*, *Potamocypris paludum*, *Trajancypris serrata*, *Amnocythere sp.*, *Herpetocypris helenae*, *Cypridopsis vidua*, *Plesiocypridopsis newtoni*. Since the MOTR method is developed only for freshwater species *Cyprideis torosa* (a typically brackish water species although it occurs sometimes in freshwater) is not calibrated and so could not be used. *Amnocythere sp.* and *Ilyocypris sp.* (for taxonomic uncertainty) and *Trajancypris serrata*, *Potamocypris paludum* and *Herpetocypris helenae* (still not calibrated) are also excluded. First results have produced a high-resolution paleotemperature curve covering the interval from 45152ka to 10696ka (sediment depth 7.7 to 3.3m) according to a chronology, which is based on 10 radiocarbon age control points. Ways of interpreting the MOTR results and correlating them with equivalent palaeotemperature curves from the region are being explored. Ongoing isotopic analyses on the ostracod shells will be used to improve the paleotemperature reconstruction.

REFERENCES

- Hijmans, R.J., Guarino, L., Cruz, M. & Rojas, E., 2001. Computer tools for spatial analysis of plant genetic resources data: 1. DIVA-GIS. Plant Genetic Resources Newsletter No. 127, 15–19.
- Horne, D.J., 2007. A Mutual Temperature Range method for Quaternary palaeoclimatic analysis using European nonmarine Ostracoda. Quaternary Science Reviews 26, 1398–1415

P 11.12

Iron fertilization in the Subantarctic Indian Ocean during the last glacial cycle and the drawdown of atmospheric CO₂

Simone Moretti¹, Samuel Jaccard², Daniel Montluçon¹, Alfredo Martínez-García³ & Timothy Ian Eglinton¹

¹ *Department of Earth Sciences, ETH Zürich, Sonneggstrasse 5, CH-8092 Zürich (smoretti@student.ethz.ch)*

² *Institute of Geological Sciences, University of Bern, Baltzerstrasse 1+3, CH-3012 Bern*

³ *Climate Geochemistry Group, Max Planck Institute for Chemistry, Hahn-Meitner-Weg 1, DE-55128 Mainz*

Following the characterization of the Pleistocene ice ages based on the study of marine sediment cores (Emiliani, 1955) and their astronomically controlled cyclicity (Hays, 1976) new observations were provided by ice core archives that suggested CO₂ varied in concert with the Milankovitch-paced waxing and waning of ice sheets and temperature shifts over Antarctica during the last 800.000 years with CO₂ variations ranging from 180 to 280 ppm (Petit et al., 1999).

Several decades of studies have been trying to understand what caused CO₂ to systematically vary in sync with ice ages and the role it played in regulating the climate of the past.

The best candidate to account for the observed CO₂ variations is the Ocean, which is by far the largest reservoir of carbon on timescales relevant to ice ages cycles (Sigman & Boyle, 2000).

The current focus is directed in particular toward the Southern Ocean, which has been an area of net outgassing of CO₂ to the atmosphere (Sarmiento & Gruber, 2006), due to the interaction of biogeochemistry and ocean circulation that results in a low-efficiency biological pump (Sigman & Haug, 2003).

A possibly mechanism that could reduce this “leak” of carbon to the atmosphere by increasing the efficiency of the biological pump is related to the “iron (Fe) fertilization hypothesis” (Martin, 1990). Iron is a limiting nutrient in the present day Southern Ocean and evidence from the Atlantic (Martínez-García et al., 2014) and Pacific (Lamy et al., 2014) Subantarctic showed an increase of productivity tightly coupled with increasing airborne Fe supply to these regions. Iron fertilization could explain up to 50% of the glacial to interglacial CO₂ shift (Martínez-García et al., 2014), provided fertilization took place equally over the whole Subantarctic, an argument that is challenged by some model simulations (Bopp et al., 2003).

In this work, we analysed a sediment core, whose record span the last glacial cycle back to MIS6, which was retrieved in the Subantarctic Indian Ocean. This sector has been relatively unexplored in terms of paleo-productivity estimates of phytoplankton related to bioavailable iron fertilization, and hence is an important location to assess whether this process was a globally distributed process able to lead to a significant drawdown of atmospheric CO₂, rather than a localised event with a minor impact on the global carbon cycle.

In order to address this question, we made use of both inorganic and organic-based proxies as tracers of past oceanographic conditions.

In particular, we analysed fundamental sediment properties like elemental composition, CaCO₃ and opal content and bulk organic carbon abundance as well as the quantification of different biomarker lipids (including alkanes, alkenones and GDGTs).

Our results shows that the concentration of iron is very likely related mostly to input from continents and that this iron is certainly related to an increase of primary production of alkenone-producing Haptophyte algae and diatoms. However, it also clear that the onset of alkenone productivity initiates before the onset of iron supply. This is supported also by the observation that opal, another tracers for paleo-productivity, is also anticipating the iron signal. We infer that the initial trigger of changes in paleo-productivity is related to a northward displacement of the polar front position and nutrient-rich Antarctic waters, which is then followed by an incipient increase of iron supply from the continents which jointly determines a strong increase of primary production in the Subantarctic Indian sector. This is consistent with the glacial increase of productivity observed in the Atlantic (Martínez-García et al., 2014) and Pacific (Lamy et al., 2014) Subantarctic sectors, suggesting that a strengthening of the biological pump during glacial times was a global scale process rather than a localised one, and hence being able to be a quantitatively important player for the drawdown of atmospheric CO₂ during glacial cycles.

REFERENCES

- Bopp, L., Karen E. K., Corinne L. Q., and Olivier A. 2003: Dust Impact on Marine Biota and Atmospheric CO₂ during Glacial Periods, *Paleoceanography* 18, no. 2: 1046.
- Emiliani, C. 1955: Pleistocene Temperatures, *The Journal of Geology*, 63(6), 538-578.
- Hays, J., Imbrie, J., & Shackleton, N. 1976: Variations in the Earth's Orbit: Pacemaker of the Ice Ages, *Science*, 194(4270), 1121-1132.
- Lamy, F., Gersonde, R., Winckler, G., Esper, O., Jaeschke, A., Kuhn, G., . . . Kilian, R. 2014: Increased Dust Deposition in the Pacific Southern Ocean During Glacial Periods, *Science*, 343, 403-407.
- Martínez-García, A., Sigman, D.M., Ren, H., Anderson, R., Straub, M., Hodell, D., Jaccard, S.L., . . . Haug, G.H. 2014: Iron Fertilization of the Subantarctic Ocean During the Last Ice Age, *Science*, 343, 1347-1350.
- Petit, J.R., Jouzel, J., Raynaud, D., Barkov, N.I., Barnola, J.-M., Basile, I., Bender, M., . . . Stievenard, M. 1999: Climate and atmospheric history of the past 420,000 years from the Vostok ice core, Antarctica, *Nature*, 399, 429-436.
- Sigman, D.M., & Boyle, E.A. 2000: Glacial/interglacial variations in atmospheric carbon dioxide, *Nature*, 407, 859-869.
- Sigman, D.M. & Haug, G.H. 2003: The biological pump in the past. In: Elderfield H (ed.) *Treatise on Geochemistry, The Oceans and Marine Geochemistry*, vol. 6, pp. 491-528. Oxford: Elsevier Pergamon.

P 11.13

Centennial-scale variability of the Early Holocene Humid Period in NW Arabia inferred from high-resolution geochemistry and microfacies of the Tayma palaeolake

Ina Neugebauer^{1,2} Birgit Plessen², Michèle Dinies³, Max Engel⁴, Rik Tjallingii² & Achim Brauer²

¹ *Département des Sciences de la Terre, University of Geneva, Rue des Maraîchers 13, CH-1205 Genève (Ina.Neugebauer@unige.ch)*

² *Sektion 5.2 Klimadynamik und Landschaftsentwicklung, GFZ German Research Centre for Geosciences, Telegrafenberg, D-14473 Potsdam*

³ *Referat Naturwissenschaften - Archäobotanik, German Archaeological Institute (DAI), Im Dol 2-6, D-14195 Berlin*

⁴ *Geographisches Institut, University of Cologne, Albertus-Magnus-Platz, D-50923 Köln*

The Early Holocene Humid Period (EHHP) caused a much increased availability of freshwater in subtropical regions suffering from hyperaridity today. Thereby, enhanced orbital summer insolation forced a strengthening and northward expansion of the African summer monsoon between ca. 10 and 6 ka BP. However, while the underlying mechanisms of the EHHP are fairly well understood and the subsequent environmental responses are documented in numerous North African lake records, most of these records fail to present better than millennial-scale changes. Moreover, palaeoclimate records from the Arabian Peninsula are extremely underrepresented.

The Tayma palaeolake is a rare archive of EHHP in northern Arabia (Dinies et al. 2015; Engel et al. 2012). Here we present a ca. 1 m thick and 700 years spanning annually laminated sediment section that was deposited in the centre of the former lake from ca. 8500 to 7800 calibrated years (cal. yrs) BP, as determined by AMS ¹⁴C dating of pollen concentrates (Dinies et al. 2015). High-resolution microfacies analyses based on thin section microscopy and μ XRF element scanning, as well as $\delta^{18}\text{O}_{\text{carb}}$ and $\delta^{13}\text{C}_{\text{carb}}$ measurements on single carbonate laminae and on bulk samples were performed in order to investigate the sedimentological and geochemical changes along the varved sequence in great detail.

The finely laminated marl sediments are mainly composed of sub-mm thick laminae of endogenic aragonite, organic matter and diatoms, as well as occasional silt-clay layers. Following an early lake phase from ca. 8700 to 8500 cal. yrs BP characterized by coarsely laminated, presumably non-annual marl sediments that are rich in ostracods, three main varved phases can be distinguished within the investigated section: (1) aragonitic-organic varves from ca. 8500 to 8150 cal. yrs BP, (2) diatom-organic varves from ca. 8150 to 7900 cal. yrs BP that frequently include aragonite laminae and occasionally gastropod and ostracod shells, and (3) clastic-organic varves from ca. 7900 to 7800 cal. yrs BP with decreasing diatom and aragonite laminae and an increasing frequency of gypsum layers. After this period, gypsum becomes abundant and fine lamination appears only sporadically. In addition, we observe an increasing trend of $\delta^{13}\text{C}_{\text{carb}}$ and decreasing $\delta^{18}\text{O}_{\text{carb}}$ during phase 1 with the highest/lowest values, respectively, during phase 2, pointing towards the maximum lake productivity and increased seasonal precipitation.

Our results indicate that the EHHP experienced pronounced centennial-scale climatic fluctuations. The EHHP was comparably short in the NW Arabian region, lasting from ca. 8700 to 7800 cal. yrs BP with the highest moisture availability at around 8200 to 7900 cal. yrs BP. A preceding dry period observed from ca. 8500 to 8300 cal. yrs BP challenges the prior idea that this dry spell, recognised in other African records at that time as well, was connected to the so-called 8.2 ka cold event in the North Atlantic realm. In addition to the earlier appearance of this dry period, its longer duration compared to the rather short 8.2 event suggests an independent trigger mechanism.

This study is a contribution to the research project "CLEAR - Holocene CLimatic Events of Northern ARabia" (<https://clear2018.wordpress.com/>).

REFERENCES

- Dinies, M., Plessen, B., Neef, R. & Kürschner, H. 2015: When the desert was green: Grassland expansion during the early Holocene in northwestern Arabia, *Quaternary International*, 382, 293-302.
- Engel, M., Brückner, H., Pint, A., Wellbrock, K., Ginau, A., Voss, P., Grottker, M., Klasen, N. & Frenzel, P. 2012: The early Holocene humid period in NW Saudi Arabia – Sediments, microfossils and palaeo-hydrological modelling, *Quaternary International*, 266, 131-141.

P 11.14

Lateglacial deglaciation of the High Tatra Mountains

Ewelina Opyrchał¹, Jerzy Zasadni¹, Piotr Kłapyta², Marcus Christl³, Susan Ivy-Ochs³

¹ Faculty of Geology, Geophysics and Environmental Protection, AGH University of Science and Technology, al. Mickiewicza 30, 30-059 Kraków, Poland (ewelinaopyrchal@gmail.com)

² Institute of Geography and Spatial Management, Jagiellonian University, ul. Gronostajowa 7, 30-387 Kraków, Poland

³ Laboratory of Ion Beam Physics (LIP), ETH Swiss Federal Institute of Technology, Zürich, Otto-Stern-Weg 5, 8093 Zürich, Switzerland

The Tatra Mountains present well developed and preserved alpine-type landscape to the north of the Alps with no contemporary glaciation. This northernmost massif in the Carpathians had been shaped by several valley glaciers in the past, however, glacial advances in the highest parts of these mountains have never been fully investigated. The aim of this study is to reconstruct a chronology of the youngest glacier advances and the timing of deglaciation of high elevated glacial cirques from the example of Veľká Studená Valley located on the southern slope of the High Tatra Mountains (Slovakia). Based on digital spatial data analysis and geomorphological mapping the valley has been investigated. We have collected samples for surface exposure dating with cosmogenic ¹⁰Be and tested selected surfaces using Schmidt hammer method. Dating methods in combination with morphostratigraphy allow to identify periods and ranges of glacier advance and retreat within the valley cirque. Preliminary results revealed two glacier advances which occurred in the late Pleistocene and both were limited to the glacial cirque. The first advance which almost entirely covered the bottom of the cirque is confirmed by several ages on an voluminous lobate latero-frontal moraine. The extent of the second advance has been marginalized and is represented by small relict talus-rock glaciers and moraines of glaciers which advanced from the cirque walls towards the center of the cirque. These two advances have remarkably different geometry and cross-cutting relations can be observed. The older advance represents a pre-Bølling–Allerød glacier activity, whereas the younger one is related to the Younger Dryas cold phase. Since no younger moraines were found, the obtained results lead to the conclusion that in the study area glaciers have never advanced during the Holocene.

P 11.15

Tracking the pace of Middle Pleistocene Revolution in the southern Alpine Foreland

Soumita Patra^a, Naki Akçar^a, Susan Ivy-Ochs^b, Giovanni Monegato^c

^a*Institute of Geological Sciences, University of Bern, Baltzerstrasse 1-3, 3012, Bern, Switzerland*

^b*Laboratory of Ion Beam Physics (LIP), ETH Zurich, Schafmattstrasse 20, 8093, Zurich, Switzerland*

^c*Department of Geosciences, University of Padova, Via Gradenigo 6, 35131 Padova, Italy*

The southern Alpine foreland, enclosed between the Adriatic Sea and the Alps, represents a key area to understand the climate and environmental transition between Mediterranean and Central Europe through the Quaternary global climate change. During the Middle Pleistocene Revolution (MPR), the structure of the glacial-interglacial cycles changed from 41 ka (low-amplitude/high-frequency) to 100 ka (high-amplitude/low-frequency) oscillations. This transition resulted in changes in landscape evolution. These changes are recorded terrestrial geo-archives, which are generally discontinuous in space and time. In the Middle Pleistocene the first major expansion of the alpine glaciers triggered a change in drainage patterns and a marked increase in erosion rates in the southern Alpine Foreland, where the MPR is commonly attributed to re-organization of the drainage system of the rivers.

During the Middle Pleistocene glaciers advanced repeatedly from the Alps to the Alpine foreland. The chronology of the records of those changes in the southern Alpine Foreland is not completely constrained. Therefore, the aim of this study is to quantify landscape evolution since the onset of Early Pleistocene based on the detailed study of glacio-fluvial deposits which was accumulated by glacial meltwater.

For this, we will apply detailed mapping, analyze the sedimentology of these sequences and calibrate their chronology with cosmogenic nuclides. We will apply both depth-profile and isochron-burial techniques with cosmogenic ^{10}Be , ^{26}Al and ^{36}Cl to date these deposits. Based on the reconstructed chronology, we will report post-depositional incision rates into bedrock. For the provenance analysis, the lithology of approximately 250 clasts from the gravel fraction (16-63 mm) will be determined and counted. Subsequently, counted gravels will be grouped into different lithological classes. In addition key lithologies will be identified. Based on the results, we will define the provenance of sediments, estimate catchment-wide erosion rates, gather information on their transport, depositional environments, date their accumulation and calculate bedrock incision rates.

P 11.16

Re-visiting radiocarbon ages of Oetzi the Ice Man

Duygu Saracoğlu*, Irka Hajdas**, Mantana Maurer**, Maria Belen Röttig**, Susan Ivy-Ochs**, Hans-Arno Synal**

¹ *Istanbul Technical University, Turkey*

² *ETH Zurich, Laboratory of Ion Beam Physics, Switzerland*

A quarter of century ago remains of a frozen and mummified body were discovered on the Hauslabjoch in the Ötztaler Alps (near the Similaun Mountain), South Tyrol, Italy in September 1991. The first step in investigation of this Ice Man was to find out how old it was. Acceleration mass spectrometry (AMS) was used for age determination because the smallest amount of the sample had to be used for dating. A fragment of tissue and the bone were submitted to the laboratory at ETH Zurich. In addition a small piece of grass was found in the Ice Man's tissue and analyzed. The mean value of all the all the measurements was 4550 ± 27 BP (Bonani et al. 1994)

The samples from the Ötztal were kept in a glass jar since November 1991 (Fig.1a). In this study we perform additional analysis on the remaining material that had been stored frozen for 25 years. First of all, the sample was controlled for contaminants by examination under the binocular microscope (Fig. 1b). At that moment, pieces of grass which was determined from the sample noted and divided from the skin and muscle tissue. The Ice Man sample is similar to Animal skin parchment, which can easily dissolve in base. Therefore, the normal acid-base-acid (ABA) treatment was to be attenuated to clean the samples (Hajdas 2008). We will present results obtained on seven additional samples.



Figure 1a (left) Sample has been stored frozen for 25 years. 1b one of the sub-samples picked out for new 2016 analysis

REFERENCES

Bonani, G., Ivy, S.D., Hajdas, I., Niklaus, T.R., Suter, M. 1994: AMS C14 age determinations of tissue, bone and grass samples from the Ötztal ice man, 2, 247-250.

P 11.17

Leaf waxes and compound-specific isotopes indicate more humid conditions in Spain during the LGM

Imke Kathrin Schäfer¹, Marcel Bliedtner¹, Lorenz Wüthrich¹, Daniel Wolf², Jana Zech¹, Dominik Faust² & Roland Zech¹

¹ *Geographisches Institut and Oeschger Centre for Climate Change Research, University of Bern, Hallertsrasse 12, CH-3007 Bern (imke.schaefer@giub.unibe.ch)*

² *Department of Geography, Technical University Dresden, Helmholtzstrasse 10, DE-01069 Dresden*

The Western Mediterranean Region increasingly suffers under the consequences of global warming, particularly extreme drought periods. To better understand these changes and to predict future ones, past climate and environmental changes provide a useful context. Here we present results of leaf wax and compound-specific isotope analyses from the ~8 m high loess paleosol sequence El Paraíso, Central Spain. Chain length patterns generally show a dominance of grass-derived $n\text{-C}_{31}$ and $n\text{-C}_{33}$ alkanes, but more deciduous tree-derived $n\text{-C}_{27}$ at ~2 m depth can be interpreted to reflect more humid conditions during the Last Glacial Maximum (LGM: ~25 ka). Most enriched $\delta^{13}\text{C}_{n\text{-alkane}}$ values before ~30 ka indicate particularly arid conditions, followed by more depleted values and more humid conditions during the LGM. The observed ~2‰ decrease in $\delta^{13}\text{C}$ since can largely be explained by the increase in atmospheric $p\text{CO}_2$. Compound-specific deuterium analyses show more enriched values during the last glacial compared to the Holocene, which probably simply reflects the enrichment of the source water (North Atlantic) and should not be interpreted as enhanced evapotranspiration. Our results (i) confirm the idea of a more humid LGM in the Western Mediterranean Region based on lake levels, fluvial records and climate modelling, (ii) show some controversy with regard to pollen records, and (iii) fuel concerns of more severe droughts in the near, warmer future.

P 11.18

Multiple stable isotope analysis of vegetable oils from the southern and northern hemispheres: increasing an archaeological/paleoclimatic database

Jorge E. Spangenberg¹

¹ *Institute of Earth Surface Dynamics (IDYST), University of Lausanne, Géopolis, CH-1015 Lausanne (jorge.spangenberg@unil.ch)*

The impact of globalization on food systems (food availability, supply, marketing, distribution, consumption, dietary patterns) in developing countries, largely caused by the growth of urban population, has important impact on food security, health and nutrition. In particular it has changed the international demand for healthy edible oils, their trade and business strategies in the EU and worldwide. This, in turn, also impacts the domestic vegetable oil production. Therefore, the characterization and authentication of vegetable oils (liquid) and fats (solid) is of prime importance for human health and economic growth. As further application, their bulk and molecular C, H and O stable isotope composition ($\delta^{13}\text{C}$, $\delta^2\text{H}$, and $\delta^{18}\text{O}$ values) can be employed as a valuable database for archaeological, palaeoclimatic and paleoenvironmental research.

The $\delta^{13}\text{C}$, $\delta^2\text{H}$, and $\delta^{18}\text{O}$ values of plants and their products are linked to photosynthetic fractionation, environmental factors and agricultural practices. The $\delta^{13}\text{C}$ values of plants record their photosynthetic origin and adaptation to environmental conditions. Northern hemisphere atmospheric $\delta^{13}\text{C}_{\text{CO}_2}$ values are more negative than southern hemisphere values, but only during the warm northern hemisphere season when atmospheric carbon fixation exceeds the rate of the release of CO_2 from fossil fuel combustion, which is also more important in the northern hemisphere (e.g., <http://cdiac.ornl.gov/trends/co2/iso-sio/graphics/iso-graphics.html>). As such crops that produce oil-containing seeds or fruits may show this interhemispheric $\delta^{13}\text{C}_{\text{CO}_2}$ difference (≤ 1 ‰). Other stable isotope ratios ($\delta^2\text{H}$, and $\delta^{18}\text{O}$) of the bulk oil alone (e.g., Iacumin et al., 2009) or combined with the molecular isotopic information (Richter et al., 2010) permit to get further insight into the geographic origin of the oils in the EU and Mediterranean countries. The variations of $\delta^2\text{H}$ and $\delta^{18}\text{O}$ values in plant and their products through their relationship with humidity-precipitation and temperature conditions during plant growth may allow characterization of the geographic origin of vegetable oils. Therefore, this multiple-stable isotope approach contributes to the assessment of commercial vegetable-oils purity and their geographical origin.

Maize, olive, sunflower, groundnut, soybean and rice oils differing in sites of growth in the southern and northern hemispheres were characterized by bulk oil stable isotopes ($\delta^{13}\text{C}_{\text{bulk}}$, $\delta^2\text{H}_{\text{bulk}}$, and $\delta^{18}\text{O}_{\text{bulk}}$) and fatty acids (FAs) concentrations and $\delta^{13}\text{C}_{\text{FA}}$ values using elemental analysis/isotope ratio mass spectrometry, gas chromatography/mass spectrometry, gas chromatography/ flame ionization detection and gas chromatography/combustion/isotope ratio mass spectrometry. Principal component analysis was applied to examine the inherent structure of the data.

The $\delta^{13}\text{C}_{\text{bulk}}$ values of maize oils (-18.4 to -14.9 ‰) are typical for C_4 plants; those of olive (-30.2 to -28.2 ‰), sunflower (-30.2 to -29.2 ‰), groundnut (-29.3 ‰), soybean (-30.6 ‰), and rice (-34.5 ‰) oils are typical for C_3 plants. The $\delta^2\text{H}_{\text{bulk}}$ values vary from -161 to -132 ‰ for maize oils and -171 to -109 ‰ for C_3 oils. The $\delta^{18}\text{O}_{\text{bulk}}$ values of all oils vary between 15.2 and 38.9 ‰. The major $\delta^{13}\text{C}_{\text{FA}}$ differences (>5 ‰) within plant species render the inter- C_3 -species comparison difficult. These differences are explained in terms of variations in the lipid biosynthetic pathways and blend of vegetable oils of different FA composition and $\delta^{13}\text{C}_{\text{FA}}$ values. The samples from the southern hemisphere are generally enriched in ^{13}C compared to those from the northern hemisphere. Differences between the southern and northern hemispheres were observed in $\delta^2\text{H}$ ($p < 0.001$) and $\delta^{18}\text{O}_{\text{bulk}}$ ($p = 0.129$) for all C_3 oils, $\delta^{13}\text{C}_{18:1}$ ($p = 0.026$) and $\delta^{18}\text{O}_{\text{bulk}}$ ($p = 0.160$) for maize oils. The results of this study show that combining bulk and molecular stable isotope ratios, fatty acid compositions and their statistical analysis help characterization of the geographic origin of oils. This methodology can be used to detect and get insight into the origin of impurities in valuable vegetable oils commercialized worldwide. 18 years ago we advanced that the carbon isotope composition of individual fatty acids in genuine olive oil (from archaeological samples) may be a molecular tracer of paleoclimatic changes in the Mediterranean basin (Spangenberg et al., 1998). The results of the present study show that these type of analysis may also help to trace intercontinental variations of single seed/species C_3 and C_4 plant products, thus providing important information for archaeological, paleoclimatic and palaeoecological studies.

REFERENCES

- Iacumin, L., Bernini, L. & Boschetti, I. 2009: Climatic factors influencing the isotope composition of Italian olive oils and geographic characterisation, *Rapid Communication in Mass Spectrometry*, 23, 448-454.
- Richter, E. K., Spangenberg, J. E., Kreuzer, M. & Leiber, F. 2010: Characterization of rapeseed (*Brassica napus*) oils by bulk C, O, H, and fatty acid C stable isotope analyses. *Journal of Agricultural and Food Chemistry*, 58, 8048-8055.
- Spangenberg, J. E., Macko, S. A. & Hunziker, J. 1998: Characterization of olive oil by carbon isotope analysis of individual fatty acids: Implications for authentication. *Journal of Agricultural and Food Chemistry*, 46, 4179-4184.

P 11.19

Subaquatic moraine amphitheatre in Lake Thun

Stefano C. Fabbri¹, Benedikt J. Weiss², Christian Hübscher², Heinrich Horstmeyer³, Cédric Schmelzbach³, Marius W. Buechi⁴, Marco Herwegh¹, Fritz Schlunegger¹, Flavio S. Anselmetti⁴

¹ *Institute of Geological Sciences, University of Bern, Baltzerstr. 1+3, CH-3012 Bern (stefano.fabbri@geo.unibe.ch)*

² *Institute of Geophysics, University of Hamburg, Bundesstr. 55, D-20146 Hamburg*

³ *Institute of Geophysics, Dept. of Earth Sciences, ETH Zürich, CH-8092 Zürich*

⁴ *Institute of Geological Sciences and Oeschger Centre for Climate Change Research, University of Bern, Baltzerstr. 1+3, CH-3012 Bern*

The combination of a recently acquired high-resolution multibeam bathymetric dataset with 2D multichannel reflection seismic data from perialpine Lake Thun reveals new insights into the evolution of the lake basin upon deglaciation and a so far unknown subaquatic moraine. These new data improve our so comprehension of the landforms associated with the ice-contact zone, the facies architecture of the sub- to proglacial units, the related depositional processes, and thus the retreat mechanisms of the Aare Glacier.

The overdeepened basin of Lake Thun was formed by a combination of tectonically predefined weak zones and glacial erosion during the last glaciation periods. Seismic stratigraphic analysis of the new data indicates that below the outermost edge of a morphologically distinct platform in the southeastern part of the lake basin ('Bödeli'), a complex ridge structure marked by strong reflection amplitudes occurs. This structure is interpreted as a stack of several subaquatic terminal moraine crests, most likely created by a slightly advancing or stagnant and grounded Aare Glacier during its overall retreat phase. Packages of overridden moraine crests are distinguishable, which smoothly transform downstream into prograding clinofolds with foresets with internally recognisable layering. They dip steeply towards the deepest part of the basin, eventually transforming into bottomsets. This stacked succession of subaquatic glacial sequences is overlain by lacustrine deposits formed by Late-Glacial and Holocene laminated muds comprising intercalated turbidites (Wirth et al. 2011).

Little is known about the exact timing and behaviour of the retreating Aare Glacier between its recessional phase from the Alpine foreland to the deglaciation of the inner-Alpine ice cap, mostly due to the lack of well-developed moraines that indicate glacier stabilization or slight readvance. Radiocarbon-dated calcareous clay gyttja of Late-Glacial Lake Amsoldingen, located adjacent to the water outlet of Lake Thun, shows a ~16.3 ka BP age (Lotter, 1985), providing a minimum age for the formation of the postglacial small lake. Higher up in the catchment, the oldest ¹⁰Be exposure ages from the Grimsel area, the accumulation area of the Aare Glacier, indicate ice-free conditions around 14-11.3 ka BP (Kelly et al., 2006; Wirsig et al., 2016). The emplacement of the subaquatic moraine complex of the Aare Glacier must have occurred between these age constraints, implying high sedimentation rates in the lake basin.

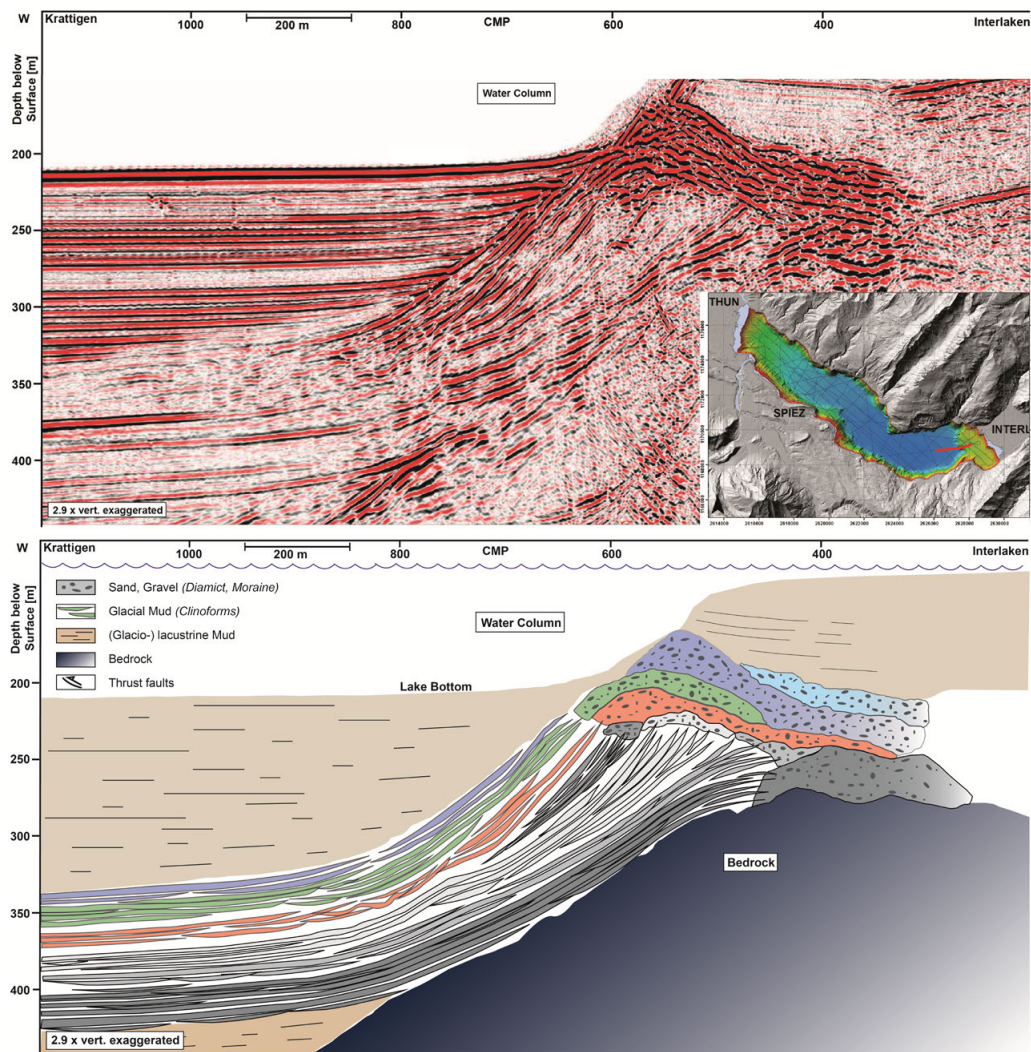


Figure 1. Top: Seismic reflection profile from the shallow subaquatic platform close to Interlaken to the main basin of Lake Thun. Bottom: Seismic sequence stratigraphic analysis indicating different stages of a retreating Aare Glacier as documented by a stack of several depositional sequences representing subaquatic moraine deposits, which translate into prograding clinoforms towards the center of the basin.

REFERENCES

- Kelly, M. A., Ivy-Ochs, S., Kubik, P. W., von Blanckenburg, F., and Schluchter, C., 2006: Chronology of deglaciation based on Be-10 dates of glacial erosional features in the Grimsel Pass region, central Swiss Alps, *Boreas*, 35, p.634-643.
- Lotter, A. F., 1985: Amsoldingensee-Late glacial and Holocene environments of a lake at the southern edge of the Swiss plateau., *Dissertation Botanicae*, 87, p.185-208.
- Wirsig, C., Zasadni, J., Ivy-Ochs, S., Christl, M., Kober, F., and Schluchter, C., 2016: A deglaciation model of the Oberhasli, Switzerland, *Journal of Quaternary Science*, 31, p.46-59.
- Wirth, S. B., Girardclos, S., Rellstab, C., and Anselmetti, F. S., 2011: The sedimentary response to a pioneer geo-engineering project: Tracking the Kander River deviation in the sediments of Lake Thun (Switzerland), *Sedimentology*, 58, p.1737-1761.

P 11.20

Multiproxy Analysis and Pedosedimentary Reconstruction of Loess-Paleosol Sequences on two Pleistocene Fluvial Terraces of the Mosel

Julian Struck^{1,3}, Sina Felicitas Sparrenberg¹, Peter Kühn², Raimund Schneider¹, Sören Thiele-Bruhn¹, Jana Zech³, Roland Zech³, Anja Zander⁴, Michael Weidenfeller⁵

¹ Soil Science / University of Trier, Germany, (julian.struck1988@gmail.com)

² Research Area Geography, Laboratory of Soil Science and Geoecology / Eberhard Karls University, Tübingen, Germany

³ Institute of Geography and Oeschger Centre for Climate Change Research / University of Bern, Switzerland

⁴ Institute of Geography / University of Cologne, Germany

⁵ Quaternary Geology / Landesamt für Geologie und Bergbau Rheinland-Pfalz, Germany

Previous studies of the lower Mosel valley focussed on the evolution and characterisation of terrace levels (Rixhon et al., 2016, 2014; Cordier et al., 2006; Müller, 1976) and on fluvial dynamics and soil development (Weidenfeller, 1990). Loess-paleosol sequences (LPSs) developed on these terraces are potentially valuable archives, but have not yet been studied in detail.

We present grain size distributions, soil physical, micromorphological and geochemical data from two LPSs in the lower Mosel valley. According to Müller (1976), the Bandemer LPS is situated on a high terrace, 145 m above the present Mosel, and the Hetzerath LPS is located on an upper middle terrace, 70 m above the present Mosel.

Four distinct paleosols were identified in the Bandemer LPS and three paleosols in the Hetzerath LPS. The surface soil at the Bandemer LPS is a Stagnic Luvisol supposed to be formed during the last Interglacial, whereas the surface soil at the Hetzerath LPS is a Stagnic Luvisol supposed to have developed during the Holocene. All buried paleosols are generally Luvisols with redoximorphic features of different intensities. Micromorphology shows evidence for several phases of clay illuviation as indicated by the presence of intact and fragmented clay coatings. Samples are also being processed for optical stimulated luminescence (OSL) dating to support the proposed long-term soil sequence development, which is indicated by very high weathering indices. To get information about changes in paleo-vegetation (grasses versus trees) n-alkanes, i.e. leaf-wax biomarkers are analysed. Further we started analysing δD on n-alkanes for paleo-hydrological reconstruction.

REFERENCES

- Cordier, S., Harmand, D., Frechen M. & Beiner M. 2006: New evidences on the Moselle terrace stratigraphy between the Meurthe confluence (Paris Basin) and Koblenz (Rhenish Massif). *Zeitschrift für Geomorphologie* 50.3, 281–304.
- Müller, M. J. 1976: Untersuchungen zur pleistozänen Entwicklungsgeschichte des Trierer Moseltals und der «Wittlicher Senke». Trier: Zentralausschuss für Deutsche Landeskunde.
- Rixhon, G., Cordier, S., Harmand, D., May, S. M., Kelterbaum, D., Dunai, T., Binnie, S. & Brückner H. 2014: Unraveling the Quaternary river incision in the Moselle valley (Rhenish Massif, Germany): new insights from cosmogenic nuclide dating ($^{10}\text{Be}/^{26}\text{Al}$) of the Main Terrace complex. *Geophysical Research Abstracts* Vol. 16, EGU2014-8081, EGU General Assembly 2014
- Rixhon, G., Cordier, S., May, S.M., Kelterbaum, D., Szemkus, N., Keulertz, R. Dunai, T., Binnie, S., Hambach, U. & Brückner, H. 2016: Potentials and pitfalls of depth profile (^{10}Be), burial isochron ($^{26}\text{Al}/^{10}\text{Be}$) and palaeomagnetic techniques for dating Early Pleistocene terrace deposits of the Moselle valley (Germany). *Geophysical Research Abstracts* Vol. 18, EGU2016-14508, EGU General Assembly 2016
- Weidenfeller, M. 1990: Jungquartäre fluviale Geomorphodynamik und Bodenentwicklung in den Talauen der Mosel bei Trier und Nennig. Dissertation, Trier.

P 11.21

Probabilistic stability evaluation and seismic triggering scenarios of submerged slopes in perialpine Lake Zurich

Michael Strupler¹, Michael Hilbe², Flavio S. Anselmetti², Timo Fleischmann³, Achim J. Kopf³ and Michael Strasser^{1,4}

¹ *Geologisches Institut, ETH Zürich, Sonneggstrasse 5, CH-8092 Zürich (michael.strupler@erdw.ethz.ch)*

² *Institut für Geologie und Oeschger Centre for Climate Change Research, Universität Bern, Baltzerstrasse 1+3, CH-3012 Bern*

³ *MARUM - Center for Marine Environmental Sciences, D- 28195 Bremen*

⁴ *Institut für Geologie, Universität Innsbruck, Innrain 52, A-6020 Innsbruck*

The assessment of geohazards in the subaqueous environment has been becoming more important in the recent years (e.g. Lee and Jones, 2014; Mueller et al., 2016; Urgeles et al., 2002). Such hazards include subaqueous landslides, which can be triggered by various processes such as earthquakes or human activity. Stability analyses of submerged slopes are crucial, yet complex steps for a hazard assessment, as many geotechnical and morphological factors need to be considered. As high costs arise and great efforts are required to have a high spatial data coverage, deterministic models with data from few sampling locations are typically used for the evaluation of slope stabilities.

We present a concept for the probabilistic stability assessment of subaqueous slopes, taking into account the spatial variability of the geotechnical data.

Our study is conducted in perialpine Lake Zurich, Switzerland, where multiple distinct subaquatic landslides with well-defined headscarps, translation areas, and mass-transport deposits can be identified.

The ages of the landslides are known and their triggering has been assigned to different mechanisms by previous studies. The subaquatic slope was investigated in great detail with geophysical, geotechnical, and sedimentological methods: 3.5 kHz pinger seismic reflection data (Strasser and Anselmetti, 2008) and a 300 kHz multibeam bathymetric dataset (1 m grid; Strupler et al. 2015) were used for the detection of landslide features, for the layout of a coring campaign, and for an in situ geotechnical testing campaign. A total of 7 Kullenberg-type piston cores (~4 cores /km²) and 21 short gravity cores (~11 cores /km²) were taken, and 39 in situ cone penetration tests (CPT; ~20 CPT /km²) were performed. The high density of geotechnical datasets allows the inclusion of the spatial variability in the slope model. A mechanical stratigraphy of the postglacial sediments on the lakefloor was constructed and is used as input for a Monte Carlo-simulated limit-equilibrium model on an infinite slope. The results show that the location of landslide-failure initiation in the model is consistent with stratigraphic analysis and failure-plane identification from sediment cores. Our model supports previously hypothesized earthquake triggering from a geotechnical perspective. The present-day sediment-charged slopes are failure-prone, even for a static case.

REFERENCES

Lee EM, Jones DKC (2014) *Landslide Risk Assessment*, 2nd edn. ICE Publishing, London

Mueller C, Mountjoy J, Power W, et al (2016) Submarine Mass Movements and their Consequences. 41:589–597. doi: 10.1007/978-3-319-20979-1

Strupler M, Hilbe M, Anselmetti FS, Strasser M (2015) Das neue Tiefenmodell des Zürichsees: Hochauflösende Darstellung der geomorphodynamischen Ereignisse im tiefen Seebecken. *Swiss Bull angew Geol* 20:71–83.

Urgeles R, Locat J, Lee HJ, Martin F (2002) The Saguenay Fjord, Quebec, Canada: integrating marine geotechnical and geophysical data for spatial seismic slope stability and hazard assessment. *Mar Geol* 185:319–340. doi: 10.1016/S0025-3227(02)00185-8

REFERENCES

- Akçar N., Yavuz V., Yeşilyurt S., Ivy-Ochs S., Reber R., Bayrakdar C., Kubik P., Zahno C., Schlunegger F & Schlüchter C., 2016. Synchronous glacier maximum extent during last glaciation over the Anatolian peninsula. In: Quaternary Glaciation in the Mediterranean Region, P. D. Hughes and J. C. Woodward (eds.), Geological Society of London Special Publications, 433, <http://doi.org/10.1144/SP433.7>
- Shakun, J.D. & Carlson, A.E. 2010. A global perspective on Last Glacial Maximum to Holocene climate change. *Quaternary Science Reviews*, 29, 1801-1816.
- Yeşilyurt, S., Akçar, N., Doğan, U., Yavuz, V., Ivy-Ochs, S., Vockenhuber, C., Schlunegger, F. & Schlüchter, C. 2016. Extensive Quaternary glaciations in eastern Turkey. EGU General Assembly 2016, Vienna, Austria.
- Yeşilyurt, S., Akçar, N., Doğan, U., Yavuz, V., Ivy-Ochs, S., Vockenhuber, C. & Schlüchter, C. 2014. Quaternary glaciations of Kavuşşahap Mountains, eastern Anatolia. 8th International Symposium on Eastern Mediterranean Geology, October 13–17, 2014, Muğla, Turkey, 139.

12. Cryospheric Sciences

M. Schwikowski, M. Heggli, M. Huss, J. Nötzli, Daniel Tobler

Swiss Snow, Ice and Permafrost Society

TALKS:

- 12.1 Brauchli T., Trujillo E., Huwald H., Lehning M.: Snowmelt observations at the slope scale and implications for the catchment response using the Alpine3D model
- 12.2 Buri P., Steiner J.F., Miles E.S., Pellicciotti F.: Modelling backwasting of supraglacial ice cliffs over a debris-covered glacier, Nepalese Himalaya
- 12.3 Calonne N., Cetti C., Fierz C., van Herwijnen A., Jaggi M., Löwe H., Matzl M., Schmid L., Schneebeli M.: A unique time series of daily and weekly snowpack measurements at Weissfluhjoch, Davos, Switzerland
- 12.4 Frehner M., Amschwand D., Gärtner-Roer I.: Rockglacier flow law determined from deformation data and geomorphological indicators: An example from the Murtèl rockglacier (Engadin, SE Switzerland)
- 12.5 Ghirlanda A., Delaloye R., Kummert M., Staub B., Braillard L.: Destabilization of the Jegi rock glacier: historical development and ongoing crisis
- 12.6 Irarrazaval I., Mariethoz G., Herman F.: Geostatistical inversion of subglacial drainage system
- 12.7 Jouvét G., Weidmann Y., Seguinot J., Funk M., Abe T., Sakakibara D., Sugiyama S.: Initiation of a major calving event on Bowdoin Glacier captured by UAV photogrammetry
- 12.8 Lindner F., Walter F., Laske G.: Seismic monitoring of the 2016 outburst flood of Lac des Faverges on Glacier de la Plaine Morte
- 12.9 Lucas C., Bühler Y., Leinss S., Marino A., Hajsek I.: Interfering reflections in ground based radar measurements: Lessons learnt from a snow depth measurement campaign
- 12.10 Machguth H., Colgan W.: Conventional and radioactive waste at the abandoned ice sheet base at Camp Century, Greenland, in a warming climate
- 12.11 Naegeli K., Damm A., Huss M., Wulf H., Schaepman M., Hoeszle M.: Glacier surface albedo derived from remotely sensed data and its importance for mass balance modelling
- 12.12 Seguinot J., Funk M., Jouvét G., Ryser C., Bauder A., Leinss S., Sakakibara D., Sugiyama S.: Tidewater glacier dynamics dominated by sliding at Bowdoin Glacier, Northwest Greenland
- 12.13 Steiner L., Baumann M., Geiger A.: Point-wise estimation of glacier surface height changes based on reflected GPS signals
- 12.14 Visnjevic V., Herman F., Podladchikov Y.: Glacier climate interaction: reconstruction of the mass balance field using ice extent data
- 12.15 Zekollari H., Huybrechts P., Noël B., van de Berg W.J., van den Broeke M.R.: Dynamics and climate sensitivity of Hans Tausen Iskappe (Greenland)

POSTERS:

- P 12.1 Avak S.E., Birrer M., Guillon M., Bartels-Rausch T., Schwikowski M., Eichler A.: Development of a Cryocell LA-ICP-MS Setup for Spatial Trace Element Analysis in High Alpine Glacier Ice
- P 12.2 Dal Farra A., Kaspari S., Schwikowski M.: Effects of particulate matter on the albedo of Alpine glaciers
- P 12.3 Brugger S.O., Gobet E., Sigl M., Osmont D., Schwikowski M., Tinner W.: FROZENFIRE – 5000 years of fire, vegetation and pollution history from the Mongolian Altai
- P 12.4 Brugger S.O., Gobet E., Sigl M., Osmont D., Schwikowski M., Tinner W.: FROZENFIRE – A high-alpine ice core record to assess vegetation and fire dynamics in Western Europe over the last millennium
- P 12.5 Osmont D., Sigl M., Wendl I., Schmidely L., Isaksson E., Grieman M., Schwikowski M.: Towards the reconstruction of forest fires through chemical analysis of black carbon in ice cores from mountain glaciers
- P 12.6 Tetzner D., Fernandoy F., Meyer H.: Stable water isotopes as climate tracers in the Laclavere Plateau, Antarctic Peninsula
- P 12.7 Barandun M., Huss M., Usabaliev R., Bolch T., Hoelzle M.: From snow cover mapping to glacier-wide mass balance on Central Asian glaciers
- P 12.8 Huber J., Zemp M., Paul F., Cook A.J.: A complete glacier inventory of the Antarctic Peninsula based on Landsat7 data from 2000–2002 and other pre-existing datasets
- P 12.9 Goerlich F., Bolch T., Mukherjee K., Pieczonka T.: Negative geodetic glacier mass balances in the Ak-Shirak range (Kyrgyzstan) between 1960s and 70s derived from Corona and Hexagon reconnaissance imagery
- P 12.10 Mölg N., Steinmann M., Zemp M.: A worldwide glacier information system to go
- P 12.11 Mölg, N., Bolch, T., Vieli, A.: Traditional photogrammetry versus modern structure-from-motion: using aerial images to derive surface elevation changes of a debris covered Alpine glacier tongue
- P 12.12 Vivero S., MacDonell S., Mernild S.: Ice-elevation changes derived by high resolution airborne and terrestrial laser scanning data of a high Andean glacier
- P 12.13 Weidmann Y., Huss M., Fischer M., Schmassmann E.: Swiss Glacier Inventory 3D, a product of the Swiss topographical landscape model
- P 12.14 Seguinot J., Jouvét G., Huss M., Funk M.: Modelling the last glacial cycle in the Alps
- P 12.15 Cohen D., Zwinger Th., Fischer U.H., Haeberli W.: Modeling glaciers and permafrost in connection with radioactive waste repositories in northern Switzerland
- P 12.16 Becker P., Funk M.: Modeling the ice flow in the Upper Valais at the Last Glacial Maximum
- P 12.17 Werder M.A., Huss M.: Bayesian inference of ice thickness
- P 12.18 Förster S., Huss M., Gudmundsson H.: Demystifying the end of the Little Ice Age: first tests simulating the Rhône Glacier with Úa

- P 12.19 Sommer C.G., Lehning M., Fierz C.: A new ring-shaped wind tunnel facility to study wind- packing of snow
- P 12.20 Capelli A., Reiweger I., Schweizer J.: Studying the acoustic emissions and the failure process during loading experiments of snow
- P 12.21 Gaume J., Löwe H.: The contact density to characterize the mechanical behavior of very loose cohesive granular materials : towards snow microstructure modeling
- P 12.22 Bavay M., Fierz C., Egger T., Lehning M.: The Open Source Snowpack modelling ecosystem
- P 12.23 Couttet M., Wever N., Bavay M., Fierz C., Lehning M.: Modelling water vapour transport in snow
- P 12.24 Schlägl S., Mott R., Lehning M.: Energy balance and melt over a patchy snow cover
- P 12.25 Preiswerk L.E., Walter F., Meier L., Funk M.: Icefalls from the Eiger West Face Monitored by Interferometric Radar and Seismometers
- P 12.26 Steiner J.F., Buri P., Miles E.S., Epp M.: Rapid growth of a terminal lake in the Glarner Alpen

12.1

Snowmelt observations at the slope scale and implications for the catchment response using the Alpine3D model

Tristan Brauchli¹, Ernesto Trujillo, Huwald Hendrik¹ & Michael Lehning²

¹ School of Architecture, Civil and Environmental Engineering, Ecole Polytechnique Fédérale de Lausanne (EPFL), Switzerland (tristan.brauchli@epfl.ch)

² WSL Institute for Snow and Avalanche Research, SLF, Davos

Snowpack and especially its melt during spring is a crucial resource for water availability in mountainous regions. A better understanding of the processes and their representation in hydrological models is therefore necessary for different purposes, such as water management, flood forecast or hydropower production. However, this remains a challenge given the complexity of the controlling processes and their relative interactions. In this study, we analyze data from snowmelt lysimeters in a small alpine catchment, the Dischma river basin (~40 km²) near Davos, Switzerland. The objective is to study relationships between snow ablation and its driving processes, morphology and watershed response. The overall goal is to improve snowmelt processes representation in distributed hydrological models. Four measurement stations installed on representative slopes monitored continuously the snowpack temperature profile, snowpack liquid water output, and soil moisture throughout the melting season. The catchment response is measured at three stream gauges, the first one at the watershed outlet and the two others at specific sub-basins outlets. The results for the water year 2015 will be presented: our analysis focuses on the snowmelt lysimeters data and the implication for the stream flow. These measurements are compared to model results obtained from the spatially distributed and physically based model Alpine3D (Lehning et al., 2006) and its recent hydrological extension StreamFlow (Gallice et al., 2016). We will notably discuss the influence of the liquid water transport scheme within the snowpack on the snowmelt response, and the spatio-temporal snow distribution over the catchment.

REFERENCES

- Gallice, A., Bavay, M., Brauchli, T., Comola, F., Lehning, M. and Huwald, H.: StreamFlow 1.0: An extension to the spatially distributed snow model Alpine3D for hydrological modeling and deterministic stream temperature prediction, *Geosci. Model Dev. Discuss.*, 1–51, doi:10.5194/gmd-2016-167, 2016.
- Lehning, M., Völksch, I., Gustafsson, D., Nguyen, T. A., Stähli, M. and Zappa, M.: ALPINE3D: a detailed model of mountain surface processes and its application to snow hydrology, *Hydrol. Process.*, 20(10), 2111–2128, doi:10.1002/hyp.6204, 2006.

12.2

Modelling backwasting of supraglacial ice cliffs over a debris-covered glacier, Nepalese Himalaya.

Pascal Buri¹, Jakob Steiner¹, Evan Miles² & Francesca Pellicciotti^{3,1}

¹ *Institute of Environmental Engineering, ETH Zürich, Stefano-Franscini-Platz 3, CH-8093 Zürich (buri@ifu.baug.ethz.ch)*

² *Scott Polar Research Institute, University of Cambridge, Lensfield Road, UK Cambridge CB2 1ER*

³ *Department of Geography, Northumbria University, Ellison Place, UK Newcastle upon Tyne NE1 8ST*

High melt rates at supraglacial ice cliffs on debris-covered tongues are thought to contribute a significant amount of the total mass losses of these glaciers, affecting their surface dynamics and downwasting considerably.

The steep slopes of the cliffs represent a non-negligible area of ice exposed to the atmosphere, with their energy balance depending on cliff aspect, steepness and surrounding topography. This results in a strong variability of melt across single cliffs and over different cliffs, and leads to complex backwasting patterns over the glacier surface.

Extrapolation of melt rates to the glacier scale from point-scale observations or models might result in misleading total volumes as the use of constant slopes and aspects neglects the topographic variability at the cliff scale. We develop a grid-based ice cliff melt model, which uses as input high resolution UAV-imagery and DEMs and on-glacier meteorological data. By using a high-resolution DEM we are able to account for shading effects on shortwave radiation and longwave emission from the surrounding, debris-covered glacier surface. Model results from detailed energy balance calculations show longwave radiation from debris being a key flux, able to counteract the net longwave flux of radiation from the sky and the ice.

Compared to existing point scale models, the model is dynamic in the sense that the ice cliff geometry is updated periodically, considering cumulative melt, reburial by debris, newly exposed slopes in the cliff's marginal sections and the influence of adjacent supraglacial ponds. The additional melt sourcing from supraglacial water bodies at the cliff's base has been observed to lead to a homogenous translation of cliff geometry by conservation of steep sections. The absence of adjacent ponds in contrast seems to lead to continuously demising cliffs instead. The simulated backwasting patterns are validated with consecutive, detailed UAV- and ground-based observations over two melt seasons. The model presented and validated in this study is a clear step forward compared to existing approaches for the simulation of cliff backwasting and can be applied to quantify the contribution of cliffs over debris-covered glaciers to their total ablation and mass balance.

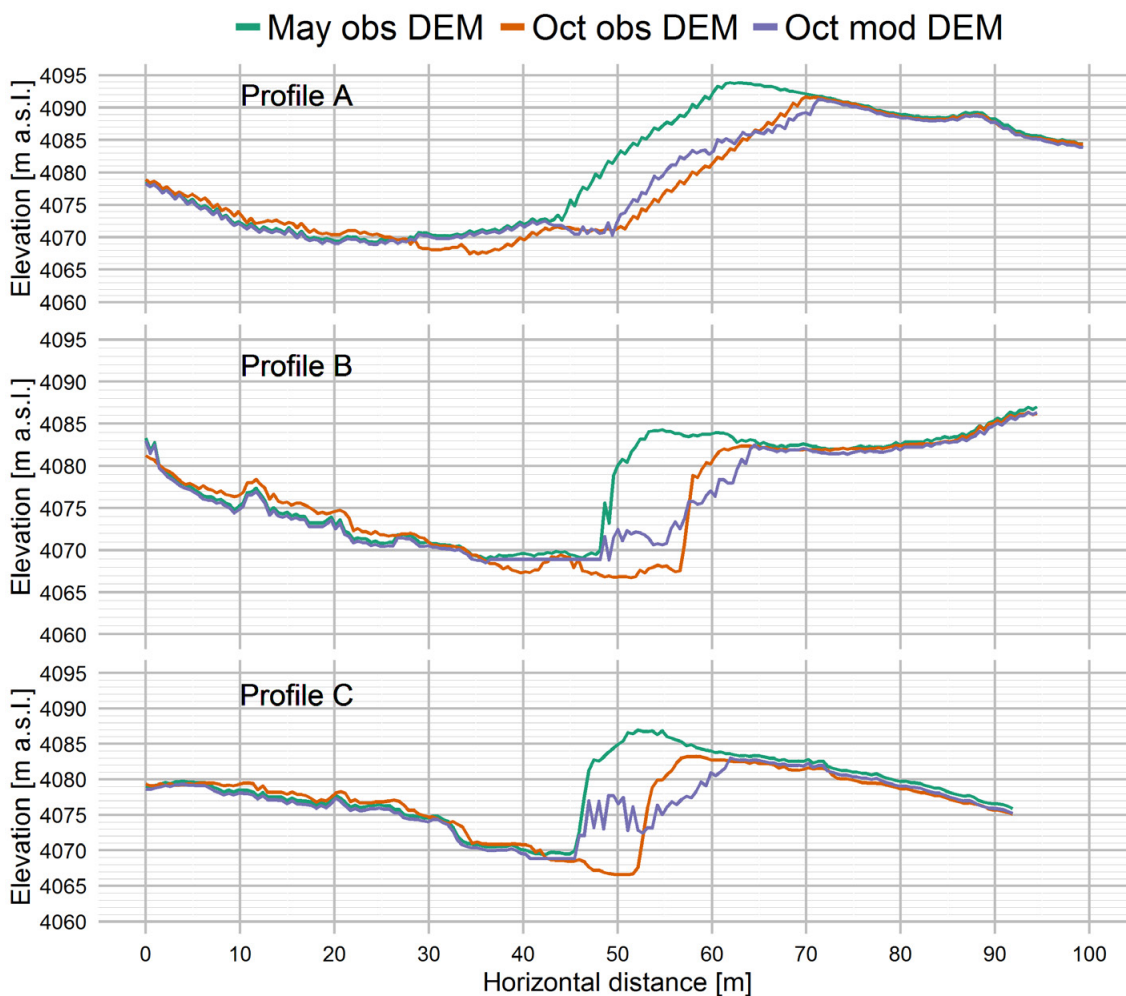


Figure 1. Elevation profiles (roughly north to south) across one cliff with an adjacent lake on Lirung Glacier, Nepal. The orthoimages are from UAV-flights in May (left) and October 2013 (right). The elevation profiles are shown below as derived from the May and October UAV-DEMs (0.6m resolution) and modelled for October 2013.

12.3

A unique time series of daily and weekly snowpack measurements at Weissfluhjoch, Davos, Switzerland

Neige Calonne¹, Cecilia Cetti¹, Charles Fierz¹, Alec van Herwijnen¹, Matthais Jaggi¹, Henning Löwe¹, Margret Matzl¹, Lino Schmid¹ and Martin Schneebeli¹

¹ WSL Institute for Snow and Avalanche Research SLF, Flüelastrasse 11, CH-7260 Davos Dorf

Recently, different efforts were dedicated to improve various components of snowpack models, notably, by including more objective parameters of snow microstructure. To contribute with a dataset for this purpose, we designed a new measurement campaign for the winter 2015-2016 at Weissfluhjoch, Switzerland. We focused on density and specific surface area (SSA) of snow, two fundamental microstructural parameters from which many physical snow properties can be estimated. Weekly measurements of density (density cutter) and SSA (*IceCube*) profiles at 3 cm vertical resolution now extend the traditional snow measurements. To investigate also short time evolutions, daily *SnowMicroPen* measurements were additionally done from which proxies of density and SSA can be calculated at 1 mm vertical resolution. Occasionally, snow samples were also taken from the snow pit for micro-tomography measurements to investigate specific snow cover features, such as weak layers, graupel or crusts at a 10 micrometers resolution. Finally, Propagation Saw Tests were performed nearly on a weekly basis.

In this paper, we present an overview of this measurement campaign carried out from December 2015 to March 2016. We show preliminary results of the density profile evolution that highlight the advantage of daily measurements compared to weekly ones when aiming at a highly continuous picture. The present dataset offers new opportunities for calibrating and validating physically based snowpack models, as well as for a better understanding of processes such as fracture propagation, snow densification, or crust formation.

12.4

Rockglacier flow law determined from deformation data and geomorphological indicators: An example from the Murtèl rockglacier (Engadin, SE Switzerland)

Marcel Frehner¹, Dominik Amschwand¹, Isabelle Gärtner-Roer²

¹ Geological Institute, ETH Zurich, Sonneggstrasse 5, CH-8092 Zurich (marcel.frehner@erdw.ethz.ch)

² Department of Geography, University of Zurich, Winterthurerstrasse 190, CH-8057 Zurich

Rockglaciers are tongue-shaped permafrost landforms creeping downslope due to gravity. They consist of unconsolidated rock fragments (silt/sand–rock boulders) with interstitial ice. Therefore, their creep behavior (i.e., rheology) may deviate from the simple and well-known flow-laws for pure ice.

During creep, rockglaciers develop typical flow structures (e.g., furrow-and-ridge morphology; Figure 1A) on time scales of decades to centuries. For the Murtèl rockglacier (upper Engadin valley, SE Switzerland), Frehner et al. (2015) reproduced these surface structures using a linear viscous (Newtonian) flow model. However, here we demonstrate why and how these flow structures provide much more detailed information about the flow law that governed rockglacier creep in the past centuries. In addition, we use the readily available deformation data (both borehole (Arenson et al., 2002; Figure 1B) and surface data) of the Murtèl rockglacier to further determine the flow law that governed rockglacier creep in the past decades and today.

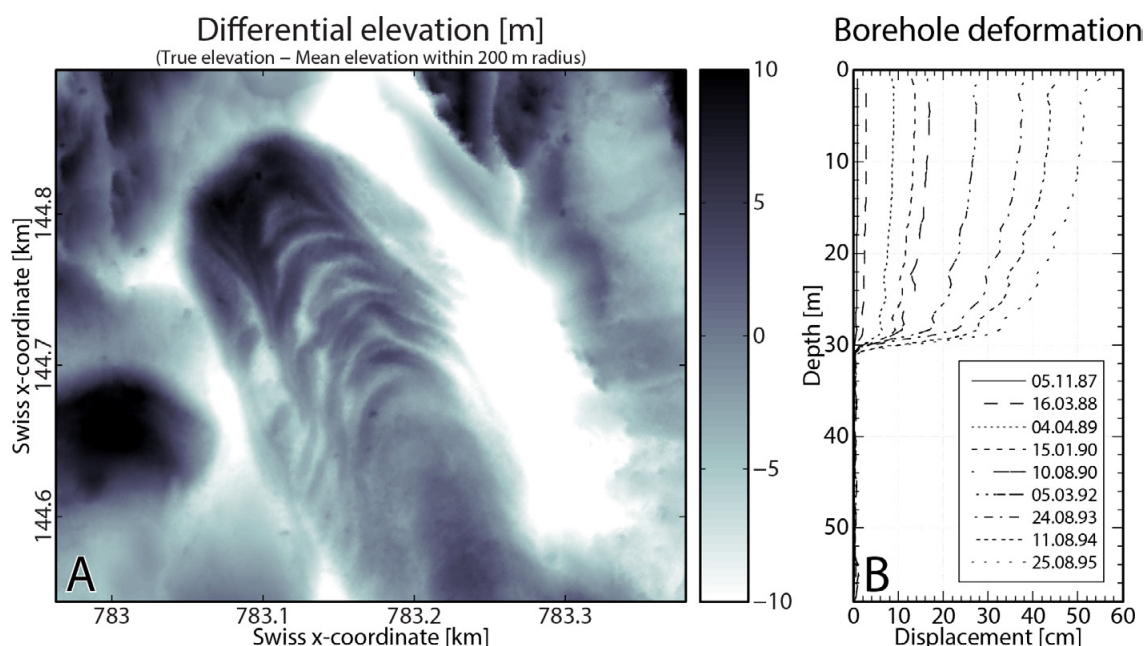


Figure 1. Base data for our study. A) Differential elevation model of the Murtèl rockglacier (Frehner et al. 2015). B) Time-lapse borehole deformation data (Arenson et al. 2002).

Both the surface flow structures (Figure 1A) and the borehole deformation data (Figure 1B) exhibit curved deformation in map view and in vertical direction, respectively. We use this curved flow geometry to constrain the viscous flow law governing the creep of the rockglacier. Linear viscous creep results in perfectly parabolic flow geometries; non-linear creep leads to non-parabolic flow geometries. Hence, by fitting theoretical functions to the curved flow geometry (Figure 2), we determine the non-linear viscous flow law that describes the rockglacier creep most adequately.

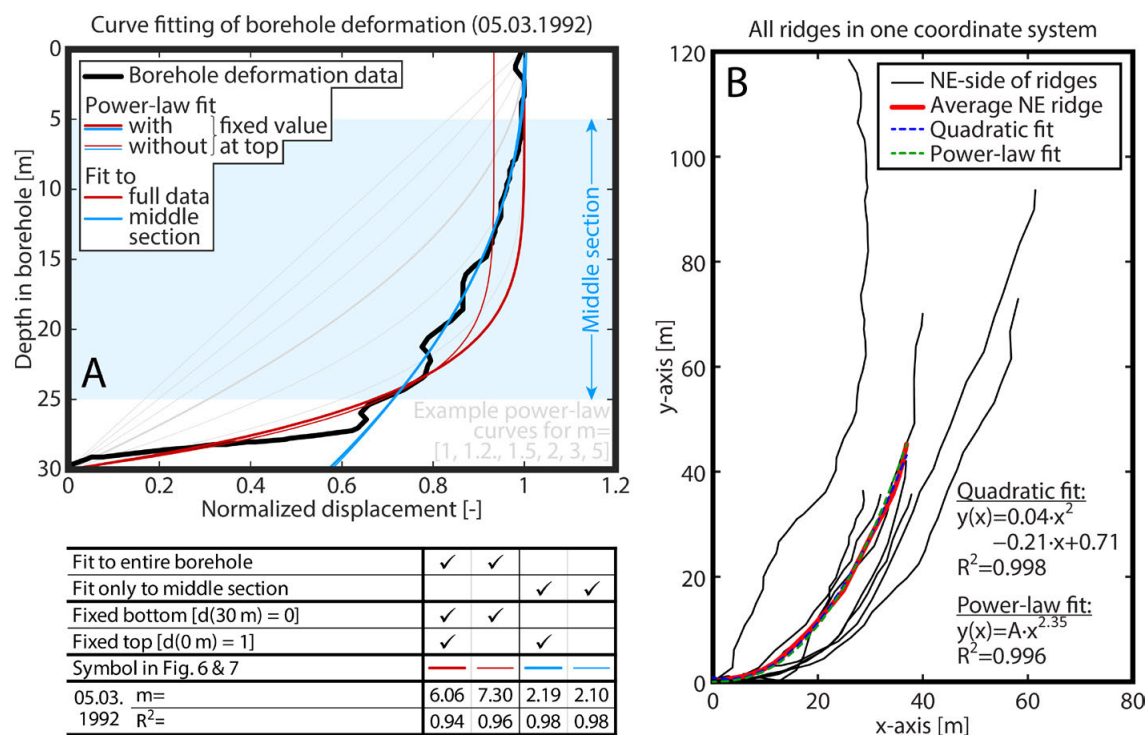


Figure 2. A) Borehole deformation curve and power-law fitting functions using different boundary conditions (curve fitting details in table). Best fits are obtained fitting only the middle section of the borehole. B) Digitized ridges on the NE side of the rockglacier (black) and calculated average ridge geometry (red). The latter is fitted with quadratic (blue) and power-law curves (green). Both fits work equally well.

Both the surface morphology (Figure 2B) and the middle section of the borehole (Figure 2A) are governed by a linear viscous rheology (i.e., close to quadratic flow geometry). However, considering the entire borehole (i.e., including the shear zone at about 30 m depth), a power-law flow law has to be used. Therefore, We interpret that the surface morphology is not controlled or influenced by the shear zone, but solely by the bulk rockglacier flow.

REFERENCES

- Arenson, L., Hoelzle, M. & Springman, S. 2002: Borehole deformation measurements and internal structure of some rock glaciers in Switzerland, *Permafrost and Periglacial Processes*, 13, 117–135.
- Frehner, M., Ling, A.H.M. & Gärtner-Roer, I. 2015: Furrow-and-ridge morphology on rockglaciers explained by gravity-driven buckle folding: A case study from the Murtèl rockglacier (Switzerland), *Permafrost and Periglacial Processes*, 26, 57–66.

12.5

Destabilization of the Jegi rock glacier: historical development and ongoing crisis

Alyssa Ghirlanda¹, Reynald Delaloye¹, Mario Kummert¹, Benno Staub¹, Luc Braillard¹

¹ *Institut de Géographie, University of Fribourg, Chemin du Musée 4, CH-1700 Fribourg (name.surname@unifr.ch)*

The so-called destabilization of a rock glacier is characterized by a fast motion rate of the landform (usually more than 2 meters per year (m/y)) and the development of crevasse(s) or landslide-like scarp(s) on its surface. It may concern the entire of a rock glacier or only a part of it. Such a destabilization phase is generally considered to be the result of the varying and combined influence of different factors (thermal, geometric, mechanic) (Delaloye et al., 2013).

The object of the study is the 720m long Jegi rock glacier, located between 2750 and 2450 m a.s.l. on the western flank of the Jegihorn summit (3206 m a.s.l.) in the western Swiss Alps. It consists of an upper tongue ending with a first front superimposed on a 150m long second tongue located below.

In 2008, the rock glacier was detected with satellite-borne DInSAR as presenting morphological and kinematical evidences of an ongoing destabilization phase between 1991 and 1999, affecting a steep section above the upper front moving in the order of 2-3 m/y since at least 1995 (Delaloye et al., 2008). Since 2009, its surface motion has been under investigation: GNSS measurements campaigns have been held twice a year since June 2009; detailed investigations have been conducted using DInSAR technologies between 2011 and 2013 (Barboux et al., 2015); two permanent GNSS sensors have been installed since 2012 and 2016.

In this context, the aim of the present study is to reconstruct the story of the Jegi rock glacier for the last 85 years as well as to detect the trigger point of the ongoing crisis and its cause. One terrestrial (1931) and twelve aerial images (1946-2015), of which eleven were ortho-rectified, have been photogrammetrically analyzed to recognize and reconstruct earlier stages of the destabilization development. The focus is on the evolution of surface morphology and horizontal velocity.

Our results points out 5 successive phases of the Jegi rock glacier destabilization development: a surge-like crisis (1) which was either distinct or bound to a destabilization phase active in 1946 and lasting at least until 1958 (2); a quiet phase with slower movements after 1958 (3); a new destabilization phase beginning between 1993 and 1995 and affecting mainly the frontal part of the upper tongue (4); a significant acceleration of the whole rock glacier with very high local displacement rate, up to 17m/y in the frontal part of the upper tongue (5). This current destabilization phase is now propagating upwards.

Even if the triggering factors of the first crisis cannot be known precisely, both following destabilization phases appear to be closely related to warm atmospheric periods (around 1950 and since about 1990). The pluri-decennial permafrost warming trend which was particularly pronounced in the Swiss Alps for the last 5 years (2011-2015) is likely to play an important role in the current acceleration. This thermal (climatic) trigger seems to be an important factor for rock glacier dynamic, as increasing velocities have been observed in most monitoring sites in the Alps (Delaloye et al., 2010).

REFERENCES

- Barboux, C., Strozzi, T., Delaloye, R., Wegmüller, U. and Collet, C. (2015). Mapping slope movements in Alpine environments using TerraSAR-X interferometric methods, *ISPRS Journal of Photogrammetry and Remote Sensing*, 109: 178-192. DOI: 10.1016/j.isprsjprs.2015.09.010
- Delaloye, R., Lambiel, C. and Gärtner-Roed, I. (2010): Overview of rock glacier kinematics research in the Swiss Alps. *Geogr. Helv.* 65, 135-145.
- Delaloye, R., Strozzi, T., Lambiel, C., Perruchoud, E. and Raetzo, H. (2008). Landslide-like development of rockglaciers detected with ERS-1/2 SAR interferometry. *Proceedings of the FRINGE 2007 Workshop, Frascati, Italy, 26-30 November 2007 (ESA SP-649, February 2008).*
- Delaloye, R., Morard, S., Barboux, C., Abbet, D., Gruber, V., Riedo, M. and Gachet, S. (2013). Rapidly moving rock glaciers in Matterthal. *Mattertal – ein Tal in Bewegung. Graf C. (Ed.) 2013. Publikation zur Jahrestagung der Schweizerischen Geomorphologischen Gesellschaft 29. Juni – 1. Juli 2011, St. Niklaus. Eidg. Forschungsanstalt WSL. P 21-31*

12.6

Geostatistical inversion of subglacial drainage system.

Inigo Irarrazaval¹, Grégoire Mariethoz¹ & Frédéric Herman¹

¹ *Institut des dynamiques de la surface terrestre, Université de Lausanne, CH-1015 Lausanne (inigo.irarrazavalbusto@unil.ch)*

Water flow at the glacier and bedrock interface plays an important role in understanding alpine catchment hydrology, glacier motion, erosion processes, as well as potential hazards such as glacial outburst floods. In general, the subglacial drainage system (channelized and distributed water flow) is not directly accessible and measurable. In addition, the transient processes of melt, freezing and the advance of the glacier, make it a very complex system. Numerical models that aim to represent the physics of this system have been built, however, existing models require to know a number of physical parameters that are usually impossible to uniquely determine based on the available data (Flowers 2015).

This work focuses on identifying ranges of parameters for a subglacial system based on inverse modeling. As such, it investigates for the first time the use of inverse geostatistical modeling for identifying inaccessible subglacial features. To this end, two innovations are proposed.

The first innovation is a methodology where subglacial features are generated using a combination of stochastic and physics-based processes. The methodology includes the generation of discrete elements such as channels incised to the ice (Röthlisberger channels) and a linked cavity system represented by distributed diffuse flow. We use a finite element groundwater model to represent pressurized flow and mass transport (Cornaton 2007).

The second innovation is the use of an inverse framework that iteratively modifies the subglacial drainage network to match the observed discharge at the outlet of the glacier and breakthrough curves from tracer experiments in moulins. At each iteration, the channel network and model parameters are perturbed to search for an ensemble of suitable solutions. This technique ensures a hydrologically coherent connectivity of the channelized elements and allows the generation of different network structures.

Overall, the proposed methodology is able to represent and identify the type of connected patterns that drive subglacial dynamics and allows conditioning to observed data. As such, this work is a step towards rigorous assessment of parameters uncertainty in subglacial modeling.

REFERENCES

Cornaton, F. 2007: Ground water : A 3-d ground water and surface water flow, mass transport and heat transfer finite element simulator. Internal report, University of Neuchâtel.

Flowers, G. E. 2015: Modelling water flow under glaciers and ice sheets. *Proceedings of the Royal Society A: Mathematical, Physical and Engineering Sciences*, 471, 20140907-20140907.

12.7

Initiation of a major calving event on Bowdoin Glacier captured by UAV photogrammetry

Guillaume Jouvet¹, Yvo Weidmann¹, Julien Seguinot¹, Martin Funk¹, Takahiro Abe², Daiki Sakakibara³, and Shin Sugiyama³

¹ ETHZ, VAW, Zurich, Switzerland (jouvet@vaw.baug.ethz.ch)

² Graduate School of Science, Hokkaido University, Sapporo, Japan

³ Institute of Low Temperature Science, Hokkaido University, Sapporo, Japan

In this study, we analyse the calving activity of Bowdoin Glacier, north-west Greenland, in 2015 by combining satellite images, UAV photogrammetry and ice flow modelling. During our 2015 summer field campaign on Bowdoin Glacier, using a long-range fixed-wing UAV (Unmanned Aerial Vehicle) we collected aerial images of the calving front before and after the initiation of a 1-km long fracture, which later induced a major calving event. Combining photogrammetrical techniques to infer georeferenced orthoimages, and feature tracking techniques, we obtained a high-resolution surface velocity field, which indicates a strong discontinuity at the crack location, see Fig. 1. A detailed analysis of the displacement field and the strain rates allowed us to map accurately the opening crack. Modelling results (see Fig. 2) indicated that the crack was about half-thickness deep, filled with water up to sea level, and getting irreversibly deeper when it was captured by the UAV. Later on, the crack deepening caused stress concentration around the tip, lateral propagation, and final collapse about two weeks later. The crack initiated in a highly crevassed area which is likely caused by a local bump of the basal topography between the medial moraine and the left margin, see Fig. 1. The asymmetry of bed at the front explains the typical calving pattern observed in spring and summer 2015, while a symmetric bed would have made calving events less predictable. Importantly, our results also evidence a subglacial depression directly behind the current calving front of Bowdoin Glacier, so that a rapid unstable retreat of the front must be expected in the coming years if the glacier keeps thinning.

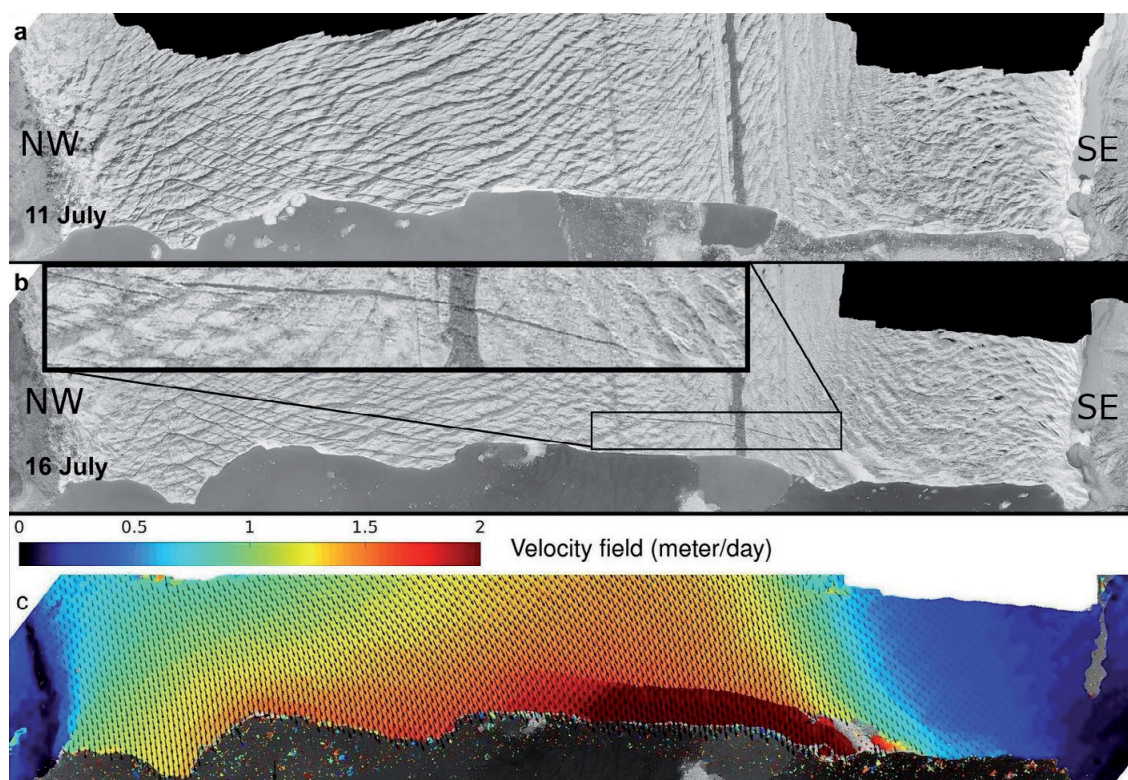


Figure 1. Calving front of Bowdoin Glacier: orthoimages obtained by UAV on the 11th (a) and the 16th (b) of July 2015, and resulting velocity field inferred by feature tracking (c), respectively. The discontinuity in the velocity field is due to the fracture, which appeared on the second orthoimage.

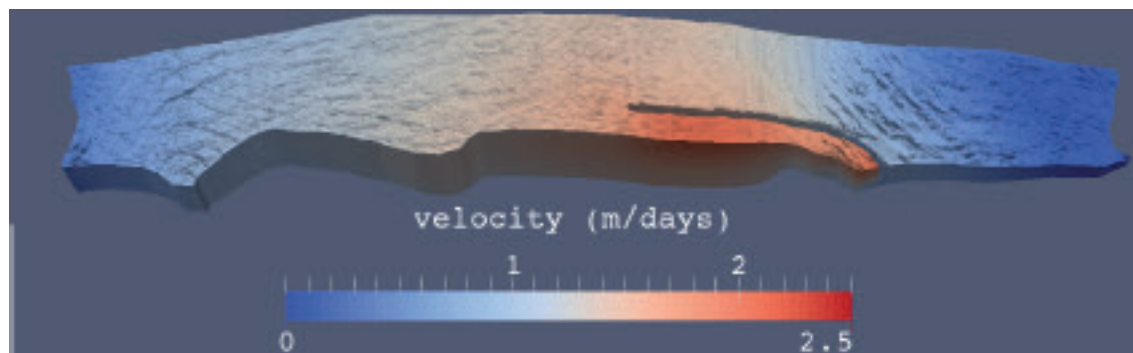


Figure 2: Velocity field modelled with ELMER/ICE.

REFERENCES

- G. Jovet, Y. Weidmann, J. Seguinot, M. Funk, T. Abe, D. Sakakibara, and S. Sugiyama. Initiation of a major calving event on Bowdoin Glacier captured by UAV photogrammetry. Preprint.
- J. C. Ryan, A. L. Hubbard, J. E. Box, J. Todd, P. Christoffersen, J. R. Carr, T. O. Holt, and N. Snooke. UAV photogrammetry and structure from motion to assess calving dynamics at store glacier, a large outlet draining the Greenland Ice Sheet. *The Cryosphere*, 9(1):1–11, 2015.
- S. Sugiyama, D. Sakakibara, S. Tsutaki, M. Maruyama, and T. Sawagaki. Glacier dynamics near the calving front of Bowdoin Glacier, northwestern Greenland. *Journal of Glaciology*, 61:223–232, 2015.

12.8

Seismic monitoring of the 2016 outburst flood of Lac des Faverges on Glacier de la Plaine Morte

Fabian Lindner¹, Fabian Walter¹ & Gabi Laske²

¹ *Laboratory of Hydraulics, Hydrology and Glaciology, ETH Zürich, Hönggerbergstr. 26, CH-8093 Zürich (lindner@vaw.baug.ethz.ch)*

² *Cecil H. and Ida M. Green Institute of Geophysics and Planetary Physics, Scripps Institution of Oceanography, University of California San Diego, 9500 Gilman Drive, La Jolla, CA 92093-0225, USA*

In recent years, Lac des Faverges – a glacier-dammed lake on Glacier de la Plaine Morte located in Switzerland's canton Bern – was subject to sudden drainage events (Huss et al., 2013). These events are of interest, as they 1) partly caused floods in the Simme valley and 2) impact the ice flow by changing subglacial hydraulic conditions. However, the drainage process is difficult to monitor with conventional approaches as borehole pressure measurements provide point measurements, only, tracer experiments give an integrated view of water routing and radar and active seismics identifying changes in subsurface water flow are laborious.

In summer 2016, we monitored Lac des Faverges using passive seismological recordings. Seismology provides continuous measurements and has shown to provide valuable insights into fracture opening, basal motion and water flow. In the context of subglacial hydraulics, turbulent water flow through englacial or subglacial conduits generates seismic signals (Gimbert et al., 2016) and water-filled void spaces can cause resonance effects which are quantifiable with seismic sensors (Roeoesli et al., 2016). Glacier seismology is advantageous as it is not a point measurement and not limited to surface processes, but capable to “look into the glacier”.

The lake reached an all-time maximum volume of ~2 Mm³ (million cubic meters) this summer, before the drainage initiated at the end of August. The peak discharge of ~1 Mm³ over the course of nine hours was recorded by six on-ice seismometers installed close to the lake and ten geophones installed along the approximate expected drainage path. With this setup we intend to study 1) the initiation mechanism of the outburst-flood, 2) the drainage path 3) the evolution of the subglacial drainage system over time.

Furthermore, with geophones placed in crevasse fields, we can investigate seismic anisotropy caused by preferred fracture and crevasse orientations in these parts of the glacier. As the water content of crevasses can change significantly during an outburst flood, the anisotropy signature (if observable) should change as well. This would elucidate variations in subglacial water pressure before, during and after the drainage process.



Figure 1. Lac des Faverges on Glacier de la Plaine Morte with view to the mountains of canton Valais.

REFERENCES

- Gimbert, F., Tsai, V. C., Amundson, J. M., Bartholomaeus, T. C., & Walter, J. I. (2016). Subseasonal changes observed in subglacial channel pressure, size, and sediment transport. *Geophysical Research Letters*, 43(8), 3786-3794.
- Huss, M., Voinesco, A., & Hoelzle, M. (2013). Implications of climate change on Glacier de la Plaine Morte, Switzerland. *Geogr. Helv.*, 68, 227-237.
- Roeoesli, C., Walter, F., Ampuero, J. P., & Kissling, E. (2016). Seismic moulin tremor. *Journal of Geophysical Research: Solid Earth*.

12.9

Interfering reflections in ground based radar measurements: Lessons learnt from a snow depth measurement campaign

Célia Lucas¹, Yves Bühler², Silvan Leinss¹, Armando Marino³, Irena Hajnsek^{1,4}

¹ *Institute of Environmental Engineering (IfU), ETH Zürich, 8093 Zürich, Switzerland (lucas@ifu.baug.ethz.ch)*

² *WSL Institute for Snow and Avalanche Research (SLF), Flüelastrasse 11, CH-7260 Davos Dorf, Switzerland*

³ *Department of Engineering and Innovation, Open University, Milton Keys, United Kingdom*

⁴ *Microwaves and Radar Institute, German Aerospace Center (DLR), Germany*

Spatially continuous snow depth information over large areas is important for different applications such as runoff predictions during snowmelt or avalanche warning. Whereas automated weather stations or manual field measurements only provide localised point measurements, imaging radar has the potential to map large regions, without the need of physically accessing the area even if the visibility is limited.

During the winter season 2015/2016 we performed a measurement campaign using our Ku-band Advanced Polarimetric Radar Interferometer (KAPRI) in Davos (GR). The south-east facing Dorfberg slope was monitored continuously by KAPRI during the entire winter season.

Ku-band radar waves are expected to penetrate up to a few meters into dry snow (Mätzler 1987, Wiesmann & Mätzler 1999), with a scattering center located close to the ground surface. As snow gets wet, free water appears in the snow which increases microwave absorption by several orders of magnitude. This limits the penetration depth to the uppermost few centimeters (Mätzler 1987, Wiesmann & Mätzler 1999). Using the interferometric capabilities of KAPRI, a digital elevation model (DEM) of a snow free, a dry and a wet snow scenario was produced. Subtracting the dry snow DEM from the wet- or snow free DEM results in a snow depth map. Reference measurements were acquired using UAS photogrammetry as described in Bühler et al (2016). The DEM Differencing technique was previously performed by Leinss (2015) using spaceborne TanDEM-X data and produced promising results in agreement with snow depth maps provided by the WSL Institute for Snow and Avalanche Research. However due to a lack of in situ reference data, the findings could not directly be validated.

During our campaign with the ground based KAPRI, we observed an interference pattern, overprinting the data and obscuring the measurement. The pattern of this signal consists of undulations in the intensity and the interferometric phase parallel to the elevation contour lines of the terrain, leading to artefacts in the derived DEMs. Due to the similarity of this signal to the pattern left by grazing cows in mountainous areas, it was dubbed “Ochsohypsen”.

To investigate to origin of the pattern, we performed an experiment at the Campus of ETH Hönggerberg, where the undulations could be reproduced and were identified as interference patterns. For this experiment KAPRI was mounted on a fork lift and measurements were performed from different heights between 0.5 and 4.6m above the ground. It was found that the wavelength of the interference pattern changes as the antenna height above the ground increases. Further analysis indicates that they emanate from an interference of direct and indirect waves reflected on the ground, similar to the overlay problem known in radar images acquired with a downward looking geometry, such as airborne or spaceborne radar images. With our experiment, we show that a similar problem arises from upward looking radar geometries where a flat ground located between the radar and the area of interest produces specular reflections.

These findings show that snow depth retrieval with the DEM Differencing methodology and the used measurement geometry is not possible due to interference of direct and indirect waves. Whereas the expected snow depth results could not be obtained, we were able to pinpoint a crucial problem for ground based radars, which impacts a large spectrum of applications. Our findings allow to avoid such problems in the future by choosing an appropriate measurement geometry and should make snow depth estimation with ground based radars possible.

REFERENCES

- Bühler, Y., Adams, M.S., Bösch, R. & Stoffel, A. 2016: Mapping snow depth in alpine terrain with unmanned aerial systems (UAS): potential and limitations, *The Cryosphere*, 10.3, 1075-1088
- Leinss, S. 2015: Depth, Anisotropy, and water equivalent of snow estimated by radar interferometry and polarimetry, Ph.D. Dissertation
- Mätzler, C. 1987: Applications of the interaction of microwaves with the natural snow cover, *Remote Sensing Reviews*, 2, 259-387
- Wiesmann, A. & Mätzler, C. 1999: Microwave emission model of layered snowpacks, *Remote Sensing of the Environment*, 70.3, 307-317

12.10

Conventional and radioactive waste at the abandoned ice sheet base at Camp Century, Greenland, in a warming climate

Horst Machguth^{1,2} and William Colgan³

¹ Department of Geography, University of Zurich, Zurich, Switzerland (horst.machguth@geo.uzh.ch)

² Department of Geosciences, University of Fribourg, Fribourg, Switzerland

³ Lassonde School of Engineering, York University, Toronto, Ontario, Canada

In 1959 the U.S. Army Corps of Engineers built Camp Century beneath the surface of the northwestern Greenland Ice Sheet (Fig. 1; Colgan et al., 2016). The camp served at studying the feasibility of “Project Iceworm”, which sought at exploring the possibility of deploying ballistic missiles within the ice sheet. The subsurface base was also the locale of major scientific endeavours, in particular the retrieval of the first ever ice core drilled to the bed of an ice sheet.

The base was abandoned with minimal decommissioning in 1967, under the assumption material and waste from six years of operation would be “preserved for eternity” by perpetually accumulating snowfall (Clark et al., 1962). However, ice sheet mass loss has accelerated under anthropogenic climate change, and current scenarios indicate continued increase in melt.

Here, we firstly review the history of Camp Century and inventory the nature and quantity of abandoned wastes. We conclude that the site likely hosts substantial quantities of physical waste, diesel fuel, radiological waste and non-trivial amounts of polychlorinated biphenyls (PCBs). Secondly, we show that a transition from net accumulation to net ablation at the site of the former camp is plausible within the next 75 years, under a business-as-usual anthropogenic emissions scenario (Representative Concentration Pathway 8.5). Net ablation would guarantee the eventual remobilization of the abandoned waste.

Buried under 35 to 70 m of firn, the abandoned waste rather calls for monitoring than immediate remediation. However, Camp Century, legally established under Danish-U.S. treaties, stands emblematic for the potential remobilization of a whole spectra of abandoned assets, resulting from climate change.



Figure 1. Location of Camp Century on Greenland, installation of the nuclear reactor that powered the camp and view into the tunnel system (image credits: US Army, National Geographic, Getty Images)

REFERENCES

- Clark, L. K., Alter, A. J., & Blake, L. J. (1962), Sanitary waste disposal for navy camps in polar regions, *J. Water Pollut. Control Fed.*, 34, 1219–1234.
- Colgan, W., Machguth, H., MacFerrin, M., Colgan, J. D., van As, D. & MacGregor, J. A. (2016), The abandoned ice sheet base at Camp Century, Greenland, in a warming climate, *Geophys. Res. Lett.*, 43, doi:10.1002/2016GL069688.

12.11

Glacier surface albedo derived from remotely sensed data and its importance for mass balance modelling

Kathrin Naegeli¹, Alexander Damm², Matthias Huss^{1,3}, Hendrik Wulf², Michael Schaepman², Martin Hoelzle¹

¹ *Department of Geosciences, University of Fribourg, Chemin du Musée 4, CH-1700 Fribourg (kathrin.naegeli@unifr.ch)*

² *Remote Sensing Laboratories, University of Zurich, Winterthurerstr. 190, CH-8057 Zurich*

³ *Laboratory of Hydraulics, Hydrology and Glaciology (VAW), ETH Zurich, Hönggerberggring 26, CH-8093 Zürich*

Glacier surface albedo is crucial to determine the amount of energy absorbed by snow/ice surfaces throughout the year. Especially in summer, when large parts of the glaciers are snow-free, the albedo of heterogeneous bare-ice surfaces substantially impacts on glacier melt rates (Naegeli et al. 2015). However, an operational data product providing broadband surface albedo suitable for rather small-scale mountain glaciers is still lacking. Hence, current glacier mass balance models rely on oversimplified homogeneous ice albedo parameters in their energy balance functions, neglecting the diverse nature of glacier surfaces and their changes over time. While in-situ measurements provide valuable point data, indicating local temporal variations in albedo, airborne- and/or satellite-based sensors offer the possibility to attribute glacier surface albedo to larger areas with reasonable spatial (<30 m) but still limited temporal resolution (Paul et al. 2005, Klok et al. 2003).

Here, we outline a methodology to derive shortwave broadband albedo for glacier surfaces based on in-situ, airborne and satellite (Sentinel-2 and Landsat 8) data. We use APEX (Airborne Prism Experiment) and in-situ reflectance measurements obtained on several Swiss glaciers to evaluate the accuracy of derived albedo products from satellite data and discuss related uncertainties, in particular the influence of spectral and spatial resolution. Applying our approach to Landsat and Sentinel-2 data, allows us to quantify the glacier albedo in high spatial resolution at regional-scale. In addition, we highlight the value and implications of such detailed albedo data for glacier mass balance modelling with focus on the summer melt season.

Our results contribute to a better understanding of spatio-temporal variations in bare-ice albedo and demonstrate the benefit of spatially distributed albedo datasets to study the heterogeneous melt behaviour of glacier surfaces. We conclude on the relevance of these recent satellite missions to extend the yet limited temporal resolution for mapping dynamic glaciological processes such as the recent darkening of glacier surfaces, and to advance and facilitate modelling approaches to study future glacier evolution.

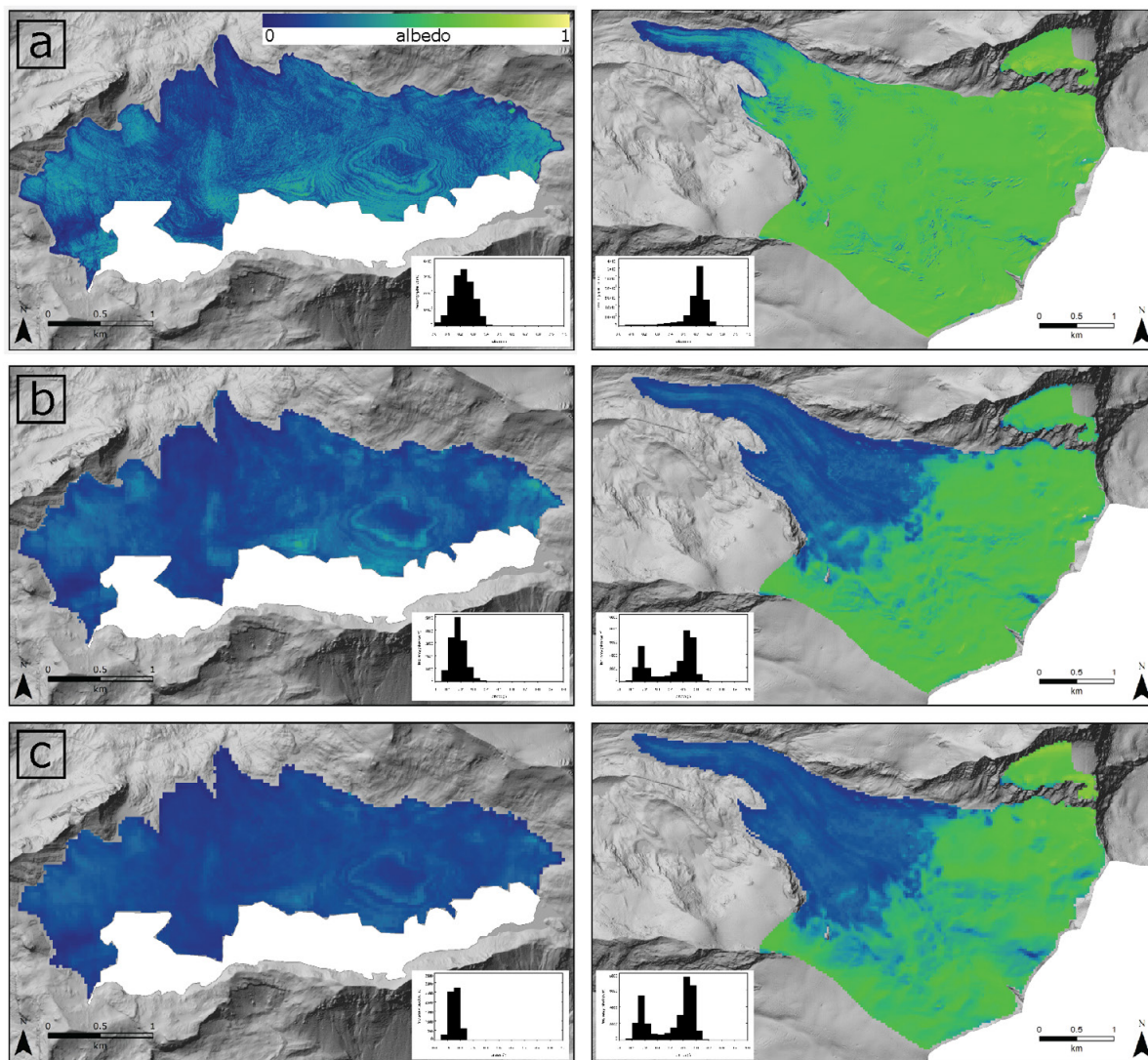


Figure 1. Albedo products of Glacier de la Plaine Morte (left), Findelengletscher (right) based on: (a) APEX data (22.08.2015), (b) Sentinel-2 data (29.08.2015) and (c) Landsat 8 data (30.08.2015). The insets show the albedo frequency distribution per glacier and product.

REFERENCES

- Klok, E.J.L., Greuell, W., & Oerlemans, J. 2003: Temporal and spatial variation of the surface albedo of Morteratschgletscher, Switzerland, as derived from 12 Landsat images. *Journal of Glaciology*, 49(167), 491–502.
- Naegeli, K., Damm, A., Huss, M., Schaepman, M. and Hoelzle, M. 2015: Imaging spectroscopy to assess the composition of ice surface materials and their impact on glacier mass balance. *Remote Sensing of Environment*, 168, 388-402. doi:10.1016/j.rse.2015.07.006
- Paul, F., Machguth, H. & Käab, A. 2005: On the impact of glacier albedo under conditions of extreme glacier melt: the summer of 2003 in the Alps. *EARSeL eProceedings*, 4(2), 139–149.

12.12

Tidewater glacier dynamics dominated by sliding at Bowdoin Glacier, Northwest Greenland

Julien Seguinot¹, Martin Funk¹, Guillaume Jouvét¹, Claudia Ryser¹, Andreas Bauder¹, Silvan Leinss², Daiki Sakakibara³ and Shin Sugiyama³

¹ Laboratory of Hydraulics, Hydrology and Glaciology, ETH Zürich, Switzerland (seguinot@vaw.baug.ethz.ch)

² Institute of Environmental Engineering, ETH Zürich, Switzerland

³ Institute of Low Temperature Science, Hokkaido University, Sapporo, Japan

The observed rapid retreat of ocean-terminating glaciers in southern Greenland in the last two decades has now propagated to the northwest. Hence, tidewater glaciers in this area, some of which have remain stable for decades, have started retreating rapidly through iceberg calving in recent years, thus allowing a monitoring and investigation of ice dynamical changes starting from the early stages of retreat.

Bowdoin Glacier, a small and relatively accessible calving glacier in Northwest Greenland, appeared to be very stable since its frontal position had been first documented by explorers in the late 19th century. However, following a two-fold increase of surface velocity in the early 2000s, the calving front of Bowdoin Glacier has experienced a rapid retreat of ca. 2 km between 2007 and 2013. Since 2013, the ice front is once again stable, yet the glacier surface continues to experience lowering at an alarming rate of ca. 6 m/a.

Here, we present a two-year record of surface velocity and englacial deformation of the tidewater glacier tongue. From July 2014 to July 2016, we monitored, 1.5 to 2 km upstream from the calving front, subglacial water pressure changes in boreholes, internal ice deformation through tilt sensors at different depths, englacial ice temperature profiles from the glacier bed to the surface, and high-resolution surface motion from GPS records. Combined with feature tracking velocities from visible (Landsat-8) and Radar (Sentinel-1A) satellite imagery, this record allows for a continuous, 20-month reconstruction of basal sliding in the vicinity of the calving front. Our results indicate that the glacier's ice is below pressure melting point except for its temperate base. Basal sliding accounts for ca. 90% of the observed surface motion. Both sliding and deformation increase by up to 100% during periods of warm weather in the annual melt season. Such speed-up events have been most pronounced in 2016, perhaps due to the continued thinning of the ice tongue.

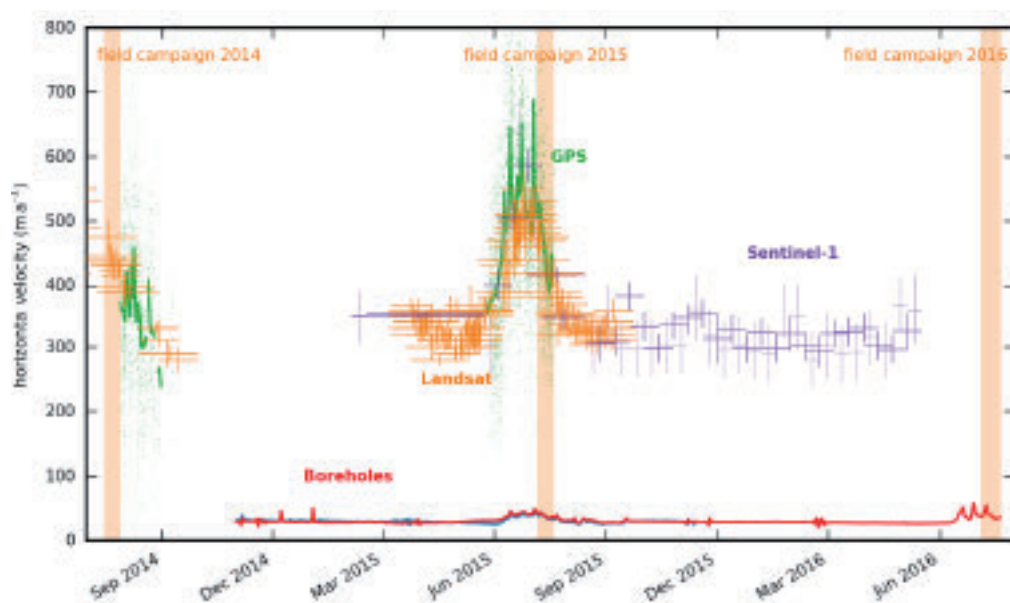


Figure 1. Bowdoin Glacier surface velocity from solar-powered GPS receiver (green), and Landsat-8 (orange) and Sentinel-1A (purple) satellite images, compared with deformation velocity from tilt sensors (red and blue).

12.13

Point-wise estimation of glacier surface height changes based on reflected GPS signals

Ladina Steiner¹, Martin Baumann² & Alain Geiger¹

¹ *Institute of Geodesy and Photogrammetry, ETH Zurich, Switzerland (ladinasteiner@ethz.ch)*

² *now at Trimble New Zealand, Christchurch 8440, New Zealand*

Observing and monitoring glacier mass balance is of great importance for future sea-level rise, regional hydrology and climate change. Radar observations or manual in-situ measurements at stakes are used to determine the mass balance seasonally to annually. Mounted on such stakes, GPS is commonly used for glacier flow measurements. In general, GPS multipath signals reflected off the surrounding surface lead to errors in accurate position estimation. GPS-reflectometry (GPS-R) is a method where these multipath signals are used to derive height information of the reflection surface and its roughness.

By using the GPS signals reflected off a glacier surface, it is possible to continuously determine the sensor's height change over the surface and thus to monitor point-wise snow accumulation and ice melt. We therefore set-up an automated GPS station on the Glacier de la Plaine Morte, Switzerland. From GPS signal reflections of approximately 50 meters around the station, a mean antenna height over the snow-covered glacier surface can be estimated. We compared these results to measurements from a sonic ranger, installed at our station. By knowing the absolute position of the GPS antenna and the antenna height over the surface, a mean height of the (snow-covered) glacier surface and thus the snow accumulation and ice melt at our location could be derived.

Our results show a high level of correlation and an accuracy within a few centimeters compared to the independent height measurements of the sonic ranger. Our method has a considerable potential to measure surface elevation changes over snow and ice at high temporal resolution without the need of installing additional specific sensors.

12.14

Glacier climate interaction: reconstruction of the mass balance field using ice extent data

Vjerran Visnjevic¹, Frederic Herman¹, Yuri Podladchikov¹

¹ *Institute of Earth Surface Dynamics, University of Lausanne, CH-1005 Lausanne (vjeran.visnjevic@unil.ch)*

With the end of the Last Glacial Maximum (LGM), about 20 000 years ago, ended the most recent long-lasting cold phase in Earth's history. This last glacial advance left a strong imprint on the landscape, such as abandoned moraines, trimlines and other glacial geomorphic features. These features provide a valuable record of local climate change on the continents. In particular, terminal moraines reflect the extent and volume of glacier ice, which itself reflects past temperature and precipitation conditions. Here we present an inverse approach we have recently developed to reconstruct the LGM mass balance from known ice extent data. The ice flow model is developed using the shallow ice approximation and the developed codes are accelerated using Graphical Processing Units capabilities (GPU). The mass balance field, \dot{b} , is the constrained variable defined by the ice surface, balance rate β and the spatially variable equilibrium line altitude field (ELA), where c is the cutoff value:

$$\dot{b} = \max(\beta \cdot (S(x, y) - ELA(x, y)), c).$$

We show that such a mass balance, and thus the spatially variable ELA field, can be inferred from the observed past ice extent and ice thickness. We start with synthetic test to demonstrate the method. We then apply the method to LGM ice extent the South Island of New Zealand. This example shows that the method is capable of constraining spatial changes in mass balance at the scale of a mountain range.

12.15

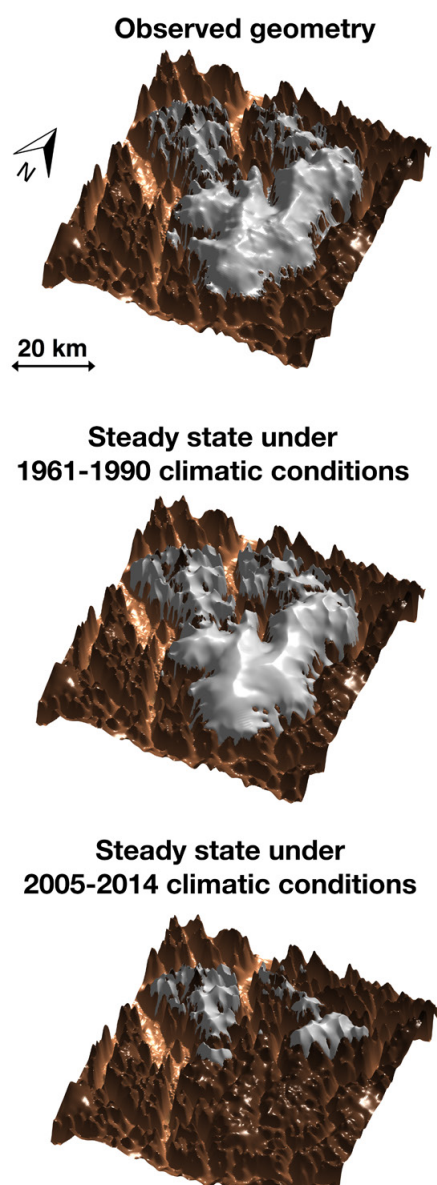
Dynamics and climate sensitivity of Hans Tausen Iskappe (Greenland)

Harry Zekollari^{1/2}, Philippe Huybrechts¹, Brice Noël³, Willem Jan van de Berg³ & Michiel R. van den Broeke³

¹ Earth System Science & Departement Geografie, Vrije Universiteit Brussel, Pleinlaan 2, 1050 Brussels, Belgium (harry.zekollari@vub.ac.be)

² Versuchsanstalt für Wasserbau, Hydrologie und Glaziologie (VAW), ETH Zürich, Hönggerberggring 26, CH-8093 Zürich, Switzerland (zharry@ethz.ch)

³ Institute for Marine and Atmospheric research Utrecht, University of Utrecht, Princetonplein 5, 3584CC Utrecht, The Netherlands



Hans Tausen Iskappe (Greenland), situated at 82.5°N, is the world's northernmost ice cap. During several field campaigns in the 70s and 90s, its ice thickness was measured, mass balance and meteorological measurements were made, and a 345 m deep ice core was drilled (Hammer, 2001). From this ice core it is known that the ice cap (largely) disappeared during the Holocene Thermal Maximum. The present-day ice cap started building up some 3500–4000 years ago in a wetter and slightly warmer climate than at present.

Here we present thermo-mechanical ice flow modelling results of the ice cap's fundamental climate sensitivity. A 3-D higher-order ice flow model, that was previously developed and applied for modelling the ice flow of the Morteratsch glacier complex (Engadine, Switzerland) (Zekollari et al., 2013, 2014; Zekollari and Huybrechts, 2015), is used. The surface mass balance model considers snowfall and meltwater runoff. Net precipitation is based on RACMO2.3 output at a 1 km horizontal resolution. Runoff is calculated from a positive degree-day model that includes water retention in the snowpack with parameters derived from field measurements. The simulations are validated and calibrated with field observations complemented with satellite derived surface velocities.

The ice cap geometry evolves to a state close to the presently observed for average 1961–1990 climate conditions, but the ice cap is found to already lose a substantial part of its volume and area under slightly warmer conditions. Sensitivity analyses point out that the ice cap's northern part, situated on a plateau, is fairly stable under changing climatic conditions, whereas the southern part is much more sensitive. Under the 2005–2014 climatic conditions the entire southern part of the ice cap disappears and the ice cap loses about 80% of its present-day volume. The future projected loss of surrounding permanent sea-ice and corresponding potential sharp precipitation increase may lead to an attenuation of the retreat and even potential stabilization of the ice cap for a warming up to around 2°C. Under such conditions the ice margin will retreat while the interior is projected to grow, leading to a steeper ice cap, which is in line with the present-day observed trends. For intermediate (+4°C) and extreme warming scenarios (+8°C) the ice cap is projected to disappear respectively around 2400 and 2200, almost irrespective of the projected precipitation regime.

Figure 1. Observed and modelled ice cap geometries

REFERENCES

- Hammer, C.U. (Ed.) 2001: The Hans Tausen Ice Cap. *Glaciology and Glacial Geology*, Meddelelse. Danish Polar Center, Copenhagen.
- Zekollari, H., Huybrechts, P., Fürst, J.J., Rybak, O. & Eisen, O. 2013: Calibration of a higher-order 3-D ice-flow model of the Morteratsch glacier complex, Engadin, Switzerland. *Annals of Glaciology*, 54, 343–351, doi:10.3189/2013AoG63A434.
- Zekollari, H., Fürst, J.J. & Huybrechts, P. 2014: Modelling the evolution of Vadret da Morteratsch, Switzerland, since the Little Ice Age and into the future. *Journal of Glaciology*, 60, 1155–1168, doi:10.3189/2014JoG14J053.
- Zekollari, H. & Huybrechts, P. 2015: On the climate–geometry imbalance, response time and volume–area scaling of an alpine glacier: insights from a 3-D flow model applied to Vadret da Morteratsch, Switzerland. *Annals of Glaciology*, 56, 51–62, doi:10.3189/2015AoG70A921.

P 12.1

Development of a Cryocell LA-ICP-MS Setup for Spatial Trace Element Analysis in High Alpine Glacier Ice

Sven Erik Avak,^{1,2,3} Mario Birrer,¹ Marcel Guillong,⁴ Thorsten Bartels-Rausch,¹ Margit Schwikowski,^{1,2,3} and Anja Eichler^{1,2}

¹ *Laboratory of Environmental Chemistry, Paul Scherrer Institute, CH-5232 Villigen PSI (sven.avak@psi.ch)*

² *Oeschger Centre for Climate Change Research, University of Bern, CH-3012 Bern*

³ *Department of Chemistry and Biochemistry, University of Bern, CH-3012 Bern*

⁴ *Institute of Geochemistry and Petrology, ETH Zurich, CH-8092 Zurich*

High alpine glaciers provide valuable information about past climate and atmospheric composition since they store a continuous record of entrapped atmospheric air and precipitation. Retrieving and analyzing ice cores from high alpine glaciers allows tracking climate variability and environmental changes over time in regions where most of the world's population lives. For instance, past changes in atmospheric pollution can be reconstructed from ice core trace element records (Schwikowski *et al.*, 2004).

Due to the current global temperature increase glaciers are rapidly retreating and even glaciers at high altitudes are in danger to melt. Percolation of meltwater alters the information originally stored in these environmental archives. A previous study (Eichler *et al.*, 2001) revealed evidence that the preservation of impurities with respect to meltwater depends on their location in the crystal ice lattice. Laser ablation inductively coupled plasma mass spectrometry (LA-ICP-MS) is the method of choice for the direct *in situ* chemical analysis of trace elements at a sub-millimeter resolution in glacier ice (Sneed *et al.*, 2015). However, there are still difficulties regarding the quantification of signals (Reinhardt *et al.*, 2001, Della Lunga *et al.*, 2014). Here, we present the setup of a newly designed cryocell compatible with a commercially available laser ablation system. This cryocell is able to simultaneously hold ice samples and frozen standard solutions for quantifying differences in concentrations of trace elements between grain boundaries and ice grain interiors. The development and optimization of frozen standards for calibration will be discussed. Application of this analytical technique will facilitate the evaluation of the potential of trace elements as environmental proxies in glaciers affected by melting.

REFERENCES

- Della Lunga, D., Müller, W., Rasmussen, S. O. & Svensson, A. 2014: Location of cation impurities in NGRIP deep ice revealed by cryo-cell UV-laser-ablation ICPMS, *Journal of Glaciology*, 60, 970-988.
- Eichler, A., Schwikowski, M., Gäggeler, H. W. 2001: Meltwater-induced relocation of chemical species in Alpine firn, *Tellus B*, 53, 192-203.
- Reinhardt, H., Kriews, M., Miller, H., Schrems, O., Lüdke, C., Hoffmann, E. & Skole, J. 2001: Laser ablation inductively coupled plasma mass spectrometry: a new tool for trace element analysis in ice cores, *Fresenius' Journal of Analytical Chemistry*, 370, 629-636.
- Schwikowski, M., Barbante, C., Doering, T., Gäggeler, H. W., Boutron, C., Schotterer, U., Tobler, L., van de Velde, K., Ferrari, C., Cozzi, G., Rosman, K., Cescon, P. 2004: Post-17th-Century Changes of European Lead Emissions Recorded in High-Altitude Alpine Snow and Ice, *Environmental Science & Technology*, 38, 957-964.
- Sneed, S. B., Mayewski, P. A., Sayre, W. G., Handley, M. J., Kurbatov, A. V., Taylor, K. C., Bohleber, P., Wagenbach, D., Erhardt, T. & Spaulding, N. E. 2015: New LA-ICP-MS cryocell and calibration technique for sub-millimeter analysis of ice cores, *Journal of Glaciology*, 61, 233-242.

P 12.2

Effects of particulate matter on the albedo of Alpine glaciers

Anna Dal Farra^{1,2,3}, Susan Kaspari⁴, Margit Schwikowski^{1,2,3}

¹ Paul Scherrer Institute, CH-5232 Villigen, Switzerland

² Oeschger Centre for Climate Change Research, University of Bern, Falkenplatz 16, CH-3012 Bern, Switzerland

³ Department of Chemistry and Biochemistry, University of Bern, Freierstrasse 3, CH-3012 Bern, Switzerland

⁴ Department of Geological Sciences, Central Washington University, 400 E University Way, WA -98926 Ellensburg

Alpine glaciers are vital components of the earth's hydrological system; the current prevailing trend shows an overall increase of their melt rates [IPCC, 2007]. Previous studies have suggested that along with rising temperatures, a decrease in surface albedo might play a role in this phenomenon [Warren, 1980].

Albedo is a property of surfaces and is defined as the proportion of incident radiation that is reflected by a surface. The surface albedo of glaciers decreases through a number of effects, such as the ageing of snow, the presence of liquid water on the surface, the exposure of the underlying bare ice and the presence of light absorbing impurities (LAI) [Gabbi, 2015]. Light absorbing impurities commonly found on glaciers include black carbon, mineral dust and colored organic material. In order to assess how each class of LAI influences the surface albedo of ice and snow a representative reflectance spectrum from each class should be defined. Instead of separating the classes of LAI and collecting the reflectance of each, which might alter their optical properties, we opted for collecting reflectance spectra from different individual particles. To achieve that, we developed a new method using the Cytoviva Hyperspectral Microscope (CHM, Cytoviva).

The CHM provides quantitative spectral analysis of nanoscale (128 nm pixel resolution) materials in the visible to near-infrared range (400 nm-1000 nm). Reflectance spectra of standard materials, such as diesel soot, fullerene, humic substances, fulvic substances and various minerals have been collected both with the CHM setup and with a commonly used spectroradiometer. The agreement between the two methods validates this powerful technique. The samples were collected on Plaine Morte glacier, a flat glacier of 7.8 km², located in the Swiss Alps between the cantons of Valais and Bern.

The glacier is easily accessible, has a strong negative mass balance and has been snow-free during the summer for the past seven years, progressively enriching a dark layer of light absorbing impurities on its surface [Huss, 2013]. An environmental sample was analyzed with the analytical method established in this work. The results comparing the reflectance spectra of all the LAI classes in this sample will show which of them has the highest effect on the albedo decrease.



Figure 1. Plaine Morte glacier with fresh snow in June 2010 [Bühlmann, 2011] with albedo value of 0.9 and in August 2015 with bare ice and an albedo of 0.2

REFERENCES

- E. Bühlmann, Master thesis: Influence of particulate matter on observed albedo reduction on Plaine Morte glacier, Swiss Alps.
- Effects of particulate matter on the albedo of Alpine glaciers
- J. Gabbi, M. Huss, A. Bauder, F. Cao, and M. Schwikowski. 2015: The impact of Saharan dust and black carbon on albedo and long term glacier mass balance, *The Cryosphere Discussion*, 9, 1133-1175.
- M. Huss, A. Voinesco, M. Hoelzle, 2013: Implications of climate change on glacier de la Plaine Morte, Switzerland, *Geographica Helvetica*, 68, 227-237.
- Vaughan, D.G., J.C. Comiso, I. Allison, J. Carrasco, G. Kaser, R. Kwok, P. Mote, T. Murray, F. Paul, J. Ren, E. Rignot, O. Solomina, K. Steffen and T. Zhang, 2013: Observations: Cryosphere. In: *Climate Change 2013: The Physical Science Basis. Contribution of Working Group I to the Fifth Assessment Report of the Intergovernmental Panel on Climate Change*.
- S. Warren, W. Wiscombe, 1980: A model for the spectral albedo of snow. II Snow containing atmospheric aerosols, *Journal of Atmospheric Sciences*, 37, 2734-2745.

P 12.3

FROZENFIRE – 5000 years of fire, vegetation and pollution history from the Mongolian Altai

Sandra O. Brugger¹, Erika Gobet¹, Michael Sigl², Dimitri Osmont², Margit Schwikowski², Willy Tinner¹

¹ *Institute of Plant Sciences and Oeschger Centre for Climate Change Research, Altenbergrain 21, 3013 Bern*

² *Paul Scherrer Institute, OFLB/109, 5232 Villigen*

Devastating, uncontrolled fires and air pollution have increasingly occurred in recent years, resulting in enormous economic costs and disruption of habitats (Moritz et al. 2014). Air pollution plumes related to extreme fire events are of growing concern due to their effect on human health (Peel et al. 2013). Nevertheless, the drivers for long-term biomass burning are still debated. For the period since 1850 a decoupling of fire-activity from temperature and human population density was proposed (i.e. the “broken hockey stick”-hypothesis). In combination with increasing fire severity in recent decades such uncertainty raises major public and scientific questions about future management strategies under global-warming conditions (Kehrwald et al. 2013).

Pollen and spores as proxies for past vegetation and land use, microscopic charcoal (>10µm) as a proxy for fire activity, and framboid organic particles (or soots) as a proxy for fossil fuel combustion preserve in ice cores over millennia (Eichler et al. 2011). We present the results of an ice core record from Tsambagarav Mountain in the Mongolian Altai (4130 m a.s.l.) covering the past 5500 years (Herren et al. 2013). A sound chronology allows a comparison of vegetation and societal responses to climatic change and fire disturbance with a focus on the last 150 years. The record reflects large scale fire and vegetation dynamics in the Mongolian steppes under a continuous impact of pastoralism over five millennia. A decline of forested areas is tentatively correlated with the rise of Dshingis Khan’s empire around 1200 AD, and a pollution signal comparable to Western Europe is reconstructed, starting in the 18th century AD, peaking in the 1960ies.

REFERENCES

- Eichler A., Tinner W., Brüttsch S., Olivier S., Papina T., Schwikowski M. (2011): An ice-core based history of Siberian forest fires since AD 1250. *Quaternary Science Reviews*, 30(9), 1027-1034.
- Herren, P. A., Eichler, A., Machguth, H., Papina, T., Tobler, L., Zapf, A., & Schwikowski, M. 2013. The onset of Neoglaciation 6000 years ago in western Mongolia revealed by an ice core from the Tsambagarav mountain range. *Quaternary Science Reviews*, 69, 59-68.
- Kehrwald, N. M., Whitlock, C., Barbante, C., Brovkin, V., Daniu, A. L., Kaplan, J. O., Marlon, J. R. 2013. Fire research: linking past, present, and future data. *Eos, Transactions, American Geophysical Union*, 94(46). (2013): Fire Research: Linking Past, Present, and Future Data. *Eos, Transactions American Geophysical Union*, 94(46), 421-422.
- Moritz M. A., Battlori E., Bradstock R. A., Gill A. M., Handmer J., Hessburg P. F., Leonard J. McCaffrey S., Odion D. C., Schoennagel T., Syphard A. D. 2014: Learning to coexist with wildfire. *Nature*, 515(7525), 58-66.
- Peel J. L., Haeuber R., Garcia V., Russell A. G., & Neas L. 2013: Impact of nitrogen and climate change interactions on ambient air pollution and human health. *Biogeochemistry*, 114(1-3), 121-134.

P 12.4

FROZENFIRE – A high-alpine ice core record to assess vegetation and fire dynamics in Western Europe over the last millennium

Sandra O. Brugger¹, Erika Gobet¹, Michael Sigl², Dimitri Osmont², Margit Schwikowski², Willy Tinner¹

¹ Institute of Plant Sciences and Oeschger Centre for Climate Change Research, Altenbergrain 21, 3013 Bern

² Paul Scherrer Institute, OFLB/109, 5232 Villigen

Wild fires are an ecological disturbance agent across ecosystems, driving vegetation dynamics and resulting in disruption of habitats (Moritz et al. 2014).

We analyze pollen and spores as proxies for vegetation composition, structure and agricultural activity, microscopic charcoal as a proxy for fire activity, and framboid organic particles (or soots) as a proxy for fossil fuel combustion which preserve in ice cores over millennia (Eichler et al. 2011).

Our high-alpine ice core (4452 m a.s.l.) from Colle Gnifetti is located in the center of Western Europe, thus allowing to assess vegetation and societal responses to climatic change and wildfire disturbance on a subcontinental scale. The record covers the last millennium with an excellent chronological control (Jenk et al. 2009, Sigl et al. 2009), particularly over the most recent 150 years - the period that experienced important climatic changes and an increasing globalization of economy.

The Colle Gnifetti record reflects large scale impacts such as extreme weather, societal innovations, agricultural crises and pollution of the industrial period in Western Europe. We aim at disentangling the role of climate, vegetation and human impacts on biomass burning in the Mediterranean realm and Western Europe to significantly advance the understanding of the regional role of wildfire events and vegetation responses under future climate change scenarios. To our knowledge we present the first long-term high-resolution palynological record of a high elevation ice core in the Alps.

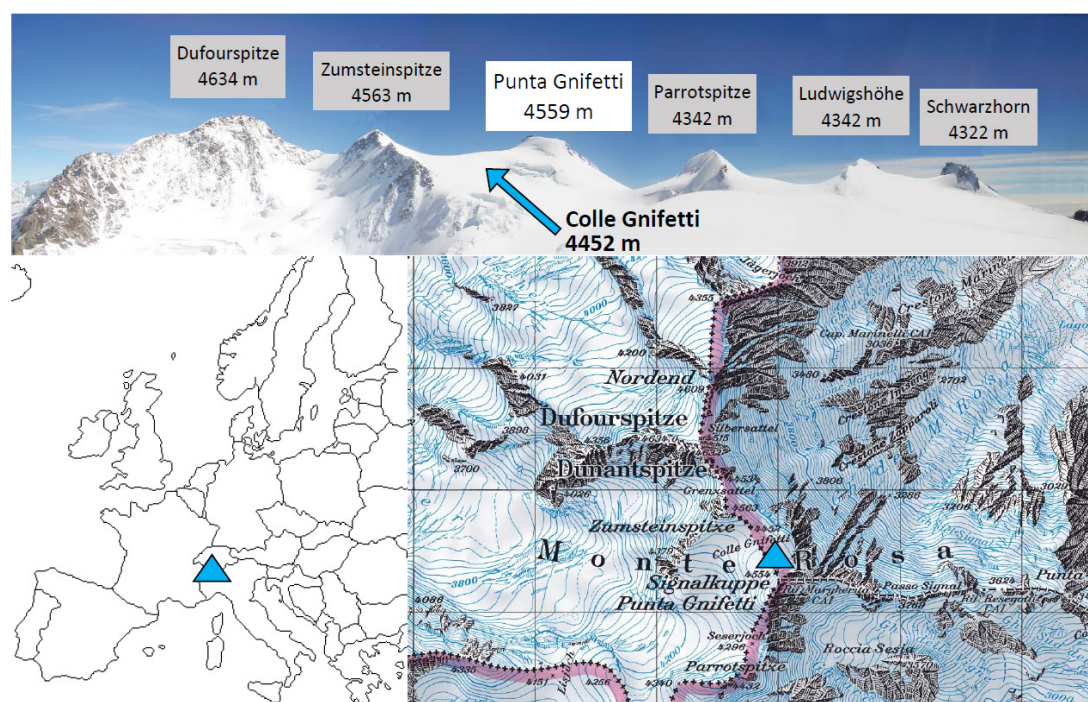


Figure 1. Panorama of the Monte Rosa and a map showing the drilling location of the ice core on the Colle Gnifetti glacier (blue triangle).

REFERENCES

- Eichler, A., Tinner, W., Brüttsch, S., Olivier, S., Papina, T., Schwikowski, M. 2011: An ice-core based history of Siberian forest fires since AD 1250. *Quaternary Science Reviews*, 30(9), 1027-1034.
- Jenk, T.M., Szidat, S., Boliuss, D., Sigl, M., Gäggeler, H.W., Wacker, L., Ruff, M., Barbante, C., Boutron, C.F., Schwikowski, M. 2009. A novel radiocarbon dating technique applied to an ice core from the Alps indicating late Pleistocene ages. *Journal of Geophysical Research: Atmospheres*, 114(D14).
- Moritz M. A., Batllori E., Bradstock R. A., Gill A. M., Handmer J., Hessburg P. F., Leonard J. McCaffrey S., Odion D. C., Schoennagel T., Syphard A. D. 2014: Learning to coexist with wildfire. *Nature*, 515(7525), 58-66.
- Sigl, M., Jenk, T. M., Kellerhals, T., Szidat, S., Gäggeler, H. W., Wacker, L., Synal, H.-A., Boutron, C., Barbante, C., Gabrieli, J., Schwikowski, M. 2009: Towards radiocarbon dating of ice cores. *Journal of Glaciology*, 55(194), 985-996.

P 12.5

Towards the reconstruction of forest fires through chemical analysis of black carbon in ice cores from mountain glaciers

Dimitri Osmont^{1,2,3}, Michael Sigl^{1,3}, Isabel Wendl¹, Loic Schmidely³, Elisabeth Isaksson⁴, Mackenzie Grieman⁵, Margit Schwikowski^{1,2,3}

¹ *Laboratory of Environmental Chemistry, Paul Scherrer Institute, CH-5232 Villigen PSI (dimitri.osmont@psi.ch)*

² *Department of Chemistry and Biochemistry, University of Bern, Freiestrasse 3, CH-3012 Bern*

³ *Oeschger Centre for Climate Change Research, University of Bern, Falkenplatz 16, CH-3012 Bern*

⁴ *Norwegian Polar Institut, Fram Centre, NO-9296 Tromsø*

⁵ *Department of Earth System Science, University of California, CA-92 697 Irvine, USA*

In recent years, the repeated occurrence of huge fire events, like the 2016 forest fires in Portugal, drew public attention to this phenomenon responsible of important damages to our infrastructures, buildings and environment, causing substantial economic losses (Moritz et al., 2014). However, even if fires occur on all vegetated continents, the long-term drivers for biomass burning are still not clearly understood because of the complexity of the interactions between climate, humans and fires. By using a compilation of more than 400 charcoal records from lake sediment cores, it has been postulated that global fire activity, after following temperature variations until 1870, abruptly showed a decoupling from its main drivers, namely temperature and population density, and dropped due to increasing human influences (Marlon et al., 2008). However, this hypothesis, called “broken fire hockey stick”, is still subject to large uncertainties inherent to the uppermost part of lake sediment cores, and needs to be confirmed by means of records from other climate archives.

In this respect, ice cores retrieved from polar and high-mountain glaciers are a very powerful tool to reconstruct paleoclimates due to the fact that glaciers behave as climate archives by trapping chemical information from the atmosphere. The inter-disciplinary Paleo Fire project aims to test the “broken fire hockey stick” hypothesis by reconstructing regional paleo fires history from multi-proxy high-mountain ice cores for the last 2000 years.

In this work, black carbon (BC) was used as a proxy for fire activity in ice cores. BC consists of aggregates of small carbonaceous spherules produced by the incomplete combustion of fossil fuels and biofuels from both anthropogenic and natural origin, including wildfires (Bond et al., 2013). BC was analyzed with a Single Particle Soot Photometer (SP2) according to the protocol given by Wendl et al. (2014).

Here, we present a BC record from the already well-dated Lomonosovfonna ice core, drilled in Svalbard in 2009, which covers 800 years of climate history. We will discuss the evolution of the anthropogenic influence in the record, which overwhelms the natural BC background since 1800, as well as the detection of forest fire events, particularly during the pre-industrial times when the BC background was low. We will compare our results to other ice-core records in order to assess its representativeness and show that Svalbard is an interesting location which brings complementary information compared to Greenland. Lastly, as BC is not only emitted by forest fires, we will combine the BC record with other forest fire proxies measured in the same ice core (ammonium, vanillic acid, p-hydroxybenzoic acid) in order to disentangle the anthropogenic sources from the fire emissions and thus obtain a more detailed picture of the paleo fire activity.

REFERENCES

- Bond, T. C., Doherty, S. J., Fahey, D. W., Forster, P. M., Berntsen, T., DeAngelo, B. J., Flanner, M. G., Ghan, S., Kärcher, B., Koch, D., Kinne, S., Kondo, Y., Quinn, P. K., Sarofim, M. C., Schultz, M. G., Schulz, M., Venkataraman, C., Zhang, H., Zhang, S., Bellouin, N., Guttikunda, S. K., Hopke, P. K., Jacobson, M. Z., Kaiser, J. W., Klimont, Z., Lohmann, U., Schwarz, J. P., Shindell, D., Storelvmo, T., Warren, S. G. & Zender, C. S. 2013: Bounding the role of black carbon in the climate system: A scientific assessment. *Journal of Geophysical Research: Atmospheres*, 118, 5380-5552.
- Marlon, J. R., Bartlein, P. J., Carcaillet, C., Gavin, D. G., Harrison, S. P., Higuera, P. E., Joos, F., Power, M. J. & Prentice, I. C. 2008: Climate and human influences on global biomass burning over the past two millennia. *Nature Geoscience*, 1, 697-702.
- Moritz, M. A., Batllori, E., Bradstock, R. A., Gill, M., Handmer, J., Hessburg, P. F., Leonard, J., McCaffrey, S., Odion, D. C., Schoennagel, T. & Syphard, A. D. 2014: Learning to coexist with wildfires. *Nature*, 515, 58-66.
- Wendl, I. A., Menking, J. A., Färber, R., Gysel, M., Kaspari, S. D., Laborde, M. J. G. & Schwikowski, M. 2014: Optimized method for black carbon analysis in ice and snow using the Single Particle Soot Photometer. *Atmospheric Measurement Techniques*, 7, 2667-2681.

P 12.6

Stable water isotopes as climate tracers in the Laclavere Plateau, Antarctic Peninsula

Dieter Tetzner¹, Francisco Fernandoy², Hanno Meyer³

¹ Center for Climate and Resilience Research, University of Chile, Santiago, Av. Blanco Encalada 2002, 8370361, Chile (dtetzner@dgf.uchile.cl / dieter.tetz@gmail.com)

² Facultad de Ingeniería, Universidad Andrés Bello, Viña del Mar, 2531015, Chile

³ Foundation Alfred Wegener Institute for Polar and Marine Research in the Helmholtz Association, Research Unit Potsdam, Potsdam, Germany

A steady positive air-temperature trend has been observed for the last half century ($>0.20^{\circ}\text{C decade}^{-1}$) at several stations from the northern Antarctic Peninsula and central West Antarctica. In the last decades the western side of the Antarctic Peninsula has presented the highest temperature increase of the southern hemisphere. Recent publications describe that the present condition is unusual for natural variability but not unprecedented (Mulvaney et al. 2012). The lack of instrumental meteorological records in this region has hindered the study of regional climatic trends. In this context the study of ice cores has become a powerful source of information because they contain records of greater temporal extension and from areas where meteorological information hasn't been retrieved. Ice cores from high-accumulation regions can significantly contribute to understand the undergoing climate variability and expand short meteorological time-series to the past.

Laclavere Plateau ($63^{\circ}27'15''\text{S} / 57^{\circ}41'53''\text{W} / 1130 \text{ m.a.s.l.}$) is situated in the northern tip of the Antarctic Peninsula and is the northern area in the Peninsula which has a height above 1000 m.a.s.l. The climatological regime in the north of the Peninsula presents a complex interaction between the different elements that form the climatic system. Meteorological conditions in this area are strongly controlled by the variation in the sea ice extension, the position of the Antarctic Circumpolar Current and the differences in the lapse rate throughout the year.

The air parcels that precipitate over the Laclavere Plateau are strongly related with the conditions that prevail on the Southern Seas at the west of the Antarctic Peninsula and in particular with the conditions present near coastal areas of the Bellingshausen Sea. Since 2008, we have studied the northern part of the Antarctic Peninsula, where several surface firn cores ($<20\text{m}$ depth) have been collected from sea level to the divide between west and east coast at the Plateau Laclavere (Fernandoy et al. 2012). The isotope signature of the cores shows a complicated signal to interpret. No clear seasonality is observed from $\delta^{18}\text{O}$ (δD). Here we show the statistical treatment that allow us to conclude that the deuterium excess ($\text{dexcess} = \delta\text{D} - 8 \delta^{18}\text{O}$), oxygen and deuterium ratios can be potentially used as a seasonal marker. We propose that variations observed in the stable isotope signal and in meteorological conditions are related with the development of an inversion layer in the lower troposphere (below 1000 m.a.s.l.) during the winter because of the formation of sea ice in the western coast of the Peninsula (Figure 1).

We estimate that the Laclavere Plateau present appropriate conditions for the conservation of the isotopic signal recorded in the snow that accumulates on its surface (mean value of $1,700 \text{ kg m}^{-2} \text{ a}^{-1}$). Therefore, we conclude that isotopic signal recovered from Laclavere's Plateau ice show that ice is a strong indicator of actual meteorological parameters, which make them capable of being proxy of local variability in atmospheric circulation, snow accumulation and temperatures above surface. The well preserved isotope signal, along with the thick ice cover over the Laclavere Plateau (surveyed by geophysical methods), project this place as a favorable spot to recover a medium depth ice core ($>250\text{m}$), from which it could be developed a paleoclimatic reconstruction covering at least half century at a high temporal resolution.

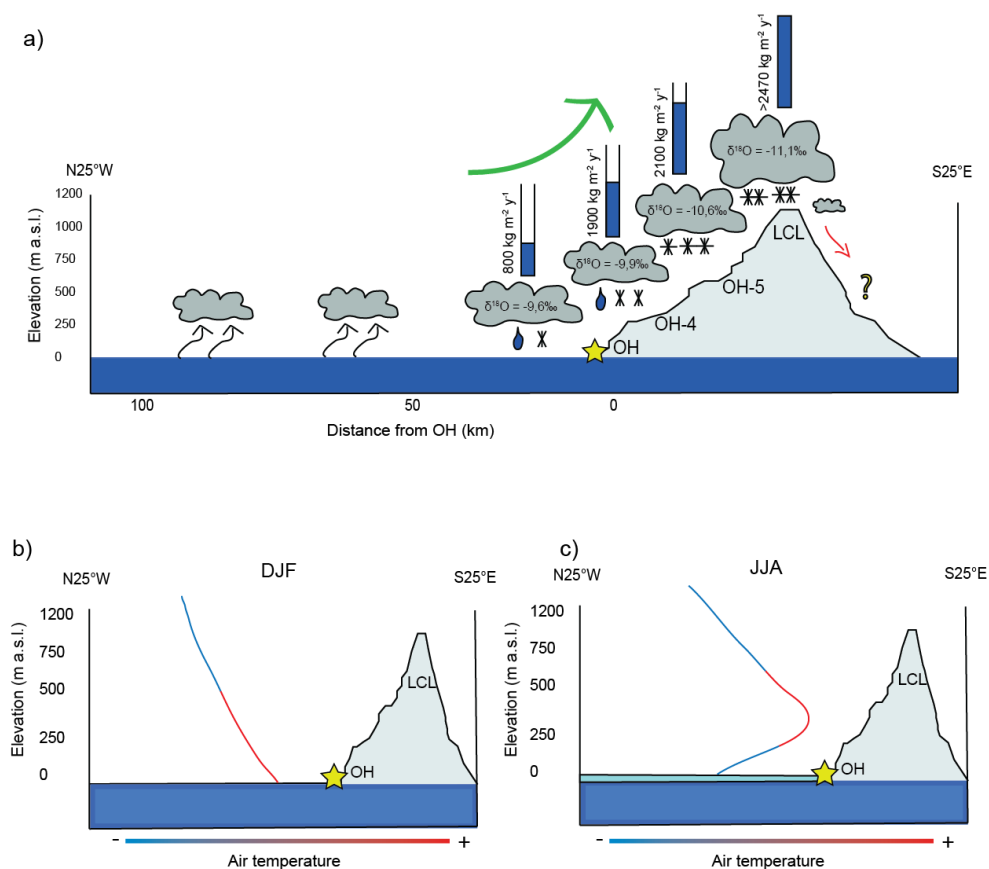


Figure 1. (a) Proposed orographic trap effect of the AP over the stable water isotope depletion and accumulation at different altitudes, (b) normal temperature gradient (adiabatic cooling) during summer season with sea ice free condition, (c) low tropospheric inversion layer proposed during sea ice covered condition in winter. OH= O'Higgins Station.

REFERENCES

- Fernandoy, F., H. Meyer, and M. Tonelli (2012), Stable water isotopes of precipitation and firn cores from the northern Antarctic Peninsula region as a proxy for climate reconstruction, *The Cryosphere*, 6(2), 313-330.
- Mulvaney, R., N. J. Abram, R. C. A. Hindmarsh, C. Arrowsmith, L. Fleet, J. Triest, L. C. Sime, O. Alemany, and S. Foord (2012), Recent Antarctic Peninsula warming relative to Holocene climate and ice-shelf history, *Nature*, 489(7414), 141-144.

P 12.7

From snow cover mapping to glacier-wide mass balance on Central Asian glaciers

Martina Barandun ¹, Matthias Huss ^{1,2}, Ryskul Usabaliev ³, Tobias Bolch ^{4,5}, Martin Hoelzle ¹

¹ Department of Geoscience, University of Fribourg, Fribourg, Switzerland (martina.barandun@unifr.ch),

² Laboratory of Hydraulics, Hydrology and Glaciology (VAW), ETH Zurich, Zurich, Switzerland,

³ Central Asian Institute of Applied Geosciences (CAIAG), Bishkek, Kyrgyzstan,

⁴ Department of Geography, University of Zurich, 8057 Zurich, Switzerland,

⁵ Institute for Cartography, Technische Universität Dresden, 01069 Dresden, Germany

A complete and representative coverage of glacier monitoring sites is necessary to enhance the understanding of regional to global response of glaciers to climate change. Accessibility and the lack of resources, however, are limiting such actions, especially in politically and economically unstable countries. Today, glacier mass balance monitoring in Central Asia is underrepresented in one of the most glacierized mountain areas in the world (Sorg and others, 2012).

In this study, a novel approach to calculate sub-seasonal mass balance based on remote snowline monitoring developed after Huss and others (2013) is applied and enhanced for selected glaciers in Central Asia (Abramov, Golubin, Batysh Sook Glacier and Glacier No. 354) from 2003 to 2015. Thereby, temporal changes of the snow cover during the ablation season are related to the winter accumulation through backwards modelling.

In a second step, a rating curve is derived to link the Snow Covered Area Fraction (SCAF) to the glacier-wide transient mass balance (Figure 1). Consequentially, the mass balance can be directly derived from the SCAF observations and thus does not depend on glaciological measurements. Snowline observation is performed remotely either on satellite (here Landsat and Terra ASTER) or camera images (Mobotix).

The approach is applied to four glaciers with direct mass balance measurements from 2011 to 2015 and with longer-term reconstructed mass balance series. Re-analysed mass balance series are used for calibration. Furthermore, the derived glacier-wide mass balance is validated with geodetic mass balances for the first decade of the 21st century. A minimum of three images is necessary to achieve reliable results and results become more robust with increased image frequency and regular distribution over the summer months.

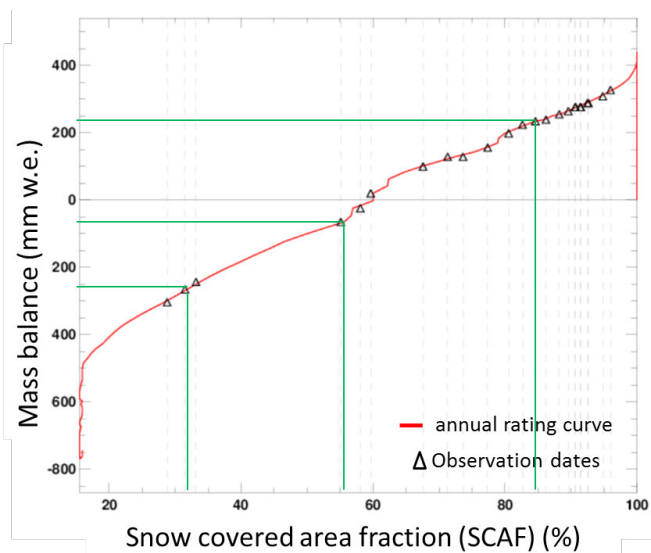


Figure 1. Relation between snow covered area fraction (SCAF) and mass balance depending on glacier geometry for Abramov Glacier (Pamir-Alay, Kyrgyzstan) in 2012. Sub-seasonal mass balance can be calculated for each observation date.

REFERENCES

- Huss, M., Sold, L., Hoelzle, M., Stokvis, M., Salzmann, N., Farinotti, D., Zemp, M., (2013) Towards remote monitoring of sub seasonal glacier mass balance. *Annals of Glaciology*, 54(63), 75-83.
- Sorg, A., Bolch, T., Stoel, M., Solomina, O., Beniston, M. (2012) Climate change impacts on glaciers and runoff in Tien Shan (Central Asia). *Nature Climate Change*, 2(10), 725-731.

P 12.8

A complete glacier inventory of the Antarctic Peninsula based on Landsat7 data from 2000–2002 and other pre-existing datasets

Jacqueline Huber¹, Michael Zemp¹, Frank Paul¹, Alison J. Cook²

¹ Department of Geography, University of Zurich–Irchel, Winterthurerstrasse 190, CH–8057 Zurich (jhuber@access.uzh.ch)

² Department of Geography, Swansea University, Singleton Park, Swansea SA2 8PP, Wales, UK

The glaciers on the Antarctic Peninsula (AP) potentially make a large contribution to sea level rise. However, this contribution was difficult to estimate, as no complete glacier inventory (outlines, attributes, separation from the ice sheet) was available so far. This work fills the gap and presents a new glacier inventory of the AP north of 70° S based on digitally combining pre-existing datasets with GIS techniques. Rock outcrops are removed from the glacier basin outlines of Cook et al. (2014) by digital intersection with the latest layer of the Antarctic Digital Database (Burton-Johnson et al., 2016). Glacier-specific topographic parameters (e.g. mean elevation, slope and aspect) as well as hypsometry have been calculated from the DEM of Cook et al. (2012). We also assigned connectivity levels to all glaciers following the concept by Rastner et al. (2012). Moreover, the bedrock dataset of Huss & Farinotti (2014) enabled us to add ice thickness and volume for each glacier.

The new inventory is available from the GLIMS database and consists of 1589 glaciers covering an area of 95 273 km², slightly more than the 90 000 km² covered by glaciers surrounding the Greenland Ice Sheet. The total ice volume is 34 590 km³ of which 1/3 is below sea level. The hypsometric curve has a bimodal shape due to the special topography of the AP consisting mainly of ice caps with outlet glaciers. Most of the glacierized area is located at 200–500 m a.s.l. with a secondary maximum at 1500–1900 m. About 63% of the area is drained by marine-terminating glaciers and ice shelf tributary glaciers cover 35% of the area. This combination results in a high sensitivity of the glaciers to climate change for several reasons: (1) only slightly rising equilibrium line altitudes would expose huge additional areas to ablation, (2) rising ocean temperatures increase melting of marine terminating glaciers, and (3) ice shelves have a buttressing effect on their feeding glaciers and their collapse would alter glacier dynamics and strongly enhance ice loss (Rott et al., 2011). The new inventory should facilitate modelling of the related effects using approaches tailored to glaciers for a more accurate determination of their future evolution and contribution to sea level rise.

REFERENCES

- Burton-Johnson, A., Black, M., Fretwell, P. T., and Kaluza-Gilbert, J. 2016: An automated methodology for differentiating rock from snow, clouds and sea in Antarctica from Landsat 8 imagery: A new rock outcrop map and area estimation for the entire Antarctic continent, *The Cryosphere*, 10, 1665–1677, doi:10.5194/tc-10-1665-2016.
- Cook, A. J., Murray, T., Luckman, A., Vaughan, D. G., and Barrand, N. E. 2012: A new 100-m Digital Elevation Model of the Antarctic Peninsula derived from ASTER Global DEM: methods and accuracy assessment, *Earth Syst. Sci. Data*, 4, 129–142, doi:10.5194/essd-4-129-2012.
- Cook, A. J., Vaughan, D. G., Luckman, A. J., and Murray, T. 2014: A new Antarctic Peninsula glacier basin inventory and observed area changes since the 1940s, *Antarctic Science*, 26, 614–624, doi:10.1017/S0954102014000200.
- Huss, M. and Farinotti, D. 2014: A high-resolution bedrock map for the Antarctic Peninsula, *The Cryosphere*, 8, 1261–1273, doi:10.5194/tc-8-1261-2014.
- Rastner, P., Bolch, T., Mölg, N., Machguth, H., Le Bris, R., and Paul, F. 2012: The first complete inventory of the local \ newline glaciers and ice caps on Greenland, *The Cryosphere*, 6, 1483–1495, doi:10.5194/tc-6-1483-2012.
- Rott, H., Müller, F., Nagler, T., and Floricioiu, D. 2011: The imbalance of glaciers after disintegration of Larsen-B ice shelf, Antarctic Peninsula, *The Cryosphere*, 5, 125–134, doi:10.5194/tc-5-125-2011.

P 12.9**Negative geodetic glacier mass balances in the Ak-Shirak range (Kyrgyzstan) between 1960s and 70s derived from Corona and Hexagon reconnaissance imagery**

Franz Goerlich², now at¹, Tobias Bolch^{1,2}, Kriti Mukherjee², Tino Pieczonka²

¹ *Geographisches Institut, University of Zurich, Winterthurerstrasse 190, CH-8057 Zürich (franz.goerlich@geo.uzh.ch)*

² *Institut für Kartographie, University of Dresden, Helmholtzstrasse 10, D-01069 Dresden*

Glacier shrinkage is a well-known phenomenon in most parts of the world and in the central Tian Shan, respectively. The resulting meltwater of Tian Shan glaciers plays a significant role for the central Asian population and a continuing glacier retreat could endanger the future water supply. With a better understanding of glacier dynamics and glacier hydrology the potential threat could be reduced.

For this purpose former research have been estimated geodetic mass balances of glaciers in High Asia for several periods starting in the 1960s using Corona reconnaissance satellite imagery on small areas (e.g. individual glaciers) or in the 1970s based on Hexagon imagery on a larger scale. Due to a particular camera model and complex distortion effects the analysis of especially complete Corona images is a challenging task.

We present a workflow to generate digital terrain models (DTMs) and orthophotos from Corona and Hexagon data including the these camera models to estimate large-scale glacier dynamics. We calculated mass balances and length changes of glaciers for an entire mountain range (Ak-Shirak) located in the central Tian Shan between 1964 (Corona), 1973 and 1980 (both Hexagon). We found negative mass balances up to -0.6 ± 0.1 m w.e.a⁻¹ and -1.1 ± 0.2 m w.e.a⁻¹ for the whole region and individual glaciers, respectively. The future work will focus on automatization approaches to analyse region-wide Corona data which would allow the interpretation of glacier dynamics in a larger context.

P 12.10**A worldwide glacier information system to go**

Nico Mölg¹, Martin Steinmann¹, Michael Zemp¹

¹ *Department of Geography, University of Zurich, Switzerland*

In the forefront of the Paris Climate Conference COP21 in December 2015, the WGMS and UNESCO jointly launched a glacier application for mobile devices. This new information system aims at bringing scientifically sound facts and figures on worldwide glacier changes to decision makers at governmental and intergovernmental levels as well as reaching out to the interested public.

The wgms Glacier App provides a map interface based on satellite images that display all the observed glaciers in the user's proximity. Basic information is provided for each glacier, including photographs and general information on size and elevation. Graphs with observation data illustrate the glacier's development, along with information on latest principal investigators and their sponsoring agencies as well as detailed explanations of the measurement types. A text search allows the user to filter the glacier by name, country, region, measurement type and the current "health" status, i.e. if the glacier has gained or lost ice over the past decade. A compass shows the closest observed glaciers in all directions from the user's current position. Finally, the card game allows the user to compete against the computer on the best monitored glaciers in the world.

Our poster provides a visual entrance point to the wgms Glacier App and, hence, provides access to fluctuation series of more than 3'700 glaciers around the world.

P 12.11

Traditional photogrammetry versus modern structure-from-motion: using aerial images to derive surface elevation changes of a debris covered Alpine glacier tongue

Nico Mölg¹, Tobias Bolch^{1,2}, Andreas Vieli¹

¹ *Department of Geography, University of Zurich, Switzerland*

² *Institute of Cartography, Technische Universität Dresden, Germany*

The debris covered glacier surface is increasing also in the Alps. It is unclear in which way an extensive debris layer influences the long-term mass change, surface characteristics and ice flow dynamics of a glacier and documentations of such a development are rare. The archive of aerial images in the Swiss Alps dates back to 1946 and contains a large number of photographs due to a regularly high observation frequency, which can be used to produce multi-temporal digital elevation models to document the glacier surface changes with time.

We have investigated the possibilities of the increasingly popular structure-from-motion technique and compared its performance to results from classical stereo photogrammetry using the same aerial images and ground control points as input. The advantages of structure-from-motion are on the one hand a simple workflow process that requires less theoretical background by the analyst and on the other hand, the capacity to handle large quantities of input data with little meta information like the position or exterior orientation information of the camera.

Results show that both techniques produce comparably homogeneous and robust results even from images with partly low quality (e.g. due to storing or scanning). The location accuracy is mostly within 5 metres and also the vertical accuracy is on average below 10 metres. With fewer input images the structure-from-motion results become noisier on water surfaces and in very steep terrain. Nevertheless, structure-from-motion is a powerful alternative to traditional photogrammetry, especially under circumstances of unknown and oblique camera positions and large quantities of input data. With both techniques we were able to retrieve a 70-year trend in surface elevation and detect surface characteristics of a debris covered glacier tongue.

P 12.12

Ice-elevation changes derived by high resolution airborne and terrestrial laser scanning data of a high Andean glacier

Sebastián Vivero^{1,2}, Shelley MacDonell² & Sebastian H. Mernild^{3,4}

¹ *Institut des dynamiques de la surface terrestre (IDYST), Université de Lausanne, Bâtiment Géopolis UNIL Mouline, CH-1015 Lausanne (sebastian.viveroandrade@unil.ch)*

² *Centro de Estudios Avanzados en Zonas Áridas (CEAZA), La Serena, Chile*

³ *Universidad de Magallanes, Punta Arenas, Chile*

⁴ *Faculty of Engineering and Science, Sogn og Fjordane University College, Sogndal, Norway*

Glaciers located in central Chile have experienced significant retreat during recent decades, mainly as a response to an elevation increase of the 0°C isotherm. Whilst most studies have only investigated frontal and areal changes, there are no detailed studies regarding elevation changes or volume losses. This gap of information restricts not only the evaluation of freshwater resource availability in the region, but also has limited the environmental assessment of glaciers located close to mining activities. This study aims to evaluate ice-elevation changes over a one-year (April 2015 to March 2016) period from 3D data collected by terrestrial and aerial laser scanning campaigns performed on Olivares Gamma glacier (33°S). Laser scanning data were processed to generate two Digital Elevation Models (DEMs) of high spatial resolution (2 m) and accuracy (better than 0.2 m). Comparisons of the two DEMs revealed widespread negative elevation changes, up to -12 m, associated with the development of an ice cliff in the lower glacier area. Averaged elevation change values close to zero are localized on the middle glacier area. In this area, field observations indicated a slightly positive mass balance of the glacier. Significant off glacier elevation changes on the west bounding moraine ridge are identified as mass movement related to either massive glacier down wasting or earthquake induced slope failure. Additionally, terrestrial and aerial scans were able to record small scale features such as penitents and crevasses, which are not normally captured by medium to coarse resolution datasets. This study shows that the combination of laser scanner and field measurements provides a good approach to study current glacier changes.

P 12.13

Swiss Glacier Inventory 3D, a product of the Swiss topographical landscape model

Yvo Weidmann^{1,5}, Matthias Huss^{1,2}, Mauro Fischer^{2,3}, Emanuel Schmassmann⁴

¹ *Laboratory of Hydraulics, Hydrology and Glaciology (VAW), ETH Zurich, Hönggerberggring 26, CH-8093 Zurich*

² *University of Fribourg, Unit of Geography, Chemin du Musée 4, 1700 Fribourg*

³ *World Glacier Monitoring Service, Department of Geography, University of Zurich, Winterthurerstrasse 190, CH-8057 Zurich*

⁴ *Federal Office of Topography swisstopo, Seftigenstrasse 264, CH-3084 Wabern*

⁵ *Geoldee Geoinformatik, Postfach 1209, CH-8038 Zurich*

The Federal Office of Topography swisstopo implements the country-wide vector-based Topographical Landscape Model (TLM) as base for the topographical maps of Switzerland in the scales larger than 1:10 000. The whole territory of Switzerland will be recorded by the year 2020. The different topics of the landscape model (land cover, roads, buildings, hydrography, ...) are entirely digitized as 3D geometries using stereo imagery in natural colours and the near-infrared channel. The recorded geometries are checked and updated if needed on a 4 to 6-year basis. With the migration of the former cartographical data model VECTOR25 towards the TLM, the subtypes *glacier* and *unconsolidated rock* are an import and reliable data source for glaciological studies.

The three main Swiss Glacier Inventories (SGI) 1850, 1973 and 2010 (Maisch et al., 2000; Fischer et al., 2010) are based on 2D reconstructions of the glacier outlines derived from historical maps, field surveys and aerial orthoimages. The demanding task of recording the outlines of all Swiss glaciers was a major obstacle for having a higher temporal resolution of inventories.

Within the framework of the GLAcier MONitoring Switzerland (GLAMOS) the feasibility of using the data of TLM as a continuous and highly reliable data source for future inventories was analysed. The analysis determined the differences between geometries of the former SGI and the TLM, the data structure of the TLM, the possible workflow, the temporal data coverage and reliability and much more. Based on the needs of GLAMOS, the requirements for the recording of glacier geometries within the TLM were formulated.

By 2016 / 2017 the requirements of GLAMOS are implemented by swisstopo. With the completion of the first edition of the TLM by 2020 a new Swiss Glacier Inventory entirely in 3D will be published (SGI2020^{3D}). With the constant update of the TLM during the next decades, a continuous glacier inventory will be available which is expected to offer a highly valuable basis for glaciological, hydrological geomorphological analyses in the Swiss Alps. Due to the integration of the workflow at the Federal Office of Topography a long-term continuance and quality is guaranteed.

REFERENCES

- Fischer, M., Huss, M., Barboux, C. & Hoelzle, M. (2014). The new Swiss Glacier Inventory SGI2010: Relevance of using high-resolution source data in areas dominated by very small glaciers *Arctic, Antarctic and Alpine Research*, 46(4), 933-945.
- Maisch, M., Wipf, A., Denneler, B., Battaglia, J., & Benz, C. (2000). Die Gletscher der Schweizer Alpen: Gletscherhochstand 1850, aktuelle Vergletscherung. *Gletscherschwund-Szenarien*, vdf Hochschulverlag AG an der ETH Zürich, Zürich.

P 12.14

Modelling the last glacial cycle in the Alps

Julien Seguinot¹, Guillaume Jouvét¹, Matthias Huss¹, Martin Funk¹

¹ Laboratory of Hydraulics, Hydrology and Glaciology, ETH Zürich, Switzerland (seguinot@vaw.baug.ethz.ch)

The European Alps, cradle of pioneer glacial studies, are one of the regions where geological markers of past glaciations are most abundant and well-studied. Such conditions make the region ideal for testing numerical glacier models based on approximated ice flow physics against field-based reconstructions, and vice-versa.

Here, we use the Parallel Ice Sheet Model (PISM) to model the entire last glacial cycle (120–0 ka) in the Alps, with a horizontal resolution of 1 km. Climate forcing is derived using present-day climate data from WorldClim, the ERA-Interim reanalysis, and time-dependent temperature offsets from the EPICA ice core record in Antarctica, which allows reproduce the two major glaciation events documented in the geological record during marine oxygen isotope stages 4 (69–62 ka) and 2 (34–18 ka).

Despite the low variability of this Antarctic-based climate forcing, our simulation depict a highly dynamic ice cap, showing that alpine glaciers may have advanced many times over the foreland during MIS 5 and 3. Cumulative basal sliding, a proxy for glacial erosion, is modelled to be highest in the deep valleys of the western Alps. However, relict uplift rates at the end of the simulation are most important in the eastern Alps where a thick ice cover persists for most of the modelled glacial cycle. Finally, the Last Glacial Maximum advance, often considered synchronous, is here modelled as a time-transgressive event, with some glacier lobes reaching their maximum as early as 27 ka, and some as late as 21 ka, which may explain some of the variability in published cosmogenic dates.

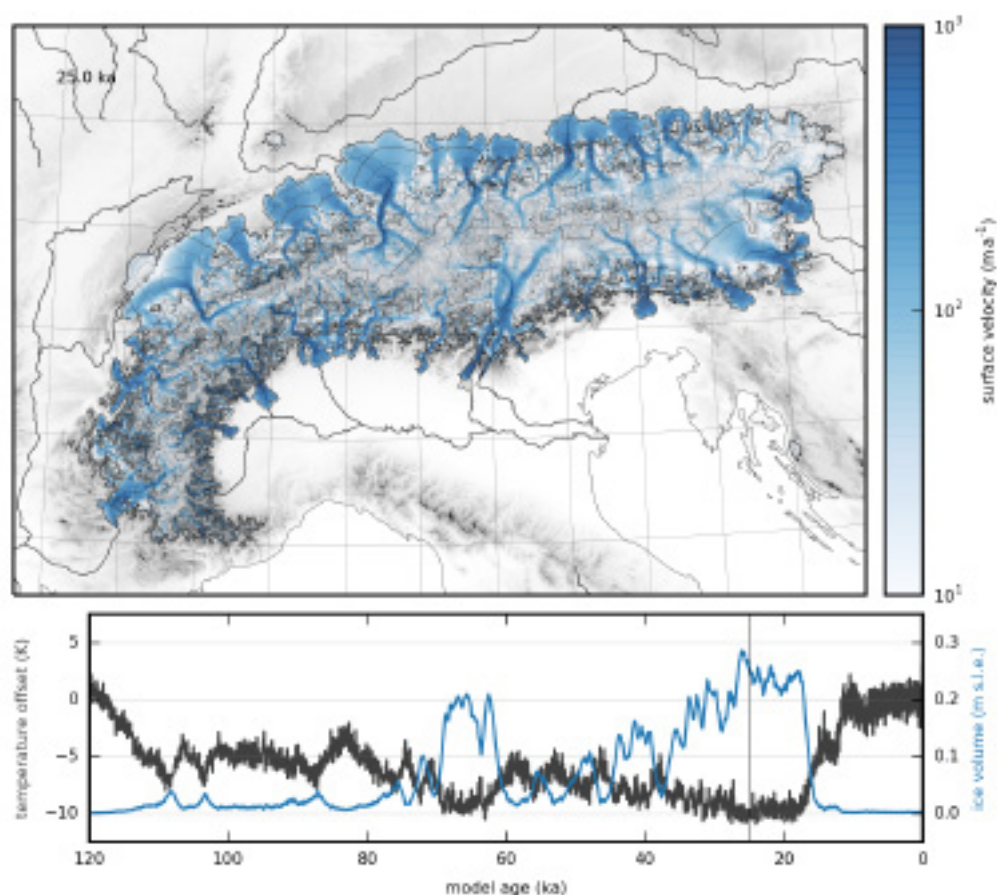


Figure 1. Modelled ice surface elevation (top panel, 200 m contours) and ice surface velocity (top panel, colour mapping) at 25 ka. Time-dependant input temperature offsets (bottom panel, black curve) and modelled sea-level equivalent ice volume (bottom panel, blue curve).

P 12.15

Modeling glaciers and permafrost in connection with radioactive waste repositories in northern Switzerland

Denis Cohen¹, Thomas Zwinger², Urs H. Fischer³, Wilfried Haeberli⁴

¹ Department of Geological and Atmospheric Sciences, Iowa State University Ames, USA

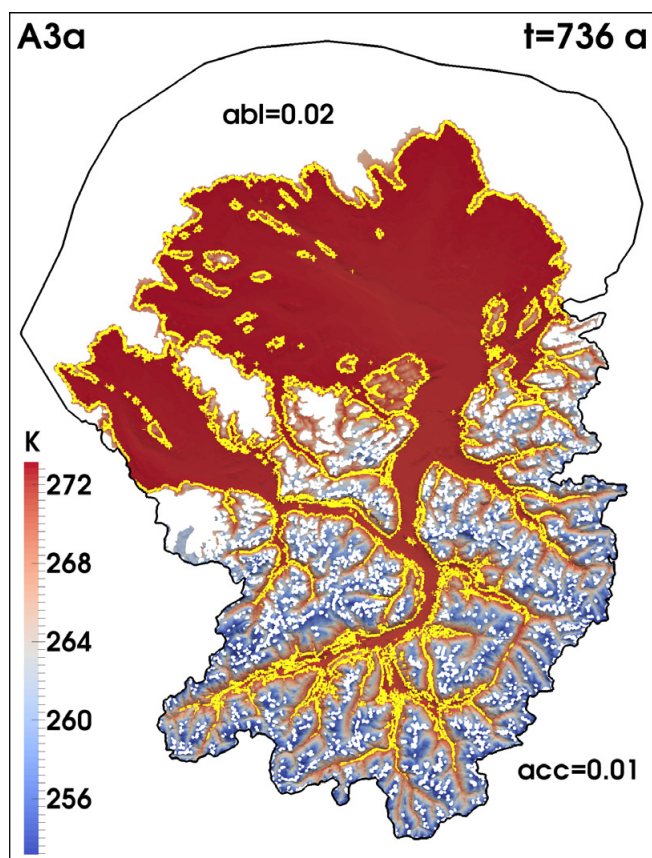
² CSC - IT Center for Science Ltd., Espoo, Finland

³ National Cooperative for the Disposal of Radioactive Waste, Nagra, Wettingen, Switzerland

⁴ Geography Department, University of Zurich, Switzerland (wilfried.haeberli@geo.uzh.ch)

The long-term management of radioactive waste produced through the use of radioactive materials in power production, industry, research and medicine entails its containment and isolation within deep geological repositories over hundreds of thousands of years. Over such extended time periods, the performance of repositories in mid- and high-latitude regions can be affected by impacts from future ice-age conditions (Fischer et al. 2014). During the LGM, central Europe experienced extremely cold and dry conditions. At this stage, flat and extended lobes of large piedmont glaciers spreading out over much of the Swiss Plateau were poly-thermal, characterized by low driving stresses (typically around 30 kPa) and surrounded by continuous periglacial permafrost (Haeberli et al. 1984) up to 150 m thick. Subsurface temperatures and groundwater flow conditions were strongly influenced by the presence of extended surface and subsurface ice. Glacial erosion in the ice-marginal zones with cold ice frozen to subglacial permafrost was probably limited due to strongly reduced basal sliding and melt-water flow. More humid conditions with higher flow velocities, increased basal sliding and stronger erosion by abrasion and melt-water effects must have prevailed during ice advance across the Swiss Plateau. Rapid down-wasting or even collapse (calving instability in lakes) is likely to have taken place during the retreat phase back into the Alpine valleys. It appears plausible to assume that similar cycles were characteristic for past ice ages in general and could also be characteristic for future ice-age conditions in northern Switzerland.

Numerical simulations of the flow of the Rhine glacier at the LGM (Figure 1) were carried out using Elmer, a finite element numerical model that solves the coupled three-dimensional heat, mass, and momentum equations for Stokes flow.



The model is initialized using the reconstructed ice geometry. After adjusting this glacier geometry in order to eliminate unphysical velocity fields resulting from reconstruction artefacts a best fit with the geomorphological reconstructions (extent) was obtained with extremely low mass balance gradients (Cohen et al. 2015). This result supports that climatic conditions of a cold desert must have existed during the LGM. Nevertheless, while the ice margins are cold and frozen to sub-glacial permafrost large parts of the modeled piedmont ice lobe are warm-based. Because the proposed sites for the radioactive waste repositories are located in the marginal zones of ice-age glaciations, the involved glacier-permafrost interactions and their influence on deep groundwater hydrology must be considered. One key aspect thereby is the question whether permafrost is already in place when the ice margin advances over it. Such a development could lead to complex transient conditions of inverse heat flow from glacier parts near melting conditions into still frozen ground. In addition, the cold ice margin with subglacial permafrost represents an important hydraulic barrier to groundwater flow and may cause elevated water pressure in the transition zone from warm- to cold-based ice. This elevated water pressure increases basal sliding and, hence, erosion further up-flow beneath warm-based parts of the glacier.

Figure 1: Modelled basal temperature of the Rhine glacier at the LGM. The yellow line outlines extent of temperate ice. Mass balance gradients used for the model run are 0.02m per 100m and year in the ablation area and 0.01m per 100m and year in the accumulation area.

REFERENCES

- Fischer, U.H., Bebiolka, A., Brandefelt, J., Follin, S., Hirschorn, S., Jensen, M., Keller, S., Kennel, I. L., Näslund, J.-O., Normani, S., Selroos, J.-O. & Vidstrand, R. 2014: Radioactive waste under conditions of future ice ages. In: Haeberli, W., Whiteman, C. (Eds): *Snow and Ice-Related Hazards, Risks and Disasters*; Elsevier, 345-393.
- Cohen, D., Haeberli, W., Fischer, U.H. & Machguth, H. 2015: Mass balance reconstruction for the Rhine glacier, Swiss Alps, at the Last Glacial Maximum from three-dimensional thermo-mechanical modeling. *Geophysical Research Abstracts* 17, EGU General Assembly 2015 .
- Haeberli, W., Rellstab, W. & Harrison, W.D. 1984: Geothermal effects of 18ka BP ice conditions in the Swiss Plateau. *Annals of Gaciology* 5, 56-60.

P 12.16

Modeling the ice flow in the Upper Valais at the Last Glacial Maximum

Patrick Becker¹, Martin Funk¹

¹ *Versuchsanstalt für Wasserbau, Hydrologie und Glaziologie (VAW), ETH Zürich, Hönggerbergstrasse 26, CH-8093 Zürich (becker@vaw.baug.ethz.ch)*

During the Last Glacial Maximum (LGM), glaciers in the Alps reached a maximum ice extent and broad sections of the foreland were covered by ice. A recent study by Becker et al. (2016) successfully simulated the lateral LGM ice cap extent using a glacier flow model to constrain the prevailing precipitation pattern with a geomorphological reconstruction of ice extent. The study demonstrates, that for a reproduction of the LGM ice cap, a more severe decrease in precipitation in the north than in the south is required. This result supports previous studies indicating a southwesterly advection of atmospheric moisture to the Alps, by a southward shift of the North Atlantic storm track during the LGM. However, the study revealed a significant overestimate in the modeled thickness of the ice thickness in the Upper Rhone valley compared to the geomorphologically based mappings by Bini et al. (2009).

We will present a detailed study, modeling this area using the Parallel Ice Sheet Model (PISM). The modeled ice thickness will be discussed as well as opportunities to narrow the gap between the modeled ice thickness and the geomorphological mappings. Also we study the relation of ice thickness, the local glacier flow field, ice surface morphology.

We find a modeled ice coverage at the Upper Rhone Valley that builds up an ice divide between the Bernese and the Valais ice domes near Brig at LGM. Thus, the drainage system of the Rhone glacier is separated into two regions. The glacier downstream of Brig drains into the direction of Lake Geneva, following the relief of the mountain ranges, according to present days river. In contrast, the glacier upstream of Brig transfluences over the Simplonpass and adjacent passes to the south. This means, that ice of the Upper Rhone Valley is forced out of the Rhone drainage basin into the drainage system of the Toce in the Piedmont region in Italy. Our findings agree well with the striations found at the top of the Simplonpass, interpreted as north-south transfluence by Kelly et al. (2004).

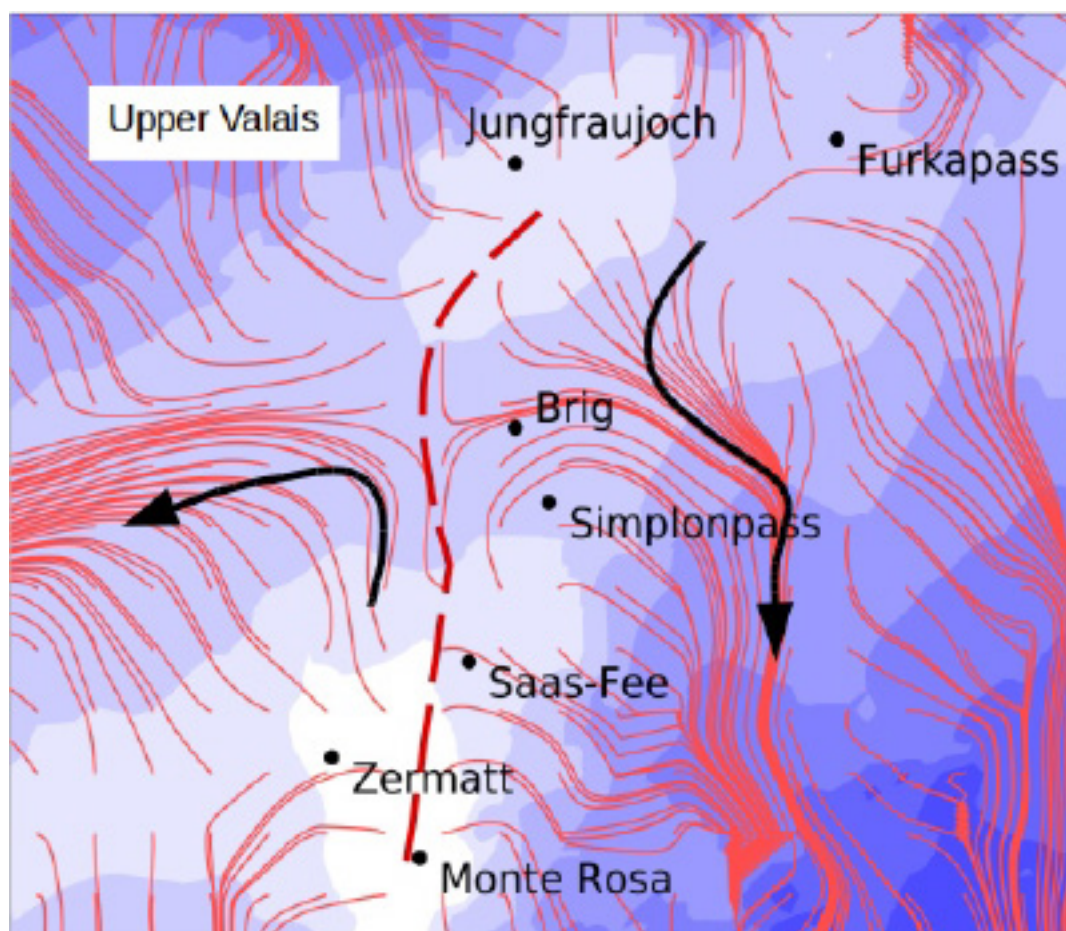


Figure 1. Modeled ice surface topography at the LGM (solid red lines = glacier flow field, red dashed line = resulting ice divide, blue shadings in the background = ice surface elevation).

REFERENCES

- Becker, P., Seguinot, J., Juvet, G. & Funk M. 2016: Last Glacial Maximum precipitation pattern in the Alps inferred from glacier modelling. *Geogr. Helv.*, 71, 173–187.
- Bini, A., Buoncristiani, J.-F., Coutterand, S., Ellwanger D., Felber, M., Florineth, D., Graf, H. R., Keller, O., Kelly M., Schlüchter, C. & Schoeneich, P. 2009: Die Schweiz während des letzteiszeitlichen Maximums (LGM)
- Kelly, J., Buoncristiani, C. & Schlüchter C. 2004: A reconstruction of the last glacial maximum (LGM) ice surface geometry in the western {S}wiss {A}lps and contiguous Alpine regions in Italy and France, *Eclogae geol. Helv.*, 97, 57-75.

P 12.17

Bayesian inference of ice thickness

Mauro A. Werder¹, Matthias Huss^{1/2}

¹ *Versuchsanstalt für Wasserbau, Hydrologie und Glaziologie (VAW), ETH Zürich, 8093 Zürich (werder@vaw.baug.ethz.ch)*

² *Unit of Geography, Université de Fribourg, 1700 Fribourg*

Knowledge about ice thickness and volume is indispensable for studying ice dynamics, future sea-level rise due to glacier melt or their contribution to regional hydrology. Accurate measurements of glacier thickness require on-site work, usually employing radar techniques. However, these field measurements are time consuming, expensive and sometime downright impossible. Conversely, measurements of the ice surface, namely elevation and flow velocity, are becoming available world-wide through remote sensing.

The model of Farinotti et al. (2009) calculates ice thicknesses based on a mass conservation approach using estimates of the surface mass balance. The presented work applies a Bayesian inference approach to estimate the parameters of a modified version of this forward model by fitting it to both measurements of surface flow speed and of ice thickness. The inverse model outputs ice thickness as well the distribution of the error. We fit the model to ten test glaciers and ice caps and quantify the improvements of thickness estimates through the usage of surface ice flow measurements.

REFERENCES

Farinotti, D., Huss, M., Bauder, A., Funk, M., and Truffer, M. (2009). A method to estimate the ice volume and ice-thickness distribution of alpine glaciers. *Journal of Glaciology*, 55(191):422-430.

P 12.18**Demystifying the end of the Little Ice Age: first tests simulating the Rhône Glacier with Úa**Simon Förster¹, Matthias Huss¹, Hilmar Gudmundsson²¹ *Laboratory of Hydraulics, Hydrology and Glaciology (VAW), ETH Zürich, Hönggerberggring 26, CH-8093 Zürich (foerster@vaw.baug.ethz.ch)*² *British Antarctic Survey, High Cross, Madingley Rd., Cambridge, CB3 0ET, UK*

At the end of the Little Ice Age (around 1850), glaciers in the Alps reached their last maximum extent. However, it is still uncertain what caused the preceding advance and the following retreat. Several studies have concluded that temperature alone cannot explain this behaviour (e.g. Nesje & Dahl 2003). Vincent et al. (2005) found that a precipitation increase of about 25% could explain the anomaly, but this is not supported by observations. Further processes have been proposed, including changes in solar radiation (due to either solar activity variations or aerosols in the atmosphere), surface impurities on ice and snow, and dynamical effects in both the atmosphere and the glaciers. We want to test some of these processes in a model study and determine their relative importance by coupling the ice flow model Úa (Gudmundsson et al. 2012) to a mass balance model.

In a first step, we are assessing the performance of Úa, which has previously been used primarily for simulations of the Greenland and Antarctic ice sheets, in the Alpine environment in the period for which observational data is available, i.e. from the late 19th century until now. The Rhône Glacier has particularly long data series of length change, surface mass balance, ice flow speed, and geometry change, and is thus used for these initial tests. We simulate the advance and retreat of the Rhône Glacier around the Little Ice Age maximum with Úa, investigate how it reacts to changes in mass balance and model parameters, and compare the results with observations.

REFERENCES

Gudmundsson, G. H., Krug, J., Durand, G., Favier, L., & Gagliardini, O. 2012: The stability of grounding lines on retrograde slopes. *The Cryosphere*, 6, 1497-1505. doi:10.5194/tc-6-1497-2012.Nesje, A. & Dahl, S. O. 2003: The «Little Ice Age» - Only temperature? *The Holocene*, 13, 139-145. doi:10.1191/0959683603hl603fa.Vincent, C., Le Meur, E., Six, D. & Funk, M. 2005: Solving the paradox of the end of the Little Ice Age in the Alps. *Geophysical Research Letters*, 32. doi:10.1029/2005GL022552.**P 12.19****A new ring-shaped wind tunnel facility to study wind-packing of snow**Christian G. Sommer^{1,2}, Michael Lehning ^{1,2} & Charles Fierz¹¹ *WSL Institute for Snow and Avalanche Research SLF, Davos, Switzerland (sommer@slf.ch)*² *CRYOS, School of Architecture, Civil and Environmental Engineering, EPFL, Lausanne, Switzerland*

A new wind tunnel was designed and built at SLF. The facility is ring-shaped to simulate an infinite fetch. This is important for experiments where the observed processes have a slow time scale (minutes to hours). The wind tunnel was developed to study the formation of wind-packed snow. Wind-packing is the process whereby wind hardens the snow and forms crusts or slabs. The facility is equipped with sensors to monitor environmental parameters such as wind speed, air temperature and air humidity. A SnowMicroPen and an industrial camera allow to measure properties of the snow surface. The facility is flexible and mobile having outer dimensions of 2.3x1.3x0.5 m. Airflow is created by a model aircraft propeller and the wind speed reaches values of up to 8 m/s. First results suggest that saltation is a necessary condition for the formation of a wind slab.

P 12.20

Studying the acoustic emissions and the failure process during loading experiments of snow

Achille Capelli¹, Ingrid Reiweger^{2,1}, Jürg Schweizer¹

¹ WSL Institute for Snow and Avalanche Research SLF, Flüelastrasse 11, 7260 Davos Dorf, (achille.capelli@slf.ch)

² Institute of Mountain Risk Engineering, Department of Civil Engineering and Natural Hazards, BOKU University of Natural Resources and Life Sciences, Vienna, Peter-Jordan-Straße 82, 1190 Wien, Austria

Acoustic emissions generated by crack formation or bond failure allow a non-destructive observation of the progressive failure of snow. Moreover, acoustic emission features often indicate imminent failure.

We developed a new apparatus for fully load-controlled snow failure experiments. Our apparatus includes six piezoelectric transducers which record the generated acoustic emissions in the ultrasonic range. The six sensors allow localizing the sources of the acoustic emissions, i.e. where the failure process starts and how it develops with time towards catastrophic failure. The quadratic snow samples have an area of 0.25 m² and a height of 10 to 20 cm and are clearly larger than samples used in previous experiments. The size of the samples, which is comparable to the critical size for the onset of crack propagation leading to dry-snow slab avalanche release, allows studying the failure nucleation process and its relation to the spatial distribution of the recorded acoustic emissions. We performed tests with homogeneous as well as layered snow samples, including a weak layer, for varying loading rates and loading angles.

We observed various signatures typical for an imminent failure. The analysis of the waiting time indicated an acceleration of the AE and, therefore, of the damage process before failure. The observed variations in the distributions of the acoustic emissions energy, i.e. a decrease of the b-value, indicated a transition from homogeneously distributed damage to localized damage toward failure. Furthermore, the changes in the energy distributions were weaker for lower stress rates, indicating a more homogeneous distribution of the damage for lower stress rates.

P 12.21

The contact density to characterize the mechanical behavior of very loose cohesive granular materials: towards snow microstructure modeling.

J. Gaume^{1,2} and H. Löwe².

¹ School of Architecture, Civil and Environmental Engineering, Ecole Polytechnique Federale de Lausanne, Switzerland

² WSL Institute for Snow and Avalanche Research SLF, Davos, Switzerland (gaume@slf.ch)

Microstructural properties are essential to characterize the mechanical behavior of loose and cohesive granular materials such as snow. In particular, mechanical properties and physical processes of porous media are often related to the volume fraction ν . Low-density microstructures typically allow for considerable structural diversity at a given volume fraction, leading to uncertainties in modeling approaches using ν -based parametrizations only.

We have conducted discrete element simulations of cohesive granular materials with initial configurations which are drawn from Baxter's sticky hard sphere (SHS) model. This method allows to control independently the initial volume fraction ν and the average coordination number Z .

We show that variations in elasticity and strength of the samples can be fully explained by the initial contact density $C = \nu Z$ over a wide range of volume fractions and coordination numbers. Hence, accounting for the contact density C allows to resolve the discrepancies in particle based modeling between samples with similar volume fractions but different microstructures.

As an application, we applied our method to the microstructure of real snow samples which have been imaged by micro-computed tomography and reconstructed using the SHS model. Our new approach opens a promising route to evaluate snow physical and mechanical properties from field measurements, for instance using the Snow Micro Penetrometer (SMP), by linking the penetration resistance to the contact density.

P 12.22

The Open Source Snowpack modelling ecosystem

Mathias Bavay¹, Charles Fierz¹, Thomas Egger², Michael Lehning¹

¹ WSL Institute for Snow and Avalanche Research SLF, Flüelastrasse 11, 7260 Davos Dorf, Switzerland (bavay@slf.ch)

² Egger Consulting GmbH, Postgasse 2/46, 1010 Vienna, Austria

As a large number of numerical snow models are available, a few stand out as quite mature and widespread. One such model is SNOWPACK, the Open Source model that is developed at the WSL Institute for Snow and Avalanche Research SLF. Over the years, various tools have been developed around SNOWPACK in order to expand its use or to integrate additional features. Today, the model is part of a whole ecosystem that has evolved to both offer seamless integration and high modularity so each tool can easily be used outside the ecosystem. Many of these Open Source tools experience their own, autonomous development and are successfully used in their own right in other models and applications.

There is Alpine3D, the spatially distributed version of SNOWPACK, that forces it with terrain-corrected radiation fields and optionally with blowing and drifting snow. This model can be used on parallel systems (either with OpenMP or MPI) and has been used for applications ranging from climate change to reindeer herding.

There is the Meteolo pre-processing library that offers fully integrated data access, data filtering, data correction, data resampling and spatial interpolations. This library is now used by several other models and applications.

There is the SnopViz snow profile visualization library and application that supports both measured and simulated snow profiles (relying on the CAAML standard) as well as time series. This JavaScript application can be used standalone without any internet connection or served on the web together with simulation results.

There is the OSPER data platform effort with a data management service (build on the Global Sensor Network (GSN) platform) as well as a data documenting system (metadata management as a wiki).

There are several distributed hydrological models for mountainous areas in ongoing development that require very little information about the soil structure based on the assumption that in steep terrain, the most relevant information is contained in the Digital Elevation Model (DEM).

There is finally a set of tools making up the operational chain to automatically run, monitor and publish SNOWPACK simulations for operational avalanche warning purposes. This tool chain has been developed with the aim of offering very low maintenance operation and very fast deployment and to easily adapt to other avalanche services.

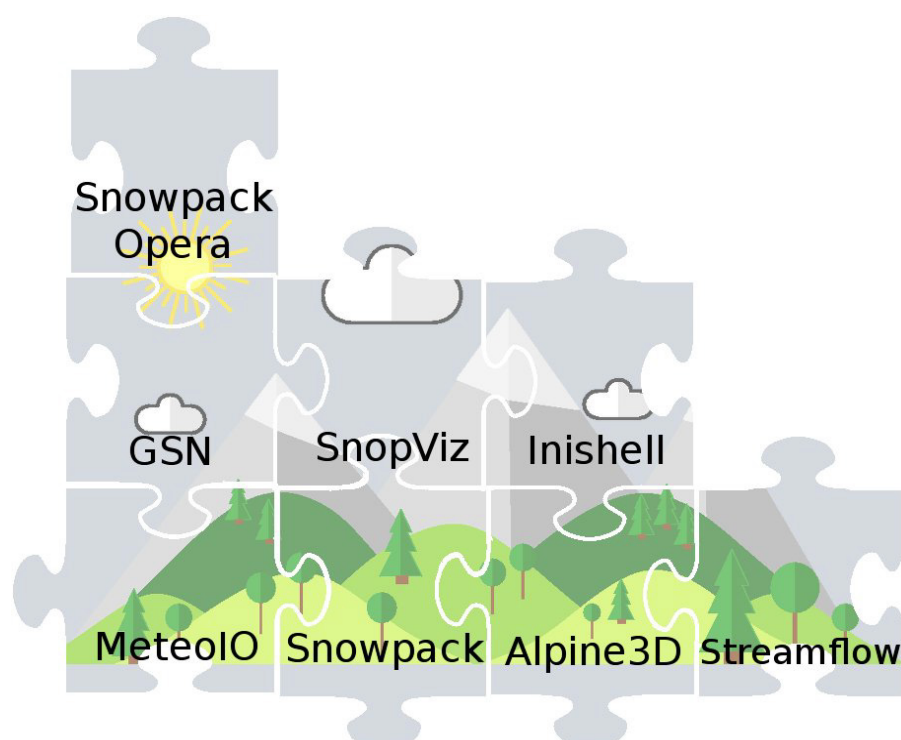


Figure 1. The components of the SNOWPACK ecosystem.

REFERENCES

- Lehning, M., Bartelt, P., Brown, R.L., Fierz, C., and Satyawali, P.K. A physical SNOWPACK model for the Swiss avalanche warning, Part II. Snow microstructure, *Cold Regions Science and Technology* 35, 2002, 147–167
- Bavay, M. and Egger, T. Meteolo 2.4.2: a preprocessing library for meteorological data. *Geosci. Model Dev.*, 7, 3135-3151, doi:10.5194/gmd-7-3135-2014, 2014.
- Gallice, A., Schaefli, B., Lehning, M., Parlange, M. B., and Huwald, H. Stream temperature prediction in ungauged basins: review of recent approaches and description of a new physics-derived statistical model, *Hydrol. Earth Syst. Sci.*, 19, 3727-3753, doi:10.5194/hess-19-3727-2015, 2015.

P 12.23

Modelling water vapour transport in snow

Margaux Couttet¹, Nander Wever², Mathias Bavay², Charles Fierz², Michael Lehning^{1,2}

¹ School of Architecture, Civil and Environmental Engineering, Ecole Polytechnique Federale de Lausanne, Lausanne, Switzerland (margaux.couttet@epfl.ch)

² WSL Institute for Snow and Avalanche Research SLF, Davos, Switzerland

In dry snow and under strong temperature gradients, snowpack metamorphism is driven by water vapor transport. Two spatial scales are considered in kinetic growth metamorphism: microscopic exchange of vapour between grains (individual dendrites scale) coupled with macroscopic vapor flux between snow layers over the entire snowpack. In SNOWPACK, a 1-dimensional physically-based snowpack model, a detailed representation of snow microstructure and metamorphism is already formulated. It includes the relationship between grain growth and water vapour flux regarding the net inter-particle vapour fluxes. Here the numerical implementation of the layer-to-layer transport of water vapour in the SNOWPACK model is presented as well as the water vapour flux across the snow-air and snow-soil interfaces. Assuming saturated conditions, the vapour flux between snow layers is expressed in terms of temperature and temperature gradients at the boundaries of the layers. Also discussed are the implications of the vertical flux between snow layers on the snowpack density and the grain types. The largest impact is observed in the basal layer of the snowpack where the formation of depth hoar occurs. Simulated results are compared to measured snow profiles in the Alps as well as observations from subarctic regions, where a significant source of water vapour is present and the snowpack is shallower compared to Alpine regions.

REFERENCES

- Lehning, M., P. Bartelt, B. Brown, C. Fierz, and P. Satyawali. "A Physical SNOWPACK Model for the Swiss Avalanche Warning: Part II. Snow Microstructure." *Cold Regions Science and Technology* 35, no. 3 (November 2002): 147–67. doi:10.1016/S0165-232X(02)00073-3.
- Sturm, M., and C. S. Benson. "Vapor Transport, Grain Growth and Depth-Hoar Development in the Subarctic Snow." *Journal of Glaciology* 43, no. 143 (1997): 42–59.
- Colbeck, S. C. "Theory of Metamorphism of Dry Snow." *Journal of Geophysical Research: Oceans* 88, no. C9 (June 20, 1983): 5475–82. doi:10.1029/JC088iC09p05475.

P 12.24

Energy balance and melt over a patchy snow cover

Sebastian Schlögl^{1,2}, Rebecca Mott¹ and Michael Lehning^{1,2}

¹ *WSL Institute for snow and avalanche research SLF, Davos, Switzerland*

² *School of Architecture, Civil and Environmental Engineering, 'Ecole Polytechnique Fédérale de Lausanne, Switzerland*

A patchy snow cover significantly alters the surface energy exchange. The two opposite effects of horizontal advection of warm air from the bare ground to the snow patch and the development of strong stability close to the ground were assessed in this study. Atmospheric, snow and hydrological models are typically limited to simulating pointwise vertical exchange between the ground and the atmosphere and do not include lateral transport close to the ground. For a patchy snow cover, this limitation leads to an underestimation of modelled melting rates at the upwind edge. We assess the relative contribution of the advective heat flux to the total surface energy balance and therefore snow melt using (i) high-resolution measurements of daily snow depth changes obtained from Terrestrial Laser Scanning, (ii) the distributed and physics-based snow model Alpine3D using standard automatic weather stations as model input, and (iii) Alpine3D, which is forced with air temperature and wind velocity fields calculated from the non-hydrostatic atmospheric model Advanced Regional Prediction model (ARPS).

Analysis of measured melt rates have shown a 5 % increase in total snow melting due to the effect of the advective heat flux for a typical spring snow distribution. We numerically investigate the effect of atmospheric flow field dynamics over a patchy snow cover on the total surface energy balance by forcing Alpine3D with fully resolved meteorological fields (air temperature and wind velocity) obtained from ARPS (i) close to the surface in order to represent the small scale variability, and (ii) above the blending height as a reference due to the fact that the model input is typically recorded above the blending height. Quantitative experimental and numerical results show how the snow melt rate increases with decreasing snow cover fraction (SCF) and decreasing mean perimeter of the snow patches.

P 12.25

Icefalls from the Eiger West Face Monitored by Interferometric Radar and Seismometers

Lukas E. Preiswerk¹, Fabian Walter¹, Lorenz Meier² & Martin Funk¹

¹ *Laboratory of Hydraulics, Hydrology and Glaciology, ETH Zürich, Switzerland, preiswerk@vaw.baug.ethz.ch*

² *GEOPRAEVENT AG, Zürich, Switzerland*

The hanging glacier in the west face of Eiger is a well-known partly cold-based unstable glacier in the Bernese Alps (Switzerland). A break-off of ice chunks from this hanging glacier might trigger dangerous combined snow/ice avalanches due to the steep slopes beneath it. Since the train to Jungfraujoch as well as several buildings and hiking paths are in the runout zone of a potential avalanche, the glacier has been monitored for the last two decades.

In fall 2015, pictures from an automated camera showed the development of an ice wedge at the glacier front and therefore an increased chance of a break-off event. In early 2016, an interferometric radar was installed to provide real-time measurements of ice velocity at the glacier front. Additionally, an array of seismometers was installed on the ice close to the potential fracture to monitor seismic emissions of even small-scale ice avalanches and englacial crevasse development.

In August 2016, the hanging glacier lost ~25'000 m³ of ice in a series of icefall events. We show that all significant events could be forecasted several days in advance based on a precursory acceleration of the glacier front, which was recorded by an interferometric radar. We also present seismological records reflecting the long-term evolution of internal damage in the weeks and months before these break-off events.

P 12.26

Rapid growth of a terminal lake in the Glarner Alpen

Jakob F. Steiner¹, Pascal Buri², Evan S. Miles³, Marco Epp⁴

¹Institute of Environmental Engineering, ETH Zurich, Zurich, Switzerland (stjakob@ethz.ch)

²Institute of Environmental Engineering, ETH Zurich, Zurich, Switzerland

³Scott Polar Research Institute, Cambridge University, Cambridge, UK

⁴Mappuls AG, Schlössli Schönegg, Wilhelmshöhe, 6003 Luzern

With receding glaciers moraine dammed terminal lakes become more common also in the European Alps, increasing continuously in size. They are an indicator for glacier mass loss and can themselves contribute to an accelerated retreat of glacier tongues. In some cases such lakes are considered a risk as moraine dams may desintegrate quickly with a rising water level or mass movements into the lake may cause a flood wave overtopping the dam.

We investigate the development of such a moraine dammed terminal lake located in the Glarner Alpen which formed initially in the 1980s and since expanded to an area of ~ 130 000 m² (Figure 1).

It is obvious from field visits that dry calving events are taking place at the glacier terminus with the terminal cliff crest continuously expanding in length. Based on available orthophotos and DEMs we document the development of the terminal lake. We estimate the contribution to the lake's runoff by precipitation and melt. Comparing to studies carried out by the group on supraglacial lakes and ice cliffs in the Himalaya and bathymetry data available for the lake we can also provide first estimates of cliff and subaqueous melt. Initial estimates on possible spill waves are also attempted.

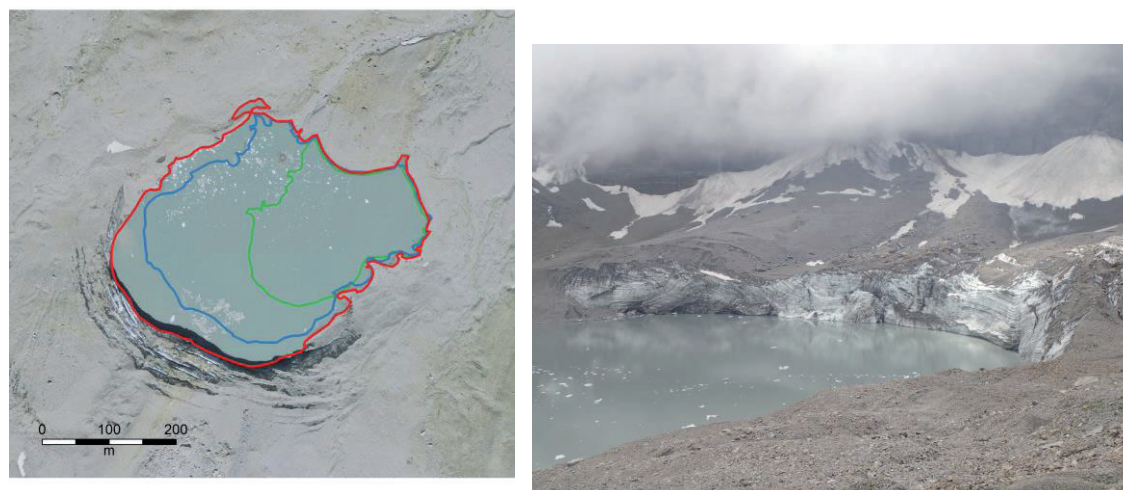


Figure 1. Expansion of the lake (2003, 2010, 2013) on the left and the ice cliff in a picture from August 2016 (right).

REFERENCES

- Hanson, B. & Hooke, R., 2000: *Glacier calving: a numerical model of forces in the calving-speed / water-depth relation*, *Journal of Glaciology*, 46
- Kirkbride, M. P., 1993: *The temporal significance of transitions from melting to calving termini at glaciers in the central Southern Alps of New Zealand*, *The Holocene*, 15, 209-231.
- Sakai, A. 2009: *Onset of calving at supraglacial lakes on debris-covered glaciers of the Nepal Himalaya*, *Journal of Glaciology*, 55
- Purdie, Jennifer and Fitzharris, Blair, 1999: *Processes and rates of ice loss at the terminus of Tasman Glacier, New Zealand*, *Global and Planetary Change*, 22
- Buri, P. et al., 2016: *A grid-based model of backwasting of supraglacial ice cliffs on debris-covered glaciers*, *Annals of Glaciology*, 57
- Miles, E. et al., 2016: *Refined energy-balance modelling of a supraglacial pond, Langtang Khola, Nepal*, *Annals of Glaciology*, 57
- Steiner, J. et al., 2015: *Modeling ice cliff backwasting on a debris covered glacier in the Nepalese Himalayas*, *Journal of Glaciology*, 61

13. Hydrology, Limnology and Hydrogeology

Pascal Blanc, Olivier Overney, Massimiliano Zappa, Michael Doering, Michael Sinreich

*Swiss Society for Hydrology and Limnology SGHL,
Swiss Hydrological Commission CHy,
Swiss Hydrogeological Society SGH*

TALKS:

- 13.1 Ammann L., Fenicia F., Doppler T., Reichert P., Stamm C.: Modelling the dynamics of in-stream herbicide concentrations: evaluation of a controlled herbicide application experiment in a headwater catchment
- 13.2 Carlier C., Wirth S., Cochand F., Staudinger M., Seibert J., Hunkeler D., Brunner P.: Groundwater and low flows in Switzerland – Assessment of water resources vulnerability to droughts using synthetic hydrogeological models
- 13.3 Costa A., Stutenbecker L., Silva T.A.A., Bakker M., Molnar P., Schlunegger F., Girardclos S., Loizeau J.-L., Lane S.N.: Temperature signal in fine sediment dynamics of the Upper Rhône basin
- 13.4 Cotte G., Vennemann T.: Tracing of Rhône River water in Lake Geneva using stable isotope composition of water
- 13.5 El Kateb A., Stalder C., Neururer C., Rüggeberg ., Spezzaferri S.: Lake Murten: Implication of high-resolution water parameter survey on lake functioning
- 13.6 Farinotti D., Pistocchi A., Huss M.: Dwindling water resources from glacierized catchments: Is mitigation possible?
- 13.7 Gerber C., Purtschert R., Hunkeler D., Sültenfuss J., Hug R.: Time lag of trend reversal after nitrate reduction measures determined by tracer measurements in the Dünnergäu, Solothurn
- 13.8 Gmünder C., Nusch S., Zimmermann S.: Use of Isotope data to quantify the interaction between the river Rhine and the groundwater at Oberriet, CH
- 13.9 Iorgulescu I., Nirel P., Higy C.: Linking hydrological and hydrochemical trends in the Arve River streamflow during the past decades
- 13.10 João P. Leitão: Keynote: New data sources as new opportunities for urban flood modelling
- 13.11 Joshua Larsen: Keynote: Streamflow responses to CO₂ – vegetation feedbacks in addition to other climatic changes
- 13.12 Luca Rossi: Keynote: Integrated water management approaches – new paradigms
- 13.13 Peter Huggenberger: Keynote: Challenges of groundwater management and protection in urban areas – Examples from the Basel area
- 13.14 Râman Vinnå L., Wüest A., Bouffard D.: Impact of nuclear produced thermal pollution on a lake with short residence time – what can models resolve?
- 13.15 Schirmer M., Musolf A., Radny D.: Mass Flux of Micropollutants in Cities – Challenges in Urban Hydrogeology
- 13.16 Seibert J., Strobl B., Etter S., Vis M., van Meerveld I.: Citizen science in hydrology: stream level observations and their potential value for constraining runoff models
- 13.17 Staudinger M., Carlier C., Cochand F., Seibert J., Brunner P.: Groundwater and low flows in Switzerland – Efforts to consider the spatial component of groundwater surface water exchange in a bucket-type hydrological model

POSTERS:

- P 13.1 Cimatoribus A., Leemin U., Barry D.A.: Transport and mixing in Lac Léman
- P 13.2 Colombo L.: Monitoring of alpine lakes: approach and results from Canton Ticino
- P 13.3 Fluixá-Sanmartín J., García Hernández J., Alesina S.: Trend of drought conditions based on meteorological index detection in the Upper Rhone River Basin, Valais, Switzerland
- P 13.4 Gies H., Wick S., Lupker M., Freymond C., Peterse F., Hagiphour N., Eglinton T.: Riverine export of organic carbon during extreme precipitation events
- P 13.5 Goyette S.: Numerical investigation with a coupled single-column lake-atmosphere model: An application to Western Switzerland
- P 13.6 Moeck C., Van Freyberg J., Schirmer M.: The effects of model complexity and calibration period on groundwater recharge predictions
- P 13.7 Nasri S., Hakdaoui M., Baghdad B.: Dynamism of spatial planning to improve management of urban expansions and the effect of water resources of Meknes city. Contribution of multisource spatial imagery
- P 13.8 Andres N., Kuhlman M., Zuend B., Federer M., Zappa M.: Hydrological-hydraulic modelling of the Lake of Zürich for future flood protection
- P 13.9 Pavia Santolamazza D., Lebreuz H.: Assessment of recent flood events at Muttenz, Switzerland
- P 13.10 Preisig G., Volken S., Gaehwiler M., Möri A., Sinreich M.: GeoQuat project: realization of groundwater volumes and vulnerability maps based on 3D parametric modeling
- P 13.11 Thomas C., Lyautey E., Ariztegui D., Dubois N., Frossard V., Pasche N., Perga M.-E., and the Life Under the Ice Scientific Team: Life under the ice: microbial diversity and methane cycling in the sediment of the ice-covered Lake Onego, Russia
- P 13.12 Thornton J.M., Mariethoz G., Brunner P.: 3D geological modelling as a basis for hydrogeological investigations in complex mountain terrain
- P 13.13 Travaglini E., Ornstein P., Moerschel J., Schneider T.: SismoRiv : Estimation du charriage en rivière à l'aide d'une mesure du bruit sismique présent dans les berges
- P 13.14 Wirth S.B., Reusch A., Bouffard D., Anselmetti F.S., Strasser M.: Pockmarks in Lake Neuchâtel
- P 13.15 Benoit L., Mariethoz G.: Rainfall structure observed by a dense network of high resolution rain gauges
- P 13.16 Beria H., Daqing Yang, Yanping Li: In a warming climate, why do we see decreasing heat influx from Russian rivers in the Arctic Ocean?
- P 13.17 Cochand F., Carlier C., Staudinger M., Seibert J., Hunkeler D., Brunner P.: Groundwater and low flows in Switzerland – Comparative physically based modelling of two Swiss catchments for assessing their low flow dynamics
- P 13.18 Consoli G., Bruder A., Lepori F., Robinson C.T.: Quantifying and predicting the effects of water abstraction on macroinvertebrate fauna and ecosystem function in alpine streams
- P 13.19 Iorgulescu I.: Differences in the present hydrological regime of two Jurassic catchments with respect to the early XXth Century
- P 13.20 Jimenez-Martinez, J: Solute mixing and chemical reactions in multiphase systems: from pore- to field-scale
- P 13.21 Metzger R.: The Surface Runoff diagnostic model for the Canton of Geneva
- P 13.22 Rusconi R., Secchi E., Willmann M., Stocker R.: Bacterial transport in saturated porous media
- P 13.23 Saletti M., Molnar P.: A multi-grain reduced-complexity model for step formation and stability in steep streams

13.1

Modelling the dynamics of in-stream herbicide concentrations: evaluation of a controlled herbicide application experiment in a headwater catchment

Lorenz Ammann¹, Fabrizio Fenicia¹, Tobias Doppler², Peter Reichert¹, Christian Stamm¹

¹ Eawag, Swiss Federal Institute of Aquatic Science and Technology, Überlandstrasse 133, CH-8600 Dübendorf (lorenz.ammann@eawag.ch)

² VSA, Swiss Water Association, Europastrasse 3, CH-8152 Glattbrugg

Diffuse pollution of water bodies by herbicides in catchments dominated by agricultural land-use is a major growing concern. While only a small fraction of the applied herbicide mass is washed off into surface waters in usual conditions, concentrations therein may reach levels proven to affect organisms (Velisek et al., 2014; Doppler et al., 2012).

Various experiments at lab and field scale have been performed to investigate the processes involved in herbicide wash off. At the scale of small catchments, however, less is known about the dynamics and interactions of those processes, which impedes the derivation of efficient mitigation measures.

We evaluate an experiment located in a small (1.2 km²) agricultural catchment in the Swiss Plateau, consisting of a controlled application of herbicides, distributed in-stream concentration measurements at high temporal resolution (Figure 1), as well as soil and ponding water samples (Doppler et al., 2012). The experiment revealed considerable spatio-temporal variation in herbicide loss rates. The objective of our study is to better understand the processes that caused this variation.

We first apply a regression analysis to identify the key controls on herbicide loss rates. Subsequently, to reproduce the dynamics and still keep parsimony, we construct a simple hydrological model with multiple non-linear reservoirs, using an extension of a flexible hydrological modelling framework (Fenicia et al., 2011). The model considers degradation and sorption of herbicides and is jointly calibrated to streamflow data and time series of herbicide concentrations.

Our preliminary results indicate that herbicide loss rates are generally higher for soils which are prone to saturation or when maximum rainfall intensity is high. With the hydrological model we are able to reproduce streamflow dynamics, whereas herbicide concentrations still pose major difficulties.

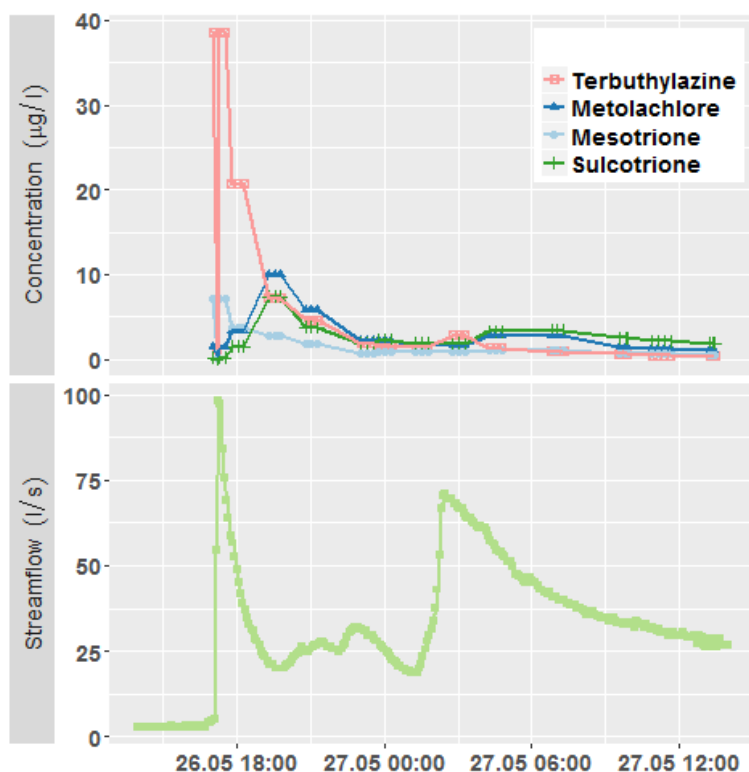


Figure 1. Observed herbicide concentration and discharge dynamics at one of the gauging stations on 6th and 7th of June, 2009.

REFERENCES

- Doppler, T., Camenzuli, L., Hirzel, G, Krauss, M., Lück, A., & Stamm, C. 2012: Spatial variability of herbicide mobilisation and transport at catchment scale: insights from a field experiment. *Hydrol. Earth Syst. Sci.* 16, 1947-1967.
- Velisek, J., Stara, A., Koutnik, D., & Machova J. 2014: Effect of Terbutylazine-2-hydroxy at Environmental Concentrations on Early Life stages of Common Carp (*Cyprinus carpio* L.). *BioMed Research International* 2014, 1-7.
- Fenicia, F., Kavetski, D., & Savenije, H. 2011: Elements of a flexible approach for conceptual hydrological modeling: 1. Motivation and theoretical development. *Water Resources Research* 47, W11510.

13.2

Groundwater and low flows in Switzerland – Part 3: Assessment of water resources vulnerability to droughts using synthetic hydrogeological models

Claire Carlier¹, Stefanie Wirth¹, Fabien Cochand¹, Maria Staudinger², Jan Seibert², Daniel Hunkeler¹, Philip Brunner¹

¹ *Centre for Hydrogeology and Geothermics (CHYN), University of Neuchâtel, Emile-Argand 11, CH-2000 Neuchâtel (claire.carlier@unine.ch)*

² *Geographisches Institut, University of Zurich, Winterthurerstrasse 190, CH-8057 Zurich*

Climate models tend to predict more frequent and intense periods with limited water availability. Even temperate and relatively humid regions like Switzerland are affected by issues related to low-flows. It is thus essential to characterise the vulnerability of watersheds to droughts in order to manage water supply. Aquifers, as a major fresh water reservoir, greatly impact hydrological catchment dynamics. Especially river low-flows are strongly dependent on the surrounding hydrogeological settings. Numerous studies have analysed watershed processes under dry conditions. However, they have mainly concentrated on stream flows.

We thus propose an integrated quantification of the impact of droughts on water resources by considering the sensitivity of both rivers and groundwater to prolonged dry periods. To achieve this, the hydrogeological and topographical controls on storage processes are characterised. The relationship between the physical properties of the catchment and its low-flow dynamics is highly complex, and no straightforward correlation can be obtained by analysing real catchment data. A modelling approach is therefore developed to systematically and independently quantify the control mechanisms of catchment parameters on river and groundwater dynamics. The physically based numerical model HydroGeoSphere is used, which simulates surface water and groundwater in a fully coupled way. Numerous synthetic models are designed with systematically varying geometry and hydrogeological parameters. Indicators describing drought vulnerability of stream flows, groundwater heads and storage volumes are proposed. A clear correlation between catchment porous storage volume and resilience to drought is observed. An attempt to link these results to real watersheds is made, analysing the flows and the geology of a selection of catchments. The validation of the synthetic results with observations would allow the development of drought sensitivity indicators based solely on physical properties of watersheds.

13.3

Temperature signal in fine sediment dynamics of the Upper Rhône basin

Anna Costa¹, Laura Stutenbecker², Tiago A. A. Silva³, Maarten Bakker⁴, Peter Molnar¹, Fritz Schlunegger², Girardclos, Stéphanie⁵, Jean-Luc Loizeau³, Stuart N. Lane⁴

¹ *Institute of Environmental Engineering, ETH Zürich, Stefano-Frascini-Platz 3, CH-8093 Zürich (costa@ifu.baug.ethz.ch)*

² *Institute of Geological Sciences, University of Bern, CH-3012 Bern*

³ *Institute F.-A. Forel, University of Geneva, CH-1290 Versoix*

⁴ *Institute of Earth Surface Dynamics, University of Lausanne, CH-1015 Lausanne*

⁵ *Section of Earth and Environmental Sciences, University of Geneva, CH-1205 Geneva*

Together with geological forcing and glacier inheritance, climate is one of the main drivers of erosional processes and sediment dynamics in alpine environments. Climatic conditions impact sediment fluxes of mountainous region, by activation/deactivation of sediment sources and by initiating specific sediment production and transport processes throughout the hydrological year. Precipitation and temperature determine, for example, the snow dynamics of alpine catchments which, in turn, impacts on the sediment regime by defining the fraction of the basin that is snow free and potentially erodible, by influencing the onset of ice-melting and the exposure of large amounts of sediment in proglacial areas. As a result, changes in climatic conditions should also influence considerably the sediment regime of such sensitive areas.

In agreement with previous studies (e.g., Beniston 1996), we identify an abrupt increase in mean air temperature (Fig. 1) during mid-1980s in the Upper Rhône basin (South-Western part of Switzerland). The main aim of this work is to analyse the potential effect of this temperature jump on the fine sediment regime of this 5,200 km² Alpine catchment.

To identify changes in the Upper Rhône basin during the last forty years, statistical tests are applied on multiple hydro-climatic and sediment related variables. Observations of basin-averaged air temperature and precipitation, discharge and suspended sediment concentration measured at the outlet of the catchment are analysed as mean annual and mean monthly values. To account for snow and ice-dynamics, spatially distributed temperature index models are calibrated and validated to simulate daily snow-melt, snow cover and ice-melt for the forty year period 1975-2015. Gridded datasets of daily precipitation and temperature with ~2x2 km² resolution, provided by Meteoswiss, are used as input for the degree-day models. Changes in fine sediment dynamics are investigated by analysing both the transport capacity of the Upper Rhône River and the evolution of specific sediment sources such as: (1) sediment entrained and transported along hillslopes and channels by snow melting, (2) sediment-rich fluxes originated in proglacial areas and by glacial erosion, (3) sediments mobilized by rainfall erosivity along snow-free hillslopes.

Simultaneously to the abrupt warming in spring and summer (Fig. 1), we identify a significant rise in suspended sediment concentration at the outlet of the basin in July and August, confirming the close link between climate and sediment dynamics. While changes in transport capacity (discharge) are not capable to explain the step-like rise in suspended sediment concentration, the analysis of specific sediment fluxes reveal that enhanced ice-melt and glacier retreat started in mid-1980s has coincided with increasing suspended sediment concentration entering the Lake Geneva. While precipitation does not show any statistically significant change over the forty year period, the combination of a remarkable reduction in snow cover duration and snowfall days in this period, especially at low and mid elevations may have also contributed to enhance suspended sediment concentration along the Rhône River. This study demonstrates the relevance of understanding processes that link climate and erosion and sediment transport, especially in the context of climate change. It also suggests the importance of adopting a more process-based approach for predicting suspended sediment load rather than traditional rating curves simply based on streamflow.

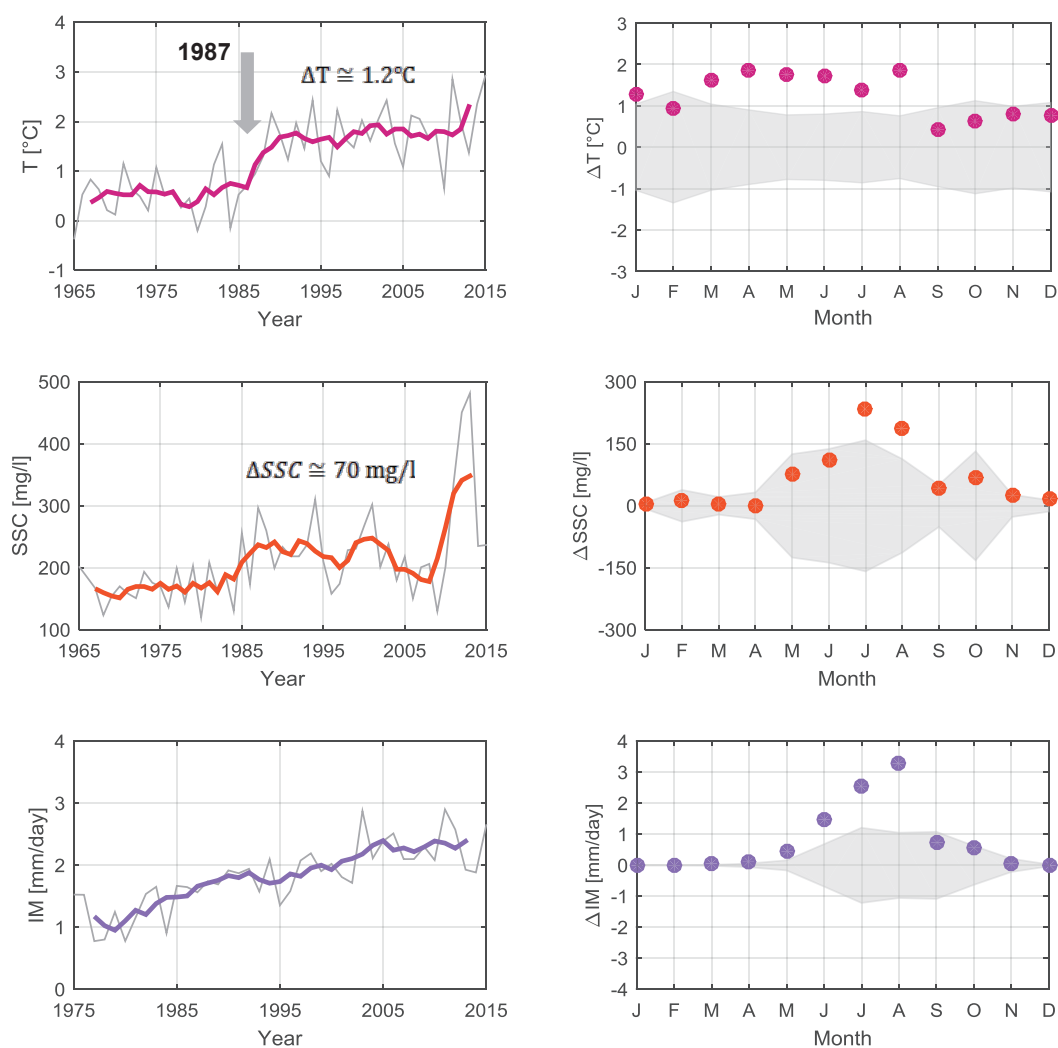


Figure 1. Time series of mean annual values (left) and monthly differences (right) between the period before and after the temperature jump (1975-1986 and 1987-2015) of basin-averaged air temperature (T), suspended sediment concentration (SSC) measured at the outlet of the basin and basin-total simulated ice-melt (IM), from top to bottom.

REFERENCES

- Beniston, M. & Rebetez, M. 1996: Regional behavior of minimum temperatures in Switzerland for the period 1979–1993, *Theor. Appl. Climatol.*, 53, 231–243.

13.4

Tracing of Rhône River water in Lake Geneva using stable isotope composition of water

Gabriel Cotte¹, Torsten Vennemann²

¹ IDYST, Université de Lausanne, Géopolis 1015 Lausanne (gabriel.cotte@unil)

² IDYST, Université de Lausanne, Géopolis 1015 Lausanne (Torsten.Vennemann@unil.ch)

It is important to determine the hydrodynamics of lake water in order to better understand nutrient transport and the distribution of potential pollutants through bodies of water.

The objective of this study is to understand the hydrodynamic mixing of Rhône River water in Lake Geneva. It has been ascertained that during the summer and fall, when the lake has an established thermal stratification, Rhône River water can flow directly to the “Petit Lac” more than 55 km away from its mouth (Halder et al., 2013). During winter, when stratification is weakened, the water from the Rhône River mixes quickly with the cold and homogeneous water of Lake Geneva. Therefore, the aim is to determine the path of the Rhône River through the lake and identify the thermal and meteorologic conditions favorable for this kind of flow.

To realise the studies objectives, water samples are taken in different sectional transects orientated North-South in different parts of the lake. Bathymetric profiles are taken at each sampling location, measuring temperature, pH, conductivity and oxygen concentration. Sampling campaigns are carried out every two months to study the lake's hydrodynamics at varying thermal conditions. For every sample, we analyse the isotope composition of the water, the dissolved inorganic carbon and the major ions. The isotopic signature of water is a strong tracing tool for ascertaining the precise origin of water molecules in the water cycle. The isotopic fractionation implies that light isotopes moved preferentially further than heavy isotopes during atmospheric disturbance travel. Altitude increases also this fractionation. So, it's possible to differentiate Lake Geneva's isotopically lighter water from the heavier Rhône River water which is mostly fed by glaciers.

The analysis of water's isotopic composition is a key tool to understand the hydrodynamic of the lake. It can ascertain not only the origin of the water, but also its residence time and nutrient or pollutant dispersion.

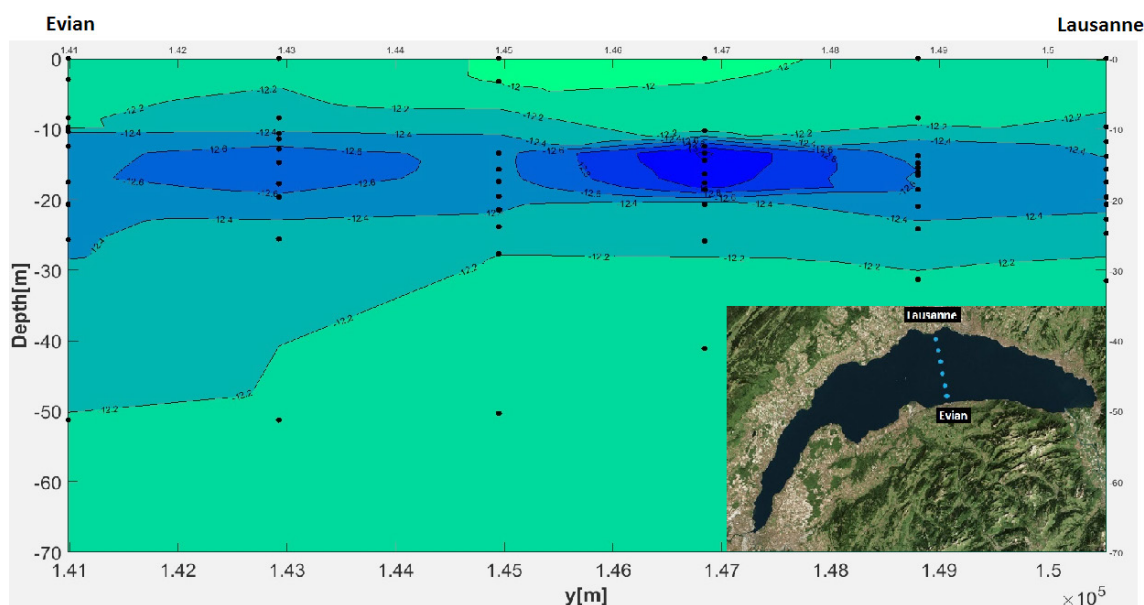


Figure 1. Isotopic composition of oxygen of water $\delta^{18}\text{O}_{\text{VSMOW}}$ (‰) measured on the Evian-Lausanne cross section in August 2015.

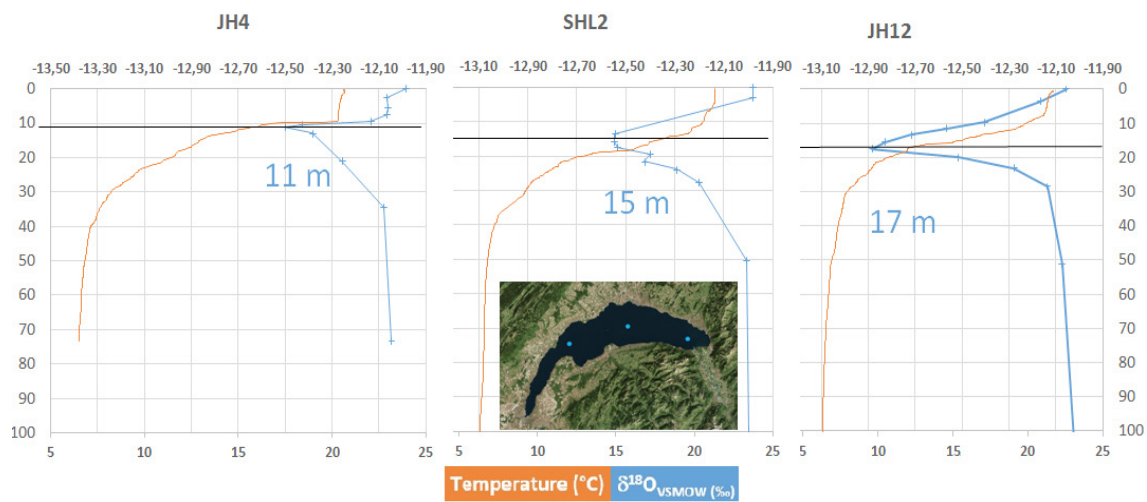


Figure 2. Isotopic composition of oxygen of water $\delta^{18}\text{O}_{\text{VSMOW}}$ (‰) measured on three profiles in August 2015.

REFERENCES

Halder J., Decrouy L. & Vennemann T. 2013 : Mixing of Rhône River water in Lake Geneva (Switzerland–France) inferred from stable hydrogen and oxygen isotope profiles, *Journal of Hydrology* 477:152–164

13.5

Lake Murten: Implication of high-resolution water parameter survey on lake functioning

El Kateb Akram, Stalder Claudio, Neururer Christoph, Rüggeberg Andres, Spezzaferri Silvia

Department of Geosciences, University of Fribourg, Chemin du Musée 6, 1700 Fribourg

Lake Murten is the smallest lake in the Lake District, located in the western part of Switzerland between the Canton of Vaud and Fribourg. Lake Murten has a total surface of 22.8 km² with a length of 8.15 km and a width of 2.8 km. The maximal depth reaches 45.5 m whereas the mean water depth is 23.3 m. Several water parameters such as pH, temperature, conductivity, dissolved oxygen of the Lake Murten are monitored by the Service de l'environnement de Fribourg (SEN) since several years. Once a month, a water profile is performed at the deepest part of the lake. Usually, strong water mass stratification is observed during the spring season until the beginning of winter. During this stratification, the bottom layer and even the entire hypolimnion get anoxic.

To better understand this process and to pinpoint the influence of the atmosphere on the water parameters, an own-developed Lander System was placed in front of the village of Mur on the south-western part of the lake at 20m water depth. The Lander system is equipped with four sensors connected to a data logger that allows continuously measurements of water temperature, pH, dissolved oxygen and electrical conductivity. Additionally, video survey was performed in the deployment area to collect information on the lake bottom.

Water parameter data were collected from the 9th April 2015 until the 10th September 2015. Detailed Atmospheric data obtained from Meteo Suisse were synchronized and compared to the monitored water parameters. A positive correlation between water temperature, dissolved oxygen and wind speed could be identified. Our results indicate that wind induces a downwelling current which gradually weakens with increasing stratification. Based on our data, the downwelling speed can be estimated to 1 m/hour. Conductivity increased up to 200 $\mu\text{S}/\text{cm}$ in September. The unusually strong precipitations of May 2015 were also monitored by the Lander. During this period the lake level rose of around 1 m coinciding with a marked increase of conductivity.

Additionally, a significant decrease of dissolved oxygen was recorded during the monitoring period. Indeed, the concentration of dissolved oxygen was at 11 mg/l in April and decreased to 3 mg/l in September. Hourly to daily dissolved oxygen fluctuations reached in some cases variations of more than 1 mg/l. Similarly to the water temperature, strong dissolved oxygen fluctuations can be attributed to wind forcing.

13.6

Dwindling water resources from glacierized catchments: Is mitigation possible?

Daniel Farinotti^{1,2}, Alberto Pistocchi³, Matthias Huss^{1,4}

¹ Laboratory of Hydraulics, Hydrology and Glaciology (VAW), ETH Zurich, Zurich, Switzerland (daniel.farinotti@ethz.ch)

² Swiss Federal Research Institute WSL, Birmensdorf, Switzerland

² European Commission, DG Joint Research Centre (JRC), Institute for Environment and Sustainability, Ispra, Italy,

³ Department of Geosciences, University of Fribourg, Fribourg, Switzerland

Ongoing glacier retreat is often source of concern for future water availability. This is especially true for summer months, when glacier contribution to runoff is highest. In most cases, studies carried out in the domain focus on the quantification of future impacts. The potential for possible mitigation strategies, on the other hand, is rarely addressed.

In our work (Farinotti et al., 2016) we started from the assumption that maintaining unaltered the runoff regime from glacierized catchments is a desirable target. From that, we quantified the degree to which the expected changes in future summer-runoff could be offset when artificially reallocating the water surplus expected during spring time (Fig. 1). Our analyses are based on results from the glacier evolution model GloGEM (Huss and Hock, 2015), that was forced with ensembles of temperature and precipitation time series derived within from the Coupled Model Intercomparison Project Phase 5 (Taylor et al., 2012).

For the end of the century and integrated over the European Alps, we estimated that potentially about 1 km³ of water could be seasonally reallocated in order to mitigate the expected changes. According to our results, this could allow offsetting as much as 65% of the changes expected in the summer runoff from presently glacierized surfaces.

In a provocative assessment, we compared the above volume to the retention volume that could be provided when installing artificial reservoirs in the areas becoming ice-free. Our analysis suggests that the installable volume exceeds the volume required for achieving the maximal possible mitigation by more than one order of magnitude.

Obviously, the proposed strategy would not compensate for the overall reduction in annual runoff. By 2070-2099, glacier ice depletion across the Alps could result in a total runoff reduction of about $0.73 \pm 0.67 \text{ km}^3 \text{ a}^{-1}$.

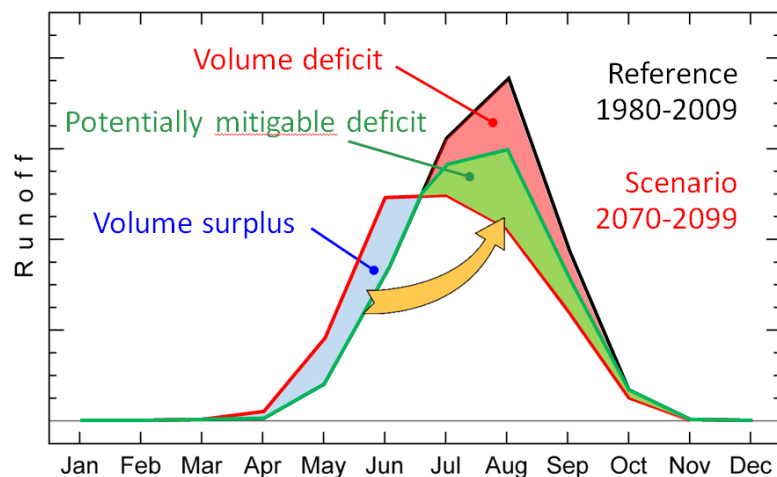


Figure 1. Illustration of the mitigation-concept used in our study. Assuming that maintaining unaltered the present runoff regime (black) is desirable, the expected regime change (red) could be mitigated by re-transferring the additional spring water (blue) to the summer months (green). Figure adapted from Farinotti et al. (2016).

REFERENCES

- Farinotti, D., Pistocchi, A., & Huss, M. 2016: From dwindling ice to headwater lakes: could dams replace glaciers in the European Alps?. *Environmental Research Letters*, 11(5), 054022.
- Huss, M., & Hock, R., 2015: A new model for global glacier change and sea-level rise. *Frontiers in Earth Science*, 3, 54.
- Taylor, K. E., Stouffer, R. J., & Meehl, G. A. 2012: An overview of CMIP5 and the experiment design. *Bulletin of the American Meteorological Society*, 93(4), 485-498.

13.7

Time lag of trend reversal after nitrate reduction measures determined by tracer measurements in the Dünnerngäu, Solothurn

Christoph Gerber¹, Roland Purtschert¹, Daniel Hunkeler², Jürgen Sültenfuss³ Rainer Hug⁴

¹ *Klima- und Umweltp Physik, Physikalisches Institut, und Oeschger Centre for Climate Change Research, Universität Bern, Sidlerstrasse 5, CH-3012 Bern (cgerber@climate.unibe.ch)*

² *Centre d'hydrogéologie et de géothermie (CHYN), Université de Neuchâtel, Rue Emile-Argand 11, CH-2000 Neuchâtel*

³ *Institut für Umweltp Physik, Abt. Ozeanographie, Universität Bremen, NW 1, Raum S-0360, Otto-Hahn-Allee, D-28359 Bremen*

⁴ *Amt für Umwelt des Kantons Solothurn, Greibenhof, Werkhofstrasse 5, CH-4509 Solothurn*

Rising nitrate concentrations due to intense agriculture threaten the quality and safety of drinking waters in many places in Switzerland and around the world. In the Dünnerngäu between Balsthal and Olten, nitrate concentrations surpassed the quality target value for nitrate concentrations of 25 mg/L (GschV) in the 1980s at several of the production wells (see Figure 1). Although nitrate concentrations did not yet exceed the tolerance value of 40 mg/L at the end of the 1990s, the "Nitratprojekt" was founded in 2000 to establish measures to reduce the input of nitrate to the groundwater. A 2D particle-tracking model was implemented to determine contributing areas of production wells, groundwater travel times, and to predict reaction times to nitrate reduction measures (Biaggi et al., 1999). In the first few years after the initiation of the "Nitratprojekt", nitrate concentrations decreased as predicted but then they stagnated or even increased again in some of the wells (Figure 1).

To better understand this discrepancy, we quantified residence times in the saturated and unsaturated zone based on time series of nitrate measurements from the pumping wells and measurements of environmental tracers (³H, ³He, ⁴He, ³⁹Ar, and ⁸⁵Kr). These measurements are interpreted by means of a lumped-parameter model that explicitly considers the unsaturated zone. Model parameters are estimated using a Bayesian inference scheme based on the Markov-Chain Monte-Carlo method (Alikhani et al., 2016). We also assess the usefulness of both the nitrate time series and the tracer data in constraining residence times and predicting nitrate concentrations. Finally, models with and without an explicit unsaturated zone were compared to identify the effect of including the unsaturated zone on estimated residence times and predicted nitrate concentrations.

We find that residence times of water and nitrate in the subsurface are longer than previously thought. The main reason is relatively long transfer times in the unsaturated zone of 2 to 10 years, which were neglected in the particle-tracking study. Generally, combining tracer data and nitrate time series leads to smaller uncertainties in nitrate predictions for wells, especially where the available nitrate time series are relatively short (Well 6 and 10 in Figure 1). For some wells, however, including tracer data results in a poorer agreement with the measured nitrate time series (especially well 5 in Figure 1). Including the tracer data results in hydrogeologically more realistic parameter sets, even if predicted nitrate concentrations look very similar to predictions from using nitrate time series alone. Finally, using nitrate time series alone, parameters of the model with an explicit unsaturated zone cannot be estimated due to high parameter correlation. Thus, environmental tracer measurements are indispensable to allow for a separation of residence times in the saturated and unsaturated zones.

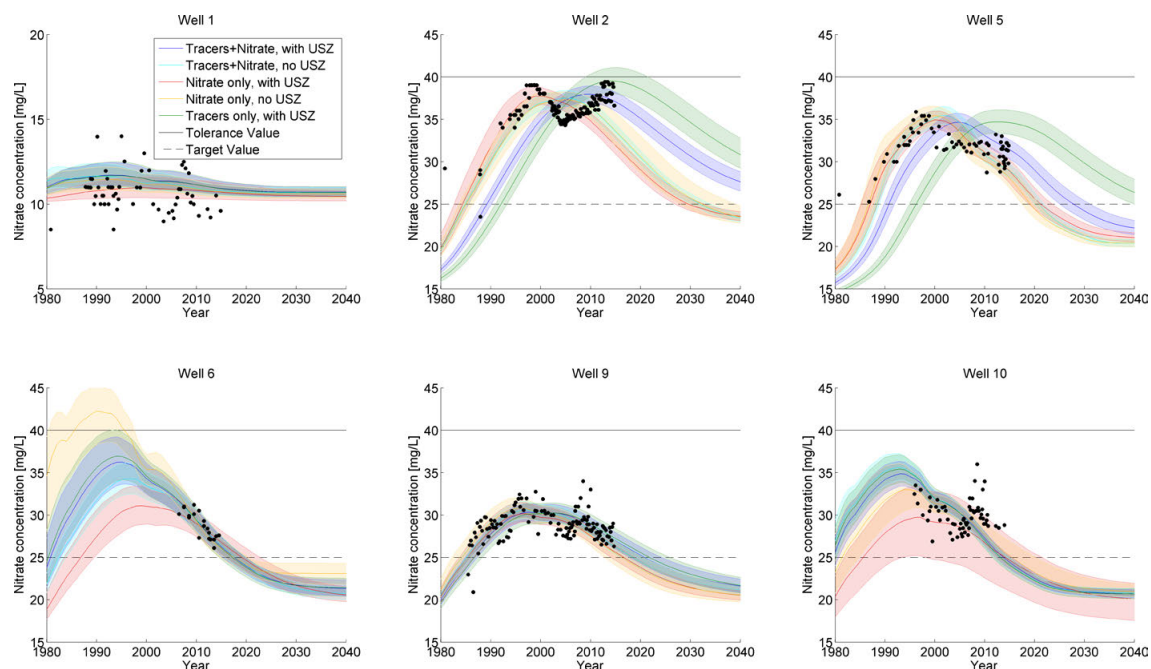


Figure 1. Measured nitrate concentrations (black dots) and median (lines) and 67% credible intervals (shaded areas) of predicted nitrate concentrations for five different scenarios.

REFERENCES

- Biaggi, D., Trösch, J. & Kuhlmann, U. 1999: Grundwassermodell Gäu, Synthesebericht und Technischer Bericht, Baudepartement Kanton Solothurn, ARGE Geotechnisches Institut/TK Consult AG, Bern/Zürich
- Alikhani, J., Deinhart, A., Visser, A., Bibby, R., Purtschert, R., Moran, J., Massoudieh, A. & Esser, B. 2016: Nitrate vulnerability projections from Bayesian inference of multiple groundwater age tracers. *Journal of Hydrology*, in press.

13.8

Use of Isotope data to quantify the interaction between the river Rhine and the groundwater at Oberriet, CH

Christian Gmünder¹, Simon Nusch¹, Stephanie Zimmermann²

¹ Simultec AG, Hardturmstrasse 261, CH-8005 Zürich (cg@simultec.ch)

² BAFU, Papiermühlestr. 172, 3063 Ittigen (stephanie.zimmermann@bafu.admin.ch)

A groundwater model has been built up to quantify the influence of the planned flood protection measures along the Alpenrhein. One of the most important questions building up the model has been the interaction between Rhine and groundwater, especially near the existing drinking water wells. The drinking water quality directly depends upon the fraction of infiltrated Rhine water.

For model calibration purposes, the electrical conductivity (EC) measures at the drinking water well “Balanggen” near Oberriet have been used. EC is quite a good tracer for quantifying the river infiltration into wells near the river, because the river water values are considerably lower than the background values in groundwater. If the well is positioned further away from the river, as this is the case at Oberriet, a mineralization takes place during the travel path to the well. This introduces a new unknown parameter to the calibration process. To omit this problem, the ¹⁸O concentrations have been used for model validation. ¹⁸O measurement values are provided by the NAQUA National Groundwater Monitoring at the “Balanggen” well. ¹⁸O concentration remains stable during groundwater passage.

Two methods were applied to validate the model. The first method is derived from a path line method developed by Cordes and Kinzelbach (1992). Because the method is based on a continuous flow field, the water balance can be calculated along the flow paths (Gmünder 2008). The method can be used to quantify the age and fraction of river water arriving at the well. 100 flow paths have been started at the well every five days during the simulation period and were tracked back in time. At the nodes where river water enters into the model, the measured ¹⁸O concentration of the river Rhine was applied to the infiltrating water.

As a second method, a mass transport model has been setup (Figure 1). Along the river Rhine, the measured ¹⁸O concentration was assigned to the water infiltrating into the groundwater. The ¹⁸O concentration at all other boundary nodes was set to a background value. At the Alpenrhein valley, background ¹⁸O values of 10.3 have been measured (Kralik et al. 2011).

A good match between simulated and measured ¹⁸O concentrations could be achieved. The simulations showed a strong time dependency of river water fraction and travel times. The mean fraction of river water is about 25%. The travel time of water infiltrated during the high-water season is between 90 and 120 days. As a by-product of the calibration process, the mineralization speed of EC could be quantified. It could be shown that ¹⁸O time series are well suited for the quantification of river infiltration to wells with a travel time of some months. The ¹⁸O concentrations should be measured monthly to detect the minimum and maximum values of the annual fluctuations.

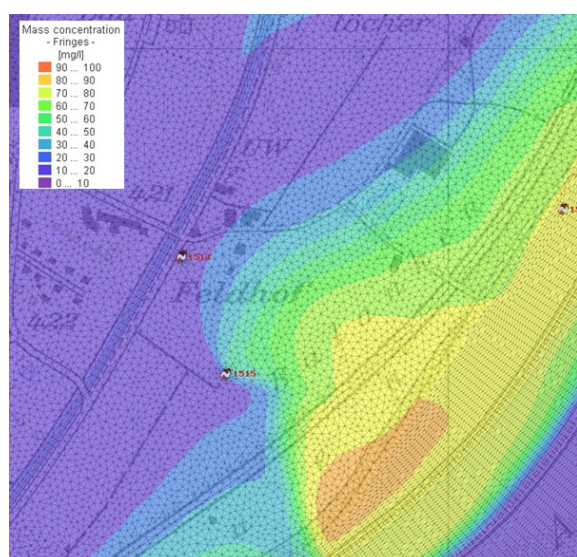


Figure 1. Snapshot of the mass concentration model. As numerical problems would arise when using the absolute ¹⁸O values, the differences between river water and background concentrations were simulated, scaling them to values between 0 and 100.

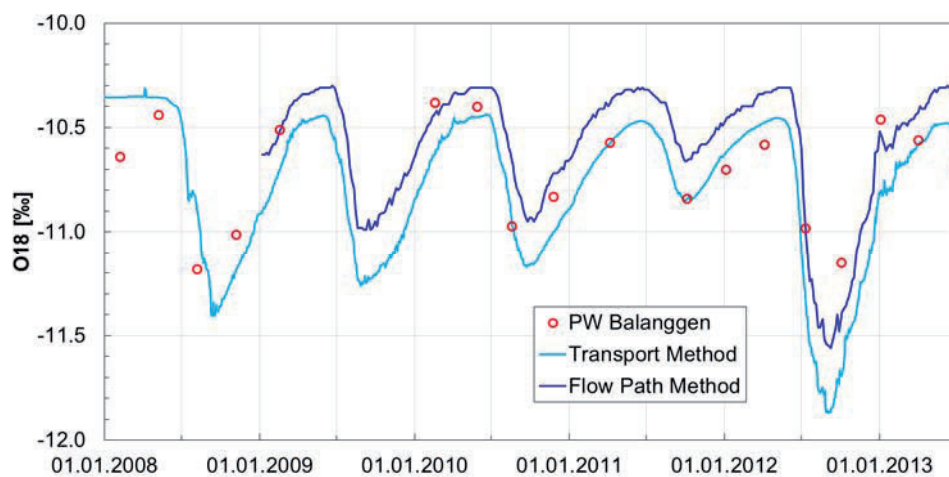


Figure 2. Comparison of the measured and simulated ^{18}O concentrations using the transport and the flow path method.

REFERENCES

- Cordes C. & Kinzelbach W. (1992): Continuous Groundwater Velocity Fields and Path Lines in Linear, Bilinear, and Trilinear Finite Elements - Water Resources Research, Vol. 28, No 11.
- Gmünder C. (2008): Modellgestützte Ermittlung der Einzugsbereiche von Grundwasserfassungen, Mitteilungen der Thurgauischen Naturforschenden Gesellschaft, Band 63.
- Kralik et al. (2011): Grundwasseralter ausgewählter Grundwasserkörper 2009/2010. Grazer Feld, Jauntal, Leibnitzer Feld, Rheintal, Unteres Salzachtal, Wulkatal. Publikation des Umweltbundesamtes, Perspektiven für Umwelt & Gesellschaft.

13.9

Linking hydrological and hydrochemical trends in the Arve River streamflow during the past decades

Ion Iorgulescu¹, Pascale Nirel² & Christophe Higy³

¹ *Direction Générale de l'Eau, Etat de Genève, rue des Gazomètres 7, CH-1205 Genève, Suisse
(Ion.Iorgulescu@etat.genève.ch)*

² *Direction Générale de l'Eau, Etat de Genève, Avenue de Ste-Clotilde 25, CH-1211 Genève, Suisse*

³ *mch-consultants, route des Lacustres 9, 1470 Estavayer-le-Lac, Suisse*

Analysis of streamflow data of the Arve River at the Bout-de-Monde (CH) gauging station over the last four decades show a statistically significant decrease in flows at the annual scale and especially during the summer seasonal maximum flows. At the same time chemical elements that have a strong inverse relationship with flow, sulphates in particular, show a significant increase especially during summer months. Other chemical elements such as Barium show a more complex behaviour. We explore the relationship between the hydrological and hydrochemical trends in the framework of a hydrochemical mixing model accounting for 'geographic' sources. While we acknowledge the limitations of this approach in a large and heterogeneous catchment such as the Arve River, we believe that it offers useful insights into the spatiotemporal sources of flow and in the mechanisms that underlie the observed temporal trends. The results are consistent with the hypothesis that the relationship between hydrological and hydrochemical behaviour is mostly controlled by shifting ratios of flowpaths across an heterogeneous catchment. The trends in the hydrological and hydrochemical fingerprints are consistent with changes in snow accumulation and melt processes and with an overall decrease in shallow pathway flows.

13.10

New data sources as new opportunities for urban flood modelling

João P. Leitão

¹ *Department of Urban Water Management, Eawag: Swiss Federal Institute of Aquatic Science and Technology, Überlandstrasse 133, CH-8600 Dübendorf (joapaulo.leitao@eawag.ch)*

The context

Floods are one of the natural hazards that causes most annually damage worldwide (approx. 30% of total natural hazards between 1900 and 2006) (Adikari and Yoshitani 2009). Due to predicted climate changes and migration to urban areas, flood events are expected to become more frequent and with increased consequences (United Nations, Department of Economic and Social Affairs, Population Division 2014). Urban floods caused by extreme rainfall (urban pluvial flood) are strongly influenced by the variability of urban land-use and by the urban layout; so, tools to accurately estimate urban flood risk, such as flood simulation models, need to include an accurate representation of the urban features (Fewtrell et al. 2011; Leitão et al. 2009), i.e., need to rely on fine-resolution (spatial and temporal) data.

New data sources are available, now what?

The digital revolution has been one of the key drivers of growth in post-industrial economies. Urban flood modelling and risk management have also strongly benefited from the recent technological advances. As an example, new opportunities are also becoming available regarding the sources of data for urban flood modelling; new technologies/ platforms, such as van-mounted LiDAR (Light Detection And Ranging) and UAVs photogrammetry, made the generation of up-to-date sub-meter Digital Elevation Models (DEMs) and orthophotos possible. These new data sources can be used to improve urban flood model results. The newly available orthophotos can help improving the capacity of estimating catchment infiltration capacity (Tokarczyk et al. 2015) and the newly available DEMs can bring additional detail to runoff modelling (Leitão et al. 2016), leading to more accurate flood modelling results. However, these new data sources pose new challenges to modelling, e.g.:

- *How deal with the increased computation time usually associated with the increase of data resolution?*
- *How to combine these new data sets with existing ones?*

Also, social networks and the Internet of Things are promising sources of urban flood information. More than ever, urban dwellers are connected to the internet with mobile devices. But *how can this large share of data be used to improve urban flood estimation?*

The future

Modelling urban pluvial floods is complex. It is not only as previously mentioned the need to take into account fine-resolution data and its impact on simulation time; data available from social media sources are highly uncertain, creating a challenges when used for, for example, model calibration. To resolve these challenges, existing methods will be upgraded so that they can take the newly available and more prone to error data sources into account. Future advances in (parallel) computational methods and in methods to deal with large quantities of data will enable us to better estimate the risk of pluvial flooding in urban areas, leading to new opportunities for model calibration and real-time flood applications.

REFERENCES

- Adikari, Y., Yoshitani, J. 2009: Global Trends in Water-Related Disasters: an insight for policymakers. International Centre for Water Hazard and Risk Management (ICHARM), UNESCO, France (available at: <http://www.unwater.org/downloads/181793E.pdf>) [Accessed: 16 September 2016]
- Fewtrell, T.J., Duncan, A., Sampson, C.C., Neal, J.C., & Bates, P.D. 2011: Benchmarking Urban Flood Models of Varying Complexity and Scale Using High Resolution Terrestrial LiDAR Data. *Physics and Chemistry of the Earth, Parts A/B/C*, 36(7-8), 281–91. doi: 10.1016/j.pce.2010.12.011
- Leitão, J. P., Boonya-Aroonnet, S., Prodanovic, D. & Maksimovic, C. 2009: The influence of digital elevation model resolution on overland flow networks for modelling urban pluvial flooding, *Water Science and Technology*, 60, 3137–3149, doi: 10.2166/wst.2009.754
- Leitão, J. P., Moy de Vitry, M., Scheidegger & A, Rieckermann, J. 2016: Assessing the quality of Digital Elevation Models obtained from mini-Unmanned Aerial Vehicles for overland flow modelling in urban areas. *Hydrology and Earth System Sciences*, 20, 1637-1653. doi: 10.5194/hess-20-1637-2016
- Tokarczyk, P., Leitao, J. P., Rieckermann, J., Schindler, K., & Blumensaat, F. 2015: High-quality observation of surface imperviousness for urban runoff modelling using UAV imagery, *Hydrology and Earth System Sciences*, 19, 4215–4228, doi: 10.5194/hess-19-4215-2015, 2015
- United Nations, Department of Economic and Social Affairs, Population Division 2014: World Urbanization Prospects: The 2014 Revision, Highlights (ST/ESA/SER.A/352). United Nations (available at: <http://esa.un.org/unpd/wup/Publications/Files/WUP2014-Highlights.pdf>) [Accessed: 16 September 2016]

13.11

Streamflow responses to CO₂ – vegetation feedbacks in addition to other climatic changes

Larsen, J., Trancoso, R., McVicar, T., McAlpine, C., Phinn, S.

Quantifying changes to the hydrological cycle and establishing their cause and effect is a significant research challenge since many of these changes often occur simultaneously. One such change is due the expected feedbacks between increasing concentrations of atmospheric CO₂, vegetation water use efficiency, and runoff. However, these feedbacks are poorly constrained, and generally not represented within land surface models. Nonetheless, they are attributed (in part) to explain the global 'greening' of water limited regions (fertilization effect) in spite of variable rainfall trends, while impacts within energy limited environments remain largely unknown. Recent predictions emphasise additional soil moisture availability as a result of increased vegetation water use efficiency, and suggest this will enhance hydrological buffering during drought. In order to test the potential impacts of these feedbacks on observational data, we assess trends in baseflow across a large climatic gradient in Australia and separate the contributions of precipitation, potential evaporation and 'other factors' on these trends. Using satellite based observations, our findings further reveal that these other factors influencing baseflow trends are best explained by an increase in photosynthetic activity. These results provide the first robust observational evidence that increasing atmospheric CO₂, and its associated vegetation feedbacks are reducing freshwater availability in already water-limited regions. In addition, these same feedbacks may be increasing baseflow within energy limited regions, which has large implications for the global distribution of available freshwater resources.

13.12

Integrated water management approaches – new paradigms

Luca Rossi^{1,2}

¹ *e-dric.ch, ch, du Rionzi 54, CH-1052 Le Mont-sur-Lausanne (luca.rossi@e-dric.ch)*

² *VSA, Swiss Water Association, bureau romand, Ch. De Mornex 3, 1003 Lausanne*

The quality of the receiving waters, lakes and rivers has improved overall in Switzerland since the 60s with the development of sewage systems, despite the demographic development and the proliferation of synthetic substances. More “soft” decisions such as substitution or prohibition of hazardous substances have also contributed to this situation. Nevertheless, many challenges are still present and are emerging in global water management. These challenges include climate change, constant increase of imperviousness on watersheds, multiplication of persistent synthetic substances, lack of financial resources ... There is a need to constantly develop new approaches, concepts and management tools.

Historically, different water sectors, directly related, were developed independently, in conjunction with the Swiss political organization. Thus, sewage system, wastewater treatment plants, and finally receiving waters are too often managed independently. This division has certainly helped in optimizing each sector, but conducted to lose the overview of the system as a whole. An integrated approach, promoting links between sectors, is necessary.

An integrated sewer network-receiving water approach was for example developed in Switzerland, related to the General Plan for Water Management (PGEE), mandatory for each commune. As part of the PGEE, urban wet-weather water management is based on the immission concept (Rossi et al, 2009), through the STORM directive (Brenni et al, 2007). For its implementation, we first need to set expectations and goals for the receiving waters and, depending on these objectives (immission), the acceptable emissions are defined (Figure 1).



Figure 1. Illustration of the “emission - immission” concept. Goals are defined in the receiving waters, in terms of « immissions », that allow to define the acceptable amount of discharges (emissions)

The receiving environment is somehow again at the center of discussions. This approach requires nevertheless skills in multiple areas, whether in urban hydrology, hydrobiology, ecotoxicology, etc. Thus, a transdisciplinary approach is necessary for its implementation.

STORM Directive is applied mainly for small streams. Only recently developments have focused on discharges in lakes. The Léman21 project (www.leman21.ch), based on the case of the Bay of Vidy in Lake Geneva, is focused on the link between micropollutants and their impacts on the lake environment. The project Elemo (www.lemo.ch) also allowed to better understand the lake environment and the link between the urban watershed and the potential impacts of substances released by human activities. Discussions are underway to define a “STORM Lake” approach, designed to better identify the impacts of urban wet-weather discharges to lake environments.

In these developments, the currents plays an essential role in estimating the impacts of discharges. 3D modeling tools in lacustrine environments, validated by field measurements, help in advancing towards a better understanding of implicated processes, but at the cost of a major effort for data acquisition and modeling. Hopefully, all lakes in Switzerland will be modeled, thus facilitating a better understanding of potential impacts.

In terms of water management, many projects are going in the direction of integrated management, including also sectors such as drinking water, hydrogeology, agriculture, recreational activities ... The main obstacle to this integrated vision, encouraged by the Confederation (Schaffner et al. 2009), is not related to technologies, but more institutional. Participants in a conference like the SGM can play a key role in integrated approaches, developing multidisciplinary research and analysis outside their research comfort zone.

Through various examples, this presentation will illustrate some case studies and will suggest ways to promote and develop an interdisciplinary and integrated approach for water management.

REFERENCES

- Brenni R., Elber F., Federer W., Fischer P., Flückiger M., Krejci V., Krummenacher R., Reichmuth U., Rossi L., Suter K. (2007). Rejets pluviaux urbains dans les eaux de surface (STORM). Directive pour la planification conceptuelle de mesures de protection. Association suisse des professionnels de la protection des eaux (VSA), Zürich, Switzerland
- Rossi L., Chèvre N, Fankhauser R, Krejci V. (2009) Probabilistic environmental risk assessment of urban wet-weather discharges: an approach developed for Switzerland. *Urban Water Journal* 6:5, 355–367.
doi:10.1080/15730620902934801
- Schaffner, Monika, Martin Pfaundler, Hugo Aschwanden, et Stefan Vollenweider. 2009. « Gestion des eaux en Suisse 2007 - Situation actuelle et thèses - Résultats de l'enquête ». OFEV, Agenda 21 pour l'eau.

13.13

Challenges of groundwater management and protection in urban areas – Examples from the Basel area

Peter Huggenberger, Horst Dresmann, Jannis Epting, Matthias Müller & Stefan Scheidler

Applied and Environmental Geology, Department of Environmental Sciences, University Basel
(peter.huggenberger@unibas.ch ; <http://aug/duw/unibas.ch>)

The urban agglomeration of Basel, located on the border with France and Germany, is one of the most dynamic economic regions in Switzerland and also constitutes an international and national transport hub. The groundwater resources of the region are located in aquifers made up of unconsolidated fluvial sediments in the valleys of the rivers Rhine, Birs and Wiese as well as in the vulnerable karst areas of the Tabular and Folded Jura. Among other impacts, the quality and quantity of groundwater is affected by the ongoing urbanization and the development of subsurface infrastructures. The densification of land use affects the availability of water resources and also leaves measurable traces in the groundwater.

Urban subsurface resources and especially urban groundwater bodies are particularly vulnerable to environmental impacts and their rational management is of major importance. Therefore, the development of optimization strategies should consider simultaneously the numerous impacts on urban subsurface resources, such as infrastructure development or groundwater and geothermal subsurface use.

Important issues of urban hydrogeology is the understanding of the changes due to the realization and operation of infrastructure projects in the underground, the use of groundwater for cooling or as a heat resource. Urban areas are also confronted with permanent use changes. This increasingly requires instruments that allow understanding and predicting the development of quantitative and qualitative issues concerning ground water resources, to recognize the impact of the various uses in a larger context and derive measures of resource protection.

Generally, infrastructure development in urban environments and associated alterations in land use only consider the benefits for the improved infrastructure itself and planning largely takes the pragmatic form of engineering for short-term economic objectives. This often leads to adverse effects concerning quantitative and qualitative issues of subsurface resources including groundwater flow regimes, induced natural hazards and use conflicts in general. Alternative approaches include the implementation of adaptive management schemes. Such schemes start with the definition of particular profiles of systems (i.e. water supply). Together with the identification of system profiles, specific targets can be defined that lead to overall goals for particular subsurface resources, in the case of groundwater i.e., the desired short and long-term development of urban groundwater resources. The conceptual approach we propose includes the combination of instruments that allow to adequately identifying influences of the various single impacts on the complete environmental system. Thereby, both impacts that only affect the system in its immediate vicinity and impacts with influence on the system on a regional scale are considered.

In recent years, the Applied and Environmental Geology group of the Basel University has developed, in cooperation and on behalf of the cantonal authorities BS and BL and in the context of transnational projects, a system of tools that make it possible to understand the current state of the different groundwater bodies in the Basel area. These tools are applied, tested and further developed in the context of the construction of subsurface transport infrastructure, thermal management of groundwater resources or scenarios techniques for the evaluation of river revitalisation measures in a transnational context.

REFERENCES

- Epting, J., Huggenberger, P., Dresmann, H., Wiesmeier, S., Zea, M. and Auckenthaler, A. 2015. Analyse von Grundwasserkörpern mit GIS. GIS-Tool GSIA - Basis für das Prozessverständnis der Interaktion von Grundwassersystemen. *Aqua & Gas* 7/8, 72-79.
- Epting, J. & Huggenberger, P. 2013. Unraveling the heat island effect observed in urban groundwater bodies - Definition of a potential natural state. *Journal of Hydrology* 501, 193-204, doi:10.1016/j.jhydrol.2013.08.002
- Huggenberger, P., Epting, J. & Scheidler, S. 2013. Concepts for the sustainable management of multi-scale flow systems: the groundwater system within the Laufen Basin, Switzerland. *Environmental Earth Sciences* 69, 645-661, doi:10.1007/s12665-013-2308-0.
- Huggenberger, P. and Epting, J. 2011. *Urban Geology - Process-oriented concept for adaptive and integrated resource management*, Springer, Basel.

13.14

Impact of nuclear produced thermal pollution on a lake with short residence time - what can models resolve?

L. Râman Vinnâ¹, A. Wüest^{1,2} and D. Bouffard¹

¹ *Physics of Aquatic Systems Laboratory, Margaretha Kamprad Chair, École Polytechnique Fédérale de Lausanne, Institute of Environmental Engineering, Lausanne CH-1015, Switzerland*

² *Eawag, Swiss Federal Institute of Aquatic Science and Technology, Surface Waters Research and Management, Kastanienbaum, Switzerland*

¹ *Corresponding author, e-mail love.ramanvinna@epfl.ch*

Introduction-Thermal pollution can have considerable influence on water temperature in freshwater systems notably affecting stratification (Kirillin et al., 2013). Consequences can be seen across the entire aquatic food web (Barnett, 1971; Cairns, 1971; Sylvester, 1972). The increased usage of aquatic systems as sinks and sources of heat necessitates detailed investigations of the impact of thermal pollution on lakes and reservoirs. Here we investigate the impact of thermal pollution on temperature and heat fluxes in the perialpine Lake Biel (7°10'E, 47°5'N, 39.3 km² and 74 m deep). The lake has a short hydraulic residence time of only 58 days and is under strong influence of the Aare tributary. The source of the thermal pollution, the Mühleberg Nuclear Power Plant, is located 20 km upstream. The plant emits 700 MW (18 W m⁻²) as cooling water into the Aare River. The aim of our study is to provide guidelines regarding model selection for studies of thermal pollution in similar aquatic systems.

Materials and methods-The thermal consequences for Lake Biel was investigated with two hydrodynamic models. The one-dimensional model SIMSTRAT (Goudsmit et al., 2002) and the three-dimensional model Delft3D-Flow <<https://oss.deltares.nl/delft3d>>. The power plant is up for decommissioning scheduled for 2019. The influence of thermal pollution was therefore investigated by running the models with and without thermal emission. The temporal variability of the lake was analyzed for a cold (April to March 2010/2011) and a warm period (April to March 2013/2014).

Results and discussion- We observe a strong seasonal dependence in the lakes response to thermal pollution. By removing the thermal pollution the lake cools down by ~ -0.3 °C between October and March. The corresponding value from April to September was ~ -0.1 °C. The impact was marginally stronger for the warm period compared to the cold period. The majority of thermal pollution (~60 %) leaves the lake through the Aare outflow. This is due to the lake's short retention time and the short distance between the Aare inflow and outflow (~8 km). Surprisingly we were able to reproduce this throughflow accurately even with the one-dimensional model. The reason being the high discharge of the Aare which quickly flushes the incoming heat out of the lake. The flushing was likewise observed in the three-dimensional model. This model could furthermore resolve the path of the river intrusion within the lake. We could identify periods where the river water travelled along the shoreline directly from the inflow to the outflow, thereby short-cutting the lake. Additionally the spatial impact of thermal pollution was, as expected, better resolved by the three-dimensional model. With observed temperature fluctuations up to -3.4 °C in Delft3D-Flow and -1.7 °C in SIMSTRAT.

We argue that three-dimensional models should be used to assess the spatial impact of extreme levels of thermal pollution, which can have severe impact on biota. For overall system assessment one-dimensional models are sufficient. However, care is required for aquatic systems with short distance between the thermal source input and outflow.

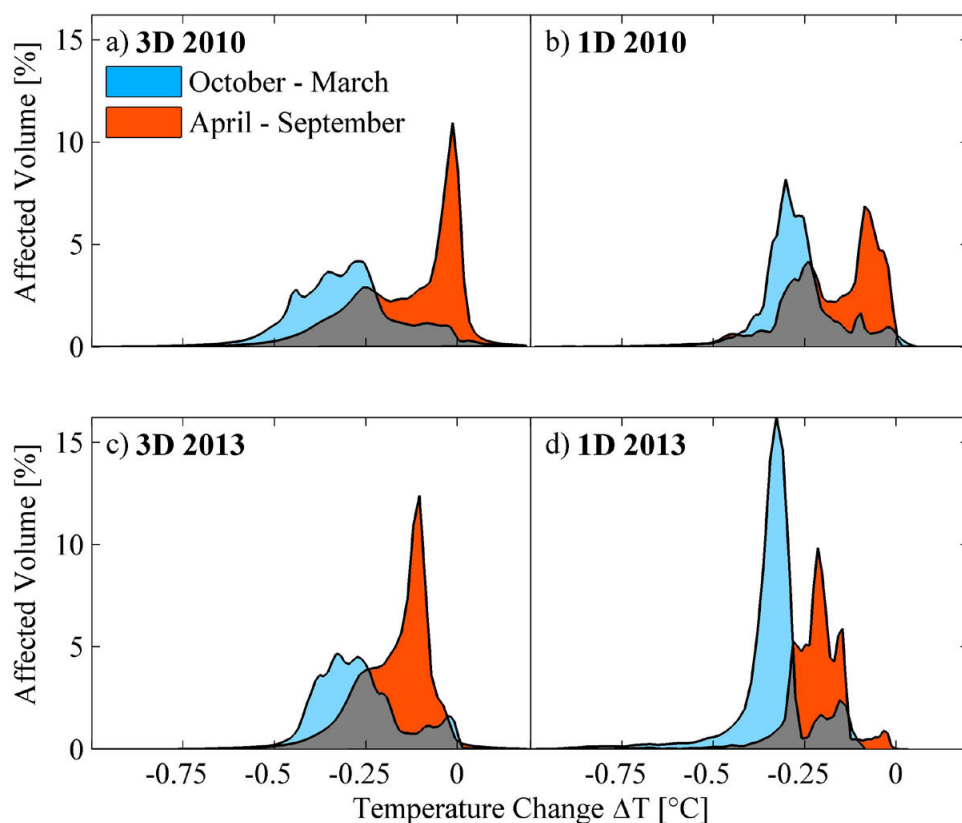


Figure 1. Temperature change in Lake Biel (ΔT) due to removal of thermal pollution. Displayed as percentage of total volume for Delft3D-Flow (a, c) and SIMSTRAT (b, d) during cold (a, b) and warm (c, d) period.

REFERENCES

- Barnett, P.R.O. (1971). Some changes in intertidal sand communities due to thermal pollution. *Proc. R. Soc. Lond. B Biol. Sci.* *177*, 353–364.
- Cairns, J. (1971). Thermal pollution: a cause for concern. *Water Pollut. Control Fed.* *43*, 55–66.
- Goudsmit, G.-H., Burchard, H., Peeters, F., and Wüest, A. (2002). Application of $k-\epsilon$ turbulence models to enclosed basins: The role of internal seiches. *J. Geophys. Res.* *107*, 3230.
- Kirillin, G., Shatwell, T., and Kasprzak, P. (2013). Consequences of thermal pollution from a nuclear plant on lake temperature and mixing regime. *J. Hydrol.* *496*, 47–56.
- Sylvester, J.R. (1972). Possible effects of thermal effluents on fish: a review. *Environ. Pollut.* *3*, 205–215.

13.15

Mass Flux of Micropollutants in Cities – Challenges in Urban Hydrogeology

Mario Schirmer¹, Andreas Musolff² & Dirk Radny¹

¹ *Eawag, the Swiss Federal Institute of Aquatic Science and Technology, Department Water Resources and Drinking Water, Ueberlandstr. 133, 8600 Dübendorf, Switzerland (mario.schirmer@eawag.ch)*

² *Helmholtz Centre for Environmental Research - UFZ, Department of Hydrogeology, Permoserstr. 15, 04318 Leipzig, Germany*

Urban areas are a focus of increasing conflict with regard to water use and water protection. More than half of the world's population (54%) and about 73% of Europeans live in cities (UN 2014). As a direct and/or indirect consequence of human activity, urban water systems are frequently polluted with organic contaminants. Many of those are related to human behaviour and activity, such as pharmaceuticals, personal care products (collectively PPCPs) and endocrine-active substances, and are increasingly found in urban water systems (Schirmer & Schirmer 2008). However, the fate and the effects of these contaminants in the environment have been widely unknown until now. Consequently, an interdisciplinary project on the assessment of risk of urban water pollution, focussing on PPCPs and endocrine-active substances, has been performed at the UFZ in collaboration with Eawag and other research partners. The aim was to explore new integrated methodologies (including flux calculations as well as chemical and biological investigations) for determining the impact of human activities on urban water systems and on processes within the urban watershed. The overall goal was to assess the risks to humans and the ecosystem, and to support the development of suitable management strategies.

Our research on urban water in large cities like Leipzig and Halle/Saale (Germany) focused on the source, distribution and transport behaviour of micropollutants as indicator substances for the anthropogenic impact on the urban water system (Schirmer et al. 2013). The micropollutants reported here are low concentrations of highly eco-toxic micropollutants including PPCPs and industrial chemicals, most of them can be endocrine disrupters. The concepts presented required a new methodology for assessing human activities on the urban water system and processes among urban watersheds. To this end, we used different approaches in relation to the hydrogeological and hydrodynamic situation of the cities of Leipzig and Halle.

In Leipzig in a first approach, we used a concept of various urban land uses and their influence on the urban water system. At both sites investigated, we demonstrated the use of indicators consisting of hydrological parameters and compound-specific patterns of complex organic substances. These indicators helped to balance urban substance fluxes and assess urban effects on surface water quality (Musolff et al. 2009).

In a further study, a new methodology to estimate mass flux from leaky sewers was developed. Using average concentrations derived by Integral Pumping Tests (IPT) up- and downstream of a leaky sewer, we calculated two mass flow rates. The difference between mass flow rates up- and downstream yields the mass flow rate per length of the sewer. For chloride, e.g., as wastewater indicator a mass flow rate $7.8 \text{ g m}_{\text{sewer}}^{-1} \text{ d}^{-1}$ was estimated.

The new methodology can be used in field studies to give average exfiltration rates from leaky sewers into groundwater for desired target substances under specific conditions. The results are more reliable than point sampling, because the heterogeneity of the exfiltration from the leaky sewer is overcome by this approach. The obtained values can be used as input for transport models in urban areas. The methodology is not suitable to obtain mass fluxes from a complete sewer network, because the effort for the operation of the pumping wells and the sample analysis in the laboratory is too large to realize it on a larger scale. The applicability of the new methodology also depends on background concentrations and exfiltration rates from the sewer. Due to dilution during pumping, a strong concentration difference between upstream groundwater and the potential source is needed to obtain reliable mass flow rates. Effects of sorption and biodegradation on the concentration distribution downstream of the leaky sewer have to be considered in future work on micropollutants.

In conclusion, identification of anthropogenic impacts on urban waters is often not easy by means of concentration measurements. In many cases, the concentration input is too low and retardation as well as degradation processes mask this influence. More promising is the investigation of the contaminant mass fluxes, although these methods are, by far, more extensive, especially as the water fluxes have to be determined using a model that integrates groundwater, surface water and soil water.

REFERENCES

- Musolff, A., Leschik, S., Möder, M., Strauch, G., Reinstorf, F. & Schirmer, M. 2009: Temporal and spatial patterns of micropollutants in urban receiving waters. *Environmental Pollution* 157 (11), 3069 – 3077.
- Schirmer, K. & Schirmer, M. 2008: Who is chasing whom? A call for a more integrated approach to reduce the load of micropollutants in the environment. *Water Science and Technology* 57(1), 145-150.
- Schirmer, M., Leschik, S. & Musolff, A. 2013: Current research in urban hydrogeology – A review. *Advances in Water Resources* 51, 280–291.
- United Nations (2014). *World Urbanization Prospects – 2014 Revision Highlights*. United Nations, New York.

13.16

Citizen science in hydrology: stream level observations and their potential value for constraining runoff models

Jan Seibert, Barbara Strobl, Simon Etter, Marc Vis and Ilja van Meerveld

Department of Geography, University of Zurich, Winterthurerstr. 190, CH-8057 Zürich

The project CrowdWater will explore opportunities for citizen science approaches in hydrology. Here, we present first results on one aspect, namely the potential value of crowd-based stream level observations for model calibration. Hydrological models with a low number of parameters are often able to simulate streamflow reasonably well but rely on model calibration, which makes their use in ungauged basins challenging. Stream levels are easier to measure than streamflow and can be observed by citizen scientists. We recently demonstrated that stream level data, instead of streamflow data, are useful for constraining a simple runoff model. This suggests that if stream level observations are available for otherwise ungauged catchments, these data can be used to constrain a runoff model and to generate simulated discharge time series from the level observations. However, the challenge with crowd-based stream level data is that observations are taken at irregular time intervals and with a limited vertical resolution. The latter is especially the case at sites where no staff gauge is available and relative stream levels are observed based on (in)visible features in the stream, such as rocks. Here, we pretend that stream level observations are available at a limited vertical resolution by transferring the data into stream level classes. The model was calibrated with these hypothetical data sets and subsequently evaluated on the observed streamflow record. Our results indicate that stream level data can result in good streamflow simulations, even with a reduced temporal resolution of the level observations. Time series of only two stream level classes, e.g. above or below a rock in the stream, were already informative, especially when the class boundary was chosen towards the highest levels. There was some added value in using up to five stream level classes but there was hardly any improvement in model performance when using more classes. These results are encouraging for citizen science projects and provide a basis for designing observation systems that collect data that are as informative as possible for deriving model-based discharge time series for previously ungauged basins.

13.17

Groundwater and low flows in Switzerland – Part 2: Efforts to consider the spatial component of groundwater surface water exchange in a bucket-type hydrological model

Maria Staudinger¹, Claire Carlier², Fabien Cochand², Jan Seibert¹, Philip Brunner²

¹ *Geographisches Institut, University of Zurich, Winterthurerstrasse 190, CH-8057 Zurich (maria.staudinger@geo.uzh.ch)*

² *Centre for Hydrogeology and Geothermics (CHYN), University of Neuchâtel, Emile-Argand 11, CH-2000 Neuchâtel*

Longer dry spells can become critical for water supply and groundwater dependent ecosystems. During these dry spells groundwater is often the most relevant source for streams. Hence, the hydrological behavior of a catchment is often dominated by groundwater surface water interactions, which can vary considerably in space and time. While classical hydrological approaches hardly consider this spatial dependence, quantitative, hydrogeological modeling approaches can couple surface runoff processes and groundwater processes. Hydrogeological modeling can help to gain an improved understanding of a catchment during low flow. However, due to their complex parametrization such hydrogeological models are not applicable for larger catchments or a set of several catchments. In these cases bucket-type hydrological models remain a practical alternative. In our project we try to combine the strengths of both the hydrogeological and bucket-type hydrological models to better understand low flow processes and ultimately to use this knowledge for low flow projections. Bucket-type hydrological models have traditionally not been developed with focus on low flow simulation. One consequence is that interactions between surface and groundwater are not explicitly considered. Water in bucket-type hydrological models is commonly simulated to flow only in one direction from the groundwater to the stream but not from the stream to the groundwater. This latter flux, however, can become important during low flow situations. We thus further developed the bucket-type hydrological model HBV to simulate low flow situations by allowing for exchange in both directions i.e. also from the stream to the groundwater. The HBV exchange box is developed by using a variety of hydrogeological models as training set. In this way processes that occur in different spatial settings within the catchment are translated to functional relationships and effective parameter values for the conceptual exchange box can be extracted. We show the development as well as the application of the HBV exchange box and compare the simulations to benchmark models without groundwater surface water interaction.

P 13.1

Transport and mixing in Lac Léman

Andrea Cimatoribus¹, Ulrich Lemmin¹ and D. Andrew Barry¹

¹ Ecological Engineering Laboratory (ECOL), IIE ENAC EPFL, Station 2, CH-1015, Lausanne (Andrea.Cimatoribus@epfl.ch)

Lake Geneva (Lac Léman) is the largest freshwater body in Western Europe. It is a deep peri-alpine lake whose importance stems from being not only an essential freshwater source in the region, but also a major tourist destination, a fishery and a waterway. Its dynamics have been the subject of long-term monitoring and study, and its response patterns to wind forcing (the major forcing) are relatively well understood (e.g. Lemmin et al. 2005). On the other hand, the large-scale organisation of the water circulation is less well known; the associated transport properties are even less clear.

The interest in the transport of water parcels inside the lake is linked to the inflow of sediments and pollutants from the tributaries, in particular from the Rhône River, the major one in terms of water and sediment discharged into the lake. Most of the sediments entering the lake through the Rhône are believed to sink in the eastern part of the lake (Giovanoli, 1990). More recently, Halder et al. (2013) traced, using stable isotopes, water parcels from the Rhône River in the entire lake basin. This study demonstrates that the water entering the lake from its main tributary has a complex distribution inside the whole basin. How this distribution is established and evolves in time is, however, mostly unknown.

The Ecological Engineering Laboratory of EPFL is trying to shed further light on this issue, by combining observational and numerical modelling tools. In particular, up to 6 Acoustic Doppler Current Profilers (ADCP's) have been simultaneously deployed at various locations inside the lake. This data, together with available historical data, is being used to validate a hydrodynamic model of the lake, implemented using Delft3D code.

Various passive-tracer release experiments were conducted using the numerical model, investigating the relative importance of wind-forcing, depth of release, stratification, and the Rhône discharge rate, for the spreading and mixing of the tracers. The preliminary numerical results confirm that the northern and southern coastal regions are preferred initial pathways for the transport of the Rhône discharge. More interestingly, the numerical simulations unmistakably show that the transport of the Rhône River water inside the lake is highly inhomogeneous in space, and highly intermittent in time, even ignoring the discharge variability itself. This intermittency should be taken into account, in particular when interpreting point measurements, isolated in time. From a practical point of view, this is likely to have an important effect on the nutrient and oxygen availability, as well as on the concentration of pollutants. From a more fundamental point of view, this study contributes to further understanding the mixing processes in rotating, stratified flows at length scales where rotation is an important but not the only dynamic process (Rossby number small but non-zero).

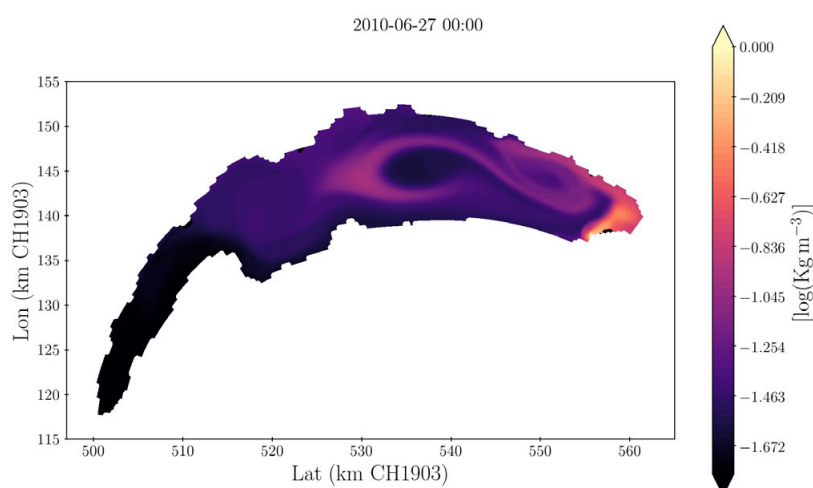


Figure 1. Filled-contours plot (logarithmic scale) of the simulated concentration of a passive tracer released from the Rhône river mouth (south-eastern end of the basin). The figure shows the results approximately 4 months after the beginning of the numerical simulation.

REFERENCES

- Giovanoli, F. 1990: Horizontal Transport and Sedimentation by Interflows and Turbidity Currents in Lake Geneva. In: Large Lakes: Ecological Structure and Function (Ed. by Tilzer M. M. & Serruya C.), Springer, Berlin, 175-195.
- Halder J., Decrouy L. & Vennemann T. W. 2013: Mixing of Rhône River water in Lake Geneva (Switzerland-France) inferred from stable hydrogen and oxygen isotope profiles, *Journal of Hydrology*, 477, 152-164.
- Lemmin, U., Mortimer, C. H. & Bäuerle, E. 2005: Internal seiche dynamics in Lake Geneva, *Limnology and Oceanography*, 50, 207-216.

P 13.2

Monitoring of alpine lakes: approach and results from Canton Ticino

L. Colombo¹, Fabio Lepori¹, M. Pozzoni¹, S. Steingruber², A. Bruder¹ & S. Pera¹

¹ *Department for Environment Constructions and Design, University of Applied Sciences and Arts of Southern Switzerland, Campus Trevano, Via Trevano, CH-6952 Canobbio (fabio.lepori@supsi.ch)*

² *Ufficio aria, clima e energie rinnovabili, SPAAS, DT Canton Ticino, Via Franco Zorzi 13, CH-6500 Bellinzona*

Alpine environments are facing global pressures including climate warming and deposition of air pollutants. The southern slope of the Central Alps (including Canton Ticino, Switzerland) is highly affected, due to its proximity to the heavily industrialised Po Valley, Italy. For example, in Canton Ticino, atmospheric deposition of nitrogen (N) ranks among the highest recorded in mountain areas worldwide (up to 30-40 kg ha yr⁻¹; Steingruber, 2015) while regional temperatures have been increasing nearly twice as fast as the global average (MeteoSwiss, 2016).

To evaluate the effects of these pressures on the alpine catchments of Canton Ticino, the Swiss Federal Office for the Environment (FOEN) has funded a twofold programme of environmental monitoring. One programme, coordinated by the canton-level environmental protection agency, comprises the extensive survey of 20 mountain lakes and three streams. The second programme, run by the University of Applied Sciences and Arts of Southern Switzerland, focuses on the catchment of one of the lakes included in the extensive survey (Lago Nero), which is however monitored more intensively. The goals of these programmes are complementary. Whereas the extensive monitoring was designed to assess the spatial extent of the impacts of atmospheric deposition, the intensive programme aims at developing predictive models of ecosystem responses to environmental change. Together, these programmes contribute to form a basis for decisions on environmental management at national and international levels. The international influence of these programmes is enhanced through the participation to working groups within the Convention on Long-range Transboundary Air Pollution of the UNECE, namely the international cooperative programmes on waters (ICP-Waters, which involves the extensive programme) and integrated monitoring (ICP-Integrated Monitoring, which involves the intensive programme).

Surveying methods vary according to the programme goals. The extensive monitoring programme places emphasis on the chemistry of surface waters during the ice-free season, although biological responses (benthic invertebrates) are also measured at a subset of lakes. The intensive programme at Lago Nero measures a wider array of ecosystem responses, including runoff quantity and chemistry, catchment soil composition and the species composition of terrestrial vegetation. Sampling frequency depends on the response, varying from nearly continuous (e.g. runoff) to every five years (e.g. soil and vegetation).

The extensive programme has been running for over 30 years and has yielded most results so far. A main goal of the programme was to assess the effects of acid deposition, which was most severe in the 1970s and 1980s. The long-term results have chronicled a remarkable recovery in the chemistry of the deposition and the water of receiving lakes, which reflects international efforts to manage sulfur (S) emissions (Rogora et al., 2013). For example, between the early 1980s and 2013, most of the lakes have displayed trends toward lower concentrations of sulfate (13 of 20 lakes) and higher alkalinity (14 of 20). However, nitrate has decreased less frequently (7 of 20), probably because N deposition has declined comparatively less and more lately than S deposition.

The intensive programme started in 2014 with a pilot study, and the results are preliminary. Nonetheless, the high N concentrations recorded at the outlet throughout the 2014-2015 hydrological year (including the vegetative season) indicate that the soils of Lago Nero's catchment have become saturated with this nutrient (Stoddard, 1994). The leaching of N to surface waters, including the lake itself, means that these waters may be affected by enriching (eutrophying) effects, including increased biomass of phytoplankton and phytobenthos, and (potentially) a reduced efficiency in the transfer of nutrients and carbon through the food web (Lepori & Robin, 2014). Future investigations will examine these responses more closely, as well as other ecosystem features, such as the timing of ice-out and snow melt, runoff generation and the temperature of surface waters.

Mountain catchments offer valuable vantage points to monitor global environmental changes, because they are often remote and free from local pressures. Moreover, because of their vulnerability, these catchments are considered to be among the most sensitive sentinels of environmental change (Beniston et al., 1997). As climate warms and N deposition increases at the global scale, monitoring programmes in mountain catchments will become increasingly important to detect the effects as early as possible and prevent damage to these important landscape features. Because the southern slope of the Alps appears to be changing particularly fast, monitoring programmes in this region might play an especially important role in detecting early signal of change.

REFERENCES

- Beniston, M., Diaz, H. F. & Bradley, R. S. 1997: Climatic change at high elevation sites: an overview. *Clim. Change* 36: 233–251.
- Lepori, F. & Robin, J. 2014: Nitrogen limitation of the phytobenthos in Alpine lakes: results from nutrient-diffusing substrata. *Freshwater Biol.*, 59, 1633-1645.
- MeteoSwiss. 2016. Trend climatici della Svizzera. www.meteosvizzera.admin.ch
- Rogora, M., Colombo, L., Lepori, F., Marchetto, A., Steingruber, S., & Tornimbeni, O. 2013: Thirty years of chemical changes in alpine acid-sensitive lakes in the Alps. *Water, Air, & Soil Pollut.* 224, 1-20.
- Steingruber, S. 2015: Deposition of Acidifying and Eutrophying Pollutants in Southern Switzerland from 1988 to 2013. *Boll. Soc. Tic. Sc. Nat.*, 103, 37-45.
- Stoddard, J.L. 1994: Long-term changes in watershed retention of nitrogen: its causes and aquatic consequences. In: Baker, L.A., ed. *Environmental chemistry of lakes and reservoirs: advances in chemistry*, Ser. No. 237. Washington, DC: American Chemical Society: 223-284.

P 13.3

Trend of drought conditions based on meteorological index detection in the Upper Rhone River Basin, Valais, Switzerland

Javier Fluixá-Sanmartín¹, Javier García Hernández¹ & Samuel Alesina¹

¹ Centre de recherche sur l'environnement alpin (CREALP), Rue de l'Industrie 45, CH-1950 Sion (javier.fluixa@crealp.vs.ch)

Drought is a phenomenon resulting from persistent low precipitations that generally affects larger areas and more people than any other natural catastrophes. It is commonly classified as meteorological (rainfall deficiency), agricultural (insufficient soil moisture) and hydrological (deficient surface and subsurface water supply) droughts. Comprehensive hydro-meteorological monitoring of drought requires a variety of indicators and indices that accurately reflect and represent the impacts being experienced during drought events.

Among different available meteorological indices, the Standardized Precipitation Index (SPI) stands out. The SPI (McKee et al. 1993) uses historical precipitation records for a given location and can be easily computed for various timescales, from 1 to 48 months or longer, with different available tools (e.g. Travaglini et al. 2016). Its analysis enables the detection of drought events, thus leading to effective monitoring (Hayes 2011). SPI can be used to identify short periods of precipitation deficiency –related to meteorological droughts– as well as long periods –related to agricultural or hydrological droughts (WMO 2012).

This approach was applied to the Upper Rhone River Basin, located in the Alps upstream of Lake Geneva, in Switzerland. Covering a surface of 5'524 km² with 658 km² of glaciers, this basin is characterized by elevations varying from 372 to 4'634 meters. Using historical rainfall data from 1981 to 2015, the SPI was calculated for 13 meteorological stations situated within and to the proximity of the basin and for timescales of 1, 6, 12 and 24 months.

The analysis of the 24 month SPI helped identifying two main consistent dry periods throughout the studied area in 2004-2005 and 2010-2011 (see example of Zermatt in Figure 1). In addition, a trend analysis using the Mann-Kendall test was performed (Figure 2) and showed a general decreasing trend of the SPI values, which indicate the worsening of dryness conditions over the study period. A Mann-Kendall test applied to the meteorological data set also indicates general decreasing of rainfall and increasing of temperature.

Based on meteorological data, the present study reveals a deterioration of climatic conditions from 1981 to 2015 in the Upper Rhone River Basin that may result in drier periods, and even in drought events, in the future. Moreover, demographic, agricultural and climate change may lead to a reduction and over-exploitation of water resources, and further threat of water supply with expected socio-economic and environmental consequences.

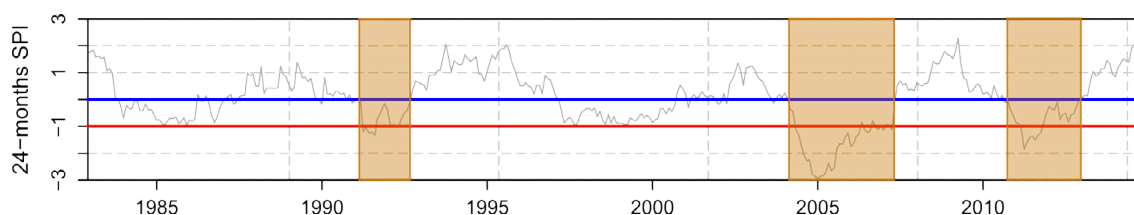


Figure 1. Evolution of SPI values resulting from the Zermatt meteorological station. Red/blue thresholds (McKee et al. 1993) used for the detection of SPI-based droughts (in orange).

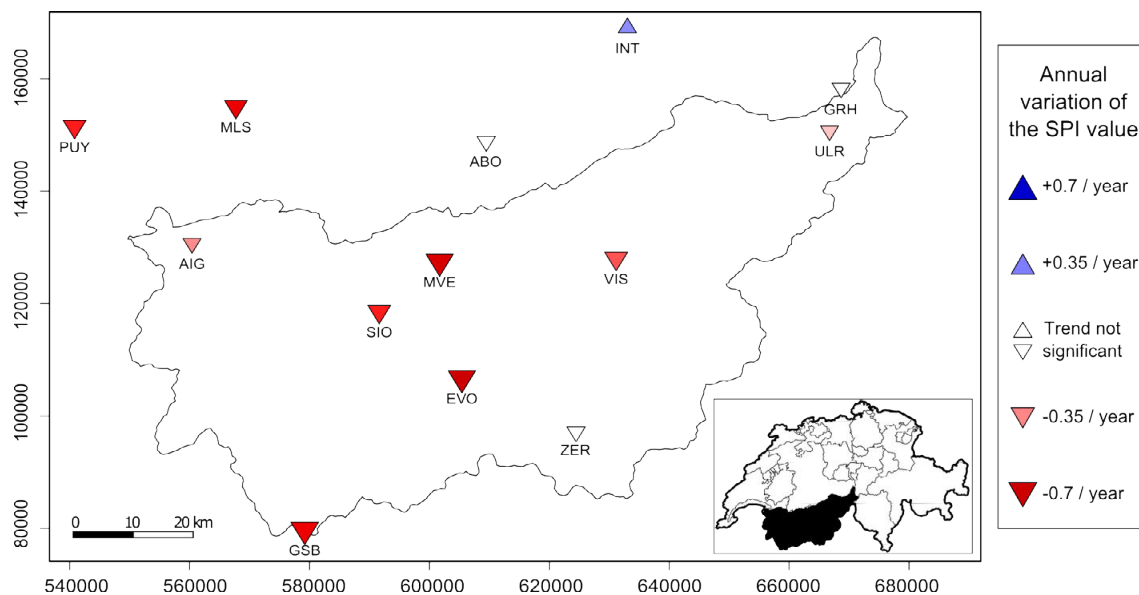


Figure 2. Trends in the SPI values between 1981 and 2015, with a 95% level of significance.

REFERENCES

- Hayes, M.J. 2011: Comparison of Major Drought Indices: Introduction. National Drought Mitigation Center.
- McKee, T.B., N.J. Doesken, and J. Kleist 1993: The relationship of drought frequency and duration to time scales. Proceedings of the 8th Conference on Applied Climatology, 17–23 January 1993, Anaheim, CA. Boston, MA, American Meteorological Society.
- Travaglini, E., Fluixá-Sanmartín, J., Alesina, S., Foehn, A. and García Hernández, J. 2016: TeREsA – User's Manual v1.0. CREALP Group, Switzerland.
- World Meteorological Organization (WMO) 2012: Standardized Precipitation Index - User Guide. WMO-No. 1090.

P 13.4

Riverine export of organic carbon during extreme precipitation events

Hannah Gies¹, Silvan Wick², Maarten Lupker¹, Chantal Freymond¹, Francien Peterse³, Negar Hagiphour¹, Timothy Eglinton

¹ *Institute of Geology, ETH Zürich, Sonneggstrasse 5, 8092 Zürich, Switzerland (hgies@ethz.ch)*

² *Eawag, Department of Water Resources and Drinking Water, Swiss Federal Institute of Aquatic Science and Technology, CH-8600 Dübendorf, Switzerland*

³ *Utrecht University, Department of Earth Sciences, 3584 CD Utrecht, the Netherlands*

The riverine export of biospheric carbon to the ocean, where it is eventually deposited in marine sediment and hence preserved from oxidation, is an important long-term carbon sequestration mechanism. In actively eroding areas, high discharge events appear to generate high export fluxes of particulate organic carbon (POC). These events mobilize larger proportions of modern organic carbon over petrographic carbon in comparison to background discharges, probably due to topsoil erosion (e.g. Hilton et al., 2012; Smith et al., 2013). However, detailed information on the sources and mechanisms of organic carbon mobilization in the stream network is still scarce.

The POC exported by three alpine headwater catchments in the Alphal (Central Swiss Alps) was sampled during rainfall and analyzed for alkanes, n-alkanoic acids and glycerol dialkyl glycerol tetraethers (GDGTs). The results were compared to samples collected during background conditions.

This study aims to describe the response of different biomarkers to rising discharges to quantify the influence of hydrology on the exported biomarker signal of the POC and, if possible, to fingerprint the sources of the carbon in the landscape that are mobilized with increasing discharge. Additionally, the results were compared to a series of samples taken further downstream, on the Sihl River, to see how the signal from the first-order tributaries impacts the composition of POC in higher order streams.

Preliminary results suggest that all biomarkers respond to changes in discharge, however the changes are small introducing large uncertainties in the carbon source fingerprinting. Nevertheless, the results point out the need to conduct biomarker studies in upstream reaches of the fluvial network at representative discharges (i.e. above average background discharges) to avoid influences from hydrology. In the Sihl River, discharge does not influence the biomarker content of POC anymore but seasonal controls seem more dominant.

REFERENCES

- Hilton, R. G., Galy, A., Hovius, N., Kao, S. J., Horng, M. J., & Chen, H. (2012): Climatic and geomorphic controls on the erosion of terrestrial biomass from subtropical mountain forest. *Global Biogeochemical Cycles*, 26(3).
- Smith, J. C., Galy, A., Hovius, N., Tye, A. M., Turowski, J. M., & Schleppe, P. (2013): Runoff-driven export of particulate organic carbon from soil in temperate forested uplands. *Earth and Planetary Science Letters*, 365, 198-208.

13.5

Numerical investigation with a coupled single-column lake-atmosphere model: An application to Western Switzerland

Stéphane Goyette

Institute for Environmental Sciences, University of Geneva, 66 boulevard Carl Vogt, 1205 Geneva

The potential of a novel atmospheric single-column model (SCM) developed in the framework of the Canadian Regional Climate Model, CRCM, driven by NCEP-NCAR reanalyses is investigated. The approach to solve the model equations and the technique described here may be implemented in any RCM system environment as a model option. The working hypothesis underlying this SCM formulation is that a substantial portion of the variability simulated in the column can be reproduced by processes operating in the vertical dimension and a lesser portion comes from processes operating in the horizontal dimension. This SCM offers interesting prospects as the horizontal and vertical resolution of the RCM is ever increasing. Due to its low computational cost, multiple simulations may be carried out in a short period of time. In this paper, a range of possible results from changing the lower boundary from land to open water surface, and varying model parameters are shown for western Switzerland (Fig. 1). The benefit of using Newtonian relaxation, or “nudging”, is demonstrated. Results show that air temperature, moisture and windspeed profiles are modified in a coherent manner in the lowest levels. Such changes are consistent with those of the surface vertical sensible, latent heat and momentum fluxes. Compared to atmospheric profiles over land, switching to and open water surface representative of Lake Geneva over the annual cycle of 1990, air temperature is increased by up to 1°C during the autumn and winter seasons, and by 0.5°C during the spring and summer seasons. Specific humidity is increased by up to 0.2 g kg⁻¹ during the autumn and winter seasons and decreased by 0.3 g kg⁻¹ during the spring and summer seasons. The increased windspeed at the surface, often more than 1.5 m s⁻¹, is due to the smaller roughness height. The surface radiation and energy budgets are also modified subsequent to the different partitioning of the latent and sensible heat fluxes, but also the solar and thermal infrared fluxes undergone significant changes. The question of how the open water and the overlying atmosphere interact and which of these “factors” has the most influence also needs attention. The sole presence of the lake is shown to be a major feature with regard to the surface energy budget components whose contributions counteract those of the lower atmosphere, thus supporting the fact that Lake Geneva acts as a damping factor to the regional climate system. It is also shown that not only did the presence of the lake and the overlying atmosphere independently modulate the surface energy budget, but also the synergistic nonlinear interaction among them, either positive or negative, was often found non-negligible. Moreover, some processes may turn out to be important on short time scales while being negligible on the long term as shown in Goyette (2016).

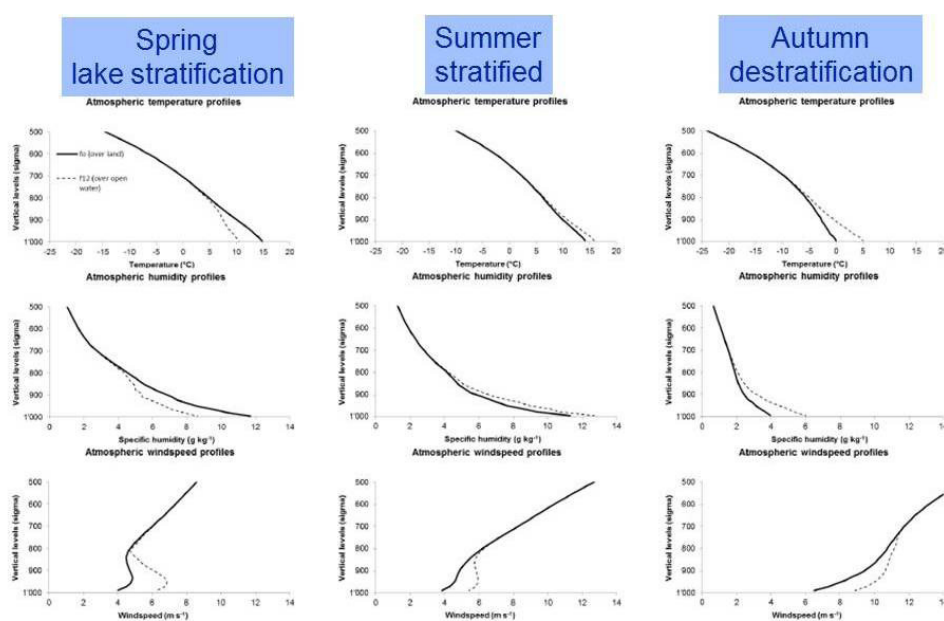


Figure 1. Atmospheric boundary-layer temperature, specific humidity, and windspeed mean profiles over land and open water surfaces for three one-month time-periods, selected for the analysis of this case study.

REFERENCES

Goyette, S., 2016: Numerical investigation with a coupled single-column lake-atmosphere model: using the Alpert–Stein factor separation methodology to assess the sensitivity of surface interactions. *Climate Dynamics* [in press].

P 13.6

The effects of model complexity and calibration period on groundwater recharge predictions

Christian Moeck¹, Jana Van Freyberg², Mario Schirmer^{1,3}

¹ *Eawag, Swiss Federal Institute of Aquatic Science and Technology, Dübendorf, Switzerland (christian.moeck@eawag.ch)*

² *ETH Zurich, Institute of Terrestrial Ecosystems, Environmental Systems Science, Zurich Switzerland*

³ *Centre of Hydrogeology and Geothermics (CHYN), University of Neuchâtel, Neuchâtel, Switzerland*

Numerous groundwater recharge models exist that vary in terms of model complexity and structure (Crosbie et al., 2011; von Freyberg et al., 2015). Complex physically based models are often considered to be more robust in the predictions, however, the computational expenses might constrain their use for certain applications (e.g., long-term predictions of climate change scenarios). A few studies indicate that model robustness in more simple models can be enhanced with longer calibration periods that contain climatically contrasting conditions (Moeck et al., 2016). In that context, an implicit assumption is made that model parameters calibrated over historical periods are also valid for the predictions. However, non-stationarity of model parameters can occur, suggesting that certain historic time periods might be more useful for the identification of the parameter space while others might be less informative. Very few studies exist which investigate the effect of chosen model complexity and calibration period on performance and robustness of groundwater recharge models.

Therefore, we systematically compared four groundwater recharge models (soil-water balance equation, lumped models and physically-based models) within a stochastic framework by using a long-term data set from a large-scale weighting lysimeter in northern Switzerland. To evaluate model robustness, all models were calibrated on lysimeter recharge data with six different calibration periods that cover a wide range of contrasting climatic conditions, i.e. from very wet to very dry. We then analysed the models' performance for climatic conditions that were very different to those during the calibration periods (differential split sample test).

We demonstrate that an acceptable model performance during the calibration period does not ensure reliable groundwater recharge predictions under contrasting climatic conditions. The deviations between simulated and observed groundwater recharge, however, is a function of the chosen model complexity. We also show that the more complex, physically-based models best reproduced observed recharge, even when calibration and prediction periods had contrasting climatic conditions. In contrast, the performance of the soil-water balance model and the lumped model depended strongly on the chosen calibration period. Our analysis suggests that the uncertainty in model parameters was less important than the model structure itself, so that the robustness of each individual model followed the degree of model complexity. It can be argued that physically-based models have a greater potential to obtain predictions beyond the range of conditions during calibration. It is however, still difficult to provide general guidelines on how to choose an optimal calibration period, since model performance seems to depend more on the model complexity and structure rather than on the calibration period. The results obtained here have important implications when using recharge models as decision-making tools in a wide range of applications (e.g. water availability, climate change impact studies, water resource management, etc.).

REFERENCES

- Crosbie, R.S. et al., 2011. Differences in future recharge estimates due to GCMs, downscaling methods and hydrological models. *Geophys Res Lett*, 38.
- Moeck, C., Brunner, P., Hunkeler, D., 2016. The influence of model structure on groundwater recharge rates in climate-change impact studies. *Hydrogeol J*: 1-14.
- von Freyberg, J., Moeck, C., Schirmer, M., 2015. Estimation of groundwater recharge and drought severity with varying model complexity. *J Hydrol*, 527: 844-857.

P 13.7

Dynamism of spatial planning to improve management of urban expansions and the effect of water resources of Meknes city. Contribution of multisource spatial imagery.

Soufyane.NASRI¹, Mustapha.HAKDAOUI¹, Bouamar.BAGHDAD¹

¹ *Remote sensing and GIS applied to Geosciences and Environment Team, Sciences Faculty Ben M'sik Casablanca, Boulevard Cdt Driss Harti, BP 7955, Ben M'Sik (s)*

¹ *Hassan II Institute of Agronomy and Veterinary Medicine Hassan II*

This work concerns the dynamics of land use in Meknes city using multi-temporal, multi-source data and multi-sensors. In order to move towards good design development of the city.

the main objective of this study is to analyze the problems caused by urban development of Meknes city, the effects of urban and peri-urban expansion on the environment by studying the environmental factors that are leading this development (climate, humidity, hydraulics, agricultural networks, etc.) and spatial factors (direction of propagation, form of city form of buildings and neighborhoods, etc.) to get ideas on the scenarios of urban expansion and management integrate new strategies to control new issues and criteria to be temporal, spatial planning for better. This work is based on several data and methods such as (multi-date imagery satellite, land uses plans, land management, and other factors).

The results are thematic satellite imagery and interpreted and analyzed maps, in order to have results in good well-planned design city for best urban management.

REFERENCES

- [1] C.M. Mertes, A. Schneider, D. Sulla-Menashe, A.J. Tatem, B. Tanf, "Detecting change in urban areas at continental scales with MODIS data 158 (2015) 331–347" Science Direct, Elsevier Inc 2014.
- [2] Wang, L., Li, C., Ying, Q., Cheng, X., Wang, X., Li, X., et al. (2012). China's urban expansion from 1990 to 2010 determined with satellite remote sensing. Chinese Science Bulletin, 57, 2802–2812.
- [3] World Bank (2014). Mapping a Decade of Urban Change: East Asia, 2000-2010. Washington DC: World Bank Publications (in press).

P 13.8

Hydrological-hydraulic modelling of the Lake of Zürich for future flood protection

Norina Andres¹, Michel Kuhlman², Benno Zuend³, Markus Federer⁴, Massimiliano Zappa¹

¹ *Swiss Federal Institute for Forest, Snow and Landscape Research WSL, Zürcherstrasse 111, 8903 Birmensdorf*

² *TK Consult AG, Hallenstrasse 10, 8008 Zürich*

³ *Pöyry Schweiz AG, Herostrasse 12, P.O. Box, 8048 Zürich*

⁴ *Office of Waste, Water, Energy and Air / WWEA, Canton of Zürich, Walcheplatz 2, 8090 Zürich*

Large parts of the city Zürich are built upon the fan delta of the river Sihl. This is a densely built up area, with partly sensible infrastructure like the central railway station and shops, all with high damage potential. During the flood in 2005 no great damages occurred, but this event showed the vulnerability of the city Zürich. A subsequent assessment indicated that there is acute need for action regarding flood management in the catchment of the lake Zürich – river Sihl – river Limmat. Based on these findings, the WWEA (cantonal Office of Waste, Water, Energy and Air of the Canton of Zürich) initiated the implementation of various short and medium term measures. In parallel the planning of a long-term flood protection of the river Sihl was launched. In a first phase different solutions were studied. Finally, two concepts were evaluated: a “bypass discharge tunnel” (DT) in the lower section of the lake Sihl, hereafter called “spillway tunnel” (ST) and a “combination solution energy” (CSE), where the hydropower plant at the lake Sihl is upgraded and additional water can be released from the lake Sihl to the lake Zürich.

With the numeric hydrological model PREVAH the discharge was simulated, which provided the input data for the hydraulic 1d-model FLORIS and a 2d-model of the river branch at the outlet of the lake Zürich. Scenarios of accumulated precipitation with return period of 300 years for durations of 48 and 72 hours have been designed and propagated through the system. By laying the focus of the rainfall over one of these sub-basins and by assigning to the remaining areas a precipitation scenario with a 50 years return period.

The hydraulic model FLORIS simulated the lake level and the discharge of the river Sihl and Limmat, both without and with the relief concepts ST, DT and CSE. Furthermore, the hydraulic 2d-model BASEMENT allowed exploring the sensitivity of the channel between the lake outlet and the river-runout power plant located at Zürichweir Platzspitz. Simulation experiments identified that ST, DT and CSE have impact on the level of the lake of Zürich. Nevertheless, the diversion of water from the Sihl catchment into the lake Zürich has for a 300-year precipitation event a comparatively small influence on the level of lake Zürich. Under the actual configuration, the lake Zürich level could additionally rise about 5 cm in case of a diversion of water from the Sihl catchment.

This study proved that the diversion of the river Sihl, either with ST, DT or CSE, would not affect drastically the residents along the lake Zürich. But the water level rise of about 5 cm might cause increased vulnerability to damages. Adequate solutions to compensate for these effects are needed. A first option in this respect is the preventive drawdown of the lake Zürich level before a possibly critical event. A timely decision in this respect based on flood forecasts could compensate for the additional flood volume stemming from the diversion of the river Sihl. Furthermore, the 2d hydraulic simulations demonstrated that several local construction measures in the river branch between the lake Zürich outlet and the weir Platzspitz could contribute to increase the outflow capacity of the lake and thus reduce the impacts of ST, DT and CSE.

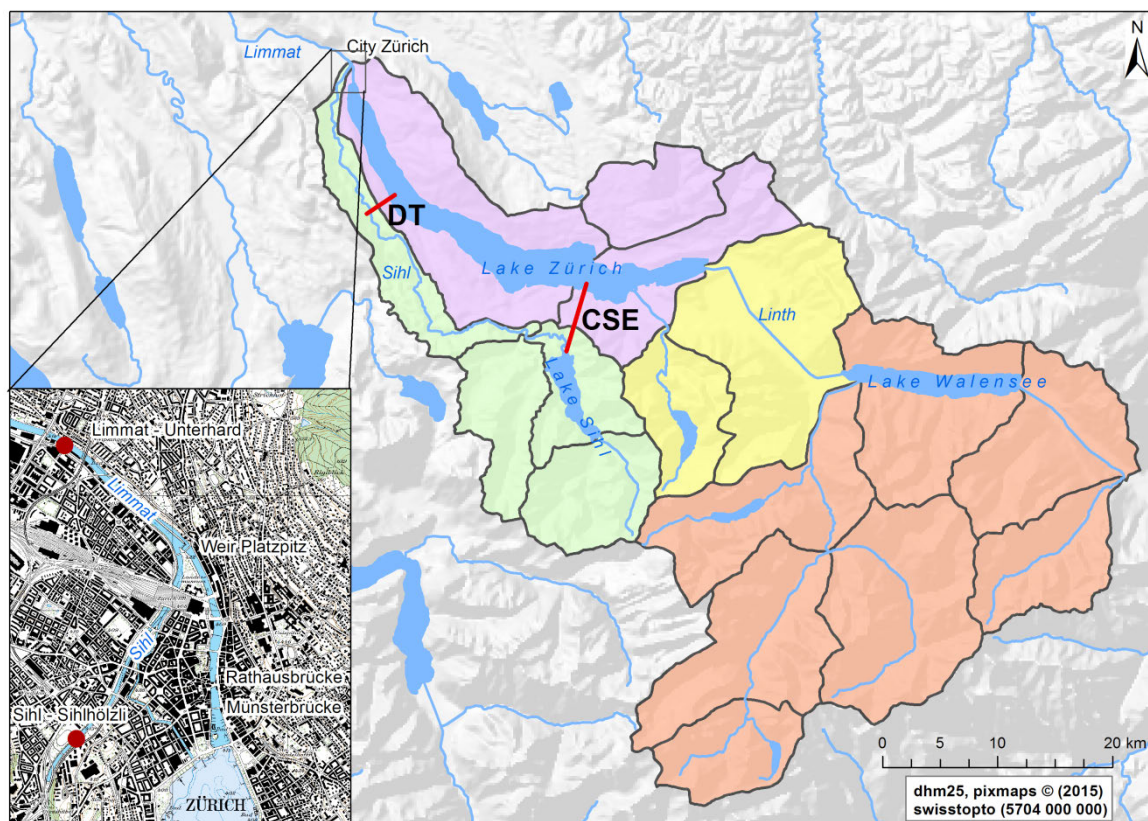


Figure 1 Catchment of river Sihl and Limmat with sub-basins "river Sihl" (green), "lake Walensee" (red), "plain of the river Linth" (yellow) and "basin of the lake Zürich" (violet); water deviation concepts: "spillway discharge tunnel" (STDT) and "combination solution energy" (CSE). Small map: confluence of river Sihl into Limmat with hydrological measurement stations at Sihlhölzli and Unterhard and with the weir Platzspitz which regulates lake Zürich. GIS elements reproduced by kind authorization of "swisstopo" (JA022265), BFS GEOSTAT/BUWAL.

P 13.9

Assessment of recent flood events at Muttenz, Switzerland.

Daniela Pavia Santolamazza¹ & Henning Lebreuz¹

¹ Institute of Civil Engineering, University of Applied Sciences and Arts Northwestern Switzerland FHNW, Gründenstrasse 40, CH-4132 Muttenz (daniela.pviasantolamazza@fhnw.ch)

On the current year intense rain events have led to flooding at the Municipality of Muttenz, on the Northwestern Switzerland. The floods took place at the point where the 'Dorfbach' stream (small drainage basin of approximately 5.5 km²) is diverted through a separate sewerage system until the Rhine River. At the inlet of the conduit, an overflow to the combined sewerage towards the treatment plant is allowed, for increasing the capacity of the water drained.

The objective of this study is not only the assessment of the capacity of the sewerage under the weather conditions of May 14th and June 25th, but also to understand the occurrences of the floods. For evaluating the sewerage system, a SWMM model is developed (using the information of the net given by the municipality). To judge the floods incidences in terms of the capacity of the sewerage, the model is run with the precipitation estimations of radar images provided by MeteoSwiss, which were improved using the measurements at the station Schweizerhalle of the 'Lufthygieneamt beider Basel'.

Precipitation events are furthermore investigated independently, rating the fallen amount of water in comparison to previous years and evaluating the catchment respond to both meteorological events. An analysis of the events' behaviour is performed to identify hydrological effects and conditions that led to the inundations, using the concept of entropy to describe the rain distribution within the days.

With this study it is possible to conclude that even though the capacity of the sewerage was not enough to drain the water of the stream, both storm events are over the established design thresholds, highlighting the necessity to understand the mechanisms that lead to floods in small drainage basins to be able to account their responses in the designs.

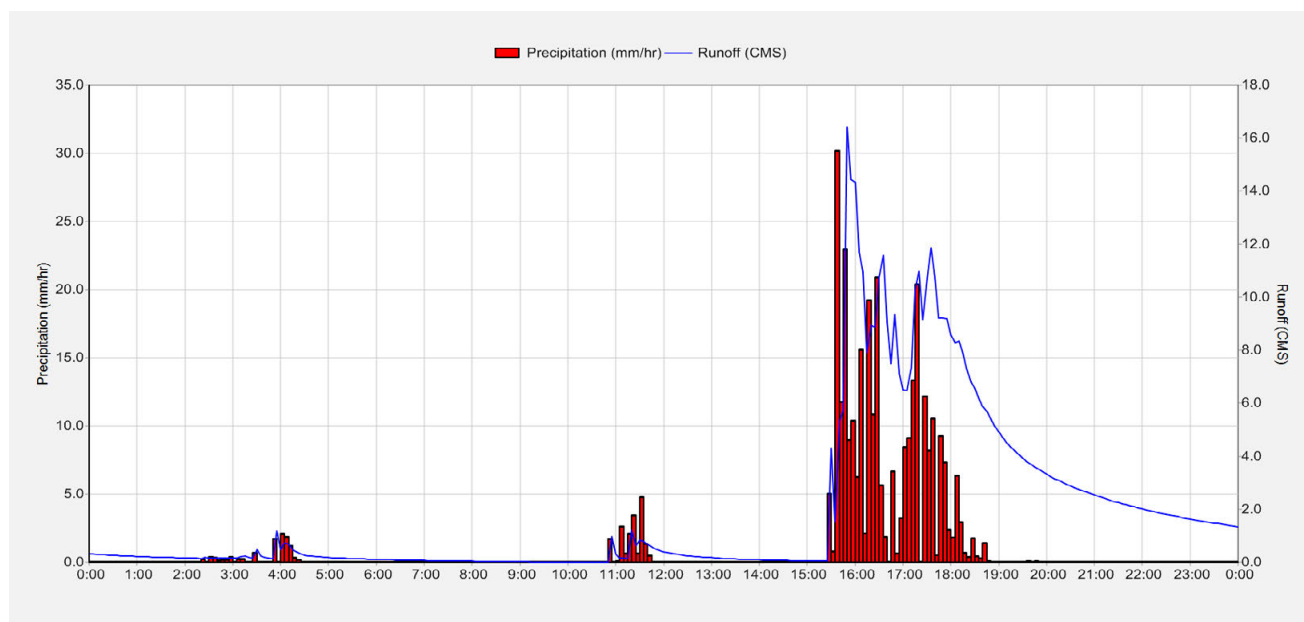


Figure 1. Rainfall-Runoff for the Dorfbach stream modelled with SWMM.

P 13.10

GeoQuat project: realization of groundwater volumes and vulnerability maps based on 3D parametric modeling

Giona Preisig¹, Stefan Volken¹, Michael Gaehwiler¹, Andreas Möri¹ & Michael Sinreich²

¹ Federal Office of Topography swisstopo, Swiss Geological Survey (SGS), Seftigenstrasse 264, CH-3084 Wabern bei Bern (Giona.Preisig@swisstopo.ch)

² Federal Office for the Environment, Hydrogeological Basics Section, Papiermühlestrasse 172, CH-3063 Bern-Ittigen

In Switzerland, Quaternary deposits have been widely explored for hydrogeological, geotechnical or geothermal purposes, in particular by means of boreholes. For instance, about half of drinking water supply comes from aquifers located in Quaternary formations. The GeoQuat project has been therefore launched by the Federal Office of Topography swisstopo in cooperation with the Federal Office for the Environment FOEN and the Federal Office of Energy SFOE in order to i) develop a system for structured storage of unconsolidated rock data (QLG database), ii) realize 3D geological and parametric models (voxel models) of Quaternary deposits, and iii) make them accessible to users working in the different fields of applied geology. The first task mainly consists in data harmonization and pre-processing, while the second and third include data processing (modeling) and post-processing. Specifics about data harmonization, pre-processing and modeling are detailed in Volken et al. (2016). In this abstract, the focus is given on the post-processing of 3D parametric models for deriving exemplified maps of groundwater volumes and groundwater vulnerability.

3D parametric models aim to simulate the heterogeneity of material properties, such as the spatial distribution of hydraulic conductivity (K). One of the simplest and straightforward method for realizing 3D parametric models is geostatistical processing coupled with voxel modeling. In this framework, a volume is subdivided into regular cells (voxels) and geostatistical algorithms, e.g. kriging, are subsequently used to interpolate available raw data to each voxel. In GeoQuat, all lithological layers in the QLG database are classified through the Unified Soil Classification System (*USCS*). On the basis of a norm (e.g. SIA SN 670'010) or on a methodology taking into account the grain size characteristics of soil materials, it is then possible to link the *USCS* of each lithological layer to a numeric value representative of the layer hydraulic conductivity (Fig. 1a). In the pilot region Birrfeld (AG) of the project GeoQuat 1'581 boreholes for a total of 19'794 lithological layers have been captured and classified. All layers have been linked to a value of hydraulic conductivity, expressed as $\log_{10}(K[\text{m/s}])$ and used as input data for building a 3D hydraulic conductivity model of the pilot region. Fig. 1b illustrates a cross section through the 3D parametric model which consists of 6'050'254 voxels of size 25x25x2m. An anisotropic searching ellipsoid has been used to favor the ordinary kriging along the direction of the glacial flow. The modeling has been realized with the software SGeMS (Remy 2004).

Once the 3D voxel model is constructed, it can be used to post-process maps whose elaboration depends on subsurface characteristics. A good example are maps of groundwater volumes and groundwater vulnerability (Fig. 1c). For the derivation of maps of groundwater volumes, the 3D hydraulic conductivity model is merged with the surfaces representing average groundwater table levels of Birrfeld aquifers. A python code (Python Software Foundation 2016) scans each vertical column of the 3D voxel model and for the permeable voxels (i.e. $K > 10^{-5}$ m/s) situated below the groundwater level, the code converts the voxel hydraulic conductivity in porosity and calculates the voxel groundwater volume. By means of a summation along the vertical column of voxels the groundwater volume is obtained for a cell of size 25x25m and the map is generated by plotting the volume of each cell (Fig. 1c). For the elaboration of maps of groundwater vulnerability, the vulnerability concept detailed in Philipp et al. (2006) has been adapted for 3D voxel models. Based on the 3D parametric model and on the average groundwater table level, a python code scans each vertical column, considers only voxels situated above the groundwater level and applies the concept of Philipp et al. (2006) to evaluate the protective effect of the top layer and of the unsaturated zone and subsequently estimates the vulnerability of a given aquifer to surface contamination.

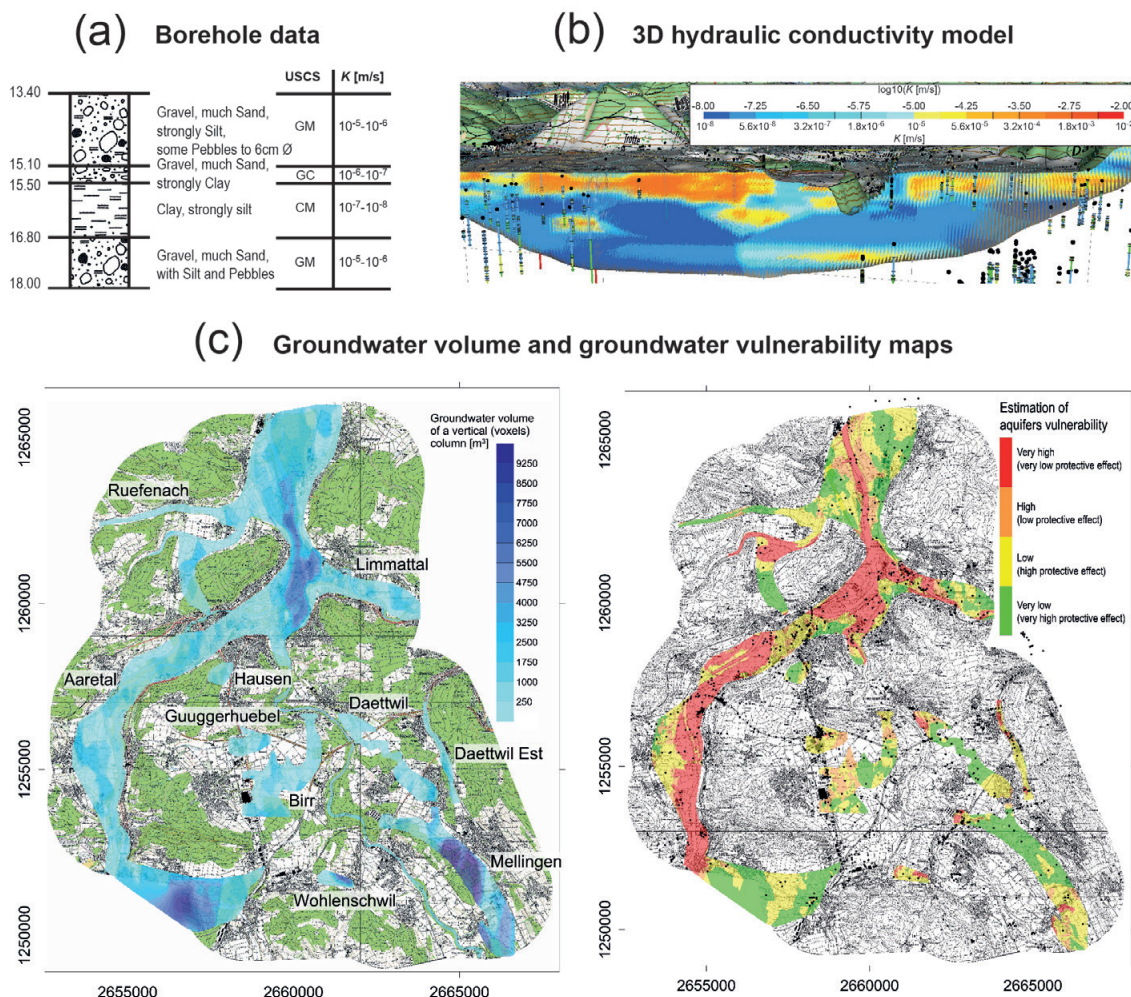


Figure 1. a) Schematics of a borehole log illustrating the link between layers lithology, USCS and K; b) cross section through the 3D hydraulic conductivity model for pilot region Birrfeld (lateral extent 4.5km, vertical exaggeration 5x) and c) post-processed groundwater volume and vulnerability maps.

REFERENCES

- Philipp, R., et al. 2006: Vulnérabilité des réservoirs aquifères – Atlas Hydrologique de la Suisse. Office fédéral de l'Environnement OFEV.
- Python Software Foundation 2016: Python 2.7, <https://www.python.org/>
- Remy, N. 2004: SGeMS – Stanford Geostatistical Modeling Software: User's Manual, <http://sgems.sourceforge.net/>
- Volken, S., Preisig, G. & Gaehwiler, M. 2016: GeoQuat: Developing a system for the sustainable management, 3D modelling and application of Quaternary deposit data. Swiss Bull. angew. Geol., 21(1), 3-16.

P 13.11

Life under the ice: microbial diversity and methane cycling in the sediment of the ice-covered Lake Onego, Russia

Camille Thomas¹, Emilie Lyautey², Daniel Ariztegui³, Nathalie Dubois⁴, Victor Frossard², Natacha Pasche⁵, Marie-Elodie Perga¹ and the Life Under the Ice Scientific Team⁶

¹ UMR CARRTEL, INRA, Thonon-les-Bains, France, camille.thomas@univ-smb.fr

² UMR CARRTEL, Université Savoie Mont Blanc, Le Bourget-du-Lac, France

³ Department of Earth Sciences, University of Geneva, Geneva, Switzerland

⁴ EAWAG, Dübendorf, Switzerland

⁵ APHYS, EPFL, Lausanne, Switzerland

⁶ Complete list of partners available at www.elemo.ch/ladoga

The largest lakes of Europe, namely lake Ladoga and lake Onego, are seasonally ice-covered, limiting studies to summer periods. Moreover, boreal lakes are important producers of methane, a large part of which is released during thawing. Within the “life under the ice” research program, our objectives are to assess for Lake Onego, during winter, the structure and diversity of the sedimentary microbial communities and their relationship with methane production and degradation. In order to do so, a 1.30 m-long core was retrieved from the ice-covered bay of Petrozavodsk in March 2015, and sampled for microbiological analyses. Its lithology was then analyzed and DNA and RNA were extracted to investigate the subsurface microbial diversity by high-throughput sequencing (HTS) of 16S rRNA genes and transcripts. Functional (*mcrA* and *pmoA*) genes and transcripts involved in methane cycle were also quantified.

Along the 130 cm core, the microbial assemblages were structured in several zones. An oxic zone between 0 and 6 cm was separated from a transitional zone between 7 and 10 cm by a sharp chemical and geological transition. At this depth, measurements of in situ ATP levels and transcripts of archaeal and bacterial 16S rRNA showed a peak in microbial activity. Below this, *mcrA* gene and transcript copies increased, implying methanogenesis. The latter was supported by congruent carbon isotopes of methane allowing to define a methane production zone between 10 and 40 cm. The transitional zone hosts methanotrophic organisms (ANME-2D) able to oxidize the produced methane anaerobically while the residual methane is almost completely consumed in the oxic zone where methanotrophs were detected (*pmoA* gene and transcripts). As a result very little methane diffused out of the sediment, making lake Onego a relatively low contributor of methane to the atmosphere. Finally, the microbial communities from the 40 to 120 cm in the core were dominated by uncultured Archaea belonging to the Miscellaneous Crenarchaeotic Groups, very common in deep ocean sediment, and allegedly well adapted to low energy environments.

P 13.12

3D geological modelling as a basis for hydrogeological investigations in complex mountain terrain

James Thornton¹, Grégoire Mariethoz² & Philip Brunner¹

¹ Centre for Hydrogeology and Geothermics, University of Neuchâtel, Rue Emile-Argand 11, 2000 Neuchâtel, Switzerland

² Institute of Earth Surface Dynamics, University of Lausanne, UNIL-Mouline, Geopolis, 1015 Lausanne, Switzerland

Physically-based hydrogeological models demand the a priori specification of a large number of uncertain parameters distributed in 3D space. Making reasonable estimations of their values at the outset helps to constrain any subsequent, automated calibration to the realm of physical plausibility. Thus, within a probabilistic framework, the parameter sets deemed “acceptable” are more likely to be useful for prediction than if no prior had been specified, assuming the selected performance criteria are appropriate. Developing predictive capability with respect to mountain hydrology is particularly pressing given the sensitivity of such regions to climatic change. Here, the ongoing development of a 3D geological model for the Nant / Anzeindaz region (Vaud Alps, Switzerland) is described. First, terrain and geological data (surface mapping and interpretive vertical cross-sections) were compiled. Then, in the GeoModeller software, the geological units were interpolated between the known reference points using geostatistics and geological rules. In the forthcoming phase, hydrological parameters shall be assigned to each unit in order to construct a physically-based, fully-coupled groundwater-surface water representation of the catchment using the HydroGeoSphere code. The presence of karstic systems in the region is expected to provide an additional challenge. Ultimately, the hydrogeological model will be employed to explore the data worth of spatially-distributed field measurements obtained using novel techniques (drone surveys of water temperature, dissolved gas concentration measurements to estimate water ages) in the processes of model parameter estimation, calibration and evaluation.

P 13.13

SismoRiv : Estimation du charriage en rivière à l'aide d'une mesure du bruit sismique présent dans les berges

Travaglini Eric ¹, Ornstein Pascal ¹, Moerschel Joseph², Schneider Thierry³

¹ Centre de recherche sur l'environnement alpin CREALP, Rue de l'industrie 45, CH-1951 Sion

² HES-So Valais, Route du Rawyl 47, CH-1950 Sion2

³ TETRAEDRE Sarl, Rue des Epancheurs 34b, CH 2012 Auvernier

Le transport solide, ou capacité d'un cours d'eau à transporter des sédiments, est le facteur principal influençant la morphodynamique des cours d'eau de montagne. L'estimation du transport sédimentaire, ou charriage, est habituellement effectuée à l'aide des formules de la littérature et suppose une relation constante entre les débits liquides et solides. Cette relation jugée satisfaisante à long terme subit une forte variabilité à court terme, la rendant inadaptée à l'analyse des événements de crue.

En 2011, le CREALP, en partenariat avec le WSL, a piloté la construction à Zinal (Val d'Anniviers, VS) d'une station de mesure expérimentale basée sur une méthode d'écoute sismique utilisant la technique des « Swiss Plate Geophones » (Rickenman 2014). Le principe est d'estimer le charriage à partir d'une mesure des vibrations émises par les sédiments lorsqu'ils impactent le fond du lit (Figure 1A). Des géophones, installés sous des plaques métalliques elles-mêmes disposées au sein d'une section bétonnée dans le lit de la rivière (Figure 1B), enregistrent ces vibrations. Une campagne de calibration réalisée entre 2012 et 2013 a permis d'établir une relation entre le signal vibratoire émis et le volume sédimentaire en transit. Bien qu'offrant de très bons résultats en matière de suivi quantitatif du transport sédimentaire, cette solution s'appuie sur un dispositif de mesure intrusif nécessitant des investissements lourds et coûteux pour sa mise en œuvre et limitant considérablement son déploiement à grande échelle.

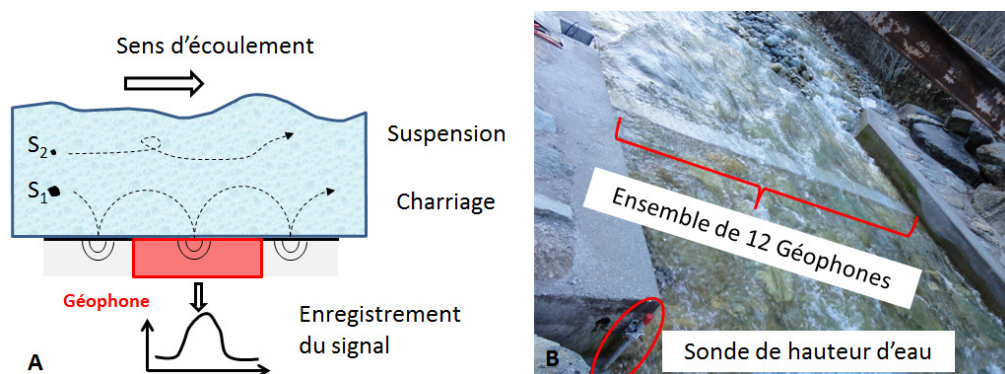


Figure 1.A) Concept de mesure des « Swiss Plate Geophones », B) Application au site expérimental de Zinal

Les recherches de Burtin et al. 2011 montrent que les flux liquides et solides transitant au sein d'un cours d'eau génèrent des vibrations qui se propagent à l'extérieur du lit. Sur la base de ces observations, confirmées par de récentes études (Gimbert et al. 2014, Larose et al. 2015), le CREALP propose une nouvelle approche axée sur l'utilisation de capteurs sismiques à bas coûts installés dans les berges de la rivière. Avec le soutien de l'OFEV dans le cadre de son programme de Promotion des technologies environnementales, une solution de mesure (SismoRiv) a été développée et testée au cours de l'été 2015 parallèlement aux mesures effectuées par la station de référence équipée des « Swiss Plate Geophones ». Ce premier test a permis d'attester la faisabilité du concept de mesure. L'analyse préliminaire des résultats obtenus confirme l'existence, au sein du signal sismique mesuré, de différentes composantes fréquentielles représentatives des fractions liquides et solides du débit. Le débit solide ($Q_{s, \text{SismoRiv}}$) déduit des mesures sismiques réalisées avec la solution SismoRiv (Figure 2) montre une bonne similitude avec les débits fournis par la station de référence ($Q_{s, \text{Ref}}$) et un gain significatif par rapport aux estimations obtenues à l'aide des formules de la littérature ($Q_{s, \text{Recking}}$). Ces premiers résultats encourageants mettent en évidence le potentiel de la solution de mesure SismoRiv pour le monitoring du charriage.

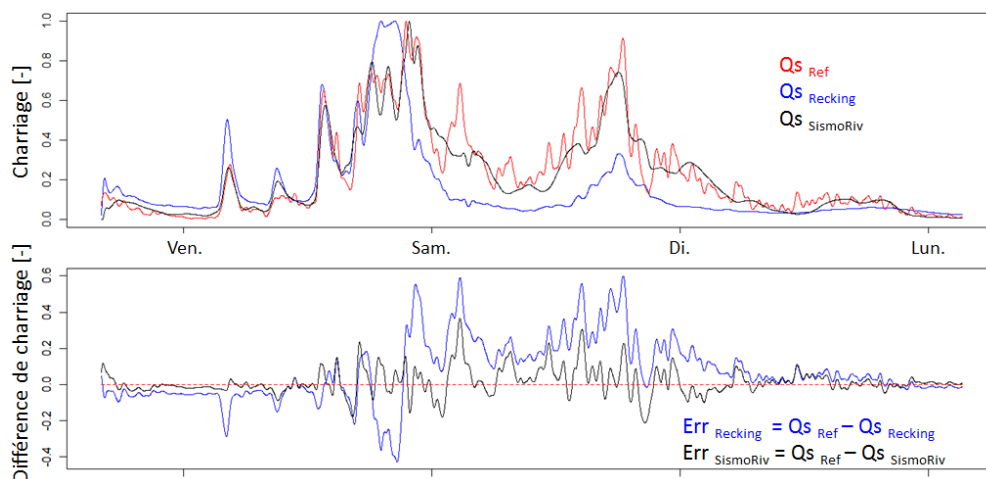


Figure 2. Comparaison d'estimations normalisées du charriage sur le site de Zinal obtenues via différentes approches météorologiques et numériques.

REFERENCES

- Burtin, A., Cattin, R., Bollinger, L., Vergne, J., Steer, P., Robert, A., Findling, N. and Tiberi, C. (2011). Towards the hydrologic and bed load monitoring from high-frequency seismic noise in a braided river: The "torrent de St Pierre", French Alps. *J. Hydrol.*, 408(1–2). 43–53. ISSN 00221694. doi: 10.1016/j.jhydrol.2011.07.014.
- Gimbert, F., Tsai, V. C. and Lamb, M. P. (2014). A physical model for seismic noise generation by turbulent flow in rivers. *J. Geophys. Res. Earth Surf.*, 119(10). 2209–2238. ISSN 2169-9011. doi: 10.1002/2014JF003201.
- Larose, E., Carrière, S., Voisin, C., Bottelin, P., Baillet, L., Guéguen, P., Walter, F., Jongmans, D., Guillier, B., Garambois, S., Gimbert, F. and Massey, C. (2015). Environmental seismology: What can we learn on earth surface processes with ambient noise? *J. Appl. Geophys.*, 116. 62–74. ISSN 0926-9851. doi: 10.1016/j.jappgeo.2015.02.001.
- Rickenmann, Dieter, Jens M. Turowski, Bruno Fritschi, Carlos Wyss, Jonathan Laronne, Ronel Barzilai, Ian Reid, et al. « Bedload Transport Measurements with Impact Plate Geophones: Comparison of Sensor Calibration in Different Gravel-Bed Streams ». *Earth Surface Processes and Landforms* 39, no 7 (15 juin 2014): 928-42. doi:10.1002/esp.3499.

P 13.14

Pockmarks in Lake Neuchâtel

Stefanie B. Wirth¹, Anna Reusch², Damien Bouffard³, Flavio S. Anselmetti⁴ & Michael Strasser⁵

¹ Centre for Hydrogeology and Geothermics, University of Neuchâtel, Rue Emile-Argand 11, CH-2000 Neuchâtel (stefanie.wirth@unine.ch)

² Department of Geosciences, University of Bremen, Gebäude GEO, Klagenfurter Strasse 2, D-28359 Bremen

³ Physics of Aquatic Systems Laboratory, EPF Lausanne, GR A0 412 (Bâtiment GR), Station 2, CH-1015 Lausanne

⁴ Institute of Geological Sciences and Oeschger Centre for Climate Change Research, University of Bern, Baltzerstrasse 1+3, CH-3012 Bern

⁵ Institute of Geology, University of Innsbruck, Innrain 52, A-6020 Innsbruck

Numerous pockmarks were discovered in Lake Neuchâtel in 2012 during the acquisition of new swath bathymetric data (Reusch et al. 2015; Reusch et al. 2016). Most prominent are four 'giant' pockmarks (80 to 160 m in diameter) located along the northern lake shore in the extension of NW-SE or NE-SW oriented faults of the Jura Mountains. In addition, numerous (>200) smaller pockmarks (up to 40 m in diameter) are present on the Molasse ridge in the central part of the lake.

One of the giant pockmarks was more closely investigated (Reusch et al. 2015). The temperature and the water oxygen isotopic composition of the sediment suspension filling the ~60 m deep pockmark crater indicates that the water originates from the karst system of the Jura Mountains. Tertiary deposits are absent or minor at the positions of the giant pockmarks, probably allowing vertical flow of artesian groundwater from the Malm aquifer through karstified Cretaceous units into the overlying Quaternary sediments (Pasquier et al. 1999; Ndiaye et al. 2014). Up to now, however, it is unknown if karst water indeed discharges into the lake via the pockmarks and how big that water volume would be. We are therefore installing a monitoring system with temperature, conductivity and pressure probes, as well as an ADCP (Acoustic Doppler Current Profiler) for continuously recording the hydro(geo)logical and sedimentological behavior of the pockmark in relation with meteorological events in the Jura Mountains. This setup should allow assessing potential vertical water flow within the pockmark crater and just above the pockmark surface.

Little is so far known about the origin and characteristics of the numerous smaller pockmarks located on an about 500 m thick package of Molasse covered by 30–40 m of Quaternary deposits (Sommaruga et al. 2012; Reusch 2016; Reusch A. and Gorin G., unpubl. seismic data). Their formation might be related to glacial erosion since some pockmark groups are aligned in a SW-NE orientation consistent with scour marks observable in the swath bathymetric data. Alternatively, fractures in the Molasse could give way to fluid and/or gas flow into the overlying Quaternary deposits. These hypotheses as well as the degree of activity of the pockmarks will be investigated in the future.

REFERENCES

- Ndiaye, M., Clerc, N., Gorin, G., Girardclos, S. & Fiore, J. 2014: Lake Neuchâtel (Switzerland) seismic stratigraphic record points to the simultaneous Würmian deglaciation of the Rhône Glacier and Jura Ice Cap. *Quat. Sci. Rev.*, 85, 1–19.
- Pasquier, F., Bouzelboudjen, M. & Zwahlen F. 1999: Carte hydrogéologique de la Suisse 1:100 000, Feuille 6 Sarine/Saane, notice explicative. Commission Géotechnique Suisse et service hydrologique et géologique national (SHGN).
- Reusch, A.M. 2016: Sublacustrine paleoseismology and fluid flow in the Western Swiss Molasse Basin: New constraints from the sedimentary archive of Lake Neuchâtel – Mass-transport deposits, subsurface sediment mobilization and geomorphology. Dissertation, ETH Zurich, Nr. 23131, <http://dx.doi.org/10.3929/ethz-a-010638214>.
- Reusch, A., Loher, M., Bouffard, D., Moernaut, J., Hellmich, F., Anselmetti, F.S., Bernasconi, S.M., Hilbe, M., Kopf, A., Lilley, M.D., Meinecke, G. & Strasser, M. 2015: Giant lacustrine pockmarks with subaqueous groundwater discharge and subsurface sediment mobilization. *Geophys. Res. Lett.*, 42, 3465–3473.
- Reusch, A., Moernaut, J., Anselmetti, F.S. & Strasser, M. 2016: Sediment mobilization deposits from episodic subsurface fluid flow—A new tool to reveal long-term earthquake records? *Geology*, 44, 243–246.
- Sommaruga, A., Eichenberger, U. & Marillier, F. 2012: Seismic Atlas of the Swiss Molasse Basin. Edited by the Swiss Geophysical Commission. *Matér. Géol. Suisse, Géophys.* 44.

P 13.15

Rainfall structure observed by a dense network of high resolution rain gauges

Lionel Benoit¹, Grégoire Mariethoz¹

¹ *Institute of Earth Surface Dynamics, University of Lausanne, UNIL-Mouline, Bâtiment Geopolis, 1015 Lausanne (lionel.benoit@unil.ch)*

Rainfall is acknowledged to be an intermittent process and to present a fluctuating intensity in space and in time. For technical reasons, its measurement involves either spatially integrated remote sensing data (e.g. weather radar images) or temporally integrated in situ data (e.g. rain gauge measurements) which lead in both cases to misestimate the variability of the rainfall process.

When the local structure of the rain is of interest, dense networks of tipping bucket rain gauges are commonly used because they allow investigating rainfall variability within a single radar pixel. Several experiments have been carried out involving more than ten rain gauges per square kilometer allowed to characterize the heterogeneity of the rain for time scales ranging from days to hours under different climates (e.g. Krajewski et al, 2003; Peleg et al, 2013). However, for shorter integration times, conclusions are biased by the limited resolution of standard tipping bucket rain gauges (0.25 to 0.1mm of rain height). As a consequence, the variability of the rainfall process at these scales is today inaccessible with these instruments.

Here we propose to use high resolution rain gauges (Driptych Pluvimates, resolution: 0.01mm of rain height) to extend the results of the previously mentioned experiments for the case of short integration times (up to one minute) using a network of 8 gauges set up on an area of about 1km². An analysis of the rainfall structure with Geostatistical tools shows that despite a strong variability, the rain field presents a degree of spatial and temporal coherence at these extremely small scales.

REFERENCES

- Krajewski WF, Ciach G, Habib E. 2003: An analysis of small-scale rainfall variability in different climatic regimes. *Hydrological Sciences Journal*, 48, 151-162.
- Peleg N, Ben-Ascher M, Morin E. 2013: Radar subpixel-scale rainfall variability and uncertainty: lessons learned from observations of a dense rain-gauge network. *Hydrology and Earth System Sciences*, 17, 2195-2208.

P 13.16

In a warming climate, why do we see decreasing heat influx from Russian rivers in the Arctic Ocean?

Harsh Beria¹, Daqing Yang², Yanping Li³

¹ *Institut des Dynamiques de la Surface Terrestre (IDYST), University of Lausanne, Lausanne, Switzerland (harsh.beria@unil.ch)*

² *National Hydrology Research Center, Environment Canada, Saskatoon, Canada*

³ *School of Environment and Sustainability and Global Institute for Water Security, University of Saskatchewan, Saskatoon, Canada*

A warmer climate brings more precipitation to the higher latitudes due to increased northward atmospheric moisture transport, leading to an increase in the river flows. Increased air temperature gradually heats up the water. Heat flux is directly proportional to both stream temperature and discharge. With higher river water temperature and river discharge, we expect an increase in the net heat flux discharge into the Arctic Ocean. Using daily streamflow and decadal (10-days) water temperature records (dating back to 1929) of six large Siberian basins, which account for about 70% of the total discharge into the Arctic Ocean, we show a long term decreasing heat flux trend. To answer the anomaly, we separated the basins by reservoir regulation. For the regulated basins, Pettitt change point approach was used to account for changes in the flow regime due to reservoir regulation. In the unregulated basins, Mann Kendall's trend test along with Sen's slope calculation was carried out to quantify long term trends in the river discharge, air temperature and heat flux time series. We found that reservoir regulation plays a key role in altering the heat flux trends downstream, with decreasing heat flux discharge in the regulated basins. In the unregulated basins, the increased heat flux trend was attributed due to a combination of increasing discharge and water temperature. Previous work showed that the impact of dams on the water temperature profile downstream can generally be assumed to be limited to a few hundred kilometres, which was validated in this study. However, changes in the downstream flow regime along with earlier spring melt alter the flux regime significantly, which can have significant impacts on the marine ecosystem and large scale ocean circulation, due to disproportionate mixing of water.

P 13.17

Groundwater and low flows in Switzerland – Part 1: Comparative physically based modelling of two Swiss catchments for assessing their low flow dynamics

Fabien Cochand¹, Claire Carlier¹, Maria Staudinger², Jan Seibert², Daniel Hunkeler¹ and Philip Brunner¹

¹ *The Centre for Hydrogeology and Geothermics of University of Neuchâtel (CHYN), Rue Emile-Argand 11, 2000 Neuchâtel, Suisse*

² *Department of Geography, University of Zurich – Irchel, Winterthurerstrasse. 190 CH-8057 Zurich, Switzerland*

In the context of a large BAFU project, we aim to understand the behaviour of two Swiss river catchments during low flow periods. Specifically, we aim to identify key catchment characteristics and processes which control low flow catchment response. The Roethenbach and the Langete catchments are characterized by the same meteorological conditions because of their geographical proximity, but have completely different river flow dynamics. The Roethenbach is characterized by high peak flows and low mean flows. Conversely, the Langete is characterized by relatively low peak flows and high mean flow rates. To understand the fundamentally different behaviour of the two catchments under future and current climate conditions, a fully-integrated surface-subsurface flow model for each catchment was developed and calibrated.

The 3D models of each catchment were developed using HydroGeoSphere (HGS). HGS is a physically-based, fully-integrated variably-saturated surface-subsurface flow model. The main advantage of an integrated model is its ability to realistically reproduce processes which play a key role during low flow periods such as surface-subsurface interactions or evapotranspiration. Calibration results showed that models were able to represent measured groundwater heads and the surface flow dynamics of each catchment. The calibrated models were then run with climatic scenarios consisting of a succession of historically observed dry periods.. Finally, the comparative analysis was carried out by comparing groundwater heads, stream flow rates and by indentifying resevoirs which maintain river flow rates during low flow. The study allows identifying the spatial and temporal dynamics of the different water storages such as bedrock, alluvial aquifer, soil or snow.

P 13.18

Quantifying and predicting the effects of water abstraction on macroinvertebrate fauna and ecosystem function in alpine streams

Gabriele Consoli^{1,2}, Andreas Bruder², Fabio Lepori² & Christopher T. Robinson³

¹ Faculty of Marine and Environmental Sciences CASEM, University of Cadiz, Avenida de la universidad de Cadiz, s/n, 11519 Puerto Real, Cádiz

² University of Applied Sciences and Arts of Southern Switzerland, Institute of Earth Sciences, Campus Trevano, 6952 Canobbio, Switzerland (gabriele.consoli@supsi.ch)

³ Eawag, Swiss Federal Institute of Aquatic Science, Department of Limnology, EAWAG/ETHZ, CH-8600 Dübendorf, Switzerland

Growing trends in global energy demand and the dramatic projections of climate change scenarios have increased the importance of renewable energy sources in the last decades. In this context hydropower plays a major role. Hydropower provides society with undeniable benefits but it is burdened by a long list of drawbacks that heavily impact stream ecosystem structure and functioning (Dynesius & Nilsson, 1994). Therefore, it is needed to increase in the electricity production efficiency and to develop effective mitigation strategies to reduce impacts on stream ecosystems. Stream benthic invertebrates play key roles in stream ecosystems and the status of their community is often used as an indicator of stream ecosystem health. Stream invertebrates are sensitive to flow alterations – a common cause of hydropower operations - as it causes modifications in the physical habitat characteristics and in resource availability (Dewson, James, & Death, 2007). To understand the health of a river, to develop effective mitigation strategies or to assess the possible impact of flow alterations, it is crucial to understand the complex relationships among the stream biota, their habitat and resources. Descriptors of these relationships are functional and structural indicators. Functional indicators have the power to expand the research out of the strict taxonomical limits, looking at the organisms but seeing also the larger systems of which they are part, involving resources and energy fluxes (Wallace & Webster, 1996). These ecosystem functions are reflected by the distribution of functional traits (such as functional feeding guilds - FFGs) within the invertebrate community.

We applied a physical habitat model (CASiMiR Benthos) to model the invertebrate community in response to gradients in discharge and their consequences on abiotic habitat conditions (bottom hydraulic forces) in two alpine streams (Fig. 1a). We used the FST-hemispheres method (Fig. 1b) (Statzner & Muller, 1989) as an indirect measure of bottom hydraulic forces. This method allows to measure complex hydraulic forces on the stream substrate and can be coupled with information on invertebrate abundance to quantify invertebrate preference to these hydraulic forces (Fig. 1c). The outcome of the habitat model is an index of hydraulic habitat suitability (HHS) (Fig. 1d) and the weighted usable area (WUA) within the reach for the investigated indicator (taxon, FFG, resources). We further assessed how discharge-related changes affect the functional composition of the invertebrate community in response to dominant resources.

Results indicate that taxa and FFGs followed patterns of distribution which were determined by bottom hydraulic forces, overall resulting in an increase of suitable habitats at increasing discharge. The analysis of FFGs habitat preferences demonstrated its integrative power in the description of community dynamics, but also a loss of sensitivity compared to taxonomical information. On the resources side, coarse particulate organic matter appeared to be abundant in patches with higher bottom forces. In contrast, fine particulate organic matter did not show any link with the physical habitat features measured. These results indicate that, despite the great amount of information provided by FFGs analysis, it is important to integrate structural and functional indicators for a more complete assessment of the impacts of environmental change on stream ecosystems.

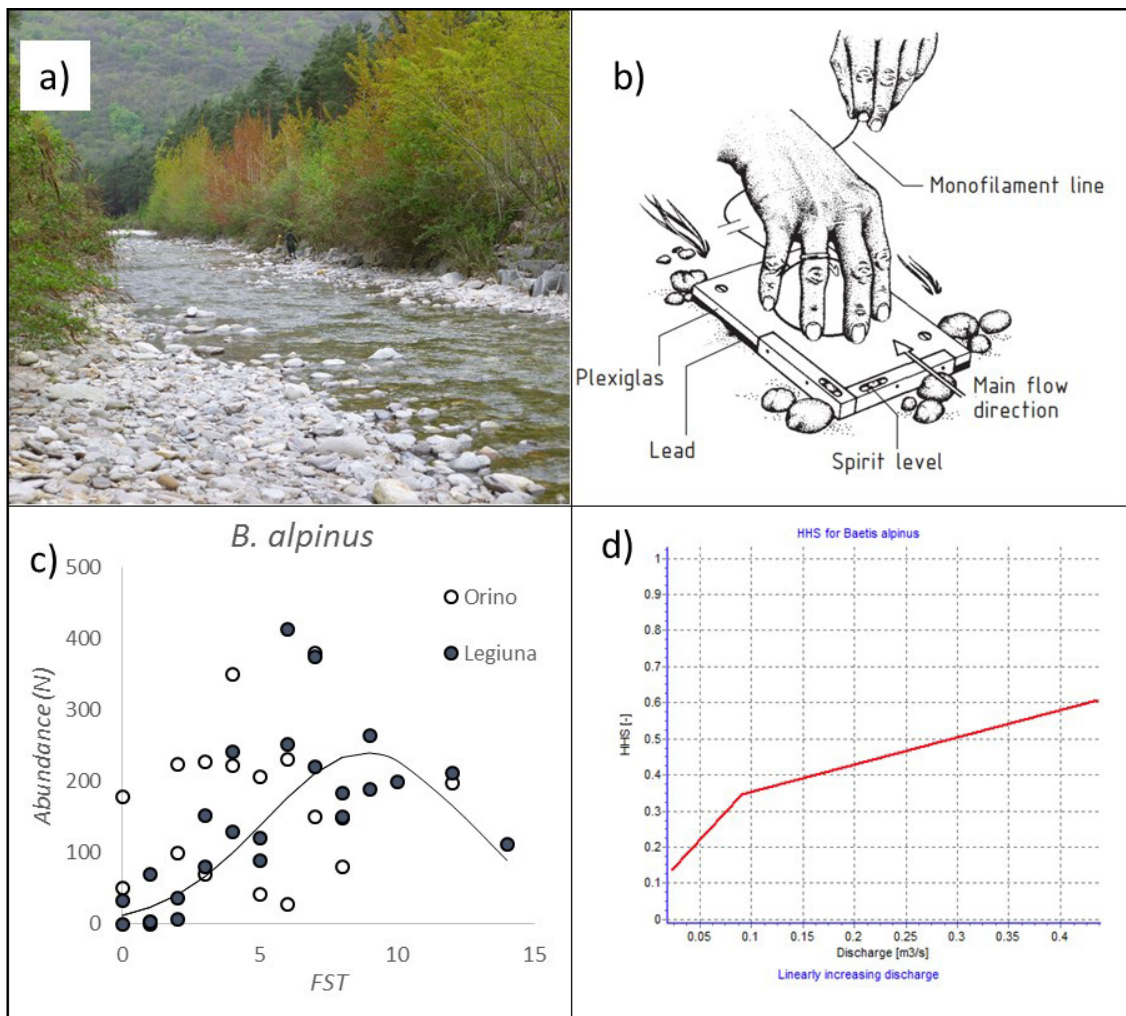


Figure 1. a) Study site on the Legiuna; b) FST hemisphere setup and placement method (from Statzner & Muller, 1989); c) Preference curve for *Baetis alpinus*; d) Hydraulic habitat suitability (HHS) for *B. alpinus* for the Orino.

REFERENCES

- Dewson, Z. S., James, A. B. W., & Death, R. G. 2007. A review of the consequences of decreased flow for instream habitat and macroinvertebrates. *Journal of the North American Benthological Society*, 26(3), 401–415.
- Dynesius, M., & Nilsson, C. 1994. Fragmentation and Flow Regulation of River Systems in. *Science*, 266, 4.
- Statzner, B., & Muller, R. 1989. Standard hemispheres as indicators of flow characteristics in lotic benthos research. *Freshwater Biology*, 21(3), 445-459.
- Wallace, J. B., & Webster, J. R. 1996. The role of macroinvertebrates in stream ecosystem function. *Annual Review of Entomology*, 41(1), 115–139.

P 13.19**Differences in the present hydrological regime of two Jurassian catchments with respect to the early XXth Century**

Ion Iorgulescu

*Direction Générale de l'Eau, Etat de Genève, rue des Gazomètres 7, CH-1205 Genève, Suisse
(lon.iorgulescu@etat.genève.ch)*

L'Allondon and La Versoix are two mid-sized adjoining catchments that originate from the Jura mountains. Altitudes range from about 1700 m a.s.l. to around 350 m a.s.l. The catchments are characterized by steep gradients in temperature and precipitation. The Allondon streamflow has been monitored continuously since 1985 at Dardagny-Les Granges. The topographic area at the gauging location is 119 km². The National Hydrological and Geological Service (SHGN) operated a stream gauge at the same location between 1918 and 1935. The analysis of the historical record reveals that, while average discharge didn't change significantly, the hydrological and flood significantly evolved over the past century. The current regime is characterized by a late winter / early spring maximum and a late summer / early autumn minimum. During winter (December to February), the monthly Pardé coefficients at the beginning of the twentieth century were considerably lower than during the last three decades, while maximum discharges were recorded later in the spring (March to May). Minimum flows correspond in both cases to late summer, but historical values were higher. The statistical analysis of maximum annual flows shows a significant increase in the mean of the distribution, while changes in dispersion are small and not significant. As a consequence, a maximum relative effect is observed for frequent floods. For example, the median annual flood is presently 46 m³/s, while during the 1918-1935 it was 31 m³/s, which represents an almost 50% increase. This evolution is associated to a change in the seasonality of the maximum annual. During the 1918-1935 period more than one in five annual floods occurred in May while none occurred in February. During the last 30 years none of the annual floods occurred in May while almost one in five occurred in February. These hydrological changes are consistent with a temperature-controlled change in the snow accumulation and melt regime. The adjoining La Versoix catchment (topographic area 88 km²) was monitored by SHGN between 1917 and 1931. Monitoring by the Cantonal Service resumed in 1996, albeit at a different location. The shorter monitoring period, the different gauging site as well as significant water diversions in the catchment make analyses more difficult. While hydrological changes appear as being less significant a similar evolution in the hydrological regimes can be observed.

P 13.20**Solute mixing and chemical reactions in multiphase systems: from pore- to field-scale**

Joaquin Jimenez-Martinez

*Department Water Resources and Drinking Water, EAWAG, 8600 Dübendorf, Switzerland
Department of Civil, Environmental and Geomatic Engineering, ETH Zurich, 8093 Zurich, Switzerland
(joaquinjimmar@gmail.com)*

Flow and transport processes in multiphase systems remain a grand scientific and engineering challenge in industrial (e.g., CO₂ sequestration, unconventional oil and gas extraction, enhanced oil recovery) as in natural systems. As a particular case, the soils and vadose zone, where air and water coexist, play a key role in the transport of chemical substances from the surface to groundwater resources. Mixing processes in porous media is a major control on fluid-fluid and fluid-solid chemical reactions. However, conventional continuum-scale theories and models oversimplify and/or ignore many important pore-scale processes. Multiphase flows, with the creation of highly heterogeneous velocity fields (i.e., regions of fluid of very low velocities, also called stagnation zones, and connected principal paths of high velocity), makes transport more complex, both conservative and reactive. We discuss recent experimental developments and theoretical approaches at different scales to quantify transport, including mixing, and reaction and their coupling with multiphase flows.

P 13.21

The Surface Runoff diagnostic model for the Canton of Geneva

Richard Metzger¹

¹ Terranum Sàrl, rue de l'Industrie 35b, CH-1030 Bussigny (richard.metzger@terranum.ch)

Among the damage to property and buildings from flooding, those caused by surface runoff during intense rainfall event (storms) are if not the majority, at least a significant part of total cost.

Although there is no legal basis requiring the authorities to take account of this risk, agencies may be asked to give an opinion on the subject.

In this context, the State of Geneva found interesting to develop a GIS tool to assess the risk of flooding due to surface runoff. This tool allows you to choose any part of the cantonal territory (building, land, local depression) and operate a dynamic modeling of surface runoff. One of the main advantage of the tool is to provide the informed user a quick and easy implementation so that it can produce an expert opinion in the shortest possible time.

The basic assumption of the surface runoff model is that it is generated by exceeding the infiltration capacity (Hortonian flow). Two infiltration functions are available:

- Initial losses and constant infiltration rate, and
- Surface runoff by local deficit of the water table (contributive area or TOPMODEL concept)

The water which has not infiltrated is then routed on the surface using a quasi 2D model.

Input data are:

- A DTM, a flow direction and a flow accumulation model;
- A rainfall event, choosen from either a long time recorded or generated serie or a catalog of events;
- The constant infiltration rate or the saturated hydraulic conductivity(TOPMODEL implementation);
- The Manning-Strickler runoff coefficient;

Both the infiltration rate/hydraulic conductivity and the Manning-Strickler codefficient can be spatialised if needed.

Model outputs are maps of maximum flow velocity and maximum flow depth. The model highlights the two main components of surface runoff hazard: runoff path concentration and water accumulation within terrain depressions.

Although the model is not new in itself, it constitutes an achievement in the sense that it allows for quick assesment of area prone to surface runoff flooding, thanks to modern GIS and GUI tools. Typically, an experienced user would perform an assesement running two or three different scenarios within 20 to 30 minuts.

This work is funded and supported by the Canton of Geneva.

REFERENCES

- Beven K.J.& Kirkby M. 1979: A physically based, variable contributing area model of basin hydrology. Hydro. Sci. Bull., 24(1), 43-69.
- Cunge, J. A. 1975: Two-dimensional Modeling of Flood Plains. Chap. 17 in Unsteady Flow in Open Channels, edited by K Yevjevich and V Mahmood, 3 vol. Fort Collins, CO: Water Resources Publications.
- Horton J. 1933: The role of infiltration in the hydrological cycle. Trans. of the Am. Geophys. Union, 14, 446-460.
- Obled C & Zin 2004, I. TOPMODEL : principes de fonctionnement et application, La Houille Blanche, Vol. 1, 65-77.

P 13.22

Bacterial transport in saturated porous media

Roberto Rusconi, Eleonora Secchi, Matthias Willmann, Roman Stocker

Department of Civil, Environmental and Geomatic Engineering, ETH Zurich, 8093 Zurich, Switzerland (rusconir@ethz.ch)

Understanding the transport of bacteria in saturated porous media is crucial for many applications ranging from the management of pumping wells subject to bio-clogging to the design of new bioremediation schemes for subsurface contamination. However, little is known about the spatial distribution of bacteria at the pore scale, particularly when small-scale heterogeneities – always present even in seemingly homogeneous aquifers – lead to preferential pathways for groundwater flow. In particular, the coupling of flow and motility has recently been shown to strongly affect bacterial transport, and this leads us to predict that subsurface flow may strongly affect the dispersal of bacteria in saturated aquifers. We present here an upscaling framework for the transport of motile bacterial in saturated porous media by combining detailed numerical simulations with controlled laboratory experiments.

Bacteria are ubiquitously exposed to fluid flow in natural environments, the human body, and artificial systems. However, the influence of flow on the transport and attachment of bacteria to surfaces and the formation of biofilms remains poorly investigated and understood. We have used microfluidic technology and mathematical modelling to study the role of fluid shear on surface colonization by pathogenic bacteria, such as *Pseudomonas aeruginosa* and *Escherichia coli*, under clinically relevant flow rates. In a first set of experiments, we discovered a novel and counterintuitive phenomenon by which the coupling of motility and shear results in a higher cell concentration near the walls of a channel and consequently in a strong enhancement of bacterial surface attachment compared to quiescent conditions. A crucial step in obtaining these results was the use of a multi-channel microfluidic device, which allowed the simultaneous monitoring of bacterial surface coverage under different shear conditions while avoiding potential confounding factors stemming from variability among cell cultures. In a second set of experiments, we studied the coupling of flow and surface topography by observing the attachment of bacteria to corrugated surfaces. In particular, we show how the topological features of the flow can promote the attachment of bacteria to specific regions of the corrugated surface, which will ultimately influence the formation of biofilms. These results highlight the intimate link between small-scale biological processes and transport in porous media.

REFERENCES

Rusconi, R., Guasto, J.S. & Stocker, R. 2014: Bacterial transport suppressed by fluid shear. *Nature Physics*, 10, 212–217.

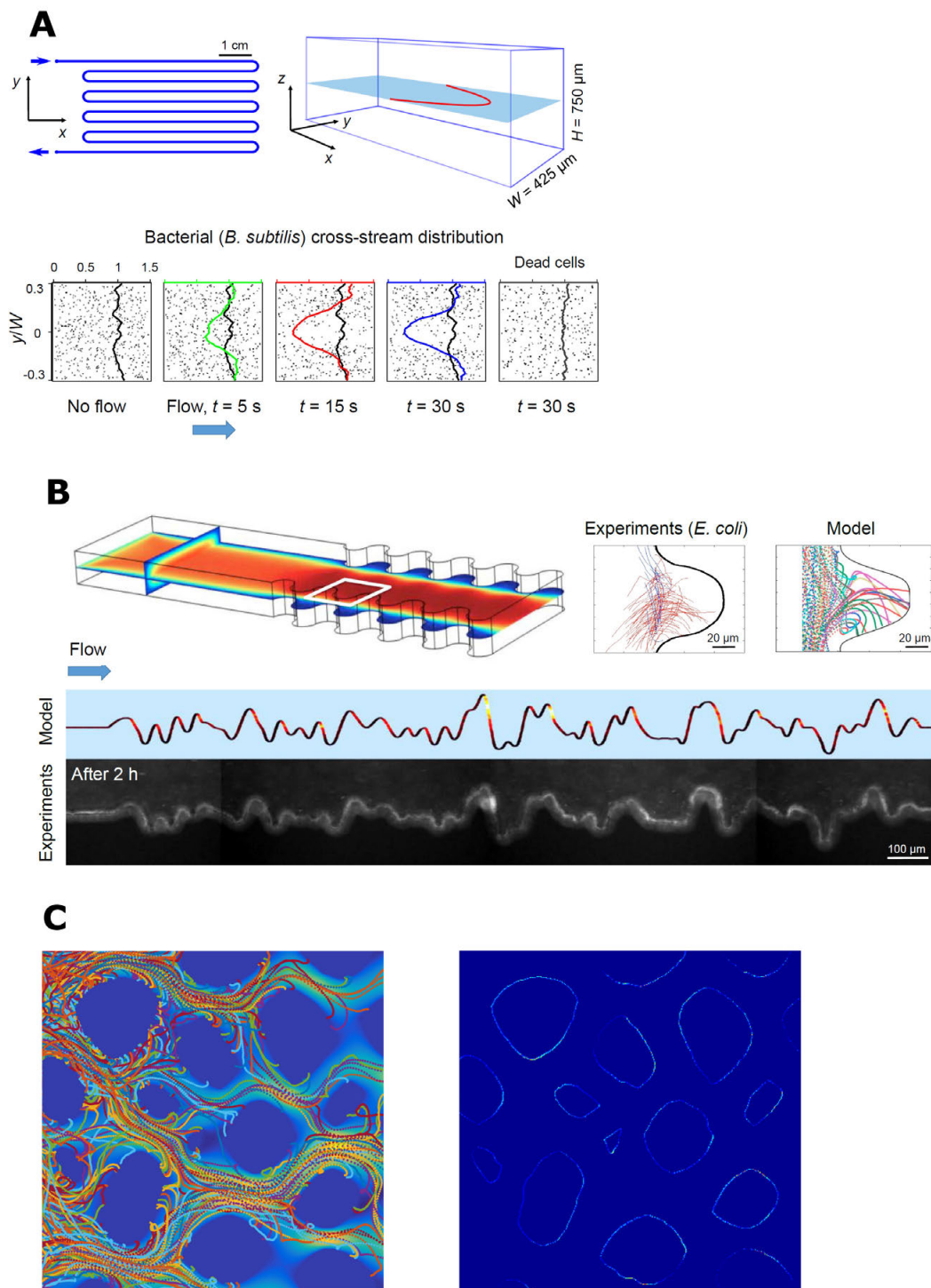


Figure 1. A, Microfluidics experiments of bacterial transport in narrow channels, showing depletion of cells in the region of low shear rate and accumulation of cells in the regions of high shear rate. B, Numerical and experimental results of bacterial transport and surface attachment in the presence of regular and randomly corrugated surfaces. C, Numerical results of bacterial transport (left-hand side) and preferential attachment (right-hand side) in a two-dimensional model of a saturated porous medium.

P 13.23

A multi-grain reduced-complexity model for step formation and stability in steep streams

Matteo Saletti¹ and Peter Molnar²

¹ *Institute of Environmental Engineering, ETH Zurich, Stefano Franscini Platz 3, CH-8093 Zurich (saletti@ifu.baug.ethz.ch)*

² *Institute of Environmental Engineering, ETH Zurich, Stefano Franscini Platz 5, CH-8093 Zurich*

We present a multi-grain particle-based reduced-complexity model to simulate sediment transport and a step-pool morphology. The model CAST (Cellular Automaton Sediment Transport) contains phenomenological parameterizations, deterministic or stochastic, of sediment supply, bed load transport, particle entrainment and deposition, and granular interactions in a cellular-automaton space for uniform size (see Figure 1.) [Saletti et al., 2016]. CAST yields realistic results, in agreement with field and laboratory observations, in terms of bed morphology, transport-rate fluctuations and particle travel distances.

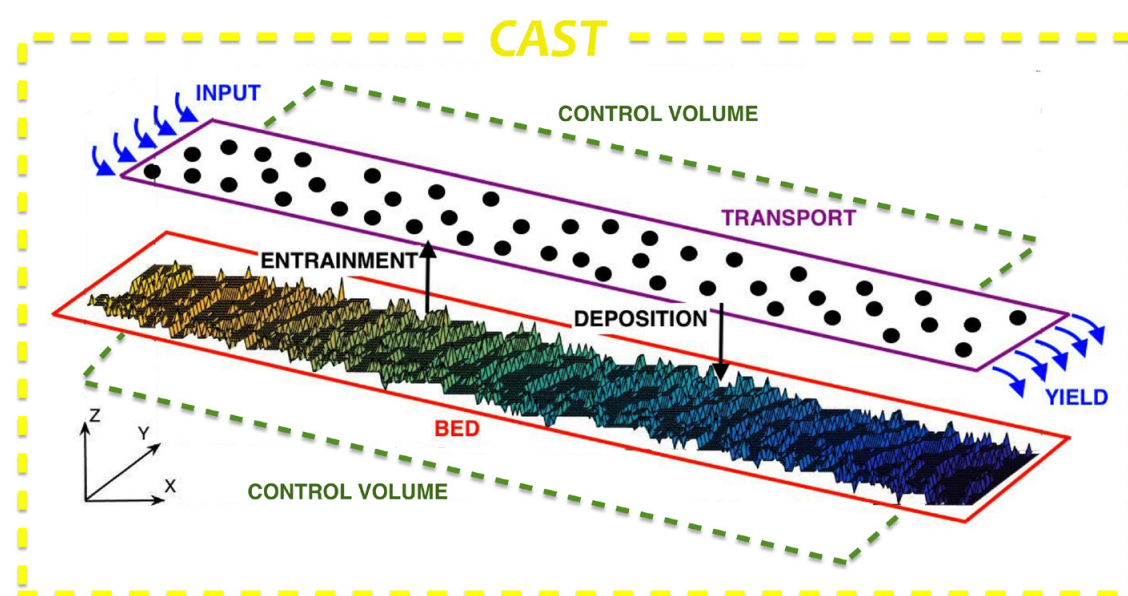


Figure 1. Diagram of CAST: spatial domain, model components and simulated processes [taken from Saletti et al., 2016].

A more sophisticated version of the model, $CAST_2$, has been developed to simulate the effect of different grain sizes by considering two types of particles: finer grains, which can be mobilized by any flow, and coarser grains, whose mobility is flow-dependent. The model has been applied to test the effect of granular forces on step formation and stability in step-pool channels, as hypothesized in the jammed-state framework by Church and Zimmermann [2007]. In $CAST_2$ the jamming of particles in motion and their enhanced stability on the bed are considered: in this way steps are effectively generated during high-flow periods and they are stable during low flows when sediment supply is small. Longitudinal profiles of the bed and the density of steps in the channel obtained in numerical simulations are consistent with field observations made at the Erlenbach, a step-pool stream in the Swiss Alps.

Finally we show the effect of (a) flood frequency and (b) randomness of inter-arrival times between floods on step density by means of longer simulations with repeated flood events. Model results show that the probability density functions of step density are more sensitive to flood frequency than randomness. Systems with high flood frequency are characterized by larger values of step density, similar to those measured in the Erlenbach, a very active and frequently perturbed fluvial system. Moreover, step density increases in high-frequency flood simulations when flood events are equally spaced, compared to the case when inter-arrival times are randomly generated.

Our results show the potential of reduced-complexity models as learning tools to gain new insight on complex feedback and poorly understood processes characterizing geomorphic systems, pointing out the importance of hydrological forcing on the formation and stability of step-pool morphology.

REFERENCES

- Church, M., and A. Zimmermann (2007), Form and stability of step-pool channels: Research progress, *Water Resour. Res.*, 43, W03415, doi:10.1029/2006WR005037.
- Saletti, M., Molnar, P., Hassan, M. A., and Burlando, P.: A reduced-complexity model for sediment transport and step-pool morphology, *Earth Surf. Dynam.*, 4, 549-566, doi:10.5194/esurf-4-549-2016, 2016.

14. Environmental Biogeochemistry of Trace Elements

Andreas Voegelin, Lenny Winkel

TALKS:

- 14.1 Aepli M., Brown A.R., Voegelin A., Hofstetter T.B., Sander M.: Reduction dynamics of iron(oxyhydr)oxides as assessed by mediated electrochemical analysis
- 14.2 Bigalke M., Schwab L., Kusunwiryawong C., Imseng M., Rehmus A., Ulrich A., Tondo P., Fleisch M., Wigggenhauser M., Frossard E., Keller A., Müller M., Wilcke W.: Fate of fertilizer-derived U in Swiss agricultural soils
- 14.3 Biswakarma J., Kang K., Schenkeveld W.D.C., Borowski S.C., Kraemer S.M., Hering J.G., Hug S.J.: Fe(II)-catalyzed ligand-controlled dissolution of iron (hydr)oxides
- 14.4 de Meyer C., Rodriguez J., Garcia P., Carpio E., Wahnfried I., Matheus J., Stengel C., Berg M.: Geogenic trace elements in groundwater resources of the Amazon region
- 14.5 Jiskra M., Sonke J., Obrist D., Agnan Y., Hedge C., Moore C., Colgrove D., Huber J., Helmig D.: Vegetation uptake drives the deposition of gaseous elemental mercury to Arctic tundra soils – Insights from stable mercury isotopes
- 14.6 Jones G.D., Winkel L.H.E.: Climate-soil interactions drive trace element concentrations in topsoils
- 14.7 Marafatto F.F., Gilbert B., Peña J.: Irradiation of Ni-laden birnessite results in pH dependent Ni release.
- 14.8 Mestrot A., Grob M., Wilcke W.: Antimony release and biomethylation in shooting range soils under flooded conditions
- 14.9 Müller E., Von Gunten U., Winkel L.: Reactions between marine bromine and organic sulfur species
- 14.10 Sarret G., Aucour A.-M., Queyron M., Tholé R., Lamboux A., Testemale D., Magnin V., Bedell J.-P.: KEYNOTE: Dynamics of Zn in urban wetland soil-plant systems: coupling EXAFS and isotopic approaches
- 14.11 ThomasArrigo L., Mikutta C., Lohmayer R., Planer-Friedrich B., Kretzschmar R.: Arsenic Cycling in Iron-rich Organic Freshwater Floccs
- 14.12 van Genuchten C.M., Pena J.: Mn(II) oxidation coupled to Fe(II) oxidation in Fenton-type reactions
- 14.13 Wang Y., Benkaddour S., Marafatto F., Peña J.: Time-Resolved characterization of Co(II) Oxidation by δ -MnO₂ using quick X-ray absorption spectroscopy
- 14.14 Wick, S., Baeyens, B., Voegelin, A.: Thallium sorption on illite and its importance in soils
- 14.15 Wigggenhauser M., Wilcke W., Bigalke M., Imseng M., Müller M., Archer C., Frossard E.: Zinc isotope fractionation during translocation in wheat

POSTERS:

- P 14.1 Beauvais-Flück R., Regier N., Slaveykova V. I., Cosio C.: *Elodea nuttallii* exposure to mercury in natural water under enhanced ultraviolet radiation
- P 14.2 Benkaddour S., Sander M., Marafatto F. F., Peña J.: Redox properties of manganese oxide minerals (birnessite)
- P 14.3 Hassler C., Vance D., Moisset S., Pascal L., Ellwood M.: Trace metal and iron isotope cycling in the meromictic Lake Cadagno
- P 14.4 Gogos A., Thalmann B., Voegelin A., Kaegi R.: Sulfidation kinetics of copper oxide nanoparticles
- P 14.5 Gonzalez Holguera J., Dossou Etui I., Peña J.: Pb, Zn and Mn sorption on biogenic MnO₂: linking sorption affinity to reactive surface sites
- P 14.6 Liu Y., Schäffer A., Lenz M.: Selenium Methylation by a Pseudomonas Species and its Transcriptomic Responses to Se Oxyanions Exposure
- P 14.7 Loreggian L., Roebbert Y., Neubert N., Weyer S., Bernier Latmani R.: Uranium isotope fractionation during abiotic reduction by magnetite
- P 14.8 Penezic A., Tercier-Waeber, M.-L., Bakker, E.: Voltammetric detection of As(V) in natural waters
- P 14.9 Senn A.-C., Kaegi R., Hug S. J., Hering J. G., Voegelin A.: Composition, structure and arsenate sequestration of iron oxidation products
- P 14.10 Viacava K., Lederballe Meibom K., Mestrot A., Bernier-Latmani R.: Arsenic biomethylation efficiency across microbial phyla

14.1

Reduction Dynamics of Iron(Oxyhydr-)Oxides as Assessed by Mediated Electrochemical Analysis

Meret Aeppli^{1,2}, Ashley R. Brown¹, Andreas Voegelin¹, Thomas B. Hofstetter¹, and Michael Sander²

¹ *Eawag, Swiss Federal Institute of Aquatic Science and Technology, Dübendorf, Switzerland*

² *Institute of Biogeochemistry and Pollutant Dynamics, Swiss Federal Institute of Technology, ETH Zürich, Switzerland*

Iron (oxyhydr-)oxides are predominant redox-active geochemical phases in many natural and engineered systems. They play key roles in the biogeochemical cycling of major and minor elements as well as in the redox transformations of organic and inorganic pollutants by undergoing electron transfer reactions with both abiotic and biotic reaction partners. To date, electron transfer to iron oxides has most commonly been studied in batch systems by reacting the oxides with chemical bulk reductants or by incubating them with iron reducing bacteria, followed by quantification of the reductant consumed or the Fe(II) formed. While electrochemical techniques have also been used to study the redox properties of oxides, measurements were often challenged by redox disequilibrium between the oxides and the working electrodes of the electrochemical cells.

In this contribution, we demonstrate the applicability of a novel electrochemical approach, mediated electrochemical reduction, to assess the kinetics and thermodynamics of iron oxide reduction. Different from traditional, non-mediated electrochemical approaches, mediated electrochemical reduction relies on the use of a dissolved electron transfer mediator in the electrochemical cell to facilitate electron transfer (and thus redox equilibration) between the working electrode and iron oxides added to the cell (Sander et al., 2015). Electron transfer to the oxides is monitored at a constant potential using chronoamperometry. As such, this approach allows for a direct and highly sensitive quantification of both the rates of electron transfer (by analysis of the shape of the reductive current peak in response to oxide addition) and the total number of electrons transferred (by integration of the reductive current peak). The use of the electrochemical cell further allows for an independent control of pH and potential during reduction.

Using mediated electrochemical reduction, we systematically studied the effects of potential and solution pH on the rates and extents of electron transfer to three iron oxides, 6-line ferrihydrite, goethite and hematite. The pH was varied between pH 5 and 8 and the applied reduction potential between -0.17 and -0.53 V (versus the standard hydrogen electrode). As expected based on reaction thermodynamics, the rates and extents of electron transfers to all three oxides decreased when increasing the pH from 5 to 8. While the decrease in rates and extents of reduction was relatively small for 6-line ferrihydrite, it was significantly more pronounced for goethite and hematite, for which the decreases occurred over a relatively narrow pH range from pH 6.5 to 8. The differences between the three tested minerals were consistent with their different thermodynamic stabilities, as reflected by the relatively high reported standard reduction potential of 6-line ferrihydrite as compared to the lower standard reduction potentials of goethite and hematite.

For all three oxides, the decreases in reactivity with increasing pH and reduction potential can be linked to the concomitant decreases in the free energies of the reductions, ΔG_r . A control on oxide reduction dynamics by the thermodynamics of the systems was further supported by the finding that reduction rates and extents of the oxides decreased when adding dissolved Fe(II) to the electrochemical cell prior to the oxides but increased in the presence of phenanthroline, a strong ligand for Fe(II).

This work is the first to show that mediated electrochemistry in chronoamperometry model can be employed to study reduction dynamics of Fe oxides. In combination with mediated potentiometric measurements (Gorski et al., 2016), mediated electrochemical reduction lays the methodological foundation for more comprehensive investigations of thermodynamic properties of Fe oxides and their effects on reactivity.

REFERENCES

- Sander M., Hofstetter T. B. and Gorski C. A. 2015: Electrochemical analyses of redox-active iron minerals: a review of nonmediated and mediated approaches. *Environmental Science & Technology*, 49, 5862-5878.
- Gorski C. A., Edwards R., Sander M., Hofstetter T. B. and Stewart S. M. 2016: Thermodynamic characterization of iron oxide-aqueous Fe²⁺ redox couples. *Environmental Science & Technology*, 50, 8538-8547.

14.2

Fate of fertilizer-derived U in Swiss agricultural soils

Moritz Bigalke¹, Lorenz Schwab¹, Charirat Kusonwiriawong¹, Martin Imseng¹, Agnes Rehmus¹, Andrea Ulrich², Patrick Tondo³, Markus Flisch³, Matthias Wigganhauser⁴, Emmanuel Frossard⁴, Armin Keller⁵, Michael Müller⁵, Wolfgang Wilcke⁶

¹ *Geographisches Institut, Universität Bern, Hallerstrasse 12, CH-3012 Bern*

² *Federal Office for Agriculture, Mattenhofstrasse 5, 3003 Bern, Switzerland*

³ *Laboratory of the Canton of Bern, Muesmattstrasse 19, 3012 Bern, Switzerland*

⁴ *Institute of Agricultural Sciences, ETH Zurich, Eschikon 33, CH-8315 Lindau, Switzerland*

⁵ *Swiss Soil Monitoring Network (NABO), Agroscope, Reckenholzstrasse 191, CH-8046 Zürich, Switzerland*

⁶ *Institute of Geography and Geoecology, Karlsruhe Institute of Technology (KIT), P.O. Box 6980, D-76049 Karlsruhe, Germany*

Many phosphate fertilizers contain high concentrations of potentially toxic elements. These elements are applied to agricultural soils together with the fertilizers and result in elevated trace element concentrations in soils and an increased risk of toxic element transfer into the food chain. Besides Cadmium, another common contaminant of P fertilizers, the uranium (U), is of high interest because of its high toxicity and possible transfer to ground and surface waters.

We assessed the contribution of fertilizer-derived U at agricultural sites in Switzerland. We compared arable to grassland sites and topsoil of arable sites to the corresponding subsoil. We analyzed all inputs and outputs of U at three arable sites in Switzerland and calculated U budgets to assess main sources of U and ^{234/238}U activity ratios and to estimate the contribution of fertilizer-derived U. Swiss arable soils are significantly enriched in U compared to grassland sites (16%) and arable topsoils are significantly enriched in U compared to the corresponding subsoils (6-9%). The U budgeting shows that phosphate fertilizers are the dominant source of U in agricultural soils (Input ca. 20 g ha⁻¹ a⁻¹). Uptake by crops and outputs by harvest are negligible. At our three field sites in Switzerland, U concentrations in soil solutions were low (<0.004-0.73 µg L⁻¹), apparently contradicting the threat of groundwater contamination. Similarly, U accumulation in the soils was small, raising the question about the fate of the fertilizer-derived U.

To answer this question, we used ^{234/238}U activity ratios. Generally ^{234/238}U activity ratios in soils are < 1, depending on the degree of weathering, while U fertilizers have distinct ^{234/238}U activity ratios of 1.00-1.05 and might affect the U-234/U-238 ratios of soils when added to the soils. The U activity ratios in the three study soils ranged 0.90-1.05 indicating a contribution of fertilizer-derived U. The fertilizer-derived U seems to mainly accumulate in the mobile (NaHCO₃- extractable) fraction. In summary, while low soil water concentrations of U do not indicate U leaching, there are a number of findings suggesting a high U mobility and U loss from the soil. Possible explanations include colloidal transport and preferential flow of U which bypassed the suction cups we used for soil solution sampling but may contribute substantially to U leaching.

14.3

Fe(II)-catalyzed ligand-controlled dissolution of iron (hydr)oxides

Jagannath Biswakarma^{1§}, Kyounglim Kang², Walter D.C. Schenkeveld², Susan C. Borowski¹, Stephan M. Kraemer², Janet G. Hering^{1§}, Stephan J. Hug¹

¹ *Eawag, Swiss Federal Institute of Aquatic Science and Technology, Ueberlandstr. 133, CH-8600, Dübendorf, Switzerland (jagannath.biswakarma@eawag.ch)*

[§] *IBP, Swiss Federal Institute of Technology (ETH) Zurich, CH-8092, Zürich, Switzerland*

² *University of Vienna, Dept. of Environmental Geosciences Center for Earth Sciences, Althanstrasse 14 (UZA II) 1090 Vienna, Austria*

The dissolution of iron (oxyhydr)oxide minerals (FeOOH) is an essential biogeochemical process that not only influences the mobility and bioavailability of Fe, but also of other elements such as P, S and As. An understanding of FeOOH dissolution reactions in environmentally relevant conditions is therefore highly important for the assessment of the behavior of Fe and other trace elements in the environment. Numerous studies have been conducted to investigate the FeOOH dissolution at pH 3-5, and synergistic effects on ligand-controlled dissolution with two or more ligands have been shown. A few previous studies found that a trace of Fe(II) can lead to a strongly accelerated ligand-controlled FeOOH dissolution in anoxic conditions at low pH. The acceleration of the dissolution rate by traces of Fe(II) with simple ligands such as EDTA has been shown to be on the order of 10-100 at low pH. Despite its possible relevance, Fe(II)-catalyzed dissolution has not been well investigated in the pH-range 6-7, which is relevant for a wide range of terrestrial and aquatic systems. The goal of our investigation is an improved understanding of reductive and non-reductive dissolution and of the mechanisms that lead to accelerated dissolution of FeOOH by Fe(II) in the near-neutral pH range.

Fe(II)-accelerated FeOOH dissolution under anoxic and oxic conditions at pH 6-7 is studied with Attenuated Total Reflectance (ATR) Fourier-Transform Infrared (FTIR) spectroscopy. ATR-FTIR is used to (a) obtain information on the quantity and structure of adsorbed ligands, (b) follow the dissolution of FeOOH over time, and (c) observe the structural changes in the bulk and on the surface of FeOOH during the dissolution process. Dissolution experiments using the ATR-FTIR technique showed a strong catalytic effect of added Fe(II) on the overall non-reductive dissolution of lepidocrocite with EDTA at pH 6 and 7. The catalytic effect was also observed with production of Fe(II) in photo-chemical and thermal reactions. Introduction of O₂ decreased the rate of dissolution and eventually inhibited the dissolution process.

We will present spectroscopic results on the adsorption of EDTA on lepidocrocite and results of the effect of added and photochemically produced Fe(II) on the kinetics of dissolution. Based on the results, we will discuss possible mechanisms and the importance of Fe(II)-catalyzed dissolution of FeOOH at the oxic-anoxic interface in various environmental systems.

14.4

Geogenic trace elements in groundwater resources of the Amazon region

Caroline de Meyer¹, Juan Rodriguez², Pilar Garcia², Edward Carpio², Ingo Wahnfried³, João Matheus³, Caroline Stengel¹, Michael Berg¹

¹ *Eawag: Swiss Federal Institute of Aquatic Science and Technology, 8600 Dübendorf, Switzerland (caroline.demeyer@eawag.ch)*

² *Facultad de Ciencias, Universidad Nacional de Ingeniería, Av. Tupac Amaru 210, Lima, Peru*

³ *Geosciences Department, Universidade Federal do Amazonas, Av. Gal. Rodrigo Otávio Jordão Ramos, 3000, Manaus, Brazil*

In the floodplains of the Amazon Basin high loads of Andean sediments are deposited under tropical conditions, providing an ideal scenario for the creation of reducing conditions in the subsurface, and hence for dissolution of arsenic and other redox sensitive elements in groundwater. However to date, the groundwater quality in the Amazon region is very poorly known. This is of particular concern because many people in both rural and urban areas depend on groundwater as their source of drinking water.

Here we present the results of two pilot studies on trace elements in groundwater of the Amazon region. We collected water from 110 domestic wells during two sampling campaigns in the Peruvian Western Amazon and in the Brazilian Central Amazon. We determined the hydrochemical characteristics including >50 parameters, such as major and minor elements, as well as arsenic speciation. We linked the chemical analyses to environmental factors such as geology, geomorphology and soil.

Trace element analyses revealed aquifers where aluminum, arsenic and/or manganese were elevated at concentrations harmful for human health. Our results show that the distribution of the trace elements is not only related to the age of the aquifer deposits but also linked to the depositional environment. We distinguish between basins drained by white water rivers, carrying a high sediment load and resulting in pH-neutral subsurface conditions, and those drained by blackwater rivers carrying a high organic load and resulting in acidic subsurface conditions.

Our study provides first insights on the presence and distribution of trace elements in groundwater resources of the Amazon floodplains. Understanding the regional geochemical mechanisms triggering the enrichment of toxic elements in groundwater forms a particularly important step to raise awareness and implement mitigation where needed.

14.5

Vegetation uptake drives the deposition of gaseous elemental mercury to Arctic tundra soils - Insights from stable mercury isotopes

Martin Jiskra¹, Jeroen E. Sonke¹, Daniel Obrist², Yannick Agnan², Christine Hedge², Christopher Moore², Dominique Colgrove³, Jaques Huber³ & Detlev Helmig³

¹ *Géosciences Environment Toulouse, OMP, CNRS, Avenue Edouard Belin 14, F-31400 Toulouse (martin.jiskra@get.obs-mip.fr)*

² *Division of Atmospheric Sciences, Desert Research Institute, 2215 Raggio Parkway, NV-89512 Reno, USA*

³ *Institute of Arctic and Alpine Research, University of Colorado, 4001 Discovery Drive, CO-80309 Boulder,*

Mercury (Hg) is a global pollutant of great concern for human and ecosystem health. The Arctic is particularly vulnerable because of the high dietary exposure of indigenous populations to Hg in fish and mammals. The deposition of Hg from the atmosphere to Earth surfaces and its re-emission determine Hg concentrations in Earth surface reservoirs, such as soils, snow, and runoff into Arctic lakes and the surface Ocean and thus in the food chain. Stable Hg isotopes are a promising new tool to identify the dominant pathways of atmospheric Hg deposition and potential re-emission processes.

In a first part we will present stable Hg isotope measurements of all major ecosystem compartments (soils, vegetation, bedrock, snow, atmosphere) of a study conducted in the Arctic tundra of northern Alaska (Toolik Field station, AK). The results suggest that vegetation uptake of gaseous elemental mercury from the atmosphere represent the dominant deposition pathway to the terrestrial ecosystem, illustrated by quasi-identical isotopic signatures of organic soils with the overlying vegetation. The deposition of oxidized atmospheric mercury species during halogen-driven atmospheric mercury depletion events (AMDE), a well-reported phenomenon on the Arctic coast during spring, however does not represent a significant source for Hg in the tundra soils. The Hg isotope signatures in the soils and the atmosphere show no indication for substantial re-emission of gaseous elemental mercury from the soils.

In a second part, the findings based on stable Hg isotopes will be compared to concentration-based measurements conducted at the same location. Both independent approaches suggest that vegetation uptake of gaseous elemental Hg represents the dominant Hg flux between the atmosphere and Arctic tundra soils and they thus represent a net sink for atmospheric Hg. Changes in environmental conditions, such as warming and thawing of permafrost due to climate change or fires could however lead to a remobilization of a large Hg pool stored in Arctic tundra soils.

14.6

Climate-soil interactions drive trace element concentrations in topsoils

Gerrad D. Jones¹, Lenny H.E. Winkel^{1 2}

¹ *Eawag: Swiss Federal Institute of Aquatic Science and Technology, 8600 Duebendorf, Switzerland
(Gerrad.Jones@eawag.ch, Lenny.Winkel@eawag.ch)*

² *Institute of Biogeochemistry and Pollution Dynamics, ETH Zurich, 8092 Zurich, Switzerland (lwinkel@ethz.ch)*

Human health is directly tied to the elemental composition of soils and their uptake by plants. While the factors governing the uptake of essential/toxic elements by plants is relatively well understood, the factors governing their broad-scale distributions in soils are less well known. Understanding the broad-scale distribution of such trace elements could be useful to minimize the adverse human health effects associated with under/over exposure to essential/toxic elements. While some soil geochemical surveys have been conducted in developed countries, the distribution of such elements is unknown throughout a vast majority of the world, and as a result, the risk of under/over exposure to these elements throughout the world is largely unknown.

Much of the work that has been done to identify the variables/mechanisms that control soil concentrations have been evaluated on small scales (e.g., soil column studies). Although many of these studies have found strong evidence linking soil physicochemical properties (e.g., pH, soil organic carbon, clay) to element distributions in soils, these studies have ignored the potential role that climate (e.g., precipitation, evapotranspiration, etc.) plays in affecting the spatial distribution of elements in soils. In addition, as the investigative scale increases from smaller-scales to continental scales, the relationships between predictor variables and element concentrations become increasingly complex, likely due to interactions among predictor variables. In addition, many of the statistical tools often used to evaluate these patterns (e.g., linear regression) are not capable of capturing the environmental complexity driving broad-scale patterns. As a result, our understanding of the processes governing the broad-scale distributions of essential/toxic elements in soils as well as the risks associated with over/under exposure to these elements is limited.

Here, we will report on a robust modeling approach used to overcome these limitations, which we used to address the following three questions: 1) what are the dominant variables driving element (e.g., As, Hg, S, Se) concentrations in top soils on continental/global scales? 2) can element concentrations be predicted in top soils in areas where geochemical surveys have not been conducted?, and 3) how stable are element concentrations in top soils given changes in environmental variables? We used different machine learning tools to investigate the complex relationships between environmental variables, interactions between environmental variables (e.g., synergistic or antagonistic), and element distributions in top soils. Using sensitivity analyses of the machine learning models, we tested multiple hypotheses of controlling mechanisms/ processes that have been proposed in the literature to explain element distributions. For the 4 elements analyzed (As, Hg, S, and Se) our analysis indicated that both direct and indirect effects of climate are the primary factors driving element distributions, while soil physicochemical properties generally play a smaller role. Previously, element concentrations in top soils have been hypothesized to be largely constant. However, given the importance of climate in controlling element distributions, it can be expected that changes in climate could result in changes in element concentrations in top soils, which could affect the nutritional content/quality of crops and therefore have potential human health impacts.

14.7

Irradiation of Ni-laden birnessite results in pH dependent Ni release.

Francesco Femi Marafatto¹, Benjamin Gilbert², Jasquelin Peña¹

¹ *Institut des Dynamiques de la Surface Terrestre, Faculte des Geosciences et de l'Environnement, Universite de Lausanne, CH-1015*

² *Earth Sciences Division, Lawrence Berkeley National Laboratory, Berkeley, CA-94720, USA*

Layer type Mn oxides (birnessites), are among the most widespread metal oxides on the earth's surface (Post, 1999). These minerals are characterized by small particle size, high specific surface area; they are also among the strongest oxidizants present in nature (Morgan, 2000). Because of these properties, birnessite minerals are linked to numerous biogeochemical cycles and influence the fate of many organic and inorganic species. Furthermore, the precipitation and dissolution of these oxides in sunlit environments can occur on diel timescales: the main formation pathway is through microbially mediated oxidation of aqueous Mn(II) to form MnO₂, whereas the (photo)reductive dissolution of MnO₂ yields aqueous Mn(II), both through the formation of intermediate Mn(III)(Sunda et al., 1983; Tebo et al., 2004).

The the photoreduction of Mn oxides has important implications regarding contaminant release (e.g., mining impacted streams) and nutrient availability (e.g., water column in marine systems). However, few studies have been carried out to date to investigate the impact of MnO₂ photoreduction on the fate of adsorbed metals. Furthermore, only recently was the mechanism and rate of birnessite photoreduction decoupled from that of organic compounds and microorganisms (Marafatto et al., 2015). The proposed mechanism of photoreduction, whereby irradiation of MnO₂ results in accumulation of Mn(III) in the interlayer region of the nanosheets, provides a framework with which to investigate the effect of sunlight on the mobility of trace elements associated with birnessite.

This work investigates the effect of visible light irradiation on the uptake and release of Ni from birnessite minerals as a function of pH. Specifically, dilute mineral suspensions were prepared with a Ni surface loading of 5% (mol Ni / mol Mn) at pH 4 and pH 8 and irradiated in a flow through system under 400 nm LED irradiation for 96 hours. The pH was kept constant with the use of automatic pH STAT titrators, and dark control experiments were run in parallel. The amount of solid-phase Mn(III) produced through photoreduction and changes in Ni surface loading were monitored for the duration of the experiment. Both dark-control and irradiated samples were collected for extended X-ray absorption fine structure (EXAFS) spectroscopy after 96 hours to investigate any changes in Ni surface speciation caused by irradiation.

Our results show that irradiation of mineral suspensions at pH 4 results in about 50% desorption of Ni, whereas no change in surface loading occurs at pH 8. However, both at pH 4 and pH 8 irradiation led to changes in the Ni bonding environment, as evidenced by Ni K-edge EXAFS spectra. In particular, the release of Ni from the mineral surface at pH 4 was accompanied by a decrease in the intensity of the coordination shell that corresponds to Ni sorbed as a corner sharing complex, suggesting a release of Ni from vacancy sites. We interpret the Ni release and change in surface coordination at pH 4 to changes in the Mn(III) content of the mineral upon photoreduction, which alters the surface coordination of Ni and induces its release to solution. At pH 8, no change in the Ni surface loading was observed, but there was a small change in the surface coordination of Ni. We interpret these results as a modification of the Ni from triple corner sharing complex site to an incorporated species on the edge sites.

The results from this study have important implications on predicting the mobility of trace elements in multiple environmental settings. In particular, birnessites in acidic environments characterized by elevated trace metal concentrations such as acid mine drainage-affected wetlands may not only be less efficient in scavenging such elements under irradiated conditions, but also release them without dissolution of the mineral. The results at pH 8, on the other hand, provide additional information on the controls of the Ni sorption mechanism in Mn oxides in seawater.

REFERENCES

- Marafatto, F.F., Strader, M.L., Gonzalez-Holguera, J., Schwartzberg, A., Gilbert, B. and Pena, J. (2015) Rate and mechanism of the photoreduction of birnessite (MnO₂) nanosheets. *Proc Natl Acad Sci U S A* 112, 4600-4605.
- Morgan, J.J. (2000) Manganese in natural waters and earth's crust: its availability to organisms. *Met Ions Biol Syst* 37, 1-34.
- Post, J. (1999) Manganese oxide minerals: Crystal structures and economic and environmental significance. *Proceedings of the National Academy of Sciences* 96, 3447-3454.
- Sunda, W.G., Huntsman, S.A. and Harvey, G.R. (1983) Photo-Reduction of Manganese Oxides in Seawater and Its Geochemical and Biological Implications. *Nature* 301, 234-236.
- Tebo, B.M., Bargar, J.R., Clement, B.G., Dick, G.J., Murray, K.J., Parker, D., Verity, R. and Webb, S.M. (2004) Biogenic manganese oxides: Properties and mechanisms of formation. *Annual Review of Earth and Planetary Sciences* 32, 287-328.

14.8

Antimony release and biomethylation in shooting range soils under flooded conditions

Adrien Mestrot¹, Matthias Grob¹ & Wolfgang Wilcke^{1,2}

¹ *Institute of Geography, University of Bern, Hallerstrasse 12, CH-3012 Bern.
(adrien.mestrot@giub.unibe.ch)*

² *Institute of Geography and Geoecology, Karlsruhe Institute of Technology, Reinhard-Baumeister-Platz 1,
DE-76131 Karlsruhe, Germany.*

Antimony (Sb) is a toxic trace element that is often compared to arsenic (As) due to similar properties. However, very little is known about the behaviour, the speciation and the biogeochemistry of this element. In Switzerland, Sb can be found at very high concentrations in soils due to shooting activities and the associated weathering of Sb-containing ammunitions. Furthermore, this Sb can be transformed into methylated Sb species through biomethylation, a biological mechanisms that is not well understood. Additionally, this mechanism can fundamentally change the mobility, availability and toxicity of Sb, especially under reduced or flooded conditions. This lack of understanding mostly stems from an absence of simple extractions and analytical methods to measure Sb and methylated Sb species such as trimethylantimony (TMSb).

In this study, we use a novel analysis method, using high pressure liquid chromatography – inductively coupled plasma mass spectrometer (HPLC-ICP-MS), to validate a soil extraction procedure that keeps the Sb speciation intact prior to analysis.

With this technique, we screened three water-influenced shooting ranges for TMSb and found concentrations of up to 1.34 mg/kg Sb in the soil, near the targets. This is the first time that TMSb is found in shooting ranges soils and furthermore, the concentrations measured are very high compared to concentrations of methylated As or even methylated mercury (Hg) usually found in polluted areas.

Finally, we incubated soils of these three shooting ranges under flooded conditions for 15 days. Our results show that after only a few days, the concentration of dissolved Sb in the porewater reaches between 0.3 and 3.5 mg/L Sb depending on the site. This represents almost 1% of the total Sb in the soil (380 mg/kg Sb). These values are very high and show that Sb is being released from polluted soils at a very high rate as opposed to previous studies. Furthermore, our HPLC-ICP-MS technique allowed us to show that after 4 to 10 days, TMSb was also formed and released in the porewater where it represented up to 8 % of the dissolved Sb.

Our results demonstrate that Sb is very mobile in water-influenced shooting ranges with high quantities being released in the porewater and therefore made available to microorganisms, plants and animals. Finally, we could also show that biomethylation plays an important role in Sb contaminated soils with high concentrations of TMSb found directly in the soils and in the porewater of incubated soils.

14.9

Reactions between marine bromine and organic sulfur species

Emanuel Müller¹, Urs von Gunten^{1,2,3}, Lenny Winkel^{1,2}

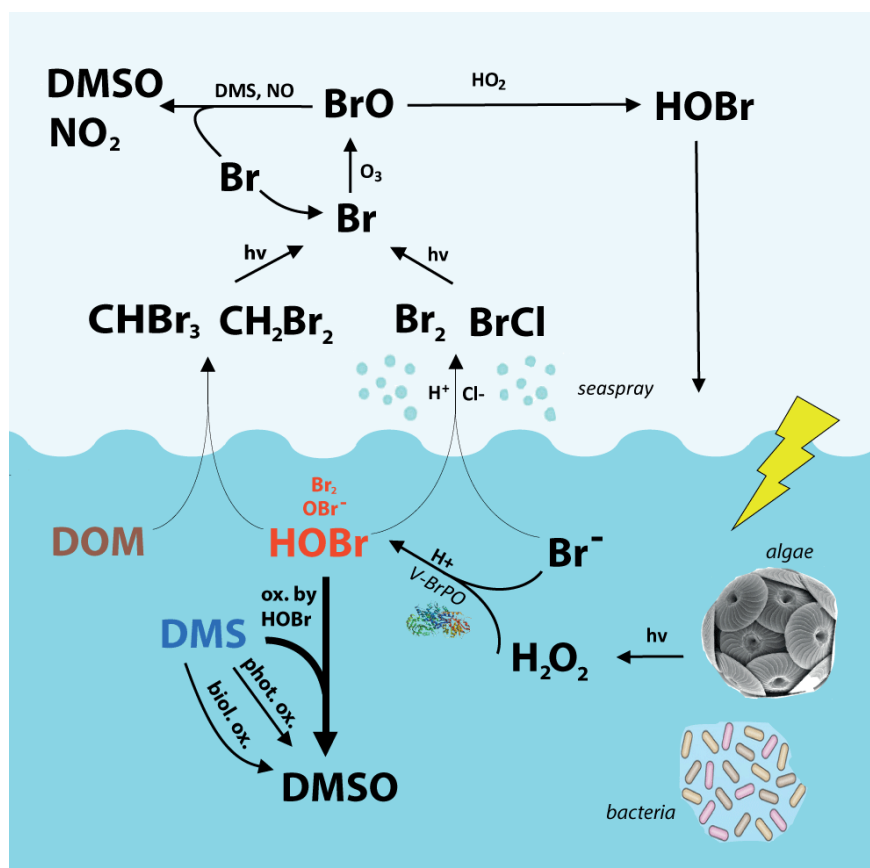
¹ Eawag, Swiss Federal Institute of Aquatic Science and Technology, Department of Water Resources and Drinking Water (W+T), Überlandstrasse 133, CH-8600 Dübendorf

² ETH Zürich, Swiss Federal Institute of Technology, Institute of Biogeochemistry and Pollutant Dynamics (IBP), Department of Environment Systems (D-USYS), Sälimstrasse 101, 8092 Zürich

³ School of Architecture, Civil and Environmental Engineering (ENAC), Ecole Polytechnique Fédérale de Lausanne, CH-1015 Lausanne, Switzerland

Marine volatile organic sulfur and bromine compounds are important players in climatic processes. A key compound in the production of volatile bromine compounds (e.g. bromoform, dibromomethane) is enzymatically produced bromine (e.g., Br₂, HOBr, OBr), via reactions with dissolved organic matter (DOM) in marine waters. Indirectly, these reactions are also important for stratospheric chemistry, as the volatile bromine species can photolyze to Br atoms, which are known to degrade ozone (see figure below). However, apart from reacting with DOM, bromine potentially also reacts with biogenic marine organic sulfur compounds (e.g. dimethylsulfoniopropionate, dimethylsulfide, dimethylsulfoxide) and could thus play an additional role in controlling concentrations of these species in marine waters. Nevertheless, the reactivity of bromine towards these species is largely unknown.

Therefore, we study the competition between reactions of HOBr with organic sulfur compounds and DOM in marine waters by determining second order rate constants for their reactions. Furthermore, experiments with a diffusion-reaction chamber model, simulating transport through membranes, as well as biotic experiments with algae and bacteria are planned. Our results will give a first answer to the question to what extent the presence and concentrations of organic sulfur species may influence the formation of brominated volatile organic compounds and thereby affect the concentrations of these and organic sulfur compounds in the marine environment.



The possible role of DMS in the bromine cycle. DMS might react fast with HOBr and reduces therefore the availability of HOBr for the production of volatile bromine species (indicated by thin arrows). The reaction between HOBr and DMS might also represent the major DMS removal process (indicated by thick arrow). Note that the volatile bromine species (i.e. Br₂, CHBr₃, CH₂Br₂, BrCl) are produced in the water before they enter the atmosphere via air-sea gas exchange. For a better overview of the main reaction processes these transport processes between marine waters and the atmosphere are not shown.

REFERENCES

- Rehder D. 2014: Vanadate-Dependent Peroxidases in Macroalgae: Function, Applications, and Environmental Impact. *Oceanography* 2, 121.
- Stefels et al. 2007: Environmental constraints on the production and removal of the climatically active gas dimethylsulphide (DMS) and implications for ecosystem modelling. *Biogeochemistry* 83, 245-275.
- Wever, R., & van der Horst M.A. 2013: The role of vanadium haloperoxidases in the formation of volatile brominated compounds and their impact on the environment. *Dalton Transactions* 42, 11778-11786.

14.10

Dynamics of Zn in urban wetland soil-plant systems: coupling EXAFS and isotopic approaches

Géraldine Sarret¹, Anne-Marie Aucour², Marine Queyron³, Romain Tholé³, Aline Lamboux², Denis Testemale⁴, Valérie Magnin¹, Jean-Philippe Bedell³

¹ ISTERre, Université Grenoble Alpes, CNRS, BP53, F-38041 Grenoble, France (geraldine.sarret@univ-grenoble-alpes.fr)

² Université de Lyon, ENS de Lyon, Université Lyon 1, CNRS, UMR 5276 LGL-TPE, F-69364 Lyon Cedex 7, France

³ Université de Lyon, ENTPE, CNRS, UMR 5023 LEHNA, 2 Rue Maurice Audin F-69518 Vaulx-en-Velin, France

⁴ ESRF, FAME Beamline, 71 rue des Martyrs, Grenoble F-38000, France

The present study is focused on zinc, a metal contaminant present at high to toxic concentrations in mining, urban and industrial environments. The study of Zn speciation in soils had shed light on Zn sequestration mechanisms and the formation of stable Zn phases (Jacquat et al., 2009 and Refs. therein). On the other hand, only a few studies have been conducted on Zn speciation in wetland soils (Bostick et al., 2001; Peltier et al., 2003). Although some studies have evaluated the transfer and mass balance between the soil and plant compartments, little is known about the dynamics of transfer between and within the soil, litter, porewater and plant compartments. This dynamic aspect is crucial in a system subject to the continuous input of metals and fast biomass turnover.

This study focused on Zn speciation and dynamics in soil-plant systems of an urban wetland receiving stormwater. A combination of EXAFS spectroscopy and Zn stable isotope measurements was applied for soil, plant organs and decaying biomass in the flooded *Typha latifolia* and alternating wet-dry *Phalaris arundinacea* zones. EXAFS spectroscopy provides a snapshot of the final form of Zn accumulated in the various compartments whereas Zn isotopic composition is the result of diffusion and cross-membrane transport all along the Zn uptake and translocation pathway and it also depends on the quantity of Zn transferred.

In both soils, Zn was present as Zn-layered double hydroxide and tetrahedral and octahedral sorbed Zn species. In addition, *T. latifolia* soil contained ZnS. An iron plaque was found on *T. latifolia* rhizome and roots. Light isotope enrichment for Zn sorbed on the plaque suggested dissolution of ZnS in the rhizosphere with subsequent sorption. For both species, light isotope enrichment from soil to plant ($\Delta^{66}\text{Zn}_{\text{plant-soil}}$ of -0.5 to -0.6‰) suggested Zn uptake via low-affinity transport systems. In the organs of both plants, a mixture of octahedral and tetrahedral Zn attributed to symplastic Zn-organic acid and apoplasmic Zn-cell wall complexes, respectively, was observed (Aucour et al., 2005). In addition, Zn-thiol species were detected in the roots, rhizome and stem of *T. latifolia*. The $\delta^{66}\text{Zn}$ values measured in the plant organs suggested that Zn was sequestered in the stem after transit through leaves. In conclusion, this study provided a complete overview of Zn cycling in urban wetland soil-plant systems, and described several changes in Zn speciation with Zn isotopic fractionation processes in a complex system. Although the two soil-plant systems showed common trends in Zn isotopic fractionation and speciation, marked differences were observed due to waterlogging and also to plant species, with a prominent role of sulfur in the waterlogged system.

REFERENCES

- Aucour A.M., Bedell J.P., Queyron, M., Magnin V., Testemale D. & Sarret G. 2015: Dynamics of Zn in an urban wetland soil-plant system: coupling isotopic and EXAFS approaches. *Geochimica et Cosmochimica Acta*, 160, 55-69.
- Bostick B. C., Hansel C. M., La Force M. J. & Fendorf S. 2001: Seasonal fluctuations in zinc speciation within a contaminated wetland. *Environ. Sci. Technol.* 35, 3823-3829.
- Jacquat O., Voegelin A. & Kretzschmar R. 2009: Soil properties controlling Zn speciation and fractionation in contaminated soils. *Geochim. Cosmochim. Acta* 73, 5256-5272.
- Peltier E. F., Webb S. M. & Gaillard J. F. 2003: Zinc and lead sequestration in an impacted wetland system. *Adv. Environ. Res.* 8, 103-112.

14.11

Arsenic Cycling in Iron-rich Organic Freshwater Flocs

Laurel ThomasArrigo¹, Christian Mikutta¹, Regina Lohmayer², Britta Planer-Friedrich² & Ruben Kretzschmar¹

¹ Soil Chemistry Group, Institute of Biogeochemistry and Pollutant Dynamics, ETH Zürich, Universitätstrasse 16, CH-8092 Zürich (laurel.thomas@usys.ethz.ch)

² Environmental Geochemistry Group, Bayreuth Center for Ecology and Environmental Research (BAYCEER), Bayreuth University, Universitätstrasse 30, DE-95447 Bayreuth

Iron-rich organic flocs are commonly identified in freshwater wetlands and tend to show high affinities for trace metal(loid)s (Elliot et al., 2012, ThomasArrigo et al., 2014 & 2016). The Fe mineral phases existing within flocs play a dominant role in trace metal(loid) sorption, with higher trace metal(loid) concentrations associated with poorly crystalline Fe(III)-(oxyhydr)oxides (Elliot et al., 2012, ThomasArrigo et al., 2014 & 2016), and lower trace metal(loid) concentrations linked to increasing Fe(III)-(oxyhydr)oxide crystallinity and organic/sulfide-associated Fe(II) (Elliot and Warren, 2014, ThomasArrigo et al., 2016). Recently, we characterized organic flocs from freshwater streambeds of the As-enriched peatland *Gola di Lago* (canton Ticino, Switzerland) using ⁵⁷Fe Mössbauer spectroscopy and synchrotron X-ray techniques and found up to 2620 mg/kg As (arsenate and arsenite) bound in monodentate-binuclear ('bridging') surface complexes to ferrihydrite (e.g., ~Fe₅HO₈•4H₂O) and disordered nano-lepidocrocite (γ-FeOOH) (ThomasArrigo et al., 2014).

Gola di Lago flocs tend to settle in the low-flow streams and may eventually become buried and exposed to sulfate-reducing conditions. Both ferrihydrite and lepidocrocite are relatively unstable Fe(III)-(oxyhydr)oxides which readily oxidize sulfide. Transformations of floc-Fe mineral phases as well as speciation changes in floc-As induced by sulfate-reducing conditions may either inhibit or enhance the mobility of As through the formation of, for example, As sulfides or thioarsenic species. For this reason, we spiked As-rich organic freshwater flocs containing ≤35 wt.% C_{org} and ≤22 wt.% Fe with 5 mM bisulfide (molar S(-II)/As and S(-II)/Fe ratios = 290-720 and 0.73-1.55, respectively) at pH 7. Using a combination of X-ray absorption spectroscopy, electron microscopy, as well as HPLC-UV and IC-ICP-MS analyses, we investigated changes in the solid- and aqueous-phase speciation of As, Fe, and S over one week.

Our results show that after reaction with bisulfide, solid-phase Fe mineral transformations were dominated by mackinawite (FeS) formation (52-81% of Fe_{solid} at day 7), with a preferential transformation of ferrihydrite over lepidocrocite, although the neoformation of lepidocrocite could not be excluded. Sulfur speciation analyses revealed that S(0) and polysulfides were almost exclusively associated with the solid phase. Arsenic released from the solid phase was dependent on the molar S(-II)/Fe ratio, with highest As releases (up to 73% of total As) found at the highest molar S(-II)/Fe ratios. Up to 33% of dissolved As was present as thioarsenates. Solid-phase As, primarily present as arsenate (47-72%), was found preferentially adsorbed to Fe(III)-(oxyhydr)oxides, despite abundant mackinawite precipitation. At higher S(-II)/Fe molar ratios (≥1.0), the formation of an orpiment-like As sulfide mineral accounted for up to 35% of solid-phase As. Despite Fe and As sulfide precipitation and the presence of residual Fe(III)-(oxyhydr)oxides, mobilization of As was recorded in all samples (As_{aq} = 0.5-7.0 μM at 7 days). Our findings show that organic freshwater flocs from the *Gola di Lago* peatland may become a source of As under sulfate-reducing conditions, and thus likely play a pivotal role in trace metal(loid) cycling in S-rich wetlands characterized by oscillating redox conditions.

REFERENCES

- Elliott, A. V. C.; Plach, J. M.; Droppo, I. G.; Warren, L. A. 2012: Comparative floc-bed sediment trace element partitioning across variably contaminated aquatic ecosystems, *Environ. Sci. Technol.*, 46, 209-216.
- ThomasArrigo, L. K.; Mikutta, C.; Byrne, J.; Barmettler, K.; Kappler, A.; Kretzschmar, R. 2014: Iron and arsenic speciation and distribution in organic flocs from streambeds of an arsenic-enriched peatland, *Environ. Sci. Technol.*, 48, 13218-13228.
- ThomasArrigo, L. K.; Mikutta, C.; Lohmayer, R.; Planer-Friedrich, B.; Kretzschmar, R. 2016: Sulfidization of organic freshwater flocs from a minerotrophic peatland: Speciation changes of iron, sulfur, and arsenic, *Environ. Sci. Technol.*, 50, 3607-3616.
- Elliott, A. V. C., & Warren, L. A. 2014: Microbial engineering of floc Fe and trace metal geochemistry in a circumneutral, remote lake, *Environ. Sci. Technol.*, 48, 6578-6587.

14.12

Mn(II) oxidation coupled to Fe(II) oxidation in Fenton-type reactions

Case M. van Genuchten¹ & Jasquelin Peña¹

¹ *Laboratoire de Géochimie Environnementale, Institut des dynamiques de la surface terrestre, University of Lausanne, Quartier UNIL-Mouline, Bâtiment Géopolis, CH-1015 Lausanne (jasquelin.pena@unil.ch)*

The oxidation of Fe(II) by O_2/H_2O_2 initiates a cascade of reactions that leads to the formation of strong, short-lived oxidants ($^{\bullet}O_2^-$, $^{\bullet}OH$, Fe(IV)). These reactive intermediates are critical players in the oxidation of chemical species including As(III), Sb(III), organic pollutants, and soil organic matter. Recent studies provide indirect evidence that Mn(II) is also susceptible to homogeneous oxidation by reactive oxidants species, such as extracellular superoxide radicals produced by bacteria and superoxide and singlet oxygen radicals generated from photochemical excitation of humic substances.

This presentation will focus on characterizing the reaction products of Fe(II)-mediated Mn(II) oxidation and will describe the factors that control the Mn(II) oxidation efficiency in Fenton-type systems. An Fe(0) electrocoagulation (EC) system, which permits precise control of the rate of Fe(II) production, was used to investigate the co-oxidation of Fe(II) and Mn(II) as a function of the rate at which iron was dosed into solution, the Fe(II) oxidant (O_2 or H_2O_2), and solution pH. Our experimental approach combines i) time-dependent Mn(II) removal experiments, ii) pyrophosphate (PP) extractions for measurements of Mn(III), and iii) Mn and Fe K-edge EXAFS spectroscopy.

The results presented in this work uncover an undocumented pathway of Mn(II) oxidation and will help form the basis of Mn(II) oxidation kinetic models in Fenton-type systems. This information is critical for accurate predictions of target compound oxidation in systems containing Mn(II), such as groundwater contaminated with As(III) and Mn(II).

14.13

Time-Resolved characterization of Co(II) Oxidation by δ -MnO₂ using quick X-ray absorption spectroscopy

Yuheng Wang¹, Sassi Benkaddour¹, Francesco Marafato¹ & Jasquelin Peña¹

¹ *Laboratoire de Géochimie Environnementale, Institut des dynamiques de la surface terrestre, University of Lausanne, Quartier UNIL-Mouline, Bâtiment Géopolis, CH-1015 Lausanne (yuheng.wang@unil.ch)*

Environmental manganese (Mn) oxides typically occur as layered-type birnessites, which contain varying amounts of Mn(II,III) and vacant Mn(IV) sites in the MnO₂ sheets. Due to the high sorptive and oxidative capacities, Mn oxides are among the most reactive soil minerals and control the mobility and bioavailability of organic and inorganic contaminants, e.g. pesticides, flame retardants, Cr, As, Se, Co etc. However, the relationship between the oxidative power of Mn oxides and their chemistry and mineralogy is still under debate in the literature.

Recently, we showed that different sites on the surface of δ -MnO₂ nanoparticles display distinct adsorption and capacity, which is controlled both by the valence (Mn(III) or Mn(IV)) and location (i.e., layer edges, layer interior vacancies, interlayer) of the site (Simanova et al., 2015a). These findings suggest that information about the kinetics of interfacial processes, as well as time-dependent speciation of surface species, is critical to understand the redox reactivity of Mn oxides. Specifically, there are two open questions: 1) at which reactive sites (vacancy sites vs. edge sites) does electron transfer occur between Mn oxides and adsorbed reductants; 2) what conditions favor Mn(III) versus Mn(IV) surface sites as a major oxidant. Our previous quick X-ray absorption spectroscopy (QXAS) study (Simanova et al., 2015b) using Co(II) to probe the redox reactivity of Mn(III)-rich δ -MnO₂ (referred to as " δ -Mn^{III,IV}O₂" hereafter) showed that at pH 6.6 Co(II) was first oxidized by Mn(III) sites at the particle edges, while the vacancy sites capped by interlayer Mn(III) atoms were largely unreactive. The limited redox reactivity of interlayer Mn(III) atoms in δ -Mn^{III,IV}O₂ can be explained by the slow electron transfer of outer-sphere complexes and the passivation of the vacancies by adsorbed Mn(III). However, the kinetics of Co(II) oxidation may be enhanced significantly if pure Mn(IV) oxide (referred to as " δ -Mn^{IV}O₂" hereafter) was used, as it possesses abundant free vacancy sites (11%).

In the present study, we carried out time-resolved QXAS analyses on the oxidation of Co(II) by δ -Mn^{IV}O₂ at pH 8, 6 and 4 maintained using pH STAT and with Co(II)/Mn(IV) molar ratio from 0.1 to 0.4. The results show that Co(II) was quickly immobilized on the surface of δ -Mn^{IV}O₂ through adsorption followed by gradual oxidation. More specifically, at pH 8 all initial soluble Co(II) was transferred to δ -Mn^{IV}O₂ in less than 10 min, whereas at pH 6 and 4 less than 70% of the initial Co(II) was sorbed after 24-hr. These findings show slowed adsorption of Co(II) on δ -Mn^{IV}O₂ in experiments at pH 6 and 4. Moreover, δ -Mn^{IV}O₂ is mainly reduced to δ -Mn^{III,IV}O₂ by Co(II) at all the three pH values and only up to 2% of initial Mn(IV) is converted to soluble Mn(II). This suggests that Mn(IV) is significantly more redox reactive than Mn(III) in δ -Mn^{III,IV}O₂ under the conditions of the present study. The outcome of the study helps to fill the knowledge gap in identifying the type of Mn valence and sites in δ -MnO₂ that most effectively oxidize contaminants, and it provides valuable information for predicting the mobility and bioavailability of contaminants in Mn-containing surface environments.

REFERENCES

- Simanova, A.A., Kwon, K.D., Bone, S.E., Bargar, J.R., Refson, K., Sposito, G. & Peña, J. 2015a: Probing the sorption reactivity of the edge surfaces in birnessite nanoparticles using nickel(II). *Geochimica et Cosmochimica Acta*, 164, 191-204.
- Simanova, A.A. and Peña, J. 2015b: Time-Resolved Investigation of Cobalt Oxidation by Mn(III)-Rich δ -MnO₂ Using Quick X-ray Absorption Spectroscopy. *Environmental Science & Technology*, 49, 10867-10876.

14.14

Thallium sorption on illite and its importance in soils

Silvan Wick¹, Bart Baeyens² & Andreas Voegelin³

¹ *Eawag, Überlandstrasse 133, CH-8600 Dübendorf (silvan.wick@eawag.ch)*

² *Paul Scherrer Institute, CH-5232 Villigen PSI (bart.baeyens@psi.ch)*

³ *Eawag, Überlandstrasse 133, CH-8600 Dübendorf (andreas.voegelin@eawag.ch)*

Thallium (Tl) is a highly toxic trace metal. In the environment, Tl occurs as monovalent Tl^I and trivalent Tl^{III}. Tl^I exhibits both chalcophilic and lithophilic character. Because Tl^I has a similar ionic radius as K⁺, it can substitute K⁺ in a wide range of K-bearing minerals. In soils and sediments, Tl^I uptake by the clay mineral illite has long been considered to be a key retention mechanism. Direct evidence for Tl uptake by illite in soils was provided by a recent spectroscopic study on geogenically Tl-rich soils (Voegelin et al. 2015). To date, however, data on Tl sorption by illite and its effect on Tl solubility in soils are lacking.

We currently investigate the sorption of Tl^I by pure illite (Illite du Puy) in batch experiments. First results confirm that Tl^I uptake by illite is highly specific and exhibits similar trends as known for Cs⁺ (Poinssot et al., 1999; Fuller et al., 2015): Limited pH dependence, marked sorption competition with Na⁺, and slow sorption/desorption kinetics. The new sorption data for Tl^I on illite will be quantitatively described in the framework of a generalized model of K⁺, Rb⁺, Cs⁺ and NH₄⁺ uptake by argillaceous rocks (Bradbury and Baeyens, 2000).

To gain direct insight into the effect of Tl sorption by illite in soils, we examine the solubility and extractability of Tl in geogenically Tl-rich soils from the Swiss Jura mountains (Voegelin et al., 2015) covering a wide range in Tl contents. Qualitatively, the results from extracts targeting soluble (10 mM CaCl₂) and exchangeable cations (1 M NH₄-acetate) are in line with Tl uptake by illite as solubility-controlling process. Additional time-resolved extracts reveal slow Tl release kinetics, probably from high-affinity sorption sites.

In continuing work, further insight into Tl uptake by illite and Tl speciation in soils will be obtained using synchrotron-based X-ray absorption spectroscopy. Our mechanistic sorption results in combination with our quantitative data will lead to an improved understanding of the uptake of Tl by illite and its impact on the mobility and bioavailability in soils.

REFERENCES

- Bradbury, M. H., Baeyens, B. (2000) A generalised sorption model for the concentration dependent uptake of caesium by argillaceous rocks, *Journal of Contaminant Hydrology*, 42, 141-163.
- Fuller, A.J., Shaw, S., Ward, M.B., Haigh, S.J., Mosselmans, J.F.W., Peacock, C.L., Stackhouse, S., Dent, A.J., Trivedi, D. and Burke, I.T. (2015) Caesium incorporation and retention in illite interlayers, *Applied Clay Science*, 108, 128-134.
- Poinssot, C., Baeyens, B. and Bradbury, M.H. (1999) Experimental and modelling studies of caesium sorption on illite, *Geochimica et Cosmochimica Acta*, 63(19-20), 3217-3227.
- Voegelin, A., Pfenninger, N., Petrikis, J., Majzlan, J., Plötze, M., Senn, A.C., Mangold, S., Steininger, R., and Gottlicher, J. (2015): Thallium speciation and extractability in a thallium- and arsenic-rich soil developed from mineralized carbonate rock, *Environmental Science and Technology*, 49, 5390-5398.

14.15

Zinc isotope fractionation during translocation in wheat

Matthias Wiggerhauser¹, Wolfgang Wilcke², Moritz Bigalke³, Martin Imseng³, Michael Müller⁴, Corey Archer⁵, Emmanuel Frossard¹

¹ Institute of Agricultural Sciences, ETH Zurich, Eschikon 33, CH-8315 Lindau, matthias.wiggerhauser@usys.ethz.ch

² Institute of Geography and Geoecology, Karlsruhe Institute of Technology (KIT), P.O. Box 6980, D-76049 Karlsruhe

³ Geographic Institute, University of Bern, Hallerstrasse 12, CH-3012 Bern

⁴ Swiss Soil Monitoring Network (NABO), Agroscope, Reckenholzstrasse 191, CH-8046 Zürich

⁵ Institute of Geochemistry and Petrology, Department of Earth Sciences, ETH Zürich, Clausiusstrasse 25, CH-8092 Zurich

Zinc (Zn) is an essential element for plants and humans. There are different strategies how plants satisfy their Zn needs which are well studied. However, there is a paucity of information on how Zn is redistributed between the various plant parts (e.g., from leaves to grain). Furthermore, uptake and redistribution processes of Zn also control plant tissue concentrations of the chemically similar and toxic element Cadmium (Cd). To better understand translocation of Zn in plants, we used Zn stable isotope ratios to elucidate biochemical processes that drive Zn translocation in the plant.

Wheat (*Triticum aestivum* L.) was grown on two agricultural soils with different pH and organic matter content under controlled conditions. Wheat plants were harvested at two different stages of growth, flowering stage and at full maturity, and were then systematically dissected for isotopic analysis into the following parts that play a distinct role in Zn redistribution processes (overview in Figure 1). Until the SGM 2016, Zn isotopes will be also analyzed in $n = 3$ individually grown plants, in xylem sap, bulk soil and in 0.1M HCl soil extracts as proxy for plant- available Zn.

Preliminary results revealed that Zn concentrations in straw strongly decreased during grain filling (straw_{flowering} 28 $\mu\text{g g}^{-1}$, straw_{fullmaturity} 13 $\mu\text{g g}^{-1}$, $n = 1$). Thus, approximately 75% of the Zn in the shoot was translocated to the grains between flowering and full maturity (grain_{fullmaturity} 39 $\mu\text{g g}^{-1}$). There was a slight difference in the Zn isotope composition in the shoots at flowering ($\delta^{66/64}\text{Zn}_{\text{JMC}} = 0.21\text{‰}$, Figure 1) and at full maturity (0.27‰). However, at full maturity, there was an enrichment of light isotopes in the grains (0.18‰) and a corresponding enrichment of heavy isotopes in the straw (0.49‰). The Zn isotope ratios of the straw parts ranged from 0.25-0.76‰ and showed distinct apparent isotope fractionation comparing the two growth stages (e.g. $\Delta_{\text{fullmaturity-flowering}}$: peduncle 0.57‰, flag leave 0.23‰). These values indicate that different plant parts did not release Zn to the grain in an equally efficient manner.

The preliminary data show that Zn isotopes are markedly fractionated during the grain filling period of wheat and potentially provide information about Zn fluxes and biogeochemical processes within wheat. At the conference, the complete data set will be discussed regarding (i) Zn fluxes in the plant during grain filling using mass balances and Zn isotope ratios, (ii) processes causing Zn isotope fractionation during translocation in wheat, and (iii) a comparison of Zn isotope fractionation with that of Cd isotopes in soil-wheat systems.

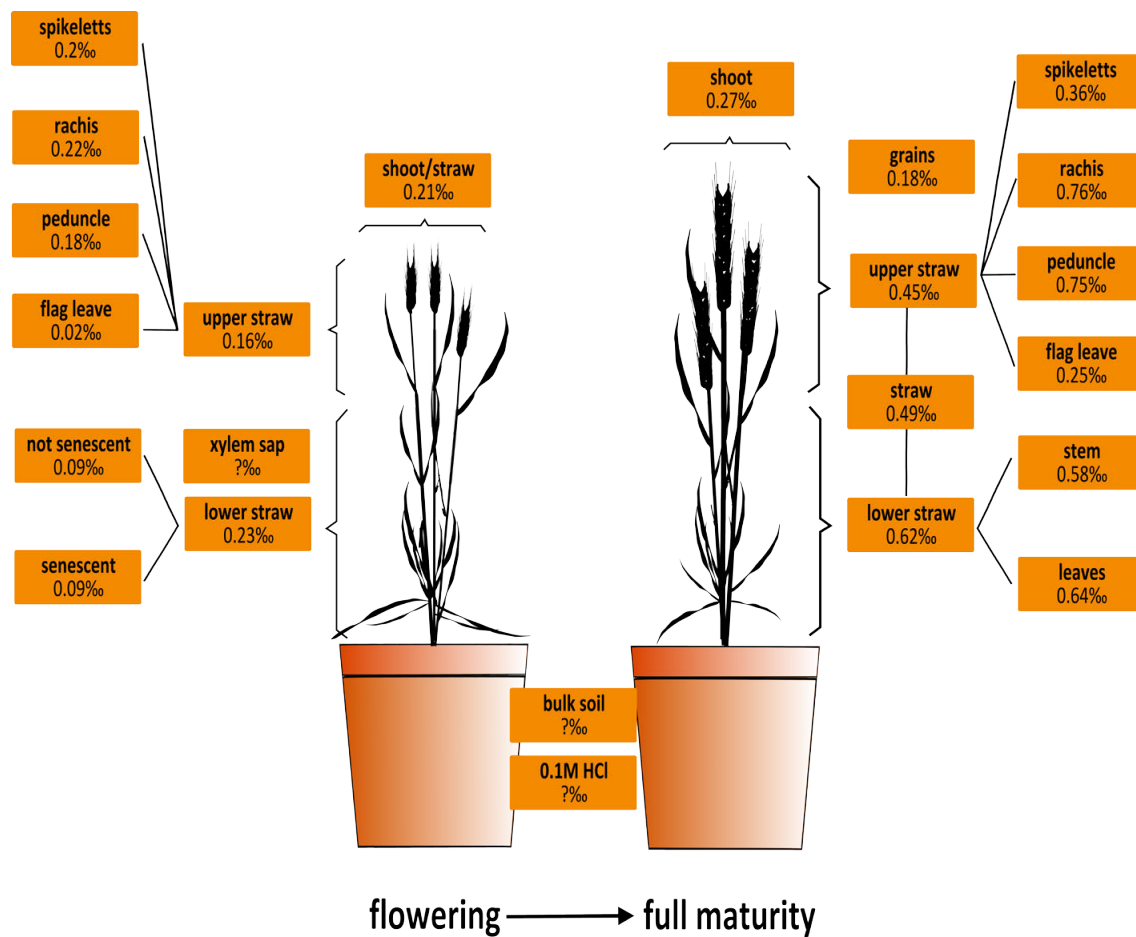


Figure 1: Zinc isotope ratios of wheat grown on arable soils under controlled conditions. Plants were harvested at flowering stage (left) and at full maturity (right). Preliminary results show $\delta^{66/64}\text{Zn}_{\text{JMC}}$ ratios in ‰ for $n = 1$ fully analyzed wheat plant per growth period. Question marks indicate that these compartments have not been measured yet.

P 14.1

***Elodea nuttallii* exposure to mercury in natural water under enhanced ultraviolet radiation**

Rebecca Beauvais-Flück, Nicole Regier, Vera I. Slaveykova, Claudia Cosio

Environmental Biogeochemistry and Ecotoxicology, Department F.-A. Forel for Environmental and Aquatic Sciences, Earth and Environmental Sciences, Faculty of Sciences, University of Geneva, 66 boulevard Carl-Vogt, CH-1205 Geneva, Switzerland

Macrophytes are aquatic plants that play a key role in primary production and nutrients biogeochemical cycles of shallow waters (e.g. lakes, ponds). Fitness of macrophytes in these environments is likely to be affected by the increase of UV-radiation occurring during severe hydrological alterations (e.g. drought) that may become more frequent and intense due to climate change. Higher UV radiation is thought to affect the growth and development of aquatic plants and also their sensitivity to metal pollution.

Mercury (Hg) is one priority contaminant of global importance. In aquatic ecosystems, the mercury problem has received special attention because of the toxicity to aquatic organisms and the accumulation in aquatic food webs. Primary producers, including aquatic macrophytes accumulate Hg directly from water and sediments.

The aim of this study was to determine how the predicted environmental changes of the 21st century will affect macrophytes. To this end, the effects of increased UV radiation, combined with Hg pollution in natural waters on both Hg bioaccumulation and its effects at the physiological and transcriptomic level were investigated in *Elodea nuttallii*. We hypothesize that organic matter present in natural waters will reduce Hg bioaccumulation and that UV and heavy metal stress have interacting effects on the macrophytes and might induce a phenomenon termed cross-tolerance.

The results demonstrated that the increasing concentrations of organic matter (1-10 mg/L Suwannee River humic acid (SRHA)) decreased Hg bioaccumulation at 10^{-9} M inorganic Hg (IHg) and methyl Hg (MeHg), but not 10^{-7} M IHg. In IHg + MeHg mixture exposure, bioaccumulation of Hg was reduced by SRHA. At the transcriptomic level, the intensity of genes signals clearly decreased with increasing SRHA, supporting that the response of those genes correlated to Hg bioavailability. In sum, the gene signatures are specific for a given chemical and linked to its bioavailability. Our data support that transcriptomic is suitable to measure bioavailability of metals.

Combined exposure to UV + Hg enhanced the stress response at the transcriptomic level in comparison with single treatments, affecting the expression level of genes involved in energy metabolism, lipid metabolism, nutrition, and redox homeostasis. Single and combined UV and Hg treatments dysregulated different genes, but with similar functions, suggesting a fine regulation of the plant to stresses triggered by Hg, UV and their combination but the lack of co-tolerance. At the physiological level, UV + Hg treatment reduced chlorophyll content and depleted antioxidant compounds such as anthocyanin and GSH/GSSG, in *E. nuttallii*. Nonetheless, combined exposure to UV + Hg resulted in about 30% reduction in Hg accumulation in shoots vs. exposure to Hg alone, which was congruent with the level of expression of several transporters' genes, as well as the UV effect on Hg bioavailability in water.

In conclusion, both organic matter and light affected bioaccumulation and stress responses in the plant: fine and contrasted interactions were evidenced at the physiological level by the different endpoints for pigments and oxidative stress affected in additive, antagonistic or synergistic manner suggesting a multilevel interaction between organic matter, Hg and UV exposure.

The findings of the present work underlined the importance of performing experimentation under environmentally realistic conditions and to consider the interplay between contaminants and environmental variables, such as light that might have confounding effects, to better understand and anticipate the effects of multiple stressors in the aquatic environment. In the context of global climate changes even lower bioaccumulation of Hg might result in higher stress level for organisms.

P 14.2

Redox properties of manganese oxide minerals (birnessite)

Sassi Benkaddour¹, Michael Sander², Francesco Femi Marafatto¹, Jasquelin Peña¹

¹ *Institute of Earth Surface Dynamics, University of Lausanne, Lausanne 1015, Switzerland (sassi.benkaddour@unil.ch)*

² *Department of Environmental Systems Science, Institute of Biogeochemistry and Pollutant Dynamics, Swiss Federal Institute of Technology (ETH) Zurich, Zurich, Switzerland (michael.sander@env.ethz.ch)*

Manganese oxide minerals are critical players in a number of biogeochemical processes and have the potential to be used in environmental remediation and materials science applications. These minerals are powerful oxidants of inorganic and organic species and have remarkably high adsorption capacities for trace and contaminant metals. The reactivity of layer-type manganese oxides (birnessite) is controlled by their structure and composition, including particle size, presence of structural defects in the form of vacancy sites, and the presence of adsorbed or structural Mn(III) (Simanova & Peña 2015; van Genuchten & Peña 2016).

The goal of this project was to investigate the redox properties for a suite of birnessite minerals that varied in terms of their structure (nm – μm sizes) and composition (0 – 20 % Mn(III): c-disordered birnessite (c-dis Bi), nanocrystalline δ-MnO₂ (δ-MnO₂), crystalline potassium birnessite (K Bi) and microcrystalline triclinic birnessite (Tc Bi). We hypothesized that both particle size as well as the crystallographic location and amount of Mn(III) in the mineral govern the mineral redox properties and thus reactivity. To test this hypothesis we developed analytical methods that are easily applicable to assess the redox state of these minerals. We then used mediated potentiometry (Sander et al. 2015; Gorski et al. 2016) to determine the reduction potentials (E_{H}) of the minerals at different pH values and concentrations of Mn²⁺. The combination of results from solid-phase characterization and electrochemical measurements will allow us to link the structure and composition of the birnessites to their oxidative capacity.

Thus far, we established two methods for the quantification of Mn(III) and the determination of the Average Manganese Oxidation Number (AMON) for a given manganese oxide. In the first method, sodium pyrophosphate (PP) is used to extract surface-bound/incorporated Mn(III) from Mn(III)-bearing MnO₂ to form Mn(III)-PP complexes. The concentration of these complexes can be quantified spectrophotometrically. In the second method, the AMON was determined by potentiometric titrations (Simanova et al. 2015): after using Mohr's salt to achieve complete reductive dissolution of the mineral to Mn²⁺, permanganate is used to back titrate the Mn²⁺ solution to Mn(III) using excess PP. While both methods are quite accurate, the PP extraction method slightly underestimates the Mn(III) content, compared to the AMON titration method (about 5% less Mn(III)), of the minerals with a low specific surface area.

To measure the reduction potential (E_{H}) as a function of suspension pH we used mediated potentiometry in which the electron transfer mediator 2,2'-azino-bis(3-ethylbenzothiazoline-6-sulphonic acid) (ABTS) was used to facilitate redox equilibration between the mineral and the working electrode (Pt). Initial observations suggest that the four minerals present different potentials, for the same conditions of pH and total Mn concentration, that depend on Mn(III) contents and -to a lesser extent- on parameters like specific surface area. A deeper investigation of the redox properties, especially focusing on potential equilibrium conditions and covering a broad range of environmental pH values will improve our ability to understand the role of manganese oxides in biogeochemical processes and pollutant dynamics. A more fundamental understanding of the relationship between mineral structure and redox properties will further allow for control and design of manganese oxides with specific redox properties.

REFERENCES

- Gorski, C.A., Edwards, R., Sander, M., Hofstetter, T.B. and Stewart, S.M. 2016: Thermodynamic Characterization of Iron Oxide–Aqueous Fe²⁺ Redox Couples. *Environmental science & technology*.
- Sander, M., Hofstetter, T.B. and Gorski C.A. 2015: Electrochemical analyses of redox-active iron minerals: a review of non-mediated and mediated approaches. *Environmental science & technology*, 49, 5862-5878.
- Simanova, A.A. and Peña, J. 2015: Time-resolved investigation of cobalt oxidation by Mn(III)-rich δ-MnO₂ using quick X-ray absorption spectroscopy. *Environmental science & technology*, 49, 10867-10876.
- Simanova, A.A., Kwon, K.D., Bone, S.E., Bargar, J.R., Refson, K., Sposito, G. and Peña, J. 2015: Probing the sorption reactivity of the edge surfaces in birnessite nanoparticles using nickel(II). *Geochimica et Cosmochimica Acta*, 164, 191-204.
- van Genuchten, C.M. and Pena, J. 2016: Sorption Selectivity of Birnessite Particle Edges: a d-PDF Analysis of Cd(II) and Pb(II) Sorption by δ-MnO₂ and Ferrihydrite. *Environmental sciences processes & impacts*.

P 14.3

Trace metal and iron isotope cycling in the meromictic Lake Cadagno

Christel Hassler¹ Derek Vance², Sophie Moisset¹ Ludovic Pascal³ Michael Ellwood⁴

¹ University of Geneva, Institute F. A. Forel, 10 rte de Suisse, 1290 Versoix, Switzerland. (Christel.Hassler@unige.ch)

² Institute of Geochemistry and Petrology, Department of Earth Sciences, ETH Zürich.

³ University of Bordeaux, EPOC, Talence, France.Genève

⁴ Research School of Earth Sciences, Australian National University, Canberra, Australia. (michael.ellwood@anu.edu.au)

Lake Cadagno is a 21 m deep alpine meromictic lake that is permanently stratified. It has two chemically distinct water layers; an oxic mixolimnion and an anoxic monimolimnion with a narrow chemocline separating the two. The chemocline is located across a narrow band between 10 to 13 m with a large chemical gradient in dissolved oxygen, redox potential, nutrients (nitrate, ammonia), dissolved and particulate trace elements (iron, manganese, vanadium, chromium, copper etc), and sulfur species. The reaction series for changes in nutrient and trace metal concentrations associated with the transition from oxic to anoxic conditions follow the “classical” sequence seen for meromictic lakes and sediment porewaters.

Iron isotope analysis of both dissolved ($\delta^{56}\text{DFe}$) and particulate ($\delta^{56}\text{PFe}$) iron revealed a very sharp transition between 11.5 and 12 m with heavier $\delta^{56}\text{DFe}$ values above ($\sim 0.75\text{‰}$) and lighter $\delta^{56}\text{DFe}$ values below the ferrocline (-0.61‰). The isotope composition of $\delta^{56}\text{PFe}$ was opposite with lighter $\delta^{56}\text{PFe}$ values (relative to $\delta^{56}\text{DFe}$) above and heavier $\delta^{56}\text{PFe}$ values below the ferrocline. Our results indicate that $\delta^{56}\text{DFe}$ fractionation is under kinetic control with the rate of reduced iron diffusion across the chemocline, and its subsequent oxidation, being the key steps in setting $\delta^{56}\text{DFe}$.

P 14.4

Sulfidation kinetics of copper oxide nanoparticles

Alexander Gogos¹, Basilius Thalmann¹, Andreas Voegelin¹ and Ralf Kaegi¹

¹ *Eawag, Swiss Federal Institute of Aquatic Science and Technology, Überlandstrasse 133, CH-8600 Dübendorf (alexander.gogos@eawag.ch)*

In addition to their use in the fields of catalysis, electronics and energy, copper oxide nanoparticles (CuO NP) are increasingly used in a variety of biocide applications, such as wood preservation, anti-fouling coatings and agricultural pesticides (Tegenaw et al., 2015). From some applications, CuO NP are directly released into the wastewater stream and reach a wastewater treatment plant (WWTP). Due to the elevated concentration of bisulfide (HS⁻) in wastewater systems, reactions with bisulfide strongly influence the speciation and bioavailability of chalcophile elements such as Cu and Ag in (treated) wastewater (Kaegi et al., 2011).

In this study, we investigated the sulfidation of CuO NP (3-13 μM) by HS⁻ (14-170 μM) in oxic solutions at pH 8.0. Reacted CuO NP were collected at selected time points and characterized using scanning transmission electron microscopy (STEM) in combination with energy dispersive X-ray (EDX) analysis. The kinetics of the reaction were determined over a range of CuO NP and HS⁻ concentrations using AgNO₃ for the selective dissolution of Cu_xS and Zincon for the spectrophotometric quantification of the released Cu²⁺.

The STEM analyses revealed a rapid transformation of crystalline CuO into amorphous Cu_xS upon reaction with bisulfide. Over time, amorphous Cu_xS recrystallized into hexagonal platelets, pointing to the formation of covellite. The formation of Cu_xS seemed to proceed in two stages: Fast initial CuO sulfidation to Cu_xS followed by a considerably slower reaction that led to a further increase of the Cu_xS fraction. Although the mechanistic details of the sulfidation of CuO still need to be fully resolved, our kinetic results clearly show that at most a few minutes are required for the transformation of half of the CuO into Cu_xS under conditions relevant for wastewater systems. Thus, CuO NP released from consumer products into wastewater are expected to be rapidly transformed into Cu_xS. With the treated effluent, part of this Cu_xS may be released into surface waters downstream of wastewater treatment plants.

REFERENCES:

- Kaegi, R., Voegelin, A., Sinnet, B., Zuleeg, S., Hagendorfer, H., Burkhardt, M. & Siegrist, H. (2011) Behavior of Metallic Silver Nanoparticles in a Pilot Wastewater Treatment Plant. *Environ. Sci. Technol.* 45, 3902-3908.
- Tegenaw, A., Tolaymat, T., Al-Abed, S., El Badawy, A., Luxton, T., Sorial, G. & Genaidy, A. (2015) Characterization and Potential Environmental Implications of Select Cu-Based Fungicides and Bactericides Employed in US Markets. *Environ. Sci. Technol.* 49, 1294-1302.

P 14.5

Pb, Zn and Mn sorption on biogenic MnO₂: linking sorption affinity to reactive surface sites

Julia Gonzalez Holguera¹, Imelda Dossou Etui¹ & Jasquelin Peña¹

¹ *Institute of Earth Surface Dynamics, University of Lausanne, CH-1015, Lausanne (julia.gonzalezholguera@unil.ch)*

Layer-type manganese oxides (MnO₂) are soil minerals that sequester metal cations on their surfaces, which makes them key players in the distribution and bioavailability of natural and anthropogenic inorganic contaminants in soils. Their remarkable sorption properties are mainly explained by a high content of vacancy sites, in which Mn(IV) are absent from octahedral sites, and the influence of edges due to the particles' small sizes. Both characteristics lead to local oxygen unsaturation and high reactivity towards metal cations.

Recently, studies of Ni sorption on a Mn(III)-enriched synthetic MnO₂ demonstrated that Mn(III) capping of vacancies could prevent Ni accessing these reactive sites, thus encouraging sorption on edges and diminishing the sorption capacity of the mineral (1). This finding is particularly relevant in natural systems, where the local presence of organic matter can induce partial reduction of Mn(IV) to Mn(III), thus increasing the Mn(III) content of natural Mn oxides. Furthermore, because the precipitation of MnO₂ in natural systems is microbially mediated, MnO₂ typically occurs admixed with microbial biomass. While the mineral is expected to control the sorption process, the biomass fraction also influences metal sorption by contributing directly to the sorption capacity of the composite, or by passivating reactive surface sites on the particle edges.

This study aims to further our mechanistic understanding of metal sorption on an environmentally relevant biogenic MnO₂ that contains both a significant Mn(III) content and an extracellular organic fraction, through batch sorption experiments and EXAFS spectroscopy. Biogenic MnO₂ was precipitated by the model bacterium *Pseudomonas putida* GB-1. Lead(II) and Zn(II) were chosen as probe ions because they are found on both sides of Mn(III) on the affinity sequence for MnO₂ surfaces (2-5). Sorption isotherms of Pb and Zn were measured on bio-mineral composites at pH 5.2 (+/- 0.3). Samples were prepared for EXAFS analysis at the Mn and Zn K-edges and Pb L3 edge, at pH 5.5 (+/- 0.2) to identify the partitioning between different sorption sites as a function of the affinity of the metal ions for the MnO₂ surface.

Both ions show high affinity for the mineral, but maximum loading of Pb was significantly higher than that for Zn ($q = 0.55$ mol Pb/ mol Mn and $q = 0.12$ mol Zn/ mol Mn respectively). Sorption of Pb(II), but not of Zn(II), was associated with the accumulation of Mn(II) in solution. This difference was explained by the ability of Pb(II), but not Zn(II), to displace Mn(II/III) from sorption sites, in accordance with the affinity sequence Zn(II) < Mn(II/III) < Pb(II) for MnO₂ (2, 3, 5). The 0.6 ($R^2 = 0.95$) ratio between Mn released and sorbed Pb suggest that Pb sorption induces disproportionation of surface bound Mn(III), with associated release of Mn(II) and crystal growth from newly formed Mn(IV). The amount of Mn(II) accumulated in solution as a function of Pb loading was used to estimate the initial Mn(II,III) found on the mineral surface. The good agreements between our estimated Mn(III) content and independent measurements of Mn(III) in biogenic MnO₂, further substantiate the mechanism conclusions.

This study investigates how the access to the different sorption sites of an environmentally relevant MnO₂ mineral varies for different incoming metal cations. Our findings demonstrate that their respective capacities to displace any previously sorbed metal ions ultimately determines the effective capacity of MnO₂ to influence the fate of different, often co-occurring, contaminants in natural systems.

REFERENCES

1. Simanova AA, Kwon KD, Bone SE, Bargar JR, Refson K, Sposito G, et al. Probing the sorption reactivity of the edge surfaces in birnessite nanoparticles using Nickel (II). *Geochim. Cosmochim. Ac.* 2015;164:191-204.
2. Murray JW. The interaction of metal ions at the manganese dioxide-solution interface. *Geochim Cosmochim. Ac.* 1975;39(4):505-19.
3. Matocha CJ, Elzinga EJ, Sparks DL. Reactivity of Pb (II) at the Mn (III, IV)(oxyhydr) oxide-water interface., *Environ. Sci. Technol.*, 2001;35(14):2967-72.
4. Villalobos M, Bargar J, Sposito G. Mechanisms of Pb (II) sorption on a biogenic manganese oxide, *Environ. Sci. Technol.*, 2005;39(2):569-76.
5. McKenzie R. The adsorption of lead and other heavy metals on oxides of manganese and iron, *Soil Research*, 1980;18(1):61-73.

P 14.6

Selenium Methylation by a *Pseudomonas* Species and its Transcriptomic Responses to Se Oxyanions Exposure

Ying Liu¹, Andreas Schäffer², Markus Lenz¹

¹ *Institute for Ecopreneurship, School of Life Sciences, University of Applied Sciences and Arts Northwestern Switzerland, Grünenstrasse 40, 4132 Muttenz, Switzerland (ying.liu@fhnw.ch)*

² *Institute for Environmental Research (Biology V), RWTH Aachen University, 52074 Aachen, Germany*

The trace element selenium (Se) which acts as a component of major metabolic pathways is essential for animals and humans health. However there are broad Se deficiencies worldwide and millions of people may be affected by the accompanying endemic diseases (Fairweather-Tait et al., 2011). Methylation and subsequent volatilization is an important Se cycle process in natural environments which may lessen available Se in soils limiting its entry into the food chain (Winkel et al., 2012). Se methylation is mostly regarded as a detoxification process for organisms since volatilization decreases the Se intracellular content. Hence most studies of Se volatilization were performed using Se concentrations 10^3 - 10^6 fold higher (mg / L) than those commonly found in the environment. A recent study revealed efficient volatilization from a natural wetland with very low Se concentrations (ng / L) (Vriens et al., 2014). It seems implausible that these concentrations may induce any specific enzymes for Se detoxification. As a consequence, Se volatilization fluxes based on laboratory experiments using high Se concentrations may have limited relevance for cycling outside of Se contaminated environments.

Here, we conducted a Se methylation study using a *Pseudomonas* strain at low $\mu\text{g} / \text{L}$ range of Se oxyanions. Methylated Se compounds were quantified by headspace SPME-GC-MS and the speciation and concentrations of Se oxyanions were measured by IC-ICP-MS. Transcriptional profiles of this strain responding to Se oxyanions exposure were analyzed by RNA-seq. Methylated Se species were detected in the culture headspace from selenite treatment but not from selenate. In the higher selenite treatment, more than half of the original Se methylated, whereas the methylation efficiency was less than one percent in lower selenite treatment.

REFERENCES

- Fairweather-Tait, S. J., Bao, Y., Broadley, M. R., Collings, R., Ford, D., Hesketh, J. E. & Hurst, R. 2011: Selenium in Human Health and Disease. *Antioxidants & Redox Signaling*, 14, 1337-1383.
- Vriens, B., Lenz, M., Charlet, L., Berg, M. & Winkel, L. H. E. 2014: Natural wetland emissions of methylated trace elements. *Nature Communications*, 5:3035.
- Winkel, L. H. E., Johnson, C. A., Lenz, M., Grundl, T., Leupin, O. X., Amini, M. & Charlet, L. 2012: Environmental Selenium Research: From Microscopic Processes to Global Understanding. *Environmental Science & Technology*, 46, 571-579

P 14.7

Uranium isotope fractionation during abiotic reduction by magnetite

Luca Loreggian¹, Yvonne Roebbert², Nadja Neubert², Stefan Weyer², Rizlan Bernier Latmani¹

¹ *Environmental Microbiology Laboratory, Ecole Polytechnique Federale de Lausanne, Route Cantonale, CH-1015 Lausanne (rizlan.bernier-latmani@epfl.ch)*

² *Institut für Mineralogie, Leibniz Universität Hannover, Callinstrasse, 30167 Hannover, Germany.*

The ratio of the two major uranium (U) isotopes, ²³⁸U and ²³⁵U, varies in natural environments depending on biogeochemical conditions [1]. This isotopic signature has been proposed as a tool to distinguish between abiotic and biotic U reduction in paleo and modern redox processes [2]. However, further research is required to fully develop this tool as a marker for reduction processes. Recent experimental findings indicate that strong U isotope fractionation (with high ²³⁸U/²³⁵U in the product) occurs during biotic U reduction, while fractionation is either negligible or opposite in direction during abiotic reduction [2].

This study aims to tackle the abiotic reduction mediated by magnetite (Fe₃O₄) which is a Fe(II)-bearing mineral frequently occurring in the subsurface. Here, we systematically monitor the isotope fractionation during reduction in batch configuration. In particular, we investigate how isotopic fractionation is affected by variable U(VI) loading and variable kinetics of reduction, by the crystallinity of the U(IV) products, and by adsorption prior to reduction.

We capture the reduction progress over time by quantifying the fraction of unreacted U(VI) with inductively coupled mass spectrometry (ICP-MS) after bicarbonate extraction as described by Alessi et al [3]. The isotopic fractionation is probed via multi-collector ICP-MS (MC ICP-MS) both in the U(IV) products and in the unreacted U(VI) fraction. U(IV) and U(VI) are separated via an anion exchange method as described by Wang et al. [4]. Ultimately, the U(IV) products in the solid phase are characterized with X-ray absorption spectroscopy to verify the extent of reduction.

Our preliminary results confirmed what was observed in a previous study [2]. U(VI) reduction by magnetite occurs in two distinct phases. During the initial short phase, most of dissolved U(VI) is reduced at a high rate, while the kinetics of reduction are slower during the second longer phase. We also observed that no isotope fractionation occurs in the first phase of reduction, while ²³⁵U is preferentially reduced in the second phase, resulting in positive $\delta^{238}\text{U}$ of the U(VI) that remains in solution (Fig. 1). The strongest fractionation is observed in the case with the highest U(VI) loading (Fig. 1A).

In order to explore how the final speciation of U(IV) affects the isotopic fractionation, we set up an experiment where U(VI) was reduced by magnetite that was pre-sorbed with phosphate. It is known that pre-sorption of phosphate onto the surface of magnetite promotes the formation of less crystalline U(IV) products at the end of reduction [5]. Even though pre-sorbed magnetite maintains its reactivity, it reduces U(VI) at a slower rate. Independently from the **slower reduction**, ²³⁵U is still preferentially reduced yielding a similar enrichment factor (Fig. 1B) and suggesting that U(IV) speciation does not affect isotopic fractionation. Further experiments are required to confirm this observation.

Finally, we assessed the contribution of adsorption to isotopic fractionation by examining U(VI) adsorption on maghemite (Fe₂O₃) as an Fe(II)-free proxy for magnetite. In fact, maghemite shares the same structure and magnetic properties with magnetite, but, because it does not harbor Fe(II), U(VI) is not reduced. Even in this case, the lighter isotope is preferentially absorbed but the extent of fractionation is lower than during reduction (Fig. 1C). Figure 1. Uranium isotope fractionation ($\delta^{238}\text{U}$) for the U(VI) aqueous fraction plotted against the fraction of unreacted U(VI) (C/C0). A: $\delta^{238}\text{U}$ during reduction by magnetite, B: $\delta^{238}\text{U}$ during U(VI) reduction by magnetite pre-sorbed with phosphate, C: ²³⁸U during U(VI) adsorption onto maghemite.

These data confirm previous findings on the direction of fractionation during abiotic reduction of U(VI) by magnetite and further evidences the role of U(VI) loading on the extent of fractionation. It also confirms previous results on uranium fractionation during adsorption to birnessite [6]. The impact of U(IV) speciation will require additional work.

REFERENCES

- [1] Weyer S. et al. 2008: Natural fractionation of ²³⁸U/²³⁵U, *Geochemica et Geologica Acta*, 72, 345-359.
- [2] Stylo M. et al. 2015: Uranium isotopes fingerprint biotic reduction, *Proceeding of the National Academy of Sciences of the United States of America*, 18, 5619-5624.
- [3] Alessi D. et al. 2012: Quantitative separation of Monomeric U(VI) reduction from UO₂ in products of U(VI) reduction.
- [4] Wang X., Johnson T. M. & Lundstrom C. 2015: Isotope fractionation during oxidation of tetravalent uranium by dissolved oxygen, *Geochimica et Cosmochimica Acta*, 150, 160-170.
- [5] Veeramani H. et al 2011: Products of abiotic U(VI) reduction by biogenic magnetite and vivianite, *Geochimica et Cosmochimica Acta*, 75, 2512-2528.
- [6] Brennecke G. A. et al. 2011: Uranium Isotope Fractionation during adsorption to Mn-Oxyhydroxides, *Environmental Science & Technology*, 45, 1370-1375.

P 14.8

Voltammetric detection of As(V) in natural waters

Abra Penezić, Mary-Lou Tercier-Waeber, Eric Bakker

Department of Inorganic and Analytic Chemistry, University of Geneva, Sciences II, 30 Quai E.-Ansermet, CH-1211 Genève (abra.penezic@unige.ch)

Arsenic is ubiquitous in the environment, with its sources being of natural and anthropogenic origin. It is classified as a group 1 human carcinogen by the International Agency for Research on Cancer (IARC Monographs, 1980), which makes monitoring the environmental levels of arsenic very important. The concentrations of arsenic in freshwater range from 1 to 130 nM and in seawater from 1 to 30 nM, and can be up to μM level in contaminated groundwater. Threshold values for arsenic in drinking water, proposed by the World Health Organisation, are around 130 nM ($1\mu\text{g/L}$).

Arsenic in the aquatic systems is present mainly in the form of inorganic trivalent arsenite species and pentavalent arsenate oxyanions. As(III) species are considered 60 times more toxic than the pentavalent species. There are reported voltammetric techniques for As(III) environmental sensing (Touilloux et al., 2015). Voltammetry enables the development of robust low cost sensors that can be adapted for in-situ measurements, making them especially attractive for environmental monitoring. Voltammetric detection of As(V) is limited to working at pH values below 2 (Gibbon-Walsh et al., 2010). An acidification step significantly complicates the development of an electrochemical sensor probe for *in situ* monitoring, and makes such tools difficult to use in arsenic speciation analysis.

In the work by Zhang et al. (2009), a polymer composed of aniline and o-aminophenol (PANOA), has been shown to electrocatalyze the reduction of As(V) in the process of arsenate removal. PANOA was shown to be electroactive in the pH range from 5.6 to 7. This idea was implemented into development of a PANOA modified gold microelectrode for As(V) detection. By using square wave anodic stripping voltammetry, As(V) can be measured after it has been reduced to As(III) at the PANOA-sensor surface vicinity. This work presents the preliminary research conducted on voltammetric detection of As(V) at pH 6. The ultimate aim is to obtain a sensor enabling direct As(V) monitoring at (sub-) nanomolar concentrations in close-to-neutral pH aquatic systems.

REFERENCES:

- IARC Monographs on the Evaluation of Carcinogenic Risks to Humans. 1980: Some Metals and Metallic Compounds, 23.
- Touilloux, R., Tercier-Waeber, M.-L. & Bakker, E. 2015: Antifouling membrane integrated renewable gold microelectrode for *in situ* detection of As(III), *Analytical Methods*, 7, 7503-7510.
- Gibbon-Walsh, K., Salaün, P. & Van den Berg, C. 2010: Arsenic speciation in natural waters by cathodic stripping voltammetry, *Analytica Chimica Acta*, 662(1), 1-8.
- Zhang, Y., Li, Q., Sun, L. & Zhai, J. J. 2009: The electrocatalytic reduction and removal of arsenate by poly(aniline-co-o-aminophenol), *Electroanalytical Chemistry*, 636, 47-52.

P 14.9

Composition, structure and arsenate sequestration of iron oxidation products

Anna-Caterina Senn¹, Ralf Kaegi¹, Stephan Hug¹, Janet Hering¹, Andreas Voegelin¹

¹ *Eawag, Swiss Federal Institute of Aquatic Science and Technology, Duebendorf, Switzerland
(anna-caterina.senn@eawag.ch)*

The oxidation of dissolved Fe(II) in oxygenated water leads to the formation of amorphous to poorly-crystalline Fe(III)-precipitates that profoundly impact the fate of nutrients and contaminants in natural and engineered aquatic systems. Dissolved phosphate (P), silicate (Si) and Ca strongly influence the structure of Fe(III)-precipitates (Voegelin et al., 2010). In this study, we quantified the interdependent effects of these solutes on the composition, structure and arsenate (As(V)) uptake of fresh and aged Fe(III)-precipitates. The precipitates were formed by oxidation of 0.5 mM Fe(II) at 12 P/Fe ratios from 0 to 2 in aerated 8 mM bicarbonate-buffered (pH 7.0) electrolyte containing 7 μ M As(V), with 8 mM Na, 4 mM Ca, 4 mM Mg or 7 mM Na + 0.5 mM Ca as electrolyte cations. Additional experiments in Na and Ca electrolyte were performed in the presence of 0.5 mM Si. After Fe oxidation and precipitation (4 h), solution and precipitates were samples for ICP-MS and Fe K-edge XAS analysis. To assess the effects of aging, precipitate suspensions reacted for 30 d at 40°C before sampling were examined as well (Senn et al., 2015, Senn et al., submitted).

The evaluation of the Fe XAS spectra of 144 precipitate samples revealed gradual variations in precipitate structure between several endmembers: (i) poorly crystalline lepidocrocite (pLp*), (ii) hydrous ferric oxide (HFO) or silicate-containing ferrihydrite (Fh-Si*) and (iii) amorphous (Ca-)Fe(III)-phosphate ((Ca)FeP*). These variations depended on P/Fe ratio, electrolyte cation and presence of Si. Enhanced co-precipitation of P in Ca-containing electrolytes could be attributed to electrostatic effects as well as to the formation of mixed Ca-Fe(III)-phosphate in which the Fe(III)-octahedra exhibited enhanced mitridatite-like corner- and edge-sharing linkage. By combining ICP-MS and LCF results, the oxyanion uptake capacity of the different precipitate types could be derived. Depending on initial P/Fe ratios, the presence of Si, and the type of electrolyte cation (and thus precipitate type), dissolved As(V) concentrations varied by up to 3 orders of magnitude.

During aging, Si and Ca slowed down Fe(III) polymerization and thereby substantially reduced P and As(V) remobilization at low P/Fe ratios compared to Si- and Ca-free suspensions. The results further emphasized that the combined effects of Ca and Si were required for most effective P and As(V) retention during precipitate aging.

The results from this study provide insight into the link between water chemistry and the structure and composition of fresh and aged Fe(III)-precipitates as well as into their As retention capacity. This knowledge is essential to assess the dynamics of As and other trace elements in natural aquatic systems and water treatment.

REFERENCES

- Voegelin, A., Kaegi, R., Frommer, J., Vantelon, D. & Hug, S.J. 2010: Effect of phosphate, silicate, and Ca on Fe(III)-precipitates formed in aerated Fe(II)- and As(III)-containing water studied by X-ray absorption spectroscopy, *Geochimica et Cosmochimica Acta*, 74, 164-186
- Senn, A.-C., Kaegi, R., Hug, S.J., Hering, J.G., Mangold, S. & Voegelin, A. 2015: Composition and structure of Fe(III)-precipitates formed by Fe(II) oxidation in water at near-neutral pH: Interdependent effects of phosphate, silicate and Ca, *Geochimica et Cosmochimica Acta*, 162, 220-246
- Senn, A.-C., Kaegi, R., Hug, S.J., Hering, J.G., Mangold, S. & Voegelin, A. submitted: Effect of aging on the structure and phosphate retention of Fe(III)-precipitates formed by Fe(II) oxidation in water, *Geochimica et Cosmochimica Acta*

P 14.10

Arsenic biomethylation efficiency across microbial phyla

Karen Viacava¹, Karin Lederballe Meibom¹, Adrien Mestrot² & Rizlan Bernier-Latmani¹

¹ Environmental Microbiology Laboratory, EPFL, Station 6, CH-1015 Lausanne (rizlan.bernier-latmani@epfl.ch)

² Trace Element Speciation and Environmental Chemistry Group (TrES Group), University of Bern, Hallerstrasse 12, CH-3012 Bern

Arsenic (As), a toxic metalloid and potent carcinogen, is ubiquitous in the environment and is released from geogenic as well as anthropogenic sources. As biomethylation, which consists of the catalyzed transfer of methyl groups to the metalloid generating both volatile and non-volatile As methyl derivatives, is also widespread. It is observed in bacteria, archaea, fungi, algae, plants and animals, including humans. The attachment of a methyl group changes the chemical and physical properties of As, influencing its biogeochemical cycling and toxicity. Nonetheless, biomethylation is far from universal and the main biological systems responsible for the biosynthesis of arsenic organocompounds remain microorganisms (Bentley & Chasteen 2002).

The reaction is catalyzed by the methyltransferase ArsM. Several specific pathways have been proposed for As methylation, but the exact mechanism remains under debate. In the classic biomethylation pathway (Challenger, 1945), sequential steps of reduction and oxidative methylation were described, with S-adenosylmethionine (SAM) serving as the methyl donor. Since, the transfer of the methyl group with no formal change in the oxidation state has been proposed and methylcobalamin has been hypothesized to be the methyl donor (Wuerfel et al. 2012).

A cornerstone of the research path to unravel the mechanism of As methylation is to identify an efficient biomethylator for detailed study. Here, we present an evaluation of the ability of six bacterial strains, pertaining to three bacterial phyla (Proteobacteria, Firmicutes, and Bacteroidetes), to synthesize methylated As compounds. We considered two *Deltaproteobacteria*: an iron reducer (*Geobacter metallireducens*), and a sulfate reducer (*Desulfovibrio vulgaris*). Further, we evaluated three Firmicutes: a dehalogenator (*Desulfitobacterium hafniense*), a saccharolytic fermenter (*Clostridium pasteurianum*), and a proteolytic fermenter (*Clostridium collagenovorans*). Finally, the only aerobic bacterium we studied is a member of the *Cytophagaceae* family and is heterotrophic (*Arsenicibacter rosenii*) (Huang et al. 2016),.

Some of these organisms (*Clostridium collagenovorans*, *Desulfovibrio vulgaris* and *Arsenicibacter rosenii*) are proven As methylators (Michalke et al. 2000; Huang et al. 2016), while the others possess genes encoding for homologues of the As(III) methyltransferase gene (ArsM), identifying them as possible As methylators.

The As methylation ability of *G. metallireducens* strain GS-15 was tested in a time-course experiment. The pure culture was inoculated into medium containing As(III) in varying concentrations (2, 5, 10 and 50 μM). As speciation analysis was performed using high performance liquid chromatography-inductively coupled plasma mass spectrometry (HPLC-ICP-MS). The presence of As(III) in the medium did not hinder the growth of the inoculated bacteria (Fig. 1). However, only inorganic As species (As(V) + As(III)) were detected in the medium to date (inset in Fig. 1).

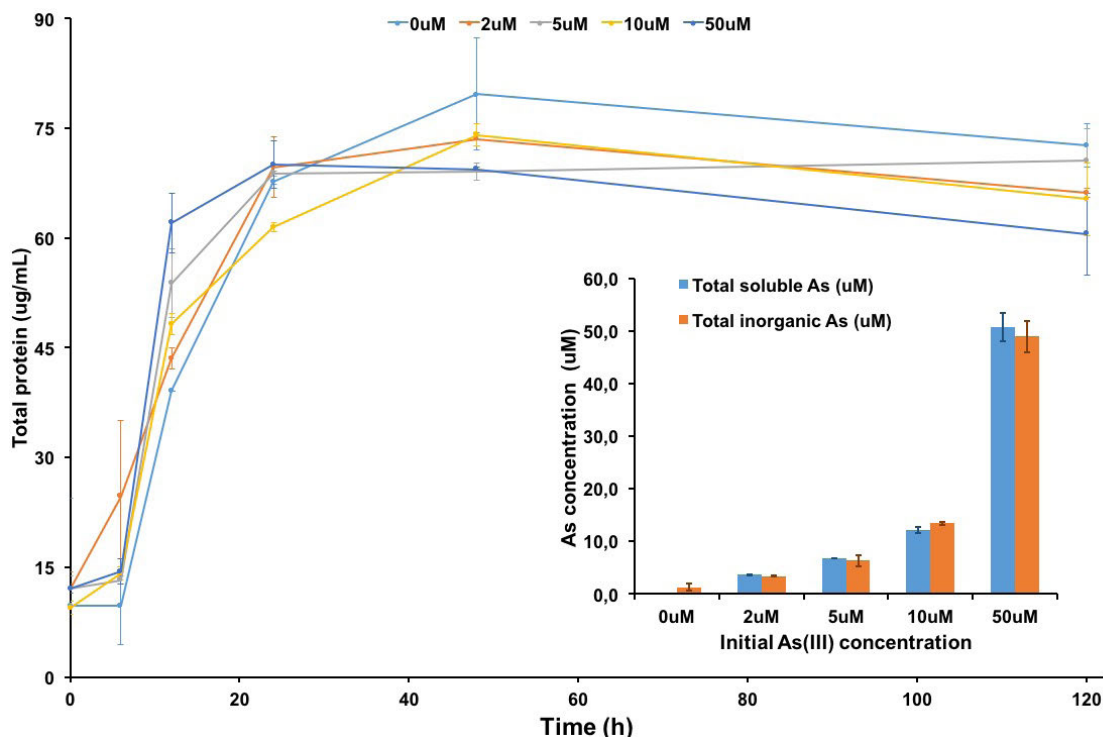


Figure 1. Cell growth measured as quantification of total protein (Thermo Scientific™ Pierce™ BCA Protein Assay). Inset: total As vs total inorganic As after 48h in the medium. The data are means \pm SD (n=2).

Ongoing work will be presented that evaluates the methylation efficiency of the other strains considered.

REFERENCES

- Bentley, R., & Chasteen, T. G. 2002: Microbial methylation of metalloids: arsenic, antimony, and bismuth. *Microbiol. Mol. Biol. Rev.* 66(2), 250–71.
- Huang, K., Chen, C., Zhang, J., Tang, Z., Shen, Q., Rosen, B. P., & Zhao, F.-J. 2016: Efficient Arsenic Methylation and Volatilization Mediated by a Novel Bacterium from an Arsenic-Contaminated Paddy Soil. *Environ Sci. Technol.* 50, 6389–6396.
- Michalke, K., Wickenheiser, E. B., Mehring, M., Hirner, A. V., & Hensel, R. 2000: Production of volatile derivatives of metal(loid)s by microflora involved in anaerobic digestion of sewage sludge. *Appl. Environ. Microbiol.* 66(7), 2791–2796.
- Wuerfel, O., Thomas, F., Schulte, M. S., Hensel, R., & Diaz-Bone, R. A. 2012: Mechanism of multi-metal(loid) methylation and hydride generation by methylcobalamin and cob(I)alamin: A side reaction of methanogenesis. *Appl. Organomet. Chem.* 26(2), 94–101.

15. Linking Trace Element and Carbon Biogeochemistry

Vera I Slaveykova, Séverine Le Faucheur and Christel S. Hassler

TALKS:

- 15.1 Bravo A.G., Ortega S.H., Bouchet S., Tolu J., Catalán N., Björn E., Bertilsson S.: Organic matter composition controls mercury methylation in aquatic ecosystems
- 15.2 Jaccard S.L., Semeniuk D.M., Maldonado M.T.: Chromium uptake and adsorption in marine phytoplankton – Implications for the marine chromium cycle
- 15.3 Jiménez-Lamana J., Slaveykova V.I.: Silver nanoparticles fate in lake water depends on the natural organic matter origin
- 15.4 Pinheiro J.P., Botero W.G., Janot N., Domingos R.F., Rocha L.S., Groenenberg J.E., Benedetti M.F.: Binding behavior of trace metals with fully purified and alkaline extracted soil humic acid
- 15.5 Rotureau E., Présent R., Billard P., Pagnout C., Duval J.F.L.: Kinetics and thermodynamics of metal partitioning at the cell-solution interface : impacts of intracellular speciation dynamics
- 15.6 Sieber M., Conway T.M., Takano S., Sohrin Y., Vance D.: The role of the Antarctic Ocean in influencing the distribution of Cd isotopes at lower latitudes in the South West Pacific
- 15.7 Vance D., Little S., de Souza G.F.: Southern Ocean biology and physical oceanography the key control on global ocean trace metal distributions

POSTERS:

- P 15.1 Cabanes D.J.E., Norman L., Santos-Echeandía J., Iversen M.H., Trimborn S., Laglera L.M., Hassler C.S.: Salp fecal pellets interaction with iron biogeochemistry
- P 15.2 de Souza G.F., Khatiwala S., Little S.H., Vance D.: Systematics of biogeochemical controls on the oceanic distribution of zinc
- P 15.3 Krishnamoorthy D., Moisset S., Cabanes D., Hassler C.: Relevance of iron speciation with respect to the distribution of humics and phytoplankton in Lake Geneva
- P 15.4 Mannerheim N., Blessing C., Oren I., Gruenzweig J., Buchmann N.: Short-term carbon allocation within the root system of the tropical tree species *Ceiba pentandra*
- P 15.5 Tribovillard N., Petit A., Quijada M., Riboulleau A., Sans-Jofre P., Thomazo C., Birgel D.: Early-diagenesis carbonate precipitation: from nodules to cone-in-cone structures
- P 15.6 Laffite A., Devarajan N, Mulaji C.K., Slaveykova V.I., Poté J.: High levels of toxic metals detected in sub-saharian rivers receiving hospital effluents: Case of Democratic Republic of Congo

15.1

Organic Matter Composition Controls Mercury Methylation in Aquatic Ecosystems

Andrea G. Bravo^{1,1}, Sonia Herrero Ortega¹, Sylvain Bouchet², Julie Tolu³, Núria Catalán¹, Erik Björn², Stefan Bertilsson¹

¹ Department of Ecology and Genetics, Limnology, Uppsala University, SE-75236 Uppsala, Sweden.

² Department of Chemistry, Umeå University, SE-90187 Umeå, Sweden.

³ Department of Ecology and Environmental Science, Umeå University SE-90187 Umeå, Sweden.

¹andrea.garcia@ebc.uu.se

One major challenge in contemporary environmental science is to identify factors controlling the formation of methylmercury (MeHg). The formation of MeHg is biotically mediated in aquatic systems. Organic matter (OM) interacts very strongly with Hg, affecting its speciation, solubility, mobility, and toxicity in the aquatic environment. OM in aquatic systems consists of a mixture of terrestrial compounds drained from the catchment and internally produced OM mainly derived from phytoplankton. Even if the effect of OM concentration on Hg methylation has been the subject of numerous studies, the influence of the molecular composition of OM remains poorly understood. Here we show the impact of terrigenous and planktonic derived OM on Hg methylation in different aquatic ecosystems. Concretely, we studied Hg methylation in sediments of 10 lakes and 9 beaver pond ecosystems. While the selected lakes receive inputs of both terrigenous and in situ OM, the sediments from beaver ponds of different ages are primarily dominated by terrigenous OM with different degradation status. We used inorganic mercury isotope tracers to determine mercury methylation and pyrolysis–gas chromatography mass spectrometry to identify and quantify 110 organic compounds in lakes sediments. We used optical measurements (spectrometry and fluorescence) to characterize the OM in the sediment overlying water of beaver pond ecosystems. Hg methylation rate constants reach the highest values in lakes dominated by protein algal derived compounds (0.038–0.075 day⁻¹, n=4) and are much lower in lake sediments enriched in terrigenous OM (0.0095–0.013, n=5) or in invertebrate chitin associated compounds (0.013, n=1). For sediments in the beaver ponds, we found a median of 0.026 day⁻¹ (IQR=0.01–0.031, n=9). The characterization of OM suggests that, in lake sediments, algal-derived compounds primarily control Hg methylation by enhancing the activity of the whole microbial community and or Hg-availability. In beaver ponds, chlorophyll-a also correlated with Hg methylation rate constants, confirming the role of algal derived OM even in systems dominated by terrestrial sources. Qualitative analysis of the sediment overlying dissolved organic matter with excitation-emission-matrix fluorescence spectroscopy, further suggests that unprocessed terrestrial organic matter also enhances Hg methylation in young ponds. We thus conclude that algal derived compounds are the main driver of Hg methylation, but in systems limited by autochthonous sources, fresh terrigenous OM play an important role on the process.

15.2

Chromium uptake and adsorption in marine phytoplankton – implications for the marine chromium cycle

Samuel L. Jaccard¹, David M. Semeniuk¹, Maria T. Maldonado²

¹ *Institute of Geological Sciences and Oeschger Center for Climate Change Research, University of Bern, Baltzerstrasse 1+3, CH-3012 Bern, Switzerland*

² *Department of Earth, Ocean, and Atmospheric Sciences, University of British Columbia, 2207 Main Mall, Vancouver, BC, Canada, V6T 1Z4*

Using the radioisotope ⁵¹Cr, we investigated the controls of cellular Cr accumulation in an array of marine phytoplankton grown in environmentally relevant Cr concentrations (1-10 nM). Given the affinity of Cr(III) for amorphous Fe-hydroxide mineral surfaces, and the formation of these mineral phases on the outside of phytoplankton cells, extracellular Cr was monitored in a model diatom species (*Thalassiosira weissflogii*) as extracellular Fe concentrations varied.

Extracellular Cr in *T. weissflogii* increased with increasing extracellular Fe, demonstrating that Cr may be removed from seawater via extracellular adsorption to phytoplankton. Short-term Cr(VI) and Cr(III) uptake experiments performed with *T. weissflogii* demonstrated that Cr(III) was the primary oxidation state adsorbing to cells and being internalized by them.

Cellular Cr:C ratios (<0.5 μmol Cr mol C⁻¹) of the eight phytoplankton species surveyed were significantly lower than previously reported Cr:C ratios in marine particles with a high biogenic component (10 to 300 μmol Cr mol C⁻¹). This indicates that Cr(III) likely accumulates in marine particles due to uptake and/or adsorption. Mass balance calculations demonstrate that surface water Cr deficits can be explained via loss of Cr(III) to exported particles, thereby providing a mechanism to account for the nutrient depth profile for Cr in modern seawater.

Given the large fractionation of stable Cr isotopes during Cr(VI) reduction, Cr(III) associated with exported organic carbon is likely enriched in lighter isotopes.

Most sedimentary Cr isotope studies have thus far neglected internal fractionating processes in the marine Cr cycle, but our data indicate that loss of Cr to exported particles may be traced in the sedimentary δ⁵³Cr record.

15.3

Silver nanoparticles fate in lake water depends on the natural organic matter origin

Javier Jiménez-Lamana^{1,2} and Vera I. Slaveykova¹

¹ *Environmental Biogeochemistry and Ecotoxicology, Institute F.-A. Forel, Faculty of Sciences, University of Geneva, Uni Carl Vogt, 66 Bvd. Carl Vogt, CH-1211 Geneva, Switzerland (vera.slaveykova@unige.ch).*

² *Present address: Laboratory of Bioinorganic Analytical and Environmental Chemistry (LCABIE), UMR5254, CNRS-UPPA, Hélioparc, 2 Av. President Angot 64053 Pau Cedex 09, France (j.jimenez-lamana@univ-pau.fr).*

The growing use and concomitant release of a variety of silver nanoparticles (AgNPs) with different sizes and surface coatings into aquatic systems is raising concerns about their environmental fate and impacts. The understanding of the AgNPs fate in the aquatic environment and the role of different modifying factors such as particle size and coating, medium composition on NPs stability and persistence is necessary to be able to evaluate their potential impacts. Natural organic matter (NOM) is considered to play a significant role in nanoparticles stability and transformations. Nevertheless, the interactions of NOM of different nature with the AgNPs are overlooked in particularly at low environmentally relevant nanoparticle concentrations (e.g. ng L⁻¹). In addition, the role of the nanoparticle surface coatings in the NP interactions with the NOM present in freshwater is still to explore.

Given the low concentrations of engineered nanomaterials in the natural water the studies of their fate requires the use of the most sensitive analytical techniques. In the present work, we use a combination of an asymmetric flow field-flow fractionation (AsFFFF), Surface plasmon resonance and single particle inductively coupled plasma mass spectrometry (SP-ICP-MS) to characterize the behaviors of AgNPs in lake water. The stability of AgNPs of three different coatings – citrate (CIT), polyvinyl pyrrolidone (PVP) and lipoic acid (LIP) and size of 20 and 50nm in lake water over time at low environmentally relevant concentrations. Well-characterized, standard aquatic humic acid (SRHA), isolated from the Suwannee River in Georgia was used as a model of NOM of pedogenic origine, while the extracellular polymeric substances produced by cyanobacterium *Synechocystis* sp. (EPS) were used as representatives of aquagenic NOM.

The results demonstrated that AgNPs stability results form a complex interplay between the surface coating characteristics and the nature of NOM rather the initial AgNP size. PVP coated AgNPs agglomerate to a lesser extent as compared with the CIT- and LIP-AgNPs. Both NOM of pedogenic and aquagenic origin increased the stability of the AgNPs (LW+EPS > LW+SRHA > LW). Moreover, the nature of NOM is an important factor as well: EPS (aquagenic origin) stabilizes lipoic acid-coated AgNPs more effectively than SRHA (pedogenic origin). The obtained results will help to the understanding of the persistence of different AgNPs in aquatic systems, when present at low environmentally relevant concentrations.

15.4

Binding behavior of trace metals with fully purified and alkaline extracted soil humic acid

José Paulo Pinheiro¹, Wander G. Botero², Noémie Janot¹, Rute F. Domingos³, Luciana S. Rocha⁴, Jan E. Groenenberg¹, Marc F. Benedetti³

¹ LIEC (UMR 7360), University of Lorraine/CNRS, 15 Avenue du Charmois, 54500 Vandoeuvre-les-Nancy, France (jose-paulo.pinhoiro@univ-lorraine.fr)

² Federal University of Alagoas (UFAL), Campus Arapiraca, 57309-005-, Arapiraca, AL, Brazil

³ Institut de Physique du Globe de Paris, Sorbonne Paris Cité, Université Paris Diderot, UMR CNRS 7154, 75205 Paris Cedex 05, France

⁴ DQF/FCT, Universidade do Algarve, Campus de Gambelas, 8005-139 Faro, Portugal

The solid solution partitioning and speciation of trace metals in terrestrial and aquatic environments is key to the understanding of their mobility, fate and bioavailability. During the last decades, large progress has been made in the development of ion binding models for modeling of metal binding to the most important adsorbing constituents in natural systems (organic matter, Al/Fe/Mn-(hydr)oxides, clays and their assemblages (Groenenberg & Lofts 2014).

The most advanced models for metal binding to organic matter, especially the alkaline extract or “humic fraction” thereof, are the Humic Ion Binding Models VI and VII, the Stockholm Humic Model (SHM) and the Non Ideal Competitive Adsorption - Donnan (NICA-Donnan) model. Model parameters for these models have been derived from proton- and metal binding experiments with purified humic- and fulvic acids which have been isolated from soils and surface waters according to various protocols.

There are, however questions with respect to the representativeness of purified humic substances for organic matter in natural systems. It has been suggested that the harsh chemical conditions of the humic substance isolation and purification may cause artifacts that influence the binding properties of the humics and Lehman and Kleber question the reality of what is called humics and suggest the adoption of a soil continuum model stating that the alkaline extraction is not representative of the soil organic matter (Lehman & Kleber 2015).

Another interesting trend is the growing interest in using alkaline soil organic matter extracts, especially those obtained from peat soils, as natural fertilizers to replace the commercially used inorganic fertilizers. The commercial version of the “natural fertilizers” is obtained using a purification similar to the IHSS procedure without the last step which consist in the attack with HCl/HF and dialysis using a 8 kD membrane.

The environmental impact of these fertilizer is thus difficult to model since the extraction and purification procedures are different from the ones used in the scientific studies to obtain the model parameters

Thus in this work we study proton and metal binding to terrestrial organic matter in fully purified (FPHA) following the IHSS procedure and the material obtained without the last step named alkaline extracted soil humic acid (AEHA) isolated from a peat soil from the Mogi river region of Ribeirão Preto, São Paulo State, Brasil.

Both materials were characterized by NMR, elemental composition and metal content by ICP-MS. Proton titrations were performed using potentiometry and metal (cadmium, lead and zinc) titrations were performed using AGNES, an electroanalytical technique which provides the free metal concentration in the sample.

The FPHA results were fitted using the NICA-Donnan model yielding the specific proton and metal binding parameters for Cd, Pb and Zn.

On the other hand the proton titrations of the AEHA were irreproducible which is imputed to the presence of clay minerals as observed by DRX and probalby amorphous iron oxi/hydroxides due to the amount of iron detected by ICP-MS in that sample.

It was observed that for the same amount of sample the binding hability of the FPHA is generally one order of magnitude higher than the AEHA. This is probably due to the smaller carbon content of the AEHA (36% vs 50% for the FPHA) and the presence of an important mineral phase in the AEHA (7% ash content vs less than 1% for the FPHA).

The differences observed in the metal binding between FP and AE humic acids indicates that the use of the FP NICA-Donnan parameters, i.e., the “generic parameters”, will most probably underestimate the free metal present in soils treated with “natural” fertilizers. Therefore, further studies are necessary to understand the differences between these two materials and to model the AE metal binding interaction.

REFERENCES

- Groenenberg, J.E.& Lofts, S. 2014: The Use of Assemblage Models to Describe Trace Element Partitioning, Speciation and Fate: A review, *Environ. Toxicol. Chem.* 33, 2181–2196.
- Lehman, J.& Kleber, M. 2015: The contentious nature of soil organic matter, *Nature*, 528, 60-68.

15.5

Kinetics and thermodynamics of metal partitioning at the cell-solution interface : impacts of intracellular speciation dynamics

Elise Rotureau¹, Romain Présent,¹ Patrick Billard¹, Christophe Pagnout¹, Jérôme F.L. Duval¹

¹ LIEC (Laboratoire Interdisciplinaire des Environnements Continentaux) UMR7360 CNRS, Université de Lorraine, Vandœuvre-lès-Nancy F-54501, France.

Understanding the toxic and essential trace compounds uptake by microorganisms under conditions relevant to natural environment is a major trigger of concern in environmental risk assessments. While toxicity assays are well documented in numerous studies where exposed ambient concentrations of metals are related to toxicology endpoints such as mortality or growth rate, predicting metal toxicity with clear account of the dynamic interplay between cell growth and metal biointerfacial partitioning is still very scarce. We recently proposed an integrative theory where metal transport, adsorption, excretion, internalisation and depletion processes are rigorously accounted for. In this presentation, the theory is briefly presented together with supporting experimental data collected on bacteria suspensions exposed to Cd(II) solutions. It is shown how a critical examination of these data with help of theory can be valuable in deciphering the mechanisms governing the partitioning of metal at biointerfaces over time. Then, the profound effects of intracellular speciation dynamics on (i) the kinetics of M depletion from outer bulk solution, (ii) the limitation of M biouptake by diffusive transport, or (iii) the nature of the equilibrium M interfacial partitioning, are demonstrated on the basis of illustrative computational examples.

REFERENCES

- Duval JFL. 2013: Dynamics of metal uptake by charged biointerphases: bioavailability and bulk depletion. *Physical Chemistry Chemical Physics* 15, 7873.
- Duval JFL, Rotureau E. 2014: Dynamics of metal uptake by charged soft biointerphases: impacts of depletion, internalisation, adsorption and excretion. *Physical Chemistry Chemical Physics* 16, 7401.
- Rotureau E., Billard P., Duval JFL. 2015 : Evaluation of metal biouptake from the analysis of bulk metal depletion kinetics at various cell concentrations: theory and application. *Environmental Science & Technology*, 49, 990.
- Duval, JFL.; Présent, RM. and Rotureau, E: Kinetic and thermodynamic determinants of trace metal partitioning at biointerfaces: contributions from intracellular speciation dynamics. *Submitted*.

15.6

The role of the Antarctic Ocean in influencing the distribution of Cd isotopes at lower latitudes in the South West Pacific

Matthias Sieber*, Tim M. Conway*, Shotaro Takano**, Yoshiki Sohrin** & Derek Vance*

¹ *Institute Geochemistry and Petrology, ETH Zürich, Clausiusstrasse 25, Zurich, 8092, Switzerland (matthias.sieber@erdw.ethz.ch)*

² *Institute Chemical Research, Kyoto University, Uji, Kyoto 611-011, Japan*

Cadmium (Cd) is a trace metal that exhibits a nutrient-type dissolved distribution in the global oceans, with a close linear correlation to dissolved phosphate [1]. Under Fe limiting conditions, this relationship changes as Cd is apparently taken up by phytoplankton preferentially to phosphate, resulting in a 'kink' in the Cd:P relationship. Previous studies have highlighted the influence of biogeochemical processes in the Southern Antarctic Ocean on basin-wide distributions of Cd throughout the lower-latitude oceans [2, 3]. Dissolved Cd stable isotope ratios ($\delta^{114}\text{Cd}$) can inform understanding of these source processes, which impart the distinctive $\delta^{114}\text{Cd}$ and Cd:P signatures to southern-sourced water masses that are then transported northwards. Although the deep oceans are relatively homogeneous for $\delta^{114}\text{Cd}$ ($\sim+0.2$ to $+0.3\text{‰}$), Antarctic Intermediate Water carries a depleted $\delta^{114}\text{Cd}$ signal ($+0.45\text{‰}$) into the far North Atlantic, whilst such a signal is seemingly absent at 30°N in the Pacific [4, 5]. Here, we present new seawater dissolved Cd stable isotope data for the South Pacific. Our method uses Nobias PA-1 chelating resin to extract metals from seawater, purification by anion exchange chromatography, and analysis by ^{111}Cd - ^{113}Cd double-spike Neptune MC-ICPMS [6]. We present further method development as well as the first water-column profiles of dissolved $\delta^{114}\text{Cd}$ from the SW Pacific Ocean, using samples collected during a recent Japanese GEOTRACES GP19 North-South transect along 170°W . These new data show that surface processes in the Antarctic Ocean (namely removal of light Cd into biological material) result in a fractionated surface $\delta^{114}\text{Cd}$ signal being transported northward to intermediate depths further north. We use our new data to investigate how the Southern Ocean influences Cd cycling in the Equatorial Oceans, comparing the Pacific to the Atlantic.

REFERENCES

- [1] de Baar, H. et al. *Mar. Chem.* 46, 261–281 (1994).
- [2] Abouchami, W. et al. *GCA* 127, 348–367 (2014).
- [3] Baars, O. et al. *Limnol. Ocean.* 59, 385–399 (2014).
- [4] Conway, T. M. & John, S. G. *GCA* 164, 262–283 (2015).
- [5] Conway, T. M. & John, S. G. *GCA* 148, 269–283 (2015).
- [6] Xue, Z. et al. *Anal. Bioanal. Chem.* 402, 883–893 (2012).

15.7

Southern Ocean biology and physical oceanography the key control on global ocean trace metal distributions

Derek Vance¹, Susan Little² & Gregory de Souza¹

¹ *Institute for Geochemistry and Petrology, Department of Earth Sciences, ETH Zürich, Clausiusstrasse 25, 8092 Zürich (derek.vance@erdw.ethz.ch)*

² *Department of Earth Science and Engineering, Imperial College London, London SW7 2BP, UK.*

Trace metals play an important role in the metabolism of phytoplankton. One prominent expression of this role is their nutrient-like depth profiles: extreme depletion of many metals in the dissolved pool of the photic zone due to phytoplankton uptake, and enrichments in the deep ocean through regeneration - bacterial respiration of photosynthetic carbon exported from the photic zone to depth. For transition metals like cadmium (Cd) and zinc (Zn) surface depletion factors of several hundred are common. A feature of the depth profiles of Zn in the ocean is that they very closely resemble those of silica (Si), another nutrient-like element by virtue of its importance to the most important phytoplankton group for export productivity in the oceans, the diatoms. However, this close correspondence of Zn and Si represents a long-standing puzzle. If one-dimensional vertical cycling between the photic zone and the deep ocean, at every point in the ocean, were to control Zn distributions they should not look like Si. Diatoms do take up large amounts of Zn. But virtually none of it is in the diatom opal, but is co-located with phosphate in the soft-parts of cells, and regenerated in the upper water column with the organic parts of those cells, not at the greater depths where Si is regenerated from opal dissolution.

Here, we put forward a new view of the oceanic Zn cycle, informed by recent abundance and isotopic data from the GEOTRACES programme, and building on ideas concerning the main controls on the Si cycle that emphasise key physical oceanographic and biological processes in the Southern Ocean. These ideas focus on the remarkable physiology of Southern Ocean diatoms, which have Zn/PO₄ ratios that are an order of magnitude greater than other oceanic phytoplankton. The uptake of both Zn and Si in this unique biogeochemical regime sets the Zn characteristics of surface and deep water bodies that are then exported to the deep and intermediate global ocean by advection. These processes split the ocean into two, an upper ocean from which Zn, and Si, has been largely stripped by focussed upwelling and biological processing in the Southern Ocean, and a deep ocean where Zn, like Si, is trapped.

P 15.1

Salp fecal pellets interaction with iron biogeochemistry

Damien Cabanes¹, Louiza Norman², Juan Santos-Echeandía³, Morten Iversen^{4,5}, Scarlett Trimborn^{4,6}, Luis Laglera⁷ & Christel Hassler¹

¹ *Institute F.- A. Forel, Earth and Environmental Sciences, University of Geneva, 66 rue Carl-Vogt, 1211 Geneva 4, Switzerland (Damien.Cabanes@unige.ch)*

² *Department of Plant Sciences, University of Cambridge, Downing Street, Cambridge, CB2 3EA, UK*

³ *CSIC Instituto de Investigaciones Marinas, Eduardo Cabello 6, 36208 Vigo, Spain*

⁴ *Alfred Wegener Institute Helmholtz Centre for Polar and Marine Research, Am Handelshafen 12, 27570 Bremerhaven, Germany*

⁵ *MARUM, University of Bremen, Leobener Strasse, 28359 Bremen, Germany*

⁶ *Marine Botany, University of Bremen, Leobener Strasse NW2, 28359 Bremen, Germany*

⁷ *FI-TRACE, Universitat de les Illes Balears, Chemistry department, Balearic Islands 07122, Spain*

Planktonic grazers such as salps may have a dominant role in iron (Fe) cycling in surface waters of the Southern Ocean (SO). Salps, have high ingestion rates and egest large, fast sinking fecal pellets (FPs) that potentially contribute to the vertical flux of carbon. In this study, we studied the impact of FPs from the most abundant salp in the SO (*Salpa thompsoni*) on Fe chemistry. During the Polarstern expedition ANT-XXVII/3, salps were incubated in 200 µm screened seawater and their FPs were collected for further experiments. To investigate whether the FPs release Fe and Fe-binding ligands to the filtered seawater (FSW), under different experimental conditions, they were either exposed in the dark or under full sunlight at in situ temperatures for 24h, or placed into the dark after a freeze/thaw treatment. We observed that none of the treatments caused release of dissolved Fe (dFe) or strong Fe ligands from the salp FPs. However, humic-substance like (HS-like) compounds, weak Fe ligands, were released at a rate of $8.22 \pm 4.72 \mu\text{g HS-like.FP-1.d-1}$. The Fe content per salp FP was $0.33 \pm 0.02 \text{ nmol dFe FP-1}$, which resulted in an estimated dFe export flux of $21 \text{ nmol Fe m-2 d-1}$ at 300 m. Overall, our results suggest that salp FPs are important for Fe export while they barely contribute to Fe recycling in SO surface waters.

P 15.2

Systematics of biogeochemical controls on the oceanic distribution of zinc

Gregory de Souza¹, Samar Khatiwala², Susan Little³ and Derek Vance¹

¹ *Institute of Geochemistry and Petrology, ETH Zurich, Clausiusstrasse 25, CH-8092 Zurich (desouza@erdw.ethz.ch)*

² *Department of Earth Sciences, University of Oxford, Oxford OX1 3AN, UK*

³ *Department of Earth Science and Engineering, Imperial College London, London SW7 2BP, UK*

Zinc (Zn) is a vital micronutrient for marine phytoplankton, most importantly due to its role as cofactor in the metalloenzyme carbonic anhydrase, which is fundamental for photosynthesis. It is thus actively cycled by biota in the sea, and exhibits the typical distribution – with low concentrations in the near-surface ocean and elevated concentrations at depth – of other biogeochemically-cycled elements in the ocean. A peculiarity of the Zn distribution that has been known since the first reliable measurements of its oceanic abundance were made (Bruland, 1980) is its close correspondence to that of silicon (Si), an element that is dominantly cycled via the opaline hard parts of marine diatoms. This similarity in large-scale distributions is surprising, since there is no *a priori* reason to expect it: Zn is required by all photosynthesizing algae, not diatoms alone; it is taken up overwhelmingly (>97%) into the soft organic tissue of phytoplankton (including diatoms) rather than into their hard parts; and upon export and remineralisation it is regenerated rapidly together with the labile major nutrients P and N, rather than with Si during dissolution of opaline hard parts.

Recently, Vance et al. (2014 & this volume) have proposed that the striking similarity between the large-scale distributions of Zn and Si comes about due to the interplay between physical ocean circulation and diatom physiology in the Southern Ocean surrounding Antarctica. This ocean region plays an inordinately important role in determining ocean tracer properties due to its importance as a region of deep-water upwelling and intermediate-/upper-ocean ventilation; and it bears diatom communities whose cellular Zn quotas, normalised to phosphorus, are 5-8 times greater than average oceanic phytoplankton. Vance et al. (2014) suggest that the remarkably high Zn:P ratio of export driven by diatom-dominated Southern Ocean floral assemblages combines with the circulation of the Southern Ocean to set the Zn (and Si) characteristics of the upper and deep ocean at the global scale.

Here, we use the transport-matrix method of Khatiwala et al. (2005) to test this hypothesis in the context of a ocean global circulation model coupled to a simple biogeochemical model of PO₄, Zn and Si cycling. The computational efficiency of this method allows us to conduct a swathe of sensitivity simulations in order to determine the factors that result in a large-scale Zn distribution that mimics that of Si even though the biogeochemical models governing these elements' cycling are entirely independent. This analysis shows that elevated Zn:P of uptake in the surface Southern Ocean is the first-order control on this similarity, as postulated by Vance et al. (2014).

REFERENCES

- Bruland, K. W. 1980: Oceanographic distributions of cadmium, zinc, nickel and copper in the North Pacific, Earth and Planetary Science Letters, 47, 176-198.
- Khatiwala, S., Visbeck, M. & Cane, M. A. 2005: Accelerated simulation of passive tracers in ocean circulation models, Ocean Modelling, 9, 51-69.
- Vance, D., Little, S., Zhao, Y., Cullen, J., de Souza, G. & Lohan, M. 2014 : The oceanic biogeochemical cycle of zinc and its isotopes: the dominance of Southern Ocean export, AGU Fall Meeting, San Francisco CA, USA.
- Vance, D., Little, S. & de Souza, G. this volume: Southern Ocean biology and physical oceanography the key control on global ocean trace metal distributions, Swiss Geoscience Meeting 2016, Geneva, Switzerland.

P 15.3

Relevance of iron speciation with respect to the distribution of humics and phytoplankton in Lake Geneva

Dineshkumar Krishnamoorthy^{1,2}, Sophie Moisset¹, Damien Cabanes¹, Christel Hassler¹.

¹ *Marine and Lake Biogeochemistry, Institute F.-A. Forel, University of Geneva, Switzerland (sophie.moisset@unige.ch).*

² *Department of Plant Science, Central University of Kerala, Kerala, India.*

It has been suggested that iron (Fe) is a potential limiting factor of phytoplanktonic cell growth in lake waters due to its really low concentration. Although the availability of Fe for phytoplankton depends significantly on its speciation, little is known about Fe speciation in natural lake water. Here, we investigated the horizontal distribution (0-270 m) and temporal variation of dissolved Fe and its chemical speciation in Lake Geneva, at two reference stations (GE3 and SHL2) from January to October 2014. Monthly sampling showed low dissolved Fe concentrations (3.94-39.40 nM and 1.43-68.23 nM at GE3 and SHL2, respectively), likely to impair with phytoplankton growth. Lake Geneva, as other warm meso-oligotrophic lake, has a marked seasonal succession of phytoplankton, resulting in important variation in *in-vivo* chlorophyll *a* (Chl *a*) levels (1.9-17.2 µg/L and 1.2-22.2 µg/L at GE3 and SHL2, respectively). Temporal evolution of the phytoplankton can be summarized in four main phases: winter (with very low levels of Chl *a* but high nutrient concentrations), spring bloom (with high levels of Chl *a* and high nutrient concentrations), clear water phase (with low levels of Chl *a* and active remineralization of nutrients) and autumnal bloom (with intermediate levels of Chl *a* and medium nutrient concentrations). Significant amount of colored dissolved organic matter (CDOM) were reported (0.4-3.7 and 0.3-1.6 mg/L at GE3 and SHL2, respectively) which are likely to impact Fe chemical speciation and affect its bioavailability to support phytoplankton growth. Indeed, humics able to bind Fe were electrochemically detected at concentrations from 6.5 to 953.3 µg/L SRFA equivalent. Marine electrochemical technique to measure Fe chemical speciation using the competitive ligand exchange adsorptive cathodic stripping voltammetry with salicylaldoxime, as the exchange ligand, was tuned to be used in freshwater. In order to unravel Fe chemical speciation under contrasted levels of Chl *a*, dissolved trace metals and humic substances, five vertical profiles per station were analyzed. Data showed that strong Fe-binding organic ligands were present, representing 2.7 to 42.7 nM organic ligands for GE3 and 2.8 to 70 nM for SHL2 with a conditional stability constant ($K_{Fe'L}$) of $10^{11.17}$ to $10^{12.74}$ for GE3 and $10^{11.19}$ to $10^{13.58}$ for SHL2, resulting in an inorganic Fe concentration from 0.30 pM to 8.7 pM for GE3 and 0.83 pM to 227 pM for SHL2 respectively. Results allow us to study, for the first time, the link between dissolved Fe (total and inorganic), its chemical speciation (stability constant and total organic ligands concentrations) with humics and Chl *a* in Lake Geneva.

P 15.4

Short-term carbon allocation within the root system of the tropical tree species *Ceiba pentandra*

Neringa Mannerheim¹, Carola Blessing², Israel Oren³, Jose Gruenzweig³, Nina Buchmann¹

¹ Institute of Agricultural Sciences, Grassland Group, ETH Zurich, neringa.mannerheim@usys.ethz.ch

² Faculty of Agriculture and Environment, University of Sydney

³ Institute of Plant Sciences, Faculty of Agriculture, Food and Environment, Hebrew University of Jerusalem

Tropical forests are responsible for the largest fraction of global biospheric CO₂ uptake from the atmosphere. They store up to 285 ± 64 Pg C in above-ground biomass, which is estimated to be >30% of Earth's terrestrial carbon stock. Large carbon sinks of tropical forests are the balance between photosynthetic CO₂ uptake and ecosystem respiration that releases CO₂ back to the atmosphere. Tree roots greatly contribute to this respiratory flux, but the extent of total root respiration and its regulation by either the environment and/or allocation of photoassimilates from the canopy to the below-ground are still largely unknown. This knowledge gap is mainly a result of the inaccessibility of the complex root systems of trees.

Here we report about a ¹³CO₂ pulse-chase experiment with *Ceiba pentandra*, also called Kapok or silk-cotton tree, grown in a unique large-scale aeroponic facility that can host trees up to 4m height and more than 6m long root systems. Here, we were able to fully access and manipulate tree shoots and roots and therefore study the short-term allocation of photoassimilates to the root system. The ¹³CO₂ pulse-labeling was applied to the top of the tree canopies and recovery of ¹³C in different plant tissues and compounds were investigated during a 118 hour chase period. At harvest, different root classes from the 3 depth categories (0-1m, 1-2m, 2-3m) were separated and ¹³C excess was estimated.

Our findings suggest that proportionally more C was allocated to the upper part of the root system, indicating the strongest sink of below-ground system. Upper woody roots (0-1m depth) contained the highest quantities of newly assimilated C and therefore indicate a good measure for C below-ground storage, while non-woody root tips indicate growing sink strength with the depth of the root system, linking to the fastest growing non-woody root tissue and the highest need of newly assimilated C for growth and respiration.

P 15.5

Early-diagenesis carbonate precipitation: from nodules to cone-in-cone structures

Nicolas Tribovillard¹, Anélia Petit¹, Melesio Quijada¹, Armelle Riboulleau¹, Pierre Sans-Jofre², Christophe Thomazo³ & Daniel Birgel⁴

¹ Laboratoire LOG, Univ-Lille & CNRS, F-59655 Villeneuve d'Ascq cedex (nicolas.tribovillard@univ-lille1.fr)

² Laboratoire Domaines océaniques, Université Bretagne Occidentale & CNRS

³ Laboratoire Biogéosciences, Université Bourgogne & CNRS

⁴ Institute of Earth Sciences, University of Hamburg

The Boulonnais area (alongshore the English Channel; North of France) displays Late Jurassic, clastic-dominated, sedimentary rocks, deposited in an embayment that was undergoing tectonic extension, in relation to the rifting of the Atlantic Ocean. The stratigraphic succession is largely made of an alternation of siltstones, (black) shales and sandstones, representing sea-level conditions oscillating from lower offshore to upper shoreface. Through the succession of rocks dominated by terrigenous facies, some fine-grained carbonate beds are intercalated. The beds are continuous or nodulous. They are interpreted as being of early diagenetic origin, resulting from bacterial activity at or closest to the sediment-water interface. The bacterial activity was stimulated by the seepage of fluids rich in dissolved organic carbon. The fluid expulsion itself was induced by synsedimentary fault movements (Tribovillard et al., 2012, 2015; Hatem et al., 2014, 2016).

Only one level of nodular authigenic carbonates also yielding cone-in-cone structures (CiC) at the nodule base has been observed. The centimetric-scale CiC grew from the base of the nodule downward.

The thin-section observations at various scales (photonic and electronic microscopes coupled to cathodoluminescence) indicate that the growth of the carbonate of the nodules as well as of the CiC occurred in one continuous phase. The chemical analyses show that the carbonate precipitated under reducing conditions. The C, O and S stable isotope signatures indicate that the precipitation of the authigenic carbonate began during earliest diagenesis, i.e., very close to the sediment water interface. The carbon of the authigenic carbonate is of organic origin. The role of sulfate-reduction reactions is evidenced with our data; however we could not detect organic molecules diagnostic of bacteria/archaea responsible for anoxic methane oxidation. Consequently, the authigenic carbonate precipitation was fueled by fluids rich in dissolved organic carbon (the presence of methane cannot be ruled out).

The fluid pressure necessary to account for the formation of CiC may be associated with the ascending movements of organic-rich fluids, induced by synsedimentary tectonics.

Our model suggests that methane seepages could be involved in the formation of CiC in many other situations.

REFERENCES

- Hatem, E., N. Tribovillard, O. Averbuch, D. Vidier, P. Sansjofre, D. Birgel, F. Guillot, 2014. Oyster patch reefs as indicators of fossil hydrocarbon seeps induced by synsedimentary faults. *Marine and Petroleum Geology*, 55, 176-185.
- Hatem, E., Tribovillard, N., Averbuch, O., Sansjofre, P., Adatte, T., Guillot, F., Ader, M., Vidier, D., 2016. Early diagenetic formation of carbonates in a clastic-dominated ramp environment impacted by synsedimentary faulting-induced fluid seepage – Evidence from the Late Jurassic Boulonnais Basin (N France). *Marine and Petroleum Geology*, 72, 12-29.
- Tribovillard, N., Sansjofre, P., Ader, M., Trentesaux, A., Averbuch, O., Barbecot, F., 2012. Early diagenetic carbonate bed formation at the sediment–water interface triggered by synsedimentary faults. *Chemical Geology*, 300–301, 1-13.
- Tribovillard, N., Hatem, E., Averbuch, O., Barbecot, F., Bout-Roumazielles, V., Trentesaux, A., 2015. Iron availability as a dominant control on the primary composition and diagenetic overprint of organic-matter-rich rocks. *Chemical Geology*, 401, 67-82.

P 15.6

High levels of toxic metals detected in sub-saharian rivers receiving hospital effluents: Case of Democratic Republic of Congo.

Amandine Laffite¹, Naresh Devarajan¹, Crispin K. Mulaji², Vera I. Slaveykova¹ & John Poté^{1,2}

¹ Faculty of Science, Earth and Environmental Science Section, F.-A. Forel Institute and Institute of Environmental Sciences, University of Geneva, Geneva, Switzerland

² Department of Chemistry, Faculty of Science, University of Kinshasa, Kinshasa, Democratic Republic of the Congo

The contamination of freshwater resources with various organic and inorganic contaminants including toxic metals, persistent organic pollutants, pathogenic organisms, antibiotic resistant bacteria and their resistant genes is still a major problem in many parts of the world. This situation is particularly alarming in developing countries in which the poor water quality continues to pose a serious threat to human health. The deterioration of freshwater resources is essentially due to the important discharge of untreated industrial effluents, agricultural and urban runoffs, mining wastewaters, uncontrolled urban landfills, improperly processed hospital effluents and domestic wastewaters which in turn pose tremendous effects and health risk to populations and environment consumers.

The aim of this research is to assess the role of untreated hospital and urban wastewaters on the contamination of urban rivers receiving systems in the city of Kinshasa Democratic Republic of Congo. Sediment samples were collected and analyzed for organic matter and toxic metals. The results highlight high concentration of toxic metals reaching the values of 47 (Cr), 4.97 (Co), 21.20 (Ni), 213.59 (Cu), 1434.78 (Zn), 2.65 (Cd), 274.19 (Pb) and 13.60 (Hg) ppm. We observed that contamination of wastewater receiving system by metal is highly linked with organic matter contamination ($0.74 < R < 0.89$, $p < 0.05$), thus suggesting a common origin of these contaminants. Interestingly, high values were also observed upstream hospital wastewater discharge (up to (Cu) 107, (Zn) 884, (Cd) 1.79 and (Hg) 1.43 ppm), indicating that hospital effluents are only one of several sources of contamination.

These high level of toxic metals in sediment indicate the human and environmental potential risks. Indeed, rivers network are currently used for domestic purposes, irrigation and recreational bathing.

16. Trace elements in aquatic ecosystems: from legacy to emerging pollutants

Montserrat Filella, Jean-Luc Loizeau

Commission of Limnology and Oceanography

TALKS:

- 16.1 M.-L. Tercier-Waeber: Keynote: In situ monitoring of trace metal speciation: needs, means and challenges
- 16.2 Y. Wang, P. Le Pape, G. Morin, E. Suvorova, B. Bártoová, M. P. Asta, M. Fruttschi, M. Ikogou, Vu Pham C. H., Phu Le Vo, T. Geraki, L. Charlet, R. Bernier-Latmani: A novel arsenic species in Mekong Delta sediments
- 16.3 M.P. Asta, Y. Wang, P. Le Pape, M. Fruttschi, K. Vicava, Phu Le Vo, A.M. Fernandez, D.M. Sánchez-Ledesma, G. Morin, R. Bernier-Latmani: Sulfur-bound species as a source of arsenic in Vietnam Delta sediments
- 16.4 P. Nirel: Keynote: 22 years of water quality survey for trace elements and?
- 16.5 E. Gascon Diez, N.D. Graham, J.-L. Loizeau: Transport, distribution, and speciation of particulate mercury in Lake Geneva, Switzerland
- 16.6 J.C. Rodríguez-Murillo, P. Nirel, M. Filella: Are trace element concentrations increasing in Lake Geneva waters?

POSTERS:

- P 16.1 D. Ciszewski: Sulphates are intensively transformed to sulphides in the hyporheic zone of the polluted sandbed river
- P 16.2 E. Gascon Diez, J.-P. Corella, T. Adatte, F. Thevenon, J.-L. Loizeau: The legacy of metal pollution related to industrial activities in a highly contaminated area of Lake Geneva (Switzerland)
- P 16.3 M.C. Casado-Martinez, M. Wild, B.I.D. Ferrari, I. Werner: A new module for the sediment compartment within the Modular Stepwise Procedure (MSK) for the assessment of water bodies in Switzerland: the ModSed project
- P 16.4 M. Filella, A. Voegelin: Network on technology-critical elements: from environmental processes to human health threats (COST action TD1407)

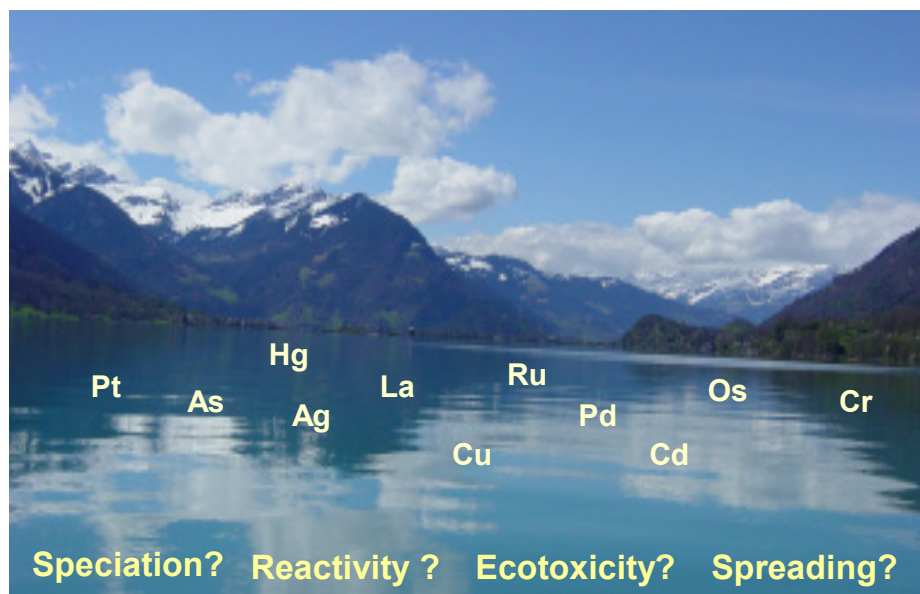
16.1

In situ Monitoring of Trace Metal Speciation: needs, means and challenges.

Mary-Lou Tercier-Waeber

Département de Chimie Minérale et Analytique, Université de Genève, Sciences II, Quai E.-Ansermet 30, CH-1211 Geneva 4 (marie-louise.tercier@unige.ch)

Trace metals are ubiquitous and persistent in the environment. Due to their specific properties they play important roles in many biogeochemical processes, where they may act as micronutrients or pollutants. In addition to more classically exploited and emitted trace metals (e.g. Zn, Cu, Pb, Cd, etc.) there is a range of elements (e.g. Platinum Group Metals, Rare Earth Elements etc.) critical to various recent and future technical applications, implying high strategic and economic value of these technology-critical elements (TCEs) on the one hand and emerging contamination of surface environments on the other. For some trace metals, the anthropogenic global cycle has already outcompeted the respective natural cycle, underlining the need to understand their environmental roles and fate. If the general biogeochemical cycles of the more classical metallic contaminants are relatively well documented, knowledge gaps on speciation, transformation processes, control factors and transfer to living organisms still persist, due to analytical limitations. For TCEs, extremely little information (or no information at all) on natural concentrations (geochemical background), speciation, reactivity, transfer dynamics, etc. exists because of the lack in analytical methods available. However, such methods are essential to develop the urgently needed capacity of surveying, observing and understanding anthropogenically modified trace metal cycles in aquatic environments.



This lecture will present examples of innovative approaches we have developed and we are currently exploring to provide robust and reliable chemical mapping probes for in situ quantification of specific trace metal species or fraction. The related challenges will be discussed.

REFERENCES

Tercier-Waeber, M.-L., Stoll, S & Slaveykova V.I. 2012: Trace metal behavior in surface waters: emphasis on dynamic speciation, sorption processes and bioavailability - Review. *Archive of Science Journal*, 65, 119-142. Cobelo-Garcia, A. 2014: Technology-critical elements: a need for evaluating the anthropogenic impact on their marine biogeochemical cycles. *Front. Mar. Sci. Conference Abstract: IMMR | International Meeting on Marine Research 2014*. (doi: 10.3389/conf.fmars.2014.02.00164).

16.2

A novel arsenic species in Mekong Delta sediments

Yuheng Wang¹, Pierre Le Pape², Guillaume Morin², Elena Suvorova¹, Barbora Bártořová¹, Maria P. Asta¹, Manon Fruttschi¹, Maya Ikogou², Vu Pham C. H.³, Phu Le Vo³, Tina Geraki⁴, Laurent Charlet⁵ and Rizlan Bernier-Latmani¹

¹ *Ecole Polytechnique Fédérale de Lausanne (EPFL), Environmental Microbiology Laboratory (EML), Station 6, CH-1015 Lausanne, Switzerland. (yuheng.wang@epfl.ch)*

² *Centre National de la Recherche Scientifique (CNRS) - Université Pierre et Marie Curie (UPMC Paris 6), Institut de Minéralogie, de Physique des Matériaux et de Cosmochimie (IMPMC, CNRS-UPMC-IRD-MNHN UMR 7590), 4 place Jussieu, 75005 Paris, France*

³ *Ho Chi Minh City University of Technology, Faculty of Environment and Natural Resources, VNU-HCM, 268 Ly Thuong Kiet, Ho Chi Minh City, Vietnam*

⁴ *Diamond Light Source, Beamline I18, Didcot, Oxfordshire OX11 0DE, United Kingdom*

⁵ *Université Grenoble Alpes, Institut des Sciences de la Terre (ISterre, UMR 5275), BP 53, F-38041 Grenoble, France*

The occurrence of elevated arsenic (As) concentrations in groundwater is common in Southeast Asian deltas and represents a significant health hazard to the health of millions. Although extensive research has been carried out to understand the mechanism of As contamination, open questions remain about (a) the persistence of an As(V) signature in the reducing sediment environment (Lowers et al., 2007; Stuckey et al., 2015), (b) the origin (authigenic or detrital) of individual As-bearing phases, and (c) their role in As cycling (Acharyya et al., 1999; Nickson et al., 1998).

In the present study, we investigate As speciation in redox-preserved sediment cores from the Mekong Delta in Vietnam to obtain a comprehensive view of the As-bearing phases in the sediments and to address the remaining questions. We characterize the sediments at a wide range of scales, including bulk mineralogical and chemical analyses, micro-scale electron microscopy and spectroscopy, and bulk and micro-scale X-ray absorption spectroscopy. We identified a novel As(V) species associated with graphite-like nanostructures. This species is identified throughout the sediment profile down to 20 m. On the other hand, As-free C nanostructures were identified in suspended particulate matter from the Mekong River, suggesting a riverine origin for the nanostructures but an authigenic origin for the novel As(V) species. Additionally, at some depths, the sediment layers also harbor arsenian pyrite and As(III) bound to thiol groups as significant fractions of total As, which correspond to a paleo-mangrove depositional environment. We propose that this newly discovered As(V) species might be key to explaining the persistence of pentavalent arsenic in reduced sediments and hypothesize that it acts as a long-term sink for As. Thus, this work opens new avenues to refine the current model for the origin, deposition, and release of arsenic in the alluvial aquifers of the Mekong Delta.

REFERENCES

- Acharyya, S.K., Chakraborty, P., Lahiri, S., Raymahashay, B.C., Guha, S. and Bhowmik, A. 1999: Arsenic poisoning in the Ganges delta. *Nature*, 401, 545-545.
- Lowers, H.A., Breit, G.N., Foster, A.L., Whitney, J., Yount, J., Uddin, M.N. and Muneem, A.A. 2007: Arsenic incorporation into authigenic pyrite, Bengal Basin sediment, Bangladesh. *Geochimica et Cosmochimica Acta*, 71, 2699-2717.
- Nickson, R., McArthur, J., Burgess, W., Ahmed, K.M., Ravenscroft, P. and Rahmann, M. 1998: Arsenic poisoning of Bangladesh groundwater. *Nature*, 395, 338-338.
- Stuckey, J.W., Schaefer, M.V., Benner, S.G. and Fendorf, S. 2015: Reactivity and speciation of mineral-associated arsenic in seasonal and permanent wetlands of the Mekong Delta. *Geochimica et Cosmochimica Acta*, 171, 143-155.

16.3

Sulfur-bound species as a source of arsenic in Vietnam Delta sediments

Maria P. Asta¹, Yuheng Wang¹, Pierre Le Pape², Manon Fruttschi¹, Karen Vicava¹, Phu Le Vo³, Ana M. Fernandez⁴, D.M. Sánchez-Ledesma⁴, Guillaume Morin², Rizlan Bernier-Latmani¹

¹ Environmental Microbiology Laboratory (EML), Ecole Polytechnique Fédérale de Lausanne, Switzerland (maria.astaandres@epfl.ch)

² Centre National de la Recherche Scientifique (CNRS) - Université Pierre et Marie Curie (UPMC Paris 6), Institut de Minéralogie, de Physique des Matériaux et de Cosmochimie (IMPMC, CNRS-UPMC-IRD-MNHN UMR 7590), 4 place Jussieu, 75005 Paris, France

³ Ho Chi Minh City University of Technology, Faculty of Environment and Natural Resources, VNU-HCM, Vietnam

⁴ Centro de Investigaciones Energéticas, Medioambientales y Tecnológicas (CIEMAT), Dpto. Medio Ambiente, Madrid, Spain

Arsenic (As) release from sediments into groundwater is a major water quality problem in South and South East Asia. The most commonly accepted model infers that influx of organic carbon results in the microbial reductive dissolution of As-bearing Fe(III) (oxyhydr)oxides (Stuckey et al., 2015). Although this mechanism is thought to be responsible for As release in some deltaic areas (Postma et al., 2010), it may not be the dominant mechanism at our study site in An Giang Province in the Mekong Delta in Vietnam. Indeed, Fe(III) (oxyhydr)oxides are depleted in the reduced sediment below 7 m (Figure 1a) and the majority of As is associated with pyrite and natural organic matter (NOM) through thiol-bonding, together with O-bound As species (Wang et al., 2016; see Figure 1b).

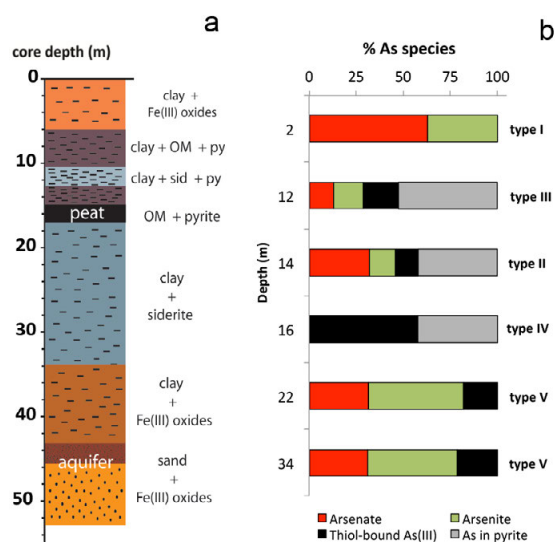


Figure 1. (a) Scheme summarizing the lithology of sediment cores (modified from Wang et al., 2016). Sediments consist of a 40 m thick clay layer overlaying the sandy aquifer. The peat layer at 16 m holds the highest As content (Table 1). (b) Speciation of As as a function of depth determined using linear combination fitting of As K-edge EXAFS data. The classification of sediment layer types are from Wang et al. (2016).

To probe the potential source(s) of arsenic in this sediment, flow-through leaching experiments were performed for each type of sediment using artificial groundwater (AGW). We found that As was released into the AGW mainly as As(III). Interestingly, there was no correlation between the amounts of As and Fe released, suggesting that microbially mediated iron reduction might not be the main mechanism of As release in these reduced sediments. Furthermore, the peat layer (Type IV) and the clay-rich layers immediately below it (Type V) released the largest fraction of As (Table 1). Moreover, As concentrations in the porewater of the squeezed sediments (to which pressure at 1.5-3.1 Mpa were applied) showed the highest values at these two layers (Table 1). These observations suggest that As species in these two layers, mainly S-bound As, may be released more readily than O-bound As species. Thus, we propose that As is likely released from S-bound As pools in the peat layer, most likely NOM-thiol bound As but also possibly As-pyrite.

Sediment	Depth	As _{solid}	% leached	As _{pore water}
	(m)	(ppm)		(µg/L)
Type I	2	21	5	<i>n.a.</i>
Type II	12	11	14	16
Type III	14	12	12	6
Type IV	16	34	40	52
Type V	22	12	23	56
	34	12	<i>n.a.</i>	8
Type VI	44	7	<i>n.a.</i>	<i>n.a.</i>

n.a.: not analyzed

Table 1. Arsenic concentrations for the various types of sediment layers (Wang et al. (2016)) obtained from leaching experiments and squeezed porewater. Dissolved arsenic concentrations were measured after filtration using 0.2 µm pore size filters.

Peat layers have been proposed as As sinks for both surface peatland (Langner et al., 2011) and buried deltaic sediment (Stuckey et al., 2015) with the formation of S-bound As. However, in the present study, we suggest for the first time that S-bound As plays a key role in arsenic cycling in the Mekong delta as a significant source for anoxic As mobilization.

REFERENCES

- Langner, P., Mikutta, C., Kretzschmar, R. 2011: Arsenic sequestration by organic sulphur in peat. *Nature Geoscience* 5, 66-73.
- Postma, D., Jessen, S., Thi Minh Hue, N., Thanh Duc, M., Bender Koch, C., Quy Nhan, P., Larsen F. 2010: Mobilization of arsenic and iron from Red River floodplain sediments, Vietnam. *Geochimica et Cosmochimica Acta* 74, 3367-3381.
- Stuckey, J.W., Schaefer, M.V., Kocar, B.D., Dittmar, J., Lezama Pacheco, J., Benner, S.G., Fendorf, S. 2015: Peat formation concentrates arsenic within sediment deposits of the Mekong Delta. *Geochimica et Cosmochimica Acta* 149, 190-205.
- Stuckey, J.W., Schaefer, M.V., Kocar, B.D., Benner, S.G., Fendorf, S. 2016: Arsenic release metabolically limited to permanently water-saturated soil in Mekong Delta. *Nature Geoscience* 9, 70-76.
- Wang, Y., Le Pape, P., Morin, G., Suvorova, E., Bartova, B. Asta, M.P., Fruttschi, M., Ikogou, M., Pham, V., Le Vo, P., Charlet, L., Bernier-Latmani, R. 2016: A carbon nanotube-associated source of arsenic in Mekong Delta sediments. *Nature Communications* (In revision).

16.4

22 years of water quality survey for trace elements and?

Pascale Nirel

Direction Générale de l'Eau, Etat de Genève, Avenue de Ste-Clotilde 25, CH-1211 Genève

22 years ago, the Canton of Geneva launched a water quality survey for trace elements project. The time frame appears long enough to assess the results and share the acquired knowledge.

Did the actions undertaken to limitate metals release succeed and to what extend ?

Long term surveys optimization: data bases and what else?

Those are some of the points we shall consider.

16.5

Transport, distribution, and speciation of particulate mercury in Lake Geneva, Switzerland.

Elena Gascon Diez, Neil D. Graham & Jean-Luc Loizeau

¹ *Department F.-A. Forel for Environmental and Aquatic Sciences and Institute for Environmental Sciences, University of Geneva, Boulevard Carl-Vogt 66, CH-1211 Geneva (Elena.Gascon@unige.ch)*

Trace metals are of major concern in lacustrine environments, in particular, mercury (Hg) which is a hazardous neurotoxic chemical that accumulates and bioamplifies through the food chain when it is present as methylmercury (MeHg). Due to its specific geochemistry, particle-bound mercury in aquatic systems is transported and/or settled on the sediment surface (Riscassi et al., 2011). In order to study the sources and dynamics of total mercury (THg) and MeHg from the shore to the deep waters of a large lake, settling particles have been collected by sediment traps during a two-year period (2010-2011) at two sites and two depths of Lake Geneva, supplemented by surface sediment sampling at the same sites and dates

Combined results of concentrations and fluxes showed that the major input of THg into the lake is the combination of the human activities and contributions from the catchment area. THg concentrations measured on particles recovered in the top and bottom sediment traps ranged between 0.073 ± 0.001 and 0.27 ± 0.01 $\mu\text{g/g}$ at NG2 (closer to the shore), and between 0.038 ± 0.001 and 0.21 ± 0.01 $\mu\text{g/g}$ at NG3 (closer to the deep lake); these concentrations in settling particles were up to 10 times higher than the natural reference value in sediments of THg in Lake Geneva (0.03 $\mu\text{g/g}$) (Arbouille et al., 1988).

Both sites followed similar seasonal patterns with the highest THg concentrations in autumn-winter and the lowest contents in summer-autumn. However, Concentration data itself is not enough to fully understand the dynamics of THg associated with particles. Variations in sediment accumulation rates (SAR) modify the particulate THg signal. Therefore, to further understand these spatial and temporal variations, THg fluxes were calculated for the top and bottom sediment traps of both NG2 and NG3. THg fluxes ranged between 0.144 ± 0.002 and 1.6 ± 0.3 $\mu\text{g/m}^2/\text{d}$ at NG2, and between 0.10 ± 0.05 and 0.89 ± 0.03 $\mu\text{g/m}^2/\text{d}$ at NG3 (Figure 1). Although the most distal sampling site (~ 3km from the shoreline) showed a decrease of total mercury fluxes, SAR and organic matter fluxes suggested that this area was still affected by the coastal region, as compared to sites in the center of the lake. Seasonal variability of THg fluxes was less pronounced than Hg concentration variability suggesting that THg concentrations were strongly influenced by the seasonal trends of sedimentation rates.

Resuspension and/or lateral advection has been observed in the bottom tier of the sediment traps (5m above the lakebed) with greater THg fluxes in the bottom trap than in the top trap at both sites (Figure 1). In addition, THg bottom fluxes were slightly greater at NG2 than at NG3, and as NG2 is about one km closer to shore, lateral advectons at this site could be due to resuspension from the shallower areas where the sediments are slightly charged with anthropogenic THg.

Regarding MeHg results, MeHg concentrations and fluxes in settling particles largely exceeded the concentrations found in sediments and contrary to THg, the largest MeHg concentrations were found during summer. Differently to THg fluxes, MeHg fluxes did not show significant differences with relation to the distance from shore. The high content of fresh planktonic organic matter found in settling particles likely enhanced the activity of the heterotrophic bacteria involved in Hg-methylation processes (Schartup et al., 2015). Thus, the MeHg found in settling particles would be related to lake internal production rather than the effect of the transport from the watershed and/or resuspension of sediments.

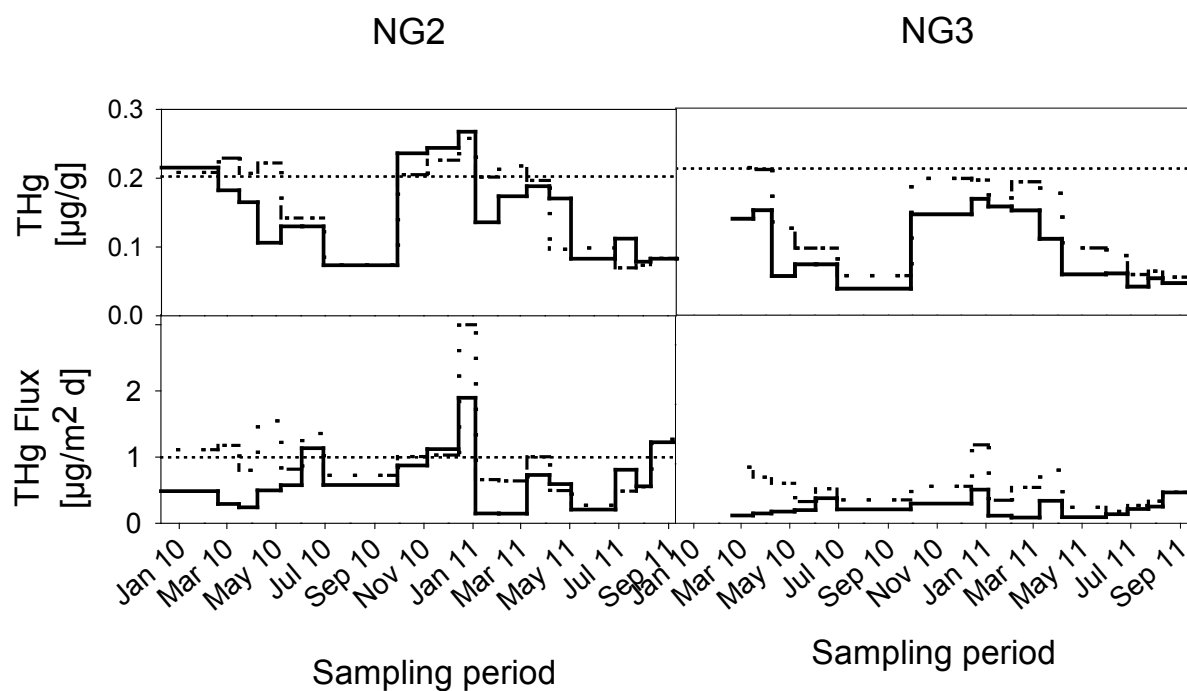


Figure 1. THg concentrations (top graphs) and fluxes (bottom graphs) in settling particles and sediments at NG2 and NG3. Solid line: top sediment trap. Dashed line: bottom sediment trap. Dotted line: mean THg concentration or flux in surface sediments during the entire period of sampling.

REFERENCES

- Arbouille, D., Howa, H., Span, D. & Vernet, J. P. 1988: Etude générale de la pollution par les métaux et repartition des nutriments dans les sédiments du Léman, Commission internationale pour la protection des eaux du Léman, Campagne 1988, 139-172.
- Riscassi, A. L., Hokanson, K. J. & Scanlon, T. M. 2011: Streamwater Particulate Mercury and Suspended Sediment Dynamics in a Forested Headwater Catchment, *Water, Air, & Soil Pollution*, 220, 23-36.
- Schartup, A. T., Ndu, U., Balcom, P. H., Mason, R. P. & Sunderland, E. M. 2015: Contrasting Effects of Marine and Terrestrially Derived Dissolved Organic Matter on Mercury Speciation and Bioavailability in Seawater, *Environmental Science & Technology*, 49, 5965-5972.

16.6

Are trace element concentrations increasing in Lake Geneva waters?

Juan Carlos Rodríguez-Murillo¹, Pascale Nirel² & Montserrat Filella³

¹ *Museo Nacional de Ciencias Naturales, CSIC, Serrano 115 dpdo., E-28006 Madrid, Spain*

² *Service de l'écologie de l'eau, Av. Sainte-Clotilde 23, CH-1211 Geneva 8, Switzerland*

³ *Institute F.-A. Forel, University of Geneva, Boulevard Carl-Vogt 66, CH-1205 Geneva, Switzerland*

It is generally assumed that the increased use of metals and other chemical elements, characteristic of the Holocene, necessarily leads to an increase in their concentrations in the different environmental compartments. It is well-known that increases in element anthropic uses are reflected in so-called environmental archives (e.g., ice, peat bogs, lake sediments) but the follow-up and the understanding of changes in surface water concentrations are more difficult. First, the detection of concentration trends in waters requires the existence of long temporal series of reliable concentration data; this represents a formidable obstacle because such series are extremely scarce. Secondly, element concentrations in lake waters are not only the result of direct inputs (e.g., water treatment plants and atmospheric deposition) but also of runoff contributions (of geological or anthropogenic origin) and reflect internal processes in soils and waters.

Luckily, concentration data exist in Lake Geneva for a certain number of elements over many years. Results for well-studied elements (Cd, Co, Mo, Pb, Sb, Sr) as well as for some technology-critical elements (Ga, Gd, Ge) will be presented. Particular attention will be paid to methodological considerations and, when possible, the reasons for the observed trends will be discussed.

P 16.1

Sulphates are intensively transformed to sulphides in the hyporheic zone of the polluted sandbed river

Dariusz Ciszewski¹

¹ AGH-University of Sciences and Technology, 30-059 Krakow, Mickiewicza St.30 Poland (ciszewski@geol.agh.edu.pl)

Hyporheic zone (HZ) is an area beneath the channel bottom where river waters mix with groundwaters. Whereas, it has been recognized that the microbial activity of this zone reduces the load of nitrates transported down the river, its role in transformation of sulphates is underestimated. It was studied in a channel bar of the strongly polluted Przemsza River, draining the industrialized part of southern Poland. In the studied reach, it is the gaining river, incised in alluvial sandy deposits as a result of adjustment to post-channelization increase of the channel gradient. The average river discharge equals to about 15 m³/s and the bed load of the sandy material form dunes about 1 m thick sparsely distributed at sheltered locations along channel banks.

Water was sampled 8 times during a year from the river itself and from piezometers installed in the channel: from the bar (HZ) at depth 0.5-1 m, from the channel bottom at depth 1-1.5 m (below the bar) and from the floodplain at the depth about 3-4 m below the ground surface, several meters from the bank. Standard chemistry of waters was analyzed using gas chromatography and the content of trace elements was analyzed by means of the ICP MS. Additionally, SEM was performed in a sediment sample from the HZ, prepared in oxygen free conditions. The variability of water chemistry was coupled with daily water flow data from a gauge station.

Content of sulphates in the HZ is always several times lower than in river waters and groundwaters, most probably due to the microbial sulphate degradation and formation of iron sulphides. It is accompanied by the very low content of dissolved sulphur in the HZ. The intensive microbial activity is confirmed also by contrastingly higher content of hydrocarbonates in the HZ than in the river and groundwaters draining the floodplain. It is the final product of microbial CO₂ production during organic matter degradation. Moreover, the HZ is characterized by the content of NH₄ two orders of magnitude higher than in groundwaters and in the river. The lack of nitrates in the HZ with their average concentrations in the river water of about 10 mg/l, proves microbially mediated denitrification processes in the sandbar. Hence, the HZ zone in the sandbar is characterized by anoxic conditions which favour iron reduction to Fe⁺² and indicate that dissolved Fe of the HZ originates from the dissolution of this element present in bed sediments probably as hydrooxides. The dissolved iron is present in the river in concentrations over 100 times lower than in the HZ and the river water seems to be the less important source of iron to the HZ. As a result of reducing conditions in the HZ, presence of organic matter, sulphates, and excess of iron, microcrystals of iron sulphides (pyrites) (Fe_{0.9}Zn_{0.1})S₂, and pyrite framboids (Fe_{0.75}Zn_{0.25})S₂ (which are bounded with clays) are formed onto quartz grains of sand.

High water flows causes a partial exchange of the sandy bar surface material. Maximum flow on September caused net sediment erosion and induced the larger penetration of river waters into the HZ (e.g. indicated by an equal conductance in the HZ and in the river), whereas the maximum flow of October caused the accretion of silty sediments, which reduced infiltration of river waters into the river bed (e.g. indicated by equal conductance in the HZ and in groundwaters).

The investigations conducted indicate that, the HZ in sandy alluvia of the strongly polluted rivers contributes to reduction of pollution load transported in the river. Sandbars can be an excellent place, however temporary variable, for transformation of sulphates to sulphides. These microbially mediated processes lead to formation of micropyrrite crystals and pyrite framboids dispersed within matrix of quartz grains.

P 16.2

The legacy of metal pollution related to industrial activities in a highly contaminated area of Lake Geneva (Switzerland)

Elena Gascon Diez¹, Juan-Pablo Corella², Thierry Adatte³, Florian Thevenon⁴ & Jean-Luc Loizeau¹

¹ Department F.-A. Forel for environmental and aquatic sciences and Institute for Environmental sciences, University of Geneva, Boulevard Carl-Vogt 66, CH-1211 Genève (Elena.Gascon@unige.ch)

² Institute of Physical Chemistry Rocasolano, CSIC, C/ Serrano 117, 28006 Madrid, Spain

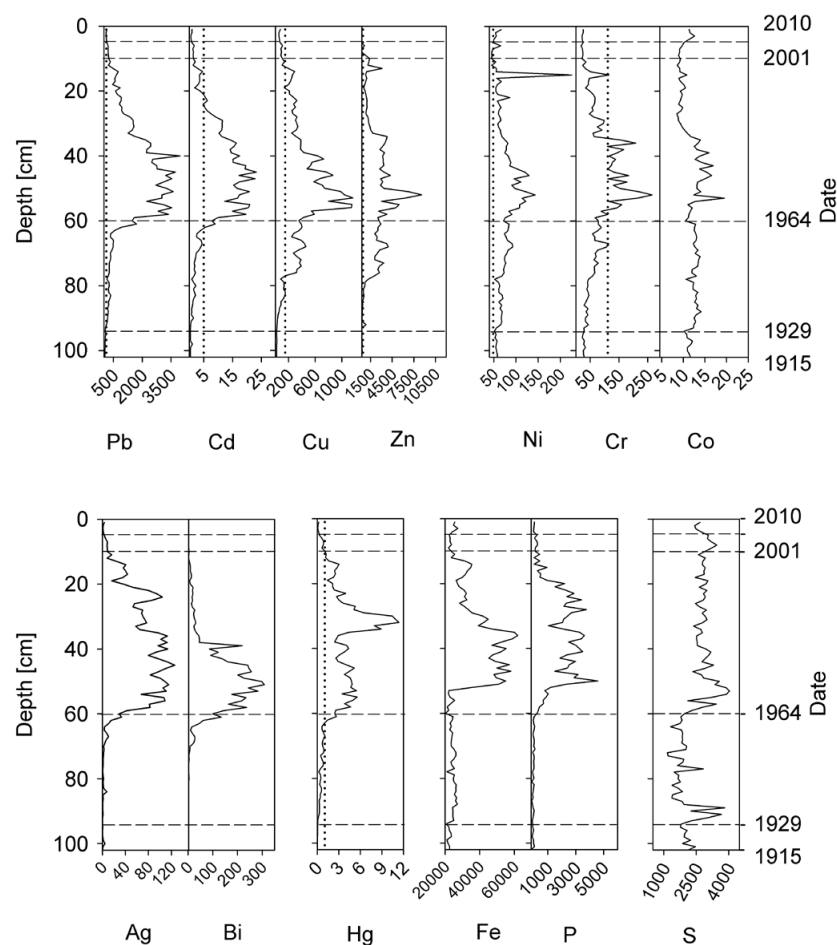
³ Institut des Sciences de la Terre, University of Lausanne, Quartier UNIL - Mouline Bâtiment Géopolis, CH-1015 Lausanne

⁴ WaterLex International Secretariat, Avenue de la Paix 7 bis, CH-1202 Genève

Toxic trace metals in (drinking) water reservoirs and lacustrine sediments can be harmful to biota and human health. Trace metals, major elements, total organic carbon (TOC), mineral carbon (MinC), Hydrogen Index, Oxygen Index, and TOC/N ratios were measured on a sediment core to reconstruct the historical environmental pollution of Vidy Bay, the most contaminated area of Lake Geneva. The study area has been affected by hazardous compounds released by the effluent of a major wastewater treatment plant (WWTP) implemented in 1964.

Pb, Cd, Cu, Zn, and Hg, the most hazardous anthropogenic trace metals, together with Ni, Cr, Co, Ag, Bi, and Fe concentrations increased throughout the 20th century following the industrial revolution in Europe of 1850 ca. The highest amounts of these toxic metals were recorded in sediments deposited between 1964 and 2001. During the period of operation of the WWTP's facilities, all trace elements highly exceeded the sediment quality guideline "probable concentration effect" (PEC) in freshwater ecosystems (MacDonald et al., 2000), with the following maximum concentrations (in mg kg⁻¹): Pb 3977, Cd 23, Cu 1166, Zn 8586, Hg 11, Ni 143, Cr 265, Ag 126, and Bi 309.

Detrital elements trends (Al, Si, Ca, Ti, Zr, Rb, and Sr) showed a clear decrease since the WWTP implementation due to a decrease in the clastic input and the WWTP releases after treatment into the lake, changing the origin and the composition of the geogenic sources in the sediments of the bay.



The nature and quality of organic matter were also clearly affected by the effluent. The TOC gained importance over MinC after 1964 in the bay. Simultaneously, the Hydrogen Index and Oxygen Index inversed their tendencies, conferring to the sediments a signal similar to algal components (Kruge et al., 2010) during the WWTP functioning period, due to settling of organic-rich particles.

The sedimentary record also revealed that, after some improvements in the wastewater treatment processes and the relocation of the outlet pipe (in 2001), the characteristics of the sediments tended to return to similar conditions to those prevailing before the WWTP implementation. However, the sediments deposited in the Vidy Bay during the second part of the 20th century represent a major contaminant legacy that constitutes a potential threat to the lake biota and human health in the case of sediment remobilization (Kremer et al., 2015).

Figure 1. Trace metals in mg kg⁻¹; and S and P in cps (analyzed by XRF). Horizontal short dashes represent the limits between stratigraphic units. Vertical dotted lines represent the PEC for each element

REFERENCES

- Kremer, K., Corella, J. P., Adatte, T., Garnier, E., Zenhäusern, G. & Girardclos, S. 2015: Origin of Turbidites In Deep Lake Geneva (France–Switzerland) In the Last 1500 Years. *Journal of sedimentary research*, 85, 1455-1465.
- Kruege, M. A., Permanyer, A., Serra, J. & Yu, D. 2010: Geochemical investigation of an offshore sewage sludge deposit, Barcelona, Catalonia, Spain. *Journal of Analytical and Applied Pyrolysis*, 89, 204-217.
- MacDonald, D. D., Ingersoll, C. G. & Berger, T. A. 2000: Development and evaluation of consensus-based sediment quality guidelines for freshwater ecosystems. *Archives of Environmental Contamination and Toxicology*, 39, 2031.

P 16.3

A new module for the sediment compartment within the Modular Stepwise Procedure (MSK) for the assessment of water bodies in Switzerland: the ModSed project

M.Carmen Casado-Martinez¹, Michel Wildi¹, Benoit J.D. Ferrari¹ & Inge Werner²

¹ Swiss Centre for Applied Ecotoxicology Eawag-EPFL, EPFL Station 2, 1015 Lausanne (carmen.casado@centreecotox.ch)

² Swiss Centre for Applied Ecotoxicology Eawag-EPFL, Überlandstrasse 133, 611 Dübendorf

Sediments are an ecologically important compartment of surface waters. According to the Swiss Water Protection Ordinance (OFEV 1998), sediments must not accumulate persistent pollutants to ensure the protection of aquatic life. Although a national program for the monitoring of sediment quality such as the one implemented for soils (NABO) is absent, existing data illustrate that sediment contamination is present in Switzerland and there are cases where it is of concern for the health of aquatic ecosystems. Despite this, to date no harmonised guidelines/methods or quality standards are available for sediment-quality monitoring.

According to a questionnaire sent to cantonal agencies, the availability of adequate sediment quality guidelines for selected chemicals to classify *in situ* sediments according to their ecotoxicological risk is a top need (Flück et al. 2011). Of second priority is the harmonisation of sampling strategies, including the preparation of samples for further analyses.

In response to the needs of cantons and other stakeholders, in January 2015 a project for the development of a “module sediment” within the framework of the Modular Stepwise Procedure (“MSK”) used in Switzerland for surface water quality monitoring was launched by the Swiss Centre for Applied Ecotoxicology, in partnership with Eawag and the Swiss Federal Office of the Environment. The new module is planned to complement existing MSK modules and thereby to achieve a more holistic assessment of Swiss surface waters by incorporating the sediment compartment.

The first project phase deals with the development of a sediment assessment system based on the chemical status and will address the two top priorities for cantons: 1) the development of a harmonized protocol for sediment sampling and pre-treatment to allow a robust interpretation of data at a pan-national level, and 2) the derivation of numerical sediment quality criteria for selected contaminants prioritized according to their presence in Swiss waters and their potential for toxicity. Here we will present the project concept, the state of implementation and the expected results relevant for the trace elements included in the project.

REFERENCES

- Office Fédéral de la Protection de l'Environnement 1998: Ordonnance du 28 octobre 1998 sur la protection des eaux (OEaux). No. RS 814.201. Berne, Suisse.
- Flück, R., Chèvre, N., & Campiche, S. 2011: Surveillance de la qualité des sédiments en Suisse : Synthèse d'un questionnaire. Septembre 2011, Centre Ecotox, Lausanne, Suisse.

P 16.4

Network on technology-critical elements: from environmental processes to human health threats (COST action TD1407)

Montserrat Filella¹ & Andreas Voegelin²

¹ *Institute F.-A. Forel, University of Geneva, Geneva, Switzerland*

² *Eawag, Swiss Federal Institute of Aquatic Science and Technology, Dübendorf, Switzerland*

Whilst considerable progress has been made in understanding the environmental fate and eco-toxicological behaviour of traditionally used trace elements, our knowledge on the environmental fate and impact of a range of trace elements that are used in an ever expanding list of emerging technologies is still limited. This group of elements includes Ga, Ge, In, Te, Nb, Ta, Ti, the Pt group elements and most of the rare earth elements, which have become essential components in a variety of applications in the fields of communication and electronics, mobility and (green) energy. Their current strategic importance is such that have now been labelled as 'energy-critical elements' or 'technology-critical elements' (TCEs). Due to their high economic relevance and the dependency of the European Union (EU) on imports, the EU has identified 14 critical materials for which, at the moment, no mining zones with an acceptable short/mid-term profit exist within Europe. These critical materials identified by the EU encompass most of the TCEs mentioned above.

The increasing use of TCEs may lead to increasing emissions into aquatic and terrestrial environments and induce significant changes in the processes associated with their biogeochemical cycling at the Earth's surface. At all stages of their life cycle, these elements and their compounds can be released into the environment and come in contact with the biosphere. However, the impact of the increasing use of many TCEs on environmental and human health is still poorly understood. For several TCEs, there are basically no data at all.

On April 2015, a new EU COST action (TD 1407) focused on the study of TCEs was launched (www.costnotice.net). The aim of the action is to create a network of scientists interested in the investigation of TCEs. The participation of scientists from the geological and environmental sciences is needed and most welcome.

17. Atmospheric Processes and Interactions with the Biosphere

Christof Ammann, Stefan Brönnimann, Lutz Merbold, Peter Waldner

*ACP – Commission on Atmospheric Chemistry and Physics,
ProClim – Forum for Climate and Global Change*

TALKS:

- 17.1 Burri S., Haeler E., Haeni M., Braun S., Walthert L., Buchmann N., Eugster W., Zweifel R.: Forest growth in Switzerland during the hot summer 2015
- 17.2 Emmel C., Eugster W., Hörtnagl L.: Carbon budgets of six different agricultural crops at the Oensingen arable land Fluxnet site
- 17.3 Fuchs K., Hoertnagl L., Eugster W., Koller P., Kaeslin F., Merbold L.: Management matters: Testing a mitigation strategy of nitrous oxide emissions on managed grassland
- 17.4 Ingensand J., Bullinger G., Composto S., Camponovo R., Spahni B., Froidevaux M., Nappez M., Varesano D.: The influence of ground surfaces on urban climate
- 17.5 Revall A., Emmel C., D'Odorico P., Buchmann N., Eugster W.: Process-based crop model simulations of carbon fluxes and stocks – an evaluation at the Oensingen cropland site
- 17.6 Sigl M., Büntgen U., Toohey M., Ludlow F., Oppenheimer C., Manning J.: Volcanism, climate and human: On an illuminative journey with an ice-core time machine
- 17.7 Van der Voort T.S., Hagedorn F., Mannu U., McIntyre C., Walthert L., Schleppi P., Eglinton T.I.: Soil carbon dynamics and fluxes across a climatic gradient from temporally-resolved radiocarbon measurements

POSTERS:

- P 17.1 Randevoson F., Cailleau G., Rajoelison G., Razakamanarivo H., Razafimbelo T., Verrecchia E.: Is grain size distribution an important factor of Oxalate-Carbonate Pathway efficiency?
- P 17.2 Matteodo M., Sebag D., Vittoz P., Verrecchia E.P.: Stability of soil organic matter in Alpine ecosystems: no relationship with vegetation

17.1

Forest growth in Switzerland during the hot summer 2015

Susanne Burri^{1,3}, Elena Haeler¹, Matthias Haeni¹, Sabine Braun², Lorenz Walther¹, Nina Buchmann³, Werner Eugster³, Roman Zweifel¹

¹ *Forest Dynamics, Swiss Federal Institute for Forest, Snow and Landscape Research WSL, Zürcherstrasse 111, CH-8903 Birmensdorf*

² *Institute for Applied Plant Biology, Sandgrubenstrasse 25/27, CH-4124 Schönenbuch*

³ *Institute of Agricultural Sciences, ETH Zurich, Universitaetstrasse 2, CH-8092 Zurich (susanne.burri@usys.ethz.ch)*

In 2015, Switzerland experienced the second warmest summer since measurement start in 1865. Temperatures were 2.4°C higher on average and precipitation amounts were regionally below average (norm period 1981-2010) (MeteoSchweiz 2015). Hence, the hot summer 2015 was a prime example for summers as projected under future climatic conditions in Switzerland (CH2011 2011). Since forests cover about one third of Switzerland, the response of forest ecosystems to such extreme events is of high interest for carbon balance, yield and finally ecosystem stability. Thus, how did trees in Switzerland experience the hot summer 2015?

Investigating such questions is what the research network TreeNet is aiming at. It uses point dendrometers to continuously measure fluctuations of stem radius on the micrometer scale. In our study, we analyzed tree growth from 56 trees across Switzerland, originating from 11 sites. The majority of the trees analyzed were *Picea abies* and *Fagus sylvatica* (the two main tree species in Switzerland), but also *Abies alba*, *Fraxinus excelsior* and *Quercus* species were included. The high temporal resolution of our measurements not only allowed deriving annual tree growth, but also, as a novel approach, to exactly define tree-specific growing periods. As a next step, we could then characterize the meteorological conditions for each tree during its growing period. We then finally compared our results to the year 2014 where, in contrast to 2015, the summer was relatively cool and wet.

At many sites the hot summer 2015 led to reduced tree growth in comparison to 2014. This effect was strongest for *Picea abies* which showed decreased growth at 5 of 6 sites and the highest growth differences between 2015 and 2014 among all species investigated. The difference was highest at lowland sites, while it was less strong or even positive at higher altitude sites. The pattern was less clear for the other species investigated, because both increased or decreased growth was observed in 2015 in comparison to 2014. Thereby, especially for *Fagus sylvatica*, trees that experienced less drought stress during the growing period (e.g. due to locally small precipitation deficits or high water holding capacities of the soil) could partly profit from the hot summer 2015 and grew slightly better in comparison to 2014.

By integrating the response of tree growth to the hot summer 2015 from numerous trees and sites across Switzerland, we received an impression of how Swiss forest ecosystems might respond to more extreme summers projected under future climate.

REFERENCES

CH2011. 2011: Swiss Climate Change Scenarios CH2011, published by C2SM, MeteoSwiss, ETH, NCCR Climate, and OcCC, Zurich, Switzerland, 88 pp.

MeteoSchweiz. 2015: Klimabulletin Sommer 2015. Zürich

17.2

Carbon budgets of six different agricultural crops at the Oensingen arable land Fluxnet site

Carmen Emmel, Werner Eugster, Lukas Hörtnagl

Institute of Agricultural Sciences, ETH Zürich, Universitätstr. 2, CH-8092 Zürich (carmen.emmel@usys.ethz.ch)

The arable land Swiss Fluxnet site at Oensingen, Solothurn (CH-Oe2) has been running since December 2003. This site provides unique data to study turbulent fluxes of carbon dioxide, water vapour and energy as well as crop yield, carbon budgets and microclimate in a typical Swiss crop production region on the Swiss Plateau. It is the only long-term Swiss Fluxnet arable land site and it belongs to the longest continuously running arable land flux sites worldwide.

The site is managed under the low pesticide integrated production (IP) farming protocol with a crop rotation focusing on winter wheat, which also includes winter barley, rapeseed, peas, potatoes and intermediate cover crops. Long-term measurements at the site include eddy covariance measurements of three-dimensional wind velocity, air temperature, carbon dioxide and water vapour concentrations as well as soil temperature, soil moisture, soil heat flux, relative humidity, incoming and outgoing short and longwave radiation and incoming photosynthetically active radiation. Additionally, management information, harvested crop and straw yields as well as carbon and nitrogen concentrations of yield and residue are available.

This study uses this rich dataset to address the following objectives:

- (1) To quantify the carbon budgets of the different crop types planted at CH-Oe2 in the past thirteen seasons,
- (2) To determine the interannual variability in the carbon budgets of winter wheat, winter barley and rapeseed,
- (3) To analyze the climatic conditions at the site during these thirteen seasons and compare them to the carbon budgets.

17.3

Management matters: Testing a mitigation strategy of nitrous oxide emissions on managed grassland

Kathrin Fuchs¹, Lukas Hoernagl¹, Werner Eugster¹, Patrick Koller¹, Florian Kaeslin¹, Lutz Merbold²

¹ *Department of Environmental Systems Science, Grassland Sciences Group, ETH Zurich, Universitätsstrasse 2, CH-8092 Zurich (kathrin.fuchs@usys.ethz.ch)*

² *Mazingira Centre, International Livestock Research Institute (ILRI), P.O. Box 30709, KE-00100 Nairobi*

The magnitude of greenhouse gas (GHG) exchange between managed grasslands and the atmosphere largely depends on management practices. While natural or extensively managed grasslands are known to function as GHG sinks intensively managed grasslands are often characterized by substantial nitrous oxide (N₂O) emissions and therefore act as net GHG emitters. One potential approach to mitigate N₂O emissions is a decrease in fertilizer inputs by replacing the needed N input by biological nitrogen fixation via legumes. However, the effect of legumes on nitrous oxide fluxes is still uncertain. In this study we aim at quantifying net GHG fluxes from two management strategies under field conditions in relation to the productivity of the fields (yield estimates). Furthermore, we aim at revealing direct drivers of N₂O exchange and developing suggestions for a more sustainable grassland management in the future.

We conducted an ecosystem-scale experiment to compare GHG fluxes from an intensively managed Swiss grassland site. The experimental approach consisted of a control parcel representing conventional management with up to 6 harvests and subsequent organic fertilizer application (N input 310 kg ha⁻¹ yr⁻¹) as well as an adjacent treatment parcel where common organic fertilizer N inputs are replaced by biological nitrogen fixation via legumes. We measured the net exchange of the three major GHGs, nitrous oxide (N₂O), methane (CH₄) and carbon dioxide (CO₂) with the eddy covariance technique in 2015. GHG flux measurements were accompanied by measurements of commonly known driver variables such as water filled pore space, soil temperature, soil oxygen concentrations and mineral N to disentangle the soil meteorological influence of N₂O fluxes from human drivers.

We measured enlarged N₂O fluxes following organic fertilizer application in the control site and unchanged N₂O emissions in the treatment site. We also observed peaks in N₂O emissions on the treatment parcel, which partly could be attributed to rain events. Net annual fluxes were about one third lower at the experimental parcel. Annual yields were 19% lower at the experimental parcel compared to the control parcel. Relatively dry conditions during the growing season affected plant growth and the timing of the management events.

Significantly lower nitrous oxide fluxes under experimental management compared to conventional management indicate that nitrous oxide emissions can be effectively reduced at very low costs with a clover-based management. Dry weather conditions are regarded as adequate to reflect future climate at the site. In order to get insights into effects under more common (i.e. wetter) weather conditions and into long-term effects, further measurements are required.

17.4

The influence of ground surfaces on urban climate

Jens Ingensand¹, Géraldine Bullinger², Sarah Composto¹, Reto Camponovo³, Bruno Spahni², Manuel Froidevaux², Marion Nappetz¹ & Damien Varesano³

¹ G2C, HEIG-VD. Rte de Cheseaux 1, CH-1401 Yverdon (jens.ingensand@heig-vd.ch)

² iTEC, HEIA-FR. Pérolles 80, CH-1705 Fribourg

³ LEEA, hepia. Rue de la Prairie 4, CH-1202 Genève

INTRODUCTION.

In the context of global climate change the term *urban heat island* (UHI) is a phenomenon that has been observed in recent years (Oke 1982). UHI have a negative influence on the water cycle and on human health. Within the same city important differences in temperature can be observed. These differences depend to a high degree on the type of ground surface (e.g. impermeable and permeable surfaces, waterbodies, parks, etc.) (Kustas 2000).

The goals of the project THER-SOL were to 1. Categorize significant types of urban ground surfaces, 2. Quantify the impact of the identified surface types on urban microclimate, 3. Identify strategies to decrease the appearance of UHI through the identification of potential surfaces where the type of surface can be changed.

STUDY SETTING.

The sectors *Mail-Jonction* and *Acacias* in the city of Geneva had been chosen. Within the limits of these sectors different types of impermeable and permeable surfaces can be found. Compared to other Swiss cities the city of Geneva is rather flat and less subjected to the influence of the relief, which may allow for an extrapolation of the results to other cities. Furthermore a rich collection of geographical data layers (e.g. surface types, solar radiation, etc.) is publicly available (SGOI 2016).

In the middle of the two sectors, within the uncovered *Plainpalais*-area, three very different surface types were identified. On these three sites experimental stations were set-up to measure different energy fluxes between the atmosphere and the surface (see Figure 1). Thermocouples and thermometers were placed at 8 cm depth to evaluate heat flux in the soil and at 3 m height to evaluate sensible heat flux and net radiation. Data was collected during ten consecutive days in summer 2015.



Figure 1: Experimental setup at Plainpalais: lawn (green dot on the map; 2nd picture), ghorr/Beaujolaïs-gravel (red dot; 3rd picture) and asphalt (blue dot; 4th picture).

RESULTS.

Significant differences were identified between the three surfaces. Sensible heat was slightly higher for the gravel-surface than for the lawn. The heat flux in the soil was more reactive on the gravel that warms up and cools down faster. Net radiation is significantly higher on the lawn, where more energy is transformed even if the gravel is darker than the lawn. This evidence suggests that permeable surfaces help decreasing heat in urban areas. Additional measures made with a backpack equipped with thermometers enabled us to quantify the thermal comfort experienced by citizens and to highlight that the areas covered by vegetation indeed are important in the context of UHI. Based on the available land-use layers we identified current permeable surfaces. We calculated that only 4% of the total surface are currently covered by vegetation (see Figure 2; 1st map). By transforming existing surfaces, such as roads, car parks, crossroads, pavements and tram tracks, an estimated 9-10% of the total surface of the study area could be made permeable.(see Figure 2; 2nd map).

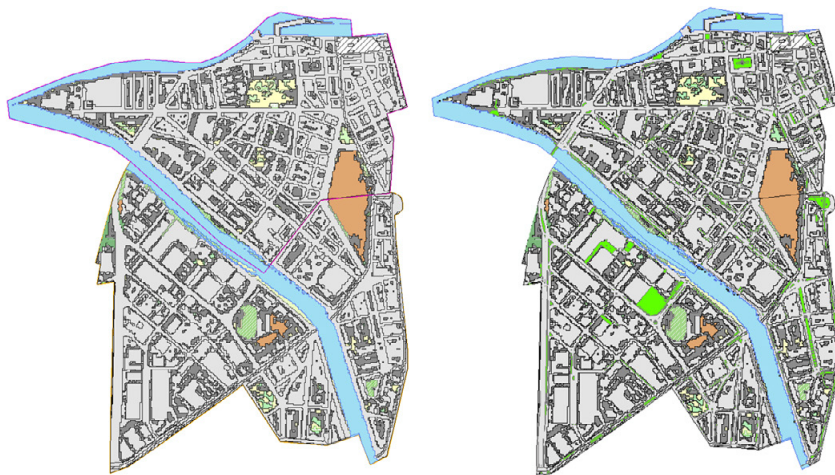


Figure 2: Current (1st map on the left) and suggested (2nd map on the right) land-use of the sectors Mail-Jonction and Acacias with vegetation (in green and yellow), waterbodies (in blue), pavements and buildings (in grey and brown).

CONCLUSIONS AND PERSPECTIVES.

This project demonstrated the significance of permeable surfaces regarding UHI. The Plainpalais area is an interesting area since very different surface types can be found here. According to our results, the ideal surface has a high soil retention capacity (storage). The cooling potential of a surface is mainly linked to its evaporation potential. It would be interesting to consider the influence of trees on UHI as well. Another possibility is to analyze the orientation and the shape of urban canyons in order to refine the results. Finally as this project focused on lawn, gravel and asphalt, it would be interesting to include other ground surface types as well.

REFERENCES

- Kustas, W. P., J. H. Prueger & al. 2000: Variability in soil heat flux from a mesquite dune site, *Agricultural and Forest Meteorology* 103(3), 249-264.
- Oke, T. R. 1982: The Energetic Basis of the Urban Heat-Island, *Quarterly Journal of the Royal Meteorological Society* 108(455), 1-24.
- SGOI (Service de géomatique et de l'organisation de l'information). 2016: Le territoire genevois à la carte (SITG), <http://ge.ch/sitg/>.

17.5

Process-based crop model simulations of carbon fluxes and stocks – an evaluation at the Oensingen cropland site

Andrew Reville¹, Carmen Emmel¹, Petra D'Odorico¹, Nina Buchmann¹, Werner Eugster¹

¹ *Institute of Agricultural Sciences, ETH Zurich, Universitätsstrasse 2, 8092 Zurich, Switzerland (Revilla@ethz.ch)*

In response to climate change mitigation strategies and food security, there is an ever-increasing requirement to understand the key drivers of the cropland carbon (C) balance. Croplands are also entirely managed ecosystems, which causes uncertainty when investigating the impacts of climate on crop growth.

Process-based crop models, driven by meteorological observations, can provide a realistic simulation and diagnosis of the variability in land-atmosphere C fluxes and yield. However, the amount of field-scale observations that are required to thoroughly assess, and subsequently improve, the accuracy of crop models are typically spatially and temporally sparse.

This research evaluates the performance of the Soil-Plant-Atmosphere Crop (SPA-Crop, Sus *et al.*, 2010) model for the simulation of daily C fluxes and stocks of multiple crop types and seasons. SPA-Crop is a detailed model, simulating ecosystem photosynthesis and water balance at fine temporal (half-hourly time-steps) and spatial scales (multiple canopy and soil layers). We first initialise the model using management information and continuous meteorological observations that are available during 10 crop growing seasons (including wheat, barley, rapeseed and pea) at a cropland site located in Oensingen, Switzerland. Second, we evaluate the daily and at-harvest cumulative model estimates of photosynthesis and net ecosystem exchanges (NEE) of C using data derived from field-scale eddy covariance measurements. Further comparisons are made between the modelled and observed yields.

Across all crop seasons we demonstrate a high agreement between the observed and modelled photosynthesis (mean $R^2 > 0.70$ and $RMSE < 2.0 \text{ gC m}^{-2} \text{ day}^{-1}$). A similarly high accuracy is shown for the NEE (mean $R^2 > 0.65$ and $RMSE < 1.5 \text{ gC m}^{-2} \text{ day}^{-1}$). Overall SPA-Crop underestimated the crop yield by around 10%.

REFERENCES

Sus, O., Williams, M., Bernhofer, C., Beziat, P., Buchmann, N., Ceschia, E., Doherty, R., Eugster, W., Grunwald, T., Kutsch, W., et al., 2010: A linked carbon cycle and crop developmental model: Description and evaluation against measurements of carbon fluxes and carbon stocks at several European agricultural sites. *Agriculture, ecosystems and environment*. 139, 402-418.

17.6

Volcanism, climate and human: On an illuminative journey with an ice-core time machine.

Michael Sigl^{1,2}, Ulf Büntgen^{2,3}, Francis Ludlow⁴, Matthew Toohey⁵, Clive Oppenheimer⁶ & Joseph Manning⁷

¹ *Laboratory of Environmental Chemistry, Paul Scherrer Institut, PSI Ost, CH-5232 Villigen (michael.sigl@psi.ch)*

² *Oeschger Centre for Climate Change Research, University of Bern, CH-3012 Bern*

³ *Swiss Federal Research Institute WSL, Zürcherstrasse 111, CH-8903 Birmensdorf*

⁴ *GEOMAR Helmholtz Centre for Ocean Research, Düsternbrooker Weg 20, D-24105 Kiel*

⁵ *School of Histories & Humanities, Trinity College, College Green, Dublin, Ireland*

⁶ *Department of Geography, University of Cambridge, Downing Pl, Cambridge, UK*

⁷ *Department of History, Yale University, 320 York Street, New Haven, USA*

By using state-of-the-art absolute and relative dating techniques and integrating information from ice cores, tree-rings and documentary records we developed a new timeline of volcanic eruptions and their aerosol forcing on climate for the past 2,500 years (Sigl et al., 2014, 2015, 2016). Ice-core composite records of sulphur from Greenland and Antarctica form the backbone of the reconstruction.

Here, we report the timing and consequences of two of the greatest volcanic episodes of the past two millennia: the so-called ‘Millennium Eruption’ of Changbaishan and the lava flood eruption of Eldgjá (Iceland). The Millennium Eruption (946 AD) was a large explosive episode, comparable to that of Tambora (Indonesia) in 1815, which is associated with the following “Year without a summer”. The Eldgjá event (939 AD), on the other hand, was a flood lava eruption, comparable to but somewhat larger than that of Laki in 1783/84.

In 536 AD, observers in Europe documented a mysterious cloud which dimmed the light of the sun for at least a year. Using a coupled aerosol-climate model, with eruption parameters constrained by our re-dated ice-core records and historical observations of the aerosol cloud, we reconstructed the radiative forcing resulting from a sequence of two major volcanic eruptions in 536 and 540 AD (Toohey et al., 2016). We estimate that the decadal-scale Northern Hemisphere (NH) radiative forcing from this volcanic “double event” was larger than that of any period in the past 2,000 years. Earth system model simulations including the volcanic forcing show peak NH mean temperature anomalies reaching more than -2 °C. Tree-ring records from Eurasia demonstrate the sudden and prolonged cooling, which took place in the beginning of the 6th century and which continued to characterize the period until around 660 AD. We thus identify the interval from 536 to about 660 AD as the Late Antique Little Ice Age (Büntgen et al., 2016). Spanning most of the NH, we suggest that this cold phase be considered as an additional factor contributing to the establishment of the Justinian plague, and transformation of the eastern Roman Empire.

We further integrate written and natural archives to show that volcanic eruptions repeatedly suppressed the agriculturally-critical Nile flood. Previous work linking eruptions to Nile flow noted coincidences in timing between Nile “failure” and a handful of historic eruptions. Using our new ice-core volcanic reconstruction with Nilometer data (the world’s longest documentary hydrological record) and qualitative flood descriptions during the Ptolemaic Era (261 to 30 BCE), we show a persistent suppression of the Nile across more than a millennium.

These examples demonstrate the sensitivity of the climate system and vulnerability of human societies to large volcanic eruptions – both major themes of a new PAGES Working Group “Volcanic Impact on Climate and Society, VICS”. Aerosol properties derived from this new ice-core based volcanic reconstruction will be employed as the default volcanic forcing series for performing transient climate model simulations of the past 1,000 and 2,000 years within the Paleoclimate Modelling Intercomparison Project (PMIP4). This will help to further improve our understanding of the volcanic influences on global and regional climate, at various temporal scales.

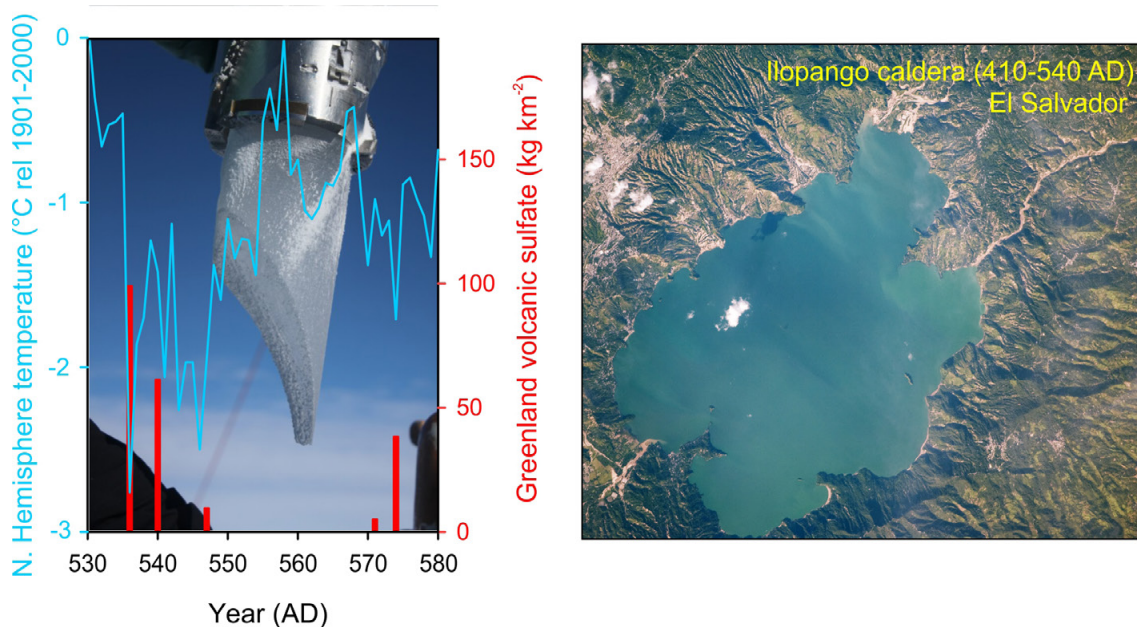


Figure 1. (Left) Greenland volcanic sulphate deposition and Northern Hemisphere June-August temperatures from 530-580 AD marking the onset of the Late Antique Little Ice Age; (right) satellite image of the caldera from the Ilopango eruption, one of the candidate events for the large 540 AD ice-core sulphate signal.

REFERENCES

- Sigl, M. et al. 2014: Insights from Antarctica on volcanic forcing during the Common Era. *Nature Climate Change* 4, 693-697.
- Sigl, M. et al. 2015: Timing and climate forcing of volcanic eruptions for the past 2,500 years. *Nature* 523, 543-549.
- Sigl, M. et al. 2016: The WAIS Divide deep ice core WD2014 chronology - Part 2: Annual-layer counting (0-31 ka BP). *Climate of the Past* 12, 769-786.
- Toohey, M., Krüger, K., Sigl, M., Stordal, F. & Svensen, H. 2016: Climatic and societal impacts of a volcanic double event at the dawn of the Middle Ages. *Climatic Change* 136, 401-412.
- Büntgen, U. et al. 2016: Cooling and societal change during the Late Antique Little Ice Age from 536 to around 660 AD. *Nature Geoscience* 9, 231-236.

17.7

Soil carbon dynamics and fluxes across a climatic gradient from temporally-resolved radiocarbon measurements

Tessa Sophia van der Voort¹, Frank Hagedorn², Utsav Mannu², Cameron McIntyre^{1,3}, Lorenz Walthert², Patrick Schleppi² and Timothy Ian Eglinton¹

¹ *Institute of Geology, ETH Zürich, Sonneggstrasse 5, 8092 Zürich, Switzerland*

² *Forest soils and Biogeochemistry, Swiss Federal Research Institute WSL, Zürcherstrasse 111, 8903 Birmensdorf, Switzerland*

³ *Department of Physics, Laboratory of Ion Beam Physics, ETH Zurich, Schaffmatstrasse 20, 9083 Zurich*

Soil organic matter (SOM) constitutes the largest terrestrial reservoir of organic carbon, and therefore quantifying soil organic matter dynamics (carbon turnover, stocks and fluxes to the atmosphere) across spatial and climatic gradients is essential for an understanding of the carbon cycle and the impacts of global change. Links between soil carbon dynamics and different climatic and compositional factors are particularly poorly understood. Radiocarbon constitutes a powerful tool for unraveling soil carbon dynamics and is increasingly used in studies of carbon turnover. Temporally-resolved radiocarbon measurements, which take advantage of “bomb-radiocarbon”-driven changes in atmospheric ¹⁴C over the last decades, enable further constraints to be placed on C turnover times. These in turn can yield more precise flux estimates for both upper and deeper soil horizons. This project combines bulk radiocarbon measurements on a suite of soil profiles spanning strong climatic (MAT 1.3-9.2 °C, MAP ~600 to 2100 mm m⁻²y⁻¹) and geologic gradients with a more in-depth approach for a subset of locations. For this subset, temporal and carbon-fraction specific radiocarbon data has been acquired for both topsoil and deeper soils. These well-studied sites are part of the Long-Term Forest Ecosystem Research (LWF) program of the Swiss Federal Institute for Forest, Snow and Landscape research (WSL). Resulting temporally-resolved turnover estimates are coupled to carbon stocks, fluxes across this wide range of forest ecosystems and are examined in the context of environmental drivers (temperature, precipitation, primary production and soil moisture) as well as texture (sand, silt and clay content). Statistical analysis on the region-scale – correlating radiocarbon signature with climatic variables such as temperature, precipitation, primary production and elevation – indicates that composition rather than climate is a key driver of $\Delta^{14}\text{C}$ signatures. Preliminary estimates of carbon turnover, stocks and fluxes derived from temporally-resolved measurements highlight the strong gradients and variability there is in carbon efflux in top- and deep soil in a range of ecosystems. Overall, this study has afforded a uniquely comprehensive dataset that improves our understanding of controls on soil carbon dynamics and carbon fluxes to the atmosphere across spatial and temporal scales, as well as the pool-specific and long-term trends in soil carbon (de)stabilization and vulnerability.

P 17.1

Is grain size distribution an important factor of Oxalate-Carbonate Pathway efficiency?

Finaritra Randevoson¹, Guillaume Cailleau¹, Gabrielle Rajoelison², Herintsitohaina Razakamanarivo³, Tantely Razafimbelo³ & Eric Verrecchia¹

¹ *Institute of Earth Dynamics, University of Lausanne, Switzerland (manohiainafinaritra.randevoson@unil.ch)*

² *Water and Forest Department, ESSA, University of Antananarivo, Madagascar*

³ *Radiolotopes Laboratory, University of Antananarivo, Madagascar*

Carbonate accumulations through the oxalate-carbonate pathway (OCP) are recently studied in Madagascar around *Tamarindus indica* (Fabaceae). Basically, OCP refers to the transformation of oxalate, a product of photosynthesis, to carbonate into the soil when oxalogenic trees, oxalotrophic bacteria, and fungi combine efficient activities. This process increases local pH and can lead to long-term carbon sequestration when occurring in Ca-carbonate free soils.

Many factors regarding to site conditions could influence the importance of OCP effects on soil such as the tree specie. Grain size distribution with its link to soil permeability may be one of these factors.

Do grain size distribution affect the OCP's efficiency? This study therefore aims at investigate the effect of grain size distribution on soil alkalization and carbonate accumulations under the influence of an OCP ecosystem.

Consequently, six tamarinds, with a diameter at breast height (i.e. DBH) of at least 65cm and 16 m high, were selected. Three soils profiles were dug around each tree. One soil profile 15 m away was established as a reference profile. Soil samples were taken from six depths in the different soil profiles. Variables such as pH_{H₂O}, grain size distributions, and carbonate detection were performed.

Reference soils data results were used to build a cluster tree using hierarchical cluster analysis highlighting two groups of soils. The first group, represented by three trees is defined as sandy soils with pH ranging from 7 to 7.5. The second group, also constituted by three trees is defined as loamy-sandy, the pH ranging from 6.5 to 7. Considering this discrimination of sites, grain size distribution under trees is assumed to be similar compared to their associated distant soils. The loamy-sandy soils present a pH shift (from assumed original conditions measured at distant sites and soils around the trees) of 1.17 ± 0.31 (n=54) higher than for sandy soils, 0.64 ± 0.58 (n=51) whereas the carbonate detected by X-Ray is less important for loamy-sandy soils ($2.9 \pm 2.46\%$, n=46) than sandy soils ($1.41 \pm 1.14\%$, n=40). In addition, field observations showed the presence of local carbonate accumulation in deeper horizon of four profiles of sandy soils.

These results suggest that the particles size fractions have somehow their importance in the downward transfer of materials and could favour carbonate accumulation in sandy soils. The higher buffering capacity of the loamy-sandy soils than sandy soils was presumed to counteract the alkalization process and could explain the pH shift difference.

Nevertheless, the more acidic pH of distant loamy-sandy soils may explain this pH shift difference. As the stability pH for calcite in the present environmental conditions is 8.4, the soil pH increase to allow carbonate to precipitate is much more important in acidic soil than basic soil.

REFERENCES

- Braissant, O., Cailleau, G., Aragno, M., & Verrecchia, E. 2004: Biogeologically induced mineralization in the tree *Milicia excelsa* (Moraceae): its causes and consequences to the environment, *Geobiology*, 2, 59-66.
- Cailleau, G., Motta, M., Bindschedler, S., Junier, P., & Verrecchia, E. 2014: Detection of active-carbonate pathway ecosystem in the Amazon Basin: Global implications of a natural potential C sink, *Catena*, 116, 132-141.
- Raharimalala, O., Buttler, A., Ramohavelo, C., Razanaka, S., Sorg, J-P., & Gobat, J-M. 2010 : Soil-vegetation patterns in secondary slash and burn successions in Central Menabe, Madagascar, *Agriculture, Ecosystems & Environment*, Volume 139, Issues 1-2, 150-158.
- Verrecchia E., Braissant O., & Cailleau G. 2006: The oxalate-carbonate pathway in soil carbon storage: the role of fungi and oxalotrophic bacteria, *Fungi in Biogeochemical Cycles*, ed. G. M. Gadd, Published by Cambridge University Press.

P 17.2

Stability of soil organic matter in Alpine ecosystems: no relationship with vegetation

Magali Matteodo¹, David Sebag^{1,2}, Pascal Vittoz¹, Eric Pascal Verrecchia¹

¹ *Institute of Earth Surface Dynamics (IDYST), University of Lausanne, Géopolis Building, 1015 Lausanne, Switzerland*

² *Normandie Univ, UNIROUEN, UNICAEN, CNRS, M2C, 76000 Rouen, France*

There is an emerging understanding of mechanisms governing soil organic matter (SOM) stability, which is challenging the historical view of carbon persistence¹. According to this alternative vision, SOM stability is not directly regulated by the molecular structure of plant inputs (i.e. the historical view), but the biotic and abiotic conditions of the surrounding environment which play a major role and mediate the influence of compound chemistry. The persistence of SOM is thus influenced by ecological conditions, controlling the access and activity of decomposers' enzymes and being ecosystem-dependent.

In this study, we investigated differences of (1) carbon content, and (2) stability of organic matter in litter and organomineral layers from the most widespread plant communities at the subalpine-alpine level of the Swiss Alps. For this purpose, 230 samples from 47 soil profiles have been analysed across seven plant communities, along a subalpine–alpine elevation gradient. Both calcareous and siliceous grasslands were studied, as well as snowbed and ridge communities. Aboveground litter and A horizons were sampled and analysed using Rock-Eval Pyrolysis, a proxy-technique commonly used for the investigation of organic matter composition and stability^{2,3}.

Results show that the litter layers of the seven plant communities are significantly different in terms of total organic carbon (TOC) content, but slightly variable in terms of stability. The situation is radically different in the organomineral horizons where the amount of organic carbon is interestingly homogeneous, as well as the SOM stability. In mineral horizons, the amount and stability of SOM are mainly driven by the geological settings, and therefore vary in the different plant communities.

These results show a clear disconnection between organic, organomineral, and mineral horizons in terms of factors governing soil organic matter stability. Consistent with the recent view of the carbon balance, plant input seems to influence the litter C dynamics (qualitatively and quantitatively) but not the SOM stability in A and mineral horizons.

REFERENCES

¹Schmidt, MWI., et al. 2011 : Persistence of soil organic matter as an ecosystem property. *Nature* 478, 49-56.

²Disnar, JR., et al. 2003: Soil organic matter (SOM) characterization by Rock-Eval pyrolysis. *Org. Geochem.* 34, 327-343.

³Sebag, D., et al. 2006: Monitoring organic matter dynamics in soil profiles by 'Rock-Eval pyrolysis' : bulk characterization and quantification of degradation. *Eur. J. of Soil Sci.* 57, 344-355.

18. Phenology and seasonality

+

19. Earth Observation addressing key Earth System processes

Convenors 18: Martine Rebetez, Christian Rixen, This Rutishauser

Convenors 19: Stefan Wunderle, Mathias Kneubühler, Brigitte Buchmann, Alain Geiger

*Swiss Commission for Phenology and Seasonality,
Swiss Commission for Remote Sensing,
Swiss Geodetic Commission*

TALKS:

- 18.1 Jing Xie, Kneubühler M., Garonna I., De Jong R., Schaepman M.E.: Altitude-dependent correlation of snow cover duration with alpine spring phenology
- 18.2 Asse D., Randin C., Chuine I., Delestrade A.: Understanding the effect of warming temperatures on spring phenology of trees in the Alps using data from a citizen science program
- 18.3 Meier M., Holzkaemper A., Fuhrer J.: Changes in the risk of spring frost damage to grapevine due to climate change in Switzerland
- 18.4 Ladd S.N., Dubois N., Schubert C.: Seasonal changes in hydrogen isotope fractionation between algal lipid biomarkers and lake surface water correspond to lipid production rates
- 19.1 Manconi A., Dini B., Loew S.: Ground deformation in the Greater Zurich Area from differential SAR interferometry
- 19.2 Milani G., Tonolla D., Robinson C., Kneubühler M., Doering M., Schaepman M.: Comparison of riverine habitat dynamic cycles conditioned by hydrological regimes under different anthropogenic pressure
- 19.3 Sternai P., Caricchi L., Castelltort S.: Erosion changes throughout glacial cycles contribute to the magma production by continental unloading and associated volcanic activity
- 19.4 Vogt M.-L., Käser D., Hunkeler D., Zwahlen F., Brunner P.: Monitoring run-off, accumulation and infiltration in the arid Ennedi mountains (Northern Chad), using remote sensing

POSTERS:

- P 18.1 Ambrosi C., Strozzi T., Scapozza C., Wegmüller U.: Landslide Hazard Assessment in the Himalayas (Nepal and Bhutan) based on Earth-Observation Data
- P 18.2 Manconi A., Wolter A., Amann F.: Measuring surface displacements from airborne imagery with Digital Image Correlation: insights from the Cuolm Da Vi deep-seated rockslide
- P 18.3 Butz C., Grosjean M., Rey F.: Tracking of seasonal to millennial variability of biogeochemical proxies in varved lake sediments using hyperspectral imaging

18.1

Altitude-dependent correlation of snow cover duration with alpine spring phenology

Jing Xie, Mathias Kneubühler, Irene Garonna, Rogier De Jong, and Michael E. Schaepman

*Remote Sensing Laboratories, Department of Geography, University of Zurich,
Winterthurerstrasse 190, CH-8057 Zurich (jing.xie@geo.uzh.ch)*

Snow cover duration plays a vital role in alpine ecosystems and has a large impact on the alpine spring phenology. However, our knowledge about the correlation of snow cover duration with alpine spring phenology is still limited, as is the dependence of this correlation on altitude.

In this study, we used satellite derived parameters such as Snow Cover Duration (SCD), and Start Of Season (SOS, namely, alpine spring phenology) of natural vegetation for the period of 2003–2014 and over the European Alps. We tested for the existence of altitude-dependent changes in the correlation between inter-annual differences (Δ) of SCD and SOS of various natural vegetation types in different climatic sub-regions from 0 to 3000 m above sea level (m a.s.l.).

The results show that both SCD and SOS significantly ($p < 0.001$) change with altitude. Less than 3% of all pixels show a significant trend ($p < 0.05$) in SCD or SOS over the study period across the entire study area. A considerable amount of pixels show significant correlation between Δ SCD and Δ SOS (25.3% of total pixels) across the entire study area. The positive correlation between Δ SCD and Δ SOS reaches high correlation values ($R > 0.7$) at high altitudes (> 2000 m a.s.l.), where predominant vegetation covers are natural grassland (NG) and sparsely vegetated areas (SV). In mid altitudes (1000–2000 m a.s.l.), where the main vegetation covers are NG and forest (i.e., broad-leaved forest (BF), coniferous forest (CF), and mixed forest (MF)), Δ SCD is positively correlated with Δ SOS above 600 m a.s.l in the northern Alps (temperate oceanic climate features), and above 1500 m a.s.l in the southern Alps (mediterranean subtropical climate features). Weak negative correlations ($-0.4 < R < 0$) between Δ SCD and Δ SOS are mainly present over forests (i.e., BF, CF and MF) at low altitudes (< 1000 m a.s.l). It is remarkable that a higher percentage of significant pixels is found in high and mid altitudes than in low altitudes.

Our findings support the hypothesis that snow cover duration is correlated with alpine spring phenology, and that this correlation varies between natural vegetation types, climatic sub-regions and altitude. Furthermore, we suggest that i) SCD shows stronger correlation with alpine spring phenology in high and mid altitudes than in low altitudes, possibly due to coupling effects of SCD associated with air temperature and underground thermal conditions, and ii) the correlation differences among sub-regions are more pronounced at mid and low altitudes and tend to disappear toward high altitudes.

18.2

Understanding the effect of warming temperatures on spring phenology of trees in the Alps using data from a citizen science program

Daphné Asse¹, Christophe Randin¹, Isabelle Chuine², Anne Delestrade³

¹ *Université de Lausanne, Department of Ecology and Evolution, Lausanne*

² *CNRS, UMR 5175 Centre d'Ecologie Fonctionnelle et Evolutive (CEFE), DREAM, Montpellier, France*

³ *Centre de Recherches sur les Ecosystèmes d'Altitude (CREA), Chamonix Mont-Blanc, France*

Mountain regions are particularly exposed to climate change and temperature. In the Alps increased twice faster than in the northern hemisphere during the 20th century (Moisselin *et al.*, 2002; Beniston, 2004; Rebetez & Reinhard, 2008). As an immediate response, spring phenological phases of plant species such as budburst and flowering, have tended to occur earlier (Defila & Clot, 2005).

In 2004, the CREA (Centre de Recherches sur les Ecosystèmes d'Altitude, Chamonix, France) initiated the citizen science program Phenoclim, which aims at assessing the long-term effects of climate changes on plant phenology over the entire French Alps. Sixty sites with phenological observations were equipped with temperature stations across a large elevational gradient.

Here we used phenological records for five tree species (birch, ash, hazel, spruce and larch) combined with measurements or projections of temperature. We first tested the effects of geographic and topo-climatic factors on the timing of spring phenological phases. We then tested the hypothesis that a lack of chilling temperature during winter delayed dormancy release and subsequently spring phenological phases. Our data are currently being used to calibrate process-based phenological models to test to which extent soil temperature (Schenker *et al.*, 2014) and photoperiod affect the timing of spring phenological phases.

We found that growing degree-days was the best predictor of the timing of spring phenological phases, with a significant contribution of chilling. Our results also suggest that spring phenological phases were consistently delayed at low elevation by a lack of chilling in fall during warm years for the three deciduous species.

REFERENCES

- Beniston, M. 2004: Climatic Change and Impacts: An Overview Focusing on Switzerland. Kluwer Academic Publishers, 296.
- Defila, C. & Clot, B. 2005: Phytophenological trends in the Swiss Alps, 1951-2002. *Meteorologische Zeitschrift*, 14, 2, 191-196.
- Moisselin, J.-M., Schneider, M., Canellas, C. & Mestre, O. 2002: Les changements climatiques en France au XXe siècle. Etude des longues séries homogénéisées de données de température et de précipitations. *Météorologie*, 38, 45-56.
- Rebetez, M. & Reinhard, M. 2008: Monthly air temperature trends in Switzerland 1901-2000 and 1975-2004. *Theoretical and Applied Climatology*, 91, 27-34.
- Schenker, G., Lenz, A., Körner, C. & Hoch, G. 2014: Physiological minimum temperatures for root growth in seven common European broad-leaved tree species. *Tree Physiology*, 34, 302-313.

18.3

Changes in the risk of spring frost damage to grapevine due to climate change in Switzerland

Michael Meier^{1/2}, Annelie Holzkaemper^{1/2} & Jürg Fuhrer^{1/2}

¹ University of Bern, Oeschger Centre for Climate Change Research, Falkenplatz 16, 3012 Bern, Switzerland
(Corresponding author : michael.meier@students.unibe.ch)

² Agroscope, Climate & Air Pollution Group, Reckenholzstrasse 191, 8046 Zürich, Switzerland

Risk for spring frost damages to grapevine is in general changing with a changing climate. While increasing temperatures generally decrease the risk of frost occurrence, they also lead to an acceleration of phenological development. This leads to a shift in the stage of budburst - during which the plant is particularly sensitive to frost damage - into a period of the year when the probability of frost occurrence is still high. Increasing temperature variability can add to this increase in the risk for spring frost damage. Therefore, although controversially at first thought, there could be a danger of increasing freezing injuries in spring.

Focusing on grapevines in the canton Valais, changes in frost risk due to climate change are modelled for two stations (i.e. Aigle/AIG and Sion/SIO). Climate projections are based upon GCM-RCM model chains from the EU-FP6 project ENSEMBLES (<http://www.ensembles-eu.org/>) and on the IPCC A1B emission scenario. Regarding budburst, two main model types are used to describe grapevine phenology: Forcing models and chilling-and-forcing models. In the former type, only forcing units with respect to temperature are summed up, starting at the same day every year. The latter type on the other hand allows for an ever changing starting point regarding forcing units accumulation, depending on when a certain threshold for the accumulation of chilling units is reached. Finally, the four indicators of frost risk are applied in combination with the 12 phenology models and 16 GCM-RCM model chains to estimate changes in frost risk for each station. Thus, covering a time span from the year 1951 to 2050 and solely focusing on the grapevine variety Chasselas, 1536 model runs are executed. The trend regarding the change of frost risk is, amongst others, calculated by conducting a linear regression. The significance of the trends is evaluated with a Mann-Kendall test.

Results show that out of the 1536 runs, 63 runs predict a significantly increasing frost risk, while 100 runs predict a significant decrease in the risk for frost damages, both at a significance level of 5%. Thus, most model runs (i.e. 1373 runs) result in insignificant trends. An analysis of variance (ANOVA) over all 1536 runs identifies the greatest sources of uncertainty of frost risk change prediction: While GCM-RCM model chains explain 47.9% of total variance, phenology models account 13.2% of total variance. If calculated for AIG and SIO individually, GCM-RCM model chains accounts for 58.4% and 63.0% of total variance, respectively. Phenology models on the other hand explain 16.6% and 13.2% of total variance for AIG and SIO, respectively. The amount of total variance explained by the frost indices is, for the ANOVA for each station as well as for the combined ANOVA, 1.5% or smaller. These results allow for further analysis of the different factors, driving the trend for frost risk.

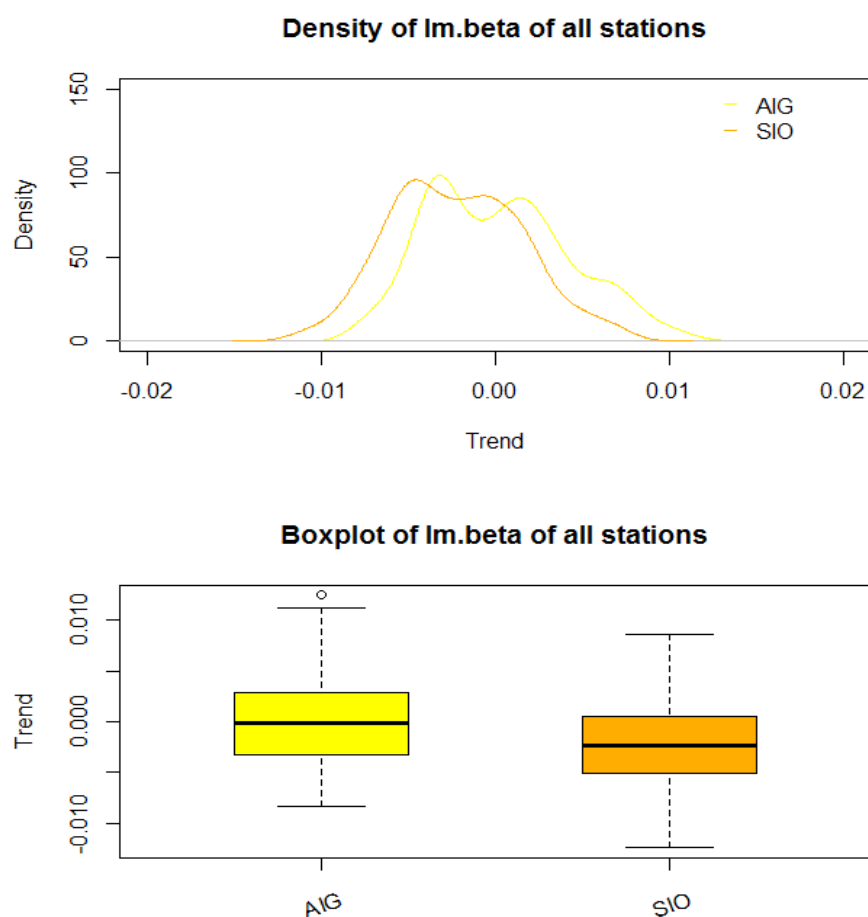


Figure 1. Density distribution and corresponding boxplots of trend according linear regression, for Aigle (AIG) and Sion (SIO).

REFERENCES

- Ball, M. C., Harris-Pascal, D., Egerton, J. J. G., & Lenné, T. (2012). Change in Cold Climate Vegetation. *Temperature adaptation in a changing climate: nature at risk*, 3, 179.
- Basler, D. (2016). Evaluating phenological models for the prediction of leaf-out dates in six temperate tree species across central Europe. *Agricultural and Forest Meteorology*, 217, 10-21.
- Chuine, I. (2000). A unified model for budburst of trees. *Journal of theoretical biology*, 207(3), 337-347.
- Fila, G., Gardiman, M., Belvini, P., Meggio, F., & Pitacco, A. (2014). A comparison of different modelling solutions for studying grapevine phenology under pre-sent and future climate scenarios. *Agricultural and Forest Meteorology*, 195, 192-205.
- Rigby, J. R., & Porporato, A. (2008). Spring frost risk in a changing climate. *Geophysical Research Letters*, 35(12).

18.4

Seasonal changes in hydrogen isotope fractionation between algal lipid biomarkers and lake surface water correspond to lipid production rates

S. Nemiah Ladd¹, Nathalie Dubois¹, Carsten Schubert¹

¹ EAWAG, Department of Surface Waters Research and Management, Seestrasse 79, CH-6047, Kastanienbaum

The hydrogen isotope composition ($^2\text{H}/^1\text{H}$) of biomarkers produced by algae is strongly influenced by the $^2\text{H}/^1\text{H}$ ratio of the water in which the organism grew. $^2\text{H}/^1\text{H}$ ratios of algal biomarkers preserved in lake sediments are thus a useful tool for reconstructing past changes in lake water isotope values, which can be used to infer hydroclimate changes. However, a number of variables can influence the magnitude of hydrogen isotope fractionation between algal lipids and their source water in laboratory cultures, particularly factors relating to growth rates. Quantifying the natural extent of these changes in field settings and identifying their causes is essential for robust application of $^2\text{H}/^1\text{H}$ ratios of algal lipids as paleohydroclimate proxies, yet these remain poorly constrained.

This work targets the effect of nutrient availability and variable growth rates on $^2\text{H}/^1\text{H}$ fractionation in algal biomarkers through a comparative study between two central Swiss lakes: eutrophic Greifensee and oligotrophic Vierwaldstättersee. Suspended particles from surface water were collected at six time points throughout the spring and summer of 2015, and hydrogen isotope values of short chain saturated and unsaturated fatty acids were measured. We paired these measurements with in situ incubations conducted with $\text{NaH}^{13}\text{CO}_3$, which were used to calculate the production rate of short chain fatty acids in lake surface water. We demonstrate that as algal productivity increased from April to June, the magnitude of $^2\text{H}/^1\text{H}$ fractionation in Greifensee increased by as much as 140 ‰ for individual fatty acids. Fractionation also increased with increasing productivity for fatty acids in Vierwaldstättersee, but the magnitude of the effect was smaller than in Greifensee. We attribute these changes to relatively greater contributions of highly depleted H from NADPH in photosystem I as temperature and light availability increased. Larger changes in $^2\text{H}/^1\text{H}$ fractionation in Greifensee than in Vierwaldstättersee may indicate a greater capacity for more productive systems to rapidly increase photosynthesis in response to warmer temperatures and more sunlight.

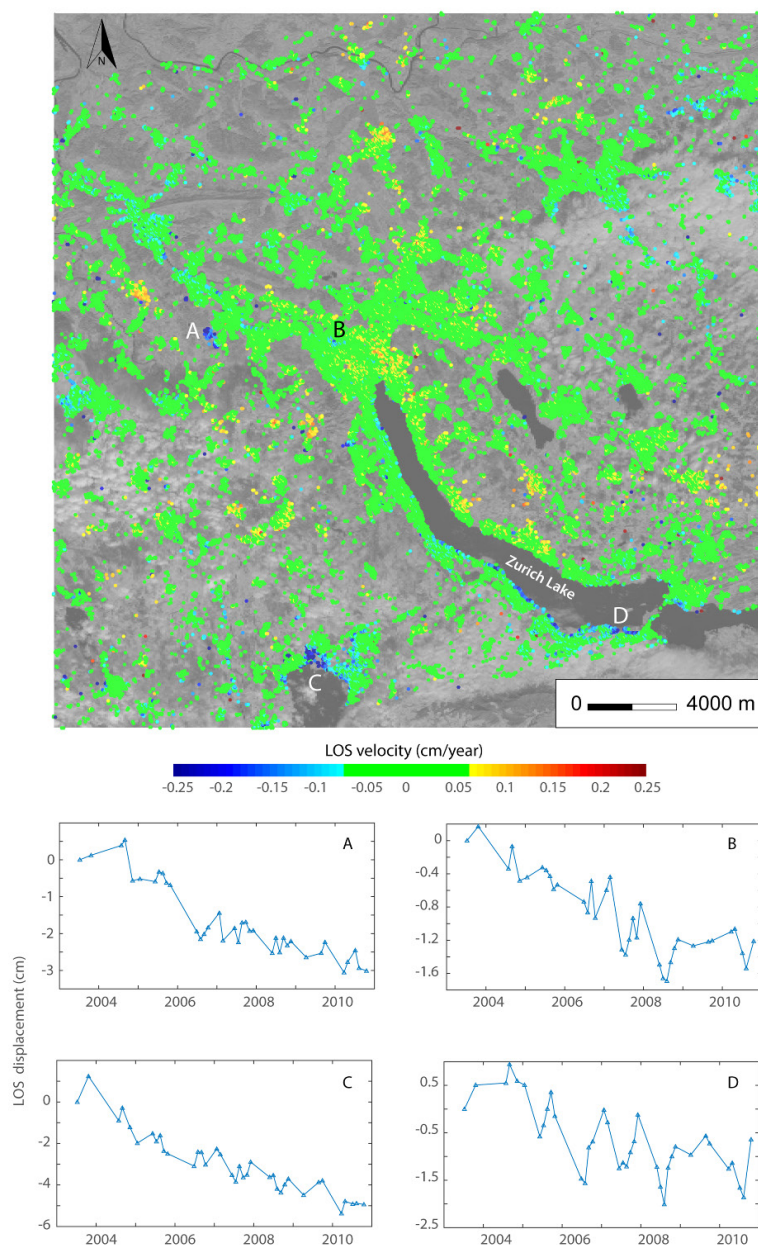
19.1

Ground deformation in the Greater Zurich Area from differential SAR interferometry

Andrea Manconi¹, Benedetta Dini & Simon Loew

¹ Swiss Federal Institute of Technology, Department of Earth Sciences, Zurich, Switzerland (andrea.manconi@erdw.ethz.ch)

Space borne Differential Synthetic Aperture Radar Interferometry (DInSAR) is a consolidated remote sensing method used for the analysis of surface deformation at regional scales. Nowadays, archived multi-temporal satellite acquisitions allows generating time series of ground deformation spanning periods as long as 20 years. Moreover, the advent of new satellite missions, such as the ESA Sentinel-1, will increase our capability to identify and monitor surface displacements over space and time. Advanced DInSAR methods have been developed in the last decade to derive ground velocity maps and displacement time series. Among several, the Small Baseline Subset (SBAS) technique combines sets of interferograms with small orbital separation (baseline) and short revisiting time to reduce the temporal decorrelation and maximize the number of coherent SAR targets. SBAS has proven to be suitable in different scenarios, with accuracies of 1 mm/year for mean surface velocities and 5 mm for displacement measurements.



In this work, we present surface velocity maps and displacement time series obtained in the Greater Zurich Area (GZA) by processing the ASAR Envisat data acquired from two different satellite orbits (ascending and descending) in the 2002-2010 time period. The SAR data was processed by leveraging a new service released within the ESA GRID-based operational environment, i.e. the unsupervised parallel implementation of the SBAS algorithm. The main advantage of this approach is that users with different backgrounds, more interested in the analysis of the surface deformation than in the details of the SAR data processing, can apply a reliable and validated state of the art algorithm without downloading large amounts of input data, nor owning costly processing hardware, or learning specific software. Despite a general overall stability, our results show interesting deformation patterns in the GZA. Here we illustrate the technique and show examples relevant to a known landslide in the Limmat valley, subsidence located in the vicinity of the Zurich and Zug lakes, as well as deformation patterns likely related to anthropic activities.

Figure 1. Surface velocity map (top) and displacement time series (A-D) computed over the Greater Zurich Area by exploiting the Parallel SBAS technique in the ESA-GRID environment. 37 Envisat ASAR images (track 487, ascending orbit) acquired between 2003 and 2010 were processed exploiting the Parallel SBAS approach. Selected time series show (A) displacement due to slope movement in Bergdietikon, (B) subsidence in the Hardbruecke-Gleisfeld area, Zurich city, (C) and (D) subsidence on the coastal area of the Zug and (D) Zurich lakes, respectively.

19.2

Comparison of riverine habitat dynamic cycles conditioned by hydrological regimes under different anthropogenic pressure

Gillian Milani¹, Diego Tonolla², Christopher Robinson³, Mathias Kneubühler¹, Michael Doering², Michael Schaeppman¹

¹ Department of Geography, Remote Sensing Laboratories, University of Zurich, Winterthurerstrasse 190, Zurich, Switzerland (gillian.milani@geo.uzh.ch)

² Institute of Integrative Ecology, Zurich University of Applied Sciences ZHAW, Wädenswil, Switzerland

³ EAWAG, Swiss Federal Institute of Aquatic Science and Technology, Dübendorf, Switzerland

Riverine environments are among the most valuable natural environments providing unique ecosystem services and high biodiversity despite their very small terrestrial coverage (Ward et al., 2002). Riverine environments of alpine and sub-alpine rivers in Switzerland and elsewhere are highly impacted by the control of hydrological regime due to the hydropower industry (Person, 2013). Since riverine environments are valuable directly and indirectly for cultural, economical and ecological purposes, it is required to decrease the current impact of the hydropower industry and find an optimum between the ecosystem services provided by the natural environment and economic and industrial services provided by the hydropower plants. It is therefore necessary to quantify the different processes happening in natural and anthropogenically impacted riverine environments (Winemiller et al., 2010).

In this context, we quantify the dynamic of land cover composition around the river channel of the Sense river, being close to a natural state, and along two reaches of the Sarine river, one under residual water conditions and the other one under hydro-peaking conditions. The classification approach used has been presented at the SGM 2015 in Basel. The method of 2015 has proved to be useful under variation of sensor properties and seasonality. Adaptations to the method have been carried out to face image mis-registration, variation of sensor types, acquisition conditions and image properties. Registration of images taken by different sensors operated on UAVs has been realized by the use of mutual information, applying an algorithm usually used in medical imagery (Pluim et al., 2003).

Here, we extract the land cover composition of multiple datasets and analyse the fraction of each land cover, their temporal changes and the main cycles of land cover changes among time and space (Figure 1).

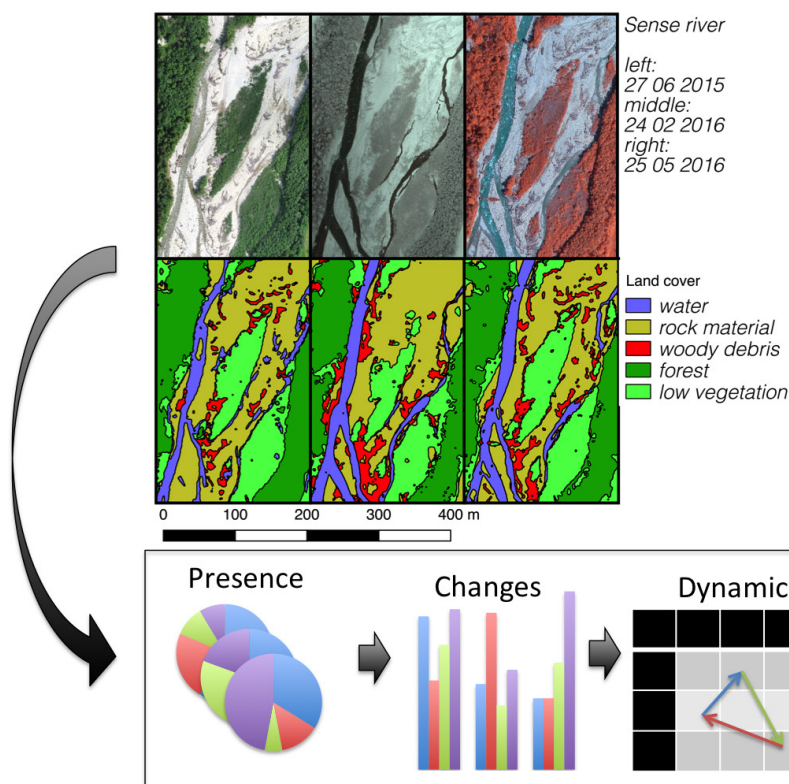


Figure 1. Example of land cover classification at varying seasons using different imagery. These classifications are then analysed to extract the dynamics of the riverine environment.

Summarized for each type of hydrological regime, the results show the differences in the land cover dynamics under various anthropogenic pressures. The quantification of the habitat dynamic through remote sensing allows an exhaustive consideration of the reach area. The main result of the study is the capability to get a robust estimate of the land cover dynamic, applicable also in ambiguous situation, i.e., where the anthropogenic pressure level is not clear. Management of hydropower plants can be supported by this study to help reaching a quantified target of health for the riverine environment. The challenge to quantify the dynamic of riverine environment is thus on the way to be solved.

REFERENCES

- Person, E. (2013). Impact of hydropeaking on fish and their habitat: EPFL-LCH.
- Pluim, J. P., Maintz, J. A., & Viergever, M. A. 2003: Mutual-information-based registration of medical images: a survey. *IEEE transactions on medical imaging*, 22, 986-1004.
- Ward, J., Tockner, K., Arscott, D., & Claret, C. 2002: Riverine landscape diversity. *Freshwater Biology*, 47, 517-539.
- Winemiller, K. O., Flecker, A. S., & Hoeninghaus, D. J. 2010: Patch dynamics and environmental heterogeneity in lotic ecosystems. *Journal of the North American Benthological Society*, 29, 84-99.

19.3

Erosion changes throughout glacial cycles contribute to the magma production by continental unloading and associated volcanic activity

Pietro Sternai¹, Luca Caricchi¹, Sébastien Castelltort¹

¹ *Département de Sciences de la Terre, University of Geneva, Rue de Maraichaire 13, CH-1205 Genève*

Observed peaks of igneous activity worldwide during the current interglacial (e.g., Huybers and Langmuir, 2009) suggest that climate oscillations affect the melting of the Earth's interior. A deglacial-triggering hypothesis (Hardarson and Fitton, 1991), according to which continental unloading owing to the melting of ice-caps during the transition to interglacials leads to enhanced magma production, is currently the most accredited explanation for this correspondence. The impact of climate oscillations on magma production, however, has been evaluated regardless of surface erosion although the density of upper crustal rocks and sediments exceeds that of ice by approximately three times. Such a density difference implies that the melting of 1 km of ice leads to the same increase of basalt production as the removal ~0.3 km of upper crustal rocks by erosion, provided that such unloading occurs during similar time intervals.

We use datasets relating to the evolution of erosion rates (e.g., Hallet et al., 1996; Herman et al., 2013) to calibrate numerical models of surface erosion processes and evaluate the relative dynamic contributions of erosion and ice building/melting to continental loading/unloading during a 100 ka glacial-interglacial climate oscillation. Assuming that the Earth possess a linear rheology, a time invariant geothermal gradient and negligible deviatoric stresses at depth, variations of the melt production at any given depth due to surface ice building/melting and erosion can be inferred from modelled loading/unloading histories beneath an eroding ice sheet responding to such a climate signal.

Our numerical experiments are capable of linking self-consistently short- and long-term observational constraints and suggest that the observed rates of glacial erosion imply comparable contributions to the magma production by continental unloading from ice melting during the deglaciation and surface erosion.

Degassing associated with mantle melting injects chemically and physically active gases and aerosol particles into the atmosphere, which affect climate and weather changes (Cole-Dai, 2010). The decompression of volatile saturated magmas also drives gas exsolution, which increases the probability of eruption and degassing events to occur as well as the amount of volatiles potentially released in the atmosphere (Jellinek and De Paolo, 2003). While many other physical and biological

feedbacks in the ocean are certainly involved, our results suggest that erosion may play a role as important as that of ice building/melting in controlling the emissions of greenhouse gases from the solid Earth across continental domains. Although the forcing of climate oscillations on submarine volcanisms is debated (Olive et al., 2015), sea-level rise following continental ice melting seems able to reduce the magma production of mid oceanic ridges (Crowley et al., 2015), in turn buffering the increased subaerial volcanic and degassing activity owing to continental unloading by the deglaciation (e.g., Huybers and Langmuir, 2009). Such a buffering mechanism, however, does not apply to continental unloading by erosion because loading by sediment deposition in the ocean is unlikely to occur atop of oceanic ridge. Therefore continental erosion may have greater net effects than ice building/melting on the CO₂ outflux and magma production from the solid Earth.

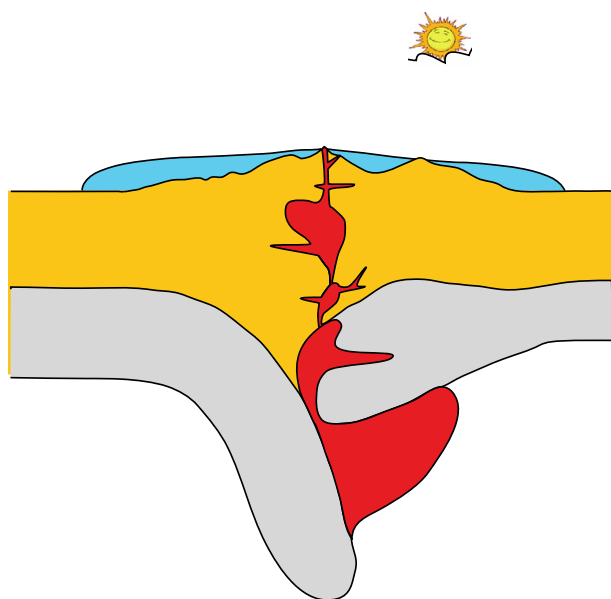


Figure 1. Schematic representation of the proposed feedback between surface and deep processes. Building and melting of erosive continental glaciers and ice-sheets throughout climate cycles control the redistribution of ice, water and rock masses across the Earth's surface and affect the magma production by mantle decompression melting. In turn, the eruption of magma at the Earth's surface affects the atmospheric greenhouse gas budget and feedbacks on climate and weather.

REFERENCES

- Cole-Dai, J. 2010. "Volcanoes and Climate." *Wiley Interdisciplinary Reviews: Climate Change* 1(6):824-839.
- Crowley, J. W., R. F. Katz, P. Huybers, C. Langmuir, and S-H Park. 2015. "Glacial cycles drive variations in the production of oceanic crust." *Science* 347(6227):1237-1240.
- Hallet, B., L. Hunter, and J. Bogen. 1996. "Rates of erosion and sediment evacuation by glaciers: A review of field data and their implications." *Global and Planetary Change* 12:213-235.
- Hardarson, B. and G. Fitton. 1991. "Increased mantle melting beneath Snaefellsjökull volcano during Late Pleistocene deglaciation." *Nature* 353:62-64.
- Herman, F., D. Seward, P. G. Valla, A. Carter, B. Kohn, S. D. Willett, and T. A. Ehlers. 2013. "Worldwide acceleration of mountain erosion under a cooling climate." *Nature* 504.
- Huybers, P. and C. Langmuir. 2009. "Feedback between deglaciation, volcanism, and atmospheric CO₂." *Earth and Planetary Science Letters* 286:479-491.
- Jellinek, A. M. and D. J. De Paolo. 2003. "A model for the origin of large silicic magma chambers: precursors of caldera-forming eruptions." *Bulletin of Volcanology* 65(5):pp.363–381.
- Lisiecki, L. E. and M. E. Raymo. 2007. "Plio–Pleistocene climate evolution: trends and transitions in glacial cycle dynamics." *Quaternary Science Reviews* 26:56-69.
- Olive, J-A., M. D., Behn, G., Ito, W. R., Buck, J., Escartín, & S., Howell. 2015. "Sensitivity of seafloor bathymetry to climate-driven fluctuations in mid-ocean ridge magma supply." *Science* 350.6258: 310-313.

19.4

Monitoring run-off, accumulation and infiltration in the arid Ennedi mountains (Northern Chad), using remote sensing

Marie-Louise Vogt¹, Daniel Käser¹, Daniel Hunkeler¹, François Zwahlen¹, Philip Brunner¹

¹ Centre d'Hydrogéologie et Géothermie (CHYN), University of Neuchâtel, Rue Emile-Argand 11, 2000 Neuchâtel

The aim of this investigation is to quantify surface water (run-off, accumulation and infiltration) and recharge dynamics occurring in the Ennedi range, Northern Chad. Despite the high aridity of the region, groundwater outcropping in the Ennedi were proved to be of modern origin (Vogt et al., 2013), indicating that recharge is currently taking place. The renewable character of the aquifer has great significance for the region, which otherwise relies on the fossil Nubian Sandstone Aquifer System (NSAS), one of the most important aquifer systems of Northern Africa.

The rainy season takes place from July to September with only about 10 days of rain. Precipitation is characterized as low frequency-low duration-high intensity rainfalls with a high spatial variability. Surface run-off is high and water is rapidly conveyed in localized accumulation zones, where eventually infiltration will occur. Focused rather than diffuse infiltration is therefore the main recharge process. Only a few field-based climatic data (precipitation, air temperature, evapotranspiration, incoming solar radiation, wind speed, etc.) and surface run-off measurements are available. Remote sensing is the only available data, but is also subject to some restrictions, namely the need of a relatively high temporal and spatial resolution which allows to evidence the natural variability occurring before, during and after the rainy season at the scale of a wadi (generally less than 100 m width). Nevertheless, remote sensing can provide spatially distributed information on precipitation, evapotranspiration and flow accumulation at the surface, which are used as a base for recharge estimation.

Infiltration rates and recharge are estimated through a water balance which uses the parameters extracted by satellite images. 17 free of clouds LandSat8OLI images (spatial resolution 30 m, temporal resolution 16 days) were selected in order to cover the entire rainy season of 2014 (testing year) for the area under investigation. Surface water/soil moisture was detected by using Normalized Difference Water Index (NDWI). Vegetation growth and shrinking during the season is well identified using Normalized Difference Vegetation Index (NDVI). A full R-code workflow was developed in order to automatically process the images for evapotranspiration estimation, based on the determination of surface albedo (Da Silva et al., 2016), land surface temperature (Du et al., 2015), evaporative fraction (Roerink et al., 2000) and finally daily evapotranspiration (Parodi, 2002). Air temperature data was retrieved from Global TempSIM (version 1.0). Rainfall estimates were extracted from the Famine Early Warning System (FEWS-NET, spatial resolution 1200 m, temporal resolution 10 days).

In 2014, precipitations were detected from 20th of July to 31st of August. In good agreement with the field observation of previous authors, higher precipitations are occurring at the southern front of the Ennedi massif (200-300 mm), while northern slopes receive 60-100 mm (western side) and less than 60 mm (eastern side). The temporal analysis of the LandSat images and NDWI index shows that water is rapidly conveyed in specific accumulation zones which correspond to, from older to younger, the Precambrian basement, the Silurian and Middle Devonian platforms (towards the south), and the Mourdi Carboniferous depression (towards the north). In such locations, despite the intense evapotranspiration, water remains visible for 1-2 months after the end of the rainy season, clearly indicating that groundwater exfiltration occurs. Such information is highly complementary to the limited amount of hydrogeological observations and will be integrated in a 3D geological model currently under construction. This model will better represent the hydrogeological connection of the Paleozoic sequence outcropping in the Ennedi and the Paleo-Mesozoic sequence composing the Nubian Sandstone Aquifer System of Northern Chad.

REFERENCES

- Da Silva, B.B., Braga, A.C., Braga, C.C., de Oliveira, L.M.M., Montenegro, S.M.G., Barbosa Jr, B. (2016): Procedures of calculation of the albedo with OLI-LandSat8 images: application to the Brazilian semi-arid, *Revista Brasileira de Engenharia Agrícola e Ambiental*, v.20, n.1, 3-8.
- Du, C., Ren, H., Qin, Q., Meng, J., Zhao, S. (2015) : A practical split-window algorithm for estimating land surface temperature from LandSat8 data, *Remote Sens.*, 7, 647-665.
- Parodi, I.G.N. (2002): AHVRR Hydrological Analysis System, Algorithms and theory, version 1.3, WRES-ITC
- Roerink, G.J., Su, Z., Menenti, M. (2000): S-SEBI A simple remote sensing algorithm to estimate the surface energy balance, *Phys. Chem. Earth (B)*, vol. 25, no.2, 147-157.
- Vogt, M.-L., Pera, S., Hamit, A., Haeberlin, Y., Bünzli, M.-A., (2013): Hydrochemical exploration of Ennedi, Northern Chad, abstract and conference 11th Swiss Geosciences Meeting, November 2013, Lausanne.

P 18.1

Landslide Hazard Assessment in the Himalayas (Nepal and Bhutan) based on Earth-Observation Data

Christian Ambrosi¹, Tazio Strozzi², Cristian Scapozza¹, Urs Wegmüller²

¹ *SUPSI - University of Applied Sciences and Arts of Southern Switzerland, Switzerland;*

² *Gamma Remote Sensing AG*

The Himalayan range is a high-risk area; natural hazards can cause damages, destructions, injuries and deaths at any time (SDC, 2009). Landslides, rockfalls, floods and earthquakes cause numerous deaths each year and destroy villages, access roads and other important infrastructures. As the Himalayas is located in a tectonically active zone, landslides and rockfalls triggered the earthquakes represent one of the most dangerous hazards. More than 3000 landslides, for example, were triggered by the earthquake of April and May 2015 (BGS, 2015).

The hazard assessment represents one of the most important actions in the disaster risk management strategy. Because a lack of diffuse field data (i.e. diffuse landslide mapping), landslide hazard maps are not available for vast regions of the Himalayas.

Based on satellite EO data valuable information to perform landslide hazard maps for two areas in Nepal (Lukla region) and Bhutan (Chomolhari/Paro region) were collected. Landslide hazard maps were performed based on geomorphological and quantitative (InSAR analysis) approach through a compilation of a landslide inventory map at regional scale by means of satellite photo-interpretation and the assessment of the state of activity of mapped phenomena based on surface displacement rates quantified from differential SAR interferometry. Regarding Lukla region, the 7.5% of the area (total of 724 km²) is affected by landslides. The 40% of mapped landslides were classified as active. The 6% of the Chomolhari area (total of 620 km²) is affected by landslides; 45% of them were classified as active. Rockslide represents for both regions the most of the mapped landslides.

The landslide hazard assessment over large regions based on EO products represents an important aspect for the disaster risk reduction not only in the whole Himalayan region but also in other mountain areas in absence of detailed landslide inventory maps.

P 18.2

Measuring surface displacements from airborne imagery with Digital Image Correlation: insights from the Cuolm Da Vi deep-seated rockslide

Andrea Manconi¹, Andrea Wolter & Florian Amann

¹ *Swiss Federal Institute of Technology, Department of Earth Sciences, Zurich, Switzerland (andrea.manconi@erdw.ethz.ch)*

Optical imagery is routinely acquired from airborne and space-borne platforms to produce accurate orthophotos and digital surface models. In engineering geology applications, these products are crucial to investigate morphological features at regional and local scales, as well as to understand their relationship with the surrounding geological and tectonic environment. Moreover, repeated acquisitions of such imagery over the same area can be leveraged to identify changes over time due to natural phenomena (e.g. erosion, faulting, mass wasting, etc.) and/or anthropic activities. Recently, a photogrammetric technique named Digital Image Correlation (DIC, known also as sub-pixel-offset or feature-tracking) has been successfully applied to several digital image sources (optical, multispectral, thermal, and radar) in order to identify and measure surface displacements over large areas.

In this work, we present the results obtained by applying the DIC approach to orthophotos generated from airborne optical imagery acquired over the Cuolm Da Vi DSGSD area (Grisons, CH) in 1999, 2003, 2010, 2013, and 2015. In this area, large surface deformations caused by the landslide activity are well-known and clearly identified from repeated field surveys and traditional in situ monitoring. We show that the results obtained from the application of DIC to multitemporal acquisitions are in good agreement with the available independent displacement data, and with engineering geological and geomorphic mapping of features. Moreover, our results highlight the development of a local deformation on the western part of the unstable slope during the period 1999-2015. On 14 March 2016, a rock fall of about 200.000 m³ occurred in this area and threatened the Val Strem and some infrastructures. Thus, the information gained from DIC on Cuolm Da Vi is valuable not only to understand the long-term evolution of the rock slope, but also to infer impending hazards.

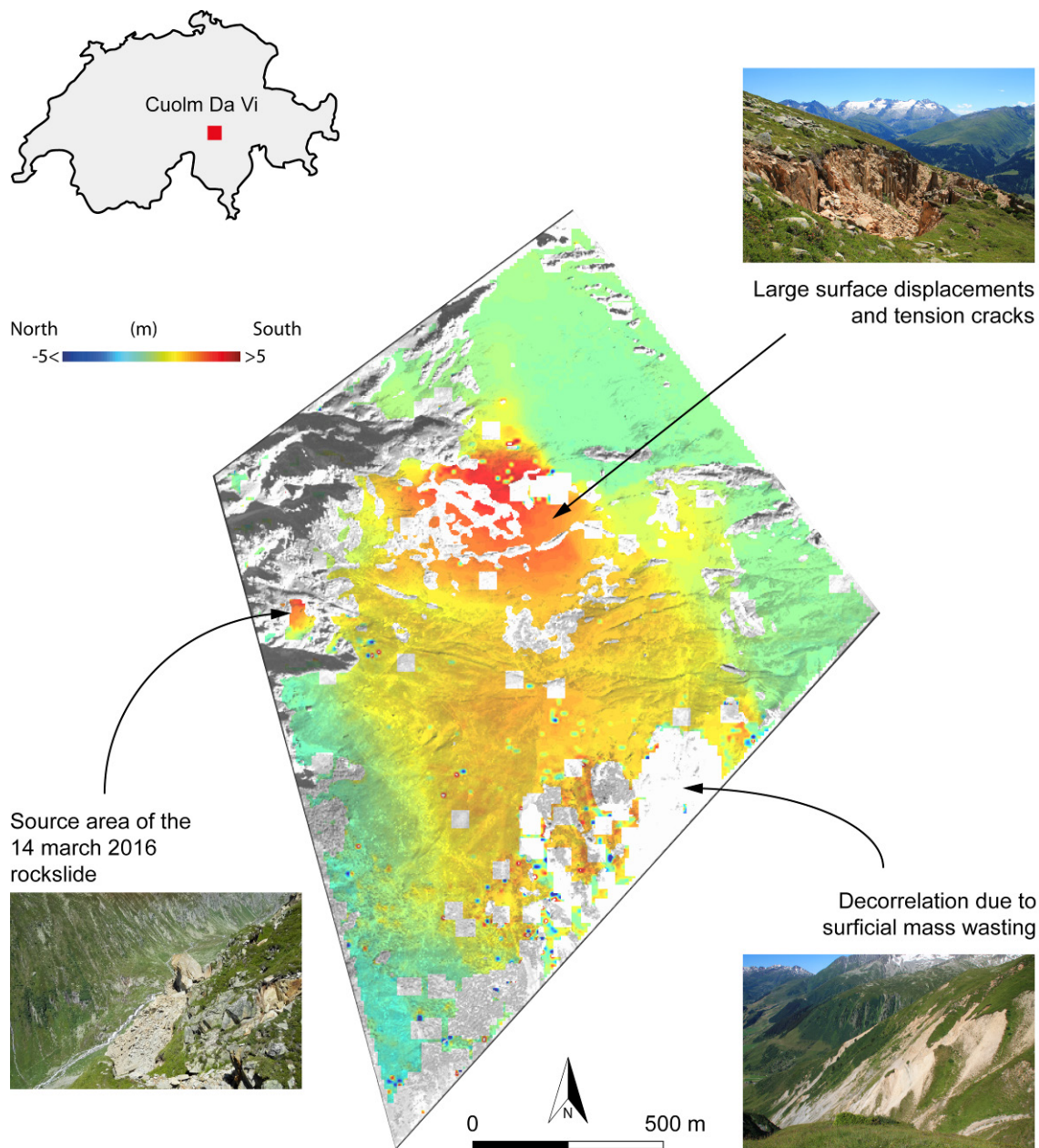


Figure 1. Surface deformation in the North-South direction revealed by applying the DIC approach to a pair of orthophotos acquired on 1999 and 2015.

P 18.3

Tracking of seasonal to millennial variability of biogeochemical proxies in varved lake sediments using hyperspectral imaging

Christoph Butz¹, Martin Grosjean¹, Fabian Rey²

¹ *Institute of Geography & Oeschger Centre For Climate Change Research, University of Bern, Erlachstr. 9a (Building 3), CH-3012 Bern (christoph.butz@giub.unibe.ch)*

² *Institute of Plant Sciences, University of Bern, Altenbergrain 21, CH-3013 Bern*

Varved lake sediments are high-resolution archives for past environmental and climate conditions. Potentially, they can serve as continuous records for seasonally resolved proxies over several millennia (Zolitschka et al. 2015). Different studies use, among other proxies, concentrations of sedimentary photopigments for paleo-temperature reconstructions. However, it is already challenging to obtain well-calibrated records with annual resolutions and even more so with seasonal resolutions. Most laboratory methods used for the analysis of lake sediments require physical subsampling, which is expensive and time-consuming (Reuss et al. 2005). Furthermore, many of these methods are destructive in the process and require large amounts of sampling material. This limits the temporal sampling resolution especially for very low sediment accumulation rates.

To address these issues we explore visual to near infrared hyperspectral imaging (VNIR HSI) as a non-destructive method to analyse lake sediments based on their reflectance spectra. In contrast to other scanning methods like x-ray fluorescence (XRF), VNIR reflectance spectrometry distinguishes between biogeochemical substances rather than single elements. Among others Rein & Sirocko (2002) have shown that reflectance spectrometry detects relative concentrations of sedimentary photopigments (e.g. chlorins, carotenoids) and clay minerals.

In this study, we use VNIR HSI to infer ecological proxy data from reflectance spectra of varved lake sediments. Hyperspectral imaging permits the measurement of an entire sediment core in a single run at high spatial (30x30µm/pixel) and spectral resolutions (~2.8nm) within the VNIR spectrum (400-1000nm). This allows the analysis of data time series and spatial mapping of sedimentary substances (e.g. chlorophylls / bacteriochlorophylls and diagenetic products as well as charcoal and clays) at sub-varve (i.e. seasonal) resolution.

Calibration of diagnostic spectral absorption bands (i.e. relative concentrations) with absolute concentrations as derived from high-performance-liquid-chromatography (HPLC) is possible with an uncertainty of 10-14% (Butz et al. 2015). This results in high-resolution datasets of absolute sedimentary pigment concentrations suitable for the analysis of seasonal pigment variability. Pigments may be used as proxies for lake productivity (i.e. chlorophylls) and meromixis (i.e. bacteriochlorophylls). Additionally, HSI can potentially detect and spatially map other key sediment facies, such as lithogenic input (e.g. clays) and fire events in the catchment (e.g. charcoal).

We demonstrate this method on varved lake sediments from northern Poland and Switzerland showing the distributions of lithogenic content and calibrated concentrations of sedimentary pigments. In combination with high-resolution XRF data, we trace cycles of green algae, anoxygenic phototrophic bacteria, endogenic calcite and lithogenic content for individual varves and for millennial periods.

REFERENCES

- Butz C, Grosjean M, Fischer D, Wunderle S, Tylmann W, Rein B. (2015): Hyperspectral imaging spectroscopy: a promising method for the biogeochemical analysis of lake sediments. *J Appl Remote Sens* 9:096031-096031.
- Rein B & Sirocko F. (2002): In-situ reflectance spectroscopy—analysing techniques for high-resolution pigment logging in sediment cores. *Int J Earth Sci* 91:950-954.
- Reuss N, Conley DJ, Bianchi TS. (2005): Preservation conditions and the use of sediment pigments as a tool for recent ecological reconstruction in four Northern European estuaries. *Mar Chem* 95:283-302.
- Zolitschka B, Francus P, Ojala AEK, Schimmelmann A. (2015): Varves in lake sediments – a review. *Quat Sci Rev* 117:1-41.

20. Geoscience and Geoinformation – From data acquisition to modelling and visualisation

Nils Oesterling, Adrian Wiget, Massimiliano Cannata, Michael Sinreich

*Swiss Geodetic Commission,
Swiss Geotechnical Commission,
Swiss Geophysical Commission,
Swiss Hydrogeological Society*

TALKS:

- 20.1 Allenbach R., Baumberger R., Di Tommaso G., Dürst Stucki M., Kuhn P., Kurmann-Matzenauer E., Michael S., Reynolds L., Wehrens P.: GeoMol-Development of 3D models of the Swiss Molasse Basin: Results and lessons learned
- 20.2 Boulicault L., Oesterling N., Minnig C., Baumberger R.: GeoTherm: the first Information System for Deep Geothermal Energy in Switzerland
- 20.3 Brentini M., Favre S.: Tools for the State of Geneva to manage its subsurface resources
- 20.4 Cannata M., Neumann J., Cardoso M., Rossetto R., Foglia L., Borsi I.: FREEWAT: open source water resource management platform
- 20.5 Fraefel M., Fischer C.: GIS-based compilation and assessment of the forestry road network in Switzerland
- 20.6 Malard A., Debache J., Jeannin P-Y., Vogel M., Randles S., Hausmann P.: Visual KARSYS – a web-tool for the documentation of karst aquifers
- 20.7 Pedrazzini G., Kinzelbach W.: Interactive online real-time groundwater model for irrigation water allocation in the Heihe mid-reaches, China
- 20.8 Rasera L.G., Mariethoz G., Lane S.N.: Geostatistical sub-pixel imaging of terrain elevation data
- 20.9 Rauch A., Sartori M., Gouffon Y., Möri A., Castellort S.: Assessing Uncertainties in Bedrock Geology Maps – a “Pre-Modelling” Approach

POSTERS:

- P 20.1 Brentini M., Favre S., Rusillon E., Moscariello A.: Tools for the State of Geneva to manage its subsurface resources: Relevance of geological data
- P 20.2 Favre S., Brentini M., Giuliani G., Lehmann A.: Tools for the State of Geneva to manage its subsurface resources: Data model design and implementation
- P 20.3 Cannata M., Mahanama S., Karyanto O., Shahid I.: 4ONSE: 4 times Open and Non-conventional technology for Sensing the Environment
- P 20.4 Heerwagen, E., Martini, R.: Cluster analysis and Multi-dimensional scaling – A combined approach to discriminate carbonate microfacies
- P 20.5 Kanevski M., Golay J., Pereira M.: Analysis of forest fires clustering using the multipoint Morisita index
- P 20.6 Leuenberger M., Parente J., Tonini M., Pereira M., Kanevski M.: Wildfire susceptibility: Comparing deterministic approach with machine learning
- P 20.7 Laib M., Kanevski M.: Analysis of wind speed data using network science measures
- P 20.8 Moradi G., Cardot R., Lane S.N. & Rennie C.D.: Field Data Collection Methods and Data Processing of the Influence of Low Momentum Ratio and the Rate of Sediment Transport Forcing on Confluence Hydrodynamics, Morphodynamics and Mixing

20.1

GeoMol - Development of 3D models of the Swiss Molasse Basin: Results and lessons learned

Robin Allenbach¹, Roland Baumberger¹, Gennaro Di Tommaso², Mirjam Dürst Stucki³, Pascal Kuhn⁴, Eva Kurmann-Matzenauer¹, C. Salomè Michael¹, Lance Reynolds¹, Philip Wehrens¹

¹ *Swiss Geological Survey, Federal Office of Topography (swisstopo), CH-3084 Wabern, robin.allenbach@swisstopo.ch*

² *Federal Office for Public Health, CH-3003 Bern*

³ *Kanton Fribourg, Department for Spatial Development, CH-1701 Fribourg*

⁴ *Kanton Bern, Department for Geoinformation, CH-3011 Bern*

Competing claims on the subsurface of the Swiss Molasse Basin, such as those for energy and repositories, and related conflicts such as property and planning in 3D, are expected to be a source of societal conflict in the near future (Baumberger & Allenbach, 2016). Geological data and information have become increasingly important to decision makers, planning authorities and even the public as solutions to subsurface development are being sought. Geoscientists are being tasked with producing 3D visualizations of the subsurface and providing suggestions on as to how it can be optimally developed (Baumberger et al., 2015).

Within the framework of the EU-funded GeoMol project (2012-2015; GeoMol Team, 2015), a large-scale geological 3D model of the Swiss Molasse Basin was produced. The model is based on the Seismic Atlas of the Swiss Molasse Basin (Sommaruga et al., 2012), includes the most important large-scale fault zones and has a resolution of 200 x 200 m (approximately 1:200'000; FM200). As a follow-up to this low-resolution model, the Swiss Geological Survey (SGS) went on to develop a high-resolution, basin-wide geological 3D model of the Swiss Molasse Basin (resolution 100 x 100 m; approximately 1:50'000; FM50).

While the large-scale FM200 was developed entirely by the SGS, the small-scale FM50 is a collaborative work by six different partners under the lead of the SGS (Universities of Basel, Bern, Fribourg, Geneva; Musée géologique du canton de Vaud). The model will be completed by the end of 2016.

Prior to GeoMol, knowledge of nation-wide geological 3D modeling at the SGS was scant and the SGS found itself in a position to not only develop methodologies, but also to test and adapt workflows. A task of these dimensions requires several independent modelling steps which surpass the scope of many off-the-shelf software packages. Since several software packages and data formats had to be handled in successive modelling steps, rules and workflows for data exchange needed to be established. Between 2013 and today the SGS has experienced, and continues to profit, from a very steep learning curve.

GeoMol CH delivers the first comprehensive geological 3D model of the Swiss Molasse basin for public access (FM200, only). It comprises Cenozoic (Plateau and Subalpine Molasse) and 12 major Mesozoic units (see Figure 1) and is described based on the SGS data models (Swiss Geological Survey, 2013; Swiss Geological Survey, 2012). Besides the two models (FM200 and FM50), the following products were also developed:

1) Top Bedrock (available at 25 × 25 m resolution); 2) Mesozoic interval-velocity model (all new, including the St.Gallen well and data supplied by the LGRB); 3) Data Coverage Maps (horizon-based, input data location maps); 4) 3D structures (set of fault zones).

Regarding the visualization and the distribution of the models, as well as the corresponding data transfer, the SGS offers various approaches, which are tailored to the needs of non-experts and experts alike.

In future development steps, models existing at the SGS will be consolidated into a 3D knowledgebase containing retrievable attributes to be used in practical applications and research (Baumberger & Allenbach, 2016). By continuously improving its 3D products from which new products can be derived and fed back to the 3D knowledgebase, the SGS aims to increase the 3D coverage of the subsurface and to eventually produce a national geological 3D model.

The geological 3D models of the deep subsurface underlying the Swiss Plateau are based on a standardized stratigraphic section. They provide harmonized data for the most important horizons and the major fault zones. During the past four years, the SGS not only acquired a huge amount of theoretical and practical knowledge in geological 3D modelling, but also achieved a high level of performance in many different subdomains (e.g. data preparation and harmonization, seismic data handling and interpretation, quality assurance and control, etc.). With the FM50, it could also be shown that collaborative 3D modelling is a viable approach to developing large geological 3D models.

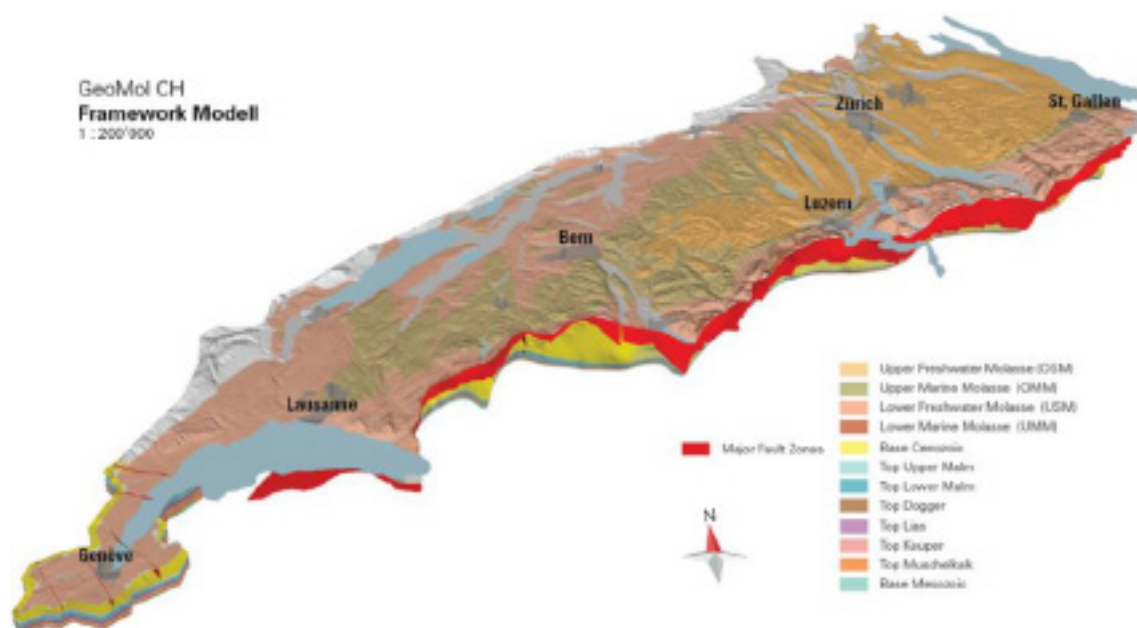


Figure 1: Large-scale, low-resolution geological 3D model of the Swiss Molasse Basin (FM200). It consists of 12 major horizons, from Base Quaternary down to Base Mesozoic. The 22 most important large-scale fault zones (Major Fault Zones) are included as well as the triangle zone of the Alpine thrust system.

REFERENCES

- Baumberger, R. & Allenbach, R. (2016): 3D model of the Swiss Molasse Basin – A first step towards a national geological 3D model; Swiss Bull. Appl. Geol. (in press), <http://www.saseg.ch>
- Baumberger R., Allenbach R. & Volken, S. (2015): From wallflower to eye-catcher: 3d geological modelling in Switzerland – more than XYZ, less than a Swiss Army knife. 3D mapping workshop at the Annual Meeting of the Geological Society of America, Baltimore, 2015.
- GeoMol Team (2015): GeoMol – Assessing subsurface potentials of the Alpine Foreland Basins for sustainable planning and use of natural resources – Project Report, 188 pp. (Augsburg, LfU)
- Swiss Geological Survey (2012): Data Model Geology, Description in UML Format and Object Catalogue, Version 2.1, ed.: Federal Office of Topography (swisstopo), Wabern.
- Swiss Geological Survey (2013): Data Model 3D Geology, Extension of the Data Model Geology, Version 2.0, ed.: Federal Office of Topography (swisstopo), Wabern.
- Sommaruga, A., Eichenberger, U. & Marillier, F. (2012): Seismic Atlas of the Swiss Molasse Basin. Edited by the Swiss Geophysical Commission. Matér. Géol. Suisse – Géophysique 44, 88 pp., 24 maps, ISSN 0253-1186

20.2

GeoTherm: the first Information System for Deep Geothermal Energy in Switzerland

L.Boulicault¹, N.Oesterling¹, C.Minnig¹, R.Baumberger¹

¹ *Federal Office of Topography swisstopo, Swiss Geological Survey, Seftigenstrasse 264, CH-3084 Wabern (lise.boulicault@swisstopo.ch)*

In Switzerland the subsurface is under the authority of the cantons. Due to this very heterogeneous legal situation, geological data is stored at different places and in different legal frameworks. Since federal data access rules are lacking, the accessibility to the data is hindered and it is difficult to obtain an accurate overview. Consequently, every project must start all over again with data acquisition which is time consuming, causes substantial costs, leads to non-sustainable data treatment, bad overall data quality (if so) and new risks in projects development.

For data relevant for deep geothermal energy the Swiss Federal Offices for Energy (SFOE) and Topography (swisstopo) identified this challenge. In early 2015, they launched the GeoTherm (2015-2019) project, which aims to collect, harmonize, store and publish the relevant data for deep geothermal energy on the Federal web-portal (map.geo.admin.ch). This project is going to be the first information system for data related to deep geothermal energy available to the public in Switzerland and contributes to the goals of the "Energy Strategy 2050". This article denotes the work in progress report after 12 months of project duration.

Collection of data relevant to deep geothermal energy

Up to now the metadata of 131 wells over 500m depth as well as 59 2D seismic lines in the public domain have been inventoried. Additionally, information about the deep geothermal projects in Switzerland have been compiled and will also be published on the internet. External partners such as universities, cantons and private companies throughout Switzerland are contacted in order to build-up a community of collaboration and information transfers.

Data harmonization and perennial backup in the Federal database

Parallel to the data inventarization, the data quality control and harmonization based on the borehole data model (Brodhag & Oesterling, 2014) are ongoing. Relevant information (e.g. well depth, porosity, temperature etc.) for the development of geothermal projects are compiled from the reports and stored in a central database. This guarantees efficient use and perennial backups of the data.

Web-publication of non-confidential data

In 2016, three new layers of data relevant to deep geothermal energy (wells deeper than 500 m, seismic lines in the public domain as well as the locations of the geothermal projects in Switzerland) will be published on the Federal geodata portal (map.geo.admin.ch). Depending on the confidentiality and legal status of the data, they will be available for full or partial (metadata only) download, respectively. Negotiations will take place with the owners of confidential data for forthcoming web-publications.

Production of a geothermal expert system

The publication of uninterpreted as well as interpreted data is only the first objective of the GeoTherm project. Based on this data and on the 3D geological model of the Swiss Molasse Basin (GeoMol project; Allenbach et al., 2016; this volume), the SFOE and swisstopo intend to produce an expert system which will contain models of sub-surface geothermal potentials including temperatures, heat flow etc. This expert system will be a tool for enhancing the comprehension of the subsurface, assisting in reducing the economic risk of geothermal (and other) projects and promoting the development of future deep geothermal projects in Switzerland.

REFERENCES:

- Allenbach, R., Baumberger, R., Di Tommaso, G., Dürst Stucki, M., Kuhn, P., Kurmann-Matzenauer, E., Michael, S., Reynolds, L., Wehrens, P. (2016): Development of 3D models of the Swiss Molasse Basin: Review and lessons learned; Abstract submitted to the Swiss Geoscience Meeting 2016
- Brodhag, S. & Oesterling, N., 2014: Datenmodell Bohrdaten. Beschreibung des Kernmodells mit Objektkatalog und UML – Modell. Version 2.0. Bundesamt für Landestopografie swisstopo

20.3

Tools for the State of Geneva to manage its subsurface resources

Maud Brentini¹, Stéphanie Favre², Elme Rusillon¹ & Andrea Moscariello¹

¹ *Department of Earth Sciences, University of Geneva, Rue des Maraîchers 13, CH-1205 Geneva (maud.brentini@unige.ch)*

² *Institute for Environmental Sciences, University of Geneva, Boulevard Carl Vogt 66, CH-1205 Geneva*

For the abstract of this talk, please refer to the abstracts of the posters P 20.1 & P 20.2

20.4

FREEWAT: open source water resource management platform

Massimiliano Cannata¹, Jakob Neumann¹, Mirko Cardoso¹, Rudy Rossetto², Laura Foglia³, Iacopo Borsi⁴

¹ *Dipartimento Ambiente Costruzione e Design, Scuola Universitaria Professionale della Svizzera Italiana - SUPSI, Canobbio, Ticino, Switzerland*

² *Scuola Superiore S. Anna, Pisa, Italy*

³ *Technischen Universität Darmstadt, Darmstadt, Germany*

⁴ *Tea Sistemi SpA, Pisa, Italy*

FREEWAT (FREE and open source tools for WATER resource management) is an HORIZON 2020 project financed by the EU Commission whose principal result will be an open source and public domain GIS integrated modelling platform for the simulation of water quantity and quality in surface water and groundwater with an integrated water management and planning module.

FREEWAT aims at promoting water resource management by simplifying the application of the Water Framework Directive and other EU and national water related Directives.

Specific objectives of the FREEWAT project are:

- to coordinate previous EU and national funded research to integrate existing software modules for water management in a single environment into the GIS based FREEWAT;
- to support the FREEWAT application in an innovative participatory approach gathering technical staff and relevant stakeholders (in primis policy and decision makers) in designing scenarios for the proper application of water policies.

From a technical point of view the FREEWAT platform is a complex QGIS plug-in which integrates the USGS MODFLOW “suite” of open source numerical models together with other tools, libraries and software to offer a seamless environment with a large number of functions and tools accessible with specific interfaces, which facilitate the model creation, calibration, running and result analysis.

The open source characteristics of the platform allow to consider FREEWAT an initiative “*ad includendum*”, as further research institutions, private developers etc. may contribute to the platform development was chosen to guarantee the sustainability of the platform. The development of 14 case studies in Europe and Africa that has been preceded by one week training and that will be implemented with a participatory approach will assure a large number of stakeholder involvement and software validation.

Free training courses are foreseen the next year in each case study country, including Switzerland, to further disseminate the platform.

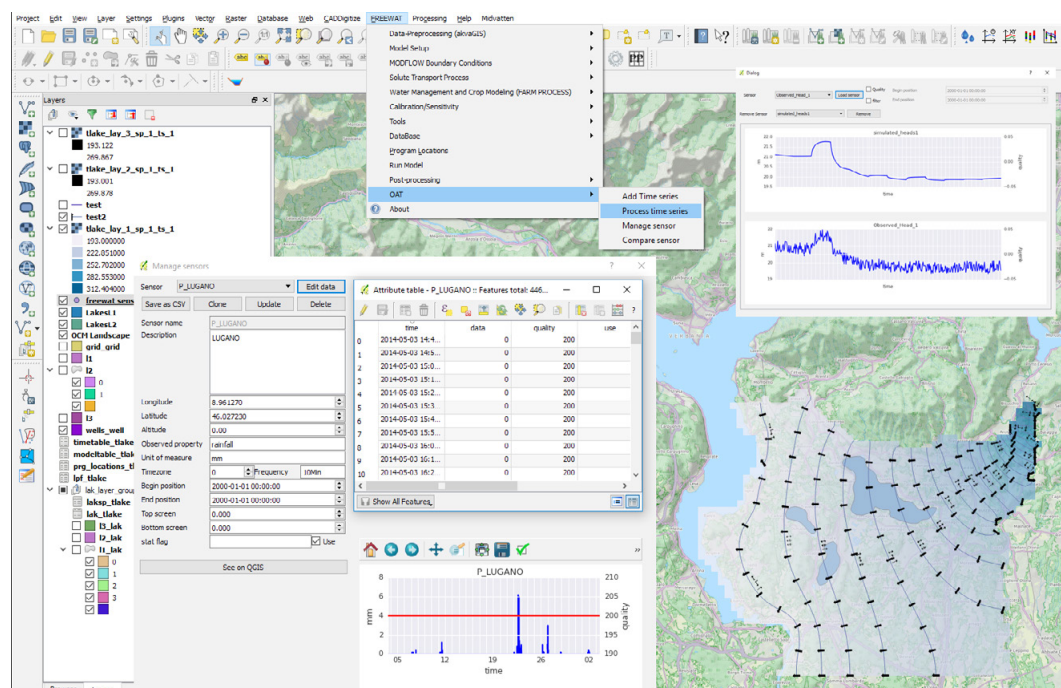


Figure 1. Screenshot of the FREEWAT interface, observation analysis tool and the lake package interface are visible.

REFERENCES

- Foglia, L., Borsi, I., Canatta, M., Velasco, V., Mehl, S., Rosetto, R. (2015). FREE and open source software tools for WATER resource management. AGU Fall Meeting, San Francisco (USA). December 2015.
- Rossetto, R., Borsi, I., Schifani, C., Bonari, E., Mogorovich P. & Primicerio M. (2013) - SID&GRID: integrating hydrological modeling in GIS environment hydroinformatics system for the management of the water resource. Rendiconti Online Società Geologica Italiana Volume 24, 282-283
- Rossetto, R., Borsi, I., Foglia, L., 2015, FREEWAT, Rend. Online Soc. Geol. It., Vol. 35 (2015), pp. 252-255, doi: 10.3301/ROL.2015.113.
- Cannata, M., Neumann, J., Cardoso, M., Rossetto, R., Foglia, L. (2016). Observation analysis tool for the FREEWAT GIS environment for water resources management, DOI: 10.7287/peerj.preprints.2127v1
- Cannata, M., Neumann, J., Cardoso, M., Rossetto, R., Foglia, L., Borsi, I. (2016). Integration of the MODFLOW Lak7 package in the FREEWAT GIS modelling environment, DOI: 10.7287/peerj.preprints.2207v1

20.5

GIS-based compilation and assessment of the forestry road network in Switzerland

Marielle Fraefel¹, Christoph Fischer²

¹ Swiss Federal Research Institute WSL, Research Group GIS, Zürcherstrasse 111, CH-8903 Birmensdorf
(marielle.fraefel@wsl.ch)

² Swiss Federal Research Institute WSL, Research Group Scientific Service NFI, Zürcherstrasse 111, CH-8903 Birmensdorf

In Switzerland, timber harvest and transportation accounts for a large share of the total wood production costs. This makes the location and dimension of forest roads an important cost factor: Generally, low forest road densities lead to longer hauling distances, thus increasing harvesting costs. In addition, roads with low bearing capability make additional trips necessary, increasing transport costs. In order to determine the most suitable and economic harvesting method and the shortest (or fastest) transport route, reliable information about forest roads is essential.

In the Swiss National Forest Inventory, information about the forest has been collected for more than 30 years (Brändli 2010). The collected data include the forest roads (for trucks) and their paving type in the entire forested area in Switzerland. In the most recent survey (2013-2014), additional data describing the width of the roads and their suitability for different truck types were collected for the first time. Roads outside the forest that connect forest roads to main (cantonal) roads were also mapped.

Data collection and the production of a digital road network required several steps. First, the road information from the previous survey, stored in attribute fields of a VECTOR25 road dataset, had to be transferred to the most current swissTLM^{3D} road data by means of a semi-automatic process. This road network was printed on maps, on which the local forest services indicated all changes since the previous interview. The changes were digitised, using various quality assurance mechanisms and consistency checks.

The result is a complete topological forest road network that also includes the main routes to the higher-order road network (Müller et al. 2016). It is used to assess the forest road density in different regions, considering different criteria (type of paving, vehicle size). Using network topology functions, we analysed the distance from sample plots to the nearest main road. In addition, we evaluated the adequacy of the Swiss forest road network for efficient timber transport, taking vehicles of various sizes into account. We found that in many areas forests are only accessible with small trucks, or cannot be accessed by road at all. With regard to timber transportation costs, the results indicate that investments in the road infrastructure might be worthwhile for some regions in Switzerland.

REFERENCES

- Brändli, U.-B. (Red.) 2010: Schweizerisches Landesforstinventar. Ergebnisse der dritten Erhebung 2004–2006. Birmensdorf, Eidgenössische Forschungsanstalt für Wald, Schnee und Landschaft WSL. Bern, Bundesamt für Umwelt, BAFU.
- Müller, K., Fraefel, M., Cioldi, F., Camin, P. & Fischer, C. 2016: Der Datensatz "Walderschliessungsstrassen 2013" des Schweizerischen Landesforstinventars. Schweizerische Zeitschrift für Forstwesen 167 / 3, 136-142.

20.6

Visual KARSYS – a web-tool for the documentation of karst aquifers

Arnauld Malard¹, Julien Debache¹, Pierre-Yves Jeannin¹, Manfred Vogel², Stephen Randles², Philipp Hausmann²

¹ SSKA | Swiss Institute for Speleology and Karst Studies, La Chaux-de-Fonds, info@isska.ch

² i4ds | Institut für 4D Technologien, Hochschule für Technik, Fachhochschule Nordwestschweiz

Visual KARSYS is a web-tool being developed for the documentation of karst aquifers and the management of groundwater resources. The tool is developed by SSKA and i4ds with inputs from various cantons and Confederation. The project is supported by the grant for Innovation and Technologic development provided by the Swiss Federal Office for Environment. The tool will help users to apply the KARSYS approach (Jeannin *et al.* 2013) by themselves through an intuitive web-based interface. It will also include a 3D-Web viewer dedicated to end-users (e.g. water authorities), who are interested in viewing and interrogating the data/results, for instance as maps for decision-making, etc. Innovations regarding the developments concern the online (hydro)geological 3D viewer, the 3D tools to process the 3D models and the connection of models and viewer to a geological data base. The talk intends to present the architecture of Visual KARSYS data base and the expected functionalities of the tool, which is still at the beginning of its development.

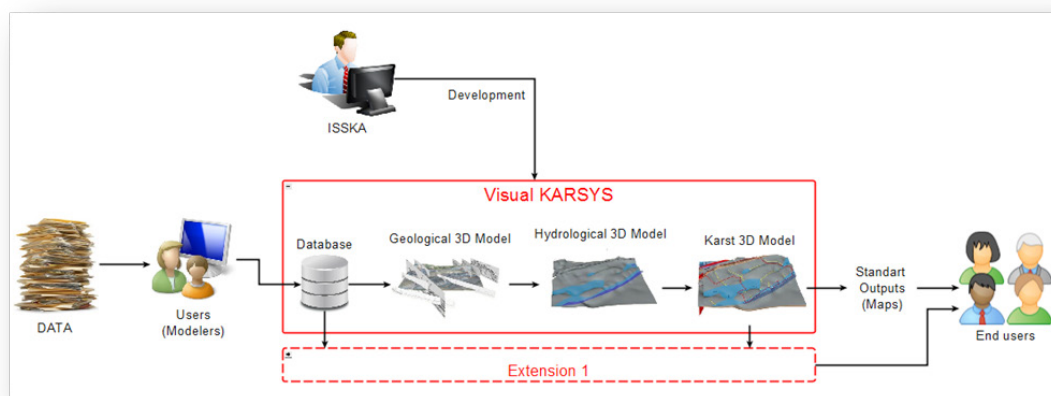


Figure 1. Overview of the organization of the Visual KARSYS web-tool

REFERENCES

Jeannin P.-Y., Eichenberger U., Sinreich M., Vouillamoz J., Malard A. et al. (2013) KARSYS: a pragmatic approach to karst hydrogeological system conceptualisation. Assessment of groundwater reserves and resources in Switzerland. *Environmental Earth Sciences*, 69(3): 999-1013 p.

20.7

Interactive online real-time groundwater model for irrigation water allocation in the Heihe mid-reaches, China

Gianni Pedrazzini¹, Wolfgang Kinzelbach¹

¹ Institut für Umweltingenieurwissenschaften, ETH Zürich

In the Heihe Basin and many other semi-arid regions in the world the ongoing introduction of smart meter IC-card systems on farmers' pumping wells will soon allow monitoring and control of abstractions with the goal of preventing further depletion of the resource. In this regard, a major interest of policy makers concerns the development of new and the improvement of existing legislation on pricing schemes and groundwater/surface water quotas. Predictive knowledge on the development of groundwater levels for different allocation schemes or climatic change scenarios is required to support decision-makers in this task.

In the past groundwater models have been a static component of investigations and their results delivered in the form of reports. We set up and integrated a groundwater model into a user-friendly web-based environment, allowing direct and easy access to the novice user. Through operating sliders the user can select an irrigation district, change irrigation patterns such as partitioning of surface- and groundwater, size of irrigation area, irrigation efficiency, as well as a number of climate related parameters. Reactive handles allow to display the results in real-time. The implemented software is all license free.

The tool is currently being introduced to irrigation district managers in the project area. Findings will be available after some practical experience to be expected in a given time. The accessibility via a web-interface is a novelty in the context of groundwater models. It allows delivering a product accessible from everywhere and from any device. The maintenance and if necessary updating of model or software can occur remotely. Feedback mechanisms between reality and prediction will be introduced and the model periodically updated through data assimilation as new data becomes available. This will render the model a dynamic tool steadily available and evolving over time.

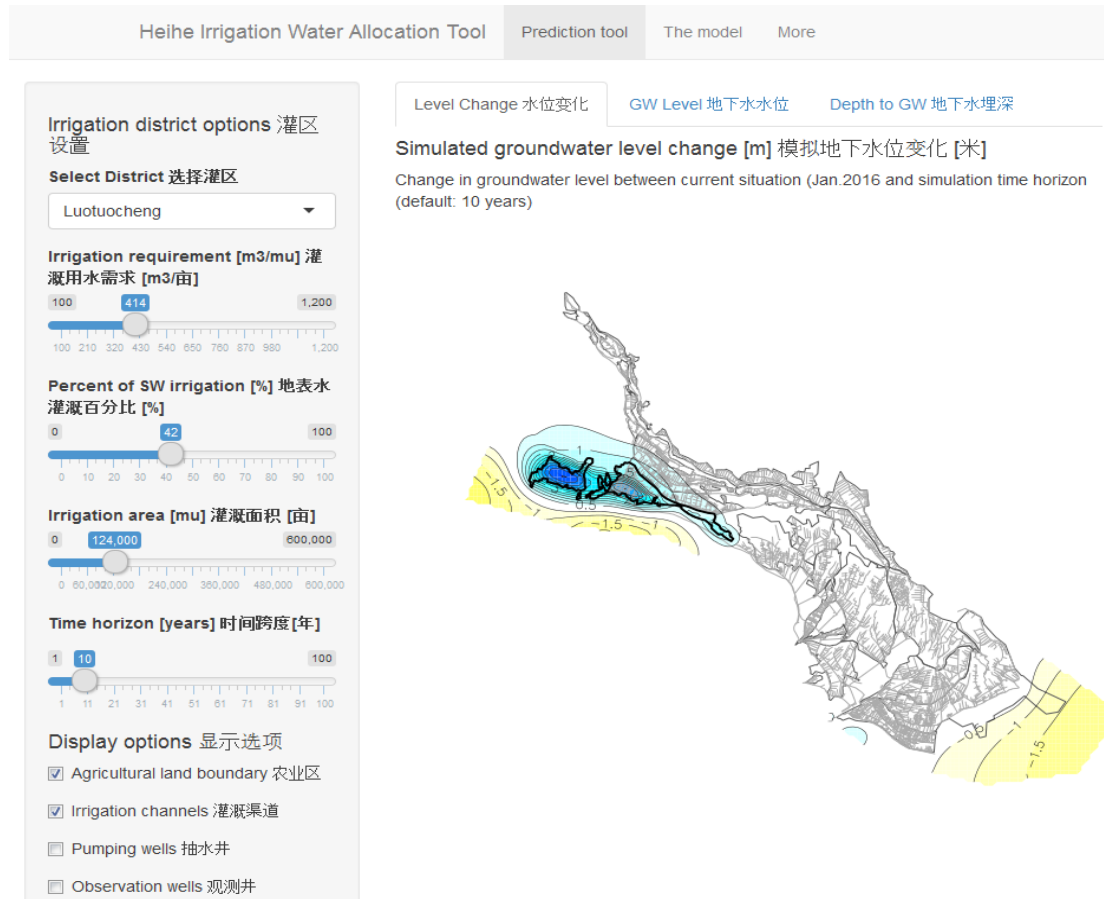


Figure 1. Screenshot of the interactive web-based user-interface allowing real-time forecasting of groundwater levels for different irrigation water allocations.

20.8

Geostatistical sub-pixel imaging of terrain elevation data

Luiz Gustavo Rasera, Gregoire Mariethoz, Stuart N. Lane

Institute of Earth Surface Dynamics, University of Lausanne, CH-1015 Lausanne (luizgustavo.rasera@unil.ch)

Fine-scale topography plays a fundamental role in controlling large-scale surface processes in mountainous environments. Connectivity patterns between gullies, for example, can affect surface water runoff in large drainage basins. High-resolution digital elevation models (HR-DEMs) are one of the most important tools for understanding and modeling these geomorphic processes.

Current remote sensing techniques enable fast and precise acquisition of HR-DEMs. Yet, sensors designed to measure terrain elevation still feature different spatial resolution and coverage capabilities. Developing algorithms for merging different data sources offers the opportunity to generate high-resolution data in areas where only coarse measurements are available.

In this work, we propose a geostatistical simulation algorithm to downscale spaceborne low-resolution digital elevation models (LR-DEMs) using HR-DEMs derived from ground-based and airborne altimetry as training data. The method relies on the use of a training image (TI), an analogue DEM to a specific target LR-DEM, which contains information at both spatial scales. High-resolution elevation patterns are retrieved from the TI to downscale the target LR-DEM through sequential simulation. Ancillary variables on LR-DEMs serve as secondary information to evaluate which topographic patterns are more likely to occur at a given location in the target DEM.

Simulated realizations exhibit the same spatial resolution as the high-resolution patterns found on the TI and also reproduce the spatial structure and statistics of the original DEM. The method is illustrated by a case study in the Swiss Alps.

20.9

Assessing Uncertainties in Bedrock Geology Maps – a “Pre-Modelling” Approach

Anna Rauch¹, Mario Sartori¹, Yves Gouffon², Andreas Möri², Sébastien Castellort¹,

¹ *Département des sciences de la Terre, Université de Genève, Rue des Maraîchers 13, CH-1205 Genève (anna.rauch@unige.ch)*

² *Office fédéral de topographie swisstopo, Service géologique, Seftigenstrasse 264, CH- 3084 Wabern*

In all fields of geology, interpreted maps (e.g., hazard-, groundwater- or bedrock geology maps) derived from observation-based geological maps are widely used as a tool to make decisions, which are not seldom of important economic, environmental or social interest. Bedrock Geology Maps (BGM) typically represent the pattern of bedrock units on the top-bedrock topography including the parts hidden below unconsolidated deposits. BGM can be derived from geological maps such as the Geological Atlas of Switzerland and become more and more important in the GeoCover vector data sets of swisstopo. Any cross section, the basis for many 3D Models, is bound to a BGM interpretation.

Based on the same geological map, different geologists usually produce different BGM interpretations. In some regions, the uncertainty related to the bedrock geometry can be so high that its use as a tool for decision-making cannot be accepted. Yet in other regions, the BGM represents bedrock interfaces with a rather high degree of confidence. This highlights the need to assess the uncertainty at any location.

Also in the area of 3D geological models, the need to express uncertainty has been recognised. So-called “implicit” modelling techniques have been developed, which use powerful statistical analyses to estimate probabilities or variabilities associated with the position of bedrock interfaces (Lindsay et al. 2012; Wellmann et al. 2010). However, many factors come into play for the construction of a 3D Model (as for a BGM). Data-based, but also knowledge-based factors are essential to carry out structural interpretation. Implicit modelling techniques integrate specific knowledge input before data interpolation (Calcagno et al. 2008). However, knowledge-based factors are by nature quasi impossible to quantify statistically.

The aim of this project is to develop a non-statistical, 3-dimensional, pre-modelling approach, in which the uncertainty model is generated based on observed input data, i.e. outcrop and borehole data, independent of any previous interpretation or model. To do so, we define a set of geometrical rules enabling the extrapolation of interfaces between rock bodies in subcropping zones according to structural principles (e.g., geometry of topography-interface intersections in outcrop zones, exclusion zones, structural measurements). Expectedly, there are many viable solutions that respect the data and the rules. The total of viable solutions for a given interface delimits the PITE (“Plausible Interface Trace Extent”), i.e. a band in which the presence of the interface trace cannot be excluded. If a PITE forms a narrow band, it can be inferred that the BGM interpretation is strongly constrained by the input data. Where a PITE remains broad, it intuitively reflects the higher uncertainty in which the choice of the interface position is to be taken. In awareness that the definition of the rules is crucial for such pre-modelling approach, numerous tests on synthetic and natural datasets in different geological settings will be undertaken.

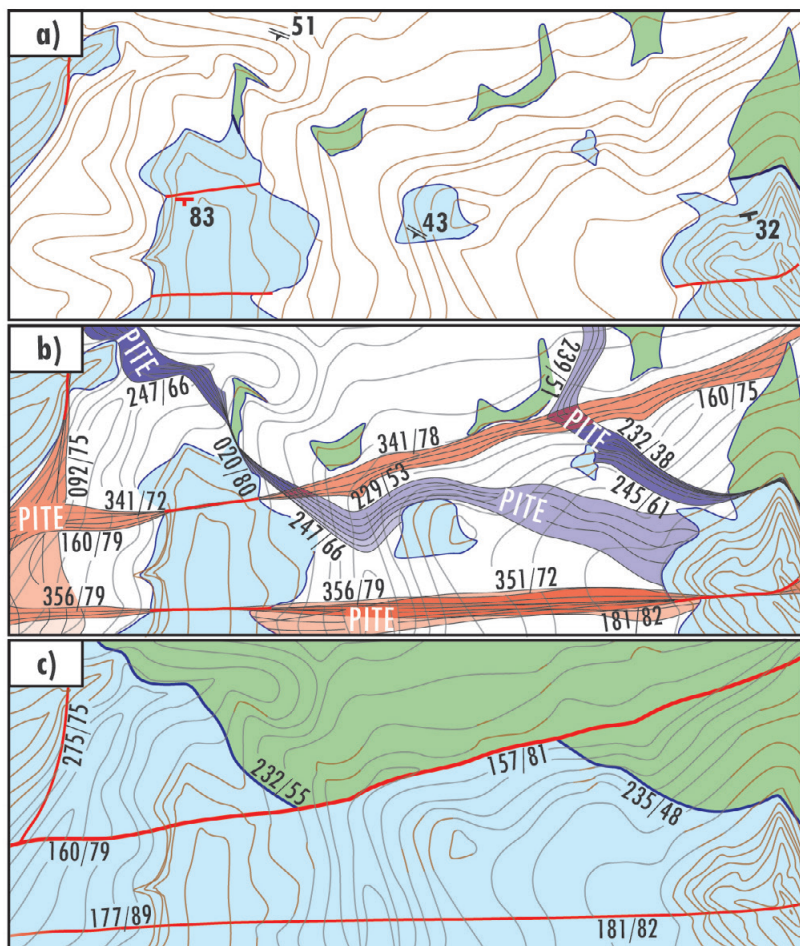


Figure 1. From the geological map to the Bedrock Geology Map (conceptual). a) Imagined geological setting showing only outcrops, faults and structural measurement data. b) Proposed uncertainty model showing PITE's (Plausible Interface Trace Extent) confined according to basic geological principles. c) One possible BGM interpretation consistent with the PITE's locations.

REFERENCES

- Calcagno, P., Chilès, J. P., Courrioux, G., & Guillen, A. 2008: Geological modelling from field data and geological knowledge. Part I. Modelling method coupling 3D potential-field interpolation and geological rules. *Physics of the Earth and Planetary Interiors* 171(1-4), 147-157.
- Lindsay, M. D., Aillères, L., Jessell, M. W., de Kemp, E. A., & Betts, P. G. 2012: Locating and quantifying geological uncertainty in three-dimensional models: Analysis of the Gippsland Basin, southeastern Australia. *Tectonophysics* 546-547, 10-27.
- Wellmann, J. F., Horowitz, F. G., Schill, E., & Regenauer-Lieb, K. 2010: Towards incorporation uncertainty of structural data in 3D geological inversion. *Tectonophysics* 490(3-4), 141-151.

P 20.1

Tools for the State of Geneva to manage its subsurface resources: Relevance of geological data

Maud Brentini¹, Stéphanie Favre², Elme Rusillon¹ & Andrea Moscariello¹

¹ *Department of Earth Sciences, University of Geneva, Rue des Maraîchers 13, CH-1205 Geneva (maud.brentini@unige.ch)*

² *Institute for Environmental Sciences, University of Geneva, Boulevard Carl Vogt 66, CH-1205 Geneva*

The use of GIS, database, web interface or OpenData services is increasingly used by geological surveys to manage their data. Until today, management of subsurface data was often regarded as less important than the interpretation and understanding of the data themselves. However, State institutions need more and more strong and secure infrastructure where surface and subsurface data are collected and stored to ensure a better understanding and management of the subsurface resources of their territory. The State of Geneva was confronted to this situation with the GEothermie2020 program. Piloted by the State of Geneva and implemented by the Services Industriels de Genève (SIG), this program aims to rework with old data, collect new one and gives, thus the opportunity to improve subsurface knowledge. Nevertheless, the actual IT infrastructure is not complete enough to centralize these data.

In the context of this program, my project consists on finding the balance between comprehensiveness and relevance of the data to integrate to the future complete database system. Geological data are numerous, various and often very heterogeneous and incorporate all data is often difficult or even impossible. One of the main challenges is to find the limit between archiving and valorising the information. The first step is, therefore, the understanding and the harmonization of regional stratigraphy. This is also a key issue to appreciate lateral variation and to design properly sedimentary body distribution through the subsurface to allow 3D modelling.

To constrain and understand better the stratigraphy and lateral variabilities of the Great Geneva Basin (GGB), nearly 50 diplomas and 10 PhD theses of the University of Geneva were consulted, enhanced by an extensive published literature search. A large work on collecting and digitizing these data was accomplished and numerous correlations sheets and stratigraphic logs were generated. In Geneva, we have a great opportunity to understand better the subsurface units by studying them in the numerous surrounding outcrops (Charollais et al., 2007, Meyer, 2000). Thus, different field campaigns on the Jura, Saleve and Vuache, were also made to complete the study.

Done over several generations, it is a real challenge to connect the different definitions, interpretations and stratigraphic associations peculiar to each author. Heterogeneities and discrepancies of the data are the main issue. Mesozoic and the Cenozoic time period form the major part of the sedimentary succession in the GGB and are principally composed of an alternation of carbonates and marls. The thicknesses and facies vary laterally across the basin. The Upper Jurassic and lower Cretaceous are the main series studied in the outcrops surrounding Geneva. However, Middle Jurassic and Lower Jurassic and Triassic series are weaker in terms of data in the area. Direct correlations with the HARMOS program, the new official Swiss stratigraphic framework (Morard, 2014, Strasser et al., 2016) are not exhaustive for all geological periods, in particular for the Jurassic and for the Triassic. Significant differences between local stratigraphic nomenclature and this new system exist and further investigations are necessary to fit to the needs. Different composite logs and a stratigraphic catalog are in progress to help the State of Geneva and the SIG in their subsurface prospections. Therefore, a clear stratigraphic framework will be available for the GGB and it will be possible to integrate homogenized data in the new IT system.

The GEothermie 2020 Program has raised the importance of harmonizing and correlating data in order to understand better the GGB subsurface geology. The future database, build on a clear geological context with relevance of the data to integrate and the accurate stratigraphic framework, will offer tools to the State of Geneva to easily find data, create correlations, modelisation and requests. Furthermore, an easier management of its subsurface resources will be possible. The development of this intelligent and interactive system for data management holds an important place, especially for such large-scale projects involving growing numbers of stakeholders.

REFERENCES

- Charollais, J., Weidmann, M., Berger, J.-P., Engesser, B., Hotellier, -F., Gorin, G., Rechenbacher, B. & Schäfer, P., 2007. La Molasse du bassin Genevois et son substratum. Archives des Sciences, vol. 60, fasc. 2-3.
- Meyer, M., 2000. Le Complexe récifal kimméridgien – tithonien du Jura méridional interne (France), évolution multifactorielle, stratigraphie et tectonique. Thèse n°3170. Terre & Environnement.
- Morard, A., 2014. Correlations beyond HARMOS: how, where, why? Swiss Geoscience Meeting 2014. Platform Geosciences, Swiss Academy of Science, SCNAT. Conference paper.
- Strasser, A., Charollais, J., Conrad, M. A., Clavel, B., Pictet, A. and Mastrangelo, B. 2016 : The Cretaceous of the Swiss Jura Mountains : an improved lithostratigraphic scheme. Swiss Journal of Geosciences, 1-20.

P 20.2

Tools for the State of Geneva to manage its subsurface resources: Data model design and implementation

Stéphanie Favre¹, Maud Brentini², Gregory Giuliani¹ & Anthony Lehmann¹

¹ *Institute for Environmental Sciences, University of Geneva, Boulevard Carl Vogt 66, CH-1205 Genève (stephanie.favre@unige.ch)*

² *Department of Earth Sciences, University of Geneva, Rue des Maraîchers 13, CH-1205 Genève (maud.brentini@unige.ch)*

Issues concerning the exploitation of the subsurface are increasingly important in the context of a sustainable territorial development (Blunier et al. 2007). A detailed and accurate knowledge of the local geology is therefore key to allow an effective exploitation and management of the existing resources. GEothermie 2020 is a program led by the State of Geneva and implemented by the Services Industriels de Genève. Aiming to develop the geothermal energy in the Geneva basin, this program offers the opportunity to improve subsurface knowledge by collecting new data, both in two and three-dimensions (2D and 3D). As owner of the subsurface, these data have to be gathered, organized and managed by the Geneva Geological Survey (Service de géologie, sols et déchets - GESDEC). Unfortunately to date, existing IT infrastructures are not sufficient to address these needs.

Funded by the State of Geneva, the main objective of this research is to develop a geological database linked to a Geographic Information System (GIS). Geological data has to be organized in a database allowing spatial requests, map production and 3D modelisation. Another main challenge relates to the link between 2D and 3D geological data, especially through the cantonal platform (ge.ch/sitg/geologie3d) that stores and displays 3D models (Gabriel et al. 2015). Furthermore, geological data must also be intersected with information on energy and territorial planning, while ensuring a monitoring of the data through time (4D).

The very first step of this study was to establish the state of the art on the current geological data management practices in Europe. In order to evaluate their Information Systems (IS), short structured questions have been sent to all European geological surveys as well as an adapted version for the cantonal and federal swiss institutes. Concerning the database and GIS development aspects, an analysis of the GESDEC's needs and constraints allowed to expand the data model previously issued from Brentini and Favre's work. These developments took place in parallel with discussions with stakeholders involved and various experts in the field of information management, geology and geothermal energy.

This preliminary study revealed that the development of a geological IS differs largely from a country to another. However, objectives and needs of geological surveys are similar. The exploitation and management of the subsurface resources of a territory requires an integrated system for geological data. In Geneva, the data model was developed according to the following themes: geology, hydrogeology, geophysics and geothermal energy (see in Figure 1). Each theme contains features that are characterized by a geometric shape (point, line or polygon), attribute tables and relations between them. The data model was designed to allow crossed requests between features through unique identifier (ID) attributes. Meanwhile, features and their attributes have been defined in a feature catalog to ensure updated metadata.

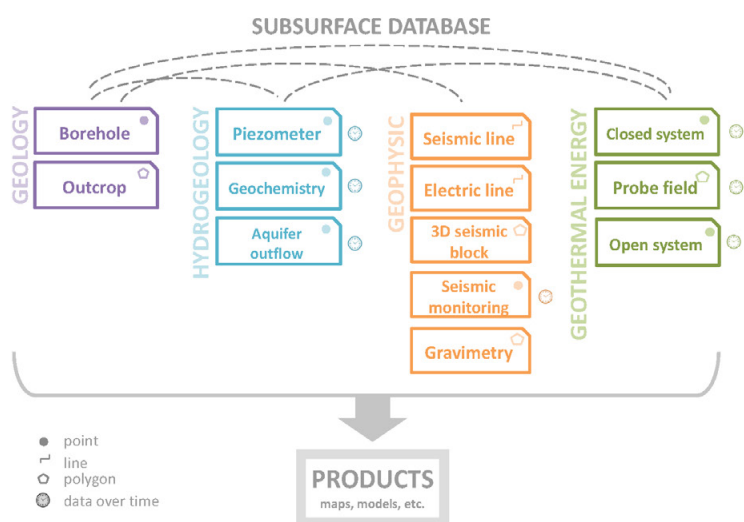


Figure 1. Global view of the subsurface database thematic data model.

The data model extension will lead to a multiple use of the subsurface database. The next step is to implement the data model in a database management system (DBMS) combined to a GIS. The whole system should be able to answer queries for the production of maps, models and protection zones, which assist an optimal management of the subsurface resources for the State of Geneva.

REFERENCES

- Blunier, P., Tacher, L. and Parriaux, A. 2007: Systemic Approach of Urban Underground Resources Exploitation. 11th ACUUS Conference: Underground Space: Expanding the Frontiers. Athens (Greece).
- Brentini, M. and Favre, S. 2014: Développement d'une base de données du sous-sol dans le cadre de GEothermie 2020: intégration des forages et lignes sismiques à Genève. Internship thesis, University of Geneva, 90p.
- Gabriel, P., Gietzel, J., Le, H., H., and Schaeben, H. 2015: GST: A Network Based Datastore for Geoscience Data and Geomodels and Its Implementation - ProMine's Contribution Towards Interoperability. Springer International Publishing Switzerland, 59-71.

P 20.3

4ONSE: 4 times Open and Non-conventional technology for Sensing the Environment

Massimiliano Cannata¹, P. K. Seneviratne Mahanama², Oka Karyanto³, Imran Shahid⁴

¹ *University of Applied Sciences and Arts of Southern Switzerland (SUPSI), Switzerland*

² *University of Moratuwa, Sri Lanka*

³ *Universitas Gadjah Mada, Indonesia*

⁴ *Institute of Space Technology, Pakistan*

4ONSE is part of the Swiss Programme for Research on Global Issues for Development (r4d programme) financed by the Swiss Agency for Development and Cooperation (SDC) and the Swiss National Science Foundation (SNSF).

The availability of complete, quality and dense monitoring hydro-meteorological data is essential to address a number of practical issues including, but not limited to, flood-water and urban drainage management, climate change impact assessment, early warning and risk management, now-casting and weather predictions. Thanks to the recent developments (Internet Of things, big data, Internet diffusion, etc.) non-conventional monitoring system based on low cost and open technologies may be a great opportunity either as a complement to standard and authoritative monitoring systems or as a vital data source in regions where traditional observation networks are in decline or missing.

In order to progress beyond the state of the art the 4ONSE project has been lunched for providing detailed information on open challenges found in literature for these kind of open and non-conventional systems, specifically: data quality, metadata accessibility and standardization. This will be achieved by integrating and further developing the available technologies to implement a fully open (data, standard, hardware and software) solution and to deploy an experimental monitoring system composed of about 30 stations which will be analysed in term of data quality; system durability; management costs; performances; sustainability. Moreover the suitability of this type of system will be evaluated in existing climatic-dependent management practices to understand its applicability, advantages and limitations.

The ultimate desired impact of 4ONSE is to strengthen the capacity of data production, usage and management in developing countries. Filling the gap that lead to monitoring network failure in developing countries will empower these countries with the ability to set-up and maintain their own climatic monitoring network. This leads, among other benefits, to: shorter reaction time in case of impending hazards, better understanding of phenomena, wiser definition of management strategies and policies and capacity to evaluate policy implementation effects. With an eye at the above strategic objective, this project intend to contribute to advance in this direction by impacting the capability of developing countries in perform researches in the field of earth observation by means of better understanding of concepts on open technologies and data capabilities. It is also important that a common sense of joint responsibility of governments, international and regional organizations, private sector and civil society is grown in order to boost this process and that the opportunity of using data from dense monitoring system and open standards is well acknowledged as a support tool for the development of new policies and activities.

P 20.4

Cluster analysis and Multi-dimensional scaling – A combined approach to discriminate carbonate microfacies

Eric Heerwagen¹ & Rossana Martini¹

¹ *Department of Earth Sciences, University of Geneva, Rue des Maraichers 13, CH-1205 Geneva (eric.heerwagen@unige.ch)*

Some decades ago, cluster analysis has been identified as a powerful tool in microfacies discrimination. In numerous case studies, mainly on the Bahamas, various authors tried to use multivariate analysis to determine, and map, microfacies belts. Their used settings (distance measure, amalgamation method, raw data, normalized data, etc.) strongly influenced the outcomes of the respective studies. That is why the recommendations for the use of cluster analysis, and its value strongly diverted. In our study, a Q-mode analysis with not normalized raw data has been performed, to identify microfacies in our samples. As distance measure Manhattan, and for amalgamation algorithm Ward was used. The final identification of the cluster, and therefore microfacies, is based on frequency data from thin section analysis, as well as on the rock texture from thin section scans. For each outcrop in Sierra del Álamo, and Barra los Tanques outcrops, eleven facies have been identified.

Additionally multi-dimensional scaling has been performed, to visualize the relationships among the groups. To create these ordination plots, the dissimilarity matrix of the cluster analysis was used. This multivariate analysis is particularly useful to assign the distinguished facies to corresponding depositional environments. Through key fossils (e.g. sponges), fix points for energy and proximity to a hypothetical shoreline were set, and trends could be identified. These two parameters allowed us to define different depositional structures of a theoretical carbonate ramp model.

Acknowledgements: This project has been funded by the Swiss National Science Foundation No. 200020-137661 and 200020-156422 to RM.

P 20.5

Analysis of forest fires clustering using the multipoint Morisita index

Mikhail Kanevski¹, Jean Golay¹, Mario Pereira²

¹ *Institute of Earth Surface Dynamics, University of Lausanne, Switzerland (Mikhail.Kanevski@unil.ch)*

² *Centre for Research and Technology of Agro-Environment and Biological Sciences, CITAB, University of Trás-os-Montes and Alto Douro, Portugal*

A new measure of clustering based on multipoint Morisita index (mMI) is applied to analyze the clustering of forest fires in Portugal. The data set consists of more than 30000 fire events covering the time period from 1975 to 2013. The distribution of forest fires is very complex and highly variable in space. The mMI is a recent development of the classical two-point Morisita index, which is usually used in spatial data analysis to characterize the clustering of point patterns. In essence, mMI is estimated by covering the region of the study by a grid and by computing how many times more likely it is that m points selected at random will be from the same grid cell than it would be in the case of a complete random Poisson process. By changing the number of grid cells (size of the grid cells), mMI characterizes the scaling properties of spatial clustering. From mMI, the data intrinsic dimension (fractal dimension) of the point distribution can be estimated as well.

In this study, the mMI of forest fires is compared with the mMI of random patterns (RPs) generated within the validity domain defined by the forest zones of Portugal. It turns out that the forest fires are highly clustered inside the validity domain in comparison with the RPs. Moreover, they demonstrate different scaling properties at different spatial scales. The results obtained from the mMI analysis are also compared with those of fractal measures of clustering – box counting and sand box counting approaches.

REFERENCES

- Golay, J., Kanevski, M., Vega Orozco, C. & Leuenberger, M., 2014: The multipoint Morisita index for the analysis of spatial patterns. *Physica A*, 406, 191-202.
- Golay, J. & Kanevski, M. 2015: A new estimator of intrinsic dimension based on the multipoint Morisita index. *Pattern Recognition*, 48, 4070-4081.

P 20.6

Wildfire susceptibility: Comparing deterministic approach with machine learning

Michael Leuenberger¹, Joana Parente², Marj Tonini¹, Mário Pereira^{2,3} & Mikhail Kanevski¹

¹ *Institute of Earth Surface Dynamics (IDYST), University of Lausanne, CH-1000 Lausanne (michael.leuenberger@unil.ch)*

² *Centro de Investigação e de Tecnologias Agro-Ambientais e Biológicas (CITAB), Universidade de Trás-os-Montes e Alto Douro, P-5000-801 Vila Real*

³ *Instituto Dom Luiz (IDL), Faculdade de Ciências da Universidade de Lisboa, Campo Grande, Edifício C8, Piso 3, P-1749-016 Lisboa*

Wildfire susceptibility is a measure of the terrain/land propensity for occurrence or spread of a wildfire due only to the terrain's intrinsic characteristics. Associated with the fire probability, the fire hazard can be determined and therefore, it is a fundamental component of the fire risk conceptual framework. Different methods and tools were tested, used and compared to model and map wildfire susceptibility. First, the deterministic and linear approach proposed by Verde & Zêzere (2010) and, second, two non-linear methods including the Extreme Learning Machine (ELM, Huang et al. 2006) and different approaches of Random Forest (RF, Breiman 2001). For comparison purposes, the same predisposing variables (slope and vegetation cover) were combined and used as predictions in all models.

The Portuguese PROF (*Planos Regionais de Ordenamento Florestal*) region of Dão-Lafões was selected as a case study because it allows reducing the size area, which is Portugal, without loss of generality. Moreover, this region belongs into the range of national average values of the number of fires and burnt area, and includes a high heterogeneity in land cover and slope. Notice that Portugal is, by far, the European country most affected by wildfires.

By means of GIS techniques, prediction maps, which represent the susceptibility of the study area to fire, were obtained. Comparison of the different methods includes the location of the pixels with similar standardized susceptibility and total validation burnt area in each of five susceptibility classes. Results obtained with all different methods are very alike and allow to obtain similar fire susceptibility maps and variables' importance ranking.

REFERENCES

Breiman, L. 2001: Random forest. *Machine Learning* 45, 5-32.

Huang, G.-B., Zhu, Q.-Y. & Siew, C.-K. 2006: Extreme learning machine: Theory and applications. *Neurocomputing* 70, 489-501.

Verde, J.C. & Zêzere, J.L. 2010: Assessment and validation of wildfire susceptibility and hazard in Portugal. *Natural Hazard and Earth System Science* 10(3), 485-497.

P 20.7

Analysis of wind speed data using network science measures

Mohamed Laib, Mikhail Kanevski

Institute of Earth Surface Dynamics, University of Lausanne, Switzerland (Mohamed.Laib@unil.ch)

Recently application of network science has gained a considerable interest in different scientific disciplines, from social networks to environmental monitoring. In this research, measures of network science are used to analyse the spatio-temporal structure of wind speed. Using more than 100 weather stations covering Switzerland, and taken at 10 minutes intervals. The correlation between these stations is used to construct networks.

The temporal evolution of these networks is studied and quantified using their density. Such analysis gives better visualization of wind speed structure, and analyses the change of connectivity over time in terms of network density. Furthermore, it is useful for investigating if there is any topographical similarity between the connected stations. Finally, the time series given by the network density over time (fig. 1) is studied. According to the Hurst exponent, the existence of long-memory dependence of connectivity between stations is confirmed. Such results can be useful on risk assessment, when the correlations are positive. It means, when a wind storm is happened in one place, it is possible to predict if the same storm will happen elsewhere.

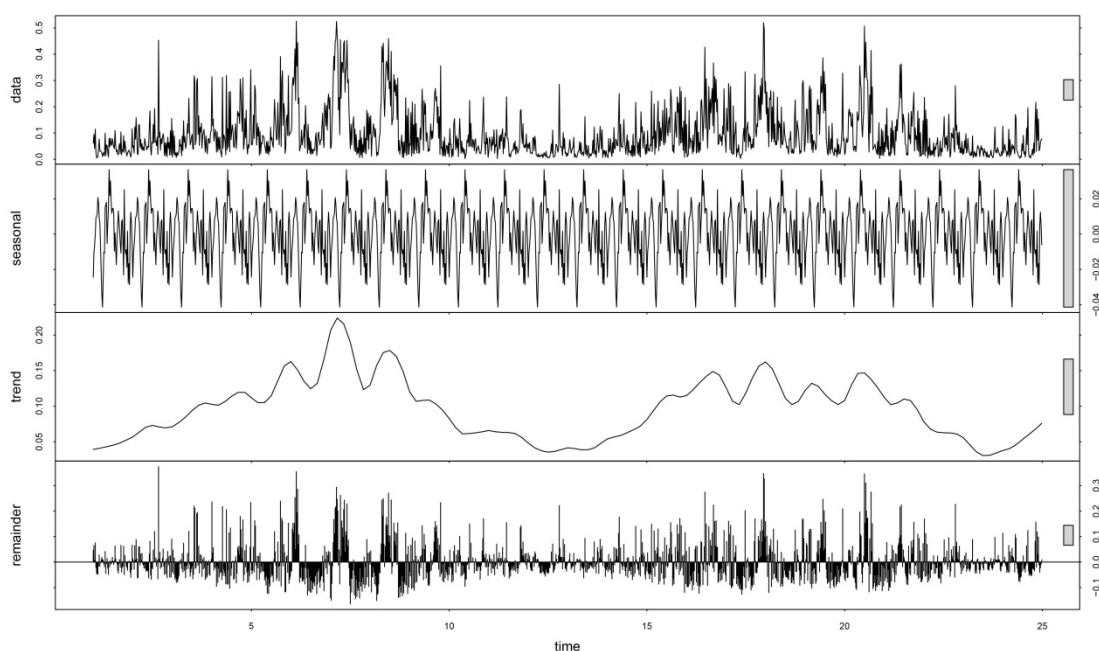


Fig 1. Time series of networks density over time.

REFERENCES

- Domino K et al., The use of copula functions for predictive analysis of correlation between extreme storm tides, *Physica A*, 413 (2014) 489 - 497.
- Hastie T., et al., *The Elements of Statistical Learning*, 2nd ed. p. 745, Springer, New York, 2009.
- Stanley Wasserman, Katherine Faust, *Social Network analysis: Methods and Applications*, p. 854, Cambridge University Press, 1994.
- Yuan N., et al., Effect of extreme value loss on long-term correlated time series, *Theo Appl Climatol* 109 (2012) 133-140.

P 20.8

Field Data Collection Methods and Data Processing of the Influence of Low Momentum Ratio and the Rate of Sediment Transport Forcing on Confluence Hydrodynamics, Morphodynamics and Mixing

Gelare Moradi¹, Romain Cardot¹, Stuart N. Lane¹ & Colin D. Rennie²

¹ Faculty of Geosciences and Environment, Institute of Earth Surface Dynamics, University of Lausanne, Quartier UNIL-Mouline, Bâtiment Géopolis, CH-1015 Lausanne (gelare.moradi@unil.ch)

² Dept. of Civil Engineering, Colonel By building, office A-015, 161 Louis Pasteur St., Ottawa, ON, K1N 6N5, CANADA

River confluences are zones where two or more rivers join and form a single channel downstream of their junction. Because of their essential role in the dynamic of fluvial networks, there has been an increase in the attention given to their hydrodynamics and morphodynamics during last three decades. Despite this increased understanding of the complex flow behavior and morphological aspects, few studies has been focused on low momentum ratio river confluences and mixing processes. As among these few studies, most of them have been driven by the mean of laboratory experiments and numerical models, a combination of field data collection and data processing is required to study the effect of low momentum ratio on flow dynamic, rive morphology and rate of mixing in river confluences.

In the present poster, the flow discharge and velocity data of two upper Rhône river confluences in Switzerland, which are characterized by low momentum ratio and a varied rate of poorly sorted sediment transport is shown. The data set is mostly collected, using spatial distributed acoustic Doppler current profiling (aDcp) measurements. The morphological changes are studied using a combination of high-resolution aerial imagery data obtained by a phantom drone and acoustic bathymetric surveys. The mixing processes are investigated by measuring the surface water temperature with a thermic camera mounted on an E-bee drone [*whereas sediment pathways can be explored through the use of the 'bottom-tracking' feature of the aDcp device (not sure there will be such results at the conference time)*].

These collected data is processed using a matlab code, Pix4D and visualization software. These processed data then can be used to describe the flow behavior, morphological aspects and mixing processes at river confluences characterized by low momentum ratio and to test laboratory derived conceptual models of flow processes at such junctions. The obtained results can be used under a wider range of forcing conditions to provide detailed data on the three-dimensional flow field and the morphology, to validate numerical models.